



کاربر گرامی..

این کتاب از کتابخانه مجازی کتابلاین دانلود شده است.برای دریافت رایگان و بدون محدودیت انواع کتاب الکترونیکی | صوتی و کتاب موبایل به آدرس زیر مراجعه کنید.(کتابلاین را تنها با این نشان و آدرس زیر بشناسید)

www.Ketabline.com

توجه:

- این کتاب رایگان بوده و خرید یا فروش آن به هر نحوی ممنوع است.

- تمامی حقوق مادی و معنوی این اثر برای نویسنده/ناشر و کتابخانه مجازی کتابلاین محفوظ است.

- در صورت وجود اشکال یا اشتباه در ساختار این کتاب یا کتابخانه میتوانید موضوع را به آدرس ایمیل زیر ارسال نمایید تا در کمتر از 12 ساعت مورد پیگیری قرار گیرد.

Info@Ketabline.com

مجموعه کتابخانه های کتابلاین:

کتابخانه موبایل | کتابخانه صوتی | کتابخانه الکترونیکی

mobilebook.ketabline.com | audiobook.ketabline.com | ebook.Ketabline.com

ketabline.com Ebook.ketabline.com

Fluid Mechanics



ketabline.com Ebook.ketabline.com

McGraw-Hill Series in Mechanical Engineering

CONSULTING EDITORS

Jack P. Holman, *Southern Methodist University*

John Lloyd, *Michigan State University*

Anderson
Computational Fluid Dynamics: The Basics with Applications

Anderson
Modern Compressible Flow: With Historical Perspective

Arora
Introduction to Optimum Design

Borman and Ragland
Combustion Engineering

Burton
Introduction to Dynamic Systems Analysis

Culp
Principles of Energy Conversion

Dieter
Engineering Design: A Materials & Processing Approach

Doebelin
Engineering Experimentation: Planning, Execution, Reporting

Driels
Linear Control Systems Engineering

Edwards and McKee
Fundamentals of Mechanical Component Design

Gebhart
Heat Conduction and Mass Diffusion

Gibson
Principles of Composite Material Mechanics

Hamrock
Fundamentals of Fluid Film Lubrication

Heywood
Internal Combustion Engine Fundamentals

Hinze
Turbulence

Histand and Alciatore
Introduction to Mechatronics and Measurement Systems

Holman
Experimental Methods for Engineers

Howell and Buckius
Fundamentals of Engineering Thermodynamics

Jaluria
Design and Optimization of Thermal Systems

Juvinall
Engineering Considerations of Stress, Strain, and Strength

Kays and Crawford
Convective Heat and Mass Transfer

Kelly
Fundamentals of Mechanical Vibrations

Kimbrell
Kinematics Analysis and Synthesis

Kreider and Rabl
Heating and Cooling of Buildings

Martin
Kinematics and Dynamics of Machines

Mattingly
Elements of Gas Turbine Propulsion

Modest
Radiative Heat Transfer

Norton
Design of Machinery

Oosthuizen and Carscallen
Compressible Fluid Flow

Oosthuizen and Naylor
Introduction to Convective Heat Transfer Analysis

Phelan
Fundamentals of Mechanical Design

Reddy
An Introduction to Finite Element Method

Rosenberg and Karnopp
Introduction to Physical Systems Dynamics

Schlichting
Boundary-Layer Theory

Shames
Mechanics of Fluids

Shigley
Kinematic Analysis of Mechanisms

Shigley and Mischke
Mechanical Engineering Design

Shigley and Uicker
Theory of Machines and Mechanisms

Stiffler
Design with Microprocessors for Mechanical Engineers

Stoecker and Jones
Refrigeration and Air Conditioning

Turns
An Introduction to Combustion: Concepts and Applications

Ullman
The Mechanical Design Process

Wark
Advanced Thermodynamics for Engineers

Wark and Richards
Thermodynamics

White
Viscous Fluid Flow

Zeid
CAD/CAM Theory and Practice



ketabline.com Ebook.ketabline.com

Fluid Mechanics

Fourth Edition

Frank M. White
University of Rhode Island

WCB McGraw-Hill

Boston Burr Ridge, IL Dubuque, IA Madison, WI New York San Francisco St. Louis
Bangkok Bogotá Caracas Lisbon London Madrid
Mexico City Milan New Delhi Seoul Singapore Sydney Taipei Toronto



ketabline.com Ebook.ketabline.com

About the Author

Frank M. White is Professor of Mechanical and Ocean Engineering at the University of Rhode Island. He studied at Georgia Tech and M.I.T. In 1966 he helped found, at URI, the first department of ocean engineering in the country. Known primarily as a teacher and writer, he has received eight teaching awards and has written four textbooks on fluid mechanics and heat transfer.

During 1979–1990 he was editor-in-chief of the *ASME Journal of Fluids Engineering* and then served from 1991 to 1997 as chairman of the ASME Board of Editors and of the Publications Committee. He is a Fellow of ASME and in 1991 received the ASME Fluids Engineering Award. He lives with his wife, Jeanne, in Narragansett, Rhode Island.



ketabline.com Ebook.ketabline.com

To Jeanne



ketabline.com Ebook.ketabline.com

Preface

General Approach

The fourth edition of this textbook sees some additions and deletions but no philosophical change. The basic outline of eleven chapters and five appendices remains the same. The triad of integral, differential, and experimental approaches is retained and is approached in that order of presentation. The book is intended for an undergraduate course in fluid mechanics, and there is plenty of material for a full year of instruction. The author covers the first six chapters and part of Chapter 7 in the introductory semester. The more specialized and applied topics from Chapters 7 to 11 are then covered at our university in a second semester. The informal, student-oriented style is retained and, if it succeeds, has the flavor of an interactive lecture by the author.

Learning Tools

Approximately 30 percent of the problem exercises, and some fully worked examples, have been changed or are new. The total number of problem exercises has increased to more than 1500 in this fourth edition. The focus of the new problems is on practical and realistic fluids engineering experiences. Problems are grouped according to topic, and some are labeled either with an asterisk (especially challenging) or a computer-disk icon (where computer solution is recommended). A number of new photographs and figures have been added, especially to illustrate new design applications and new instruments.

Professor John Cimbala, of Pennsylvania State University, contributed many of the new problems. He had the great idea of setting *comprehensive problems* at the end of each chapter, covering a broad range of concepts, often from several different chapters. These comprehensive problems grow and recur throughout the book as new concepts arise. Six more open-ended design projects have been added, making 15 projects in all. The projects allow the student to set sizes and parameters and achieve good design with more than one approach.

An entirely new addition is a set of 95 multiple-choice problems suitable for preparing for the Fundamentals of Engineering (FE) Examination. These FE problems come at the end of Chapters 1 to 10. Meant as a realistic practice for the actual FE Exam, they are engineering problems with five suggested answers, all of them plausible, but only one of them correct.



ketabline.com Ebook.ketabline.com

New to this book, and to any fluid mechanics textbook, is a special appendix, Appendix E, Introduction to the Engineering Equation Solver (EES), which is keyed to many examples and problems throughout the book. The author finds EES to be an extremely attractive tool for applied engineering problems. Not only does it solve arbitrarily complex systems of equations, written in any order or form, but also it has built-in property evaluations (density, viscosity, enthalpy, entropy, etc.), linear and nonlinear regression, and easily formatted parameter studies and publication-quality plotting. The author is indebted to Professors Sanford Klein and William Beckman, of the University of Wisconsin, for invaluable and continuous help in preparing this EES material. The book is now available with or without an EES problems disk. The EES engine is available to adopters of the text with the problems disk.

Another welcome addition, especially for students, is Answers to Selected Problems. Over 600 answers are provided, or about 43 percent of all the regular problem assignments. Thus a compromise is struck between sometimes having a specific numerical goal and sometimes directly applying yourself and hoping for the best result.

Content Changes

There are revisions in every chapter. Chapter 1—which is purely introductory and could be assigned as reading—has been toned down from earlier editions. For example, the discussion of the fluid acceleration vector has been moved entirely to Chapter 4. Four brief new sections have been added: (1) the uncertainty of engineering data, (2) the use of EES, (3) the FE Examination, and (4) recommended problem-solving techniques.

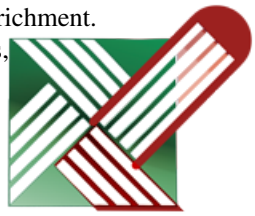
Chapter 2 has an improved discussion of the stability of floating bodies, with a fully derived formula for computing the metacentric height. Coverage is confined to static fluids and rigid-body motions. An improved section on pressure measurement discusses modern microsensors, such as the fused-quartz bourdon tube, micromachined silicon capacitive and piezoelectric sensors, and tiny (2 mm long) silicon resonant-frequency devices.

Chapter 3 tightens up the energy equation discussion and retains the plan that Bernoulli's equation comes *last,* after control-volume mass, linear momentum, angular momentum, and energy studies. Although some texts begin with an entire chapter on the Bernoulli equation, this author tries to stress that it is a dangerously restricted relation which is often misused by both students and graduate engineers.

In Chapter 4 a few inviscid and viscous flow examples have been added to the basic partial differential equations of fluid mechanics. More extensive discussion continues in Chapter 8.

Chapter 5 is more successful when one selects scaling variables before using the pi theorem. Nevertheless, students still complain that the problems are too ambiguous and lead to too many different parameter groups. Several problem assignments now contain a few hints about selecting the repeating variables to arrive at traditional pi groups.

In Chapter 6, the "alternate forms of the Moody chart" have been resurrected as problem assignments. Meanwhile, the three basic pipe-flow problems—pressure drop, flow rate, and pipe sizing—can easily be handled by the EES software, and examples are given. Some newer flowmeter descriptions have been added for further enrichment. Chapter 7 has added some new data on drag and resistance of various bodies, biological systems which adapt to the flow of wind and water.



ketabline.com Ebook.ketabline.com

Chapter 8 picks up from the sample plane potential flows of Section 4.10 and plunges right into inviscid-flow analysis, especially aerodynamics. The discussion of numerical methods, or computational fluid dynamics (CFD), both inviscid and viscous, steady and unsteady, has been greatly expanded. Chapter 9, with its myriad complex algebraic equations, illustrates the type of examples and problem assignments which can be solved more easily using EES. A new section has been added about the suborbital X-33 and VentureStar vehicles.

In the discussion of open-channel flow, Chapter 10, we have further attempted to make the material more attractive to civil engineers by adding real-world comprehensive problems and design projects from the author's experience with hydropower projects. More emphasis is placed on the use of friction factors rather than on the Manning roughness parameter. Chapter 11, on turbomachinery, has added new material on compressors and the delivery of gases. Some additional fluid properties and formulas have been included in the appendices, which are otherwise much the same.

Supplements

The all new **Instructor's Resource CD** contains a PowerPoint presentation of key text figures as well as additional helpful teaching tools. The list of films and videos, formerly App. C, is now omitted and relegated to the **Instructor's Resource CD.**

The **Solutions Manual** provides complete and detailed solutions, including problem statements and artwork, to the end-of-chapter problems. It may be photocopied for posting or preparing transparencies for the classroom.

EES Software

The Engineering Equation Solver (EES) was developed by Sandy Klein and Bill Beckman, both of the University of Wisconsin—Madison. A combination of equation-solving capability and engineering property data makes EES an extremely powerful tool for your students. EES (pronounced "ease") enables students to solve problems, especially design problems, and to ask "what if" questions. EES can do optimization, parametric analysis, linear and nonlinear regression, and provide publication-quality plotting capability. Simple to master, this software allows you to enter equations in any form and in any order. It automatically rearranges the equations to solve them in the most efficient manner.

EES is particularly useful for fluid mechanics problems since much of the property data needed for solving problems in these areas are provided in the program. Air tables are built-in, as are psychometric functions and Joint Army Navy Air Force (JANAF) table data for many common gases. Transport properties are also provided for all substances. EES allows the user to enter property data or functional relationships written in Pascal, C, C++, or Fortran. The EES engine is available free to qualified adopters via a password-protected website, to those who adopt the text with the problems disk. The program is updated every semester.

The EES software problems disk provides examples of typical problems in this text. Problems solved are denoted in the text with a disk symbol. Each fully documented solution is actually an EES program that is run using the EES engine. Each program provides detailed comments and on-line help. These programs illustrate the use of EES and help the student master the important concepts without the ca[illegible] that has been previously required.



ketabline.com Ebook.ketabline.com

Acknowledgments

So many people have helped me, in addition to Professors John Cimbala, Sanford Klein, and William Beckman, that I cannot remember or list them all. I would like to express my appreciation to many reviewers and correspondents who gave detailed suggestions and materials: Osama Ibrahim, University of Rhode Island; Richard Lessmann, University of Rhode Island; William Palm, University of Rhode Island; Deborah Pence, University of Rhode Island; Stuart Tison, National Institute of Standards and Technology; Paul Lupke, Druck Inc.; Ray Worden, Russka, Inc.; Amy Flanagan, Russka, Inc.; Søren Thalund, Greenland Tourism a/s; Eric Bjerregaard, Greenland Tourism a/s; Martin Girard, DH Instruments, Inc.; Michael Norton, Nielsen-Kellerman Co.; Lisa Colomb, Johnson-Yokogawa Corp.; K. Eisele, Sulzer Innotec, Inc.; Z. Zhang, Sultzer Innotec, Inc.; Helen Reed, Arizona State University; F. Abdel Azim El-Sayed, Zagazig University; Georges Aigret, Chimay, Belgium; X. He, Drexel University; Robert Loerke, Colorado State University; Tim Wei, Rutgers University; Tom Conlisk, Ohio State University; David Nelson, Michigan Technological University; Robert Granger, U.S. Naval Academy; Larry Pochop, University of Wyoming; Robert Kirchhoff, University of Massachusetts; Steven Vogel, Duke University; Capt. Jason Durfee, U.S. Military Academy; Capt. Mark Wilson, U.S. Military Academy; Sheldon Green, University of British Columbia; Robert Martinuzzi, University of Western Ontario; Joel Ferziger, Stanford University; Kishan Shah, Stanford University; Jack Hoyt, San Diego State University; Charles Merkle, Pennsylvania State University; Ram Balachandar, University of Saskatchewan; Vincent Chu, McGill University; and David Bogard, University of Texas at Austin.

The editorial and production staff at WCB McGraw-Hill have been most helpful throughout this project. Special thanks go to Debra Riegert, Holly Stark, Margaret Rathke, Michael Warrell, Heather Burbridge, Sharon Miller, Judy Feldman, and Jennifer Frazier. Finally, I continue to enjoy the support of my wife and family in these writing efforts.



ketabline.com Ebook.ketabline.com

Contents

Preface xi

Chapter 1
Introduction 3

1.1 Preliminary Remarks 3
1.2 The Concept of a Fluid 4
1.3 The Fluid as a Continuum 6
1.4 Dimensions and Units 7
1.5 Properties of the Velocity Field 14
1.6 Thermodynamic Properties of a Fluid 16
1.7 Viscosity and Other Secondary Properties 22
1.8 Basic Flow-Analysis Techniques 35
1.9 Flow Patterns: Streamlines, Streaklines, and Pathlines 37
1.10 The Engineering Equation Solver 41
1.11 Uncertainty of Experimental Data 42
1.12 The Fundamentals of Engineering (FE) Examination 43
1.13 Problem-Solving Techniques 44
1.14 History and Scope of Fluid Mechanics 44
Problems 46
Fundamentals of Engineering Exam Problems 53
Comprehensive Problems 54
References 55

Chapter 2
Pressure Distribution in a Fluid 59

2.1 Pressure and Pressure Gradient 59
2.2 Equilibrium of a Fluid Element 61
2.3 Hydrostatic Pressure Distributions 63
2.4 Application to Manometry 70
2.5 Hydrostatic Forces on Plane Surfaces 74
2.6 Hydrostatic Forces on Curved Surfaces 79
2.7 Hydrostatic Forces in Layered Fluids 82
2.8 Buoyancy and Stability 84
2.9 Pressure Distribution in Rigid-Body Motion 89
2.10 Pressure Measurement 97
Summary 100
Problems 102
Word Problems 125
Fundamentals of Engineering Exam Problems 125
Comprehensive Problems 126
Design Projects 127
References 127

Chapter 3
Integral Relations for a Control Volume 129

3.1 Basic Physical Laws of Fluid Mechanics 129
3.2 The Reynolds Transport Theorem 133
3.3 Conservation of Mass 141
3.4 The Linear Momentum Equation 146
3.5 The Angular-Momentum Theorem 158
3.6 The Energy Equation 163
3.7 Frictionless Flow: The Bernoulli Equation 174
Summary 183
Problems 184
Word Problems 210
Fundamentals of Engineering Exam Problems 210
Comprehensive Problems 211
Design Project 212
References 213



ketabline.com Ebook.ketabline.com

Chapter 4
Differential Relations for a Fluid Particle 215

4.1 The Acceleration Field of a Fluid 215
4.2 The Differential Equation of Mass Conservation 217
4.3 The Differential Equation of Linear Momentum 223
4.4 The Differential Equation of Angular Momentum 230
4.5 The Differential Equation of Energy 231
4.6 Boundary Conditions for the Basic Equations 234
4.7 The Stream Function 238
4.8 Vorticity and Irrotationality 245
4.9 Frictionless Irrotational Flows 247
4.10 Some Illustrative Plane Potential Flows 252
4.11 Some Illustrative Incompressible Viscous Flows 258
Summary 263
Problems 264
Word Problems 273
Fundamentals of Engineering Exam Problems 273
Comprehensive Applied Problem 274
References 275

Chapter 5
Dimensional Analysis and Similarity 277

5.1 Introduction 277
5.2 The Principle of Dimensional Homogeneity 280
5.3 The Pi Theorem 286
5.4 Nondimensionalization of the Basic Equations 292
5.5 Modeling and Its Pitfalls 301
Summary 311
Problems 311
Word Problems 318
Fundamentals of Engineering Exam Problems 319
Comprehensive Problems 319
Design Projects 320
References 321

Chapter 6
Viscous Flow in Ducts 325

6.1 Reynolds-Number Regimes 325
6.2 Internal versus External Viscous Flows 330
6.3 Semiempirical Turbulent Shear Correlations 333
6.4 Flow in a Circular Pipe 338
6.5 Three Types of Pipe-Flow Problems 351
6.6 Flow in Noncircular Ducts 357
6.7 Minor Losses in Pipe Systems 367
6.8 Multiple-Pipe Systems 375
6.9 Experimental Duct Flows: Diffuser Performance 381
6.10 Fluid Meters 385
Summary 404
Problems 405
Word Problems 420
Fundamentals of Engineering Exam Problems 420
Comprehensive Problems 421
Design Projects 422
References 423

Chapter 7
Flow Past Immersed Bodies 427

7.1 Reynolds-Number and Geometry Effects 427
7.2 Momentum-Integral Estimates 431
7.3 The Boundary-Layer Equations 434
7.4 The Flat-Plate Boundary Layer 436
7.5 Boundary Layers with Pressure Gradient 445
7.6 Experimental External Flows 451
Summary 476
Problems 476
Word Problems 489
Fundamentals of Engineering Exam Problems 489
Comprehensive Problems 490
Design Project 491
References 491

Chapter 8
Potential Flow and Computational Fluid Dynamics 495

8.1 Introduction and Review 495
8.2 Elementary Plane-Flow Solutions 498
8.3 Superposition of Plane-Flow Solutions 500
8.4 Plane Flow Past Closed-Body Shapes 507
8.5 Other Plane Potential Flows 516
8.6 Images 521
8.7 Airfoil Theory 523
8.8 Axisymmetric Potential Flow 534
8.9 Numerical Analysis 540
Summary 555



ketabline.com Ebook.ketabline.com

Problems 555
Word Problems 566
Comprehensive Problems 566
Design Projects 567
References 567

Chapter 9
Compressible Flow 571

9.1 Introduction 571
9.2 The Speed of Sound 575
9.3 Adiabatic and Isentropic Steady Flow 578
9.4 Isentropic Flow with Area Changes 583
9.5 The Normal-Shock Wave 590
9.6 Operation of Converging and Diverging Nozzles 598
9.7 Compressible Duct Flow with Friction 603
9.8 Frictionless Duct Flow with Heat Transfer 613
9.9 Two-Dimensional Supersonic Flow 618
9.10 Prandtl-Meyer Expansion Waves 628
Summary 640
Problems 641
Word Problems 653
Fundamentals of Engineering Exam Problems 653
Comprehensive Problems 654
Design Projects 654
References 655

Chapter 10
Open-Channel Flow 659

10.1 Introduction 659
10.2 Uniform Flow; the Chézy Formula 664
10.3 Efficient Uniform-Flow Channels 669
10.4 Specific Energy; Critical Depth 671
10.5 The Hydraulic Jump 678
10.6 Gradually Varied Flow 682
10.7 Flow Measurement and Control by Weirs 687
Summary 695
Problems 695
Word Problems 706
Fundamentals of Engineering Exam Problems 707
Comprehensive Problems 707
Design Projects 707
References 708

Chapter 11
Turbomachinery 711

11.1 Introduction and Classification 711
11.2 The Centrifugal Pump 714
11.3 Pump Performance Curves and Similarity Rules 720
11.4 Mixed- and Axial-Flow Pumps: The Specific Speed 729
11.5 Matching Pumps to System Characteristics 735
11.6 Turbines 742
Summary 755
Problems 755
Word Problems 765
Comprehensive Problems 766
Design Project 767
References 767

Appendix A **Physical Properties of Fluids** 769

Appendix B **Compressible-Flow Tables** 774

Appendix C **Conversion Factors** 791

Appendix D **Equations of Motion in Cylindrical Coordinates** 793

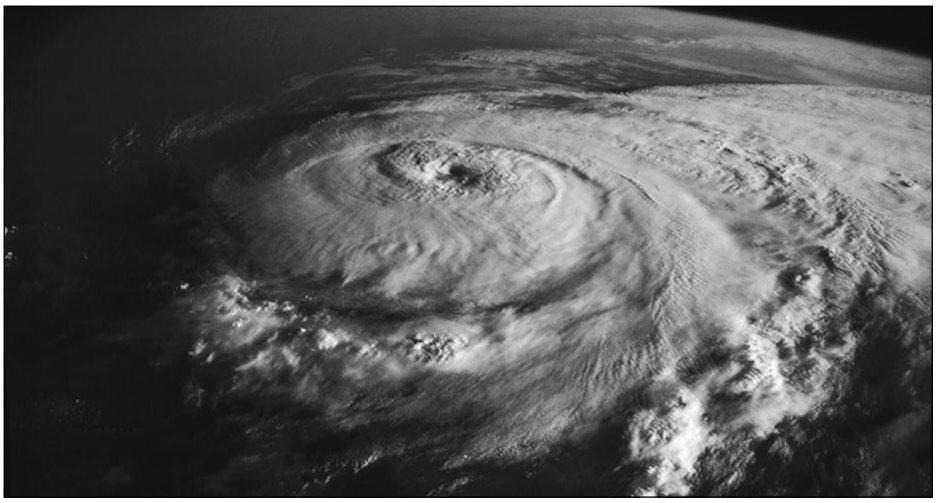
Appendix E **Introduction to EES** 795

Answers to Selected Problems 806

Index 813



ketabline.com Ebook.ketabline.com



Hurricane Elena in the Gulf of Mexico. Unlike most small-scale fluids engineering applications, hurricanes are strongly affected by the Coriolis acceleration due to the rotation of the earth, which causes them to swirl counterclockwise in the Northern Hemisphere. The physical properties and boundary conditions which govern such flows are discussed in the present chapter. *(Courtesy of NASA/Color-Pic Inc./E.R. Degginger/Color-Pic Inc.)*



ketabline.com Ebook.ketabline.com

Chapter 1
Introduction

1.1 Preliminary Remarks

Fluid mechanics is the study of fluids either in motion (fluid *dynamics*) or at rest (fluid *statics*) and the subsequent effects of the fluid upon the boundaries, which may be either solid surfaces or interfaces with other fluids. Both gases and liquids are classified as fluids, and the number of fluids engineering applications is enormous: breathing, blood flow, swimming, pumps, fans, turbines, airplanes, ships, rivers, windmills, pipes, missiles, icebergs, engines, filters, jets, and sprinklers, to name a few. When you think about it, almost everything on this planet either is a fluid or moves within or near a fluid.

The essence of the subject of fluid flow is a judicious compromise between theory and experiment. Since fluid flow is a branch of mechanics, it satisfies a set of well-documented basic laws, and thus a great deal of theoretical treatment is available. However, the theory is often frustrating, because it applies mainly to idealized situations which may be invalid in practical problems. The two chief obstacles to a workable theory are geometry and viscosity. The basic equations of fluid motion (Chap. 4) are too difficult to enable the analyst to attack arbitrary geometric configurations. Thus most textbooks concentrate on flat plates, circular pipes, and other easy geometries. It is possible to apply numerical computer techniques to complex geometries, and specialized textbooks are now available to explain the new *computational fluid dynamics* (CFD) approximations and methods [1, 2, 29].[1] This book will present many theoretical results while keeping their limitations in mind.

The second obstacle to a workable theory is the action of viscosity, which can be neglected only in certain idealized flows (Chap. 8). First, viscosity increases the difficulty of the basic equations, although the boundary-layer approximation found by Ludwig Prandtl in 1904 (Chap. 7) has greatly simplified viscous-flow analyses. Second, viscosity has a destabilizing effect on all fluids, giving rise, at frustratingly small velocities, to a disorderly, random phenomenon called *turbulence*. The theory of turbulent flow is crude and heavily backed up by experiment (Chap. 6), yet it can be quite serviceable as an engineering estimate. Textbooks now present digital-computer techniques for turbulent-flow analysis [32], but they are based strictly upon empirical assumptions regarding the time mean of the turbulent stress field.

[1]Numbered references appear at the end of each chapter.



ketabline.com Ebook.ketabline.com

Thus there is theory available for fluid-flow problems, but in all cases it should be backed up by experiment. Often the experimental data provide the main source of information about specific flows, such as the drag and lift of immersed bodies (Chap. 7). Fortunately, fluid mechanics is a highly visual subject, with good instrumentation [4, 5, 35], and the use of dimensional analysis and modeling concepts (Chap. 5) is widespread. Thus experimentation provides a natural and easy complement to the theory. You should keep in mind that theory and experiment should go hand in hand in all studies of fluid mechanics.

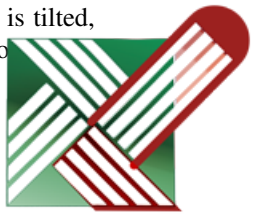
1.2 The Concept of a Fluid

From the point of view of fluid mechanics, all matter consists of only two states, fluid and solid. The difference between the two is perfectly obvious to the layperson, and it is an interesting exercise to ask a layperson to put this difference into words. The technical distinction lies with the reaction of the two to an applied shear or tangential stress. *A solid can resist a shear stress by a static deformation; a fluid cannot*. Any shear stress applied to a fluid, no matter how small, will result in motion of that fluid. The fluid moves and deforms continuously as long as the shear stress is applied. As a corollary, we can say that a fluid at rest must be in a state of zero shear stress, a state often called the hydrostatic stress condition in structural analysis. In this condition, Mohr's circle for stress reduces to a point, and there is no shear stress on any plane cut through the element under stress.

Given the definition of a fluid above, every layperson also knows that there are two classes of fluids, *liquids* and *gases*. Again the distinction is a technical one concerning the effect of cohesive forces. A liquid, being composed of relatively close-packed molecules with strong cohesive forces, tends to retain its volume and will form a free surface in a gravitational field if unconfined from above. Free-surface flows are dominated by gravitational effects and are studied in Chaps. 5 and 10. Since gas molecules are widely spaced with negligible cohesive forces, a gas is free to expand until it encounters confining walls. A gas has no definite volume, and when left to itself without confinement, a gas forms an atmosphere which is essentially hydrostatic. The hydrostatic behavior of liquids and gases is taken up in Chap. 2. Gases cannot form a free surface, and thus gas flows are rarely concerned with gravitational effects other than buoyancy.

Figure 1.1 illustrates a solid block resting on a rigid plane and stressed by its own weight. The solid sags into a static deflection, shown as a highly exaggerated dashed line, resisting shear without flow. A free-body diagram of element A on the side of the block shows that there is shear in the block along a plane cut at an angle θ through A. Since the block sides are unsupported, element A has zero stress on the left and right sides and compression stress $\sigma = -p$ on the top and bottom. Mohr's circle does not reduce to a point, and there is nonzero shear stress in the block.

By contrast, the liquid and gas at rest in Fig. 1.1 require the supporting walls in order to eliminate shear stress. The walls exert a compression stress of $-p$ and reduce Mohr's circle to a point with zero shear everywhere, i.e., the hydrostatic condition. The liquid retains its volume and forms a free surface in the container. If the walls are removed, shear develops in the liquid and a big splash results. If the container is tilted, shear again develops, waves form, and the free surface seeks a horizontal co



ketabline.com Ebook.ketabline.com

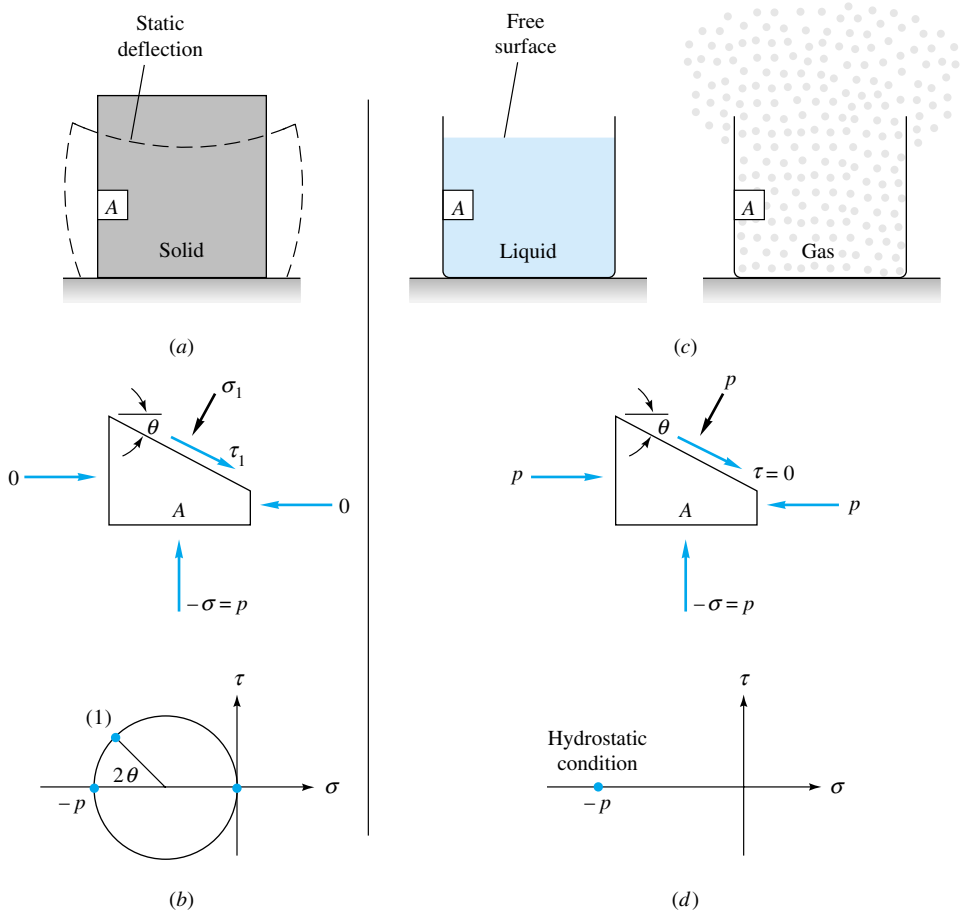


Fig. 1.1 A solid at rest can resist shear. (*a*) Static deflection of the solid; (*b*) equilibrium and Mohr's circle for solid element *A*. A fluid cannot resist shear. (*c*) Containing walls are needed; (*d*) equilibrium and Mohr's circle for fluid element *A*.

tion, pouring out over the lip if necessary. Meanwhile, the gas is unrestrained and expands out of the container, filling all available space. Element *A* in the gas is also hydrostatic and exerts a compression stress $-p$ on the walls.

In the above discussion, clear decisions could be made about solids, liquids, and gases. Most engineering fluid-mechanics problems deal with these clear cases, i.e., the common liquids, such as water, oil, mercury, gasoline, and alcohol, and the common gases, such as air, helium, hydrogen, and steam, in their common temperature and pressure ranges. There are many borderline cases, however, of which you should be aware. Some apparently "solid" substances such as asphalt and lead resist shear stress for short periods but actually deform slowly and exhibit definite fluid behavior over long periods. Other substances, notably colloid and slurry mixtures, resist small shear stresses but "yield" at large stress and begin to flow as fluids do. Specialized textbooks are devoted to this study of more general deformation and flow, a field called *rheology* [6]. Also, liquids and gases can coexist in two-phase mixtures, such as steam-water mixtures or water with entrapped air bubbles. Specialized textbooks p

ketabline.com Ebook.ketabline.com

of such *two-phase flows* [7]. Finally, there are situations where the distinction between a liquid and a gas blurs. This is the case at temperatures and pressures above the so-called *critical point* of a substance, where only a single phase exists, primarily resembling a gas. As pressure increases far above the critical point, the gaslike substance becomes so dense that there is some resemblance to a liquid and the usual thermodynamic approximations like the perfect-gas law become inaccurate. The critical temperature and pressure of water are $T_c = 647$ K and $p_c = 219$ atm,[2] so that typical problems involving water and steam are below the critical point. Air, being a mixture of gases, has no distinct critical point, but its principal component, nitrogen, has $T_c = 126$ K and $p_c = 34$ atm. Thus typical problems involving air are in the range of high temperature and low pressure where air is distinctly and definitely a gas. This text will be concerned solely with clearly identifiable liquids and gases, and the borderline cases discussed above will be beyond our scope.

1.3 The Fluid as a Continuum

We have already used technical terms such as *fluid pressure* and *density* without a rigorous discussion of their definition. As far as we know, fluids are aggregations of molecules, widely spaced for a gas, closely spaced for a liquid. The distance between molecules is very large compared with the molecular diameter. The molecules are not fixed in a lattice but move about freely relative to each other. Thus fluid density, or mass per unit volume, has no precise meaning because the number of molecules occupying a given volume continually changes. This effect becomes unimportant if the unit volume is large compared with, say, the cube of the molecular spacing, when the number of molecules within the volume will remain nearly constant in spite of the enormous interchange of particles across the boundaries. If, however, the chosen unit volume is too large, there could be a noticeable variation in the bulk aggregation of the particles. This situation is illustrated in Fig. 1.2, where the "density" as calculated from molecular mass δm within a given volume $\delta \mathcal{V}$ is plotted versus the size of the unit volume. There is a limiting volume $\delta \mathcal{V}^*$ below which molecular variations may be important and

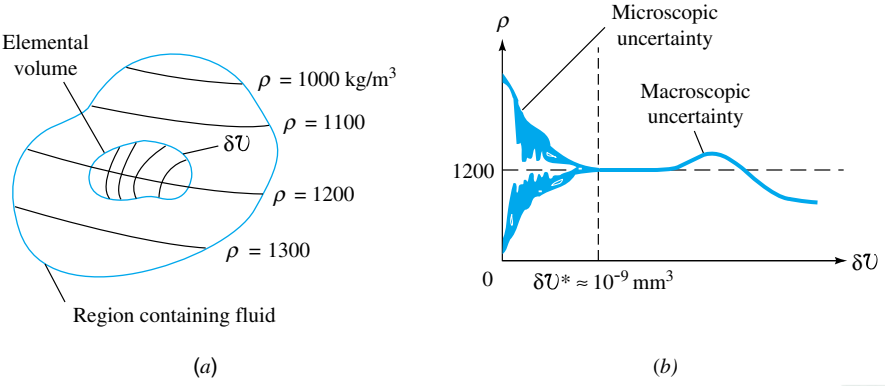


Fig. 1.2 The limit definition of continuum fluid density: (*a*) an elemental volume in a fluid region of variable continuum density; (*b*) calculated density versus size of the elemental volume.

[2]One atmosphere equals 2116 lbf/ft^2 = 101,300 Pa.



ketabline.com Ebook.ketabline.com

above which aggregate variations may be important. The *density* ρ of a fluid is best defined as

$$\rho = \lim_{\delta\mathcal{V}\to\delta\mathcal{V}^*} \frac{\delta m}{\delta\mathcal{V}} \tag{1.1}$$

The limiting volume $\delta\mathcal{V}^*$ is about 10^{-9} mm^3 for all liquids and for gases at atmospheric pressure. For example, 10^{-9} mm^3 of air at standard conditions contains approximately 3×10^7 molecules, which is sufficient to define a nearly constant density according to Eq. (1.1). Most engineering problems are concerned with physical dimensions much larger than this limiting volume, so that density is essentially a point function and fluid properties can be thought of as varying continually in space, as sketched in Fig. 1.2*a*. Such a fluid is called a *continuum,* which simply means that its variation in properties is so smooth that the differential calculus can be used to analyze the substance. We shall assume that continuum calculus is valid for all the analyses in this book. Again there are borderline cases for gases at such low pressures that molecular spacing and mean free path[3] are comparable to, or larger than, the physical size of the system. This requires that the continuum approximation be dropped in favor of a molecular theory of rarefied-gas flow [8]. In principle, all fluid-mechanics problems can be attacked from the molecular viewpoint, but no such attempt will be made here. Note that the use of continuum calculus does not preclude the possibility of discontinuous jumps in fluid properties across a free surface or fluid interface or across a shock wave in a compressible fluid (Chap. 9). Our calculus in Chap. 4 must be flexible enough to handle discontinuous boundary conditions.

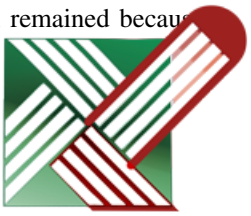
1.4 Dimensions and Units

A *dimension* is the measure by which a physical variable is expressed quantitatively. A *unit* is a particular way of attaching a number to the quantitative dimension. Thus length is a dimension associated with such variables as distance, displacement, width, deflection, and height, while centimeters and inches are both numerical units for expressing length. Dimension is a powerful concept about which a splendid tool called *dimensional analysis* has been developed (Chap. 5), while units are the nitty-gritty, the number which the customer wants as the final answer.

Systems of units have always varied widely from country to country, even after international agreements have been reached. Engineers need numbers and therefore unit systems, and the numbers must be accurate because the safety of the public is at stake. You cannot design and build a piping system whose diameter is D and whose length is L. And U.S. engineers have persisted too long in clinging to British systems of units. There is too much margin for error in most British systems, and many an engineering student has flunked a test because of a missing or improper conversion factor of 12 or 144 or 32.2 or 60 or 1.8. Practicing engineers can make the same errors. The writer is aware from personal experience of a serious preliminary error in the design of an aircraft due to a missing factor of 32.2 to convert pounds of mass to slugs.

In 1872 an international meeting in France proposed a treaty called the Metric Convention, which was signed in 1875 by 17 countries including the United States. It was an improvement over British systems because its use of base 10 is the foundation of our number system, learned from childhood by all. Problems still remained becau

[3]The mean distance traveled by molecules between collisions.



ketabline.com Ebook.ketabline.com

even the metric countries differed in their use of kiloponds instead of dynes or newtons, kilograms instead of grams, or calories instead of joules. To standardize the metric system, a General Conference of Weights and Measures attended in 1960 by 40 countries proposed the *International System of Units* (SI). We are now undergoing a painful period of transition to SI, an adjustment which may take many more years to complete. The professional societies have led the way. Since July 1, 1974, SI units have been required by all papers published by the American Society of Mechanical Engineers, which prepared a useful booklet explaining the SI [9]. The present text will use SI units together with British gravitational (BG) units.

Primary Dimensions

In fluid mechanics there are only four *primary dimensions* from which all other dimensions can be derived: mass, length, time, and temperature.[4] These dimensions and their units in both systems are given in Table 1.1. Note that the kelvin unit uses no degree symbol. The braces around a symbol like $\{M\}$ mean "the dimension" of mass. All other variables in fluid mechanics can be expressed in terms of $\{M\}$, $\{L\}$, $\{T\}$, and $\{\Theta\}$. For example, acceleration has the dimensions $\{LT^{-2}\}$. The most crucial of these secondary dimensions is force, which is directly related to mass, length, and time by Newton's second law

$$\mathbf{F} = m\mathbf{a} \tag{1.2}$$

From this we see that, dimensionally, $\{F\} = \{MLT^{-2}\}$. A constant of proportionality is avoided by defining the force unit exactly in terms of the primary units. Thus we define the newton and the pound of force

$$\begin{aligned} 1 \text{ newton of force} &= 1 \text{ N} \equiv 1 \text{ kg} \cdot \text{m/s}^2 \\ 1 \text{ pound of force} &= 1 \text{ lbf} \equiv 1 \text{ slug} \cdot \text{ft/s}^2 = 4.4482 \text{ N} \end{aligned} \tag{1.3}$$

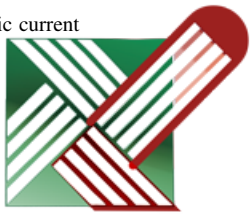
In this book the abbreviation *lbf* is used for pound-force and *lb* for pound-mass. If instead one adopts other force units such as the dyne or the poundal or kilopond or adopts other mass units such as the gram or pound-mass, a constant of proportionality called g_c must be included in Eq. (1.2). We shall not use g_c in this book since it is not necessary in the SI and BG systems.

A list of some important secondary variables in fluid mechanics, with dimensions derived as combinations of the four primary dimensions, is given in Table 1.2. A more complete list of conversion factors is given in App. C.

Table 1.1 Primary Dimensions in SI and BG Systems

Primary dimension	SI unit	BG unit	Conversion factor
Mass $\{M\}$	Kilogram (kg)	Slug	1 slug = 14.5939 kg
Length $\{L\}$	Meter (m)	Foot (ft)	1 ft = 0.3048 m
Time $\{T\}$	Second (s)	Second (s)	1 s = 1 s
Temperature $\{\Theta\}$	Kelvin (K)	Rankine (°R)	1 K = 1.8°R

[4] If electromagnetic effects are important, a fifth primary dimension must be included, electric current $\{I\}$, whose SI unit is the ampere (A).



ketabline.com Ebook.ketabline.com

Table 1.2 Secondary Dimensions in Fluid Mechanics

Secondary dimension	SI unit	BG unit	Conversion factor
Area $\{L^2\}$	m^2	ft^2	1 m^2 = 10.764 ft^2
Volume $\{L^3\}$	m^3	ft^3	1 m^3 = 35.315 ft^3
Velocity $\{LT^{-1}\}$	m/s	ft/s	1 ft/s = 0.3048 m/s
Acceleration $\{LT^{-2}\}$	m/s^2	ft/s^2	1 ft/s^2 = 0.3048 m/s^2
Pressure or stress $\{ML^{-1}T^{-2}\}$	Pa = N/m^2	lbf/ft^2	1 lbf/ft^2 = 47.88 Pa
Angular velocity $\{T^{-1}\}$	s^{-1}	s^{-1}	1 s^{-1} = 1 s^{-1}
Energy, heat, work $\{ML^2T^{-2}\}$	J = N · m	ft · lbf	1 ft · lbf = 1.3558 J
Power $\{ML^2T^{-3}\}$	W = J/s	ft · lbf/s	1 ft · lbf/s = 1.3558 W
Density $\{ML^{-3}\}$	kg/m^3	$slugs/ft^3$	1 $slug/ft^3$ = 515.4 kg/m^3
Viscosity $\{ML^{-1}T^{-1}\}$	kg/(m · s)	slugs/(ft · s)	1 slug/(ft · s) = 47.88 kg/(m · s)
Specific heat $\{L^2T^{-2}\Theta^{-1}\}$	$m^2/(s^2 \cdot K)$	$ft^2/(s^2 \cdot °R)$	1 $m^2/(s^2 \cdot K)$ = 5.980 $ft^2/(s^2 \cdot °R)$

EXAMPLE 1.1

A body weighs 1000 lbf when exposed to a standard earth gravity $g = 32.174$ ft/s^2. (*a*) What is its mass in kg? (*b*) What will the weight of this body be in N if it is exposed to the moon's standard acceleration $g_{moon} = 1.62$ m/s^2? (*c*) How fast will the body accelerate if a net force of 400 lbf is applied to it on the moon or on the earth?

Solution

Part (a) Equation (1.2) holds with F = weight and $a = g_{earth}$:

$$F = W = mg = 1000 \text{ lbf} = (m \text{ slugs})(32.174 \text{ ft/s}^2)$$

or

$$m = \frac{1000}{32.174} = (31.08 \text{ slugs})(14.5939 \text{ kg/slug}) = 453.6 \text{ kg} \qquad \textit{Ans. (a)}$$

The change from 31.08 slugs to 453.6 kg illustrates the proper use of the conversion factor 14.5939 kg/slug.

Part (b) The mass of the body remains 453.6 kg regardless of its location. Equation (1.2) applies with a new value of a and hence a new force

$$F = W_{moon} = mg_{moon} = (453.6 \text{ kg})(1.62 \text{ m/s}^2) = 735 \text{ N} \qquad \textit{Ans. (b)}$$

Part (c) This problem does not involve weight or gravity or position and is simply a direct application of Newton's law with an unbalanced force:

$$F = 400 \text{ lbf} = ma = (31.08 \text{ slugs})(a \text{ ft/s}^2)$$

or

$$a = \frac{400}{31.08} = 12.43 \text{ ft/s}^2 = 3.79 \text{ m/s}^2 \qquad \textit{Ans. (c)}$$

This acceleration would be the same on the moon or earth or anywhere.



ketabline.com Ebook.ketabline.com

Many data in the literature are reported in inconvenient or arcane units suitable only to some industry or specialty or country. The engineer should convert these data to the SI or BG system before using them. This requires the systematic application of conversion factors, as in the following example.

EXAMPLE 1.2

An early viscosity unit in the cgs system is the poise (abbreviated P), or g/(cm · s), named after J. L. M. Poiseuille, a French physician who performed pioneering experiments in 1840 on water flow in pipes. The viscosity of water (fresh or salt) at 293.16 K = 20°C is approximately $\mu = 0.01$ P. Express this value in (*a*) SI and (*b*) BG units.

Solution

Part (a)

$$\mu = [0.01 \text{ g/(cm} \cdot \text{s)}] \frac{1 \text{ kg}}{1000 \text{ g}} (100 \text{ cm/m}) = 0.001 \text{ kg/(m} \cdot \text{s)} \qquad \textit{Ans. (a)}$$

Part (b)

$$\mu = [0.001 \text{ kg/(m} \cdot \text{s)}] \frac{1 \text{ slug}}{14.59 \text{ kg}} (0.3048 \text{ m/ft})$$

$$= 2.09 \times 10^{-5} \text{ slug/(ft} \cdot \text{s)} \qquad \textit{Ans. (b)}$$

Note: Result (*b*) could have been found directly from (*a*) by dividing (*a*) by the viscosity conversion factor 47.88 listed in Table 1.2.

We repeat our advice: Faced with data in unusual units, convert them immediately to either SI or BG units because (1) it is more professional and (2) theoretical equations in fluid mechanics are *dimensionally consistent* and require no further conversion factors when these two fundamental unit systems are used, as the following example shows.

EXAMPLE 1.3

A useful theoretical equation for computing the relation between pressure, velocity, and altitude in a steady flow of a nearly inviscid, nearly incompressible fluid with negligible heat transfer and shaft work[5] is the *Bernoulli relation,* named after Daniel Bernoulli, who published a hydrodynamics textbook in 1738:

$$p_0 = p + \tfrac{1}{2}\rho V^2 + \rho g Z \tag{1}$$

where p_0 = stagnation pressure
p = pressure in moving fluid
V = velocity
ρ = density
Z = altitude
g = gravitational acceleration

[5]That's an awful lot of assumptions, which need further study in Chap. 3.



ketabline.com Ebook.ketabline.com

(*a*) Show that Eq. (1) satisfies the principle of dimensional homogeneity, which states that all additive terms in a physical equation must have the same dimensions. (*b*) Show that consistent units result without additional conversion factors in SI units. (*c*) Repeat (*b*) for BG units.

Solution

Part (a) We can express Eq. (1) dimensionally, using braces by entering the dimensions of each term from Table 1.2:

$$\{ML^{-1}T^{-2}\} = \{ML^{-1}T^{-2}\} + \{ML^{-3}\}\{L^2T^{-2}\} + \{ML^{-3}\}\{LT^{-2}\}\{L\}$$

$$= \{ML^{-1}T^{-2}\} \text{ for all terms} \qquad \textit{Ans. (a)}$$

Part (b) Enter the SI units for each quantity from Table 1.2:

$$\{\text{N/m}^2\} = \{\text{N/m}^2\} + \{\text{kg/m}^3\}\{\text{m}^2/\text{s}^2\} + \{\text{kg/m}^3\}\{\text{m/s}^2\}\{\text{m}\}$$

$$= \{\text{N/m}^2\} + \{\text{kg/(m} \cdot \text{s}^2)\}$$

The right-hand side looks bad until we remember from Eq. (1.3) that $1\ \text{kg} = 1\ \text{N} \cdot \text{s}^2/\text{m}$.

$$\{\text{kg/(m} \cdot \text{s}^2)\} = \frac{\{\text{N} \cdot \text{s}^2/\text{m}\}}{\{\text{m} \cdot \text{s}^2\}} = \{\text{N/m}^2\} \qquad \textit{Ans. (b)}$$

Thus all terms in Bernoulli's equation will have units of pascals, or newtons per square meter, when SI units are used. No conversion factors are needed, which is true of all theoretical equations in fluid mechanics.

Part (c) Introducing BG units for each term, we have

$$\{\text{lbf/ft}^2\} = \{\text{lbf/ft}^2\} + \{\text{slugs/ft}^3\}\{\text{ft}^2/\text{s}^2\} + \{\text{slugs/ft}^3\}\{\text{ft/s}^2\}\{\text{ft}\}$$

$$= \{\text{lbf/ft}^2\} + \{\text{slugs/(ft} \cdot \text{s}^2)\}$$

But, from Eq. (1.3), $1\ \text{slug} = 1\ \text{lbf} \cdot \text{s}^2/\text{ft}$, so that

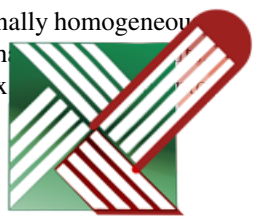
$$\{\text{slugs/(ft} \cdot \text{s}^2)\} = \frac{\{\text{lbf} \cdot \text{s}^2/\text{ft}\}}{\{\text{ft} \cdot \text{s}^2\}} = \{\text{lbf/ft}^2\} \qquad \textit{Ans. (c)}$$

All terms have the unit of pounds-force per square foot. No conversion factors are needed in the BG system either.

There is still a tendency in English-speaking countries to use pound-force per square inch as a pressure unit because the numbers are more manageable. For example, standard atmospheric pressure is $14.7\ \text{lbf/in}^2 = 2116\ \text{lbf/ft}^2 = 101{,}300$ Pa. The pascal is a small unit because the newton is less than $\frac{1}{4}$ lbf and a square meter is a very large area. It is felt nevertheless that the pascal will gradually gain universal acceptance; e.g., repair manuals for U.S. automobiles now specify pressure measurements in pascals.

Consistent Units

Note that not only must all (fluid) mechanics equations be dimensionally homogeneou
one must also use *consistent units;* that is, each additive term must h
There is no trouble doing this with the SI and BG systems, as in Ex



ketabline.com Ebook.ketabline.com

those who try to mix colloquial English units. For example, in Chap. 9, we often use the assumption of steady adiabatic compressible gas flow:

$$h + \tfrac{1}{2}V^2 = \text{constant}$$

where h is the fluid enthalpy and $V^2/2$ is its kinetic energy. Colloquial thermodynamic tables might list h in units of British thermal units per pound (Btu/lb), whereas V is likely used in ft/s. It is completely erroneous to add Btu/lb to ft^2/s^2. The proper unit for h in this case is ft · lbf/slug, which is identical to ft^2/s^2. The conversion factor is 1 Btu/lb $\approx$ 25,040 ft^2/s^2 = 25,040 ft · lbf/slug.

Homogeneous versus Dimensionally Inconsistent Equations

All theoretical equations in mechanics (and in other physical sciences) are *dimensionally homogeneous*; i.e., each additive term in the equation has the same dimensions. For example, Bernoulli's equation (1) in Example 1.3 is dimensionally homogeneous: Each term has the dimensions of pressure or stress of $\{F/L^2\}$. Another example is the equation from physics for a body falling with negligible air resistance:

$$S = S_0 + V_0 t + \tfrac{1}{2}gt^2$$

where S_0 is initial position, V_0 is initial velocity, and g is the acceleration of gravity. Each term in this relation has dimensions of length $\{L\}$. The factor $\frac{1}{2}$, which arises from integration, is a pure (dimensionless) number, $\{1\}$. The exponent 2 is also dimensionless.

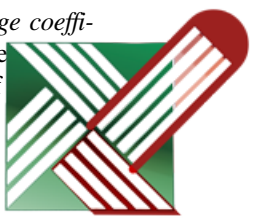
However, the reader should be warned that many empirical formulas in the engineering literature, arising primarily from correlations of data, are dimensionally inconsistent. Their units cannot be reconciled simply, and some terms may contain hidden variables. An example is the formula which pipe valve manufacturers cite for liquid volume flow rate Q (m^3/s) through a partially open valve:

$$Q = C_V\left(\frac{\Delta p}{\text{SG}}\right)^{1/2}$$

where Δp is the pressure drop across the valve and SG is the specific gravity of the liquid (the ratio of its density to that of water). The quantity C_V is the *valve flow coefficient,* which manufacturers tabulate in their valve brochures. Since SG is dimensionless $\{1\}$, we see that this formula is totally inconsistent, with one side being a flow rate $\{L^3/T\}$ and the other being the square root of a pressure drop $\{M^{1/2}/L^{1/2}T\}$. It follows that C_V must have dimensions, and rather odd ones at that: $\{L^{7/2}/M^{1/2}\}$. Nor is the resolution of this discrepancy clear, although one hint is that the values of C_V in the literature increase nearly as the square of the size of the valve. The presentation of experimental data in homogeneous form is the subject of *dimensional analysis* (Chap. 5). There we shall learn that a homogeneous form for the valve flow relation is

$$Q = C_d A_{\text{opening}}\left(\frac{\Delta p}{\rho}\right)^{1/2}$$

where ρ is the liquid density and A the area of the valve opening. The *discharge coefficient* C_d is dimensionless and changes only slightly with valve size. Please belie til we establish the fact in Chap. 5—that this latter is a *much* better formulation of



ketabline.com Ebook.ketabline.com

Meanwhile, we conclude that dimensionally inconsistent equations, though they abound in engineering practice, are misleading and vague and even dangerous, in the sense that they are often misused outside their range of applicability.

Convenient Prefixes in Powers of 10

Engineering results often are too small or too large for the common units, with too many zeros one way or the other. For example, to write $p = 114{,}000{,}000$ Pa is long and awkward. Using the prefix "M" to mean 10^6, we convert this to a concise $p = 114$ MPa (megapascals). Similarly, $t = 0.000000003$ s is a proofreader's nightmare compared to the equivalent $t = 3$ ns (nanoseconds). Such prefixes are common and convenient, in both the SI and BG systems. A complete list is given in Table 1.3.

Table 1.3 Convenient Prefixes for Engineering Units

Multiplicative factor	Prefix	Symbol
10^{12}	tera	T
10^{9}	giga	G
10^{6}	mega	M
10^{3}	kilo	k
10^{2}	hecto	h
10	deka	da
10^{-1}	deci	d
10^{-2}	centi	c
10^{-3}	milli	m
10^{-6}	micro	μ
10^{-9}	nano	n
10^{-12}	pico	p
10^{-15}	femto	f
10^{-18}	atto	a

EXAMPLE 1.4

In 1890 Robert Manning, an Irish engineer, proposed the following empirical formula for the average velocity V in uniform flow due to gravity down an open channel (BG units):

$$V = \frac{1.49}{n} R^{2/3} S^{1/2} \tag{1}$$

where R = hydraulic radius of channel (Chaps. 6 and 10)
S = channel slope (tangent of angle that bottom makes with horizontal)
n = Manning's roughness factor (Chap. 10)

and n is a constant for a given surface condition for the walls and bottom of the channel. (*a*) Is Manning's formula dimensionally consistent? (*b*) Equation (1) is commonly taken to be valid in BG units with n taken as dimensionless. Rewrite it in SI form.

Solution

Part (a)

Introduce dimensions for each term. The slope S, being a tangent or ratio, is dimensionless, denoted by {unity} or {1}. Equation (1) in dimensional form is

$$\left\{\frac{L}{T}\right\} = \left\{\frac{1.49}{n}\right\}\{L^{2/3}\}\{1\}$$

This formula cannot be consistent unless $\{1.49/n\} = \{L^{1/3}/T\}$. If n is dimensionless (and it is never listed with units in textbooks), then the numerical value 1.49 must have units. This can be tragic to an engineer working in a different unit system unless the discrepancy is properly documented. In fact, Manning's formula, though popular, is inconsistent both dimensionally and physically and does not properly account for channel-roughness effects except in a narrow range of parameters, for water only.

Part (b)

From part (*a*), the number 1.49 must have dimensions $\{L^{1/3}/T\}$ and thus in BG units equals 1.49 $\text{ft}^{1/3}/\text{s}$. By using the SI conversion factor for length we have

$$(1.49\ \text{ft}^{1/3}/\text{s})(0.3048\ \text{m/ft})^{1/3} = 1.00\ \text{m}^{1/3}/\text{s}$$

Therefore Manning's formula in SI becomes

$$V = \frac{1.0}{n} R^{2/3} S^{1/2}$$



ketabline.com Ebook.ketabline.com

with R in m and V in m/s. Actually, we misled you: This is the way Manning, a metric user, first proposed the formula. It was later converted to BG units. Such dimensionally inconsistent formulas are dangerous and should either be reanalyzed or treated as having very limited application.

1.5 Properties of the Velocity Field

In a given flow situation, the determination, by experiment or theory, of the properties of the fluid as a function of position and time is considered to be the *solution* to the problem. In almost all cases, the emphasis is on the space-time distribution of the fluid properties. One rarely keeps track of the actual fate of the specific fluid particles.[6] This treatment of properties as continuum-field functions distinguishes fluid mechanics from solid mechanics, where we are more likely to be interested in the trajectories of individual particles or systems.

Eulerian and Lagrangian Desciptions

There are two different points of view in analyzing problems in mechanics. The first view, appropriate to fluid mechanics, is concerned with the field of flow and is called the *eulerian* method of description. In the eulerian method we compute the pressure field $p(x, y, z, t)$ of the flow pattern, not the pressure changes $p(t)$ which a particle experiences as it moves through the field.

The second method, which follows an individual particle moving through the flow, is called the *lagrangian* description. The lagrangian approach, which is more appropriate to solid mechanics, will not be treated in this book. However, certain numerical analyses of sharply bounded fluid flows, such as the motion of isolated fluid droplets, are very conveniently computed in lagrangian coordinates [1].

Fluid-dynamic measurements are also suited to the eulerian system. For example, when a pressure probe is introduced into a laboratory flow, it is fixed at a specific position (x, y, z). Its output thus contributes to the description of the eulerian pressure field $p(x, y, z, t)$. To simulate a lagrangian measurement, the probe would have to move downstream at the fluid particle speeds; this is sometimes done in oceanographic measurements, where flowmeters drift along with the prevailing currents.

The two different descriptions can be contrasted in the analysis of traffic flow along a freeway. A certain length of freeway may be selected for study and called the field of flow. Obviously, as time passes, various cars will enter and leave the field, and the identity of the specific cars within the field will constantly be changing. The traffic engineer ignores specific cars and concentrates on their average velocity as a function of time and position within the field, plus the flow rate or number of cars per hour passing a given section of the freeway. This engineer is using an eulerian description of the traffic flow. Other investigators, such as the police or social scientists, may be interested in the path or speed or destination of specific cars in the field. By following a specific car as a function of time, they are using a lagrangian description of the flow.

The Velocity Field

Foremost among the properties of a flow is the velocity field $\mathbf{V}(x, y, z, t)$. In fact, determining the velocity is often tantamount to solving a flow problem, since other prop-

[6] One example where fluid-particle paths are important is in water-quality analysis of the fate contaminant discharges.



ketabline.com Ebook.ketabline.com

erties follow directly from the velocity field. Chapter 2 is devoted to the calculation of the pressure field once the velocity field is known. Books on heat transfer (for example, Ref. 10) are essentially devoted to finding the temperature field from known velocity fields.

In general, velocity is a vector function of position and time and thus has three components u, v, and w, each a scalar field in itself:

$$\mathbf{V}(x, y, z, t) = \mathbf{i}u(x, y, z, t) + \mathbf{j}v(x, y, z, t) + \mathbf{k}w(x, y, z, t) \tag{1.4}$$

The use of u, v, and w instead of the more logical component notation V_x, V_y, and V_z is the result of an almost unbreakable custom in fluid mechanics.

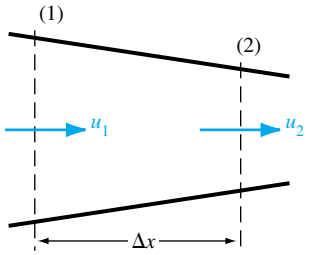
Several other quantities, called *kinematic properties,* can be derived by mathematically manipulating the velocity field. We list some kinematic properties here and give more details about their use and derivation in later chapters:

1.	Displacement vector:	$\mathbf{r} = \int \mathbf{V}\, dt$	(Sec. 1.9)
2.	Acceleration:	$\mathbf{a} = \dfrac{d\mathbf{V}}{dt}$	(Sec. 4.1)
3.	Volume rate of flow:	$Q = \int (\mathbf{V} \cdot \mathbf{n})\, dA$	(Sec. 3.2)
4.	Volume expansion rate:	$\dfrac{1}{\forall}\dfrac{d\forall}{dt} = \nabla \cdot \mathbf{V}$	(Sec. 4.2)
5.	Local angular velocity:	$\omega = \frac{1}{2}\nabla \times \mathbf{V}$	(Sec. 4.8)

We will not illustrate any problems regarding these kinematic properties at present. The point of the list is to illustrate the type of vector operations used in fluid mechanics and to make clear the dominance of the velocity field in determining other flow properties. *Note:* The fluid *acceleration,* item 2 above, is not as simple as it looks and actually involves four different terms due to the use of the chain rule in calculus (see Sec. 4.1).

EXAMPLE 1.5

Fluid flows through a contracting section of a duct, as in Fig. E1.5. A velocity probe inserted at section (1) measures a steady value $u_1 = 1$ m/s, while a similar probe at section (2) records a steady $u_2 = 3$ m/s. Estimate the fluid acceleration, if any, if $\Delta x = 10$ cm.



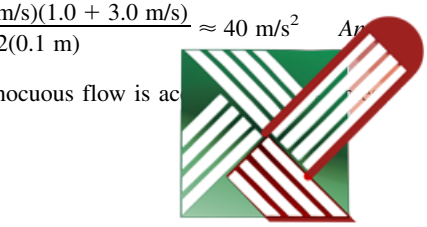
E1.5

Solution

The flow is *steady* (not time-varying), but fluid particles clearly increase in velocity as they pass from (1) to (2). This is the concept of *convective acceleration* (Sec. 4.1). We may estimate the acceleration as a velocity change Δu divided by a time change $\Delta t = \Delta x/u_{\text{avg}}$:

$$a_x \approx \frac{\text{velocity change}}{\text{time change}} \approx \frac{u_2 - u_1}{\Delta x/[\frac{1}{2}(u_1 + u_2)]} = \frac{(3.0 - 1.0 \text{ m/s})(1.0 + 3.0 \text{ m/s})}{2(0.1 \text{ m})} \approx 40 \text{ m/s}^2 \quad \textit{An}$$

A simple estimate thus indicates that this seemingly innocuous flow is ac



ketabline.com Ebook.ketabline.com

the acceleration of gravity. In the limit as Δx and Δt become very small, the above estimate reduces to a partial-derivative expression for convective x-acceleration:

$$a_{x,\text{convective}} = \lim_{\Delta t \to 0} \frac{\Delta u}{\Delta t} = u\frac{\partial u}{\partial x}$$

In three-dimensional flow (Sec. 4.1) there are *nine* of these convective terms.

1.6 Thermodynamic Properties of a Fluid

While the velocity field **V** is the most important fluid property, it interacts closely with the thermodynamic properties of the fluid. We have already introduced into the discussion the three most common such properties

1. Pressure p
2. Density ρ
3. Temperature T

These three are constant companions of the velocity vector in flow analyses. Four other thermodynamic properties become important when work, heat, and energy balances are treated (Chaps. 3 and 4):

4. Internal energy e
5. Enthalpy $h = \hat{u} + p/\rho$
6. Entropy s
7. Specific heats c_p and c_v

In addition, friction and heat conduction effects are governed by the two so-called *transport properties:*

8. Coefficient of viscosity μ
9. Thermal conductivity k

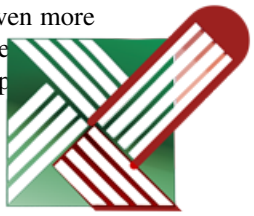
All nine of these quantities are true thermodynamic properties which are determined by the thermodynamic condition or *state* of the fluid. For example, for a single-phase substance such as water or oxygen, two basic properties such as pressure and temperature are sufficient to fix the value of all the others:

$$\rho = \rho(p, T) \qquad h = h(p, T) \qquad \mu = \mu(p, T) \tag{1.5}$$

and so on for every quantity in the list. Note that the specific volume, so important in thermodynamic analyses, is omitted here in favor of its inverse, the density ρ.

Recall that thermodynamic properties describe the state of a *system,* i.e., a collection of matter of fixed identity which interacts with its surroundings. In most cases here the system will be a small fluid element, and all properties will be assumed to be continuum properties of the flow field: $\rho = \rho(x, y, z, t)$, etc.

Recall also that thermodynamics is normally concerned with *static* systems, whereas fluids are usually in variable motion with constantly changing properties. Do the properties retain their meaning in a fluid flow which is technically not in equilibrium? The answer is yes, from a statistical argument. In gases at normal pressure (and even more so for liquids), an enormous number of molecular collisions occur over a ve
distance of the order of 1 μm, so that a fluid subjected to sudden changes rap



ketabline.com Ebook.ketabline.com

justs itself toward equilibrium. We therefore assume that all the thermodynamic properties listed above exist as point functions in a flowing fluid and follow all the laws and state relations of ordinary equilibrium thermodynamics. There are, of course, important nonequilibrium effects such as chemical and nuclear reactions in flowing fluids which are not treated in this text.

Pressure

Pressure is the (compression) stress at a point in a static fluid (Fig. 1.1). Next to velocity, the pressure p is the most dynamic variable in fluid mechanics. Differences or *gradients* in pressure often drive a fluid flow, especially in ducts. In low-speed flows, the actual magnitude of the pressure is often not important, unless it drops so low as to cause vapor bubbles to form in a liquid. For convenience, we set many such problem assignments at the level of 1 atm = 2116 lbf/ft^2 = 101,300 Pa. High-speed (compressible) gas flows (Chap. 9), however, are indeed sensitive to the magnitude of pressure.

Temperature

Temperature T is a measure of the internal energy level of a fluid. It may vary considerably during high-speed flow of a gas (Chap. 9). Although engineers often use Celsius or Fahrenheit scales for convenience, many applications in this text require *absolute* (Kelvin or Rankine) temperature scales:

$$°R = °F + 459.69$$
$$K = °C + 273.16$$

If temperature differences are strong, *heat transfer* may be important [10], but our concern here is mainly with dynamic effects. We examine heat-transfer principles briefly in Secs. 4.5 and 9.8.

Density

The density of a fluid, denoted by ρ (lowercase Greek rho), is its mass per unit volume. Density is highly variable in gases and increases nearly proportionally to the pressure level. Density in liquids is nearly constant; the density of water (about 1000 kg/m^3) increases only 1 percent if the pressure is increased by a factor of 220. Thus most liquid flows are treated analytically as nearly "incompressible."

In general, liquids are about three orders of magnitude more dense than gases at atmospheric pressure. The heaviest common liquid is mercury, and the lightest gas is hydrogen. Compare their densities at 20°C and 1 atm:

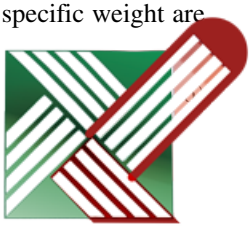
$$\text{Mercury:}\quad \rho = 13{,}580 \text{ kg/m}^3 \qquad \text{Hydrogen:}\quad \rho = 0.0838 \text{ kg/m}^3$$

They differ by a factor of 162,000! Thus the physical parameters in various liquid and gas flows might vary considerably. The differences are often resolved by the use of *dimensional analysis* (Chap. 5). Other fluid densities are listed in Tables A.3 and A.4 (in App. A).

Specific Weight

The *specific weight* of a fluid, denoted by γ (lowercase Greek gamma), is its weight per unit volume. Just as a mass has a weight $W = mg$, density and specific weight are simply related by gravity:

$$\gamma = \rho g$$



ketabline.com Ebook.ketabline.com

The units of γ are weight per unit volume, in lbf/ft^3 or N/m^3. In standard earth gravity, $g = 32.174$ ft/s^2 $= 9.807$ m/s^2. Thus, e.g., the specific weights of air and water at 20°C and 1 atm are approximately

$$\gamma_{air} = (1.205 \text{ kg/m}^3)(9.807 \text{ m/s}^2) = 11.8 \text{ N/m}^3 = 0.0752 \text{ lbf/ft}^3$$

$$\gamma_{water} = (998 \text{ kg/m}^3)(9.807 \text{ m/s}^2) = 9790 \text{ N/m}^3 = 62.4 \text{ lbf/ft}^3$$

Specific weight is very useful in the hydrostatic-pressure applications of Chap. 2. Specific weights of other fluids are given in Tables A.3 and A.4.

Specific Gravity

Specific gravity, denoted by SG, is the ratio of a fluid density to a standard reference fluid, water (for liquids), and air (for gases):

$$\text{SG}_{gas} = \frac{\rho_{gas}}{\rho_{air}} = \frac{\rho_{gas}}{1.205 \text{ kg/m}^3} \tag{1.7}$$

$$\text{SG}_{liquid} = \frac{\rho_{liquid}}{\rho_{water}} = \frac{\rho_{liquid}}{998 \text{ kg/m}^3}$$

For example, the specific gravity of mercury (Hg) is $\text{SG}_{Hg} = 13{,}580/998 \approx 13.6$. Engineers find these dimensionless ratios easier to remember than the actual numerical values of density of a variety of fluids.

Potential and Kinetic Energies

In thermostatics the only energy in a substance is that stored in a system by molecular activity and molecular bonding forces. This is commonly denoted as *internal energy* $\hat{u}$. A commonly accepted adjustment to this static situation for fluid flow is to add two more energy terms which arise from newtonian mechanics: the potential energy and kinetic energy.

The potential energy equals the work required to move the system of mass m from the origin to a position vector $\mathbf{r} = \mathbf{i}x + \mathbf{j}y + \mathbf{k}z$ against a gravity field $\mathbf{g}$. Its value is $-m\mathbf{g} \cdot \mathbf{r}$, or $-\mathbf{g} \cdot \mathbf{r}$ per unit mass. The kinetic energy equals the work required to change the speed of the mass from zero to velocity V. Its value is $\frac{1}{2}mV^2$ or $\frac{1}{2}V^2$ per unit mass. Then by common convention the total stored energy e per unit mass in fluid mechanics is the sum of three terms:

$$e = \hat{u} + \tfrac{1}{2}V^2 + (-\mathbf{g} \cdot \mathbf{r}) \tag{1.8}$$

Also, throughout this book we shall define z as upward, so that $\mathbf{g} = -g\mathbf{k}$ and $\mathbf{g} \cdot \mathbf{r} = -gz$. Then Eq. (1.8) becomes

$$e = \hat{u} + \tfrac{1}{2}V^2 + gz \tag{1.9}$$

The molecular internal energy $\hat{u}$ is a function of T and p for the single-phase pure substance, whereas the potential and kinetic energies are kinematic properties.

State Relations for Gases

Thermodynamic properties are found both theoretically and experimentally t
lated to each other by state relations which differ for each substance. As me



ketabline.com Ebook.ketabline.com

we shall confine ourselves here to single-phase pure substances, e.g., water in its liquid phase. The second most common fluid, air, is a mixture of gases, but since the mixture ratios remain nearly constant between 160 and 2200 K, in this temperature range air can be considered to be a pure substance.

All gases at high temperatures and low pressures (relative to their critical point) are in good agreement with the *perfect-gas law*

$$p = \rho RT \qquad R = c_p - c_v = \text{gas constant} \tag{1.10}$$

Since Eq. (1.10) is dimensionally consistent, R has the same dimensions as specific heat, $\{L^2T^{-2}\Theta^{-1}\}$, or velocity squared per temperature unit (kelvin or degree Rankine). Each gas has its own constant R, equal to a universal constant Λ divided by the molecular weight

$$R_{\text{gas}} = \frac{\Lambda}{M_{\text{gas}}} \tag{1.11}$$

where $\Lambda = 49{,}700\ \text{ft}^2/(\text{s}^2 \cdot {}^\circ\text{R}) = 8314\ \text{m}^2/(\text{s}^2 \cdot \text{K})$. Most applications in this book are for air, with $M = 28.97$:

$$R_{\text{air}} = 1717\ \text{ft}^2/(\text{s}^2 \cdot {}^\circ\text{R}) = 287\ \text{m}^2/(\text{s}^2 \cdot \text{K}) \tag{1.12}$$

Standard atmospheric pressure is 2116 lbf/ft^2, and standard temperature is 60°F = 520°R. Thus standard air density is

$$\rho_{\text{air}} = \frac{2116}{(1717)(520)} = 0.00237\ \text{slug/ft}^3 = 1.22\ \text{kg/m}^3 \tag{1.13}$$

This is a nominal value suitable for problems.

One proves in thermodynamics that Eq. (1.10) requires that the internal molecular energy $\hat{u}$ of a perfect gas vary only with temperature: $\hat{u} = \hat{u}(T)$. Therefore the specific heat c_v also varies only with temperature:

$$c_v = \left(\frac{\partial \hat{u}}{\partial T}\right)_\rho = \frac{d\hat{u}}{dT} = c_v(T)$$

or

$$d\hat{u} = c_v(T)\, dT \tag{1.14}$$

In like manner h and c_p of a perfect gas also vary only with temperature:

$$h = \hat{u} + \frac{p}{\rho} = \hat{u} + RT = h(T)$$

$$c_p = \left(\frac{\partial h}{\partial T}\right)_p = \frac{dh}{dT} = c_p(T) \tag{1.15}$$

$$dh = c_p(T)\, dT$$

The ratio of specific heats of a perfect gas is an important dimensionless parameter in compressible-flow analysis (Chap. 9)

$$k = \frac{c_p}{c_v} = k(T) \geq 1$$



ketabline.com Ebook.ketabline.com

As a first approximation in airflow analysis we commonly take c_p, c_v, and k to be constant

$$k_{\text{air}} \approx 1.4$$

$$c_v = \frac{R}{k-1} \approx 4293 \text{ ft}^2/(\text{s}^2 \cdot {}^\circ\text{R}) = 718 \text{ m}^2/(\text{s}^2 \cdot \text{K}) \tag{1.17}$$

$$c_p = \frac{kR}{k-1} \approx 6010 \text{ ft}^2/(\text{s}^2 \cdot {}^\circ\text{R}) = 1005 \text{ m}^2/(\text{s}^2 \cdot \text{K})$$

Actually, for all gases, c_p and c_v increase gradually with temperature, and k decreases gradually. Experimental values of the specific-heat ratio for eight common gases are shown in Fig. 1.3.

Many flow problems involve steam. Typical steam operating conditions are relatively close to the critical point, so that the perfect-gas approximation is inaccurate. The properties of steam are therefore available in tabular form [13], but the error of using the perfect-gas law is sometimes not great, as the following example shows.

EXAMPLE 1.6

Estimate ρ and c_p of steam at 100 lbf/in^2 and 400°F (*a*) by a perfect-gas approximation and (*b*) from the ASME steam tables [13].

Solution

Part (a) First convert to BG units: $p = 100$ lbf/in^2 = 14,400 lb/ft^2, $T = 400°\text{F} = 860°\text{R}$. From Table A.4 the molecular weight of H_2O is $2M_H + M_O = 2(1.008) + 16.0 = 18.016$. Then from Eq. (1.11) the gas constant of steam is approximately

$$R = \frac{49{,}700}{18.016} = 2759 \text{ ft}^2/(\text{s}^2 \cdot {}^\circ\text{R})$$

whence, from the perfect-gas law,

$$\rho \approx \frac{p}{RT} = \frac{14{,}400}{2759(860)} = 0.00607 \text{ slug/ft}^3 \qquad \textit{Ans. (a)}$$

From Fig. 1.3, k for steam at 860°R is approximately 1.30. Then from Eq. (1.17),

$$c_p \approx \frac{kR}{k-1} = \frac{1.30(2759)}{1.30-1} = 12{,}000 \text{ ft}^2/(\text{s}^2 \cdot {}^\circ\text{R}) \qquad \textit{Ans. (a)}$$

Part (b) From Ref. 13, the specific volume v of steam at 100 lbf/in^2 and 400°F is 4.935 ft^3/lbm. Then the density is the inverse of this, converted to slugs:

$$\rho = \frac{1}{v} = \frac{1}{(4.935 \text{ ft}^2/\text{lbm})(32.174 \text{ lbm/slug})} = 0.00630 \text{ slug/ft}^3 \qquad \textit{Ans. (b)}$$

This is about 4 percent higher than our ideal-gas estimate in part (*a*).

Reference 13 lists the value of c_p of steam at 100 lbf/in^2 and 400°F as 0.535 Btu/(lbm · °F). Convert this to BG units:

$$c_p = [0.535 \text{ Btu/(lbm} \cdot {}^\circ\text{R)}](778.2 \text{ ft} \cdot \text{lbf/Btu})(32.174 \text{ lbm/slug})$$

$$= 13{,}400 \text{ ft} \cdot \text{lbf/(slug} \cdot {}^\circ\text{R)} = 13{,}400 \text{ ft}^2/(\text{s}^2 \cdot {}^\circ\text{R})$$



ketabline.com Ebook.ketabline.com

This is about 11 percent higher than our ideal-gas estimate in part (*a*). The chief reason for the discrepancy is that this temperature and this pressure are quite close to the critical point and saturation line of steam. At higher temperatures and lower pressures, say, 800°F and 50 lbf/in^2, the perfect-gas law gives ρ and c_p of steam within an accuracy of ± 1 percent.

Note that the use of pound-mass and British thermal units in the traditional steam tables requires continual awkward conversions to BG units. Newer tables and disks are in SI units.

State Relations for Liquids

The writer knows of no "perfect-liquid law" comparable to that for gases. Liquids are nearly incompressible and have a single reasonably constant specific heat. Thus an idealized state relation for a liquid is

$$\rho \approx \text{const} \qquad c_p \approx c_v \approx \text{const} \qquad dh \approx c_p\, dT \tag{1.18}$$

Most of the flow problems in this book can be attacked with these simple assumptions. Water is normally taken to have a density of 1.94 slugs/ft^3 and a specific heat $c_p = 25{,}200$ ft^2/(s$^2 \cdot$ °R). The steam tables may be used if more accuracy is required.

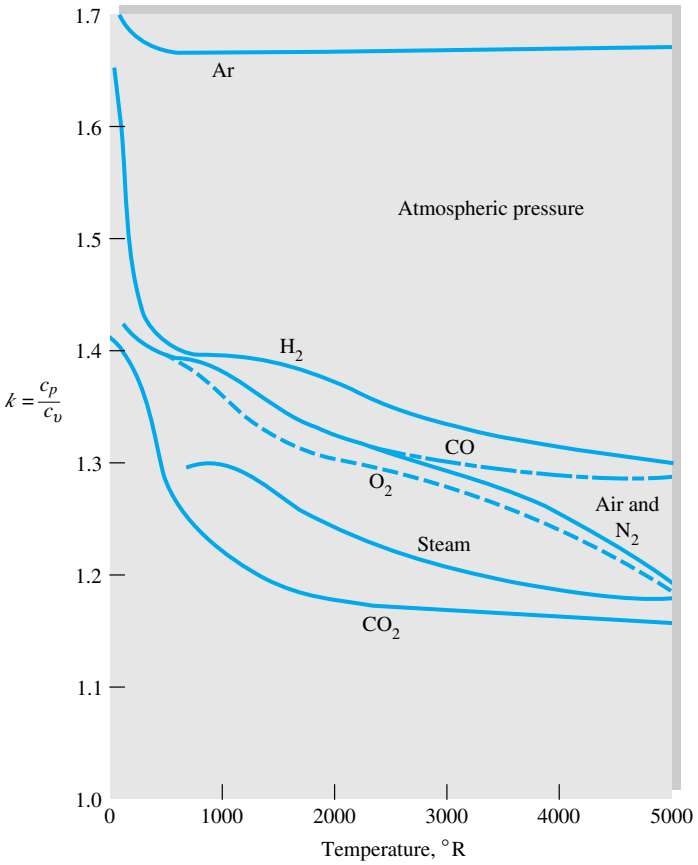


Fig. 1.3 Specific-heat ratio of eight common gases as a function of temperature. *(Data from Ref. 12.)*



ketabline.com Ebook.ketabline.com

The density of a liquid usually decreases slightly with temperature and increases moderately with pressure. If we neglect the temperature effect, an empirical pressure-density relation for a liquid is

$$\frac{p}{p_a} \approx (B + 1)\left(\frac{\rho}{\rho_a}\right)^n - B \tag{1.19}$$

where B and n are dimensionless parameters which vary slightly with temperature and p_a and ρ_a are standard atmospheric values. Water can be fitted approximately to the values $B \approx 3000$ and $n \approx 7$.

Seawater is a variable mixture of water and salt and thus requires three thermodynamic properties to define its state. These are normally taken as pressure, temperature, and the *salinity* $\hat{S}$, defined as the weight of the dissolved salt divided by the weight of the mixture. The average salinity of seawater is 0.035, usually written as 35 parts per 1000, or 35 ‰. The average density of seawater is 2.00 slugs/ft^3. Strictly speaking, seawater has three specific heats, all approximately equal to the value for pure water of 25,200 ft^2/(s^2 · °R) = 4210 m^2/(s^2 · K).

EXAMPLE 1.7

The pressure at the deepest part of the ocean is approximately 1100 atm. Estimate the density of seawater at this pressure.

Solution

Equation (1.19) holds for either water or seawater. The ratio p/p_a is given as 1100:

$$1100 \approx (3001)\left(\frac{\rho}{\rho_a}\right)^7 - 3000$$

or

$$\frac{\rho}{\rho_a} = \left(\frac{4100}{3001}\right)^{1/7} = 1.046$$

Assuming an average surface seawater density $\rho_a = 2.00$ slugs/ft^3, we compute

$$\rho \approx 1.046(2.00) = 2.09 \text{ slugs/ft}^3 \qquad \textit{Ans.}$$

Even at these immense pressures, the density increase is less than 5 percent, which justifies the treatment of a liquid flow as essentially incompressible.

1.7 Viscosity and Other Secondary Properties

The quantities such as pressure, temperature, and density discussed in the previous section are *primary* thermodynamic variables characteristic of any system. There are also certain secondary variables which characterize specific fluid-mechanical behavior. The most important of these is viscosity, which relates the local stresses in a moving fluid to the strain rate of the fluid element.

Viscosity

When a fluid is sheared, it begins to move at a strain rate inversely proportio
property called its *coefficient of viscosity* μ. Consider a fluid element sheare



ketabline.com Ebook.ketabline.com

plane by a single shear stress τ, as in Fig. 1.4*a*. The shear strain angle $\delta\theta$ will continuously grow with time as long as the stress τ is maintained, the upper surface moving at speed δu larger than the lower. Such common fluids as water, oil, and air show a linear relation between applied shear and resulting strain rate

$$\tau \propto \frac{\delta\theta}{\delta t} \tag{1.20}$$

From the geometry of Fig. 1.4*a* we see that

$$\tan \delta\theta = \frac{\delta u\ \delta t}{\delta y} \tag{1.21}$$

In the limit of infinitesimal changes, this becomes a relation between shear strain rate and velocity gradient

$$\frac{d\theta}{dt} = \frac{du}{dy} \tag{1.22}$$

From Eq. (1.20), then, the applied shear is also proportional to the velocity gradient for the common linear fluids. The constant of proportionality is the viscosity coefficient μ

$$\tau = \mu\frac{d\theta}{dt} = \mu\frac{du}{dy} \tag{1.23}$$

Equation (1.23) is dimensionally consistent; therefore μ has dimensions of stress-time: $\{FT/L^2\}$ or $\{M/(LT)\}$. The BG unit is slugs per foot-second, and the SI unit is kilograms per meter-second. The linear fluids which follow Eq. (1.23) are called *newtonian fluids,* after Sir Isaac Newton, who first postulated this resistance law in 1687.

We do not really care about the strain angle $\theta(t)$ in fluid mechanics, concentrating instead on the velocity distribution $u(y)$, as in Fig. 1.4*b*. We shall use Eq. (1.23) in Chap. 4 to derive a differential equation for finding the velocity distribution $u(y)$—and, more generally, $\mathbf{V}(x, y, z, t)$—in a viscous fluid. Figure 1.4*b* illustrates a shear layer, or *boundary layer,* near a solid wall. The shear stress is proportional to the slope of the

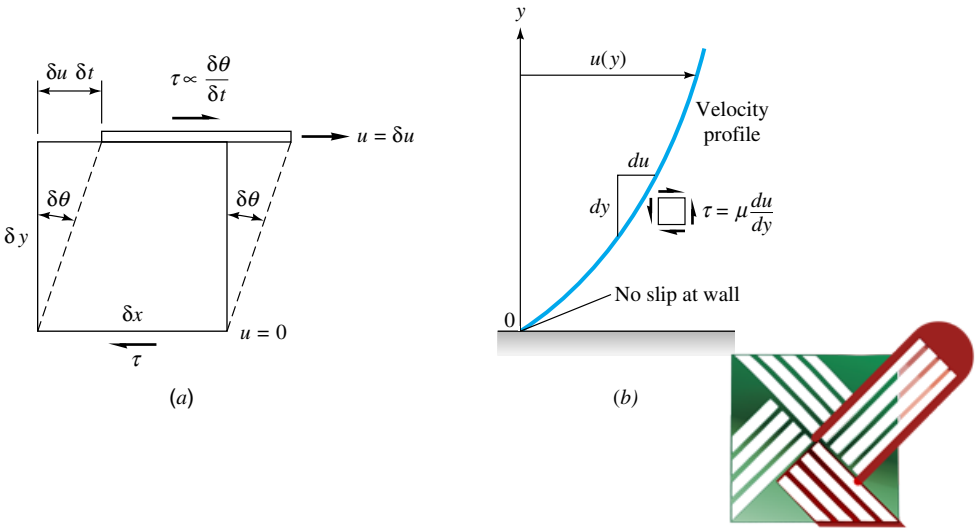


Fig. 1.4 Shear stress causes continuous shear deformation in a fluid: (*a*) a fluid element straining at a rate $\delta\theta/\delta t$; (*b*) newtonian shear distribution in a shear layer near a wall.

ketabline.com Ebook.ketabline.com

Table 1.4 Viscosity and Kinematic Viscosity of Eight Fluids at 1 atm and 20°C

Fluid	μ, kg/(m · s)†	Ratio $\mu/\mu(H_2)$	ρ, kg/m³	ν m²/s†	Ratio ν/ν(Hg)
Hydrogen	8.8 E–6	1.0	0.084	1.05 E–4	920
Air	1.8 E–5	2.1	1.20	1.51 E–5	130
Gasoline	2.9 E–4	33	680	4.22 E–7	3.7
Water	1.0 E–3	114	998	1.01 E–6	8.7
Ethyl alcohol	1.2 E–3	135	789	1.52 E–6	13
Mercury	1.5 E–3	170	13,580	1.16 E–7	1.0
SAE 30 oil	0.29	33,000	891	3.25 E–4	2,850
Glycerin	1.5	170,000	1,264	1.18 E–3	10,300

†1 kg/(m · s) = 0.0209 slug/(ft · s); 1 m²/s = 10.76 ft²/s.

velocity profile and is greatest at the wall. Further, at the wall, the velocity u is zero relative to the wall: This is called the *no-slip condition* and is characteristic of all viscous-fluid flows.

The viscosity of newtonian fluids is a true thermodynamic property and varies with temperature and pressure. At a given state (p, T) there is a vast range of values among the common fluids. Table 1.4 lists the viscosity of eight fluids at standard pressure and temperature. There is a variation of six orders of magnitude from hydrogen up to glycerin. Thus there will be wide differences between fluids subjected to the same applied stresses.

Generally speaking, the viscosity of a fluid increases only weakly with pressure. For example, increasing p from 1 to 50 atm will increase μ of air only 10 percent. Temperature, however, has a strong effect, with μ increasing with T for gases and decreasing for liquids. Figure A.1 (in App. A) shows this temperature variation for various common fluids. It is customary in most engineering work to neglect the pressure variation.

The variation $\mu(p, T)$ for a typical fluid is nicely shown by Fig. 1.5, from Ref. 14, which normalizes the data with the *critical-point state* (μ_c, p_c, T_c). This behavior, called the *principle of corresponding states,* is characteristic of all fluids, but the actual numerical values are uncertain to ±20 percent for any given fluid. For example, values of $\mu(T)$ for air at 1 atm, from Table A.2, fall about 8 percent low compared to the "low-density limit" in Fig. 1.5.

Note in Fig. 1.5 that changes with temperature occur very rapidly near the critical point. In general, critical-point measurements are extremely difficult and uncertain.

The Reynolds Number

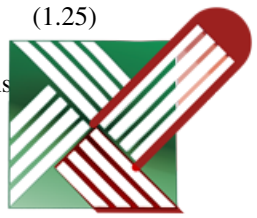
As we shall see in Chaps. 5 through 7, the primary parameter correlating the viscous behavior of all newtonian fluids is the dimensionless *Reynolds number:*

$$\mathrm{Re} = \frac{\rho V L}{\mu} = \frac{V L}{\nu} \tag{1.24}$$

where V and L are characteristic velocity and length scales of the flow. The second form of Re illustrates that the ratio of μ to ρ has its own name, the *kinematic viscosity:*

$$\nu = \frac{\mu}{\rho} \tag{1.25}$$

It is called kinematic because the mass units cancel, leaving only the dimensions



ketabline.com Ebook.ketabline.com

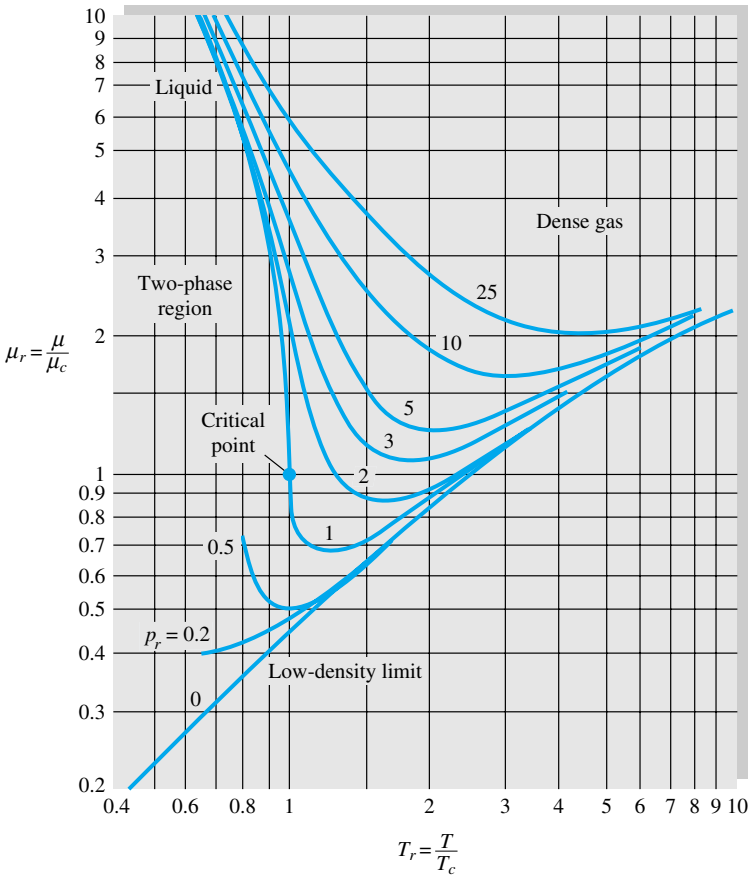


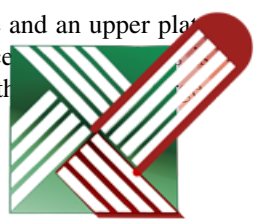
Fig. 1.5 Fluid viscosity nondimensionalized by critical-point properties. This generalized chart is characteristic of all fluids but is only accurate to ±20 percent. *(From Ref. 14.)*

Generally, the first thing a fluids engineer should do is estimate the Reynolds number range of the flow under study. Very low Re indicates viscous *creeping* motion, where inertia effects are negligible. Moderate Re implies a smoothly varying *laminar* flow. High Re probably spells *turbulent* flow, which is slowly varying in the time-mean but has superimposed strong random high-frequency fluctuations. Explicit numerical values for low, moderate, and high Reynolds numbers cannot be stated here. They depend upon flow geometry and will be discussed in Chaps. 5 through 7.

Table 1.4 also lists values of ν for the same eight fluids. The pecking order changes considerably, and mercury, the heaviest, has the smallest viscosity relative to its own weight. All gases have high ν relative to thin liquids such as gasoline, water, and alcohol. Oil and glycerin still have the highest ν, but the ratio is smaller. For a given value of V and L in a flow, these fluids exhibit a spread of four orders of magnitude in the Reynolds number.

Flow between Plates

A classic problem is the flow induced between a fixed lower plate and an upper pla moving steadily at velocity **V**, as shown in Fig. 1.6. The clearance h, and the fluid is newtonian and does not slip at either plate. If th



ketabline.com Ebook.ketabline.com

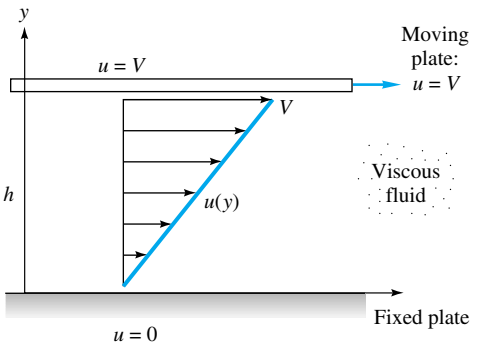


Fig. 1.6 Viscous flow induced by relative motion between two parallel plates.

this steady shearing motion will set up a velocity distribution $u(y)$, as shown, with $v = w = 0$. The fluid acceleration is zero everywhere.

With zero acceleration and assuming no pressure variation in the flow direction, you should show that a force balance on a small fluid element leads to the result that the shear stress is constant throughout the fluid. Then Eq. (1.23) becomes

$$\frac{du}{dy} = \frac{\tau}{\mu} = \text{const}$$

which we can integrate to obtain

$$u = a + by$$

The velocity distribution is linear, as shown in Fig. 1.6, and the constants a and b can be evaluated from the no-slip condition at the upper and lower walls:

$$u = \begin{cases} 0 = a + b(0) & \text{at } y = 0 \\ V = a + b(h) & \text{at } y = h \end{cases}$$

Hence $a = 0$ and $b = V/h$. Then the velocity profile between the plates is given by

$$u = V\frac{y}{h} \tag{1.26}$$

as indicated in Fig. 1.6. Turbulent flow (Chap. 6) does not have this shape.

Although viscosity has a profound effect on fluid motion, the actual viscous stresses are quite small in magnitude even for oils, as shown in the following example.

EXAMPLE 1.8

Suppose that the fluid being sheared in Fig. 1.6 is SAE 30 oil at 20°C. Compute the shear stress in the oil if $V = 3$ m/s and $h = 2$ cm.

Solution

The shear stress is found from Eq. (1.23) by differentiating Eq. (1.26):

$$\tau = \mu\frac{du}{dy} = \frac{\mu V}{h}$$



ketabline.com Ebook.ketabline.com

From Table 1.4 for SAE 30 oil, $\mu = 0.29$ kg/(m · s). Then, for the given values of V and h, Eq. (1) predicts

$$\tau = \frac{[0.29 \text{ kg/(m} \cdot \text{s)}](3 \text{ m/s})}{0.02 \text{ m}} = 43 \text{ kg/(m} \cdot \text{s}^2\text{)}$$

$$= 43 \text{ N/m}^2 = 43 \text{ Pa} \qquad \textit{Ans.}$$

Although oil is very viscous, this is a modest shear stress, about 2400 times less than atmospheric pressure. Viscous stresses in gases and thin liquids are even smaller.

Variation of Viscosity with Temperature

Temperature has a strong effect and pressure a moderate effect on viscosity. The viscosity of gases and most liquids increases slowly with pressure. Water is anomalous in showing a very slight decrease below 30°C. Since the change in viscosity is only a few percent up to 100 atm, we shall neglect pressure effects in this book.

Gas viscosity increases with temperature. Two common approximations are the power law and the Sutherland law:

$$\frac{\mu}{\mu_0} \approx \begin{cases} \left(\dfrac{T}{T_0}\right)^n & \text{power law} \\ \dfrac{(T/T_0)^{3/2}(T_0 + S)}{T + S} & \text{Sutherland law} \end{cases} \tag{1.27}$$

where μ_0 is a known viscosity at a known absolute temperature T_0 (usually 273 K). The constants n and S are fit to the data, and both formulas are adequate over a wide range of temperatures. For air, $n \approx 0.7$ and $S \approx 110$ K $= 199$°R. Other values are given in Ref. 3.

Liquid viscosity decreases with temperature and is roughly exponential, $\mu \approx ae^{-bT}$; but a better fit is the empirical result that ln μ is quadratic in $1/T$, where T is absolute temperature

$$\ln\frac{\mu}{\mu_0} \approx a + b\left(\frac{T_0}{T}\right) + c\left(\frac{T_0}{T}\right)^2 \tag{1.28}$$

For water, with $T_0 = 273.16$ K, $\mu_0 = 0.001792$ kg/(m · s), suggested values are $a = -1.94$, $b = -4.80$, and $c = 6.74$, with accuracy about ± 1 percent. The viscosity of water is tabulated in Table A.1. Curve-fit viscosity formulas for 355 organic liquids are given by Yaws et al. [34]. For further viscosity data, see Refs. 28 and 36.

Thermal Conductivity

Just as viscosity relates applied stress to resulting strain rate, there is a property called *thermal conductivity* k which relates the vector rate of heat flow per unit area $\mathbf{q}$ to the vector gradient of temperature ∇T. This proportionality, observed experimentally for fluids and solids, is known as *Fourier's law of heat conduction*

$$\mathbf{q} = -k\nabla T \tag{1.29a}$$

which can also be written as three scalar equations

$$q_x = -k\frac{\partial T}{\partial x} \qquad q_y = -k\frac{\partial T}{\partial y} \qquad q_z = -k\frac{\partial T}{\partial z}$$



ketabline.com Ebook.ketabline.com

The minus sign satisfies the convention that heat flux is positive in the direction of decreasing temperature. Fourier's law is dimensionally consistent, and k has SI units of joules per second-meter-kelvin. Thermal conductivity k is a thermodynamic property and varies with temperature and pressure in much the same way as viscosity. The ratio k/k_0 can be correlated with T/T_0 in the same manner as Eqs. (1.27) and (1.28) for gases and liquids, respectively.

Further data on viscosity and thermal-conductivity variations can be found in Ref. 11.

Nonnewtonian Fluids

Fluids which do not follow the linear law of Eq. (1.23) are called *nonnewtonian* and are treated in books on rheology [6]. Figure 1.7*a* compares four examples with a newtonian fluid. A *dilatant,* or shear-thickening, fluid increases resistance with increasing applied stress. Alternately, a *pseudoplastic,* or shear-thinning, fluid decreases resistance with increasing stress. If the thinning effect is very strong, as with the dashed-line curve, the fluid is termed *plastic*. The limiting case of a plastic substance is one which requires a finite yield stress before it begins to flow. The linear-flow *Bingham plastic* idealization is shown, but the flow behavior after yield may also be nonlinear. An example of a yielding fluid is toothpaste, which will not flow out of the tube until a finite stress is applied by squeezing.

A further complication of nonnewtonian behavior is the transient effect shown in Fig. 1.7*b*. Some fluids require a gradually increasing shear stress to maintain a constant strain rate and are called *rheopectic*. The opposite case of a fluid which thins out with time and requires decreasing stress is termed *thixotropic*. We neglect nonnewtonian effects in this book; see Ref. 6 for further study.

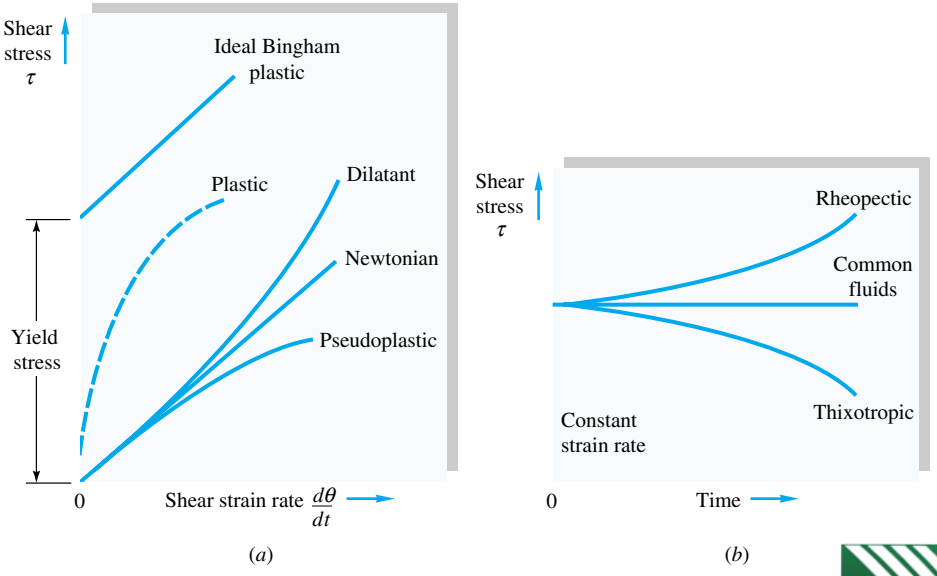


Fig. 1.7 Rheological behavior of various viscous materials: (*a*) stress versus strain rate; (*b*) effect of time on applied stress.

ketabline.com Ebook.ketabline.com

Surface Tension

A liquid, being unable to expand freely, will form an *interface* with a second liquid or gas. The physical chemistry of such interfacial surfaces is quite complex, and whole textbooks are devoted to this specialty [15]. Molecules deep within the liquid repel each other because of their close packing. Molecules at the surface are less dense and attract each other. Since half of their neighbors are missing, the mechanical effect is that the surface is in tension. We can account adequately for surface effects in fluid mechanics with the concept of surface tension.

If a cut of length dL is made in an interfacial surface, equal and opposite forces of magnitude $\Upsilon\, dL$ are exposed normal to the cut and parallel to the surface, where Υ is called the *coefficient of surface tension*. The dimensions of Υ are $\{F/L\}$, with SI units of newtons per meter and BG units of pounds-force per foot. An alternate concept is to open up the cut to an area dA; this requires work to be done of amount $\Upsilon\, dA$. Thus the coefficient Υ can also be regarded as the surface energy per unit area of the interface, in $\text{N} \cdot \text{m/m}^2$ or $\text{ft} \cdot \text{lbf/ft}^2$.

The two most common interfaces are water-air and mercury-air. For a clean surface at 20°C = 68°F, the measured surface tension is

$$\Upsilon = \begin{cases} 0.0050 \text{ lbf/ft} = 0.073 \text{ N/m} & \text{air-water} \\ 0.033 \text{ lbf/ft} = 0.48 \text{ N/m} & \text{air-mercury} \end{cases} \tag{1.30}$$

These are design values and can change considerably if the surface contains contaminants like detergents or slicks. Generally Υ decreases with liquid temperature and is zero at the critical point. Values of Υ for water are given in Fig. 1.8.

If the interface is curved, a mechanical balance shows that there is a pressure difference across the interface, the pressure being higher on the concave side, as illustrated in Fig. 1.9. In Fig. 1.9*a,* the pressure increase in the interior of a liquid cylinder is balanced by two surface-tension forces

$$2RL\, \Delta p = 2\Upsilon L$$

or

$$\Delta p = \frac{\Upsilon}{R} \tag{1.31}$$

We are not considering the weight of the liquid in this calculation. In Fig. 1.9*b,* the pressure increase in the interior of a spherical droplet balances a ring of surface-tension force

$$\pi R^2\, \Delta p = 2\pi R \Upsilon$$

or

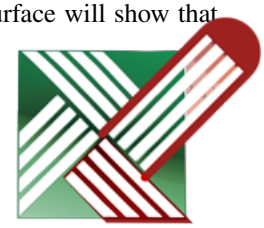
$$\Delta p = \frac{2\Upsilon}{R} \tag{1.32}$$

We can use this result to predict the pressure increase inside a soap bubble, which has *two* interfaces with air, an inner and outer surface of nearly the same radius R:

$$\Delta p_{\text{bubble}} \approx 2\, \Delta p_{\text{droplet}} = \frac{4\Upsilon}{R} \tag{1.33}$$

Figure 1.9*c* shows the general case of an arbitrarily curved interface whose principal radii of curvature are R_1 and R_2. A force balance normal to the surface will show that the pressure increase on the concave side is

$$\Delta p = \Upsilon(R_1^{-1} + R_2^{-1})$$



ketabline.com Ebook.ketabline.com

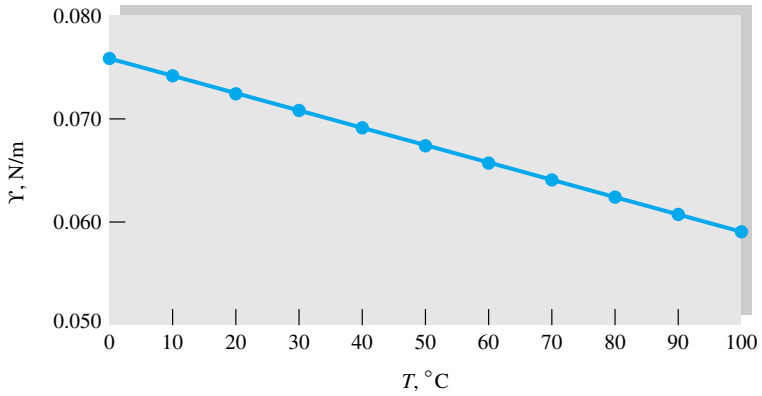


Fig. 1.8 Surface tension of a clean air-water interface. Data from Table A.5.

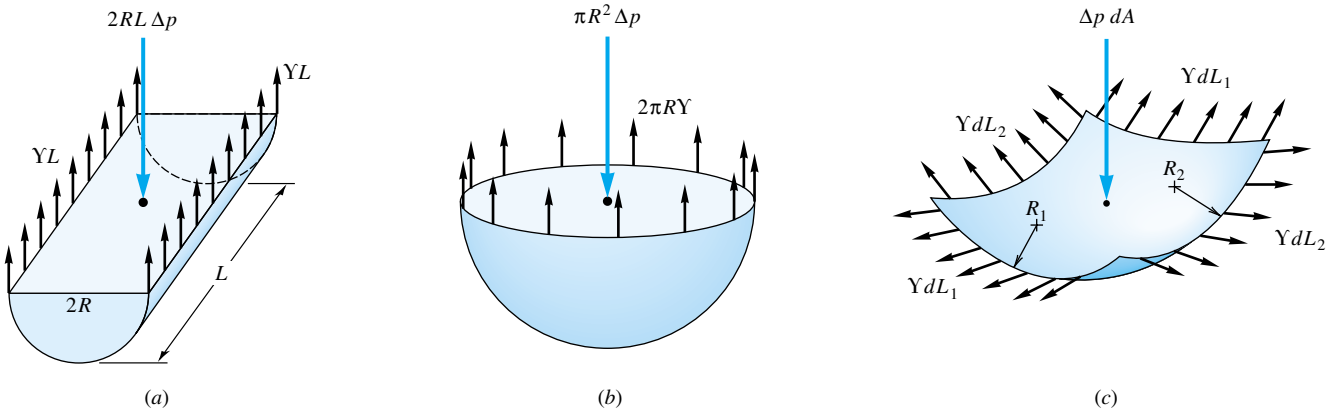


Fig. 1.9 Pressure change across a curved interface due to surface tension: (*a*) interior of a liquid cylinder; (*b*) interior of a spherical droplet; (*c*) general curved interface.

Equations (1.31) to (1.33) can all be derived from this general relation; e.g., in Eq. (1.31), $R_1 = R$ and $R_2 = \infty$.

A second important surface effect is the *contact angle* θ which appears when a liquid interface intersects with a solid surface, as in Fig. 1.10. The force balance would then involve both Υ and θ. If the contact angle is less than 90°, the liquid is said to *wet* the solid; if $\theta > 90°$, the liquid is termed *nonwetting*. For example, water wets soap but does not wet wax. Water is extremely wetting to a clean glass surface, with $\theta \approx 0°$. Like Υ, the contact angle θ is sensitive to the actual physicochemical conditions of the solid-liquid interface. For a clean mercury-air-glass interface, $\theta = 130°$.

Example 1.9 illustrates how surface tension causes a fluid interface to rise or fall in a capillary tube.



ketabline.com Ebook.ketabline.com

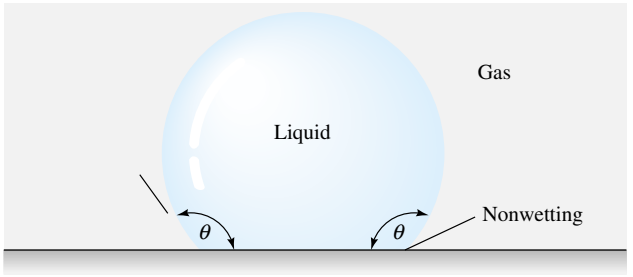


Fig. 1.10 Contact-angle effects at liquid-gas-solid interface. If $\theta < 90°$, the liquid "wets" the solid; if $\theta > 90°$, the liquid is nonwetting.

EXAMPLE 1.9

Derive an expression for the change in height h in a circular tube of a liquid with surface tension Υ and contact angle θ, as in Fig. E1.9.

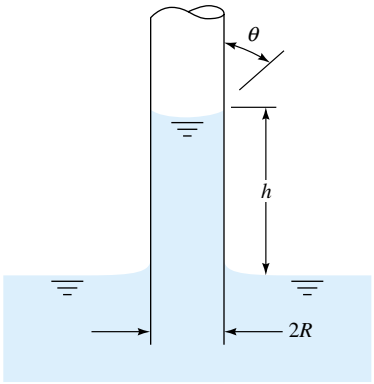


Fig. E1.9

Solution

The vertical component of the ring surface-tension force at the interface in the tube must balance the weight of the column of fluid of height h

$$2\pi R\Upsilon \cos\theta = \gamma\pi R^2 h$$

Solving for h, we have the desired result

$$h = \frac{2\Upsilon \cos\theta}{\gamma R} \qquad \textit{Ans.}$$

Thus the capillary height increases inversely with tube radius R and is positive if $\theta < 90°$ (wetting liquid) and negative (capillary depression) if $\theta > 90°$.

Suppose that $R = 1$ mm. Then the capillary rise for a water-air-glass interface, $\theta \approx 0°$, $\Upsilon = 0.073$ N/m, and $\rho = 1000$ kg/m^3 is

$$h = \frac{2(0.073\ \text{N/m})(\cos 0°)}{(1000\ \text{kg/m}^3)(9.81\ \text{m/s}^2)(0.001\ \text{m})} = 0.015\ (\text{N}\cdot\text{s}^2)/\text{kg} = 0.015\ \text{m} = 1.5\ \text{cm}$$

For a mercury-air-glass interface, with $\theta = 130°$, $\Upsilon = 0.48$ N/m, and $\rho = 13{,}600$ kg/m^3, the capillary rise is

$$h = \frac{2(0.48)(\cos 130°)}{13{,}600(9.81)(0.001)} = -0.46\ \text{cm}$$

When a small-diameter tube is used to make pressure measurements (Chap. 2), these capillary effects must be corrected for.

Vapor Pressure

Vapor pressure is the pressure at which a liquid boils and is in equilibrium with its own vapor. For example, the vapor pressure of water at 68°F is 49 lbf/ft^2, while th of mercury is only 0.0035 lbf/ft^2. If the liquid pressure is great



ketabline.com Ebook.ketabline.com

pressure, the only exchange between liquid and vapor is evaporation at the interface. If, however, the liquid pressure falls below the vapor pressure, vapor bubbles begin to appear in the liquid. If water is heated to 212°F, its vapor pressure rises to 2116 lbf/ft^2, and thus water at normal atmospheric pressure will boil. When the liquid pressure is dropped below the vapor pressure due to a flow phenomenon, we call the process *cavitation*. As we shall see in Chap. 2, if water is accelerated from rest to about 50 ft/s, its pressure drops by about 15 lbf/in^2, or 1 atm. This can cause cavitation.

The dimensionless parameter describing flow-induced boiling is the *cavitation number*

$$\text{Ca} = \frac{p_a - p_v}{\frac{1}{2}\rho V^2} \tag{1.35}$$

where p_a = ambient pressure
p_v = vapor pressure
V = characteristic flow velocity

Depending upon the geometry, a given flow has a critical value of Ca below which the flow will begin to cavitate. Values of surface tension and vapor pressure of water are given in Table A.5. The vapor pressure of water is plotted in Fig. 1.11.

Figure 1.12*a* shows cavitation bubbles being formed on the low-pressure surfaces of a marine propeller. When these bubbles move into a higher-pressure region, they collapse implosively. Cavitation collapse can rapidly spall and erode metallic surfaces and eventually destroy them, as shown in Fig. 1.12*b*.

No-Slip and No-Temperature-Jump Conditions

When a fluid flow is bounded by a solid surface, molecular interactions cause the fluid in contact with the surface to seek momentum and energy equilibrium with that surface. All liquids essentially are in equilibrium with the surface they contact. All gases are, too,

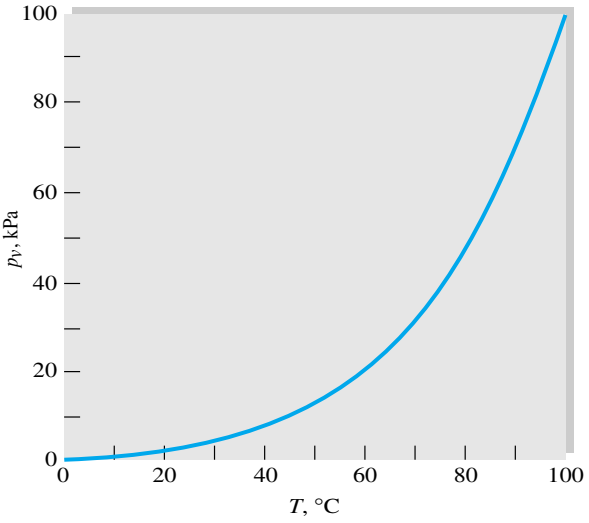


Fig. 1.11 Vapor pressure of water. Data from Table A.5.



ketabline.com Ebook.ketabline.com

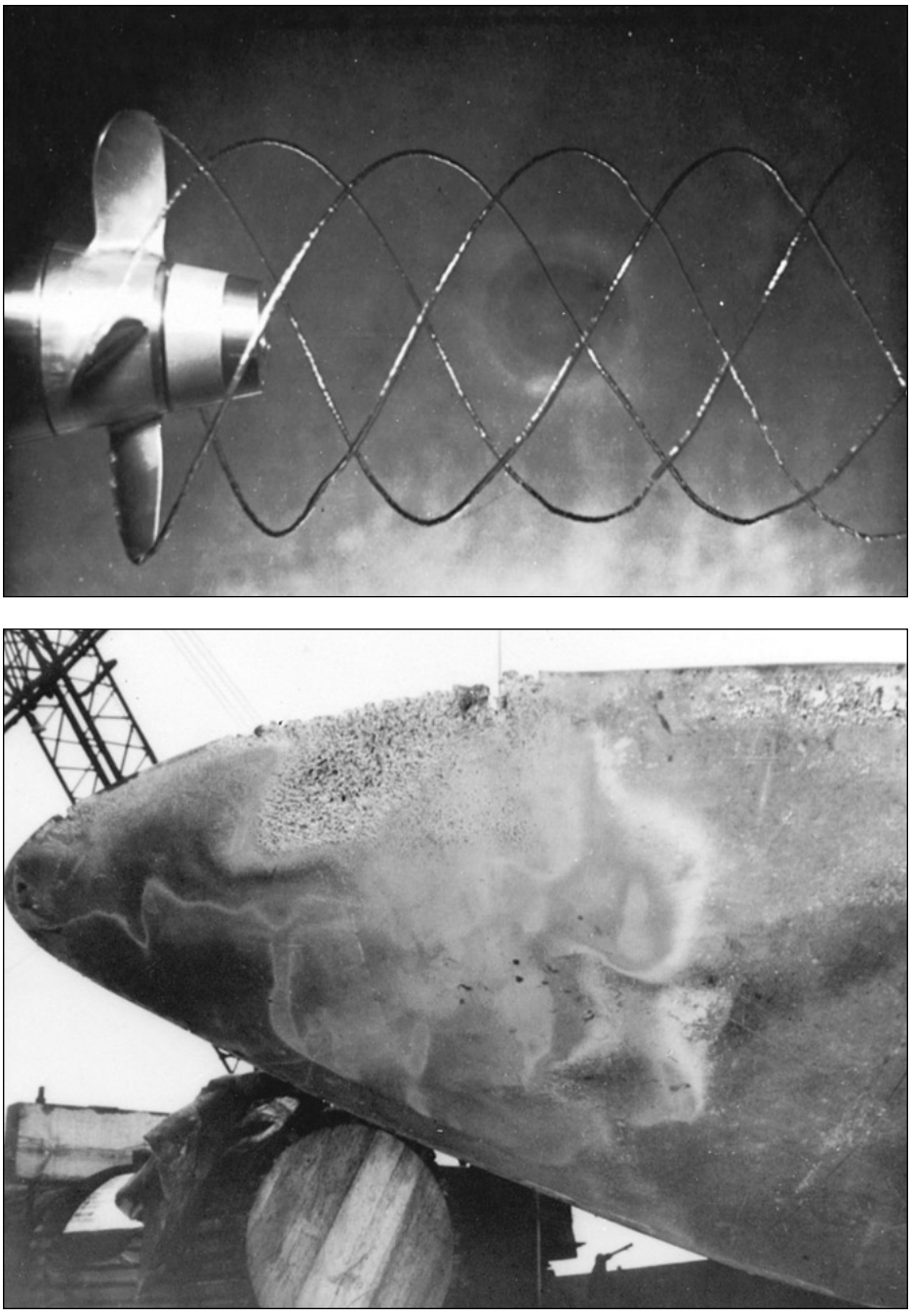


Fig. 1.12 Two aspects of cavitation bubble formation in liquid flows: (*a*) Beauty: spiral bubble sheets form from the surface of a marine propeller. *(Courtesy of the Garfield Thomas Water Tunnel, Pennsylvania State University);* (*b*) ugliness: collapsing bubbles erode a propeller surface. *(Courtesy of Thomas T. Huang, David Taylor Research Center.)*



ketabline.com Ebook.ketabline.com

except under the most rarefied conditions [8]. Excluding rarefied gases, then, all fluids at a point of contact with a solid take on the velocity and temperature of that surface

$$\mathbf{V}_{\text{fluid}} \equiv \mathbf{V}_{\text{wall}} \qquad T_{\text{fluid}} \equiv T_{\text{wall}} \tag{1.36}$$

These are called the *no-slip* and *no-temperature-jump conditions,* respectively. They serve as *boundary conditions* for analysis of fluid flow past a solid surface (Chap. 6). Figure 1.13 illustrates the no-slip condition for water flow past the top and bottom surfaces of a fixed thin plate. The flow past the upper surface is disorderly, or turbulent, while the lower surface flow is smooth, or laminar.[7] In both cases there is clearly no slip at the wall, where the water takes on the zero velocity of the fixed plate. The velocity profile is made visible by the discharge of a line of hydrogen bubbles from the wire shown stretched across the flow.

To decrease the mathematical difficulty, the no-slip condition is partially relaxed in the analysis of inviscid flow (Chap. 8). The flow is allowed to "slip" past the surface but not to permeate through the surface

$$V_{\text{normal}}(\text{fluid}) \equiv V_{\text{normal}}(\text{solid}) \tag{1.37}$$

while the tangential velocity V_t is allowed to be independent of the wall. The analysis is much simpler, but the flow patterns are highly idealized.

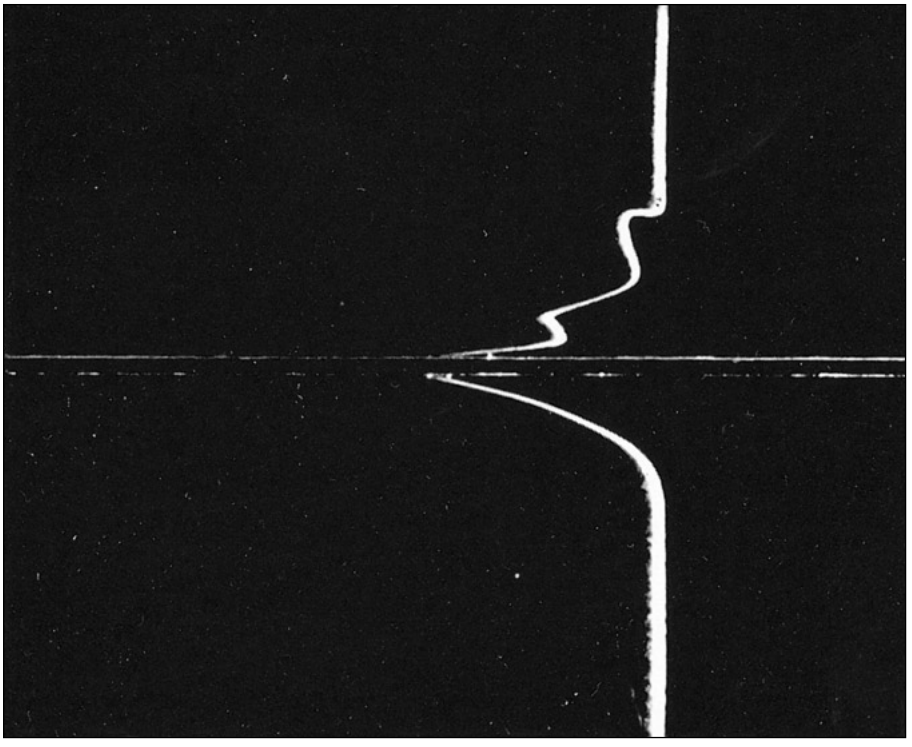


Fig. 1.13 The no-slip condition in water flow past a thin fixed plate. The upper flow is turbulent; the lower flow is laminar. The velocity profile is made visible by a line of hydrogen bubbles discharged from the wire across the flow. *[From* Illustrated Experiments in Fluid Mechanics *(The NCFMF Book of Film Notes), National Committee for Fluid Mechanics Films, Education Development Center, Inc., copyright 1972.]*

[7]Laminar and turbulent flows are studied in Chaps. 6 and 7.



ketabline.com Ebook.ketabline.com

Speed of Sound

In gas flow, one must be aware of *compressibility* effects (significant density changes caused by the flow). We shall see in Sec. 4.2 and in Chap. 9 that compressibility becomes important when the flow velocity reaches a significant fraction of the speed of sound of the fluid. The *speed of sound a* of a fluid is the rate of propagation of small-disturbance pressure pulses ("sound waves") through the fluid. In Chap. 9 we shall show, from momentum and thermodynamic arguments, that the speed of sound is defined by

$$a^2 = \left(\frac{\partial p}{\partial \rho}\right)_s = k\left(\frac{\partial p}{\partial \rho}\right)_T \qquad k = \frac{c_p}{c_v} \tag{1.38}$$

This is true for either a liquid or a gas, but it is for *gases* that the problem of compressibility occurs. For an ideal gas, Eq. (1.10), we obtain the simple formula

$$a_{\text{ideal gas}} = (kRT)^{1/2} \tag{1.39}$$

where R is the gas constant, Eq. (1.11), and T the absolute temperature. For example, for air at 20°C, $a = \{(1.40)[287\ \text{m}^2/(\text{s}^2 \cdot \text{K})](293\ \text{K})\}^{1/2} \approx 343$ m/s (1126 ft/s = 768 mi/h). If, in this case, the air velocity reaches a significant fraction of a, say, 100 m/s, then we must account for compressibility effects (Chap. 9). Another way to state this is to account for compressibility when the *Mach number* Ma $= V/a$ of the flow reaches about 0.3.

The speed of sound of water is tabulated in Table A.5. The speed of sound of air (or any approximately perfect gas) is simply calculated from Eq. (1.39).

1.8 Basic Flow-Analysis Techniques

There are three basic ways to attack a fluid-flow problem. They are equally important for a student learning the subject, and this book tries to give adequate coverage to each method:

1. Control-volume, or *integral* analysis (Chap. 3)
2. Infinitesimal system, or *differential* analysis (Chap. 4)
3. Experimental study, or *dimensional* analysis (Chap. 5)

In all cases, the flow must satisfy the three basic laws of mechanics[8] plus a thermodynamic state relation and associated boundary conditions:

1. Conservation of mass (continuity)
2. Linear momentum (Newton's second law)
3. First law of thermodynamics (conservation of energy)
4. A state relation like $\rho = \rho(p, T)$
5. Appropriate boundary conditions at solid surfaces, interfaces, inlets, and exits

In integral and differential analyses, these five relations are modeled mathematically and solved by computational methods. In an experimental study, the fluid itself performs this task without the use of any mathematics. In other words, these laws are believed to be fundamental to physics, and no fluid flow is known to violate them.

[8]In fluids which are variable mixtures of components, such as seawater, a fourth [illegible] *conservation of species*. For an example of salt conservation analysis, see Chap. 4, [illegible]



ketabline.com Ebook.ketabline.com

A control volume is a finite region, chosen carefully by the analyst, with open boundaries through which mass, momentum, and energy are allowed to cross. The analyst makes a budget, or balance, between the incoming and outgoing fluid and the resultant changes within the control volume. The result is a powerful tool but a crude one. Details of the flow are normally washed out or ignored in control-volume analyses. Nevertheless, the control-volume technique of Chap. 3 never fails to yield useful and quantitative information to the engineering analyst.

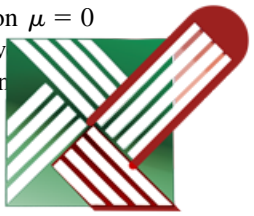
When the conservation laws are written for an infinitesimal system of fluid in motion, they become the basic differential equations of fluid flow. To apply them to a specific problem, one must integrate these equations mathematically subject to the boundary conditions of the particular problem. Exact analytic solutions are often possible only for very simple geometries and boundary conditions (Chap. 4). Otherwise, one attempts numerical integration on a digital computer, i.e., a summing procedure for finite-sized systems which one hopes will approximate the exact integral calculus [1]. Even computer analysis often fails to provide an accurate simulation, because of either inadequate storage or inability to model the finely detailed flow structure characteristic of irregular geometries or turbulent-flow patterns. Thus differential analysis sometimes promises more than it delivers, although we can successfully study a number of classic and useful solutions.

A properly planned experiment is very often the best way to study a practical engineering flow problem. Guidelines for planning flow experiments are given in Chap. 5. For example, no theory presently available, whether differential or integral, calculus or computer, is able to make an accurate computation of the aerodynamic drag and side force of an automobile moving down a highway with crosswinds. One must solve the problem by experiment. The experiment may be *full-scale*: One can test a real automobile on a real highway in real crosswinds. For that matter, there are wind tunnels in existence large enough to hold a full-scale car without significant blockage effects. Normally, however, in the design stage, one tests a small-model automobile in a small wind tunnel. Without proper interpretation, the model results may be poor and mislead the designer (Chap. 5). For example, the model may lack important details such as surface finish or underbody protuberances. The "wind" produced by the tunnel propellers may lack the turbulent gustiness of real winds. It is the job of the fluid-flow analyst, using such techniques as dimensional analysis, to plan an experiment which gives an accurate estimate of full-scale or *prototype* results expected in the final product.

It is possible to classify flows, but there is no general agreement on how to do it. Most classifications deal with the assumptions made in the proposed flow analysis. They come in pairs, and we normally assume that a given flow is either

Steady	or	unsteady	(1.40*a*)
Inviscid	or	viscous	(1.40*b*)
Incompressible	or	compressible	(1.40*c*)
Gas	or	liquid	(1.40*d*)

As Fig. 1.14 indicates, we choose one assumption from each pair. We may have a steady viscous compressible gas flow or an unsteady inviscid ($\mu = 0$) incompressible liquid flow. Although there is no such thing as a truly inviscid fluid, the assumption $\mu = 0$ gives adequate results in many analyses (Chap. 8). Often the assumptions ov
flow may be viscous in the boundary layer near a solid surface (Fig. 1.13) an



ketabline.com Ebook.ketabline.com



Fig. 1.14 Ready for a flow analysis? Then choose one assumption from each box.

tively inviscid away from the surface. The viscous part of the flow may be laminar or transitional or turbulent or combine patches of all three types of viscous flow. A flow may involve both a gas and a liquid and the free surface, or interface, between them (Chap. 10). A flow may be compressible in one region and have nearly constant density in another. Nevertheless, Eq. (1.40) and Fig. 1.14 give the basic binary assumptions of flow analysis, and Chaps. 6 to 10 try to separate them and isolate the basic effect of each assumption.

1.9 Flow Patterns: Streamlines, Streaklines, and Pathlines

Fluid mechanics is a highly visual subject. The patterns of flow can be visualized in a dozen different ways, and you can view these sketches or photographs and learn a great deal qualitatively and often quantitatively about the flow.

Four basic types of line patterns are used to visualize flows:

1. A *streamline* is a line everywhere tangent to the velocity vector at a given instant.
2. A *pathline* is the actual path traversed by a given fluid particle.
3. A *streakline* is the locus of particles which have earlier passed through a prescribed point.
4. A *timeline* is a set of fluid particles that form a line at a given instant.

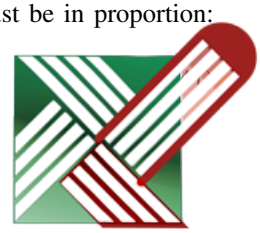
The streamline is convenient to calculate mathematically, while the other three are easier to generate experimentally. Note that a streamline and a timeline are instantaneous lines, while the pathline and the streakline are generated by the passage of time. The velocity profile shown in Fig. 1.13 is really a timeline generated earlier by a single discharge of bubbles from the wire. A pathline can be found by a time exposure of a single marked particle moving through the flow. Streamlines are difficult to generate experimentally in unsteady flow unless one marks a great many particles and notes their direction of motion during a very short time interval [17, p. 35]. In steady flow the situation simplifies greatly:

Streamlines, pathlines, and streaklines are identical in steady flow.

In fluid mechanics the most common mathematical result for visualization purposes is the streamline pattern. Figure 1.15*a* shows a typical set of streamlines, and Fig. 1.15*b* shows a closed pattern called a *streamtube*. By definition the fluid within a streamtube is confined there because it cannot cross the streamlines; thus the streamtube walls need not be solid but may be fluid surfaces.

Figure 1.16 shows an arbitrary velocity vector. If the elemental arc length dr of a streamline is to be parallel to $\mathbf{V}$, their respective components must be in proportion:

Streamline: $$\frac{dx}{u} = \frac{dy}{v} = \frac{dz}{w} = \frac{dr}{V}$$



ketabline.com Ebook.ketabline.com

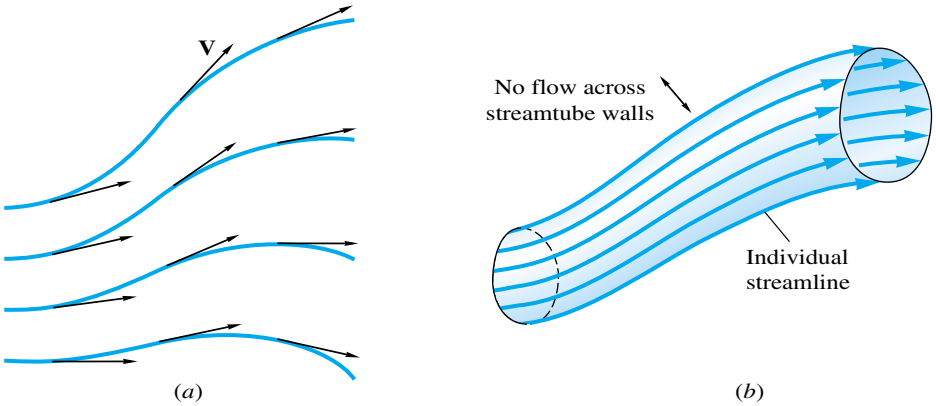


Fig. 1.15 The most common method of flow-pattern presentation: (*a*) Streamlines are everywhere tangent to the local velocity vector; (*b*) a streamtube is formed by a closed collection of streamlines.

If the velocities (u, v, w) are known functions of position and time, Eq. (1.41) can be integrated to find the streamline passing through the initial point (x_0, y_0, z_0, t_0). The method is straightforward for steady flows (Example 1.10) but may be laborious for unsteady flow.

The pathline, or displacement of a particle, is defined by integration of the velocity components, as mentioned in Sec. 1.5:

$$\text{Pathline:} \qquad x = \int u\,dt \qquad y = \int v\,dt \qquad z = \int w\,dt \tag{1.42}$$

Given (u, v, w) as known functions of position and time, the integration is begun at a specified initial position (x_0, y_0, z_0, t_0). Again the integration may be laborious.

Streaklines, easily generated experimentally with smoke, dye, or bubble releases, are very difficult to compute analytically. See Ref. 18 for mathematical details.

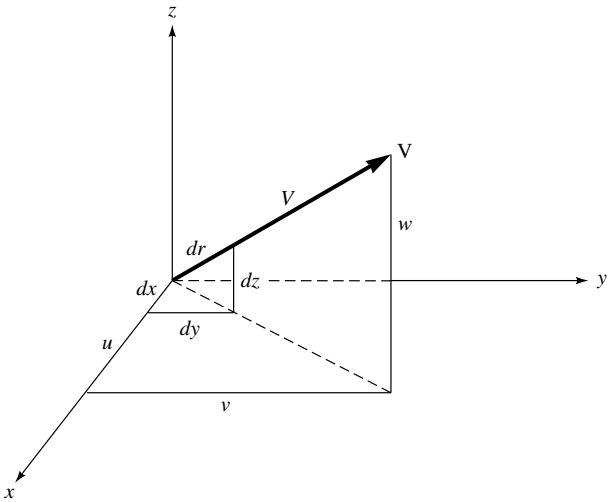


Fig. 1.16 Geometric relations for defining a streamline.



ketabline.com Ebook.ketabline.com

EXAMPLE 1.10

Given the steady two-dimensional velocity distribution

$$u = Kx \qquad v = -Ky \qquad w = 0 \tag{1}$$

where K is a positive constant, compute and plot the streamlines of the flow, including directions, and give some possible interpretations of the pattern.

Solution

Since time does not appear explicitly in Eq. (1), the motion is steady, so that streamlines, pathlines, and streaklines will coincide. Since $w = 0$ everywhere, the motion is two dimensional, in the xy plane. The streamlines can be computed by substituting the expressions for u and v into Eq. (1.41):

$$\frac{dx}{Kx} = -\frac{dy}{Ky}$$

or

$$\int \frac{dx}{x} = -\int \frac{dy}{y}$$

Integrating, we obtain $\ln x = -\ln y + \ln C$, or

$$xy = C \qquad \textit{Ans.} \tag{2}$$

This is the general expression for the streamlines, which are hyperbolas. The complete pattern is plotted in Fig. E1.10 by assigning various values to the constant C. The arrowheads can be determined only by returning to Eqs. (1) to ascertain the velocity component directions, assuming K is positive. For example, in the upper right quadrant ($x > 0$, $y > 0$), u is positive and v is negative; hence the flow moves down and to the right, establishing the arrowheads as shown.

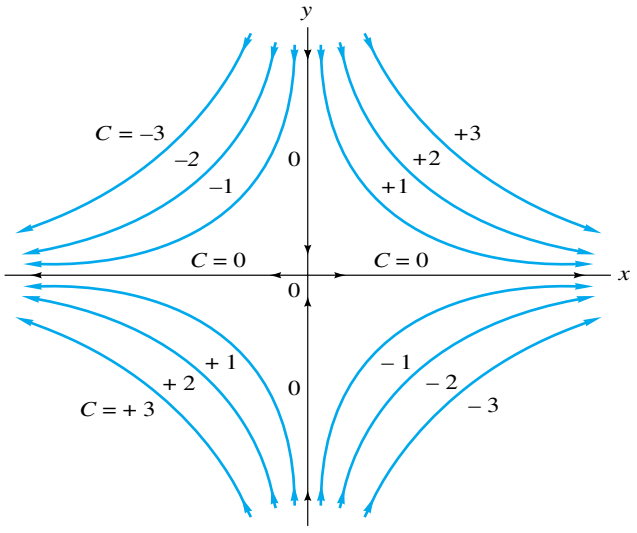


Fig. E1.10 Streamlines for the velocity distribution given by Eq. (1), for $K > 0$.



ketabline.com Ebook.ketabline.com

Note that the streamline pattern is entirely independent of constant K. It could represent the impingement of two opposing streams, or the upper half could simulate the flow of a single downward stream against a flat wall. Taken in isolation, the upper right quadrant is similar to the flow in a 90° corner. This is definitely a realistic flow pattern and is discussed again in Chap. 8.

Finally note the peculiarity that the two streamlines ($C = 0$) have opposite directions and intersect. This is possible only at a point where $u = v = w = 0$, which occurs at the origin in this case. Such a point of zero velocity is called a *stagnation point*.

A streakline can be produced experimentally by the continuous release of marked particles (dye, smoke, or bubbles) from a given point. Figure 1.17 shows two examples. The flow in Fig. 1.17*b* is unsteady and periodic due to the flapping of the plate against the oncoming stream. We see that the dash-dot streakline does not coincide with either the streamline or the pathline passing through the same release point. This is characteristic of unsteady flow, but in Fig. 1.17*a* the smoke filaments form streaklines which are identical to the streamlines and pathlines. We noted earlier that this coincidence of lines is always true of steady flow: Since the velocity never changes magnitude or direction at any point, every particle which comes along repeats the behavior of its earlier neighbors.

Methods of experimental flow visualization include the following:

1. Dye, smoke, or bubble discharges
2. Surface powder or flakes on liquid flows
3. Floating or neutral-density particles
4. Optical techniques which detect density changes in gas flows: shadowgraph, schlieren, and interferometer
5. Tufts of yarn attached to boundary surfaces
6. Evaporative coatings on boundary surfaces
7. Luminescent fluids or additives

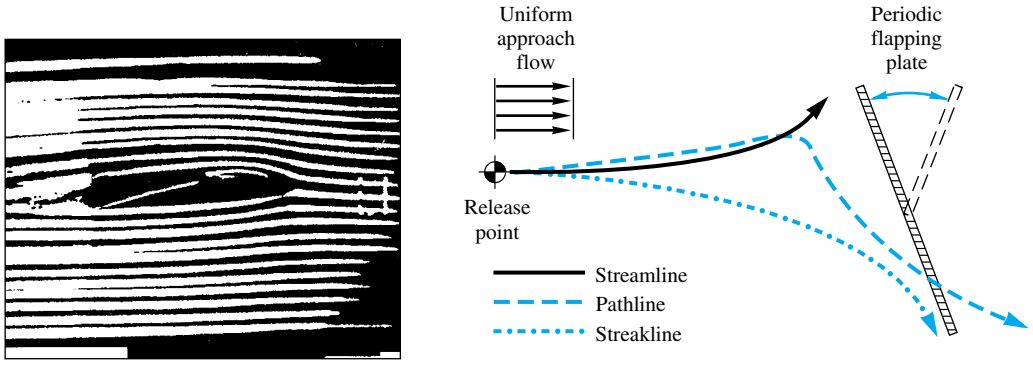


Fig. 1.17 Experimental visualization of steady and unsteady flow: (*a*) steady flow past an airfoil visualized by smoke filaments *(C. A. A. SCIENTIFIC—Prime Movers Laboratory Systems);* (*b*) unsteady flow past an oscillating plate with a point bubble release (from an experiment in Ref. 17).



ketabline.com Ebook.ketabline.com

The mathematical implications of flow-pattern analysis are discussed in detail in Ref. 18. References 19 and 20 are beautiful albums of photographs. References 21 and 22 are monographs on flow visualization.

1.10 The Engineering Equation Solver



Most of the examples and exercises in this text are amenable to direct calculation without guessing or iteration or looping. Until recently, only such direct problem assignments, whether "plug-and-chug" or more subtle, were appropriate for undergraduate engineering courses. However, the recent introduction of computer software *solvers* makes almost any set of algebraic relations viable for analysis and solution. The solver recommended here is the *Engineering Equation Solver* (EES) developed by Klein and Beckman [33] and described in Appendix E.

Any software solver should handle a purely mathematical set of relations, such as the one posed in Ref. 33: $X \ln(X) = Y^3$, $X^{1/2} = 1/Y$. Submit that pair to any commercial solver and you will no doubt receive the answer: $X = 1.467$, $Y = 0.826$. However, for engineers, in the author's opinion, EES is superior to most solvers because (1) equations can be entered in any order; (2) scores of mathematical formulas are built-in, such as the Bessel functions; and (3) thermophysical properties of many fluids are built-in, such as the steam tables [13]. Both metric and English units are allowed. Equations need not be written in the traditional BASIC or FORTRAN style. For example, $X - Y + 1 = 0$ is perfectly satisfactory; there is no need to retype this as $X = Y - 1$.

For example, reconsider Example 1.7 as an EES exercise. One would first enter the reference properties p_0 and ρ_0 plus the curve-fit constants B and n:

```
Pz = 1.0
Rhoz = 2.0
B = 3000
n = 7
```

Then specify the given pressure ratio and the curve-fit relation, Eq. (1.19), for the equation of state of water:

```
P = 1100*Pz
P/Pz = (B + 1)*(Rho/Rhoz)^n - B
```

If you request an initial opinion from the CHECK/FORMAT menu, EES states that there are six equations in six unknowns and there are no obvious difficulties. Then request SOLVE from the menu and EES quickly prints out Rho = 2.091, the correct answer as seen already in Ex. 1.7. It also prints out values of the other five variables. Occasionally EES reports "unable to converge" and states what went wrong (division by zero, square root of a negative number, etc.). One needs only to improve the guesses and ranges of the unknowns in Variable Information to assist EES to the solution.

In subsequent chapters we will illustrate some implicit (iterative) examples by using EES and will also assign some advanced problem exercises for which EES is an ideal approach. The use of an engineering solver, notably EES, is recommended to all engineers in this era of the personal computer.



ketabline.com Ebook.ketabline.com

1.11 Uncertainty of Experimental Data

Earlier in this chapter we referred to the *uncertainty* of the principle of corresponding states in discussing Fig. 1.5. Uncertainty is a fact of life in engineering. We rarely know any engineering properties or variables to an extreme degree of accuracy. Therefore, we need to know the *uncertainty* U of our data, usually defined as the band within which the experimenter is 95 percent confident that the true value lies (Refs. 30, 31). In Fig. 1.5, we were given that the uncertainty of μ/μ_c is $U \approx \pm 20$ percent.

Fluid mechanics is heavily dependent upon experimentation, and the data uncertainty is needed before we can use it for prediction or design purposes. Sometimes uncertainty completely changes our viewpoint. As an offbeat example, suppose that astronomers reported that the length of the earth year was 365.25 days "give or take a couple of months." First, that would make the five-figure accuracy ridiculous, and the year would better be stated as $Y \approx 365 \pm 60$ days. Second, we could no longer plan confidently or put together accurate calendars. Scheduling Christmas vacation would be chancy.

Multiple variables make uncertainty estimates cumulative. Suppose a given result P depends upon N variables, $P = P(x_1, x_2, x_3, \ldots, x_N)$, each with its own uncertainty; for example, x_1 has uncertainty δx_1. Then, by common agreement among experimenters, the total uncertainty of P is calculated as a root-mean-square average of all effects:

$$\delta P = \left[\left(\frac{\partial P}{\partial x_1}\delta x_1\right)^2 + \left(\frac{\partial P}{\partial x_2}\delta x_2\right)^2 + \cdots + \left(\frac{\partial P}{\partial x_N}\delta x_N\right)^2\right]^{1/2} \tag{1.43}$$

This calculation is statistically much more probable than simply adding linearly the various uncertainties δx_i, thereby making the unlikely assumption that all variables simultaneously attain maximum error. Note that it is the responsibility of the experimenter to establish and report accurate estimates of all the relevant uncertainties δx_i.

If the quantity P is a simple power-law expression of the other variables, for example, $P = \text{Const}\ x_1^{n_1}x_2^{n_2}x_3^{n_3}\ldots$, then each derivative in Eq. (1.43) is proportional to P and the relevant power-law exponent and is inversely proportional to that variable.

If $P = \text{Const}\ x_1^{n_1}x_2^{n_2}x_3^{n_3}\ldots$, then

$$\frac{\partial P}{\partial x_1} = \frac{n_1 P}{x_1}, \frac{\partial P}{\partial x_2} = \frac{n_2 P}{x_2}, \frac{\partial P}{\partial x_3} = \frac{n_3 P}{x_3}, \cdots$$

Thus, from Eq. (1.43),

$$\frac{\delta P}{P} = \left[\left(n_1\frac{\delta x_1}{x_1}\right)^2 + \left(n_2\frac{\delta x_2}{x_2}\right)^2 + \left(n_3\frac{\delta x_3}{x_3}\right)^2 + \cdots\right]^{1/2} \tag{1.44}$$

Evaluation of δP is then a straightforward procedure, as in the following example.

EXAMPLE 1.11

The so-called dimensionless Moody pipe-friction factor f, plotted in Fig. 6.13, is calculated in experiments from the following formula involving pipe diameter D, pressure drop Δp, density ρ, volume flow rate Q, and pipe length L:

$$f = \frac{\pi^2}{32}\frac{D^5\Delta p}{\rho Q^2 L}$$



ketabline.com Ebook.ketabline.com

Measurement uncertainties are given for a certain experiment: for D: 0.5 percent, Δp: 2.0 percent, ρ: 1.0 percent, Q: 3.5 percent, and L: 0.4 percent. Estimate the overall uncertainty of the friction factor f.

Solution

The coefficient $\pi^2/32$ is assumed to be a pure theoretical number, with no uncertainty. The other variables may be collected using Eqs. (1.43) and (1.44):

$$U = \frac{\delta f}{f} = \left[\left(5\frac{\delta D}{D}\right)^2 + \left(1\frac{\delta \Delta p}{\Delta p}\right)^2 + \left(1\frac{\delta \rho}{\rho}\right)^2 + \left(2\frac{\delta Q}{Q}\right)^2 + \left(1\frac{\delta L}{L}\right)^2\right]^{1/2}$$

$$= [\{5(0.5\%)\}^2 + (2.0\%)^2 + (1.0\%)^2 + \{2(3.5\%)\}^2 + (0.4\%)^2]^{1/2} \approx 7.8\% \qquad \textit{Ans.}$$

By far the dominant effect in this particular calculation is the 3.5 percent error in Q, which is amplified by doubling, due to the power of 2 on flow rate. The diameter uncertainty, which is quintupled, would have contributed more had δD been larger than 0.5 percent.

1.12 The Fundamentals of Engineering (FE) Examination

The road toward a professional engineer's license has a first stop, the Fundamentals of Engineering Examination, known as the FE exam. It was formerly known as the Engineer-in-Training (E-I-T) Examination. This 8-h national test will probably soon be required of all engineering graduates, not just for licensure, but as a student-assessment tool. The 120-problem morning session covers many general studies:

Chemistry	Computers	Dynamics
Electric circuits	Engineering economics	***Fluid Mechanics***
Materials science	Mathematics	Mechanics of materials
Statics	Thermodynamics	Ethics

For the 60-problem afternoon session you may choose chemical, civil, electrical, industrial, or mechanical engineering or take more general-engineering problems for remaining disciplines. As you can see, *fluid mechanics* is central to the FE exam. Therefore, this text includes a number of end-of-chapter FE problems where appropriate.

The format for the FE exam questions is multiple-choice, usually with five selections, chosen carefully to tempt you with plausible answers if you used incorrect units or forgot to double or halve something or are missing a factor of π, etc. In some cases, the selections are unintentionally ambiguous, such as the following example from a previous exam:

Transition from laminar to turbulent flow occurs at a Reynolds number of
(A) 900 (B) 1200 (C) 1500 (D) 2100 (E) 3000

The "correct" answer was graded as (D), Re = 2100. Clearly the examiner was thinking, but forgot to specify, Re_d for *flow in a smooth circular pipe,* since (see Chaps. 6 and 7) transition is highly dependent upon geometry, surface roughness, and the length scale used in the definition of Re. The moral is not to get peevish a simply to go with the flow (pun intended) and decide which a



ketabline.com Ebook.ketabline.com

undergraduate-training situation. Every effort has been made to keep the FE exam questions in this text unambiguous.

1.13 Problem-Solving Techniques

Fluid flow analysis generates a plethora of problems, 1500 in this text alone! To solve these problems, one must deal with various equations, data, tables, assumptions, unit systems, and numbers. The writer recommends these problem-solving steps:

1. Gather all the given system parameters and data in one place.
2. Find, from tables or charts, all needed fluid property data: ρ, μ, c_p, k, Υ, etc.
3. Use SI units (N, s, kg, m) if possible, and no conversion factors will be necessary.
4. Make sure what is *asked*. It is all too common for students to answer the wrong question, for example, reporting mass flow instead of volume flow, pressure instead of pressure gradient, drag force instead of lift force. Engineers are expected to read carefully.
5. Make a detailed sketch of the system, with everything clearly labeled.
6. Think carefully and then list your *assumptions*. Here knowledge is power; you should not guess the answer. You must be able to decide correctly if the flow can be considered steady or unsteady, compressible or incompressible, one-dimensional, or multidimensional, viscous or inviscid, and whether a control volume or partial differential equations are needed.
7. Based on steps 1 to 6 above, write out the appropriate equations, data correlations, and fluid state relations for your problem. If the algebra is straightforward, solve for what is *asked*. If the equations are complicated, e.g., nonlinear or too plentiful, use the Engineering Equation Solver (EES).
8. Report your solution clearly, with proper units listed and to the proper number of significant figures (usually two or three) that the overall uncertainty of the data will allow.

1.14 History and Scope of Fluid Mechanics

Like most scientific disciplines, fluid mechanics has a history of erratically occurring early achievements, then an intermediate era of steady fundamental discoveries in the eighteenth and nineteenth centuries, leading to the twentieth-century era of "modern practice," as we self-centeredly term our limited but up-to-date knowledge. Ancient civilizations had enough knowledge to solve certain flow problems. Sailing ships with oars and irrigation systems were both known in prehistoric times. The Greeks produced quantitative information. Archimedes and Hero of Alexandria both postulated the parallelogram law for addition of vectors in the third century B.C. Archimedes (285–212 B.C.) formulated the laws of buoyancy and applied them to floating and submerged bodies, actually deriving a form of the differential calculus as part of the analysis. The Romans built extensive aqueduct systems in the fourth century B.C. but left no records showing any quantitative knowledge of design principles.

From the birth of Christ to the Renaissance there was a steady improvement in the design of such flow systems as ships and canals and water conduits but no recorded evidence of fundamental improvements in flow analysis. Then Leonardo d
(1452–1519) derived the equation of conservation of mass in one-dimensiona



ketabline.com Ebook.ketabline.com

flow. Leonardo was an excellent experimentalist, and his notes contain accurate descriptions of waves, jets, hydraulic jumps, eddy formation, and both low-drag (streamlined) and high-drag (parachute) designs. A Frenchman, Edme Mariotte (1620–1684), built the first wind tunnel and tested models in it.

Problems involving the momentum of fluids could finally be analyzed after Isaac Newton (1642–1727) postulated his laws of motion and the law of viscosity of the linear fluids now called newtonian. The theory first yielded to the assumption of a "perfect" or frictionless fluid, and eighteenth-century mathematicians (Daniel Bernoulli, Leonhard Euler, Jean d'Alembert, Joseph-Louis Lagrange, and Pierre-Simon Laplace) produced many beautiful solutions of frictionless-flow problems. Euler developed both the differential equations of motion and their integrated form, now called the Bernoulli equation. D'Alembert used them to show his famous paradox: that a body immersed in a frictionless fluid has zero drag. These beautiful results amounted to overkill, since perfect-fluid assumptions have very limited application in practice and most engineering flows are dominated by the effects of viscosity. Engineers began to reject what they regarded as a totally unrealistic theory and developed the science of *hydraulics,* relying almost entirely on experiment. Such experimentalists as Chézy, Pitot, Borda, Weber, Francis, Hagen, Poiseuille, Darcy, Manning, Bazin, and Weisbach produced data on a variety of flows such as open channels, ship resistance, pipe flows, waves, and turbines. All too often the data were used in raw form without regard to the fundamental physics of flow.

At the end of the nineteenth century, unification between experimental *hydraulics* and theoretical *hydrodynamics* finally began. William Froude (1810–1879) and his son Robert (1846–1924) developed laws of model testing, Lord Rayleigh (1842–1919) proposed the technique of dimensional analysis, and Osborne Reynolds (1842–1912) published the classic pipe experiment in 1883 which showed the importance of the dimensionless Reynolds number named after him. Meanwhile, viscous-flow theory was available but unexploited, since Navier (1785–1836) and Stokes (1819–1903) had successfully added newtonian viscous terms to the equations of motion. The resulting Navier-Stokes equations were too difficult to analyze for arbitrary flows. Then, in 1904, a German engineer, Ludwig Prandtl (1875–1953), published perhaps the most important paper ever written on fluid mechanics. Prandtl pointed out that fluid flows with small viscosity, e.g., water flows and airflows, can be divided into a thin viscous layer, or *boundary layer,* near solid surfaces and interfaces, patched onto a nearly inviscid outer layer, where the Euler and Bernoulli equations apply. Boundary-layer theory has proved to be the single most important tool in modern flow analysis. The twentieth-century foundations for the present state of the art in fluid mechanics were laid in a series of broad-based experiments and theories by Prandtl and his two chief friendly competitors, Theodore von Kármán (1881–1963) and Sir Geoffrey I. Taylor (1886–1975). Many of the results sketched here from a historical point of view will, of course, be discussed in this textbook. More historical details can be found in Refs. 23 to 25.

Since the earth is 75 percent covered with water and 100 percent covered with air, the scope of fluid mechanics is vast and touches nearly every human endeavor. The sciences of meteorology, physical oceanography, and hydrology are concerned with naturally occurring fluid flows, as are medical studies of breathing and blood circulation. All transportation problems involve fluid motion, with well-developed specialties in aerodynamics of aircraft and rockets and in naval hydrodynamics of ships and submarines. Almost all our electric energy is developed either from w



ketabline.com Ebook.ketabline.com

steam flow through turbine generators. All combustion problems involve fluid motion, as do the more classic problems of irrigation, flood control, water supply, sewage disposal, projectile motion, and oil and gas pipelines. The aim of this book is to present enough fundamental concepts and practical applications in fluid mechanics to prepare you to move smoothly into any of these specialized fields of the science of flow—and then be prepared to move out again as new technologies develop.

Problems

Most of the problems herein are fairly straightforward. More difficult or open-ended assignments are labeled with an asterisk as in Prob. 1.18. Problems labeled with an EES icon (for example, Prob. 2.62), will benefit from the use of the Engineering Equation Solver (EES), while problems labeled with a computer disk may require the use of a computer. The standard end-of-chapter problems 1.1 to 1.85 (categorized in the problem list below) are followed by fundamentals of engineering (FE) exam problems FE3.1 to FE3.10, and comprehensive problems C1.1 to C1.4.

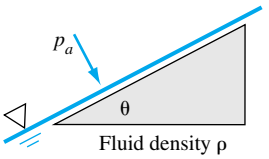
Problem Distribution

Section	Topic	Problems
1.1, 1.2, 1.3	Fluid-continuum concept	1.1–1.3
1.4	Dimensions, units, dynamics	1.4–1.20
1.5	Velocity field	1.21–1.23
1.6	Thermodynamic properties	1.24–1.37
1.7	Viscosity; no-slip condition	1.38–1.61
1.7	Surface tension	1.62–1.71
1.7	Vapor pressure; cavitation	1.72–1.75
1.7	Speed of sound; Mach number	1.76–1.78
1.8,9	Flow patterns, streamlines, pathlines	1.79–1.84
1.10	History of fluid mechanics	1.85

P1.1 A gas at 20°C may be considered *rarefied,* deviating from the continuum concept, when it contains less than 10^{12} molecules per cubic millimeter. If Avogadro's number is 6.023 E23 molecules per mole, what absolute pressure (in Pa) for air does this represent?

P1.2 Table A.6 lists the density of the standard atmosphere as a function of altitude. Use these values to estimate, crudely—say, within a factor of 2—the number of molecules of air in the entire atmosphere of the earth.

P1.3 For the triangular element in Fig. P1.3, show that a *tilted* free liquid surface, in contact with an atmosphere at pressure p_a, must undergo shear stress and hence begin to flow. *Hint:* Account for the weight of the fluid and show that a no-shear condition will cause horizontal forces to be out of balance.



P1.3

P1.4 A beaker approximates a right circular cone of diameter 7 in and height 9 in. When filled with liquid, it weighs 70 oz. When empty, it weighs 14 oz. Estimate the density of this liquid in both SI and BG units.

P1.5 The *mean free path* of a gas, ℓ, is defined as the average distance traveled by molecules between collisions. A proposed formula for estimating ℓ of an ideal gas is

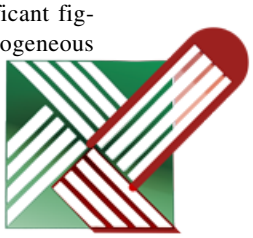
$$\ell = 1.26\frac{\mu}{\rho\sqrt{RT}}$$

What are the dimensions of the constant 1.26? Use the formula to estimate the mean free path of air at 20°C and 7 kPa. Would you consider air *rarefied* at this condition?

P1.6 In the $\{MLT\Theta\}$ system, what is the dimensional representation of (*a*) enthalpy, (*b*) mass rate of flow, (*c*) bending moment, (*d*) angular velocity, (*e*) modulus of elasticity; (*f*) Poisson's ratio?

P1.7 A small village draws 1.5 acre · ft/day of water from its reservoir. Convert this average water usage to (*a*) gallons per minute and (*b*) liters per second.

P1.8 Suppose we know little about the strength of materials but are told that the bending stress σ in a beam is *proportional* to the beam half-thickness y and also depends upon the bending moment M and the beam area moment of inertia I. We also learn that, for the particular case $M = 2900$ in · lbf, $y = 1.5$ in, and $I = 0.4$ in^4, the predicted stress is 75 MPa. Using this information and dimensional reasoning only, find, to three significant figures, the only possible dimensionally homogeneous formula $\sigma = y\,f(M, I)$.



ketabline.com Ebook.ketabline.com

P1.9 The *kinematic viscosity* of a fluid is the ratio of viscosity to density, $\nu = \mu/\rho$. What is the only possible dimensionless group combining ν with velocity V and length L? What is the name of this grouping? (More information on this will be given in Chap. 5.)

P1.10 The Stokes-Oseen formula [18] for drag force F on a sphere of diameter D in a fluid stream of low velocity V, density ρ, and viscosity μ, is

$$F = 3\pi\mu DV + \frac{9\pi}{16}\rho V^2 D^2$$

Is this formula dimensionally homogeneous?

P1.11 Engineers sometimes use the following formula for the volume rate of flow Q of a liquid flowing through a hole of diameter D in the side of a tank:

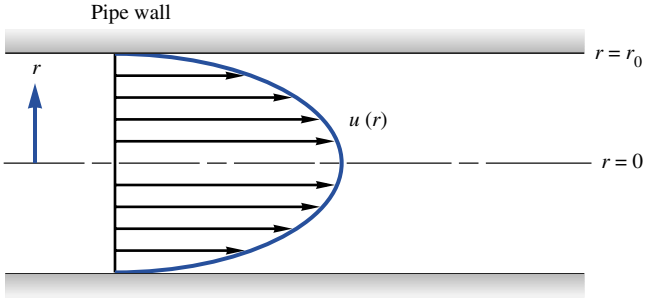
$$Q = 0.68\, D^2\sqrt{gh}$$

where g is the acceleration of gravity and h is the height of the liquid surface above the hole. What are the dimensions of the constant 0.68?

P1.12 For low-speed (laminar) steady flow through a circular pipe, as shown in Fig. P1.12, the velocity u varies with radius and takes the form

$$u = B\frac{\Delta p}{\mu}(r_0^2 - r^2)$$

where μ is the fluid viscosity and Δp is the pressure drop from entrance to exit. What are the dimensions of the constant B?



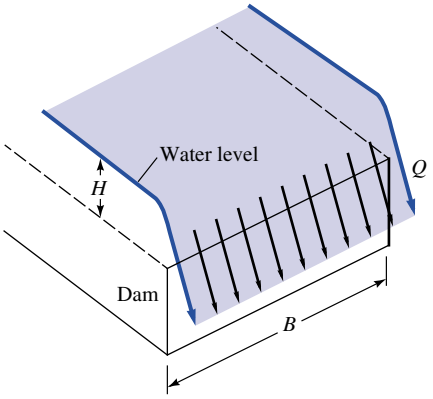
P1.12

P1.13 The efficiency η of a pump is defined as the (dimensionless) ratio of the power developed by the flow to the power required to drive the pump:

$$\eta = \frac{Q\Delta p}{\text{input power}}$$

where Q is the volume rate of flow and Δp is the pressure rise produced by the pump. Suppose that a certain pump develops a pressure rise of 35 lbf/in^2 when its flow rate is 40 L/s. If the input power is 16 hp, what is the efficiency?

***P1.14** Figure P1.14 shows the flow of water over a dam. The volume flow Q is known to depend only upon crest width B, acceleration of gravity g, and upstream water height H above the dam crest. It is further known that Q is proportional to B. What is the form of the only possible dimensionally homogeneous relation for this flow rate?



P1.14

P1.15 As a practical application of Fig. P1.14, often termed a sharp-crested weir, civil engineers use the following formula for flow rate: $Q \approx 3.3BH^{3/2}$, with Q in ft^3/s and B and H in feet. Is this formula dimensionally homogeneous? If not, try to explain the difficulty and how it might be converted to a more homogeneous form.

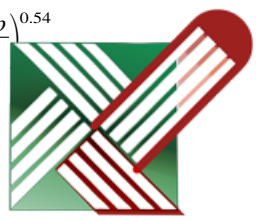
P1.16 Algebraic equations such as Bernoulli's relation, Eq. (1) of Ex. 1.3, are dimensionally consistent, but what about differential equations? Consider, for example, the boundary-layer x-momentum equation, first derived by Ludwig Prandtl in 1904:

$$\rho u\frac{\partial u}{\partial x} + \rho v\frac{\partial u}{\partial y} = -\frac{\partial p}{\partial x} + \rho g_x + \frac{\partial \tau}{\partial y}$$

where τ is the boundary-layer shear stress and g_x is the component of gravity in the x direction. Is this equation dimensionally consistent? Can you draw a general conclusion?

P1.17 The Hazen-Williams hydraulics formula for volume rate of flow Q through a pipe of diameter D and length L is given by

$$Q \approx 61.9\, D^{2.63}\left(\frac{\Delta p}{L}\right)^{0.54}$$



ketabline.com Ebook.ketabline.com

where Δp is the pressure drop required to drive the flow. What are the dimensions of the constant 61.9? Can this formula be used with confidence for various liquids and gases?

***P1.18** For small particles at low velocities, the first term in the Stokes-Oseen drag law, Prob. 1.10, is dominant; hence, $F \approx KV$, where K is a constant. Suppose a particle of mass m is constrained to move horizontally from the initial position $x = 0$ with initial velocity V_0. Show (*a*) that its velocity will decrease exponentially with time and (*b*) that it will stop after traveling a distance $x = mV_0/K$.

***P1.19** For larger particles at higher velocities, the quadratic term in the Stokes-Oseen drag law, Prob. 1.10, is dominant; hence, $F \approx CV^2$, where C is a constant. Repeat Prob. 1.18 to show that (*a*) its velocity will decrease as $1/(1 + CV_0t/m)$ and (*b*) it will never quite stop in a finite time span.

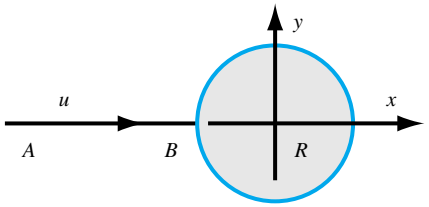
P1.20 A baseball, with $m = 145$ g, is thrown directly upward from the initial position $z = 0$ and $V_0 = 45$ m/s. The air drag on the ball is CV^2, as in Prob. 1.19, where $C \approx 0.0013$ N · s^2/m^2. Set up a differential equation for the ball motion, and solve for the instantaneous velocity $V(t)$ and position $z(t)$. Find the maximum height z_{max} reached by the ball, and compare your results with the classical case of zero air drag.

P1.21 A velocity field is given by $\mathbf{V} = Kx\mathbf{i} - Ky\mathbf{j} + 0\mathbf{k}$, where K is a positive constant. Evaluate (*a*) $\nabla \cdot \nabla$ and (*b*) $\nabla \times \mathbf{V}$.

***P1.22** According to the theory of Chap. 8, as a uniform stream approaches a cylinder of radius R along the symmetry line AB in Fig. P1.22, the velocity has only one component:

$$u = U_\infty\left(1 - \frac{R^2}{x^2}\right) \text{ for } -\infty < x \leq -R$$

where U_∞ is the stream velocity far from the cylinder. Using the concepts from Ex. 1.5, find (*a*) the maximum flow deceleration along AB and (*b*) its location.



P1.22

P1.23 Experiment with a faucet (kitchen or otherwise) to determine typical flow rates Q in m^3/h, perhaps timing the discharge of a known volume. Try to achieve an exit jet condition which is (*a*) smooth and round and (*b*) disorderly and fluctuating. Measure the supply-pipe diameter (look under the sink). For both cases, calculate the average flow velocity, $V_{avg} = Q/A_{cross\text{-}section}$ and the dimensionless Reynolds number of the flow, $\text{Re} = \rho V_{avg} D/\mu$. Comment on your results.

P1.24 Air at 1 atm and 20°C has an internal energy of approximately 2.1 E5 J/kg. If this air moves at 150 m/s at an altitude $z = 8$ m, what is its total energy, in J/kg, relative to the datum $z = 0$? Are any energy contributions negligible?

P1.25 A tank contains 0.9 m^3 of helium at 200 kPa and 20°C. Estimate the total mass of this gas, in kg, (*a*) on earth and (*b*) on the moon. Also, (*c*) how much heat transfer, in MJ, is required to expand this gas at constant temperature to a new volume of 1.5 m^3?

P1.26 When we in the United States say a car's tire is filled "to 32 lb," we mean that its internal pressure is 32 lbf/in^2 above the ambient atmosphere. If the tire is at sea level, has a volume of 3.0 ft^3, and is at 75°F, estimate the total weight of air, in lbf, inside the tire.

P1.27 For steam at 40 lbf/in^2, some values of temperature and specific volume are as follows, from Ref. 13:

T, °F	400	500	600	700	800
v, ft^3/lbm	12.624	14.165	15.685	17.195	18.699

Is steam, for these conditions, nearly a perfect gas, or is it wildly nonideal? If reasonably perfect, find a least-squares† value for the gas constant R, in m^2/(s^2 · K), estimate the percent error in this approximation, and compare with Table A.4.

P1.28 Wet atmospheric air at 100 percent relative humidity contains saturated water vapor and, by Dalton's law of partial pressures,

$$p_{atm} = p_{dry\ air} + p_{water\ vapor}$$

Suppose this wet atmosphere is at 40°C and 1 atm. Calculate the density of this 100 percent humid air, and compare it with the density of dry air at the same conditions.

P1.29 A compressed-air tank holds 5 ft^3 of air at 120 lbf/in^2 "gage," that is, above atmospheric pressure. Estimate the energy, in ft-lbf, required to compress this air from the atmosphere, assuming an ideal isothermal process.

P1.30 Repeat Prob. 1.29 if the tank is filled with compressed *water* instead of air. Why is the result thousands of times less than the result of 215,000 ft · lbf in Prob. 1.29?

***P1.31** The density of (fresh) water at 1 atm, over the temperature range 0 to 100°C, is given in Table A.1. Fit these values to a least-squares† equation of the form $\rho = a + bT + cT^2$, with T in °C, and estimate its accuracy. Use your formula to compute the density of water at 45°C, and compare your result with the accepted experimental value of 990.1 kg/m^3.

† The concept of "least-squares" error is very important and learned by everyone.



ketabline.com Ebook.ketabline.com

P1.32 A blimp is approximated by a prolate spheroid 90 m long and 30 m in diameter. Estimate the weight of 20°C gas within the blimp for (*a*) helium at 1.1 atm and (*b*) air at 1.0 atm. What might the *difference* between these two values represent (see Chap. 2)?

***P1.33** Experimental data for the density of mercury versus pressure at 20°C are as follows:

p, atm	1	500	1,000	1,500	2,000
ρ, kg/m^3	13,545	13,573	13,600	13,625	13,653

Fit this data to the empirical state relation for liquids, Eq. (1.22), to find the best values of B and n for mercury. Then, assuming the data are nearly isentropic, use these values to estimate the speed of sound of mercury at 1 atm and compare with Table 9.1.

P1.34 If water occupies 1 m^3 at 1 atm pressure, estimate the pressure required to reduce its volume by 5 percent.

P1.35 In Table A.4, most common gases (air, nitrogen, oxygen, hydrogen) have a specific heat ratio $k \approx 1.40$. Why do argon and helium have such high values? Why does NH_3 have such a low value? What is the lowest k for any gas that you know of?

P1.36 The isentropic bulk modulus B of a fluid is defined as the isentropic change in pressure per fractional change in density:

$$B = \rho\left(\frac{\partial p}{\partial \rho}\right)_s$$

What are the dimensions of B? Using theoretical $p(\rho)$ relations, estimate the bulk modulus of (*a*) N_2O, assumed to be an ideal gas, and (*b*) water, at 20°C and 1 atm.

P1.37 A near-ideal gas has a molecular weight of 44 and a specific heat $c_v = 610$ J/(kg · K). What are (*a*) its specific heat ratio, k, and (*b*) its speed of sound at 100°C?

P1.38 In Fig. 1.6, if the fluid is glycerin at 20°C and the width between plates is 6 mm, what shear stress (in Pa) is required to move the upper plate at 5.5 m/s? What is the Reynolds number if L is taken to be the distance between plates?

P1.39 Knowing μ for air at 20°C from Table 1.4, estimate its viscosity at 500°C by (*a*) the power law and (*b*) the Sutherland law. Also make an estimate from (*c*) Fig. 1.5. Compare with the accepted value of $\mu \approx 3.58$ E-5 kg/m · s.

***P1.40** For liquid viscosity as a function of temperature, a simplification of the log-quadratic law of Eq. (1.31) is *Andrade's equation* [11], $\mu \approx A \exp(B/T)$, where (A, B) are curve-fit constants and T is absolute temperature. Fit this relation to the data for water in Table A.1 and estimate the percent error of the approximation.

P1.41 Some experimental values of the viscosity of argon gas at 1 atm are as follows:

T, K	300	400	500	600	700	800
μ, kg/(m · s)	2.27 E-5	2.85 E-5	3.37 E-5	3.83 E-5	4.25 E-5	4.64 E-5

Fit these value to either (*a*) a power law or (*b*) the Sutherland law, Eq. (1.30).

P1.42 Experimental values for the viscosity of helium at 1 atm are as follows:

T, K	200	400	600	800	1000	1200
μ, kg/(m · s)	1.50 E-5	2.43 E-5	3.20 E-5	3.88 E-5	4.50 E-5	5.08 E-5

Fit these values to either (*a*) a power law or (*b*) the Sutherland law, Eq. (1.30).

***P1.43** Yaws et al. [34] suggest the following curve-fit formula for viscosity versus temperature of organic liquids:

$$\log_{10} \mu \approx A + \frac{B}{T} + CT + DT^2$$

with T in absolute units. (*a*) Can this formula be criticized on dimensional grounds? (*b*) Disregarding (*a*), indicate analytically how the curve-fit constants A, B, C, D could be found from N data points (μ_i, T_i) using the method of least squares. Do not actually carry out a calculation.

P1.44 The values for SAE 30 oil in Table 1.4 are strictly "representative," not exact, because lubricating oils vary considerably according to the type of crude oil from which they are refined. The Society of Automotive Engineers [26] allows certain kinematic viscosity *ranges* for all lubricating oils: for SAE 30, $9.3 < \nu < 12.5$ mm^2/s at 100°C. SAE 30 oil density can also vary ±2 percent from the tabulated value of 891 kg/m^3. Consider the following data for an acceptable grade of SAE 30 oil:

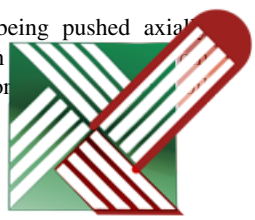
T, °C	0	20	40	60	80	100
μ, kg/(m · s)	2.00	0.40	0.11	0.042	0.017	0.0095

How does this oil compare with the plot in Appendix Fig. A.1? How well does the data fit Andrade's equation in Prob. 1.40?

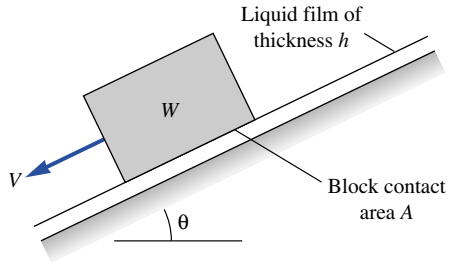
P1.45 A block of weight W slides down an inclined plane while lubricated by a thin film of oil, as in Fig. P1.45. The film contact area is A and its thickness is h. Assuming a linear velocity distribution in the film, derive an expression for the "terminal" (zero-acceleration) velocity V of the block.

P1.46 Find the terminal velocity of the block in Fig. P1.45 if the block mass is 6 kg, $A = 35$ cm^2, $\theta = 15°$, and the film is 1-mm-thick SAE 30 oil at 20°C.

P1.47 A shaft 6.00 cm in diameter is being pushed axial through a bearing sleeve 6.02 cm in long. The clearance, assumed unifor



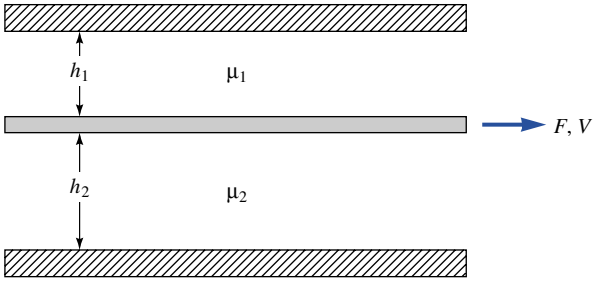
ketabline.com Ebook.ketabline.com



P1.45

whose properties are $\nu = 0.003$ m^2/s and SG = 0.88. Estimate the force required to pull the shaft at a steady velocity of 0.4 m/s.

P1.48 A thin plate is separated from two fixed plates by very viscous liquids μ_1 and μ_2, respectively, as in Fig. P1.48. The plate spacings h_1 and h_2 are unequal, as shown. The contact area is A between the center plate and each fluid. (*a*) Assuming a linear velocity distribution in each fluid, derive the force F required to pull the plate at velocity V. (*b*) Is there a necessary *relation* between the two viscosities, μ_1 and μ_2?



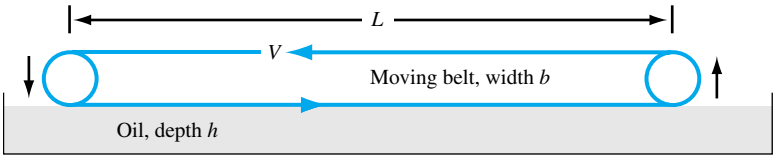
P1.48

P1.49 The shaft in Prob. 1.47 is now fixed axially and rotated inside the sleeve at 1500 r/min. Estimate (*a*) the torque (N · m) and (*b*) the power (kW) required to rotate the shaft.

P1.50 An amazing number of commercial and laboratory devices have been developed to measure the viscosity of fluids, as described in Ref. 27. The concentric rotating shaft of Prob. 1.49 is an example of a *rotational viscometer*. Let the inner and outer cylinders have radii r_i and r_o, respectively, with total sleeve length L. Let the rotational rate be Ω (rad/s) and the applied torque be M. Derive a theoretical relation for the viscosity of the clearance fluid, μ, in terms of these parameters.

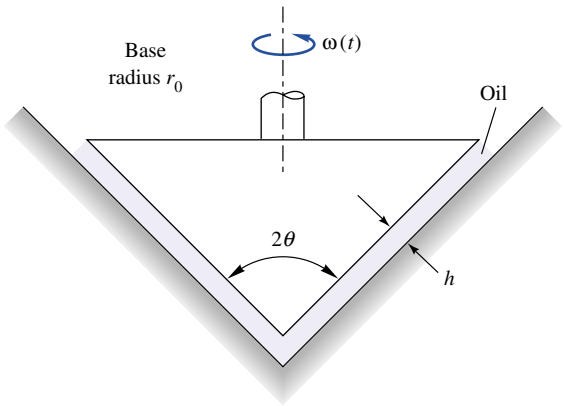
P1.51 Use the theory of Prob. 1.50 (or derive an ad hoc expression if you like) for a shaft 8 cm long, rotating at 1200 r/min, with $r_i = 2.00$ cm and $r_o = 2.05$ cm. If the measured torque is 0.293 N · m, what is the fluid viscosity? Suppose that the uncertainties of the experiment are as follows: L (±0.5 mm), M (±0.003 N · m), Ω (±1 percent), and r_i or r_o (±0.02 mm). What is the uncertainty in the measured viscosity?

P1.52 The belt in Fig. P1.52 moves at a steady velocity V and skims the top of a tank of oil of viscosity μ, as shown. Assuming a linear velocity profile in the oil, develop a simple formula for the required belt-drive power P as a function of (h, L, V, b, μ). What belt-drive power P, in watts, is required if the belt moves at 2.5 m/s over SAE 30W oil at 20°C, with $L = 2$ m, $b = 60$ cm, and $h = 3$ cm?



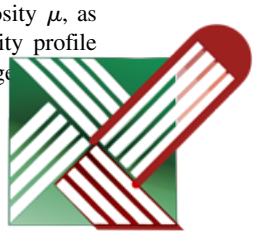
P1.52

***P1.53** A solid cone of angle 2θ, base r_0, and density ρ_c is rotating with initial angular velocity ω_0 inside a conical seat, as shown in Fig. P1.53. The clearance h is filled with oil of viscosity μ. Neglecting air drag, derive an analytical expression for the cone's angular velocity $\omega(t)$ if there is no applied torque.

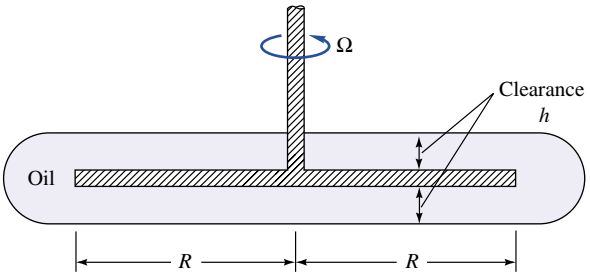


P1.53

***P1.54** A disk of radius R rotates at an angular velocity Ω inside a disk-shaped container filled with oil of viscosity μ, as shown in Fig. P1.54. Assuming a linear velocity profile and neglecting shear stress on the outer disk edge, derive a formula for the viscous torque on the disk.



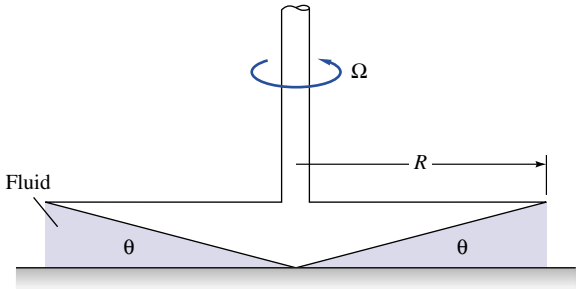
ketabline.com Ebook.ketabline.com



P1.54

***P1.55** The device in Fig. P1.54 is called a *rotating disk viscometer* [27]. Suppose that $R = 5$ cm and $h = 1$ mm. If the torque required to rotate the disk at 900 r/min is 0.537 N · m, what is the viscosity of the fluid? If the uncertainty in each parameter (M, R, h, Ω) is ±1 percent, what is the overall uncertainty in the viscosity?

***P1.56** The device in Fig. P1.56 is called a *cone-plate viscometer* [27]. The angle of the cone is very small, so that $\sin\theta \approx \theta$, and the gap is filled with the test liquid. The torque M to rotate the cone at a rate Ω is measured. Assuming a linear velocity profile in the fluid film, derive an expression for fluid viscosity μ as a function of (M, R, Ω, θ).



P1.56

***P1.57** For the cone-plate viscometer of Fig. P1.56, suppose that $R = 6$ cm and $\theta = 3°$. If the torque required to rotate the cone at 600 r/min is 0.157 N · m, what is the viscosity of the fluid? If the uncertainty in each parameter (M, R, Ω, θ) is ±1 percent, what is the overall uncertainty in the viscosity?

***P1.58** The laminar-pipe-flow example of Prob. 1.12 can be used to design a *capillary viscometer* [27]. If Q is the volume flow rate, L is the pipe length, and Δp is the pressure drop from entrance to exit, the theory of Chap. 6 yields a formula for viscosity:

$$\mu = \frac{\pi r_0^4 \Delta p}{8LQ}$$

Pipe end effects are neglected [27]. Suppose our capillary has $r_0 = 2$ mm and $L = 25$ cm. The following flow rate and pressure drop data are obtained for a certain fluid:

Q, m³/h	0.36	0.72	1.08	1.44	1.80
Δp, kPa	159	318	477	1274	1851

What is the viscosity of the fluid? *Note:* Only the first three points give the proper viscosity. What is peculiar about the last two points, which were measured accurately?

P1.59 A solid cylinder of diameter D, length L, and density ρ_s falls due to gravity inside a tube of diameter D_0. The clearance, $D_0 - D << D$, is filled with fluid of density ρ and viscosity μ. Neglect the air above and below the cylinder. Derive a formula for the terminal fall velocity of the cylinder. Apply your formula to the case of a steel cylinder, $D = 2$ cm, $D_0 = 2.04$ cm, L = 15 cm, with a film of SAE 30 oil at 20°C.

P1.60 For Prob. 1.52 suppose that $P = 0.1$ hp when $V = 6$ ft/s, $L = 4.5$ ft, $b = 22$ in, and $h = 7/8$ in. Estimate the viscosity of the oil, in kg/(m · s). If the uncertainty in each parameter (P, L, b, h, V) is ±1 percent, what is the overall uncertainty in the viscosity?

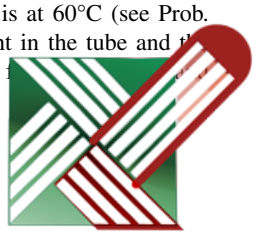
***P1.61** An air-hockey puck has a mass of 50 g and is 9 cm in diameter. When placed on the air table, a 20°C air film, of 0.12-mm thickness, forms under the puck. The puck is struck with an initial velocity of 10 m/s. Assuming a linear velocity distribution in the air film, how long will it take the puck to (*a*) slow down to 1 m/s and (*b*) stop completely? Also, (*c*) how far along this extremely long table will the puck have traveled for condition (*a*)?

P1.62 The hydrogen bubbles which produced the velocity profiles in Fig. 1.13 are quite small, $D \approx 0.01$ mm. If the hydrogen-water interface is comparable to air-water and the water temperature is 30°C estimate the excess pressure within the bubble.

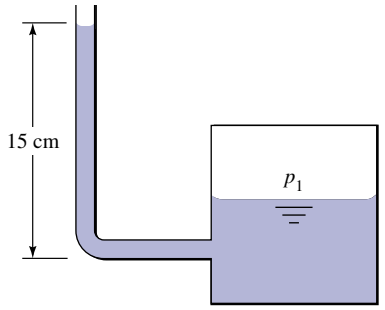
P1.63 Derive Eq. (1.37) by making a force balance on the fluid interface in Fig. 1.9*c*.

P1.64 At 60°C the surface tension of mercury and water is 0.47 and 0.0662 N/m, respectively. What capillary height changes will occur in these two fluids when they are in contact with air in a clean glass tube of diameter 0.4 mm?

P1.65 The system in Fig. P1.65 is used to calculate the pressure p_1 in the tank by measuring the 15-cm height of liquid in the 1-mm-diameter tube. The fluid is at 60°C (see Prob. 1.64). Calculate the true fluid height in the tube and the percent error due to capillarity if the fluid is (*a*) water or (*b*) mercury.



ketabline.com Ebook.ketabline.com

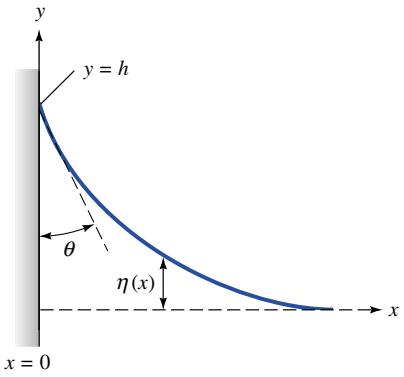


P1.65

P1.66 A thin wire ring, 3 cm in diameter, is lifted from a water surface at 20°C. Neglecting the wire weight, what is the force required to lift the ring? Is this a good way to measure surface tension? Should the wire be made of any particular material?

P1.67 Experiment with a capillary tube, perhaps borrowed from the chemistry department, to verify, in clean water, the rise due to surface tension predicted by Example 1.9. Add small amounts of liquid soap to the water, and report to the class whether detergents significantly lower the surface tension. What practical difficulties do detergents present?

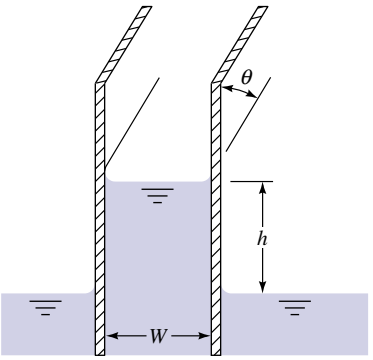
***P1.68** Make an analysis of the shape $\eta(x)$ of the water-air interface near a plane wall, as in Fig. P1.68, assuming that the slope is small, $R^{-1} \approx d^2\eta/dx^2$. Also assume that the pressure difference across the interface is balanced by the specific weight and the interface height, $\Delta p \approx \rho g \eta$. The boundary conditions are a wetting contact angle θ at $x = 0$ and a horizontal surface $\eta = 0$ as $x \to \infty$. What is the maximum height h at the wall?



P1.68

P1.69 A solid cylindrical needle of diameter d, length L, and density ρ_n may float in liquid of surface tension Y. Neglect buoyancy and assume a contact angle of 0°. Derive a formula for the maximum diameter d_{max} able to float in the liquid. Calculate d_{max} for a steel needle (SG = 7.84) in water at 20°C.

P1.70 Derive an expression for the capillary height change h for a fluid of surface tension Y and contact angle θ between two vertical parallel plates a distance W apart, as in Fig. P1.70. What will h be for water at 20°C if $W = 0.5$ mm?



P1.70

***P1.71** A soap bubble of diameter D_1 coalesces with another bubble of diameter D_2 to form a single bubble D_3 with the same amount of air. Assuming an isothermal process, derive an expression for finding D_3 as a function of D_1, D_2, p_{atm}, and Y.

P1.72 Early mountaineers boiled water to estimate their altitude. If they reach the top and find that water boils at 84°C, approximately how high is the mountain?

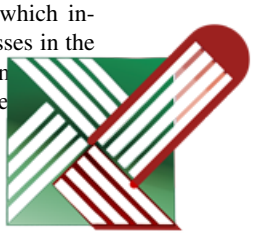
P1.73 A small submersible moves at velocity V, in fresh water at 20°C, at a 2-m depth, where ambient pressure is 131 kPa. Its critical cavitation number is known to be $C_a = 0.25$. At what velocity will cavitation bubbles begin to form on the body? Will the body cavitate if $V = 30$ m/s and the water is cold (5°C)?

P1.74 A propeller is tested in a water tunnel at 20°C as in Fig. 1.12*a*. The lowest pressure on the blade can be estimated by a form of Bernoulli's equation (Ex. 1.3):

$$p_{min} \approx p_0 - \tfrac{1}{2}\rho V^2$$

where $p_0 = 1.5$ atm and $V =$ tunnel velocity. If we run the tunnel at $V = 18$ m/s, can we be sure that there will be no cavitation? If not, can we change the water temperature and avoid cavitation?

P1.75 Oil, with a vapor pressure of 20 kPa, is delivered through a pipeline by equally spaced pumps, each of which increases the oil pressure by 1.3 MPa. Friction losses in the pipe are 150 Pa per meter of pipe. What is the m
possible pump spacing to avoid cavitation of the



ketabline.com Ebook.ketabline.com

P1.76 An airplane flies at 555 mi/h. At what altitude in the standard atmosphere will the airplane's Mach number be exactly 0.8?

***P1.77** The density of 20°C gasoline varies with pressure approximately as follows:

p, atm	1	500	1000	1500
ρ, lbm/ft^3	42.45	44.85	46.60	47.98

Use these data to estimate (*a*) the speed of sound (m/s) and (*b*) the bulk modulus (MPa) of gasoline at 1 atm.

P1.78 Sir Isaac Newton measured the speed of sound by timing the difference between seeing a cannon's puff of smoke and hearing its boom. If the cannon is on a mountain 5.2 mi away, estimate the air temperature in degrees Celsius if the time difference is (*a*) 24.2 s and (*b*) 25.1 s.

P1.79 Examine the photographs in Figs. 1.12*a*, 1.13, 5.2*a*, 7.14*a*, and 9.10*b* and classify them according to the boxes in Fig. 1.14.

***P1.80** A two-dimensional steady velocity field is given by $u = x^2 - y^2$, $v = -2xy$. Derive the streamline pattern and sketch a few streamlines in the upper half plane. *Hint:* The differential equation is exact.

P1.81 Repeat Ex. 1.10 by letting the velocity components increase linearly with time:

$$\mathbf{V} = Kxt\mathbf{i} - Kyt\mathbf{j} + 0\mathbf{k}$$

Find and sketch, for a few representative times, the instantaneous streamlines. How do they differ from the steady flow lines in Ex. 1.10?

P1.82 A velocity field is given by $u = V\cos\theta$, $v = V\sin\theta$, and $w = 0$, where V and θ are constants. Derive a formula for the streamlines of this flow.

***P1.83** A two-dimensional unsteady velocity field is given by $u = x(1 + 2t)$, $v = y$. Find the equation of the time-varying streamlines which all pass through the point (x_0, y_0) at some time t. Sketch a few of these.

***P1.84** Repeat Prob. 1.83 to find and sketch the equation of the *pathline* which passes through (x_0, y_0) at time $t = 0$.

P1.85 Do some reading and report to the class on the life and achievements, especially vis-à-vis fluid mechanics, of

(*a*) Evangelista Torricelli (1608–1647)
(*b*) Henri de Pitot (1695–1771)
(*c*) Antoine Chézy (1718–1798)
(*d*) Gotthilf Heinrich Ludwig Hagen (1797–1884)
(*e*) Julius Weisbach (1806–1871)
(*f*) George Gabriel Stokes (1819–1903)
(*g*) Moritz Weber (1871–1951)
(*h*) Theodor von Kármán (1881–1963)
(*i*) Paul Richard Heinrich Blasius (1883–1970)
(*j*) Ludwig Prandtl (1875–1953)
(*k*) Osborne Reynolds (1842–1912)
(*l*) John William Strutt, Lord Rayleigh (1842–1919)
(*m*) Daniel Bernoulli (1700–1782)
(*n*) Leonhard Euler (1707–1783)

Fundamentals of Engineering Exam Problems

FE1.1 The absolute viscosity μ of a fluid is primarily a function of
(*a*) Density, (*b*) Temperature, (*c*) Pressure, (*d*) Velocity, (*e*) Surface tension

FE1.2 If a uniform solid body weighs 50 N in air and 30 N in water, its specific gravity is
(*a*) 1.5, (*b*) 1.67, (*c*) 2.5, (*d*) 3.0, (*e*) 5.0

FE1.3 Helium has a molecular weight of 4.003. What is the weight of 2 m^3 of helium at 1 atm and 20°C?
(*a*) 3.3 N, (*b*) 6.5 N, (*c*) 11.8 N, (*d*) 23.5 N, (*e*) 94.2 N

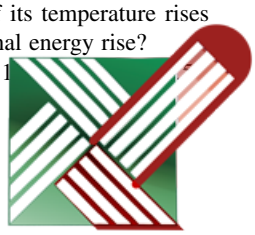
FE1.4 An oil has a kinematic viscosity of 1.25 E-4 m^2/s and a specific gravity of 0.80. What is its dynamic (absolute) viscosity in kg/(m · s)?
(*a*) 0.08, (*b*) 0.10, (*c*) 0.125, (*d*) 1.0, (*e*) 1.25

FE1.5 Consider a soap bubble of diameter 3 mm. If the surface tension coefficient is 0.072 N/m and external pressure is 0 Pa gage, what is the bubble's internal gage pressure?
(*a*) −24 Pa, (*b*) +48 Pa, (*c*) +96 Pa, (*d*) +192 Pa, (*e*) −192 Pa

FE1.6 The only possible dimensionless group which combines velocity V, body size L, fluid density ρ, and surface tension coefficient σ is
(*a*) $L\rho\sigma/V$, (*b*) $\rho VL^2/\sigma$, (*c*) $\rho\sigma V^2/L$, (*d*) $\sigma LV^2/\rho$, (*e*) $\rho LV^2/\sigma$

FE1.7 Two parallel plates, one moving at 4 m/s and the other fixed, are separated by a 5-mm-thick layer of oil of specific gravity 0.80 and kinematic viscosity 1.25 E-4 m^2/s. What is the average shear stress in the oil?
(*a*) 80 Pa, (*b*) 100 Pa, (*c*) 125 Pa, (*d*) 160 Pa, (*e*) 200 Pa

FE1.8 Carbon dioxide has a specific heat ratio of 1.30 and a gas constant of 189 J/(kg · °C). If its temperature rises from 20 to 45°C, what is its internal energy rise?
(*a*) 12.6 kJ/kg, (*b*) 15.8 kJ/kg, (*c*) 1[illegible] kJ/kg, (*e*) 25.1 kJ/kg



ketabline.com Ebook.ketabline.com

FE1.9 A certain water flow at 20°C has a critical cavitation number, where bubbles form, $Ca \approx 0.25$, where $Ca = 2(p_a - p_{vap})/\rho V^2$. If $p_a = 1$ atm and the vapor pressure is 0.34 pounds per square inch absolute (psia), for what water velocity will bubbles form?
(*a*) 12 mi/h, (*b*) 28 mi/h, (*c*) 36 mi/h, (*d*) 55 mi/h, (*e*) 63 mi/h

FE1.10 A steady incompressible flow, moving through a contraction section of length L, has a one-dimensional average velocity distribution given by $u \approx U_0(1 + 2x/L)$. What is its convective acceleration at the end of the contraction, $x = L$?
(*a*) U_0^2/L, (*b*) $2U_0^2/L$, (*c*) $3U_0^2/L$, (*d*) $4U_0^2/L$, (*e*) $6U_0^2/L$

Comprehensive Problems

C1.1 Sometimes equations can be developed and practical problems can be solved by knowing nothing more than the dimensions of the key parameters in the problem. For example, consider the heat loss through a window in a building. Window efficiency is rated in terms of "*R* value" which has units of $(ft^2 \cdot h \cdot °F)/Btu$. A certain manufacturer advertises a double-pane window with an *R* value of 2.5. The same company produces a triple-pane window with an *R* value of 3.4. In either case the window dimensions are 3 ft by 5 ft. On a given winter day, the temperature difference between the inside and outside of the building is 45°F.

(*a*) Develop an equation for the amount of heat lost in a given time period Δt, through a window of area A, with *R* value R, and temperature difference ΔT. How much heat (in Btu) is lost through the double-pane window in one 24-h period?

(*b*) How much heat (in Btu) is lost through the triple-pane window in one 24-h period?

(*c*) Suppose the building is heated with propane gas, which costs $1.25 per gallon. The propane burner is 80 percent efficient. Propane has approximately 90,000 Btu of available energy per gallon. In that same 24-h period, how much money would a homeowner save per window by installing triple-pane rather than double-pane windows?

(*d*) Finally, suppose the homeowner buys 20 such triple-pane windows for the house. A typical winter has the equivalent of about 120 heating days at a temperature difference of 45°F. Each triple-pane window costs $85 more than the double-pane window. Ignoring interest and inflation, how many years will it take the homeowner to make up the additional cost of the triple-pane windows from heating bill savings?

C1.2 When a person ice skates, the surface of the ice actually melts beneath the blades, so that he or she skates on a thin sheet of water between the blade and the ice.

(*a*) Find an expression for total friction force on the bottom of the blade as a function of skater velocity V, blade length L, water thickness (between the blade and the ice) h, water viscosity μ, and blade width W.

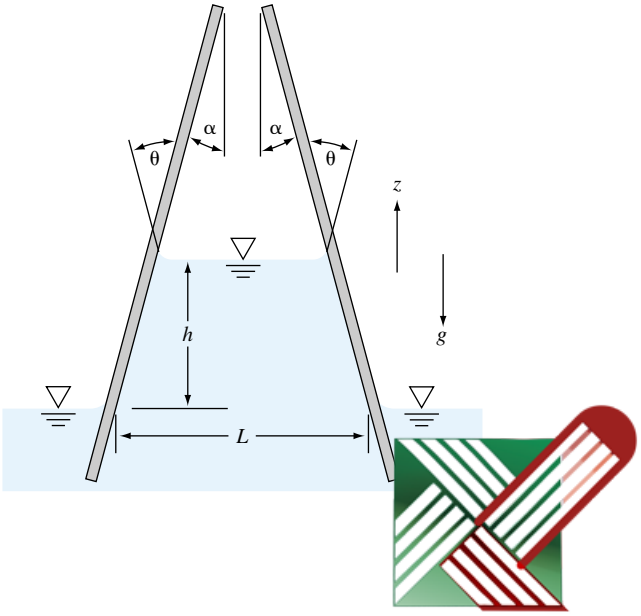
(*b*) Suppose an ice skater of total mass m is skating along at a constant speed of V_0 when she suddenly stands stiff with her skates pointed directly forward, allowing herself to coast to a stop. Neglecting friction due to air resistance, how far will she travel before she comes to a stop? (Remember, she is coasting on *two* skate blades.) Give your answer for the total distance traveled, x, as a function of V_0, m, L, h, μ, and W.

(*c*) Find x for the case where $V_0 = 4.0$ m/s, $m = 100$ kg, $L = 30$ cm, $W = 5.0$ mm, and $h = 0.10$ mm. Do you think our assumption of negligible air resistance is a good one?

C1.3 Two thin flat plates, tilted at an angle α, are placed in a tank of liquid of known surface tension Υ and contact angle θ, as shown in Fig. C1.3. At the free surface of the liquid in the tank, the two plates are a distance L apart and have width b into the page. The liquid rises a distance h between the plates, as shown.

(a) What is the total upward (z-directed) force, due to surface tension, acting on the liquid column between the plates?

(b) If the liquid density is ρ, find an expression for surface tension Υ in terms of the other variables.



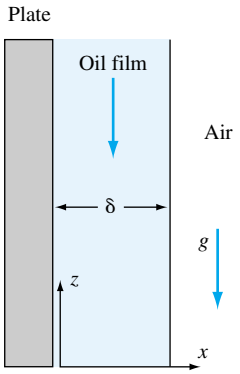
C1.3

ketabline.com Ebook.ketabline.com

C1.4 Oil of viscosity μ and density ρ drains steadily down the side of a tall, wide vertical plate, as shown in Fig. C1.4. In the region shown, *fully developed* conditions exist; that is, the velocity profile shape and the film thickness δ are independent of distance z along the plate. The vertical velocity w becomes a function only of x, and the shear resistance from the atmosphere is negligible.

(a) Sketch the approximate shape of the velocity profile $w(x)$, considering the boundary conditions at the wall and at the film surface.

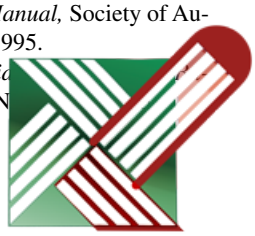
(b) Suppose film thickness δ, and the slope of the velocity profile at the wall, $(dw/dx)_{wall}$, are measured by a laser Doppler anemometer (to be discussed in Chap. 6). Find an expression for the viscosity of the oil as a function of ρ, δ, $(dw/dx)_{wall}$, and the gravitational accleration g. Note that, for the coordinate system given, both w and $(dw/dx)_{wall}$ are negative.



C1.4

References

1. J. C. Tannehill, D. A. Anderson, and R. H. Pletcher, *Computational Fluid Mechanics and Heat Transfer,* 2d ed., Taylor and Francis, Bristol, PA, 1997.
2. S. V. Patankar, *Numerical Heat Transfer and Fluid Flow,* McGraw-Hill, New York, 1980.
3. F. M. White, *Viscous Fluid Flow,* 2d ed., McGraw-Hill, New York, 1991.
4. R. J. Goldstein (ed.), *Fluid Mechanics Measurements,* 2d ed., Taylor and Francis, Bristol, PA, 1997.
5. R. A. Granger, *Experiments in Fluid Mechanics,* Oxford University Press, 1995.
6. H. A. Barnes, J. F. Hutton, and K. Walters, *An Introduction to Rheology,* Elsevier, New York, 1989.
7. A. E. Bergeles and S. Ishigai, *Two-Phase Flow Dynamics and Reactor Safety,* McGraw-Hill, New York, 1981.
8. G. N. Patterson, *Introduction to the Kinetic Theory of Gas Flows,* University of Toronto Press, Toronto, 1971.
9. *ASME Orientation and Guide for Use of Metric Units,* 9th ed., American Society of Mechanical Engineers, New York, 1982.
10. J. P. Holman, *Heat Transfer,* 8th ed., McGraw-Hill, New York, 1997.
11. R. C. Reid, J. M. Prausnitz, and T. K. Sherwood, *The Properties of Gases and Liquids,* 4th ed., McGraw-Hill, New York, 1987.
12. J. Hilsenrath et al., "Tables of Thermodynamic and Transport Properties," *U. S. Nat. Bur. Stand. Circ. 564,* 1955; reprinted by Pergamon, New York, 1960.
13. R. A. Spencer et al., *ASME Steam Tables with Mollier Chart,* 6th ed., American Society of Mechanical Engineers, New York, 1993.
14. O. A. Hougen and K. M. Watson, *Chemical Process Principles Charts,* Wiley, New York, 1960.
15. A. W. Adamson, *Physical Chemistry of Surfaces,* 5th ed., Interscience, New York, 1990.
16. J. A. Knauss, *Introduction to Physical Oceanography,* Prentice-Hall, Englewood Cliffs, NJ, 1978.
17. National Committee for Fluid Mechanics Films, *Illustrated Experiments in Fluid Mechanics,* M.I.T. Press, Cambridge, MA, 1972.
18. I. G. Currie, *Fundamental Mechanics of Fluids,* 2d ed., McGraw-Hill, New York, 1993.
19. M. van Dyke, *An Album of Fluid Motion,* Parabolic Press, Stanford, CA, 1982.
20. Y. Nakayama (ed.), *Visualized Flow,* Pergamon Press, Oxford, 1988.
21. W. J. Yang (ed.), *Handbook of Flow Visualization,* Hemisphere, New York, 1989.
22. W. Merzkirch, *Flow Visualization,* 2d ed., Academic, New York, 1987.
23. H. Rouse and S. Ince, *History of Hydraulics,* Iowa Institute of Hydraulic Research, Univ. of Iowa, Iowa City, 1957; reprinted by Dover, New York, 1963.
24. H. Rouse, *Hydraulics in the United States 1776–1976,* Iowa Institute of Hydraulic Research, Univ. of Iowa, Iowa City, 1976.
25. G. Garbrecht, *Hydraulics and Hydraulic Research: An Historical Review,* Gower Pub., Aldershot, UK, 1987.
26. *1986 SAE Handbook,* 4 vols., Society of Automotive Engineers, Warrendale, PA.
27. J. R. van Wazer, *Viscosity and Flow Measurement,* Interscience, New York, 1963.
28. *SAE Fuels and Lubricants Standards Manual,* Society of Automotive Engineers, Warrendale, PA, 1995.
29. John D. Anderson, *Computational Fluid*
sics with Applications, McGraw-Hill, N

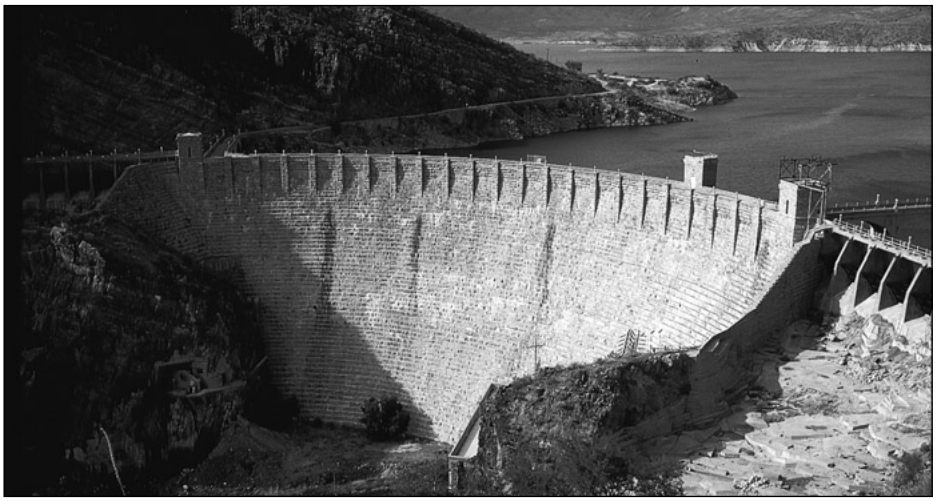


ketabline.com Ebook.ketabline.com

30. H. W. Coleman and W. G. Steele, *Experimentation and Uncertainty Analysis for Engineers,* John Wiley, New York, 1989.
31. R. J. Moffatt, "Describing the Uncertainties in Experimental Results," *Experimental Thermal and Fluid Science,* vol., 1, 1988, pp. 3–17.
32. Paul A. Libby, *An Introduction to Turbulence,* Taylor and Francis, Bristol, PA, 1996.
33. Sanford Klein and William Beckman, *Engineering Equation Solver (EES),* F-Chart Software, Middleton, WI, 1997.
34. C. L. Yaws, X. Lin, and L. Bu, "Calculate Viscosities for 355 Compounds. An Equation Can Be Used to Calculate Liquid Viscosity as a Function of Temperature," *Chemical Engineering,* vol. 101, no. 4, April 1994, pp. 119–128.
35. Frank E. Jones, *Techniques and Topics in Flow Measurement,* CRC Press, Boca Raton, FL, 1995.
36. Carl L. Yaws, *Handbook of Viscosity,* 3 vols., Gulf Publishing, Houston, TX, 1994.



ketabline.com Ebook.ketabline.com



Roosevelt Dam in Arizona. Hydrostatic pressure, due to the weight of a standing fluid, can cause enormous forces and moments on large-scale structures such as a dam. Hydrostatic fluid analysis is the subject of the present chapter. *(Courtesy of Dr. E.R. Degginger/Color-Pic Inc.)*



ketabline.com Ebook.ketabline.com

Chapter 2
Pressure Distribution in a Fluid

Motivation. Many fluid problems do not involve motion. They concern the pressure distribution in a static fluid and its effect on solid surfaces and on floating and submerged bodies.

When the fluid velocity is zero, denoted as the *hydrostatic condition*, the pressure variation is due only to the weight of the fluid. Assuming a known fluid in a given gravity field, the pressure may easily be calculated by integration. Important applications in this chapter are (1) pressure distribution in the atmosphere and the oceans, (2) the design of manometer pressure instruments, (3) forces on submerged flat and curved surfaces, (4) buoyancy on a submerged body, and (5) the behavior of floating bodies. The last two result in Archimedes' principles.

If the fluid is moving in *rigid-body motion*, such as a tank of liquid which has been spinning for a long time, the pressure also can be easily calculated, because the fluid is free of shear stress. We apply this idea here to simple rigid-body accelerations in Sec. 2.9. Pressure measurement instruments are discussed in Sec. 2.10. As a matter of fact, pressure also can be easily analyzed in arbitrary (nonrigid-body) motions $\mathbf{V}(x, y, z, t)$, but we defer that subject to Chap. 4.

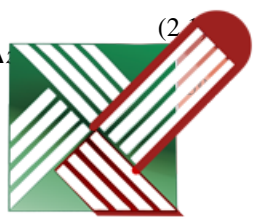
2.1 Pressure and Pressure Gradient

In Fig. 1.1 we saw that a fluid at rest cannot support shear stress and thus Mohr's circle reduces to a point. In other words, the normal stress on any plane through a fluid element at rest is equal to a unique value called the *fluid pressure* p, taken positive for compression by common convention. This is such an important concept that we shall review it with another approach.

Figure 2.1 shows a small wedge of fluid at rest of size Δx by Δz by Δs and depth b into the paper. There is no shear by definition, but we postulate that the pressures p_x, p_z, and p_n may be different on each face. The weight of the element also may be important. Summation of forces must equal zero (no acceleration) in both the x and z directions.

$$\Sigma F_x = 0 = p_x b\,\Delta z - p_n b\,\Delta s \sin\theta$$

$$\Sigma F_z = 0 = p_z b\,\Delta x - p_n b\,\Delta s \cos\theta - \tfrac{1}{2}\gamma b\,\Delta x\,\Delta z \qquad (2.$$



ketabline.com Ebook.ketabline.com

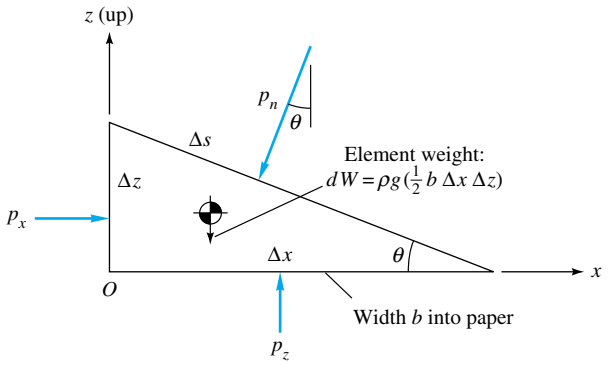


Fig. 2.1 Equilibrium of a small wedge of fluid at rest.

but the geometry of the wedge is such that

$$\Delta s \sin \theta = \Delta z \qquad \Delta s \cos \theta = \Delta x \tag{2.2}$$

Substitution into Eq. (2.1) and rearrangement give

$$p_x = p_n \qquad p_z = p_n + \tfrac{1}{2}\gamma\, \Delta z \tag{2.3}$$

These relations illustrate two important principles of the hydrostatic, or shear-free, condition: (1) There is no pressure change in the horizontal direction, and (2) there is a vertical change in pressure proportional to the density, gravity, and depth change. We shall exploit these results to the fullest, starting in Sec. 2.3.

In the limit as the fluid wedge shrinks to a "point," $\Delta z \to 0$ and Eqs. (2.3) become

$$p_x = p_z = p_n = p \tag{2.4}$$

Since θ is arbitrary, we conclude that the pressure p at a point in a static fluid is independent of orientation.

What about the pressure at a point in a moving fluid? If there are strain rates in a moving fluid, there will be viscous stresses, both shear and normal in general (Sec. 4.3). In that case (Chap. 4) the pressure is defined as the average of the three normal stresses σ_{ii} on the element

$$p = -\tfrac{1}{3}(\sigma_{xx} + \sigma_{yy} + \sigma_{zz}) \tag{2.5}$$

The minus sign occurs because a compression stress is considered to be negative whereas p is positive. Equation (2.5) is subtle and rarely needed since the great majority of viscous flows have negligible viscous normal stresses (Chap. 4).

Pressure Force on a Fluid Element

Pressure (or any other stress, for that matter) causes no net force on a fluid element unless it varies *spatially*.[1] To see this, consider the pressure acting on the two x faces in Fig. 2.2. Let the pressure vary arbitrarily

$$p = p(x, y, z, t) \tag{2.6}$$

[1] An interesting application for a large element is in Fig. 3.7.



ketabline.com Ebook.ketabline.com

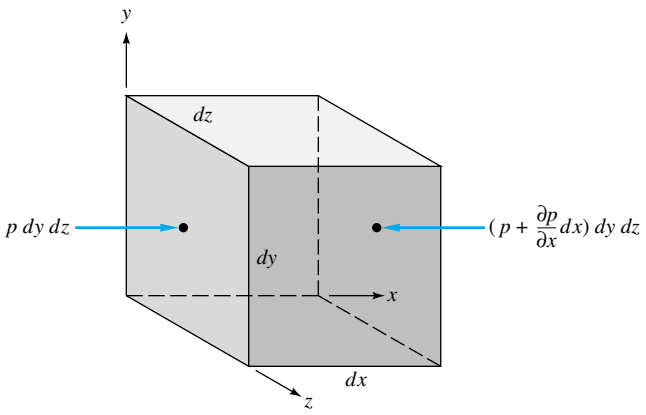


Fig. 2.2 Net x force on an element due to pressure variation.

The net force in the x direction on the element in Fig. 2.2 is given by

$$dF_x = p\ dy\ dz - \left(p + \frac{\partial p}{\partial x}\ dx\right) dy\ dz = -\frac{\partial p}{\partial x}\ dx\ dy\ dz \tag{2.7}$$

In like manner the net force dF_y involves $-\partial p/\partial y$, and the net force dF_z concerns $-\partial p/\partial z$. The total net-force vector on the element due to pressure is

$$d\mathbf{F}_{\text{press}} = \left(-\mathbf{i}\frac{\partial p}{\partial x} - \mathbf{j}\frac{\partial p}{\partial y} - \mathbf{k}\frac{\partial p}{\partial z}\right) dx\ dy\ dz \tag{2.8}$$

We recognize the term in parentheses as the negative vector gradient of p. Denoting $\mathbf{f}$ as the net force per unit element volume, we rewrite Eq. (2.8) as

$$\mathbf{f}_{\text{press}} = -\nabla p \tag{2.9}$$

Thus it is not the pressure but the pressure *gradient* causing a net force which must be balanced by gravity or acceleration or some other effect in the fluid.

2.2 Equilibrium of a Fluid Element

The pressure gradient is a *surface* force which acts on the sides of the element. There may also be a *body* force, due to electromagnetic or gravitational potentials, acting on the entire mass of the element. Here we consider only the gravity force, or weight of the element

$$d\mathbf{F}_{\text{grav}} = \rho\mathbf{g}\ dx\ dy\ dz$$
$$\text{or} \qquad \mathbf{f}_{\text{grav}} = \rho\mathbf{g} \tag{2.10}$$

In general, there may also be a surface force due to the gradient, if any, of the viscous stresses. For completeness, we write this term here without derivation and consider it more thoroughly in Chap. 4. For an incompressible fluid with constant viscosity, the net viscous force is

$$\mathbf{f}_{\text{VS}} = \mu\left(\frac{\partial^2 \mathbf{V}}{\partial x^2} + \frac{\partial^2 \mathbf{V}}{\partial y^2} + \frac{\partial^2 \mathbf{V}}{\partial z^2}\right) = \mu\nabla^2\mathbf{V} \tag{2.11}$$

where VS stands for viscous stresses and μ is the coefficient of vis
1. Note that the term $\mathbf{g}$ in Eq. (2.10) denotes the acceleration of gr



ketabline.com Ebook.ketabline.com

ing toward the center of the earth. On earth the average magnitude of **g** is 32.174 ft/s^2 = 9.807 m/s^2.

The total vector resultant of these three forces—pressure, gravity, and viscous stress—must either keep the element in equilibrium or cause it to move with acceleration **a**. From Newton's law, Eq. (1.2), we have

$$\rho\mathbf{a} = \Sigma\,\mathbf{f} = \mathbf{f}_{\text{press}} + \mathbf{f}_{\text{grav}} + \mathbf{f}_{\text{visc}} = -\nabla p + \rho\mathbf{g} + \mu\nabla^2\mathbf{V} \tag{2.12}$$

This is one form of the differential momentum equation for a fluid element, and it is studied further in Chap. 4. Vector addition is implied by Eq. (2.12): The acceleration reflects the local balance of forces and is not necessarily parallel to the local-velocity vector, which reflects the direction of motion at that instant.

This chapter is concerned with cases where the velocity and acceleration are known, leaving one to solve for the pressure variation in the fluid. Later chapters will take up the more general problem where pressure, velocity, and acceleration are all unknown. Rewrite Eq. (2.12) as

$$\nabla p = \rho(\mathbf{g} - \mathbf{a}) + \mu\nabla^2\mathbf{V} = \mathbf{B}(x, y, z, t) \tag{2.13}$$

where **B** is a short notation for the vector sum on the right-hand side. If **V** and $\mathbf{a} = d\mathbf{V}/dt$ are known functions of space and time and the density and viscosity are known, we can solve Eq. (2.13) for $p(x, y, z, t)$ by direct integration. By components, Eq. (2.13) is equivalent to three simultaneous first-order differential equations

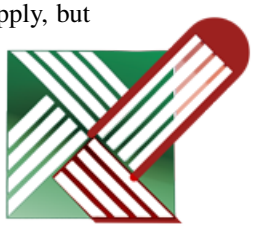
$$\frac{\partial p}{\partial x} = B_x(x, y, z, t) \qquad \frac{\partial p}{\partial y} = B_y(x, y, z, t) \qquad \frac{\partial p}{\partial z} = B_z(x, y, z, t) \tag{2.14}$$

Since the right-hand sides are known functions, they can be integrated systematically to obtain the distribution $p(x, y, z, t)$ except for an unknown function of time, which remains because we have no relation for $\partial p/\partial t$. This extra function is found from a condition of known time variation $p_0(t)$ at some point (x_0, y_0, z_0). If the flow is steady (independent of time), the unknown function is a constant and is found from knowledge of a single known pressure p_0 at a point (x_0, y_0, z_0). If this sounds complicated, it is not; we shall illustrate with many examples. Finding the pressure distribution from a known velocity distribution is one of the easiest problems in fluid mechanics, which is why we put it in Chap. 2.

Examining Eq. (2.13), we can single out at least four special cases:

1. **Flow at rest or at constant velocity:** The acceleration and viscous terms vanish identically, and p depends only upon gravity and density. This is the *hydrostatic* condition. See Sec. 2.3.
2. **Rigid-body translation and rotation:** The viscous term vanishes identically, and p depends only upon the term $\rho(\mathbf{g} - \mathbf{a})$. See Sec. 2.9.
3. **Irrotational motion ($\nabla \times \mathbf{V} \equiv \mathbf{0}$):** The viscous term vanishes identically, and an exact integral called *Bernoulli's equation* can be found for the pressure distribution. See Sec. 4.9.
4. **Arbitrary viscous motion:** Nothing helpful happens, no general rules apply, but still the integration is quite straightforward. See Sec. 6.4.

Let us consider cases 1 and 2 here.



ketabline.com Ebook.ketabline.com

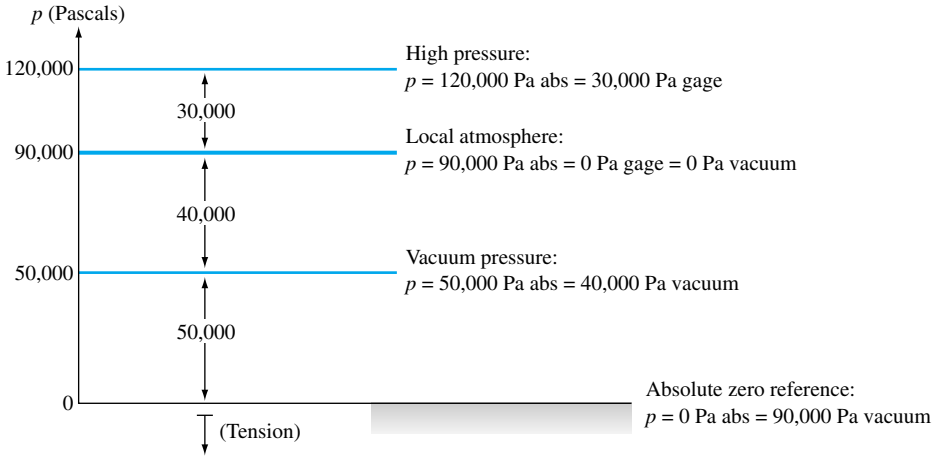


Fig. 2.3 Illustration of absolute, gage, and vacuum pressure readings.

Gage Pressure and Vacuum Pressure: Relative Terms

Before embarking on examples, we should note that engineers are apt to specify pressures as (1) the *absolute* or total magnitude or (2) the value *relative* to the local ambient atmosphere. The second case occurs because many pressure instruments are of *differential* type and record, not an absolute magnitude, but the difference between the fluid pressure and the atmosphere. The measured pressure may be either higher or lower than the local atmosphere, and each case is given a name:

1. $p > p_a$ *Gage* pressure: $p(\text{gage}) = p - p_a$
2. $p < p_a$ *Vacuum* pressure: $p(\text{vacuum}) = p_a - p$

This is a convenient shorthand, and one later adds (or subtracts) atmospheric pressure to determine the absolute fluid pressure.

A typical situation is shown in Fig. 2.3. The local atmosphere is at, say, 90,000 Pa, which might reflect a storm condition in a sea-level location or normal conditions at an altitude of 1000 m. Thus, on this day, p_a = 90,000 Pa absolute = 0 Pa gage = 0 Pa vacuum. Suppose gage 1 in a laboratory reads p_1 = 120,000 Pa absolute. This value may be reported as a *gage* pressure, p_1 = 120,000 − 90,000 = 30,000 Pa *gage*. (One must also record the atmospheric pressure in the laboratory, since p_a changes gradually.) Suppose gage 2 reads p_2 = 50,000 Pa absolute. Locally, this is a *vacuum* pressure and might be reported as p_2 = 90,000 − 50,000 = 40,000 Pa *vacuum*. Occasionally, in the Problems section, we will specify gage or vacuum pressure to keep you alert to this common engineering practice.

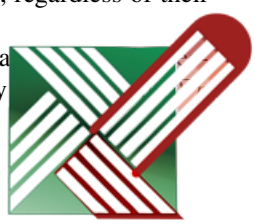
2.3 Hydrostatic Pressure Distributions

If the fluid is at rest or at constant velocity, $\mathbf{a} = 0$ and $\nabla^2\mathbf{V} = 0$. Equation (2.13) for the pressure distribution reduces to

$$\nabla p = \rho\mathbf{g} \tag{2.15}$$

This is a *hydrostatic* distribution and is correct for all fluids at rest, regardless of their viscosity, because the viscous term vanishes identically.

Recall from vector analysis that the vector ∇p expresses the ma
tion of the maximum spatial rate of increase of the scalar property



ketabline.com Ebook.ketabline.com

is perpendicular everywhere to surfaces of constant p. Thus Eq. (2.15) states that a fluid in hydrostatic equilibrium will align its constant-pressure surfaces everywhere normal to the local-gravity vector. The maximum pressure increase will be in the direction of gravity, i.e., "down." If the fluid is a liquid, its free surface, being at atmospheric pressure, will be normal to local gravity, or "horizontal." You probably knew all this before, but Eq. (2.15) is the proof of it.

In our customary coordinate system z is "up." Thus the local-gravity vector for small-scale problems is

$$\mathbf{g} = -g\mathbf{k} \tag{2.16}$$

where g is the magnitude of local gravity, for example, 9.807 m/s^2. For these coordinates Eq. (2.15) has the components

$$\frac{\partial p}{\partial x} = 0 \qquad \frac{\partial p}{\partial y} = 0 \qquad \frac{\partial p}{\partial z} = -\rho g = -\gamma \tag{2.17}$$

the first two of which tell us that p is independent of x and y. Hence $\partial p/\partial z$ can be replaced by the total derivative dp/dz, and the hydrostatic condition reduces to

$$\frac{dp}{dz} = -\gamma$$

or

$$p_2 - p_1 = -\int_1^2 \gamma \, dz \tag{2.18}$$

Equation (2.18) is the solution to the hydrostatic problem. The integration requires an assumption about the density and gravity distribution. Gases and liquids are usually treated differently.

We state the following conclusions about a hydrostatic condition:

> Pressure in a continuously distributed uniform static fluid varies only with vertical distance and is independent of the shape of the container. The pressure is the same at all points on a given horizontal plane in the fluid. The pressure increases with depth in the fluid.

An illustration of this is shown in Fig. 2.4. The free surface of the container is atmospheric and forms a horizontal plane. Points a, b, c, and d are at equal depth in a horizon-

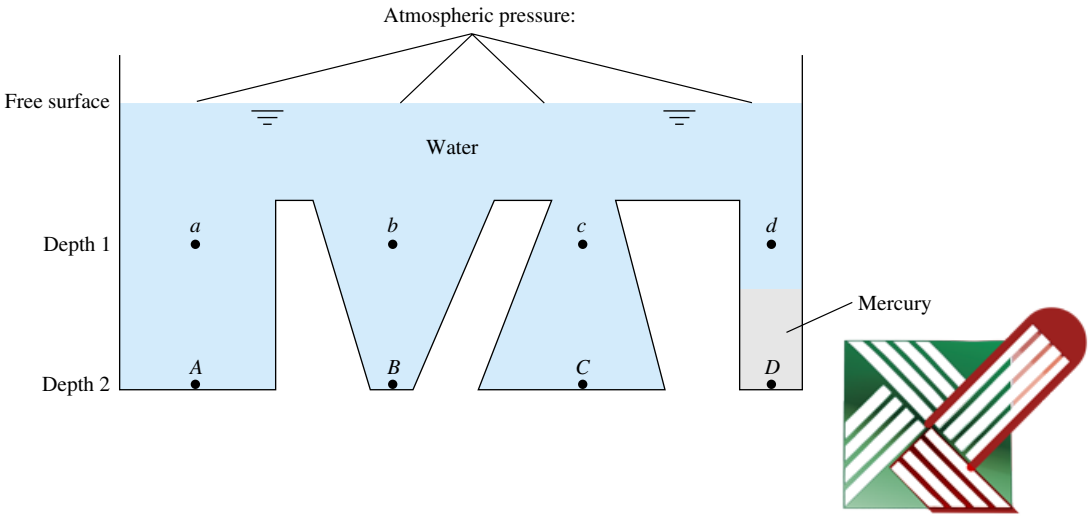


Fig. 2.4 Hydrostatic-pressure distribution. Points a, b, c, and d are at equal depths in water and therefore have identical pressures. Points A, B, and C are also at equal depths in water and have identical pressures higher than a, b, c, and d. Point D has a different pressure from A, B, and C because it is not connected to them by a water path.

ketabline.com Ebook.ketabline.com

tal plane and are interconnected by the same fluid, water; therefore all points have the same pressure. The same is true of points A, B, and C on the bottom, which all have the same higher pressure than at a, b, c, and d. However, point D, although at the same depth as A, B, and C, has a different pressure because it lies beneath a different fluid, mercury.

Effect of Variable Gravity

For a spherical planet of uniform density, the acceleration of gravity varies inversely as the square of the radius from its center

$$g = g_0\left(\frac{r_0}{r}\right)^2 \tag{2.19}$$

where r_0 is the planet radius and g_0 is the surface value of g. For earth, $r_0 \approx 3960$ statute mi ≈ 6400 km. In typical engineering problems the deviation from r_0 extends from the deepest ocean, about 11 km, to the atmospheric height of supersonic transport operation, about 20 km. This gives a maximum variation in g of $(6400/6420)^2$, or 0.6 percent. We therefore neglect the variation of g in most problems.

Hydrostatic Pressure in Liquids

Liquids are so nearly incompressible that we can neglect their density variation in hydrostatics. In Example 1.7 we saw that water density increases only 4.6 percent at the deepest part of the ocean. Its effect on hydrostatics would be about half of this, or 2.3 percent. Thus we assume constant density in liquid hydrostatic calculations, for which Eq. (2.18) integrates to

Liquids:
$$p_2 - p_1 = -\gamma(z_2 - z_1) \tag{2.20}$$

or
$$z_1 - z_2 = \frac{p_2}{\gamma} - \frac{p_1}{\gamma}$$

We use the first form in most problems. The quantity γ is called the *specific weight* of the fluid, with dimensions of weight per unit volume; some values are tabulated in Table 2.1. The quantity p/γ is a length called the *pressure head* of the fluid.

For lakes and oceans, the coordinate system is usually chosen as in Fig. 2.5, with $z = 0$ at the free surface, where p equals the surface atmospheric pressure p_a. When

Table 2.1 Specific Weight of Some Common Fluids

Fluid	Specific weight γ at 68°F = 20°C, lbf/ft^3	Specific weight γ at 68°F = 20°C, N/m^3
Air (at 1 atm)	0.0752	11.8
Ethyl alcohol	49.2	7,733
SAE 30 oil	55.5	8,720
Water	62.4	9,790
Seawater	64.0	10,050
Glycerin	78.7	12,360
Carbon tetrachloride	99.1	15,570
Mercury	846	133,100



ketabline.com Ebook.ketabline.com

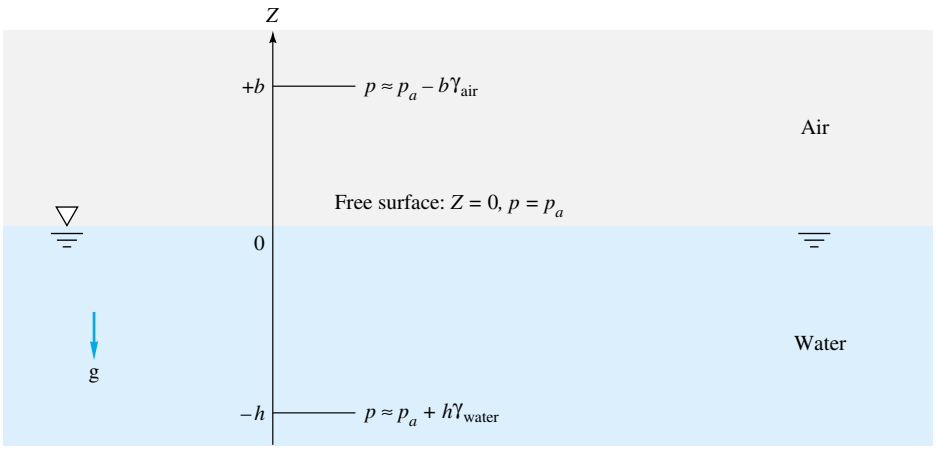


Fig. 2.5 Hydrostatic-pressure distribution in oceans and atmospheres.

we introduce the reference value $(p_1, z_1) = (p_a, 0)$, Eq. (2.20) becomes, for p at any (negative) depth z,

Lakes and oceans: $$p = p_a - \gamma z \tag{2.21}$$

where γ is the average specific weight of the lake or ocean. As we shall see, Eq. (2.21) holds in the atmosphere also with an accuracy of 2 percent for heights z up to 1000 m.

EXAMPLE 2.1

Newfound Lake, a freshwater lake near Bristol, New Hampshire, has a maximum depth of 60 m, and the mean atmospheric pressure is 91 kPa. Estimate the absolute pressure in kPa at this maximum depth.

Solution

From Table 2.1, take $\gamma \approx 9790$ N/m^3. With $p_a = 91$ kPa and $z = -60$ m, Eq. (2.21) predicts that the pressure at this depth will be

$$p = 91 \text{ kN/m}^2 - (9790 \text{ N/m}^3)(-60 \text{ m}) \frac{1 \text{ kN}}{1000 \text{ N}}$$

$$= 91 \text{ kPa} + 587 \text{ kN/m}^2 = 678 \text{ kPa} \qquad \textit{Ans.}$$

By omitting p_a we could state the result as $p = 587$ kPa (gage).

The Mercury Barometer

The simplest practical application of the hydrostatic formula (2.20) is the barometer (Fig. 2.6), which measures atmospheric pressure. A tube is filled with mercury and inverted while submerged in a reservoir. This causes a near vacuum in the closed upper end because mercury has an extremely small vapor pressure at room temperatures (0.16 Pa at 20°C). Since atmospheric pressure forces a mercury column to rise a di into the tube, the upper mercury surface is at zero pressure.



ketabline.com Ebook.ketabline.com

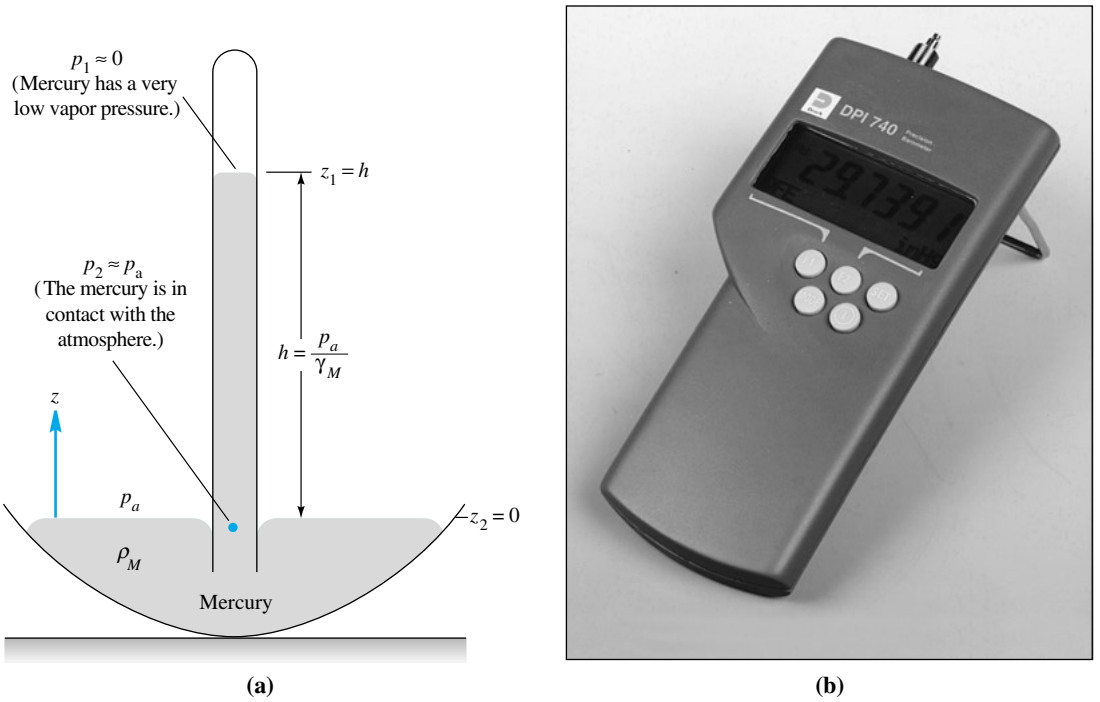


Fig. 2.6 A barometer measures local absolute atmospheric pressure: (*a*) the height of a mercury column is proportional to p_{atm}; (*b*) a modern portable barometer, with digital readout, uses the resonating silicon element of Fig. 2.28*c*. *(Courtesy of Paul Lupke, Druck Inc.)*

From Fig. 2.6, Eq. (2.20) applies with $p_1 = 0$ at $z_1 = h$ and $p_2 = p_a$ at $z_2 = 0$:

$$p_a - 0 = -\gamma_M(0 - h)$$

or

$$h = \frac{p_a}{\gamma_M} \tag{2.22}$$

At sea-level standard, with $p_a = 101{,}350$ Pa and $\gamma_M = 133{,}100$ N/m^3 from Table 2.1, the barometric height is $h = 101{,}350/133{,}100 = 0.761$ m or 761 mm. In the United States the weather service reports this as an atmospheric "pressure" of 29.96 inHg (inches of mercury). Mercury is used because it is the heaviest common liquid. A water barometer would be 34 ft high.

Hydrostatic Pressure in Gases

Gases are compressible, with density nearly proportional to pressure. Thus density must be considered as a variable in Eq. (2.18) if the integration carries over large pressure changes. It is sufficiently accurate to introduce the perfect-gas law $p = \rho RT$ in Eq. (2.18)

$$\frac{dp}{dz} = -\rho g = -\frac{p}{RT}\, g$$



ketabline.com Ebook.ketabline.com

Separate the variables and integrate between points 1 and 2:

$$\int_1^2 \frac{dp}{p} = \ln\frac{p_2}{p_1} = -\frac{g}{R}\int_1^2 \frac{dz}{T} \tag{2.23}$$

The integral over z requires an assumption about the temperature variation $T(z)$. One common approximation is the *isothermal atmosphere*, where $T = T_0$:

$$p_2 = p_1 \exp\left[-\frac{g(z_2 - z_1)}{RT_0}\right] \tag{2.24}$$

The quantity in brackets is dimensionless. (Think that over; it must be dimensionless, right?) Equation (2.24) is a fair approximation for earth, but actually the earth's mean atmospheric temperature drops off nearly linearly with z up to an altitude of about 36,000 ft (11,000 m):

$$T \approx T_0 - Bz \tag{2.25}$$

Here T_0 is sea-level temperature (absolute) and B is the *lapse rate*, both of which vary somewhat from day to day. By international agreement [1] the following standard values are assumed to apply from 0 to 36,000 ft:

$$T_0 = 518.69°\text{R} = 288.16\ \text{K} = 15°\text{C}$$

$$B = 0.003566°\text{R/ft} = 0.00650\ \text{K/m} \tag{2.26}$$

This lower portion of the atmosphere is called the *troposphere.* Introducing Eq. (2.25) into (2.23) and integrating, we obtain the more accurate relation

$$p = p_a\left(1 - \frac{Bz}{T_0}\right)^{g/(RB)} \qquad \text{where } \frac{g}{RB} = 5.26\ \text{(air)} \tag{2.27}$$

in the troposphere, with $z = 0$ at sea level. The exponent $g/(RB)$ is dimensionless (again it must be) and has the standard value of 5.26 for air, with $R = 287\ \text{m}^2/(\text{s}^2 \cdot \text{K})$.

The U.S. standard atmosphere [1] is sketched in Fig. 2.7. The pressure is seen to be nearly zero at $z = 30$ km. For tabulated properties see Table A.6.

EXAMPLE 2.2

If sea-level pressure is 101,350 Pa, compute the standard pressure at an altitude of 5000 m, using (*a*) the exact formula and (*b*) an isothermal assumption at a standard sea-level temperature of 15°C. Is the isothermal approximation adequate?

Solution

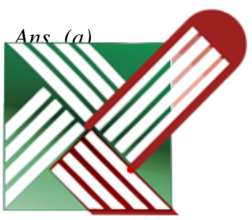
Part (a) Use absolute temperature in the exact formula, Eq. (2.27):

$$p = p_a\left[1 - \frac{(0.00650\ \text{K/m})(5000\ \text{m})}{288.16\ \text{K}}\right]^{5.26} = (101{,}350\ \text{Pa})(0.8872)^{5.26}$$

$$= 101{,}350(0.52388) = 54{,}000\ \text{Pa}$$

Ans. (a)

This is the standard-pressure result given at $z = 5000$ m in Table A.6.



ketabline.com Ebook.ketabline.com

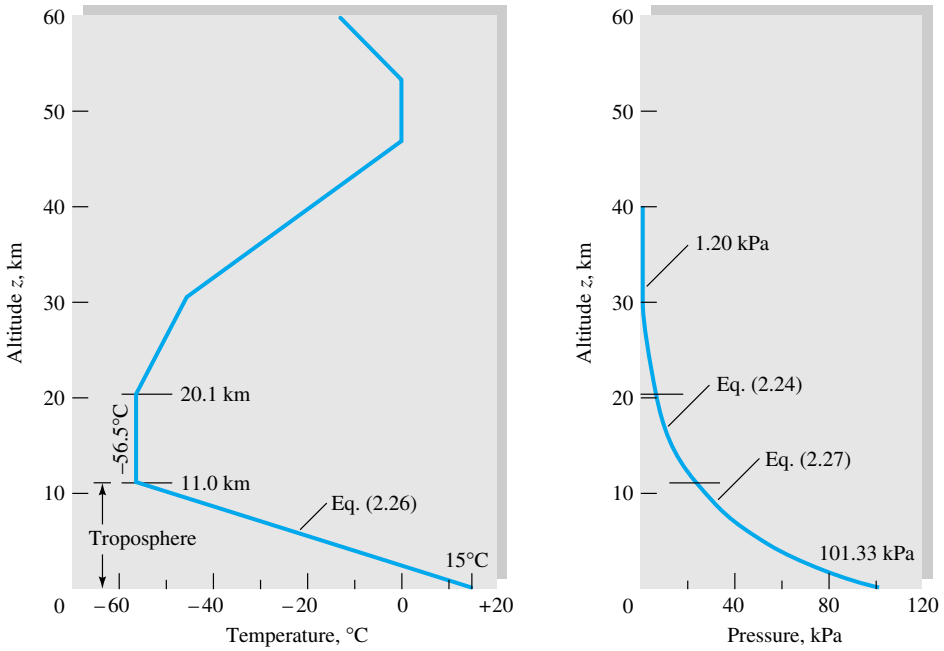


Fig. 2.7 Temperature and pressure distribution in the U.S. standard atmosphere. *(From Ref. 1.)*

Part (b) If the atmosphere were isothermal at 288.16 K, Eq. (2.24) would apply:

$$p \approx p_a \exp\left(-\frac{gz}{RT}\right) = (101{,}350 \text{ Pa}) \exp\left\{-\frac{(9.807 \text{ m/s}^2)(5000 \text{ m})}{[287 \text{ m}^2/(\text{s}^2 \cdot \text{K})](288.16 \text{ K})}\right\}$$

$$= (101{,}350 \text{ Pa}) \exp(-0.5929) \approx 60{,}100 \text{ Pa} \qquad \textit{Ans. (b)}$$

This is 11 percent higher than the exact result. The isothermal formula is inaccurate in the troposphere.

Is the Linear Formula Adequate for Gases?

The linear approximation from Eq. (2.20) or (2.21), $\Delta p \approx \gamma \, \Delta z$, is satisfactory for liquids, which are nearly incompressible. It may be used even over great depths in the ocean. For gases, which are highly compressible, it is valid only over moderate changes in altitude.

The error involved in using the linear approximation (2.21) can be evaluated by expanding the exact formula (2.27) into a series

$$\left(1 - \frac{Bz}{T_0}\right)^n = 1 - n\frac{Bz}{T_0} + \frac{n(n-1)}{2!}\left(\frac{Bz}{T_0}\right)^2 - \cdots \tag{2.28}$$

where $n = g/(RB)$. Introducing these first three terms of the series into Eq. (2.27) and rearranging, we obtain

$$p = p_a - \gamma_a z\left(1 - \frac{n-1}{2}\frac{Bz}{T_0} + \cdots\right)$$



ketabline.com Ebook.ketabline.com

Thus the error in using the linear formula (2.21) is small if the second term in parentheses in (2.29) is small compared with unity. This is true if

$$z \ll \frac{2T_0}{(n-1)B} = 20{,}800 \text{ m} \tag{2.30}$$

We thus expect errors of less than 5 percent if z or δz is less than 1000 m.

2.4 Application to Manometry

From the hydrostatic formula (2.20), a change in elevation $z_2 - z_1$ of a liquid is equivalent to a change in pressure $(p_2 - p_1)/\gamma$. Thus a static column of one or more liquids or gases can be used to measure pressure differences between two points. Such a device is called a *manometer*. If multiple fluids are used, we must change the density in the formula as we move from one fluid to another. Figure 2.8 illustrates the use of the formula with a column of multiple fluids. The pressure change through each fluid is calculated separately. If we wish to know the total change $p_5 - p_1$, we add the successive changes $p_2 - p_1$, $p_3 - p_2$, $p_4 - p_3$, and $p_5 - p_4$. The intermediate values of p cancel, and we have, for the example of Fig. 2.8,

$$p_5 - p_1 = -\gamma_0(z_2 - z_1) - \gamma_w(z_3 - z_2) - \gamma_G(z_4 - z_3) - \gamma_M(z_5 - z_4) \tag{2.31}$$

No additional simplification is possible on the right-hand side because of the different densities. Notice that we have placed the fluids in order from the lightest on top to the heaviest at bottom. This is the only stable configuration. If we attempt to layer them in any other manner, the fluids will overturn and seek the stable arrangement.

A Memory Device: Up Versus Down

The basic hydrostatic relation, Eq. (2.20), is mathematically correct but vexing to engineers, because it combines two negative signs to have the pressure increase downward. When calculating hydrostatic pressure changes, engineers work instinctively by simply having the pressure increase downward and decrease upward. Thus they use the following mnemonic, or memory, device, first suggested to the writer by Professor John

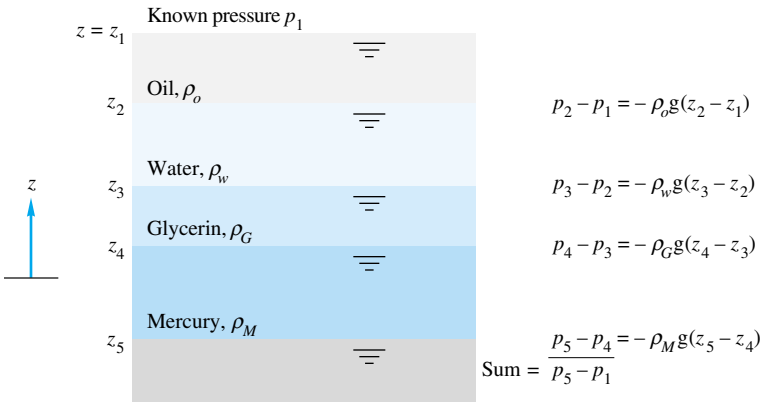


Fig. 2.8 Evaluating pressure changes through a column of multiple fluids.



ketabline.com Ebook.ketabline.com

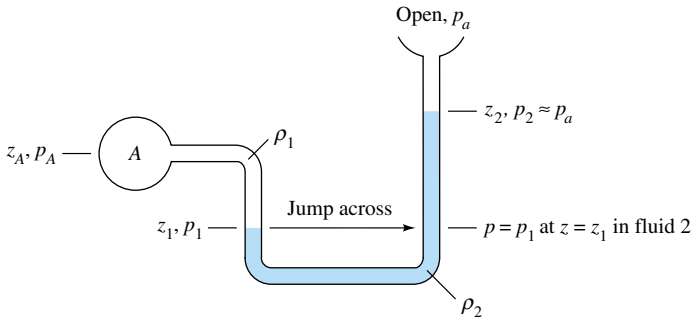


Fig. 2.9 Simple open manometer for measuring p_A relative to atmospheric pressure.

Foss of Michigan State University:

$$p_{down} = p^{up} + \gamma |\Delta z| \tag{2.32}$$

Thus, without worrying too much about which point is "z_1" and which is "z_2", the formula simply increases or decreases the pressure according to whether one is moving down or up. For example, Eq. (2.31) could be rewritten in the following "multiple increase" mode:

$$p_5 = p_1 + \gamma_0 |z_1 - z_2| + \gamma_w |z_2 - z_3| + \gamma_G |z_3 - z_4| + \gamma_M |z_4 - z_5|$$

That is, keep adding on pressure increments as you move down through the layered fluid. A different application is a manometer, which involves both "up" and "down" calculations.

Figure 2.9 shows a simple open manometer for measuring p_A in a closed chamber relative to atmospheric pressure p_a, in other words, measuring the gage pressure. The chamber fluid ρ_1 is combined with a second fluid ρ_2, perhaps for two reasons: (1) to protect the environment from a corrosive chamber fluid or (2) because a heavier fluid ρ_2 will keep z_2 small and the open tube can be shorter. One can, of course, apply the basic hydrostatic formula (2.20). Or, more simply, one can begin at A, apply Eq. (2.32) "down" to z_1, jump across fluid 2 (see Fig. 2.9) to the same pressure p_1, and then use Eq. (2.32) "up" to level z_2:

$$p_A + \gamma_1 |z_A - z_1| - \gamma_2 |z_1 - z_2| = p_2 \approx p_{\text{atm}} \tag{2.33}$$

The physical reason that we can "jump across" at section 1 in that a continuous length of the same fluid connects these two equal elevations. The hydrostatic relation (2.20) requires this equality as a form of Pascal's law:

> Any two points at the same elevation in a continuous mass of the same static fluid will be at the same pressure.

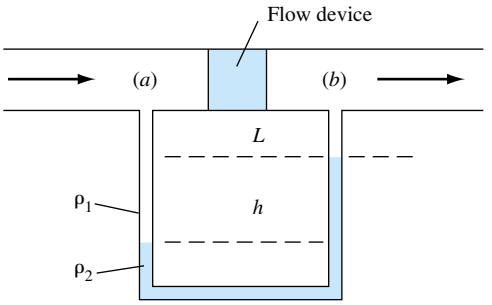
This idea of jumping across to equal pressures facilitates multiple-fluid problems.

EXAMPLE 2.3

The classic use of a manometer is when two U-tube legs are of equal len
and the measurement involves a pressure difference across two horizontal p



ketabline.com Ebook.ketabline.com



E2.3

plication is to measure pressure change across a flow device, as shown. Derive a formula for the pressure difference $p_a - p_b$ in terms of the system parameters in Fig. E2.3.

Solution

Using our "up-down" concept as in Eq. (2.32), start at (a), evaluate pressure changes around the U-tube, and end up at (b):

$$p_a + \rho_1 gL + \rho_1 gh - \rho_2 gh - \rho_1 gL = p_b$$

or

$$p_a - p_b = (\rho_2 - \rho_1)gh \qquad \textit{Ans.}$$

The measurement only includes h, the manometer reading. Terms involving L drop out. Note the appearance of the *difference* in densities between manometer fluid and working fluid. It is a common student error to fail to subtract out the working fluid density ρ_1—a serious error if both fluids are liquids and less disastrous numerically if fluid 1 is a gas. Academically, of course, such an error is always considered serious by fluid mechanics instructors.

Although Ex. 2.3, because of its popularity in engineering experiments, is sometimes considered to be the "manometer formula," it is best *not* to memorize it but rather to adapt Eq. (2.20) or (2.32) to each new multiple-fluid hydrostatics problem. For example, Fig. 2.10 illustrates a multiple-fluid manometer problem for finding the

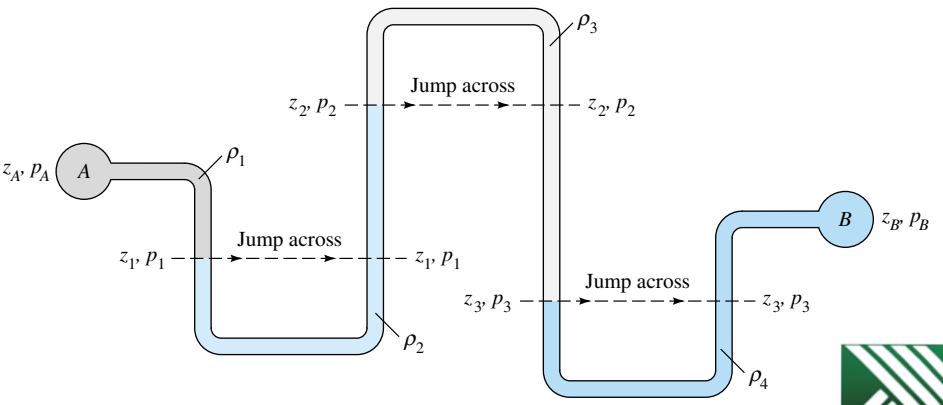


Fig. 2.10 A complicated multiple-fluid manometer to relate p_A to p_B. This system is not especially practical but makes a good homework or examination problem.

ketabline.com Ebook.ketabline.com

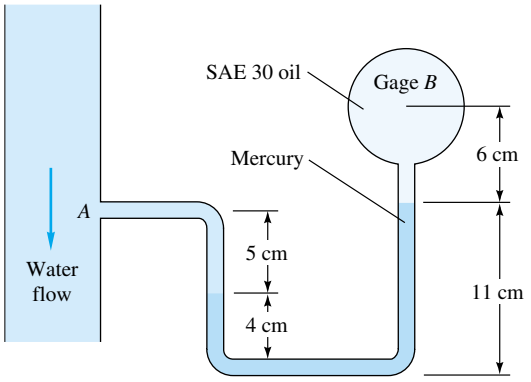
difference in pressure between two chambers A and B. We repeatedly apply Eq. (2.20), jumping across at equal pressures when we come to a continuous mass of the same fluid. Thus, in Fig. 2.10, we compute four pressure differences while making three jumps:

$$\begin{aligned} p_A - p_B &= (p_A - p_1) + (p_1 - p_2) + (p_2 - p_3) + (p_3 - p_B) \\ &= -\gamma_1(z_A - z_1) - \gamma_2(z_1 - z_2) - \gamma_3(z_2 - z_3) - \gamma_4(z_3 - z_B) \end{aligned} \tag{2.34}$$

The intermediate pressures $p_{1,2,3}$ cancel. It looks complicated, but really it is merely *sequential*. One starts at A, goes down to 1, jumps across, goes up to 2, jumps across, goes down to 3, jumps across, and finally goes up to B.

EXAMPLE 2.4

Pressure gage B is to measure the pressure at point A in a water flow. If the pressure at B is 87 kPa, estimate the pressure at A, in kPa. Assume all fluids are at 20°C. See Fig. E2.4.



E2.4

Solution

First list the specific weights from Table 2.1 or Table A.3:

$$\gamma_{water} = 9790 \text{ N/m}^3 \qquad \gamma_{mercury} = 133{,}100 \text{ N/m}^3 \qquad \gamma_{oil} = 8720 \text{ N/m}^3$$

Now proceed from A to B, calculating the pressure change in each fluid and adding:

$$p_A - \gamma_W(\Delta z)_W - \gamma_M(\Delta z)_M - \gamma_O(\Delta z)_O = p_B$$

or $$p_A - (9790 \text{ N/m}^3)(-0.05 \text{ m}) - (133{,}100 \text{ N/m}^3)(0.07 \text{ m}) - (8720 \text{ N/m}^3)(0.06 \text{ m})$$

$$= p_A + 489.5 \text{ Pa} - 9317 \text{ Pa} - 523.2 \text{ Pa} = p_B = 87{,}000 \text{ Pa}$$

where we replace N/m^2 by its short name, Pa. The value $\Delta z_M = 0.07$ m is the net elevation change in the mercury (11 cm − 4 cm). Solving for the pressure at point A, we obtain

$$p_A = 96{,}351 \text{ Pa} = 96.4 \text{ kPa} \qquad \textit{Ans.}$$

The intermediate six-figure result of 96,351 Pa is utterly fatuous, since the measurements cannot be made that accurately.



ketabline.com Ebook.ketabline.com

In making these manometer calculations we have neglected the capillary-height changes due to surface tension, which were discussed in Example 1.9. These effects cancel if there is a fluid interface, or *meniscus*, on both sides of the U-tube, as in Fig. 2.9. Otherwise, as in the right-hand U-tube of Fig. 2.10, a capillary correction can be made or the effect can be made negligible by using large-bore (≥ 1 cm) tubes.

2.5 Hydrostatic Forces on Plane Surfaces

A common problem in the design of structures which interact with fluids is the computation of the hydrostatic force on a plane surface. If we neglect density changes in the fluid, Eq. (2.20) applies and the pressure on any submerged surface varies linearly with depth. For a plane surface, the linear stress distribution is exactly analogous to combined bending and compression of a beam in strength-of-materials theory. The hydrostatic problem thus reduces to simple formulas involving the centroid and moments of inertia of the plate cross-sectional area.

Figure 2.11 shows a plane panel of arbitrary shape completely submerged in a liquid. The panel plane makes an arbitrary angle θ with the horizontal free surface, so that the depth varies over the panel surface. If h is the depth to any element area dA of the plate, from Eq. (2.20) the pressure there is $p = p_a + \gamma h$.

To derive formulas involving the plate shape, establish an xy coordinate system in the plane of the plate with the origin at its centroid, plus a dummy coordinate ξ down from the surface in the plane of the plate. Then the total hydrostatic force on one side of the plate is given by

$$F = \int p\, dA = \int (p_a + \gamma h)\, dA = p_a A + \gamma \int h\, dA \tag{2.35}$$

The remaining integral is evaluated by noticing from Fig. 2.11 that $h = \xi \sin \theta$ and,

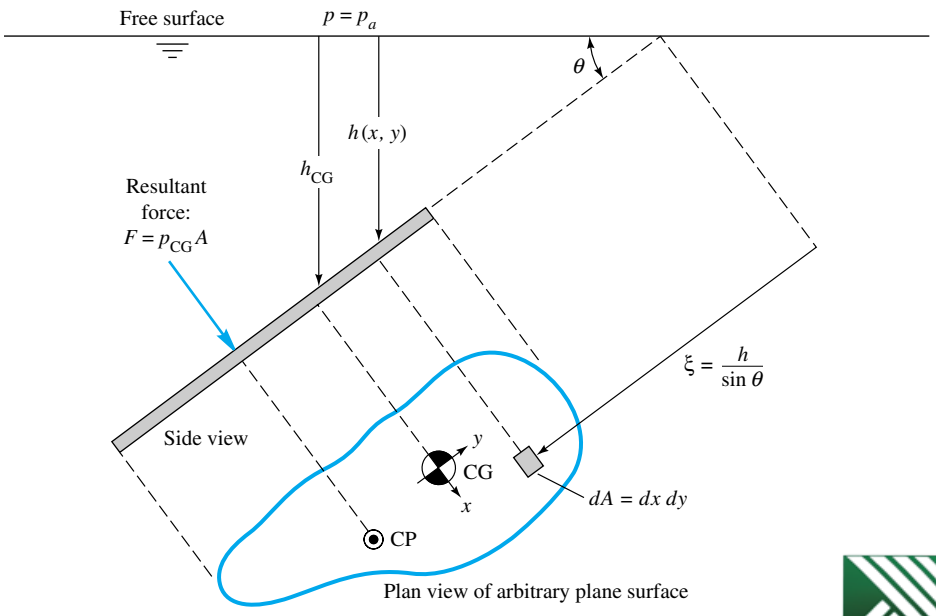


Fig. 2.11 Hydrostatic force and center of pressure on an arbitrary plane surface of area A inclined at an angle θ below the free surface.



ketabline.com Ebook.ketabline.com

by definition, the centroidal slant distance from the surface to the plate is

$$\xi_{CG} = \frac{1}{A}\int \xi \, dA \tag{2.36}$$

Therefore, since θ is constant along the plate, Eq. (2.35) becomes

$$F = p_a A + \gamma \sin\theta \int \xi \, dA = p_a A + \gamma \sin\theta \, \xi_{CG} A \tag{2.37}$$

Finally, unravel this by noticing that $\xi_{CG} \sin\theta = h_{CG}$, the depth straight down from the surface to the plate centroid. Thus

$$F = p_a A + \gamma h_{CG} A = (p_a + \gamma h_{CG})A = p_{CG} A \tag{2.38}$$

The force on one side of any plane submerged surface in a uniform fluid equals the pressure at the plate centroid times the plate area, independent of the shape of the plate or the angle θ at which it is slanted.

Equation (2.38) can be visualized physically in Fig. 2.12 as the resultant of a linear stress distribution over the plate area. This simulates combined compression and bending of a beam of the same cross section. It follows that the "bending" portion of the stress causes no force if its "neutral axis" passes through the plate centroid of area. Thus the remaining "compression" part must equal the centroid stress times the plate area. This is the result of Eq. (2.38).

However, to balance the bending-moment portion of the stress, the resultant force F does not act through the centroid but below it toward the high-pressure side. Its line of action passes through the *center of pressure* CP of the plate, as sketched in Fig. 2.11. To find the coordinates (x_{CP}, y_{CP}), we sum moments of the elemental force $p\,dA$ about the centroid and equate to the moment of the resultant F. To compute y_{CP}, we equate

$$Fy_{CP} = \int yp \, dA = \int y(p_a + \gamma\xi \sin\theta) \, dA = \gamma \sin\theta \int y\xi \, dA \tag{2.39}$$

The term $\int p_a y \, dA$ vanishes by definition of centroidal axes. Introducing $\xi = \xi_{CG} - y$,

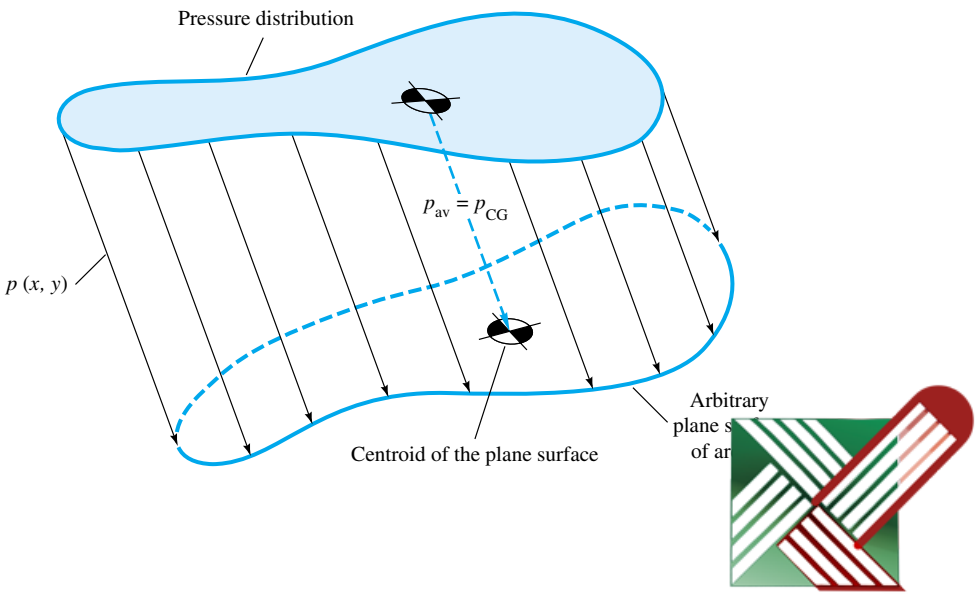


Fig. 2.12 The hydrostatic-pressure force on a plane surface is equal, regardless of its shape, to the resultant of the three-dimensional linear pressure distribution on that surface $F = p_{CG}A$.

ketabline.com Ebook.ketabline.com

we obtain

$$Fy_{CP} = \gamma \sin\theta\left(\xi_{CG}\int y\,dA - \int y^2\,dA\right) = -\gamma \sin\theta\, I_{xx} \tag{2.40}$$

where again $\int y\,dA = 0$ and I_{xx} is the area moment of inertia of the plate area about its centroidal x axis, computed in the plane of the plate. Substituting for F gives the result

$$y_{CP} = -\gamma \sin\theta \frac{I_{xx}}{p_{CG}A} \tag{2.41}$$

The negative sign in Eq. (2.41) shows that y_{CP} is below the centroid at a deeper level and, unlike F, depends upon angle θ. If we move the plate deeper, y_{CP} approaches the centroid because every term in Eq. (2.41) remains constant except p_{CG}, which increases.

The determination of x_{CP} is exactly similar:

$$Fx_{CP} = \int xp\,dA = \int x[p_a + \gamma(\xi_{CG} - y)\sin\theta]\,dA$$

$$= -\gamma \sin\theta \int xy\,dA = -\gamma \sin\theta\, I_{xy} \tag{2.42}$$

where I_{xy} is the product of inertia of the plate, again computed in the plane of the plate. Substituting for F gives

$$x_{CP} = -\gamma \sin\theta \frac{I_{xy}}{p_{CG}A} \tag{2.43}$$

For positive I_{xy}, x_{CP} is negative because the dominant pressure force acts in the third, or lower left, quadrant of the panel. If $I_{xy} = 0$, usually implying symmetry, $x_{CP} = 0$ and the center of pressure lies directly below the centroid on the y axis.

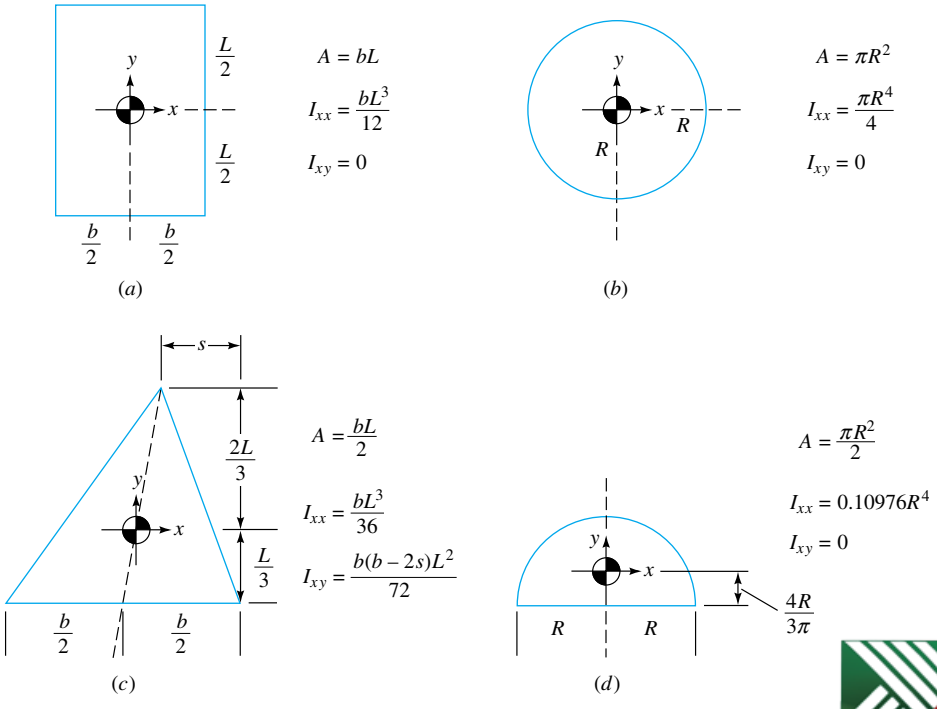


Fig. 2.13 Centroidal moments of inertia for various cross sections: (*a*) rectangle, (*b*) circle, (*c*) triangle, and (*d*) semicircle.



ketabline.com Ebook.ketabline.com

Gage-Pressure Formulas

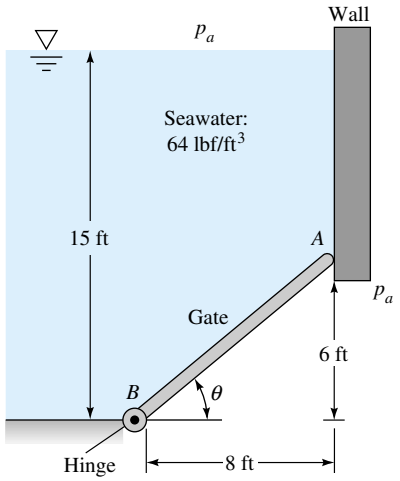
In most cases the ambient pressure p_a is neglected because it acts on both sides of the plate; e.g., the other side of the plate is inside a ship or on the dry side of a gate or dam. In this case $p_{CG} = \gamma h_{CG}$, and the center of pressure becomes independent of specific weight

$$F = \gamma h_{CG} A \qquad y_{CP} = -\frac{I_{xx} \sin\theta}{h_{CG} A} \qquad x_{CP} = -\frac{I_{xy} \sin\theta}{h_{CG} A} \tag{2.44}$$

Figure 2.13 gives the area and moments of inertia of several common cross sections for use with these formulas.

EXAMPLE 2.5

The gate in Fig. E2.5*a* is 5 ft wide, is hinged at point *B*, and rests against a smooth wall at point *A*. Compute (*a*) the force on the gate due to seawater pressure, (*b*) the horizontal force *P* exerted by the wall at point *A*, and (*c*) the reactions at the hinge *B*.



E2.5a

Solution

Part (a) By geometry the gate is 10 ft long from *A* to *B*, and its centroid is halfway between, or at elevation 3 ft above point *B*. The depth h_{CG} is thus 15 − 3 = 12 ft. The gate area is 5(10) = 50 ft^2. Neglect p_a as acting on both sides of the gate. From Eq. (2.38) the hydrostatic force on the gate is

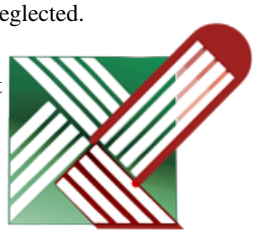
$$F = p_{CG} A = \gamma h_{CG} A = (64 \text{ lbf/ft}^3)(12 \text{ ft})(50 \text{ ft}^2) = 38{,}400 \text{ lbf} \qquad \textit{Ans. (a)}$$

Part (b) First we must find the center of pressure of *F*. A free-body diagram of the gate is shown in Fig. E2.5*b*. The gate is a rectangle, hence

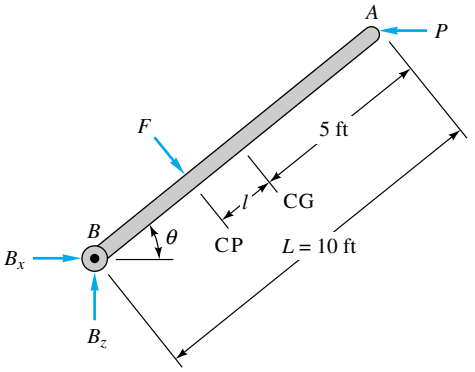
$$I_{xy} = 0 \qquad \text{and} \qquad I_{xx} = \frac{bL^3}{12} = \frac{(5 \text{ ft})(10 \text{ ft})^3}{12} = 417 \text{ ft}^4$$

The distance *l* from the CG to the CP is given by Eq. (2.44) since p_a is neglected.

$$l = -y_{CP} = +\frac{I_{xx} \sin\theta}{h_{CG} A} = \frac{(417 \text{ ft}^4)(\frac{6}{10})}{(12 \text{ ft})(50 \text{ ft}^2)} = 0.417 \text{ ft}$$



ketabline.com Ebook.ketabline.com



E2.5b

The distance from point B to force F is thus $10 - l - 5 = 4.583$ ft. Summing moments counterclockwise about B gives

$$PL \sin \theta - F(5 - l) = P(6 \text{ ft}) - (38{,}400 \text{ lbf})(4.583 \text{ ft}) = 0$$

or $$P = 29{,}300 \text{ lbf} \qquad \textit{Ans. (b)}$$

Part (c) With F and P known, the reactions B_x and B_z are found by summing forces on the gate

$$\sum F_x = 0 = B_x + F \sin \theta - P = B_x + 38{,}400(0.6) - 29{,}300$$

or $$B_x = 6300 \text{ lbf}$$

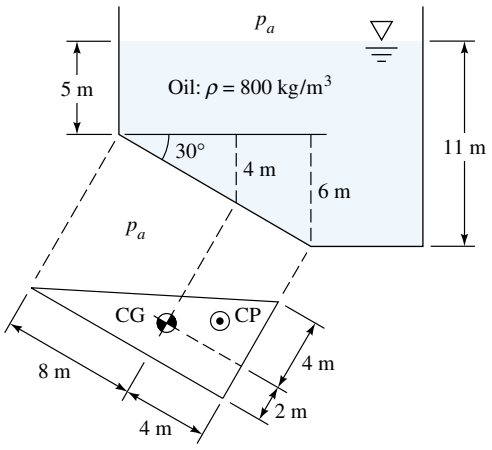
$$\sum F_z = 0 = B_z - F \cos \theta = B_z - 38{,}400(0.8)$$

or $$B_z = 30{,}700 \text{ lbf} \qquad \textit{Ans. (c)}$$

This example should have reviewed your knowledge of statics.

EXAMPLE 2.6

A tank of oil has a right-triangular panel near the bottom, as in Fig. E2.6. Omitting p_a, find the (a) hydrostatic force and (b) CP on the panel.



E2.6



ketabline.com Ebook.ketabline.com

Solution

Part (a) The triangle has properties given in Fig. 2.13*c*. The centroid is one-third up (4 m) and one-third over (2 m) from the lower left corner, as shown. The area is

$$\tfrac{1}{2}(6\text{ m})(12\text{ m}) = 36\text{ m}^2$$

The moments of inertia are

$$I_{xx} = \frac{bL^3}{36} = \frac{(6\text{ m})(12\text{ m})^3}{36} = 288\text{ m}^4$$

and

$$I_{xy} = \frac{b(b-2s)L^2}{72} = \frac{(6\text{ m})[6\text{ m} - 2(6\text{ m})](12\text{ m})^2}{72} = -72\text{ m}^4$$

The depth to the centroid is $h_{CG} = 5 + 4 = 9$ m; thus the hydrostatic force from Eq. (2.44) is

$$F = \rho g h_{CG} A = (800\text{ kg/m}^3)(9.807\text{ m/s}^2)(9\text{ m})(36\text{ m}^2)$$

$$= 2.54 \times 10^6\text{ (kg} \cdot \text{m)/s}^2 = 2.54 \times 10^6\text{ N} = 2.54\text{ MN} \qquad \textit{Ans. (a)}$$

Part (b) The CP position is given by Eqs. (2.44):

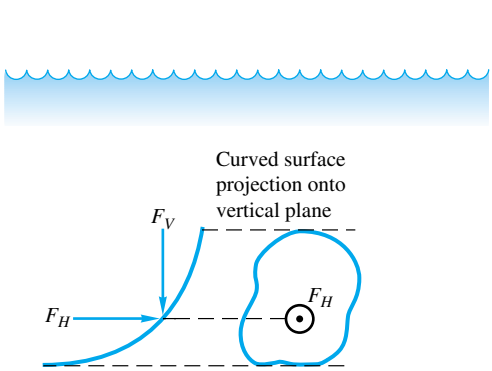
$$y_{CP} = -\frac{I_{xx}\sin\theta}{h_{CG}A} = -\frac{(288\text{ m}^4)(\sin 30^\circ)}{(9\text{ m})(36\text{ m}^2)} = -0.444\text{ m}$$

$$x_{CP} = -\frac{I_{xy}\sin\theta}{h_{CG}A} = -\frac{(-72\text{ m}^4)(\sin 30^\circ)}{(9\text{ m})(36\text{ m}^2)} = +0.111\text{ m} \qquad \textit{Ans. (b)}$$

The resultant force $F = 2.54$ MN acts through this point, which is down and to the right of the centroid, as shown in Fig. E2.6.

2.6 Hydrostatic Forces on Curved Surfaces

The resultant pressure force on a curved surface is most easily computed by separating it into horizontal and vertical components. Consider the arbitrary curved surface sketched in Fig. 2.14*a*. The incremental pressure forces, being normal to the local area element, vary in direction along the surface and thus cannot be added numerically. We



(*a*)

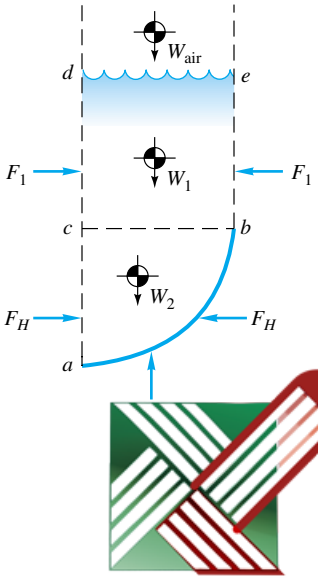


Fig. 2.14 Computation of hydrostatic force on a curved surface: (*a*) submerged curved surface; (*b*) free-body diagram of fluid above the curved surface.

ketabline.com Ebook.ketabline.com

could sum the separate three components of these elemental pressure forces, but it turns out that we need not perform a laborious three-way integration.

Figure 2.14*b* shows a free-body diagram of the column of fluid contained in the vertical projection above the curved surface. The desired forces F_H and F_V are exerted by the surface on the fluid column. Other forces are shown due to fluid weight and horizontal pressure on the vertical sides of this column. The column of fluid must be in static equilibrium. On the upper part of the column *bcde*, the horizontal components F_1 exactly balance and are not relevant to the discussion. On the lower, irregular portion of fluid *abc* adjoining the surface, summation of horizontal forces shows that the desired force F_H due to the curved surface is exactly equal to the force F_H on the vertical left side of the fluid column. This left-side force can be computed by the plane-surface formula, Eq. (2.38), based on a vertical projection of the area of the curved surface. This is a general rule and simplifies the analysis:

> The horizontal component of force on a curved surface equals the force on the plane area formed by the projection of the curved surface onto a vertical plane normal to the component.

If there are two horizontal components, both can be computed by this scheme.

Summation of vertical forces on the fluid free body then shows that

$$F_V = W_1 + W_2 + W_{\text{air}} \tag{2.45}$$

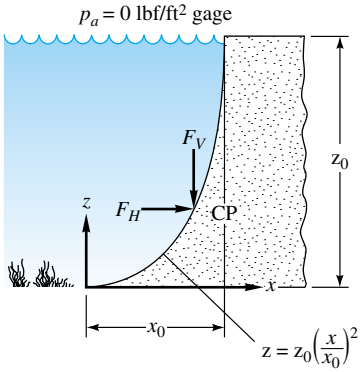
We can state this in words as our second general rule:

> The vertical component of pressure force on a curved surface equals in magnitude and direction the weight of the entire column of fluid, both liquid and atmosphere, above the curved surface.

Thus the calculation of F_V involves little more than finding centers of mass of a column of fluid—perhaps a little integration if the lower portion *abc* has a particularly vexing shape.

EXAMPLE 2.7

A dam has a parabolic shape $z/z_0 = (x/x_0)^2$ as shown in Fig. E2.7*a*, with $x_0 = 10$ ft and $z_0 = 24$ ft. The fluid is water, $\gamma = 62.4$ lbf/ft^3, and atmospheric pressure may be omitted. Compute the



E2.7a



ketabline.com Ebook.ketabline.com

forces F_H and F_V on the dam and the position CP where they act. The width of the dam is 50 ft.

Solution

The vertical projection of this curved surface is a rectangle 24 ft high and 50 ft wide, with its centroid halfway down, or $h_{CG} = 12$ ft. The force F_H is thus

$$F_H = \gamma h_{CG} A_{proj} = (62.4 \text{ lbf/ft}^3)(12 \text{ ft})(24 \text{ ft})(50 \text{ ft})$$

$$= 899{,}000 \text{ lbf} = 899 \times 10^3 \text{ lbf} \qquad \textit{Ans.}$$

The line of action of F_H is below the centroid by an amount

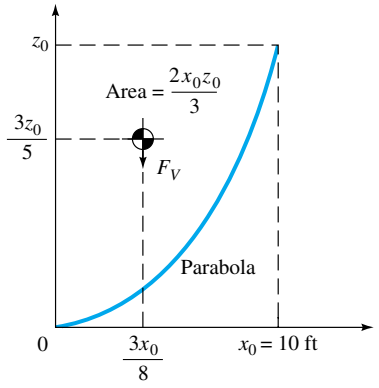
$$y_{CP} = -\frac{I_{xx} \sin\theta}{h_{CG} A_{proj}} = -\frac{\frac{1}{12}(50 \text{ ft})(24 \text{ ft})^3 (\sin 90°)}{(12 \text{ ft})(24 \text{ ft})(50 \text{ ft})} = -4 \text{ ft}$$

Thus F_H is 12 + 4 = 16 ft, or two-thirds, down from the free surface or 8 ft from the bottom, as might have been evident by inspection of the triangular pressure distribution.

The vertical component F_V equals the weight of the parabolic portion of fluid above the curved surface. The geometric properties of a parabola are shown in Fig. E2.7*b*. The weight of this amount of water is

$$F_V = \gamma(\tfrac{2}{3} x_0 z_0 b) = (62.4 \text{ lbf/ft}^3)(\tfrac{2}{3})(10 \text{ ft})(24 \text{ ft})(50 \text{ ft})$$

$$= 499{,}000 \text{ lbf} = 499 \times 10^3 \text{ lbf} \qquad \textit{Ans.}$$



E2.7b

This acts downward on the surface at a distance $3x_0/8 = 3.75$ ft over from the origin of coordinates. Note that the vertical distance $3z_0/5$ in Fig. E2.7*b* is irrelevant.

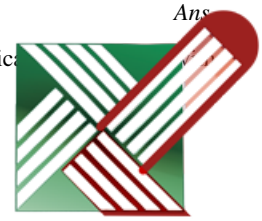
The total resultant force acting on the dam is

$$F = (F_H^2 + F_V^2)^{1/2} = [(499)^2 + (899)^2]^{1/2} = 1028 \times 10^3 \text{ lbf}$$

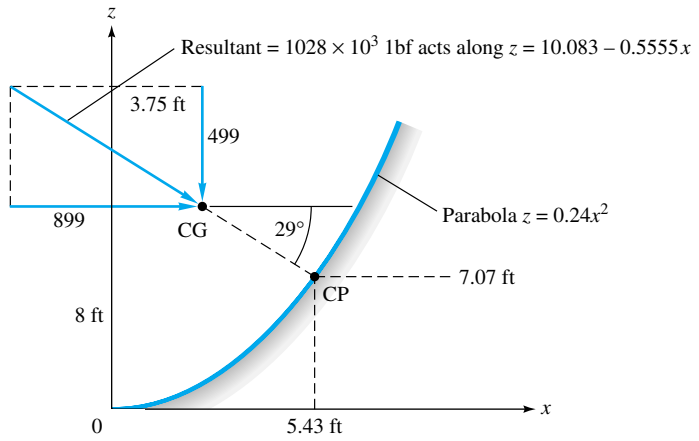
As seen in Fig. E2.7*c*, this force acts down and to the right at an angle of $29° = \tan^{-1} \frac{499}{899}$. The force F passes through the point $(x, z) = (3.75 \text{ ft}, 8 \text{ ft})$. If we move down along the 29° line until we strike the dam, we find an equivalent center of pressure on the dam at

$$x_{CP} = 5.43 \text{ ft} \qquad z_{CP} = 7.07 \text{ ft} \qquad \textit{Ans.}$$

This definition of CP is rather artificial, but this is an unavoidable complica
a curved surface.



ketabline.com Ebook.ketabline.com



E2.7c

2.7 Hydrostatic Forces in Layered Fluids

The formulas for plane and curved surfaces in Secs. 2.5 and 2.6 are valid only for a fluid of uniform density. If the fluid is layered with different densities, as in Fig. 2.15, a single formula cannot solve the problem because the slope of the linear pressure distribution changes between layers. However, the formulas apply separately to each layer, and thus the appropriate remedy is to compute and sum the separate layer forces and moments.

Consider the slanted plane surface immersed in a two-layer fluid in Fig. 2.15. The slope of the pressure distribution becomes steeper as we move down into the denser

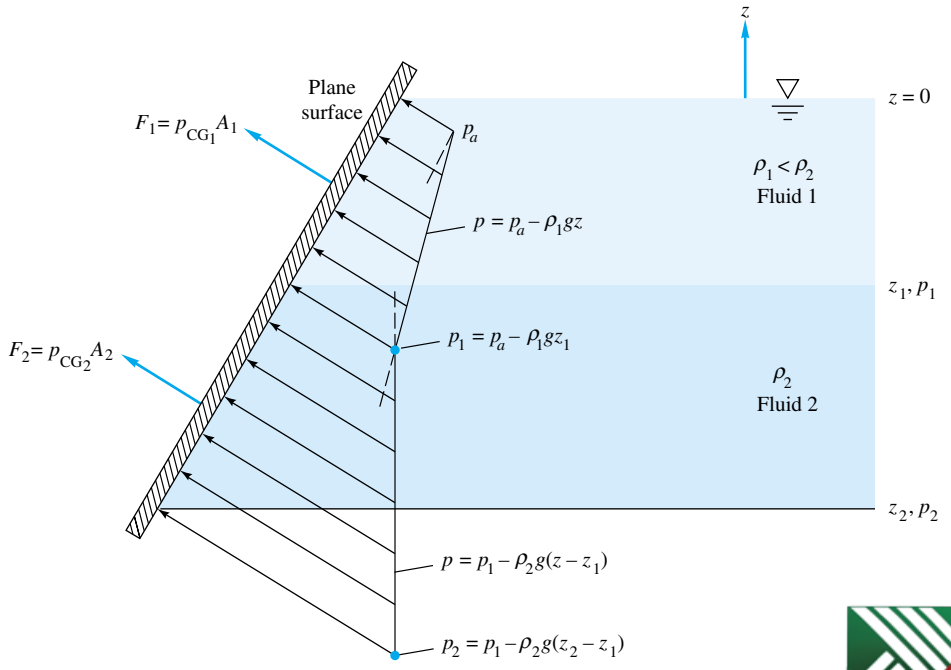


Fig. 2.15 Hydrostatic forces on a surface immersed in a layered fluid must be summed in separate pieces.



ketabline.com Ebook.ketabline.com

second layer. The total force on the plate does *not* equal the pressure at the centroid times the plate area, but the plate portion in each layer does satisfy the formula, so that we can sum forces to find the total:

$$F = \Sigma F_i = \Sigma p_{CG_i} A_i \tag{2.46}$$

Similarly, the centroid of the plate portion in each layer can be used to locate the center of pressure on that portion

$$y_{CP_i} = -\frac{\rho_i g \sin \theta_i I_{xx_i}}{p_{CG_i} A_i} \qquad x_{CP_i} = -\frac{\rho_i g \sin \theta_i I_{xy_i}}{p_{CG_i} A_i} \tag{2.47}$$

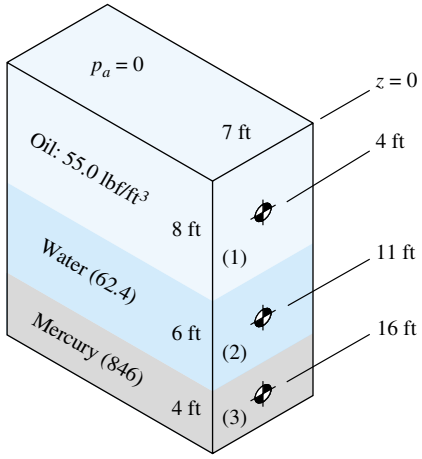
These formulas locate the center of pressure of that particular F_i with respect to the centroid of that particular portion of plate in the layer, not with respect to the centroid of the entire plate. The center of pressure of the total force $F = \Sigma F_i$ can then be found by summing moments about some convenient point such as the surface. The following example will illustrate.

EXAMPLE 2.8

A tank 20 ft deep and 7 ft wide is layered with 8 ft of oil, 6 ft of water, and 4 ft of mercury. Compute (*a*) the total hydrostatic force and (*b*) the resultant center of pressure of the fluid on the right-hand side of the tank.

Solution

Part (a) Divide the end panel into three parts as sketched in Fig. E2.8, and find the hydrostatic pressure at the centroid of each part, using the relation (2.38) in steps as in Fig. E2.8:



E2.8

$$P_{CG_1} = (55.0 \text{ lbf/ft}^3)(4 \text{ ft}) = 220 \text{ lbf/ft}^2$$

$$p_{CG_2} = (55.0)(8) + 62.4(3) = 627 \text{ lbf/ft}^2$$

$$p_{CG_3} = (55.0)(8) + 62.4(6) + 846(2) = 2506 \text{ lbf/ft}^2$$



ketabline.com Ebook.ketabline.com

These pressures are then multiplied by the respective panel areas to find the force on each portion:

$$F_1 = p_{CG_1}A_1 = (220 \text{ lbf/ft}^2)(8 \text{ ft})(7 \text{ ft}) = 12{,}300 \text{ lbf}$$

$$F_2 = p_{CG_2}A_2 = 627(6)(7) = 26{,}300 \text{ lbf}$$

$$F_3 = p_{CG_3}A_3 = 2506(4)(7) = \underline{70{,}200 \text{ lbf}}$$

$$F = \Sigma F_i = 108{,}800 \text{ lbf} \qquad \textit{Ans. (a)}$$

Part (b) Equations (2.47) can be used to locate the CP of each force F_i, noting that $\theta = 90°$ and $\sin\theta = 1$ for all parts. The moments of inertia are $I_{xx_1} = (7 \text{ ft})(8 \text{ ft})^3/12 = 298.7 \text{ ft}^4$, $I_{xx_2} = 7(6)^3/12 = 126.0 \text{ ft}^4$, and $I_{xx_3} = 7(4)^3/12 = 37.3 \text{ ft}^4$. The centers of pressure are thus at

$$y_{CP_1} = -\frac{\rho_1 g I_{xx_1}}{F_1} = -\frac{(55.0 \text{ lbf/ft}^3)(298.7 \text{ ft}^4)}{12{,}300 \text{ lbf}} = -1.33 \text{ ft}$$

$$y_{CP_2} = -\frac{62.4(126.0)}{26{,}300} = -0.30 \text{ ft} \qquad y_{CP_3} = -\frac{846(37.3)}{70{,}200} = -0.45 \text{ ft}$$

This locates $z_{CP_1} = -4 - 1.33 = -5.33$ ft, $z_{CP_2} = -11 - 0.30 = -11.30$ ft, and $z_{CP_3} = -16 - 0.45 = -16.45$ ft. Summing moments about the surface then gives

$$\Sigma F_i z_{CP_i} = F z_{CP}$$

or $$12{,}300(-5.33) + 26{,}300(-11.30) + 70{,}200(-16.45) = 108{,}800 z_{CP}$$

or $$z_{CP} = -\frac{1{,}518{,}000}{108{,}800} = -13.95 \text{ ft} \qquad \textit{Ans. (b)}$$

The center of pressure of the total resultant force on the right side of the tank lies 13.95 ft below the surface.

2.8 Buoyancy and Stability

The same principles used to compute hydrostatic forces on surfaces can be applied to the net pressure force on a completely submerged or floating body. The results are the two laws of buoyancy discovered by Archimedes in the third century B.C.:

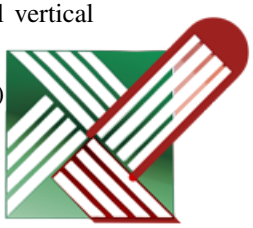
1. A body immersed in a fluid experiences a vertical buoyant force equal to the weight of the fluid it displaces.
2. A floating body displaces its own weight in the fluid in which it floats.

These two laws are easily derived by referring to Fig. 2.16. In Fig. 2.16*a*, the body lies between an upper curved surface 1 and a lower curved surface 2. From Eq. (2.45) for vertical force, the body experiences a net upward force

$$\begin{aligned} F_B &= F_V(2) - F_V(1) \\ &= (\text{fluid weight above 2}) - (\text{fluid weight above 1}) \\ &= \text{weight of fluid equivalent to body volume} \end{aligned} \qquad (2.48)$$

Alternatively, from Fig. 2.16*b*, we can sum the vertical forces on elemental vertical slices through the immersed body:

$$F_B = \int_{\text{body}} (p_2 - p_1)\, dA_H = -\gamma \int (z_2 - z_1)\, dA_H = (\gamma)(\text{body volume})$$



ketabline.com Ebook.ketabline.com

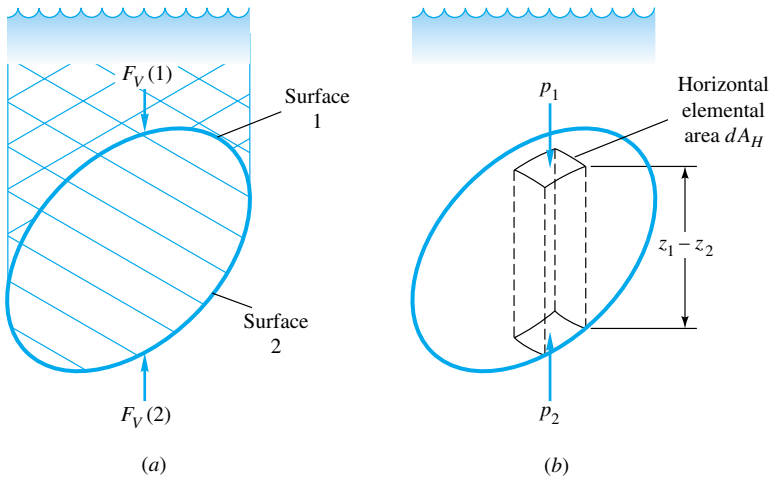


Fig. 2.16 Two different approaches to the buoyant force on an arbitrary immersed body: (*a*) forces on upper and lower curved surfaces; (*b*) summation of elemental vertical-pressure forces.

These are identical results and equivalent to law 1 above.

Equation (2.49) assumes that the fluid has uniform specific weight. The line of action of the buoyant force passes through the center of volume of the displaced body; i.e., its center of mass is computed as if it had uniform density. This point through which F_B acts is called the *center of buoyancy*, commonly labeled B or CB on a drawing. Of course, the point B may or may not correspond to the actual center of mass of the body's own material, which may have variable density.

Equation (2.49) can be generalized to a layered fluid (LF) by summing the weights of each layer of density ρ_i displaced by the immersed body:

$$(F_B)_{\text{LF}} = \Sigma\, \rho_i g(\text{displaced volume})_i \tag{2.50}$$

Each displaced layer would have its own center of volume, and one would have to sum moments of the incremental buoyant forces to find the center of buoyancy of the immersed body.

Since liquids are relatively heavy, we are conscious of their buoyant forces, but gases also exert buoyancy on any body immersed in them. For example, human beings have an average specific weight of about 60 lbf/ft^3. We may record the weight of a person as 180 lbf and thus estimate the person's total volume as 3.0 ft^3. However, in so doing we are neglecting the buoyant force of the air surrounding the person. At standard conditions, the specific weight of air is 0.0763 lbf/ft^3; hence the buoyant force is approximately 0.23 lbf. If measured in vacuo, the person would weigh about 0.23 lbf more. For balloons and blimps the buoyant force of air, instead of being negligible, is the controlling factor in the design. Also, many flow phenomena, e.g., natural convection of heat and vertical mixing in the ocean, are strongly dependent upon seemingly small buoyant forces.

Floating bodies are a special case; only a portion of the body is submerged, with the remainder poking up out of the free surface. This is illustrated in Fig. 2.17, where the shaded portion is the displaced volume. Equation (2.49) is modified to apply to this smaller volume

$$F_B = (\gamma)(\text{displaced volume}) = \text{floating-body weig}$$



ketabline.com Ebook.ketabline.com

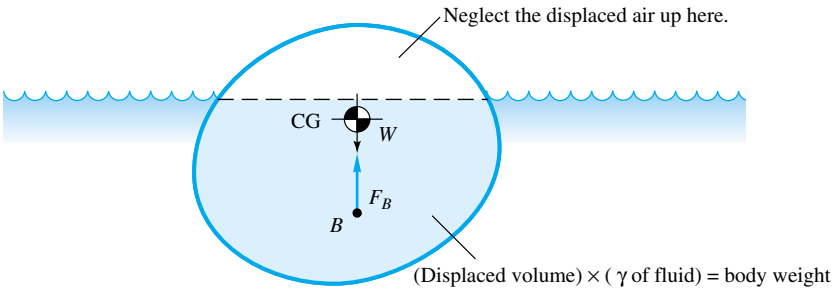
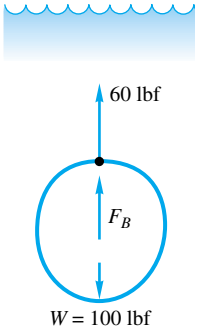


Fig. 2.17 Static equilibrium of a floating body.

Not only does the buoyant force equal the body weight, but also they are *collinear* since there can be no net moments for static equilibrium. Equation (2.51) is the mathematical equivalent of Archimedes' law 2, previously stated.

EXAMPLE 2.9

A block of concrete weighs 100 lbf in air and "weighs" only 60 lbf when immersed in fresh water (62.4 lbf/ft^3). What is the average specific weight of the block?



E2.9

Solution

A free-body diagram of the submerged block (see Fig. E2.9) shows a balance between the apparent weight, the buoyant force, and the actual weight

$$\Sigma F_z = 0 = 60 + F_B - 100$$

or

$$F_B = 40 \text{ lbf} = (62.4 \text{ lbf/ft}^3)(\text{block volume, ft}^3)$$

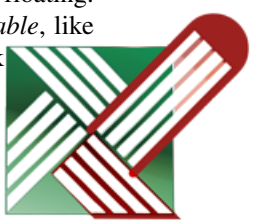
Solving gives the volume of the block as $40/62.4 = 0.641$ ft^3. Therefore the specific weight of the block is

$$\gamma_{\text{block}} = \frac{100 \text{ lbf}}{0.641 \text{ ft}^3} = 156 \text{ lbf/ft}^3 \qquad \textit{Ans.}$$

Occasionally, a body will have exactly the right weight and volume for its ratio to equal the specific weight of the fluid. If so, the body will be *neutrally buoyant* and will remain at rest at any point where it is immersed in the fluid. Small neutrally buoyant particles are sometimes used in flow visualization, and a neutrally buoyant body called a *Swallow float* [2] is used to track oceanographic currents. A submarine can achieve positive, neutral, or negative buoyancy by pumping water in or out of its ballast tanks.

Stability

A floating body as in Fig. 2.17 may not approve of the position in which it is floating. If so, it will overturn at the first opportunity and is said to be statically *unstable*, like a pencil balanced upon its point. The least disturbance will cause it to seek equilibrium position which is stable. Engineers must design to avoid floating



ketabline.com Ebook.ketabline.com

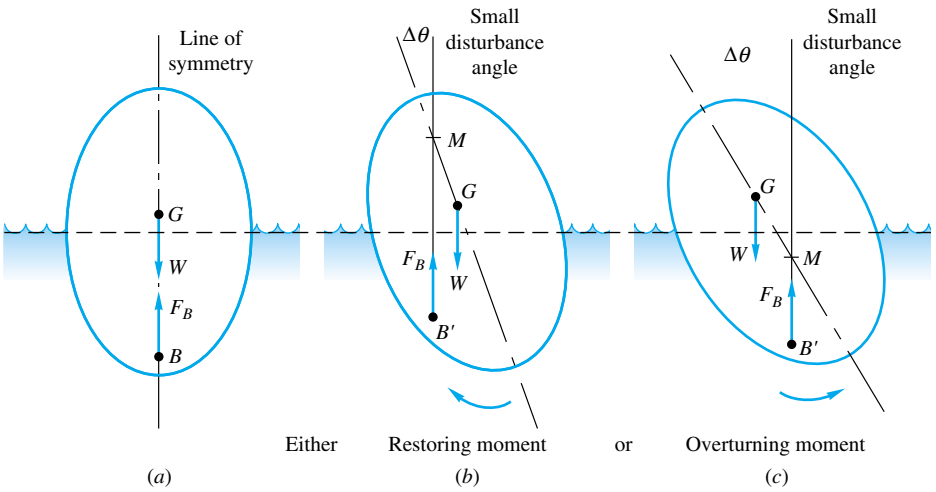


Fig. 2.18 Calculation of the metacenter M of the floating body shown in (a). Tilt the body a small angle $\Delta\theta$. Either (b) B' moves far out (point M above G denotes stability); or (c) B' moves slightly (point M below G denotes instability).

ity. The only way to tell for sure whether a floating position is stable is to "disturb" the body a slight amount mathematically and see whether it develops a restoring moment which will return it to its original position. If so, it is stable; if not, unstable. Such calculations for arbitrary floating bodies have been honed to a fine art by naval architects [3], but we can at least outline the basic principle of the static-stability calculation. Figure 2.18 illustrates the computation for the usual case of a symmetric floating body. The steps are as follows:

1. The basic floating position is calculated from Eq. (2.51). The body's center of mass G and center of buoyancy B are computed.
2. The body is tilted a small angle $\Delta\theta$, and a new waterline is established for the body to float at this angle. The new position B' of the center of buoyancy is calculated. A vertical line drawn upward from B' intersects the line of symmetry at a point M, called the *metacenter*, which is independent of $\Delta\theta$ for small angles.
3. If point M is above G, that is, if the *metacentric height* $\overline{MG}$ is positive, a restoring moment is present and the original position is stable. If M is below G (negative $\overline{MG}$, the body is unstable and will overturn if disturbed. Stability increases with increasing $\overline{MG}$.

Thus the metacentric height is a property of the cross section for the given weight, and its value gives an indication of the stability of the body. For a body of varying cross section and draft, such as a ship, the computation of the metacenter can be very involved.

Stability Related to Waterline Area

Naval architects [3] have developed the general stability concepts from Fig. 2.18 into a simple computation involving the area moment of inertia of the *waterline area* about the axis of tilt. The derivation assumes that the body has a smooth shape variation (no discontinuities) near the waterline and is derived from Fig. 2.19.

The y-axis of the body is assumed to be a line of symmetry. Tiltin
angle θ then submerges small wedge Obd and uncovers an equal wed



ketabline.com Ebook.ketabline.com

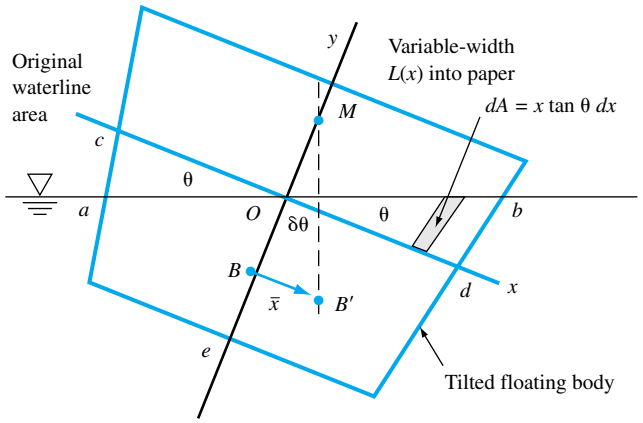


Fig. 2.19 A floating body tilted through a small angle θ. The movement $\bar{x}$ of the center of buoyancy B is related to the waterline area moment of inertia.

The new position B' of the center of buoyancy is calculated as the centroid of the submerged portion *aObde* of the body:

$$\bar{x}\,\forall_{abOde} = \int_{cOdea} x\,d\forall + \int_{Obd} x\,d\forall - \int_{cOa} x\,d\forall = 0 + \int_{Obd} x\,(L\,dA) - \int_{cOa} x\,(L\,dA)$$

$$= 0 + \int_{Obd} x\,L\,(x\tan\theta\,dx) - \int_{cOa} xL\,(-x\tan\theta\,dx) = \tan\theta \int_{\text{waterline}} x^2\,dA_{\text{waterline}} = I_O \tan\theta$$

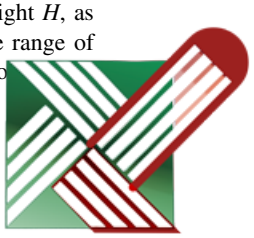
where I_O is the area moment of inertia of the *waterline footprint* of the body about its tilt axis O. The first integral vanishes because of the symmetry of the original submerged portion *cOdea*. The remaining two "wedge" integrals combine into I_O when we notice that $L\,dx$ equals an element of *waterline area*. Thus we determine the desired distance from M to B:

$$\frac{\bar{x}}{\overline{MB}} = \frac{I_O}{\forall_{\text{submerged}}} = \overline{MG} + \overline{GB} \qquad \text{or} \qquad \overline{MG} = \frac{I_O}{\forall_{\text{sub}}} - \overline{GB} \tag{2.52}$$

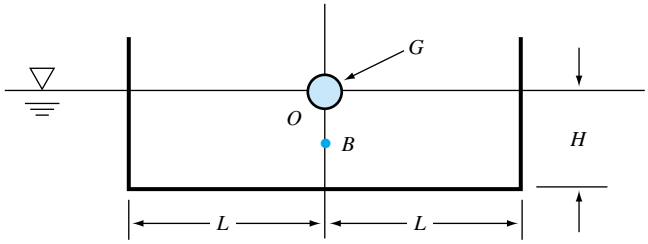
The engineer would determine the distance from G to B from the basic shape and design of the floating body and then make the calculation of I_O and the submerged volume $\forall_{\text{sub}}$. If the metacentric height MG is positive, the body is stable for small disturbances. Note that if $\overline{GB}$ is negative, that is, B is *above* G, the body is always stable.

EXAMPLE 2.10

A barge has a uniform rectangular cross section of width $2L$ and vertical draft of height H, as in Fig. E2.10. Determine (*a*) the metacentric height for a small tilt angle and (*b*) the range of ratio L/H for which the barge is statically stable if G is exactly at the waterline as sho



ketabline.com Ebook.ketabline.com



E2.10

Solution

If the barge has length b into the paper, the waterline area, relative to tilt axis O, has a base b and a height $2L$; therefore, $I_O = b(2L)^3/12$. Meanwhile, $\upsilon_{sub} = 2LbH$. Equation (2.52) predicts

$$\overline{MG} = \frac{I_O}{\upsilon_{sub}} - \overline{GB} = \frac{8bL^3/12}{2LbH} - \frac{H}{2} = \frac{L^2}{3H} - \frac{H}{2} \qquad \textit{Ans. (a)}$$

The barge can thus be stable only if

$$L^2 > 3H^2/2 \qquad \text{or} \qquad 2L > 2.45H \qquad \textit{Ans. (b)}$$

The wider the barge relative to its draft, the more stable it is. Lowering G would help also.

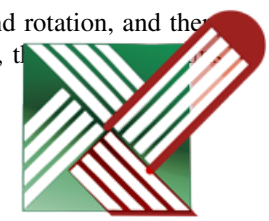
Even an expert will have difficulty determining the floating stability of a buoyant body of irregular shape. Such bodies may have two or more stable positions. For example, a ship may float the way we like it, so that we can sit upon the deck, or it may float upside down (capsized). An interesting mathematical approach to floating stability is given in Ref. 11. The author of this reference points out that even simple shapes, e.g., a cube of uniform density, may have a great many stable floating orientations, not necessarily symmetric. Homogeneous circular cylinders can float with the axis of symmetry tilted from the vertical.

Floating instability occurs in nature. Living fish generally swim with their plane of symmetry vertical. After death, this position is unstable and they float with their flat sides up. Giant icebergs may overturn after becoming unstable when their shapes change due to underwater melting. Iceberg overturning is a dramatic, rarely seen event.

Figure 2.20 shows a typical North Atlantic iceberg formed by calving from a Greenland glacier which protruded into the ocean. The exposed surface is rough, indicating that it has undergone further calving. Icebergs are frozen fresh, bubbly, glacial water of average density 900 kg/m^3. Thus, when an iceberg is floating in seawater, whose average density is 1025 kg/m^3, approximately 900/1025, or seven-eighths, of its volume lies below the water.

2.9 Pressure Distribution in Rigid-Body Motion

In rigid-body motion, all particles are in combined translation and rotation, and there is no relative motion between particles. With no relative motion, t



ketabline.com Ebook.ketabline.com

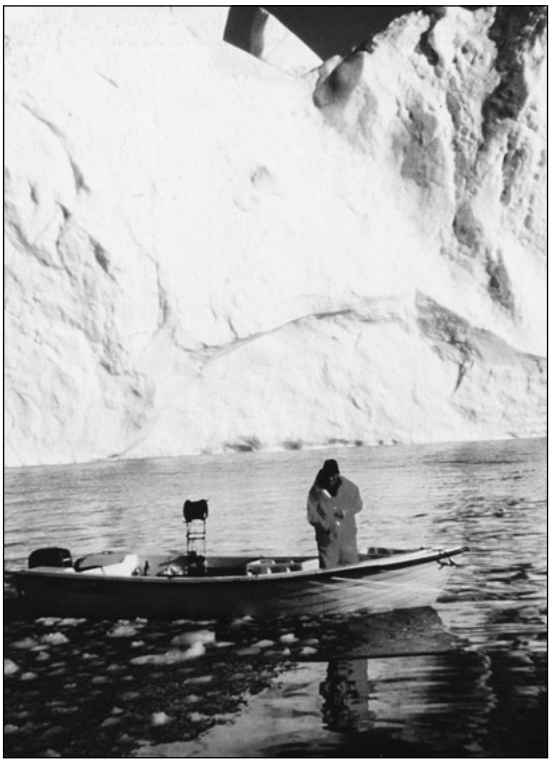


Fig. 2.20 A North Atlantic iceberg formed by calving from a Greenland glacier. These, and their even larger Antarctic sisters, are the largest floating bodies in the world. Note the evidence of further calving fractures on the front surface. *(Courtesy of Søren Thalund, Greenland tourism a/s Iiulissat, Greenland.)*

or strain rates, so that the viscous term $\mu\nabla^2\mathbf{V}$ in Eq. (2.13) vanishes, leaving a balance between pressure, gravity, and particle acceleration

$$\nabla p = \rho(\mathbf{g} - \mathbf{a}) \tag{2.53}$$

The pressure gradient acts in the direction $\mathbf{g} - \mathbf{a}$, and lines of constant pressure (including the free surface, if any) are perpendicular to this direction. The general case of combined translation and rotation of a rigid body is discussed in Chap. 3, Fig. 3.12. If the center of rotation is at point O and the translational velocity is V_0 at this point, the velocity of an arbitrary point P on the body is given by[2]

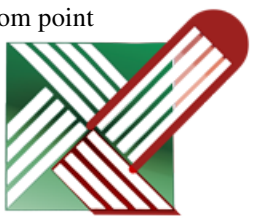
$$\mathbf{V} = \mathbf{V}_0 + \boldsymbol{\Omega} \times \mathbf{r}_0$$

where $\boldsymbol{\Omega}$ is the angular-velocity vector and $\mathbf{r}_0$ is the position of point P. Differentiating, we obtain the most general form of the acceleration of a rigid body:

$$\mathbf{a} = \frac{d\mathbf{V}_0}{dt} + \boldsymbol{\Omega} \times (\boldsymbol{\Omega} \times \mathbf{r}_0) + \frac{d\boldsymbol{\Omega}}{dt} \times \mathbf{r}_0 \tag{2.54}$$

Looking at the right-hand side, we see that the first term is the translational acceleration; the second term is the *centripetal acceleration*, whose direction is from point

[2] For a more detailed derivation of rigid-body motion, see Ref. 4, Sec. 2.7.



ketabline.com Ebook.ketabline.com

P perpendicular toward the axis of rotation; and the third term is the linear acceleration due to changes in the angular velocity. It is rare for all three of these terms to apply to any one fluid flow. In fact, fluids can rarely move in rigid-body motion unless restrained by confining walls for a long time. For example, suppose a tank of water is in a car which starts a constant acceleration. The water in the tank would begin to slosh about, and that sloshing would damp out very slowly until finally the particles of water would be in approximately rigid-body acceleration. This would take so long that the car would have reached hypersonic speeds. Nevertheless, we can at least discuss the pressure distribution in a tank of rigidly accelerating water. The following is an example where the water in the tank will reach uniform acceleration rapidly.

EXAMPLE 2.11

A tank of water 1 m deep is in free fall under gravity with negligible drag. Compute the pressure at the bottom of the tank if $p_a = 101$ kPa.

Solution

Being unsupported in this condition, the water particles tend to fall downward as a rigid hunk of fluid. In free fall with no drag, the downward acceleration is $\mathbf{a} = \mathbf{g}$. Thus Eq. (2.53) for this situation gives $\nabla p = \rho(\mathbf{g} - \mathbf{g}) = 0$. The pressure in the water is thus *constant everywhere* and equal to the atmospheric pressure 101 kPa. In other words, the walls are doing no service in sustaining the pressure distribution which would normally exist.

Uniform Linear Acceleration

In this general case of uniform rigid-body acceleration, Eq. (2.53) applies, $\mathbf{a}$ having the same magnitude and direction for all particles. With reference to Fig. 2.21, the parallelogram sum of $\mathbf{g}$ and $-\mathbf{a}$ gives the direction of the pressure gradient or greatest rate of increase of p. The surfaces of constant pressure must be perpendicular to this and are thus tilted at a downward angle θ such that

$$\theta = \tan^{-1}\frac{a_x}{g + a_z} \tag{2.55}$$

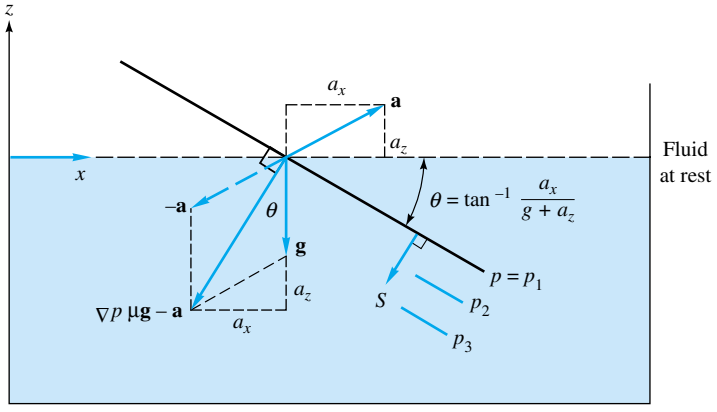


Fig. 2.21 Tilting of constant-pressure surfaces in a tank of liquid in rigid-body acceleration.



ketabline.com Ebook.ketabline.com

One of these tilted lines is the free surface, which is found by the requirement that the fluid retain its volume unless it spills out. The rate of increase of pressure in the direction $\mathbf{g} - \mathbf{a}$ is greater than in ordinary hydrostatics and is given by

$$\frac{dp}{ds} = \rho G \qquad \text{where } G = [a_x^2 + (g + a_z)^2]^{1/2} \tag{2.56}$$

These results are independent of the size or shape of the container as long as the fluid is continuously connected throughout the container.

EXAMPLE 2.12

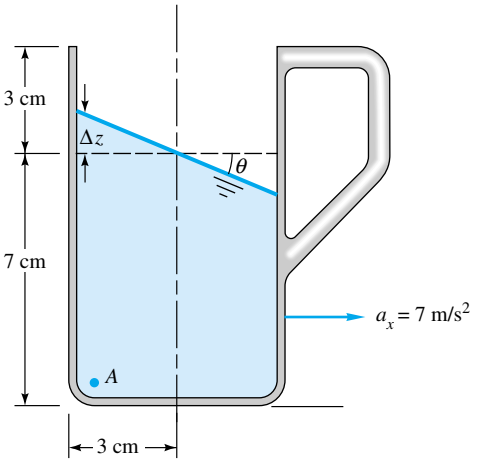
A drag racer rests her coffee mug on a horizontal tray while she accelerates at 7 m/s^2. The mug is 10 cm deep and 6 cm in diameter and contains coffee 7 cm deep at rest. (*a*) Assuming rigid-body acceleration of the coffee, determine whether it will spill out of the mug. (*b*) Calculate the gage pressure in the corner at point A if the density of coffee is 1010 kg/m^3.

Solution

Part (a) The free surface tilts at the angle θ given by Eq. (2.55) regardless of the shape of the mug. With $a_z = 0$ and standard gravity,

$$\theta = \tan^{-1}\frac{a_x}{g} = \tan^{-1}\frac{7.0}{9.81} = 35.5^\circ$$

If the mug is symmetric about its central axis, the volume of coffee is conserved if the tilted surface intersects the original rest surface exactly at the centerline, as shown in Fig. E2.12.



E2.12

Thus the deflection at the left side of the mug is

$$z = (3\text{ cm})(\tan\theta) = 2.14\text{ cm} \qquad \textit{Ans. (a)}$$

This is less than the 3-cm clearance available, so the coffee will not spill unless it was sloshed during the start-up of acceleration.

Part (b) When at rest, the gage pressure at point A is given by Eq. (2.20):

$$p_A = \rho g(z_{\text{surf}} - z_A) = (1010\text{ kg/m}^3)(9.81\text{ m/s}^2)(0.07\text{ m}) = 694\text{ N/m}^2 = 694\text{ Pa}$$



ketabline.com Ebook.ketabline.com

During acceleration, Eq. (2.56) applies, with $G = [(7.0)^2 + (9.81)^2]^{1/2} = 12.05$ m/s^2. The distance Δs down the normal from the tilted surface to point A is

$$\Delta s = (7.0 + 2.14)(\cos\theta) = 7.44 \text{ cm}$$

Thus the pressure at point A becomes

$$p_A = \rho G\, \Delta s = 1010(12.05)(0.0744) = 906 \text{ Pa} \qquad \textit{Ans. (b)}$$

which is an increase of 31 percent over the pressure when at rest.

Rigid-Body Rotation

As a second special case, consider rotation of the fluid about the z axis without any translation, as sketched in Fig. 2.22. We assume that the container has been rotating long enough at constant Ω for the fluid to have attained rigid-body rotation. The fluid acceleration will then be the centripetal term in Eq. (2.54). In the coordinates of Fig. 2.22, the angular-velocity and position vectors are given by

$$\boldsymbol{\Omega} = \mathbf{k}\Omega \qquad r_0 = \mathbf{i}_r r \tag{2.57}$$

Then the acceleration is given by

$$\boldsymbol{\Omega} \times (\boldsymbol{\Omega} \times \mathbf{r}_0) = -r\Omega^2 \mathbf{i}_r \tag{2.58}$$

as marked in the figure, and Eq. (2.53) for the force balance becomes

$$\nabla p = \mathbf{i}_r \frac{\partial p}{\partial r} + \mathbf{k}\frac{\partial p}{\partial z} = \rho(\mathbf{g} - \mathbf{a}) = \rho(-g\mathbf{k} + r\Omega^2 \mathbf{i}_r) \tag{2.59}$$

Equating like components, we find the pressure field by solving two first-order partial differential equations

$$\frac{\partial p}{\partial r} = \rho r \Omega^2 \qquad \frac{\partial p}{\partial z} = -\gamma \tag{2.60}$$

This is our first specific example of the generalized three-dimensional problem described by Eqs. (2.14) for more than one independent variable. The right-hand sides of

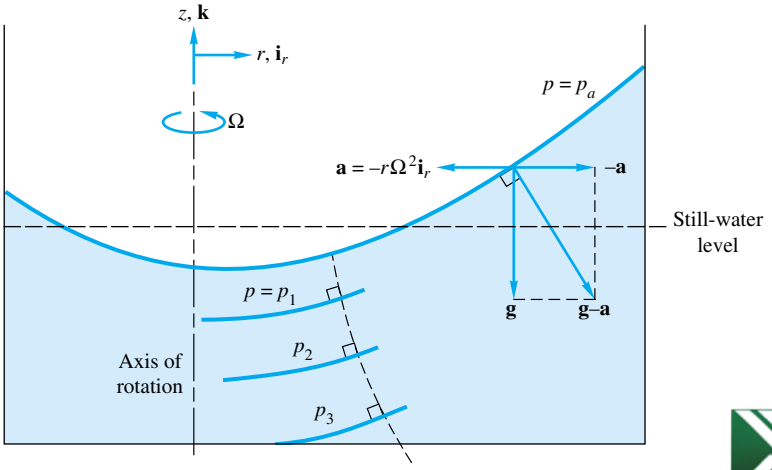


Fig. 2.22 Development of paraboloid constant-pressure surfaces in a fluid in rigid-body rotation. The dashed line along the direction of maximum pressure increase is an exponential curve.



ketabline.com Ebook.ketabline.com

(2.60) are known functions of r and z. One can proceed as follows: Integrate the first equation "partially," i.e., holding z constant, with respect to r. The result is

$$p = \tfrac{1}{2}\rho r^2\Omega^2 + f(z) \tag{2.61}$$

where the "constant" of integration is actually a function $f(z)$.[†] Now differentiate this with respect to z and compare with the second relation of (2.60):

$$\frac{\partial p}{\partial z} = 0 + f'(z) = -\gamma$$

or

$$f(z) = -\gamma z + C \tag{2.62a}$$

where C is a constant. Thus Eq. (2.61) now becomes

$$p = \text{const} - \gamma z + \tfrac{1}{2}\rho r^2\Omega^2 \tag{2.62b}$$

This is the pressure distribution in the fluid. The value of C is found by specifying the pressure at one point. If $p = p_0$ at $(r, z) = (0, 0)$, then $C = p_0$. The final desired distribution is

$$p = p_0 - \gamma_z + \tfrac{1}{2}\rho r^2\Omega^2 \tag{2.63}$$

The pressure is linear in z and parabolic in r. If we wish to plot a constant-pressure surface, say, $p = p_1$, Eq. (2.63) becomes

$$z = \frac{p_0 - p_1}{\gamma} + \frac{r^2\Omega^2}{2g} = a + br^2 \tag{2.64}$$

Thus the surfaces are paraboloids of revolution, concave upward, with their minimum point on the axis of rotation. Some examples are sketched in Fig. 2.22.

As in the previous example of linear acceleration, the position of the free surface is found by conserving the volume of fluid. For a noncircular container with the axis of rotation off-center, as in Fig. 2.22, a lot of laborious mensuration is required, and a single problem will take you all weekend. However, the calculation is easy for a cylinder rotating about its central axis, as in Fig. 2.23. Since the volume of a paraboloid is

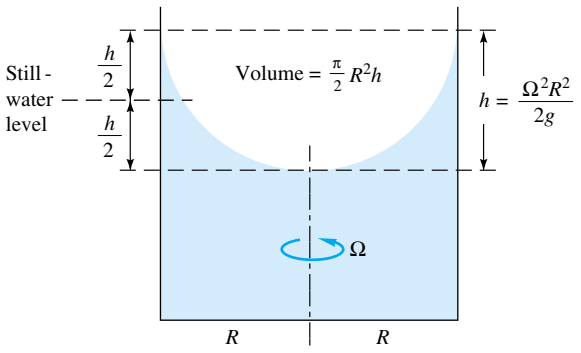


Fig. 2.23 Determining the free-surface position for rotation of a cylinder of fluid about its central axis.

[†]This is because $f(z)$ vanishes when differentiated with respect to r. If you don't see this, you review your calculus.



ketabline.com Ebook.ketabline.com

one-half the base area times its height, the still-water level is exactly halfway between the high and low points of the free surface. The center of the fluid drops an amount $h/2 = \Omega^2 R^2/(4g)$, and the edges rise an equal amount.

EXAMPLE 2.13

The coffee cup in Example 2.12 is removed from the drag racer, placed on a turntable, and rotated about its central axis until a rigid-body mode occurs. Find (*a*) the angular velocity which will cause the coffee to just reach the lip of the cup and (*b*) the gage pressure at point *A* for this condition.

Solution

Part (a) The cup contains 7 cm of coffee. The remaining distance of 3 cm up to the lip must equal the distance $h/2$ in Fig. 2.23. Thus

$$\frac{h}{2} = 0.03 \text{ m} = \frac{\Omega^2 R^2}{4g} = \frac{\Omega^2 (0.03 \text{ m})^2}{4(9.81 \text{ m/s}^2)}$$

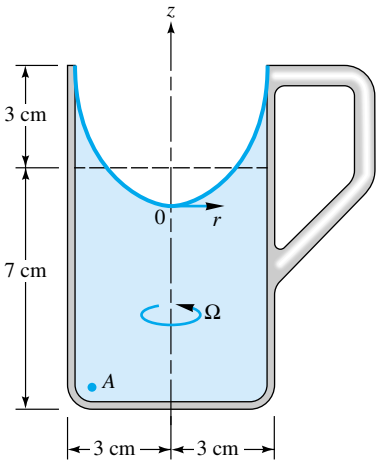
Solving, we obtain

$$\Omega^2 = 1308 \qquad \text{or} \qquad \Omega = 36.2 \text{ rad/s} = 345 \text{ r/min} \qquad \textit{Ans. (a)}$$

Part (b) To compute the pressure, it is convenient to put the origin of coordinates r and z at the bottom of the free-surface depression, as shown in Fig. E2.13. The gage pressure here is $p_0 = 0$, and point *A* is at $(r, z) = (3 \text{ cm}, -4 \text{ cm})$. Equation (2.63) can then be evaluated

$$p_A = 0 - (1010 \text{ kg/m}^3)(9.81 \text{ m/s}^2)(-0.04 \text{ m})$$
$$+ \tfrac{1}{2}(1010 \text{ kg/m}^3)(0.03 \text{ m})^2(1308 \text{ rad}^2/\text{s}^2)$$
$$= 396 \text{ N/m}^2 + 594 \text{ N/m}^2 = 990 \text{ Pa} \qquad \textit{Ans. (b)}$$

This is about 43 percent greater than the still-water pressure $p_A = 694$ Pa.

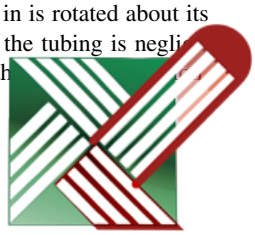


E2.13

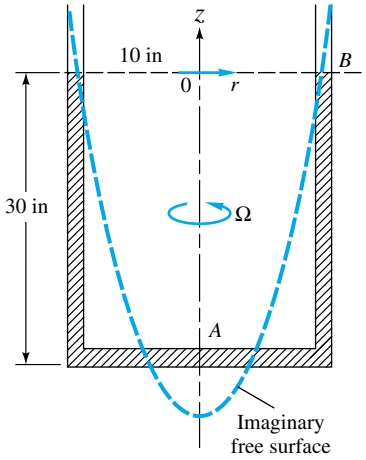
Here, as in the linear-acceleration case, it should be emphasized that the paraboloid pressure distribution (2.63) sets up in *any* fluid under rigid-body rotation, regardless of the shape or size of the container. The container may even be closed and filled with fluid. It is only necessary that the fluid be continuously interconnected throughout the container. The following example will illustrate a peculiar case in which one can visualize an imaginary free surface extending outside the walls of the container.

EXAMPLE 2.14

A U-tube with a radius of 10 in and containing mercury to a height of 30 in is rotated about its center at 180 r/min until a rigid-body mode is achieved. The diameter of the tubing is negligible. Atmospheric pressure is 2116 lbf/ft^2. Find the pressure at point *A* in th
See Fig. E2.14.



ketabline.com Ebook.ketabline.com



E2.14

Solution

Convert the angular velocity to radians per second:

$$\Omega = (180 \text{ r/min}) \frac{2\pi \text{ rad/r}}{60 \text{ s/min}} = 18.85 \text{ rad/s}$$

From Table 2.1 we find for mercury that $\gamma = 846$ lbf/ft^3 and hence $\rho = 846/32.2 = 26.3$ slugs/ft^3. At this high rotation rate, the free surface will slant upward at a fierce angle [about 84°; check this from Eq. (2.64)], but the tubing is so thin that the free surface will remain at approximately the same 30-in height, point B. Placing our origin of coordinates at this height, we can calculate the constant C in Eq. (2.62b) from the condition $p_B = 2116$ lbf/ft^2 at $(r, z) = (10 \text{ in}, 0)$:

$$p_B = 2116 \text{ lbf/ft}^2 = C - 0 + \tfrac{1}{2}(26.3 \text{ slugs/ft}^3)(\tfrac{10}{12} \text{ ft})^2(18.85 \text{ rad/s})^2$$

or

$$C = 2116 - 3245 = -1129 \text{ lbf/ft}^2$$

We then obtain p_A by evaluating Eq. (2.63) at $(r, z) = (0, -30 \text{ in})$:

$$p_A = -1129 - (846 \text{ lbf/ft}^3)(-\tfrac{30}{12} \text{ ft}) = -1129 + 2115 = 986 \text{ lbf/ft}^2 \qquad \textit{Ans.}$$

This is less than atmospheric pressure, and we can see why if we follow the free-surface paraboloid down from point B along the dashed line in the figure. It will cross the horizontal portion of the U-tube (where p will be atmospheric) and fall *below* point A. From Fig. 2.23 the actual drop from point B will be

$$h = \frac{\Omega^2 R^2}{2g} = \frac{(18.85)^2(\frac{10}{12})^2}{2(32.2)} = 3.83 \text{ ft} = 46 \text{ in}$$

Thus p_A is about 16 inHg below atmospheric pressure, or about $\frac{16}{12}(846) = 1128$ lbf/ft^2 below $p_a = 2116$ lbf/ft^2, which checks with the answer above. When the tube is at rest,

$$p_A = 2116 - 846(-\tfrac{30}{12}) = 4231 \text{ lbf/ft}^2$$

Hence rotation has reduced the pressure at point A by 77 percent. Further rotation can reduce p_A to near-zero pressure, and cavitation can occur.

An interesting by-product of this analysis for rigid-body rotation is that the lines everywhere parallel to the pressure gradient form a family of curved surfaces, as sketched in Fig. 2.22. They are everywhere orthogonal to the constant-pressure surfaces, and hence their slope is the negative inverse of the slope computed from Eq. (2.64):

$$\left.\frac{dz}{dr}\right|_{\text{GL}} = -\frac{1}{(dz/dr)_{p=\text{const}}} = -\frac{1}{r\Omega^2/g}$$

where GL stands for gradient line

or

$$\frac{dz}{dr} = -\frac{g}{r\Omega^2} \qquad (2.65)$$



ketabline.com Ebook.ketabline.com

Separating the variables and integrating, we find the equation of the pressure-gradient surfaces

$$r = C_1 \exp\left(-\frac{\Omega^2 z}{g}\right) \tag{2.66}$$

Notice that this result and Eq. (2.64) are independent of the density of the fluid. In the absence of friction and Coriolis effects, Eq. (2.66) defines the lines along which the apparent net gravitational field would act on a particle. Depending upon its density, a small particle or bubble would tend to rise or fall in the fluid along these exponential lines, as demonstrated experimentally in Ref. 5. Also, buoyant streamers would align themselves with these exponential lines, thus avoiding any stress other than pure tension. Figure 2.24 shows the configuration of such streamers before and during rotation.

2.10 Pressure Measurement

Pressure is a derived property. It is the force per unit area as related to fluid molecular bombardment of a surface. Thus most pressure instruments only *infer* the pressure by calibration with a primary device such as a deadweight piston tester. There are many such instruments, both for a static fluid and a moving stream. The instrumentation texts in Refs. 7 to 10, 12, and 13 list over 20 designs for pressure measurement instruments. These instruments may be grouped into four categories:

1. *Gravity-based:* barometer, manometer, deadweight piston.
2. *Elastic deformation:* bourdon tube (metal and quartz), diaphragm, bellows, strain-gage, optical beam displacement.
3. *Gas behavior:* gas compression (McLeod gage), thermal conductance (Pirani gage), molecular impact (Knudsen gage), ionization, thermal conductivity, air piston.
4. *Electric output:* resistance (Bridgman wire gage), diffused strain gage, capacitative, piezoelectric, magnetic inductance, magnetic reluctance, linear variable differential transformer (LVDT), resonant frequency.

The gas-behavior gages are mostly special-purpose instruments used for certain scientific experiments. The deadweight tester is the instrument used most often for calibrations; for example, it is used by the U.S. National Institute for Standards and Technology (NIST). The barometer is described in Fig. 2.6.

The manometer, analyzed in Sec. 2.4, is a simple and inexpensive hydrostatic-principle device with no moving parts except the liquid column itself. Manometer measurements must not disturb the flow. The best way to do this is to take the measurement through a *static hole* in the wall of the flow, as illustrated for the two instruments in Fig. 2.25. The hole should be normal to the wall, and burrs should be avoided. If the hole is small enough (typically 1-mm diameter), there will be no flow into the measuring tube once the pressure has adjusted to a steady value. Thus the flow is almost undisturbed. An oscillating flow pressure, however, can cause a large error due to possible dynamic response of the tubing. Other devices of smaller dimensions are used for dynamic-pressure measurements. Note that the manometers in Fig. 2.25 are arrange to measure the absolute pressures p_1 and p_2. If the pressure differe



ketabline.com Ebook.ketabline.com

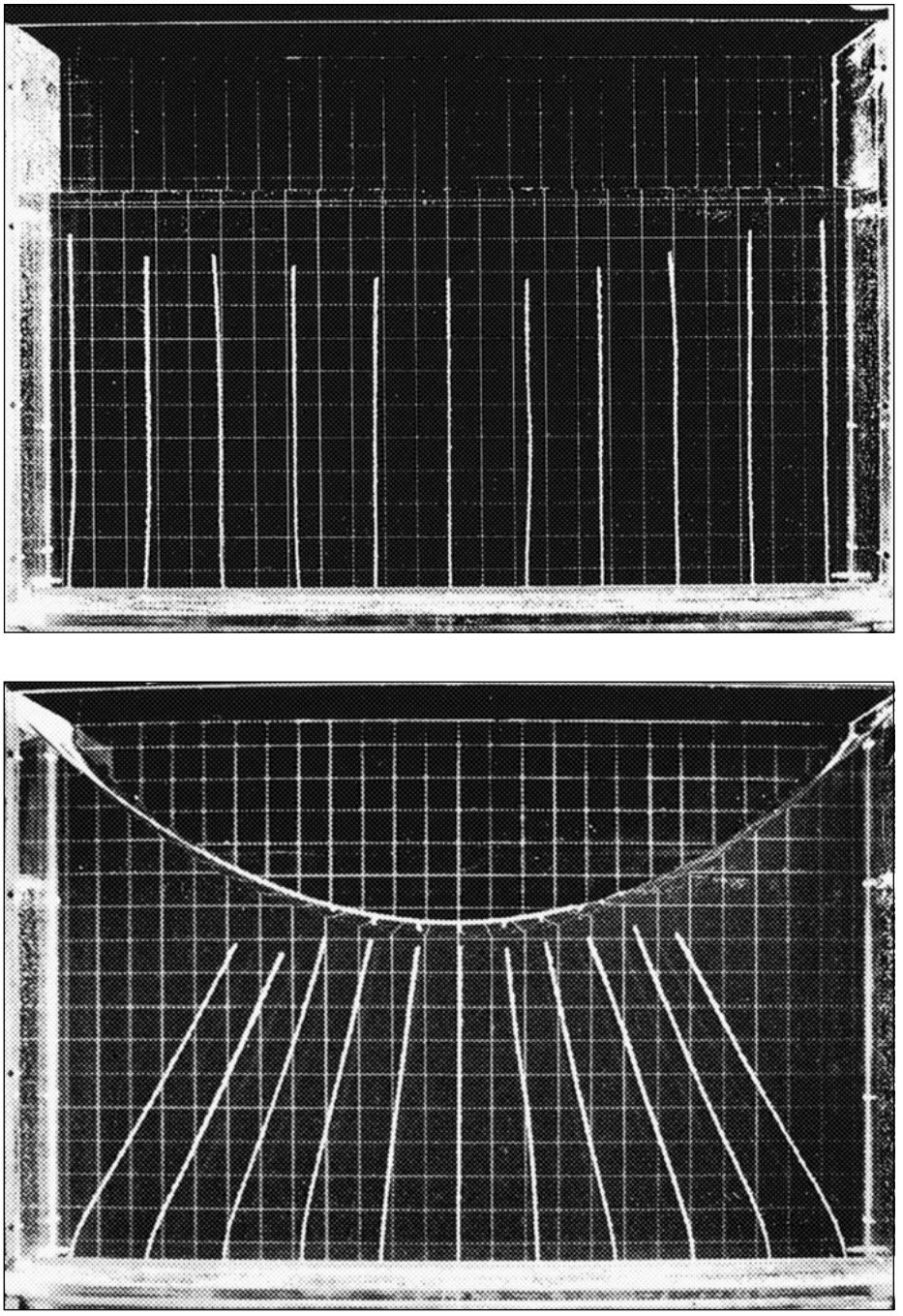


Fig. 2.24 Experimental demonstration with buoyant streamers of the fluid force field in rigid-body rotation: (*top*) fluid at rest (streamers hang vertically upward); (*bottom*) rigid-body rotation (streamers are aligned with the direction of maximum pressure gradient). (*From Ref. 5, courtesy of R. Ian Fletcher.*)



ketabline.com Ebook.ketabline.com

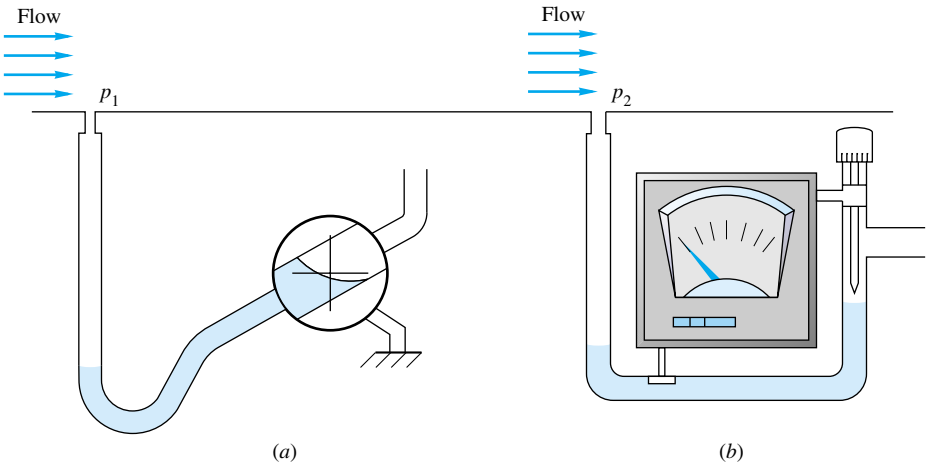


Fig. 2.25 Two types of accurate manometers for precise measurements: (*a*) tilted tube with eyepiece; (*b*) micrometer pointer with ammeter detector.

sired, a significant error is incurred by subtracting two independent measurements, and it would be far better to connect both ends of one instrument to the two static holes p_1 and p_2 so that one manometer reads the difference directly. In category 2, elastic-deformation instruments, a popular, inexpensive, and reliable device is the *bourdon tube,* sketched in Fig. 2.26. When pressurized internally, a curved tube with flattened cross section will deflect outward. The deflection can be measured by a linkage attached to a calibrated dial pointer, as shown. Or the deflection can be used to drive electric-output sensors, such as a variable transformer. Similarly, a membrane or *diaphragm* will deflect under pressure and can either be sensed directly or used to drive another sensor.

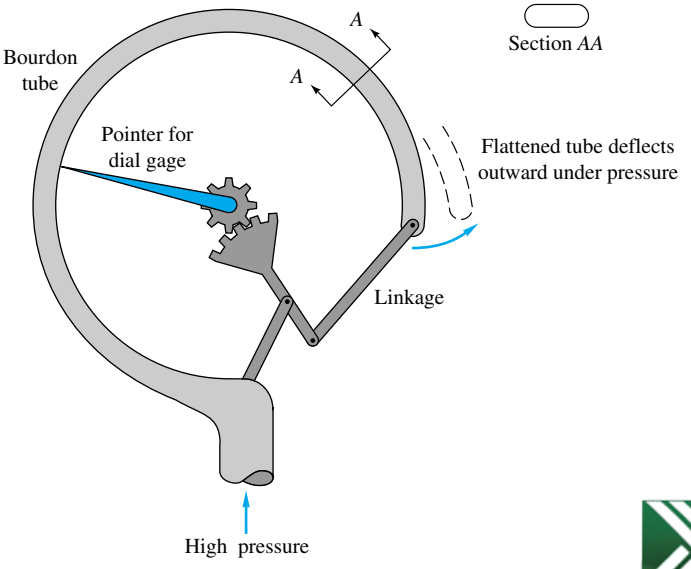


Fig. 2.26 Schematic of a bourdon-tube device for mechanical measurement of high pressures.



ketabline.com Ebook.ketabline.com

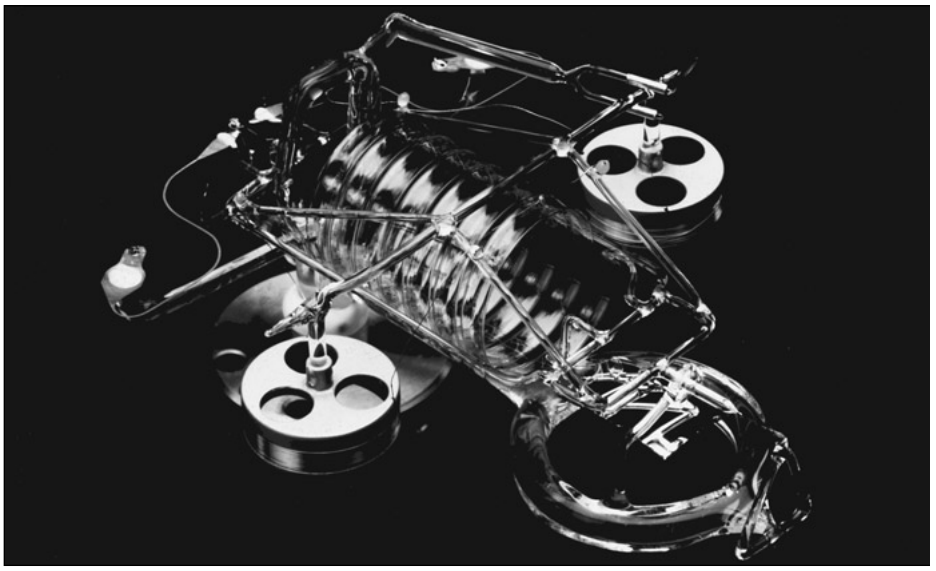


Fig. 2.27 The fused-quartz, force-balanced bourdon tube is the most accurate pressure sensor used in commercial applications today. (*Courtesy of Ruska Instrument Corporation, Houston, TX.*)

An interesting variation of Fig. 2.26 is the *fused-quartz, forced-balanced bourdon tube,* shown in Fig. 2.27, whose deflection is sensed optically and returned to a zero reference state by a magnetic element whose output is proportional to the fluid pressure. The fused-quartz, forced-balanced bourdon tube is reported to be one of the most accurate pressure sensors ever devised, with uncertainty of the order of ± 0.003 percent.

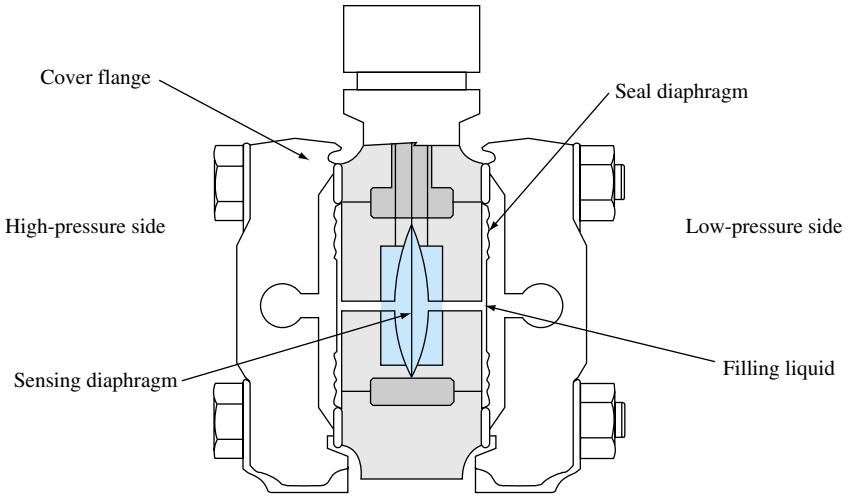
The last category, *electric-output* sensors, is extremely important in engineering because the data can be stored on computers and freely manipulated, plotted, and analyzed. Three examples are shown in Fig. 2.28, the first being the *capacitive* sensor in Fig. 2.28*a*. The differential pressure deflects the silicon diaphragm and changes the capacitancce of the liquid in the cavity. Note that the cavity has spherical end caps to prevent overpressure damage. In the second type, Fig. 2.28*b*, strain gages and other sensors are diffused or etched onto a chip which is stressed by the applied pressure. Finally, in Fig. 2.28*c*, a micromachined silicon sensor is arranged to deform under pressure such that its natural vibration frequency is proportional to the pressure. An oscillator excites the element's resonant frequency and converts it into appropriate pressure units. For further information on pressure sensors, see Refs. 7 to 10, 12, and 13.

Summary

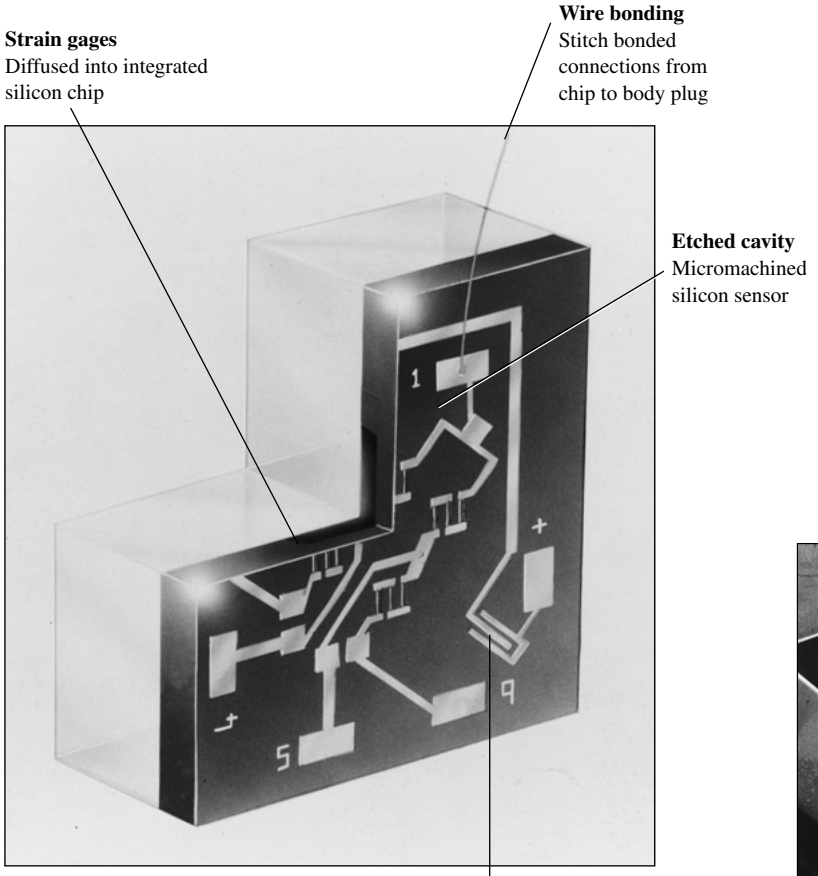
This chapter has been devoted entirely to the computation of pressure distributions and the resulting forces and moments in a static fluid or a fluid with a known velocity field. All hydrostatic (Secs. 2.3 to 2.8) and rigid-body (Sec. 2.9) problems are solved in this manner and are classic cases which every student should understand. In arbitrary viscous flows, both pressure and velocity are unknowns and are solved together as a system of equations in the chapters which follow.



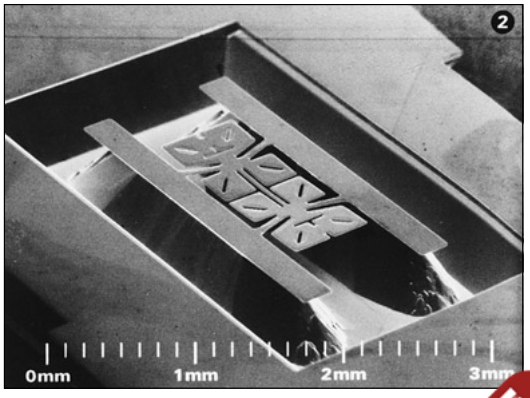
ketabline.com Ebook.ketabline.com



(*a*)



(*b*)



(*c*)

Fig. 2.28 Pressure sensors with electric output: (*a*) a silicon diaphragm whose deflection changes the cavity capacitance (*Courtesy of Johnson-Yokogawa Inc.*); (*b*) a silicon strain gage which is stressed by applied pressure; (*c*) a micromachined silicon element which resonates at a frequency proportional to applied pressure. *[(b) and (c) are courtesy of Druck, Inc., Fairfield, CT.]*

ketabline.com Ebook.ketabline.com

Problems

Most of the problems herein are fairly straightforward. More difficult or open-ended assignments are indicated with an asterisk, as in Prob. 2.8. Problems labeled with an EES icon (for example, Prob. 2.62), will benefit from the use of the Engineering Equation Solver (EES), while problems labeled with a disk icon may require the use of a computer. The standard end-of-chapter problems 2.1 to 2.158 (categorized in the problem list below) are followed by word problems W2.1 to W2.8, fundamentals of engineering exam problems FE2.1 to FE2.10, comprehensive problems C2.1 to C2.4, and design projects D2.1 and D2.2.

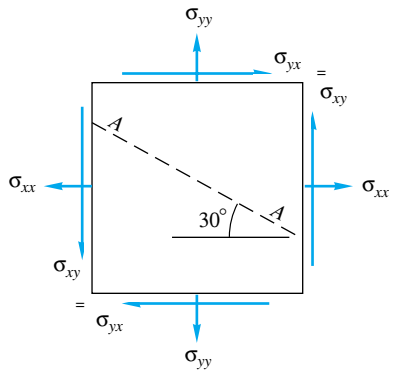
Problem Distribution

Section	Topic	Problems
2.1, 2.2	Stresses; pressure gradient; gage pressure	2.1–2.6
2.3	Hydrostatic pressure; barometers	2.7–2.23
2.3	The atmosphere	2.24–2.29
2.4	Manometers; multiple fluids	2.30–2.47
2.5	Forces on plane surfaces	2.48–2.81
2.6	Forces on curved surfaces	2.82–2.100
2.7	Forces in layered fluids	2.101–2.102
2.8	Buoyancy; Archimedes' principles	2.103–2.126
2.8	Stability of floating bodies	2.127–2.136
2.9	Uniform acceleration	2.137–2.151
2.9	Rigid-body rotation	2.152–2.158
2.10	Pressure measurements	None

P2.1 For the two-dimensional stress field shown in Fig. P2.1 it is found that

$$\sigma_{xx} = 3000 \text{ lbf/ft}^2 \quad \sigma_{yy} = 2000 \text{ lbf/ft}^2 \quad \sigma_{xy} = 500 \text{ lbf/ft}^2$$

Find the shear and normal stresses (in lbf/ft^2) acting on plane AA cutting through the element at a 30° angle as shown.



P2.1

P2.2 For the two-dimensional stress field shown in Fig. P2.1 suppose that

$$\sigma_{xx} = 2000 \text{ lbf/ft}^2 \quad \sigma_{yy} = 3000 \text{ lbf/ft}^2 \quad \sigma_n(AA) = 2500 \text{ lbf/ft}^2$$

Compute (*a*) the shear stress σ_{xy} and (*b*) the shear stress on plane AA.

P2.3 Derive Eq. (2.18) by using the differential element in Fig. 2.2 with z "up," no fluid motion, and pressure varying only in the z direction.

P2.4 In a certain two-dimensional fluid flow pattern the lines of constant pressure, or *isobars,* are defined by the expression $P_0 - Bz + Cx^2 = \text{constant}$, where B and C are constants and p_0 is the (constant) pressure at the origin, $(x, z) = (0, 0)$. Find an expression $x = f(z)$ for the family of lines which are everywhere parallel to the local pressure gradient $\overline{V}_p$.

P2.5 Atlanta, Georgia, has an average altitude of 1100 ft. On a standard day (Table A.6), pressure gage A in a laboratory experiment reads 93 kPa and gage B reads 105 kPa. Express these readings in gage pressure or vacuum pressure (Pa), whichever is appropriate.

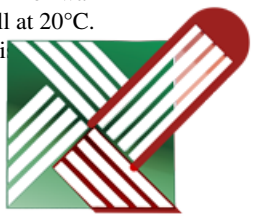
P2.6 Any pressure reading can be expressed as a length or *head,* $h = p/\rho g$. What is standard sea-level pressure expressed in (*a*) ft of ethylene glycol, (*b*) in Hg, (*c*) m of water, and (*d*) mm of methanol? Assume all fluids are at 20°C.

P2.7 The deepest known point in the ocean is 11,034 m in the Mariana Trench in the Pacific. At this depth the specific weight of seawater is approximately 10,520 N/m^3. At the surface, $\gamma \approx 10{,}050$ N/m^3. Estimate the absolute pressure at this depth, in atm.

P2.8 *Dry adiabatic lapse rate* (DALR) is defined as the negative value of atmospheric temperature gradient, dT/dz, when temperature and pressure vary in an isentropic fashion. Assuming air is an ideal gas, DALR $= -dT/dz$ when $T = T_0(p/p_0)^a$, where exponent $a = (k - 1)/k$, $k = c_p/c_v$ is the ratio of specific heats, and T_0 and p_0 are the temperature and pressure at sea level, respectively. (*a*) Assuming that hydrostatic conditions exist in the atmosphere, show that the dry adiabatic lapse rate is constant and is given by DALR $= g(k - 1)/(kR)$, where R is the ideal gas constant for air. (*b*) Calculate the numerical value of DALR for air in units of °C/km.

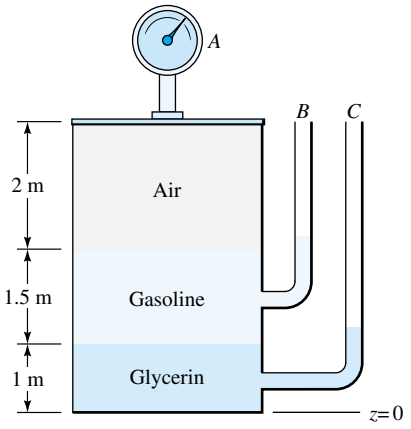
***P2.9** For a liquid, integrate the hydrostatic relation, Eq. (2.18), by assuming that the *isentropic bulk modulus,* $B = \rho(\partial p/\partial \rho)_s$, is constant—see Eq. (9.18). Find an expression for $p(z)$ and apply the Mariana Trench data as in Prob. 2.7, using $B_{seawater}$ from Table A.3.

P2.10 A closed tank contains 1.5 m of SAE 30 oil, 1 m of water, 20 cm of mercury, and an air space on top, all at 20°C. The absolute pressure at the bottom of the tank i
What is the pressure in the air space?



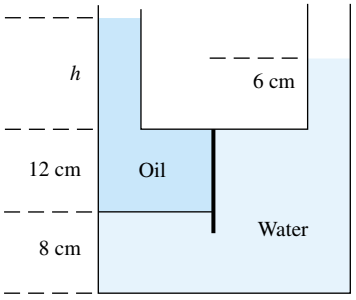
ketabline.com Ebook.ketabline.com

P2.11 In Fig. P2.11, pressure gage A reads 1.5 kPa (gage). The fluids are at 20°C. Determine the elevations z, in meters, of the liquid levels in the open piezometer tubes B and C.



P2.11

P2.12 In Fig. P2.12 the tank contains water and immiscible oil at 20°C. What is h in cm if the density of the oil is 898 kg/m^3?

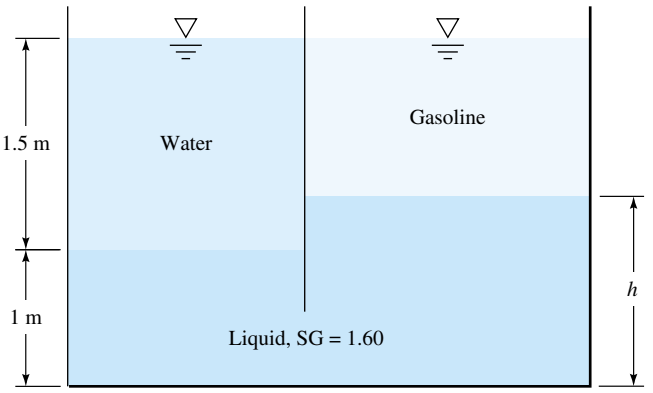


P2.12

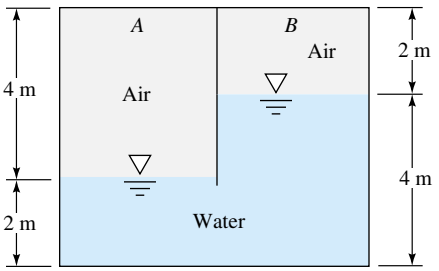
P2.13 In Fig. P2.13 the 20°C water and gasoline surfaces are open to the atmosphere and at the same elevation. What is the height h of the third liquid in the right leg?

P2.14 The closed tank in Fig. P2.14 is at 20°C. If the pressure at point A is 95 kPa absolute, what is the absolute pressure at point B in kPa? What percent error do you make by neglecting the specific weight of the air?

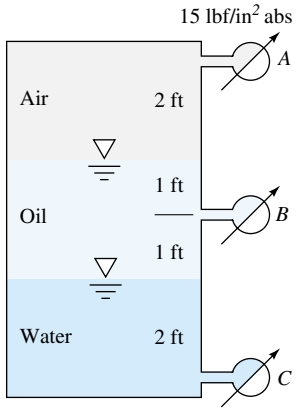
P2.15 The air-oil-water system in Fig. P2.15 is at 20°C. Knowing that gage A reads 15 lbf/in^2 absolute and gage B reads 1.25 lbf/in^2 less than gage C, compute (*a*) the specific weight of the oil in lbf/ft^3 and (*b*) the actual reading of gage C in lbf/in^2 absolute.



P2.13



P2.14



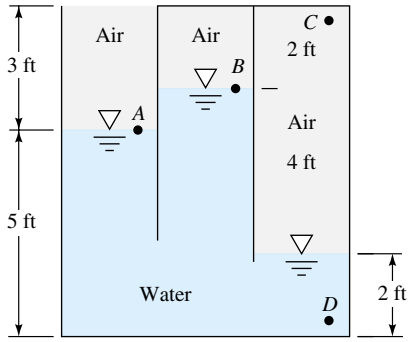
P2.15

P2.16 A closed inverted cone, 100 cm high with diameter 60 cm at the top, is filled with air at 20°C and 1 atm. Water at 20°C is introduced at the bottom (the vertex) to compress the air isothermally until a gage at the top of the cone reads 30 kPa (gage). Estimate (*a*) the amount of water need (cm^3) and (*b*) the resulting absolute p of the cone (kPa).



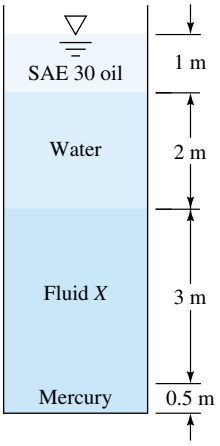
ketabline.com Ebook.ketabline.com

P2.17 The system in Fig. P2.17 is at 20°C. If the pressure at point A is 1900 lbf/ft^2, determine the pressures at points B, C, and D in lbf/ft^2.



P2.17

P2.18 The system in Fig. P2.18 is at 20°C. If atmospheric pressure is 101.33 kPa and the pressure at the bottom of the tank is 242 kPa, what is the specific gravity of fluid X?

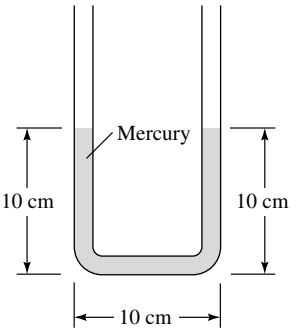


P2.18

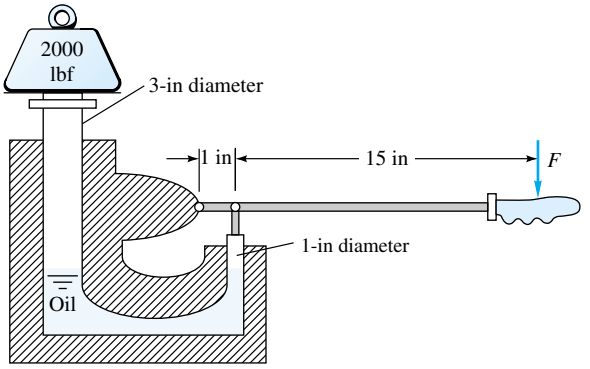
P2.19 The U-tube in Fig. P2.19 has a 1-cm ID and contains mercury as shown. If 20 cm^3 of water is poured into the right-hand leg, what will the free-surface height in each leg be after the sloshing has died down?

P2.20 The hydraulic jack in Fig. P2.20 is filled with oil at 56 lbf/ft^3. Neglecting the weight of the two pistons, what force F on the handle is required to support the 2000-lbf weight for this design?

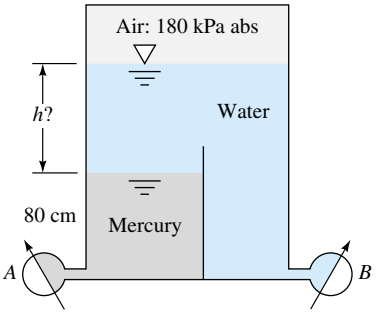
P2.21 At 20°C gage A reads 350 kPa absolute. What is the height h of the water in cm? What should gage B read in kPa absolute? See Fig. P2.21.



P2.19



P2.20



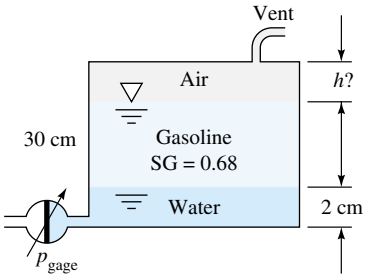
P2.21

P2.22 The fuel gage for a gasoline tank in a car reads proportional to the bottom gage pressure as in Fig. P2.22. If the tank is 30 cm deep and accidentally contains 2 cm of water plus gasoline, how many centimeters of air remain at the top when the gage erroneously reads "full"?

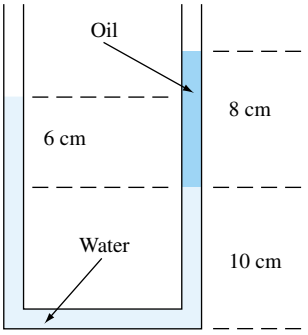
P2.23 In Fig. P2.23 both fluids are at 20°C. If surface tension effects are negligible, what is the density of the oil, in kg/m^3?

P2.24 In Prob. 1.2 we made a crude integration of the density distribution $\rho(z)$ in Table A.6 and estimated the the earth's atmosphere to be $m \approx 6$ E18 kg. Ca

ketabline.com Ebook.ketabline.com



P2.22



P2.23

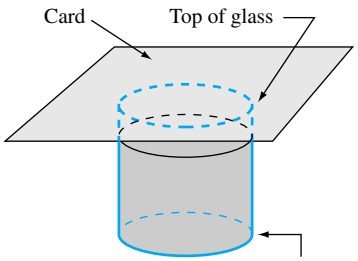
sult be used to estimate sea-level pressure on the earth? Conversely, can the actual sea-level pressure of 101.35 kPa be used to make a more accurate estimate of the atmospheric mass?

P2.25 Venus has a mass of 4.90 E24 kg and a radius of 6050 km. Its atmosphere is 96 percent CO_2, but let us assume it to be 100 percent. Its surface temperature averages 730 K, decreasing to 250 K at an altitude of 70 km. The average surface pressure is 9.1 MPa. Estimate the atmospheric pressure of Venus at an altitude of 5 km.

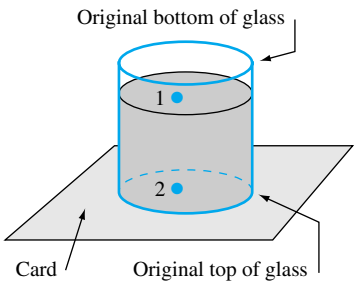
P2.26 Investigate the effect of doubling the lapse rate on atmospheric pressure. Compare the standard atmosphere (Table A.6) with a lapse rate twice as high, $B_2 = 0.0130$ K/m. Find the altitude at which the pressure deviation is (a) 1 percent and (b) 5 percent. What do you conclude?

P2.27 Conduct an experiment to illustrate atmospheric pressure. *Note:* Do this over a sink or you may get wet! Find a drinking glass with a very smooth, uniform rim at the top. Fill the glass nearly full with water. Place a smooth, light, flat plate on top of the glass such that the entire rim of the glass is covered. A glossy postcard works best. A small index card or one flap of a greeting card will also work. See Fig. P2.27*a*.

(*a*) Hold the card against the rim of the glass and turn the glass upside down. Slowly release pressure on the card. Does the water fall out of the glass? Record your experimental observations. (*b*) Find an expression for the pressure at points 1 and 2 in Fig. P2.27*b*. Note that the glass is now inverted, so the original top rim of the glass is at the bottom of the picture, and the original bottom of the glass is at the top of the picture. The weight of the card can be neglected.



P2.27a



P2.27b

(*c*) Estimate the theoretical maximum glass height such that this experiment could still work, i.e., such that the water would not fall out of the glass.

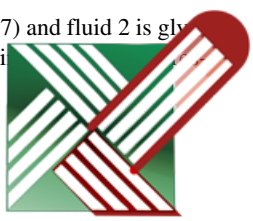
P2.28 Earth's atmospheric conditions vary somewhat. On a certain day the sea-level temperature is 45°F and the sea-level pressure is 28.9 inHg. An airplane overhead registers an air temperature of 23°F and a pressure of 12 lbf/in^2. Estimate the plane's altitude, in feet.

***P2.29** Under some conditions the atmosphere is *adiabatic*, $p \approx (\text{const})(\rho^k)$, where k is the specific heat ratio. Show that, for an adiabatic atmosphere, the pressure variation is given by

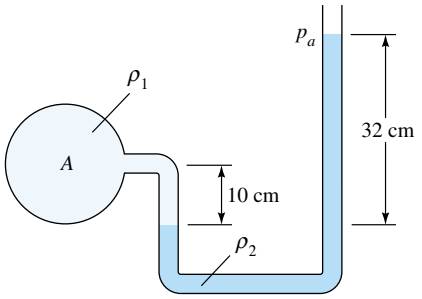
$$p = p_0\left[1 - \frac{(k-1)gz}{kRT_0}\right]^{k/(k-1)}$$

Compare this formula for air at $z = 5000$ m with the standard atmosphere in Table A.6.

P2.30 In Fig. P2.30 fluid 1 is oil (SG = 0.87) and fluid 2 is gly
erin at 20°C. If $p_a = 98$ kPa, determi
sure at point A.

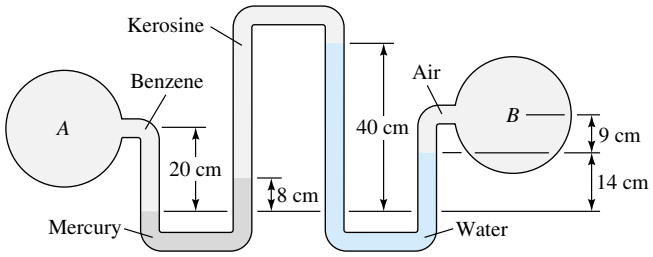


ketabline.com Ebook.ketabline.com



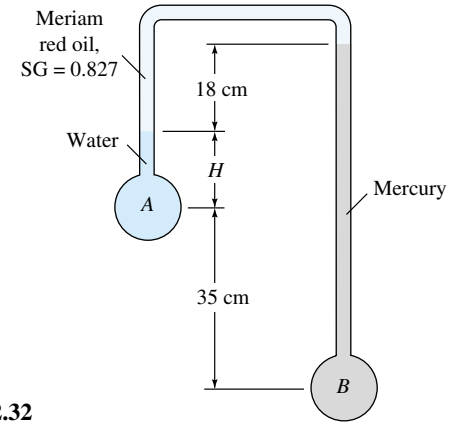
P2.30

P2.31 In Fig. P2.31 all fluids are at 20°C. Determine the pressure difference (Pa) between points A and B.



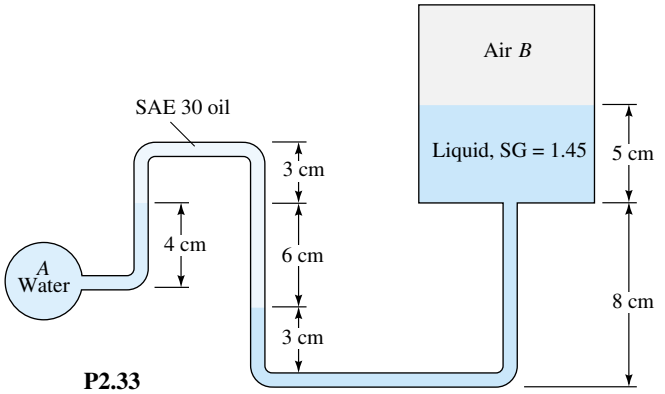
P2.31

P2.32 For the inverted manometer of Fig. P2.32, all fluids are at 20°C. If $p_B - p_A = 97$ kPa, what must the height H be in cm?



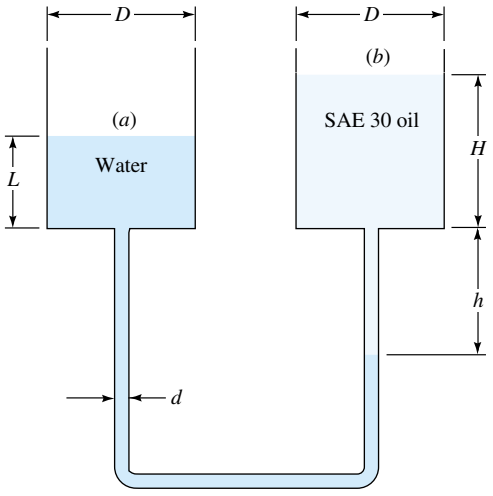
P2.32

P2.33 In Fig. P2.33 the pressure at point A is 25 lbf/in^2. All fluids are at 20°C. What is the air pressure in the closed chamber B, in Pa?



P2.33

***P2.34** Sometimes manometer dimensions have a significant effect. In Fig. P2.34 containers (*a*) and (*b*) are cylindrical and conditions are such that $p_a = p_b$. Derive a formula for the pressure difference $p_a - p_b$ when the oil-water interface on the right rises a distance $\Delta h < h$, for (*a*) $d \ll D$ and (*b*) $d = 0.15D$. What is the percent change in the value of Δp?



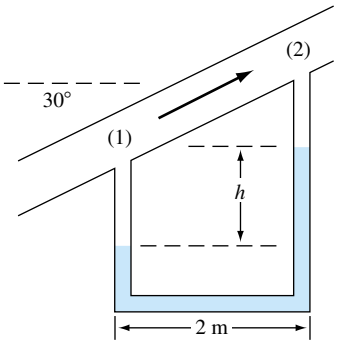
P2.34

P2.35 Water flows upward in a pipe slanted at 30°, as in Fig. P2.35. The mercury manometer reads $h = 12$ cm. Both fluids are at 20°C. What is the pressure difference $p_1 - p_2$ in the pipe?

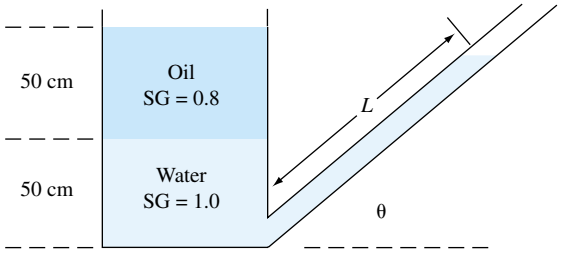
P2.36 In Fig. P2.36 both the tank and the tube are open to the atmosphere. If $L = 2.13$ m, what is the angle of tilt θ of the tube?

P2.37 The inclined manometer in Fig. P2.37 contains red manometer oil, SG = 0.827. Assume that the

ketabline.com Ebook.ketabline.com

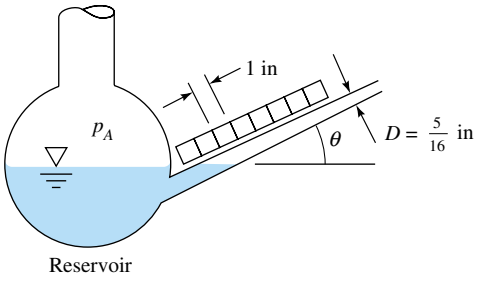


P2.35



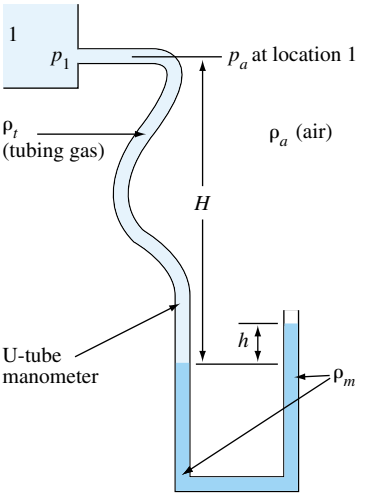
P2.36

is very large. If the inclined arm is fitted with graduations 1 in apart, what should the angle θ be if each graduation corresponds to 1 lbf/ft^2 gage pressure for p_A?



P2.37

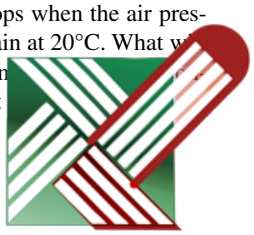
P2.38 An interesting article appeared in the *AIAA Journal* (vol. 30, no. 1, January 1992, pp. 279–280). The authors explain that the air inside fresh plastic tubing can be up to 25 percent more dense than that of the surroundings, due to outgassing or other contaminants introduced at the time of manufacture. Most researchers, however, assume that the tubing is filled with room air at standard air density, which can lead to significant errors when using this kind of tubing to measure pressures. To illustrate this, consider a U-tube manometer with manometer fluid ρ_m. One side of the manometer is open to the air, while the other is connected to new tubing which extends to pressure measurement location 1, some height H higher in elevation than the surface of the manometer liquid. For consistency, let ρ_a be the density of the air in the room, ρ_t be the density of the gas inside the tube, ρ_m be the density of the manometer liquid, and h be the height difference between the two sides of the manometer. See Fig. P2.38. (*a*) Find an expression for the gage pressure at the measurement point. *Note:* When calculating gage pressure, use the local atmospheric pressure at the elevation of the measurement point. You may assume that $h \ll H$; i.e., assume the gas in the entire left side of the manometer is of density ρ_t. (*b*) Write an expression for the error caused by assuming that the gas inside the tubing has the same density as that of the surrounding air. (*c*) How much error (in Pa) is caused by ignoring this density difference for the following conditions: $\rho_m = 860$ kg/m^3, $\rho_a = 1.20$ kg/m^3, $\rho_t = 1.50$ kg/m^3, $H = 1.32$ m, and $h = 0.58$ cm? (*d*) Can you think of a simple way to avoid this error?



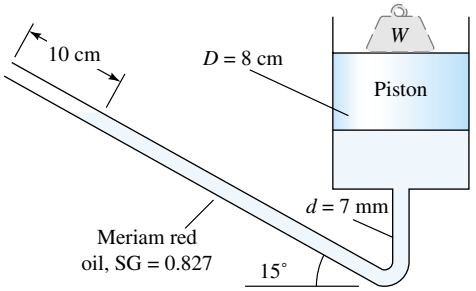
P2.38

P2.39 An 8-cm-diameter piston compresses manometer oil into an inclined 7-mm-diameter tube, as shown in Fig. P2.39. When a weight W is added to the top of the piston, the oil rises an additional distance of 10 cm up the tube, as shown. How large is the weight, in N?

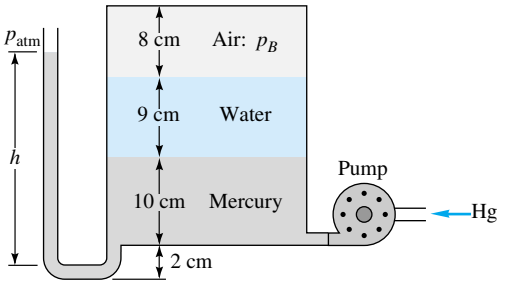
P2.40 A pump slowly introduces mercury into the bottom of the closed tank in Fig. P2.40. At the instant shown, the air pressure $p_B = 80$ kPa. The pump stops when the air pressure rises to 110 kPa. All fluids remain at 20°C. What will be the manometer reading h at that time? The tank is connected to standard sea-level ambient



ketabline.com Ebook.ketabline.com

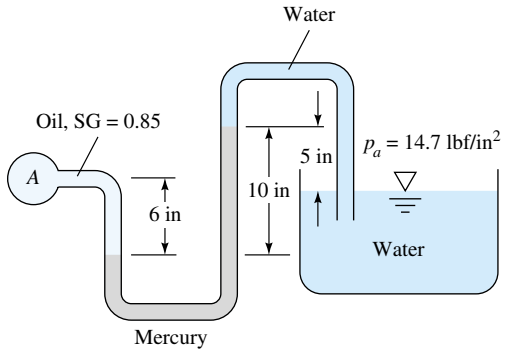


P2.39



P2.40

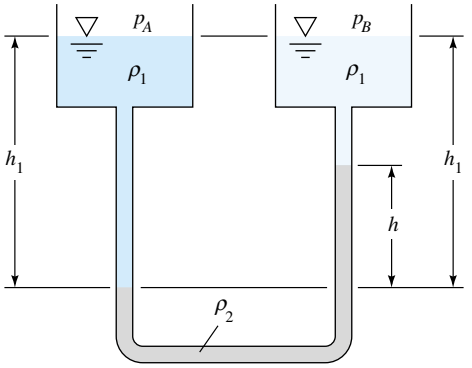
P2.41 The system in Fig. P2.41 is at 20°C. Compute the pressure at point A in lbf/ft^2 absolute.



P2.41

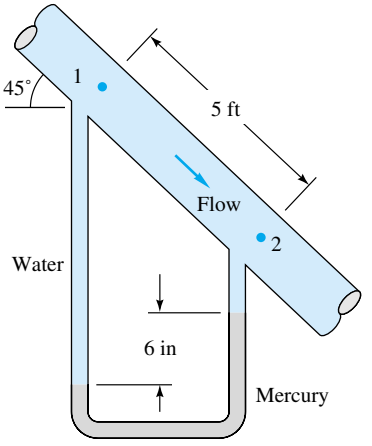
P2.42 Very small pressure differences $p_A - p_B$ can be measured accurately by the two-fluid differential manometer in Fig. P2.42. Density ρ_2 is only slightly larger than that of the upper fluid ρ_1. Derive an expression for the proportionality between h and $p_A - p_B$ if the reservoirs are very large.

***P2.43** A mercury manometer, similar to Fig. P2.35, records $h \approx$ 1.2, 4.9, and 11.0 mm when the water velocities in the pipe are V = 1.0, 2.0, and 3.0 m/s, respectively. Determine if these data can be correlated in the form $p_1 - p_2 \approx C_f \rho V^2$, where C_f is dimensionless.



P2.42

P2.44 Water flows downward in a pipe at 45°, as shown in Fig. P2.44. The pressure drop $p_1 - p_2$ is partly due to gravity and partly due to friction. The mercury manometer reads a 6-in height difference. What is the total pressure drop $p_1 - p_2$ in lbf/in^2? What is the pressure drop due to friction only between 1 and 2 in lbf/in^2? Does the manometer reading correspond only to friction drop? Why?



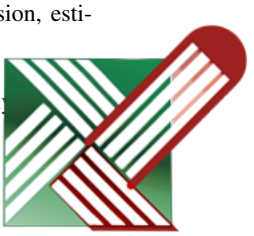
P2.44

P2.45 In Fig. P2.45, determine the gage pressure at point A in Pa. Is it higher or lower than atmospheric?

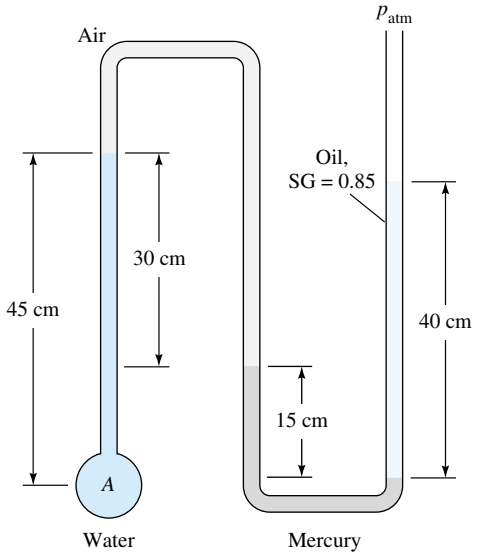
P2.46 In Fig. P2.46 both ends of the manometer are open to the atmosphere. Estimate the specific gravity of fluid X.

P2.47 The cylindrical tank in Fig. P2.47 is being filled with water at 20°C by a pump developing an exit pressure of 175 kPa. At the instant shown, the air pressure is 110 kPa and H = 35 cm. The pump stops when it can no longer raise the water pressure. For isothermal air compression, estimate H at that time.

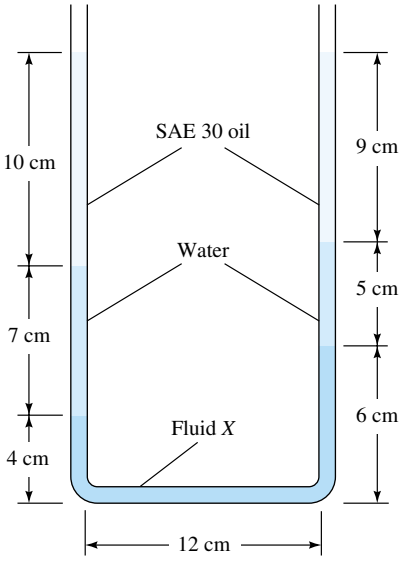
P2.48 Conduct the following experiment to illustrate
sure. Find a thin wooden ruler (approximately



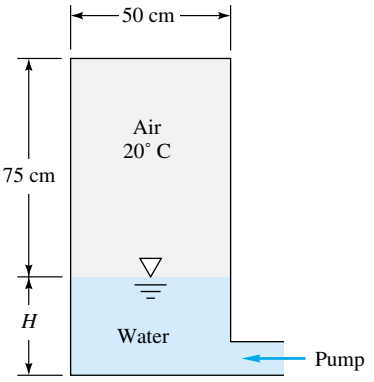
ketabline.com Ebook.ketabline.com



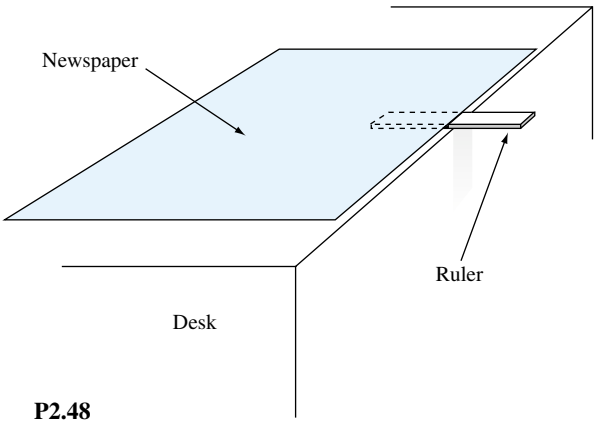
P2.45



P2.46



P2.47



P2.48

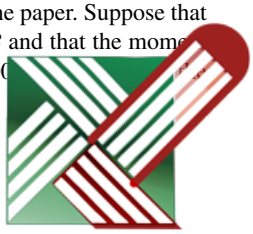
length) or a thin wooden paint stirrer. Place it on the edge of a desk or table with a little less than half of it hanging over the edge lengthwise. Get two full-size sheets of newspaper; open them up and place them on top of the ruler, covering only the portion of the ruler resting on the desk as illustrated in Fig. P2.48. (*a*) Estimate the total force on top of the newspaper due to air pressure in the room. (*b*) *Careful*! To avoid potential injury, make sure nobody is standing directly in front of the desk. Perform a karate chop on the portion of the ruler sticking out over the edge of the desk. Record your results. (*c*) Explain your results.

P2.49 A water tank has a circular panel in its vertical wall. The panel has a radius of 50 cm, and its center is 2 m below the surface. Neglecting atmospheric pressure, determine the water force on the panel and its line of action.

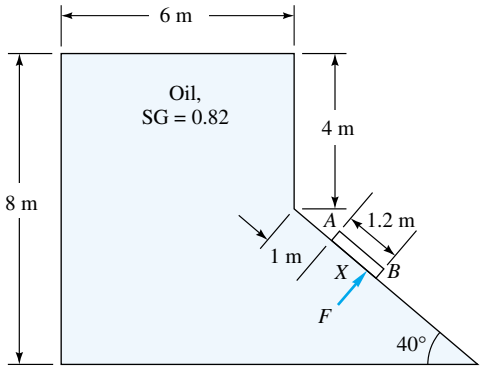
P2.50 A vat filled with oil (SG = 0.85) is 7 m long and 3 m deep and has a trapezoidal cross section 2 m wide at the bottom and 4 m wide at the top. Compute (*a*) the weight of oil in the vat, (*b*) the force on the vat bottom, and (*c*) the force on the trapezoidal end panel.

P2.51 Gate *AB* in Fig. P2.51 is 1.2 m long and 0.8 m into the paper. Neglecting atmospheric pressure, compute the force *F* on the gate and its center-of-pressure position *X*.

***P2.52** Suppose that the tank in Fig. P2.51 is filled with liquid *X*, not oil. Gate *AB* is 0.8 m wide into the paper. Suppose that liquid *X* causes a force *F* on gate *AB* and that the mome of this force about point *B* is 26,500 specific gravity of liquid *X*?

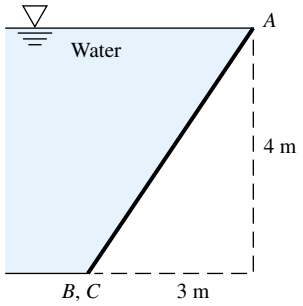


ketabline.com Ebook.ketabline.com



P2.51

P2.53 Panel *ABC* in the slanted side of a water tank is an isosceles triangle with the vertex at *A* and the base $BC = 2$ m, as in Fig. P2.53. Find the water force on the panel and its line of action.



P2.53

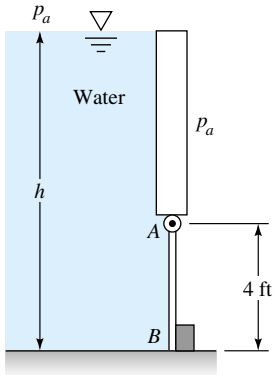
P2.54 If, instead of water, the tank in Fig. P2.53 is filled with liquid *X*, the liquid force on panel *ABC* is found to be 115 kN. What is the density of liquid *X*? The line of action is found to be the same as in Prob. 2.53. Why?

P2.55 Gate *AB* in Fig. P2.55 is 5 ft wide into the paper, hinged at *A*, and restrained by a stop at *B*. The water is at 20°C. Compute (*a*) the force on stop *B* and (*b*) the reactions at *A* if the water depth $h = 9.5$ ft.

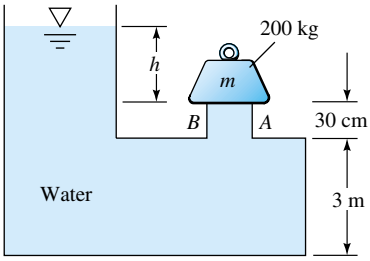
P2.56 In Fig. P2.55, gate *AB* is 5 ft wide into the paper, and stop *B* will break if the water force on it equals 9200 lbf. For what water depth *h* is this condition reached?

P2.57 In Fig. P2.55, gate *AB* is 5 ft wide into the paper. Suppose that the fluid is liquid *X*, not water. Hinge *A* breaks when its reaction is 7800 lbf, and the liquid depth is $h = 13$ ft. What is the specific gravity of liquid *X*?

P2.58 In Fig. P2.58, the cover gate *AB* closes a circular opening 80 cm in diameter. The gate is held closed by a 200-kg mass as shown. Assume standard gravity at 20°C. At what water level *h* will the gate be dislodged? Neglect the weight of the gate.

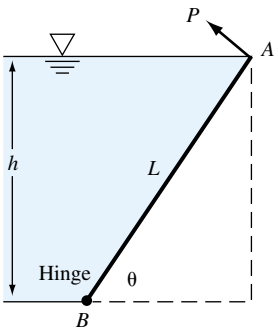


P2.55



P2.58

***P2.59** Gate AB has length *L*, width *b* into the paper, is hinged at B, and has negligible weight. The liquid level *h* remains at the top of the gate for any angle θ. Find an analytic expression for the force *P*, perpendicular to AB, required to keep the gate in equilibrium in Fig. P2.59.



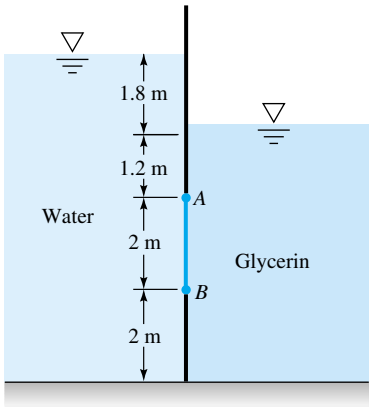
P2.59

***P2.60** Find the net hydrostatic force per unit width on the rectangular gate *AB* in Fig. P2.60 and its line of action.

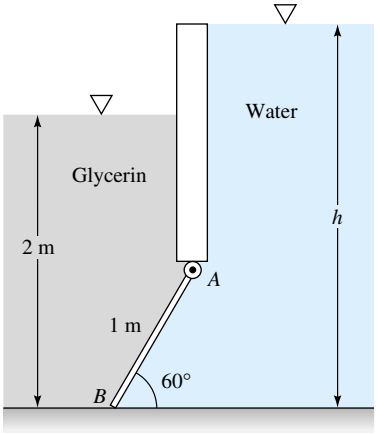
***P2.61** Gate *AB* in Fig. P2.61 is a homogeneous mass of 180 kg, 1.2 m wide into the paper, hinged at *A*, and resting on a smooth bottom at *B*. All fluids are at 20°C. For what water depth *h* will the force at point *B* be zero?



ketabline.com Ebook.ketabline.com

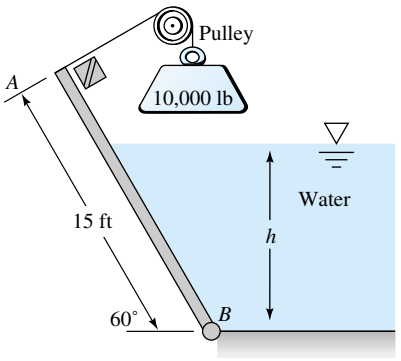


P2.60



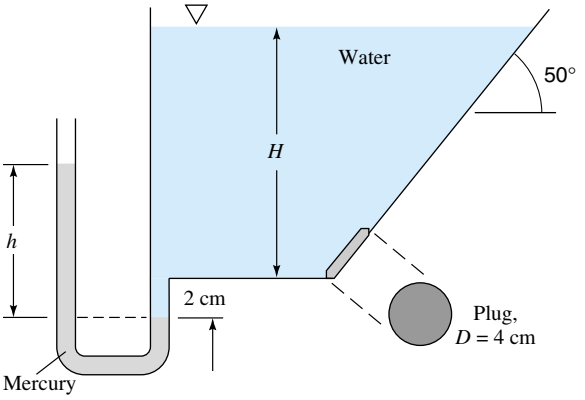
P2.61

P2.62 Gate AB in Fig. P2.62 is 15 ft long and 8 ft wide into the paper and is hinged at B with a stop at A. The water is at 20°C. The gate is 1-in-thick steel, SG = 7.85. Compute the water level h for which the gate will start to fall.



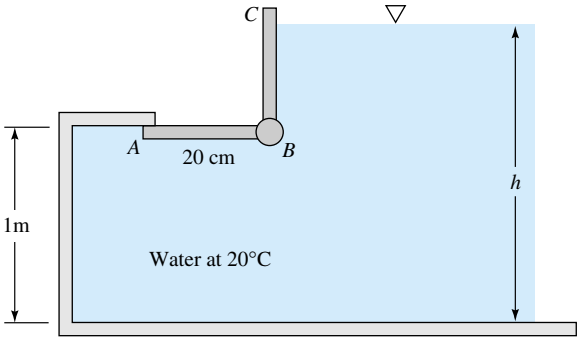
P2.62

P2.63 The tank in Fig. P2.63 has a 4-cm-diameter plug at the bottom on the right. All fluids are at 20°C. The plug will pop out if the hydrostatic force on it is 25 N. For this condition, what will be the reading h on the mercury manometer on the left side?



P2.63

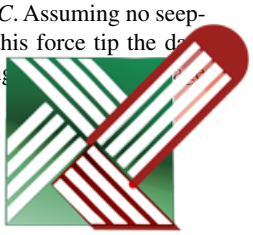
***P2.64** Gate ABC in Fig. P2.64 has a fixed hinge line at B and is 2 m wide into the paper. The gate will open at A to release water if the water depth is high enough. Compute the depth h for which the gate will begin to open.



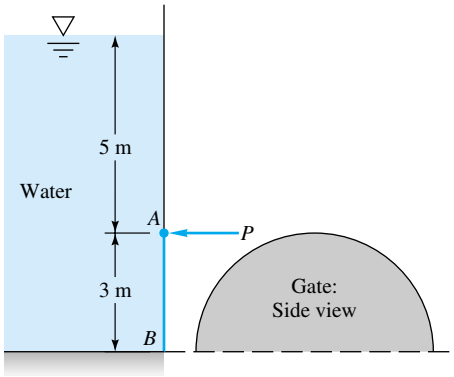
P2.64

***P2.65** Gate AB in Fig. P2.65 is semicircular, hinged at B, and held by a horizontal force P at A. What force P is required for equilibrium?

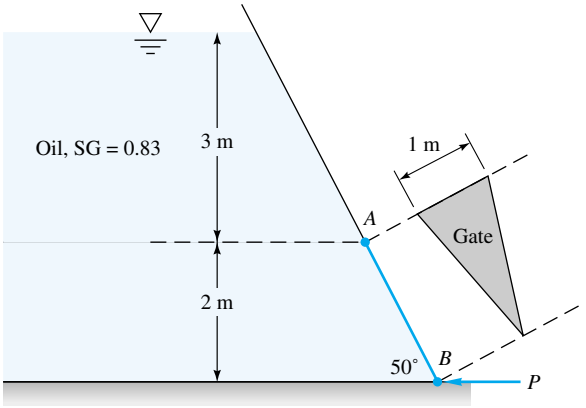
P2.66 Dam ABC in Fig. P2.66 is 30 m wide into the paper and made of concrete (SG = 2.4). Find the hydrostatic force on surface AB and its moment about C. Assuming no seepage of water under the dam, could this force tip the da over? How does your argument chang under the dam?



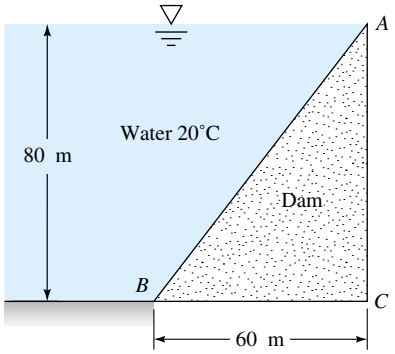
ketabline.com Ebook.ketabline.com



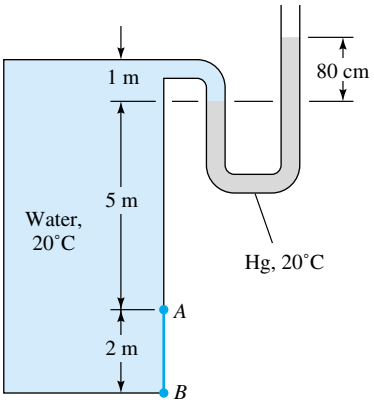
P2.65



P2.68



P2.66



P2.69

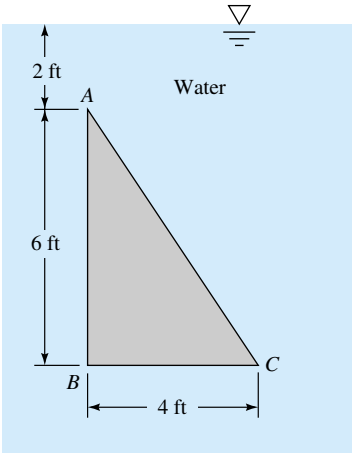
***P2.67** Generalize Prob. 2.66 as follows. Denote length AB as H, length BC as L, and angle ABC as θ. Let the dam material have specific gravity SG. The width of the dam is b. Assume no seepage of water under the dam. Find an analytic relation between SG and the critical angle θ_c for which the dam will just tip over to the right. Use your relation to compute θ_c for the special case SG = 2.4 (concrete).

P2.68 Isosceles triangle gate AB in Fig. P2.68 is hinged at A and weighs 1500 N. What horizontal force P is required at point B for equilibrium?

***P2.69** The water tank in Fig. P2.69 is pressurized, as shown by the mercury-manometer reading. Determine the hydrostatic force per unit depth on gate AB.

P2.70 Calculate the force and center of pressure on one side of the vertical triangular panel ABC in Fig. P2.70. Neglect p_{atm}.

***P2.71** In Fig. P2.71 gate AB is 3 m wide into the paper and is connected by a rod and pulley to a concrete sphere (SG =

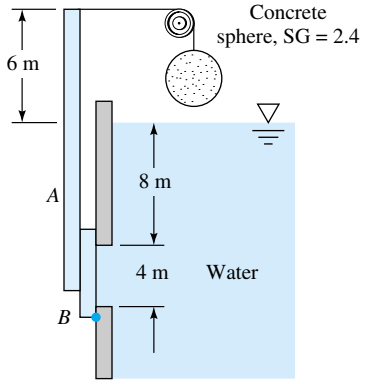


P2.70



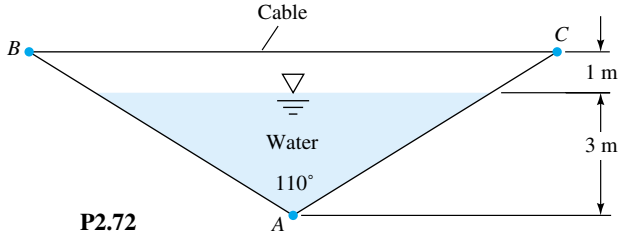
ketabline.com Ebook.ketabline.com

2.40). What diameter of the sphere is just sufficient to keep the gate closed?



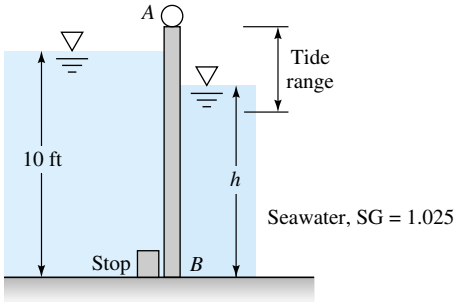
P2.71

P2.72 The V-shaped container in Fig. P2.72 is hinged at A and held together by cable BC at the top. If cable spacing is 1 m into the paper, what is the cable tension?



P2.72

P2.73 Gate AB is 5 ft wide into the paper and opens to let fresh water out when the ocean tide is dropping. The hinge at A is 2 ft above the freshwater level. At what ocean level h will the gate first open? Neglect the gate weight.



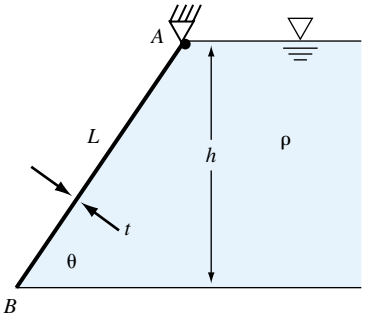
P2.73

***P2.74** In "soft" liquids (low bulk modulus β), it may be necessary to account for liquid compressibility in hydrostatic calculations. An approximate density relation would be

$$dp \approx \frac{\beta}{\rho}\, d\rho = a^2\, d\rho \qquad \text{or} \qquad p \approx p_0 + a^2(\rho - \rho_0)$$

where a is the speed of sound and (p_0, ρ_0) are the conditions at the liquid surface $z = 0$. Use this approximation to show that the density variation with depth in a soft liquid is $\rho = \rho_0 e^{-gz/a^2}$ where g is the acceleration of gravity and z is positive upward. Then consider a vertical wall of width b, extending from the surface ($z = 0$) down to depth $z = -h$. Find an analytic expression for the hydrostatic force F on this wall, and compare it with the incompressible result $F = \rho_0 g h^2 b/2$. Would the center of pressure be below the incompressible position $z = -2h/3$?

***P2.75** Gate AB in Fig. P2.75 is hinged at A, has width b into the paper, and makes smooth contact at B. The gate has density ρ_s and uniform thickness t. For what gate density ρ_s, expressed as a function of (h, t, ρ, θ), will the gate just begin to lift off the bottom? Why is your answer independent of gate length L and width b?



P2.75

***P2.76** Consider the angled gate ABC in Fig. P2.76, hinged at C and of width b into the paper. Derive an analytic formula for the horizontal force P required at the top for equilibrium, as a function of the angle θ.

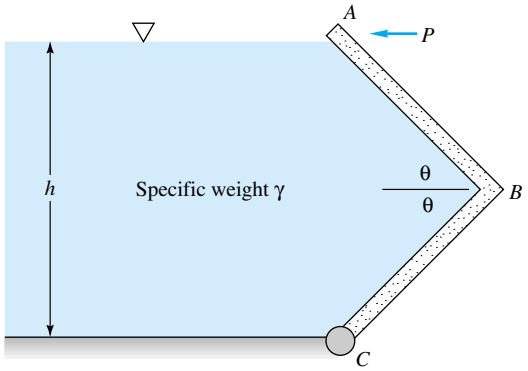
P2.77 The circular gate ABC in Fig. P2.77 has a 1-m radius and is hinged at B. Compute the force P just sufficient to keep the gate from opening when $h = 8$ m. Neglect atmospheric pressure.

P2.78 Repeat Prob. 2.77 to derive an analytic expression for P as a function of h. Is there anything unusual about your solution?

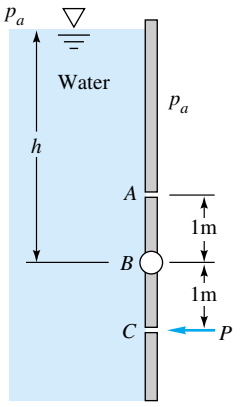
P2.79 Gate ABC in Fig. P2.79 is 1 m square and is hinged at
It will open automatically when the w
high enough. Determine the lowest



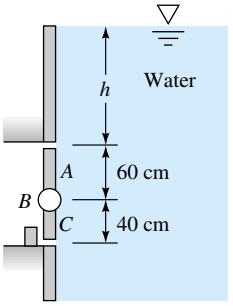
ketabline.com Ebook.ketabline.com



P2.76



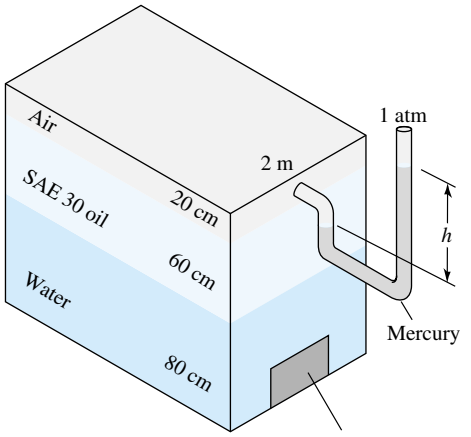
P2.77



P2.79

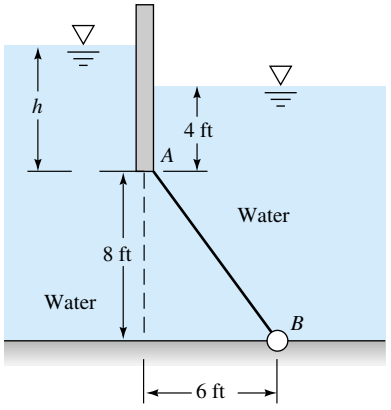
gate will open. Neglect atmospheric pressure. Is this result independent of the liquid density?

P2.80 For the closed tank in Fig. P2.80, all fluids are at 20°C, and the airspace is pressurized. It is found that the net outward hydrostatic force on the 30-by 40-cm panel at the bottom of the water layer is 8450 N. Estimate (*a*) the pressure in the airspace and (*b*) the reading *h* on the mercury manometer.



P2.80

P2.81 Gate *AB* in Fig. P2.81 is 7 ft into the paper and weighs 3000 lbf when submerged. It is hinged at *B* and rests against a smooth wall at *A*. Determine the water level *h* at the left which will just cause the gate to open.

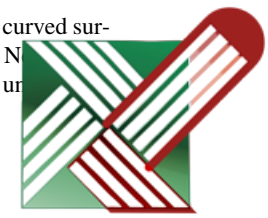


P2.81

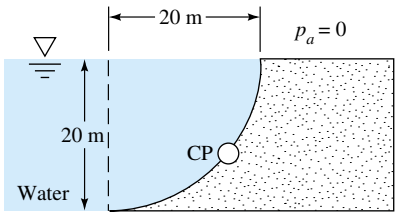
***P2.82** The dam in Fig. P2.82 is a quarter circle 50 m wide into the paper. Determine the horizontal and vertical components of the hydrostatic force against the dam and the point CP where the resultant strikes the dam.

***P2.83** Gate *AB* in Fig. P2.83 is a quarter circle 10 ft wide into the paper and hinged at *B*. Find the force *F* just sufficient to keep the gate from opening. The gate is uniform and weighs 3000 lbf.

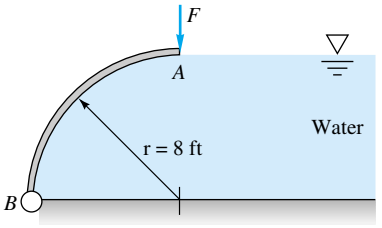
P2.84 Determine (*a*) the total hydrostatic force on the curved surface *AB* in Fig. P2.84 and (*b*) its line of action. N
mospheric pressure, and let the surface have ur



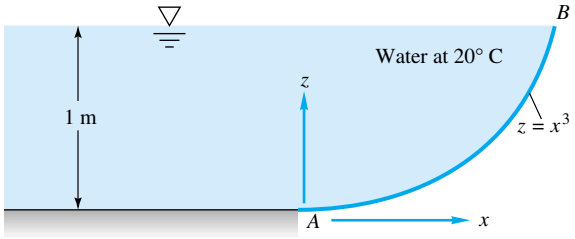
ketabline.com Ebook.ketabline.com



P2.82

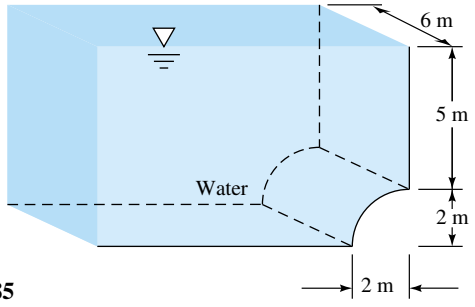


P2.83



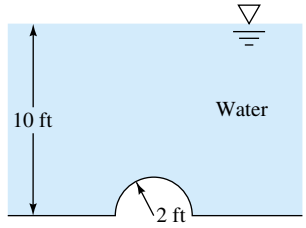
P2.84

P2.85 Compute the horizontal and vertical components of the hydrostatic force on the quarter-circle panel at the bottom of the water tank in Fig. P2.85.



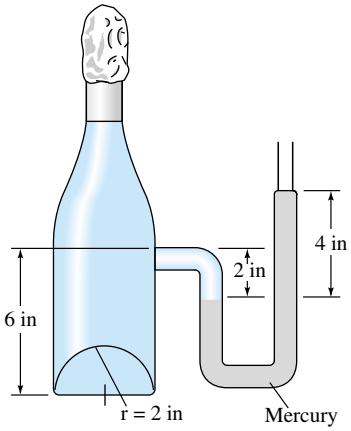
P2.85

P2.86 Compute the horizontal and vertical components of the hydrostatic force on the hemispherical bulge at the bottom of the tank in Fig. P2.86.



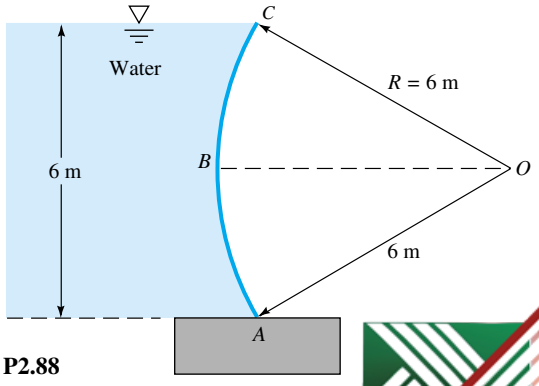
P2.86

P2.87 The bottle of champagne (SG = 0.96) in Fig. P2.87 is under pressure, as shown by the mercury-manometer reading. Compute the net force on the 2-in-radius hemispherical end cap at the bottom of the bottle.



P2.87

***P2.88** Gate *ABC* is a circular arc, sometimes called a *Tainter gate*, which can be raised and lowered by pivoting about point *O*. See Fig. P2.88. For the position shown, determine (*a*) the hydrostatic force of the water on the gate and (*b*) its line of action. Does the force pass through point *O*?

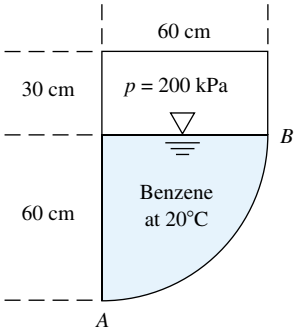


P2.88



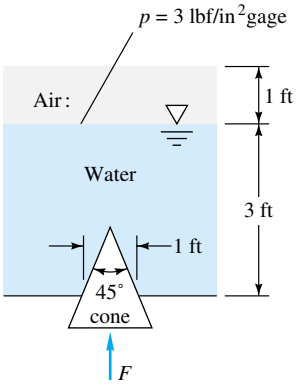
ketabline.com Ebook.ketabline.com

P2.89 The tank in Fig. P2.89 contains benzene and is pressurized to 200 kPa (gage) in the air gap. Determine the vertical hydrostatic force on circular-arc section *AB* and its line of action.



P2.89

P2.90 A 1-ft-diameter hole in the bottom of the tank in Fig. P2.90 is closed by a conical 45° plug. Neglecting the weight of the plug, compute the force F required to keep the plug in the hole.

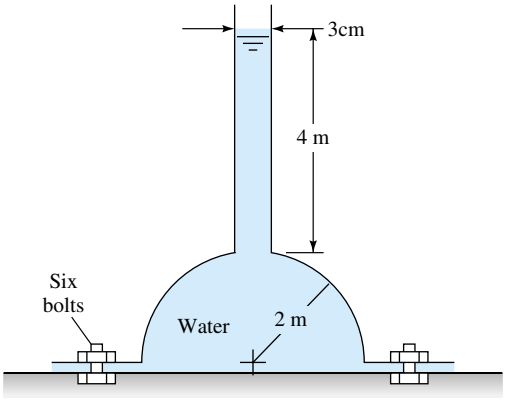


P2.90

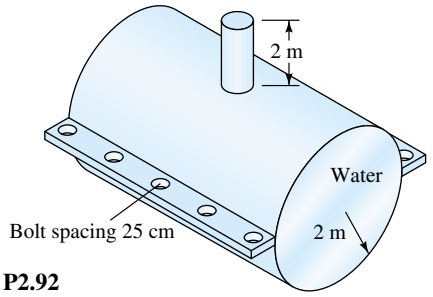
P2.91 The hemispherical dome in Fig. P2.91 weighs 30 kN and is filled with water and attached to the floor by six equally spaced bolts. What is the force in each bolt required to hold down the dome?

P2.92 A 4-m-diameter water tank consists of two half cylinders, each weighing 4.5 kN/m, bolted together as shown in Fig. P2.92. If the support of the end caps is neglected, determine the force induced in each bolt.

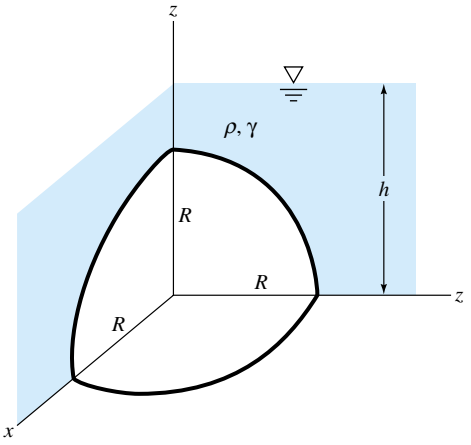
***P2.93** In Fig. P2.93, a one-quadrant spherical shell of radius R is submerged in liquid of specific gravity γ and depth $h > R$. Find an analytic expression for the resultant hydrostatic force, and its line of action, on the shell surface.



P2.91



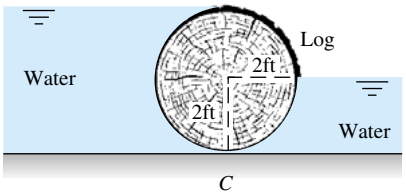
P2.92



P2.93

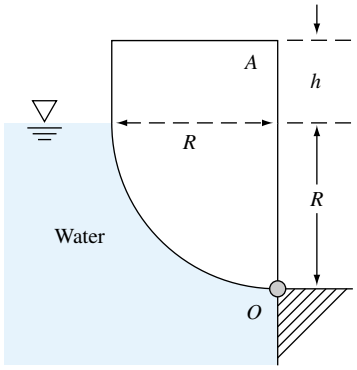
P2.94 The 4-ft-diameter log (SG = 0.80) in Fig. P2.94 is 8 ft long into the paper and dams water as shown. the net vertical and horizontal reactions at point

ketabline.com Ebook.ketabline.com



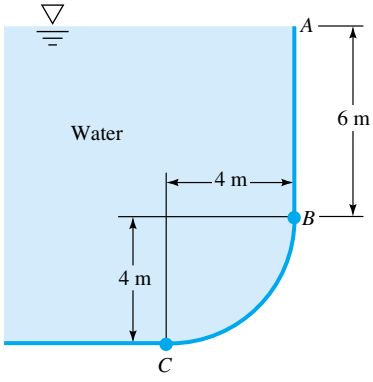
P2.94

***P2.95** The uniform body A in Fig. P2.95 has width b into the paper and is in static equilibrium when pivoted about hinge O. What is the specific gravity of this body if (*a*) $h = 0$ and (*b*) $h = R$?



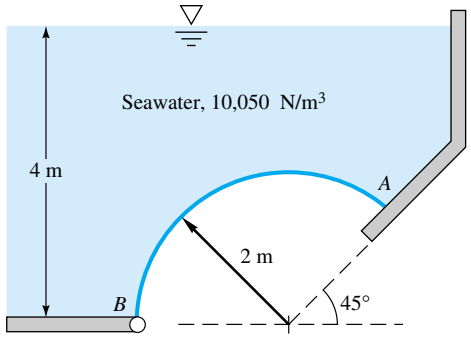
P2.95

P2.96 The tank in Fig. P2.96 is 3 m wide into the paper. Neglecting atmospheric pressure, compute the hydrostatic (*a*) horizontal force, (*b*) vertical force, and (*c*) resultant force on quarter-circle panel BC.



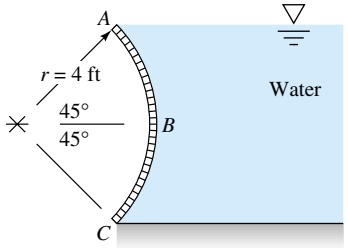
P2.96

P2.97 Gate AB in Fig. P2.97 is a three-eighths circle, 3 m wide into the paper, hinged at B, and resting against a smooth wall at A. Compute the reaction forces at points A and B.



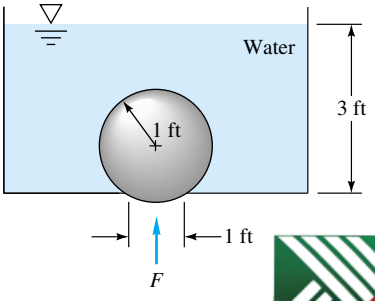
P2.97

P2.98 Gate ABC in Fig. P2.98 is a quarter circle 8 ft wide into the paper. Compute the horizontal and vertical hydrostatic forces on the gate and the line of action of the resultant force.



P2.98

P2.99 A 2-ft-diameter sphere weighing 400 lbf closes a 1-ft-diameter hole in the bottom of the tank in Fig. P2.99. Compute the force F required to dislodge the sphere from the hole.

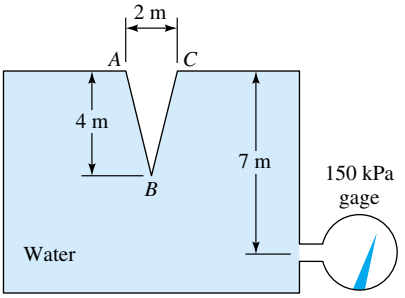


P2.99



ketabline.com Ebook.ketabline.com

P2.100 Pressurized water fills the tank in Fig. P2.100. Compute the net hydrostatic force on the conical surface *ABC*.



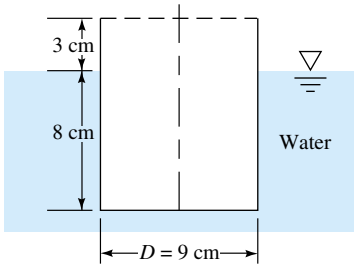
P2.100

P2.101 A fuel truck has a tank cross section which is approximately elliptical, with a 3-m horizontal major axis and a 2-m vertical minor axis. The top is vented to the atmosphere. If the tank is filled half with water and half with gasoline, what is the hydrostatic force on the flat elliptical end panel?

P2.102 In Fig. P2.80 suppose that the manometer reading is $h = 25$ cm. What will be the net hydrostatic force on the complete end wall, which is 160 cm high and 2 m wide?

P2.103 The hydrogen bubbles in Fig. 1.13 are very small, less than a millimeter in diameter, and rise slowly. Their drag in still fluid is approximated by the first term of Stokes' expression in Prob. 1.10: $F = 3\pi\mu VD$, where V is the rise velocity. Neglecting bubble weight and setting bubble buoyancy equal to drag, (*a*) derive a formula for the *terminal* (zero acceleration) rise velocity V_{term} of the bubble and (*b*) determine V_{term} in m/s for water at 20°C if $D = 30\ \mu$m.

P2.104 The can in Fig. P2.104 floats in the position shown. What is its weight in N?



P2.104

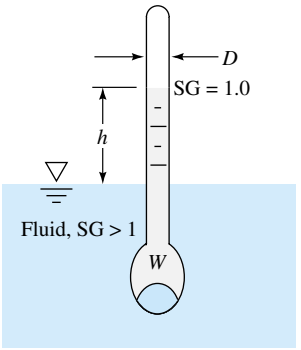
P2.105 It is said that Archimedes discovered the buoyancy laws when asked by King Hiero of Syracuse to determine whether his new crown was pure gold (SG = 19.3). Archimedes measured the weight of the crown in air to be 11.8 N and its weight in water to be 10.9 N. Was it pure gold?

P2.106 It is found that a 10-cm cube of aluminum (SG = 2.71) will remain neutral under water (neither rise nor fall) if it is tied by a string to a submerged 18-cm-diameter sphere of buoyant foam. What is the specific weight of the foam, in N/m^3?

P2.107 Repeat Prob. 2.62, assuming that the 10,000-lbf weight is aluminum (SG = 2.71) and is hanging submerged in the water.

P2.108 A piece of yellow pine wood (SG = 0.65) is 5 cm square and 2.2 m long. How many newtons of lead (SG = 11.4) should be attached to one end of the wood so that it will float vertically with 30 cm out of the water?

P2.109 A *hydrometer* floats at a level which is a measure of the specific gravity of the liquid. The stem is of constant diameter D, and a weight in the bottom stabilizes the body to float vertically, as shown in Fig. P2.109. If the position $h = 0$ is pure water (SG = 1.0), derive a formula for h as a function of total weight W, D, SG, and the specific weight γ_0 of water.

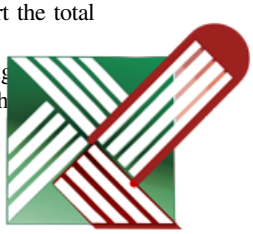


P2.109

P2.110 An average table tennis ball has a diameter of 3.81 cm and a mass of 2.6 g. Estimate the (small) depth at which this ball will float in water at 20°C and sea level standard air if air buoyancy is (*a*) neglected and (*b*) included.

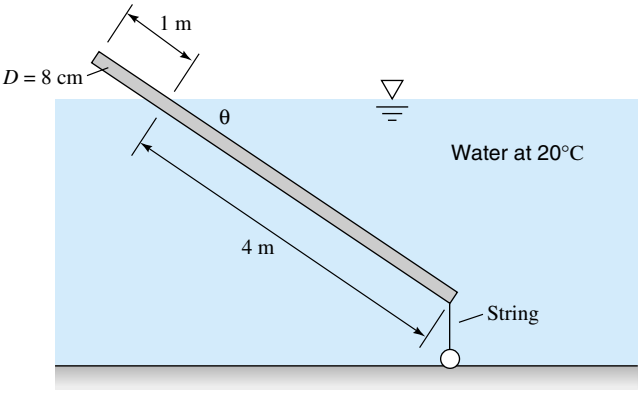
P2.111 A hot-air balloon must be designed to support basket, cords, and one person for a total weight of 1300 N. The balloon material has a mass of 60 g/m^2. Ambient air is at 25°C and 1 atm. The hot air inside the balloon is at 70°C and 1 atm. What diameter spherical balloon will just support the total weight? Neglect the size of the hot-air inlet vent.

P2.112 The uniform 5-m-long round wooden rod in Fig. is tied to the bottom by a string. Determine (*a*) th



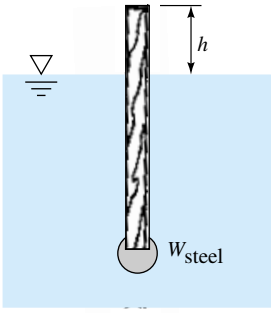
ketabline.com Ebook.ketabline.com

in the string and (*b*) the specific gravity of the wood. Is it possible for the given information to determine the inclination angle θ? Explain.



P2.112

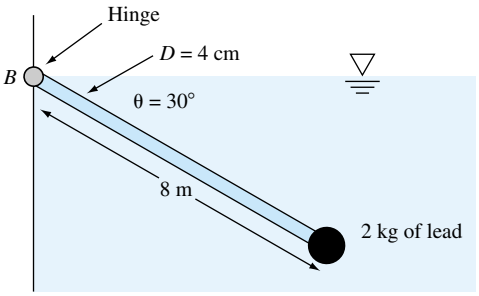
P2.113 A *spar buoy* is a buoyant rod weighted to float and protrude vertically, as in Fig. P2.113. It can be used for measurements or markers. Suppose that the buoy is maple wood (SG = 0.6), 2 in by 2 in by 12 ft, floating in seawater (SG = 1.025). How many pounds of steel (SG = 7.85) should be added to the bottom end so that $h = 18$ in?



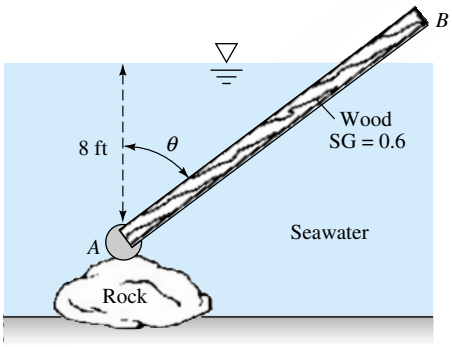
P2.113

P2.114 The uniform rod in Fig. P2.114 is hinged at point *B* on the waterline and is in static equilibrium as shown when 2 kg of lead (SG = 11.4) are attached to its end. What is the specific gravity of the rod material? What is peculiar about the rest angle $\theta = 30$?

P2.115 The 2-in by 2-in by 12-ft spar buoy from Fig. P2.113 has 5 lbm of steel attached and has gone aground on a rock, as in Fig. P2.115. Compute the angle θ at which the buoy will lean, assuming that the rock exerts no moments on the spar.

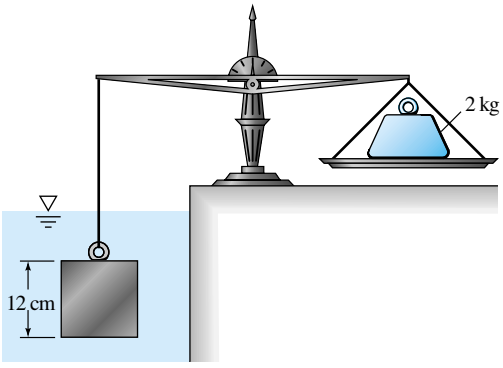


P2.114



P2.115

P2.116 The homogeneous 12-cm cube in Fig. 2.116 is balanced by a 2-kg mass on the beam scale when the cube is immersed in 20°C ethanol. What is the specific gravity of the cube?



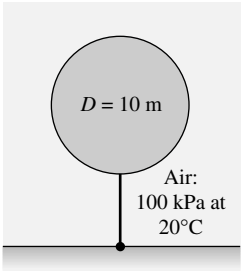
P2.116

P2.117 The balloon in Fig. P2.117 is filled w
surized to 135 kPa and 20°C. The ba



ketabline.com Ebook.ketabline.com

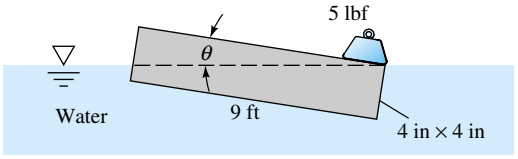
mass of 85 g/m^2. Estimate (*a*) the tension in the mooring line and (*b*) the height in the standard atmosphere to which the balloon will rise if the mooring line is cut.



P2.117

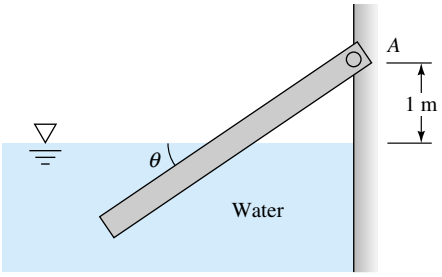
P2.118 A 14-in-diameter hollow sphere is made of steel (SG = 7.85) with 0.16-in wall thickness. How high will this sphere float in 20°C water? How much weight must be added inside to make the sphere neutrally buoyant?

P2.119 When a 5-lbf weight is placed on the end of the uniform floating wooden beam in Fig. P2.119, the beam tilts at an angle θ with its upper right corner at the surface, as shown. Determine (*a*) the angle θ and (*b*) the specific gravity of the wood. (*Hint:* Both the vertical forces and the moments about the beam centroid must be balanced.)



P2.119

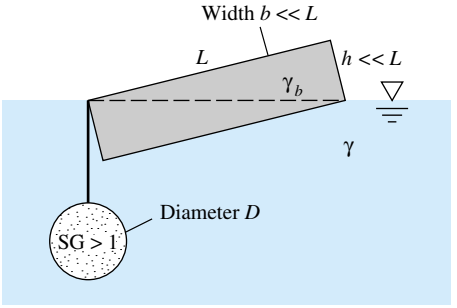
P2.120 A uniform wooden beam (SG = 0.65) is 10 cm by 10 cm by 3 m and is hinged at *A*, as in Fig. P2.120. At what angle θ will the beam float in the 20°C water?



P2.120

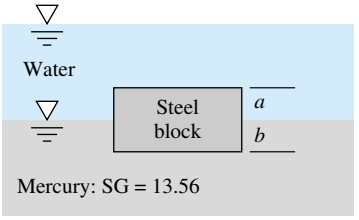
P2.121 The uniform beam in Fig. P2.121, of size *L* by *h* by *b* and with specific weight γ_b, floats exactly on its diagonal when a heavy uniform sphere is tied to the left corner, as shown. Show that this can only happen (*a*) when $\gamma_b = \gamma/3$ and (*b*) when the sphere has size

$$D = \left[\frac{Lhb}{\pi(\mathrm{SG} - 1)}\right]^{1/3}$$



P2.121

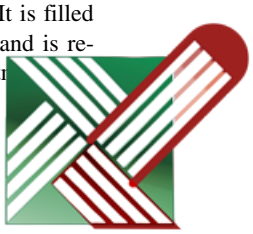
P2.122 A uniform block of steel (SG = 7.85) will "float" at a mercury-water interface as in Fig. P2.122. What is the ratio of the distances *a* and *b* for this condition?



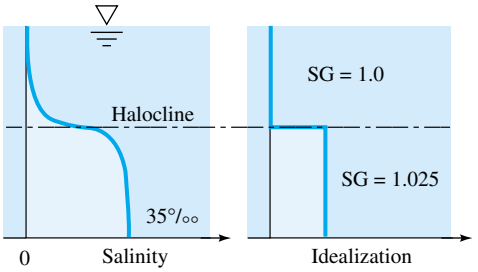
P2.122

P2.123 In an estuary where fresh water meets and mixes with seawater, there often occurs a stratified salinity condition with fresh water on top and salt water on the bottom, as in Fig. P2.123. The interface is called a *halocline*. An idealization of this would be constant density on each side of the halocline as shown. A 35-cm-diameter sphere weighing 50 lbf would "float" near such a halocline. Compute the sphere position for the idealization in Fig. P2.123.

P2.124 A balloon weighing 3.5 lbf is 6 ft in diameter. It is filled with hydrogen at 18 lbf/in^2 absolute and 60°F and is released. At what altitude in the U.S. standard atm will this balloon be neutrally buoyant?



ketabline.com Ebook.ketabline.com



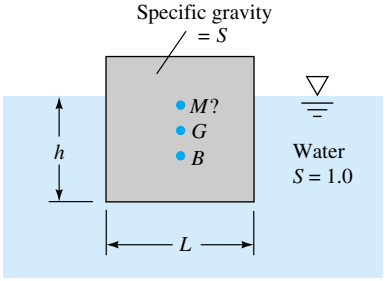
P2.123

P2.125 Suppose that the balloon in Prob. 2.111 is constructed to have a diameter of 14 m, is filled at sea level with hot air at 70°C and 1 atm, and is released. If the air inside the balloon remains constant and the heater maintains it at 70°C, at what altitude in the U.S. standard atmosphere will this balloon be neutrally buoyant?

***P2.126** A cylindrical can of weight W, radius R, and height H is open at one end. With its open end down, and while filled with atmospheric air (p_{atm}, T_{atm}), the can is eased down vertically into liquid, of density ρ, which enters and compresses the air isothermally. Derive a formula for the height h to which the liquid rises when the can is submerged with its top (closed) end a distance d from the surface.

***P2.127** Consider the 2-in by 2-in by 10-ft spar buoy of Prob. 2.113. How many pounds of steel (SG = 7.85) should be added at the bottom to ensure vertical floating with a metacentric height $\overline{MG}$ of (*a*) zero (neutral stability) or (*b*) 1 ft (reasonably stable)?

P2.128 An iceberg can be idealized as a cube of side length L, as in Fig. P2.128. If seawater is denoted by $S = 1.0$, then glacier ice (which forms icebergs) has $S = 0.88$. Determine if this "cubic" iceberg is stable for the position shown in Fig. P2.128.



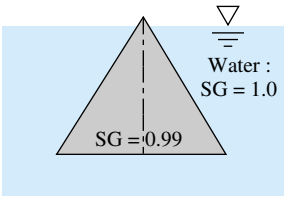
P2.128

P2.129 The iceberg idealization in Prob. 2.128 may become unstable if its sides melt and its height exceeds its width. In Fig. P2.128 suppose that the height is L and the depth into the paper is L, but the width in the plane of the paper is $H < L$. Assuming $S = 0.88$ for the iceberg, find the ratio H/L for which it becomes neutrally stable, i.e., about to overturn.

P2.130 Consider a wooden cylinder (SG = 0.6) 1 m in diameter and 0.8 m long. Would this cylinder be stable if placed to float with its axis vertical in oil (SG = 0.8)?

P2.131 A barge is 15 ft wide and 40 ft long and floats with a draft of 4 ft. It is piled so high with gravel that its center of gravity is 2 ft above the waterline. Is it stable?

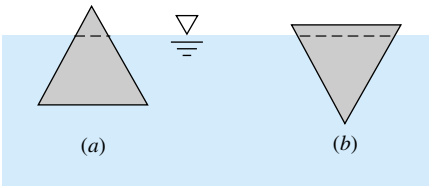
P2.132 A solid right circular cone has SG = 0.99 and floats vertically as in Fig. P2.132. Is this a stable position for the cone?



P2.132

P2.133 Consider a uniform right circular cone of specific gravity $S < 1$, floating with its vertex *down* in water ($S = 1$). The base radius is R and the cone height is H. Calculate and plot the stability $\overline{MG}$ of this cone, in dimensionless form, versus H/R for a range of $S < 1$.

P2.134 When floating in water (SG = 1.0), an equilateral triangular body (SG = 0.9) might take one of the two positions shown in Fig. P2.134. Which is the more stable position? Assume large width into the paper.



P2.134

P2.135 Consider a homogeneous right circular cylinder of length L, radius R, and specific gravity SG, floating in water (SG = 1). Show that the body will be stable with its axis vertical if

$$\frac{R}{L} > [2\text{SG}(1 - \text{SG})]^{1/2}$$



ketabline.com Ebook.ketabline.com

P2.136 Consider a homogeneous right circular cylinder of length L, radius R, and specific gravity SG = 0.5, floating in water (SG = 1). Show that the body will be stable with its axis horizontal if $L/R > 2.0$.

P2.137 A tank of water 4 m deep receives a constant upward acceleration a_z. Determine (*a*) the gage pressure at the tank bottom if $a_z = 5$ m^2/s and (*b*) the value of a_z which causes the gage pressure at the tank bottom to be 1 atm.

P2.138 A 12-fl-oz glass, of 3-in diameter, partly full of water, is attached to the edge of an 8-ft-diameter merry-go-round which is rotated at 12 r/min. How full can the glass be before water spills? (*Hint:* Assume that the glass is much smaller than the radius of the merry-go-round.)

P2.139 The tank of liquid in Fig. P2.139 accelerates to the right with the fluid in rigid-body motion. (*a*) Compute a_x in m/s^2. (*b*) Why doesn't the solution to part (*a*) depend upon the density of the fluid? (*c*) Determine the gage pressure at point *A* if the fluid is glycerin at 20°C.

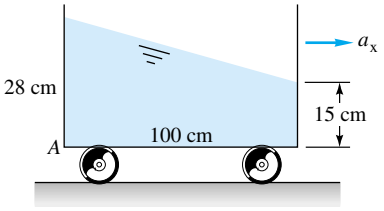


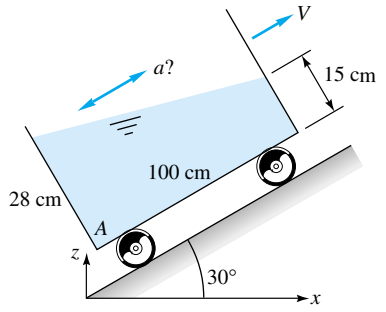
Fig. P2.139

P2.140 Suppose that the elliptical-end fuel tank in Prob. 2.101 is 10 m long and filled completely with fuel oil ($\rho = 890$ kg/m^3). Let the tank be pulled along a horizontal road. For rigid-body motion, find the acceleration, and its direction, for which (*a*) a constant-pressure surface extends from the top of the front end wall to the bottom of the back end and (*b*) the top of the back end is at a pressure 0.5 atm lower than the top of the front end.

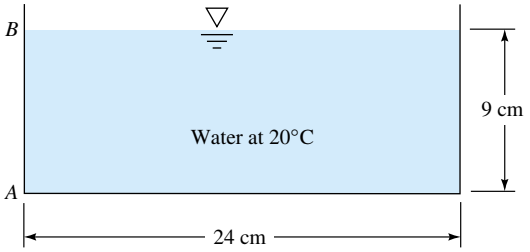
P2.141 The same tank from Prob. 2.139 is now moving with constant acceleration up a 30° inclined plane, as in Fig. P2.141. Assuming rigid-body motion, compute (*a*) the value of the acceleration *a*, (*b*) whether the acceleration is up or down, and (*c*) the gage pressure at point *A* if the fluid is mercury at 20°C.

P2.142 The tank of water in Fig. P2.142 is 12 cm wide into the paper. If the tank is accelerated to the right in rigid-body motion at 6.0 m/s^2, compute (*a*) the water depth on side *AB* and (*b*) the water-pressure force on panel *AB*. Assume no spilling.

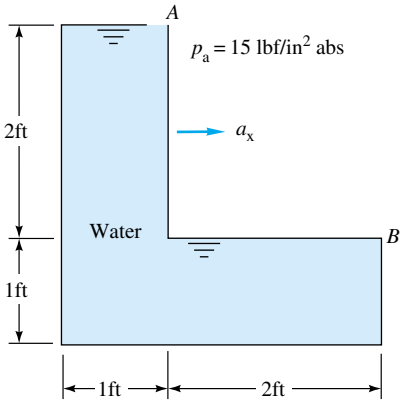
P2.143 The tank of water in Fig. P2.143 is full and open to the atmosphere at point *A*. For what acceleration a_x in ft/s^2 will the pressure at point *B* be (*a*) atmospheric and (*b*) zero absolute?



P2.141



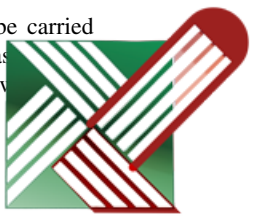
P2.142



P2.143

P2.144 Consider a hollow cube of side length 22 cm, filled completely with water at 20°C. The top surface of the cube is horizontal. One top corner, point *A*, is open through a small hole to a pressure of 1 atm. Diagonally opposite to point *A* is top corner *B*. Determine and discuss the various rigid-body accelerations for which the water at point *B* begins to cavitate, for (*a*) horizontal motion and (*b*) vertical motion.

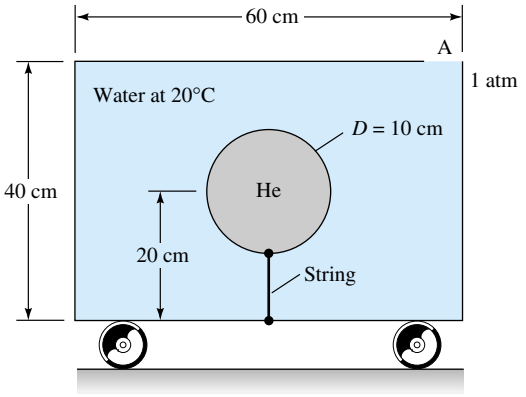
P2.145 A fish tank 14 in deep by 16 by 27 in is to be carried in a car which may experience accelerations as
6 m/s^2. What is the maximum water depth which



ketabline.com Ebook.ketabline.com

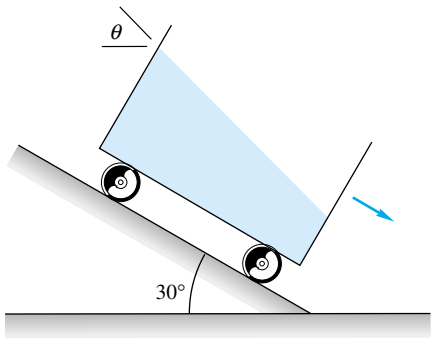
spilling in rigid-body motion? What is the proper alignment of the tank with respect to the car motion?

P2.146 The tank in Fig. P2.146 is filled with water and has a vent hole at point *A*. The tank is 1 m wide into the paper. Inside the tank, a 10-cm balloon, filled with helium at 130 kPa, is tethered centrally by a string. If the tank accelerates to the right at 5 m/s^2 in rigid-body motion, at what angle will the balloon lean? Will it lean to the right or to the left?



P2.146

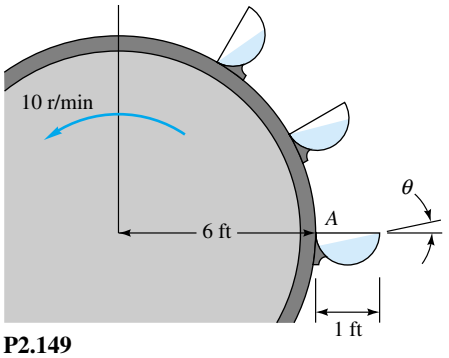
P2.147 The tank of water in Fig. P2.147 accelerates uniformly by freely rolling down a 30° incline. If the wheels are frictionless, what is the angle θ? Can you explain this interesting result?



P2.147

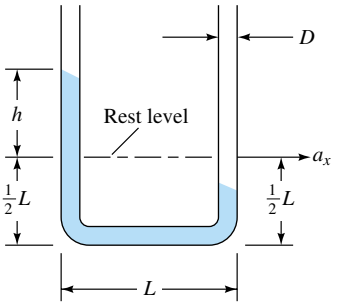
P2.148 A child is holding a string onto which is attached a helium-filled balloon. (*a*) The child is standing still and suddenly accelerates forward. In a frame of reference moving with the child, which way will the balloon tilt, forward or backward? Explain. (*b*) The child is now sitting in a car which is stopped at a red light. The helium-filled balloon is not in contact with any part of the car (seats, ceiling, etc.) but is held in place by the string, which is in turn held by the child. All the windows in the car are closed. When the traffic light turns green, the car accelerates forward. In a frame of reference moving with the car and child, which way will the balloon tilt, forward or backward? Explain. (*c*) Purchase or borrow a helium-filled balloon. Conduct a scientific experiment to see if your predictions in parts (*a*) and (*b*) above are correct. If not, explain.

P2.149 The 6-ft-radius waterwheel in Fig. P2.149 is being used to lift water with its 1-ft-diameter half-cylinder blades. If the wheel rotates at 10 r/min and rigid-body motion is assumed, what is the water surface angle θ at position *A*?



P2.149

P2.150 A cheap accelerometer, probably worth the price, can be made from a U-tube as in Fig. P2.150. If $L = 18$ cm and $D = 5$ mm, what will h be if $a_x = 6$ m/s^2? Can the scale markings on the tube be linear multiples of a_x?



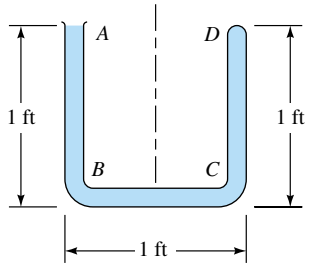
P2.150

P2.151 The U-tube in Fig. P2.151 is open a
If accelerated to the right at uniform



ketabline.com Ebook.ketabline.com

will cause the pressure at point C to be atmospheric? The fluid is water (SG = 1.0).



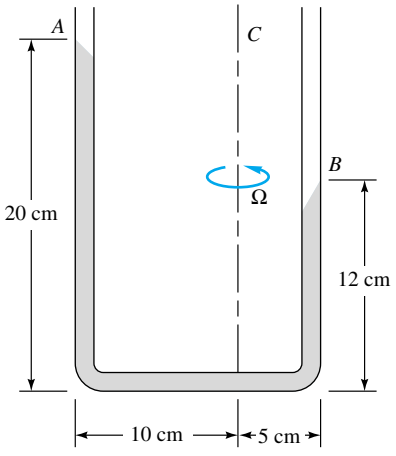
P2.151

P2.152 A 16-cm-diameter open cylinder 27 cm high is full of water. Compute the rigid-body rotation rate about its central axis, in r/min, (*a*) for which one-third of the water will spill out and (*b*) for which the bottom will be barely exposed.

P2.153 Suppose the U-tube in Fig. P2.150 is not translated but rather rotated about its right leg at 95 r/min. What will be the level h in the left leg if $L = 18$ cm and $D = 5$ mm?

P2.154 A very deep 18-cm-diameter can contains 12 cm of water overlaid with 10 cm of SAE 30 oil. If the can is rotated in rigid-body motion about its central axis at 150 r/min, what will be the shapes of the air-oil and oil-water interfaces? What will be the maximum fluid pressure in the can in Pa (gage)?

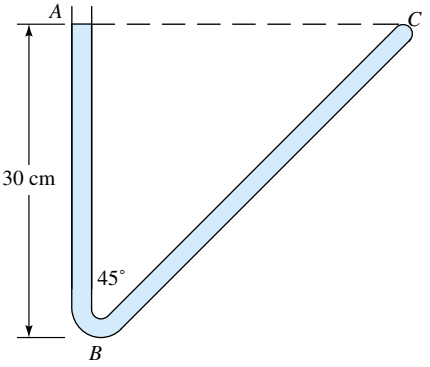
P2.155 For what uniform rotation rate in r/min about axis C will the U-tube in Fig. P2.155 take the configuration shown? The fluid is mercury at 20°C.



P2.155

P2.156 Suppose that the U-tube of Fig. P2.151 is rotated about axis DC. If the fluid is water at 122°F and atmospheric pressure is 2116 lbf/ft^2 absolute, at what rotation rate will the fluid within the tube begin to vaporize? At what point will this occur?

P2.157 The 45° V-tube in Fig. P2.157 contains water and is open at A and closed at C. What uniform rotation rate in r/min about axis AB will cause the pressure to be equal at points B and C? For this condition, at what point in leg BC will the pressure be a minimum?



P2.157

***P2.158** It is desired to make a 3-m-diameter parabolic telescope mirror by rotating molten glass in rigid-body motion until the desired shape is achieved and then cooling the glass to a solid. The focus of the mirror is to be 4 m from the mirror, measured along the centerline. What is the proper mirror rotation rate, in r/min, for this task?



ketabline.com Ebook.ketabline.com

Word Problems

W2.1 Consider a hollow cone with a vent hole in the vertex at the top, along with a hollow cylinder, open at the top, with the same base area as the cone. Fill both with water to the top. The *hydrostatic paradox* is that both containers have the same force on the bottom due to the water pressure, although the cone contains 67 percent less water. Can you explain the paradox?

W2.2 Can the temperature ever *rise* with altitude in the real atmosphere? Wouldn't this cause the air pressure to *increase* upward? Explain the physics of this situation.

W2.3 Consider a submerged curved surface which consists of a two-dimensional circular arc of arbitrary angle, arbitrary depth, and arbitrary orientation. Show that the resultant hydrostatic pressure force on this surface must pass through the center of curvature of the arc.

W2.4 Fill a glass approximately 80 percent with water, and add a large ice cube. Mark the water level. The ice cube, having SG $\approx$ 0.9, sticks up out of the water. Let the ice cube melt with negligible evaporation from the water surface. Will the water level be higher than, lower than, or the same as before?

W2.5 A ship, carrying a load of steel, is trapped while floating in a small closed lock. Members of the crew want to get out, but they can't quite reach the top wall of the lock. A crew member suggests throwing the steel overboard in the lock, claiming the ship will then rise and they can climb out. Will this plan work?

W2.6 Consider a balloon of mass m floating neutrally in the atmosphere, carrying a person/basket of mass $M > m$. Discuss the stability of this system to disturbances.

W2.7 Consider a helium balloon on a string tied to the seat of your stationary car. The windows are closed, so there is no air motion within the car. The car begins to accelerate forward. Which way will the balloon lean, forward or backward? (*Hint:* The acceleration sets up a horizontal pressure gradient in the air within the car.)

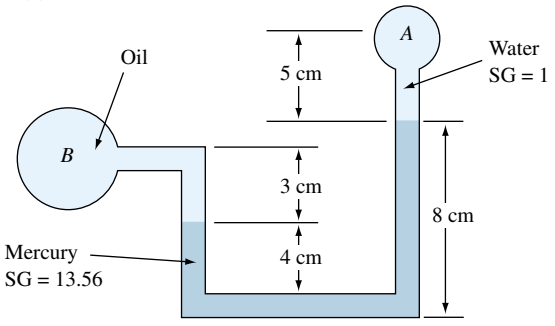
W2.8 Repeat your analysis of Prob. W2.7 to let the car move at constant velocity and go around a curve. Will the balloon lean in, toward the center of curvature, or out?

Fundamentals of Engineering Exam Problems

FE2.1 A gage attached to a pressurized nitrogen tank reads a gage pressure of 28 in of mercury. If atmospheric pressure is 14.4 psia, what is the absolute pressure in the tank?
(*a*) 95 kPa, (*b*) 99 kPa, (*c*) 101 kPa, (*d*) 194 kPa,
(*e*) 203 kPa

FE2.2 On a sea-level standard day, a pressure gage, moored below the surface of the ocean (SG = 1.025), reads an absolute pressure of 1.4 MPa. How deep is the instrument?
(*a*) 4 m, (*b*) 129 m, (*c*) 133 m, (*d*) 140 m, (*e*) 2080 m

FE2.3 In Fig. FE2.3, if the oil in region *B* has SG = 0.8 and the absolute pressure at point A is 1 atm, what is the absolute pressure at point *B*?
(*a*) 5.6 kPa, (*b*) 10.9 kPa, (*c*) 106.9 kPa, (*d*) 112.2 kPa,
(*e*) 157.0 kPa



FE2.3

FE2.4 In Fig. FE2.3, if the oil in region *B* has SG = 0.8 and the absolute pressure at point *B* is 14 psia, what is the absolute pressure at point *B*?
(*a*) 11 kPa, (*b*) 41 kPa, (*c*) 86 kPa, (*d*) 91 kPa, (*e*) 101 kPa

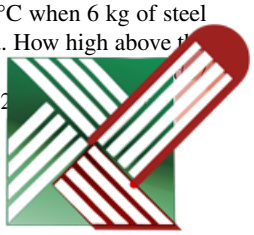
FE2.5 A tank of water (SG = 1,.0) has a gate in its vertical wall 5 m high and 3 m wide. The top edge of the gate is 2 m below the surface. What is the hydrostatic force on the gate?
(*a*) 147 kN, (*b*) 367 kN, (*c*) 490 kN, (*d*) 661 kN,
(*e*) 1028 kN

FE2.6 In Prob. FE2.5 above, how far below the surface is the center of pressure of the hydrostatic force?
(*a*) 4.50 m, (*b*) 5.46 m, (*c*) 6.35 m, (*d*) 5.33 m, (*e*) 4.96 m

FE2.7 A solid 1-m-diameter sphere floats at the interface between water (SG = 1.0) and mercury (SG = 13.56) such that 40 percent is in the water. What is the specific gravity of the sphere?
(*a*) 6.02, (*b*) 7.28, (*c*) 7.78, (*d*) 8.54, (*e*) 12.56

FE2.8 A 5-m-diameter balloon contains helium at 125 kPa absolute and 15°C, moored in sea-level standard air. If the gas constant of helium is 2077 $m^2/(s^2 \cdot K)$ and balloon material weight is neglected, what is the net lifting force of the balloon?
(*a*) 67 N, (*b*) 134 N, (*c*) 522 N, (*d*) 653 N, (*e*) 787 N

FE2.9 A square wooden (SG = 0.6) rod, 5 cm by 5 cm by 10 m long, floats vertically in water at 20°C when 6 kg of steel (SG = 7.84) are attached to one end. How high above t
water surface does the wooden end
(*a*) 0.6 m, (*b*) 1.6 m, (*c*) 1.9 m, (*d*) 2

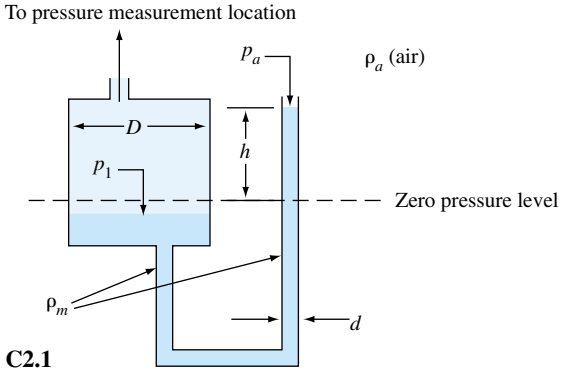


ketabline.com Ebook.ketabline.com

FE2.10 A floating body will be stable when its (*a*) center of gravity is above its center of buoyancy, (*b*) center of buoyancy is below the waterline, (*c*) center of buoyancy is above its metacenter, (*d*) metacenter is above its center of buoyancy, (*e*) metacenter is above its center of gravity

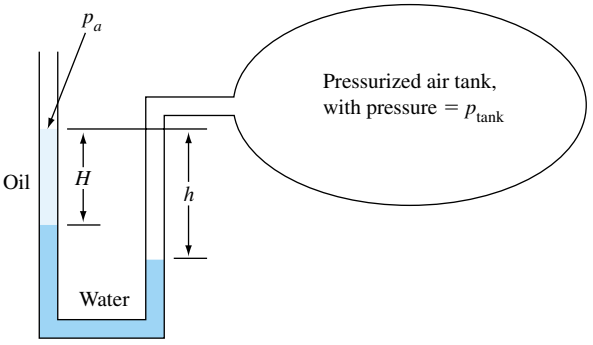
Comprehensive Problems

C2.1 Some manometers are constructed as in Fig. C2.1, where one side is a large reservoir (diameter D) and the other side is a small tube of diameter d, open to the atmosphere. In such a case, the height of manometer liquid on the reservoir side does not change appreciably. This has the advantage that only one height needs to be measured rather than two. The manometer liquid has density ρ_m while the air has density ρ_a. Ignore the effects of surface tension. When there is no pressure difference across the manometer, the elevations on both sides are the same, as indicated by the dashed line. Height h is measured from the zero pressure level as shown. (*a*) When a high pressure is applied to the left side, the manometer liquid in the large reservoir goes down, while that in the tube at the right goes up to conserve mass. Write an exact expression for $p_{1\text{gage}}$, taking into account the movement of the surface of the reservoir. Your equation should give $p_{1\text{gage}}$ as a function of h, ρ_m, and the physical parameters in the problem, h, d, D, and gravity constant g. (*b*) Write an approximate expression for $p_{1\text{gage}}$, neglecting the change in elevation of the surface of the reservoir liquid. (*c*) Suppose $h = 0.26$ m in a certain application. If $p_a = 101{,}000$ Pa and the manometer liquid has a density of 820 kg/m^3, estimate the ratio D/d required to keep the error of the approximation of part (*b*) within 1 percent of the exact measurement of part (*a*). Repeat for an error within 0.1 percent.



C2.1

C2.2 A prankster has added oil, of specific gravity SG_0, to the left leg of the manometer in Fig. C2.2. Nevertheless, the U-tube is still useful as a pressure-measuring device. It is attached to a pressurized tank as shown in the figure. (*a*) Find an expression for h as a function of H and other parameters in the problem. (*b*) Find the special case of your result in (*a*) when $p_{\text{tank}} = p_a$. (*c*) Suppose $H = 5.0$ cm, p_a is 101.2kPa, p_{tank} is 1.82 kPa higher than p_a, and $SG_0 = 0.85$. Calculate h in cm, ignoring surface tension effects and neglecting air density effects.



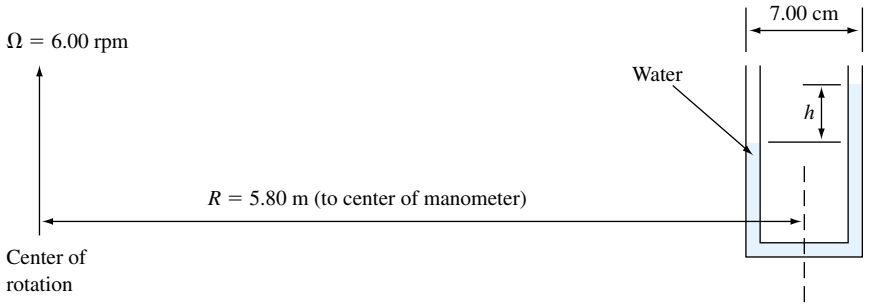
C2.2

C2.3 Professor F. Dynamics, riding the merry-go-round with his son, has brought along his U-tube manometer. (You never know when a manometer might come in handy.) As shown in Fig. C2.3, the merry-go-round spins at constant angular velocity and the manometer legs are 7 cm apart. The manometer center is 5.8 m from the axis of rotation. Determine the height difference h in two ways: (*a*) approximately, by assuming rigid body translation with **a** equal to the average manometer acceleration; and (*b*) exactly, using rigid-body rotation theory. How good is the approximation?

C2.4 A student sneaks a glass of cola onto a roller coaster ride. The glass is cylindrical, twice as tall as it is wide, and filled to the brim. He wants to know what percent of the cola he should drink before the ride begins, so that none of it spills during the big drop, in which the roller coaster achieves 0.55-g acceleration at a 45° angle below the horizontal. Make the calculation for him, neglecting sloshing and assuming that the glass is vertical at all times.



ketabline.com Ebook.ketabline.com



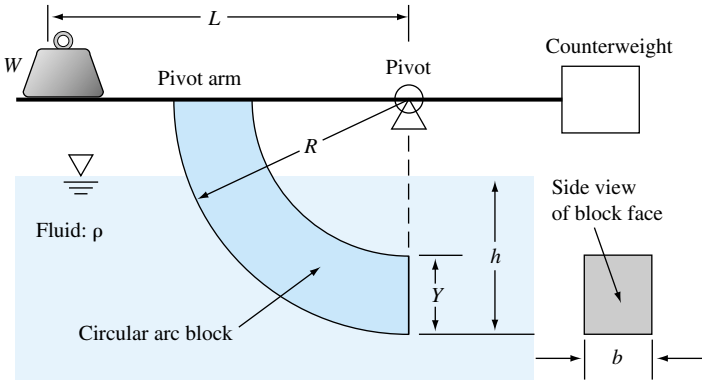
C2.3

Design Projects

D2.1 It is desired to have a bottom-moored, floating system which creates a nonlinear force in the mooring line as the water level rises. The design force F need only be accurate in the range of seawater depths h between 6 and 8 m, as shown in the accompanying table. Design a buoyant system which will provide this force distribution. The system should be practical, i.e., of inexpensive materials and simple construction.

h, m	F, N	h, m	F, N
6.00	400	7.25	554
6.25	437	7.50	573
6.50	471	7.75	589
6.75	502	8.00	600
7.00	530		

D2.2 A laboratory apparatus used in some universities is shown in Fig. D2.2. The purpose is to measure the hydrostatic force on the flat face of the circular-arc block and compare it with the theoretical value for given depth h. The counterweight is arranged so that the pivot arm is horizontal when the block is not submerged, whence the weight W can be correlated with the hydrostatic force when the submerged arm is again brought to horizontal. First show that the apparatus concept is valid in principle; then derive a formula for W as a function of h in terms of the system parameters. Finally, suggest some appropriate values of Y, L, etc., for a suitable appartus and plot theoretical W versus h for these values.



D2.2

References

1. *U.S. Standard Atmosphere*, 1976, Government Printing Office, Washington, DC, 1976.
2. G. Neumann and W. J. Pierson, Jr., *Principles of Physical Oceanography*, Prentice-Hall, Englewood Cliffs, NJ, 1966.
3. T. C. Gillmer and B. Johnson, *Introduction to Naval Architecture,* Naval Institute Press, Annapolis, MD, 1982.
4. D. T. Greenwood, *Principles of Dynamics*, 2d ed., Prentice-Hall, Englewood Cliffs, NJ, 1988.
5. R. I. Fletcher, "The Apparent Field of Gravity in a Rotating Fluid System," *Am. J. Phys.,* vol. 40, pp. 959–965, July 1972.
6. National Committee for Fluid Mechanics Films, *Illustrated Experiments in Fluid Mechanics*, M.I.T. Press, Cambridge, MA, 1972.
7. J. P. Holman, *Experimental Methods for Engineers*, 6th ed., McGraw-Hill, New York, 1993.
8. R. P. Benedict, *Fundamentals of Temperature, Pressure, and Flow Measurement*, 3d ed., Wiley, New York, 1984.
9. T. G. Beckwith and R. G. Marangoni, *Mechanical Measurements*, 4th ed., Addison-Wesley, Reading, MA, 1990.
10. J. W. Dally, W. F. Riley, and K. G. McConnell, *Instrumentation for Engineering Measurements*, Wiley, New York, 1984.
11. E. N. Gilbert, "How Things Float," *Am. Math. Monthly,* vol. 98, no. 3, pp. 201–216, 1991.
12. R. J. Figliola and D. E. Beasley, *Theory and Design for Mechanical Measurements,* 2d ed., Wiley, New York, 1994.
13. R. W. Miller, *Flow Measurement Engineering Handbook,* 3d ed., McGraw-Hill, New York, 1996.



ketabline.com Ebook.ketabline.com

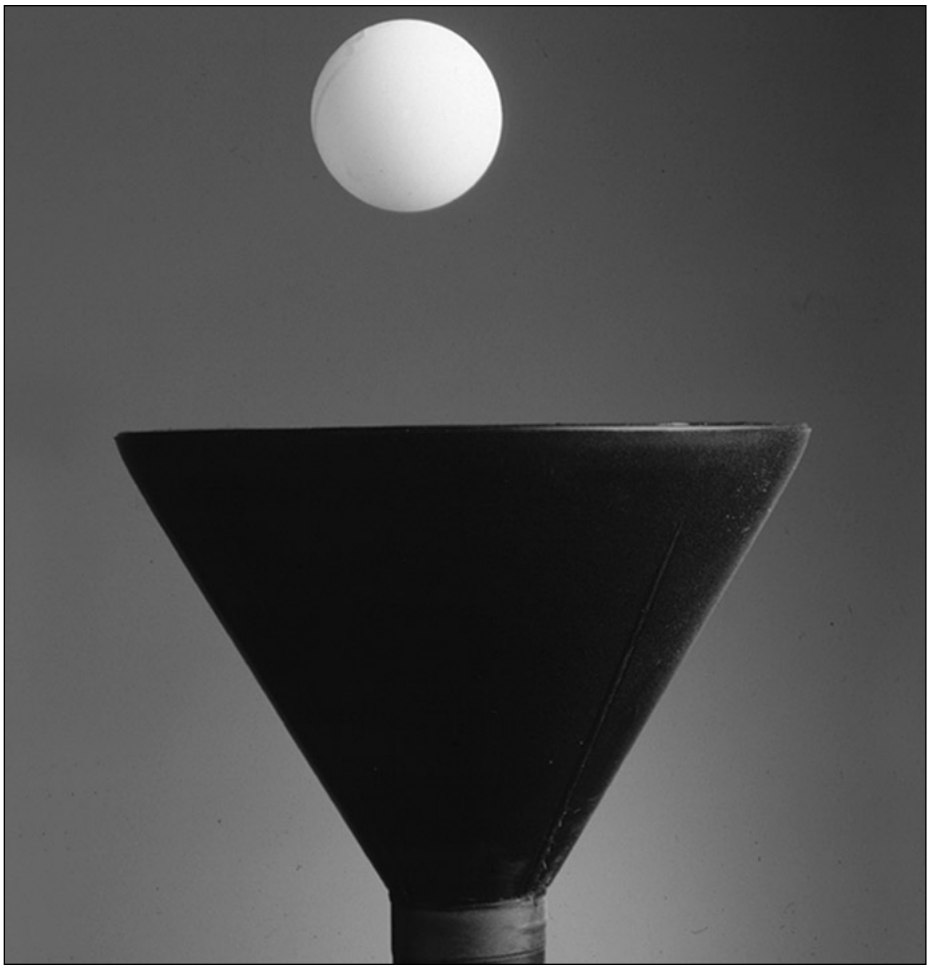


Table tennis ball suspended by an air jet. The control volume momentum principle, studied in this chapter, requires a force to change the direction of a flow. The jet flow deflects around the ball, and the force is the ball's weight. *(Courtesy of Paul Silverman/Fundamental Photographs)*



ketabline.com Ebook.ketabline.com

Chapter 3
Integral Relations for a Control Volume

Motivation. In analyzing fluid motion, we might take one of two paths: (1) seeking to describe the detailed flow pattern at every point (x, y, z) in the field or (2) working with a finite region, making a balance of flow in versus flow out, and determining gross flow effects such as the force or torque on a body or the total energy exchange. The second is the "control-volume" method and is the subject of this chapter. The first is the "differential" approach and is developed in Chap. 4.

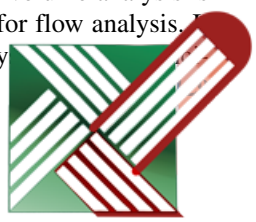
We first develop the concept of the control volume, in nearly the same manner as one does in a thermodynamics course, and we find the rate of change of an arbitrary gross fluid property, a result called the *Reynolds transport theorem*. We then apply this theorem, in sequence, to mass, linear momentum, angular momentum, and energy, thus deriving the four basic control-volume relations of fluid mechanics. There are many applications, of course. The chapter then ends with a special case of frictionless, shaft-work-free momentum and energy: the *Bernoulli equation*. The Bernoulli equation is a wonderful, historic relation, but it is extremely restrictive and should always be viewed with skepticism and care in applying it to a real (viscous) fluid motion.

3.1 Basic Physical Laws of Fluid Mechanics

It is time now to really get serious about flow problems. The fluid-statics applications of Chap. 2 were more like fun than work, at least in my opinion. Statics problems basically require only the density of the fluid and knowledge of the position of the free surface, but most flow problems require the analysis of an arbitrary state of variable fluid motion defined by the geometry, the boundary conditions, and the laws of mechanics. This chapter and the next two outline the three basic approaches to the analysis of arbitrary flow problems:

1. Control-volume, or large-scale, analysis (Chap. 3)
2. Differential, or small-scale, analysis (Chap. 4)
3. Experimental, or dimensional, analysis (Chap. 5)

The three approaches are roughly equal in importance, but control-volume analysis is "more equal," being the single most valuable tool to the engineer for flow analysis. It gives "engineering" answers, sometimes gross and crude but alway



ketabline.com Ebook.ketabline.com

ple, the differential approach of Chap. 4 can be used for any problem, but in practice the lack of mathematical tools and the inability of the digital computer to model small-scale processes make the differential approach rather limited. Similarly, although the dimensional analysis of Chap. 5 can be applied to any problem, the lack of time and money and generality often makes experimentation a limited approach. But a control-volume analysis takes about half an hour and gives useful results. Thus, in a trio of approaches, the control volume is best. Oddly enough, it is the newest of the three. Differential analysis began with Euler and Lagrange in the eighteenth century, and dimensional analysis was pioneered by Lord Rayleigh in the late nineteenth century, but the control volume, although proposed by Euler, was not developed on a rigorous basis as an analytical tool until the 1940s.

Systems versus Control Volumes

All the laws of mechanics are written for a *system*, which is defined as an arbitrary quantity of mass of fixed identity. Everything external to this system is denoted by the term *surroundings*, and the system is separated from its surroundings by its *boundaries*. The laws of mechanics then state what happens when there is an interaction between the system and its surroundings.

First, the system is a fixed quantity of mass, denoted by m. Thus the mass of the system is conserved and does not change.[1] This is a law of mechanics and has a very simple mathematical form, called *conservation of mass*:

$$m_{\text{syst}} = \text{const} \qquad \text{or} \qquad \frac{dm}{dt} = 0 \tag{3.1}$$

This is so obvious in solid-mechanics problems that we often forget about it. In fluid mechanics, we must pay a lot of attention to mass conservation, and it takes a little analysis to make it hold.

Second, if the surroundings exert a net force $\mathbf{F}$ on the system, Newton's second law states that the mass will begin to accelerate[2]

$$\mathbf{F} = m\mathbf{a} = m\frac{d\mathbf{V}}{dt} = \frac{d}{dt}(m\mathbf{V}) \tag{3.2}$$

In Eq. (2.12) we saw this relation applied to a differential element of viscous incompressible fluid. In fluid mechanics Newton's law is called the linear-momentum relation. Note that it is a vector law which implies the three scalar equations $F_x = ma_x$, $F_y = ma_y$, and $F_z = ma_z$.

Third, if the surroundings exert a net moment $\mathbf{M}$ about the center of mass of the system, there will be a rotation effect

$$\mathbf{M} = \frac{d\mathbf{H}}{dt} \tag{3.3}$$

where $\mathbf{H} = \Sigma(\mathbf{r} \times \mathbf{V})\ \delta m$ is the angular momentum of the system about its center of

[1] We are neglecting nuclear reactions, where mass can be changed to energy.
[2] We are neglecting relativistic effects, where Newton's law must be modified.



ketabline.com Ebook.ketabline.com

mass. Here we call Eq. (3.3) the angular-momentum relation. Note that it is also a vector equation implying three scalar equations such as $M_x = dH_x/dt$.

For an arbitrary mass and arbitrary moment, **H** is quite complicated and contains nine terms (see, e.g., Ref. 1, p. 285). In elementary dynamics we commonly treat only a rigid body rotating about a fixed x axis, for which Eq. (3.3) reduces to

$$M_x = I_x \frac{d}{dt}(\omega_x) \tag{3.4}$$

where ω_x is the angular velocity of the body and I_x is its mass moment of inertia about the x axis. Unfortunately, fluid systems are not rigid and rarely reduce to such a simple relation, as we shall see in Sec. 3.5.

Fourth, if heat dQ is added to the system or work dW is done by the system, the system energy dE must change according to the energy relation, or first law of thermodynamics,

$$dQ - dW = dE \tag{3.5}$$

or

$$\frac{dQ}{dt} - \frac{dW}{dt} = \frac{dE}{dt}$$

Like mass conservation, Eq. (3.1), this is a scalar relation having only a single component.

Finally, the second law of thermodynamics relates entropy change dS to heat added dQ and absolute temperature T:

$$dS \geq \frac{dQ}{T} \tag{3.6}$$

This is valid for a system and can be written in control-volume form, but there are almost no practical applications in fluid mechanics except to analyze flow-loss details (see Sec. 9.5).

All these laws involve thermodynamic properties, and thus we must supplement them with state relations $p = p(\rho, T)$ and $e = e(\rho, T)$ for the particular fluid being studied, as in Sec. 1.6.

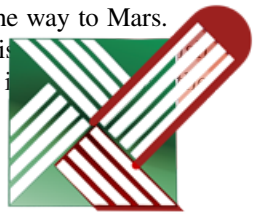
The purpose of this chapter is to put our four basic laws into the control-volume form suitable for arbitrary regions in a flow:

1. Conservation of mass (Sec. 3.3)
2. The linear-momentum relation (Sec. 3.4)
3. The angular-momentum relation (Sec. 3.5)
4. The energy equation (Sec. 3.6)

Wherever necessary to complete the analysis we also introduce a state relation such as the perfect-gas law.

Equations (3.1) to (3.6) apply to either fluid or solid systems. They are ideal for solid mechanics, where we follow the same system forever because it represents the product we are designing and building. For example, we follow a beam as it deflects under load. We follow a piston as it oscillates. We follow a rocket system all the way to Mars.

But fluid systems do not demand this concentrated attention. It is to follow the ultimate path of a specific particle of fluid. Instead i



ketabline.com Ebook.ketabline.com

fluid forms the environment whose effect on our product we wish to know. For the three examples cited above, we wish to know the wind loads on the beam, the fluid pressures on the piston, and the drag and lift loads on the rocket. This requires that the basic laws be rewritten to apply to a specific *region* in the neighborhood of our product. In other words, where the fluid particles in the wind go after they leave the beam is of little interest to a beam designer. The user's point of view underlies the need for the control-volume analysis of this chapter.

Although thermodynamics is not at all the main topic of this book, it would be a shame if the student did not review at least the first law and the state relations, as discussed, e.g., in Refs. 6 and 7.

In analyzing a control volume, we convert the system laws to apply to a specific region which the system may occupy for only an instant. The system passes on, and other systems come along, but no matter. The basic laws are reformulated to apply to this local region called a control volume. All we need to know is the flow field in this region, and often simple assumptions will be accurate enough (e.g., uniform inlet and/or outlet flows). The flow conditions away from the control volume are then irrelevant. The technique for making such localized analyses is the subject of this chapter.

Volume and Mass Rate of Flow

All the analyses in this chapter involve evaluation of the volume flow Q or mass flow $\dot{m}$ passing through a surface (imaginary) defined in the flow.

Suppose that the surface S in Fig. 3.1*a* is a sort of (imaginary) wire mesh through which the fluid passes without resistance. How much volume of fluid passes through S in unit time? If, typically, $\mathbf{V}$ varies with position, we must integrate over the elemental surface dA in Fig. 3.1*a*. Also, typically $\mathbf{V}$ may pass through dA at an angle θ off the normal. Let $\mathbf{n}$ be defined as the unit vector normal to dA. Then the amount of fluid swept through dA in time dt is the volume of the slanted parallelopiped in Fig. 3.1*b*:

$$d\mathcal{V} = V\,dt\,dA\,\cos\theta = (\mathbf{V}\cdot\mathbf{n})\,dA\,dt$$

The integral of $d\mathcal{V}/dt$ is the total volume rate of flow Q through the surface S

$$Q = \int_S (\mathbf{V}\cdot\mathbf{n})\,dA = \int_S V_n\,dA \tag{3.7}$$

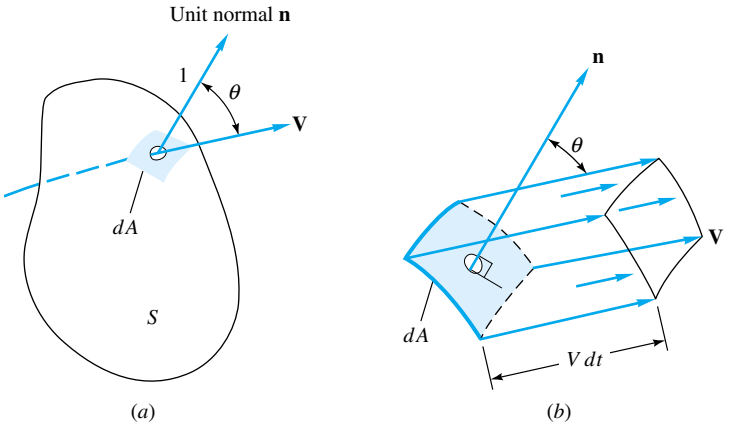


Fig. 3.1 Volume rate of flow through an arbitrary surface: (*a*) an elemental area dA on the surface; (*b*) the incremental volume swept through dA equals $V\,dt\,dA\,\cos\theta$.



ketabline.com Ebook.ketabline.com

We could replace $\mathbf{V} \cdot \mathbf{n}$ by its equivalent, V_n, the component of $\mathbf{V}$ normal to dA, but the use of the dot product allows Q to have a sign to distinguish between inflow and outflow. By convention throughout this book we consider $\mathbf{n}$ to be the *outward* normal unit vector. Therefore $\mathbf{V} \cdot \mathbf{n}$ denotes outflow if it is positive and inflow if negative. This will be an extremely useful housekeeping device when we are computing volume and mass flow in the basic control-volume relations.

Volume flow can be multiplied by density to obtain the mass flow $\dot{m}$. If density varies over the surface, it must be part of the surface integral

$$\dot{m} = \int_S \rho(\mathbf{V} \cdot \mathbf{n})\, dA = \int_S \rho V_n\, dA$$

If density is constant, it comes out of the integral and a direct proportionality results:

Constant density: $\dot{m} = \rho Q$

3.2 The Reynolds Transport Theorem

To convert a system analysis to a control-volume analysis, we must convert our mathematics to apply to a specific region rather than to individual masses. This conversion, called the *Reynolds transport theorem*, can be applied to all the basic laws. Examining the basic laws (3.1) to (3.3) and (3.5), we see that they are all concerned with the time derivative of fluid properties m, $\mathbf{V}$, $\mathbf{H}$, and E. Therefore what we need is to relate the time derivative of a system property to the rate of change of that property within a certain region.

The desired conversion formula differs slightly according to whether the control volume is fixed, moving, or deformable. Figure 3.2 illustrates these three cases. The fixed control volume in Fig. 3.2*a* encloses a stationary region of interest to a nozzle designer. The control surface is an abstract concept and does not hinder the flow in any way. It slices through the jet leaving the nozzle, circles around through the surrounding atmosphere, and slices through the flange bolts and the fluid within the nozzle. This particular control volume exposes the stresses in the flange bolts, which contribute to applied forces in the momentum analysis. In this sense the control volume resembles the *free-body* concept, which is applied to systems in solid-mechanics analyses.

Figure 3.2*b* illustrates a moving control volume. Here the ship is of interest, not the ocean, so that the control surface chases the ship at ship speed V. The control volume is of fixed volume, but the relative motion between water and ship must be considered.

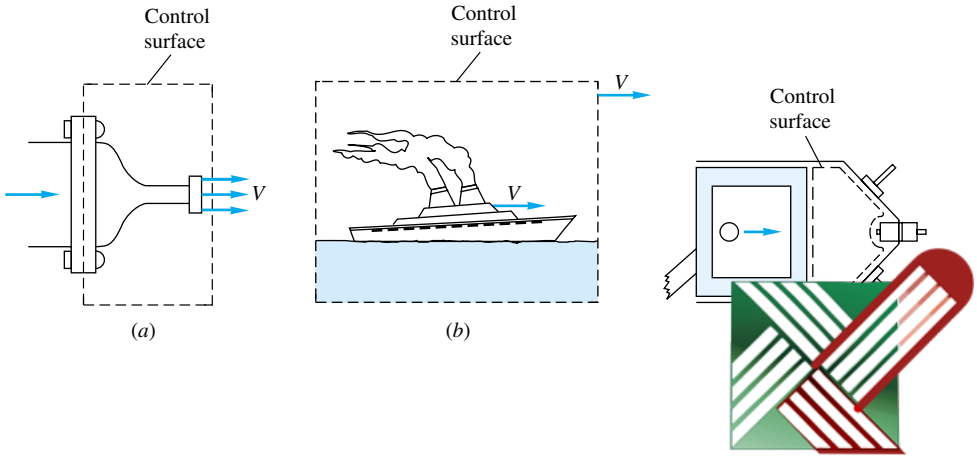


Fig. 3.2 Fixed, moving, and deformable control volumes: (*a*) fixed control volume for nozzle-stress analysis; (*b*) control volume moving at ship speed for drag-force analysis; (*c*) control volume deforming within cylinder for transient pressure-variation analysis.

ketabline.com Ebook.ketabline.com

If V is constant, this relative motion is a steady-flow pattern, which simplifies the analysis.[3] If V is variable, the relative motion is unsteady, so that the computed results are time-variable and certain terms enter the momentum analysis to reflect the noninertial frame of reference.

Figure 3.2*c* shows a deforming control volume. Varying relative motion at the boundaries becomes a factor, and the rate of change of shape of the control volume enters the analysis. We begin by deriving the fixed-control-volume case, and we consider the other cases as advanced topics.

One-Dimensional Fixed Control Volume

As a simple first example, consider a duct or streamtube with a nearly one-dimensional flow $V = V(x)$, as shown in Fig. 3.3. The selected control volume is a portion of the duct which happens to be filled exactly by system 2 at a particular instant t. At time $t + dt$, system 2 has begun to move out, and a sliver of system 1 has entered from the left. The shaded areas show an outflow sliver of volume $A_bV_b\,dt$ and an inflow volume $A_aV_a\,dt$.

Now let B be any property of the fluid (energy, momentum, etc.), and let $\beta = dB/dm$ be the *intensive* value or the amount of B per unit mass in any small portion of the fluid. The total amount of B in the control volume is thus

$$B_{CV} = \int_{CV} \beta\rho\, d\mathcal{V} \qquad \beta = \frac{dB}{dm} \tag{3.8}$$

[3] A *wind tunnel* uses a fixed model to simulate flow over a body moving through a fluid. A *tow tank* uses a moving model to simulate the same situation.

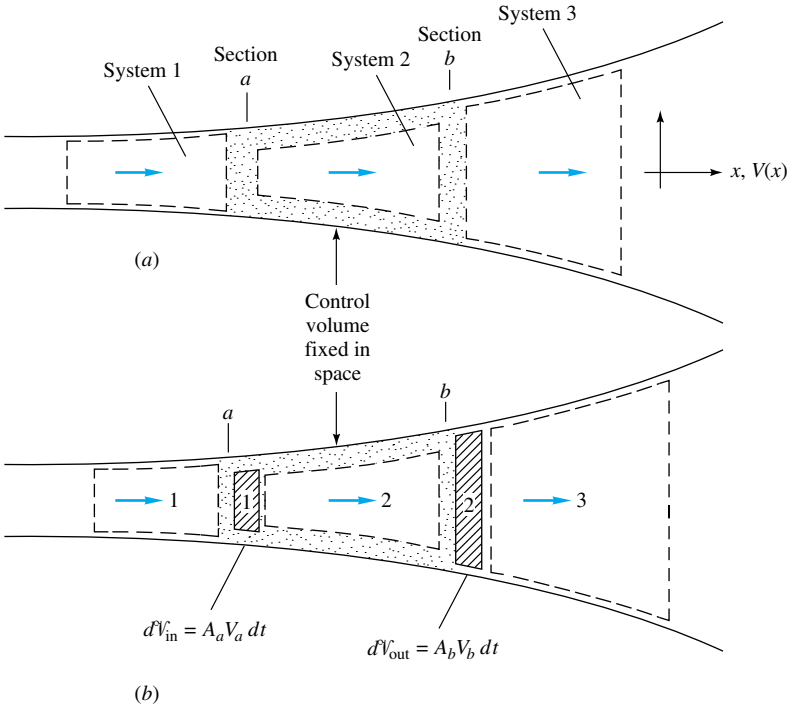


Fig. 3.3 Example of inflow and outflow as three systems pass through a control volume: (*a*) System 2 fills the control volume at time t; (*b*) at time $t + dt$ system 2 begins to leave and system 1 enters.



ketabline.com Ebook.ketabline.com

where $\rho\, d\mathcal{V}$ is a differential mass of the fluid. We want to relate the rate of change of B_{CV} to the rate of change of the amount of B in system 2 which happens to coincide with the control volume at time t. The time derivative of B_{CV} is defined by the calculus limit

$$\begin{aligned}\frac{d}{dt}(B_{CV}) &= \frac{1}{dt}B_{CV}(t+dt) - \frac{1}{dt}B_{CV}(t)\\ &= \frac{1}{dt}[B_2(t+dt) - (\beta\rho\, d\mathcal{V})_{out} + (\beta\rho d\mathcal{V})_{in}] - \frac{1}{dt}[B_2(t)]\\ &= \frac{1}{dt}[B_2(t+dt) - B_2(t)] - (\beta\rho AV)_{out} + (\beta\rho AV)_{in}\end{aligned}$$

The first term on the right is the rate of change of B within system 2 at the instant it occupies the control volume. By rearranging the last line of the above equation, we have the desired conversion formula relating changes in any property B of a local system to one-dimensional computations concerning a fixed control volume which instantaneously encloses the system.

$$\frac{d}{dt}(B_{syst}) = \frac{d}{dt}\left(\int_{CV} \beta\rho\, d\mathcal{V}\right) + (\beta\rho AV)_{out} - (\beta\rho AV)_{in} \tag{3.9}$$

This is the one-dimensional Reynolds transport theorem for a fixed volume. The three terms on the right-hand side are, respectively,

1. The rate of change of B within the control volume
2. The flux of B passing out of the control surface
3. The flux of B passing into the control surface

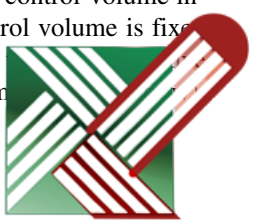
If the flow pattern is steady, the first term vanishes. Equation (3.9) can readily be generalized to an arbitrary flow pattern, as follows.

Arbitrary Fixed Control Volume

Figure 3.4 shows a generalized fixed control volume with an arbitrary flow pattern passing through. The only additional complication is that there are variable slivers of inflow and outflow of fluid all about the control surface. In general, each differential area dA of surface will have a different velocity $\mathbf{V}$ making a different angle θ with the local normal to dA. Some elemental areas will have inflow volume $(VA\cos\theta)_{in}\, dt$, and others will have outflow volume $(VA\cos\theta)_{out}\, dt$, as seen in Fig. 3.4. Some surfaces might correspond to streamlines ($\theta = 90°$) or solid walls ($\mathbf{V} = 0$) with neither inflow nor outflow. Equation (3.9) generalizes to

$$\frac{d}{dt}(B_{syst}) = \frac{d}{dt}\left(\int_{CV} \beta\rho d\mathcal{V}\right) + \int_{CS} \beta\rho V\cos\theta\, dA_{out} - \int_{CS} \beta\rho V\cos\theta\, dA_{in} \tag{3.10}$$

This is the Reynolds transport theorem for an arbitrary fixed control volume. By letting the property B be mass, momentum, angular momentum, or energy, we can rewrite all the basic laws in control-volume form. Note that all three of the control-volume integrals are concerned with the intensive property β. Since the control volume is fixed in space, the elemental volumes $d\mathcal{V}$ do not vary with time, so that [illegible] of the volume integral vanishes unless either β or ρ varies with tim[illegible]



ketabline.com Ebook.ketabline.com

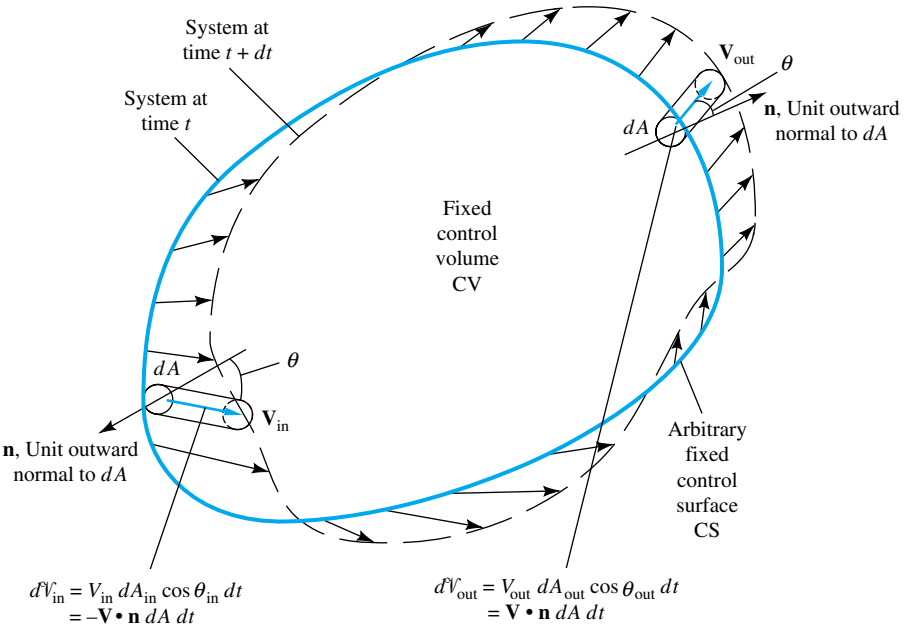


Fig. 3.4 Generalization of Fig. 3.3 to an arbitrary control volume with an arbitrary flow pattern.

Equation (3.10) expresses the basic formula that a system derivative equals the rate of change of B within the control volume plus the flux of B out of the control surface minus the flux of B into the control surface. The quantity B (or β) may be any vector or scalar property of the fluid. Two alternate forms are possible for the flux terms. First we may notice that $V \cos\theta$ is the component of V normal to the area element of the control surface. Thus we can write

$$\text{Flux terms} = \int_{CS} \beta\rho V_n\, dA_{out} - \int_{CS} \beta\rho V_n\, dA_{in} = \int_{CS} \beta\, d\dot{m}_{out} - \int_{CS} \beta\, d\dot{m}_{in} \qquad (3.11a)$$

where $d\dot{m} = \rho V_n\, dA$ is the differential mass flux through the surface. Form (3.11a) helps visualize what is being calculated.

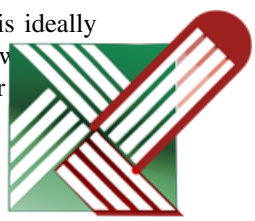
A second alternate form offers elegance and compactness as advantages. If $\mathbf{n}$ is defined as the *outward* normal unit vector everywhere on the control surface, then $\mathbf{V} \cdot \mathbf{n} = V_n$ for outflow and $\mathbf{V} \cdot \mathbf{n} = -V_n$ for inflow. Therefore the flux terms can be represented by a single integral involving $\mathbf{V} \cdot \mathbf{n}$ which accounts for both positive outflow and negative inflow

$$\text{Flux terms} = \int_{CS} \beta\rho(\mathbf{V} \cdot \mathbf{n})\, dA \qquad (3.11b)$$

The compact form of the Reynolds transport theorem is thus

$$\frac{d}{dt}(B_{syst}) = \frac{d}{dt}\left(\int_{CV} \beta\rho\, d\mathcal{V}\right) + \int_{CV} \beta\rho(\mathbf{V} \cdot \mathbf{n})\, dA \qquad (3.12)$$

This is beautiful but only occasionally useful, when the coordinate system is ideally suited to the control volume selected. Otherwise the computations are easier w
flux of B out is added and the flux of B in is subtracted, according to (3.10) or



ketabline.com Ebook.ketabline.com

The time-derivative term can be written in the equivalent form

$$\frac{d}{dt}\left(\int_{CV} \beta\rho \, d\mathcal{V}\right) = \int_{CV} \frac{\partial}{\partial t}(\beta\rho) \, d\mathcal{V} \tag{3.13}$$

for the fixed control volume since the volume elements do not vary.

Control Volume Moving at Constant Velocity

If the control volume is moving uniformly at velocity $\mathbf{V}_s$, as in Fig. 3.2*b*, an observer fixed to the control volume will see a relative velocity $\mathbf{V}_r$ of fluid crossing the control surface, defined by

$$\mathbf{V}_r = \mathbf{V} - \mathbf{V}_s \tag{3.14}$$

where $\mathbf{V}$ is the fluid velocity relative to the same coordinate system in which the control volume motion $\mathbf{V}_s$ is observed. Note that Eq. (3.14) is a vector subtraction. The flux terms will be proportional to $\mathbf{V}_r$, but the volume integral is unchanged because the control volume moves as a fixed shape without deforming. The Reynolds transport theorem for this case of a uniformly moving control volume is

$$\frac{d}{dt}(B_{syst}) = \frac{d}{dt}\left(\int_{CV} \beta\rho \, d\mathcal{V}\right) + \int_{CS} \beta\rho(\mathbf{V}_r \cdot \mathbf{n}) \, dA \tag{3.15}$$

which reduces to Eq. (3.12) if $\mathbf{V}_s \equiv 0$.

Control Volume of Constant Shape but Variable Velocity[4]

If the control volume moves with a velocity $\mathbf{V}_s(t)$ which retains its shape, then the volume elements do not change with time but the boundary relative velocity $\mathbf{V}_r = \mathbf{V}(\mathbf{r}, t) - \mathbf{V}_s(t)$ becomes a somewhat more complicated function. Equation (3.15) is unchanged in form, but the area integral may be more laborious to evaluate.

Arbitrarily Moving and Deformable Control Volume[5]

The most general situation is when the control volume is both moving and deforming arbitrarily, as illustrated in Fig. 3.5. The flux of volume across the control surface is again proportional to the relative normal velocity component $\mathbf{V}_r \cdot \mathbf{n}$, as in Eq. (3.15). However, since the control surface has a deformation, its velocity $\mathbf{V}_s = \mathbf{V}_s(\mathbf{r}, t)$, so that the relative velocity $\mathbf{V}_r = \mathbf{V}(\mathbf{r}, t) - \mathbf{V}_s(\mathbf{r}, t)$ is or can be a complicated function, even though the flux integral is the same as in Eq. (3.15). Meanwhile, the volume integral in Eq. (3.15) must allow the volume elements to distort with time. Thus the time derivative must be applied *after* integration. For the deforming control volume, then, the transport theorem takes the form

$$\frac{d}{dt}(B_{syst}) = \frac{d}{dt}\left(\int_{CV} \beta\rho \, d\mathcal{V}\right) + \int_{CS} \beta\rho(\mathbf{V}_r \cdot \mathbf{n}) \, dA \tag{3.16}$$

This is the most general case, which we can compare with the equivalent form for a fixed control volume

[4]This section may be omitted without loss of continuity.
[5]This section may be omitted without loss of continuity.



ketabline.com Ebook.ketabline.com

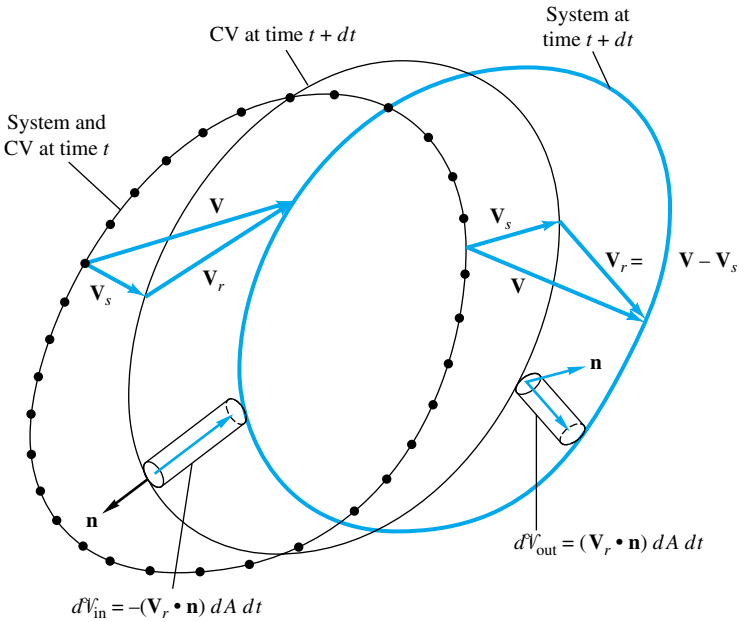


Fig. 3.5 Relative-velocity effects between a system and a control volume when both move and deform. The system boundaries move at velocity $\mathbf{V}$, and the control surface moves at velocity $\mathbf{V}_s$.

$$\frac{d}{dt}(B_{\text{syst}}) = \int_{\text{CV}} \frac{\partial}{\partial t}(\beta\rho)\, d\forall + \int_{\text{CS}} \beta\rho(\mathbf{V} \cdot \mathbf{n})\, dA \tag{3.17}$$

The moving and deforming control volume, Eq. (3.16), contains only two complications: (1) The time derivative of the first integral on the right must be taken outside, and (2) the second integral involves the *relative* velocity $\mathbf{V}_r$ between the fluid system and the control surface. These differences and mathematical subtleties are best shown by examples.

One-Dimensional Flux-Term Approximations

In many applications, the flow crosses the boundaries of the control surface only at certain simplified inlets and exits which are approximately *one-dimensional*; i.e., the flow properties are nearly uniform over the cross section of the inlet or exit. Then the double-integral flux terms required in Eq. (3.16) reduce to a simple sum of positive (exit) and negative (inlet) product terms involving the flow properties at each cross section

$$\int_{\text{CS}} \beta\rho(\mathbf{V}_r \cdot \mathbf{n})\, dA = \sum(\beta_i \rho_i V_{ri} A_i)_{\text{out}} - \sum(\beta_i \rho_i V_{ri} A_i)_{\text{in}} \tag{3.18}$$

An example of this situation is shown in Fig. 3.6. There are inlet flows at sections 1 and 4 and outflows at sections 2, 3, and 5. For this particular problem Eq. (3.18) would be

$$\int_{\text{CS}} \beta\rho(\mathbf{V}_r \cdot \mathbf{n})\, dA = \beta_2\rho_2 V_{r2} A_2 + \beta_3\rho_3 V_{r3} A_3 + \beta_5\rho_5 V_{r5} A_5 - \beta_1\rho_1 V_{r1} A_1 - \beta_4\rho_4 V_{r4} A_4$$



ketabline.com Ebook.ketabline.com

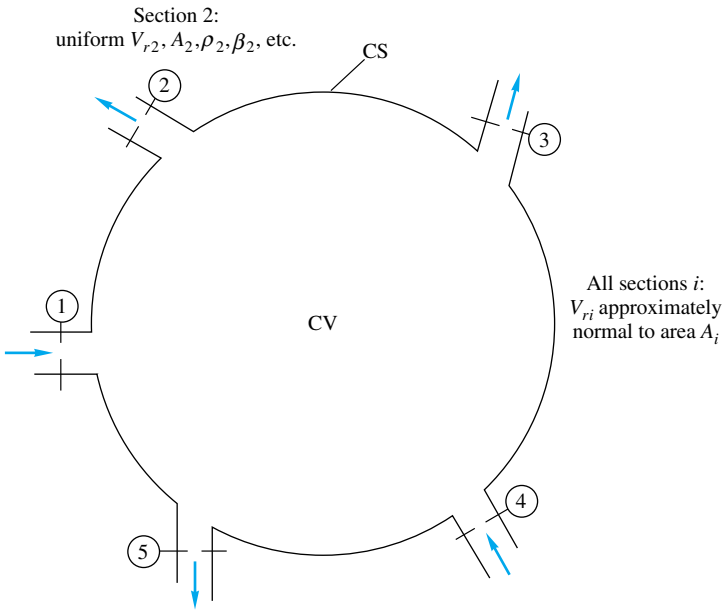
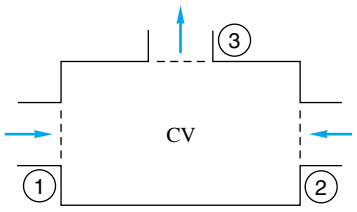


Fig. 3.6 A control volume with simplified one-dimensional inlets and exits.

with no contribution from any other portion of the control surface because there is no flow across the boundary.

EXAMPLE 3.1

A fixed control volume has three one-dimensional boundary sections, as shown in Fig. E3.1. The flow within the control volume is steady. The flow properties at each section are tabulated below. Find the rate of change of energy of the system which occupies the control volume at this instant.



E3.1

Section	Type	ρ, kg/m^3	V, m/s	A, m^2	e, J/kg
1	Inlet	800	5.0	2.0	300
2	Inlet	800	8.0	3.0	100
3	Outlet	800	17.0	2.0	150

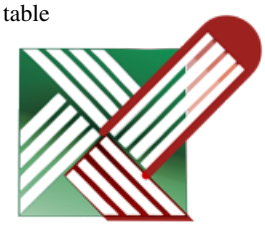
Solution

The property under study here is energy, and so $B = E$ and $\beta = dE/dm = e$, the energy per unit mass. Since the control volume is fixed, Eq. (3.17) applies:

$$\left(\frac{dE}{dt}\right)_{\text{syst}} = \int_{\text{CV}} \frac{\partial}{\partial t}(e\rho)\, d\mathcal{V} + \int_{\text{CS}} e\rho(\mathbf{V}\cdot\mathbf{n})\, dA$$

The flow within is steady, so that $\partial(e\rho)/\partial t \equiv 0$ and the volume integral vanishes. The area integral consists of two inlet sections and one outlet section, as given in the table

$$\left(\frac{dE}{dt}\right)_{\text{syst}} = -e_1\rho_1 A_1 V_1 - e_2\rho_2 A_2 V_2 + e_3\rho_3 A_3 V_3$$



ketabline.com Ebook.ketabline.com

Introducing the numerical values from the table, we have

$$\left(\frac{dE}{dt}\right)_{\text{syst}} = -(300 \text{ J/kg})(800 \text{ kg/m}^3)(2 \text{ m}^2)(5 \text{ m/s}) - 100(800)(3)(8) + 150(800)(2)(17)$$

$$= (-2{,}400{,}000 - 1{,}920{,}000 + 4{,}080{,}000) \text{ J/s}$$

$$= -240{,}000 \text{ J/s} = -0.24 \text{ MJ/s} \qquad \textit{Ans.}$$

Thus the system is losing energy at the rate of 0.24 MJ/s = 0.24 MW. Since we have accounted for all fluid energy crossing the boundary, we conclude from the first law that there must be heat loss through the control surface or the system must be doing work on the environment through some device not shown. Notice that the use of SI units leads to a consistent result in joules per second without any conversion factors. We promised in Chap. 1 that this would be the case.

Note: This problem involves energy, but suppose we check the balance of mass also. Then B = mass m, and $B = dm/dm$ = unity. Again the volume integral vanishes for steady flow, and Eq. (3.17) reduces to

$$\left(\frac{dm}{dt}\right)_{\text{syst}} = \int_{\text{CS}} \rho(\mathbf{V} \cdot \mathbf{n})\, dA = -\rho_1 A_1 V_1 - \rho_2 A_2 V_2 + \rho_3 A_3 V_3$$

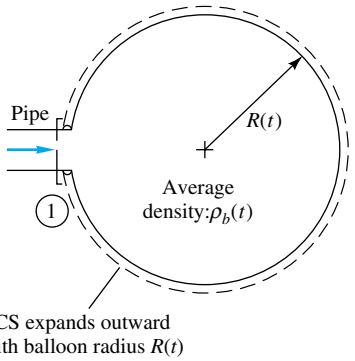
$$= -(800 \text{ kg/m}^3)(2 \text{ m}^2)(5 \text{ m/s}) - 800(3)(8) + 800(17)(2)$$

$$= (-8000 - 19{,}200 + 27{,}200) \text{ kg/s} = 0 \text{ kg/s}$$

Thus the system mass does not change, which correctly expresses the law of conservation of system mass, Eq. (3.1).

EXAMPLE 3.2

The balloon in Fig. E3.2 is being filled through section 1, where the area is A_1, velocity is V_1, and fluid density is ρ_1. The average density within the balloon is $\rho_b(t)$. Find an expression for the rate of change of system mass within the balloon at this instant.



E3.2

Solution

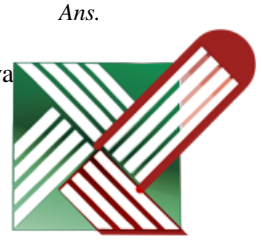
It is convenient to define a deformable control surface just outside the balloon, expanding at the same rate $R(t)$. Equation (3.16) applies with $V_r = 0$ on the balloon surface and $V_r = V_1$ at the pipe entrance. For mass change, we take $B = m$ and $\beta = dm/dm = 1$. Equation (3.16) becomes

$$\left(\frac{dm}{dt}\right)_{\text{syst}} = \frac{d}{dt}\left(\int_{\text{CS}} \rho\, d\mathcal{V}\right) + \int_{\text{CS}} \rho(\mathbf{V}_r \cdot \mathbf{n})\, dA$$

Mass flux occurs only at the inlet, so that the control-surface integral reduces to the single negative term $-\rho_1 A_1 V_1$. The fluid mass within the control volume is approximately the average density times the volume of a sphere. The equation thus becomes

$$\left(\frac{dm}{dt}\right)_{\text{syst}} = \frac{d}{dt}\left(\rho_b \frac{4}{3}\pi R^3\right) - \rho_1 A_1 V_1 \qquad \textit{Ans.}$$

This is the desired result for the system mass rate of change. Actually, by the conserva



ketabline.com Ebook.ketabline.com

(3.1), this change must be zero. Thus the balloon density and radius are related to the inlet mass flux by

$$\frac{d}{dt}(\rho_b R^3) = \frac{3}{4\pi}\rho_1 A_1 V_1$$

This is a first-order differential equation which could form part of an engineering analysis of balloon inflation. It cannot be solved without further use of mechanics and thermodynamics to relate the four unknowns ρ_b, ρ_1, V_1, and R. The pressure and temperature and the elastic properties of the balloon would also have to be brought into the analysis.

For advanced study, many more details of the analysis of deformable control volumes can be found in Hansen [4] and Potter and Foss [5].

3.3 Conservation of Mass

The Reynolds transport theorem, Eq. (3.16) or (3.17), establishes a relation between system rates of change and control-volume surface and volume integrals. But system derivatives are related to the basic laws of mechanics, Eqs. (3.1) to (3.5). Eliminating system derivatives between the two gives the control-volume, or *integral*, forms of the laws of mechanics of fluids. The dummy variable B becomes, respectively, mass, linear momentum, angular momentum, and energy.

For conservation of mass, as discussed in Examples 3.1 and 3.2, $B = m$ and $\beta = dm/dm = 1$. Equation (3.1) becomes

$$\left(\frac{dm}{dt}\right)_{\text{syst}} = 0 = \frac{d}{dt}\left(\int_{\text{CV}} \rho \, d\mathcal{V}\right) + \int_{\text{CS}} \rho(\mathbf{V_r} \cdot \mathbf{n}) \, dA \tag{3.20}$$

This is the integral mass-conservation law for a deformable control volume. For a fixed control volume, we have

$$\int_{\text{CV}} \frac{\partial \rho}{\partial t} \, d\mathcal{V} + \int_{\text{CS}} \rho(\mathbf{V} \cdot \mathbf{n}) \, dA = 0 \tag{3.21}$$

If the control volume has only a number of one-dimensional inlets and outlets, we can write

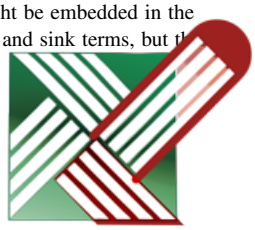
$$\int_{\text{CV}} \frac{\partial \rho}{\partial t} \, d\mathcal{V} + \sum_i (\rho_i A_i V_i)_{\text{out}} - \sum_i (\rho_i A_i V_i)_{\text{in}} = 0 \tag{3.22}$$

Other special cases occur. Suppose that the flow within the control volume is steady; then $\partial\rho/\partial t \equiv 0$, and Eq. (3.21) reduces to

$$\int_{\text{CS}} \rho(\mathbf{V} \cdot \mathbf{n}) \, dA = 0 \tag{3.23}$$

This states that in steady flow the mass flows entering and leaving the control volume must balance exactly.[6] If, further, the inlets and outlets are one-dimensional, we have

[6]Throughout this section we are neglecting *sources* or *sinks* of mass which might be embedded in the control volume. Equations (3.20) and (3.21) can readily be modified to add source and sink terms, but this is rarely necessary.



ketabline.com Ebook.ketabline.com

for steady flow

$$\sum_i (\rho_i A_i V_i)_{\text{in}} = \sum_i (\rho_i A_i V_i)_{\text{out}} \tag{3.24}$$

This simple approximation is widely used in engineering analyses. For example, referring to Fig. 3.6, we see that if the flow in that control volume is steady, the three outlet mass fluxes balance the two inlets:

$$\text{Outflow} = \text{inflow}$$
$$\rho_2 A_2 V_2 + \rho_3 A_3 V_3 + \rho_5 A_5 V_5 = \rho_1 A_1 V_1 + \rho_4 A_4 V_4 \tag{3.25}$$

The quantity ρAV is called the *mass flow* $\dot{m}$ passing through the one-dimensional cross section and has consistent units of kilograms per second (or slugs per second) for SI (or BG) units. Equation (3.25) can be rewritten in the short form

$$\dot{m}_2 + \dot{m}_3 + \dot{m}_5 = \dot{m}_1 + \dot{m}_4 \tag{3.26}$$

and, in general, the steady-flow–mass-conservation relation (3.23) can be written as

$$\sum_i (\dot{m}_i)_{\text{out}} = \sum_i (\dot{m}_i)_{\text{in}} \tag{3.27}$$

If the inlets and outlets are not one-dimensional, one has to compute $\dot{m}$ by integration over the section

$$\dot{m}_{\text{cs}} = \int_{\text{cs}} \rho(\mathbf{V} \cdot \mathbf{n})\, dA \tag{3.28}$$

where "cs" stands for cross section. An illustration of this is given in Example 3.4.

Incompressible Flow

Still further simplification is possible if the fluid is incompressible, which we may define as having density variations which are negligible in the mass-conservation requirement.[7] As we saw in Chap. 1, all liquids are nearly incompressible, and gas flows can *behave* as if they were incompressible, particularly if the gas velocity is less than about 30 percent of the speed of sound of the gas.

Again consider the fixed control volume. If the fluid is nearly incompressible, $\partial\rho/\partial t$ is negligible and the volume integral in Eq. (3.21) may be neglected, after which the density can be slipped outside the surface integral and divided out since it is nonzero. The result is a conservation law for incompressible flows, whether steady or unsteady:

$$\int_{\text{CS}} (\mathbf{V} \cdot \mathbf{n})\, dA = 0 \tag{3.29}$$

If the inlets and outlets are one-dimensional, we have

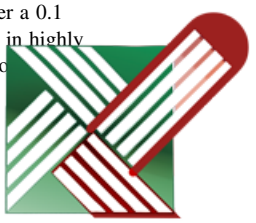
$$\sum_i (V_i A_i)_{\text{out}} = \sum_i (V_i A_i)_{\text{in}} \tag{3.30}$$

or

$$\sum Q_{\text{out}} = \sum Q_{\text{in}}$$

where $Q_i = V_i A_i$ is called the *volume flow* passing through the given cross section.

[7] Be warned that there is subjectivity in specifying incompressibility. Oceanographers consider a 0.1 percent density variation very significant, while aerodynamicists often neglect density variations in highly compressible, even hypersonic, gas flows. Your task is to justify the incompressible approximation you make it.



ketabline.com Ebook.ketabline.com

Again, if consistent units are used, $Q = VA$ will have units of cubic meters per second (SI) or cubic feet per second (BG). If the cross section is not one-dimensional, we have to integrate

$$Q_{CS} = \int_{CS} (\mathbf{V} \cdot \mathbf{n})\, dA \tag{3.31}$$

Equation (3.31) allows us to define an *average velocity* V_{av} which, when multiplied by the section area, gives the correct volume flow

$$V_{av} = \frac{Q}{A} = \frac{1}{A} \int (\mathbf{V} \cdot \mathbf{n})\, dA \tag{3.32}$$

This could be called the *volume-average velocity*. If the density varies across the section, we can define an average density in the same manner:

$$\rho_{av} = \frac{1}{A} \int \rho\, dA \tag{3.33}$$

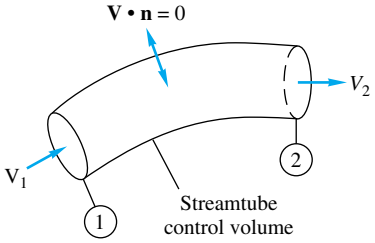
But the mass flow would contain the product of density and velocity, and the average product $(\rho V)_{av}$ would in general have a different value from the product of the averages

$$(\rho V)_{av} = \frac{1}{A} \int \rho(\mathbf{V} \cdot \mathbf{n})\, dA \approx \rho_{av} V_{av} \tag{3.34}$$

We illustrate average velocity in Example 3.4. We can often neglect the difference or, if necessary, use a correction factor between mass average and volume average.

EXAMPLE 3.3

Write the conservation-of-mass relation for steady flow through a streamtube (flow everywhere parallel to the walls) with a single one-dimensional exit 1 and inlet 2 (Fig. E3.3).



E3.3

Solution

For steady flow Eq. (3.24) applies with the single inlet and exit

$$\dot{m} = \rho_1 A_1 V_1 = \rho_2 A_2 V_2 = \text{const}$$

Thus, in a streamtube in steady flow, the mass flow is constant across every section of the tube. If the density is constant, then

$$Q = A_1 V_1 = A_2 V_2 = \text{const} \qquad \text{or} \qquad V_2 = \frac{A_1}{A_2} V_1$$

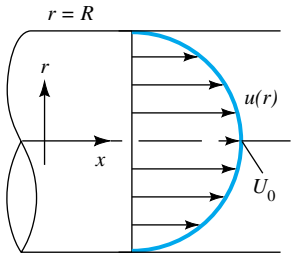
The volume flow is constant in the tube in steady incompressible flow, and the velocity increases as the section area decreases. This relation was derived by Leonardo da Vinci in 1500.

EXAMPLE 3.4

For steady viscous flow through a circular tube (Fig. E3.4), the axial velo
approximately by



ketabline.com Ebook.ketabline.com



E3.4

$$u = U_0\left(1 - \frac{r}{R}\right)^m$$

so that u varies from zero at the wall ($r = R$), or no slip, up to a maximum $u = U_0$ at the centerline $r = 0$. For highly viscous (laminar) flow $m \approx \frac{1}{2}$, while for less viscous (turbulent) flow $m \approx \frac{1}{7}$. Compute the average velocity if the density is constant.

Solution

The average velocity is defined by Eq. (3.32). Here $\mathbf{V} = \mathbf{i}u$ and $\mathbf{n} = \mathbf{i}$, and thus $\mathbf{V} \cdot \mathbf{n} = u$. Since the flow is symmetric, the differential area can be taken as a circular strip $dA = 2\,\pi r\,dr$. Equation (3.32) becomes

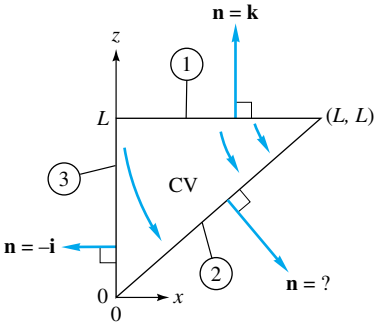
$$V_{av} = \frac{1}{A}\int u\,dA = \frac{1}{\pi R^2}\int_0^R U_0\left(1 - \frac{r}{R}\right)^m 2\pi r\,dr$$

or

$$V_{av} = U_0\,\frac{2}{(1+m)(2+m)} \qquad \textit{Ans.}$$

For the laminar-flow approximation, $m \approx \frac{1}{2}$ and $V_{av} \approx 0.53U_0$. (The exact laminar theory in Chap. 6 gives $V_{av} = 0.50U_0$.) For turbulent flow, $m \approx \frac{1}{7}$ and $V_{av} \approx 0.82U_0$. (There is no exact turbulent theory, and so we accept this approximation.) The turbulent velocity profile is more uniform across the section, and thus the average velocity is only slightly less than maximum.

EXAMPLE 3.5



Depth b into paper

E3.5

Consider the constant-density velocity field

$$u = \frac{V_0 x}{L} \qquad v = 0 \qquad w = -\frac{V_0 z}{L}$$

similar to Example 1.10. Use the triangular control volume in Fig. E3.5, bounded by (0, 0), (L, L), and (0, L), with depth b into the paper. Compute the volume flow through sections 1, 2, and 3, and compare to see whether mass is conserved.

Solution

The velocity field everywhere has the form $\mathbf{V} = \mathbf{i}u + \mathbf{k}w$. This must be evaluated along each section. We save section 2 until last because it looks tricky. Section 1 is the plane $z = L$ with depth b. The unit outward normal is $\mathbf{n} = \mathbf{k}$, as shown. The differential area is a strip of depth b varying with x: $dA = b\,dx$. The normal velocity is

$$(\mathbf{V} \cdot \mathbf{n})_1 = (\mathbf{i}u + \mathbf{k}w) \cdot \mathbf{k} = w\big|_1 = -\frac{V_0 z}{L}\bigg|_{z=L} = -V_0$$

The volume flow through section 1 is thus, from Eq. (3.31),

$$Q_1 = \int_1 (\mathbf{V} \cdot \mathbf{n})\,dA = \int_0^L (-V_0)b\,dx = -V_0 bL$$



ketabline.com Ebook.ketabline.com

Since this is negative, section 1 is a net inflow. Check the units: V_0bL is a velocity times an area; OK.

Section 3 is the plane $x = 0$ with depth b. The unit normal is $\mathbf{n} = -\mathbf{i}$, as shown, and $dA = b\,dz$. The normal velocity is

$$(\mathbf{V}\cdot\mathbf{n})_3 = (\mathbf{i}u + \mathbf{k}w)\cdot(-\mathbf{i}) = -u\big|_3 = -\frac{V_0 x}{L}\bigg|_{s=0} = 0 \qquad \textit{Ans. 3}$$

Thus $V_n \equiv 0$ all along section 3; hence $Q_3 = 0$.

Finally, section 2 is the plane $x = z$ with depth b. The normal direction is to the right $\mathbf{i}$ and down $-\mathbf{k}$ but must have *unit* value; thus $\mathbf{n} = (1/\sqrt{2})(\mathbf{i} - \mathbf{k})$. The differential area is either $dA = \sqrt{2}b\,dx$ or $dA = \sqrt{2}b\,dz$. The normal velocity is

$$(\mathbf{V}\cdot\mathbf{n})_2 = (\mathbf{i}u + \mathbf{k}w)\cdot\frac{1}{\sqrt{2}}(\mathbf{i} - \mathbf{k}) = \frac{1}{\sqrt{2}}(u - w)_2$$

$$= \frac{1}{\sqrt{2}}\left[V_0\frac{x}{L} - \left(-V_0\frac{z}{L}\right)\right]_{x=z} = \frac{\sqrt{2}V_0 x}{L} \quad \text{or} \quad \frac{\sqrt{2}V_0 z}{L}$$

Then the volume flow through section 2 is

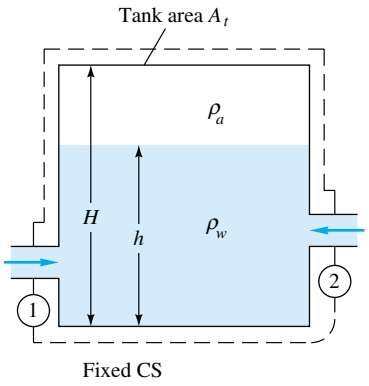
$$Q_2 = \int_2 (\mathbf{V}\cdot\mathbf{n})\,dA = \int_0^L \frac{\sqrt{2}V_0 x}{L}(\sqrt{2}b\,dx) = V_0 bL \qquad \textit{Ans. 2}$$

This answer is positive, indicating an outflow. These are the desired results. We should note that the volume flow is zero through the front and back triangular faces of the prismatic control volume because $V_n = v = 0$ on those faces.

The sum of the three volume flows is

$$Q_1 + Q_2 + Q_3 = -V_0 bL + V_0 bL + 0 = 0$$

Mass is conserved in this constant-density flow, and there are no net sources or sinks within the control volume. This is a very realistic flow, as described in Example 1.10



E3.6

EXAMPLE 3.6

The tank in Fig. E3.6 is being filled with water by two one-dimensional inlets. Air is trapped at the top of the tank. The water height is h. (*a*) Find an expression for the change in water height dh/dt. (*b*) Compute dh/dt if $D_1 = 1$ in, $D_2 = 3$ in, $V_1 = 3$ ft/s, $V_2 = 2$ ft/s, and $A_t = 2$ ft^2, assuming water at 20°C.

Solution

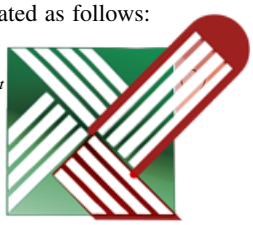
Part (a)

A suggested control volume encircles the tank and cuts through the two inlets. The flow within is unsteady, and Eq. (3.22) applies with no outlets and two inlets:

$$\frac{d}{dt}\left(\int_{CV}\rho\,d\mathcal{V}\right) - \rho_1 A_1 V_1 - \rho_2 A_2 V_2 = 0 \qquad (1)$$

Now if A_t is the tank cross-sectional area, the unsteady term can be evaluated as follows:

$$\frac{d}{dt}\left(\int_{CV}\rho\,d\mathcal{V}\right) = \frac{d}{dt}(\rho_w A_t h) + \frac{d}{dt}[\rho_a A_t(H - h)] = \rho_w A_t$$



ketabline.com Ebook.ketabline.com

The ρ_a term vanishes because it is the rate of change of air mass and is zero because the air is trapped at the top. Substituting (2) into (1), we find the change of water height

$$\frac{dh}{dt} = \frac{\rho_1 A_1 V_1 + \rho_2 A_2 V_2}{\rho_w A_t} \qquad \textit{Ans. (a)}$$

For water, $\rho_1 = \rho_2 = \rho_w$, and this result reduces to

$$\frac{dh}{dt} = \frac{A_1 V_1 + A_2 V_2}{A_t} = \frac{Q_1 + Q_2}{A_t} \tag{3}$$

Part (b) The two inlet volume flows are

$$Q_1 = A_1 V_1 = \tfrac{1}{4}\pi(\tfrac{1}{12}\text{ ft})^2(3\text{ ft/s}) = 0.016\text{ ft}^3/\text{s}$$
$$Q_2 = A_2 V_2 = \tfrac{1}{4}\pi(\tfrac{3}{12}\text{ ft})^2(2\text{ ft/s}) = 0.098\text{ ft}^3/\text{s}$$

Then, from Eq. (3),

$$\frac{dh}{dt} = \frac{(0.016 + 0.098)\text{ ft}^3/\text{s}}{2\text{ ft}^2} = 0.057\text{ ft/s} \qquad \textit{Ans. (b)}$$

Suggestion: Repeat this problem with the top of the tank open.

An illustration of a mass balance with a deforming control volume has already been given in Example 3.2.

The control-volume mass relations, Eq. (3.20) or (3.21), are fundamental to all fluid-flow analyses. They involve only velocity and density. Vector directions are of no consequence except to determine the normal velocity at the surface and hence whether the flow is *in* or *out*. Although your specific analysis may concern forces or moments or energy, you must always make sure that mass is balanced as part of the analysis; otherwise the results will be unrealistic and probably rotten. We shall see in the examples which follow how mass conservation is constantly checked in performing an analysis of other fluid properties.

3.4 The Linear Momentum Equation

In Newton's law, Eq. (3.2), the property being differentiated is the linear momentum $m\mathbf{V}$. Therefore our dummy variable is $\mathbf{B} = m\mathbf{V}$ and $\boldsymbol{\beta} = d\mathbf{B}/dm = \mathbf{V}$, and application of the Reynolds transport theorem gives the linear-momentum relation for a deformable control volume

$$\frac{d}{dt}(m\mathbf{V})_{\text{syst}} = \sum \mathbf{F} = \frac{d}{dt}\left(\int_{\text{CV}} \mathbf{V}\rho\, d\mathcal{V}\right) + \int_{\text{CS}} \mathbf{V}\rho(\mathbf{V}_r \cdot \mathbf{n})\, dA \tag{3.35}$$

The following points concerning this relation should be strongly emphasized:

1. The term $\mathbf{V}$ is the fluid velocity relative to an *inertial* (nonaccelerating) coordinate system; otherwise Newton's law must be modified to include noninertial relative-acceleration terms (see the end of this section).
2. The term $\Sigma\,\mathbf{F}$ is the *vector* sum of all forces acting on the control-volume material considered as a free body; i.e., it includes surface forces on all fluids



ketabline.com Ebook.ketabline.com

solids cut by the control surface plus all body forces (gravity and electromagnetic) acting on the masses within the control volume.

3. The entire equation is a vector relation; both the integrals are vectors due to the term **V** in the integrands. The equation thus has three components. If we want only, say, the x component, the equation reduces to

$$\sum F_x = \frac{d}{dt}\left(\int_{CV} u\rho \, d\forall\right) + \int_{CS} u\rho(\mathbf{V}_r \cdot \mathbf{n}) \, dA \tag{3.36}$$

and similarly, ΣF_y and ΣF_z would involve v and w, respectively. Failure to account for the vector nature of the linear-momentum relation (3.35) is probably the greatest source of student error in control-volume analyses.

For a fixed control volume, the relative velocity $\mathbf{V}_r \equiv \mathbf{V}$, and

$$\sum \mathbf{F} = \frac{d}{dt}\left(\int_{CV} \mathbf{V}\rho \, d\forall\right) + \int_{CS} \mathbf{V}\rho(\mathbf{V} \cdot \mathbf{n}) \, dA \tag{3.37}$$

Again we stress that this is a vector relation and that **V** must be an inertial-frame velocity. Most of the momentum analyses in this text are concerned with Eq. (3.37).

One-Dimensional Momentum Flux

By analogy with the term *mass flow* used in Eq. (3.28), the surface integral in Eq. (3.37) is called the *momentum-flux term.* If we denote momentum by **M**, then

$$\dot{\mathbf{M}}_{CS} = \int_{sec} \mathbf{V}\rho(\mathbf{V} \cdot \mathbf{n}) \, dA \tag{3.38}$$

Because of the dot product, the result will be negative for inlet momentum flux and positive for outlet flux. If the cross section is one-dimensional, **V** and ρ are uniform over the area and the integrated result is

$$\dot{\mathbf{M}}_{sec\,i} = \mathbf{V}_i(\rho_i V_{ni} A_i) = \dot{m}_i \mathbf{V}_i \tag{3.39}$$

for outlet flux and $-\dot{m}_i \mathbf{V}_i$ for inlet flux. Thus if the control volume has only one-dimensional inlets and outlets, Eq. (3.37) reduces to

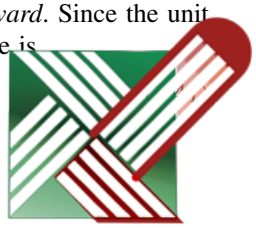
$$\sum \mathbf{F} = \frac{d}{dt}\left(\int_{CV} \mathbf{V}\rho \, d\forall\right) + \sum(\dot{m}_i \mathbf{V}_i)_{out} - \sum(\dot{m}_i \mathbf{V}_i)_{in} \tag{3.40}$$

This is a commonly used approximation in engineering analyses. It is crucial to realize that we are dealing with vector sums. Equation (3.40) states that the net vector force on a fixed control volume equals the rate of change of vector momentum within the control volume plus the vector sum of outlet momentum fluxes minus the vector sum of inlet fluxes.

Net Pressure Force on a Closed Control Surface

Generally speaking, the surface forces on a control volume are due to (1) forces exposed by cutting through solid bodies which protrude through the surface and (2) forces due to pressure and viscous stresses of the surrounding fluid. The computation of pressure force is relatively simple, as shown in Fig. 3.7. Recall from Chap. 2 that the external pressure force on a surface is normal to the surface and *inward*. Since the unit vector **n** is defined as *outward*, one way to write the pressure force is

$$\mathbf{F}_{press} = \int_{CS} p(-\mathbf{n}) \, dA$$



ketabline.com Ebook.ketabline.com

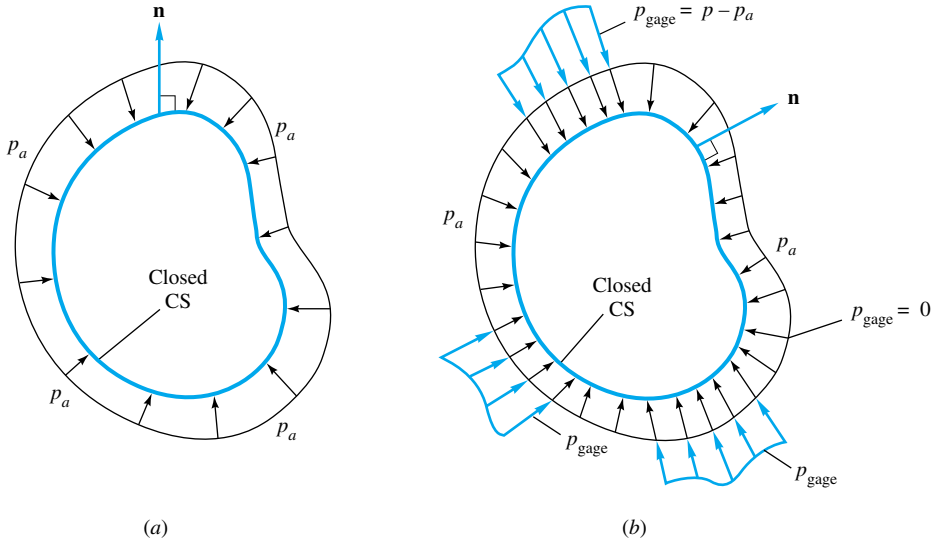


Fig. 3.7 Pressure-force computation by subtracting a uniform distribution: (*a*) uniform pressure, $\mathbf{F} = -p_a \int \mathbf{n}\, dA \equiv 0$; (*b*) nonuniform pressure, $\mathbf{F} = -\int (p - p_a)\mathbf{n}\, dA$.

Now if the pressure has a uniform value p_a all around the surface, as in Fig. 3.7*a*, the net pressure force is zero

$$\mathbf{F}_{UP} = \int p_a(-\mathbf{n})\, dA = -p_a \int \mathbf{n}\, dA \equiv 0 \tag{3.42}$$

where the subscript UP stands for uniform pressure. This result is *independent of the shape of the surface*[8] as long as the surface is closed and all our control volumes are closed. Thus a seemingly complicated pressure-force problem can be simplified by subtracting any convenient uniform pressure p_a and working only with the pieces of gage pressure which remain, as illustrated in Fig. 3.7*b*. Thus Eq. (3.41) is entirely equivalent to

$$\mathbf{F}_{press} = \int_{CS} (p - p_a)(-\mathbf{n})\, dA = \int_{CS} p_{gage}(-\mathbf{n})\, dA$$

This trick can mean quite a saving in computation.

EXAMPLE 3.7

A control volume of a nozzle section has surface pressures of 40 lbf/in^{2}absolute at section 1 and atmospheric pressure of 15 lbf/in^{2}absolute at section 2 and on the external rounded part of the nozzle, as in Fig. E3.7*a*. Compute the net pressure force if $D_1 = 3$ in and $D_2 = 1$ in.

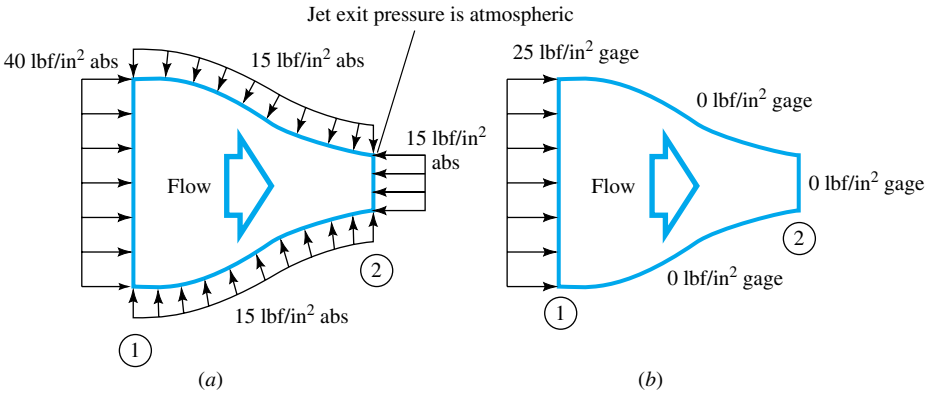
Solution

We do not have to bother with the outer surface if we subtract 15 lbf/in^2 from all surfaces. This leaves 25 lbf/in^{2}gage at section 1 and 0 lbf/in^2 gage everywhere else, as in Fig. E3.7*b*.

[8]Can you prove this? It is a consequence of Gauss' theorem from vector analysis.



ketabline.com Ebook.ketabline.com



E3.7

Then the net pressure force is computed from section 1 only

$$\mathbf{F} = p_{g1}(-\mathbf{n})_1 A_1 = (25 \text{ lbf/in}^2)\frac{\pi}{4}(3 \text{ in})^2\mathbf{i} = 177\mathbf{i} \text{ lbf} \qquad \textit{Ans.}$$

Notice that we did not change inches to feet in this case because, with pressure in pounds-force per square inch and area in square inches, the product gives force directly in pounds. More often, though, the change back to standard units is necessary and desirable. *Note:* This problem computes pressure force only. There are probably other forces involved in Fig. E3.7, e.g., nozzle-wall stresses in the cuts through sections 1 and 2 and the weight of the fluid within the control volume.

Pressure Condition at a Jet Exit

Figure E3.7 illustrates a pressure boundary condition commonly used for jet exit-flow problems. When a fluid flow leaves a confined internal duct and exits into an ambient "atmosphere," its free surface is exposed to that atmosphere. Therefore the jet itself will essentially be at atmospheric pressure also. This condition was used at section 2 in Fig. E3.7.

Only two effects could maintain a pressure difference between the atmosphere and a free exit jet. The first is surface tension, Eq. (1.31), which is usually negligible. The second effect is a *supersonic* jet, which can separate itself from an atmosphere with expansion or compression waves (Chap. 9). For the majority of applications, therefore, we shall set the pressure in an exit jet as atmospheric.

EXAMPLE 3.8

A fixed control volume of a streamtube in steady flow has a uniform inlet flow (ρ_1, A_1, V_1) and a uniform exit flow (ρ_2, A_2, V_2), as shown in Fig. 3.8. Find an expression for the net force on the control volume.

Solution

Equation (3.40) applies with one inlet and exit

$$\sum \mathbf{F} = \dot{m}_2\mathbf{V}_2 - \dot{m}_1\mathbf{V}_1 = (\rho_2 A_2 V_2)\mathbf{V}_2 - (\rho_1 A_1 V_1)\mathbf{V}_1$$



ketabline.com Ebook.ketabline.com

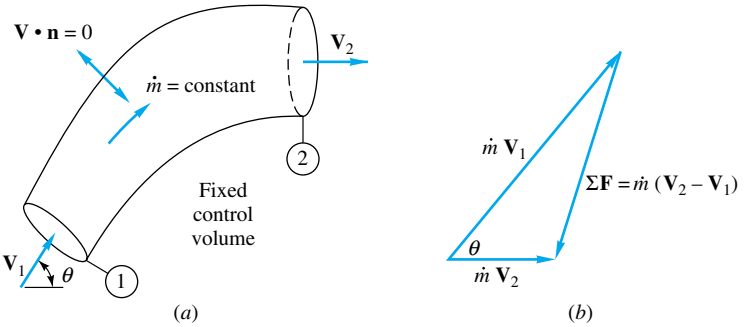


Fig. 3.8 Net force on a one-dimensional streamtube in steady flow: (*a*) streamtube in steady flow; (*b*) vector diagram for computing net force.

The volume-integral term vanishes for steady flow, but from conservation of mass in Example 3.3 we saw that

$$\dot{m}_1 = \dot{m}_2 = \dot{m} = \text{const}$$

Therefore a simple form for the desired result is

$$\sum \mathbf{F} = \dot{m}\,(\mathbf{V}_2 - \mathbf{V}_1) \qquad \textit{Ans.}$$

This is a *vector* relation and is sketched in Fig. 3.8*b*. The term $\Sigma\,\mathbf{F}$ represents the net force acting on the control volume due to all causes; it is needed to balance the change in momentum of the fluid as it turns and decelerates while passing through the control volume.

EXAMPLE 3.9

As shown in Fig. 3.9*a*, a fixed vane turns a water jet of area A through an angle θ without changing its velocity magnitude. The flow is steady, pressure is p_a everywhere, and friction on the vane is negligible. (*a*) Find the components F_x and F_y of the applied vane force. (*b*) Find expressions for the force magnitude F and the angle ϕ between F and the horizontal; plot them versus θ.

Solution

Part (a) The control volume selected in Fig. 3.9*a* cuts through the inlet and exit of the jet and through the vane support, exposing the vane force **F**. Since there is no cut along the vane-jet interface,

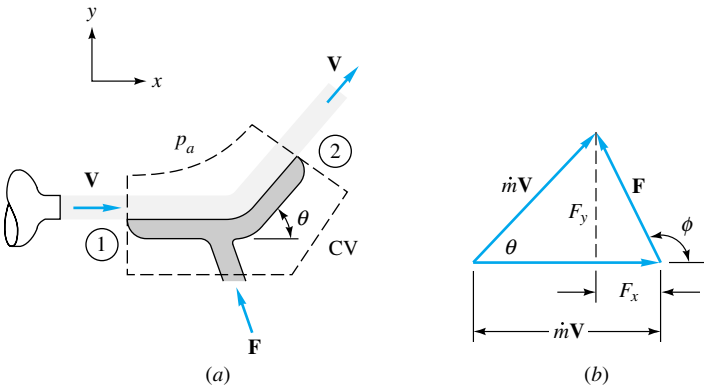


Fig. 3.9 Net applied force on a fixed jet-turning vane: (*a*) geometry of the vane turning the water jet; (*b*) vector diagram for the net force.



ketabline.com Ebook.ketabline.com

vane friction is internally self-canceling. The pressure force is zero in the uniform atmosphere. We neglect the weight of fluid and the vane weight within the control volume. Then Eq. (3.40) reduces to

$$\mathbf{F}_{\text{vane}} = \dot{m}_2\mathbf{V}_2 - \dot{m}_1\mathbf{V}_1$$

But the magnitude $V_1 = V_2 = V$ as given, and conservation of mass for the streamtube requires $\dot{m}_1 = \dot{m}_2 = \dot{m} = \rho AV$. The vector diagram for force and momentum change becomes an isosceles triangle with legs $\dot{m}\mathbf{V}$ and base $\mathbf{F}$, as in Fig. 3.9*b*. We can readily find the force components from this diagram

$$F_x = \dot{m}V(\cos\,\theta - 1) \qquad F_y = \dot{m}V\,\sin\,\theta \qquad \textit{Ans. (a)}$$

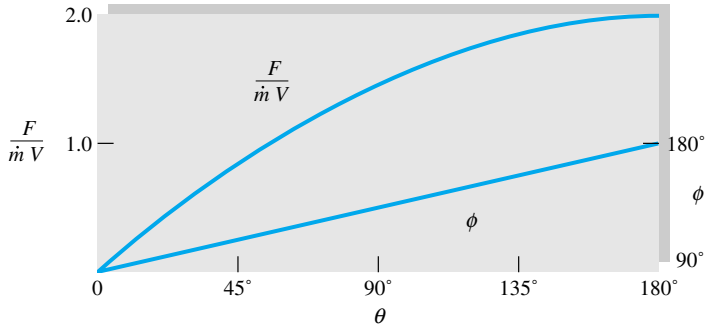
where $\dot{m}V = \rho AV^2$ for this case. This is the desired result.

Part (b) The force magnitude is obtained from part (*a*):

$$F = (F_x^2 + F_y^2)^{1/2} = \dot{m}V[\sin^2\theta + (\cos\,\theta - 1)^2]^{1/2} = 2\dot{m}V\,\sin\frac{\theta}{2} \qquad \textit{Ans. (b)}$$

From the geometry of Fig. 3.9*b* we obtain

$$\phi = 180^\circ - \tan^{-1}\frac{F_y}{F_x} = 90^\circ + \frac{\theta}{2} \qquad \textit{Ans. (b)}$$



E3.9

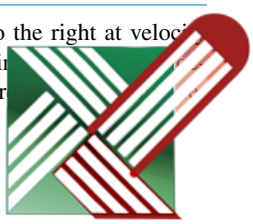
These can be plotted versus θ as shown in Fig. E3.9. Two special cases are of interest. First, the maximum force occurs at $\theta = 180^\circ$, that is, when the jet is turned around and thrown back in the opposite direction with its momentum completely reversed. This force is $2\dot{m}V$ and acts to the *left*; that is, $\phi = 180^\circ$. Second, at very small turning angles ($\theta < 10^\circ$) we obtain approximately

$$F \approx \dot{m}V\theta \qquad \phi \approx 90^\circ$$

The force is linearly proportional to the turning angle and acts nearly normal to the jet. This is the principle of a lifting vane, or airfoil, which causes a slight change in the oncoming flow direction and thereby creates a lift force normal to the basic flow.

EXAMPLE 3.10

A water jet of velocity V_j impinges normal to a flat plate which moves to the right at velocity V_c, as shown in Fig. 3.10*a*. Find the force required to keep the plate moving if the jet density is 1000 kg/m^3, the jet area is 3 cm^2, and V_j and V_c ar



ketabline.com Ebook.ketabline.com

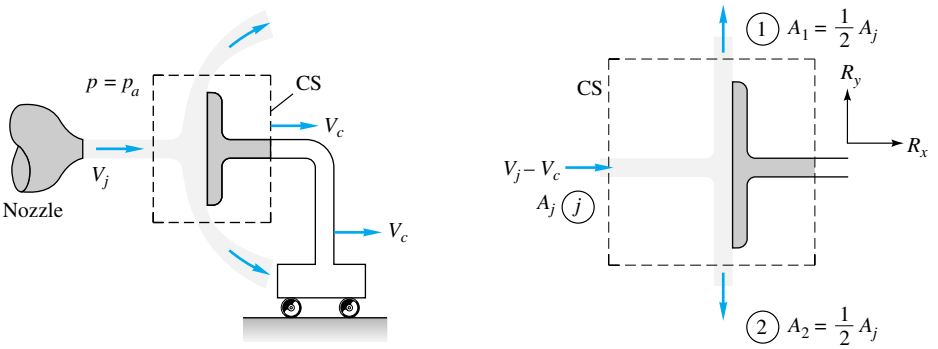


Fig. 3.10 Force on a plate moving at constant velocity: (*a*) jet striking a moving plate normally; (*b*) control volume fixed relative to the plate.

spectively. Neglect the weight of the jet and plate, and assume steady flow with respect to the moving plate with the jet splitting into an equal upward and downward half-jet.

Solution

The suggested control volume in Fig. 3.10*a* cuts through the plate support to expose the desired forces R_x and R_y. This control volume moves at speed V_c and thus is fixed relative to the plate, as in Fig. 3.10*b*. We must satisfy both mass and momentum conservation for the assumed steady-flow pattern in Fig. 3.10*b*. There are two outlets and one inlet, and Eq. (3.30) applies for mass conservation

$$\dot{m}_{\text{out}} = \dot{m}_{\text{in}}$$

or
$$\rho_1 A_1 V_1 + \rho_2 A_2 V_2 = \rho_j A_j (V_j - V_c) \tag{1}$$

We assume that the water is incompressible $\rho_1 = \rho_2 = \rho_j$, and we are given that $A_1 = A_2 = \frac{1}{2}A_j$. Therefore Eq. (1) reduces to

$$V_1 + V_2 = 2(V_j - V_c) \tag{2}$$

Strictly speaking, this is all that mass conservation tells us. However, from the symmetry of the jet deflection and the neglect of fluid weight, we conclude that the two velocities V_1 and V_2 must be equal, and hence (2) becomes

$$V_1 = V_2 = V_j - V_c \tag{3}$$

For the given numerical values, we have

$$V_1 = V_2 = 20 - 15 = 5 \text{ m/s}$$

Now we can compute R_x and R_y from the two components of momentum conservation. Equation (3.40) applies with the unsteady term zero

$$\sum F_x = R_x = \dot{m}_1 u_1 + \dot{m}_2 u_2 - \dot{m}_j u_j \tag{4}$$

where from the mass analysis, $\dot{m}_1 = \dot{m}_2 = \frac{1}{2}\dot{m}_j = \frac{1}{2}\rho_j A_j (V_j - V_c)$. Now check the flow directions at each section: $u_1 = u_2 = 0$, and $u_j = V_j - V_c = 5$ m/s. Thus Eq. (4) becomes

$$R_x = -\dot{m}_j u_j = -[\rho_j A_j (V_j - V_c)](V_j - V_c)$$



ketabline.com Ebook.ketabline.com

For the given numerical values we have

$$R_x = -(1000\ \text{kg/m}^3)(0.0003\ \text{m}^2)(5\ \text{m/s})^2 = -7.5\ (\text{kg} \cdot \text{m})/\text{s}^2 = -7.5\ \text{N} \qquad \textit{Ans.}$$

This acts to the *left*; i.e., it requires a restraining force to keep the plate from accelerating to the right due to the continuous impact of the jet. The vertical force is

$$F_y = R_y = \dot{m}_1 v_1 + \dot{m}_2 v_2 - \dot{m}_j v_j$$

Check directions again: $v_1 = V_1$, $v_2 = -V_2$, $v_j = 0$. Thus

$$R_y = \dot{m}_1(V_1) + \dot{m}_2(-V_2) = \tfrac{1}{2}\dot{m}_j(V_1 - V_2) \qquad (6)$$

But since we found earlier that $V_1 = V_2$, this means that $R_y = 0$, as we could expect from the symmetry of the jet deflection.[9] Two other results are of interest. First, the relative velocity at section 1 was found to be 5 m/s up, from Eq. (3). If we convert this to absolute motion by adding on the control-volume speed $V_c = 15$ m/s to the right, we find that the absolute velocity $\mathbf{V}_1 = 15\mathbf{i} + 5\mathbf{j}$ m/s, or 15.8 m/s at an angle of 18.4° upward, as indicated in Fig. 3.10*a*. Thus the absolute jet speed changes after hitting the plate. Second, the computed force R_x does not change if we assume the jet deflects in all radial directions along the plate surface rather than just up and down. Since the plate is normal to the x axis, there would still be zero outlet x-momentum flux when Eq. (4) was rewritten for a radial-deflection condition.

EXAMPLE 3.11

The previous example treated a plate at normal incidence to an oncoming flow. In Fig. 3.11 the plate is parallel to the flow. The stream is not a jet but a broad river, or *free stream*, of uniform velocity $\mathbf{V} = U_0\mathbf{i}$. The pressure is assumed uniform, and so it has no net force on the plate. The plate does not block the flow as in Fig. 3.10, so that the only effect is due to boundary shear, which was neglected in the previous example. The no-slip condition at the wall brings the fluid there to a halt, and these slowly moving particles retard their neighbors above, so that at the end of the plate there is a significant retarded shear layer, or *boundary layer*, of thickness $y = \delta$. The

[9]Symmetry can be a powerful tool if used properly. Try to learn more about the uses and misuses of symmetry conditions. Here we doggedly computed the results without invoking symmetry.

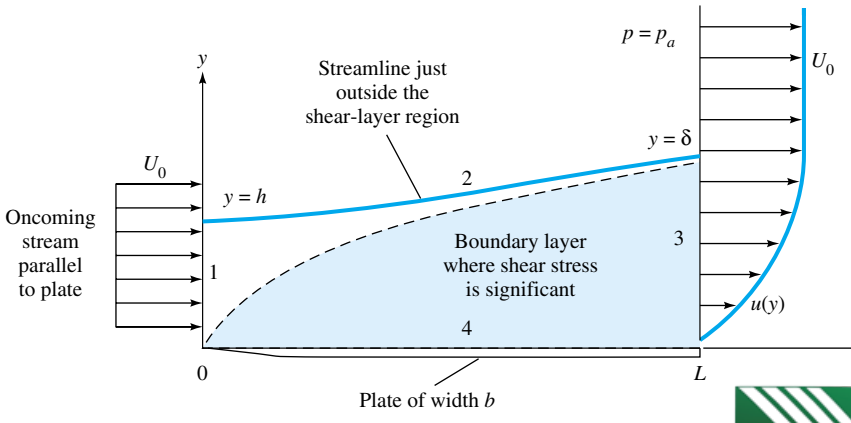


Fig. 3.11 Control-volume analysis of drag force on a flat plate due to boundary shear.

ketabline.com Ebook.ketabline.com

viscous stresses along the wall can sum to a finite drag force on the plate. These effects are illustrated in Fig. 3.11. The problem is to make an integral analysis and find the drag force D in terms of the flow properties ρ, U_0, and δ and the plate dimensions L and b.[†]

Solution

Like most practical cases, this problem requires a combined mass and momentum balance. A proper selection of control volume is essential, and we select the four-sided region from 0 to h to δ to L and back to the origin 0, as shown in Fig. 3.11. Had we chosen to cut across horizontally from left to right along the height $y = h$, we would have cut through the shear layer and exposed unknown shear stresses. Instead we follow the streamline passing through $(x, y) = (0, h)$, which is outside the shear layer and also has no mass flow across it. The four control-volume sides are thus

1. From (0, 0) to (0, h): a one-dimensional inlet, $\mathbf{V} \cdot \mathbf{n} = -U_0$
2. From (0, h) to (L, δ): a streamline, no shear, $\mathbf{V} \cdot \mathbf{n} \equiv 0$
3. From (L, δ) to (L, 0): a two-dimensional outlet, $\mathbf{V} \cdot \mathbf{n} = +u(y)$
4. From (L, 0) to (0, 0): a streamline just above the plate surface, $\mathbf{V} \cdot \mathbf{n} = 0$, shear forces summing to the drag force $-D\mathbf{i}$ acting from the plate onto the retarded fluid

The pressure is uniform, and so there is no net pressure force. Since the flow is assumed incompressible and steady, Eq. (3.37) applies with no unsteady term and fluxes only across sections 1 and 3:

$$\sum F_x = -D = \rho \int_1 u(\mathbf{V} \cdot \mathbf{n})\, dA + \rho \int_3 u(\mathbf{V} \cdot \mathbf{n})\, dA$$

$$= \rho \int_0^h U_0(-U_0)b\, dy + \rho \int_0^\delta u(+u)b\, dy$$

Evaluating the first integral and rearranging give

$$D = \rho U_0^2 bh - \rho b \int_0^\delta u^2 dy \tag{1}$$

This could be considered the answer to the problem, but it is not useful because the height h is not known with respect to the shear-layer thickness δ. This is found by applying mass conservation, since the control volume forms a streamtube

$$\rho \int_{CS} (\mathbf{V} \cdot \mathbf{n})\, dA = 0 = \rho \int_0^h (-U_0)b\, dy + \rho \int_0^\delta ub\, dy$$

or

$$U_0 h = \int_0^\delta u\, dy \tag{2}$$

after canceling b and ρ and evaluating the first integral. Introduce this value of h into Eq. (1) for a much cleaner result

$$D = \rho b \int_0^\delta u(U_0 - u)\, dy \Big|_{x=L} \qquad \textit{Ans.}\ (3)$$

This result was first derived by Theodore von Kármán in 1921.[10] It relates the friction drag on

[†]The general analysis of such wall-shear problems, called *boundary-layer theory*, is treated in Sec. 7.3.

[10]The autobiography of this great twentieth-century engineer and teacher [2] is recommended for historical and scientific insight.



ketabline.com Ebook.ketabline.com

one side of a flat plate to the integral of the *momentum defect* $u(U_0 - u)$ across the trailing cross section of the flow past the plate. Since $U_0 - u$ vanishes as y increases, the integral has a finite value. Equation (3) is an example of *momentum-integral theory* for boundary layers, which is treated in Chap. 7. To illustrate the magnitude of this drag force, we can use a simple parabolic approximation for the outlet-velocity profile $u(y)$ which simulates low-speed, or *laminar*, shear flow

$$u \approx U_0\left(\frac{2y}{\delta} - \frac{y^2}{\delta^2}\right) \qquad \text{for } 0 \le y \le \delta \tag{4}$$

Substituting into Eq. (3) and letting $\eta = y/\delta$ for convenience, we obtain

$$D = \rho b U_0^2 \delta \int_0^1 (2\eta - \eta^2)(1 - 2\eta + \eta^2)\, d\eta = \tfrac{2}{15}\rho U_0^2 b\delta \tag{5}$$

This is within 1 percent of the accepted result from laminar boundary-layer theory (Chap. 7) in spite of the crudeness of the Eq. (4) approximation. This is a happy situation and has led to the wide use of Kármán's integral theory in the analysis of viscous flows. Note that D increases with the shear-layer thickness δ, which itself increases with plate length and the viscosity of the fluid (see Sec. 7.4).

Momentum-Flux Correction Factor

For flow in a duct, the axial velocity is usually nonuniform, as in Example 3.4. For this case the simple momentum-flux calculation $\int u\rho(\mathbf{V}\cdot\mathbf{n})\, dA = \dot{m}V = \rho AV^2$ is somewhat in error and should be corrected to $\beta\rho AV^2$, where β is the dimensionless momentum-flux correction factor, $\beta \ge 1$.

The factor β accounts for the variation of u^2across the duct section. That is, we compute the exact flux and set it equal to a flux based on average velocity in the duct

$$\rho\int u^2 dA = \beta\dot{m}V_{\text{av}} = \beta\rho AV_{\text{av}}^2$$

or

$$\beta = \frac{1}{A}\int \left(\frac{u}{V_{\text{av}}}\right)^2 dA \tag{3.43a}$$

Values of β can be computed based on typical duct velocity profiles similar to those in Example 3.4. The results are as follows:

Laminar flow:

$$u = U_0\left(1 - \frac{r^2}{R^2}\right) \qquad \beta = \frac{4}{3} \tag{3.43b}$$

Turbulent flow:

$$u \approx U_0\left(1 - \frac{r}{R}\right)^m \qquad \frac{1}{9} \le m \le \frac{1}{5}$$

$$\beta = \frac{(1+m)^2(2+m)^2}{2(1+2m)(2+2m)} \tag{3.43c}$$

The turbulent correction factors have the following range of values:

Turbulent flow:

m	$\frac{1}{5}$	$\frac{1}{6}$	$\frac{1}{7}$	$\frac{1}{8}$	$\frac{1}{9}$
β	1.037	1.027	1.020	1.016	1.0



ketabline.com Ebook.ketabline.com

These are so close to unity that they are normally neglected. The laminar correction may sometimes be important.

To illustrate a typical use of these correction factors, the solution to Example 3.8 for nonuniform velocities at sections 1 and 2 would be given as

$$\sum \mathbf{F} = \dot{m}(\beta_2 \mathbf{V}_2 - \beta_1 \mathbf{V}_1) \tag{3.43d}$$

Note that the basic parameters and vector character of the result are not changed at all by this correction.

Noninertial Reference Frame[11]

All previous derivations and examples in this section have assumed that the coordinate system is inertial, i.e., at rest or moving at constant velocity. In this case the rate of change of velocity equals the absolute acceleration of the system, and Newton's law applies directly in the form of Eqs. (3.2) and (3.35).

In many cases it is convenient to use a *noninertial*, or accelerating, coordinate system. An example would be coordinates fixed to a rocket during takeoff. A second example is any flow on the earth's surface, which is accelerating relative to the fixed stars because of the rotation of the earth. Atmospheric and oceanographic flows experience the so-called *Coriolis acceleration*, outlined below. It is typically less than $10^{-5}g$, where g is the acceleration of gravity, but its accumulated effect over distances of many kilometers can be dominant in geophysical flows. By contrast, the Coriolis acceleration is negligible in small-scale problems like pipe or airfoil flows.

Suppose that the fluid flow has velocity $\mathbf{V}$ relative to a noninertial xyz coordinate system, as shown in Fig. 3.12. Then $d\mathbf{V}/dt$ will represent a noninertial acceleration which must be added vectorially to a relative acceleration $\mathbf{a}_{\text{rel}}$ to give the absolute acceleration $\mathbf{a}_i$ relative to some inertial coordinate system XYZ, as in Fig. 3.12. Thus

$$\mathbf{a}_i = \frac{d\mathbf{V}}{dt} + \mathbf{a}_{\text{rel}} \tag{3.44}$$

[11]This section may be omitted without loss of continuity.

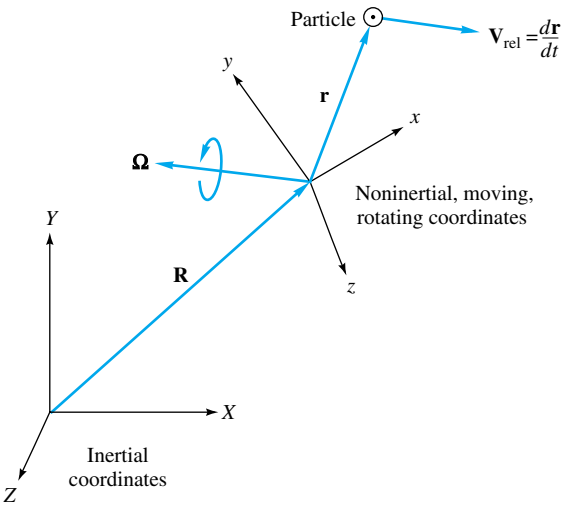


Fig. 3.12 Geometry of fixed versus accelerating coordinates.



ketabline.com Ebook.ketabline.com

Since Newton's law applies to the absolute acceleration,

$$\sum \mathbf{F} = m\mathbf{a}_i = m\left(\frac{d\mathbf{V}}{dt} + \mathbf{a}_{\text{rel}}\right)$$

or

$$\sum \mathbf{F} - m\mathbf{a}_{\text{rel}} = m\frac{d\mathbf{V}}{dt} \tag{3.45}$$

Thus Newton's law in noninertial coordinates xyz is equivalent to adding more "force" terms $-m\mathbf{a}_{\text{rel}}$ to account for noninertial effects. In the most general case, sketched in Fig. 3.12, the term $\mathbf{a}_{\text{rel}}$ contains four parts, three of which account for the angular velocity $\boldsymbol{\Omega}(t)$ of the inertial coordinates. By inspection of Fig. 3.12, the absolute displacement of a particle is

$$\mathbf{S}_i = \mathbf{r} + \mathbf{R} \tag{3.46}$$

Differentiation gives the absolute velocity

$$\mathbf{V}_i = \mathbf{V} + \frac{d\mathbf{R}}{dt} + \boldsymbol{\Omega} \times \mathbf{r} \tag{3.47}$$

A second differentiation gives the absolute acceleration:

$$\mathbf{a}_i = \frac{d\mathbf{V}}{dt} + \frac{d^2\mathbf{R}}{dt^2} + \frac{d\boldsymbol{\Omega}}{dt} \times \mathbf{r} + 2\boldsymbol{\Omega} \times \mathbf{V} + \boldsymbol{\Omega} \times (\boldsymbol{\Omega} \times \mathbf{r}) \tag{3.48}$$

By comparison with Eq. (3.44), we see that the last four terms on the right represent the additional relative acceleration:

1. $d^2\mathbf{R}/dt^2$ is the acceleration of the noninertial origin of coordinates xyz.
2. $(d\boldsymbol{\Omega}/dt) \times \mathbf{r}$ is the angular-acceleration effect.
3. $2\boldsymbol{\Omega} \times \mathbf{V}$ is the Coriolis acceleration.
4. $\boldsymbol{\Omega} \times (\boldsymbol{\Omega} \times \mathbf{r})$ is the centripetal acceleration, directed from the particle normal to the axis of rotation with magnitude $\Omega^2 L$, where L is the normal distance to the axis.[12]

Equation (3.45) differs from Eq. (3.2) only in the added inertial forces on the left-hand side. Thus the control-volume formulation of linear momentum in noninertial coordinates merely adds inertial terms by integrating the added relative acceleration over each differential mass in the control volume

$$\sum \mathbf{F} - \int_{\text{CV}} \mathbf{a}_{\text{rel}}\, dm = \frac{d}{dt}\left(\int_{\text{CV}} \mathbf{V}\rho\, d\mathcal{V}\right) + \int_{\text{CS}} \mathbf{V}\rho(\mathbf{V}_r \cdot \mathbf{n})\, dA \tag{3.49}$$

where

$$\mathbf{a}_{\text{rel}} = \frac{d^2\mathbf{R}}{dt^2} + \frac{d\boldsymbol{\Omega}}{dt} \times \mathbf{r} + 2\boldsymbol{\Omega} \times \mathbf{V} + \boldsymbol{\Omega} \times (\boldsymbol{\Omega} \times \mathbf{r})$$

This is the noninertial equivalent to the inertial form given in Eq. (3.35). To analyze such problems, one must have knowledge of the displacement $\mathbf{R}$ and angular velocity $\boldsymbol{\Omega}$ of the noninertial coordinates.

If the control volume is nondeformable, Eq. (3.49) reduces to

[12] A complete discussion of these noninertial coordinate terms is given, e.g., in R



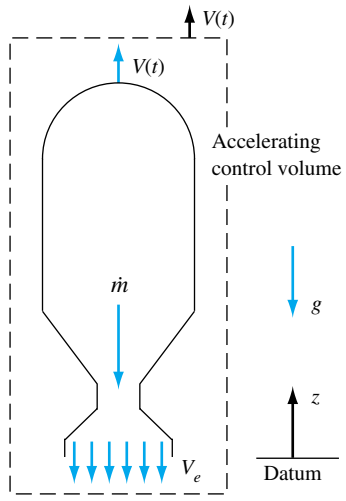
ketabline.com Ebook.ketabline.com

$$\sum \mathbf{F} - \int_{CV} \mathbf{a}_{rel}\, dm = \frac{d}{dt}\left(\int_{CV} \mathbf{V}\rho\, d\mathcal{V}\right) + \int_{CS} \mathbf{V}\rho(\mathbf{V}\cdot\mathbf{n})\, dA \tag{3.50}$$

In other words, the right-hand side reduces to that of Eq. (3.37).

EXAMPLE 3.12

A classic example of an accelerating control volume is a rocket moving straight up, as in Fig. E3.12. Let the initial mass be M_0, and assume a steady exhaust mass flow $\dot{m}$ and exhaust velocity V_e relative to the rocket, as shown. If the flow pattern within the rocket motor is steady and air drag is neglected, derive the differential equation of vertical rocket motion $V(t)$ and integrate using the initial condition $V = 0$ at $t = 0$.



E3.12

Solution

The appropriate control volume in Fig. E3.12 encloses the rocket, cuts through the exit jet, and accelerates upward at rocket speed $V(t)$. The z-momentum equation (3.49) becomes

$$\sum F_z - \int a_{rel}\, dm = \frac{d}{dt}\left(\int_{CV} w\, d\dot{m}\right) + (\dot{m}w)_e$$

or
$$-mg - m\frac{dV}{dt} = 0 + \dot{m}V_e \qquad \text{with} \quad m = m(t) = M_0 - \dot{m}t$$

The term $a_{rel} = dV/dt$ of the rocket. The control volume integral vanishes because of the steady rocket-flow conditions. Separate the variables and integrate, assuming $V = 0$ at $t = 0$:

$$\int_0^V dV = \dot{m}V_e \int_0^t \frac{dt}{M_0 - \dot{m}t} - g\int_0^t dt \quad \text{or} \quad V(t) = -V_e \ln\left(1 - \frac{\dot{m}t}{M_0}\right) - gt \qquad \textit{Ans.}$$

This is a classic approximate formula in rocket dynamics. The first term is positive and, if the fuel mass burned is a large fraction of initial mass, the final rocket velocity can exceed V_e.

3.5 The Angular-Momentum Theorem[13]

A control-volume analysis can be applied to the angular-momentum relation, Eq. (3.3), by letting our dummy variable **B** be the angular-momentum vector **H**. However, since the system considered here is typically a group of nonrigid fluid particles of variable velocity, the concept of mass moment of inertia is of no help and we have to calculate the instantaneous angular momentum by integration over the elemental masses dm. If O is the point about which moments are desired, the angular momentum about O is given by

$$\mathbf{H}_O = \int_{syst} (\mathbf{r} \times \mathbf{V})\, dm \tag{3.51}$$

where **r** is the position vector from 0 to the elemental mass dm and **V** is the velocity of that element. The amount of angular momentum per unit mass is thus seen to be

$$\boldsymbol{\beta} = \frac{d\mathbf{H}_O}{dm} = \mathbf{r} \times \mathbf{V}$$

[13]This section may be omitted without loss of continuity.



ketabline.com Ebook.ketabline.com

The Reynolds transport theorem (3.16) then tells us that

$$\left.\frac{d\mathbf{H}_O}{dt}\right|_{\text{syst}} = \frac{d}{dt}\left[\int_{\text{CV}} (\mathbf{r} \times \mathbf{V})\rho \, d\mathcal{V}\right] + \int_{\text{CS}} (\mathbf{r} \times \mathbf{V})\rho(\mathbf{V}_r \cdot \mathbf{n}) \, dA \tag{3.52}$$

for the most general case of a deformable control volume. But from the angular-momentum theorem (3.3), this must equal the sum of all the moments about point O applied to the control volume

$$\frac{d\mathbf{H}_O}{dt} = \sum \mathbf{M}_O = \sum (\mathbf{r} \times \mathbf{F})_O$$

Note that the total moment equals the summation of moments of all applied forces about point O. Recall, however, that this law, like Newton's law (3.2), assumes that the particle velocity $\mathbf{V}$ is relative to an *inertial* coordinate system. If not, the moments about point O of the relative acceleration terms $\mathbf{a}_{\text{rel}}$ in Eq. (3.49) must also be included

$$\sum \mathbf{M}_O = \sum (\mathbf{r} \times \mathbf{F})_O - \int_{\text{CV}} (\mathbf{r} \times \mathbf{a}_{\text{rel}}) \, dm \tag{3.53}$$

where the four terms constituting $\mathbf{a}_{\text{rel}}$ are given in Eq. (3.49). Thus the most general case of the angular-momentum theorem is for a deformable control volume associated with a noninertial coordinate system. We combine Eqs. (3.52) and (3.53) to obtain

$$\sum (\mathbf{r} \times \mathbf{F})_0 - \int_{\text{CV}} (\mathbf{r} \times \mathbf{a}_{\text{rel}}) \, dm = \frac{d}{dt}\left[\int_{\text{CV}} (\mathbf{r} \times \mathbf{V})\rho \, d\mathcal{V}\right] + \int_{\text{CS}} (\mathbf{r} \times \mathbf{V})\rho(\mathbf{V}_r \cdot \mathbf{n}) \, dA \tag{3.54}$$

For a nondeformable inertial control volume, this reduces to

$$\sum \mathbf{M}_0 = \frac{\partial}{\partial t}\left[\int_{\text{CV}} (\mathbf{r} \times \mathbf{V})\rho \, d\mathcal{V}\right] + \int_{\text{CS}} (\mathbf{r} \times \mathbf{V})\rho(\mathbf{V} \cdot \mathbf{n}) \, dA \tag{3.55}$$

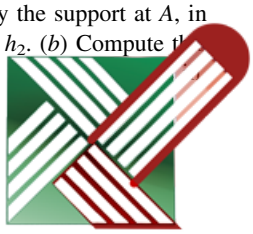
Further, if there are only one-dimensional inlets and exits, the angular-momentum flux terms evaluated on the control surface become

$$\int_{\text{CS}} (\mathbf{r} \times \mathbf{V})\rho(\mathbf{V} \cdot \mathbf{n}) \, dA = \sum (\mathbf{r} \times \mathbf{V})_{\text{out}} \dot{m}_{\text{out}} - \sum (\mathbf{r} \times \mathbf{V})_{\text{in}} \dot{m}_{\text{in}} \tag{3.56}$$

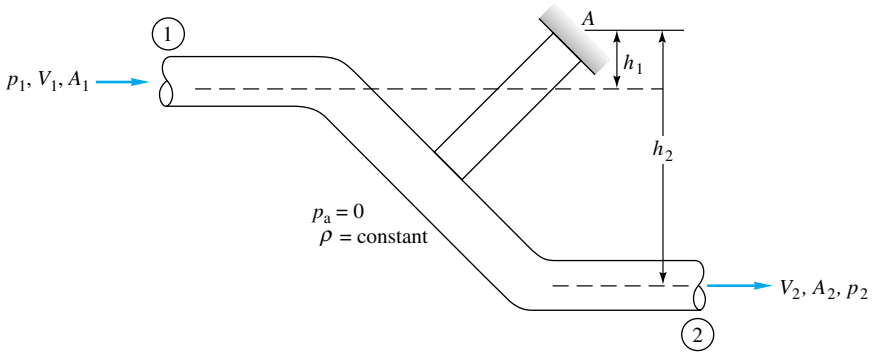
Although at this stage the angular-momentum theorem can be considered to be a supplementary topic, it has direct application to many important fluid-flow problems involving torques or moments. A particularly important case is the analysis of rotating fluid-flow devices, usually called *turbomachines* (Chap. 11).

EXAMPLE 3.13

As shown in Fig. E3.13*a*, a pipe bend is supported at point A and connected to a flow system by flexible couplings at sections 1 and 2. The fluid is incompressible, and ambient pressure p_a is zero. (*a*) Find an expression for the torque T which must be resisted by the support at A, in terms of the flow properties at sections 1 and 2 and the distances h_1 and h_2. (*b*) Compute the torque if $D_1 = D_2 = 3$ in, $p_1 = 100$ lbf/in^2 gage, $p_2 = 80$ lbf/in^2 gage, V_1 $h_2 = 10$ in, and $\rho = 1.94$ slugs/ft^3.



ketabline.com Ebook.ketabline.com



E3.13a

Solution

Part (a) The control volume chosen in Fig. E3.13*b* cuts through sections 1 and 2 and through the support at A, where the torque T_A is desired. The flexible-couplings description specifies that there is no torque at either section 1 or 2, and so the cuts there expose no moments. For the angular-momentum terms $\mathbf{r} \times \mathbf{V}$, $\mathbf{r}$ should be taken from point A to sections 1 and 2. Note that the gage pressure forces p_1A_1 and p_2A_2 both have moments about A. Equation (3.55) with one-dimensional flux terms becomes

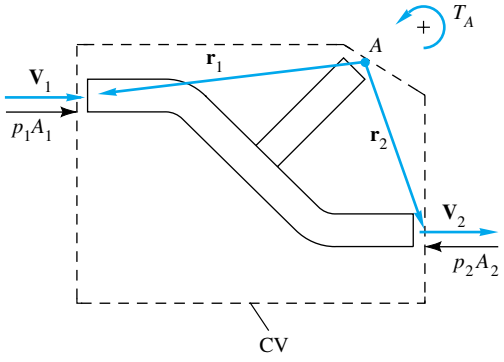
$$\sum \mathbf{M}_A = \mathbf{T}_A + \mathbf{r}_1 \times (-p_1A_1\mathbf{n}_1) + \mathbf{r}_2 \times (-p_2A_2\mathbf{n}_2)$$
$$= (\mathbf{r}_2 \times \mathbf{V}_2)(+\dot{m}_{\text{out}}) + (\mathbf{r}_1 \times \mathbf{V}_1)(-\dot{m}_{\text{in}}) \tag{1}$$

Figure E3.13*c* shows that all the cross products are associated either with $r_1 \sin \theta_1 = h_1$ or $r_2 \sin \theta_2 = h_2$, the perpendicular distances from point A to the pipe axes at 1 and 2. Remember that $\dot{m}_{\text{in}} = \dot{m}_{\text{out}}$ from the steady-flow continuity relation. In terms of counterclockwise moments, Eq. (1) then becomes

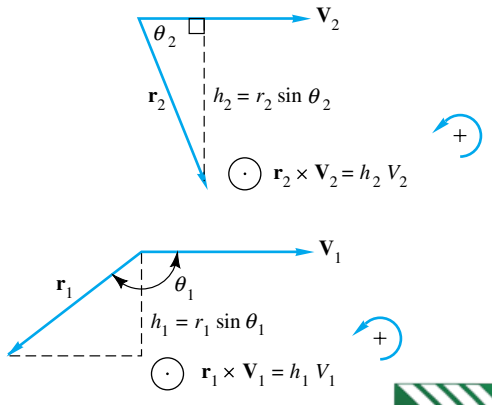
$$T_A + p_1A_1h_1 - p_2A_2h_2 = \dot{m}(h_2V_2 - h_1V_1) \tag{2}$$

Rewriting this, we find the desired torque to be

$$T_A = h_2(p_2A_2 + \dot{m}V_2) - h_1(p_1A_1 + \dot{m}V_1) \qquad \textit{Ans. (a)} \tag{3}$$



E3.13b



E3.13c



ketabline.com Ebook.ketabline.com

counterclockwise. The quantities p_1 and p_2 are gage pressures. Note that this result is independent of the shape of the pipe bend and varies only with the properties at sections 1 and 2 and the distances h_1 and h_2.†

Part (b) The inlet and exit areas are the same:

$$A_1 = A_2 = \frac{\pi}{4}(3)^2 = 7.07 \text{ in}^2 = 0.0491 \text{ ft}^2$$

Since the density is constant, we conclude from continuity that $V_2 = V_1 = 40$ ft/s. The mass flow is

$$\dot{m} = \rho A_1 V_1 = 1.94(0.0491)(40) = 3.81 \text{ slug/s}$$

Equation (3) can be evaluated as

$$T_A = (\tfrac{10}{12} \text{ ft})[80(7.07) \text{ lbf} + 3.81(40) \text{ lbf}] - (\tfrac{2}{12} \text{ ft})[100(7.07) \text{ lbf} + 3.81(40) \text{ lbf}]$$

$$= 598 - 143 = 455 \text{ ft} \cdot \text{lbf counterclockwise} \qquad \textit{Ans. (b)}$$

We got a little daring there and multiplied p in lbf/in^2 gage times A in in^2 to get lbf without changing units to lbf/ft^2 and ft^2.

EXAMPLE 3.14

Figure 3.13 shows a schematic of a centrifugal pump. The fluid enters axially and passes through the pump blades, which rotate at angular velocity ω; the velocity of the fluid is changed from V_1 to V_2 and its pressure from p_1 to p_2. (*a*) Find an expression for the torque T_O which must be applied to these blades to maintain this flow. (*b*) The power supplied to the pump would be $P = \omega T_O$. To illustrate numerically, suppose $r_1 = 0.2$ m, $r_2 = 0.5$ m, and $b = 0.15$ m. Let the pump rotate at 600 r/min and deliver water at 2.5 m^3/s with a density of 1000 kg/m^3. Compute the idealized torque and power supplied.

Solution

Part (a) The control volume is chosen to be the angular region between sections 1 and 2 where the flow passes through the pump blades (see Fig. 3.13). The flow is steady and assumed incompressible. The contribution of pressure to the torque about axis O is zero since the pressure forces at 1 and 2 act radially through O. Equation (3.55) becomes

$$\sum \mathbf{M}_O = \mathbf{T}_O = (\mathbf{r}_2 \times \mathbf{V}_2)\dot{m}_{\text{out}} - (\mathbf{r}_1 \times \mathbf{V}_1)\dot{m}_{\text{in}} \qquad (1)$$

where steady-flow continuity tells us that

$$\dot{m}_{\text{in}} = \rho V_{n1} 2\pi r_1 b = \dot{m}_{\text{out}} = \rho V_{n2} \pi r_2 b = \rho Q$$

The cross product $\mathbf{r} \times \mathbf{V}$ is found to be clockwise about O at both sections:

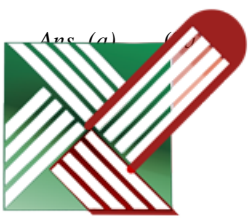
$$\mathbf{r}_2 \times \mathbf{V}_2 = r_2 V_{t2} \sin 90^\circ \, \mathbf{k} = r_2 V_{t2} \mathbf{k} \qquad \text{clockwise}$$

$$\mathbf{r}_1 \times \mathbf{V}_1 = r_1 V_{t1} \mathbf{k} \qquad \text{clockwise}$$

Equation (1) thus becomes the desired formula for torque

$$\boldsymbol{T}_O = \rho Q(r_2 V_{t2} - r_1 V_{t1})\mathbf{k} \qquad \text{clockwise} \qquad \textit{Ans. (a)}$$

†Indirectly, the pipe-bend shape probably affects the pressure change from p_1 to



ketabline.com Ebook.ketabline.com

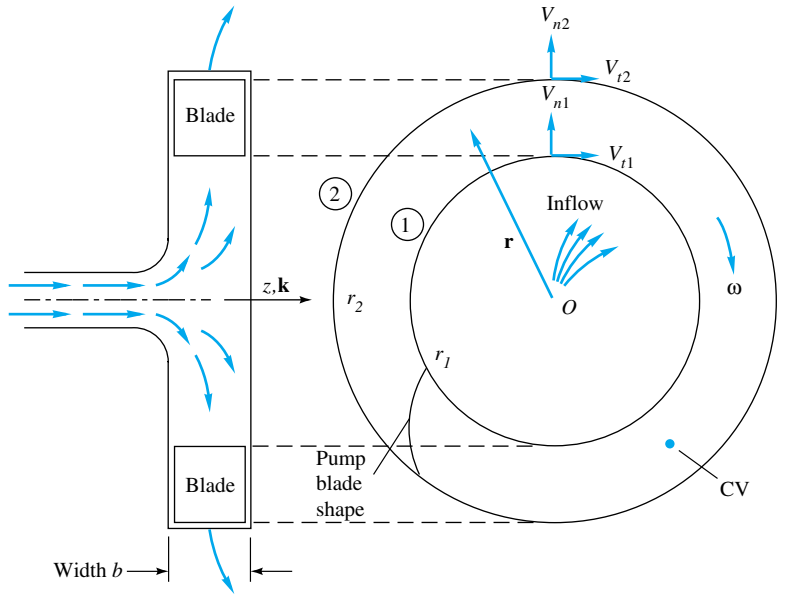


Fig. 3.13 Schematic of a simplified centrifugal pump.

This relation is called *Euler's turbine formula*. In an idealized pump, the inlet and outlet tangential velocities would match the blade rotational speeds $V_{t1} = \omega r_1$ and $V_{t2} = \omega r_2$. Then the formula for torque supplied becomes

$$T_O = \rho Q \omega (r_2^2 - r_1^2) \qquad \text{clockwise} \tag{2b}$$

Part (b) Convert ω to $600(2\pi/60) = 62.8$ rad/s. The normal velocities are not needed here but follow from the flow rate

$$V_{n1} = \frac{Q}{2\pi r_1 b} = \frac{2.5\ m^3/\text{s}}{2\pi(0.2\ \text{m})(0.15\ \text{m})} = 13.3\ \text{m/s}$$

$$V_{n2} = \frac{Q}{2\pi r_2 b} = \frac{2.5}{2\pi(0.5)(0.15)} = 5.3\ \text{m/s}$$

For the idealized inlet and outlet, tangential velocity equals tip speed

$$V_{t1} = \omega r_1 = (62.8\ \text{rad/s})(0.2\ \text{m}) = 12.6\ \text{m/s}$$

$$V_{t2} = \omega r_2 = 62.8(0.5) = 31.4\ \text{m/s}$$

Equation (2*a*) predicts the required torque to be

$$T_O = (1000\ \text{kg/m}^3)(2.5\ \text{m}^3/\text{s})[(0.5\ \text{m})(31.4\ \text{m/s}) - (0.2\ \text{m})(12.6\ \text{m/s})]$$

$$= 33{,}000\ (\text{kg} \cdot \text{m}^2)/\text{s}^2 = 33{,}000\ \text{N} \cdot \text{m} \qquad \textit{Ans.}$$

The power required is

$$P = \omega T_O = (62.8\ \text{rad/s})(33{,}000\ \text{N} \cdot \text{m}) = 2{,}070{,}000\ (\text{N} \cdot \text{m})/\text{s}$$

$$= 2.07\ \text{MW}\ (2780\ \text{hp}) \qquad \textit{Ans.}$$

In actual practice the tangential velocities are considerably less than the impeller-tip speeds, and the design power requirements for this pump may be only 1 MW or less.



ketabline.com Ebook.ketabline.com

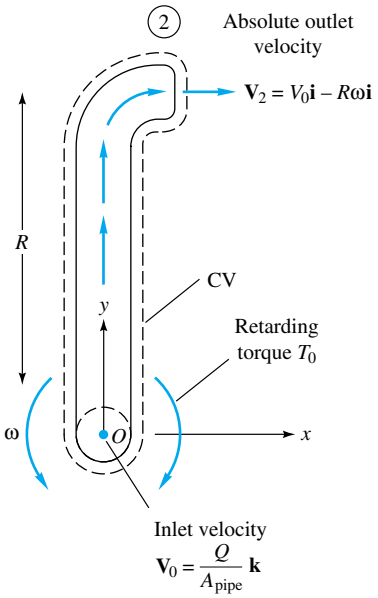


Fig. 3.14 View from above of a single arm of a rotating lawn sprinkler.

EXAMPLE 3.15

Figure 3.14 shows a lawn-sprinkler arm viewed from above. The arm rotates about O at constant angular velocity ω. The volume flux entering the arm at O is Q, and the fluid is incompressible. There is a retarding torque at O, due to bearing friction, of amount $-T_O\mathbf{k}$. Find an expression for the rotation ω in terms of the arm and flow properties.

Solution

The entering velocity is $V_0\mathbf{k}$, where $V_0 = Q/A_{pipe}$. Equation (3.55) applies to the control volume sketched in Fig. 3.14 only if $\mathbf{V}$ is the absolute velocity relative to an inertial frame. Thus the exit velocity at section 2 is

$$\mathbf{V}_2 = V_0\mathbf{i} - R\omega\mathbf{i}$$

Equation (3.55) then predicts that, for steady flow,

$$\sum \mathbf{M}_O = -T_O\mathbf{k} = (\mathbf{r}_2 \times \mathbf{V}_2)\dot{m}_{out} - (\mathbf{r}_1 \times \mathbf{V}_1)\dot{m}_{in} \tag{1}$$

where, from continuity, $\dot{m}_{out} = \dot{m}_{in} = \rho Q$. The cross products with reference to point O are

$$\mathbf{r}_2 \times \mathbf{V}_2 = R\mathbf{j} \times (V_0 - R\omega)\mathbf{i} = (R^2\omega - RV_0)\mathbf{k}$$

$$\mathbf{r}_1 \times \mathbf{V}_1 = 0\mathbf{j} \times V_0\mathbf{k} = 0$$

Equation (1) thus becomes

$$-T_O\mathbf{k} = \rho Q(R^2\omega - RV_0)\mathbf{k}$$

$$\omega = \frac{V_O}{R} - \frac{T_O}{\rho Q R^2} \qquad \textit{Ans.}$$

The result may surprise you: Even if the retarding torque T_O is negligible, the arm rotational speed is limited to the value V_0/R imposed by the outlet speed and the arm length.

3.6 The Energy Equation[14]

As our fourth and final basic law, we apply the Reynolds transport theorem (3.12) to the first law of thermodynamics, Eq. (3.5). The dummy variable B becomes energy E, and the energy per unit mass is $\beta = dE/dm = e$. Equation (3.5) can then be written for a fixed control volume as follows:[15]

$$\frac{dQ}{dt} - \frac{dW}{dt} = \frac{dE}{dt} = \frac{d}{dt}\left(\int_{CV} e\rho\, d\mathcal{V}\right) + \int_{CS} e\rho(\mathbf{V}\cdot\mathbf{n})\, dA \tag{3.57}$$

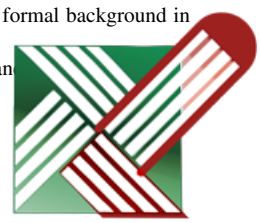
Recall that positive Q denotes heat added to the system and positive W denotes work done by the system.

The system energy per unit mass e may be of several types:

$$e = e_{internal} + e_{kinetic} + e_{potential} + e_{other}$$

[14]This section should be read for information and enrichment even if you lack formal background in thermodynamics.

[15]The energy equation for a deformable control volume is rather complicated and here. See Refs. 4 and 5 for further details.



ketabline.com Ebook.ketabline.com

where e_{other} could encompass chemical reactions, nuclear reactions, and electrostatic or magnetic field effects. We neglect e_{other} here and consider only the first three terms as discussed in Eq. (1.9), with z defined as "up":

$$e = \hat{u} + \tfrac{1}{2}V^2 + gz \tag{3.58}$$

The heat and work terms could be examined in detail. If this were a heat-transfer book, dQ/dT would be broken down into conduction, convection, and radiation effects and whole chapters written on each (see, e.g., Ref. 3). Here we leave the term untouched and consider it only occasionally.

Using for convenience the overdot to denote the time derivative, we divide the work term into three parts:

$$\dot{W} = \dot{W}_{\text{shaft}} + \dot{W}_{\text{press}} + \dot{W}_{\text{viscous stresses}} = \dot{W}_s + \dot{W}_p + \dot{W}_v$$

The work of gravitational forces has already been included as potential energy in Eq. (3.58). Other types of work, e.g., those due to electromagnetic forces, are excluded here.

The shaft work isolates that portion of the work which is deliberately done by a machine (pump impeller, fan blade, piston, etc.) protruding through the control surface into the control volume. No further specification other than $\dot{W}_s$ is desired at this point, but calculations of the work done by turbomachines will be performed in Chap. 11.

The rate of work $\dot{W}_p$ done on pressure forces occurs at the surface only; all work on internal portions of the material in the control volume is by equal and opposite forces and is self-canceling. The pressure work equals the pressure force on a small surface element dA times the normal velocity component into the control volume

$$d\dot{W}_p = -(p\ dA)V_{n,\text{in}} = -p(-\mathbf{V}\cdot\mathbf{n})\ dA$$

The total pressure work is the integral over the control surface

$$\dot{W}_p = \int_{\text{CS}} p(\mathbf{V}\cdot\mathbf{n})\ dA \tag{3.59}$$

A cautionary remark: If part of the control surface is the surface of a machine part, we prefer to delegate that portion of the pressure to the *shaft work* term $\dot{W}_s$, not to $\dot{W}_p$, which is primarily meant to isolate the fluid-flow pressure-work terms.

Finally, the shear work due to viscous stresses occurs at the control surface, the internal work terms again being self-canceling, and consists of the product of each viscous stress (one normal and two tangential) and the respective velocity component

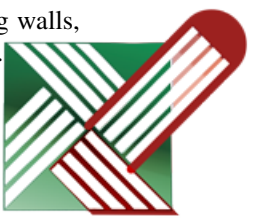
$$d\dot{W}_v = -\boldsymbol{\tau}\cdot\mathbf{V}\ dA$$

or

$$\dot{W}_v = -\int_{\text{CS}} \boldsymbol{\tau}\cdot\mathbf{V}\ dA \tag{3.60}$$

where $\boldsymbol{\tau}$ is the stress vector on the elemental surface dA. This term may vanish or be negligible according to the particular type of surface at that part of the control volume:

Solid surface. For all parts of the control surface which are solid confining walls, $\mathbf{V} = 0$ from the viscous no-slip condition; hence $\dot{W}_v$ = zero identically.



ketabline.com Ebook.ketabline.com

Surface of a machine. Here the viscous work is contributed by the machine, and so we absorb this work in the term $\dot{W}_s$.

An inlet or outlet. At an inlet or outlet, the flow is approximately normal to the element dA; hence the only viscous-work term comes from the normal stress $\tau_{nn}V_n\,dA$. Since viscous normal stresses are extremely small in all but rare cases, e.g., the interior of a shock wave, it is customary to neglect viscous work at inlets and outlets of the control volume.

Streamline surface. If the control surface is a streamline such as the upper curve in the boundary-layer analysis of Fig. 3.11, the viscous-work term must be evaluated and retained if shear stresses are significant along this line. In the particular case of Fig. 3.11, the streamline is outside the boundary layer, and viscous work is negligible.

The net result of the above discussion is that the rate-of-work term in Eq. (3.57) consists essentially of

$$\dot{W} = \dot{W}_s + \int_{CS} p(\mathbf{V}\cdot\mathbf{n})\,dA - \int_{CS} (\tau\cdot\mathbf{V})_{SS}\,dA \tag{3.61}$$

where the subscript SS stands for stream surface. When we introduce (3.61) and (3.58) into (3.57), we find that the pressure-work term can be combined with the energy-flux term since both involve surface integrals of $\mathbf{V}\cdot\mathbf{n}$. The control-volume energy equation thus becomes

$$\dot{Q} - \dot{W}_s - (\dot{W}_v)_{SS} = \frac{\partial}{\partial t}\left(\int_{CV} ep\,d\mathcal{V}\right) + \int_{CS}\left(e + \frac{p}{\rho}\right)\rho(\mathbf{V}\cdot\mathbf{n})\,dA \tag{3.62}$$

Using e from (3.58), we see that the enthalpy $\hat{h} = \hat{u} + p/\rho$ occurs in the control-surface integral. The final general form for the energy equation for a fixed control volume becomes

$$\dot{Q} - \dot{W}_s - \dot{W}_v = \frac{\partial}{\partial t}\left[\int_{CV}\left(\hat{u} + \tfrac{1}{2}V^2 + gz\right)\rho\,d\mathcal{V}\right] + \int_{CS}\left(\hat{h} + \tfrac{1}{2}V^2 + gz\right)\rho(\mathbf{V}\cdot\mathbf{n})\,dA \tag{3.63}$$

As mentioned above, the shear-work term $\dot{W}_v$ is rarely important.

One-Dimensional Energy-Flux Terms

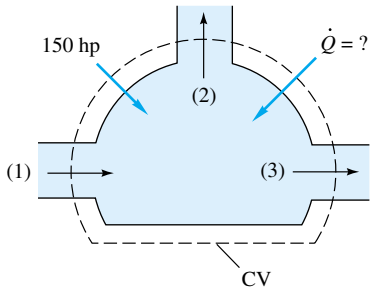
If the control volume has a series of one-dimensional inlets and outlets, as in Fig. 3.6, the surface integral in (3.63) reduces to a summation of outlet fluxes minus inlet fluxes

$$\int_{CS}(\hat{h} + \tfrac{1}{2}V^2 + gz)\rho(\mathbf{V}\cdot\mathbf{n})\,dA = \sum(\hat{h} + \tfrac{1}{2}V^2 + gz)_{out}\dot{m}_{out} - \sum(\hat{h} + \tfrac{1}{2}V^2 + gz)_{in}\dot{m}_{in} \tag{3.64}$$

where the values of $\hat{h}$, $\frac{1}{2}V^2$, and gz are taken to be averages over e



ketabline.com Ebook.ketabline.com



E3.16

EXAMPLE 3.16

A steady-flow machine (Fig. E3.16) takes in air at section 1 and discharges it at sections 2 and 3. The properties at each section are as follows:

Section	A, ft^2	Q, ft^3/s	T, °F	p, lbf/in^2 abs	z, ft
1	0.4	100	70	20	1.0
2	1.0	40	100	30	4.0
3	0.25	50	200	?	1.5

Work is provided to the machine at the rate of 150 hp. Find the pressure p_3 in lbf/in^2 absolute and the heat transfer $\dot{Q}$ in Btu/s. Assume that air is a perfect gas with $R = 1715$ and $c_p = 6003$ ft · lbf/(slug · °R).

Solution

The control volume chosen cuts across the three desired sections and otherwise follows the solid walls of the machine. Therefore the shear-work term W_v is negligible. We have enough information to compute $V_i = Q_i/A_i$ immediately

$$V_1 = \frac{100}{0.4} = 250 \text{ ft/s} \qquad V_2 = \frac{40}{1.0} = 40 \text{ ft/s} \qquad V_3 = \frac{50}{0.25} = 200 \text{ ft/s}$$

and the densities $\rho_i = p_i/(RT_i)$

$$\rho_1 = \frac{20(144)}{1715(70 + 460)} = 0.00317 \text{ slug/ft}^3$$

$$\rho_2 = \frac{30(144)}{1715(560)} = 0.00450 \text{ slug/ft}^3$$

but ρ_3 is determined from the steady-flow continuity relation:

$$\dot{m}_1 = \dot{m}_2 + \dot{m}_3$$

$$\rho_1 Q_1 = \rho_2 Q_2 + \rho_3 Q_3 \tag{1}$$

$$0.00317(100) = 0.00450(40) + \rho_3(50)$$

or

$$50\rho_3 = 0.317 - 0.180 = 0.137 \text{ slug/s}$$

$$\rho_3 = \frac{0.137}{50} = 0.00274 \text{ slug/ft}^3 = \frac{144p_3}{1715(660)}$$

$$p_3 = 21.5 \text{ lbf/in}^2 \text{ absolute} \qquad \textit{Ans.}$$

Note that the volume flux $Q_1 \neq Q_2 + Q_3$ because of the density changes.

For steady flow, the volume integral in (3.63) vanishes, and we have agreed to neglect viscous work. With one inlet and two outlets, we obtain

$$\dot{Q} - \dot{W}_s = -\dot{m}_1(\hat{h}_1 + \tfrac{1}{2}V_1^2 + gz_1) + \dot{m}_2(\hat{h}_2 + \tfrac{1}{2}V_2^2 + gz_2) + \dot{m}_3(\hat{h}_3 + \tfrac{1}{2}V_3^2 + gz_3) \tag{2}$$

where $\dot{W}_s$ is given in hp and can be quickly converted to consistent BG units:

$$\dot{W}_s = -150 \text{ hp } [550 \text{ ft} \cdot \text{lbf/(s} \cdot \text{hp)}]$$

$$= -82{,}500 \text{ ft} \cdot \text{lbf/s} \qquad \text{negative work on system}$$



ketabline.com Ebook.ketabline.com

For a perfect gas with constant c_p, $\hat{h} = c_pT$ plus an arbitrary constant. It is instructive to separate the flux terms in Eq. (2) above to examine their magnitudes:

Enthalpy flux:

$$\begin{aligned} c_p(-\dot{m}_1T_1 + \dot{m}_2T_2 + \dot{m}_3T_3) &= [6003 \text{ ft} \cdot \text{lbf/(slug} \cdot {}^\circ\text{R)}][(-0.317 \text{ slug/s})(530 {}^\circ\text{R}) \\ &\quad + 0.180(560) + 0.137(660)] \\ &= -1{,}009{,}000 + 605{,}000 + 543{,}000 \\ &= +139{,}000 \text{ ft} \cdot \text{lbf/s} \end{aligned}$$

Kinetic-energy flux:

$$\begin{aligned} -\dot{m}_1(\tfrac{1}{2}V_1^2) + \dot{m}_2(\tfrac{1}{2}V_2^2) + \dot{m}_3(\tfrac{1}{2}V_3^2) &= \tfrac{1}{2}[-0.317(250)^2 + 0.180(40)^2 + 0.137(200)^2] \\ &= -9900 + 150 + 2750 = -7000 \text{ ft} \cdot \text{lbf/s} \end{aligned}$$

Potential-energy flux:

$$\begin{aligned} g(-\dot{m}_1z_1 + \dot{m}_2z_2 + \dot{m}_3z_3) &= 32.2[-0.317(1.0) + 0.180(4.0) + 0.137(1.5)] \\ &= -10 + 23 + 7 = +20 \text{ ft} \cdot \text{lbf/s} \end{aligned}$$

These are typical effects: The potential-energy flux is negligible in gas flows, the kinetic-energy flux is small in low-speed flows, and the enthalpy flux is dominant. It is only when we neglect heat-transfer effects that the kinetic and potential energies become important. Anyway, we can now solve for the heat flux

$$\dot{Q} = -82{,}500 + 139{,}000 - 7000 + 20 = 49{,}520 \text{ ft} \cdot \text{lbf/s} \tag{3}$$

Converting, we get

$$\dot{Q} = \frac{49{,}520}{778.2 \text{ ft} \cdot \text{lbf/Btu}} = +63.6 \text{ Btu/s} \qquad \textit{Ans.}$$

The Steady-Flow Energy Equation

For steady flow with one inlet and one outlet, both assumed one-dimensional, Eq. (3.63) reduces to a celebrated relation used in many engineering analyses. Let section 1 be the inlet and section 2 the outlet. Then

$$\dot{Q} - \dot{W}_s - \dot{W}_v = -\dot{m}_1(\hat{h}_1 + \tfrac{1}{2}V_1^2 + gz_1) + \dot{m}_2(\hat{h}_2 + \tfrac{1}{2}V_2^2 + gz_2) \tag{3.65}$$

But, from continuity, $\dot{m}_1 = \dot{m}_2 = \dot{m}$, and we can rearrange (3.65) as follows:

$$\hat{h}_1 + \tfrac{1}{2}V_1^2 + gz_1 = (\hat{h}_2 + \tfrac{1}{2}V_2^2 + gz_2) - q + w_s + w_v \tag{3.66}$$

where $q = \dot{Q}/\dot{m} = dQ/dm$, the heat transferred to the fluid per unit mass. Similarly, $w_s = \dot{W}_s/\dot{m} = dW_s/dm$ and $w_v = \dot{W}_v/\dot{m} = dW_v/dm$. Equation (3.66) is a general form of the *steady-flow energy equation*, which states that the upstream *stagnation enthalpy* $H_1 = (\hat{h} + \frac{1}{2}V^2 + gz)_1$ differs from the downstream value H_2 only if there is heat transfer, shaft work, or viscous work as the fluid passes between sections 1 and 2. Recall that q is positive if heat is added to the control volume and that w_s is positive if work is done by the fluid on the surroundings.



ketabline.com Ebook.ketabline.com

Each term in Eq. (3.66) has the dimensions of energy per unit mass, or velocity squared, which is a form commonly used by mechanical engineers. If we divide through by g, each term becomes a length, or head, which is a form preferred by civil engineers. The traditional symbol for head is h, which we do not wish to confuse with enthalpy. Therefore we use internal energy in rewriting the head form of the energy relation:

$$\frac{p_1}{\gamma} + \frac{\hat{u}_1}{g} + \frac{V_1^2}{2g} + z_1 = \frac{p_2}{\gamma} + \frac{\hat{u}_2}{g} + \frac{V_1^2}{2g} + z_2 - h_q + h_s + h_v \tag{3.67}$$

where $h_q = q/g$, $h_s = w_s/g$, and $h_v = w_v/g$ are the head forms of the heat added, shaft work done, and viscous work done, respectively. The term p/γ is called *pressure head* and the term $V^2/2g$ is denoted as *velocity head.*

Friction Losses in Low-Speed Flow

A very common application of the steady-flow energy equation is for low-speed flow with no shaft work and negligible viscous work, such as liquid flow in pipes. For this case Eq. (3.67) may be written in the form

$$\frac{p_1}{\gamma} + \frac{V_1^2}{2g} + z_1 = \left(\frac{p_2}{\gamma} + \frac{V_2^2}{2g} + z_2\right) + \frac{\hat{u}_2 - \hat{u}_1 - q}{g} \tag{3.68}$$

The term in parentheses is called the useful head or *available head* or *total head* of the flow, denoted as h_0. The last term on the right is the difference between the available head upstream and downstream and is normally *positive*, representing the loss in head due to friction, denoted as h_f. Thus, in low-speed (nearly incompressible) flow with one inlet and one exit, we may write

$$\left(\frac{p}{\gamma} + \frac{V^2}{2g} + z\right)_{\text{in}} = \left(\frac{p}{\gamma} + \frac{V^2}{2g} + z\right)_{\text{out}} + h_{\text{friction}} - h_{\text{pump}} + h_{\text{turbine}} \tag{3.69}$$

Most of our internal-flow problems will be solved with the aid of Eq. (3.69). The h terms are all positive; that is, friction loss is always positive in real (viscous) flows, a pump adds energy (increases the left-hand side), and a turbine extracts energy from the flow. If h_p and/or h_t are included, the pump and/or turbine must lie *between* points 1 and 2. In Chaps. 5 and 6 we shall develop methods of correlating h_f losses with flow parameters in pipes, valves, fittings, and other internal-flow devices.

EXAMPLE 3.17

Gasoline at 20°C is pumped through a smooth 12-cm-diameter pipe 10 km long, at a flow rate of 75 m^3/h (330 gal/min). The inlet is fed by a pump at an absolute pressure of 24 atm. The exit is at standard atmospheric pressure and is 150 m higher. Estimate the frictional head loss h_f, and compare it to the velocity head of the flow $V^2/(2g)$. (These numbers are quite realistic for liquid flow through long pipelines.)

Solution

For gasoline at 20°C, from Table A.3, $\rho = 680$ kg/m^3, or $\gamma = (680)(9.81) = 6670$ N/m
is no shaft work; hence Eq. (3.69) applies and can be evaluated:



ketabline.com Ebook.ketabline.com

$$\frac{p_{in}}{\gamma} + \frac{V_{in}^2}{2g} + z_{in} = \frac{p_{out}}{\gamma} + \frac{V_{out}^2}{2g} + z_{out} + h_f \tag{1}$$

The pipe is of uniform cross section, and thus the average velocity everywhere is

$$V_{in} = V_{out} = \frac{Q}{A} = \frac{(75/3600)\ \text{m}^3/\text{s}}{(\pi/4)(0.12\ \text{m})^2} \approx 1.84\ \text{m/s}$$

Being equal at inlet and exit, this term will cancel out of Eq. (1) above, but we are asked to compute the velocity head of the flow for comparison purposes:

$$\frac{V^2}{2g} = \frac{(1.84\ \text{m/s})^2}{2(9.81\ \text{m/s}^2)} \approx 0.173\ \text{m}$$

Now we are in a position to evaluate all terms in Eq. (1) except the friction head loss:

$$\frac{(24)(101{,}350\ \text{N/m}^2)}{6670\ \text{N/m}^3} + 0.173\ \text{m} + 0\ \text{m} = \frac{101{,}350\ \text{N/m}^2}{6670\ \text{N/m}^3} + 0.173\ \text{m} + 150\ \text{m} + h_f$$

or
$$h_f = 364.7 - 15.2 - 150 \approx 199\ \text{m} \qquad \textit{Ans.}$$

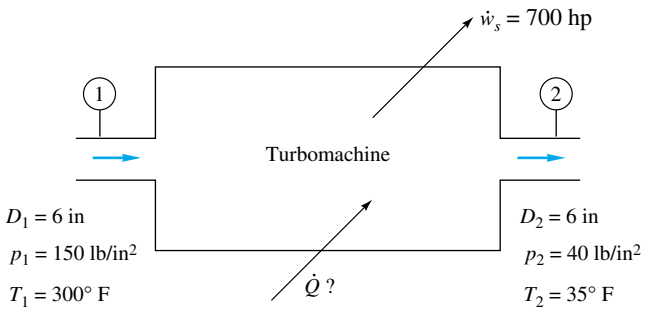
The friction head is larger than the elevation change Δz, and the pump must drive the flow against both changes, hence the high inlet pressure. The ratio of friction to velocity head is

$$\frac{h_f}{V^2/(2g)} \approx \frac{199\ \text{m}}{0.173\ \text{m}} \approx 1150 \qquad \textit{Ans.}$$

This high ratio is typical of long pipelines. (Note that we did not make direct use of the 10,000-m pipe length, whose effect is hidden within h_f.) In Chap. 6 we can state this problem in a more direct fashion: Given the flow rate, fluid, and pipe size, what inlet pressure is needed? Our correlations for h_f will lead to the estimate $p_{\text{inlet}} \approx 24$ atm, as stated above.

EXAMPLE 3.18

Air [$R = 1715$, $c_p = 6003$ ft · lbf/(slug · °R)] flows steadily, as shown in Fig. E3.18, through a turbine which produces 700 hp. For the inlet and exit conditions shown, estimate (*a*) the exit velocity V_2 and (*b*) the heat transferred $\dot{Q}$ in Btu/h.



E3.18



ketabline.com Ebook.ketabline.com

Solution

Part (a) The inlet and exit densities can be computed from the perfect-gas law:

$$\rho_1 = \frac{p_1}{RT_1} = \frac{150(144)}{1715(460 + 300)} = 0.0166 \text{ slug/ft}^3$$

$$\rho_2 = \frac{p_2}{RT_2} = \frac{40(144)}{1715(460 + 35)} = 0.00679 \text{ slug/ft}^3$$

The mass flow is determined by the inlet conditions

$$\dot{m} = \rho_1 A_1 V_1 = (0.0166)\frac{\pi}{4}\left(\frac{6}{12}\right)^2(100) = 0.325 \text{ slug/s}$$

Knowing mass flow, we compute the exit velocity

$$\dot{m} = 0.325 = \rho_2 A_2 V_2 = (0.00679)\frac{\pi}{4}\left(\frac{6}{12}\right)^2 V_2$$

or $$V_2 = 244 \text{ ft/s} \qquad \textit{Ans. (a)}$$

Part (b) The steady-flow energy equation (3.65) applies with $\dot{W}_v = 0$, $z_1 = z_2$, and $\hat{h} = c_pT$:

$$\dot{Q} - \dot{W}_s = \dot{m}(c_pT_2 + \tfrac{1}{2}V_2^2 - c_pT_1 - \tfrac{1}{2}V_1^2)$$

Convert the turbine work to foot-pounds-force per second with the conversion factor 1 hp = 550 ft · lbf/s. The turbine work is positive

$$\dot{Q} - 700(550) = 0.325[6003(495) + \tfrac{1}{2}(244)^2 - 6003(760) - \tfrac{1}{2}(100)^2]$$

$$= -510{,}000 \text{ ft} \cdot \text{lbf/s}$$

or $$\dot{Q} = -125{,}000 \text{ ft} \cdot \text{lbf/s}$$

Convert this to British thermal units as follows:

$$\dot{Q} = (-125{,}000 \text{ ft} \cdot \text{lbf/s})\frac{3600 \text{ s/h}}{778.2 \text{ ft} \cdot \text{lbf/Btu}}$$

$$= -576{,}000 \text{ Btu/h} \qquad \textit{Ans. (b)}$$

The negative sign indicates that this heat transfer is a *loss* from the control volume.

Kinetic-Energy Correction Factor

Often the flow entering or leaving a port is not strictly one-dimensional. In particular, the velocity may vary over the cross section, as in Fig. E3.4. In this case the kinetic-energy term in Eq. (3.64) for a given port should be modified by a dimensionless correction factor α so that the integral can be proportional to the square of the average velocity through the port

$$\int_{\text{port}} (\tfrac{1}{2}V^2)\rho(\mathbf{V} \cdot \mathbf{n})\, dA \equiv \alpha(\tfrac{1}{2}V_{\text{av}}^2)\dot{m}$$

where $$V_{\text{av}} = \frac{1}{A}\int u\, dA \qquad \text{for incompressible flow}$$



ketabline.com Ebook.ketabline.com

If the density is also variable, the integration is very cumbersome; we shall not treat this complication. By letting u be the velocity normal to the port, the first equation above becomes, for incompressible flow,

$$\tfrac{1}{2}\rho \int u^3 dA = \tfrac{1}{2}\rho\alpha V_{\text{av}}^3 A$$

or

$$\alpha = \frac{1}{A}\int \left(\frac{u}{V_{\text{av}}}\right)^3 dA \tag{3.70}$$

The term α is the kinetic-energy correction factor, having a value of about 2.0 for fully developed laminar pipe flow and from 1.04 to 1.11 for turbulent pipe flow. The complete incompressible steady-flow energy equation (3.69), including pumps, turbines, and losses, would generalize to

$$\left(\frac{p}{\rho g} + \frac{\alpha}{2g}V^2 + z\right)_{\text{in}} = \left(\frac{p}{\rho g} + \frac{\alpha}{2g}V^2 + z\right)_{\text{out}} + h_{\text{turbine}} - h_{\text{pump}} + h_{\text{friction}} \tag{3.71}$$

where the head terms on the right (h_t, h_p, h_f) are all numerically positive. All additive terms in Eq. (3.71) have dimensions of length $\{L\}$. In problems involving turbulent pipe flow, it is common to assume that $\alpha \approx 1.0$. To compute numerical values, we can use these approximations to be discussed in Chap. 6:

Laminar flow:

$$u = U_0\left[1 - \left(\frac{r}{R}\right)^2\right]$$

from which

$$V_{\text{av}} = 0.5U_0$$

and

$$\alpha = 2.0 \tag{3.72}$$

Turbulent flow:

$$u \approx U_0\left(1 - \frac{r}{R}\right)^m \qquad m \approx \frac{1}{7}$$

from which, in Example 3.4,

$$V_{\text{av}} = \frac{2U_0}{(1+m)(2+m)}$$

Substituting into Eq. (3.70) gives

$$\alpha = \frac{(1+m)^3(2+m)^3}{4(1+3m)(2+3m)} \tag{3.73}$$

and numerical values are as follows:

Turbulent flow:

m	$\frac{1}{5}$	$\frac{1}{6}$	$\frac{1}{7}$	$\frac{1}{8}$	$\frac{1}{9}$
α	1.106	1.077	1.058	1.046	1.037

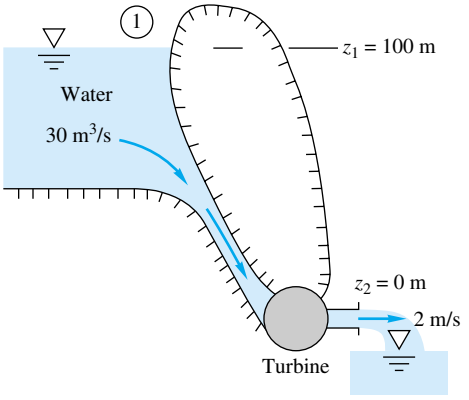
These values are only slightly different from unity and are often ne
tary turbulent-flow analyses. However, α should never be neglecte



ketabline.com Ebook.ketabline.com

EXAMPLE 3.19

A hydroelectric power plant (Fig. E3.19) takes in 30 m^3/s of water through its turbine and discharges it to the atmosphere at $V_2 = 2$ m/s. The head loss in the turbine and penstock system is $h_f = 20$ m. Assuming turbulent flow, $\alpha \approx 1.06$, estimate the power in MW extracted by the turbine.



E3.19

Solution

We neglect viscous work and heat transfer and take section 1 at the reservoir surface (Fig. E3.19), where $V_1 \approx 0$, $p_1 = p_{atm}$, and $z_1 = 100$ m. Section 2 is at the turbine outlet. The steady-flow energy equation (3.71) becomes, in head form,

$$\frac{p_1}{\gamma} + \frac{\alpha_1 V_1^2}{2g} + z_1 = \frac{p_2}{\gamma} + \frac{\alpha_2 V_2^2}{2g} + z_2 + h_t + h_f$$

$$\frac{p_a}{\gamma} + \frac{1.06(0)^2}{2(9.81)} + 100 \text{ m} = \frac{p_a}{\gamma} + \frac{1.06(2.0 \text{ m/s})^2}{2(9.81 \text{ m/s}^2)} + 0 \text{ m} + h_t + 20 \text{ m}$$

The pressure terms cancel, and we may solve for the turbine head (which is positive):

$$h_t = 100 - 20 - 0.2 \approx 79.8 \text{ m}$$

The turbine extracts about 79.8 percent of the 100-m head available from the dam. The total power extracted may be evaluated from the water mass flow:

$$P = \dot{m} w_s = (\rho Q)(g h_t) = (998 \text{ kg/m}^3)(30 \text{ m}^3/\text{s})(9.81 \text{ m/s}^2)(79.8 \text{ m})$$

$$= 23.4 \text{ E6 kg} \cdot \text{m}^2/\text{s}^3 = 23.4 \text{ E6 N} \cdot \text{m/s} = 23.4 \text{ MW} \qquad \textit{Ans. 7}$$

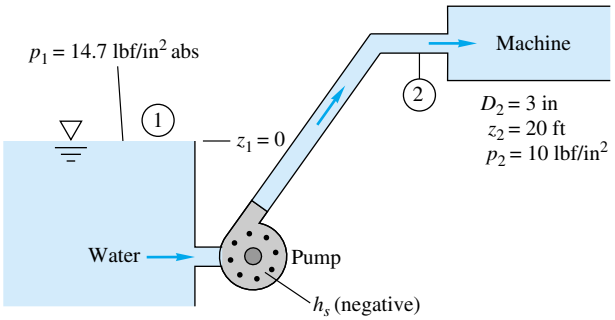
The turbine drives an electric generator which probably has losses of about 15 percent, so the net power generated by this hydroelectric plant is about 20 MW.

EXAMPLE 3.20

The pump in Fig. E3.20 delivers water (62.4 lbf/ft^3) at 3 ft^3/s to a machine at section 2 which is 20 ft higher than the reservoir surface. The losses between 1 and 2 are given by $h_f = I$



ketabline.com Ebook.ketabline.com



E3.20

where $K \approx 7.5$ is a dimensionless loss coefficient (see Sec. 6.7). Take $\alpha \approx 1.07$. Find the horsepower required for the pump if it is 80 percent efficient.

Solution

If the reservoir is large, the flow is steady, with $V_1 \approx 0$. We can compute V_2 from the given flow rate and the pipe diameter:

$$V_2 = \frac{Q}{A_2} = \frac{3 \text{ ft}^3/\text{s}}{(\pi/4)(\frac{3}{12} \text{ ft})^2} = 61.1 \text{ ft/s}$$

The viscous work is zero because of the solid walls and near-one-dimensional inlet and exit. The steady-flow energy equation (3.71) becomes

$$\frac{p_1}{\gamma} + \frac{\alpha_1 V_1^2}{2g} + z_1 = \frac{p_2}{\gamma} + \frac{\alpha_2 V_2^2}{2g} + z_2 + h_s + h_f$$

Introducing $V_1 \approx 0$, $z_1 = 0$, and $h_f = KV_2^2/(2g)$, we may solve for the pump head:

$$h_s = \frac{p_1 - p_2}{\gamma} - z_2 - (\alpha_2 + K)\left(\frac{V_2^2}{2g}\right)$$

The pressures should be in lbf/ft^2 for consistent units. For the given data, we obtain

$$h_s = \frac{(14.7 - 10.0)(144) \text{ lbf/ft}^2}{62.4 \text{ lbf/ft}^3} - 20 \text{ ft} - (1.07 + 7.5)\frac{(61.1 \text{ ft/s})^2}{2(32.2 \text{ ft/s}^2)}$$

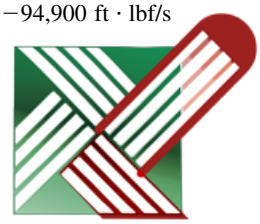
$$= 11 - 20 - 497 = -506 \text{ ft}$$

The pump head is negative, indicating work done *on* the fluid. As in Example 3.19, the power delivered is computed from

$$P = \dot{m} w_s = \rho Q g h_s = (1.94 \text{ slug/ft}^3)(3.0 \text{ ft}^3/\text{s})(32.2 \text{ ft/s}^2)(-507 \text{ ft}) = -94{,}900 \text{ ft} \cdot \text{lbf/s}$$

or

$$\text{hp} = \frac{94{,}900 \text{ ft} \cdot \text{lbf/s}}{550 \text{ ft} \cdot \text{lbf/(s} \cdot \text{hp)}} \approx 173 \text{ hp}$$



ketabline.com Ebook.ketabline.com

We drop the negative sign when merely referring to the "power" required. If the pump is 80 percent efficient, the input power required to drive it is

$$P_{\text{input}} = \frac{P}{\text{efficiency}} = \frac{173 \text{ hp}}{0.8} \approx 216 \text{ hp} \qquad \textit{Ans.}$$

The inclusion of the kinetic-energy correction factor α in this case made a difference of about 1 percent in the result.

3.7 Frictionless Flow: The Bernoulli Equation

Closely related to the steady-flow energy equation is a relation between pressure, velocity, and elevation in a frictionless flow, now called the *Bernoulli equation*. It was stated (vaguely) in words in 1738 in a textbook by Daniel Bernoulli. A complete derivation of the equation was given in 1755 by Leonhard Euler. The Bernoulli equation is very famous and very widely used, but one should be wary of its restrictions—all fluids are viscous and thus all flows have friction to some extent. To use the Bernoulli equation correctly, one must confine it to regions of the flow which are nearly frictionless. This section (and, in more detail, Chap. 8) will address the proper use of the Bernoulli relation.

Consider Fig. 3.15, which is an elemental fixed streamtube control volume of variable area $A(s)$ and length ds, where s is the streamline direction. The properties (ρ, V, p) may vary with s and time but are assumed to be uniform over the cross section A. The streamtube orientation θ is arbitrary, with an elevation change $dz = ds \sin\theta$. Friction on the streamtube walls is shown and then neglected—a very restrictive assumption.

Conservation of mass (3.20) for this elemental control volume yields

$$\frac{d}{dt}\left(\int_{\text{CV}} \rho \, d\mathcal{V}\right) + \dot{m}_{\text{out}} - \dot{m}_{\text{in}} = 0 \approx \frac{\partial \rho}{\partial t} \, d\mathcal{V} + d\dot{m}$$

where $\dot{m} = \rho AV$ and $d\mathcal{V} \approx A \, ds$. Then our desired form of mass conservation is

$$d\dot{m} = d(\rho AV) = -\frac{\partial \rho}{\partial t} A \, ds \tag{3.74}$$

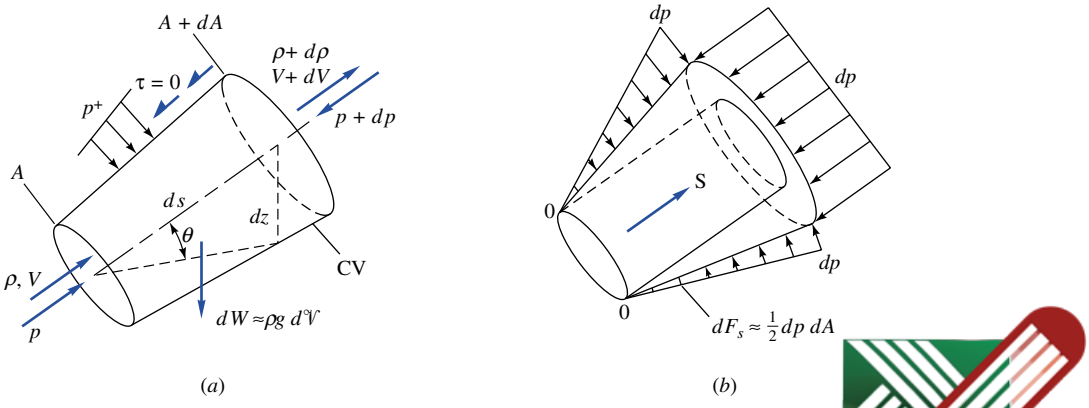


Fig. 3.15 The Bernoulli equation for frictionless flow along a streamline: (*a*) forces and fluxes; (*b*) net pressure force after uniform subtraction of p.

ketabline.com Ebook.ketabline.com

This relation does not require an assumption of frictionless flow.

Now write the linear-momentum relation (3.37) in the streamwise direction:

$$\sum dF_s = \frac{d}{dt}\left(\int_{CV} V\rho\, d\mathcal{V}\right) + (\dot{m}V)_{out} - (\dot{m}V)_{in} \approx \frac{\partial}{\partial t}(\rho V)\, A\, ds + d(\dot{m}V)$$

where $V_s = V$ itself because s is the streamline direction. If we neglect the shear force on the walls (frictionless flow), the forces are due to pressure and gravity. The streamwise gravity force is due to the weight component of the fluid within the control volume:

$$dF_{s,grav} = -dW \sin\theta = -\gamma A\, ds \sin\theta = -\gamma A\, dz$$

The pressure force is more easily visualized, in Fig. 3.15*b*, by first subtracting a uniform value p from all surfaces, remembering from Fig. 3.7 that the net force is not changed. The pressure along the slanted side of the streamtube has a streamwise component which acts not on A itself but on the outer ring of area increase dA. The net pressure force is thus

$$dF_{s,press} = \tfrac{1}{2}\, dp\, dA - dp(A + dA) \approx -A\, dp$$

to first order. Substitute these two force terms into the linear-momentum relation:

$$\sum dF_s = -\gamma A\, dz - A\, dp = \frac{\partial}{\partial t}(\rho V)\, A\, ds + d(\dot{m}V)$$

$$= \frac{\partial \rho}{\partial t} VA\, ds + \frac{\partial V}{\partial t}\rho A\, ds + \dot{m}\, dV + V\, d\dot{m}$$

The first and last terms on the right cancel by virtue of the continuity relation (3.74). Divide what remains by ρA and rearrange into the final desired relation:

$$\frac{\partial V}{\partial t} ds + \frac{dp}{\rho} + V\, dV + g\, dz = 0 \tag{3.75}$$

This is Bernoulli's equation for *unsteady frictionless flow along a streamline*. It is in differential form and can be integrated between any two points 1 and 2 on the streamline:

$$\int_1^2 \frac{\partial V}{\partial t} ds + \int_1^2 \frac{dp}{\rho} + \frac{1}{2}(V_2^2 - V_1^2) + g(z_2 - z_1) = 0 \tag{3.76}$$

To evaluate the two remaining integrals, one must estimate the unsteady effect $\partial V/\partial t$ and the variation of density with pressure. At this time we consider only steady ($\partial V/\partial t = 0$) incompressible (constant-density) flow, for which Eq. (3.76) becomes

$$\frac{p_2 - p_1}{\rho} + \frac{1}{2}(V_2^2 - V_1^2) + g(z_2 - z_1) = 0$$

or

$$\frac{p_1}{\rho} + \frac{1}{2}V_1^2 + gz_1 = \frac{p_2}{\rho} + \frac{1}{2}V_2^2 + gz_2 = \text{const} \tag{3.77}$$

This is the Bernoulli equation for steady frictionless incompress
streamline.



ketabline.com Ebook.ketabline.com

Relation between the Bernoulli and Steady-Flow Energy Equations

Equation (3.77) is a widely used form of the Bernoulli equation for incompressible steady frictionless streamline flow. It is clearly related to the steady-flow energy equation for a streamtube (flow with one inlet and one outlet), from Eq. (3.66), which we state as follows:

$$\frac{p_1}{\rho} + \frac{\alpha_1 V_1^2}{2} + gz_1 = \frac{p_2}{\rho} + \frac{\alpha_2 V_2^2}{2} + gz_2 + (\hat{u}_2 - \hat{u}_1 - q) + w_s + w_v \qquad (3.78)$$

This relation is much more general than the Bernoulli equation, because it allows for (1) friction, (2) heat transfer, (3) shaft work, and (4) viscous work (another frictional effect).

If we compare the Bernoulli equation (3.77) with the energy equation (3.78), we see that the Bernoulli equation contains even more restrictions than might first be realized. The complete list of assumptions for Eq. (3.77) is as follows:

1. *Steady flow*—a common assumption applicable to many flows.
2. *Incompressible flow*—acceptable if the flow Mach number is less than 0.3.
3. *Frictionless flow*—very restrictive, solid walls introduce friction effects.
4. *Flow along a single streamline*—different streamlines may have different "Bernoulli constants" $w_0 = p/\rho + V^2/2 + gz$, depending upon flow conditions.
5. *No shaft work between 1 and 2*—no pumps or turbines on the streamline.
6. *No heat transfer between 1 and 2*—either added or removed.

Thus our warning: Be wary of misuse of the Bernoulli equation. Only a certain limited set of flows satisfies all six assumptions above. The usual momentum or "mechanical force" derivation of the Bernoulli equation does not even reveal items 5 and 6, which are thermodynamic limitations. The basic reason for restrictions 5 and 6 is that heat transfer and work transfer, in real fluids, are married to frictional effects, which therefore invalidate our assumption of frictionless flow.

Figure 3.16 illustrates some practical limitations on the use of Bernoulli's equation (3.77). For the wind-tunnel model test of Fig. 3.16*a*, the Bernoulli equation is valid in the core flow of the tunnel but not in the tunnel-wall boundary layers, the model surface boundary layers, or the wake of the model, all of which are regions with high friction.

In the propeller flow of Fig. 3.16*b*, Bernoulli's equation is valid both upstream and downstream, but with a different constant $w_0 = p/\rho + V^2/2 + gz$, caused by the work addition of the propeller. The Bernoulli relation (3.77) is not valid near the propeller blades or in the helical vortices (not shown, see Fig. 1.12*a*) shed downstream of the blade edges. Also, the Bernoulli constants are higher in the flowing "slipstream" than in the ambient atmosphere because of the slipstream kinetic energy.

For the chimney flow of Fig. 3.16*c*, Eq. (3.77) is valid before and after the fire, but with a change in Bernoulli constant that is caused by heat addition. The Bernoulli equation is not valid within the fire itself or in the chimney-wall boundary layers.

The moral is to apply Eq. (3.77) only when all six restrictions can be satisfied: steady incompressible flow along a streamline with no friction losses, no heat transfer, and no shaft work between sections 1 and 2.



ketabline.com Ebook.ketabline.com

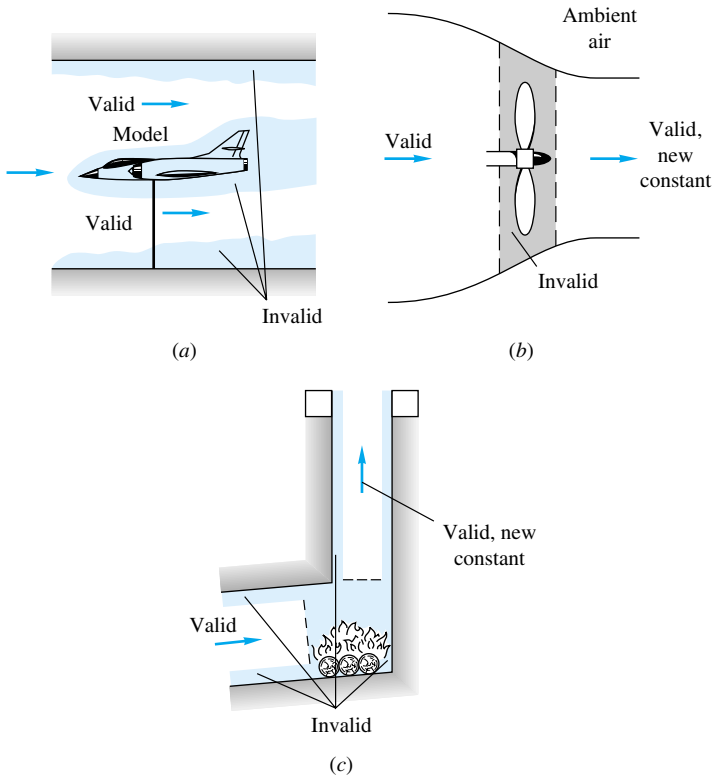


Fig. 3.16 Illustration of regions of validity and invalidity of the Bernoulli equation: (*a*) tunnel model, (*b*) propeller, (*c*) chimney.

Hydraulic and Energy Grade Lines

A useful visual interpretation of Bernoulli's equation is to sketch two grade lines of a flow. The *energy grade line* (EGL) shows the height of the total Bernoulli constant $h_0 = z + p/\gamma + V^2/(2g)$. In frictionless flow with no work or heat transfer, Eq. (3.77), the EGL has constant height. The *hydraulic grade line* (HGL) shows the height corresponding to elevation and pressure head $z + p/\gamma$, that is, the EGL minus the velocity head $V^2/(2g)$. The HGL is the height to which liquid would rise in a piezometer tube (see Prob. 2.11) attached to the flow. In an open-channel flow the HGL is identical to the free surface of the water.

Figure 3.17 illustrates the EGL and HGL for frictionless flow at sections 1 and 2 of a duct. The piezometer tubes measure the static-pressure head $z + p/\gamma$ and thus outline the HGL. The pitot stagnation-velocity tubes measure the total head $z + p/\gamma + V^2/(2g)$, which corresponds to the EGL. In this particular case the EGL is constant, and the HGL rises due to a drop in velocity.

In more general flow conditions, the EGL will drop slowly due to friction losses and will drop sharply due to a substantial loss (a valve or obstruction) or due to work extraction (to a turbine). The EGL can rise only if there is work addition (as from a pump or propeller). The HGL generally follows the behavior of the EGL with respect to losses or work transfer, and it rises and/or falls if the velocity decreases and/or increases.



ketabline.com Ebook.ketabline.com

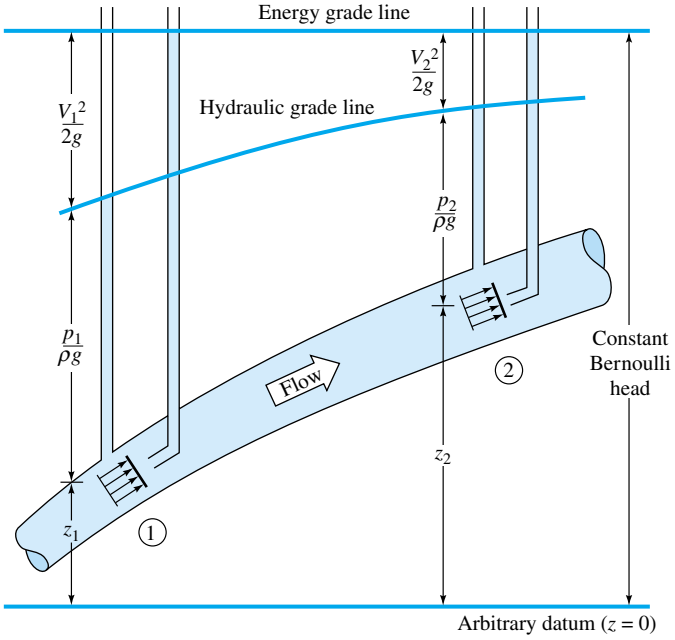


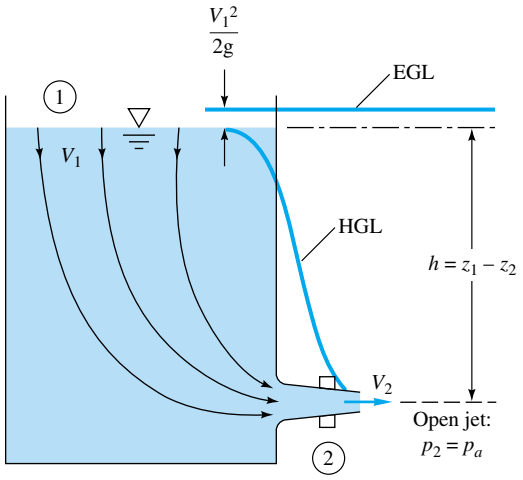
Fig. 3.17 Hydraulic and energy grade lines for frictionless flow in a duct.

As mentioned before, no conversion factors are needed in computations with the Bernoulli equation if consistent SI or BG units are used, as the following examples will show.

In all Bernoulli-type problems in this text, we consistently take point 1 upstream and point 2 downstream.

EXAMPLE 3.21

Find a relation between nozzle discharge velocity $V^2$and tank free-surface height h as in Fig. E3.21. Assume steady frictionless flow.



E3.21



ketabline.com Ebook.ketabline.com

Solution

As mentioned, we always choose point 1 upstream and point 2 downstream. Try to choose points 1 and 2 where maximum information is known or desired. Here we select point 1 as the tank free surface, where elevation and pressure are known, and point 2 as the nozzle exit, where again pressure and elevation are known. The two unknowns are V_1 and V_2.

Mass conservation is usually a vital part of Bernoulli analyses. If A_1 is the tank cross section and A_2 the nozzle area, this is approximately a one-dimensional flow with constant density, Eq. (3.30),

$$A_1V_1 = A_2V_2 \tag{1}$$

Bernoulli's equation (3.77) gives

$$\frac{p_1}{\rho} + \tfrac{1}{2}V_1^2 + gz_1 = \frac{p_2}{\rho} + \tfrac{1}{2}V_2^2 + gz_2$$

But since sections 1 and 2 are both exposed to atmospheric pressure $p_1 = p_2 = p_a$, the pressure terms cancel, leaving

$$V_2^2 - V_1^2 = 2g(z_1 - z_2) = 2gh \tag{2}$$

Eliminating V_1 between Eqs. (1) and (2), we obtain the desired result:

$$V_2^2 = \frac{2gh}{1 - A_2^2/A_1^2} \qquad \textit{Ans.}\ (3)$$

Generally the nozzle area A_2 is very much smaller than the tank area A_1, so that the ratio A_2^2/A_1^2 is doubly negligible, and an accurate approximation for the outlet velocity is

$$V_2 \approx (2gh)^{1/2} \qquad \textit{Ans.}\ (4)$$

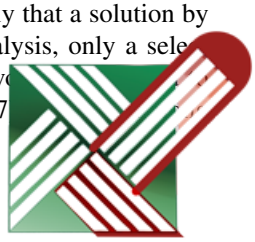
This formula, discovered by Evangelista Torricelli in 1644, states that the discharge velocity equals the speed which a frictionless particle would attain if it fell freely from point 1 to point 2. In other words, the potential energy of the surface fluid is entirely converted to kinetic energy of efflux, which is consistent with the neglect of friction and the fact that no net pressure work is done. Note that Eq. (4) is independent of the fluid density, a characteristic of gravity-driven flows.

Except for the wall boundary layers, the streamlines from 1 to 2 all behave in the same way, and we can assume that the Bernoulli constant h_0 is the same for all the core flow. However, the outlet flow is likely to be nonuniform, not one-dimensional, so that the average velocity is only approximately equal to Torricelli's result. The engineer will then adjust the formula to include a dimensionless *discharge coefficient* c_d

$$(V_2)_{\text{av}} = \frac{Q}{A_2} = c_d(2gh)^{1/2} \tag{5}$$

As discussed in Sec. 6.10, the discharge coefficient of a nozzle varies from about 0.6 to 1.0 as a function of (dimensionless) flow conditions and nozzle shape.

Before proceeding with more examples, we should note carefully that a solution by Bernoulli's equation (3.77) does *not* require a control-volume analysis, only a sele tion of two points 1 and 2 along a given streamline. The control v derive the differential relation (3.75), but the integrated form (3.77



ketabline.com Ebook.ketabline.com

the streamline for frictionless flow with no heat transfer or shaft work, and a control volume is not necessary.

EXAMPLE 3.22

Rework Example 3.21 to account, at least approximately, for the unsteady-flow condition caused by the draining of the tank.

Solution

Essentially we are asked to include the unsteady integral term involving $\partial V/\partial t$ from Eq. (3.76). This will result in a new term added to Eq. (2) from Example 3.21:

$$2\int_1^2 \frac{\partial V}{\partial t}\,ds + V_2^2 - V_1^2 = 2gh \tag{1}$$

Since the flow is incompressible, the continuity equation still retains the simple form $A_1V_1 = A_2V_2$ from Example 3.21. To integrate the unsteady term, we must estimate the acceleration all along the streamline. Most of the streamline is in the tank region where $\partial V/\partial t \approx dV_1/dt$. The length of the average streamline is slightly longer than the nozzle depth h. A crude estimate for the integral is thus

$$\int_1^2 \frac{\partial V}{\partial t}\,ds \approx \int_1^2 \frac{dV_1}{dt}\,ds \approx -\frac{dV_1}{dt}\,h \tag{2}$$

But since A_1 and A_2 are constant, $dV_1/dt \approx (A_2/A_1)(dV_2/dt)$. Substitution into Eq. (1) gives

$$-2h\frac{A_2}{A_1}\frac{dV_2}{dt} + V_2^2\left(1 - \frac{A_2^2}{A_1^2}\right) \approx 2gh \tag{3}$$

This is a first-order differential equation for $V_2(t)$. It is complicated by the fact that the depth h is variable; therefore $h = h(t)$, as determined by the variation in $V_1(t)$

$$h(t) = h_0 - \int_0^t V_1\,dt \tag{4}$$

Equations (3) and (4) must be solved simultaneously, but the problem is well posed and can be handled analytically or numerically. We can also estimate the size of the first term in Eq. (3) by using the approximation $V_2 \approx (2gh)^{1/2}$ from the previous example. After differentiation, we obtain

$$2h\frac{A_2}{A_1}\frac{dV_2}{dt} \approx -\left(\frac{A_2}{A_1}\right)^2 V_2^2 \tag{5}$$

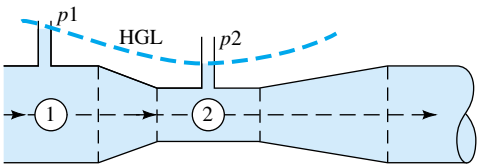
which is negligible if $A_2 \ll A_1$, as originally postulated.

EXAMPLE 3.23

A constriction in a pipe will cause the velocity to rise and the pressure to fall at section 2 in the throat. The pressure difference is a measure of the flow rate through the pipe. The smoothly necked-down system shown in Fig. E3.23 is called a *venturi tube*. Find an expressio mass flux in the tube as a function of the pressure change.



ketabline.com Ebook.ketabline.com



E3.23

Solution

Bernoulli's equation is assumed to hold along the center streamline

$$\frac{p_1}{\rho} + \tfrac{1}{2}V_1^2 + gz_1 = \frac{p_2}{\rho} + \tfrac{1}{2}V_2^2 + gz_2$$

If the tube is horizontal, $z_1 = z_2$ and we can solve for V_2:

$$V_2^2 - V_1^2 = \frac{2\,\Delta p}{\rho} \qquad \Delta p = p_1 - p_2 \tag{1}$$

We relate the velocities from the incompressible continuity relation

$$A_1V_1 = A_2V_2$$

or

$$V_1 = \beta^2 V_2 \qquad \beta = \frac{D_2}{D_1} \tag{2}$$

Combining (1) and (2), we obtain a formula for the velocity in the throat

$$V_2 = \left[\frac{2\,\Delta p}{\rho(1-\beta^4)}\right]^{1/2} \tag{3}$$

The mass flux is given by

$$\dot{m} = \rho A_2 V_2 = A_2\left(\frac{2\rho\,\Delta p}{1-\beta^4}\right)^{1/2} \tag{4}$$

This is the ideal frictionless mass flux. In practice, we measure $\dot{m}_{\text{actual}} = c_d\dot{m}_{\text{ideal}}$ and correlate the discharge coefficient c_d.

EXAMPLE 3.24

A 10-cm fire hose with a 3-cm nozzle discharges 1.5 m^3/min to the atmosphere. Assuming frictionless flow, find the force F_B exerted by the flange bolts to hold the nozzle on the hose.

Solution

We use Bernoulli's equation and continuity to find the pressure p_1 upstream of the nozzle and then we use a control-volume momentum analysis to compute the bolt force, as in Fig. E3.24.

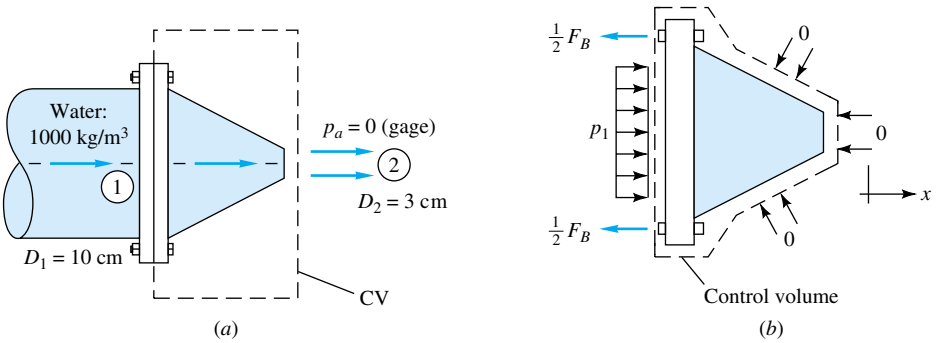
The flow from 1 to 2 is a constriction exactly similar in effect to the venturi in Example 3.23 for which Eq. (1) gave

$$p_1 = p_2 + \tfrac{1}{2}\rho(V_2^2 - V_1^2)$$



ketabline.com Ebook.ketabline.com

E3.24



The velocities are found from the known flow rate $Q = 1.5$ m^3/min or 0.025 m^3/s:

$$V_2 = \frac{Q}{A_2} = \frac{0.025 \text{ m}^3/\text{s}}{(\pi/4)(0.03 \text{ m})^2} = 35.4 \text{ m/s}$$

$$V_1 = \frac{Q}{A_1} = \frac{0.025 \text{ m}^3/\text{s}}{(\pi/4)(0.1 \text{ m})^2} = 3.2 \text{ m/s}$$

We are given $p_2 = p_a = 0$ gage pressure. Then Eq. (1) becomes

$$p_1 = \tfrac{1}{2}(1000 \text{ kg/m}^3)[(35.4^2 - 3.2^2) \text{ m}^2/\text{s}^2]$$

$$= 620{,}000 \text{ kg/(m} \cdot \text{s}^2) = 620{,}000 \text{ Pa gage}$$

The control-volume force balance is shown in Fig. E3.24*b*:

$$\sum F_x = -F_B + p_1 A_1$$

and the zero gage pressure on all other surfaces contributes no force. The x-momentum flux is $+\dot{m}V_2$ at the outlet and $-\dot{m}V_1$ at the inlet. The steady-flow momentum relation (3.40) thus gives

$$-F_B + p_1 A_1 = \dot{m}(V_2 - V_1)$$

or

$$F_B = p_1 A_1 - \dot{m}(V_2 - V_1) \tag{2}$$

Substituting the given numerical values, we find

$$\dot{m} = \rho Q = (1000 \text{ kg/m}^3)(0.025 \text{ m}^3/\text{s}) = 25 \text{ kg/s}$$

$$A_1 = \frac{\pi}{4} D_1^2 = \frac{\pi}{4} (0.1 \text{ m})^2 = 0.00785 \text{ m}^2$$

$$F_B = (620{,}000 \text{ N/m}^2)(0.00785 \text{ m}^2) - (25 \text{ kg/s})[(35.4 - 3.2) \text{ m/s}]$$

$$= 4872 \text{ N} - 805 \text{ (kg} \cdot \text{m)/s}^2 = 4067 \text{ N (915 lbf)} \quad \textit{Ans.}$$

This gives an idea of why it takes more than one firefighter to hold a fire hose at full discharge.

Notice from these examples that the solution of a typical problem i
Bernoulli's equation almost always leads to a consideration of the continuity



ketabline.com Ebook.ketabline.com

as an equal partner in the analysis. The only exception is when the complete velocity distribution is already known from a previous or given analysis, but that means that the continuity relation has already been used to obtain the given information. The point is that the continuity relation is always an important element in a flow analysis.

Summary

This chapter has analyzed the four basic equations of fluid mechanics: conservation of (1) mass, (2) linear momentum, (3) angular momentum, and (4) energy. The equations were attacked "in the large," i.e., applied to whole regions of a flow. As such, the typical analysis will involve an approximation of the flow field within the region, giving somewhat crude but always instructive quantitative results. However, the basic control-volume relations are rigorous and correct and will give exact results if applied to the exact flow field.

There are two main points to a control-volume analysis. The first is the selection of a proper, clever, workable control volume. There is no substitute for experience, but the following guidelines apply. The control volume should cut through the place where the information or solution is desired. It should cut through places where maximum information is already known. If the momentum equation is to be used, it should *not* cut through solid walls unless absolutely necessary, since this will expose possible unknown stresses and forces and moments which make the solution for the desired force difficult or impossible. Finally, every attempt should be made to place the control volume in a frame of reference where the flow is steady or quasi-steady, since the steady formulation is much simpler to evaluate.

The second main point to a control-volume analysis is the reduction of the analysis to a case which applies to the problem at hand. The 24 examples in this chapter give only an introduction to the search for appropriate simplifying assumptions. You will need to solve 24 or 124 more examples to become truly experienced in simplifying the problem just enough and no more. In the meantime, it would be wise for the beginner to adopt a very general form of the control-volume conservation laws and then make a series of simplifications to achieve the final analysis. Starting with the general form, one can ask a series of questions:

1. Is the control volume nondeforming or nonaccelerating?
2. Is the flow field steady? Can we change to a steady-flow frame?
3. Can friction be neglected?
4. Is the fluid incompressible? If not, is the perfect-gas law applicable?
5. Are gravity or other body forces negligible?
6. Is there heat transfer, shaft work, or viscous work?
7. Are the inlet and outlet flows approximately one-dimensional?
8. Is atmospheric pressure important to the analysis? Is the pressure hydrostatic on any portions of the control surface?
9. Are there reservoir conditions which change so slowly that the velocity and time rates of change can be neglected?

In this way, by approving or rejecting a list of basic simplifications one can avoid pulling Bernoulli's equation off the shelf when it do



ketabline.com Ebook.ketabline.com

Problems

Most of the problems herein are fairly straightforward. More difficult or open-ended assignments are labeled with an asterisk. Problems labeled with an EES icon, for example, Prob. 3.5, will benefit from the use of the Engineering Equation Solver (EES), while figures labeled with a computer disk may require the use of a computer. The standard end-of-chapter problems 3.1 to 3.182 (categorized in the problem list below) are followed by word problems W3.1 to W3.7, fundamentals of engineering (FE) exam problems FE3.1 to FE3.10, comprehensive problems C3.1 to C3.4, and design project D3.1.

Problem Distribution

Section	Topic	Problems
3.1	Basic physical laws; volume flow	3.1–3.8
3.2	The Reynolds transport theorem	3.9–3.11
3.3	Conservation of mass	3.12–3.38
3.4	The linear momentum equation	3.39–3.109
3.5	The angular momentum theorem	3.110–3.125
3.6	The energy equation	3.126–3.146
3.7	The Bernoulli equation	3.147–3.182

P3.1 Discuss Newton's second law (the linear-momentum relation) in these three forms:

$$\sum \mathbf{F} = m\mathbf{a} \qquad \sum \mathbf{F} = \frac{d}{dt}(m\mathbf{V})$$

$$\sum \mathbf{F} = \frac{d}{dt}\left(\int_{\text{system}} \mathbf{V}\rho\, d\mathcal{V}\right)$$

Are they all equally valid? Are they equivalent? Are some forms better for fluid mechanics as opposed to solid mechanics?

P3.2 Consider the angular-momentum relation in the form

$$\sum \mathbf{M}_O = \frac{d}{dt}\left[\int_{\text{system}} (\mathbf{r} \times \mathbf{V})\rho\, d\mathcal{V}\right]$$

What does **r** mean in this relation? Is this relation valid in both solid and fluid mechanics? Is it related to the *linear*-momentum equation (Prob. 3.1)? In what manner?

P3.3 For steady low-Reynolds-number (laminar) flow through a long tube (see Prob. 1.12), the axial velocity distribution is given by $u = C(R^2 - r^2)$, where R is the tube radius and $r \le R$. Integrate $u(r)$ to find the total volume flow Q through the tube.

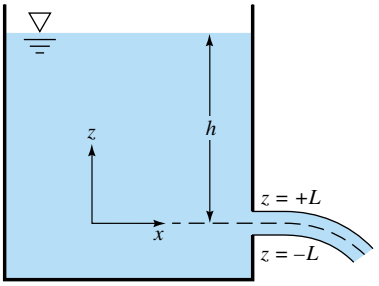
P3.4 Discuss whether the following flows are steady or unsteady: (*a*) flow near an automobile moving at 55 mi/h, (*b*) flow of the wind past a water tower, (*c*) flow in a pipe as the downstream valve is opened at a uniform rate, (*d*) river flow over the spillway of a dam, and (*e*) flow in the ocean beneath a series of uniform propagating surface waves. Elaborate if these questions seem ambiguous.

***P3.5** A theory proposed by S. I. Pai in 1953 gives the following velocity values $u(r)$ for turbulent (high-Reynolds-number) airflow in a 4-cm-diameter tube:

r, cm	0	0.25	0.5	0.75	1.0	1.25	1.5	1.75	2.0
u, m/s	6.00	5.97	5.88	5.72	5.51	5.23	4.89	4.43	0.00

Comment on these data vis-à-vis laminar flow, Prob. 3.3. Estimate, as best you can, the total volume flow Q through the tube, in m^3/s.

P3.6 When a gravity-driven liquid jet issues from a slot in a tank, as in Fig. P3.6, an approximation for the exit velocity distribution is $u \approx \sqrt{2g(h - z)}$, where h is the depth of the jet centerline. Near the slot, the jet is horizontal, two-dimensional, and of thickness $2L$, as shown. Find a general expression for the total volume flow Q issuing from the slot; then take the limit of your result if $L \ll h$.

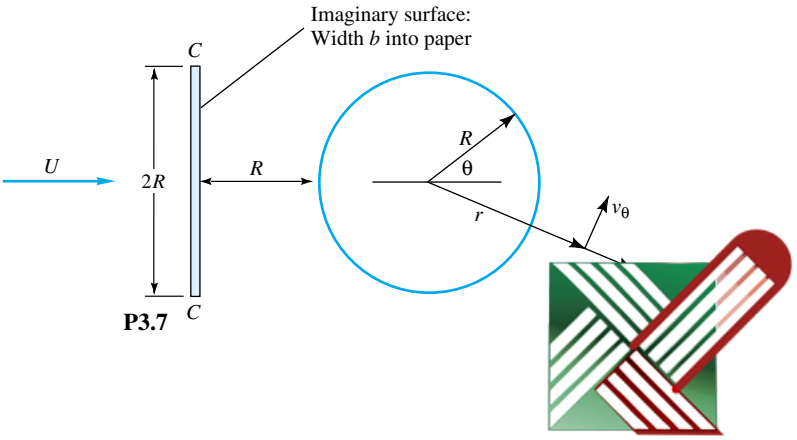


P3.6

P3.7 Consider flow of a uniform stream U toward a circular cylinder of radius R, as in Fig. P3.7. An approximate theory for the velocity distribution near the cylinder is developed in Chap. 8, in polar coordinates, for $r \ge R$:

$$v_r = U\cos\theta\left(1 - \frac{R^2}{r^2}\right) \qquad v_\theta = -U\sin\theta\left(1 + \frac{R^2}{r^2}\right)$$

where the positive directions for radial (v_r) and circumferential (v_θ) velocities are shown in Fig. P3.7. Compute the volume flow Q passing through the (imaginary) surface CC in the figure. (*Comment*: If CC were far upstream of the cylinder, the flow would be $Q = 2URb$.)



P3.7

ketabline.com Ebook.ketabline.com

P3.8 Consider the two-dimensional stagnation flow of Example 1.10, where $u = Kx$ and $v = -Ky$, with $K > 0$. Evaluate the volume flow Q, per unit depth into the paper, passing through the rectangular surface normal to the paper which stretches from $(x, y) = (0, 0)$ to $(1, 1)$.

P3.9 A laboratory test tank contains seawater of salinity S and density ρ. Water enters the tank at conditions (S_1, ρ_1, A_1, V_1) and is assumed to mix immediately in the tank. Tank water leaves through an outlet A_2 at velocity V_2. If salt is a "conservative" property (neither created nor destroyed), use the Reynolds transport theorem to find an expression for the rate of change of salt mass M_{salt} within the tank.

P3.10 Laminar steady flow, through a tube of radius R and length L, is being heated at the wall. The fluid entered the tube at uniform temperature $T_0 = T_w/3$. As the fluid exits the tube, its axial velocity and enthalpy profiles are approximated by

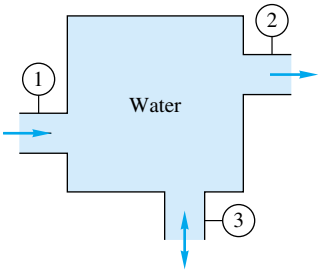
$$u = U_0\left(1 - \frac{r^2}{R^2}\right) \qquad h = \frac{c_p T_w}{2}\left(1 + \frac{r^2}{R^2}\right)$$

$$c_p = \text{const}$$

(a) Sketch these profiles and comment on their physical realism. (b) Compute the total flux of enthalpy through the exit section.

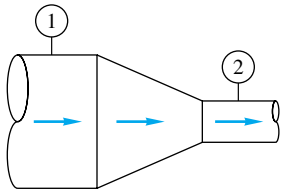
P3.11 A room contains dust of uniform concentration $C = \rho_{dust}/\rho$. It is to be cleaned up by introducing fresh air at velocity V_i through a duct of area A_i on one wall and exhausting the room air at velocity V_0 through a duct A_0 on the opposite wall. Find an expression for the instantaneous rate of change of dust mass within the room.

P3.12 Water at 20°C flows steadily through a closed tank, as in Fig. P3.12. At section 1, $D_1 = 6$ cm and the volume flow is 100 m^3/h. At section 2, $D_2 = 5$ cm and the average velocity is 8 m/s. If $D_3 = 4$ cm, what is (a) Q_3 in m^3/h and (b) average V_3 in m/s?



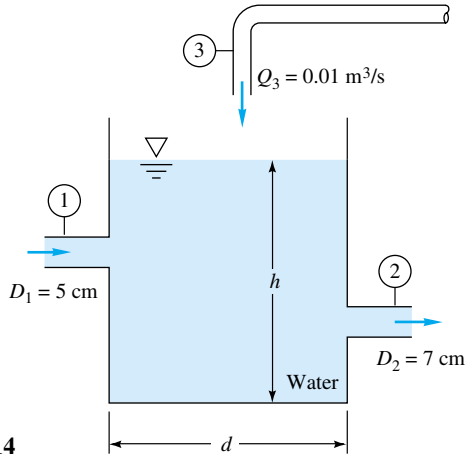
P3.12

P3.13 Water at 20°C flows steadily at 40 kg/s through the nozzle in Fig. P3.13. If $D_1 = 18$ cm and $D_2 = 5$ cm, compute the average velocity, in m/s, at (a) section 1 and (b) section 2.



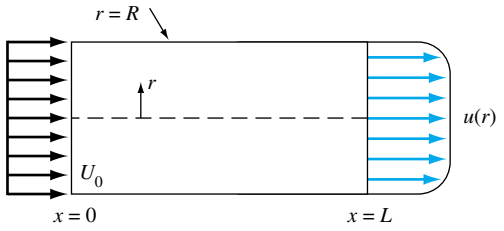
P3.13

P3.14 The open tank in Fig. P3.14 contains water at 20°C and is being filled through section 1. Assume incompressible flow. First derive an analytic expression for the water-level change dh/dt in terms of arbitrary volume flows (Q_1, Q_2, Q_3) and tank diameter d. Then, if the water level h is constant, determine the exit velocity V_2 for the given data $V_1 = 3$ m/s and $Q_3 = 0.01$ m^3/s.



P3.14

P3.15 Water, assumed incompressible, flows steadily through the round pipe in Fig. P3.15. The entrance velocity is constant, $u = U_0$, and the exit velocity approximates turbulent flow, $u = u_{max}(1 - r/R)^{1/7}$. Determine the ratio U_0/u_{max} for this flow.

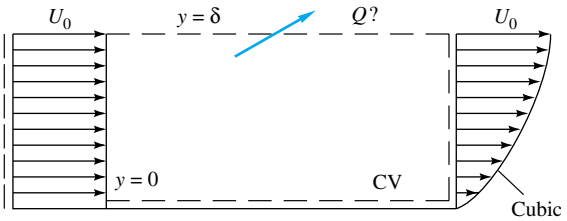


P3.15

P3.16 An incompressible fluid flows past
plate, as in Fig. P3.16, with a uniform
and a cubic polynomial exit profile



ketabline.com Ebook.ketabline.com



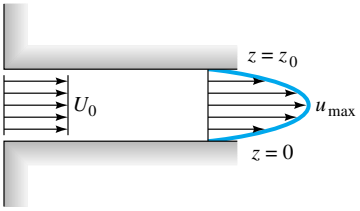
Solid plate, width b into paper

P3.16

$$u \approx U_0\left(\frac{3\eta - \eta^3}{2}\right) \qquad \text{where } \eta = \frac{y}{\delta}$$

Compute the volume flow Q across the top surface of the control volume.

P3.17 Incompressible steady flow in the inlet between parallel plates in Fig. P3.17 is uniform, $u = U_0 = 8$ cm/s, while downstream the flow develops into the parabolic laminar profile $u = az(z_0 - z)$, where a is a constant. If $z_0 = 4$ cm and the fluid is SAE 30 oil at 20°C, what is the value of u_{max} in cm/s?

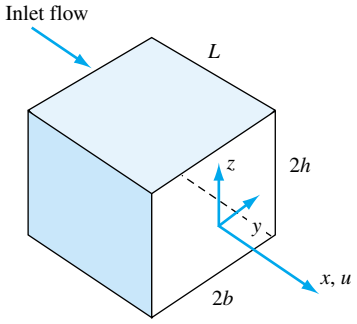


P3.17

P3.18 An incompressible fluid flows steadily through the rectangular duct in Fig. P3.18. The exit velocity profile is given approximately by

$$u = u_{max}\left(1 - \frac{y^2}{b^2}\right)\left(1 - \frac{z^2}{h^2}\right)$$

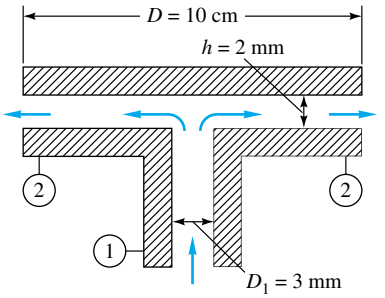
(*a*) Does this profile satisfy the correct boundary conditions for viscous fluid flow? (*b*) Find an analytical expression for the volume flow Q at the exit. (*c*) If the inlet flow is 300 ft^3/min, estimate u_{max} in m/s for $b = h = 10$ cm.



P3.18

P3.19 A partly full water tank admits water at 20°C and 85 N/s weight flow while ejecting water on the other side at 5500 cm^3/s. The air pocket in the tank has a vent at the top and is at 20°C and 1 atm. If the fluids are approximately incompressible, how much air in N/h is passing through the vent? In which direction?

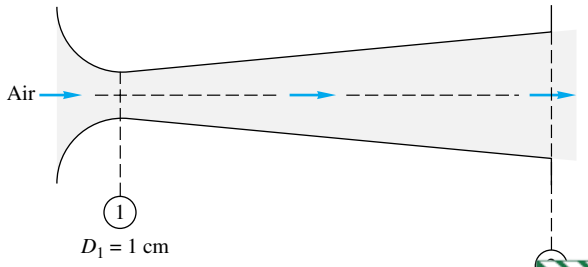
P3.20 Oil (SG = 0.89) enters at section 1 in Fig. P3.20 at a weight flow of 250 N/h to lubricate a thrust bearing. The steady oil flow exits radially through the narrow clearance between thrust plates. Compute (*a*) the outlet volume flux in mL/s and (*b*) the average outlet velocity in cm/s.



P3.20

P3.21 A dehumidifier brings in saturated wet air (100 percent relative humidity) at 30°C and 1 atm, through an inlet of 8-cm diameter and average velocity 3 m/s. After some of the water vapor condenses and is drained off at the bottom, the somewhat drier air leaves at approximately 30°C, 1 atm, and 50 percent relative humidity. For steady operation, estimate the amount of water drained off in kg/h. (This problem is idealized from a real dehumidifier.)

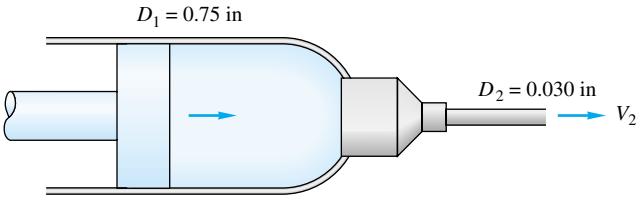
P3.22 The converging-diverging nozzle shown in Fig. P3.22 expands and accelerates dry air to supersonic speeds at the exit, where $p_2 = 8$ kPa and $T_2 = 240$ K. At the throat, $p_1 = 284$ kPa, $T_1 = 665$ K, and $V_1 = 517$ m/s. For steady compressible flow of an ideal gas, estimate (*a*) the mass flow in kg/h, (*b*) the velocity V_2, and (*c*) the Mach number Ma_2.



P3.22

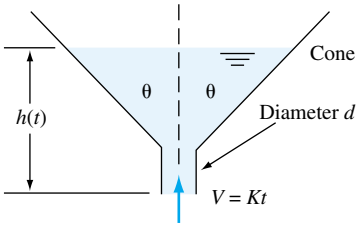
ketabline.com Ebook.ketabline.com

P3.23 The hypodermic needle in Fig. P3.23 contains a liquid serum (SG = 1.05). If the serum is to be injected steadily at 6 cm^3/s, how fast in in/s should the plunger be advanced (*a*) if leakage in the plunger clearance is neglected and (*b*) if leakage is 10 percent of the needle flow?



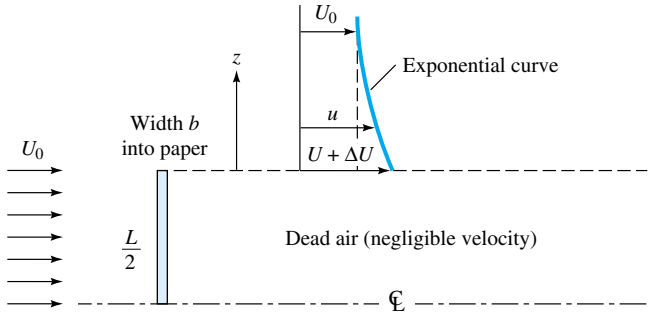
P3.23

***P3.24** Water enters the bottom of the cone in Fig. P3.24 at a uniformly increasing average velocity $V = Kt$. If d is very small, derive an analytic formula for the water surface rise $h(t)$ for the condition $h = 0$ at $t = 0$. Assume incompressible flow.



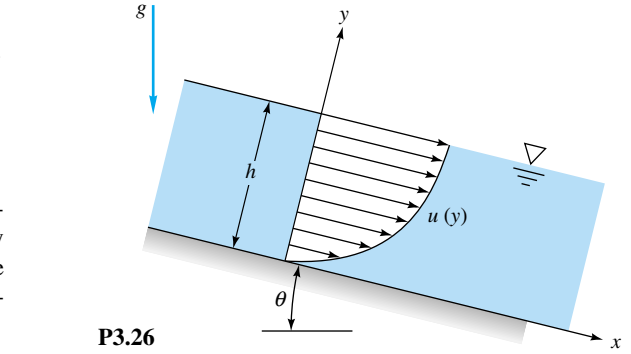
P3.24

P3.25 As will be discussed in Chaps. 7 and 8, the flow of a stream U_0 past a blunt flat plate creates a broad low-velocity wake behind the plate. A simple model is given in Fig. P3.25, with only half of the flow shown due to symmetry. The velocity profile behind the plate is idealized as "dead air" (near-zero velocity) behind the plate, plus a higher velocity, decaying vertically above the wake according to the variation $u \approx U_0 + \Delta U\, e^{-z/L}$, where L is the plate height and $z = 0$ is the top of the wake. Find ΔU as a function of stream speed U_0.



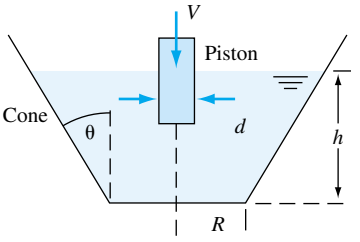
P3.25

P3.26 A thin layer of liquid, draining from an inclined plane, as in Fig. P3.26, will have a laminar velocity profile $u \approx U_0(2y/h - y^2/h^2)$, where U_0 is the surface velocity. If the plane has width b into the paper, determine the volume rate of flow in the film. Suppose that $h = 0.5$ in and the flow rate per foot of channel width is 1.25 gal/min. Estimate U_0 in ft/s.



P3.26

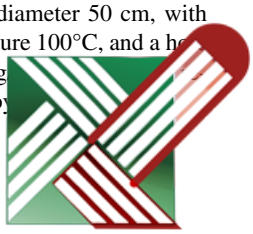
***P3.27** The cone frustum in Fig. P3.27 contains incompressible liquid to depth h. A solid piston of diameter d penetrates the surface at velocity V. Derive an analytic expression for the rate of rise dh/dt of the liquid surface.



P3.27

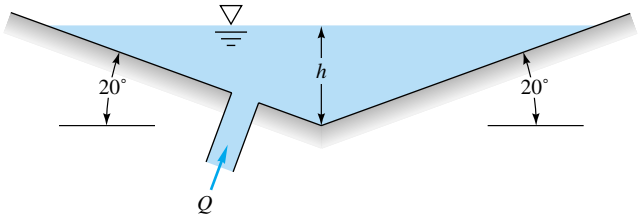
P3.28 Consider a cylindrical water tank of diameter D and water depth h. According to elementary theory, the flow rate from a small hole of area A in the bottom of the tank would be $Q \approx CA\sqrt{2gh}$, where $C \approx 0.61$. If the initial water level is h_0 and the hole is opened, derive an expression for the time required for the water level to drop to $\frac{1}{3}h_0$.

P3.29 In elementary compressible-flow theory (Chap. 9), compressed air will exhaust from a small hole in a tank at the mass flow rate $\dot{m} \approx C\rho$, where ρ is the air density in the tank and C is a constant. If ρ_0 is the initial density in a tank of volume $\mathcal{V}$, derive a formula for the density change $\rho(t)$ after the hole is opened. Apply your formula to the following case: a spherical tank of diameter 50 cm, with initial pressure 300 kPa and temperature 100°C, and a h whose initial exhaust rate is 0.01 kg quired for the tank density to drop b



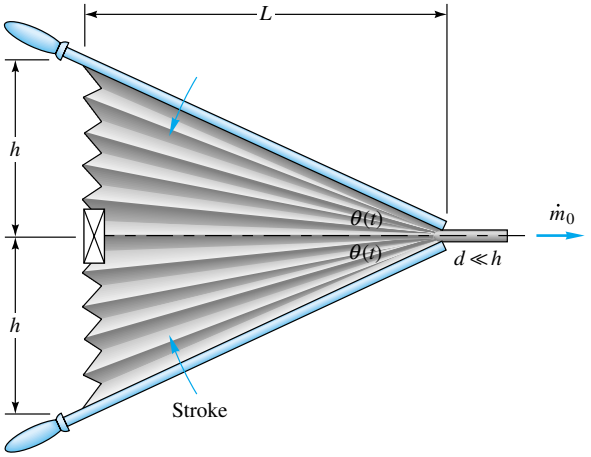
ketabline.com Ebook.ketabline.com

***P3.30** The V-shaped tank in Fig. P3.30 has width b into the paper and is filled from the inlet pipe at volume flow Q. Derive expressions for (*a*) the rate of change dh/dt and (*b*) the time required for the surface to rise from h_1 to h_2.



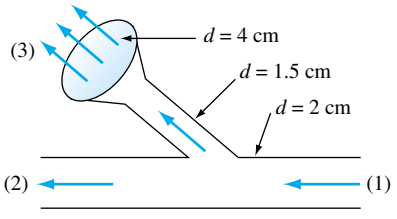
P3.30

P3.31 A bellows may be modeled as a deforming wedge-shaped volume as in Fig. P3.31. The check valve on the left (pleated) end is closed during the stroke. If b is the bellows width into the paper, derive an expression for outlet mass flow $\dot{m}_0$ as a function of stroke $\theta(t)$.



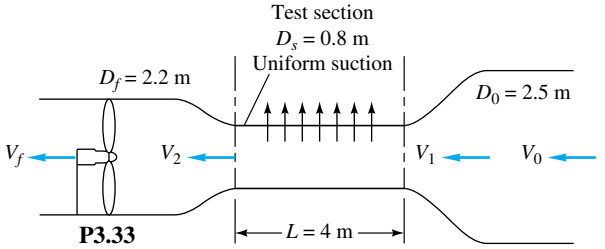
P3.31

P3.32 Water at 20°C flows steadily through the piping junction in Fig. P3.32, entering section 1 at 20 gal/min. The average velocity at section 2 is 2.5 m/s. A portion of the flow is diverted through the showerhead, which contains 100 holes of 1-mm diameter. Assuming uniform shower flow, estimate the exit velocity from the showerhead jets.



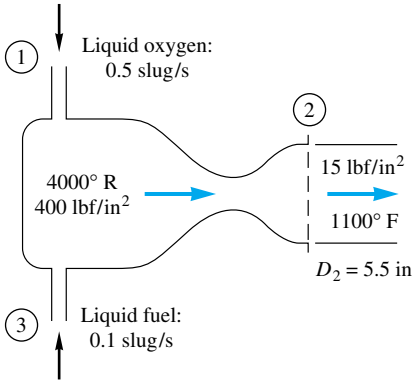
P3.32

P3.33 In some wind tunnels the test section is perforated to suck out fluid and provide a thin viscous boundary layer. The test section wall in Fig. P3.33 contains 1200 holes of 5-mm diameter each per square meter of wall area. The suction velocity through each hole is $V_s = 8$ m/s, and the test-section entrance velocity is $V_1 = 35$ m/s. Assuming incompressible steady flow of air at 20°C, compute (*a*) V_0, (*b*) V_2, and (*c*) V_f, in m/s.



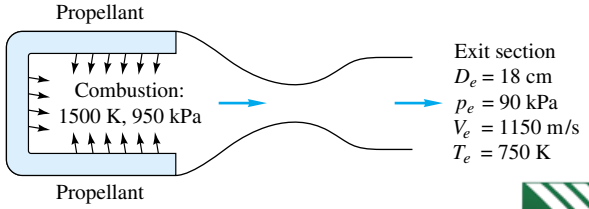
P3.33

P3.34 A rocket motor is operating steadily, as shown in Fig. P3.34. The products of combustion flowing out the exhaust nozzle approximate a perfect gas with a molecular weight of 28. For the given conditions calculate V_2 in ft/s.



P3.34

P3.35 In contrast to the liquid rocket in Fig. P3.34, the solid-propellant rocket in Fig. P3.35 is self-contained and has no entrance ducts. Using a control-volume analysis for the conditions shown in Fig. P3.35, compute the rate of mass loss of the propellant, assuming that the exit gas has a molecular weight of 28.

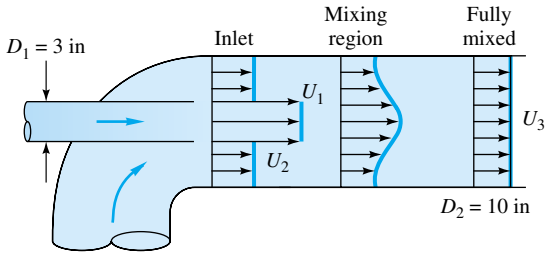


P3.35



ketabline.com Ebook.ketabline.com

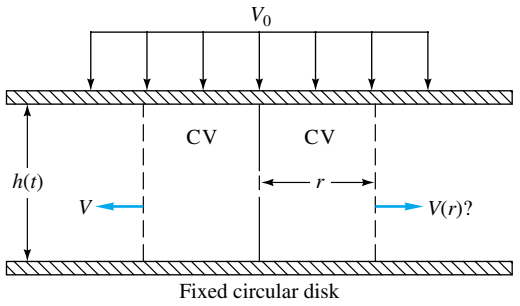
P3.36 The jet pump in Fig. P3.36 injects water at $U_1 = 40$ m/s through a 3-in-pipe and entrains a secondary flow of water $U_2 = 3$ m/s in the annular region around the small pipe. The two flows become fully mixed downstream, where U_3 is approximately constant. For steady incompressible flow, compute U_3 in m/s.



P3.36

P3.37 A solid steel cylinder, 4.5 cm in diameter and 12 cm long, with a mass of 1500 g, falls concentrically through a 5-cm-diameter vertical container filled with oil (SG = 0.89). Assuming the oil is incompressible, estimate the oil average velocity in the annular clearance between cylinder and container (*a*) relative to the container and (*b*) relative to the cylinder.

P3.38 An incompressible fluid in Fig. P3.38 is being squeezed outward between two large circular disks by the uniform downward motion V_0 of the upper disk. Assuming one-dimensional radial outflow, use the control volume shown to derive an expression for $V(r)$.

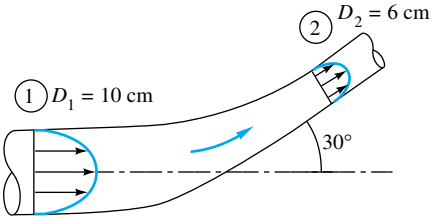


P3.38

P3.39 For the elbow duct in Fig. P3.39, SAE 30 oil at 20°C enters section 1 at 350 N/s, where the flow is laminar, and exits at section 2, where the flow is turbulent:

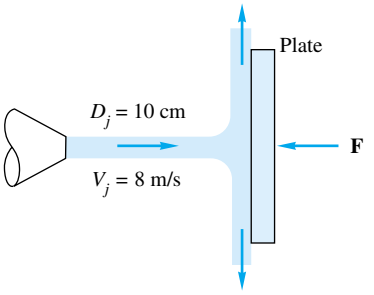
$$u_1 \approx V_{av,1}\left(1 - \frac{r^2}{R_1^2}\right) \qquad u_2 \approx V_{av,2}\left(1 - \frac{r}{R_2}\right)^{1/7}$$

Assuming steady incompressible flow, compute the force, and its direction, of the oil on the elbow due to momentum change only (no pressure change or friction effects) for (*a*) unit momentum-flux correction factors and (*b*) actual correction factors β_1 and β_2.



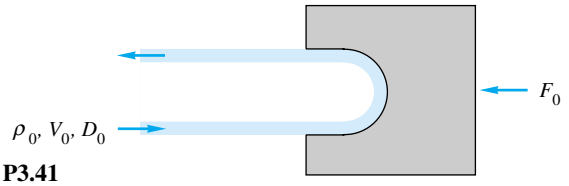
P3.39

P3.40 The water jet in Fig. P3.40 strikes normal to a fixed plate. Neglect gravity and friction, and compute the force F in newtons required to hold the plate fixed.



P3.40

P3.41 In Fig. P3.41 the vane turns the water jet completely around. Find an expression for the maximum jet velocity V_0 if the maximum possible support force is F_0.



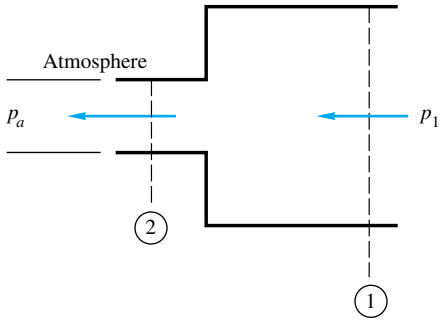
P3.41

P3.42 A liquid of density ρ flows through the sudden contracti
in Fig. P3.42 and exits to the atmosph
conditions (p_1, V_1, D_1) at section 1 an



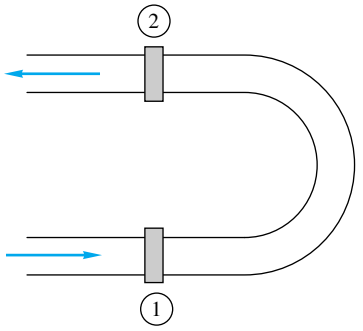
ketabline.com Ebook.ketabline.com

tion 2. Find an expression for the force F exerted by the fluid on the contraction.



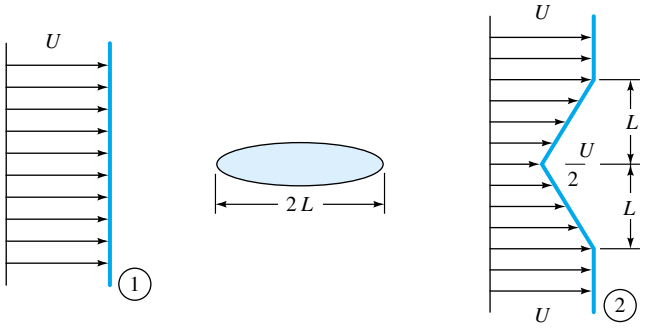
P3.42

P3.43 Water at 20°C flows through a 5-cm-diameter pipe which has a 180° vertical bend, as in Fig. P3.43. The total length of pipe between flanges 1 and 2 is 75 cm. When the weight flow rate is 230 N/s, $p_1 = 165$ kPa and $p_2 = 134$ kPa. Neglecting pipe weight, determine the total force which the flanges must withstand for this flow.



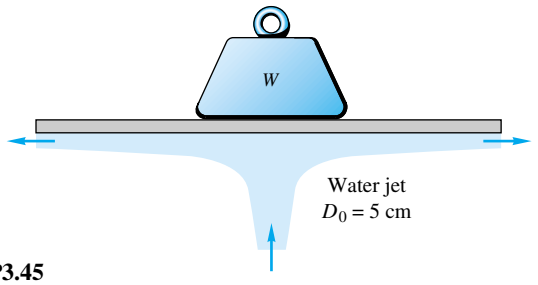
P3.43

***P3.44** When a uniform stream flows past an immersed thick cylinder, a broad low-velocity *wake* is created downstream, idealized as a V shape in Fig. P3.44. Pressures p_1 and p_2 are approximately equal. If the flow is two-dimensional and incompressible, with width b into the paper, derive a formula for the drag force F on the cylinder. Rewrite your result in the form of a dimensionless *drag coefficient* based on body length $C_D = F/(\rho U^2 bL)$.



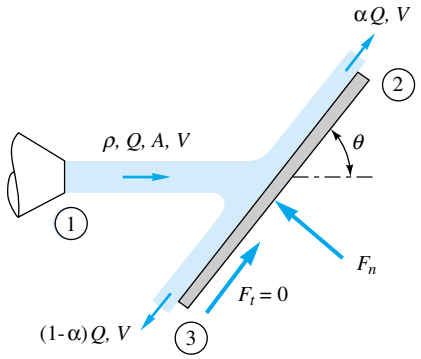
P3.44

P3.45 In Fig. P3.45 a perfectly balanced weight and platform are supported by a steady water jet. If the total weight supported is 700 N, what is the proper jet velocity?



P3.45

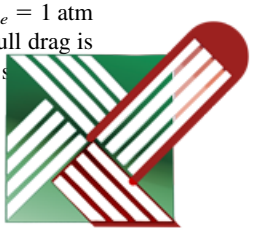
P3.46 When a jet strikes an inclined fixed plate, as in Fig. P3.46, it breaks into two jets at 2 and 3 of equal velocity $V = V_{\text{jet}}$ but unequal fluxes αQ at 2 and $(1 - \alpha)Q$ at section 3, α being a fraction. The reason is that for frictionless flow the fluid can exert no tangential force F_t on the plate. The condition $F_t = 0$ enables us to solve for α. Perform this analysis, and find α as a function of the plate angle θ. Why doesn't the answer depend upon the properties of the jet?



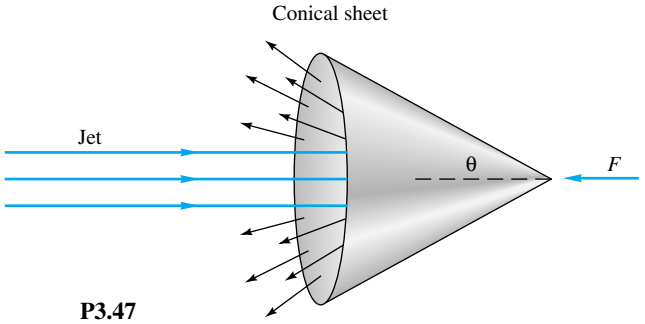
P3.46

P3.47 A liquid jet of velocity V_j and diameter D_j strikes a fixed hollow cone, as in Fig. P3.47, and deflects back as a conical sheet at the same velocity. Find the cone angle θ for which the restraining force $F = \frac{3}{2}\rho A_j V_j^2$.

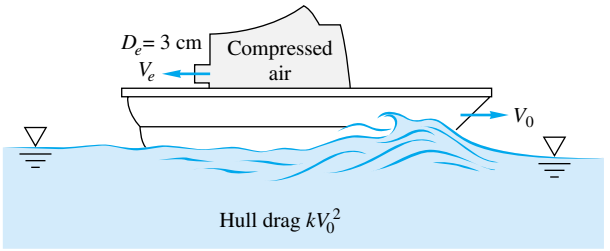
P3.48 The small boat in Fig. P3.48 is driven at a steady speed V_0 by a jet of compressed air issuing from a 3-cm-diameter hole at $V_e = 343$ m/s. Jet exit conditions are $p_e = 1$ atm and $T_e = 30$°C. Air drag is negligible, and the hull drag is kV_0^2, where $k \approx 19$ N · s^2/m^2. Estimate the boat s in m/s.



ketabline.com Ebook.ketabline.com

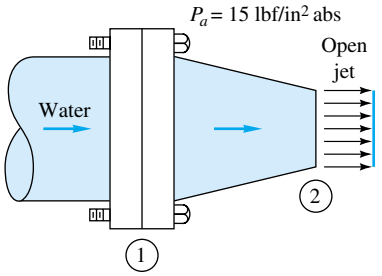


P3.47



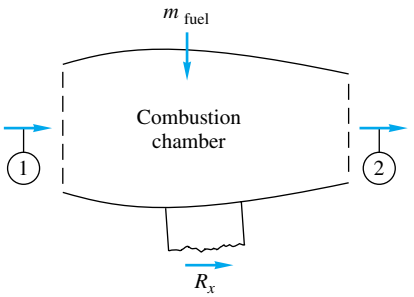
P3.48

P3.49 The horizontal nozzle in Fig. P3.49 has $D_1 = 12$ in and $D_2 = 6$ in, with inlet pressure $p_1 = 38$ lbf/in^{2}absolute and $V_2 = 56$ ft/s. For water at 20°C, compute the horizontal force provided by the flange bolts to hold the nozzle fixed.



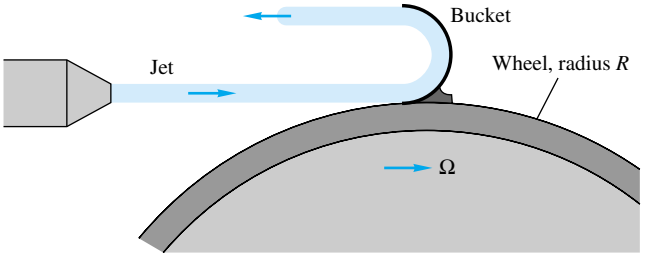
P3.49

P3.50 The jet engine on a test stand in Fig. P3.50 admits air at 20°C and 1 atm at section 1, where $A_1 = 0.5$ m^2 and $V_1 = 250$ m/s. The fuel-to-air ratio is 1:30. The air leaves section 2 at atmospheric pressure and higher temperature, where $V_2 = 900$ m/s and $A_2 = 0.4$ m^2. Compute the horizontal test stand reaction R_x needed to hold this engine fixed.



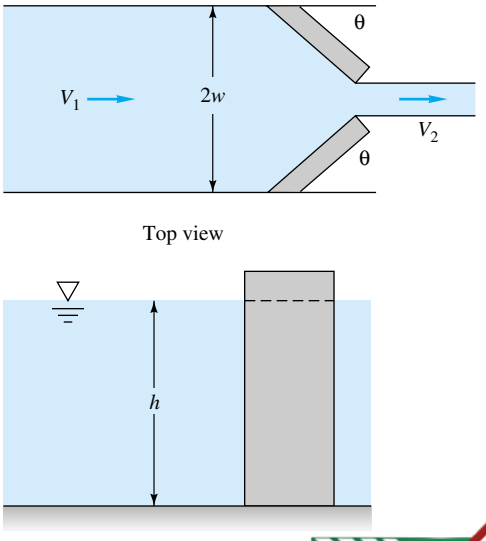
P3.50

P3.51 A liquid jet of velocity V_j and area A_j strikes a single 180° bucket on a turbine wheel rotating at angular velocity Ω, as in Fig. P3.51. Derive an expression for the power P delivered to this wheel at this instant as a function of the system parameters. At what angular velocity is the maximum power delivered? How would your analysis differ if there were many, many buckets on the wheel, so that the jet was continually striking at least one bucket?



P3.51

P3.52 The vertical gate in a water channel is partially open, as in Fig. P3.52. Assuming no change in water level and a hydrostatic pressure distribution, derive an expression for the streamwise force F_x on one-half of the gate as a function of (ρ, h, w, θ, V_1). Apply your result to the case of water at 20°C, $V_1 = 0.8$ m/s, $h = 2$ m, $w = 1.5$ m, and $\theta = 50°$.



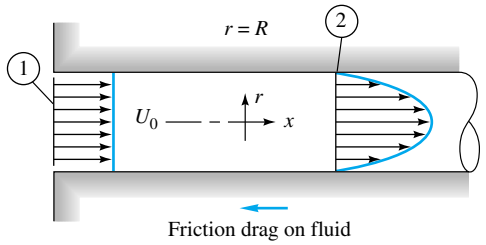
P3.52

ketabline.com Ebook.ketabline.com

P3.53 Consider incompressible flow in the entrance of a circular tube, as in Fig. P3.53. The inlet flow is uniform, $u_1 = U_0$. The flow at section 2 is developed pipe flow. Find the wall drag force F as a function of (p_1, p_2, ρ, U_0, R) if the flow at section 2 is

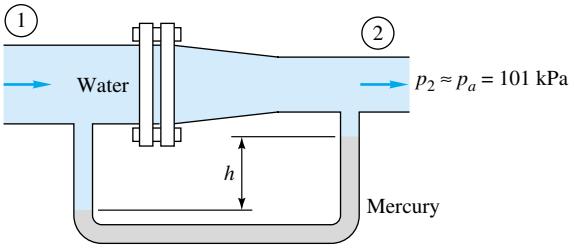
(a) Laminar: $u_2 = u_{max}\left(1 - \frac{r^2}{R^2}\right)$

(b) Turbulent: $u_2 \approx u_{max}\left(1 - \frac{r}{R}\right)^{1/7}$



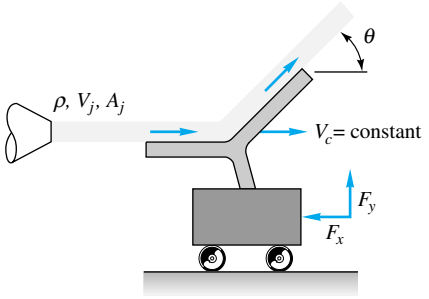
P3.53

P3.54 For the pipe-flow-reducing section of Fig. P3.54, $D_1 = 8$ cm, $D_2 = 5$ cm, and $p_2 = 1$ atm. All fluids are at 20°C. If $V_1 = 5$ m/s and the manometer reading is $h = 58$ cm, estimate the total force resisted by the flange bolts.



P3.54

P3.55 In Fig. P3.55 the jet strikes a vane which moves to the right at constant velocity V_c on a frictionless cart. Compute (a) the force F_x required to restrain the cart and (b) the power P delivered to the cart. Also find the cart velocity for which (c) the force F_x is a maximum and (d) the power P is a maximum.



P3.55

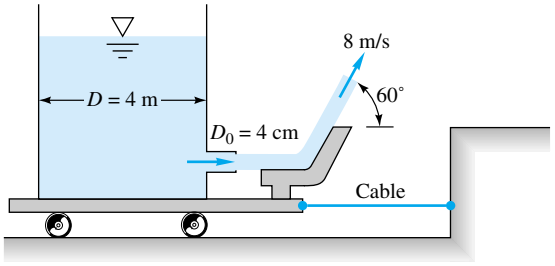
P3.56 For the flat-plate boundary-layer flow of Fig. 3.11, assume that the exit profile is given by $u \approx U_0 \sin[\pi y/(2\delta)]$ for water flow at 20°C: $U_0 = 3$ m/s, $\delta = 2$ mm, and $L = 45$ cm. Estimate the total drag force on the plate, in N, per unit depth into the paper.

***P3.57** Laminar-flow theory [Ref. 3 of Chap. 1, p. 260] gives the following expression for the wake behind a flat plate of length L (see Fig. P3.44 for a crude sketch of wake):

$$u = U\left[1 - \frac{0.664}{\pi}\left(\frac{L}{x}\right)^{1/2} \exp\left(-\frac{y^2 \rho U}{4x\mu}\right)\right]$$

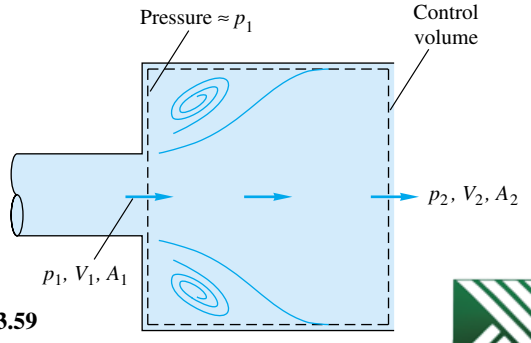
where U is the stream velocity, x is distance downstream of the plate, and $y = 0$ is the plane of the plate. Sketch two wake profiles, for $u_{min} = 0.9U$ and $u_{min} = 0.8U$. For these two profiles, evaluate the momentum-flux *defect*, i.e., the difference between the momentum of a uniform stream U and the actual wake profile. Comment on your results.

P3.58 The water tank in Fig. P3.58 stands on a frictionless cart and feeds a jet of diameter 4 cm and velocity 8 m/s, which is deflected 60° by a vane. Compute the tension in the supporting cable.



P3.58

P3.59 When a pipe flow suddenly expands from A_1 to A_2, as in Fig. P3.59, low-speed, low-friction eddies appear in the



P3.59



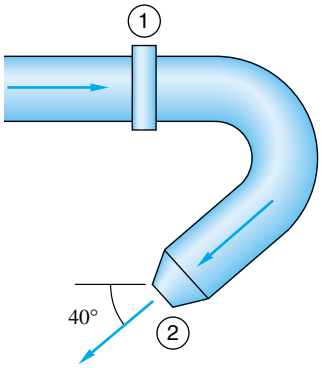
ketabline.com Ebook.ketabline.com

corners and the flow gradually expands to A_2 downstream. Using the suggested control volume for incompressible steady flow and assuming that $p \approx p_1$ on the corner annular ring as shown, show that the downstream pressure is given by

$$p_2 = p_1 + \rho V_1^2 \frac{A_1}{A_2}\left(1 - \frac{A_1}{A_2}\right)$$

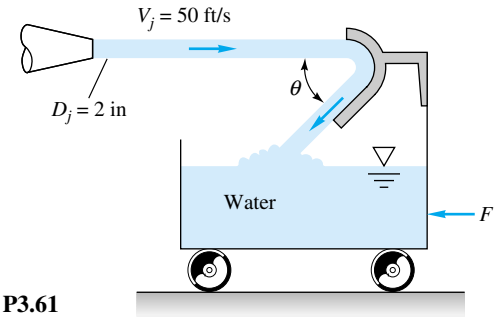
Neglect wall friction.

P3.60 Water at 20°C flows through the elbow in Fig. P3.60 and exits to the atmosphere. The pipe diameter is $D_1 = 10$ cm, while $D_2 = 3$ cm. At a weight flow rate of 150 N/s, the pressure $p_1 = 2.3$ atm (gage). Neglecting the weight of water and elbow, estimate the force on the flange bolts at section 1.



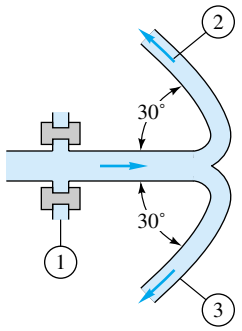
P3.60

P3.61 A 20°C water jet strikes a vane mounted on a tank with frictionless wheels, as in Fig. P3.61. The jet turns and falls into the tank without spilling out. If $\theta = 30°$, evaluate the horizontal force F required to hold the tank stationary.



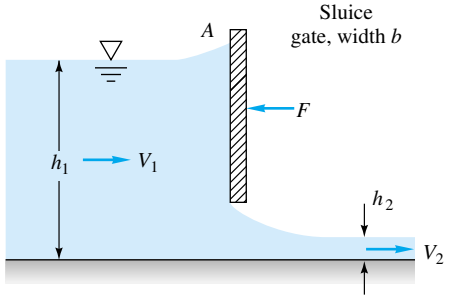
P3.61

P3.62 Water at 20°C exits to the standard sea-level atmosphere through the split nozzle in Fig. P3.62. Duct areas are $A_1 = 0.02$ m^2 and $A_2 = A_3 = 0.008$ m^2. If $p_1 = 135$ kPa (absolute) and the flow rate is $Q_2 = Q_3 = 275$ m^3/h, compute the force on the flange bolts at section 1.



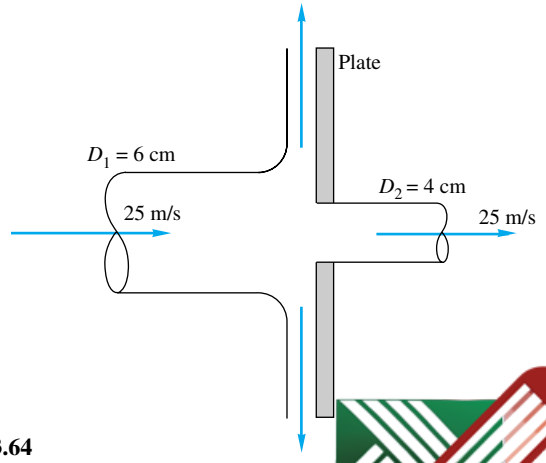
P3.62

***P3.63** The sluice gate in Fig. P3.63 can control and measure flow in open channels. At sections 1 and 2, the flow is uniform and the pressure is hydrostatic. The channel width is b into the paper. Neglecting bottom friction, derive an expression for the force F required to hold the gate. For what condition h_2/h_1 is the force largest? For very low velocity $V_1^2 \ll gh_1$, for what value of h_2/h_1 will the force be one-half of the maximum?



P3.63

P3.64 The 6-cm-diameter 20°C water jet in Fig. P3.64 strikes a plate containing a hole of 4-cm diameter. Part of the jet

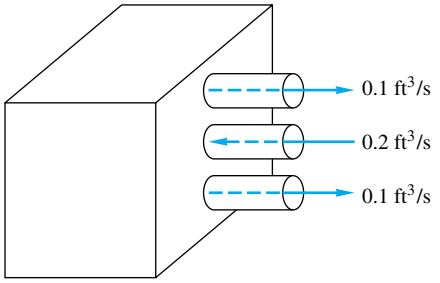


P3.64

ketabline.com Ebook.ketabline.com

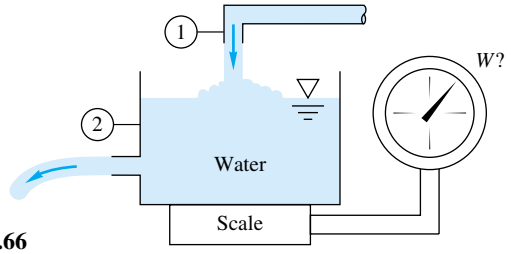
passes through the hole, and part is deflected. Determine the horizontal force required to hold the plate.

P3.65 The box in Fig. P3.65 has three 0.5-in holes on the right side. The volume flows of 20°C water shown are steady, but the details of the interior are not known. Compute the force, if any, which this water flow causes on the box.



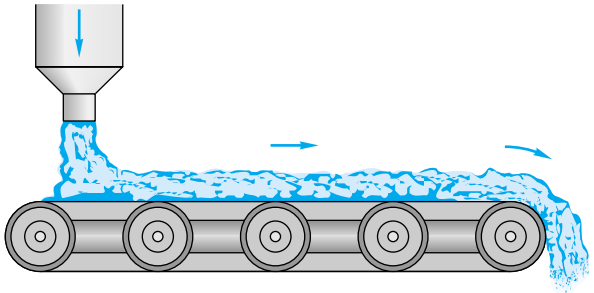
P3.65

P3.66 The tank in Fig. P3.66 weighs 500 N empty and contains 600 L of water at 20°C. Pipes 1 and 2 have equal diameters of 6 cm and equal steady volume flows of 300 m³/h. What should the scale reading W be in N?



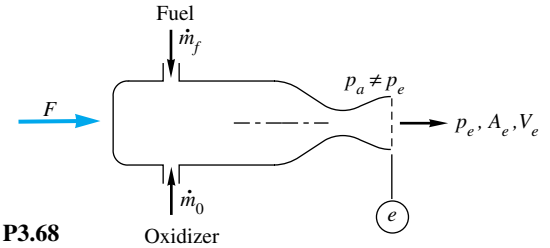
P3.66

P3.67 Gravel is dumped from a hopper, at a rate of 650 N/s, onto a moving belt, as in Fig. P3.67. The gravel then passes off the end of the belt. The drive wheels are 80 cm in diameter and rotate clockwise at 150 r/min. Neglecting system friction and air drag, estimate the power required to drive this belt.



P3.67

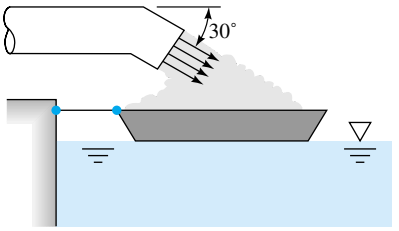
P3.68 The rocket in Fig. P3.68 has a supersonic exhaust, and the exit pressure p_e is not necessarily equal to p_a. Show that the force F required to hold this rocket on the test stand is $F = \rho_e A_e V_e^2 + A_e(p_e - p_a)$. Is this force F what we term the *thrust* of the rocket?



P3.68

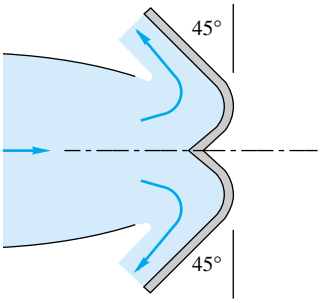
P3.69 The solution to Prob. 3.22 is a mass flow of 218 kg/h with $V_2 = 1060$ m/s and $\text{Ma}_2 = 3.41$. If the conical section 1–2 in Fig. P3.22 is 12 cm long, estimate the force on these conical walls caused by this high-speed gas flow.

P3.70 The dredger in Fig. P3.70 is loading sand (SG = 2.6) onto a barge. The sand leaves the dredger pipe at 4 ft/s with a weight flux of 850 lbf/s. Estimate the tension on the mooring line caused by this loading process.



P3.70

P3.71 Suppose that a deflector is deployed at the exit of the jet engine of Prob. 3.50, as shown in Fig. P3.71. What will the reaction R_x on the test stand be now? Is this reaction sufficient to serve as a braking force during airplane landing?



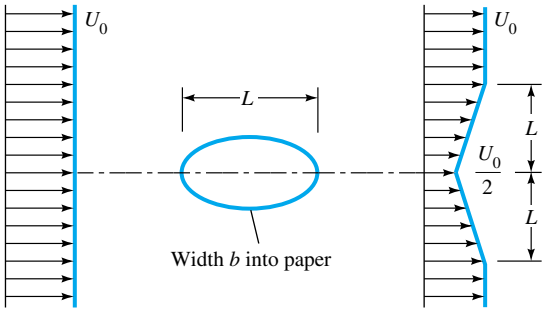
P3.71

***P3.72** When immersed in a uniform stream, a thick cylinder creates a broad downstream wake, as ide



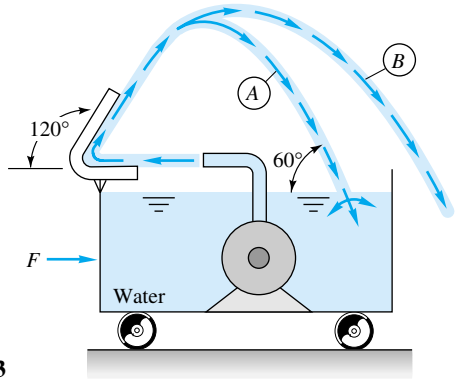
ketabline.com Ebook.ketabline.com

Fig. P3.72. The pressure at the upstream and downstream sections are approximately equal, and the fluid is water at 20°C. If $U_0 = 4$ m/s and $L = 80$ cm, estimate the drag force on the cylinder per unit width into the paper. Also compute the dimensionless drag coefficient $C_D = 2F/(\rho U_0^2 bL)$.



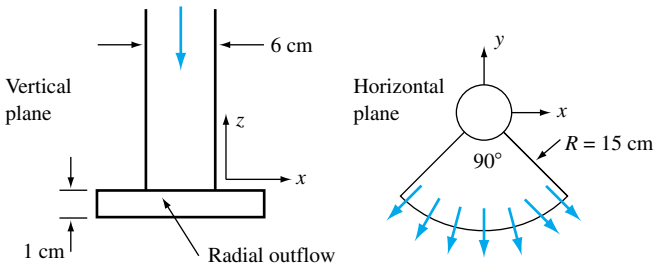
P3.72

P3.73 A pump in a tank of water at 20°C directs a jet at 45 ft/s and 200 gal/min against a vane, as shown in Fig. P3.73. Compute the force F to hold the cart stationary if the jet follows (*a*) path A or (*b*) path B. The tank holds 550 gal of water at this instant.



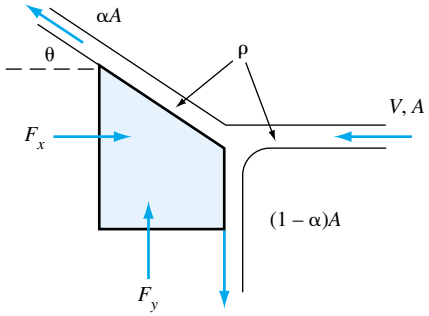
P3.73

P3.74 Water at 20°C flows down through a vertical, 6-cm-diameter tube at 300 gal/min, as in Fig. P3.74. The flow then turns horizontally and exits through a 90° radial duct segment 1 cm thick, as shown. If the radial outflow is uniform and steady, estimate the forces (F_x, F_y, F_z) required to support this system against fluid momentum changes.



P3.74

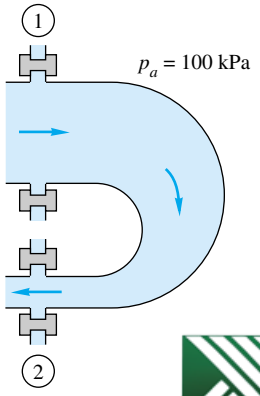
***P3.75** A jet of liquid of density ρ and area A strikes a block and splits into two jets, as in Fig. P3.75. Assume the same velocity V for all three jets. The upper jet exits at an angle θ and area αA. The lower jet is turned 90° downward. Neglecting fluid weight, (*a*) derive a formula for the forces (F_x, F_y) required to support the block against fluid momentum changes. (*b*) Show that $F_y = 0$ only if $\alpha \geq 0.5$. (*c*) Find the values of α and θ for which both F_x and F_y are zero.



P3.75

***P3.76** The rocket engine of Prob. 3.35 has an initial mass of 250 kg and is mounted on the rear of a 1300-kg racing car. The rocket is fired up, and the car accelerates on level ground. If the car has an air drag of kV^2, where $k \approx 0.65$ N · s^2/m^2, and rolling resistance cV, where $c \approx 16$ N · s/m, estimate the velocity of the car after it travels 0.25 mi (1320 ft).

P3.77 Water at 20°C flows steadily through a reducing pipe bend, as in Fig. P3.77. Known conditions are $p_1 = 350$ kPa, $D_1 = 25$ cm, $V_1 = 2.2$ m/s, $p_2 = 120$ kPa, and $D_2 = 8$ cm. Neglecting bend and water weight, estimate the total force which must be resisted by the flange bolts.

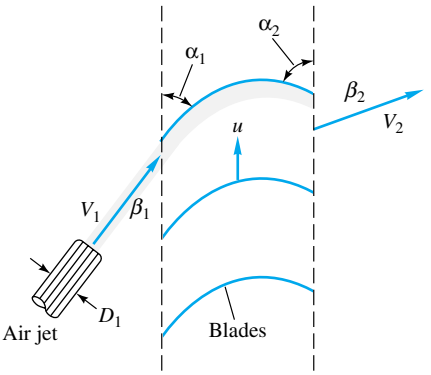


P3.77



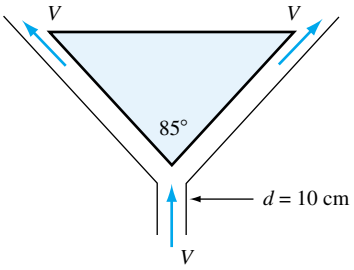
ketabline.com Ebook.ketabline.com

P3.78 A fluid jet of diameter D_1 enters a cascade of moving blades at absolute velocity V_1 and angle β_1, and it leaves at absolute velocity V_1 and angle β_2, as in Fig. P3.78. The blades move at velocity u. Derive a formula for the power P delivered to the blades as a function of these parameters.



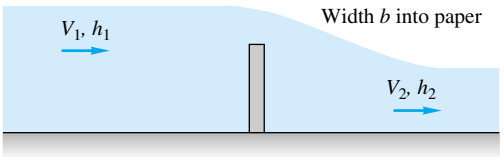
P3.78

P3.79 Air at 20°C and 1 atm enters the bottom of an 85° conical flowmeter duct at a mass flow of 0.3 kg/s, as shown in Fig. P3.79. It is able to support a centered conical body by steady annular flow around the cone, as shown. The air velocity at the upper edge of the body equals the entering velocity. Estimate the weight of the body, in newtons.



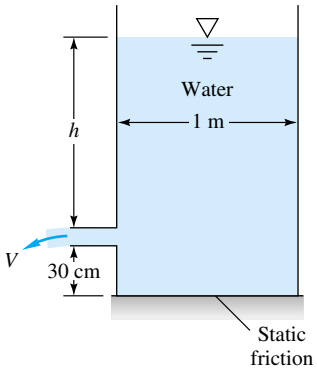
P3.79

P3.80 A river of width b and depth h_1 passes over a submerged obstacle, or "drowned weir," in Fig. P3.80, emerging at a new flow condition (V_2, h_2). Neglect atmospheric pressure, and assume that the water pressure is hydrostatic at both sections 1 and 2. Derive an expression for the force exerted by the river on the obstacle in terms of V_1, h_1, h_2, b, ρ, and g. Neglect water friction on the river bottom.



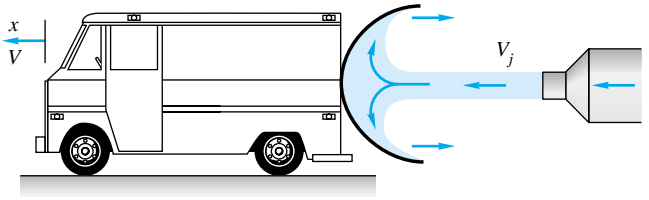
P3.80

P3.81 Torricelli's idealization of efflux from a hole in the side of a tank is $V = \sqrt{2gh}$, as shown in Fig. P3.81. The cylindrical tank weighs 150 N when empty and contains water at 20°C. The tank bottom is on very smooth ice (static friction coefficient $\zeta \approx 0.01$). The hole diameter is 9 cm. For what water depth h will the tank just begin to move to the right?



P3.81

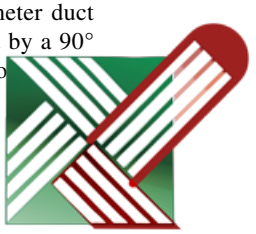
***P3.82** The model car in Fig. P3.82 weighs 17 N and is to be accelerated from rest by a 1-cm-diameter water jet moving at 75 m/s. Neglecting air drag and wheel friction, estimate the velocity of the car after it has moved forward 1 m.



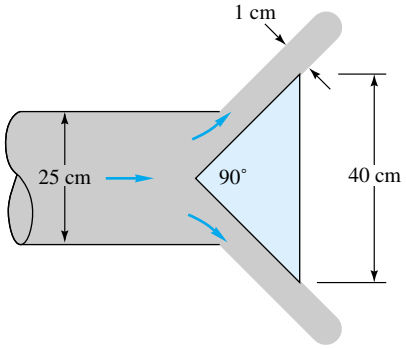
P3.82

P3.83 Gasoline at 20°C is flowing at $V_1 = 12$ m/s in a 5-cm-diameter pipe when it encounters a 1-m length of uniform radial wall suction. At the end of this suction region, the average fluid velocity has dropped to $V_2 = 10$ m/s. If $p_1 = 120$ kPa, estimate p_2 if the wall friction losses are neglected.

P3.84 Air at 20°C and 1 atm flows in a 25-cm-diameter duct at 15 m/s, as in Fig. P3.84. The exit is choked by a 90° cone, as shown. Estimate the force of the airflo
cone.

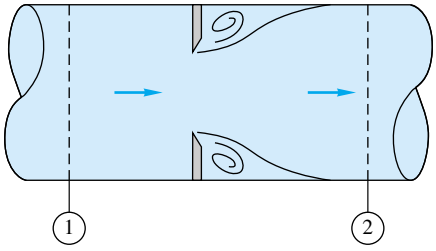


ketabline.com Ebook.ketabline.com



P3.84

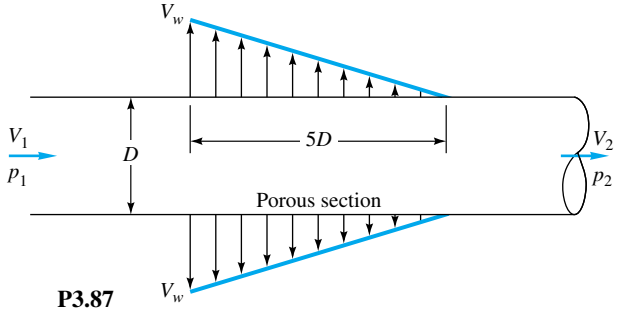
P3.85 The thin-plate orifice in Fig. P3.85 causes a large pressure drop. For 20°C water flow at 500 gal/min, with pipe $D = 10$ cm and orifice $d = 6$ cm, $p_1 - p_2 \approx 145$ kPa. If the wall friction is negligible, estimate the force of the water on the orifice plate.



P3.85

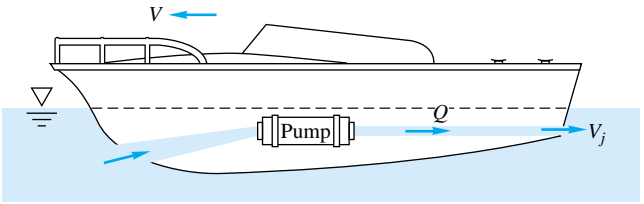
P3.86 For the water-jet pump of Prob. 3.36, add the following data: $p_1 = p_2 = 25$ lbf/in^2, and the distance between sections 1 and 3 is 80 in. If the average wall shear stress between sections 1 and 3 is 7 lbf/ft^2, estimate the pressure p_3. Why is it higher than p_1?

P3.87 Figure P3.87 simulates a *manifold* flow, with fluid removed from a porous wall or perforated section of pipe. Assume incompressible flow with negligible wall friction and small suction $V_w \ll V_1$. If (p_1, V_1, V_w, ρ, D) are known, derive expressions for (*a*) V_2 and (*b*) p_2.



P3.87

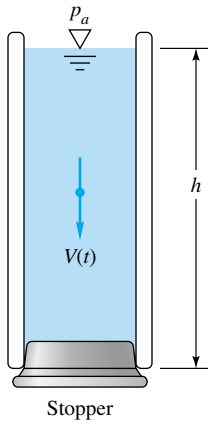
P3.88 The boat in Fig. P3.88 is jet-propelled by a pump which develops a volume flow rate Q and ejects water out the stern at velocity V_j. If the boat drag force is $F = kV^2$, where k is a constant, develop a formula for the steady forward speed V of the boat.



P3.88

P3.89 Consider Fig. P3.36 as a general problem for analysis of a mixing ejector pump. If all conditions (p, ρ, V) are known at sections 1 and 2 and if the wall friction is negligible, derive formulas for estimating (*a*) V_3 and (*b*) p_3.

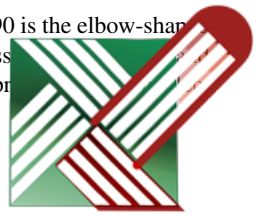
P3.90 As shown in Fig. P3.90, a liquid column of height h is confined in a vertical tube of cross-sectional area A by a stopper. At $t = 0$ the stopper is suddenly removed, exposing the bottom of the liquid to atmospheric pressure. Using a control-volume analysis of mass and vertical momentum, derive the differential equation for the downward motion $V(t)$ of the liquid. Assume one-dimensional, incompressible, frictionless flow.



P3.90

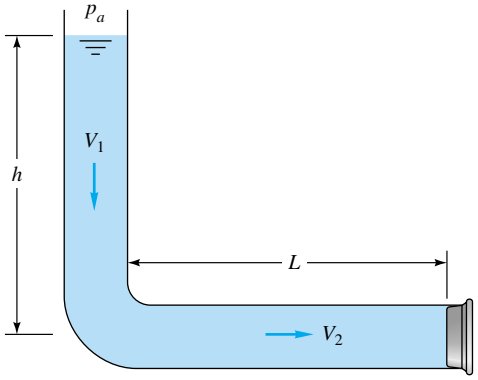
P3.91 Extend Prob. 3.90 to include a linear (laminar) average wall shear stress resistance of the form $\tau \approx cV$, where c is a constant. Find the differential equation for dV/dt and then solve for $V(t)$, assuming for simplicity that the wall area remains constant.

***P3.92** A more involved version of Prob. 3.90 is the elbow-shar
tube in Fig. P3.92, with constant cross
diameter $D \ll h$, L. Assume incompr



ketabline.com Ebook.ketabline.com

friction, and derive a differential equation for dV/dt when the stopper is opened. *Hint:* Combine two control volumes, one for each leg of the tube.



P3.92

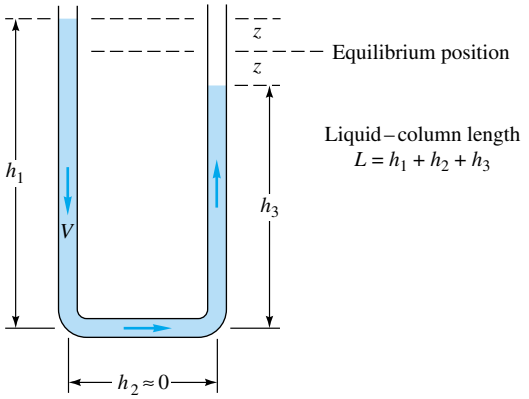
P3.93 Extend Prob. 3.92 to include a linear (laminar) average wall shear stress resistance of the form $\tau \approx cV$, where c is a constant. Find the differential equation for dV/dt and then solve for $V(t)$, assuming for simplicity that the wall area remains constant.

P3.94 Attempt a numerical solution of Prob. 3.93 for SAE 30 oil at 20°C. Let $h = 20$ cm, $L = 15$ cm, and $D = 4$ mm. Use the laminar shear approximation from Sec. 6.4: $\tau \approx 8\mu V/D$, where μ is the fluid viscosity. Account for the decrease in wall area wetted by the fluid. Solve for the time required to empty (*a*) the vertical leg and (*b*) the horizontal leg.

P3.95 Attempt a numerical solution of Prob. 3.93 for mercury at 20°C. Let $h = 20$ cm, $L = 15$ cm, and $D = 4$ mm. For mercury the flow will be *turbulent*, with the wall shear stress estimated from Sec. 6.4: $\tau \approx 0.005\rho V^2$, where ρ is the fluid density. Account for the decrease in wall area wetted by the fluid. Solve for the time required to empty (*a*) the vertical leg and (*b*) the horizontal leg. Compare with a frictionless flow solution.

P3.96 Extend Prob. 3.90 to the case of the liquid motion in a frictionless U-tube whose liquid column is displaced a distance Z upward and then released, as in Fig. P3.96. Neglect the short horizontal leg and combine control-volume analyses for the left and right legs to derive a single differential equation for $V(t)$ of the liquid column.

***P3.97** Extend Prob. 3.96 to include a linear (laminar) average wall shear stress resistance of the form $\tau \approx 8\mu V/D$, where μ is the fluid viscosity. Find the differential equation for dV/dt and then solve for $V(t)$, assuming an initial displacement $z = z_0$, $V = 0$ at $t = 0$. The result should be a damped oscillation tending toward $z = 0$.



P3.96

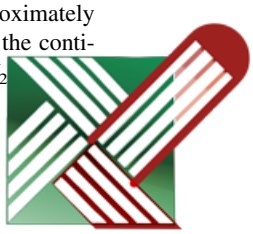
***P3.98** As an extension of Example 3.10, let the plate and its cart (see Fig. 3.10*a*) be unrestrained horizontally, with frictionless wheels. Derive (*a*) the equation of motion for cart velocity $V_c(t)$ and (*b*) a formula for the time required for the cart to accelerate from rest to 90 percent of the jet velocity (assuming the jet continues to strike the plate horizontally). (*c*) Compute numerical values for part (*b*) using the conditions of Example 3.10 and a cart mass of 2 kg.

P3.99 Suppose that the rocket motor of Prob. 3.34 is attached to a missile which starts from rest at sea level and moves straight up, as in Fig. E3.12. If the system weighs 950 lbf, which includes 300 lbf of fuel and oxidizer, estimate the velocity and height of the missile (*a*) after 10 s and (*b*) after 20 s. Neglect air drag.

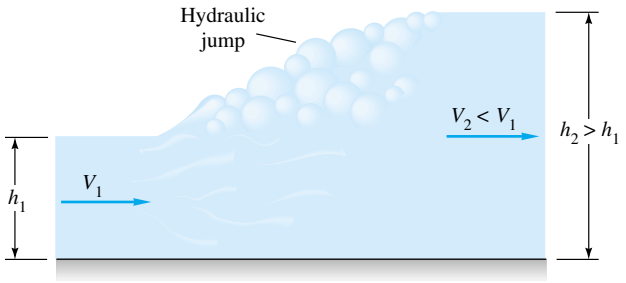
P3.100 Suppose that the solid-propellant rocket of Prob. 3.35 is built into a missile of diameter 70 cm and length 4 m. The system weighs 1800 N, which includes 700 N of propellant. Neglect air drag. If the missile is fired vertically from rest at sea level, estimate (*a*) its velocity and height at fuel burnout and (*b*) the maximum height it will attain.

P3.101 Modify Prob. 3.100 by accounting for air drag on the missile $F \approx C\rho D^2V^2$, where $C \approx 0.02$, ρ is the air density, D is the missile diameter, and V is the missile velocity. Solve numerically for (*a*) the velocity and altitude at burnout and (*b*) the maximum altitude attained.

P3.102 As can often be seen in a kitchen sink when the faucet is running, a high-speed channel flow (V_1, h_1) may "jump" to a low-speed, low-energy condition (V_2, h_2) as in Fig. P3.102. The pressure at sections 1 and 2 is approximately hydrostatic, and wall friction is negligible. Use the continuity and momentum relations to find h_2 and V_2 of (h_1, V_1).



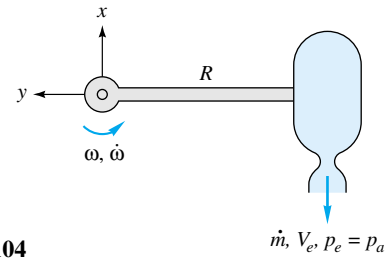
ketabline.com Ebook.ketabline.com



P3.102

***P3.103** Suppose that the solid-propellant rocket of Prob. 3.35 is mounted on a 1000-kg car to propel it up a long slope of 15°. The rocket motor weighs 900 N, which includes 500 N of propellant. If the car starts from rest when the rocket is fired, and if air drag and wheel friction are neglected, estimate the maximum distance that the car will travel up the hill.

P3.104 A rocket is attached to a rigid horizontal rod hinged at the origin as in Fig. P3.104. Its initial mass is M_0, and its exit properties are $\dot{m}$ and V_e relative to the rocket. Set up the differential equation for rocket motion, and solve for the angular velocity $\omega(t)$ of the rod. Neglect gravity, air drag, and the rod mass.

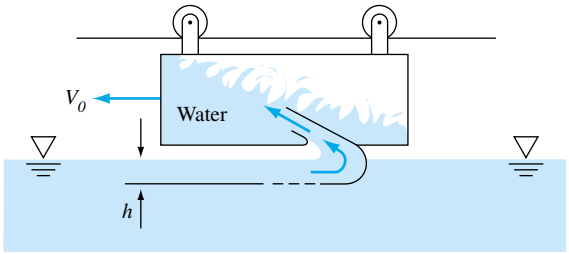


P3.104

P3.105 Extend Prob. 3.104 to the case where the rocket has a linear air drag force $F = cV$, where c is a constant. Assuming no burnout, solve for $\omega(t)$ and find the *terminal* angular velocity, i.e., the final motion when the angular acceleration is zero. Apply to the case $M_0 = 6$ kg, $R = 3$ m, $m = 0.05$ kg/s, $V_e = 1100$ m/s, and $c = 0.075$ N · s/m to find the angular velocity after 12 s of burning.

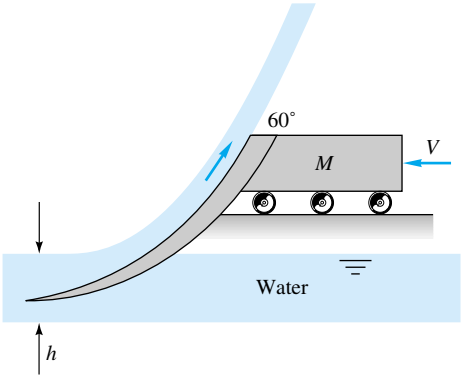
P3.106 Extend Prob. 3.104 to the case where the rocket has a quadratic air drag force $F = kV^2$, where k is a constant. Assuming no burnout, solve for $\omega(t)$ and find the *terminal* angular velocity, i.e., the final motion when the angular acceleration is zero. Apply to the case $M_0 = 6$ kg, $R = 3$ m, $m = 0.05$ kg/s, $V_e = 1100$ m/s, and $k = 0.0011$ N · s^2/m^2 to find the angular velocity after 12 s of burning.

P3.107 The cart in Fig. P3.107 moves at constant velocity $V_0 = 12$ m/s and takes on water with a scoop 80 cm wide which dips $h = 2.5$ cm into a pond. Neglect air drag and wheel friction. Estimate the force required to keep the cart moving.



P3.107

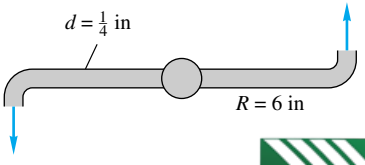
***P3.108** A rocket sled of mass M is to be decelerated by a scoop, as in Fig. P3.108, which has width b into the paper and dips into the water a depth h, creating an upward jet at 60°. The rocket thrust is T to the left. Let the initial velocity be V_0, and neglect air drag and wheel friction. Find an expression for $V(t)$ of the sled for (a) $T = 0$ and (b) finite $T \neq 0$.



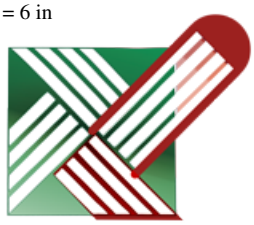
P3.108

P3.109 Apply Prob. 3.108 to the following case: $M_{total} = 900$ kg, $b = 60$ cm, $h = 2$ cm, $V_0 = 120$ m/s, with the rocket of Prob. 3.35 attached and burning. Estimate V after 3 s.

P3.110 The horizontal lawn sprinkler in Fig. P3.110 has a water flow rate of 4.0 gal/min introduced vertically through the center. Estimate (a) the retarding torque required to keep the arms from rotating and (b) the rotation rate (r/min) if there is no retarding torque.



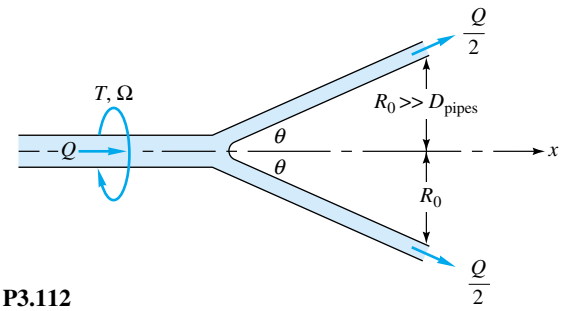
P3.110



ketabline.com Ebook.ketabline.com

P3.111 In Prob. 3.60 find the torque caused around flange 1 if the center point of exit 2 is 1.2 m directly below the flange center.

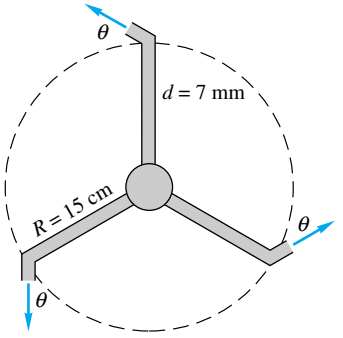
P3.112 The wye joint in Fig. P3.112 splits the pipe flow into equal amounts $Q/2$, which exit, as shown, a distance R_0 from the axis. Neglect gravity and friction. Find an expression for the torque T about the x-axis required to keep the system rotating at angular velocity Ω.



P3.112

P3.113 Modify Example 3.14 so that the arm starts from rest and spins up to its final rotation speed. The moment of inertia of the arm about O is I_0. Neglecting air drag, find $d\omega/dt$ and integrate to determine the angular velocity $\omega(t)$, assuming $\omega = 0$ at $t = 0$.

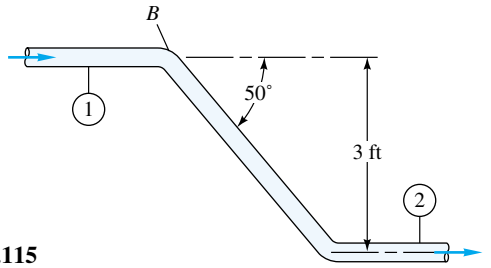
P3.114 The three-arm lawn sprinkler of Fig. P3.114 receives 20°C water through the center at 2.7 m^3/h. If collar friction is negligible, what is the steady rotation rate in r/min for (*a*) $\theta = 0°$ and (*b*) $\theta = 40°$?



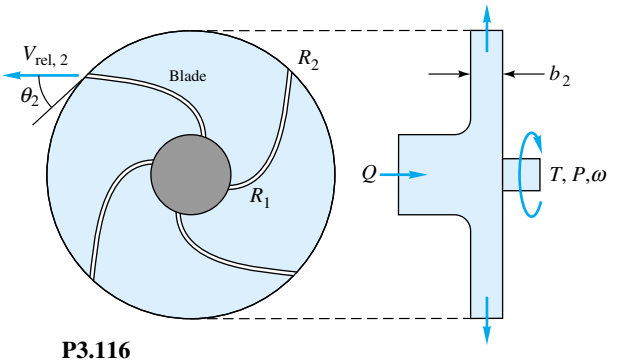
P3.114

P3.115 Water at 20°C flows at 30 gal/min through the 0.75-in-diameter double pipe bend of Fig. P3.115. The pressures are $p_1 = 30$ lbf/in^2 and $p_2 = 24$ lbf/in^2. Compute the torque T at point B necessary to keep the pipe from rotating.

P3.116 The centrifugal pump of Fig. P3.116 has a flow rate Q and exits the impeller at an angle θ_2 relative to the blades, as shown. The fluid enters axially at section 1. Assuming incompressible flow at shaft angular velocity ω, derive a formula for the power P required to drive the impeller.

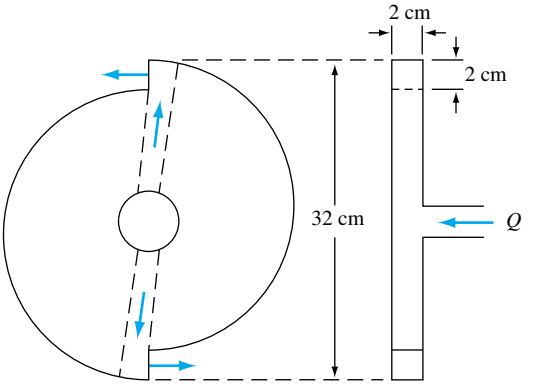


P3.115



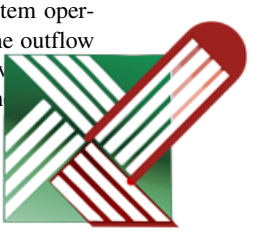
P3.116

P3.117 A simple turbomachine is constructed from a disk with two internal ducts which exit tangentially through square holes, as in Fig. P3.117. Water at 20°C enters normal to the disk at the center, as shown. The disk must drive, at 250 r/min, a small device whose retarding torque is 1.5 N · m. What is the proper mass flow of water, in kg/s?



P3.117

P3.118 Reverse the flow in Fig. P3.116, so that the system operates as a radial-inflow *turbine*. Assuming that the outflow into section 1 has no tangential velocity, derive an expression for the power P extracted by the turbine

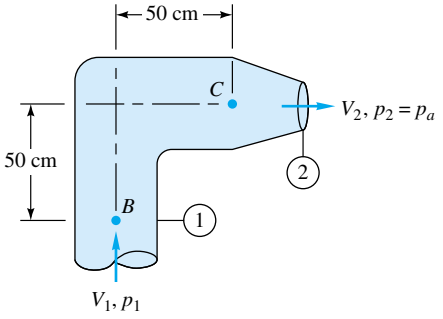


ketabline.com Ebook.ketabline.com

P3.119 Revisit the turbine cascade system of Prob. 3.78, and derive a formula for the power P delivered, using the *angular*-momentum theorem of Eq. (3.55).

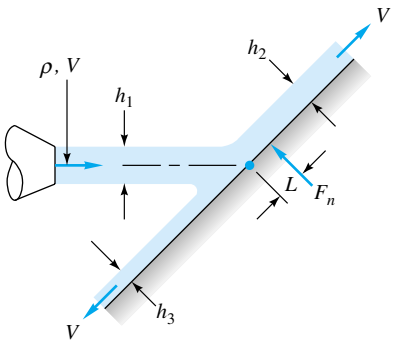
P3.120 A centrifugal pump impeller delivers 4000 gal/min of water at 20°C with a shaft rotation rate of 1750 r/min. Neglect losses. If $r_1 = 6$ in, $r_2 = 14$ in, $b_1 = b_2 = 1.75$ in, $V_{t1} = 10$ ft/s, and $V_{t2} = 110$ ft/s, compute the absolute velocities (*a*) V_1 and (*b*) V_2 and (*c*) the horsepower required. (*d*) Compare with the ideal horsepower required.

P3.121 The pipe bend of Fig. P3.121 has $D_1 = 27$ cm and $D_2 = 13$ cm. When water at 20°C flows through the pipe at 4000 gal/min, $p_1 = 194$ kPa (gage). Compute the torque required at point B to hold the bend stationary.



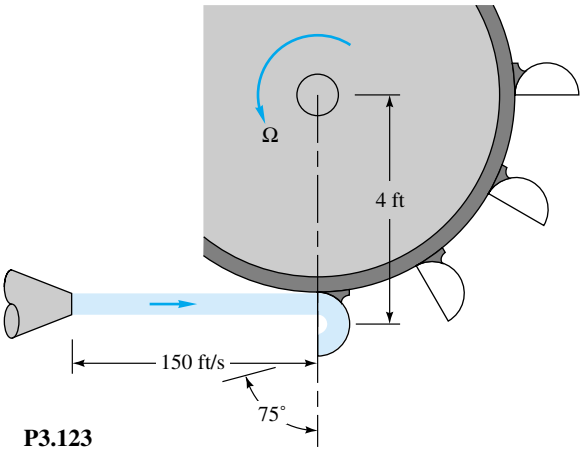
P3.121

***P3.122** Extend Prob. 3.46 to the problem of computing the center of pressure L of the normal face F_n, as in Fig. P3.122. (At the center of pressure, no moments are required to hold the plate at rest.) Neglect friction. Express your result in terms of the sheet thickness h_1 and the angle θ between the plate and the oncoming jet 1.



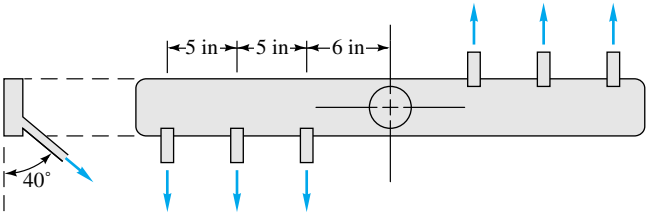
P3.122

P3.123 The waterwheel in Fig. P3.123 is being driven at 200 r/min by a 150-ft/s jet of water at 20°C. The jet diameter is 2.5 in. Assuming no losses, what is the horsepower developed by the wheel? For what speed Ω r/min will the horsepower developed be a maximum? Assume that there are many buckets on the waterwheel.



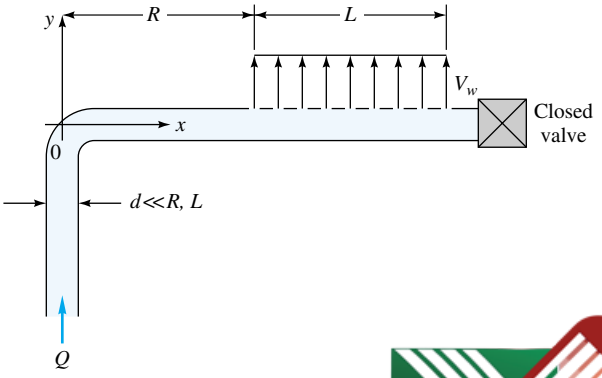
P3.123

P3.124 A rotating dishwasher arm delivers at 60°C to six nozzles, as in Fig. P3.124. The total flow rate is 3.0 gal/min. Each nozzle has a diameter of $\frac{3}{16}$ in. If the nozzle flows are equal and friction is neglected, estimate the steady rotation rate of the arm, in r/min.



P3.124

***P3.125** A liquid of density ρ flows through a 90° bend as shown in Fig. P3.125 and issues vertically from a uniformly porous section of length L. Neglecting pipe and liquid weight, derive an expression for the torque M at point 0 required to hold the pipe stationary.

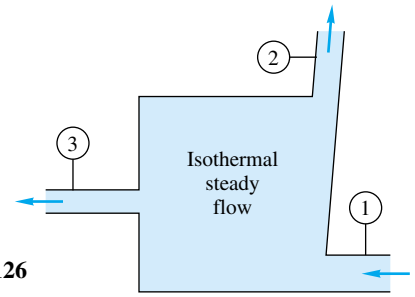


P3.125



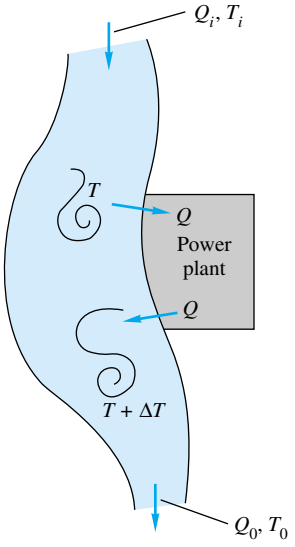
ketabline.com Ebook.ketabline.com

P3.126 There is a steady isothermal flow of water at 20°C through the device in Fig. P3.126. Heat-transfer, gravity, and temperature effects are negligible. Known data are $D_1 = 9$ cm, $Q_1 = 220$ m^3/h, $p_1 = 150$ kPa, $D_2 = 7$ cm, $Q_2 = 100$ m^3/h, $p_2 = 225$ kPa, $D_3 = 4$ cm, and $p_3 = 265$ kPa. Compute the rate of shaft work done for this device and its direction.



P3.126

P3.127 A power plant on a river, as in Fig. P3.127, must eliminate 55 MW of waste heat to the river. The river conditions upstream are $Q_i = 2.5$ m^3/s and $T_i = 18$°C. The river is 45 m wide and 2.7 m deep. If heat losses to the atmosphere and ground are negligible, estimate the downstream river conditions (Q_0, T_0).

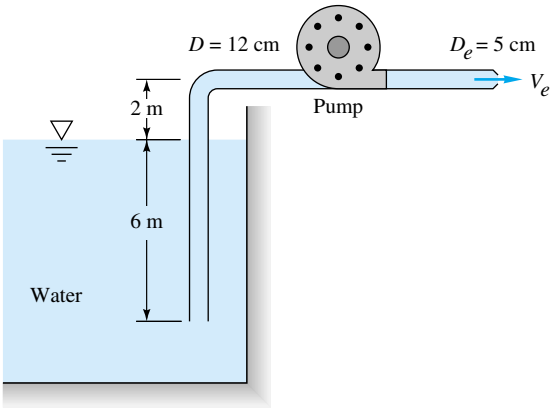


P3.127

P3.128 For the conditions of Prob. 3.127, if the power plant is to heat the nearby river water by no more than 12°C, what should be the minimum flow rate Q, in m^3/s, through the plant heat exchanger? How will the value of Q affect the downstream conditions (Q_0, T_0)?

P3.129 Multnomah Falls in the Columbia River Gorge has a sheer drop of 543 ft. Using the steady-flow energy equation, estimate the water temperature change in °F caused by this drop.

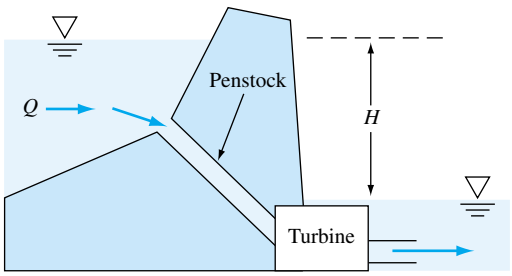
P3.130 When the pump in Fig. P3.130 draws 220 m^3/h of water at 20°C from the reservoir, the total friction head loss is 5 m. The flow discharges through a nozzle to the atmosphere. Estimate the pump power in kW delivered to the water.



P3.130

P3.131 When the pump in Fig. P3.130 delivers 25 kW of power to the water, the friction head loss is 4 m. Estimate (*a*) the exit velocity V_e and (*b*) the flow rate Q.

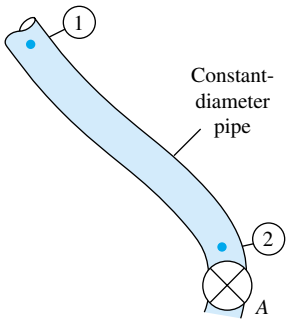
P3.132 Consider a turbine extracting energy from a penstock in a dam, as in Fig. P3.132. For turbulent pipe flow (Chap. 6), the friction head loss is approximately $h_f = CQ^2$, where the constant C depends upon penstock dimensions and the properties of water. Show that, for a given penstock geometry and variable river flow Q, the maximum turbine power possible in this case is $P_{max} = 2\rho g H Q/3$ and occurs when the flow rate is $Q = \sqrt{H/(3C)}$.



P3.132

P3.133 The long pipe in Fig. P3.133 is filled with water at 20°C. When valve A is closed, $p_1 - p_2 = 75$ kPa. When is open and water flows at 500 m^3/h, $p_1 - p_2 =$

ketabline.com Ebook.ketabline.com

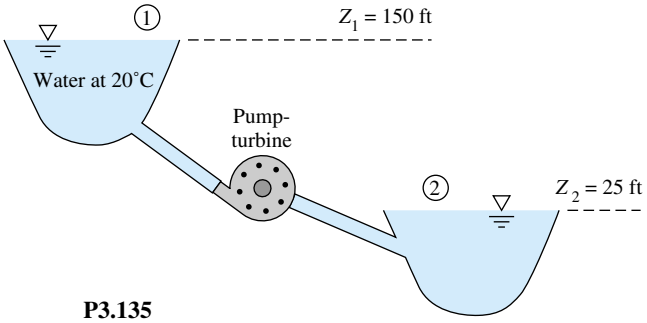


P3.133

What is the friction head loss between 1 and 2, in m, for the flowing condition?

P3.134 A 36-in-diameter pipeline carries oil (SG = 0.89) at 1 million barrels per day (bbl/day) (1 bbl = 42 U.S. gal). The friction head loss is 13 ft/1000 ft of pipe. It is planned to place pumping stations every 10 mi along the pipe. Estimate the horsepower which must be delivered to the oil by each pump.

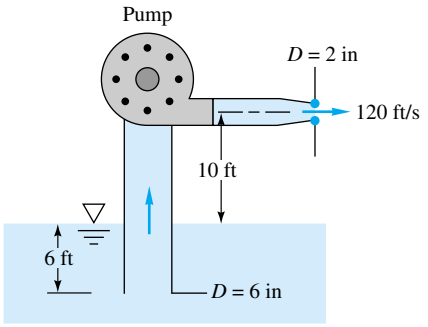
P3.135 The *pump-turbine* system in Fig. P3.135 draws water from the upper reservoir in the daytime to produce power for a city. At night, it pumps water from lower to upper reservoirs to restore the situation. For a design flow rate of 15,000 gal/min in either direction, the friction head loss is 17 ft. Estimate the power in kW (*a*) extracted by the turbine and (*b*) delivered by the pump.



P3.135

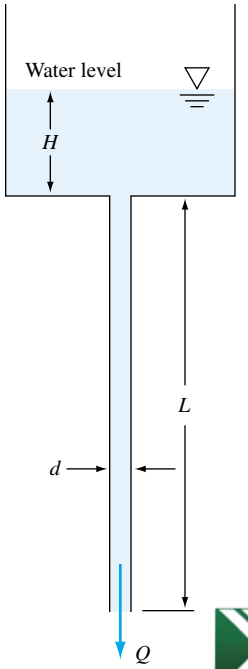
P3.136 A pump is to deliver water at 20°C from a pond to an elevated tank. The pump is 1 m above the pond, and the tank free surface is 20 m above the pump. The head loss in the system is $h_f \approx cQ^2$, where $c = 0.08$ h^2/m^5. If the pump is 72 percent efficient and is driven by a 500-W motor, what flow rate Q m^3/h will result?

P3.137 A fireboat draws seawater (SG = 1.025) from a submerged pipe and discharges it through a nozzle, as in Fig. P3.137. The total head loss is 6.5 ft. If the pump efficiency is 75 percent, what horsepower motor is required to drive it?



P3.137

***P3.138** Students in the fluid mechanics laboratory at Penn State use a very simple device to measure the viscosity of water as a function of temperature. The viscometer, shown in Fig. P3.138, consists of a tank, a long vertical capillary tube, a graduated cylinder, a thermometer, and a stopwatch. Because the tube has such a small diameter, the flow remains laminar. Because the tube is so long, entrance losses are negligible. It will be shown in Chap. 6 that the laminar head loss through a long pipe is given by $h_{f,\text{ laminar}} = (32\mu LV)/(\rho g d^2)$, where V is the average speed through the pipe. (*a*) In a given experiment, diameter d, length L, and water level height H are known, and volume flow rate Q is measured with the stopwatch and graduated cylinder. The temperature of the water is also measured. The water density at this tempera-



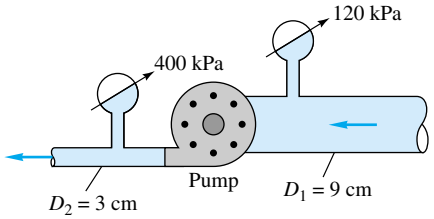
P3.138



ketabline.com Ebook.ketabline.com

ture is obtained by weighing a known volume of water. Write an expression for the viscosity of the water as a function of these variables. (*b*) Here are some actual data from an experiment: $T = 16.5°C$, $\rho = 998.7$ kg/m^3, $d = 0.041$ in, $Q = 0.310$ mL/s, $L = 36.1$ in, and $H = 0.153$ m. Calculate the viscosity of the water in kg/(m · s) based on these experimental data. (*c*) Compare the experimental result with the published value of μ at this temperature, and report a percentage error. (*d*) Compute the percentage error in the calculation of μ which would occur if a student forgot to include the kinetic energy flux correction factor in part (*b*) above (compare results with and without inclusion of kinetic energy flux correction factor). Explain the importance (or lack of importance) of kinetic energy flux correction factor in a problem such as this.

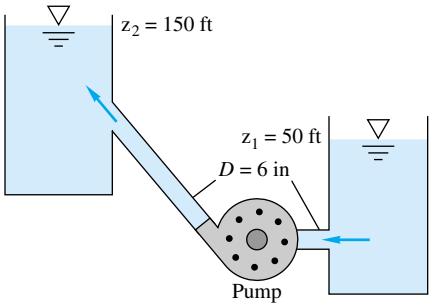
P3.139 The horizontal pump in Fig. P3.139 discharges 20°C water at 57 m^3/h. Neglecting losses, what power in kW is delivered to the water by the pump?



P3.139

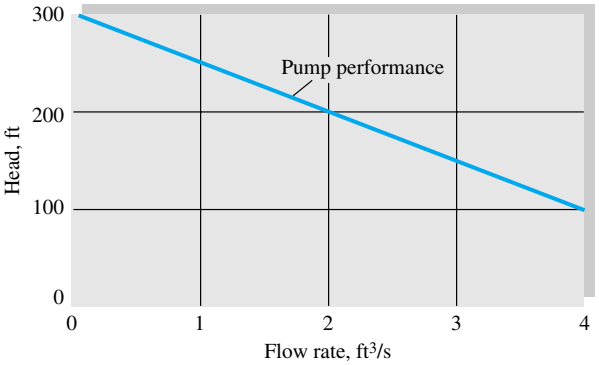
P3.140 Steam enters a horizontal turbine at 350 lbf/in^2 absolute, 580°C, and 12 ft/s and is discharged at 110 ft/s and 25°C saturated conditions. The mass flow is 2.5 lbm/s, and the heat losses are 7 Btu/lb of steam. If head losses are negligible, how much horsepower does the turbine develop?

P3.141 Water at 20°C is pumped at 1500 gal/min from the lower to the upper reservoir, as in Fig. P3.141. Pipe friction losses are approximated by $h_f \approx 27V^2/(2g)$, where V is the average velocity in the pipe. If the pump is 75 percent efficient, what horsepower is needed to drive it?



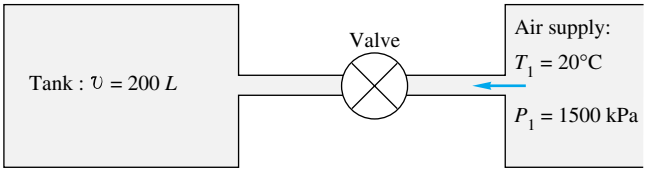
P3.141

P3.142 A typical pump has a head which, for a given shaft rotation rate, varies with the flow rate, resulting in a *pump performance curve* as in Fig. P3.142. Suppose that this pump is 75 percent efficient and is used for the system in Prob. 3.141. Estimate (*a*) the flow rate, in gal/min, and (*b*) the horsepower needed to drive the pump.



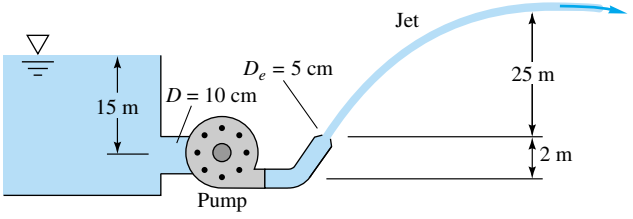
P3.142

P3.143 The insulated tank in Fig. P3.143 is to be filled from a high-pressure air supply. Initial conditions in the tank are $T = 20°C$ and $p = 200$ kPa. When the valve is opened, the initial mass flow rate into the tank is 0.013 kg/s. Assuming an ideal gas, estimate the initial rate of temperature rise of the air in the tank.



P3.143

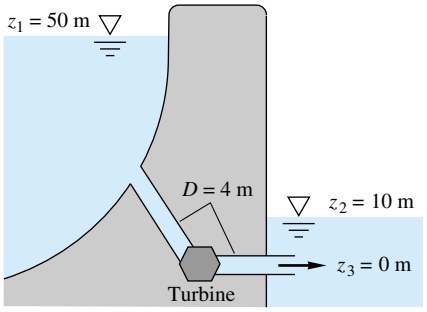
P3.144 The pump in Fig. P3.144 creates a 20°C water jet oriented to travel a maximum horizontal distance. System friction head losses are 6.5 m. The jet may be approximated by the trajectory of frictionless particles. What power must be delivered by the pump?



P3.144

P3.145 The large turbine in Fig. P3.145 diverts the river flow under a dam as shown. System friction losses $3.5V^2/(2g)$, where V is the average velocity in th

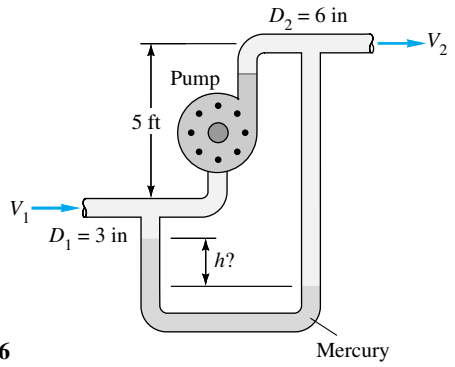
ketabline.com Ebook.ketabline.com



P3.145

pipe. For what river flow rate in m^3/s will the power extracted be 25 MW? Which of the *two* possible solutions has a better "conversion efficiency"?

P3.146 Kerosine at 20°C flows through the pump in Fig. P3.146 at 2.3 ft^3/s. Head losses between 1 and 2 are 8 ft, and the pump delivers 8 hp to the flow. What should the mercury-manometer reading h ft be?



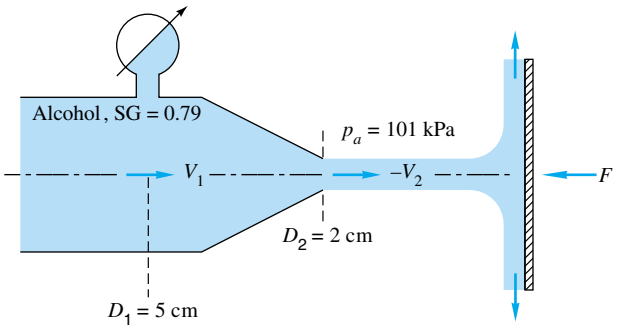
P3.146

P3.147 Repeat Prob. 3.49 by assuming that p_1 is unknown and using Bernoulli's equation with no losses. Compute the new bolt force for this assumption. What is the head loss between 1 and 2 for the data of Prob. 3.49?

P3.148 Reanalyze Prob. 3.54 to estimate the manometer reading h if Bernoulli's equation is valid with zero losses. For the reading $h \approx 58$ cm in Prob. 3.54, what is the head loss between sections 1 and 2?

P3.149 A jet of alcohol strikes the vertical plate in Fig. P3.149. A force $F \approx 425$ N is required to hold the plate stationary. Assuming there are no losses in the nozzle, estimate (*a*) the mass flow rate of alcohol and (*b*) the absolute pressure at section 1.

P3.150 Verify that Bernoulli's equation is not valid for the sudden expansion of Prob. 3.59 and that the actual head loss is given by



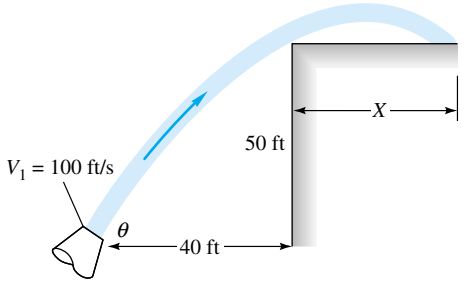
P3.149

$$h_f \approx \frac{V_1^2}{2g}\left(1 - \frac{A_1}{A_2}\right)^2$$

See Sec. 6.7 for further details.

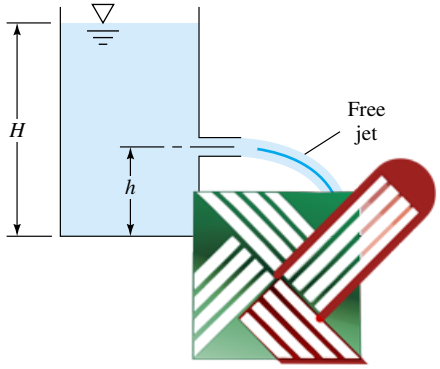
P3.151 In Prob. 3.63 the velocity approaching the sluice gate was assumed to be known. If Bernoulli's equation is valid with no losses, derive an expression for V_1 as a function of only h_1, h_2, and g.

P3.152 A free liquid jet, as in Fig. P3.152, has constant ambient pressure and small losses; hence from Bernoulli's equation $z + V^2/(2g)$ is constant along the jet. For the fire nozzle in the figure, what are (*a*) the minimum and (*b*) the maximum values of θ for which the water jet will clear the corner of the building? For which case will the jet velocity be higher when it strikes the roof of the building?



P3.152

P3.153 For the container of Fig. P3.153 use Bernoulli's equation to derive a formula for the distance X where the free jet

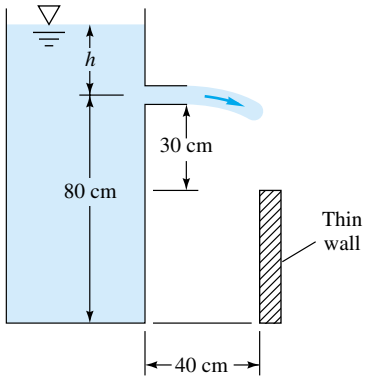


P3.153

ketabline.com Ebook.ketabline.com

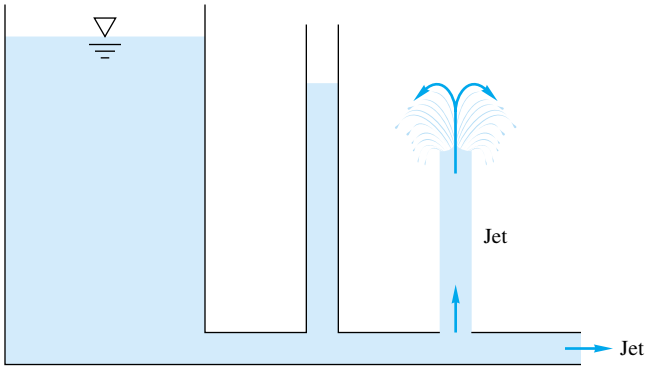
leaving horizontally will strike the floor, as a function of h and H. For what ratio h/H will X be maximum? Sketch the three trajectories for $h/H = 0.4$, 0.5, and 0.6.

P3.154 In Fig. P3.154 the exit nozzle is horizontal. If losses are negligible, what should the water level h cm be for the free jet to just clear the wall?



P3.154

P3.155 Bernoulli's 1738 treatise *Hydrodynamica* contains many excellent sketches of flow patterns related to his frictionless relation. One, however, redrawn here as Fig. P3.155, seems physically misleading. Can you explain what might be wrong with the figure?

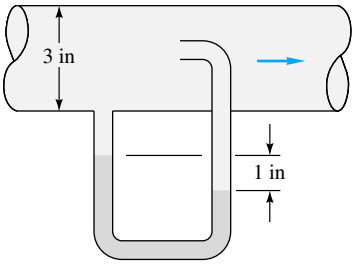


P3.155

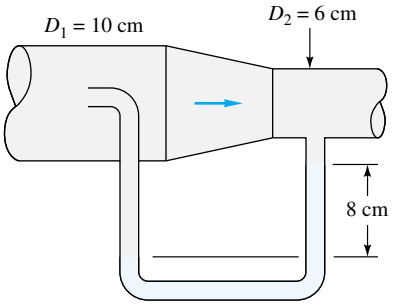
P3.156 A blimp cruises at 75 mi/h through sea-level standard air. A differential pressure transducer connected between the nose and the side of the blimp registers 950 Pa. Estimate (*a*) the absolute pressure at the nose and (*b*) the absolute velocity of the air near the blimp side.

P3.157 The manometer fluid in Fig. P3.157 is mercury. Estimate the volume flow in the tube if the flowing fluid is (*a*) gasoline and (*b*) nitrogen, at 20°C and 1 atm.

P3.158 In Fig. P3.158 the flowing fluid is CO_2 at 20°C. Neglect losses. If $p_1 = 170$ kPa and the manometer fluid is Meriam



P3.157

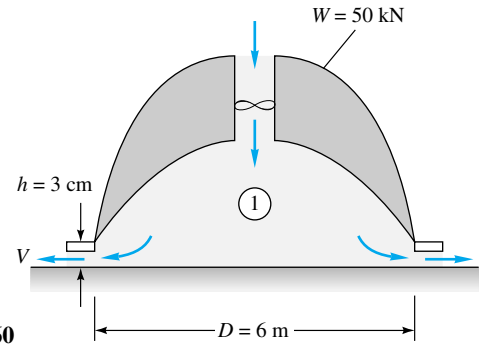


P3.158

red oil (SG = 0.827), estimate (*a*) p_2 and (*b*) the gas flow rate in m^3/h.

P3.159 Our 0.625-in-diameter hose is too short, and it is 125 ft from the 0.375-in-diameter nozzle exit to the garden. If losses are neglected, what is the minimum gage pressure required, inside the hose, to reach the garden?

P3.160 The air-cushion vehicle in Fig. P3.160 brings in sea-level standard air through a fan and discharges it at high velocity through an annular skirt of 3-cm clearance. If the vehicle weighs 50 kN, estimate (*a*) the required airflow rate and (*b*) the fan power in kW.

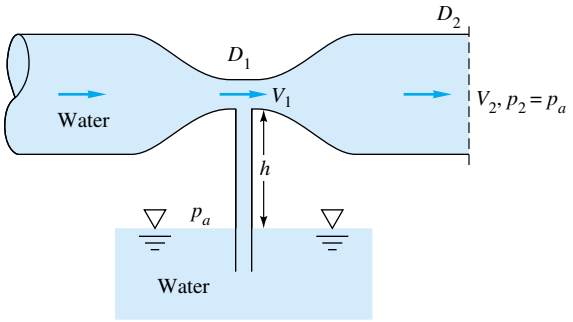


P3.160

P3.161 A necked-down section in a pipe flow, called a *venturi*, develops a low throat pressure which can aspirate
ward from a reservoir, as in Fig. P3.161. Using B



ketabline.com Ebook.ketabline.com

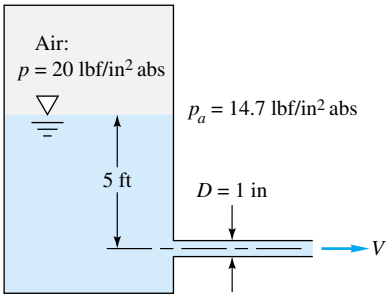


P3.161

equation with no losses, derive an expression for the velocity V_1 which is just sufficient to bring reservoir fluid into the throat.

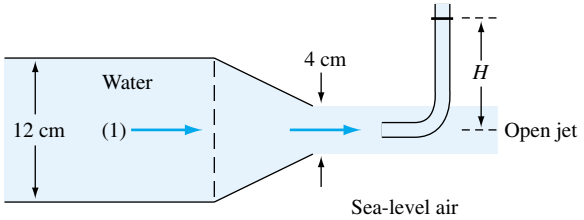
P3.162 Suppose you are designing an air hockey table. The table is 3.0×6.0 ft in area, with $\frac{1}{16}$-in-diameter holes spaced every inch in a rectangular grid pattern (2592 holes total). The required jet speed from each hole is estimated to be 50 ft/s. Your job is to select an appropriate blower which will meet the requirements. Estimate the volumetric flow rate (in ft^3/min) and pressure rise (in lb/in^2) required of the blower. *Hint:* Assume that the air is stagnant in the large volume of the manifold under the table surface, and neglect any frictional losses.

P3.163 The liquid in Fig. P3.163 is kerosine at 20°C. Estimate the flow rate from the tank for (*a*) no losses and (*b*) pipe losses $h_f \approx 4.5V^2/(2g)$.



P3.163

P3.164 In Fig. P3.164 the open jet of water at 20°C exits a nozzle into sea-level air and strikes a stagnation tube as shown.



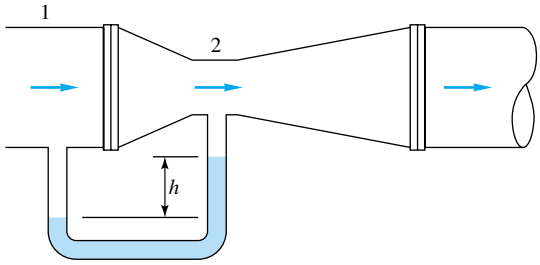
P3.164

If the pressure at the centerline at section 1 is 110 kPa, and losses are neglected, estimate (*a*) the mass flow in kg/s and (*b*) the height H of the fluid in the stagnation tube.

P3.165 A *venturi meter*, shown in Fig. P3.165, is a carefully designed constriction whose pressure difference is a measure of the flow rate in a pipe. Using Bernoulli's equation for steady incompressible flow with no losses, show that the flow rate Q is related to the manometer reading h by

$$Q = \frac{A_2}{\sqrt{1 - (D_2/D_1)^4}} \sqrt{\frac{2gh(\rho_M - \rho)}{\rho}}$$

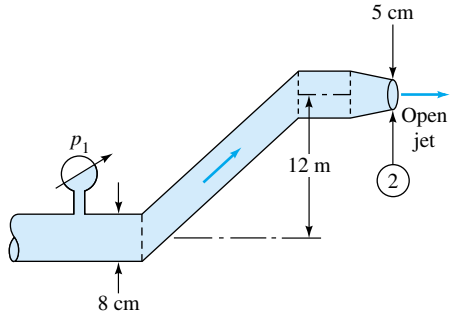
where ρ_M is the density of the manometer fluid.



P3.165

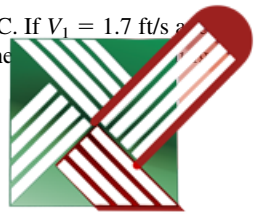
P3.166 An open-circuit wind tunnel draws in sea-level standard air and accelerates it through a contraction into a 1-m by 1-m test section. A differential transducer mounted in the test section wall measures a pressure difference of 45 mm of water between the inside and outside. Estimate (*a*) the test section velocity in mi/h and (*b*) the absolute pressure on the front nose of a small model mounted in the test section.

P3.167 In Fig. P3.167 the fluid is gasoline at 20°C at a weight flux of 120 N/s. Assuming no losses, estimate the gage pressure at section 1.

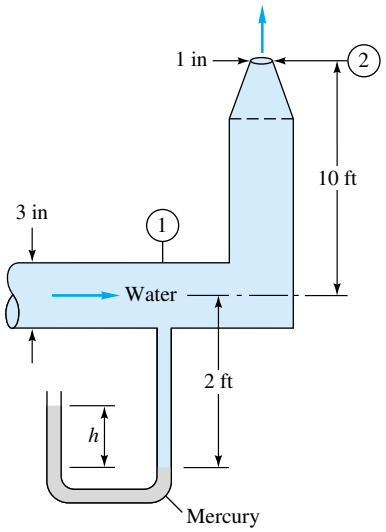


P3.167

P3.168 In Fig. P3.168 both fluids are at 20°C. If $V_1 = 1.7$ ft/s a
losses are neglected, what should the
h ft be?

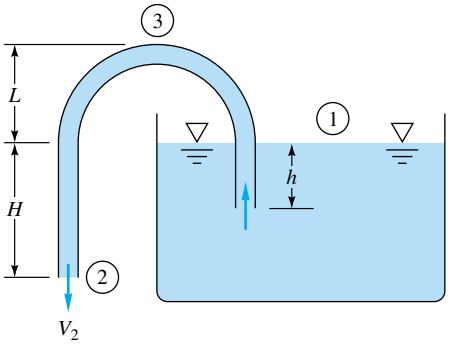


ketabline.com Ebook.ketabline.com



P3.168

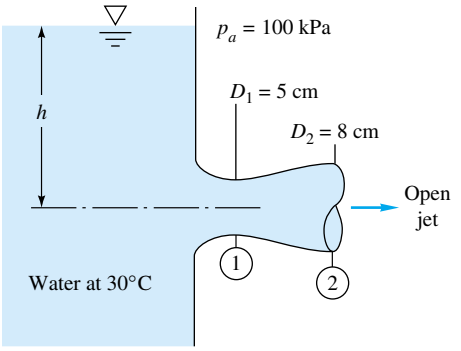
P3.169 Once it has been started by sufficient suction, the *siphon* in Fig. P3.169 will run continuously as long as reservoir fluid is available. Using Bernoulli's equation with no losses, show (*a*) that the exit velocity V_2 depends only upon gravity and the distance H and (*b*) that the lowest (vacuum) pressure occurs at point 3 and depends on the distance $L + H$.



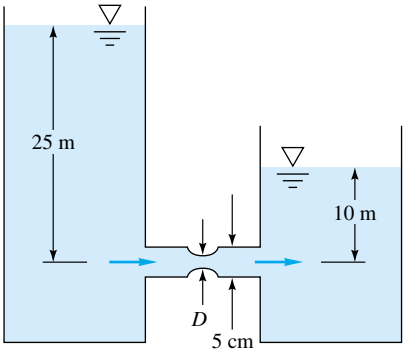
P3.169

P3.170 If losses are neglected in Fig. P3.170, for what water level h will the flow begin to form vapor cavities at the throat of the nozzle?

***P3.171** For the 40°C water flow in Fig. P3.171, estimate the volume flow through the pipe, assuming no losses; then explain what is wrong with this seemingly innocent question. If the actual flow rate is $Q = 40$ m^3/h, compute (*a*) the head loss in ft and (*b*) the constriction diameter D which causes cavitation, assuming that the throat divides the head loss equally and that changing the constriction causes no additional losses.

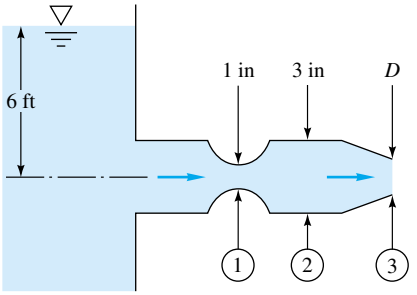


P3.170



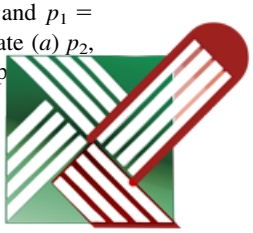
P3.171

P3.172 The 35°C water flow of Fig. P3.172 discharges to sea-level standard atmosphere. Neglecting losses, for what nozzle diameter D will cavitation begin to occur? To avoid cavitation, should you increase or decrease D from this critical value?

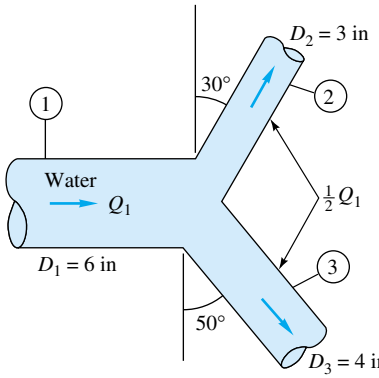


P3.172

P3.173 The horizontal wye fitting in Fig. P3.173 splits the 20°C water flow rate equally. If $Q_1 = 5$ ft^3/s and $p_1 = 25$ lbf/in^2(gage) and losses are neglected, estimate (*a*) p_2, (*b*) p_3, and (*c*) the vector force required to keep in place.

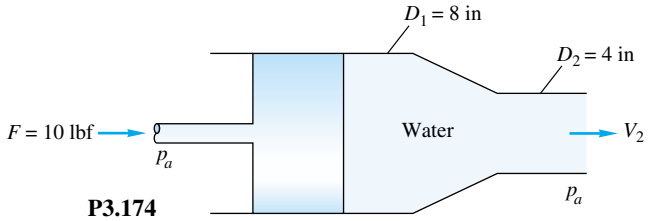


ketabline.com Ebook.ketabline.com



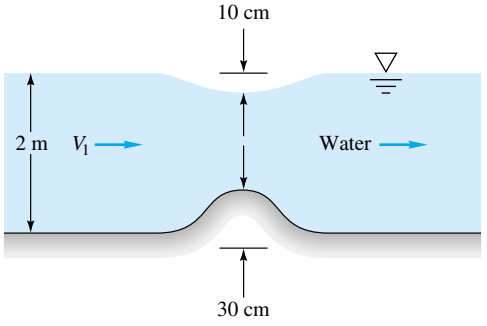
P3.173

P3.174 In Fig. P3.174 the piston drives water at 20°C. Neglecting losses, estimate the exit velocity V_2 ft/s. If D_2 is further constricted, what is the maximum possible value of V_2?



P3.174

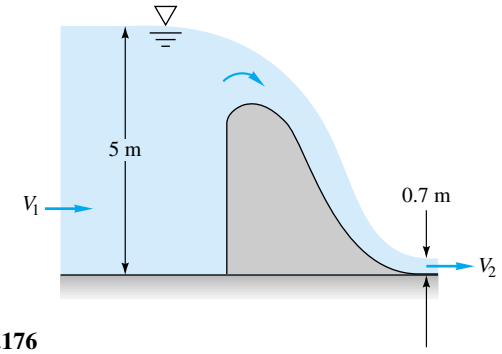
P3.175 If the approach velocity is not too high, a hump in the bottom of a water channel causes a dip Δh in the water level, which can serve as a flow measurement. If, as shown in Fig. P3.175, $\Delta h = 10$ cm when the bump is 30 cm high, what is the volume flow Q_1 per unit width, assuming no losses? In general, is Δh proportional to Q_1?



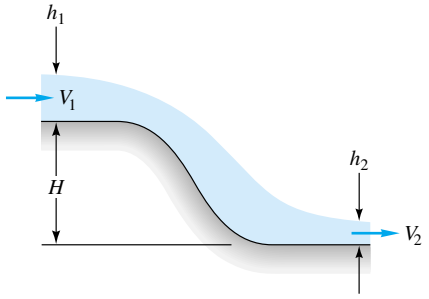
P3.175

P3.176 In the spillway flow of Fig. P3.176, the flow is assumed uniform and hydrostatic at sections 1 and 2. If losses are neglected, compute (*a*) V_2 and (*b*) the force per unit width of the water on the spillway.

P3.177 For the water-channel flow of Fig. P3.177, $h_1 = 1.5$ m, $H = 4$ m, and $V_1 = 3$ m/s. Neglecting losses and assuming uniform flow at sections 1 and 2, find the downstream depth h_2, and show that *two* realistic solutions are possible.

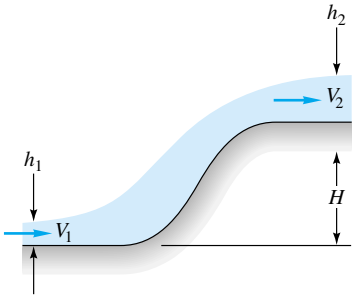


P3.176



P3.177

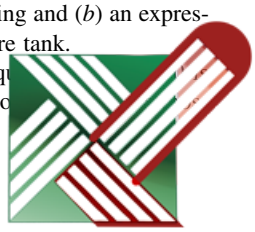
P3.178 For the water-channel flow of Fig. P3.178, $h_1 = 0.45$ ft, $H = 2.2$ ft, and $V_1 = 16$ ft/s. Neglecting losses and assuming uniform flow at sections 1 and 2, find the downstream depth h_2; show that *two* realistic solutions are possible.



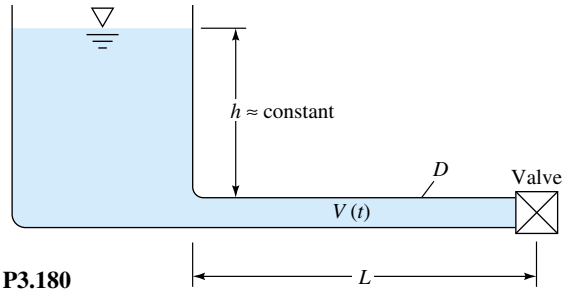
P3.178

***P3.179** A cylindrical tank of diameter D contains liquid to an initial height h_0. At time $t = 0$ a small stopper of diameter d is removed from the bottom. Using Bernoulli's equation with no losses, derive (*a*) a differential equation for the free-surface height $h(t)$ during draining and (*b*) an expression for the time t_0 to drain the entire tank.

***P3.180** The large tank of incompressible liq
at rest when, at $t = 0$, the valve is o



ketabline.com Ebook.ketabline.com



P3.180

phere. Assuming $h \approx$ constant (negligible velocities and accelerations in the tank), use the unsteady frictionless Bernoulli equation to derive and solve a differential equation for $V(t)$ in the pipe.

***P3.181** Modify Prob. 3.180 as follows. Let the top of the tank be enclosed and under constant gage pressure p_0. Repeat the analysis to find $V(t)$ in the pipe.

P3.182 The incompressible-flow form of Bernoulli's relation, Eq. (3.77), is accurate only for Mach numbers less than about 0.3. At higher speeds, variable density must be accounted for. The most common assumption for compressible fluids is *isentropic flow of an ideal gas*, or $p = C\rho^k$, where $k = c_p/c_v$. Substitute this relation into Eq. (3.75), integrate, and eliminate the constant C. Compare your compressible result with Eq. (3.77) and comment.

Word Problems

W3.1 Derive a control-volume form of the *second* law of thermodynamics. Suggest some practical uses for your relation in analyzing real fluid flows.

W3.2 Suppose that it is desired to estimate volume flow Q in a pipe by measuring the axial velocity $u(r)$ at specific points. For cost reasons only *three* measuring points are to be used. What are the best radii selections for these three points?

W3.3 Consider water flowing by gravity through a short pipe connecting two reservoirs whose surface levels differ by an amount Δz. Why does the incompressible frictionless Bernoulli equation lead to an absurdity when the flow rate through the pipe is computed? Does the paradox have something to do with the length of the short pipe? Does the paradox disappear if we round the entrance and exit edges of the pipe?

W3.4 Use the steady-flow energy equation to analyze flow through a water faucet whose supply pressure is p_0. What physical mechanism causes the flow to vary continuously from zero to maximum as we open the faucet valve?

W3.5 Consider a long sewer pipe, half full of water, sloping downward at angle θ. Antoine Chézy in 1768 determined that the average velocity of such an open-channel flow should be $V \approx C\sqrt{R \tan \theta}$, where R is the pipe radius and C is a constant. How does this famous formula relate to the steady-flow energy equation applied to a length L of the channel?

W3.6 Put a table tennis ball in a funnel, and attach the small end of the funnel to an air supply. You probably won't be able to blow the ball either up or down out of the funnel. Explain why.

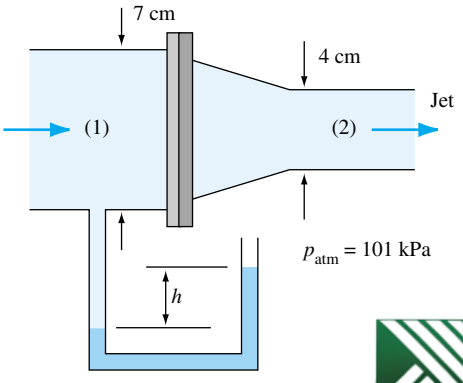
W3.7 How does a *siphon* work? Are there any limitations (e.g., how high or how low can you siphon water away from a tank)? Also, how far—could you use a flexible tube to siphon water from a tank to a point 100 ft away?

Fundamentals of Engineering Exam Problems

FE3.1 In Fig. FE3.1 water exits from a nozzle into atmospheric pressure of 101 kPa. If the flow rate is 160 gal/min, what is the average velocity at section 1?
(*a*) 2.6 m/s, (*b*) 0.81 m/s, (*c*) 93 m/s, (*d*) 23 m/s,
(*e*) 1.62 m/s

FE3.2 In Fig. FE3.1 water exits from a nozzle into atmospheric pressure of 101 kPa. If the flow rate is 160 gal/min and friction is neglected, what is the gage pressure at section 1?
(*a*) 1.4 kPa, (*b*) 32 kPa, (*c*) 43 kPa, (*d*) 29 kPa,
(*e*) 123 kPa

FE3.3 In Fig. FE3.1 water exits from a nozzle into atmospheric pressure of 101 kPa. If the exit velocity is $V_2 = 8$ m/s and



FE3.1

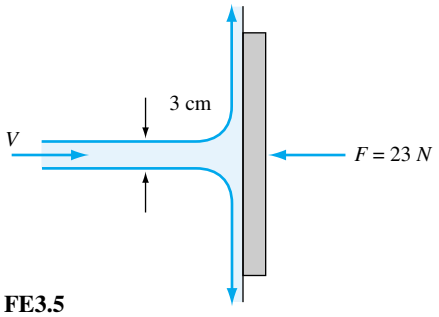


ketabline.com Ebook.ketabline.com

friction is neglected, what is the axial flange force required to keep the nozzle attached to pipe 1?
(*a*) 11 N, (*b*) 56 N, (*c*) 83 N, (*d*) 123 N, (*e*) 110 N

FE3.4 In Fig. FE3.1 water exits from a nozzle into atmospheric pressure of 101 kPa. If the manometer fluid has a specific gravity of 1.6 and $h = 66$ cm, with friction neglected, what is the average velocity at section 2?
(*a*) 4.55 m/s, (*b*) 2.4 m/s, (*c*) 2.95 m/s, (*d*) 5.55 m/s, (*e*) 3.4 m/s

FE3.5 A jet of water 3 cm in diameter strikes normal to a plate as in Fig. FE3.5. If the force required to hold the plate is 23 N, what is the jet velocity?
(*a*) 2.85 m/s, (*b*) 5.7 m/s, (*c*) 8.1 m/s, (*d*) 4.0 m/s, (*e*) 23 m/s

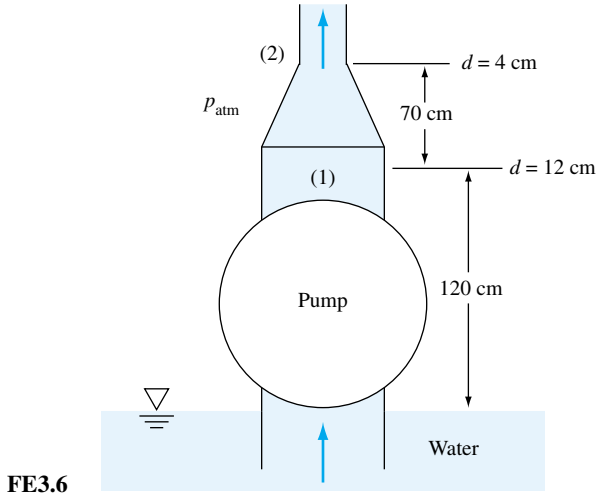


FE3.5

FE3.6 A fireboat pump delivers water to a vertical nozzle with a 3:1 diameter ratio, as in Fig. FE3.6. If friction is neglected and the flow rate is 500 gal/min, how high will the outlet water jet rise?
(*a*) 2.0 m, (*b*) 9.8 m, (*c*) 32 m, (*d*) 64 m, (*e*) 98 m

FE3.7 A fireboat pump delivers water to a vertical nozzle with a 3:1 diameter ratio, as in Fig. FE3.6. If friction is neglected and the pump increases the pressure at section 1 to 51 kPa (gage), what will be the resulting flow rate?
(*a*) 187 gal/min, (*b*) 199 gal/min, (*c*) 214 gal/min, (*d*) 359 gal/min, (*e*) 141 gal/min

FE3.8 A fireboat pump delivers water to a vertical nozzle with a 3:1 diameter ratio, as in Fig. FE3.6. If duct and nozzle friction are neglected and the pump provides 12.3 ft of head to the flow, what will be the outlet flow rate?
(*a*) 85 gal/min, (*b*) 120 gal/min, (*c*) 154 gal/min, (*d*) 217 gal/min, (*e*) 285 gal/min



FE3.6

FE3.9 Water flowing in a smooth 6-cm-diameter pipe enters a venturi contraction with a throat diameter of 3 cm. Upstream pressure is 120 kPa. If cavitation occurs in the throat at a flow rate of 155 gal/min, what is the estimated fluid vapor pressure, assuming ideal frictionless flow?
(*a*) 6 kPa, (*b*) 12 kPa, (*c*) 24 kPa, (*d*) 31 kPa, (*e*) 52 kPa

FE3.10 Water flowing in a smooth 6-cm-diameter pipe enters a venturi contraction with a throat diameter of 4 cm. Upstream pressure is 120 kPa. If the pressure in the throat is 50 kPa, what is the flow rate, assuming ideal frictionless flow?
(*a*) 7.5 gal/min, (*b*) 236 gal/min, (*c*) 263 gal/min, (*d*) 745 gal/min, (*e*) 1053 gal/min

Comprehensive Problems

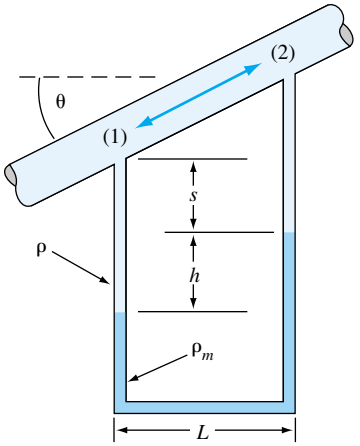
C3.1 In a certain industrial process, oil of density ρ flows through the inclined pipe in Fig. C3.1. A *U*-tube manometer, with fluid density ρ_m, measures the pressure difference between points 1 and 2, as shown. The pipe flow is steady, so that the fluids in the manometer are stationary. (*a*) Find an analytic expression for $p_1 - p_2$ in terms of the system parameters. (*b*) Discuss the conditions on h necessary for there to be no flow in the pipe. (*c*) What about flow *up*, from 1 to 2? (*d*) What about flow *down*, from 2 to 1?

C3.2 A rigid tank of volume $v = 1.0$ m^3 is initially filled with air at 20°C and $p_0 = 100$ kPa. At time $t = 0$, a vacuum pump is turned on and evacuates air at a constant volume flow rate $Q = 80$ L/min (regardless of the pressure). Assume an ideal gas and an isothermal process. (*a*) Set up a differential equation for this flow. (*b*) Solve this equation for t as a function of (v, Q, p, p_0). (*c*) Compute the time in minutes to pump the tank down to $p = 20$ kPa. *Hint:* Your answer should lie between 15 and 25 min.

C3.3 Suppose the same steady water jet as in Prob. 3.40 (jet velocity 8 m/s and jet diameter 10 cm) impinges instead a cup cavity as shown in Fig. C3.3. 180° and exits, due to friction, at l



ketabline.com Ebook.ketabline.com

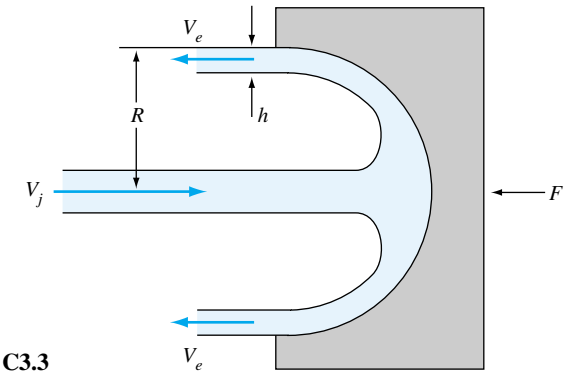


C3.1

4 m/s. (Looking from the left, the exit jet is a circular annulus of outer radius R and thickness h, flowing toward the viewer.) The cup has a radius of curvature of 25 cm. Find (*a*) the thickness h of the exit jet and (*b*) the force F required to hold the cupped object in place. (*c*) Compare part (*b*) to Prob. 3.40, where $F \approx 500$ N, and give a physical explanation as to why F has changed.

C3.4

The air flow underneath an air hockey puck is very complex, especially since the air jets from the air hockey



C3.3

table impinge on the underside of the puck at various points nonsymmetrically. A reasonable approximation is that at any given time, the gage pressure on the bottom of the puck is halfway between zero (i.e., atmospheric pressure) and the stagnation pressure of the impinging jets. (Stagnation pressure is defined as $p_0 = \frac{1}{2}\rho V_{\text{jet}}^2$.) (*a*) Find the jet velocity V_{jet} required to support an air hockey puck of weight W and diameter d. Give your answer in terms of W, d, and the density ρ of the air. (*b*) For $W = 0.05$ lbf and $d = 2.5$ in, estimate the required jet velocity in ft/s.

Design Project

D3.1

Let us generalize Probs. 3.141 and 3.142, in which a pump performance curve was used to determine the flow rate between reservoirs. The particular pump in Fig. P3.142 is one of a family of pumps of similar shape, whose dimensionless performance is as follows:

Head:

$$\phi \approx 6.04 - 161\zeta \qquad \phi = \frac{gh}{n^2 D_p^2} \quad \text{and} \quad \zeta = \frac{Q}{nD_p^3}$$

Efficiency:

$$\eta \approx 70\zeta - 91{,}500\zeta^3 \qquad \eta = \frac{\text{power to water}}{\text{power input}}$$

where h_p is the pump head (ft), n is the shaft rotation rate (r/s), and D_p is the impeller diameter (ft). The range of validity is $0 < \zeta < 0.027$. The pump of Fig. P3.142 had $D_p = 2$ ft in diameter and rotated at $n = 20$ r/s (1200 r/min). The solution to Prob. 3.142, namely, $Q \approx 2.57$ ft^3/s and $h_p \approx 172$ ft, corresponds to $\phi \approx 3.46$, $\zeta \approx 0.016$, $\eta \approx 0.75$ (or 75 percent), and power to the water $= \rho g Q h_p \approx 27{,}500$ ft · lbf/s (50 hp). Please check these numerical values before beginning this project.

Now restudy Prob. 3.142 to select a *low-cost* pump which rotates at a rate no slower than 600 r/min and delivers no less than 1.0 ft^3/s of water. Assume that the cost of the pump is linearly proportional to the power input required. Comment on any limitations to your results.



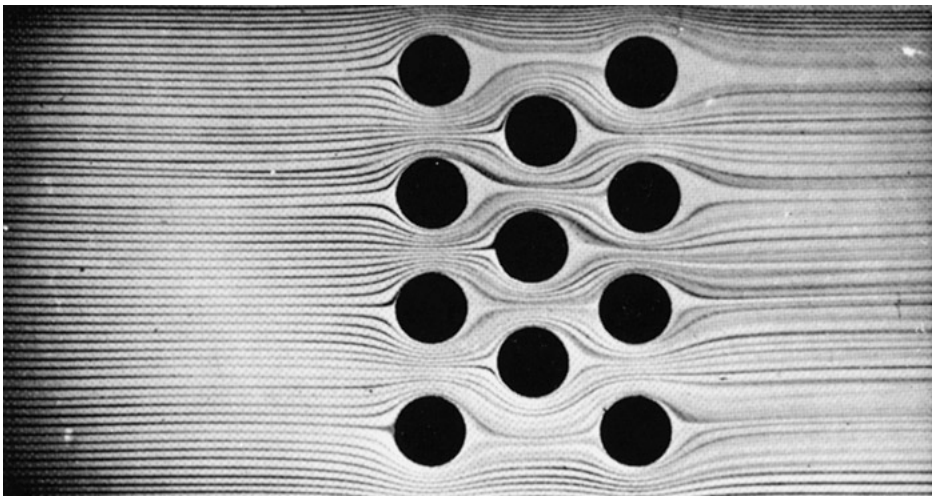
ketabline.com Ebook.ketabline.com

References

1. D. T. Greenwood, *Principles of Dynamics*, Prentice-Hall, Englewood Cliffs, NJ, 1965.
2. T. von Kármán, *The Wind and Beyond*, Little, Brown, Boston, 1967.
3. J. P. Holman, *Heat Transfer*, 7th ed., McGraw-Hill, New York, 1990.
4. A. G. Hansen, *Fluid Mechanics*, Wiley, New York, 1967.
5. M. C. Potter and J. F. Foss, *Fluid Mechanics*, Ronald, New York, 1975.
6. G. J. Van Wylen and R. E. Sonntag, *Fundamentals of Classical Thermodynamics,* 3d ed., Wiley, New York, 1985.
7. W. C. Reynolds and H. C. Perkins, *Engineering Thermodynamics*, 2d ed., McGraw-Hill, New York, 1977.



ketabline.com Ebook.ketabline.com



Inviscid potential flow past an array of cylinders. The mathematics of potential theory, presented in this chapter, is both beautiful and manageable, but results may be unrealistic when there are solid boundaries. See Figure 8.13b for the real (viscous) flow pattern. *(Courtesy of Tecquipment Ltd., Nottingham, England)*



ketabline.com Ebook.ketabline.com

Chapter 4
Differential Relations for a Fluid Particle

Motivation. In analyzing fluid motion, we might take one of two paths: (1) seeking an estimate of gross effects (mass flow, induced force, energy change) over a *finite* region or control volume or (2) seeking the point-by-point details of a flow pattern by analyzing an *infinitesimal* region of the flow. The former or gross-average viewpoint was the subject of Chap. 3.

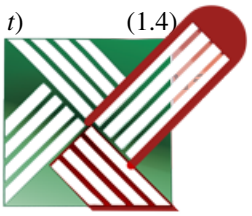
This chapter treats the second in our trio of techniques for analyzing fluid motion, small-scale, or *differential*, analysis. That is, we apply our four basic conservation laws to an infinitesimally small control volume or, alternately, to an infinitesimal fluid system. In either case the results yield the basic *differential equations* of fluid motion. Appropriate *boundary conditions* are also developed.

In their most basic form, these differential equations of motion are quite difficult to solve, and very little is known about their general mathematical properties. However, certain things can be done which have great educational value. First, e.g., as shown in Chap. 5, the equations (even if unsolved) reveal the basic dimensionless parameters which govern fluid motion. Second, as shown in Chap. 6, a great number of useful solutions can be found if one makes two simplifying assumptions: (1) steady flow and (2) incompressible flow. A third and rather drastic simplification, frictionless flow, makes our old friend the Bernoulli equation valid and yields a wide variety of idealized, or *perfect-fluid*, possible solutions. These idealized flows are treated in Chap. 8, and we must be careful to ascertain whether such solutions are in fact realistic when compared with actual fluid motion. Finally, even the difficult general differential equations now yield to the approximating technique known as *numerical analysis*, whereby the derivatives are simulated by algebraic relations between a finite number of grid points in the flow field which are then solved on a digital computer. Reference 1 is an example of a textbook devoted entirely to numerical analysis of fluid motion.

4.1 The Acceleration Field of a Fluid

In Sec. 1.5 we established the cartesian vector form of a velocity field which varies in space and time:

$$\mathbf{V}(\mathbf{r}, t) = \mathbf{i}u(x, y, z, t) + \mathbf{j}v(x, y, z, t) + \mathbf{k}w(x, y, z, t) \tag{1.4}$$



ketabline.com Ebook.ketabline.com

This is the most important variable in fluid mechanics: Knowledge of the velocity vector field is nearly equivalent to *solving* a fluid-flow problem. Our coordinates are fixed in space, and we observe the fluid as it passes by—as if we had scribed a set of coordinate lines on a glass window in a wind tunnel. This is the *eulerian* frame of reference, as opposed to the lagrangian frame, which follows the moving position of individual particles.

To write Newton's second law for an infinitesimal fluid system, we need to calculate the acceleration vector field **a** of the flow. Thus we compute the total time derivative of the velocity vector:

$$\mathbf{a} = \frac{d\mathbf{V}}{dt} = \mathbf{i}\frac{du}{dt} + \mathbf{j}\frac{dv}{dt} + \mathbf{k}\frac{dw}{dt}$$

Since each scalar component (u, v, w) is a function of the four variables (x, y, z, t), we use the chain rule to obtain each scalar time derivative. For example,

$$\frac{du(x, y, z, t)}{dt} = \frac{\partial u}{\partial t} + \frac{\partial u}{\partial x}\frac{dx}{dt} + \frac{\partial u}{\partial y}\frac{dy}{dt} + \frac{\partial u}{\partial z}\frac{dz}{dt}$$

But, by definition, dx/dt is the local velocity component u, and $dy/dt = v$, and $dz/dt = w$. The total derivative of u may thus be written in the compact form

$$\frac{du}{dt} = \frac{\partial u}{\partial t} + u\frac{\partial u}{\partial x} + v\frac{\partial u}{\partial y} + w\frac{\partial u}{\partial z} = \frac{\partial u}{\partial t} + (\mathbf{V}\cdot\boldsymbol{\nabla})u \tag{4.1}$$

Exactly similar expressions, with u replaced by v or w, hold for dv/dt or dw/dt. Summing these into a vector, we obtain the total acceleration:

$$\mathbf{a} = \frac{d\mathbf{V}}{dt} = \underbrace{\frac{\partial \mathbf{V}}{\partial t}}_{\text{Local}} + \underbrace{\left(u\frac{\partial \mathbf{V}}{\partial x} + v\frac{\partial \mathbf{V}}{\partial y} + w\frac{\partial \mathbf{V}}{\partial z}\right)}_{\text{Convective}} = \frac{\partial \mathbf{V}}{\partial t} + (\mathbf{V}\cdot\boldsymbol{\nabla})\mathbf{V} \tag{4.2}$$

The term $\partial\mathbf{V}/\partial t$ is called the *local acceleration*, which vanishes if the flow is steady, i.e., independent of time. The three terms in parentheses are called the *convective acceleration*, which arises when the particle moves through regions of spatially varying velocity, as in a nozzle or diffuser. Flows which are nominally "steady" may have large accelerations due to the convective terms.

Note our use of the compact dot product involving $\mathbf{V}$ and the gradient operator $\boldsymbol{\nabla}$:

$$u\frac{\partial}{\partial x} + v\frac{\partial}{\partial y} + w\frac{\partial}{\partial z} = \mathbf{V}\cdot\boldsymbol{\nabla} \qquad \text{where} \qquad \boldsymbol{\nabla} = \mathbf{i}\frac{\partial}{\partial x} + \mathbf{j}\frac{\partial}{\partial y} + \mathbf{k}\frac{\partial}{\partial z}$$

The total time derivative—sometimes called the *substantial* or *material* derivative—concept may be applied to any variable, e.g., the pressure:

$$\frac{dp}{dt} = \frac{\partial p}{\partial t} + u\frac{\partial p}{\partial x} + v\frac{\partial p}{\partial y} + w\frac{\partial p}{\partial z} = \frac{\partial p}{\partial t} + (\mathbf{V}\cdot\boldsymbol{\nabla})p \tag{4.3}$$

Wherever convective effects occur in the basic laws involving mass, momentum, or energy, the basic differential equations become nonlinear and are usually more complicated than flows which do not involve convective changes.

We emphasize that this total time derivative follows a particle of fixed identi
ing it convenient for expressing laws of particle mechanics in the eulerian fl



ketabline.com Ebook.ketabline.com

description. The operator d/dt is sometimes assigned a special symbol such as D/Dt as a further reminder that it contains four terms and follows a fixed particle.

EXAMPLE 4.1

Given the eulerian velocity-vector field

$$\mathbf{V} = 3t\mathbf{i} + xz\mathbf{j} + ty^2\mathbf{k}$$

find the acceleration of a particle.

Solution

First note the specific given components

$$u = 3t \qquad v = xz \qquad w = ty^2$$

Then evaluate the vector derivatives required for Eq. (4.2)

$$\frac{\partial \mathbf{V}}{\partial t} = \mathbf{i}\frac{\partial u}{\partial t} + \mathbf{j}\frac{\partial v}{\partial t} + \mathbf{k}\frac{\partial w}{\partial t} = 3\mathbf{i} + y^2\mathbf{k}$$

$$\frac{\partial \mathbf{V}}{\partial x} = z\mathbf{j} \qquad \frac{\partial \mathbf{V}}{\partial y} = 2ty\mathbf{k} \qquad \frac{\partial \mathbf{V}}{\partial z} = x\mathbf{j}$$

This could have been worse: There are only five terms in all, whereas there could have been as many as twelve. Substitute directly into Eq. (4.2):

$$\frac{d\mathbf{V}}{dt} = (3\mathbf{i} + y^2\mathbf{k}) + (3t)(z\mathbf{j}) + (xz)(2ty\mathbf{k}) + (ty^2)(x\mathbf{j})$$

Collect terms for the final result

$$\frac{d\mathbf{V}}{dt} = 3\mathbf{i} + (3tz + txy^2)\mathbf{j} + (2xyzt + y^2)\mathbf{k} \qquad \textit{Ans.}$$

Assuming that $\mathbf{V}$ is valid everywhere as given, this acceleration applies to all positions and times within the flow field.

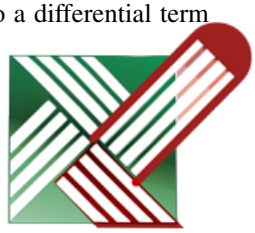
4.2 The Differential Equation of Mass Conservation

All the basic differential equations can be derived by considering either an elemental control volume or an elemental system. Here we choose an infinitesimal fixed control volume (dx, dy, dz), as in Fig. 4.1, and use our basic control-volume relations from Chap. 3. The flow through each side of the element is approximately one-dimensional, and so the appropriate mass-conservation relation to use here is

$$\int_{\text{CV}} \frac{\partial \rho}{\partial t}\, d\mathcal{V} + \sum_i (\rho_i A_i V_i)_{\text{out}} - \sum_i (\rho_i A_i V_i)_{\text{in}} = 0 \qquad (3.22)$$

The element is so small that the volume integral simply reduces to a differential term

$$\int_{\text{CV}} \frac{\partial \rho}{\partial t}\, d\mathcal{V} \approx \frac{\partial \rho}{\partial t}\, dx\, dy\, dz$$



ketabline.com Ebook.ketabline.com

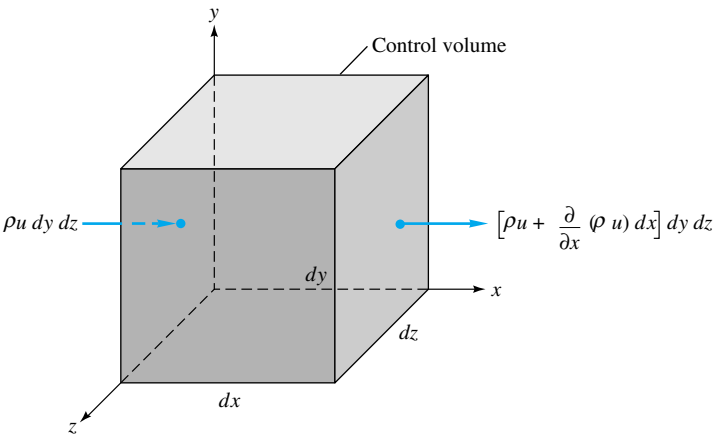


Fig. 4.1 Elemental cartesian fixed control volume showing the inlet and outlet mass flows on the x faces.

The mass-flow terms occur on all six faces, three inlets and three outlets. We make use of the field or continuum concept from Chap. 1, where all fluid properties are considered to be uniformly varying functions of time and position, such as $\rho = \rho(x, y, z, t)$. Thus, if T is the temperature on the left face of the element in Fig. 4.1, the right face will have a slightly different temperature $T + (\partial T/\partial x)\, dx$. For mass conservation, if ρu is known on the left face, the value of this product on the right face is $\rho u + (\partial \rho u/\partial x)\, dx$.

Figure 4.1 shows only the mass flows on the x or left and right faces. The flows on the y (bottom and top) and the z (back and front) faces have been omitted to avoid cluttering up the drawing. We can list all these six flows as follows:

Face	Inlet mass flow	Outlet mass flow
x	$\rho u\, dy\, dz$	$\left[\rho u + \frac{\partial}{\partial x}(\rho u)\, dx\right] dy\, dz$
y	$\rho v\, dx\, dz$	$\left[\rho v + \frac{\partial}{\partial y}(\rho v)\, dy\right] dx\, dz$
z	$\rho w\, dx\, dy$	$\left[\rho w + \frac{\partial}{\partial z}(\rho w)\, dz\right] dx\, dy$

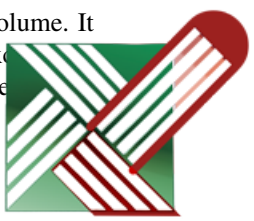
Introduce these terms into Eq. (3.22) above and we have

$$\frac{\partial \rho}{\partial t}\, dx\, dy\, dz + \frac{\partial}{\partial x}(\rho u)\, dx\, dy\, dz + \frac{\partial}{\partial y}(\rho v)\, dx\, dy\, dz + \frac{\partial}{\partial z}(\rho w)\, dx\, dy\, dz = 0$$

The element volume cancels out of all terms, leaving a partial differential equation involving the derivatives of density and velocity

$$\frac{\partial \rho}{\partial t} + \frac{\partial}{\partial x}(\rho u) + \frac{\partial}{\partial y}(\rho v) + \frac{\partial}{\partial z}(\rho w) = 0 \tag{4.4}$$

This is the desired result: conservation of mass for an infinitesimal control volume. It is often called the *equation of continuity* because it requires no assumptions ex the density and velocity are continuum functions. That is, the flow may be eithe



ketabline.com Ebook.ketabline.com

or unsteady, viscous or frictionless, compressible or incompressible.[1] However, the equation does not allow for any source or sink singularities within the element.

The vector-gradient operator

$$\nabla = \mathbf{i}\frac{\partial}{\partial x} + \mathbf{j}\frac{\partial}{\partial y} + \mathbf{k}\frac{\partial}{\partial z}$$

enables us to rewrite the equation of continuity in a compact form, not that it helps much in finding a solution. The last three terms of Eq. (4.4) are equivalent to the divergence of the vector $\rho\mathbf{V}$

$$\frac{\partial}{\partial x}(\rho u) + \frac{\partial}{\partial y}(\rho v) + \frac{\partial}{\partial z}(\rho w) \equiv \nabla \cdot (\rho \mathbf{V}) \tag{4.5}$$

so that the compact form of the continuity relation is

$$\frac{\partial \rho}{\partial t} + \nabla \cdot (\rho \mathbf{V}) = 0 \tag{4.6}$$

In this vector form the equation is still quite general and can readily be converted to other than cartesian coordinate systems.

Cylindrical Polar Coordinates

The most common alternative to the cartesian system is the *cylindrical polar* coordinate system, sketched in Fig. 4.2. An arbitrary point P is defined by a distance z along the axis, a radial distance r from the axis, and a rotation angle θ about the axis. The three independent velocity components are an axial velocity v_z, a radial velocity v_r, and a circumferential velocity v_θ, which is positive counterclockwise, i.e., in the direction

[1] One case where Eq. (4.4) might need special care is *two-phase flow*, where the density is discontinuous between the phases. For further details on this case, see, e.g., Ref. 2.

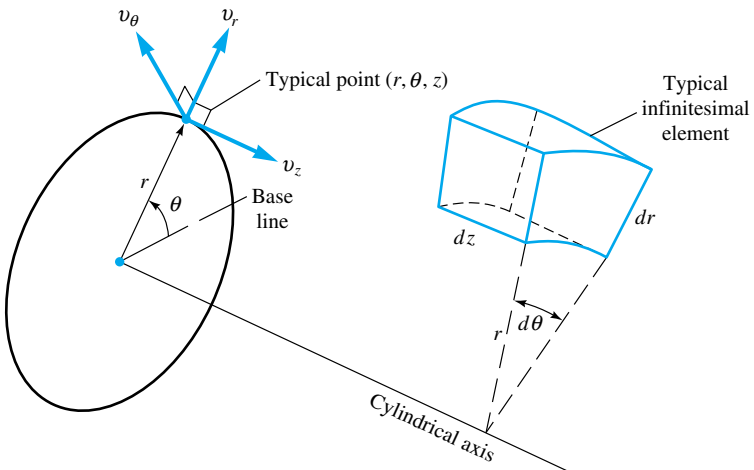


Fig. 4.2 Definition sketch for the cylindrical coordinate system.

ketabline.com Ebook.ketabline.com

of increasing θ. In general, all components, as well as pressure and density and other fluid properties, are continuous functions of r, θ, z, and t.

The divergence of any vector function $\mathbf{A}(r, \theta, z, t)$ is found by making the transformation of coordinates

$$r = (x^2 + y^2)^{1/2} \qquad \theta = \tan^{-1} \frac{y}{x} \qquad z = z \tag{4.7}$$

and the result is given here without proof[2]

$$\boldsymbol{\nabla} \cdot \mathbf{A} = \frac{1}{r} \frac{\partial}{\partial r} (rA_r) + \frac{1}{r} \frac{\partial}{\partial \theta} (A_\theta) + \frac{\partial}{\partial z} (A_z) \tag{4.8}$$

The general continuity equation (4.6) in cylindrical polar coordinates is thus

$$\frac{\partial \rho}{\partial t} + \frac{1}{r} \frac{\partial}{\partial r} (r\rho v_r) + \frac{1}{r} \frac{\partial}{\partial \theta} (\rho v_\theta) + \frac{\partial}{\partial z} (\rho v_z) = 0 \tag{4.9}$$

There are other orthogonal curvilinear coordinate systems, notably *spherical polar* coordinates, which occasionally merit use in a fluid-mechanics problem. We shall not treat these systems here except in Prob. 4.12.

There are also other ways to derive the basic continuity equation (4.6) which are interesting and instructive. Ask your instructor about these alternate approaches.

Steady Compressible Flow

If the flow is steady, $\partial/\partial t \equiv 0$ and all properties are functions of position only. Equation (4.6) reduces to

Cartesian:
$$\frac{\partial}{\partial x} (\rho u) + \frac{\partial}{\partial y} (\rho v) + \frac{\partial}{\partial z} (\rho w) = 0$$

Cylindrical:
$$\frac{1}{r} \frac{\partial}{\partial r} (r\rho v_r) + \frac{1}{r} \frac{\partial}{\partial \theta} (\rho v_\theta) + \frac{\partial}{\partial z} (\rho v_z) = 0 \tag{4.10}$$

Since density and velocity are both variables, these are still nonlinear and rather formidable, but a number of special-case solutions have been found.

Incompressible Flow

A special case which affords great simplification is incompressible flow, where the density changes are negligible. Then $\partial\rho/\partial t \approx 0$ regardless of whether the flow is steady or unsteady, and the density can be slipped out of the divergence in Eq. (4.6) and divided out. The result is

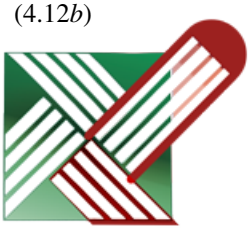
$$\boldsymbol{\nabla} \cdot \mathbf{V} = 0 \tag{4.11}$$

valid for steady or unsteady incompressible flow. The two coordinate forms are

Cartesian:
$$\frac{\partial u}{\partial x} + \frac{\partial v}{\partial y} + \frac{\partial w}{\partial z} = 0 \tag{4.12a}$$

Cylindrical:
$$\frac{1}{r} \frac{\partial}{\partial r} (rv_r) + \frac{1}{r} \frac{\partial}{\partial \theta} (v_\theta) + \frac{\partial}{\partial z} (v_z) = 0 \tag{4.12b}$$

[2] See, e.g., Ref. 3, p. 783.



ketabline.com Ebook.ketabline.com

These are *linear* differential equations, and a wide variety of solutions are known, as discussed in Chaps. 6 to 8. Since no author or instructor can resist a wide variety of solutions, it follows that a great deal of time is spent studying incompressible flows. Fortunately, this is exactly what should be done, because most practical engineering flows are approximately incompressible, the chief exception being the high-speed gas flows treated in Chap. 9.

When is a given flow approximately incompressible? We can derive a nice criterion by playing a little fast and loose with density approximations. In essence, we wish to slip the density out of the divergence in Eq. (4.6) and approximate a typical term as, e.g.,

$$\frac{\partial}{\partial x}(\rho u) \approx \rho \frac{\partial u}{\partial x} \tag{4.13}$$

This is equivalent to the strong inequality

$$\left| u \frac{\partial \rho}{\partial x} \right| \ll \left| \rho \frac{\partial u}{\partial x} \right|$$

or

$$\left| \frac{\delta \rho}{\rho} \right| \ll \left| \frac{\delta V}{V} \right| \tag{4.14}$$

As we shall see in Chap. 9, the pressure change is approximately proportional to the density change and the square of the speed of sound a of the fluid

$$\delta p \approx a^2 \, \delta \rho \tag{4.15}$$

Meanwhile, if elevation changes are negligible, the pressure is related to the velocity change by Bernoulli's equation (3.75)

$$\delta p \approx -\rho V \, \delta V \tag{4.16}$$

Combining Eqs. (4.14) to (4.16), we obtain an explicit criterion for incompressible flow:

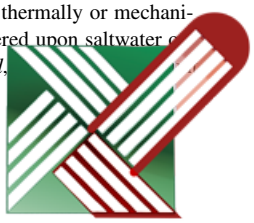
$$\frac{V^2}{a^2} = \mathrm{Ma}^2 \ll 1 \tag{4.17}$$

where $\mathrm{Ma} = V/a$ is the dimensionless *Mach number* of the flow. How small is small? The commonly accepted limit is

$$\mathrm{Ma} \leq 0.3 \tag{4.18}$$

For air at standard conditions, a flow can thus be considered incompressible if the velocity is less than about 100 m/s (330 ft/s). This encompasses a wide variety of airflows: automobile and train motions, light aircraft, landing and takeoff of high-speed aircraft, most pipe flows, and turbomachinery at moderate rotational speeds. Further, it is clear that almost all liquid flows are incompressible, since flow velocities are small and the speed of sound is very large.[3]

[3]An exception occurs in geophysical flows, where a density change is imposed thermally or mechanically rather than by the flow conditions themselves. An example is fresh water layered upon saltwater or warm air layered upon cold air in the atmosphere. We say that the fluid is *stratified*. Gravity is important for vertical density changes in Eq. (4.6) even if the velocities are small.



ketabline.com Ebook.ketabline.com

Before attempting to analyze the continuity equation, we shall proceed with the derivation of the momentum and energy equations, so that we can analyze them as a group. A very clever device called the *stream function* can often make short work of the continuity equation, but we shall save it until Sec. 4.7.

One further remark is appropriate: The continuity equation is always important and must always be satisfied for a rational analysis of a flow pattern. Any newly discovered momentum or energy "solution" will ultimately crash in flames when subjected to critical analysis if it does not also satisfy the continuity equation.

EXAMPLE 4.2

Under what conditions does the velocity field

$$\mathbf{V} = (a_1x + b_1y + c_1z)\mathbf{i} + (a_2x + b_2y + c_2z)\mathbf{j} + (a_3x + b_3y + c_3z)\mathbf{k}$$

where a_1, b_1, etc. = const, represent an incompressible flow which conserves mass?

Solution

Recalling that $\mathbf{V} = u\mathbf{i} + v\mathbf{j} + w\mathrm{k}$, we see that $u = (a_1x + b_1y + c_1z)$, etc. Substituting into Eq. (4.12*a*) for incompressible continuity, we obtain

$$\frac{\partial}{\partial x}(a_1x + b_1y + c_1z) + \frac{\partial}{\partial y}(a_2x + b_2y + c_2z) + \frac{\partial}{\partial z}(a_3x + b_3y + c_3z) = 0$$

or

$$a_1 + b_2 + c_3 = 0 \qquad \textit{Ans.}$$

At least two of constants a_1, b_2, and c_3 must have opposite signs. Continuity imposes no restrictions whatever on constants b_1, c_1, a_2, c_2, a_3, and b_3, which do not contribute to a mass increase or decrease of a differential element.

EXAMPLE 4.3

An incompressible velocity field is given by

$$u = a(x^2 - y^2) \qquad v \text{ unknown} \qquad w = b$$

where a and b are constants. What must the form of the velocity component v be?

Solution

Again Eq. (4.12*a*) applies

$$\frac{\partial}{\partial x}(ax^2 - ay^2) + \frac{\partial v}{\partial y} + \frac{\partial b}{\partial z} = 0$$

or

$$\frac{\partial v}{\partial y} = -2ax \tag{1}$$

This is easily integrated partially with respect to y

$$v(x, y, z, t) = -2axy + f(x, z, t)$$



ketabline.com Ebook.ketabline.com

This is the only possible form for v which satisfies the incompressible continuity equation. The function of integration f is entirely arbitrary since it vanishes when v is differentiated with respect to y.[†]

EXAMPLE 4.4

A centrifugal impeller of 40-cm diameter is used to pump hydrogen at 15°C and 1-atm pressure. What is the maximum allowable impeller rotational speed to avoid compressibility effects at the blade tips?

Solution

The speed of sound of hydrogen for these conditions is $a = 1300$ m/s. Assume that the gas velocity leaving the impeller is approximately equal to the impeller-tip speed

$$V = \Omega r = \tfrac{1}{2}\Omega D$$

Our rule of thumb, Eq. (4.18), neglects compressibility if

$$V = \tfrac{1}{2}\Omega D \leq 0.3a = 390 \text{ m/s}$$

or $$\tfrac{1}{2}\Omega(0.4 \text{ m}) \leq 390 \text{ m/s} \qquad \Omega \leq 1950 \text{ rad/s}$$

Thus we estimate the allowable speed to be quite large

$$\Omega \leq 310 \text{ r/s } (18{,}600 \text{ r/min}) \qquad \textit{Ans.}$$

An impeller moving at this speed in air would create shock waves at the tips but not in a light gas like hydrogen.

4.3 The Differential Equation of Linear Momentum

Having done it once in Sec. 4.2 for mass conservation, we can move along a little faster this time. We use the same elemental control volume as in Fig. 4.1, for which the appropriate form of the linear-momentum relation is

$$\sum \mathbf{F} = \frac{\partial}{\partial t}\left(\int_{CV} \mathbf{V}\rho \, d\mathcal{V}\right) + \sum (\dot{m}_i \mathbf{V}_i)_{\text{out}} - \sum (\dot{m}_i \mathbf{V}_i)_{\text{in}} \tag{3.40}$$

Again the element is so small that the volume integral simply reduces to a derivative term

$$\frac{\partial}{\partial t}\left(\int_{CV} \mathbf{V}\rho \, d\mathcal{V}\right) \approx \frac{\partial}{\partial t}(\rho \mathbf{V}) \, dx \, dy \, dz \tag{4.19}$$

The momentum fluxes occur on all six faces, three inlets and three outlets. Referring again to Fig. 4.1, we can form a table of momentum fluxes by exact analogy with the discussion which led up to the equation for net mass flux:

[†]This is a very realistic flow which simulates the turning of an inviscid fluid thr
Examples 4.7 and 4.9.



ketabline.com Ebook.ketabline.com

Faces	Inlet momentum flux	Outlet momentum flux
x	$\rho u\mathbf{V}\, dy\, dz$	$\left[\rho u\mathbf{V} + \frac{\partial}{\partial x}(\rho u\mathbf{V})\, dx\right] dy\, dz$
y	$\rho v\mathbf{V}\, dx\, dz$	$\left[\rho v\mathbf{V} + \frac{\partial}{\partial y}(\rho v\mathbf{V})\, dy\right] dx\, dz$
z	$\rho w\mathbf{V}\, dx\, dy$	$\left[\rho w\mathbf{V} + \frac{\partial}{\partial z}(\rho w\mathbf{V})\, dz\right] dx\, dy$

Introduce these terms and Eq. (4.19) into Eq. (3.40), and get the intermediate result

$$\sum \mathbf{F} = dx\, dy\, dz\left[\frac{\partial}{\partial t}(\rho\mathbf{V}) + \frac{\partial}{\partial x}(\rho u\mathbf{V}) + \frac{\partial}{\partial y}(\rho v\mathbf{V}) + \frac{\partial}{\partial z}(\rho w\mathbf{V})\right] \tag{4.20}$$

Note that this is a vector relation. A simplification occurs if we split up the term in brackets as follows:

$$\frac{\partial}{\partial t}(\rho\mathbf{V}) + \frac{\partial}{\partial x}(\rho u\mathbf{V}) + \frac{\partial}{\partial y}(\rho v\mathbf{V}) + \frac{\partial}{\partial z}(\rho w\mathbf{V})$$
$$= \mathbf{V}\left[\frac{\partial \rho}{\partial t} + \boldsymbol{\nabla}\cdot(\rho\mathbf{V})\right] + \rho\left(\frac{\partial \mathbf{V}}{\partial t} + u\frac{\partial \mathbf{V}}{\partial x} + v\frac{\partial \mathbf{V}}{\partial y} + w\frac{\partial \mathbf{V}}{\partial z}\right) \tag{4.21}$$

The term in brackets on the right-hand side is seen to be the equation of continuity, Eq. (4.6), which vanishes identically. The long term in parentheses on the right-hand side is seen from Eq. (4.2) to be the total acceleration of a particle which instantaneously occupies the control volume

$$\frac{\partial \mathbf{V}}{\partial t} + u\frac{\partial \mathbf{V}}{\partial x} + v\frac{\partial \mathbf{V}}{\partial y} + w\frac{\partial \mathbf{V}}{\partial z} = \frac{d\mathbf{V}}{dt} \tag{4.2}$$

Thus we have now reduced Eq. (4.20) to

$$\sum \mathbf{F} = \rho\frac{d\mathbf{V}}{dt}\, dx\, dy\, dz \tag{4.22}$$

It might be good for you to stop and rest now and think about what we have just done. What is the relation between Eqs. (4.22) and (3.40) for an infinitesimal control volume? Could we have *begun* the analysis at Eq. (4.22)?

Equation (4.22) points out that the net force on the control volume must be of differential size and proportional to the element volume. These forces are of two types, *body* forces and *surface* forces. Body forces are due to external fields (gravity, magnetism, electric potential) which act upon the entire mass within the element. The only body force we shall consider in this book is gravity. The gravity force on the differential mass $\rho\, dx\, dy\, dz$ within the control volume is

$$d\mathbf{F}_{\text{grav}} = \rho\mathbf{g}\, dx\, dy\, dz \tag{4.23}$$

where $\mathbf{g}$ may in general have an arbitrary orientation with respect to the coordinate system. In many applications, such as Bernoulli's equation, we take z "u
$\mathbf{g} = -g\mathbf{k}$.



ketabline.com Ebook.ketabline.com

The surface forces are due to the stresses on the sides of the control surface. These stresses, as discussed in Chap. 2, are the sum of hydrostatic pressure plus viscous stresses τ_{ij} which arise from motion with velocity gradients

$$\sigma_{ij} = \begin{vmatrix} -p + \tau_{xx} & \tau_{yx} & \tau_{zx} \\ \tau_{xy} & -p + \tau_{yy} & \tau_{zy} \\ \tau_{xz} & \tau_{yz} & -p + \tau_{zz} \end{vmatrix} \tag{4.24}$$

The subscript notation for stresses is given in Fig. 4.3.

It is not these stresses but their *gradients*, or differences, which cause a net force on the differential control surface. This is seen by referring to Fig. 4.4, which shows

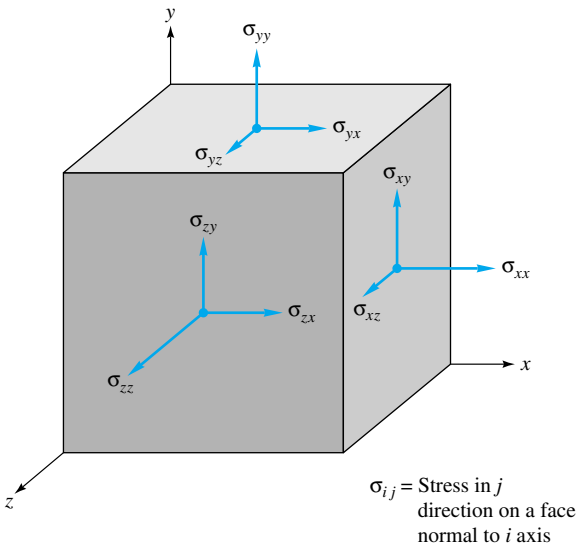


Fig. 4.3 Notation for stresses.

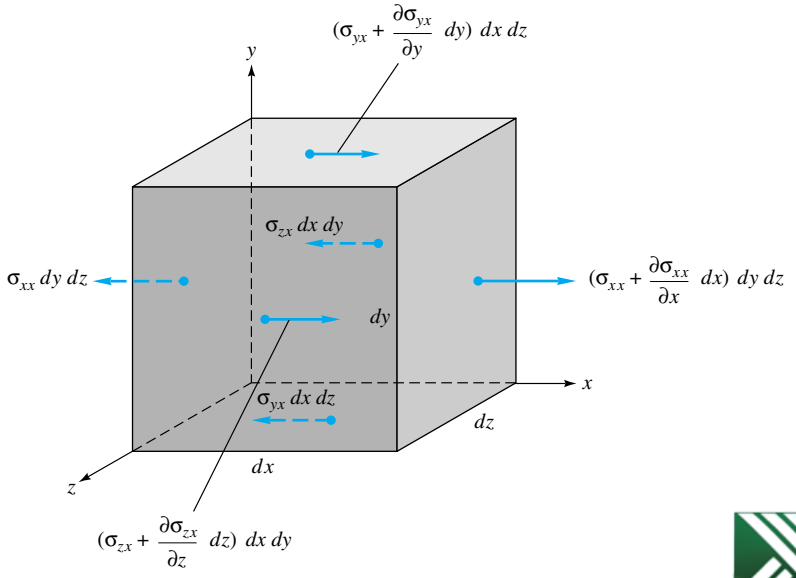


Fig. 4.4 Elemental cartesian fixed control volume showing the surface forces in the x direction only.



ketabline.com Ebook.ketabline.com

only the x-directed stresses to avoid cluttering up the drawing. For example, the leftward force $\sigma_{xx}\,dy\,dz$ on the left face is balanced by the rightward force $\sigma_{xx}\,dy\,dz$ on the right face, leaving only the net rightward force $(\partial\sigma_{xx}/\partial x)\,dx\,dy\,dz$ on the right face. The same thing happens on the other four faces, so that the net surface force in the x direction is given by

$$dF_{x,\text{surf}} = \left[\frac{\partial}{\partial x}(\sigma_{xx}) + \frac{\partial}{\partial y}(\sigma_{yx}) + \frac{\partial}{\partial z}(\sigma_{zx})\right] dx\,dy\,dz \tag{4.25}$$

We see that this force is proportional to the element volume. Notice that the stress terms are taken from the *top row* of the array in Eq. (4.24). Splitting this row into pressure plus viscous stresses, we can rewrite Eq. (4.25) as

$$\frac{dF_x}{d\mathcal{V}} = -\frac{\partial p}{\partial x} + \frac{\partial}{\partial x}(\tau_{xx}) + \frac{\partial}{\partial y}(\tau_{yx}) + \frac{\partial}{\partial z}(\tau_{zx}) \tag{4.26}$$

In exactly similar manner, we can derive the y and z forces per unit volume on the control surface

$$\frac{dF_y}{d\mathcal{V}} = -\frac{\partial p}{\partial y} + \frac{\partial}{\partial x}(\tau_{xy}) + \frac{\partial}{\partial y}(\tau_{yy}) + \frac{\partial}{\partial z}(\tau_{zy})$$

$$\frac{dF_z}{d\mathcal{V}} = -\frac{\partial p}{\partial z} + \frac{\partial}{\partial x}(\tau_{xz}) + \frac{\partial}{\partial y}(\tau_{yz}) + \frac{\partial}{\partial z}(\tau_{zz}) \tag{4.27}$$

Now we multiply Eqs. (4.26) and (4.27) by **i**, **j**, and **k**, respectively, and add to obtain an expression for the net vector surface force

$$\left(\frac{d\mathbf{F}}{d\mathcal{V}}\right)_{\text{surf}} = -\boldsymbol{\nabla} p + \left(\frac{d\mathbf{F}}{d\mathcal{V}}\right)_{\text{viscous}} \tag{4.28}$$

where the viscous force has a total of nine terms:

$$\begin{aligned}\left(\frac{d\mathbf{F}}{d\mathcal{V}}\right)_{\text{viscous}} &= \mathbf{i}\left(\frac{\partial\tau_{xx}}{\partial x} + \frac{\partial\tau_{yx}}{\partial y} + \frac{\partial\tau_{zx}}{\partial z}\right) \\ &\quad + \mathbf{j}\left(\frac{\partial\tau_{xy}}{\partial x} + \frac{\partial\tau_{yy}}{\partial y} + \frac{\partial\tau_{zy}}{\partial z}\right) \\ &\quad + \mathbf{k}\left(\frac{\partial\tau_{xz}}{\partial x} + \frac{\partial\tau_{yz}}{\partial y} + \frac{\partial\tau_{zz}}{\partial z}\right)\end{aligned} \tag{4.29}$$

Since each term in parentheses in (4.29) represents the divergence of a stress-component vector acting on the x, y, and z faces, respectively, Eq. (4.29) is sometimes expressed in divergence form

$$\left(\frac{d\mathbf{F}}{d\mathcal{V}}\right)_{\text{viscous}} = \boldsymbol{\nabla}\cdot\boldsymbol{\tau}_{ij} \tag{4.30}$$

where

$$\tau_{ij} = \begin{bmatrix}\tau_{xx} & \tau_{yx} & \tau_{zx} \\ \tau_{xy} & \tau_{yy} & \tau_{zy} \\ \tau_{xz} & \tau_{yz} & \tau_{zz}\end{bmatrix} \tag{4.31}$$



ketabline.com Ebook.ketabline.com

is the viscous-stress tensor acting on the element. The surface force is thus the sum of the *pressure-gradient* vector and the divergence of the viscous-stress tensor. Substituting into Eq. (4.22) and utilizing Eq. (4.23), we have the basic differential momentum equation for an infinitesimal element

$$\rho\mathbf{g} - \boldsymbol{\nabla} p + \boldsymbol{\nabla} \cdot \boldsymbol{\tau}_{ij} = \rho \frac{d\mathbf{V}}{dt} \tag{4.32}$$

where

$$\frac{d\mathbf{V}}{dt} = \frac{\partial \mathbf{V}}{\partial t} + u\frac{\partial \mathbf{V}}{\partial x} + v\frac{\partial \mathbf{V}}{\partial y} + w\frac{\partial \mathbf{V}}{\partial z} \tag{4.33}$$

We can also express Eq. (4.32) in words:

Gravity force per unit volume + pressure force per unit volume
+ viscous force per unit volume = density × acceleration (4.34)

Equation (4.32) is so brief and compact that its inherent complexity is almost invisible. It is a *vector* equation, each of whose component equations contains nine terms. Let us therefore write out the component equations in full to illustrate the mathematical difficulties inherent in the momentum equation:

$$\begin{aligned}
\rho g_x - \frac{\partial p}{\partial x} + \frac{\partial \tau_{xx}}{\partial x} + \frac{\partial \tau_{yx}}{\partial y} + \frac{\partial \tau_{zx}}{\partial z} &= \rho\left(\frac{\partial u}{\partial t} + u\frac{\partial u}{\partial x} + v\frac{\partial u}{\partial y} + w\frac{\partial u}{\partial z}\right) \\
\rho g_y - \frac{\partial p}{\partial y} + \frac{\partial \tau_{xy}}{\partial x} + \frac{\partial \tau_{yy}}{\partial y} + \frac{\partial \tau_{zy}}{\partial z} &= \rho\left(\frac{\partial v}{\partial t} + u\frac{\partial v}{\partial x} + v\frac{\partial v}{\partial y} + w\frac{\partial v}{\partial z}\right) \\
\rho g_z - \frac{\partial p}{\partial z} + \frac{\partial \tau_{xz}}{\partial x} + \frac{\partial \tau_{yz}}{\partial y} + \frac{\partial \tau_{zz}}{\partial z} &= \rho\left(\frac{\partial w}{\partial t} + u\frac{\partial w}{\partial x} + v\frac{\partial w}{\partial y} + w\frac{\partial w}{\partial z}\right)
\end{aligned} \tag{4.35}$$

This is the differential momentum equation in its full glory, and it is valid for any fluid in any general motion, particular fluids being characterized by particular viscous-stress terms. Note that the last three "convective" terms on the right-hand side of each component equation in (4.35) are nonlinear, which complicates the general mathematical analysis.

Inviscid Flow: Euler's Equation

Equation (4.35) is not ready to use until we write the viscous stresses in terms of velocity components. The simplest assumption is frictionless flow $\tau_{ij} = 0$, for which Eq. (4.35) reduces to

$$\rho\mathbf{g} - \boldsymbol{\nabla} p = \rho \frac{d\mathbf{V}}{dt} \tag{4.36}$$

This is Euler's equation for inviscid flow. We show in Sec. 4.9 that Euler's equation can be integrated along a streamline to yield the frictionless Bernoulli equation, (3.75) or (3.77). The complete analysis of inviscid flow fields, using continuity and the Bernoulli relation, is given in Chap. 8.

Newtonian Fluid: Navier-Stokes Equations

For a newtonian fluid, as discussed in Sec. 1.7, the viscous stresses the element strain rates and the coefficient of viscosity. For incom



ketabline.com Ebook.ketabline.com

generalization of Eq. (1.23) to three-dimensional viscous flow is[4]

$$\tau_{xx} = 2\mu \frac{\partial u}{\partial x} \qquad \tau_{yy} = 2\mu \frac{\partial v}{\partial y} \qquad \tau_{zz} = 2\mu \frac{\partial w}{\partial z}$$

$$\tau_{xy} = \tau_{yx} = \mu\left(\frac{\partial u}{\partial y} + \frac{\partial v}{\partial x}\right) \quad \tau_{xz} = \tau_{zx} = \mu\left(\frac{\partial w}{\partial x} + \frac{\partial u}{\partial z}\right) \tag{4.37}$$

$$\tau_{yz} = \tau_{zy} = \mu\left(\frac{\partial v}{\partial z} + \frac{\partial w}{\partial y}\right)$$

where μ is the viscosity coefficient. Substitution into Eq. (4.35) gives the differential momentum equation for a newtonian fluid with constant density and viscosity

$$\begin{aligned}
\rho g_x - \frac{\partial p}{\partial x} + \mu\left(\frac{\partial^2 u}{\partial x^2} + \frac{\partial^2 u}{\partial y^2} + \frac{\partial^2 u}{\partial z^2}\right) &= \rho \frac{du}{dt} \\
\rho g_y - \frac{\partial p}{\partial y} + \mu\left(\frac{\partial^2 v}{\partial x^2} + \frac{\partial^2 v}{\partial y^2} + \frac{\partial^2 v}{\partial z^2}\right) &= \rho \frac{dv}{dt} \\
\rho g_z - \frac{\partial p}{\partial z} + \mu\left(\frac{\partial^2 w}{\partial x^2} + \frac{\partial^2 w}{\partial y^2} + \frac{\partial^2 w}{\partial z^2}\right) &= \rho \frac{dw}{dt}
\end{aligned} \tag{4.38}$$

These are the *Navier-Stokes equations*, named after C. L. M. H. Navier (1785–1836) and Sir George G. Stokes (1819–1903), who are credited with their derivation. They are second-order nonlinear partial differential equations and are quite formidable, but surprisingly many solutions have been found to a variety of interesting viscous-flow problems, some of which are discussed in Sec. 4.11 and in Chap. 6 (see also Refs. 4 and 5). For compressible flow, see eq. (2.29) of Ref. 5.

Equation (4.38) has four unknowns: p, u, v, and w. It should be combined with the incompressible continuity relation (4.12) to form four equations in these four unknowns. We shall discuss this again in Sec. 4.6, which presents the appropriate boundary conditions for these equations.

EXAMPLE 4.5

Take the velocity field of Example 4.3, with $b = 0$ for algebraic convenience

$$u = a(x^2 - y^2) \qquad v = -2axy \qquad w = 0$$

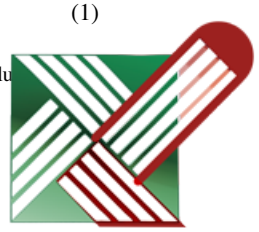
and determine under what conditions it is a solution to the Navier-Stokes momentum equation (4.38). Assuming that these conditions are met, determine the resulting pressure distribution when z is "up" ($g_x = 0$, $g_y = 0$, $g_z = -g$).

Solution

Make a direct substitution of u, v, w into Eq. (4.38):

$$\rho(0) - \frac{\partial p}{\partial x} + \mu(2a - 2a) = 2a^2\rho(x^3 + xy^2) \tag{1}$$

[4]When compressibility is significant, additional small terms arise containing the element volu pansion rate and a *second* coefficient of viscosity; see Refs. 4 and 5 for details.



ketabline.com Ebook.ketabline.com

$$\rho(0) - \frac{\partial p}{\partial y} + \mu(0) = 2a^2\rho(x^2y + y^3) \tag{2}$$

$$\rho(-g) - \frac{\partial p}{\partial z} + \mu(0) = 0 \tag{3}$$

The viscous terms vanish identically (although μ is *not* zero). Equation (3) can be integrated partially to obtain

$$p = -\rho g z + f_1(x, y) \tag{4}$$

i.e., the pressure is hydrostatic in the z direction, which follows anyway from the fact that the flow is two-dimensional ($w = 0$). Now the question is: Do Eqs. (1) and (2) show that the given velocity field *is* a solution? One way to find out is to form the mixed derivative $\partial^2 p/(\partial x\, \partial y)$ from (1) and (2) separately and then compare them.

Differentiate Eq. (1) with respect to y

$$\frac{\partial^2 p}{\partial x\, \partial y} = -4a^2\rho xy \tag{5}$$

Now differentiate Eq. (2) with respect to x

$$\frac{\partial^2 p}{\partial x\, \partial y} = -\frac{\partial}{\partial x}\left[2a^2\rho(x^2y + y^3)\right] = -4a^2\rho xy \tag{6}$$

Since these are identical, the given velocity field is an *exact* solution to the Navier-Stokes equation. *Ans.*

To find the pressure distribution, substitute Eq. (4) into Eqs. (1) and (2), which will enable us to find $f_1(x, y)$

$$\frac{\partial f_1}{\partial x} = -2a^2\rho(x^3 + xy^2) \tag{7}$$

$$\frac{\partial f_1}{\partial y} = -2a^2\rho(x^2y + y^3) \tag{8}$$

Integrate Eq. (7) partially with respect to x

$$f_1 = -\tfrac{1}{2}a^2\rho(x^4 + 2x^2y^2) + f_2(y) \tag{9}$$

Differentiate this with respect to y and compare with Eq. (8)

$$\frac{\partial f_1}{\partial y} = -2a^2\rho x^2 y + f_2'(y) \tag{10}$$

Comparing (8) and (10), we see they are equivalent if

$$f_2'(y) = -2a^2\rho y^3$$

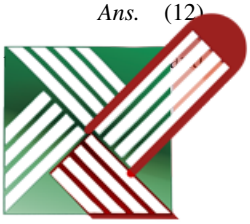
or

$$f_2(y) = -\tfrac{1}{2}a^2\rho y^4 + C \tag{11}$$

where C is a constant. Combine Eqs. (4), (9), and (11) to give the complete expression for pressure distribution

$$p(x, y, z) = -\rho g z - \tfrac{1}{2}a^2\rho(x^4 + y^4 + 2x^2y^2) + C \qquad \textit{Ans.} \tag{12}$$

This is the desired solution. Do you recognize it? Not unless you go back and square the velocity components:



ketabline.com Ebook.ketabline.com

$$u^2 + v^2 + w^2 = V^2 = a^2(x^4 + y^4 + 2x^2y^2) \tag{13}$$

Comparing with Eq. (12), we can rewrite the pressure distribution as

$$p + \tfrac{1}{2}\rho V^2 + \rho g z = C \tag{14}$$

This is Bernoulli's equation (3.77). That is no accident, because the velocity distribution given in this problem is one of a family of flows which are solutions to the Navier-Stokes equation and which satisfy Bernoulli's incompressible equation everywhere in the flow field. They are called *irrotational flows*, for which curl $\mathbf{V} = \nabla \times \mathbf{V} \equiv 0$. This subject is discussed again in Sec. 4.9.

4.4 The Differential Equation of Angular Momentum

Having now been through the same approach for both mass and linear momentum, we can go rapidly through a derivation of the differential angular-momentum relation. The appropriate form of the integral angular-momentum equation for a fixed control volume is

$$\sum \mathbf{M}_O = \frac{\partial}{\partial t}\left[\int_{\text{CV}} (\mathbf{r} \times \mathbf{V})\rho \, d\mathcal{V}\right] + \int_{\text{CS}} (\mathbf{r} \times \mathbf{V})\rho(\mathbf{V} \cdot \mathbf{n}) \, dA \tag{3.55}$$

We shall confine ourselves to an axis O which is parallel to the z axis and passes through the centroid of the elemental control volume. This is shown in Fig. 4.5. Let θ be the angle of rotation about O of the fluid within the control volume. The only stresses which have moments about O are the shear stresses τ_{xy} and τ_{yx}. We can evaluate the moments about O and the angular-momentum terms about O. A lot of algebra is involved, and we give here only the result

$$\left[\tau_{xy} - \tau_{yx} + \frac{1}{2}\frac{\partial}{\partial x}(\tau_{xy})\,dx - \frac{1}{2}\frac{\partial}{\partial y}(\tau_{yx})\,dy\right] dx\,dy\,dz$$

$$= \frac{1}{12}\rho(dx\,dy\,dz)(dx^2 + dy^2)\frac{d^2\theta}{dt^2} \tag{4.39}$$

Assuming that the angular acceleration $d^2\theta/dt^2$ is not infinite, we can neglect all higher-

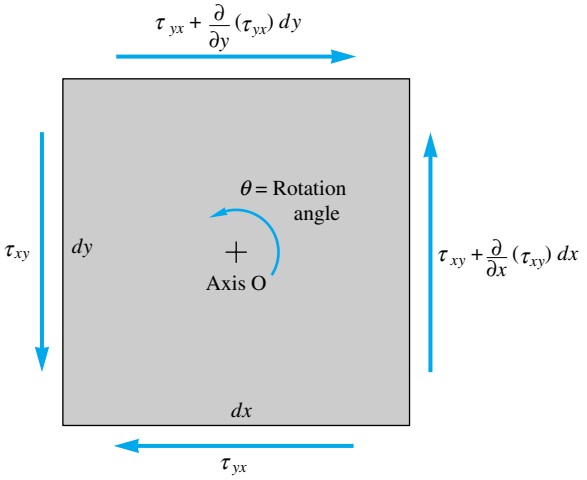


Fig. 4.5 Elemental cartesian fixed control volume showing shear stresses which may cause a net angular acceleration about axis O.



ketabline.com Ebook.ketabline.com

order differential terms, which leaves a finite and interesting result

$$\tau_{xy} \approx \tau_{yx} \tag{4.40}$$

Had we summed moments about axes parallel to y or x, we would have obtained exactly analogous results

$$\tau_{xz} \approx \tau_{zx} \qquad \tau_{yz} \approx \tau_{zy} \tag{4.41}$$

There is *no* differential angular-momentum equation. Application of the integral theorem to a differential element gives the result, well known to students of stress analysis, that the shear stresses are symmetric: $\tau_{ij} = \tau_{ji}$. This is the only result of this section.[5] There is no differential equation to remember, which leaves room in your brain for the next topic, the differential energy equation.

4.5 The Differential Equation of Energy[6]

We are now so used to this type of derivation that we can race through the energy equation at a bewildering pace. The appropriate integral relation for the fixed control volume of Fig. 4.1 is

$$\dot{Q} - \dot{W}_s - \dot{W}_v = \frac{\partial}{\partial t}\left(\int_{\text{CV}} e\rho \, d\mathcal{V}\right) + \int_{\text{CS}} \left(e + \frac{p}{\rho}\right)\rho(\mathbf{V} \cdot \mathbf{n}) \, dA \tag{3.63}$$

where $\dot{W}_s = 0$ because there can be no infinitesimal shaft protruding into the control volume. By analogy with Eq. (4.20), the right-hand side becomes, for this tiny element,

$$\dot{Q} - \dot{W}_v = \left[\frac{\partial}{\partial t}(\rho e) + \frac{\partial}{\partial x}(\rho u \zeta) + \frac{\partial}{\partial y}(\rho v \zeta) + \frac{\partial}{\partial z}(\rho w \zeta)\right] dx \, dy \, dz \tag{4.42}$$

where $\zeta = e + p/\rho$. When we use the continuity equation by analogy with Eq. (4.21), this becomes

$$\dot{Q} - \dot{W}_v = \left(\rho \frac{de}{dt} + \mathbf{V} \cdot \boldsymbol{\nabla} p\right) dx \, dy \, dz \tag{4.43}$$

To evaluate $\dot{Q}$, we neglect radiation and consider only heat conduction through the sides of the element. The heat flow by conduction follows Fourier's law from Chap. 1

$$\mathbf{q} = -k \, \boldsymbol{\nabla} T \tag{1.29a}$$

where k is the coefficient of thermal conductivity of the fluid. Figure 4.6 shows the heat flow passing through the x faces, the y and z heat flows being omitted for clarity. We can list these six heat-flux terms:

Faces	Inlet heat flux	Outlet heat flux
x	$q_x \, dy \, dz$	$\left[q_x + \frac{\partial}{\partial x}(q_x) \, dx\right] dy \, dz$
y	$q_y \, dx \, dz$	$\left[q_y + \frac{\partial}{\partial y}(q_y) \, dy\right] dx \, dz$
z	$q_z \, dx \, dy$	$\left[q_z + \frac{\partial}{\partial z}(q_z) \, dz\right] dx \, dy$

[5]We are neglecting the possibility of a finite *couple* being applied to the element by some powerful external force field. See, e.g., Ref. 6, p. 217.

[6]This section may be omitted without loss of continuity.



ketabline.com Ebook.ketabline.com

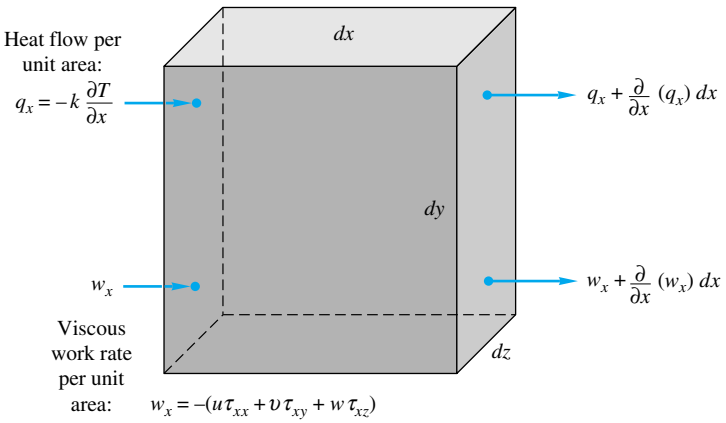


Fig. 4.6 Elemental cartesian control volume showing heat-flow and viscous-work-rate terms in the x direction.

By adding the inlet terms and subtracting the outlet terms, we obtain the net heat added to the element

$$\dot{Q} = -\left[\frac{\partial}{\partial x}(q_x) + \frac{\partial}{\partial y}(q_y) + \frac{\partial}{\partial z}(q_z)\right] dx\,dy\,dz = -\nabla \cdot \mathbf{q}\,dx\,dy\,dz \qquad (4.44)$$

As expected, the heat flux is proportional to the element volume. Introducing Fourier's law from Eq. (1.29), we have

$$\dot{Q} = \nabla \cdot (k\,\nabla T)\,dx\,dy\,dz \qquad (4.45)$$

The rate of work done by viscous stresses equals the product of the stress component, its corresponding velocity component, and the area of the element face. Figure 4.6 shows the work rate on the left x face is

$$\dot{W}_{v,\mathrm{LF}} = w_x\,dy\,dz \qquad \text{where } w_x = -(u\tau_{xx} + v\tau_{xy} + w\tau_{xz}) \qquad (4.46)$$

(where the subscript LF stands for left face) and a slightly different work on the right face due to the gradient in w_x. These work fluxes could be tabulated in exactly the same manner as the heat fluxes in the previous table, with w_x replacing q_x, etc. After outlet terms are subtracted from inlet terms, the net viscous-work rate becomes

$$\begin{aligned}\dot{W}_v = -\Bigg[&\frac{\partial}{\partial x}(u\tau_{xx} + v\tau_{xy} + w\tau_{xz}) + \frac{\partial}{\partial y}(u\tau_{yx} + v\tau_{yy} + w\tau_{yz}) \\ &+ \frac{\partial}{\partial z}(u\tau_{zx} + v\tau_{zy} + w\tau_{zz})\Bigg]\,dx\,dy\,dz \\ = -\nabla \cdot (\mathbf{V} \cdot \boldsymbol{\tau}_{ij})\,&dx\,dy\,dz \end{aligned} \qquad (4.47)$$

We now substitute Eqs. (4.45) and (4.47) into Eq. (4.43) to obtain one form of the differential energy equation

$$\rho\frac{de}{dt} + \mathbf{V} \cdot \nabla p = \nabla \cdot (k\,\nabla T) + \nabla \cdot (\mathbf{V} \cdot \boldsymbol{\tau}_{ij}) \qquad \text{where } e = \hat{u} + \tfrac{1}{2}V^2 + gz \qquad (4.48)$$

A more useful form is obtained if we split up the viscous-work term

$$\nabla \cdot (\mathbf{V} \cdot \boldsymbol{\tau}_{ij}) \equiv \mathbf{V} \cdot (\nabla \cdot \boldsymbol{\tau}_{ij}) + \Phi$$



ketabline.com Ebook.ketabline.com

where Φ is short for the *viscous-dissipation function*.[7] For a newtonian incompressible viscous fluid, this function has the form

$$\Phi = \mu\left[2\left(\frac{\partial u}{\partial x}\right)^2 + 2\left(\frac{\partial v}{\partial y}\right)^2 + 2\left(\frac{\partial w}{\partial z}\right)^2 + \left(\frac{\partial v}{\partial x} + \frac{\partial u}{\partial y}\right)^2 + \left(\frac{\partial w}{\partial y} + \frac{\partial v}{\partial z}\right)^2 + \left(\frac{\partial u}{\partial z} + \frac{\partial w}{\partial x}\right)^2\right] \tag{4.50}$$

Since all terms are quadratic, viscous dissipation is always positive, so that a viscous flow always tends to lose its available energy due to dissipation, in accordance with the second law of thermodynamics.

Now substitute Eq. (4.49) into Eq. (4.48), using the linear-momentum equation (4.32) to eliminate $\nabla \cdot \boldsymbol{\tau}_{ij}$. This will cause the kinetic and potential energies to cancel, leaving a more customary form of the general differential energy equation

$$\rho \frac{d\hat{u}}{dt} + p(\nabla \cdot \mathbf{V}) = \nabla \cdot (k \nabla T) + \Phi \tag{4.51}$$

This equation is valid for a newtonian fluid under very general conditions of unsteady, compressible, viscous, heat-conducting flow, except that it neglects radiation heat transfer and internal *sources* of heat that might occur during a chemical or nuclear reaction.

Equation (4.51) is too difficult to analyze except on a digital computer [1]. It is customary to make the following approximations:

$$d\hat{u} \approx c_v \, dT \qquad c_v, \, \mu, \, k, \, \rho \approx \text{const} \tag{4.52}$$

Equation (4.51) then takes the simpler form

$$\rho c_v \frac{dT}{dt} = k\nabla^2 T + \Phi \tag{4.53}$$

which involves temperature T as the sole primary variable plus velocity as a secondary variable through the total time-derivative operator

$$\frac{dT}{dt} = \frac{\partial T}{\partial t} + u\frac{\partial T}{\partial x} + v\frac{\partial T}{\partial y} + w\frac{\partial T}{\partial z} \tag{4.54}$$

A great many interesting solutions to Eq. (4.53) are known for various flow conditions, and extended treatments are given in advanced books on viscous flow [4, 5] and books on heat transfer [7, 8].

One well-known special case of Eq. (4.53) occurs when the fluid is at rest or has negligible velocity, where the dissipation Φ and convective terms become negligible

$$\rho c_v \frac{\partial T}{\partial t} = k \nabla^2 T \tag{4.55}$$

This is called the *heat-conduction equation* in applied mathematics and is valid for solids and fluids at rest. The solution to Eq. (4.55) for various conditions is a large part of courses and books on heat transfer.

This completes the derivation of the basic differential equations of fluid moti

[7] For further details, see, e.g., Ref. 5, p. 72.



ketabline.com Ebook.ketabline.com

4.6 Boundary Conditions for the Basic Equations

There are three basic differential equations of fluid motion, just derived. Let us summarize them here:

Continuity:
$$\frac{\partial \rho}{\partial t} + \nabla \cdot (\rho \mathbf{V}) = 0 \tag{4.56}$$

Momentum:
$$\rho \frac{d\mathbf{V}}{dt} = \rho \mathbf{g} - \nabla p + \nabla \cdot \boldsymbol{\tau}_{ij} \tag{4.57}$$

Energy:
$$\rho \frac{d\hat{u}}{dt} + p(\nabla \cdot \mathbf{V}) = \nabla \cdot (k \nabla T) + \Phi \tag{4.58}$$

where Φ is given by Eq. (4.50). In general, the density is variable, so that these three equations contain five unknowns, ρ, V, p, $\hat{u}$, and T. Therefore we need two additional relations to complete the system of equations. These are provided by data or algebraic expressions for the state relations of the thermodynamic properties

$$\rho = \rho(p, T) \qquad \hat{u} = \hat{u}(p, T) \tag{4.59}$$

For example, for a perfect gas with constant specific heats, we complete the system with

$$\rho = \frac{p}{RT} \qquad \hat{u} = \int c_v \, dT \approx c_v T + \text{const} \tag{4.60}$$

It is shown in advanced books [4, 5] that this system of equations (4.56) to (4.59) is well posed and can be solved analytically or numerically, subject to the proper boundary conditions.

What are the proper boundary conditions? First, if the flow is unsteady, there must be an *initial condition* or initial spatial distribution known for each variable:

At $t = 0$:
$$\rho, V, p, \hat{u}, T = \text{known } f(x, y, z) \tag{4.61}$$

Thereafter, for all times t to be analyzed, we must know something about the variables at each *boundary* enclosing the flow.

Figure 4.7 illustrates the three most common types of boundaries encountered in fluid-flow analysis: a solid wall, an inlet or outlet, a liquid-gas interface.

First, for a solid, impermeable wall, there is no slip and no temperature jump in a viscous heat-conducting fluid

$$\mathbf{V}_{\text{fluid}} = \mathbf{V}_{\text{wall}} \qquad T_{\text{fluid}} = T_{\text{wall}} \qquad \text{solid wall} \tag{4.62}$$

The only exception to Eq. (4.62) occurs in an extremely rarefied gas flow, where slippage can be present [5].

Second, at any inlet or outlet section of the flow, the complete distribution of velocity, pressure, and temperature must be known for all times:

Inlet or outlet:
$$\text{Known } \mathbf{V}, p, T \tag{4.63}$$

These inlet and outlet sections can be and often are at $\pm \infty$, simulating a body immersed in an infinite expanse of fluid.

Finally, the most complex conditions occur at a liquid-gas interface, or free surface, as sketched in Fig. 4.7. Let us denote the interface by

Interface:
$$z = \eta(x, y, t)$$



ketabline.com Ebook.ketabline.com

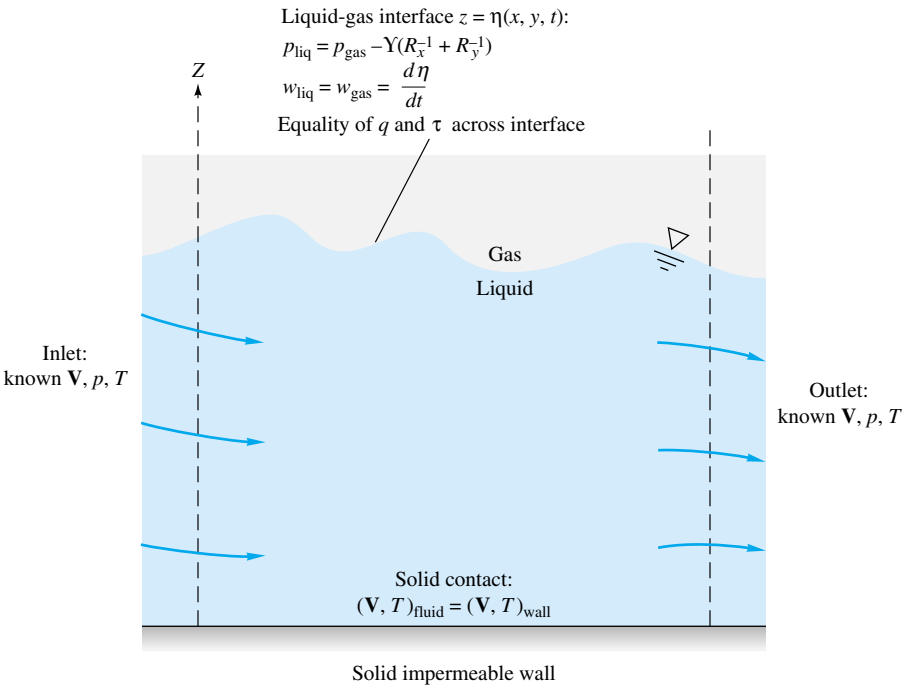


Fig. 4.7 Typical boundary conditions in a viscous heat-conducting fluid-flow analysis.

Then there must be equality of vertical velocity across the interface, so that no holes appear between liquid and gas:

$$w_{\text{liq}} = w_{\text{gas}} = \frac{d\eta}{dt} = \frac{\partial \eta}{\partial t} + u\frac{\partial \eta}{\partial x} + v\frac{\partial \eta}{\partial y} \tag{4.65}$$

This is called the *kinematic boundary condition*.

There must be mechanical equilibrium across the interface. The viscous-shear stresses must balance

$$(\tau_{zy})_{\text{liq}} = (\tau_{zy})_{\text{gas}} \qquad (\tau_{zx})_{\text{liq}} = (\tau_{zx})_{\text{gas}} \tag{4.66}$$

Neglecting the viscous normal stresses, the pressures must balance at the interface except for surface-tension effects

$$p_{\text{liq}} = p_{\text{gas}} - \Upsilon(R_x^{-1} + R_y^{-1}) \tag{4.67}$$

which is equivalent to Eq. (1.34). The radii of curvature can be written in terms of the free-surface position η

$$R_x^{-1} + R_y^{-1} = \frac{\partial}{\partial x}\left[\frac{\partial \eta/\partial x}{\sqrt{1 + (\partial \eta/\partial x)^2 + (\partial \eta/\partial y)^2}}\right] + \frac{\partial}{\partial y}\left[\frac{\partial \eta/\partial y}{\sqrt{1 + (\partial \eta/\partial x)^2 + (\partial \eta/\partial y)^2}}\right]$$



ketabline.com Ebook.ketabline.com

Finally, the heat transfer must be the same on both sides of the interface, since no heat can be stored in the infinitesimally thin interface

$$(q_z)_{\text{liq}} = (q_z)_{\text{gas}} \tag{4.69}$$

Neglecting radiation, this is equivalent to

$$\left(k\,\frac{\partial T}{\partial z}\right)_{\text{liq}} = \left(k\,\frac{\partial T}{\partial z}\right)_{\text{gas}} \tag{4.70}$$

This is as much detail as we wish to give at this level of exposition. Further and even more complicated details on fluid-flow boundary conditions are given in Refs. 5 and 9.

Simplified Free-Surface Conditions

In the introductory analyses given in this book, such as open-channel flows in Chap. 10, we shall back away from the exact conditions (4.65) to (4.69) and assume that the upper fluid is an "atmosphere" which merely exerts pressure upon the lower fluid, with shear and heat conduction negligible. We also neglect nonlinear terms involving the slopes of the free surface. We then have a much simpler and linear set of conditions at the surface

$$p_{\text{liq}} \approx p_{\text{gas}} - \Upsilon\left(\frac{\partial^2 \eta}{\partial x^2} + \frac{\partial^2 \eta}{\partial y^2}\right) \qquad w_{\text{liq}} \approx \frac{\partial \eta}{\partial t}$$

$$\left(\frac{\partial V}{\partial z}\right)_{\text{liq}} \approx 0 \qquad \left(\frac{\partial T}{\partial z}\right)_{\text{liq}} \approx 0 \tag{4.71}$$

In many cases, such as open-channel flow, we can also neglect surface tension, so that

$$p_{\text{liq}} \approx p_{\text{atm}} \tag{4.72}$$

These are the types of approximations which will be used in Chap. 10. The nondimensional forms of these conditions will also be useful in Chap. 5.

Incompressible Flow with Constant Properties

Flow with constant ρ, μ, and k is a basic simplification which will be used, e.g., throughout Chap. 6. The basic equations of motion (4.56) to (4.58) reduce to:

Continuity: $$\boldsymbol{\nabla} \cdot \mathbf{V} = 0 \tag{4.73}$$

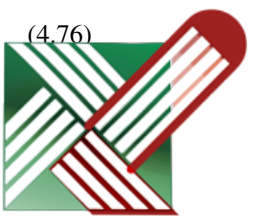
Momentum: $$\rho \frac{d\mathbf{V}}{dt} = \rho \mathbf{g} - \boldsymbol{\nabla} p + \mu\, \nabla^2 \mathbf{V} \tag{4.74}$$

Energy: $$\rho c_v \frac{dT}{dt} = k\, \nabla^2 T + \Phi \tag{4.75}$$

Since ρ is constant, there are only three unknowns: p, $\mathbf{V}$, and T. The system is closed.[8] Not only that, the system splits apart: Continuity and momentum are independent of T. Thus we can solve Eqs. (4.73) and (4.74) entirely separately for the pressure and velocity, using such boundary conditions as

Solid surface: $$\mathbf{V} = \mathbf{V}_{\text{wall}} \tag{4.76}$$

[8]For this system, what are the thermodynamic equivalents to Eq. (4.59)?



ketabline.com Ebook.ketabline.com

Inlet or outlet: Known $\mathbf{V}$, p (4.77)

Free surface: $p \approx p_a \qquad w \approx \dfrac{\partial \eta}{\partial t}$ (4.78)

Later, entirely at our leisure,[9] we can solve for the temperature distribution from Eq. (4.75), which depends upon velocity $\mathbf{V}$ through the dissipation Φ and the total time-derivative operator d/dt.

Inviscid-Flow Approximations

Chapter 8 assumes inviscid flow throughout, for which the viscosity $\mu = 0$. The momentum equation (4.74) reduces to

$$\rho \frac{d\mathbf{V}}{dt} = \rho \mathbf{g} - \nabla p \tag{4.79}$$

This is *Euler's equation*; it can be integrated along a streamline to obtain Bernoulli's equation (see Sec. 4.9). By neglecting viscosity we have lost the second-order derivative of $\mathbf{V}$ in Eq. (4.74); therefore we must relax one boundary condition on velocity. The only mathematically sensible condition to drop is the no-slip condition at the wall. We let the flow slip parallel to the wall but do not allow it to flow into the wall. The proper inviscid condition is that the normal velocities must match at any solid surface:

Inviscid flow: $(V_n)_{\text{fluid}} = (V_n)_{\text{wall}}$ (4.80)

In most cases the wall is fixed; therefore the proper inviscid-flow condition is

$$V_n = 0 \tag{4.81}$$

There is *no* condition whatever on the tangential velocity component at the wall in inviscid flow. The tangential velocity will be part of the solution, and the correct value will appear after the analysis is completed (see Chap. 8).

EXAMPLE 4.6

For steady incompressible laminar flow through a long tube, the velocity distribution is given by

$$v_z = U\left(1 - \frac{r^2}{R^2}\right) \qquad v_r = v_\theta = 0$$

where U is the maximum, or centerline, velocity and R is the tube radius. If the wall temperature is constant at T_w and the temperature $T = T(r)$ only, find $T(r)$ for this flow.

Solution

With $T = T(r)$, Eq. (4.75) reduces for steady flow to

$$\rho c_v v_r \frac{dT}{dr} = \frac{k}{r}\frac{d}{dr}\left(r\frac{dT}{dr}\right) + \mu\left(\frac{dv_z}{dr}\right)^2 \tag{1}$$

[9]Since temperature is entirely *uncoupled* by this assumption, we may never get a here and may ask you to wait until a course on heat transfer.



ketabline.com Ebook.ketabline.com

But since $v_r = 0$ for this flow, the convective term on the left vanishes. Introduce v_z into Eq. (1) to obtain

$$\frac{k}{r}\frac{d}{dr}\left(r\frac{dT}{dr}\right)^2 = -\mu\left(\frac{dv_z}{dr}\right)^2 = -\frac{4U^2\mu r^2}{R^4} \tag{2}$$

Multiply through by r/k and integrate once:

$$r\frac{dT}{dr} = -\frac{\mu U^2 r^4}{kR^4} + C_1 \tag{3}$$

Divide through by r and integrate once again:

$$T = -\frac{\mu U^2 r^4}{4kR^4} + C_1 \ln r + C_2 \tag{4}$$

Now we are in position to apply our boundary conditions to evaluate C_1 and C_2.

First, since the logarithm of zero is $-\infty$, the temperature at $r = 0$ will be infinite unless

$$C_1 = 0 \tag{5}$$

Thus we eliminate the possibility of a logarithmic singularity. The same thing will happen if we apply the *symmetry* condition $dT/dr = 0$ at $r = 0$ to Eq. (3). The constant C_2 is then found by the wall-temperature condition at $r = R$

$$T = T_w = -\frac{\mu U^2}{4k} + C_2$$

or

$$C_2 = T_w + \frac{\mu U^2}{4k} \tag{6}$$

The correct solution is thus

$$T(r) = T_w + \frac{\mu U^2}{4k}\left(1 - \frac{r^4}{R^4}\right) \qquad \textit{Ans.} \tag{7}$$

which is a fourth-order parabolic distribution with a maximum value $T_0 = T_w + \mu U^2/(4k)$ at the centerline.

4.7 The Stream Function

We have seen in Sec. 4.6 that even if the temperature is uncoupled from our system of equations of motion, we must solve the continuity and momentum equations simultaneously for pressure and velocity. The *stream function* ψ is a clever device which allows us to wipe out the continuity equation and solve the momentum equation directly for the single variable ψ.

The stream-function idea works only if the continuity equation (4.56) can be reduced to *two* terms. In general, we have *four* terms:

Cartesian:
$$\frac{\partial \rho}{\partial t} + \frac{\partial}{\partial x}(\rho u) + \frac{\partial}{\partial y}(\rho v) + \frac{\partial}{\partial z}(\rho w) = 0 \tag{4.82a}$$

Cylindrical:
$$\frac{\partial \rho}{\partial t} + \frac{1}{r}\frac{\partial}{\partial r}(r\rho v_r) + \frac{1}{r}\frac{\partial}{\partial \theta}(\rho v_\theta) + \frac{\partial}{\partial z}(\rho v_z) = 0$$



ketabline.com Ebook.ketabline.com

First, let us eliminate unsteady flow, which is a peculiar and unrealistic application of the stream-function idea. Reduce either of Eqs. (4.82) to any *two* terms. The most common application is incompressible flow in the xy plane

$$\frac{\partial u}{\partial x} + \frac{\partial v}{\partial y} = 0 \tag{4.83}$$

This equation is satisfied *identically* if a function $\psi(x, y)$ is defined such that Eq. (4.83) becomes

$$\frac{\partial}{\partial x}\left(\frac{\partial \psi}{\partial y}\right) + \frac{\partial}{\partial y}\left(-\frac{\partial \psi}{\partial x}\right) \equiv 0 \tag{4.84}$$

Comparison of (4.83) and (4.84) shows that this new function ψ must be defined such that

$$u = \frac{\partial \psi}{\partial y} \qquad v = -\frac{\partial \psi}{\partial x} \tag{4.85}$$

or

$$\mathbf{V} = \mathbf{i}\frac{\partial \psi}{\partial y} - \mathbf{j}\frac{\partial \psi}{\partial x}$$

Is this legitimate? Yes, it is just a mathematical trick of replacing two variables (u and v) by a single higher-order function ψ. The vorticity, or curl $\mathbf{V}$, is an interesting function

$$\text{curl } \mathbf{V} = 2\mathbf{k}\omega_z = -\mathbf{k}\nabla^2\psi \qquad \text{where} \qquad \nabla^2\psi = \frac{\partial^2 \psi}{\partial x^2} + \frac{\partial^2 \psi}{\partial y^2} \tag{4.86}$$

Thus, if we take the curl of the momentum equation (4.74) and utilize Eq. (4.86), we obtain a single equation for ψ

$$\frac{\partial \psi}{\partial y}\frac{\partial}{\partial x}(\nabla^2\psi) - \frac{\partial \psi}{\partial x}\frac{\partial}{\partial y}(\nabla^2\psi) = \nu\nabla^2(\nabla^2\psi) \tag{4.87}$$

where $\nu = \mu/\rho$ is the kinematic viscosity. This is partly a victory and partly a defeat: Eq. (4.87) is scalar and has only one variable, ψ, but it now contains *fourth*-order derivatives and probably will require computer analysis. There will be four boundary conditions required on ψ. For example, for the flow of a uniform stream in the x direction past a solid body, the four conditions would be

$$\begin{aligned} &\text{At infinity:} && \frac{\partial \psi}{\partial y} = U_\infty \qquad \frac{\partial \psi}{\partial x} = 0 \\ &\text{At the body:} && \frac{\partial \psi}{\partial y} = \frac{\partial \psi}{\partial x} = 0 \end{aligned} \tag{4.88}$$

Many examples of numerical solution of Eqs. (4.87) and (4.88) are given in Ref. 1.

One important application is inviscid *irrotational* flow in the xy plane, where $\omega_z \equiv 0$. Equations (4.86) and (4.87) reduce to

$$\nabla^2\psi = \frac{\partial^2 \psi}{\partial x^2} + \frac{\partial^2 \psi}{\partial y^2} = 0 \tag{4.89}$$

This is the second-order *Laplace equation* (Chap. 8), for which many analytical techniques are known. Also, boundary conditions like Eq. (



ketabline.com Ebook.ketabline.com

At infinity: $$\psi = U_\infty y + \text{const} \tag{4.90}$$

At the body: $$\psi = \text{const}$$

It is well within our capability to find some useful solutions to Eqs. (4.89) and (4.90), which we shall do in Chap. 8.

Geometric Interpretation of ψ

The fancy mathematics above would serve by itself to make the stream function immortal and always useful to engineers. Even better, though, ψ has a beautiful geometric interpretation: Lines of constant ψ are *streamlines* of the flow. This can be shown as follows. From Eq. (1.41) the definition of a streamline in two-dimensional flow is

$$\frac{dx}{u} = \frac{dy}{v}$$

or $$u\,dy - v\,dx = 0 \qquad \text{streamline} \tag{4.91}$$

Introducing the stream function from Eq. (4.85), we have

$$\frac{\partial \psi}{\partial x}\,dx + \frac{\partial \psi}{\partial y}\,dy = 0 = d\psi \tag{4.92}$$

Thus the change in ψ is zero along a streamline, or

$$\psi = \text{const along a streamline} \tag{4.93}$$

Having found a given solution $\psi(x, y)$, we can plot lines of constant ψ to give the streamlines of the flow.

There is also a physical interpretation which relates ψ to volume flow. From Fig. 4.8, we can compute the volume flow dQ through an element ds of control surface of unit depth

$$dQ = (\mathbf{V} \cdot \mathbf{n})\,dA = \left(\mathbf{i}\frac{\partial \psi}{\partial y} - \mathbf{j}\frac{\partial \psi}{\partial x}\right) \cdot \left(\mathbf{i}\frac{dy}{ds} - \mathbf{j}\frac{dx}{ds}\right) ds(1)$$

$$= \frac{\partial \psi}{\partial x}\,dx + \frac{\partial \psi}{\partial y}\,dy = d\psi \tag{4.94}$$

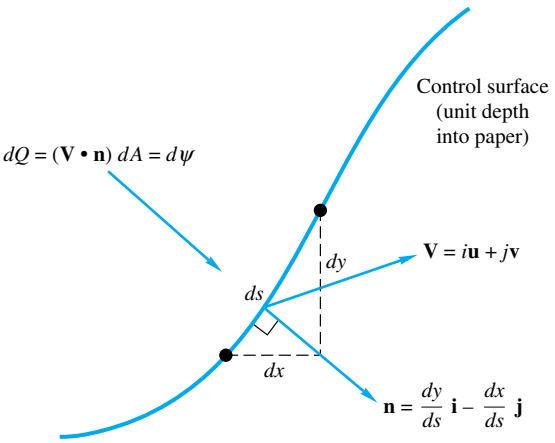


Fig. 4.8 Geometric interpretation of stream function: volume flow through a differential portion of a control surface.



ketabline.com Ebook.ketabline.com

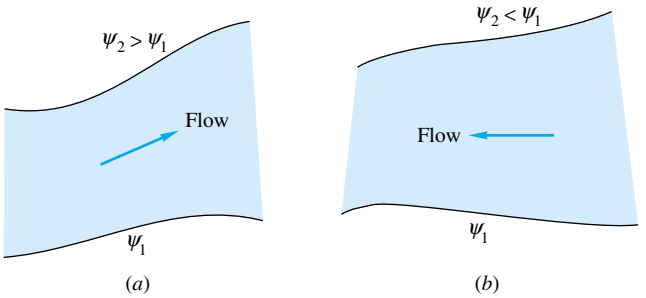


Fig. 4.9 Sign convention for flow in terms of change in stream function: (*a*) flow to the right if ψ_U is greater; (*b*) flow to the left if ψ_L is greater.

Thus the change in ψ across the element is numerically equal to the volume flow through the element. The volume flow between any two points in the flow field is equal to the change in stream function between those points:

$$Q_{1\to 2} = \int_1^2 (\mathbf{V}\cdot\mathbf{n})\, dA = \int_1^2 d\psi = \psi_2 - \psi_1 \tag{4.95}$$

Further, the direction of the flow can be ascertained by noting whether ψ increases or decreases. As sketched in Fig. 4.9, the flow is to the right if ψ_U is greater than ψ_L, where the subscripts stand for upper and lower, as before; otherwise the flow is to the left.

Both the stream function and the velocity potential were invented by the French mathematician Joseph Louis Lagrange and published in his treatise on fluid mechanics in 1781.

EXAMPLE 4.7

If a stream function exists for the velocity field of Example 4.5

$$u = a(x^2 - y^2) \quad v = -2axy \quad w = 0$$

find it, plot it, and interpret it.

Solution

Since this flow field was shown expressly in Example 4.3 to satisfy the equation of continuity, we are pretty sure that a stream function does exist. We can check again to see if

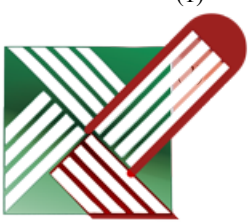
$$\frac{\partial u}{\partial x} + \frac{\partial v}{\partial y} = 0$$

Substitute: $2ax + (-2ax) = 0$ checks

Therefore we are certain that a stream function exists. To find ψ, we simply set

$$u = \frac{\partial \psi}{\partial y} = ax^2 - ay^2 \tag{1}$$

$$v = -\frac{\partial \psi}{\partial x} = -2axy$$



ketabline.com Ebook.ketabline.com

and work from either one toward the other. Integrate (1) partially

$$\psi = ax^2y - \frac{ay^3}{3} + f(x) \tag{3}$$

Differentiate (3) with respect to x and compare with (2)

$$\frac{\partial \psi}{\partial x} = 2axy + f'(x) = 2axy \tag{4}$$

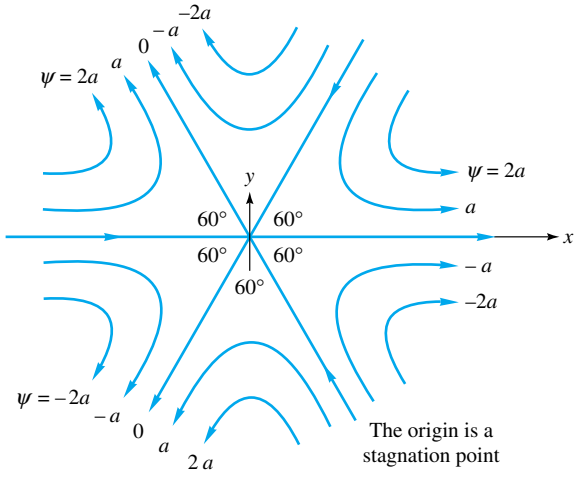
Therefore $f'(x) = 0$, or $f =$ constant. The complete stream function is thus found

$$\psi = a\left(x^2y - \frac{y^3}{3}\right) + C \qquad \textit{Ans.} \tag{5}$$

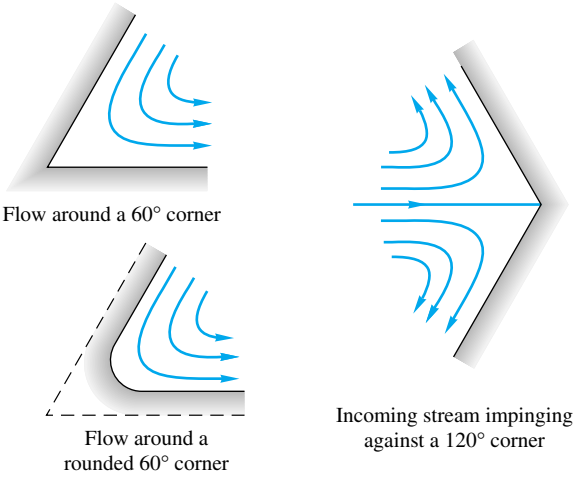
To plot this, set $C = 0$ for convenience and plot the function

$$3x^2y - y^3 = \frac{3\psi}{a} \tag{6}$$

for constant values of ψ. The result is shown in Fig. E4.7*a* to be six 60° wedges of circulating motion, each with identical flow patterns except for the arrows. Once the streamlines are labeled, the flow directions follow from the sign convention of Fig. 4.9. How can the flow be interpreted? Since there is slip along all streamlines, no streamline can truly represent a solid surface in a viscous flow. However, the flow could represent the impingement of three incoming streams at 60, 180, and 300°. This would be a rather unrealistic yet exact solution to the Navier-Stokes equation, as we showed in Example 4.5.



E4.7a



E4.7b

By allowing the flow to slip as a frictionless approximation, we could let any given streamline be a body shape. Some examples are shown in Fig. E4.7*b*.

A stream function also exists in a variety of other physical situations wh
two coordinates are needed to define the flow. Three examples are illustrated



ketabline.com Ebook.ketabline.com

Steady Plane Compressible Flow

Suppose now that the density is variable but that $w = 0$, so that the flow is in the xy plane. Then the equation of continuity becomes

$$\frac{\partial}{\partial x}(\rho u) + \frac{\partial}{\partial y}(\rho v) = 0 \tag{4.96}$$

We see that this is in exactly the same form as Eq. (4.84). Therefore a compressible-flow stream function can be defined such that

$$\rho u = \frac{\partial \psi}{\partial y} \qquad \rho v = -\frac{\partial \psi}{\partial x} \tag{4.97}$$

Again lines of constant ψ are streamlines of the flow, but the change in ψ is now equal to the *mass* flow, not the volume flow

$$d\dot{m} = \rho(\mathbf{V} \cdot \mathbf{n})\, dA = d\psi$$

or

$$\dot{m}_{1\to 2} = \int_1^2 \rho(\mathbf{V} \cdot \mathbf{n})\, dA = \psi_2 - \psi_1 \tag{4.98}$$

The sign convention on flow direction is the same as in Fig. 4.9. This particular stream function combines density with velocity and must be substituted into not only momentum but also the energy and state relations (4.58) and (4.59) with pressure and temperature as companion variables. Thus the compressible stream function is not a great victory, and further assumptions must be made to effect an analytical solution to a typical problem (see, e.g., Ref. 5, chap. 7).

Incompressible Plane Flow in Polar Coordinates

Suppose that the important coordinates are r and θ, with $v_z = 0$, and that the density is constant. Then Eq. (4.82*b*) reduces to

$$\frac{1}{r}\frac{\partial}{\partial r}(r v_r) + \frac{1}{r}\frac{\partial}{\partial \theta}(v_\theta) = 0 \tag{4.99}$$

After multiplying through by r, we see that this is the same as the analogous form of Eq. (4.84)

$$\frac{\partial}{\partial r}\left(\frac{\partial \psi}{\partial \theta}\right) + \frac{\partial}{\partial \theta}\left(-\frac{\partial \psi}{\partial r}\right) = 0 \tag{4.100}$$

By comparison of (4.99) and (4.100) we deduce the form of the incompressible polar-coordinate stream function

$$v_r = \frac{1}{r}\frac{\partial \psi}{\partial \theta} \qquad v_\theta = -\frac{\partial \psi}{\partial r} \tag{4.101}$$

Once again lines of constant ψ are streamlines, and the change in ψ is the *volume flow* $Q_{1\to 2} = \psi_2 - \psi_1$. The sign convention is the same as in Fig. 4.9. This type of stream function is very useful in analyzing flows with cylinders, vortices, sources, and sinks (Chap. 8).

Incompressible Axisymmetric Flow

As a final example, suppose that the flow is three-dimensional (v_r, v cumferential variations, $v_\theta = \partial/\partial\theta = 0$ (see Fig. 4.2 for definition of



ketabline.com Ebook.ketabline.com

a flow is termed *axisymmetric*, and the flow pattern is the same when viewed on any meridional plane through the axis of revolution z. For incompressible flow, Eq. (4.82*b*) becomes

$$\frac{1}{r}\frac{\partial}{\partial r}(rv_r) + \frac{\partial}{\partial z}(v_z) = 0 \tag{4.102}$$

This doesn't seem to work: Can't we get rid of the one r outside? But when we realize that r and z are independent coordinates, Eq. (4.102) can be rewritten as

$$\frac{\partial}{\partial r}(rv_r) + \frac{\partial}{\partial z}(rv_z) = 0 \tag{4.103}$$

By analogy with Eq. (4.84), this has the form

$$\frac{\partial}{\partial r}\left(-\frac{\partial \psi}{\partial z}\right) + \frac{\partial}{\partial z}\left(\frac{\partial \psi}{\partial r}\right) = 0 \tag{4.104}$$

By comparing (4.103) and (4.104), we deduce the form of an incompressible axisymmetric stream function $\psi(r, z)$

$$v_r = -\frac{1}{r}\frac{\partial \psi}{\partial z} \qquad v_z = \frac{1}{r}\frac{\partial \psi}{\partial r} \tag{4.105}$$

Here again lines of constant ψ are streamlines, but there is a factor (2π) in the volume flow: $Q_{1\to 2} = 2\pi(\psi_2 - \psi_1)$. The sign convention on flow is the same as in Fig. 4.9.

EXAMPLE 4.8

Investigate the stream function in polar coordinates

$$\psi = U \sin\theta\left(r - \frac{R^2}{r}\right) \tag{1}$$

where U and R are constants, a velocity and a length, respectively. Plot the streamlines. What does the flow represent? Is it a realistic solution to the basic equations?

Solution

The streamlines are lines of constant ψ, which has units of square meters per second. Note that $\psi/(UR)$ is dimensionless. Rewrite Eq. (1) in dimensionless form

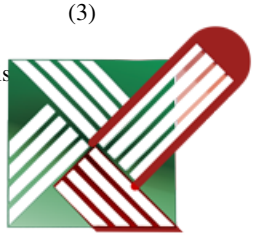
$$\frac{\psi}{UR} = \sin\theta\left(\eta - \frac{1}{\eta}\right) \qquad \eta = \frac{r}{R} \tag{2}$$

Of particular interest is the special line $\psi = 0$. From Eq. (1) or (2) this occurs when (*a*) $\theta = 0$ or 180° and (*b*) $r = R$. Case (*a*) is the x-axis, and case (*b*) is a circle of radius R, both of which are plotted in Fig. E4.8.

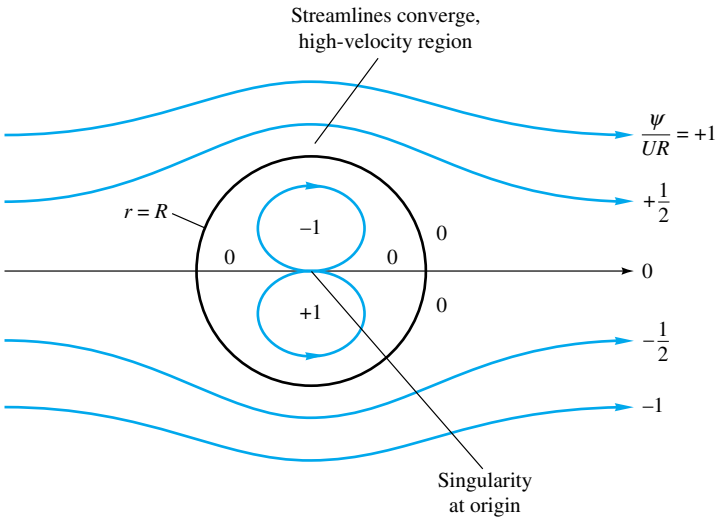
For any other nonzero value of ψ it is easiest to pick a value of r and solve for θ:

$$\sin\theta = \frac{\psi/(UR)}{r/R - R/r} \tag{3}$$

In general, there will be two solutions for θ because of the symmetry about the y-axis ample take $\psi/(UR) = +1.0$:



ketabline.com Ebook.ketabline.com



E4.8

Guess r/R	3.0	2.5	2.0	1.8	1.7	1.618
Compute θ	22° 158°	28° 152°	42° 138°	54° 156°	64° 116°	90°

This line is plotted in Fig. E4.8 and passes over the circle $r = R$. You have to watch it, though, because there is a second curve for $\psi/(UR) = +1.0$ for small $r < R$ below the x-axis:

Guess r/R	0.618	0.6	0.5	0.4	0.3	0.2	0.1
Compute θ	−90°	−70° −110°	−42° −138°	−28° −152°	−19° −161°	−12° −168°	−6° −174°

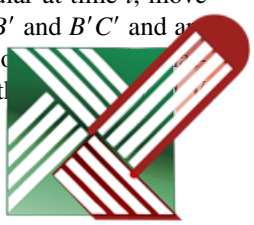
This second curve plots as a closed curve inside the circle $r = R$. There is a singularity of infinite velocity and indeterminate flow direction at the origin. Figure E4.8 shows the full pattern.

The given stream function, Eq. (1), is an exact and classic solution to the momentum equation (4.38) for frictionless flow. Outside the circle $r = R$ it represents two-dimensional inviscid flow of a uniform stream past a circular cylinder (Sec. 8.3). Inside the circle it represents a rather unrealistic trapped circulating motion of what is called a *line doublet*.

4.8 Vorticity and Irrotationality

The assumption of zero fluid angular velocity, or irrotationality, is a very useful simplification. Here we show that angular velocity is associated with the curl of the local-velocity vector.

The differential relations for deformation of a fluid element can be derived by examining Fig. 4.10. Two fluid lines AB and BC, initially perpendicular at time t, move and deform so that at $t + dt$ they have slightly different lengths $A'B'$ and $B'C'$ and a slightly off the perpendicular by angles $d\alpha$ and $d\beta$. Such deformati ically because A, B, and C have slightly different velocities when t



ketabline.com Ebook.ketabline.com

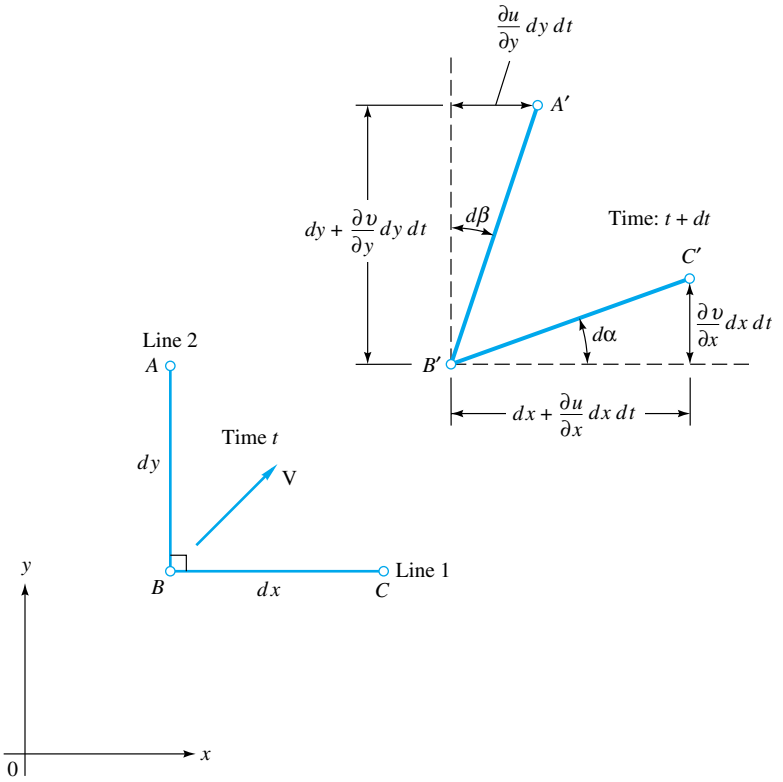


Fig. 4.10 Angular velocity and strain rate of two fluid lines deforming in the *xy* plane.

has spatial gradients. All these differential changes in the motion of *A*, *B*, and *C* are noted in Fig. 4.10.

We define the angular velocity ω_z about the *z* axis as the average rate of counterclockwise turning of the two lines

$$\omega_z = \frac{1}{2}\left(\frac{d\alpha}{dt} - \frac{d\beta}{dt}\right) \tag{4.106}$$

But from Fig. 4.10, $d\alpha$ and $d\beta$ are each directly related to velocity derivatives in the limit of small dt

$$\begin{aligned} d\alpha &= \lim_{dt\to 0}\left[\tan^{-1}\frac{(\partial v/\partial x)\,dx\,dt}{dx + (\partial u/\partial x)\,dx\,dt}\right] = \frac{\partial v}{\partial x}\,dt \\ d\beta &= \lim_{dt\to 0}\left[\tan^{-1}\frac{(\partial u/\partial y)\,dy\,dt}{dy + (\partial v/\partial y)\,dy\,dt}\right] = \frac{\partial u}{\partial y}\,dt \end{aligned} \tag{4.107}$$

Combining Eqs. (4.106) and (4.107) gives the desired result:

$$\omega_z = \frac{1}{2}\left(\frac{\partial v}{\partial x} - \frac{\partial u}{\partial y}\right) \tag{4.108}$$

In exactly similar manner we determine the other two rates:

$$\omega_x = \frac{1}{2}\left(\frac{\partial w}{\partial y} - \frac{\partial v}{\partial z}\right) \qquad \omega_y = \frac{1}{2}\left(\frac{\partial u}{\partial z} - \frac{\partial w}{\partial x}\right)$$



ketabline.com Ebook.ketabline.com

The vector $\omega = \mathbf{i}\omega_x + \mathbf{j}\omega_y + \mathbf{k}\omega_z$ is thus one-half the curl of the velocity vector

$$\omega = \frac{1}{2}(\text{curl } \mathbf{V}) = \frac{1}{2}\begin{vmatrix} \mathbf{i} & \mathbf{j} & \mathbf{k} \\ \dfrac{\partial}{\partial x} & \dfrac{\partial}{\partial y} & \dfrac{\partial}{\partial z} \\ u & v & w \end{vmatrix} \tag{4.110}$$

Since the factor of $\frac{1}{2}$ is annoying, many workers prefer to use a vector twice as large, called the *vorticity*:

$$\boldsymbol{\zeta} = 2\boldsymbol{\omega} = \text{curl } \mathbf{V} \tag{4.111}$$

Many flows have negligible or zero vorticity and are called *irrotational*

$$\text{curl } \mathbf{V} \equiv 0 \tag{4.112}$$

The next section expands on this idea. Such flows can be incompressible or compressible, steady or unsteady.

We may also note that Fig. 4.10 demonstrates the *shear-strain rate* of the element, which is defined as the rate of closure of the initially perpendicular lines

$$\dot{\epsilon}_{xy} = \frac{d\alpha}{dt} + \frac{d\beta}{dt} = \frac{\partial v}{\partial x} + \frac{\partial u}{\partial y} \tag{4.113}$$

When multiplied by viscosity μ, this equals the shear stress τ_{xy} in a newtonian fluid, as discussed earlier in Eqs. (4.37). Appendix E lists strain-rate and vorticity components in cylindrical coordinates.

4.9 Frictionless Irrotational Flows

When a flow is both frictionless and irrotational, pleasant things happen. First, the momentum equation (4.38) reduces to Euler's equation

$$\rho \frac{d\mathbf{V}}{dt} = \rho\mathbf{g} - \boldsymbol{\nabla} p \tag{4.114}$$

Second, there is a great simplification in the acceleration term. Recall from Sec. 4.1 that acceleration has two terms

$$\frac{d\mathbf{V}}{dt} = \frac{\partial \mathbf{V}}{\partial t} + (\mathbf{V} \cdot \boldsymbol{\nabla})\mathbf{V} \tag{4.2}$$

A beautiful vector identity exists for the second term [11]:

$$(\mathbf{V} \cdot \boldsymbol{\nabla})\mathbf{V} \equiv \boldsymbol{\nabla}(\tfrac{1}{2}V^2) + \boldsymbol{\zeta} \times \mathbf{V} \tag{4.115}$$

where $\zeta = \text{curl } \mathbf{V}$ from Eq. (4.111) is the fluid vorticity.

Now combine (4.114) and (4.115), divide by ρ, and rearrange on the left-hand side. Dot the entire equation into an arbitrary vector displacement $d\mathbf{r}$:

$$\left[\frac{\partial \mathbf{V}}{\partial t} + \boldsymbol{\nabla}\left(\frac{1}{2}V^2\right) + \boldsymbol{\zeta} \times \mathbf{V} + \frac{1}{\rho}\boldsymbol{\nabla} p - \mathbf{g}\right] \cdot d\mathbf{r} = 0 \tag{4.116}$$

Nothing works right unless we can get rid of the third term. We want

$$(\boldsymbol{\zeta} \times \mathbf{V}) \cdot (d\mathbf{r}) \equiv 0$$



ketabline.com Ebook.ketabline.com

This will be true under various conditions:

1. $\mathbf{V}$ is zero; trivial, no flow (hydrostatics).
2. $\boldsymbol{\zeta}$ is zero; irrotational flow.
3. $d\mathbf{r}$ is perpendicular to $\boldsymbol{\zeta} \times \mathbf{V}$; this is rather specialized and rare.
4. $d\mathbf{r}$ is parallel to $\mathbf{V}$; we integrate *along a streamline* (see Sec. 3.7).

Condition 4 is the common assumption. If we integrate along a streamline in frictionless compressible flow and take, for convenience, $\mathbf{g} = -g\mathbf{k}$, Eq. (4.116) reduces to

$$\frac{\partial \mathbf{V}}{\partial t} \cdot d\mathbf{r} + d\left(\frac{1}{2} V^2\right) + \frac{dp}{\rho} + g\, dz = 0 \tag{4.118}$$

Except for the first term, these are exact differentials. Integrate between any two points 1 and 2 along the streamline:

$$\int_1^2 \frac{\partial V}{\partial t}\, ds + \int_1^2 \frac{dp}{\rho} + \frac{1}{2}(V_2^2 - V_1^2) + g(z_2 - z_1) = 0 \tag{4.119}$$

where ds is the arc length along the streamline. Equation (4.119) is Bernoulli's equation for frictionless unsteady flow along a streamline and is identical to Eq. (3.76). For incompressible steady flow, it reduces to

$$\frac{p}{\rho} + \frac{1}{2} V^2 + gz = \text{constant along streamline} \tag{4.120}$$

The constant may vary from streamline to streamline unless the flow is also irrotational (assumption 2). For irrotational flow $\zeta = 0$, the offending term Eq. (4.117) vanishes regardless of the direction of $d\mathbf{r}$, and Eq. (4.120) then holds all over the flow field with the same constant.

Velocity Potential

Irrotationality gives rise to a scalar function ϕ similar and complementary to the stream function ψ. From a theorem in vector analysis [11], a vector with zero curl must be the gradient of a scalar function

$$\text{If} \qquad \boldsymbol{\nabla} \times \mathbf{V} \equiv 0 \qquad \text{then} \qquad \mathbf{V} = \boldsymbol{\nabla}\phi \tag{4.121}$$

where $\phi = \phi(x, y, z, t)$ is called the *velocity potential function*. Knowledge of ϕ thus immediately gives the velocity components

$$u = \frac{\partial \phi}{\partial x} \qquad v = \frac{\partial \phi}{\partial y} \qquad w = \frac{\partial \phi}{\partial z} \tag{4.122}$$

Lines of constant ϕ are called the *potential lines* of the flow.

Note that ϕ, unlike the stream function, is fully three-dimensional and not limited to two coordinates. It reduces a velocity problem with three unknowns u, v, and w to a single unknown potential ϕ; many examples are given in Chap. 8 and Sec. 4.10. The velocity potential also simplifies the unsteady Bernoulli equation (4.118) because if ϕ exists, we obtain

$$\frac{\partial \mathbf{V}}{\partial t} \cdot d\mathbf{r} = \frac{\partial}{\partial t}(\boldsymbol{\nabla}\phi) \cdot d\mathbf{r} = d\left(\frac{\partial \phi}{\partial t}\right)$$



ketabline.com Ebook.ketabline.com

Equation (4.118) then becomes a relation between ϕ and p

$$\frac{\partial \phi}{\partial t} + \int \frac{dp}{\rho} + \frac{1}{2} |\nabla \phi|^2 + gz = \text{const} \tag{4.124}$$

This is the unsteady irrotational Bernoulli equation. It is very important in the analysis of accelerating flow fields (see, e.g., Refs. 10 and 15), but the only application in this text will be in Sec. 9.3 for steady flow.

Orthogonality of Streamlines and Potential Lines

If a flow is both irrotational and described by only two coordinates, ψ and ϕ both exist and the streamlines and potential lines are everywhere mutually perpendicular except at a stagnation point. For example, for incompressible flow in the xy plane, we would have

$$u = \frac{\partial \psi}{\partial y} = \frac{\partial \phi}{\partial x} \tag{4.125}$$

$$v = -\frac{\partial \psi}{\partial x} = \frac{\partial \phi}{\partial y} \tag{4.126}$$

Can you tell by inspection not only that these relations imply orthogonality but also that ϕ and ψ satisfy Laplace's equation?[10] A line of constant ϕ would be such that the change in ϕ is zero

$$d\phi = \frac{\partial \phi}{\partial x} dx + \frac{\partial \phi}{\partial y} dy = 0 = u\, dx + v\, dy \tag{4.127}$$

Solving, we have

$$\left(\frac{dy}{dx}\right)_{\phi=\text{const}} = -\frac{u}{v} = -\frac{1}{(dy/dx)_{\psi=\text{const}}} \tag{4.128}$$

Equation (4.128) is the mathematical condition that lines of constant ϕ and ψ be mutually orthogonal. It may not be true at a stagnation point, where both u and v are zero, so that their ratio in Eq. (4.128) is indeterminate.

Generation of Rotationality

This is the second time we have discussed Bernoulli's equation under different circumstances (the first was in Sec. 3.7). Such reinforcement is useful, since this is probably the most widely used equation in fluid mechanics. It requires frictionless flow with no shaft work or heat transfer between sections 1 and 2. The flow may or may not be irrotational, the latter being an easier condition, allowing a universal Bernoulli constant.

The only remaining question is: *When* is a flow irrotational? In other words, when does a flow have negligible angular velocity? The exact analysis of fluid rotationality under arbitrary conditions is a topic for advanced study, e.g., Ref. 10, sec. 8.5; Ref. 9, sec. 5.2; and Ref. 5, sec. 2.10. We shall simply state those results here without proof.

A fluid flow which is initially irrotational may become rotational if

1. There are significant viscous forces induced by jets, wakes, or solid boundaries. In this case Bernoulli's equation will not be valid in such viscous regions.

[10] Equations (4.125) and (4.126) are called the *Cauchy-Riemann equations* and a
plex-variable theory.



ketabline.com Ebook.ketabline.com

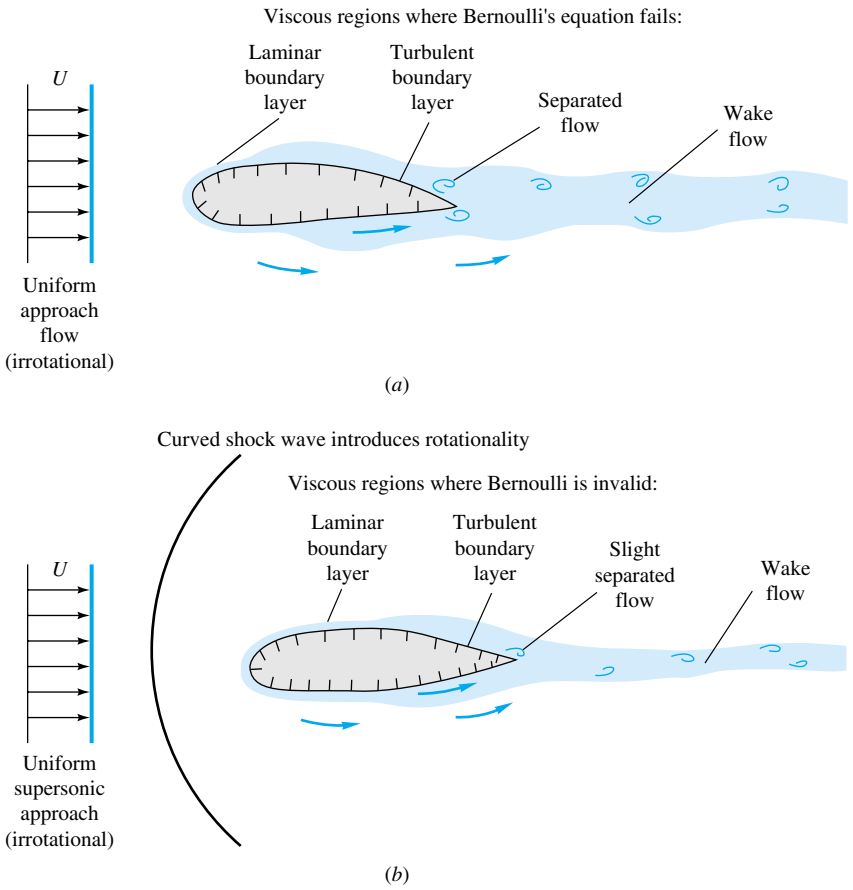


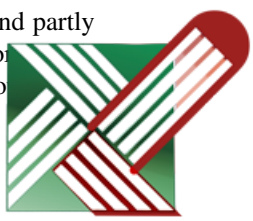
Fig. 4.11 Typical flow patterns illustrating viscous regions patched onto nearly frictionless regions: (*a*) low subsonic flow past a body ($U \ll a$); frictionless, irrotational potential flow outside the boundary layer (Bernoulli and Laplace equations valid); (*b*) supersonic flow past a body ($U > a$); frictionless, rotational flow outside the boundary layer (Bernoulli equation valid, potential flow invalid).

2. There are entropy gradients caused by curved shock waves (see Fig. 4.11*b*).
3. There are density gradients caused by *stratification* (uneven heating) rather than by pressure gradients.
4. There are significant *noninertial* effects such as the earth's rotation (the Coriolis acceleration).

In cases 2 to 4, Bernoulli's equation still holds along a streamline if friction is negligible. We shall not study cases 3 and 4 in this book. Case 2 will be treated briefly in Chap. 9 on gas dynamics. Primarily we are concerned with case 1, where rotation is induced by viscous stresses. This occurs near solid surfaces, where the no-slip condition creates a boundary layer through which the stream velocity drops to zero, and in jets and wakes, where streams of different velocities meet in a region of high shear.

Internal flows, such as pipes and ducts, are mostly viscous, and the wall layers grow to meet in the core of the duct. Bernoulli's equation does not hold in such flows unless it is modified for viscous losses.

External flows, such as a body immersed in a stream, are partly viscous and partly inviscid, the two regions being patched together at the edge of the shear layer or ary layer. Two examples are shown in Fig. 4.11. Figure 4.11*a* shows a lo



ketabline.com Ebook.ketabline.com

subsonic flow past a body. The approach stream is irrotational; i.e., the curl of a constant is zero, but viscous stresses create a rotational shear layer beside and downstream of the body. Generally speaking (see Chap. 6), the shear layer is laminar, or smooth, near the front of the body and turbulent, or disorderly, toward the rear. A separated, or deadwater, region usually occurs near the trailing edge, followed by an unsteady turbulent wake extending far downstream. Some sort of laminar or turbulent viscous theory must be applied to these viscous regions; they are then patched onto the outer flow, which is frictionless and irrotational. If the stream Mach number is less than about 0.3, we can combine Eq. (4.122) with the incompressible continuity equation (4.73).

$$\boldsymbol{\nabla} \cdot \mathbf{V} = \boldsymbol{\nabla} \cdot (\boldsymbol{\nabla}\phi) = 0$$

or

$$\nabla^2\phi = 0 = \frac{\partial^2\phi}{\partial x^2} + \frac{\partial^2\phi}{\partial y^2} + \frac{\partial^2\phi}{\partial z^2} \tag{4.129}$$

This is Laplace's equation in three dimensions, there being no restraint on the number of coordinates in potential flow. A great deal of Chap. 8 will be concerned with solving Eq. (4.129) for practical engineering problems; it holds in the entire region of Fig. 4.11*a* outside the shear layer.

Figure 4.11*b* shows a supersonic flow past a body. A curved shock wave generally forms in front, and the flow downstream is *rotational* due to entropy gradients (case 2). We can use Euler's equation (4.114) in this frictionless region but not potential theory. The shear layers have the same general character as in Fig. 4.11*a* except that the separation zone is slight or often absent and the wake is usually thinner. Theory of separated flow is presently qualitative, but we can make quantitative estimates of laminar and turbulent boundary layers and wakes.

EXAMPLE 4.9

If a velocity potential exists for the velocity field of Example 4.5

$$u = a(x^2 - y^2) \qquad v = -2axy \qquad w = 0$$

find it, plot it, and compare with Example 4.7.

Solution

Since $w = 0$, the curl of $\mathbf{V}$ has only one z component, and we must show that it is zero:

$$(\boldsymbol{\nabla} \times \mathbf{V})_z = 2\omega_z = \frac{\partial v}{\partial x} - \frac{\partial u}{\partial y} = \frac{\partial}{\partial x}(-2axy) - \frac{\partial}{\partial y}(ax^2 - ay^2)$$

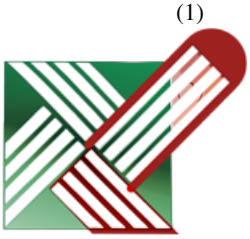
$$= -2ay + 2ay = 0 \qquad \text{checks} \qquad \textit{Ans.}$$

The flow is indeed irrotational. A potential exists.

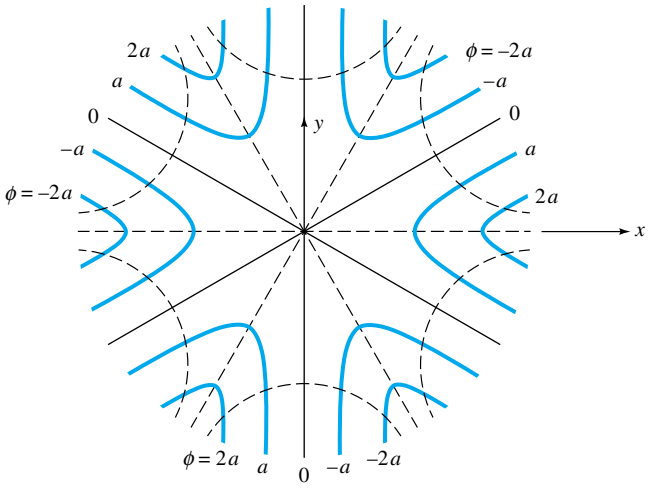
To find $\phi(x, y)$, set

$$u = \frac{\partial\phi}{\partial x} = ax^2 - ay^2 \tag{1}$$

$$v = \frac{\partial\phi}{\partial y} = -2axy$$



ketabline.com Ebook.ketabline.com



E4.9

Integrate (1)

$$\phi = \frac{ax^3}{3} - axy^2 + f(y) \tag{3}$$

Differentiate (3) and compare with (2)

$$\frac{\partial \phi}{\partial y} = -2axy + f'(y) = -2axy \tag{4}$$

Therefore $f' = 0$, or $f =$ constant. The velocity potential is

$$\phi = \frac{ax^3}{3} - axy^2 + C \qquad \textit{Ans.}$$

Letting $C = 0$, we can plot the ϕ lines in the same fashion as in Example 4.7. The result is shown in Fig. E4.9 (no arrows on ϕ). For this particular problem, the ϕ lines form the same pattern as the ψ lines of Example 4.7 (which are shown here as dashed lines) but are displaced 30°. The ϕ and ψ lines are everywhere perpendicular except at the origin, a stagnation point, where they are 30° apart. We expected trouble at the stagnation point, and there is no general rule for determining the behavior of the lines at that point.

4.10 Some Illustrative Plane Potential Flows

Chapter 8 is devoted entirely to a detailed study of inviscid incompressible flows, especially those which possess both a stream function and a velocity potential. As sketched in Fig. 4.11*a*, inviscid flow is valid away from solid surfaces, and this inviscid pattern is "patched" onto the near-wall viscous layers—an idea developed in Chap. 7. Various body shapes can be simulated by the inviscid-flow pattern. Here we discuss plane flows, three of which are illustrated in Fig. 4.12.

Uniform Stream in the *x* Direction

A uniform stream $\mathbf{V} = \mathbf{i}U$, as in Fig. 4.12*a*, possesses both a stream function and a velocity potential, which may be found as follows:

$$u = U = \frac{\partial \phi}{\partial x} = \frac{\partial \psi}{\partial y} \qquad v = 0 = \frac{\partial \phi}{\partial y} = -\frac{\partial \psi}{\partial x}$$



ketabline.com Ebook.ketabline.com

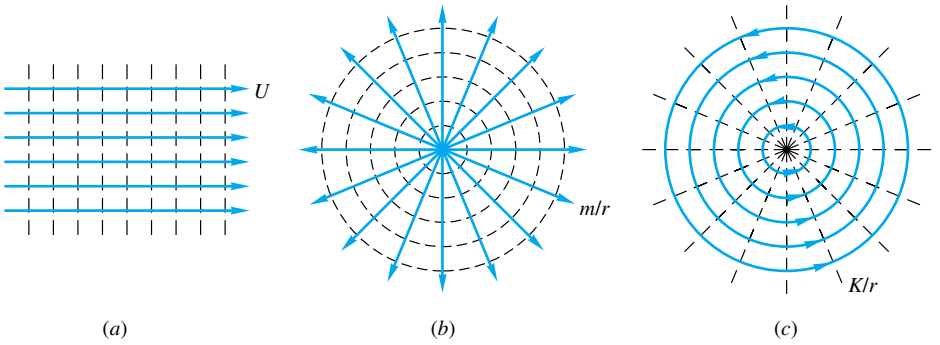


Fig. 4.12 Three elementary plane potential flows. Solid lines are streamlines; dashed lines are potential lines.

We may integrate each expression and discard the constants of integration, which do not affect the velocities in the flow. The results are

$$\text{Uniform stream } \mathbf{i}U: \qquad \psi = Uy \qquad \phi = Ux \tag{4.130}$$

The streamlines are horizontal straight lines ($y = \text{const}$), and the potential lines are vertical ($x = \text{const}$), i.e., orthogonal to the streamlines, as expected.

Line Source or Sink at the Origin

Suppose that the z-axis were a sort of thin-pipe manifold through which fluid issued at total rate Q uniformly along its length b. Looking at the xy plane, we would see a cylindrical radial outflow or *line source*, as sketched in Fig. 4.12*b*. Plane polar coordinates are appropriate (see Fig. 4.2), and there is no circumferential velocity. At any radius r, the velocity is

$$v_r = \frac{Q}{2\pi rb} = \frac{m}{r} = \frac{1}{r}\frac{\partial \psi}{\partial \theta} = \frac{\partial \phi}{\partial r} \qquad v_\theta = 0 = -\frac{\partial \psi}{\partial r} = \frac{1}{r}\frac{\partial \phi}{\partial \theta}$$

where we have used the polar-coordinate forms of the stream function and the velocity potential. Integrating and again discarding the constants of integration, we obtain the proper functions for this simple radial flow:

$$\text{Line source or sink:} \qquad \psi = m\theta \qquad \phi = m \ln r \tag{4.131}$$

where $m = Q/(2\pi b)$ is a constant, positive for a source, negative for a sink. As shown in Fig. 4.12*b*, the streamlines are radial spokes (constant θ), and the potential lines are circles (constant r).

Line Irrotational Vortex

A (two-dimensional) line vortex is a purely circulating steady motion, $v_\theta = f(r)$ only, $v_r = 0$. This satisfies the continuity equation identically, as may be checked from Eq. (4.12*b*). We may also note that a variety of velocity distributions $v_\theta(r)$ satisfy the θ-momentum equation of a viscous fluid, Eq. (E.6). We may show, as a problem exercise, that only one function $v_\theta(r)$ is *irrotational*, i.e., curl $\mathbf{V} = 0$, and that is $v_\theta = K/r$, where K is a constant. This is sometimes called a *free vortex*, for which the stream function and velocity may be found:

$$v_r = 0 = \frac{1}{r}\frac{\partial \psi}{\partial \theta} = \frac{\partial \phi}{\partial r} \qquad v_\theta = \frac{K}{r} = -\frac{\partial \psi}{\partial r} = \frac{1}{r}\frac{\partial}{\partial}$$



ketabline.com Ebook.ketabline.com

We may again integrate to determine the appropriate functions:

$$\psi = -K \ln r \qquad \phi = K\theta \tag{4.132}$$

where K is a constant called the *strength* of the vortex. As shown in Fig. 4.12*c*, the streamlines are circles (constant r), and the potential lines are radial spokes (constant θ). Note the similarity between Eqs. (4.131) and (4.132). A free vortex is a sort of reversed image of a source. The "bathtub vortex," formed when water drains through a bottom hole in a tank, is a good approximation to the free-vortex pattern.

Superposition: Source Plus an Equal Sink

Each of the three elementary flow patterns in Fig. 4.12 is an incompressible irrotational flow and therefore satisfies both plane "potential flow" equations $\nabla^2\psi = 0$ and $\nabla^2\phi = 0$. Since these are linear partial differential equations, any *sum* of such basic solutions is also a solution. Some of these composite solutions are quite interesting and useful.

For example, consider a source $+m$ at $(x, y) = (-a, 0)$, combined with a sink of equal strength $-m$, placed at $(+a, 0)$, as in Fig. 4.13. The resulting stream function is simply the sum of the two. In cartesian coordinates,

$$\psi = \psi_{\text{source}} + \psi_{\text{sink}} = m \tan^{-1} \frac{y}{x + a} - m \tan^{-1} \frac{y}{x - a}$$

Similarly, the composite velocity potential is

$$\phi = \phi_{\text{source}} + \phi_{\text{sink}} = \frac{1}{2} m \ln [(x + a)^2 + y^2] - \frac{1}{2} m \ln [(x - a)^2 + y^2]$$

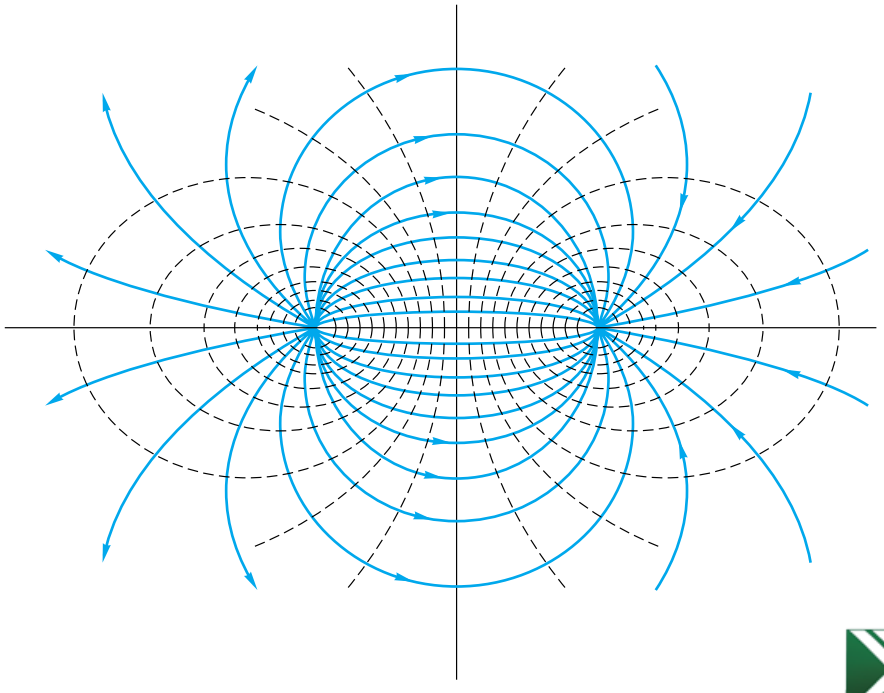


Fig. 4.13 Potential flow due to a line source plus an equal line sink, from Eq. (4.133). Solid lines are streamlines; dashed lines are potential lines.



ketabline.com Ebook.ketabline.com

By using trigonometric and logarithmic identities, these may be simplified to

$$\text{Source plus sink:} \qquad \psi = -m \tan^{-1} \frac{2ay}{x^2 + y^2 - a^2}$$

$$\phi = \frac{1}{2} m \ln \frac{(x + a)^2 + y^2}{(x - a)^2 + y^2} \tag{4.133}$$

These lines are plotted in Fig. 4.13 and are seen to be two families of orthogonal circles, with the streamlines passing through the source and sink and the potential lines encircling them. They are harmonic (laplacian) functions which are exactly analogous in electromagnetic theory to the electric-current and electric-potential patterns of a magnet with poles at $(\pm a, 0)$.

Sink Plus a Vortex at the Origin

An interesting flow pattern, approximated in nature, occurs by superposition of a sink and a vortex, both centered at the origin. The composite stream function and velocity potential are

$$\text{Sink plus vortex:} \qquad \psi = m\theta - K \ln r \qquad \phi = m \ln r + K\theta \tag{4.134}$$

When plotted, these form two orthogonal families of logarithmic spirals, as shown in Fig. 4.14. This is a fairly realistic simulation of a tornado (where the sink flow moves up the z-axis into the atmosphere) or a rapidly draining bathtub vortex. At the center of a real (viscous) vortex, where Eq. (4.134) predicts infinite velocity, the actual circulating flow is highly *rotational* and approximates solid-body rotation $v_\theta \approx Cr$.

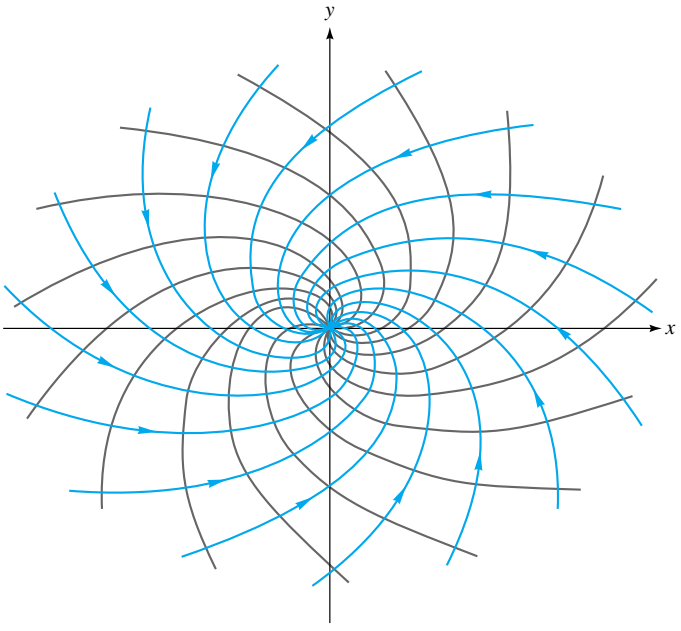


Fig. 4.14 Superposition of a sink plus a vortex, Eq. (4.134), simulates a tornado.



ketabline.com Ebook.ketabline.com

Uniform Stream Plus a Sink at the Origin: The Rankine Half-Body

If we superimpose a uniform x-directed stream against an isolated source, a half-body shape appears. If the source is at the origin, the combined stream function is, in polar coordinates,

$$\text{Uniform stream plus source:} \qquad \psi = Ur \sin \theta + m\theta \tag{4.135}$$

We can set this equal to various constants and plot the streamlines, as shown in Fig. 4.15. A curved, roughly elliptical, *half-body* shape appears, which separates the source flow from the stream flow. The body shape, which is named after the Scottish engineer W. J. M. Rankine (1820–1872), is formed by the particular streamlines $\psi = \pm \pi m$. The half-width of the body far downstream is $\pi m/U$. The upper surface may be plotted from the relation

$$r = \frac{m(\pi - \theta)}{U \sin \theta} \tag{4.136}$$

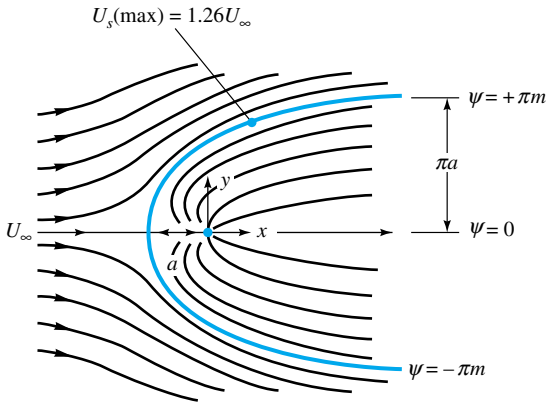


Fig. 4.15 Superposition of a source plus a uniform stream forms a Rankine half-body.

It is not a true ellipse. The nose of the body, which is a "stagnation" point where $V = 0$, stands at $(x, y) = (-a, 0)$, where $a = m/U$. The streamline $\psi = 0$ also crosses this point—recall that streamlines can cross only at a stagnation point.

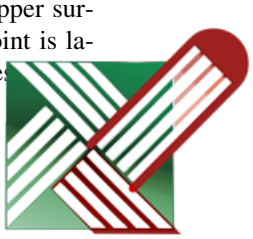
The cartesian velocity components are found by differentiation:

$$u = \frac{\partial \psi}{\partial y} = U + \frac{m}{r} \cos \theta \qquad v = -\frac{\partial \psi}{\partial x} = \frac{m}{r} \sin \theta \tag{4.137}$$

Setting $u = v = 0$, we find a single stagnation point at $\theta = 180°$ and $r = m/U$, or $(x, y) = (-m/U, 0)$, as stated. The resultant velocity at any point is

$$V^2 = u^2 + v^2 = U^2\left(1 + \frac{a^2}{r^2} + \frac{2a}{r} \cos \theta\right) \tag{4.138}$$

where we have substituted $m = Ua$. If we evaluate the velocities along the upper surface $\psi = \pi m$, we find a maximum value $U_{s,\max} \approx 1.26U$ at $\theta = 63°$. This point is labeled in Fig. 4.15 and, by Bernoulli's equation, is the point of minimum pres

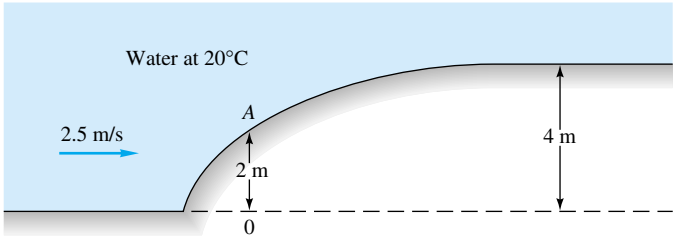


ketabline.com Ebook.ketabline.com

the body surface. After this point, the surface flow decelerates, the pressure rises, and the viscous layer grows thicker and more susceptible to "flow separation," as we shall see in Chap. 7.

EXAMPLE 4.10

The bottom of a river has a 4-m-high bump which approximates a Rankine half-body, as in Fig. E4.10. The pressure at point B on the bottom is 130 kPa, and the river velocity is 2.5 m/s. Use inviscid theory to estimate the water pressure at point A on the bump, which is 2 m above point B.



E4.10

Solution

As in all inviscid theories, we ignore the low-velocity boundary layers which form on solid surfaces due to the no-slip condition. From Eq. (4.136) and Fig. 4.15, the downstream bump half-height equals πa. Therefore, for our case, $a = (4\text{ m})/\pi = 1.27$ m. We have to find the spot where the bump height is half that much, $h = 2\text{ m} = \pi a/2$. From Eq. (4.136) we may compute

$$r = h_A = \frac{a(\pi - \theta)}{\sin\theta} = \frac{\pi}{2}a \qquad \text{or} \qquad \theta = \frac{\pi}{2} = 90^\circ$$

Thus point A in Fig. E4.10 is directly above the (initially unknown) origin of coordinates (labeled O in Fig. E4.10) and is 1.27 m to the right of the nose of the bump. With $r = \pi a/2$ and $\theta = \pi/2$ known, we compute the velocity at point A from Eq. (4.138):

$$V_A^2 = U^2\left[1 + \frac{a^2}{(\pi a/2)^2} + \frac{2a}{\pi a/2}\cos\frac{\pi}{2}\right] = 1.405U^2$$

or

$$V_A \approx 1.185U = 1.185(2.5\text{ m/s}) = 2.96\text{ m/s}$$

For water at 20°C, take $\rho = 998$ kg/m^2 and $\gamma = 9790$ N/m^3. Now, since the velocity and elevation are known at point A, we are in a position to use Bernoulli's inviscid, incompressible-flow equation (4.120) to estimate p_A from the known properties at point B (on the same streamline):

$$\frac{p_A}{\gamma} + \frac{V_A^2}{2g} + z_A \approx \frac{p_B}{\gamma} + \frac{V_B^2}{2g} + z_B$$

or

$$\frac{p_A}{9790\text{ N/m}^3} + \frac{(2.96\text{ m/s})^2}{2(9.81\text{ m/s}^2)} + 2\text{ m} \approx \frac{130{,}000}{9790} + \frac{(2.5)^2}{2(9.81)} + 0$$

Solving, we find

$$p_A = (13.60 - 2.45)(9790) \approx 109{,}200\text{ Pa}$$



ketabline.com Ebook.ketabline.com

If the approach velocity is uniform, this should be a pretty good approximation, since water is relatively inviscid and its boundary layers are thin.

4.11 Some Illustrative Incompressible Viscous Flows

The inviscid flows of Sec. 4.10 do *not* satisfy the no-slip condition. They "slip" at the wall but do not flow through the wall. To look at fully viscous no-slip conditions, we must attack the complete Navier-Stokes equation (4.74), and the result is usually not at all irrotational, nor does a velocity potential exist. We look here at three cases: (1) flow between parallel plates due to a moving upper wall, (2) flow between parallel plates due to pressure gradient, and (3) flow between concentric cylinders when the inner one rotates. Other cases will be given as problem assignments or considered in Chap. 6. Extensive solutions for viscous flows are discussed in Refs. 4 and 5.

Couette Flow between a Fixed and a Moving Plate

Consider two-dimensional incompressible plane ($\partial/\partial z = 0$) viscous flow between parallel plates a distance $2h$ apart, as shown in Fig. 4.16. We assume that the plates are very wide and very long, so that the flow is essentially axial, $u \neq 0$ but $v = w = 0$. The present case is Fig. 4.16*a*, where the upper plate moves at velocity V but there is no pressure gradient. Neglect gravity effects. We learn from the continuity equation (4.73) that

$$\frac{\partial u}{\partial x} + \frac{\partial v}{\partial y} + \frac{\partial w}{\partial z} = 0 = \frac{\partial u}{\partial x} + 0 + 0 \qquad \text{or} \qquad u = u(y) \text{ only}$$

Thus there is a single nonzero axial-velocity component which varies only across the channel. The flow is said to be *fully developed* (far downstream of the entrance). Substitute $u = u(y)$ into the x-component of the Navier-Stokes momentum equation (4.74) for two-dimensional (x, y) flow:

$$\rho\left(u\frac{\partial u}{\partial x} + v\frac{\partial u}{\partial y}\right) = -\frac{\partial p}{\partial x} + \rho g_x + \mu\left(\frac{\partial^2 u}{\partial x^2} + \frac{\partial^2 u}{\partial y^2}\right)$$

or

$$\rho(0 + 0) = 0 + 0 + \mu\left(0 + \frac{d^2u}{dy^2}\right) \tag{4.139}$$

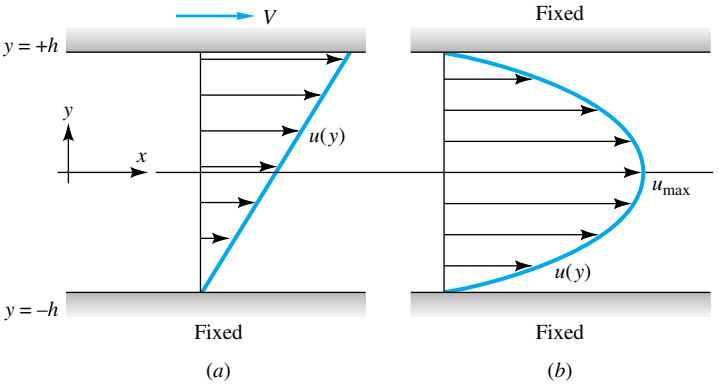


Fig. 4.16 Incompressible viscous flow between parallel plates: (*a*) no pressure gradient, upper plate moving; (*b*) pressure gradient $\partial p/\partial x$ with both plates fixed.



ketabline.com Ebook.ketabline.com

Most of the terms drop out, and the momentum equation simply reduces to

$$\frac{d^2u}{dy^2} = 0 \qquad \text{or} \qquad u = C_1y + C_2$$

The two constants are found by applying the no-slip condition at the upper and lower plates:

At $y = +h$: $\qquad u = V = C_1h + C_2$

At $y = -h$: $\qquad u = 0 = C_1(-h) + C_2$

or $\qquad C_1 = \dfrac{V}{2h} \qquad \text{and} \qquad C_2 = \dfrac{V}{2}$

Therefore the solution for this case (*a*), flow between plates with a moving upper wall, is

$$u = \frac{V}{2h}\,y + \frac{V}{2} \qquad -h \le y \le +h \tag{4.140}$$

This is *Couette flow* due to a moving wall: a linear velocity profile with no-slip at each wall, as anticipated and sketched in Fig. 4.16*a*. Note that the origin has been placed in the center of the channel, for convenience in case (*b*) below.

What we have just presented is a rigorous derivation of the more informally discussed flow of Fig. 1.6 (where y and h were defined differently).

Flow due to Pressure Gradient between Two Fixed Plates

Case (*b*) is sketched in Fig. 4.16*b*. Both plates are fixed ($V = 0$), but the pressure varies in the x direction. If $v = w = 0$, the continuity equation leads to the same conclusion as case (*a*), namely, that $u = u(y)$ only. The x-momentum equation (4.138) changes only because the pressure is variable:

$$\mu\frac{d^2u}{dy^2} = \frac{\partial p}{\partial x} \tag{4.141}$$

Also, since $v = w = 0$ and gravity is neglected, the y- and z-momentum equations lead to

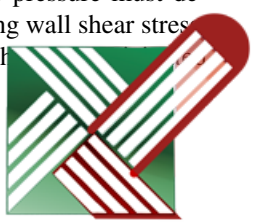
$$\frac{\partial p}{\partial y} = 0 \qquad \text{and} \qquad \frac{\partial p}{\partial z} = 0 \qquad \text{or} \qquad p = p(x) \text{ only}$$

Thus the pressure gradient in Eq. (4.141) is the total and only gradient:

$$\mu\frac{d^2u}{dy^2} = \frac{dp}{dx} = \text{const} < 0 \tag{4.142}$$

Why did we add the fact that dp/dx is *constant*? Recall a useful conclusion from the theory of separation of variables: If two quantities are equal and one varies only with y and the other varies only with x, then they must both equal the same constant. Otherwise they would not be independent of each other.

Why did we state that the constant is *negative*? Physically, the pressure must decrease in the flow direction in order to drive the flow against resisting wall shear stres
Thus the velocity profile $u(y)$ must have negative curvature everywh
and sketched in Fig. 4.16*b*.



ketabline.com Ebook.ketabline.com

The solution to Eq. (4.142) is accomplished by double integration:

$$u = \frac{1}{\mu}\frac{dp}{dx}\frac{y^2}{2} + C_1 y + C_2$$

The constants are found from the no-slip condition at each wall:

$$\text{At } y = \pm h: \quad u = 0 \quad \text{or} \quad C_1 = 0 \quad \text{and} \quad C_2 = -\frac{dp}{dx}\frac{h^2}{2\mu}$$

Thus the solution to case (*b*), flow in a channel due to pressure gradient, is

$$u = -\frac{dp}{dx}\frac{h^2}{2\mu}\left(1 - \frac{y^2}{h^2}\right) \tag{4.143}$$

The flow forms a *Poiseuille* parabola of constant negative curvature. The maximum velocity occurs at the centerline $y = 0$:

$$u_{\max} = -\frac{dp}{dx}\frac{h^2}{2\mu} \tag{4.144}$$

Other (laminar) flow parameters are computed in the following example.

EXAMPLE 4.11

For case (*b*) above, flow between parallel plates due to the pressure gradient, compute (*a*) the wall shear stress, (*b*) the stream function, (*c*) the vorticity, (*d*) the velocity potential, and (*e*) the average velocity.

Solution

All parameters can be computed from the basic solution, Eq. (4.143), by mathematical manipulation.

(*a*) The wall shear follows from the definition of a newtonian fluid, Eq. (4.37):

$$\tau_w = \tau_{xy\ \text{wall}} = \mu\left(\frac{\partial u}{\partial y} + \frac{\partial v}{\partial x}\right)\Big|_{y=\pm h} = \mu\frac{\partial}{\partial y}\left[\left(-\frac{dp}{dx}\right)\left(\frac{h^2}{2\mu}\right)\left(1 - \frac{y^2}{h^2}\right)\right]\Big|_{y=\pm h}$$

$$= \pm\frac{dp}{dx}h = \mp\frac{2\mu u_{\max}}{h} \qquad \textit{Ans. (a)}$$

The wall shear has the same magnitude at each wall, but by our sign convention of Fig. 4.3, the upper wall has negative shear stress.

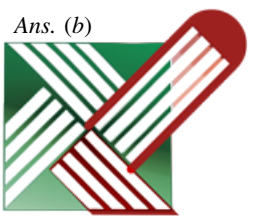
(*b*) Since the flow is plane, steady, and incompressible, a stream function exists:

$$u = \frac{\partial \psi}{\partial y} = u_{\max}\left(1 - \frac{y^2}{h^2}\right) \qquad v = -\frac{\partial \psi}{\partial x} = 0$$

Integrating and setting $\psi = 0$ at the centerline for convenience, we obtain

$$\psi = u_{\max}\left(y - \frac{y^3}{3h^2}\right) \qquad \textit{Ans. (b)}$$

At the walls, $y = \pm h$ and $\psi = \pm 2u_{\max}h/3$, respectively.



ketabline.com Ebook.ketabline.com

(*c*) In plane flow, there is only a single nonzero vorticity component:

$$\zeta_z = (\text{curl } \mathbf{V})_z = \frac{\partial v}{\partial x} - \frac{\partial u}{\partial y} = \frac{2u_{\max}}{h^2}\, y \qquad \textit{Ans. (c)}$$

The vorticity is highest at the wall and is positive (counterclockwise) in the upper half and negative (clockwise) in the lower half of the fluid. Viscous flows are typically full of vorticity and are not at all irrotational.

(*d*) From part (*c*), the vorticity is finite. Therefore the flow is not irrotational, and the velocity potential *does not exist*. *Ans. (d)*

(*e*) The average velocity is defined as $V_{\text{av}} = Q/A$, where $Q = \int u\, dA$ over the cross section. For our particular distribution $u(y)$ from Eq. (4.143), we obtain

$$V_{\text{av}} = \frac{1}{A}\int u\, dA = \frac{1}{b(2h)}\int_{-h}^{+h} u_{\max}\left(1 - \frac{y^2}{h^2}\right) b\, dy = \frac{2}{3}\, u_{\max} \qquad \textit{Ans. (e)}$$

In plane Poiseuille flow between parallel plates, the average velocity is two-thirds of the maximum (or centerline) value. This result could also have been obtained from the stream function derived in part (*b*). From Eq. (4.95),

$$Q_{\text{channel}} = \psi_{\text{upper}} - \psi_{\text{lower}} = \frac{2u_{\max}h}{3} - \left(-\frac{2u_{\max}h}{3}\right) = \frac{4}{3}\, u_{\max}h \text{ per unit width}$$

whence $V_{\text{av}} = Q/A_{b=1} = (4u_{\max}h/3)/(2h) = 2u_{\max}/3$, the same result.

This example illustrates a statement made earlier: Knowledge of the velocity vector **V** [as in Eq. (4.143)] is essentially the *solution* to a fluid-mechanics problem, since all other flow properties can then be calculated.

Flow between Long Concentric Cylinders

Consider a fluid of constant (ρ, μ) between two concentric cylinders, as in Fig. 4.17. There is no axial motion or end effect $v_z = \partial/\partial z = 0$. Let the inner cylinder rotate at angular velocity Ω_i. Let the outer cylinder be fixed. There is circular symmetry, so the velocity does not vary with θ and varies only with r.

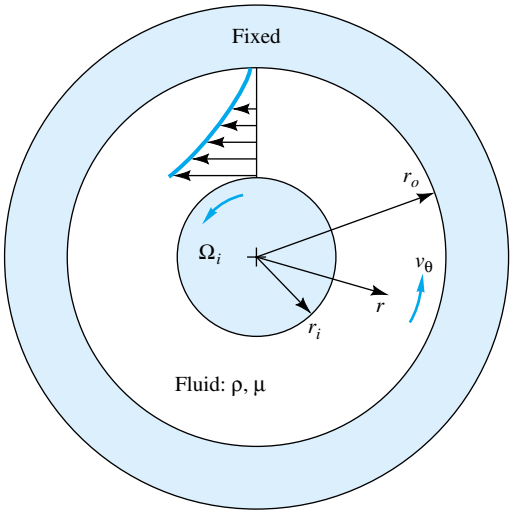


Fig. 4.17 Coordinate system for incompressible viscous flow between a fixed outer cylinder and a steadily rotating inner cylinder.



ketabline.com Ebook.ketabline.com

The continuity equation for this problem is Eq. (D.2):

$$\frac{1}{r}\frac{\partial}{\partial r}(rv_r) + \frac{1}{r}\frac{\partial v_\theta}{\partial \theta} = 0 = \frac{1}{r}\frac{d}{dr}(rv_r) \qquad \text{or} \qquad rv_r = \text{const}$$

Note that v_θ does not vary with θ. Since $v_r = 0$ at both the inner and outer cylinders, it follows that $v_r = 0$ everywhere and the motion can only be purely circumferential, $v_\theta = v_\theta(r)$. The θ-momentum equation (D.6) becomes

$$\rho(\mathbf{V}\cdot\nabla)v_\theta + \frac{\rho v_r v_\theta}{r} = -\frac{1}{r}\frac{\partial p}{\partial \theta} + \rho g_\theta + \mu\left(\nabla^2 v_\theta - \frac{v_\theta}{r^2}\right)$$

For the conditions of the present problem, all terms are zero except the last. Therefore the basic differential equation for flow between rotating cylinders is

$$\nabla^2 v_\theta = \frac{1}{r}\frac{d}{dr}\left(r\frac{dv_\theta}{dr}\right) = \frac{v_\theta}{r^2} \tag{4.145}$$

This is a linear second-order ordinary differential equation with the solution

$$v_\theta = C_1 r + \frac{C_2}{r}$$

The constants are found by the no-slip condition at the inner and outer cylinders:

Outer, at $r = r_o$: $$v_\theta = 0 = C_1 r_o + \frac{C_2}{r_o}$$

Inner, at $r = r_i$: $$v_\theta = \Omega_i r_i = C_1 r_i + \frac{C_2}{r_i}$$

The final solution for the velocity distribution is

Rotating inner cylinder: $$v_\theta = \Omega_i r_i \frac{r_o/r - r/r_o}{r_o/r_i - r_i/r_o} \tag{4.146}$$

The velocity profile closely resembles the sketch in Fig. 4.17. Variations of this case, such as a rotating outer cylinder, are given in the problem assignments.

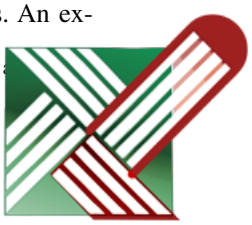
Instability of Rotating Inner Cylinder Flow

The classic *Couette-flow* solution[11] of Eq. (4.146) describes a physically satisfying concave, two-dimensional, laminar-flow velocity profile as in Fig. 4.17. The solution is mathematically exact for an incompressible fluid. However, it becomes unstable at a relatively low rate of rotation of the inner cylinder, as shown in 1923 in a classic paper by G. I. Taylor [17]. At a critical value of what is now called the *Taylor number*, denoted Ta,

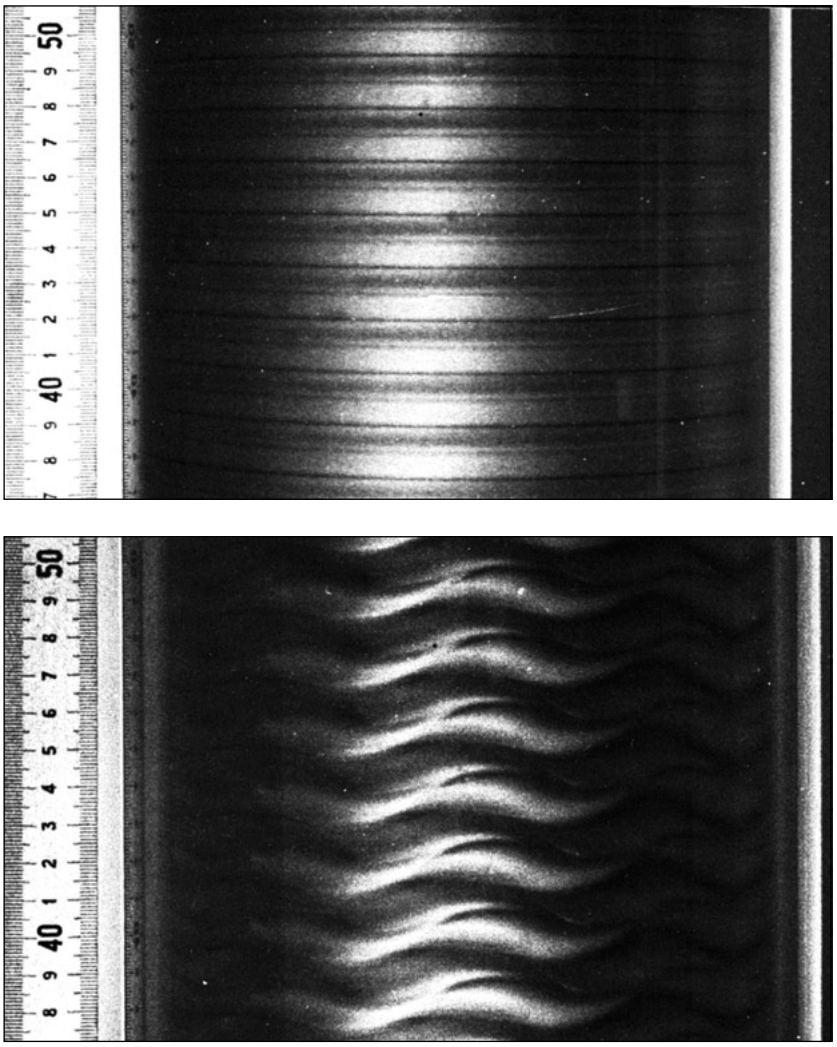
$$\text{Ta}_{\text{crit}} = \frac{r_i(r_o - r_i)^3\Omega_i^2}{\nu^2} \approx 1700 \tag{4.147}$$

the plane flow of Fig. 4.17 vanishes and is replaced by a laminar *three-dimensional* flow pattern consisting of rows of nearly square alternating toroidal vortices. An ex-

[11]Named after M. Couette, whose pioneering paper in 1890 established rotating cylinders as a still used today, for measuring the viscosity of fluids.



ketabline.com Ebook.ketabline.com



(*a*)

(*b*)

Fig. 4.18 Experimental verification of the instability of flow between a fixed outer and a rotating inner cylinder. (*a*) Toroidal Taylor vortices exist at 1.16 times the critical speed; (*b*) at 8.5 times the critical speed, the vortices are doubly periodic. (*After Koschmieder, Ref. 18.*) This instability does not occur if only the outer cylinder rotates.

perimental demonstration of toroidal "Taylor vortices" is shown in Fig. 4.18*a*, measured at Ta $\approx$ 1.16 Ta_{crit} by Koschmieder [18]. At higher Taylor numbers, the vortices also develop a circumferential periodicity but are still laminar, as illustrated in Fig. 4.18*b*. At still higher Ta, turbulence ensues. This interesting instability reminds us that the Navier-Stokes equations, being nonlinear, do admit to multiple (nonunique) laminar solutions in addition to the usual instabilities associated with turbulence and chaotic dynamic systems.

Summary

This chapter complements Chap. 3 by using an infinitesimal control volume to deri
the basic partial differential equations of mass, momentum, and e
These equations, together with thermodynamic state relations for th



ketabline.com Ebook.ketabline.com

priate boundary conditions, in principle can be solved for the complete flow field in any given fluid-mechanics problem. Except for Chap. 9, in most of the problems to be studied here an incompressible fluid with constant viscosity is assumed.

In addition to deriving the basic equations of mass, momentum, and energy, this chapter introduced some supplementary ideas—the stream function, vorticity, irrotationality, and the velocity potential—which will be useful in coming chapters, especially Chap. 8. Temperature and density variations will be neglected except in Chap. 9, where compressibility is studied.

This chapter ended by discussing a few classical solutions for inviscid flows (uniform stream, source, sink, vortex, half-body) and for viscous flows (Couette flow due to moving walls and Poiseuille flow due to pressure gradient). Whole books [11, 13] are written on the basic equations of fluid mechanics. Whole books [4, 5, 15] are written on classical solutions to fluid-flow problems. Reference 12 contains 360 solved problems which relate fluid mechanics to the whole of continuum mechanics. This does not mean that all problems can be readily solved mathematically, even with the modern digital-computer codes now available. Often the geometry and boundary conditions are so complex that experimentation (Chap. 5) is a necessity.

Problems

Most of the problems herein are fairly straightforward. More difficult or open-ended assignments are labeled with an asterisk. Problems labeled with an EES icon will benefit from the use of the Engineering Equation Solver (EES), while problems labeled with a computer disk may require the use of a computer. The standard end-of-chapter problems 4.1 to 4.91 (categorized in the problem list below) are followed by word problems W4.1 to W4.10, fundamentals of engineering exam problems FE4.1 to FE4.3, and comprehensive problem C4.1.

Problem distribution

Section	Topic	Problems
4.1	The acceleration of a fluid	4.1–4.8
4.2	The continuity equation	4.9–4.25
4.3	Linear momentum: Navier-Stokes	4.26–4.37
4.4	Angular momentum: couple stresses	4.38
4.5	The differential energy equation	4.39–4.42
4.6	Boundary conditions	4.43–4.46
4.7	Stream function	4.47–4.55
4.8	Vorticity, irrotationality	4.56–4.60
4.9	Velocity potential	4.61–4.67
4.10	Plane potential flows	4.68–4.78
4.11	Incompressible viscous flows	4.79–4.91

P4.1 An idealized velocity field is given by the formula

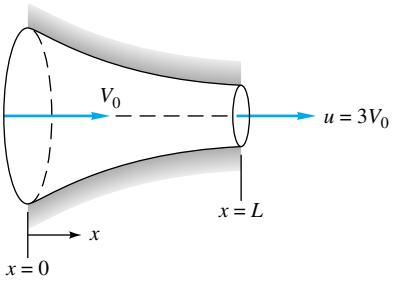
$$\mathbf{V} = 4tx\mathbf{i} - 2t^2y\mathbf{j} + 4xz\mathbf{k}$$

Is this flow field steady or unsteady? Is it two- or three-dimensional? At the point $(x, y, z) = (-1, 1, 0)$, compute (a) the acceleration vector and (b) any unit vector normal to the acceleration.

P4.2 Flow through the converging nozzle in Fig. P4.2 can be approximated by the one-dimensional velocity distribution

$$u \approx V_0\left(1 + \frac{2x}{L}\right) \qquad v \approx 0 \qquad w \approx 0$$

(a) Find a general expression for the fluid acceleration in the nozzle. (b) For the specific case $V_0 = 10$ ft/s and $L = 6$ in, compute the acceleration, in g's, at the entrance and at the exit.

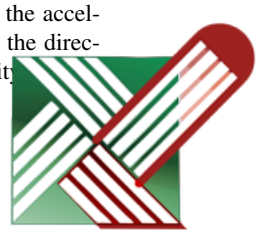


P4.2

P4.3 A two-dimensional velocity field is given by

$$\mathbf{V} = (x^2 - y^2 + x)\mathbf{i} - (2xy + y)\mathbf{j}$$

in arbitrary units. At $(x, y) = (1, 2)$, compute (a) the accelerations a_x and a_y, (b) the velocity component in the direction $\theta = 40°$, (c) the direction of maximum velocity the direction of maximum acceleration.



ketabline.com Ebook.ketabline.com

P4.4 Suppose that the temperature field $T = 4x^2 - 3y^3$, in arbitrary units, is associated with the velocity field of Prob. 4.3. Compute the rate of change dT/dt at $(x, y) = (2, 1)$.

P4.5 The velocity field near a stagnation point (see Example 1.10) may be written in the form

$$u = \frac{U_0 x}{L} \qquad v = -\frac{U_0 y}{L} \qquad U_0 \text{ and } L \text{ are constants}$$

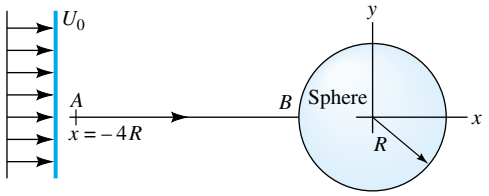
(a) Show that the acceleration vector is purely radial. (b) For the particular case $L = 1.5$ m, if the acceleration at (x, y) = (1 m, 1 m) is 25 m/s^2, what is the value of U_0?

P4.6 Assume that flow in the converging nozzle of Fig. P4.2 has the form $\mathbf{V} = V_0[1 + (2x)/L]\mathbf{i}$. Compute ($a$) the fluid acceleration at $x = L$ and (b) the time required for a fluid particle to travel from $x = 0$ to $x = L$.

P4.7 Consider a sphere of radius R immersed in a uniform stream U_0, as shown in Fig. P4.7. According to the theory of Chap. 8, the fluid velocity along streamline AB is given by

$$\mathbf{V} = u\mathbf{i} = U_0\left(1 + \frac{R^3}{x^3}\right)\mathbf{i}$$

Find (a) the position of maximum fluid acceleration along AB and (b) the time required for a fluid particle to travel from A to B.

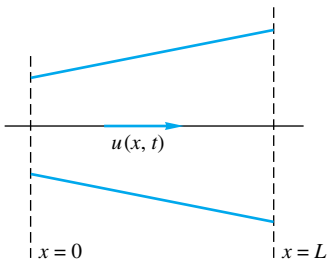


P4.7

P4.8 When a valve is opened, fluid flows in the expansion duct of Fig. 4.8 according to the approximation

$$\mathbf{V} = \mathbf{i}U\left(1 - \frac{x}{2L}\right)\tanh\frac{Ut}{L}$$

Find (a) the fluid acceleration at (x, t) = (L, L/U) and (b) the time for which the fluid acceleration at $x = L$ is zero. Why does the fluid acceleration become negative after condition (b)?



P4.8

P4.9 A velocity field is given by $\mathbf{V} = (3y^2 - 3x^2)\mathbf{i} + Cxy\mathbf{j} + 0\mathbf{k}$. Determine the value of the constant C if the flow is to be (a) incompressible and (b) irrotational.

P4.10 Write the special cases of the equation of continuity for (a) steady compressible flow in the yz plane, (b) unsteady incompressible flow in the xz plane, (c) unsteady compressible flow in the y direction only, (d) steady compressible flow in plane polar coordinates.

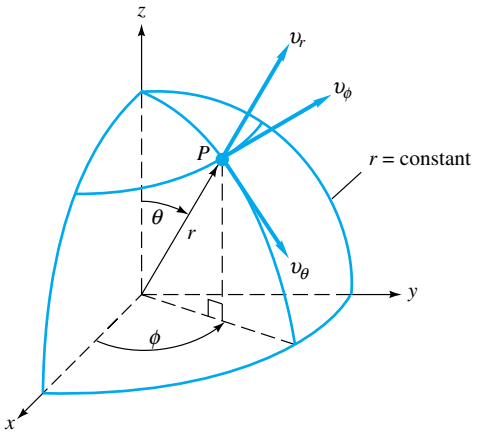
P4.11 Derive Eq. (4.12b) for cylindrical coordinates by considering the flux of an incompressible fluid in and out of the elemental control volume in Fig. 4.2.

P4.12 Spherical polar coordinates (r, θ, ϕ) are defined in Fig. P4.12. The cartesian transformations are

$$x = r \sin\theta \cos\phi$$

$$y = r \sin\theta \sin\phi$$

$$z = r \cos\theta$$



P4.12

The cartesian incompressible continuity relation (4.12a) can be transformed to the spherical polar form

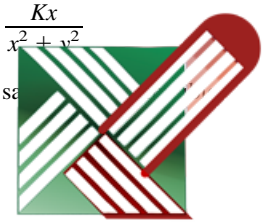
$$\frac{1}{r^2}\frac{\partial}{\partial r}(r^2 v_r) + \frac{1}{r\sin\theta}\frac{\partial}{\partial\theta}(v_\theta \sin\theta) + \frac{1}{r\sin\theta}\frac{\partial}{\partial\phi}(v_\phi) = 0$$

What is the most general form of v_r when the flow is purely radial, that is, v_θ and v_ϕ are zero?

P4.13 A two-dimensional velocity field is given by

$$u = -\frac{Ky}{x^2 + y^2} \qquad v = \frac{Kx}{x^2 + y^2}$$

where K is constant. Does this field sa



ketabline.com Ebook.ketabline.com

continuity? Transform these velocities to polar components v_r and v_θ. What might the flow represent?

P4.14 For incompressible polar-coordinate flow, what is the most general form of a purely circulatory motion, $v_\theta = v_\theta(r, \theta, t)$ and $v_r = 0$, which satisfies continuity?

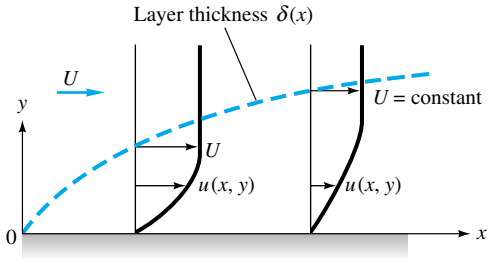
P4.15 What is the most general form of a purely radial polar-coordinate incompressible-flow pattern, $v_r = v_r(r, \theta, t)$ and $v_\theta = 0$, which satisfies continuity?

P4.16 An incompressible steady-flow pattern is given by $u = x^3 + 2z^2$ and $w = y^3 - 2yz$. What is the most general form of the third component, $v(x, y, z)$, which satisfies continuity?

P4.17 A reasonable approximation for the two-dimensional incompressible laminar boundary layer on the flat surface in Fig. P4.17 is

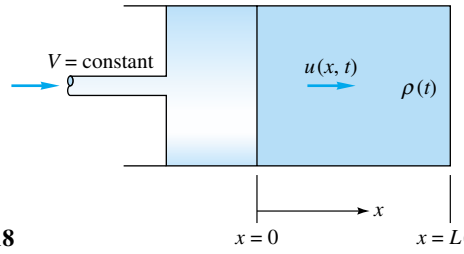
$$u = U\left(\frac{2y}{\delta} - \frac{y^2}{\delta^2}\right) \qquad \text{for } y \le \delta \qquad \text{where } \delta = Cx^{1/2},\ C = \text{const}$$

(a) Assuming a no-slip condition at the wall, find an expression for the velocity component $v(x, y)$ for $y \le \delta$. (b) Then find the maximum value of v at the station $x = 1$ m, for the particular case of airflow, when $U = 3$ m/s and $\delta = 1.1$ cm.



P4.17

P4.18 A piston compresses gas in a cylinder by moving at constant speed V, as in Fig. P4.18. Let the gas density and length at $t = 0$ be ρ_0 and L_0, respectively. Let the gas velocity vary linearly from $u = V$ at the piston face to $u = 0$ at $x = L$. If the gas density varies only with time, find an expression for $\rho(t)$.

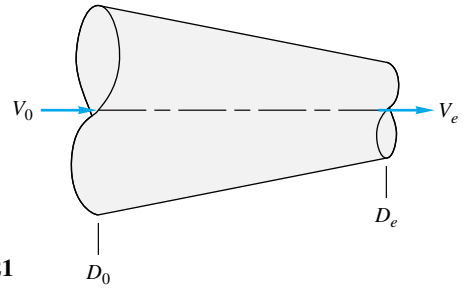


P4.18

P4.19 An incompressible flow field has the cylindrical components $v_\theta = Cr$, $v_z = K(R^2 - r^2)$, $v_r = 0$, where C and K are constants and $r \le R$, $z \le L$. Does this flow satisfy continuity? What might it represent physically?

P4.20 A two-dimensional incompressible velocity field has $u = K(1 - e^{-ay})$, for $x \le L$ and $0 \le y \le \infty$. What is the most general form of $v(x, y)$ for which continuity is satisfied and $v = v_0$ at $y = 0$? What are the proper dimensions for constants K and a?

P4.21 Air flows under steady, approximately one-dimensional conditions through the conical nozzle in Fig. P4.21. If the speed of sound is approximately 340 m/s, what is the minimum nozzle-diameter ratio D_e/D_0 for which we can safely neglect compressibility effects if $V_0 = (a)$ 10 m/s and (b) 30 m/s?



P4.21

P4.22 Air at a certain temperature and pressure flows through a contracting nozzle of length L whose area decreases linearly, $A \approx A_0[1 - x/(2L)]$. The air average velocity increases nearly linearly from 76 m/s at $x = 0$ to 167 m/s at $x = L$. If the density at $x = 0$ is 2.0 kg/m^3, estimate the density at $x = L$.

P4.23 A tank volume $\mathcal{V}$ contains gas at conditions (ρ_0, p_0, T_0). At time $t = 0$ it is punctured by a small hole of area A. According to the theory of Chap. 9, the mass flow out of such a hole is approximately proportional to A and to the tank pressure. If the tank temperature is assumed constant and the gas is ideal, find an expression for the variation of density within the tank.

***P4.24** Reconsider Fig. P4.17 in the following general way. It is known that the boundary layer thickness $\delta(x)$ increases monotonically and that there is no slip at the wall ($y = 0$). Further, $u(x, y)$ merges smoothly with the outer stream flow, where $u \approx U =$ constant outside the layer. Use these facts to prove that (a) the component $v(x, y)$ is positive everywhere within the layer, (b) v increases parabolically with y very near the wall, and (c) v is a maximum at $y = \delta$.

P4.25 An incompressible flow in polar coordinates is given by

$$v_r = K\cos\theta\left(1 - \frac{b}{r^2}\right)$$

$$v_\theta = -K\sin\theta\left(1 + \frac{b}{r^2}\right)$$

Does this field satisfy continuity? For consisten

ketabline.com Ebook.ketabline.com

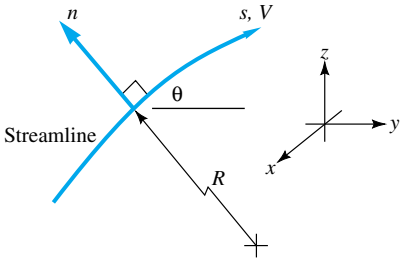
should the dimensions of constants K and b be? Sketch the surface where $v_r = 0$ and interpret.

***P4.26** Curvilinear, or streamline, coordinates are defined in Fig. P4.26, where n is normal to the streamline in the plane of the radius of curvature R. Show that Euler's frictionless momentum equation (4.36) in streamline coordinates becomes

$$\frac{\partial V}{\partial t} + V\frac{\partial V}{\partial s} = -\frac{1}{\rho}\frac{\partial p}{\partial s} + g_s \tag{1}$$

$$-V\frac{\partial \theta}{\partial t} - \frac{V^2}{R} = -\frac{1}{\rho}\frac{\partial p}{\partial n} + g_n \tag{2}$$

Further show that the integral of Eq. (1) with respect to s is none other than our old friend Bernoulli's equation (3.76).



P4.26

P4.27 A frictionless, incompressible steady-flow field is given by

$$\mathbf{V} = 2xy\mathbf{i} - y^2\mathbf{j}$$

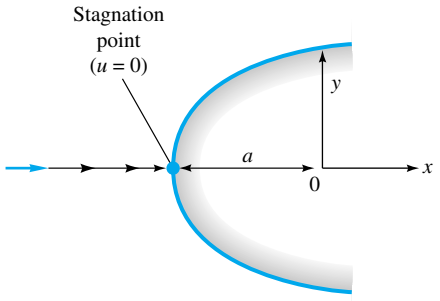
in arbitrary units. Let the density be ρ_0 = constant and neglect gravity. Find an expression for the pressure gradient in the x direction.

P4.28 If z is "up," what are the conditions on constants a and b for which the velocity field $u = ay$, $v = bx$, $w = 0$ is an exact solution to the continuity and Navier-Stokes equations for incompressible flow?

P4.29 Consider a steady, two-dimensional, incompressible flow of a newtonian fluid in which the velocity field is known, i.e., $u = -2xy$, $v = y^2 - x^2$, $w = 0$. (*a*) Does this flow satisfy conservation of mass? (*b*) Find the pressure field, $p(x, y)$ if the pressure at the point $(x = 0, y = 0)$ is equal to p_a.

P4.30 Show that the two-dimensional flow field of Example 1.10 is an exact solution to the incompressible Navier-Stokes equations (4.38). Neglecting gravity, compute the pressure field $p(x, y)$ and relate it to the absolute velocity $V^2 = u^2 + v^2$. Interpret the result.

P4.31 EES According to potential theory (Chap. 8) for the flow approaching a rounded two-dimensional body, as in Fig. P4.31, the velocity approaching the stagnation point is given by $u = U(1 - a^2/x^2)$, where a is the nose radius and U is the velocity far upstream. Compute the value and position of the maximum viscous normal stress along this streamline.



P4.31

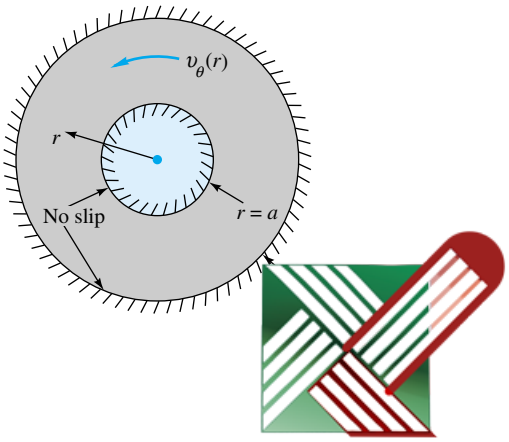
Is this also the position of maximum fluid deceleration? Evaluate the maximum viscous normal stress if the fluid is SAE 30 oil at 20°C, with $U = 2$ m/s and $a = 6$ cm.

P4.32 The answer to Prob. 4.14 is $v_\theta = f(r)$ only. Do not reveal this to your friends if they are still working on Prob. 4.14. Show that this flow field is an exact solution to the Navier-Stokes equations (4.38) for only two special cases of the function $f(r)$. Neglect gravity. Interpret these two cases physically.

P4.33 From Prob. 4.15 the purely radial polar-coordinate flow which satisfies continuity is $v_r = f(\theta)/r$, where f is an arbitrary function. Determine what particular forms of $f(\theta)$ satisfy the full Navier-Stokes equations in polar-coordinate form from Eqs. (D.5) and (D.6).

P4.34 The fully developed laminar-pipe-flow solution of Prob. 3.53, $v_z = u_{max}(1 - r^2/R^2)$, $v_\theta = 0$, $v_r = 0$, is an exact solution to the cylindrical Navier-Stokes equations (App. D). Neglecting gravity, compute the pressure distribution in the pipe $p(r, z)$ and the shear-stress distribution $\tau(r, z)$, using R, u_{max}, and μ as parameters. Why does the maximum shear occur at the wall? Why does the density not appear as a parameter?

P4.35 From the Navier-Stokes equations for incompressible flow in polar coordinates (App. D for cylindrical coordinates), find the most general case of purely circulating motion $v_\theta(r)$, $v_r = v_z = 0$, for flow with no slip between two fixed concentric cylinders, as in Fig. P4.35.



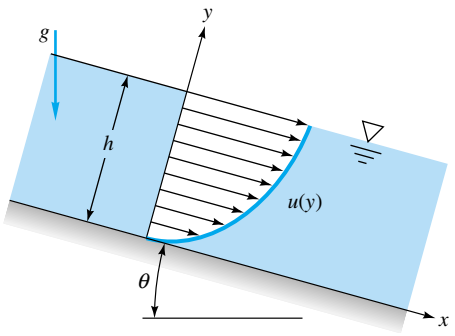
P4.35

ketabline.com Ebook.ketabline.com

P4.36 A constant-thickness film of viscous liquid flows in laminar motion down a plate inclined at angle θ, as in Fig. P4.36. The velocity profile is

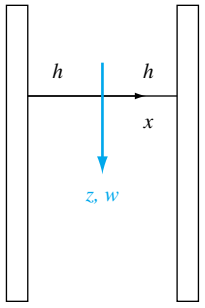
$$u = Cy(2h - y) \qquad v = w = 0$$

Find the constant C in terms of the specific weight and viscosity and the angle θ. Find the volume flux Q per unit width in terms of these parameters.



P4.36

***P4.37** A viscous liquid of constant ρ and μ falls due to gravity between two plates a distance $2h$ apart, as in Fig. P4.37. The flow is fully developed, with a single velocity component $w = w(x)$. There are no applied pressure gradients, only gravity. Solve the Navier-Stokes equation for the velocity profile between the plates.

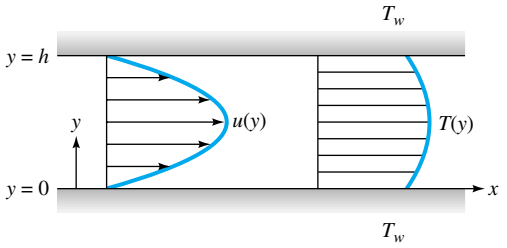


P4.37

P4.38 Reconsider the angular-momentum balance of Fig. 4.5 by adding a concentrated *body couple* C_z about the z axis [6]. Determine a relation between the body couple and shear stress for equilibrium. What are the proper dimensions for C_z? (Body couples are important in continuous media with microstructure, such as granular materials.)

P4.39 Problems involving viscous dissipation of energy are dependent on viscosity μ, thermal conductivity k, stream velocity U_0, and stream temperature T_0. Group these parameters into the dimensionless *Brinkman number*, which is proportional to μ.

P4.40 As mentioned in Sec. 4.11, the velocity profile for laminar flow between two plates, as in Fig. P4.40, is



P4.40

$$u = \frac{4u_{max}y(h - y)}{h^2} \qquad v = w = 0$$

If the wall temperature is T_w at both walls, use the incompressible-flow energy equation (4.75) to solve for the temperature distribution $T(y)$ between the walls for steady flow.

***P4.41** The approximate velocity profile in Prob. 3.18 and Fig. P3.18 for steady laminar flow through a duct, was suggested as

$$u = u_{max}\left(1 - \frac{y^2}{b^2}\right)\left(1 - \frac{z^2}{h^2}\right)$$

With $v = w = 0$, it satisfied the no-slip condition and gave a reasonable volume-flow estimate (which was the point of Prob. 3.18). Show, however, that it does *not* satsify the x-momentum Navier-Stokes equation for duct flow with constant pressure gradient $\partial p/\partial x < 0$. For extra credit, explain briefly how the actual exact solution to this problem is obtained (see, for example, Ref. 5, pp. 120–121).

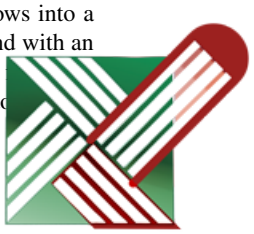
P4.42 In duct-flow problems with heat transfer, one often defines an average fluid temperature. Consider the duct flow of Fig. P4.40 of width b into the paper. Using a control-volume integral analysis with constant density and specific heat, derive an expression for the temperature arising if the entire duct flow poured into a bucket and was stirred uniformly. Assume arbitrary $u(y)$ and $T(y)$. This average is called the *cup-mixing temperature* of the flow.

P4.43 For the draining liquid film of Fig. P4.36, what are the appropriate boundary conditions (*a*) at the bottom $y = 0$ and (*b*) at the surface $y = h$?

P4.44 Suppose that we wish to analyze the sudden pipe-expansion flow of Fig. P3.59, using the full continuity and Navier-Stokes equations. What are the proper boundary conditions to handle this problem?

P4.45 Suppose that we wish to analyze the U-tube oscillation flow of Fig. P3.96, using the full continuity and Navier-Stokes equations. What are the proper boundary conditions to handle this problem?

P4.46 Fluid from a large reservoir at temperature T_0 flows into a circular pipe of radius R. The pipe walls are wound with an electric-resistance coil which delivers heat to the rate q_w (energy per unit wall area). If we wish to



ketabline.com Ebook.ketabline.com

this problem by using the full continuity, Navier-Stokes, and energy equations, what are the proper boundary conditions for the analysis?

P4.47 A two-dimensional incompressible flow is given by the velocity field $\mathbf{V} = 3y\mathbf{i} + 2x\mathbf{j}$, in arbitrary units. Does this flow satisfy continuity? If so, find the stream function $\psi(x, y)$ and plot a few streamlines, with arrows.

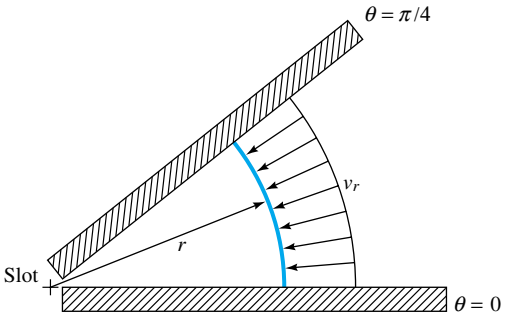
P4.48 Determine the incompressible two-dimensional stream function $\psi(x, y)$ which represents the flow field given in Example 1.10.

P4.49 Investigate the stream function $\psi = K(x^2 - y^2)$, K = constant. Plot the streamlines in the full xy plane, find any stagnation points, and interpret what the flow could represent.

P4.50 Investigate the polar-coordinate stream function $\psi = Kr^{1/2} \sin \frac{1}{2}\theta$, K = constant. Plot the streamlines in the full xy plane, find any stagnation points, and interpret.

P4.51 Investigate the polar-coordinate stream function $\psi = Kr^{2/3} \sin (2\theta/3)$, K = constant. Plot the streamlines in all except the bottom right quadrant, and interpret.

P4.52 A two-dimensional, incompressible, frictionless fluid is guided by wedge-shaped walls into a small slot at the origin, as in Fig. P4.52. The width into the paper is b, and the volume flow rate is Q. At any given distance r from the slot, the flow is radial inward, with constant velocity. Find an expression for the polar-coordinate stream function of this flow.



P4.52

P4.53 For the fully developed laminar-pipe-flow solution of Prob. 4.34, find the axisymmetric stream function $\psi(r, z)$. Use this result to determine the average velocity $V = Q/A$ in the pipe as a ratio of u_{max}.

P4.54 An incompressible stream function is defined by

$$\psi(x, y) = \frac{U}{L^2}(3x^2y - y^3)$$

where U and L are (positive) constants. Where in this chapter are the streamlines of this flow plotted? Use this stream function to find the volume flow Q passing through the rectangular surface whose corners are defined by $(x, y, z) =$ $(2L, 0, 0)$, $(2L, 0, b)$, $(0, L, b)$, and $(0, L, 0)$. Show the direction of Q.

***P4.55** In spherical polar coordinates, as in Fig. P4.12, the flow is called *axisymmetric* if $v_\phi \equiv 0$ and $\partial/\partial\phi \equiv 0$, so that $v_r = v_r(r, \theta)$ and $v_\theta = v_\theta(r, \theta)$. Show that a stream function $\psi(r, \theta)$ exists for this case and is given by

$$v_r = \frac{1}{r^2 \sin \theta}\frac{\partial \psi}{\partial \theta} \qquad v_\theta = -\frac{1}{r \sin \theta}\frac{\partial \psi}{\partial r}$$

This is called the *Stokes stream function* [5, p. 204].

P4.56 Investigate the velocity potential $\phi = Kxy$, K = constant. Sketch the potential lines in the full xy plane, find any stagnation points, and sketch in by eye the orthogonal streamlines. What could the flow represent?

P4.57 Determine the incompressible two-dimensional velocity potential $\phi(x, y)$ which represents the flow field given in Example 1.10. Sketch a few potential lines and streamlines.

P4.58 Show that the incompressible velocity potential in plane polar coordinates $\phi(r, \theta)$ is such that

$$v_r = \frac{\partial \phi}{\partial r} \qquad v_\theta = \frac{1}{r}\frac{\partial \phi}{\partial \theta}$$

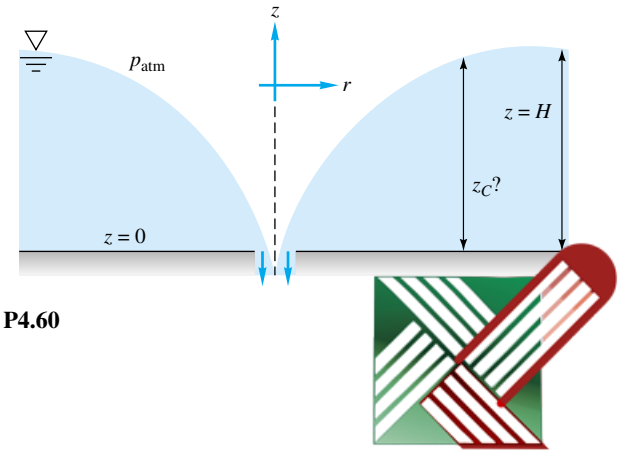
Further show that the angular velocity about the z-axis in such a flow would be given by

$$2\omega_z = \frac{1}{r}\frac{\partial}{\partial r}(rv_\theta) - \frac{1}{r}\frac{\partial}{\partial \theta}(v_r)$$

Finally show that ϕ as defined above satisfies Laplace's equation in polar coordinates for incompressible flow.

P4.59 Consider the simple flow defined by $\mathbf{V} = x\mathbf{i} - y\mathbf{j}$, in arbitrary units. At $t = 0$, consider the rectangular fluid element defined by the lines $x = 2$, $x = 3$ and $y = 2$, $y = 3$. Determine, and draw to scale, the location of this fluid element at $t = 0.5$ unit. Relate this new element shape to whether the flow is irrotational or incompressible.

P4.60 Liquid drains from a small hole in a tank, as shown in Fig. P4.60, such that the velocity field set up is given by $v_r \approx 0$, $v_z \approx 0$, $v_\theta = \omega R^2/r$, where $z = H$ is the depth of the water



P4.60

ketabline.com Ebook.ketabline.com

far from the hole. Is this flow pattern rotational or irrotational? Find the depth z_C of the water at the radius $r = R$.

P4.61 Investigate the polar-coordinate velocity potential $\phi = Kr^{1/2} \cos \frac{1}{2}\theta$, K = constant. Plot the potential lines in the full xy plane, sketch in by eye the orthogonal streamlines, and interpret.

P4.62 Show that the linear Couette flow between plates in Fig. 1.6 has a stream function but no velocity potential. Why is this so?

P4.63 Find the two-dimensional velocity potential $\phi(r, \theta)$ for the polar-coordinate flow pattern $v_r = Q/r$, $v_\theta = K/r$, where Q and K are constants.

P4.64 Show that the velocity potential $\phi(r, z)$ in axisymmetric cylindrical coordinates (see Fig. 4.2) is defined such that

$$v_r = \frac{\partial \phi}{\partial r} \qquad v_z = \frac{\partial \phi}{\partial z}$$

Further show that for incompressible flow this potential satisfies Laplace's equation in (r, z) coordinates.

P4.65 A two-dimensional incompressible flow is defined by

$$u = -\frac{Ky}{x^2 + y^2} \qquad v = \frac{Kx}{x^2 + y^2}$$

where K = constant. Is this flow irrotational? If so, find its velocity potential, sketch a few potential lines, and interpret the flow pattern.

P4.66 A plane polar-coordinate velocity potential is defined by

$$\phi = \frac{K \cos \theta}{r} \qquad K = \text{const}$$

Find the stream function for this flow, sketch some streamlines and potential lines, and interpret the flow pattern.

P4.67 A stream function for a plane, irrotational, polar-coordinate flow is

$$\psi = C\theta - K \ln r \qquad C \text{ and } K = \text{const}$$

Find the velocity potential for this flow. Sketch some streamlines and potential lines, and interpret the flow pattern.

P4.68 Find the stream function and plot some streamlines for the combination of a line source m at $(x, y) = (0, +a)$ and an equal line source placed at $(0, -a)$.

P4.69 Find the stream function and plot some streamlines for the combination of a counterclockwise line vortex K at $(x, y) = (+a, 0)$ and an equal line vortex placed at $(-a, 0)$.

***P4.70** Superposition of a source of strength m at $(-a, 0)$ and a sink (source of strength $-m$) at $(a, 0)$ was discussed briefly in this chapter, where it was shown that the velocity potential function is

$$\phi = \frac{1}{2} m \cdot \ln \frac{(x + a)^2 + y^2}{(x - a)^2 + y^2}$$

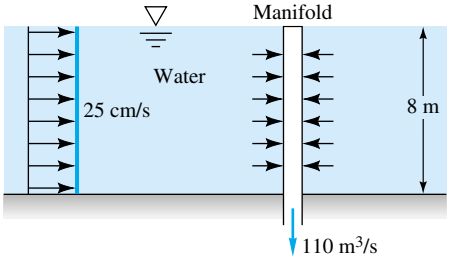
A *doublet* is formed in the limit as a goes to zero (the source and sink come together) while at the same time their strengths m and $-m$ go to infinity and minus infinity, respectively, with the product $a \cdot m$ remaining constant. (*a*) Find the limiting value of velocity potential for the doublet. *Hint*: Expand the natural logarithm as an infinite series of the form

$$\ln \frac{1 + \epsilon}{1 - \epsilon} = 2\left(\epsilon + \frac{\epsilon^3}{3} + \cdots\right)$$

as ϵ goes to zero. (*b*) Rewrite your result for ϕ_{doublet} in cylindrical coordinates.

P4.71 Find the stream function and plot some streamlines for the combination of a counterclockwise line vortex K at $(x, y) = (+a, 0)$ and an opposite (clockwise) line vortex placed at $(-a, 0)$.

P4.72 A coastal power plant takes in cooling water through a vertical perforated manifold, as in Fig. P4.72. The total volume flow intake is 110 m^3/s. Currents of 25 cm/s flow past the manifold, as shown. Estimate (*a*) how far downstream and (*b*) how far normal to the paper the effects of the intake are felt in the ambient 8-m-deep waters.



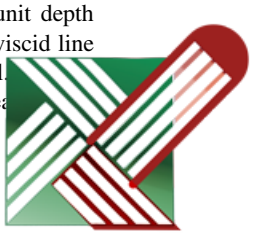
P4.72

P4.73 A two-dimensional Rankine half-body, 8 cm thick, is placed in a water tunnel at 20°C. The water pressure far upstream along the body centerline is 120 kPa. What is the nose radius of the half-body? At what tunnel flow velocity will cavitation bubbles begin to form on the surface of the body?

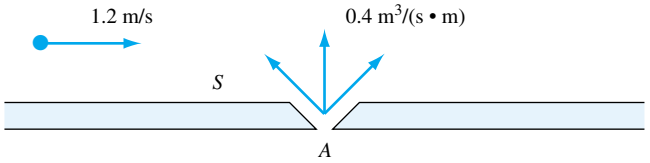
P4.74 Find the stream function and plot some streamlines for the combination of a uniform stream $\mathbf{i}U$ and a clockwise line vortex $-K$ at the origin. Are there any stagnation points in the flow field?

***P4.75** Find the stream function and plot some streamlines for the combination of a line source $2m$ at $(x, y) = (+a, 0)$ and a line source m at $(-a, 0)$. Are there any stagnation points in the flow field?

P4.76 Air flows at 1.2 m/s along a flat surface when it encounters a jet of air issuing from the horizontal wall at point A, as in Fig. 4.76. The jet volume flow is 0.4 m^3/s per unit depth into the paper. If the jet is approximated as an inviscid line source, (*a*) locate the stagnation point S on the wall far vertically will the jet flow extend into the strea



ketabline.com Ebook.ketabline.com



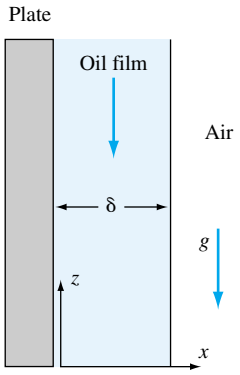
P4.76

P4.77 A tornado is simulated by a line sink $m = -1000$ m^2/s plus a line vortex $K = +1600$ m^2/s. Find the angle between any streamline and a radial line, and show that it is independent of both r and θ. If this tornado forms in sea-level standard air, at what radius will the local pressure be equivalent to 29 inHg?

P4.78 The solution to Prob. 4.68 (do not reveal!) can represent a line source m at $(0, +a)$ near a horizontal wall ($y = 0$). [The other source at $(0, -a)$ represents an "image" to create the wall.] Find (a) the magnitude of the maxinun flow velocity along the wall and (b) the point of minimum pressure along the wall. *Hint*: Use Bernoulli's equation.

***P4.79** Study the combined effect of the two viscous flows in Fig. 4.16. That is, find $u(y)$ when the upper plate moves at speed V and there is also a constant pressure gradient (dp/dx). Is superposition possible? If so, explain why. Plot representative velocity profiles for (a) zero, (b) positive, and (c) negative pressure gradients for the same upper-wall speed V.

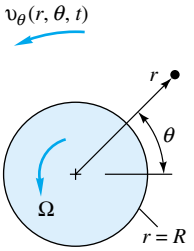
***P4.80** Oil, of density ρ and viscosity μ, drains steadily down the side of a vertical plate, as in Fig. P4.80. After a development region near the top of the plate, the oil film will become independent of z and of constant thickness δ. Assume that $w = w(x)$ only and that the atmosphere offers no shear resistance to the surface of the film. (a) Solve the Navier-Stokes equation for $w(x)$, and sketch its approximate shape. (b) Suppose that film thickness δ and the slope of the velocity profile at the wall $[\partial w/\partial x]_{\text{wall}}$ are measured with a laser-Doppler anemometer (Chap. 6). Find an expression for oil viscosity μ as a function of $(\rho, \delta, g, [\partial w/\partial x]_{\text{wall}})$.



P4.80

P4.81 Modify the analysis of Fig. 4.17 to find the velocity u_θ when the inner cylinder is fixed and the outer cylinder rotates at angular velocity Ω_0. May this solution be *added* to Eq. (4.146) to represent the flow caused when both inner and outer cylinders rotate? Explain your conclusion.

***P4.82** A solid circular cylinder of radius R rotates at angular velocity Ω in a viscous incompressible fluid which is at rest far from the cylinder, as in Fig. P4.82. Make simplifying assumptions and derive the governing differential equation and boundary conditions for the velocity field v_θ in the fluid. Do not solve unless you are obsessed with this problem. What is the steady-state flow field for this problem?

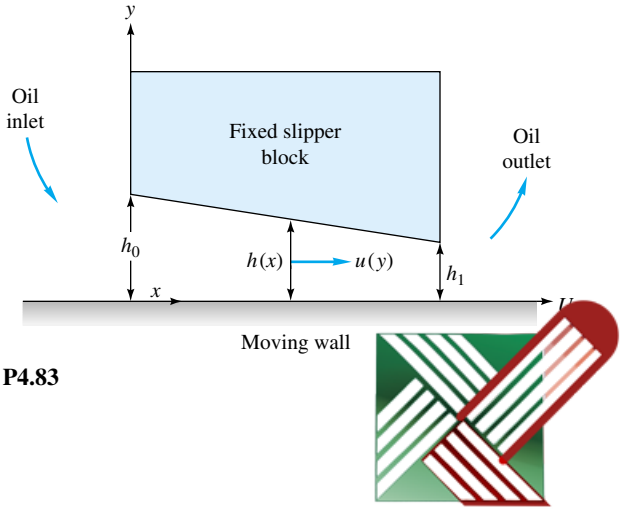


P4.82

P4.83 The flow pattern in bearing lubrication can be illustrated by Fig. P4.83, where a viscous oil (ρ, μ) is forced into the gap $h(x)$ between a fixed slipper block and a wall moving at velocity U. If the gap is thin, $h \ll L$, it can be shown that the pressure and velocity distributions are of the form $p = p(x)$, $u = u(y)$, $v = w = 0$. Neglecting gravity, reduce the Navier-Stokes equations (4.38) to a single differential equation for $u(y)$. What are the proper boundary conditions? Integrate and show that

$$u = \frac{1}{2\mu}\frac{dp}{dx}(y^2 - yh) + U\left(1 - \frac{y}{h}\right)$$

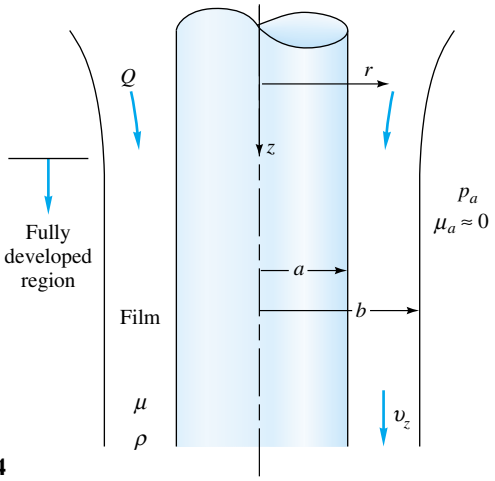
where $h = h(x)$ may be an arbitrary slowly varying gap width. (For further information on lubrication theory, see Ref. 16.)



P4.83

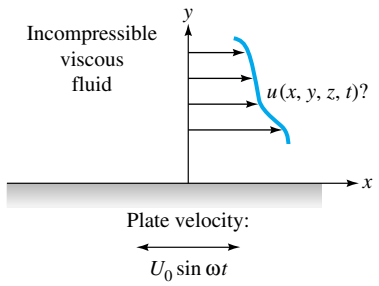
ketabline.com Ebook.ketabline.com

***P4.84** Consider a viscous film of liquid draining uniformly down the side of a vertical rod of radius a, as in Fig. P4.84. At some distance down the rod the film will approach a terminal or *fully developed* draining flow of constant outer radius b, with $v_z = v_z(r)$, $v_\theta = v_r = 0$. Assume that the atmosphere offers no shear resistance to the film motion. Derive a differential equation for v_z, state the proper boundary conditions, and solve for the film velocity distribution. How does the film radius b relate to the total film volume flow rate Q?



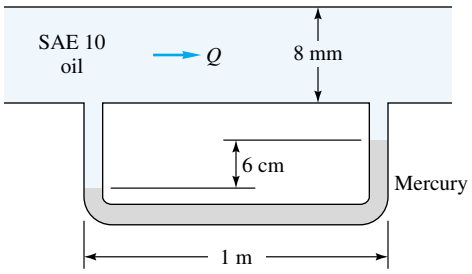
P4.84

P4.85 A flat plate of essentially infinite width and breadth oscillates sinusoidally in its own plane beneath a viscous fluid, as in Fig. P4.85. The fluid is at rest far above the plate. Making as many simplifying assumptions as you can, set up the governing differential equation and boundary conditions for finding the velocity field u in the fluid. Do not solve (if you *can* solve it immediately, you might be able to get exempted from the balance of this course with credit).



P4.85

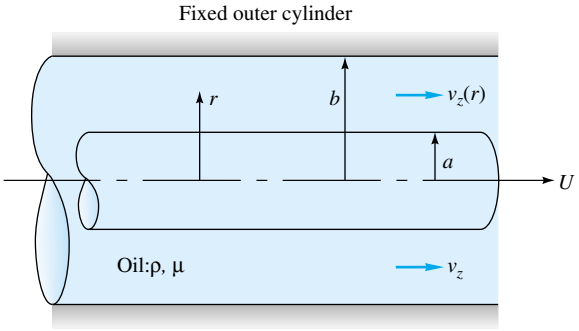
P4.86 SAE 10 oil at 20°C flows between parallel plates 8 cm apart, as in Fig. P4.86. A mercury manometer, with wall pressure taps 1 m apart, registers a 6-cm height, as shown. Estimate the flow rate of oil for this condition.



P4.86

P4.87 Suppose in Fig. 4.17 that neither cylinder is rotating. The fluid has constant (ρ, μ, k, c_p). What, then, is the steady-flow solution for $v_\theta(r)$? For this condition, suppose that the inner and outer cylinder surface temperatures are T_i and T_o, respectively. Simplify the differential energy equation appropriately for this problem, state the boundary conditions, and find the temperature distribution in the fluid. Neglect gravity.

P4.88 The viscous oil in Fig. P4.88 is set into steady motion by a concentric inner cylinder moving axially at velocity U inside a fixed outer cylinder. Assuming constant pressure and density and a purely axial fluid motion, solve Eqs. (4.38) for the fluid velocity distribution $v_z(r)$. What are the proper boundary conditions?

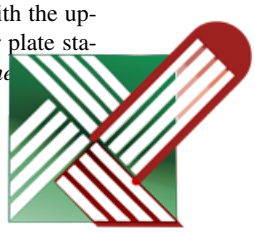


P4.88

***P4.89** Modify Prob. 4.88 so that the outer cylinder also moves to the *left* at constant speed V. Find the velocity distribution $v_z(r)$. For what ratio V/U will the wall shear stress be the same at both cylinder surfaces?

P4.90 A 5-cm-diameter rod is pulled steadily at 2 m/s through a fixed cylinder whose clearance is filled with SAE 10 oil at 20°C, as in Fig. P4.90. Estimate the (steady) force required to pull the inner rod.

***P4.91** Consider two-dimensional, incompressible, steady Couette flow (flow between two infinite parallel plates with the upper plate moving at constant speed and the lower plate stationary, as in Fig. 4.16*a*). Let the fluid be *nonne*
with its viscous stresses given by



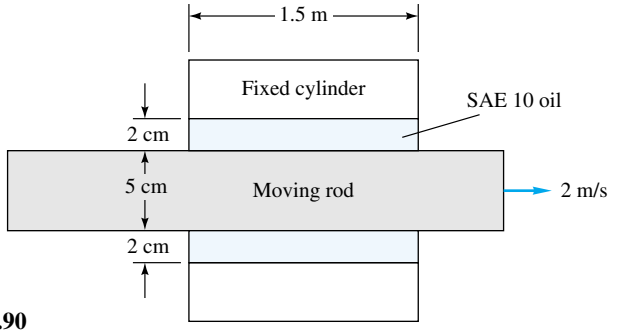
ketabline.com Ebook.ketabline.com

$$\tau_{xx} = a\left(\frac{\partial u}{\partial x}\right)^c \qquad \tau_{yy} = a\left(\frac{\partial v}{\partial y}\right)^c \qquad \tau_{zz} = a\left(\frac{\partial w}{\partial z}\right)^c$$

$$\tau_{xy} = \tau_{yx} = \tfrac{1}{2}a\left(\frac{\partial u}{\partial y} + \frac{\partial v}{\partial x}\right)^c \qquad \tau_{xz} = \tau_{zx} = \tfrac{1}{2}a\left(\frac{\partial u}{\partial z} + \frac{\partial w}{\partial x}\right)^c$$

$$\tau_{yz} = \tau_{zy} = \tfrac{1}{2}a\left(\frac{\partial v}{\partial z} + \frac{\partial w}{\partial y}\right)^c$$

where a and c are constants of the fluid. Make all the same assumptions as in the derivation of Eq. (4.140). (*a*) Find the velocity profile $u(y)$. (*b*) How does the velocity profile for this case compare to that of a newtonian fluid?



P4.90

Word Problems

W4.1 The total acceleration of a fluid particle is given by Eq. (4.2) in the eulerian system, where **V** is a known function of space and time. Explain how we might evaluate particle acceleration in the lagrangian frame, where particle position **r** is a known function of time and initial position, $\mathbf{r} = \text{fcn}(\mathbf{r}_0, t)$. Can you give an illustrative example?

W4.2 Is it true that the continuity relation, Eq. (4.6), is valid for both viscous and inviscid, newtonian and nonnewtonian, compressible and incompressible flow? If so, are there *any* limitations on this equation?

W4.3 Consider a CD compact disk rotating at angular velocity Ω. Does it have *vorticity* in the sense of this chapter? If so, how much vorticity?

W4.4 How much acceleration can fluids endure? Are fluids like astronauts, who feel that 5*g* is severe? Perhaps use the flow pattern of Example 4.8, at $r = R$, to make some estimates of fluid-acceleration magnitudes.

W4.5 State the conditions (there are more than one) under which the analysis of temperature distribution in a flow field can be completely uncoupled, so that a separate analysis for velocity and pressure is possible. Can we do this for both laminar and turbulent flow?

W4.6 Consider liquid flow over a dam or weir. How might the boundary conditions and the flow pattern change when we compare water flow over a large prototype to SAE 30 oil flow over a tiny scale model?

W4.7 What is the difference between the stream function ψ and our method of finding the streamlines from Sec. 1.9? Or are they essentially the same?

W4.8 Under what conditions do both the stream function ψ and the velocity potential ϕ exist for a flow field? When does one exist but not the other?

W4.9 How might the remarkable three-dimensional Taylor instability of Fig. 4.18 be predicted? Discuss a general procedure for examining the stability of a given flow pattern.

W4.10 Consider an irrotational, incompressible, axisymmetric ($\partial/\partial\theta = 0$) flow in (r, z) coordinates. Does a stream function exist? If so, does it satisfy Laplace's equation? Are lines of constant ψ equal to the flow streamlines? Does a velocity potential exist? If so, does it satisfy Laplace's equation? Are lines of constant ϕ everywhere perpendicular to the ψ lines?

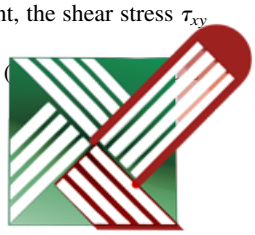
Fundamentals of Engineering Exam Problems

This chapter is not a favorite of the people who prepare the FE Exam. Probably not a single problem from this chapter will appear on the exam, but if some did, they might be like these.

FE4.1 Given the steady, incompressible velocity distribution $\mathbf{V} = 3x\mathbf{i} + Cy\mathbf{j} + 0\mathbf{k}$, where C is a constant, if conservation of mass is satisfied, the value of C should be
(*a*) 3, (*b*) 3/2, (*c*) 0, (*d*) −3/2, (*e*) −3

FE4.2 Given the steady velocity distribution $\mathbf{V} = 3x\mathbf{i} + 0\mathbf{j} + Cy\mathbf{k}$, where C is a constant, if the flow is irrotational, the value of C should be
(*a*) 3, (*b*) 3/2, (*c*) 0, (*d*) −3/2, (*e*) −3

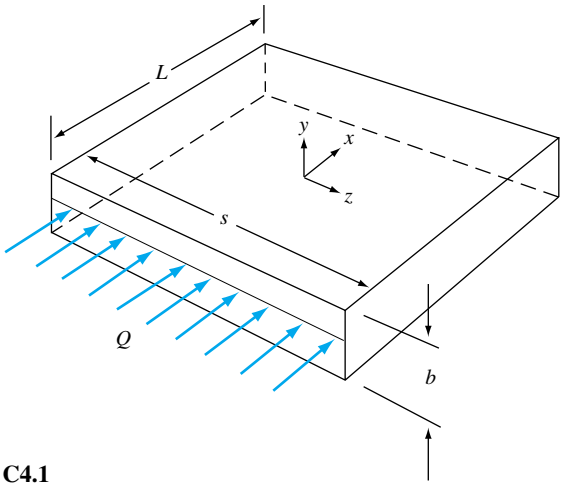
FE4.3 Given the steady, incompressible velocity distribution $\mathbf{V} = 3x\mathbf{i} + Cy\mathbf{j} + 0\mathbf{k}$, where C is a constant, the shear stress τ_{xy} at the point (x, y, z) is given by
(*a*) 3μ, (*b*) $(3x + Cy)\mu$, (
(*e*) $(3 + C)\mu$



ketabline.com Ebook.ketabline.com

Comprehensive Problem

C4.1 In a certain medical application, water at room temperature and pressure flows through a rectangular channel of length $L = 10$ cm, width $s = 1.0$ cm, and gap thickness $b = 0.30$ mm as in Fig. C4.1. The volume flow rate is sinusoidal with amplitude $\hat{Q} = 0.50$ mL/s and frequency $f = 20$ Hz, i.e., $Q = \hat{Q} \sin(2\pi ft)$.
(*a*) Calculate the maximum Reynolds number ($\mathrm{Re} = Vb/\nu$) based on maximum average velocity and gap thickness. Channel flow like this remains laminar for Re less than about 2000. If Re is greater than about 2000, the flow will be turbulent. Is this flow laminar or turbulent? (*b*) In this problem, the frequency is low enough that at any given time, the flow can be solved as if it were steady at the given flow rate. (This is called a quasi-steady assumption.) At any arbitrary instant of time, find an expression for streamwise velocity u as a function of y, μ, dp/dx, and b, where dp/dx is the pressure gradient required to push the flow through the channel at volume flow rate Q. In addition, estimate the maximum magnitude of velocity component u. (*c*) At any instant of time, find a relationship between volume flow rate Q and pressure gradient dp/dx. Your answer should be given as an expression for Q as a function of dp/dx, s, b, and viscosity μ. (*d*) Estimate the wall shear stress, τ_w as a function of $\hat{Q}$, f, μ, b, s, and time (t). (*e*) Finally, for the numbers given in the problem statement, estimate the amplitude of the wall shear stress, $\hat{\tau}_w$, in N/m^2.



C4.1

References

1. D. A. Anderson, J. C. Tannehill, and R. H. Pletcher, *Computational Fluid Mechanics and Heat Transfer*, 2d ed., McGraw-Hill, New York, 1997.
2. G. B. Wallis, *One-Dimensional Two-Phase Flow*, McGraw-Hill, New York, 1969.
3. S. M. Selby, *CRC Handbook of Tables for Mathematics*, 4th ed., CRC Press Inc., Cleveland, OH, 1976.
4. H. Schlichting, *Boundary Layer Theory*, 7th ed., McGraw-Hill, New York, 1979.
5. F. M. White, *Viscous Fluid Flow*, 2d ed., McGraw-Hill, New York, 1991.
6. L. E. Malvern, *Introduction to Mechanics of a Continuous Medium*, Prentice-Hall, Englewood Cliffs, NJ, 1969.
7. J. P. Holman, *Heat Transfer*, 8th ed., McGraw-Hill, New York, 1997.
8. W. M. Kays and M. E. Crawford, *Convective Heat and Mass Transfer*, 3d ed., McGraw-Hill, New York, 1993.
9. G. K. Batchelor, *An Introduction to Fluid Dynamics*, Cambridge University Press, Cambridge, England, 1967.
10. L. Prandtl and O. G. Tietjens, *Fundamentals of Hydro- and Aeromechanics*, Dover, New York, 1957.
11. R. Aris, *Vectors, Tensors, and the Basic Equations of Fluid Mechanics*, Prentice-Hall, Englewood Cliffs, NJ, 1962.
12. G. E. Mase, *Continuum Mechanics*, Schaum's Outline Series, McGraw-Hill, New York, 1970.
13. W. F. Hughes and E. W. Gaylord, *Basic Equations of Engineering Science*, Schaum's Outline Series, McGraw-Hill, New York, 1964.
14. G. Astarita and G. Marrucci, *Principles of Non-Newtonian Fluid Mechanics*, McGraw-Hill, New York, 1974.
15. H. Lamb, *Hydrodynamics*, 6th ed., Dover, New York, 1945.
16. A. Szeri, *Tribology: Friction, Lubrication, and Wear*, McGraw-Hill, New York, 1980.
17. G. I. Taylor, "Stability of a Viscous Liquid Contained between Two Rotating Cylinders," *Philos. Trans. Roy. Soc. London Ser. A*, vol. 223, 1923, pp. 289–343.
18. E. L. Koschmieder, "Turbulent Taylor Vortex Flow," *J. Fluid Mech.*, vol. 93, pt. 3, 1979, pp. 515–527.



ketabline.com Ebook.ketabline.com



Wind tunnel test of an F-18 fighter plane model. Testing of models is imperative in the design of complex, expensive fluids-engineering devices. Such tests use the principles of dimensional analysis and modeling from this chapter. *(Courtesy of Mark E. Gibson/Visuals Unlimited)*



ketabline.com Ebook.ketabline.com

Chapter 5
Dimensional Analysis and Similarity

Motivation. In this chapter we discuss the planning, presentation, and interpretation of experimental data. We shall try to convince you that such data are best presented in *dimensionless* form. Experiments which might result in tables of output, or even multiple volumes of tables, might be reduced to a single set of curves—or even a single curve—when suitably nondimensionalized. The technique for doing this is *dimensional analysis*.

Chapter 3 presented gross control-volume balances of mass, momentum, and energy which led to estimates of global parameters: mass flow, force, torque, total heat transfer. Chapter 4 presented infinitesimal balances which led to the basic partial differential equations of fluid flow and some particular solutions. These two chapters covered *analytical* techniques, which are limited to fairly simple geometries and well-defined boundary conditions. Probably one-third of fluid-flow problems can be attacked in this analytical or theoretical manner.

The other two-thirds of all fluid problems are too complex, both geometrically and physically, to be solved analytically. They must be tested by experiment. Their behavior is reported as experimental data. Such data are much more useful if they are expressed in compact, economic form. Graphs are especially useful, since tabulated data cannot be absorbed, nor can the trends and rates of change be observed, by most engineering eyes. These are the motivations for dimensional analysis. The technique is traditional in fluid mechanics and is useful in all engineering and physical sciences, with notable uses also seen in the biological and social sciences.

Dimensional analysis can also be useful in theories, as a compact way to present an analytical solution or output from a computer model. Here we concentrate on the presentation of experimental fluid-mechanics data.

5.1 Introduction

Basically, dimensional analysis is a method for reducing the number and complexity of experimental variables which affect a given physical phenomenon, by using a sort of compacting technique. If a phenomenon depends upon n dimensional variables, dimensional analysis will reduce the problem to only k *dimensionless* variables, where the reduction $n - k = 1$, 2, 3, or 4, depending upon the problem complexity. Gene ally $n - k$ equals the number of different dimensions (sometimes



ketabline.com Ebook.ketabline.com

mary or fundamental dimensions) which govern the problem. In fluid mechanics, the four basic dimensions are usually taken to be mass M, length L, time T, and temperature Θ, or an $MLT\Theta$ system for short. Sometimes one uses an $FLT\Theta$ system, with force F replacing mass.

Although its purpose is to reduce variables and group them in dimensionless form, dimensional analysis has several side benefits. The first is enormous savings in time and money. Suppose one knew that the force F on a particular body immersed in a stream of fluid depended only on the body length L, stream velocity V, fluid density ρ, and fluid viscosity μ, that is,

$$F = f(L, V, \rho, \mu) \tag{5.1}$$

Suppose further that the geometry and flow conditions are so complicated that our integral theories (Chap. 3) and differential equations (Chap. 4) fail to yield the solution for the force. Then we must find the function $f(L, V, \rho, \mu)$ experimentally.

Generally speaking, it takes about 10 experimental points to define a curve. To find the effect of body length in Eq. (5.1), we have to run the experiment for 10 lengths L. For each L we need 10 values of V, 10 values of ρ, and 10 values of μ, making a grand total of 10^4, or 10,000, experiments. At \$50 per experiment—well, you see what we are getting into. However, with dimensional analysis, we can immediately reduce Eq. (5.1) to the equivalent form

$$\frac{F}{\rho V^2 L^2} = g\left(\frac{\rho VL}{\mu}\right) \tag{5.2}$$

or

$$C_F = g(\mathrm{Re})$$

i.e., the dimensionless *force coefficient* $F/(\rho V^2 L^2)$ is a function only of the dimensionless *Reynolds number* $\rho VL/\mu$. We shall learn exactly how to make this reduction in Secs. 5.2 and 5.3.

The function g is different mathematically from the original function f, but it contains all the same information. Nothing is lost in a dimensional analysis. And think of the savings: We can establish g by running the experiment for only 10 values of the single variable called the Reynolds number. We do not have to vary L, V, ρ, or μ separately but only the *grouping* $\rho VL/\mu$. This we do merely by varying velocity V in, say, a wind tunnel or drop test or water channel, and there is no need to build 10 different bodies or find 100 different fluids with 10 densities and 10 viscosities. The cost is now about \$500, maybe less.

A second side benefit of dimensional analysis is that it helps our thinking and planning for an experiment or theory. It suggests dimensionless ways of writing equations before we waste money on computer time to find solutions. It suggests variables which can be discarded; sometimes dimensional analysis will immediately reject variables, and at other times it groups them off to the side, where a few simple tests will show them to be unimportant. Finally, dimensional analysis will often give a great deal of insight into the form of the physical relationship we are trying to study.

A third benefit is that dimensional analysis provides *scaling laws* which can convert data from a cheap, small *model* to design information for an expensive, large *prototype*. We do not build a million-dollar airplane and see whether it has enough force. We measure the lift on a small model and use a scaling law to predict th



ketabline.com Ebook.ketabline.com

the full-scale prototype airplane. There are rules we shall explain for finding scaling laws. When the scaling law is valid, we say that a condition of *similarity* exists between the model and the prototype. In the simple case of Eq. (5.1), similarity is achieved if the Reynolds number is the same for the model and prototype because the function g then requires the force coefficient to be the same also:

$$\text{If} \quad \text{Re}_m = \text{Re}_p \quad \text{then} \quad C_{Fm} = C_{Fp} \tag{5.3}$$

where subscripts m and p mean model and prototype, respectively. From the definition of force coefficient, this means that

$$\frac{F_p}{F_m} = \frac{\rho_p}{\rho_m}\left(\frac{V_p}{V_m}\right)^2\left(\frac{L_p}{L_m}\right)^2 \tag{5.4}$$

for data taken where $\rho_p V_p L_p/\mu_p = \rho_m V_m L_m/\mu_m$. Equation (5.4) is a scaling law: If you measure the model force at the model Reynolds number, the prototype force at the same Reynolds number equals the model force times the density ratio times the velocity ratio squared times the length ratio squared. We shall give more examples later.

Do you understand these introductory explanations? Be careful; learning dimensional analysis is like learning to play tennis: There are levels of the game. We can establish some ground rules and do some fairly good work in this brief chapter, but dimensional analysis in the broad view has many subtleties and nuances which only time and practice and maturity enable you to master. Although dimensional analysis has a firm physical and mathematical foundation, considerable art and skill are needed to use it effectively.

EXAMPLE 5.1

A copepod is a water crustacean approximately 1 mm in diameter. We want to know the drag force on the copepod when it moves slowly in fresh water. A scale model 100 times larger is made and tested in glycerin at $V = 30$ cm/s. The measured drag on the model is 1.3 N. For similar conditions, what are the velocity and drag of the actual copepod in water? Assume that Eq. (5.1) applies and the temperature is 20°C.

Solution

From Table A.3 the fluid properties are:

Water (prototype): $\mu_p = 0.001$ kg/(m · s) $\rho_p = 998$ kg/m^3

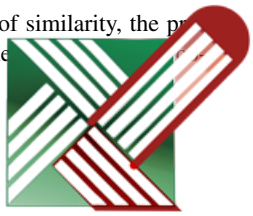
Glycerin (model): $\mu_m = 1.5$ kg/(m · s) $\rho_m = 1263$ kg/m^3

The length scales are $L_m = 100$ mm and $L_p = 1$ mm. We are given enough model data to compute the Reynolds number and force coefficient

$$\text{Re}_m = \frac{\rho_m V_m L_m}{\mu_m} = \frac{(1263 \text{ kg/m}^3)(0.3 \text{ m/s})(0.1 \text{ m})}{1.5 \text{ kg/(m} \cdot \text{s)}} = 25.3$$

$$C_{Fm} = \frac{F_m}{\rho_m V_m{}^2 L_m{}^2} = \frac{1.3 \text{ N}}{(1263 \text{ kg/m}^3)(0.3 \text{ m/s})^2(0.1 \text{ m})^2} = 1.14$$

Both these numbers are dimensionless, as you can check. For conditions of similarity, the prototype Reynolds number must be the same, and Eq. (5.2) then requires the force coefficient to be the same



ketabline.com Ebook.ketabline.com

$$\text{Re}_p = \text{Re}_m = 25.3 = \frac{998V_p(0.001)}{0.001}$$

or $$V_p = 0.0253 \text{ m/s} = 2.53 \text{ cm/s} \qquad \textit{Ans.}$$

$$C_{Fp} = C_{Fm} = 1.14 = \frac{F_p}{998(0.0253)^2(0.001)^2}$$

or $$F_p = 7.31 \times 10^{-7} \text{ N} \qquad \textit{Ans.}$$

It would obviously be difficult to measure such a tiny drag force.

Historically, the first person to write extensively about units and dimensional reasoning in physical relations was Euler in 1765. Euler's ideas were far ahead of his time, as were those of Joseph Fourier, whose 1822 book *Analytical Theory of Heat* outlined what is now called the *principle of dimensional homogeneity* and even developed some similarity rules for heat flow. There were no further significant advances until Lord Rayleigh's book in 1877, *Theory of Sound,* which proposed a "method of dimensions" and gave several examples of dimensional analysis. The final breakthrough which established the method as we know it today is generally credited to E. Buckingham in 1914 [29], whose paper outlined what is now called the *Buckingham pi theorem* for describing dimensionless parameters (see Sec. 5.3). However, it is now known that a Frenchman, A. Vaschy, in 1892 and a Russian, D. Riabouchinsky, in 1911 had independently published papers reporting results equivalent to the pi theorem. Following Buckingham's paper, P. W. Bridgman published a classic book in 1922 [1], outlining the general theory of dimensional analysis. The subject continues to be controversial because there is so much art and subtlety in using dimensional analysis. Thus, since Bridgman there have been at least 24 books published on the subject [2 to 25]. There will probably be more, but seeing the whole list might make some fledgling authors think twice. Nor is dimensional analysis limited to fluid mechanics or even engineering. Specialized books have been written on the application of dimensional analysis to metrology [26], astrophysics [27], economics [28], building scale models [36], chemical processing pilot plants [37], social sciences [38], biomedical sciences [39], pharmacy [40], fractal geometry [41], and even the growth of plants [42].

5.2 The Principle of Dimensional Homogeneity

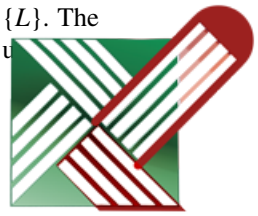
In making the remarkable jump from the five-variable Eq. (5.1) to the two-variable Eq. (5.2), we were exploiting a rule which is almost a self-evident axiom in physics. This rule, the *principle of dimensional homogeneity* (PDH), can be stated as follows:

> If an equation truly expresses a proper relationship between variables in a physical process, it will be *dimensionally homogeneous;* i.e., each of its additive terms will have the same dimensions.

All the equations which are derived from the theory of mechanics are of this form. For example, consider the relation which expresses the displacement of a falling body

$$S = S_0 + V_0 t + \tfrac{1}{2} g t^2 \tag{5.5}$$

Each term in this equation is a displacement, or length, and has dimensions $\{L\}$. The equation is dimensionally homogeneous. Note also that any consistent set of u
be used to calculate a result.



ketabline.com Ebook.ketabline.com

Consider Bernoulli's equation for incompressible flow

$$\frac{p}{\rho} + \frac{1}{2}V^2 + gz = \text{const} \tag{5.6}$$

Each term, including the constant, has dimensions of velocity squared, or $\{L^2T^{-2}\}$. The equation is dimensionally homogeneous and gives proper results for any consistent set of units.

Students count on dimensional homogeneity and use it to check themselves when they cannot quite remember an equation during an exam. For example, which is it:

$$S = \tfrac{1}{2}gt^2? \qquad \text{or} \qquad S = \tfrac{1}{2}g^2t? \tag{5.7}$$

By checking the dimensions, we reject the second form and back up our faulty memory. We are exploiting the principle of dimensional homogeneity, and this chapter simply exploits it further.

Equations (5.5) and (5.6) also illustrate some other factors that often enter into a dimensional analysis:

Dimensional variables are the quantities which actually vary during a given case and would be plotted against each other to show the data. In Eq. (5.5), they are S and t; in Eq. (5.6) they are p, V, and z. All have dimensions, and all can be nondimensionalized as a dimensional-analysis technique.

Dimensional constants may vary from case to case but are held constant during a given run. In Eq. (5.5) they are S_0, V_0, and g, and in Eq. (5.6) they are ρ, g, and C. They all have dimensions and conceivably could be nondimensionalized, but they are normally used to help nondimensionalize the variables in the problem.

Pure constants have no dimensions and never did. They arise from mathematical manipulations. In both Eqs. (5.5) and (5.6) they are $\frac{1}{2}$ and the exponent 2, both of which came from an integration: $\int t\,dt = \frac{1}{2}t^2$, $\int V\,dV = \frac{1}{2}V^2$. Other common dimensionless constants are π and e.

Note that integration and differentiation of an equation may change the dimensions but not the homogeneity of the equation. For example, integrate or differentiate Eq. (5.5):

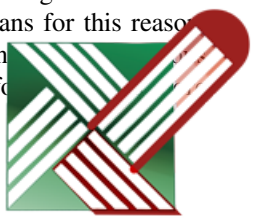
$$\int S\,dt = S_0t + \tfrac{1}{2}V_0t^2 + \tfrac{1}{6}gt^3 \tag{5.8a}$$

$$\frac{dS}{dt} = V_0 + gt \tag{5.8b}$$

In the integrated form (5.8*a*) every term has dimensions of $\{LT\}$, while in the derivative form (5.8*b*) every term is a velocity $\{LT^{-1}\}$.

Finally, there are some physical variables that are naturally dimensionless by virtue of their definition as ratios of dimensional quantities. Some examples are strain (change in length per unit length), Poisson's ratio (ratio of transverse strain to longitudinal strain), and specific gravity (ratio of density to standard water density). All angles are dimensionless (ratio of arc length to radius) and should be taken in radians for this reaso

The motive behind dimensional analysis is that any dimension equation can be written in an entirely equivalent nondimensional fo



ketabline.com Ebook.ketabline.com

compact. Usually there is more than one method of presenting one's dimensionless data or theory. Let us illustrate these concepts more thoroughly by using the falling-body relation (5.5) as an example.

Ambiguity: The Choice of Variables and Scaling Parameters[1]

Equation (5.5) is familiar and simple, yet illustrates most of the concepts of dimensional analysis. It contains five terms (S, S_0, V_0, t, g) which we may divide, in our thinking, into variables and parameters. The *variables* are the things which we wish to plot, the basic output of the experiment or theory: in this case, S versus t. The *parameters* are those quantities whose effect upon the variables we wish to know: in this case S_0, V_0, and g. Almost any engineering study can be subdivided in this manner.

To nondimensionalize our results, we need to know how many dimensions are contained among our variables and parameters: in this case, only two, length $\{L\}$ and time $\{T\}$. Check each term to verify this:

$$\{S\} = \{S_0\} = \{L\} \qquad \{t\} = \{T\} \qquad \{V_0\} = \{LT^{-1}\} \qquad \{g\} = \{LT^{-2}\}$$

Among our parameters, we therefore select two to be *scaling parameters,* used to define dimensionless variables. What remains will be the "basic" parameter(s) whose effect we wish to show in our plot. These choices will not affect the content of our data, only the form of their presentation. Clearly there is ambiguity in these choices, something that often vexes the beginning experimenter. But the ambiguity is deliberate. Its purpose is to show a particular effect, and the choice is yours to make.

For the falling-body problem, we select any two of the three parameters to be scaling parameters. Thus we have three options. Let us discuss and display them in turn.

Option 1: Scaling parameters S_0 and V_0: the effect of gravity g.

First use the scaling parameters (S_0, V_0) to define dimensionless (*) displacement and time. There is only one suitable definition for each:[2]

$$S^* = \frac{S}{S_0} \qquad t^* = \frac{V_0 t}{S_0} \tag{5.9}$$

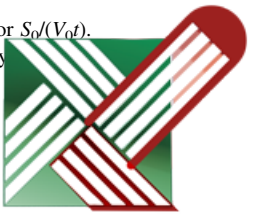
Substitute these variables into Eq. (5.5) and clean everything up until each term is dimensionless. The result is our first option:

$$S^* = 1 + t^* + \frac{1}{2}\alpha t^{*2} \qquad \alpha = \frac{gS_0}{V_0^2} \tag{5.10}$$

This result is shown plotted in Fig. 5.1*a*. There is a single dimensionless parameter α, which shows here the effect of gravity. It cannot show the direct effects of S_0 and V_0, since these two are hidden in the ordinate and abscissa. We see that gravity increases the parabolic rate of fall for $t^* > 0$, but not the initial slope at $t^* = 0$. We would learn the same from falling-body data, and the plot, within experimental accuracy, would look like Fig. 5.1*a*.

[1] I am indebted to Prof. Jacques Lewalle of Syracuse University for suggesting, outlining, and clarifying this entire discussion.

[2] Make them *proportional* to S and t. Do not define dimensionless terms upside down: S_0/S or $S_0/(V_0t)$. The plots will look funny, users of your data will be confused, and your supervisor will be angry. a good idea.



ketabline.com Ebook.ketabline.com

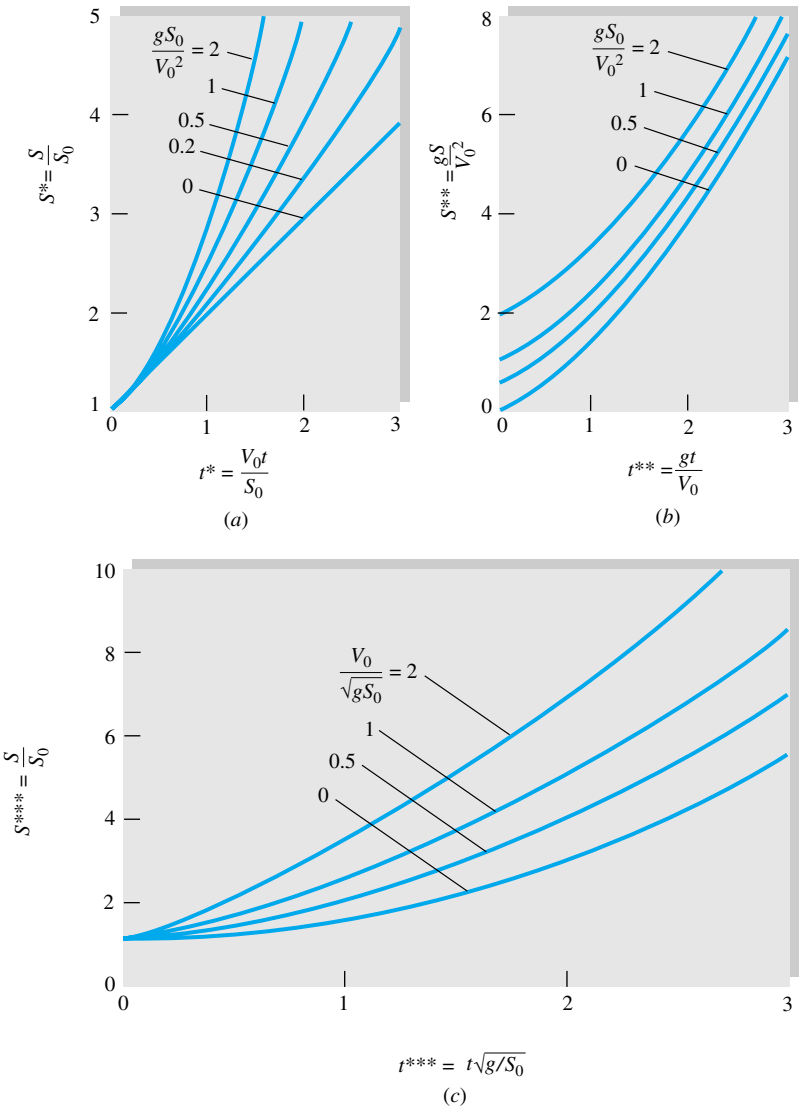


Fig. 5.1 Three entirely equivalent dimensionless presentations of the falling-body problem, Eq. (5.5): the effect of (*a*) gravity, (*b*) initial displacement, and (*c*) initial velocity. All plots contain the same information.

Option 2: Scaling parameters V_0 and g: the effect of initial displacement S_0.

Now use the new scaling parameters (V_0, g) to define dimensionless (**) displacement and time. Again there is only one suitable definition:

$$S^{**} = \frac{Sg}{V_0^2} \qquad t^{**} = t\frac{g}{V_0} \tag{5.11}$$

Substitute these variables into Eq. (5.5) and clean everything up again. The result is our second option:

$$S^{**} = \alpha + t^{**} + \frac{1}{2}t^{**2} \qquad \alpha = \frac{gS_0}{V_0^2}$$



ketabline.com Ebook.ketabline.com

This result is plotted in Fig. 5.1*b*. The same single parameter α again appears and here shows the effect of initial *displacement,* which merely moves the curves upward without changing their shape.

Option 3: Scaling parameters S_0 and g: the effect of initial speed V_0.

Finally use the scaling parameters (S_0, g) to define dimensionless (***) displacement and time. Again there is only one suitable definition:

$$S^{***} = \frac{S}{S_0} \qquad t^{***} = t\left(\frac{g}{S_0}\right)^{1/2} \tag{5.13}$$

Substitute these variables into Eq. (5.5) and clean everything up as usual. The result is our third and final option:

$$S^{***} = 1 + \beta t^{***} + \frac{1}{2}t^{***2} \qquad \beta = \frac{1}{\sqrt{\alpha}} = \frac{V_0}{\sqrt{gS_0}} \tag{5.14}$$

This final presentation is shown in Fig. 5.1*c*. Once again the parameter α appears, but we have redefined it upside down, $\beta = 1/\sqrt{\alpha}$, so that our display parameter V_0 is in the numerator and is linear. This is our free choice and simply improves the display. Figure 5.1*c* shows that initial *velocity* increases the falling displacement and that the increase is proportional to time.

Note that, in all three options, the same parameter α appears but has a different meaning: dimensionless gravity, initial displacement, and initial velocity. The graphs, which contain exactly the same information, change their appearance to reflect these differences.

Whereas the original problem, Eq. (5.5), involved five quantities, the dimensionless presentations involve only three, having the form

$$S' = \text{fcn}(t', \alpha) \qquad \alpha = \frac{gS_0}{V_0^2} \tag{5.15}$$

The reduction $5 - 3 = 2$ should equal the number of fundamental dimensions involved in the problem $\{L, T\}$. This idea led to the pi theorem (Sec. 5.3).

The choice of scaling variables is left to the user, and the resulting dimensionless parameters have differing interpretations. For example, in the dimensionless drag-force formulation, Eq. (5.2), it is now clear that the scaling parameters were ρ, V, and L, since they appear in both the drag coefficient and the Reynolds number. Equation (5.2) can thus be interpreted as the variation of dimensionless *force* with dimensionless *viscosity,* with the scaling-parameter effects mixed between C_F and Re and therefore not immediately evident.

Suppose that we wish to study drag force versus *velocity*. Then we would not use V as a scaling parameter. We would use (ρ, μ, L) instead, and the final dimensionless function would become

$$C_F' = \frac{\rho F}{\mu^2} = \text{fcn}(\text{Re}) \qquad \text{Re} = \frac{\rho VL}{\mu} \tag{5.16}$$

In plotting these data, we would not be able to discern the effect of ρ or μ, si
appear in both dimensionless groups. The grouping C_F' again would mean din



ketabline.com Ebook.ketabline.com

less force, and Re is now interpreted as either dimensionless velocity or size.[3] The plot would be quite different compared to Eq. (5.2), although it contains exactly the same information. The development of parameters such as C_F' and Re from the initial variables is the subject of the pi theorem (Sec. 5.3).

Some Peculiar Engineering Equations

The foundation of the dimensional-analysis method rests on two assumptions: (1) The proposed physical relation is dimensionally homogeneous, and (2) all the relevant variables have been included in the proposed relation.

If a relevant variable is missing, dimensional analysis will fail, giving either algebraic difficulties or, worse, yielding a dimensionless formulation which does not resolve the process. A typical case is Manning's open-channel formula, discussed in Example 1.4:

$$V = \frac{1.49}{n} R^{2/3} S^{1/2} \tag{1}$$

Since V is velocity, R is a radius, and n and S are dimensionless, the formula is not dimensionally homogeneous. This should be a warning that (1) the formula changes if the *units* of V and R change and (2) if valid, it represents a very special case. Equation (1) in Example 1.4 (see above) predates the dimensional-analysis technique and is valid only for water in rough channels at moderate velocities and large radii in BG units.

Such dimensionally inhomogeneous formulas abound in the hydraulics literature. Another example is the Hazen-Williams formula [30] for volume flow of water through a straight smooth pipe

$$Q = 61.9 D^{2.63} \left(\frac{dp}{dx} \right)^{0.54} \tag{5.17}$$

where D is diameter and dp/dx is the pressure gradient. Some of these formulas arise because numbers have been inserted for fluid properties and other physical data into perfectly legitimate homogeneous formulas. We shall not give the units of Eq. (5.17) to avoid encouraging its use.

On the other hand, some formulas are "constructs" which cannot be made dimensionally homogeneous. The "variables" they relate cannot be analyzed by the dimensional-analysis technique. Most of these formulas are raw empiricisms convenient to a small group of specialists. Here are three examples:

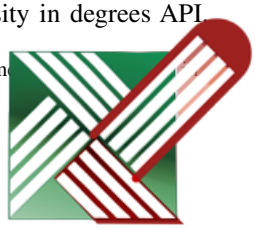
$$B = \frac{25{,}000}{100 - R} \tag{5.18}$$

$$S = \frac{140}{130 + \text{API}} \tag{5.19}$$

$$0.0147 D_E - \frac{3.74}{D_E} = 0.26 t_R - \frac{172}{t_R} \tag{5.20}$$

Equation (5.18) relates the Brinell hardness B of a metal to its Rockwell hardness R. Equation (5.19) relates the specific gravity S of an oil to its density in degrees API.

[3] We were lucky to achieve a size effect because in this case L, a scaling param the drag coefficient.



ketabline.com Ebook.ketabline.com

Equation (5.20) relates the viscosity of a liquid in D_E, or degrees Engler, to its viscosity t_R in Saybolt seconds. Such formulas have a certain usefulness when communicated between fellow specialists, but we cannot handle them here. Variables like Brinell hardness and Saybolt viscosity are not suited to an $MLT\Theta$ dimensional system.

5.3 The Pi Theorem

There are several methods of reducing a number of dimensional variables into a smaller number of dimensionless groups. The scheme given here was proposed in 1914 by Buckingham [29] and is now called the *Buckingham pi theorem*. The name *pi* comes from the mathematical notation Π, meaning a product of variables. The dimensionless groups found from the theorem are power products denoted by Π_1, Π_2, Π_3, etc. The method allows the pis to be found in sequential order without resorting to free exponents.

The first part of the pi theorem explains what reduction in variables to expect:

> If a physical process satisfies the PDH and involves n dimensional variables, it can be reduced to a relation between only k dimensionless variables or Π's. The reduction $j = n - k$ equals the maximum number of variables which do not form a pi among themselves and is always less than or equal to the number of dimensions describing the variables.

Take the specific case of force on an immersed body: Eq. (5.1) contains five variables F, L, U, ρ, and μ described by three dimensions $\{MLT\}$. Thus $n = 5$ and $j \leq 3$. Therefore it is a good guess that we can reduce the problem to k pis, with $k = n - j \geq 5 - 3 = 2$. And this is exactly what we obtained: two dimensionless variables $\Pi_1 = C_F$ and $\Pi_2 = \text{Re}$. On rare occasions it may take more pis than this minimum (see Example 5.5).

The second part of the theorem shows how to find the pis one at a time:

> Find the reduction j, then select j scaling variables which do not form a pi among themselves.[4] Each desired pi group will be a power product of these j variables plus one additional variable which is assigned any convenient nonzero exponent. Each pi group thus found is independent.

To be specific, suppose that the process involves five variables

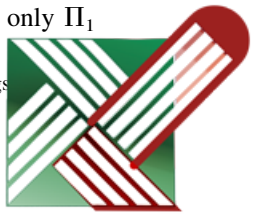
$$v_1 = f(v_2, v_3, v_4, v_5)$$

Suppose that there are three dimensions $\{MLT\}$ and we search around and find that indeed $j = 3$. Then $k = 5 - 3 = 2$ and we expect, from the theorem, two and only two pi groups. Pick out three convenient variables which do *not* form a pi, and suppose these turn out to be v_2, v_3, and v_4. Then the two pi groups are formed by power products of these three plus one additional variable, either v_1 or v_5:

$$\Pi_1 = (v_2)^a(v_3)^b(v_4)^c v_1 = M^0L^0T^0 \qquad \Pi_2 = (v_2)^a(v_3)^b(v_4)^c v_5 = M^0L^0T^0$$

Here we have arbitrarily chosen v_1 and v_5, the added variables, to have unit exponents. Equating exponents of the various dimensions is guaranteed by the theorem to give unique values of a, b, and c for each pi. And they are independent because only Π_1

[4] Make a clever choice here because all pis will contain these j variables in various groupings



ketabline.com Ebook.ketabline.com

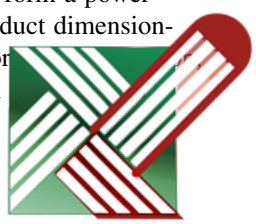
Table 5.1 Dimensions of Fluid-Mechanics Properties

Quantity	Symbol	Dimensions	
		MLTΘ	*FLTΘ*
Length	L	L	L
Area	A	L^2	L^2
Volume	$\mathcal{V}$	L^3	L^3
Velocity	V	LT^{-1}	LT^{-1}
Acceleration	dV/dt	LT^{-2}	LT^{-2}
Speed of sound	a	LT^{-1}	LT^{-1}
Volume flow	Q	L^3T^{-1}	L^3T^{-1}
Mass flow	$\dot{m}$	MT^{-1}	FTL^{-1}
Pressure, stress	p, σ	$ML^{-1}T^{-2}$	FL^{-2}
Strain rate	$\dot{\epsilon}$	T^{-1}	T^{-1}
Angle	θ	None	None
Angular velocity	ω	T^{-1}	T^{-1}
Viscosity	μ	$ML^{-1}T^{-1}$	FTL^{-2}
Kinematic viscosity	ν	L^2T^{-1}	L^2T^{-1}
Surface tension	Υ	MT^{-2}	FL^{-1}
Force	F	MLT^{-2}	F
Moment, torque	M	ML^2T^{-2}	FL
Power	P	ML^2T^{-3}	FLT^{-1}
Work, energy	W, E	ML^2T^{-2}	FL
Density	ρ	ML^{-3}	FT^2L^{-4}
Temperature	T	Θ	Θ
Specific heat	c_p, c_v	$L^2T^{-2}\Theta^{-1}$	$L^2T^{-2}\Theta^{-1}$
Specific weight	γ	$ML^{-2}T^{-2}$	FL^{-3}
Thermal conductivity	k	$MLT^{-3}\Theta^{-1}$	$FT^{-1}\Theta^{-1}$
Expansion coefficient	β	Θ^{-1}	Θ^{-1}

contains v_1 and only Π_2 contains v_5. It is a very neat system once you get used to the procedure. We shall illustrate it with several examples.

Typically, six steps are involved:

1. List and count the n variables involved in the problem. If any important variables are missing, dimensional analysis will fail.
2. List the dimensions of each variable according to {MLTΘ} or {FLTΘ}. A list is given in Table 5.1.
3. Find j. Initially guess j equal to the number of different dimensions present, and look for j variables which do not form a pi product. If no luck, reduce j by 1 and look again. With practice, you will find j rapidly.
4. Select j scaling parameters which do not form a pi product. Make sure they please you and have some generality if possible, because they will then appear in every one of your pi groups. Pick density or velocity or length. Do not pick surface tension, e.g., or you will form six different independent Weber-number parameters and thoroughly annoy your colleagues.
5. Add one additional variable to your j repeating variables, and form a power product. Algebraically find the exponents which make the product dimensionless. Try to arrange for your output or *dependent* variables (for torque, power) to appear in the numerator, and your plots will



ketabline.com Ebook.ketabline.com

this sequentially, adding one new variable each time, and you will find all $n - j = k$ desired pi products.

6. Write the final dimensionless function, and check your work to make sure all pi groups are dimensionless.

EXAMPLE 5.2

Repeat the development of Eq. (5.2) from Eq. (5.1), using the pi theorem.

Solution

Step 1 Write the function and count variables:

$$F = f(L, U, \rho, \mu) \quad \text{there are five variables } (n = 5)$$

Step 2 List dimensions of each variable. From Table 5.1

F	L	U	ρ	μ
$\{MLT^{-2}\}$	$\{L\}$	$\{LT^{-1}\}$	$\{ML^{-3}\}$	$\{ML^{-1}T^{-1}\}$

Step 3 Find j. No variable contains the dimension Θ, and so j is less than or equal to 3 (MLT). We inspect the list and see that L, U, and ρ cannot form a pi group because only ρ contains mass and only U contains time. Therefore j does equal 3, and $n - j = 5 - 3 = 2 = k$. The pi theorem guarantees for this problem that there will be exactly two independent dimensionless groups.

Step 4 Select repeating j variables. The group L, U, ρ we found in step 3 will do fine.

Step 5 Combine L, U, ρ with one additional variable, in sequence, to find the two pi products.

First add force to find Π_1. You may select *any* exponent on this additional term as you please, to place it in the numerator or denominator to any power. Since F is the output, or dependent, variable, we select it to appear to the first power in the numerator:

$$\Pi_1 = L^a U^b \rho^c F = (L)^a (LT^{-1})^b (ML^{-3})^c (\, MLT^{-2}) = M^0 L^0 T^0$$

Equate exponents:

Length: $\quad a + b - 3c + 1 = 0$

Mass: $\quad c + 1 = 0$

Time: $\quad -b \qquad -2 = 0$

We can solve explicitly for

$$a = -2 \qquad b = -2 \qquad c = -1$$

Therefore

$$\Pi_1 = L^{-2} U^{-2} \rho^{-1} F = \frac{F}{\rho U^2 L^2} = C_F \qquad \textit{Ans.}$$

This is exactly the right pi group as in Eq. (5.2). By varying the exponent on F, we co found other equivalent groups such as $UL\rho^{1/2}/F^{1/2}$.



ketabline.com Ebook.ketabline.com

Finally, add viscosity to L, U, and ρ to find Π_2. Select any power you like for viscosity. By hindsight and custom, we select the power -1 to place it in the denominator:

$$\Pi_2 = L^a U^b \rho^c \mu^{-1} = L^a (LT^{-1})^b (ML^{-3})^c (ML^{-1}T^{-1})^{-1} = M^0 L^0 T^0$$

Equate exponents:

Length: $$a + b - 3c + 1 = 0$$

Mass: $$c - 1 = 0$$

Time: $$-b \qquad + 1 = 0$$

from which we find

$$a = b = c = 1$$

Therefore $$\Pi_2 = L^1 U^1 \rho^1 \mu^{-1} = \frac{\rho UL}{\mu} = \text{Re} \qquad \textit{Ans.}$$

We know we are finished; this is the second and last pi group. The theorem guarantees that the functional relationship must be of the equivalent form

$$\frac{F}{\rho U^2 L^2} = g\left(\frac{\rho UL}{\mu}\right) \qquad \textit{Ans.}$$

which is exactly Eq. (5.2).

EXAMPLE 5.3

Reduce the falling-body relationship, Eq. (5.5), to a function of dimensionless variables. Why are there three different formulations?

Solution

Write the function and count variables

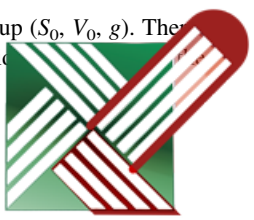
$$S = f(t, S_0, V_0, g) \quad \text{five variables } (n = 5)$$

List the dimensions of each variable, from Table 5.1:

S	t	S_0	V_0	g
$\{L\}$	$\{T\}$	$\{L\}$	$LT^{-1}\}$	$\{LT^{-2}\}$

There are only two primary dimensions (L, T), so that $j \leq 2$. By inspection we can easily find two variables which cannot be combined to form a pi, for example, V_0 and g. Then $j = 2$, and we expect $5 - 2 = 3$ pi products. Select j variables among the parameters S_0, V_0, and g. Avoid S and t since they are the dependent variables, which should not be repeated in pi groups.

There are three different options for repeating variables among the group (S_0, V_0, g). Therefore we can obtain three different dimensionless formulations, just as we did for the falling-body equation in Sec. 5.2. Take each option in turn:



ketabline.com Ebook.ketabline.com

1. Choose S_0 and V_0 as repeating variables. Combine them in turn with (S, t, g):

$$\Pi_1 = S^1 S_0^a V_0^b \quad \Pi_2 = t^1 S_0^c V_0^d \quad \Pi_3 = g^1 S_0^e V_0^f$$

Set each power product equal to L^0T^0, and solve for the exponents (a, b, c, d, e, f). Please allow us to give the results here, and you may check the algebra as an exercise:

$$a = -1 \quad b = 0 \quad c = -1 \quad d = 1 \quad e = 1 \quad f = -2$$

$$\Pi_1 = S^* = \frac{S}{S_0} \qquad \Pi_2 = t^* = \frac{V_0 t}{S_0} \qquad \Pi_3 = \alpha = \frac{gS_0}{V_0^2} \qquad \textit{Ans.}$$

Thus, for option 1, we know that $S^* = \text{fcn}(t^*, \alpha)$. We have found, by dimensional analysis, the same variables as in Eq. (5.10). But here there is no *formula* for the functional relation — we might have to experiment with falling bodies to establish Fig. 5.1*a*.

2. Choose V_0 and g as repeating variables. Combine them in turn with (S, t, S_0):

$$\Pi_1 = S^1 V_0^a g^b \quad \Pi_2 = t^1 V_0^c g^d \quad \Pi_3 = S_0^1 V_0^e g^f$$

Set each power product equal to L^0T^0, and solve for the exponents (a, b, c, d, e, f). Once more allow us to give the results here, and you may check the algebra as an exercise.

$$a = -2 \quad b = 1 \quad c = -1 \quad d = 1 \quad e = 1 \quad f = -2$$

$$\Pi_1 = S^{**} = \frac{Sg}{V_0^2} \quad \Pi_2 = t^{**} = \frac{tg}{V_0} \quad \Pi_3 = \alpha = \frac{gS_0}{V_0^2} \qquad \textit{Ans.}$$

Thus, for option 2, we now know that $S^{**} = \text{fcn}(t^{**}, \alpha)$. We have found, by dimensional analysis, the same groups as in Eq. (5.12). The data would plot as in Fig. 5.1*b*.

3. Finally choose S_0 and g as repeating variables. Combine them in turn with (S, t, V_0):

$$\Pi_1 = S^1 S_0^a g^b \quad \Pi_2 = t^1 S_0^c g^d \quad \Pi_3 = V_0^1 S_0^e g^f$$

Set each power product equal to L^0T^0, and solve for the exponents (a, b, c, d, e, f). One more time allow us to give the results here, and you may check the algebra as an exercise:

$$a = -1 \quad b = 0 \quad c = -\frac{1}{2} \quad d = \frac{1}{2} \quad e = -\frac{1}{2} \quad f = -\frac{1}{2}$$

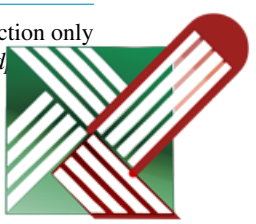
$$\Pi_1 = S^{***} = \frac{S}{S_0} \quad \Pi_2 = t^{***} = t\sqrt{\frac{g}{S_0}} \quad \Pi_3 = \beta = \frac{V_0}{\sqrt{gS_0}} \qquad \textit{Ans.}$$

Thus, for option 3, we now know that $S^{***} = \text{fcn}(t^{***}, \beta = 1/\sqrt{\alpha})$. We have found, by dimensional analysis, the same groups as in Eq. (5.14). The data would plot as in Fig. 5.1*c*.

Dimensional analysis here has yielded the same pi groups as the use of scaling parameters with Eq. (5.5). Three different formulations appeared, because we could choose three different pairs of repeating variables to complete the pi theorem.

EXAMPLE 5.4

At low velocities (laminar flow), the volume flow Q through a small-bore tube is a function only of the tube radius R, the fluid viscosity μ, and the pressure drop per unit tube length d ing the pi theorem, find an appropriate dimensionless relationship.



ketabline.com Ebook.ketabline.com

Solution

Write the given relation and count variables:

$$Q = f\left(R,\ \mu,\ \frac{dp}{dx}\right) \quad \text{four variables } (n = 4)$$

Make a list of the dimensions of these variables from Table 5.1:

Q	R	μ	dp/dx
$\{L^3T^{-1}\}$	$\{L\}$	$\{ML^{-1}T^{-1}\}$	$\{ML^{-2}T^{-2}\}$

There are three primary dimensions (M, L, T), hence $j \leq 3$. By trial and error we determine that R, μ, and dp/dx cannot be combined into a pi group. Then $j = 3$, and $n - j = 4 - 3 = 1$. There is only *one* pi group, which we find by combining Q in a power product with the other three:

$$\Pi_1 = R^a\mu^b\left(\frac{dp}{dx}\right)^c Q^1 = (L)^a(ML^{-1}T^{-1})^b(ML^{-2}T^{-2})^c(L^3T^{-1})$$

$$= M^0L^0T^0$$

Equate exponents:

Mass: $$b + c = 0$$

Length: $$a - b - 2c + 3 = 0$$

Time: $$-b - 2c - 1 = 0$$

Solving simultaneously, we obtain $a = -4$, $b = 1$, $c = -1$. Then

$$\Pi_1 = R^{-4}\mu^1\left(\frac{dp}{dx}\right)^{-1} Q$$

or $$\Pi_1 = \frac{Q\mu}{R^4(dp/dx)} = \text{const} \qquad \textit{Ans.}$$

Since there is only one pi group, it must equal a dimensionless constant. This is as far as dimensional analysis can take us. The laminar-flow theory of Sec. 6.4 shows that the value of the constant is $\pi/8$.

EXAMPLE 5.5

Assume that the tip deflection δ of a cantilever beam is a function of the tip load P, beam length L, area moment of inertia I, and material modulus of elasticity E; that is, $\delta = f(P, L, I, E)$. Rewrite this function in dimensionless form, and comment on its complexity and the peculiar value of j.

Solution

List the variables and their dimensions:

δ	P	L	I	E
$\{L\}$	$\{MLT^{-2}\}$	$\{L\}$	$\{L^4\}$	$\{ML^{-1}T^{-2}\}$



ketabline.com Ebook.ketabline.com

There are five variables ($n = 5$) and three primary dimensions (M, L, T), hence $j \leq 3$. But try as we may, we *cannot* find any combination of three variables which does not form a pi group. This is because $\{M\}$ and $\{T\}$ occur only in P and E and only in the same form, $\{MT^{-2}\}$. Thus we have encountered a special case of $j = 2$, which is less than the number of dimensions (M, L, T). To gain more insight into this peculiarity, you should rework the problem, using the (F, L, T) system of dimensions.

With $j = 2$, we select L and E as two variables which cannot form a pi group and then add other variables to form the three desired pis:

$$\Pi_1 = L^a E^b I^1 = (L)^a (ML^{-1}T^{-2})^b (L^4) = M^0 L^0 T^0$$

from which, after equating exponents, we find that $a = -4$, $b = 0$, or $\Pi_1 = I/L^4$. Then

$$\Pi_2 = L^a E^b \mathrm{P}^1 = (L)^a (ML^{-1}T^{-2})^b (MLT^{-2}) = M^0 L^0 T^0$$

from which we find $a = -2$, $b = -1$, or $\Pi_2 = P/(EL^2)$, and

$$\Pi_3 = L^a E^b \delta^1 = (L)^a (ML^{-1}T^{-2})^b (L) = M^0 L^0 T^0$$

from which $a = -1$, $b = 0$, or $\Pi_3 = \delta/L$. The proper dimensionless function is $\Pi_3 = f(\Pi_2, \Pi_1)$, or

$$\frac{\delta}{L} = f\left(\frac{P}{EL^2}, \frac{I}{L^4}\right) \qquad \textit{Ans.} \quad (1)$$

This is a complex three-variable function, but dimensional analysis alone can take us no further.

We can "improve" Eq. (1) by taking advantage of some physical reasoning, as Langhaar points out [8, p. 91]. For small elastic deflections, δ is proportional to load P and inversely proportional to moment of inertia I. Since P and I occur separately in Eq. (1), this means that Π_3 must be proportional to Π_2 and inversely proportional to Π_1. Thus, for these conditions,

$$\frac{\delta}{L} = (\text{const})\,\frac{P}{EL^2}\,\frac{L^4}{I}$$

or

$$\delta = (\text{const})\,\frac{PL^3}{EI} \qquad (2)$$

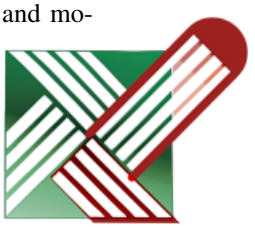
This could not be predicted by a pure dimensional analysis. Strength-of-materials theory predicts that the value of the constant is $\frac{1}{3}$.

5.4 Nondimensionalization of the Basic Equations

We could use the pi-theorem method of the previous section to analyze problem after problem, finding the dimensionless parameters which govern in each case. Textbooks on dimensional analysis [for example, 7] do this. An alternate and very powerful technique is to attack the basic equations of flow from Chap. 4. Even though these equations cannot be solved in general, they will reveal basic dimensionless parameters, e.g., Reynolds number, in their proper form and proper position, giving clues to when they are negligible. The boundary conditions must also be nondimensionalized.

Let us briefly apply this technique to the incompressible-flow continuity and momentum equations with constant viscosity:

Continuity: $$\boldsymbol{\nabla} \cdot \mathbf{V} = 0$$



ketabline.com Ebook.ketabline.com

Momentum: $$\rho\frac{d\mathbf{V}}{dt} = \rho\mathbf{g} - \boldsymbol{\nabla}p + \mu\nabla^2\mathbf{V} \tag{5.21b}$$

Typical boundary conditions for these two equations are

Fixed solid surface: $$\mathbf{V} = 0$$

Inlet or outlet: $$\text{Known } \mathbf{V}, p \tag{5.22}$$

Free surface, $z = \eta$: $$w = \frac{d\eta}{dt} \quad p = p_a - \Upsilon(R_x^{-1} + R_y^{-1})$$

We omit the energy equation (4.75) and assign its dimensionless form in the problems (Probs. 5.42 and 5.45).

Equations (5.21) and (5.22) contain the three basic dimensions M, L, and T. All variables p, $\mathbf{V}$, x, y, z, and t can be nondimensionalized by using density and two reference constants which might be characteristic of the particular fluid flow:

$$\text{Reference velocity} = U \qquad \text{Reference length} = L$$

For example, U may be the inlet or upstream velocity and L the diameter of a body immersed in the stream.

Now define all relevant dimensionless variables, denoting them by an asterisk:

$$\mathbf{V}^* = \frac{\mathbf{V}}{U}$$

$$x^* = \frac{x}{L} \quad y^* = \frac{y}{L} \quad z^* = \frac{z}{L} \tag{5.23}$$

$$t^* = \frac{tU}{L} \quad p^* = \frac{p + \rho gz}{\rho U^2}$$

All these are fairly obvious except for p^*, where we have slyly introduced the gravity effect, assuming that z is up. This is a hindsight idea suggested by Bernoulli's equation (3.77).

Since ρ, U, and L are all constants, the derivatives in Eqs. (5.21) can all be handled in dimensionless form with dimensional coefficients. For example,

$$\frac{\partial u}{\partial x} = \frac{\partial(Uu^*)}{\partial(Lx^*)} = \frac{U}{L}\frac{\partial u^*}{\partial x^*}$$

Substitute the variables from Eqs. (5.23) into Eqs. (5.21) and (5.22) and divide through by the leading dimensional coefficient, in the same way as we handled Eq. (5.12). The resulting dimensionless equations of motion are:

Continuity: $$\boldsymbol{\nabla}^* \cdot \mathbf{V}^* = 0 \tag{5.24a}$$

Momentum: $$\frac{d\mathbf{V}^*}{dt^*} = -\boldsymbol{\nabla}^* p^* + \frac{\mu}{\rho UL}\nabla^{*2}(\mathbf{V}^*) \tag{5.24b}$$

The dimensionless boundary conditions are:

Fixed solid surface: $$\mathbf{V}^* = 0$$

Inlet or outlet: $$\text{Known } \mathbf{V}^*, p^*$$



ketabline.com Ebook.ketabline.com

Free surface, $z^* = \eta^*$: $$w^* = \frac{d\eta^*}{dt^*} \tag{5.25}$$

$$p^* = \frac{p_a}{\rho U^2} + \frac{gL}{U^2} z^* - \frac{\Upsilon}{\rho U^2 L} (R_x^{*-1} + R_y^{*-1})$$

These equations reveal a total of four dimensionless parameters, one in the momentum equation and three in the free-surface-pressure boundary condition.

Dimensionless Parameters

In the continuity equation there are no parameters. The momentum equation contains one, generally accepted as the most important parameter in fluid mechanics:

$$\text{Reynolds number Re} = \frac{\rho UL}{\mu}$$

It is named after Osborne Reynolds (1842–1912), a British engineer who first proposed it in 1883 (Ref. 4 of Chap. 6). The Reynolds number is always important, with or without a free surface, and can be neglected only in flow regions away from high-velocity gradients, e.g., away from solid surfaces, jets, or wakes.

The no-slip and inlet-exit boundary conditions contain no parameters. The free-surface-pressure condition contains three:

$$\text{Euler number (pressure coefficient) Eu} = \frac{p_a}{\rho U^2}$$

This is named after Leonhard Euler (1707–1783) and is rarely important unless the pressure drops low enough to cause vapor formation (cavitation) in a liquid. The Euler number is often written in terms of pressure differences: $\text{Eu} = \Delta p/(\rho U^2)$. If Δp involves vapor pressure p_v, it is called the *cavitation number* $\text{Ca} = (p_a - p_v)/(\rho U^2)$.

The second pressure parameter is much more important:

$$\text{Froude number Fr} = \frac{U^2}{gL}$$

It is named after William Froude (1810–1879), a British naval architect who, with his son Robert, developed the ship-model towing-tank concept and proposed similarity rules for free-surface flows (ship resistance, surface waves, open channels). The Froude number is the dominant effect in free-surface flows and is totally unimportant if there is no free surface. Chapter 10 investigates Froude number effects in detail.

The final free-surface parameter is

$$\text{Weber number We} = \frac{\rho U^2 L}{\Upsilon}$$

It is named after Moritz Weber (1871–1951) of the Polytechnic Institute of Berlin, who developed the laws of similitude in their modern form. It was Weber who named Re and Fr after Reynolds and Froude. The Weber number is important only if it is of order unity or less, which typically occurs when the surface curvature is comparable in size to the liquid depth, e.g., in droplets, capillary flows, ripple waves, and ve hydraulic models. If We is large, its effect may be neglected.



ketabline.com Ebook.ketabline.com

If there is no free surface, Fr, Eu, and We drop out entirely, except for the possibility of cavitation of a liquid at very small Eu. Thus, in low-speed viscous flows with no free surface, the Reynolds number is the only important dimensionless parameter.

Compressibility Parameters

In high-speed flow of a gas there are significant changes in pressure, density, and temperature which must be related by an equation of state such as the perfect-gas law, Eq. (1.10). These thermodynamic changes introduce two additional dimensionless parameters mentioned briefly in earlier chapters:

$$\text{Mach number Ma} = \frac{U}{a} \qquad \text{Specific-heat ratio } k = \frac{c_p}{c_v}$$

The Mach number is named after Ernst Mach (1838–1916), an Austrian physicist. The effect of k is only slight to moderate, but Ma exerts a strong effect on compressible-flow properties if it is greater than about 0.3. These effects are studied in Chap. 9.

Oscillating Flows

If the flow pattern is oscillating, a seventh parameter enters through the inlet boundary condition. For example, suppose that the inlet stream is of the form

$$u = U \cos \omega t$$

Nondimensionalization of this relation results in

$$\frac{u}{U} = u^* = \cos\left(\frac{\omega L}{U} t^*\right)$$

The argument of the cosine contains the new parameter

$$\text{Strouhal number St} = \frac{\omega L}{U}$$

The dimensionless forces and moments, friction, and heat transfer, etc., of such an oscillating flow would be a function of both Reynolds and Strouhal numbers. This parameter is named after V. Strouhal, a German physicist who experimented in 1878 with wires singing in the wind.

Some flows which you might guess to be perfectly steady actually have an oscillatory pattern which is dependent on the Reynolds number. An example is the periodic vortex shedding behind a blunt body immersed in a steady stream of velocity U. Figure 5.2*a* shows an array of alternating vortices shed from a circular cylinder immersed in a steady crossflow. This regular, periodic shedding is called a *Kármán vortex street*, after T. von Kármán, who explained it theoretically in 1912. The shedding occurs in the range $10^2 < \text{Re} < 10^7$, with an average Strouhal number $\omega d/(2\pi U) \approx 0.21$. Figure 5.2*b* shows measured shedding frequencies.

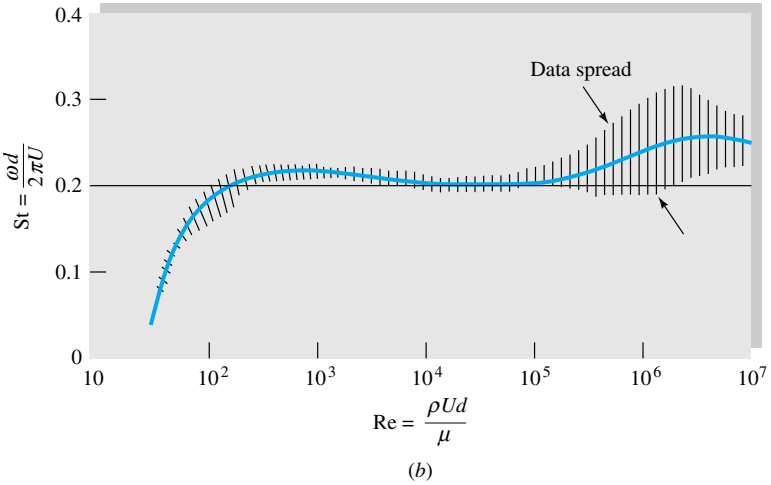
Resonance can occur if a vortex shedding frequency is near a body's structural-vibration frequency. Electric transmission wires sing in the wind, undersea mooring lines gallop at certain current speeds, and slender structures flutter at critical wind or vehicle speeds. A striking example is the disastrous failure of the Tacoma Narrows suspension bridge in 1940, when wind-excited vortex shedding caused natural torsional oscillations of the bridge.



ketabline.com Ebook.ketabline.com



(*a*)



(*b*)

Fig. 5.2 Vortex shedding from a circular cylinder: (*a*) vortex street behind a circular cylinder *(from Ref. 33, courtesy of U.S. Naval Research Laboratory);* (*b*) experimental shedding frequencies *(data from Refs. 31 and 32).*

Other Dimensionless Parameters

We have discussed seven important parameters in fluid mechanics, and there are others. Four additional parameters arise from nondimensionalization of the energy equation (4.75) and its boundary conditions. These four (Prandtl number, Eckert number, Grashof number, and wall-temperature ratio) are listed in Table 5.2 just in case you fail to solve Prob. 5.42. Another important and rather sneaky parameter is the wall-roughness ratio ϵ/L (in Table 5.2).[5] Slight changes in surface roughness have a strik-

[5] Roughness is easy to overlook because it is a slight geometric effect which does not appear equations of motion.



ketabline.com Ebook.ketabline.com

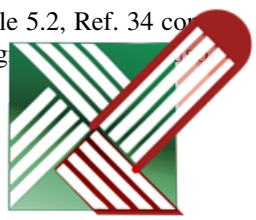
Table 5.2 Dimensionless Groups in Fluid Mechanics

Parameter	Definition	Qualitative ratio of effects	Importance
Reynolds number	$\mathrm{Re} = \frac{\rho U L}{\mu}$	$\frac{\text{Inertia}}{\text{Viscosity}}$	Always
Mach number	$\mathrm{Ma} = \frac{U}{a}$	$\frac{\text{Flow speed}}{\text{Sound speed}}$	Compressible flow
Froude number	$\mathrm{Fr} = \frac{U^2}{gL}$	$\frac{\text{Inertia}}{\text{Gravity}}$	Free-surface flow
Weber number	$\mathrm{We} = \frac{\rho U^2 L}{\Upsilon}$	$\frac{\text{Inertia}}{\text{Surface tension}}$	Free-surface flow
Cavitation number (Euler number)	$\mathrm{Ca} = \frac{p - p_v}{\rho U^2}$	$\frac{\text{Pressure}}{\text{Inertia}}$	Cavitation
Prandtl number	$\mathrm{Pr} = \frac{\mu c_p}{k}$	$\frac{\text{Dissipation}}{\text{Conduction}}$	Heat convection
Eckert number	$\mathrm{Ec} = \frac{U^2}{c_p T_0}$	$\frac{\text{Kinetic energy}}{\text{Enthalpy}}$	Dissipation
Specific-heat ratio	$k = \frac{c_p}{c_v}$	$\frac{\text{Enthalpy}}{\text{Internal energy}}$	Compressible flow
Strouhal number	$\mathrm{St} = \frac{\omega L}{U}$	$\frac{\text{Oscillation}}{\text{Mean speed}}$	Oscillating flow
Roughness ratio	$\frac{\epsilon}{L}$	$\frac{\text{Wall roughness}}{\text{Body length}}$	Turbulent, rough walls
Grashof number	$\mathrm{Gr} = \frac{\beta \Delta T g L^3 \rho^2}{\mu^2}$	$\frac{\text{Buoyancy}}{\text{Viscosity}}$	Natural convection
Temperature ratio	$\frac{T_w}{T_0}$	$\frac{\text{Wall temperature}}{\text{Stream temperature}}$	Heat transfer
Pressure coefficient	$C_p = \frac{p - p_\infty}{\frac{1}{2}\rho U^2}$	$\frac{\text{Static pressure}}{\text{Dynamic pressure}}$	Aerodynamics, hydrodynamics
Lift coefficient	$C_L = \frac{L}{\frac{1}{2}\rho U^2 A}$	$\frac{\text{Lift force}}{\text{Dynamic force}}$	Aerodynamics, hydrodynamics
Drag coefficient	$C_D = \frac{D}{\frac{1}{2}\rho U^2 A}$	$\frac{\text{Drag force}}{\text{Dynamic force}}$	Aerodynamics, hydrodynamics

ing effect in the turbulent-flow or high-Reynolds-number range, as we shall see in Chap. 6 and in Fig. 5.3.

This book is primarily concerned with Reynolds-, Mach-, and Froude-number effects, which dominate most flows. Note that we discovered all these parameters (except ϵ/L) simply by nondimensionalizing the basic equations without actually solving them.

If the reader is not satiated with the 15 parameters given in Table 5.2, Ref. 34 contains a list of over 300 dimensionless parameters in use in eng
Ref. 35.



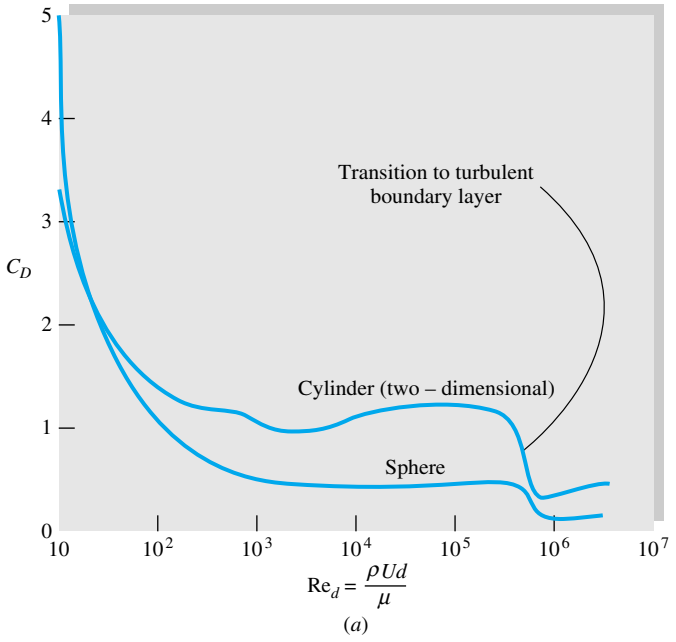
ketabline.com Ebook.ketabline.com

A Successful Application

Dimensional analysis is fun, but does it work? Yes; if all important variables are included in the proposed function, the dimensionless function found by dimensional analysis will collapse all the data onto a single curve or set of curves.

An example of the success of dimensional analysis is given in Fig. 5.3 for the measured drag on smooth cylinders and spheres. The flow is normal to the axis of the cylinder, which is extremely long, $L/d \to \infty$. The data are from many sources, for both liquids and gases, and include bodies from several meters in diameter down to fine wires and balls less than 1 mm in size. Both curves in Fig. 5.3*a* are entirely experimental; the analysis of immersed body drag is one of the weakest areas of modern fluid-mechanics theory. Except for some isolated digital-computer calculations, there is no theory for cylinder and sphere drag except *creeping flow,* $\text{Re} < 1$.

The Reynolds number of both bodies is based upon diameter, hence the notation Re_d. But the drag coefficients are defined differently:



Cylinder length effect ($10^4 < \text{Re} < 10^5$)	
L/d	C_D
∞	1.20
40	0.98
20	0.91
10	0.82
5	0.74
3	0.72
2	0.68
1	0.64

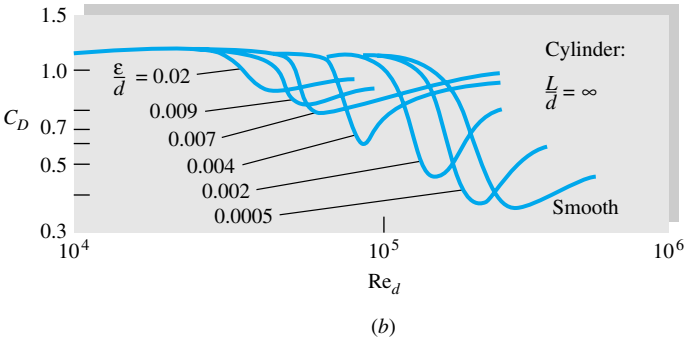


Fig. 5.3 The proof of practical dimensional analysis: drag coefficients of a cylinder and sphere: (*a*) drag coefficient of a smooth cylinder and sphere (data from many sources); (*b*) increased roughness causes earlier transition to a turbulent boundary layer.



ketabline.com Ebook.ketabline.com

$$C_D = \begin{cases} \dfrac{\text{drag}}{\frac{1}{2}\rho U^2 L d} & \text{cylinder} \\ \dfrac{\text{drag}}{\frac{1}{2}\rho U^2 \frac{1}{4}\pi d^2} & \text{sphere} \end{cases} \tag{5.26}$$

They both have a factor $\frac{1}{2}$ as a traditional tribute to Bernoulli and Euler, and both are based on the projected area, i.e., the area one sees when looking toward the body from upstream. The usual definition of C_D is thus

$$C_D = \frac{\text{drag}}{\frac{1}{2}\rho U^2(\text{projected area})} \tag{5.27}$$

However, one should carefully check the definitions of C_D, Re, etc., before using data in the literature. Airfoils, e.g., use the planform area.

Figure 5.3*a* is for long, smooth cylinders. If wall roughness and cylinder length are included as variables, we obtain from dimensional analysis a complex three-parameter function

$$C_D = f\left(\text{Re}_d, \frac{\epsilon}{d}, \frac{L}{d}\right) \tag{5.28}$$

To describe this function completely would require 1000 or more experiments. Therefore it is customary to explore the length and roughness effects separately to establish trends.

The table with Fig. 5.3*a* shows the length effect with zero wall roughness. As length decreases, the drag decreases by up to 50 percent. Physically, the pressure is "relieved" at the ends as the flow is allowed to skirt around the tips instead of deflecting over and under the body.

Figure 5.3*b* shows the effect of wall roughness for an infinitely long cylinder. The sharp drop in drag occurs at lower Re_d as roughness causes an earlier transition to a turbulent boundary layer on the surface of the body. Roughness has the same effect on sphere drag, a fact which is exploited in sports by deliberate dimpling of golf balls to give them less drag at their flight $\text{Re}_d \approx 10^5$.

Figure 5.3 is a typical experimental study of a fluid-mechanics problem, aided by dimensional analysis. As time and money and demand allow, the complete three-parameter relation (5.28) could be filled out by further experiments.

EXAMPLE 5.6

The capillary rise h of a liquid in a tube varies with tube diameter d, gravity g, fluid density ρ, surface tension Υ, and the contact angle θ. (*a*) Find a dimensionless statement of this relation. (*b*) If $h = 3$ cm in a given experiment, what will h be in a similar case if the diameter and surface tension are half as much, the density is twice as much, and the contact angle is the same?

Solution

Part (a) Step 1 Write down the function and count variables:

$$h = f(d, g, \rho, \Upsilon, \theta) \qquad n = 6 \text{ variables}$$



ketabline.com Ebook.ketabline.com

Step 2 List the dimensions $\{FLT\}$ from Table 5.2:

h	d	g	ρ	Υ	θ
$\{L\}$	$\{L\}$	$\{LT^{-2}\}$	$\{FT^2L^{-4}\}$	$\{FL^{-1}\}$	none

Step 3 Find j. Several groups of three form no pi: Υ, ρ, and g or ρ, g, and d. Therefore $j = 3$, and we expect $n - j = 6 - 3 = 3$ dimensionless groups. One of these is obviously θ, which is already dimensionless:

$$\Pi_3 = \theta \qquad \textit{Ans. (a)}$$

If we had carelessly chosen to search for it by using steps 4 and 5, we would still find $\Pi_3 = \theta$.

Step 4 Select j repeating variables which do not form a pi group: ρ, g, d.

Step 5 Add one additional variable in sequence to form the pis:

Add h: $$\Pi_1 = \rho^a g^b d^c h = (FT^2L^{-4})^a (LT^{-2})^b (L)^c (L) = F^0L^0T^0$$

Solve for

$$a = b = 0 \qquad c = -1$$

Therefore $$\Pi_1 = \rho^0 g^0 d^{-1} h = \frac{h}{d} \qquad \textit{Ans. (a)}$$

Finally add Υ, again selecting its exponent to be 1:

$$\Pi_2 = \rho^a g^b d^c \Upsilon = (FT^2L^{-4})^a (LT^{-2})^b (L)^c (FL^{-1}) = F^0L^0T^0$$

Solve for

$$a = b = -1 \quad c = -2$$

Therefore $$\Pi_2 = \rho^{-1} g^{-1} d^{-2} \Upsilon = \frac{\Upsilon}{\rho g d^2} \qquad \textit{Ans. (a)}$$

Step 6 The complete dimensionless relation for this problem is thus

$$\frac{h}{d} = F\left(\frac{\Upsilon}{\rho g d^2},\ \theta\right) \qquad \textit{Ans. (a)} \quad (1)$$

This is as far as dimensional analysis goes. Theory, however, establishes that h is proportional to Υ. Since Υ occurs only in the second parameter, we can slip it outside

$$\left(\frac{h}{d}\right)_{\text{actual}} = \frac{\Upsilon}{\rho g d^2} F_1(\theta) \qquad \text{or} \qquad \frac{h \rho g d}{\Upsilon} = F_1(\theta)$$

Example 1.9 showed theoretically that $F_1(\theta) = 4 \cos \theta$.

Part (b) We are given h_1 for certain conditions d_1, Υ_1, ρ_1, and θ_1. If $h_1 = 3$ cm, what is h_2 for $d_2 = \frac{1}{2}d_1$, $\Upsilon_2 = \frac{1}{2}\Upsilon_1$, $\rho_2 = 2\rho_1$, and $\theta_2 = \theta_1$? We know the functional relation, Eq. (1), must still hold at condition 2

$$\frac{h_2}{d_2} = F\left(\frac{\Upsilon_2}{\rho_2 g d_2^2},\ \theta_2\right)$$

But

$$\frac{\Upsilon_2}{\rho_2 g d_2^2} = \frac{\frac{1}{2}\Upsilon_1}{2\rho_1 g (\frac{1}{2}d_1)^2} = \frac{\Upsilon_1}{\rho_1 g d_1^2}$$



ketabline.com Ebook.ketabline.com

Therefore, functionally,

$$\frac{h_2}{d_2} = F\left(\frac{\Upsilon_1}{\rho_1 g d_1^2}, \theta_1\right) = \frac{h_1}{d_1}$$

We are given a condition 2 which is exactly similar to condition 1, and therefore a scaling law holds

$$h_2 = h_1\frac{d_2}{d_1} = (3\text{ cm})\frac{\frac{1}{2}d_1}{d_1} = 1.5\text{ cm} \qquad \textit{Ans. (b)}$$

If the pi groups had not been exactly the same for both conditions, we would have had to know more about the functional relation F to calculate h_2.

5.5 Modeling and Its Pitfalls

So far we have learned about dimensional homogeneity and the pi-theorem method, using power products, for converting a homogeneous physical relation to dimensionless form. This is straightforward mathematically, but there are certain engineering difficulties which need to be discussed.

First, we have more or less taken for granted that the variables which affect the process can be listed and analyzed. Actually, selection of the important variables requires considerable judgment and experience. The engineer must decide, e.g., whether viscosity can be neglected. Are there significant temperature effects? Is surface tension important? What about wall roughness? Each pi group which is retained increases the expense and effort required. Judgment in selecting variables will come through practice and maturity; this book should provide some of the necessary experience.

Once the variables are selected and the dimensional analysis is performed, the experimenter seeks to achieve *similarity* between the model tested and the prototype to be designed. With sufficient testing, the model data will reveal the desired dimensionless function between variables

$$\Pi_1 = f(\Pi_2, \Pi_3, \ldots \Pi_k) \tag{5.29}$$

With Eq. (5.29) available in chart, graphical, or analytical form, we are in a position to ensure complete similarity between model and prototype. A formal statement would be as follows:

> Flow conditions for a model test are completely similar if all relevant dimensionless parameters have the same corresponding values for the model and the prototype.

This follows mathematically from Eq. (5.29). If $\Pi_{2m} = \Pi_{2p}$, $\Pi_{3m} = \Pi_{3p}$, etc., Eq. (5.29) guarantees that the desired output Π_{1m} will equal Π_{1p}. But this is easier said than done, as we now discuss.

Instead of complete similarity, the engineering literature speaks of particular types of similarity, the most common being geometric, kinematic, dynamic, and thermal. Let us consider each separately.

Geometric Similarity

Geometric similarity concerns the length dimension $\{L\}$ and must
any sensible model testing can proceed. A formal definition is as f



ketabline.com Ebook.ketabline.com

A model and prototype are *geometrically similar* if and only if all body dimensions in all three coordinates have the same linear-scale ratio.

Note that *all* length scales must be the same. It is as if you took a photograph of the prototype and reduced it or enlarged it until it fitted the size of the model. If the model is to be made one-tenth the prototype size, its length, width, and height must each be one-tenth as large. Not only that, but also its entire shape must be one-tenth as large, and technically we speak of *homologous* points, which are points that have the same relative location. For example, the nose of the prototype is homologous to the nose of the model. The left wingtip of the prototype is homologous to the left wingtip of the model. Then geometric similarity requires that all homologous points be related by the same linear-scale ratio. This applies to the fluid geometry as well as the model geometry.

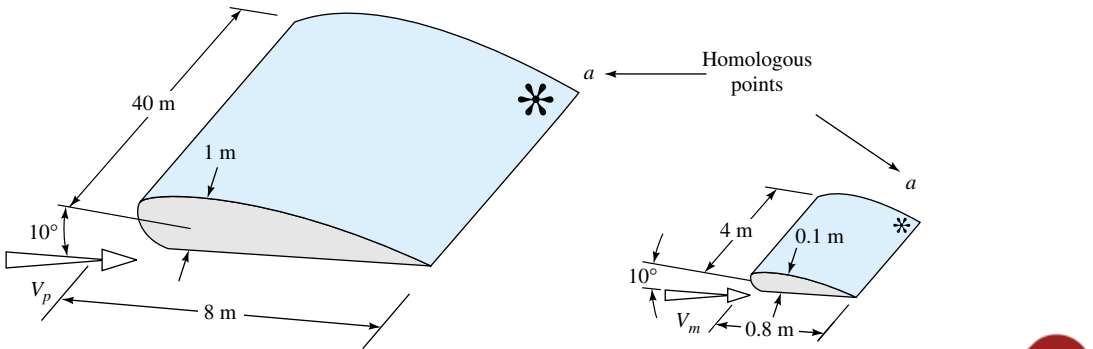
All angles are preserved in geometric similarity. All flow directions are preserved. The orientations of model and prototype with respect to the surroundings must be identical.

Figure 5.4 illustrates a prototype wing and a one-tenth-scale model. The model lengths are all one-tenth as large, but its angle of attack with respect to the free stream is the same: 10° not 1°. All physical details on the model must be scaled, and some are rather subtle and sometimes overlooked:

1. The model nose radius must be one-tenth as large.
2. The model surface roughness must be one-tenth as large.
3. If the prototype has a 5-mm boundary-layer trip wire 1.5 m from the leading edge, the model should have a 0.5-mm trip wire 0.15 m from its leading edge.
4. If the prototype is constructed with protruding fasteners, the model should have homologous protruding fasteners one-tenth as large.

And so on. Any departure from these details is a violation of geometric similarity and must be justified by experimental comparison to show that the prototype behavior was not significantly affected by the discrepancy.

Models which appear similar in shape but which clearly violate geometric similarity should not be compared except at your own risk. Figure 5.5 illustrates this point.



(a) (b)

Fig. 5.4 Geometric similarity in model testing: (*a*) prototype; (*b*) one-tenth-scale model.

ketabline.com Ebook.ketabline.com

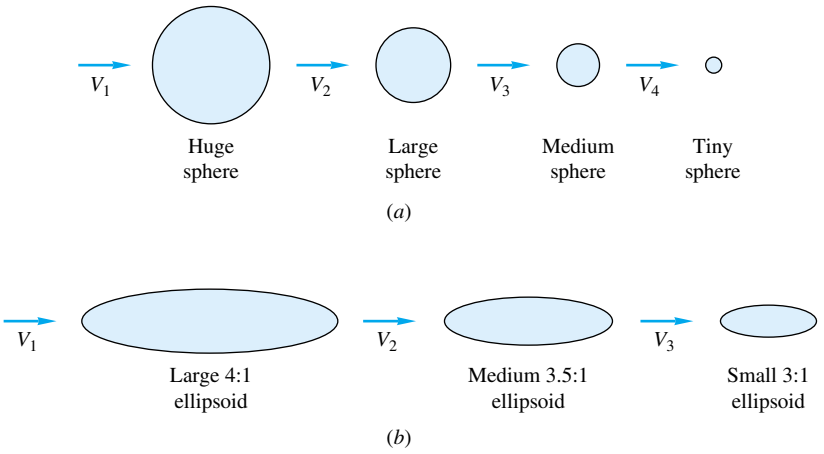


Fig. 5.5 Geometric similarity and dissimilarity of flows: (*a*) similar; (*b*) dissimilar.

The spheres in Fig. 5.5*a* are all geometrically similar and can be tested with a high expectation of success if the Reynolds number or Froude number, etc., is matched. But the ellipsoids in Fig. 5.5*b* merely *look* similar. They actually have different linear-scale ratios and therefore cannot be compared in a rational manner, even though they may have identical Reynolds and Froude numbers, etc. The data will not be the same for these ellipsoids, and any attempt to "compare" them is a matter of rough engineering judgment.

Kinematic Similarity

Kinematic similarity requires that the model and prototype have the same length-scale ratio and the same time-scale ratio. The result is that the velocity-scale ratio will be the same for both. As Langhaar [8] states it:

> The motions of two systems are kinematically similar if homologous particles lie at homologous points at homologous times.

Length-scale equivalence simply implies geometric similarity, but time-scale equivalence may require additional dynamic considerations such as equivalence of the Reynolds and Mach numbers.

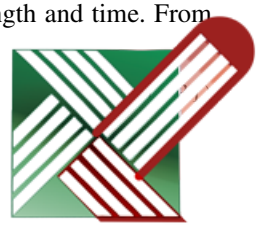
One special case is incompressible frictionless flow with no free surface, as sketched in Fig. 5.6*a*. These perfect-fluid flows are kinematically similar with independent length and time scales, and no additional parameters are necessary (see Chap. 8 for further details).

Frictionless flows with a free surface, as in Fig. 5.6*b*, are kinematically similar if their Froude numbers are equal

$$\mathrm{Fr}_m = \frac{V_m^2}{gL_m} = \frac{V_p^2}{gL_p} = \mathrm{Fr}_p \tag{5.30}$$

Note that the Froude number contains only length and time dimensions and hence is a purely kinematic parameter which fixes the relation between length and time. From Eq. (5.30), if the length scale is

$$L_m = \alpha L_p$$



ketabline.com Ebook.ketabline.com

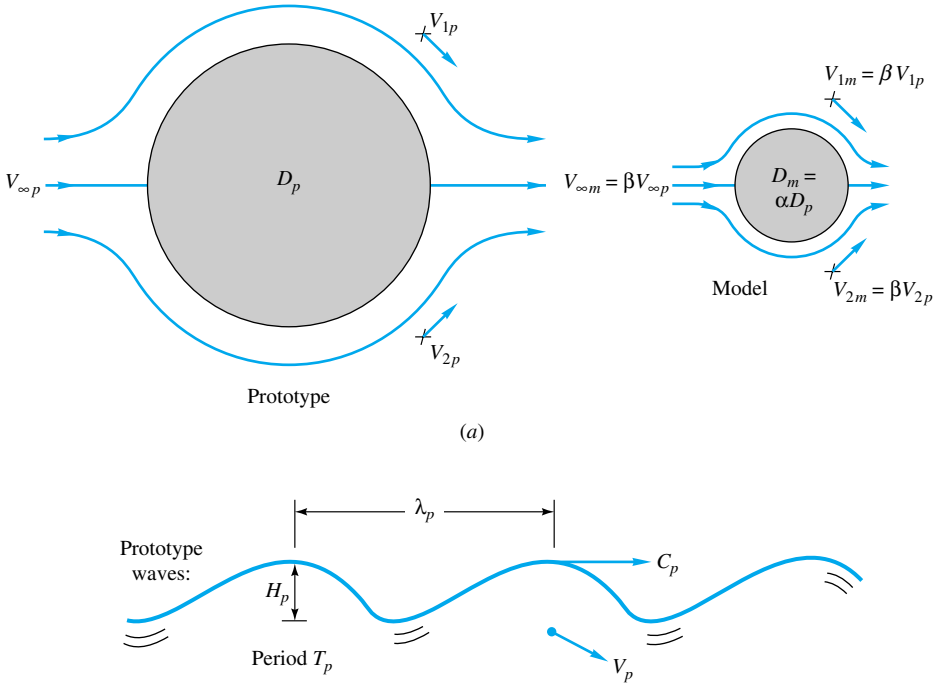


Fig. 5.6 Frictionless low-speed flows are kinematically similar: (*a*) Flows with no free surface are kinematically similar with independent length- and time-scale ratios; (*b*) free-surface flows are kinematically similar with length and time scales related by the Froude number.

where α is a dimensionless ratio, the velocity scale is

$$\frac{V_m}{V_p} = \left(\frac{L_m}{L_p}\right)^{1/2} = \sqrt{\alpha} \tag{5.32}$$

and the time scale is

$$\frac{T_m}{T_p} = \frac{L_m/V_m}{L_p/V_p} = \sqrt{\alpha} \tag{5.33}$$

These Froude-scaling kinematic relations are illustrated in Fig. 5.6*b* for wave-motion modeling. If the waves are related by the length scale α, then the wave period, propagation speed, and particle velocities are related by $\sqrt{\alpha}$.

If viscosity, surface tension, or compressibility is important, kinematic similarity is dependent upon the achievement of dynamic similarity.

Dynamic Similarity

Dynamic similarity exists when the model and the prototype have the same scale ratio, time-scale ratio, and force-scale (or mass-scale) ratio. Again geome

ketabline.com Ebook.ketabline.com

ilarity is a first requirement; without it, proceed no further. Then dynamic similarity exists, simultaneous with kinematic similarity, if the model and prototype force and pressure coefficients are identical. This is ensured if:

1. For compressible flow, the model and prototype Reynolds number and Mach number and specific-heat ratio are correspondingly equal.
2. For incompressible flow
   a. With no free surface: model and prototype Reynolds numbers are equal.
   b. With a free surface: model and prototype Reynolds number, Froude number, and (if necessary) Weber number and cavitation number are correspondingly equal.

Mathematically, Newton's law for any fluid particle requires that the sum of the pressure force, gravity force, and friction force equal the acceleration term, or inertia force,

$$\mathbf{F}_p + \mathbf{F}_g + \mathbf{F}_f = \mathbf{F}_i$$

The dynamic-similarity laws listed above ensure that each of these forces will be in the same ratio and have equivalent directions between model and prototype. Figure 5.7 shows an example for flow through a sluice gate. The force polygons at homologous points have exactly the same shape if the Reynolds and Froude numbers are equal (neglecting surface tension and cavitation, of course). Kinematic similarity is also ensured by these model laws.

Discrepancies in Water and Air Testing

The perfect dynamic similarity shown in Fig. 5.7 is more of a dream than a reality because true equivalence of Reynolds and Froude numbers can be achieved only by dramatic changes in fluid properties, whereas in fact most model testing is simply done with water or air, the cheapest fluids available.

First consider hydraulic model testing with a free surface. Dynamic similarity requires equivalent Froude numbers, Eq. (5.30), *and* equivalent Reynolds numbers

$$\frac{V_m L_m}{\nu_m} = \frac{V_p L_p}{\nu_p} \tag{5.34}$$

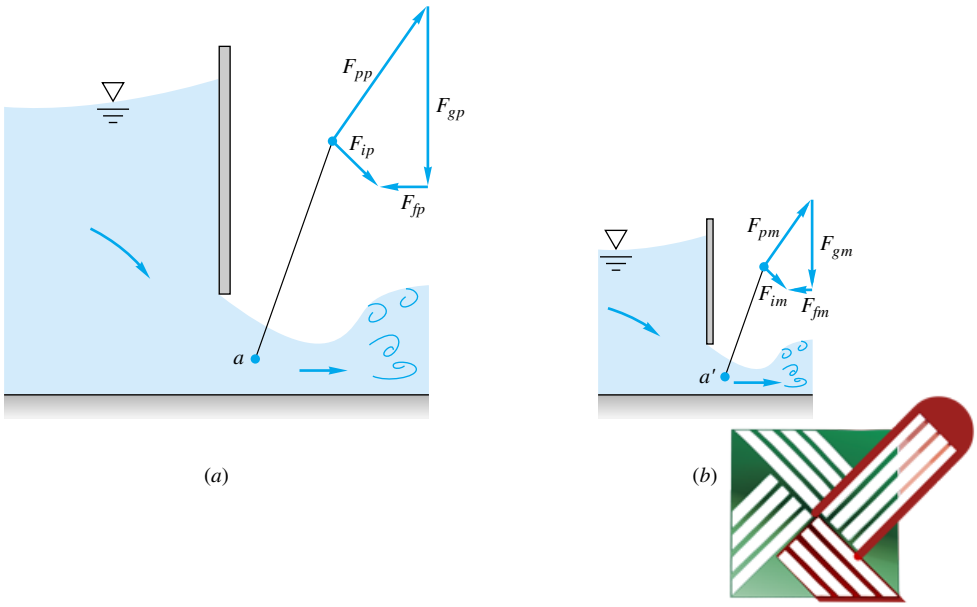


Fig. 5.7 Dynamic similarity in sluice-gate flow. Model and prototype yield identical homologous force polygons if the Reynolds and Froude numbers are the same corresponding values: (*a*) prototype; (*b*) model.

ketabline.com Ebook.ketabline.com

But both velocity and length are constrained by the Froude number, Eqs. (5.31) and (5.32). Therefore, for a given length-scale ratio α, Eq. (5.34) is true only if

$$\frac{\nu_m}{\nu_p} = \frac{L_m}{L_p}\frac{V_m}{V_p} = \alpha\sqrt{\alpha} = \alpha^{3/2} \tag{5.35}$$

For example, for a one-tenth-scale model, $\alpha = 0.1$ and $\alpha^{3/2} = 0.032$. Since ν_p is undoubtedly water, we need a fluid with only 0.032 times the kinematic viscosity of water to achieve dynamic similarity. Referring to Table 1.4, we see that this is impossible: Even mercury has only one-ninth the kinematic viscosity of water, and a mercury hydraulic model would be expensive and bad for your health. In practice, water is used for both the model and the prototype, and the Reynolds-number similarity (5.34) is unavoidably violated. The Froude number is held constant since it is the dominant parameter in free-surface flows. Typically the Reynolds number of the model flow is too small by a factor of 10 to 1000. As shown in Fig. 5.8, the low-Reynolds-number model data are used to estimate by extrapolation the desired high-Reynolds-number prototype data. As the figure indicates, there is obviously considerable uncertainty in using such an extrapolation, but there is no other practical alternative in hydraulic model testing.

Second, consider aerodynamic model testing in air with no free surface. The important parameters are the Reynolds number and the Mach number. Equation (5.34) should be satisfied, plus the compressibility criterion

$$\frac{V_m}{a_m} = \frac{V_p}{a_p} \tag{5.36}$$

Elimination of V_m/V_p between (5.34) and (5.36) gives

$$\frac{\nu_m}{\nu_p} = \frac{L_m}{L_p}\frac{a_m}{a_p} \tag{5.37}$$

Since the prototype is no doubt an air operation, we need a wind-tunnel fluid of low viscosity and high speed of sound. Hydrogen is the only practical example, but clearly it is too expensive and dangerous. Therefore wind tunnels normally operate with air as the working fluid. Cooling and pressurizing the air will bring Eq. (5.37) into better

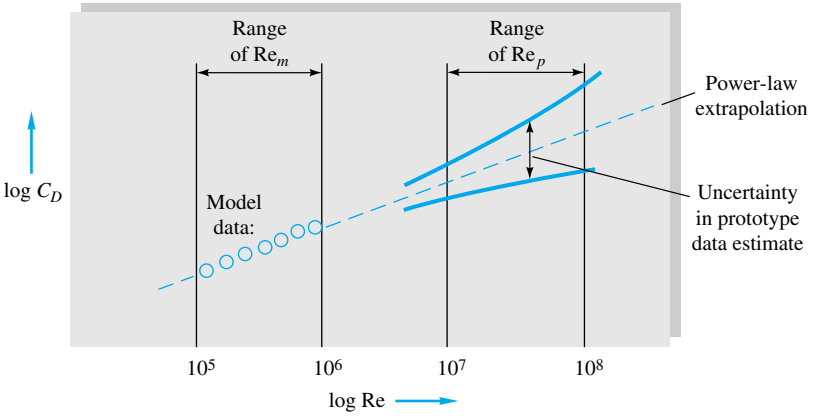


Fig. 5.8 Reynolds-number extrapolation, or scaling, of hydraulic data with equal Froude numbers.



ketabline.com Ebook.ketabline.com



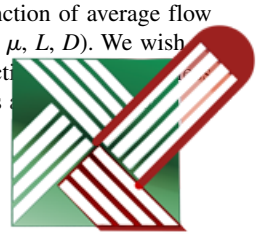
Fig. 5.9 Hydraulic model of a barrier-beach inlet at Little River, South Carolina. Such models of necessity violate geometric similarity and do not model the Reynolds number of the prototype inlet. *(Courtesy of U.S. Army Engineer Waterways Experiment Station).*

agreement but not enough to satisfy a length-scale reduction of, say, one-tenth. Therefore Reynolds-number scaling is also commonly violated in aerodynamic testing, and an extrapolation like that in Fig. 5.8 is required here also.

Finally, a serious discrepancy of another type occurs in hydraulic models of natural flow systems such as rivers, harbors, estuaries, and embayments. Such flows have large horizontal dimensions and small relative vertical dimensions. If we were to scale an estuary model by a uniform linear length ratio of, say, 1:1000, the resulting model would be only a few millimeters deep and dominated by entirely spurious surface-tension or Weber-number effects. Therefore such hydraulic models commonly violate *geometric* similarity by "distorting" the vertical scale by a factor of 10 or more. Figure 5.9 shows a hydraulic model of a barrier-beach inlet in South Carolina. The horizontal scale reduction is 1:300, but the vertical scale is only 1:60. Since a deeper channel flows more efficiently, the model channel bottom is deliberately roughened more than the natural channel to correct for the geometric discrepancy. Thus the friction effect of the discrepancy can be corrected, but its effect on, say, dispersion of heat and mass is less well known.

EXAMPLE 5.7

The pressure drop due to friction for flow in a long smooth pipe is a function of average flow velocity, density, viscosity, and pipe length and diameter: $\Delta p = \text{fcn}(V, \rho, \mu, L, D)$. We wish to know how Δp varies with V. (*a*) Use the pi theorem to rewrite this functional form. (*b*) Then plot this function, using the following data for three pipes



ketabline.com Ebook.ketabline.com

D, cm	L, m	Q, m^3/h	Δp, Pa	ρ, kg/m^3	μ, kg/(m · s)	V, m/s*
1.0	5.0	0.3	4,680	680†	2.92 E-4†	1.06
1.0	7.0	0.6	22,300	680†	2.92 E-4†	2.12
1.0	9.0	1.0	70,800	680†	2.92 E-4†	3.54
2.0	4.0	1.0	2,080	998‡	0.0010‡	0.88
2.0	6.0	2.0	10,500	998‡	0.0010‡	1.77
2.0	8.0	3.1	30,400	998‡	0.0010‡	2.74
3.0	3.0	0.5	540	13,550§	1.56 E-3§	0.20
3.0	4.0	1.0	2,480	13,550§	1.56 E-3§	0.39
3.0	5.0	1.7	9,600	13,550§	1.56 E-3§	0.67

*$V = Q/A$, $A = \pi D^2/4$.

†Gasoline.

‡Water.

§Mercury.

(c) Suppose it is further known that Δp is proportional to L (which is quite true for long pipes with well-rounded entrances). Use this information to simplify and improve the pi-theorem formulation. Plot the dimensionless data in this improved manner and comment upon the results.

Solution

There are six variables with three primary dimensions involved $\{MLT\}$. Therefore we expect that $j = 6 - 3 = 3$ pi groups. We are correct, for we can find three variables which do not form a pi product, for example, (ρ, V, L). Carefully select three (j) repeating variables, but not including Δp or V, which we plan to plot versus each other. We select (ρ, μ, D), and the pi theorem guarantees that three independent power-product groups will occur:

$$\Pi_1 = \rho^a \mu^b D^c \, \Delta p \qquad \Pi_2 = \rho^d \mu^e D^f V \qquad \Pi_3 = \rho^g \mu^h D^i L$$

or

$$\Pi_1 = \frac{\rho D^2 \, \Delta p}{\mu^2} \qquad \Pi_2 = \frac{\rho V D}{\mu} \qquad \Pi_3 = \frac{L}{D}$$

We have omitted the algebra of finding (a, b, c, d, e, f, g, h, i) by setting all exponents to zero M^0, L^0, T^0. Therefore we wish to plot the dimensionless relation

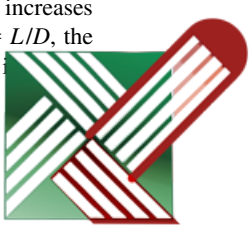
$$\frac{\rho D^2 \, \Delta p}{\mu^2} = \text{fcn}\left(\frac{\rho V D}{\mu}, \frac{L}{D}\right) \qquad \textit{Ans. (a)}$$

We plot Π_1 versus Π_2 with Π_3 as a parameter. There will be nine data points. For example, the first row in the data above yields

$$\frac{\rho D^2 \, \Delta p}{\mu^2} = \frac{(680)(0.01)^2(4680)}{(2.92 \text{ E-4})^2} = 3.73 \text{ E9}$$

$$\frac{\rho V D}{\mu} = \frac{(680)(1.06)(0.01)}{2.92 \text{ E-4}} = 24{,}700 \qquad \frac{L}{D} = 500$$

The nine data points are plotted as the open circles in Fig. 5.10. The values of L/D are listed for each point, and we see a significant length effect. In fact, if we connect the only two points which have the same L/D (= 200), we could see (and cross-plot to verify) that Δp increases linearly with L, as stated in the last part of the problem. Since L occurs only in $\Pi_3 = L/D$, the function $\Pi_1 = \text{fcn}(\Pi_2, \Pi_3)$ must reduce to $\Pi_1 = (L/D)\,\text{fcn}(\Pi_2)$, or simply a function of only *two* parameters:



ketabline.com Ebook.ketabline.com

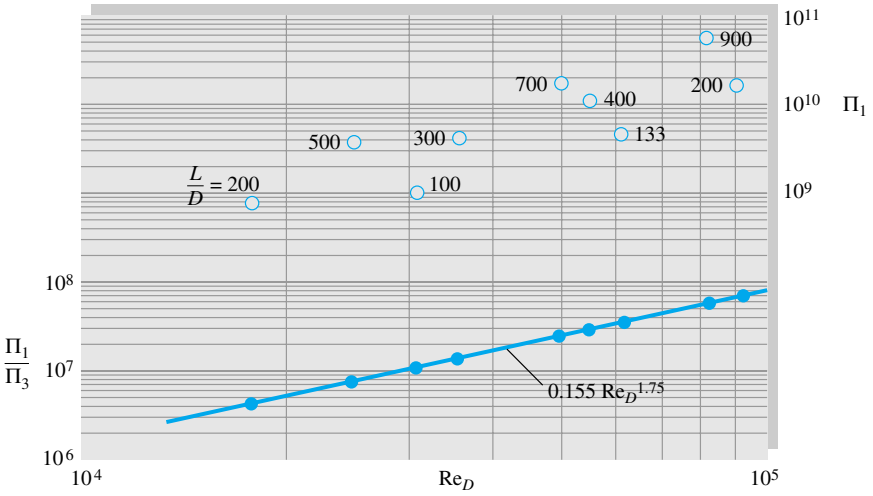


Fig. 5.10 Two different correlations of the data in Example 5.7: Open circles when plotting $\rho D^2\,\Delta p/\mu^2$ versus Re_D, L/D is a parameter; once it is known that Δp is proportional to L, a replot (solid circles) of $\rho D^3\,\Delta p/(L\mu^2)$ versus Re_D collapses into a single power-law curve.

$$\frac{\rho D^3\,\Delta p}{L\mu^2} = \text{fcn}\left(\frac{\rho VD}{\mu}\right) \qquad \text{flow in a long pipe} \qquad \textit{Ans. (c)}$$

We now modify each data point in Fig. 5.10 by dividing it by its L/D value. For example, for the first row of data, $\rho D^3\,\Delta p/(L\mu^2) = (3.73\ \text{E9})/500 = 7.46\ \text{E6}$. We replot these new data points as solid circles in Fig. 5.10. They correlate almost perfectly into a straight-line power-law function:

$$\frac{\rho D^3\,\Delta p}{L\mu^2} \approx 0.155\left(\frac{\rho VD}{\mu}\right)^{1.75} \qquad \textit{Ans. (c)}$$

All newtonian smooth pipe flows should correlate in this manner. This example is a variation of the first completely successful dimensional analysis, pipe-flow friction, performed by Prandtl's student Paul Blasius, who published a related plot in 1911. For this range of (turbulent-flow) Reynolds numbers, the pressure drop increases approximately as $V^{1.75}$.

EXAMPLE 5.8

The smooth-sphere data plotted in Fig. 5.3*a* represent dimensionless drag versus dimensionless *viscosity*, since (ρ, V, d) were selected as scaling or repeating variables. (*a*) Replot these data to display the effect of dimensionless *velocity* on the drag. (*b*) Use your new figure to predict the terminal (zero-acceleration) velocity of a 1-cm-diameter steel ball (SG = 7.86) falling through water at 20°C.

Solution

To display the effect of velocity, we must not use V as a repeating variable. Instead we choose (ρ, μ, d) as our j variables to nondimensionalize Eq. (5.1), $F = \text{fcn}(d, V, \rho, \mu)$. (See Example 5.2 for an alternate approach to this problem.) The pi groups form as follows:

$$\Pi_1 = \rho^a\mu^b d^c F = \frac{\rho F}{\mu^2} \qquad \Pi_2 = \rho^e\mu^f d^g V = \frac{\rho Vd}{\mu}$$



ketabline.com Ebook.ketabline.com

That is, $a = 1, b = -2, c = 0, e = 1, f = -1$, and $g = 1$, by using our power-product techniques of Examples 5.2 to 5.6. Therefore a plot of $\rho F/\mu^2$ versus Re will display the direct effect of velocity on sphere drag. This replot is shown as Fig. 5.11. The drag increases rapidly with velocity up to transition, where there is a slight drop, after which it increases more quickly than ever. If the force is known, we may predict the velocity from the figure.

For water at 20°C, take $\rho = 998$ kg/m^3 and $\mu = 0.001$ kg/(m · s). For steel, $\rho_s = 7.86\rho_{\text{water}} \approx 7840$ kg/m^3. For terminal velocity, the drag equals the net weight of the sphere in water. Thus

$$F = W_{\text{net}} = (\rho_s - \rho_w)g\frac{\pi}{6}d^3 = (7840 - 998)(9.81)\left(\frac{\pi}{6}\right)(0.01)^3 = 0.0351 \text{ N}$$

Therefore the ordinate of Fig. 5.11 is known:

$$\text{Falling steel sphere:} \qquad \frac{\rho F}{\mu^2} = \frac{(998 \text{ kg/m}^3)(0.0351 \text{ N})}{[0.001 \text{ kg/(m} \cdot \text{s)}]^2} \approx 3.5 \text{ E7}$$

From Fig. 5.11, at $\rho F/\mu^2 \approx 3.5$ E7, a magnifying glass reveals that $\text{Re}_d \approx 2$ E4. Then a crude estimate of the terminal fall velocity is

$$\frac{\rho V d}{\mu} \approx 20{,}000 \qquad \text{or} \qquad V \approx \frac{20{,}000[0.001 \text{ kg/(m} \cdot \text{s)}]}{(998 \text{ kg/m}^3)(0.01 \text{ m})} \approx 2.0 \frac{\text{m}}{\text{s}} \qquad \textit{Ans. (b)}$$

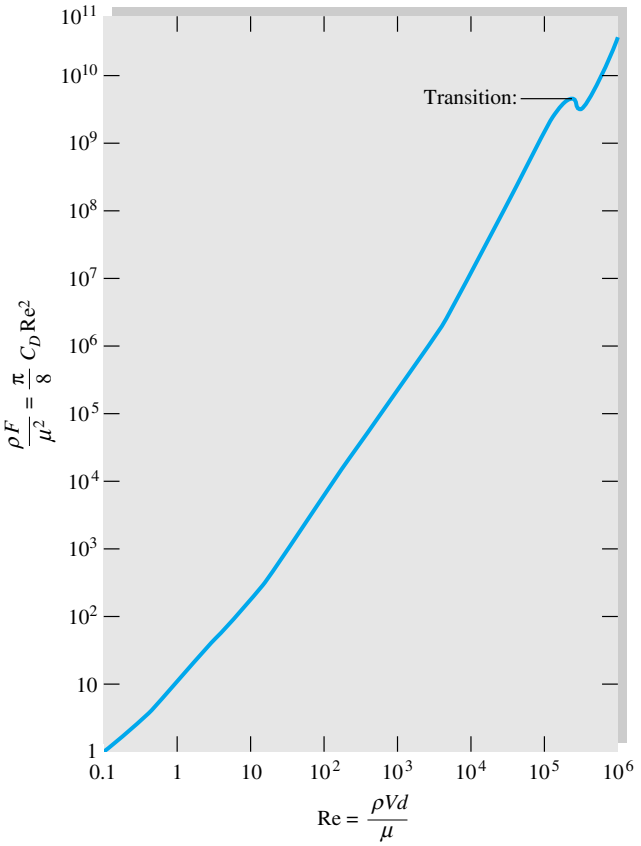


Fig. 5.11 Cross-plot of sphere-drag data from Fig. 5.3*a* to isolate diameter and velocity.



ketabline.com Ebook.ketabline.com

Better accuracy could be obtained by expanding the scale of Fig. 5.11 in the region of the given force coefficient. However, there is considerable uncertainty in published drag data for spheres, so the predicted fall velocity is probably uncertain by at least ± 5 percent.

Note that we found the answer directly from Fig. 5.11. We could use Fig. 5.3*a* also but would have to iterate between the ordinate and abscissa to obtain the final result, since V is contained in both plotted variables.

Summary

Chapters 3 and 4 presented integral and differential methods of mathematical analysis of fluid flow. This chapter introduces the third and final method: experimentation, as supplemented by the technique of dimensional analysis. Tests and experiments are used both to strengthen existing theories and to provide useful engineering results when theory is inadequate.

The chapter begins with a discussion of some familiar physical relations and how they can be recast in dimensionless form because they satisfy the principle of dimensional homogeneity. A general technique, the pi theorem, is then presented for systematically finding a set of dimensionless parameters by grouping a list of variables which govern any particular physical process. Alternately, direct application of dimensional analysis to the basic equations of fluid mechanics yields the fundamental parameters governing flow patterns: Reynolds number, Froude number, Prandtl number, Mach number, and others.

It is shown that model testing in air and water often leads to scaling difficulties for which compromises must be made. Many model tests do not achieve true dynamic similarity. The chapter ends by pointing out that classic dimensionless charts and data can be manipulated and recast to provide direct solutions to problems that would otherwise be quite cumbersome and laboriously iterative.

Problems

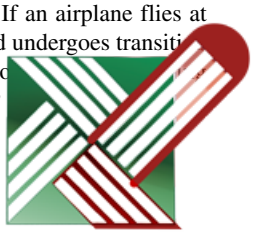
Most of the problems herein are fairly straightforward. More difficult or open-ended assignments are labeled with an asterisk. Problems labeled with an EES icon, for example, Prob. 5.61, will benefit from the use of the Engineering Equation Solver (EES), while problems labeled with a computer icon may require the use of a computer. The standard end-of-chapter problems 5.1 to 5.91 (categorized in the problem list below) are followed by word problems W5.1 to W5.10, fundamentals of engineering exam problems FE5.1 to FE5.10, comprehensive applied problems C5.1 to C5.4, and design projects D5.1 and D5.2.

Problem distribution

Section	Topic	Problems
5.1	Introduction	5.1–5.6
5.2	Choosing proper scaling parameters	5.7–5.9
5.2	The principle of dimensional homogeneity	5.10–5.17
5.3	The pi theorem	5.18–5.41
5.4	Nondimensionalizing the basic equations	5.42–5.47
5.4	Data for spheres and cylinders	5.48–5.57
5.5	Scaling of model data	5.58–5.74
5.5	Froude- and Mach-number scaling	5.75–5.84
5.5	Inventive rescaling of the data	5.85–5.91

P5.1 For axial flow through a circular tube, the Reynolds number for transition to turbulence is approximately 2300 [see Eq. (6.2)], based upon the diameter and average velocity. If $d = 5$ cm and the fluid is kerosine at 20°C, find the volume flow rate in m^3/h which causes transition.

P5.2 In flow past a thin flat body such as an airfoil, transition to turbulence occurs at about Re = 1 E6, based on the distance x from the leading edge of the wing. If an airplane flies at 450 mi/h at 8-km standard altitude and undergoes transiti at the 12 percent chord position, how lo length from leading to trailing edge)?



ketabline.com Ebook.ketabline.com

P5.3 An airplane has a chord length $L = 1.2$ m and flies at a Mach number of 0.7 in the standard atmosphere. If its Reynolds number, based on chord length, is 7 E6, how high is it flying?

P5.4 When tested in water at 20°C flowing at 2 m/s, an 8-cm-diameter sphere has a measured drag of 5 N. What will be the velocity and drag force on a 1.5-m-diameter weather balloon moored in sea-level standard air under dynamically similar conditions?

P5.5 An automobile has a characteristic length and area of 8 ft and 60 ft^2, respectively. When tested in sea-level standard air, it has the following measured drag force versus speed:

V, mi/h	20	40	60
Drag, lbf	31	115	249

The same car travels in Colorado at 65 mi/h at an altitude of 3500 m. Using dimensional analysis, estimate (*a*) its drag force and (*b*) the horsepower required to overcome air drag.

***P5.6** SAE 10 oil at 20°C flows past an 8-cm-diameter sphere. At flow velocities of 1, 2, and 3 m/s, the measured sphere drag forces are 1.5, 5.3, and 11.2 N, respectively. Estimate the drag force if the same sphere is tested at a velocity of 15 m/s in glycerin at 20°C.

P5.7 A body is dropped on the moon ($g = 1.62$ m/s^2) with an initial velocity of 12 m/s. By using option 2 variables, Eq. (5.11), the ground impact occurs at $t^{**} = 0.34$ and $S^{**} = 0.84$. Estimate (*a*) the initial displacement, (*b*) the final displacement, and (*c*) the time of impact.

P5.8 The Bernoulli equation (5.6) can be written in the form

$$p = p_0 - \tfrac{1}{2}\rho V^2 - \rho g z \qquad (1)$$

where p_0 is the "stagnation" pressure at zero velocity and elevation. (*a*) State how many scaling variables are needed to nondimensionalize this equation. (*b*) Suppose that we wish to nondimensionalize Eq. (1) in order to plot dimensionless pressure versus velocity, with elevation as a parameter. Select the proper scaling variables and carry out and plot the resulting dimensionless relation.

P5.9 Modify Prob. 5.8 as follows. Suppose that we wish to nondimensionalize Eq. (1) in order to plot dimensionless pressure versus gravity, with velocity as a parameter. Select the proper scaling variables and carry out and plot the resulting dimensionless relation.

P5.10 Determine the dimension $\{MLT\Theta\}$ of the following quantities:

$$(a)\ \rho u \frac{\partial u}{\partial x} \qquad (b)\ \int_1^2 (p - p_0)\, dA \qquad (c)\ \rho c_p \frac{\partial^2 T}{\partial x\, \partial y}$$

$$(d)\ \iiint \rho \frac{\partial u}{\partial t} dx\, dy\, dz$$

All quantities have their standard meanings; for example, ρ is density.

P5.11 For a particle moving in a circle, its centripetal acceleration takes the form $a = \text{fcn}(V, R)$, where V is its velocity and R the radius of its path. By pure dimensional reasoning, rewrite this function in algebraic form.

P5.12 The velocity of sound a of a gas varies with pressure p and density ρ. Show by dimensional reasoning that the proper form must be $a = (\text{const})(p/\rho)^{1/2}$.

P5.13 The speed of propagation C of a capillary wave in deep water is known to be a function only of density ρ, wavelength λ, and surface tension Υ. Find the proper functional relationship, completing it with a dimensionless constant. For a given density and wavelength, how does the propagation speed change if the surface tension is doubled?

P5.14 Consider laminar flow over a flat plate. The boundary layer thickness δ grows with distance x down the plate and is also a function of free-stream velocity U, fluid viscosity μ, and fluid density ρ. Find the dimensionless parameters for this problem, being sure to rearrange if neessary to agree with the standard dimensionless groups in fluid mechanics, as given in Table 5.2.

P5.15 It is desired to measure the drag on an airplane whose velocity is 300 mi/h. Is it feasible to test a one-twentieth-scale model of the plane in a wind tunnel at the same pressure and temperature to determine the prototype drag coefficient?

P5.16 Convection heat-transfer data are often reported as a *heat-transfer coefficient* h, defined by

$$\dot{Q} = hA\,\Delta T$$

where $\dot{Q}$ = heat flow, J/s
A = surface area, m^2
ΔT = temperature difference, K

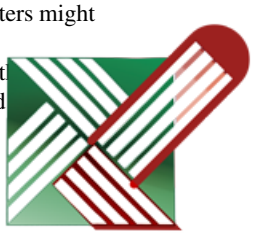
The dimensionless form of h, called the *Stanton number*, is a combination of h, fluid density ρ, specific heat c_p, and flow velocity V. Derive the Stanton number if it is proportional to h.

P5.17 In some heat-transfer textbooks, e.g., J. P. Holman, *Heat Transfer,* 5th ed., McGraw-Hill, 1981, p. 285, simplified formulas are given for the heat-transfer coefficient from Prob. 5.16 for buoyant or *natural* convection over hot surfaces. An example formula is

$$h = 1.42\left(\frac{\Delta T}{L}\right)^{1/4}$$

where L is the length of the hot surface. Comment on the dimensional homogeneity of this formula. What might be the SI units of constants 1.42 and $\frac{1}{4}$? What parameters might be missing or hidden?

P5.18 Under laminar conditions, the volume flow Q t
small triangular-section pore of side length b and



ketabline.com Ebook.ketabline.com

is a function of viscosity μ, pressure drop per unit length $\Delta p/L$, and b. Using the pi theorem, rewrite this relation in dimensionless form. How does the volume flow change if the pore size b is doubled?

P5.19 The period of oscillation T of a water surface wave is assumed to be a function of density ρ, wavelength λ, depth h, gravity g, and surface tension Υ. Rewrite this relationship in dimensionless form. What results if Υ is negligible? *Hint:* Take λ, ρ, and g as repeating variables.

P5.20 The power input P to a centrifugal pump is assumed to be a function of the volume flow Q, impeller diameter D, rotational rate Ω, and the density ρ and viscosity μ of the fluid. Rewrite this as a dimensionless relationship. *Hint:* Take Ω, ρ, and D as repeating variables.

P5.21 In Example 5.1 we used the pi theorem to develop Eq. (5.2) from Eq. (5.1). Instead of merely listing the primary dimensions of each variable, some workers list the *powers* of each primary dimension for each variable in an array:

$$\begin{array}{c} \\ M \\ L \\ T \end{array}\begin{array}{c} \begin{array}{ccccc} F & L & U & \rho & \mu \end{array} \\ \begin{bmatrix} 1 & 0 & 0 & 1 & 1 \\ 1 & 1 & 1 & -3 & -1 \\ -2 & 0 & -1 & 0 & -1 \end{bmatrix} \end{array}$$

This array of exponents is called the *dimensional matrix* for the given function. Show that the *rank* of this matrix (the size of the largest nonzero determinant) is equal to $j = n - k$, the desired reduction between original variables and the pi groups. This is a general property of dimensional matrices, as noted by Buckingham [29].

P5.22 When freewheeling, the angular velocity Ω of a windmill is found to be a function of the windmill diameter D, the wind velocity V, the air density ρ, the windmill height H as compared to the atmospheric boundary layer height L, and the number of blades N:

$$\Omega = \text{fcn}\left(D, V, \rho, \frac{H}{L}, N\right)$$

Viscosity effects are negligible. Find appropriate pi groups for this problem and rewrite the function above in dimensionless form.

P5.23 The period T of vibration of a beam is a function of its length L, area moment of inertia I, modulus of elasticity E, density ρ, and Poisson's ratio σ. Rewrite this relation in dimensionless form. What further reduction can we make if E and I can occur only in the product form EI? *Hint:* Take L, ρ, and E as repeating variables.

P5.24 The lift force F on a missile is a function of its length L, velocity V, diameter D, angle of attack α, density ρ, viscosity μ, and speed of sound a of the air. Write out the dimensional matrix of this function and determine its rank. (See Prob. 5.21 for an explanation of this concept.) Rewrite the function in terms of pi groups.

P5.25 When a viscous fluid is confined between two long concentric cylinders as in Fig. 4.17, the torque per unit length T' required to turn the inner cylinder at angular velocity Ω is a function of Ω, cylinder radii a and b, and viscosity μ. Find the equivalent dimensionless function. What happens to the torque if both a and b are doubled?

P5.26 A pendulum has an oscillation period T which is assumed to depend upon its length L, bob mass m, angle of swing θ, and the acceleration of gravity. A pendulum 1 m long, with a bob mass of 200 g, is tested on earth and found to have a period of 2.04 s when swinging at 20°. (*a*) What is its period when it swings at 45°? A similarly constructed pendulum, with $L = 30$ cm and $m = 100$ g, is to swing on the moon ($g = 1.62$ m/s^2) at $\theta = 20°$. (*b*) What will be its period?

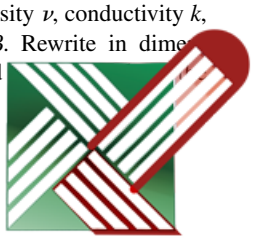
P5.27 In studying sand transport by ocean waves, A. Shields in 1936 postulated that the threshold wave-induced bottom shear stress τ required to move particles depends upon gravity g, particle size d and density ρ_p, and water density ρ and viscosity μ. Find suitable dimensionless groups of this problem, which resulted in 1936 in the celebrated Shields sand-transport diagram.

P5.28 A simply supported beam of diameter D, length L, and modulus of elasticity E is subjected to a fluid crossflow of velocity V, density ρ, and viscosity μ. Its center deflection δ is assumed to be a function of all these variables. (*a*) Rewrite this proposed function in dimensionless form. (*b*) Suppose it is known that δ is independent of μ, inversely proportional to E, and dependent only upon ρV^2, not ρ and V separately. Simplify the dimensionless function accordingly. *Hint:* Take L, ρ, and V as repeating variables.

P5.29 When fluid in a pipe is accelerated linearly from rest, it begins as laminar flow and then undergoes transition to turbulence at a time t_{tr} which depends upon the pipe diameter D, fluid acceleration a, density ρ, and viscosity μ. Arrange this into a dimensionless relation between t_{tr} and D.

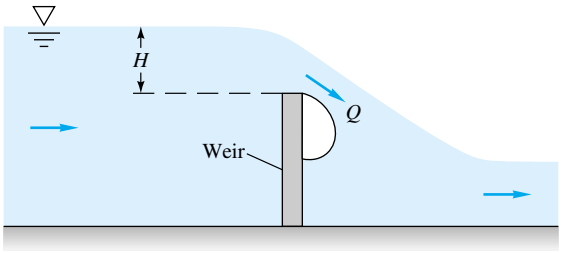
P5.30 In forced convection, the heat-transfer coefficient h, as defined in Prob. 5.16, is known to be a function of stream velocity U, body size L, and fluid properties ρ, μ, c_p, and k. Rewrite this function in dimensionless form, and note by name any parameters you recognize. *Hint:* Take L, ρ, k, and μ as repeating variables.

P5.31 The heat-transfer rate per unit area q to a body from a fluid in natural or gravitational convection is a function of the temperature difference ΔT, gravity g, body length L, and three fluid properties: kinematic viscosity ν, conductivity k, and thermal expansion coefficient β. Rewrite in dimensionless form if it is known that g and β appear only in the product $g\beta$.



ketabline.com Ebook.ketabline.com

P5.32 A *weir* is an obstruction in a channel flow which can be calibrated to measure the flow rate, as in Fig. P5.32. The volume flow Q varies with gravity g, weir width b into the paper, and upstream water height H above the weir crest. If it is known that Q is proportional to b, use the pi theorem to find a unique functional relationship $Q(g, b, H)$.

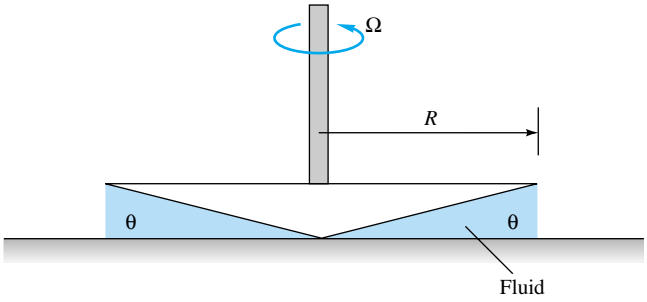


P5.32

P5.33 A spar buoy (see Prob. 2.113) has a period T of vertical (heave) oscillation which depends upon the waterline cross-sectional area A, buoy mass m, and fluid specific weight γ. How does the period change due to doubling of (*a*) the mass and (*b*) the area? Instrument buoys should have long periods to avoid wave resonance. Sketch a possible long-period buoy design.

P5.34 To good approximation, the thermal conductivity k of a gas (see Ref. 8 of Chap. 1) depends only upon the density ρ, mean free path ℓ, gas constant R, and absolute temperature T. For air at 20°C and 1 atm, $k \approx 0.026$ W/(m · K) and $\ell \approx 6.5$ E-8 m. Use this information to determine k for hydrogen at 20°C and 1 atm if $\ell \approx 1.2$ E-7 m.

P5.35 The torque M required to turn the cone-plate viscometer in Fig. P5.35 depends upon the radius R, rotation rate Ω, fluid viscosity μ, and cone angle θ. Rewrite this relation in dimensionless form. How does the relation simplify it if it is known that M is proportional to θ?



P5.35

P5.36 The rate of heat loss, $\dot{Q}_{\text{loss}}$ through a window or wall is a function of the temperature difference between inside and outside ΔT, the window surface area A, and the R value of the window which has units of (ft^2 · h · °F)/Btu. (*a*) Using Buckingham pi theorem, find an expression for rate of heat loss as a function of the other three parameters in the problem. (*b*) If the temperature difference ΔT doubles, by what factor does the rate of heat loss increase?

P5.37 The pressure difference Δp across an explosion or blast wave is a function of the distance r from the blast center, time t, speed of sound a of the medium, and total energy E in the blast. Rewrite this relation in dimensionless form (see Ref. 18, chap. 4, for further details of blast-wave scaling). How does Δp change if E is doubled?

P5.38 The size d of droplets produced by a liquid spray nozzle is thought to depend upon the nozzle diameter D, jet velocity U, and the properties of the liquid ρ, μ, and Υ. Rewrite this relation in dimensionless form. *Hint:* Take D, ρ, and U as repeating variables.

P5.39 In turbulent flow past a flat surface, the velocity u near the wall varies approximately logarithmically with distance y from the wall and also depends upon viscosity μ, density ρ, and wall shear stress τ_w. For a certain airflow at 20°C and 1 atm, $\tau_w = 0.8$ Pa and $u = 15$ m/s at $y = 3.6$ mm. Use this information to estimate the velocity u at $y = 6$ mm.

P5.40 Reconsider the slanted-plate surface tension problem (see Fig. C1.1) as an exercise in dimensional analysis. Let the capillary rise h be a function only of fluid properties, gravity, bottom width, and the two angles in Fig. C1.1. That is, $h = \text{fcn}(\rho, \Upsilon, g, L, \alpha, \theta)$. (*a*) Use the pi theorem to rewrite this function in terms of dimensionless parameters. (*b*) Verify that the exact solution from Prob. C1.1 is consistent with your result in part (*a*).

P5.41 A certain axial-flow turbine has an output torque M which is proportional to the volume flow rate Q and also depends upon the density ρ, rotor diameter D, and rotation rate Ω. How does the torque change due to a doubling of (*a*) D and (*b*) Ω?

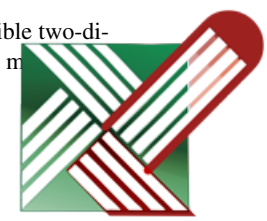
P5.42 Nondimensionalize the energy equation (4.75) and its boundary conditions (4.62), (4.63), and (4.70) by defining $T^* = T/T_0$, where T_0 is the inlet temperature, assumed constant. Use other dimensionless variables as needed from Eqs. (5.23). Isolate all dimensionless parameters you find, and relate them to the list given in Table 5.2.

P5.43 The differential equation of salt conservation for flowing seawater is

$$\frac{\partial S}{\partial t} + u\frac{\partial S}{\partial x} + v\frac{\partial S}{\partial y} + w\frac{\partial S}{\partial z} = \kappa\left(\frac{\partial^2 S}{\partial x^2} + \frac{\partial^2 S}{\partial y^2} + \frac{\partial^2 S}{\partial z^2}\right)$$

where κ is a (constant) coefficient of diffusion, with typical units of square meters per second, and S is the salinity in parts per thousand. Nondimensionalize this equation and discuss any parameters which appear.

P5.44 The differential energy equation for incompressible two-dimensional flow through a "Darcy-type" porous m
approximately



ketabline.com Ebook.ketabline.com

$$\rho c_p \frac{\sigma}{\mu}\frac{\partial p}{\partial x}\frac{\partial T}{\partial x} + \rho c_p \frac{\sigma}{\mu}\frac{\partial p}{\partial y}\frac{\partial T}{\partial y} + k\frac{\partial^2 T}{\partial y^2} = 0$$

where σ is the *permeability* of the porous medium. All other symbols have their usual meanings. (*a*) What are the appropriate dimensions for σ? (*b*) Nondimensionalize this equation, using (L, U, ρ, T_0) as scaling constants, and discuss any dimensionless parameters which arise.

P5.45 In natural-convection problems, the variation of density due to the temperature difference ΔT creates an important buoyancy term in the momentum equation (5.30). To first-order accuracy, the density variation would be $\rho \approx \rho_0(1 - \beta\,\Delta T)$, where β is the thermal-expansion coefficient. The momentum equation thus becomes

$$\rho_0 \frac{d\mathbf{V}}{dt} = -\boldsymbol{\nabla}(p + \rho_0 g z) + \rho_0 \beta\,\Delta T\, g\mathbf{k} + \mu\,\nabla^2\mathbf{V}$$

where we have assumed that z is up. Nondimensionalize this equation, using Eqs. (5.23), and relate the parameters you find to the list in Table 5.2.

P5.46 The differential equation for compressible inviscid flow of a gas in the xy plane is

$$\frac{\partial^2\phi}{\partial t^2} + \frac{\partial}{\partial t}(u^2 + v^2) + (u^2 - a^2)\frac{\partial^2\phi}{\partial x^2} + (v^2 - a^2)\frac{\partial^2\phi}{\partial y^2} + 2uv\frac{\partial^2\phi}{\partial x\,\partial y} = 0$$

where ϕ is the velocity potential and a is the (variable) speed of sound of the gas. Nondimensionalize this relation, using a reference length L and the inlet speed of sound a_0 as parameters for defining dimensionless variables.

P5.47 The differential equation for small-amplitude vibrations $y(x, t)$ of a simple beam is given by

$$\rho A\frac{\partial^2 y}{\partial t^2} + EI\frac{\partial^4 y}{\partial x^4} = 0$$

where ρ = beam material density
A = cross-sectional area
I = area moment of inertia
E = Young's modulus

Use only the quantities ρ, E, and A to nondimensionalize y, x, and t, and rewrite the differential equation in dimensionless form. Do any parameters remain? Could they be removed by further manipulation of the variables?

P5.48 A smooth steel (SG = 7.86) sphere is immersed in a stream of ethanol at 20°C moving at 1.5 m/s. Estimate its drag in N from Fig. 5.3*a*. What stream velocity would quadruple its drag? Take $D = 2.5$ cm.

P5.49 The sphere in Prob. 5.48 is dropped in gasoline at 20°C. Ignoring its acceleration phase, what will its terminal (constant) fall velocity be, from Fig. 5.3*a*?

P5.50 When a micro-organism moves in a viscous fluid, it turns out that fluid density has nearly negligible influence on the drag force felt by the micro-organism. Such flows are called *creeping flows*. The only important parameters in the problem are the velocity of motion U, the viscosity of the fluid μ, and the length scale of the body. Here assume the micro-organism's body diameter d as the appropriate length scale. (*a*) Using the Buckingham pi theorem, generate an expression for the drag force D as a function of the other parameters in the problem. (*b*) The drag coefficient discussed in this chapter $C_D = D/(\frac{1}{2}\rho U^2 A)$ is not appropriate for this kind of flow. Define instead a more appropriate drag coefficient, and call it C_c (for creeping flow). (*c*) For a spherically shaped micro-organism, the drag force can be calculated exactly from the equations of motion for creeping flow. The result is $D = 3\pi\mu U d$. Write expressions for both forms of the drag coefficient, C_c and C_D, for a sphere under conditions of creeping flow.

P5.51 A ship is towing a sonar array which approximates a submerged cylinder 1 ft in diameter and 30 ft long with its axis normal to the direction of tow. If the tow speed is 12 kn (1 kn = 1.69 ft/s), estimate the horsepower required to tow this cylinder. What will be the frequency of vortices shed from the cylinder? Use Figs. 5.2 and 5.3.

P5.52 A 1-in-diameter telephone wire is mounted in air at 20°C and has a natural vibration frequency of 12 Hz. What wind velocity in ft/s will cause the wire to sing? At this condition what will the average drag force per unit wire length be?

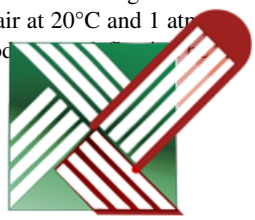
P5.53 Vortex shedding can be used to design a *vortex flowmeter* (Fig. 6.32). A blunt rod stretched across the pipe sheds vortices whose frequency is read by the sensor downstream. Suppose the pipe diameter is 5 cm and the rod is a cylinder of diameter 8 mm. If the sensor reads 5400 counts per minute, estimate the volume flow rate of water in m^3/h. How might the meter react to other liquids?

P5.54 A fishnet is made of 1-mm-diameter strings knotted into 2×2 cm squares. Estimate the horsepower required to tow 300 ft^2 of this netting at 3 kn in seawater at 20°C. The net plane is normal to the flow direction.

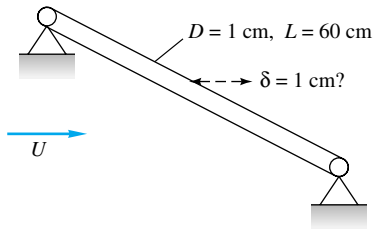
P5.55 The radio antenna on a car begins to vibrate wildly at 500 Hz when the car is driven at 55 mi/h. Estimate the diameter of the antenna.

P5.56 A wooden flagpole, of diameter 5 in and height 30 ft, fractures at its base in hurricane winds at sea level. If the fracture stress is 3500 lbf/in^2, estimate the wind velocity in mi/h.

P5.57 The simply supported 1040 carbon-steel rod of Fig. P5.57 is subjected to a crossflow stream of air at 20°C and 1 atm. For what stream velocity U will the rod [illegible] approximately 1 cm?



ketabline.com Ebook.ketabline.com



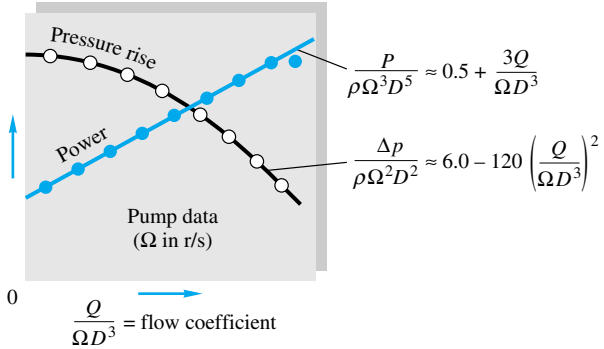
P5.57

P5.58 For the steel rod of Prob. 5.57, at what airstream velocity U will the rod begin to vibrate laterally in resonance in its first mode (a half sine wave)? *Hint:* Consult a vibration text under "lateral beam vibration."

P5.59 We wish to know the drag of a blimp which will move in 20°C air at 6 m/s. If a one-thirtieth-scale model is tested in water at 20°C, what should the water velocity be? At this velocity, if the measured water drag on the model is 2700 N, what is the drag on the prototype blimp and the power required to propel it?

P5.60 A prototype water pump has an impeller diameter of 2 ft and is designed to pump 12 ft^3/s at 750 r/min. A 1-ft-diameter model pump is tested in 20°C air at 1800 r/min, and Reynolds-number effects are found to be negligible. For similar conditions, what will the volume flow of the model be in ft^3/s? If the model pump requires 0.082 hp to drive it, what horsepower is required for the prototype?

P5.61 If viscosity is neglected, typical pump-flow results from Prob. 5.20 are shown in Fig. P5.61 for a model pump tested in water. The pressure rise decreases and the power required increases with the dimensionless flow coefficient. Curve-fit expressions are given for the data. Suppose a similar pump of 12-cm diameter is built to move gasoline at 20°C and a flow rate of 25 m^3/h. If the pump rotation speed is 30 r/s, find (*a*) the pressure rise and (*b*) the power required.



P5.61

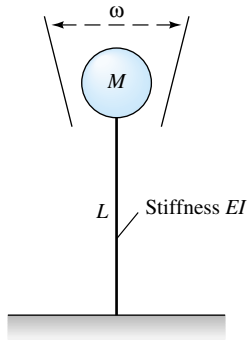
***P5.62** Modify Prob. 5.61 so that the rotation speed is unknown but $D = 12$ cm and $Q = 25$ m^3/h. What is the maximum rotation speed for which the power will not exceed 300 W? What will the pressure rise be for this condition?

***P5.63** The pressure drop per unit length $\Delta p/L$ in smooth pipe flow is known to be a function only of the average velocity V, diameter D, and fluid properties ρ and μ. The following data were obtained for flow of water at 20°C in an 8-cm-diameter pipe 50 m long:

Q, m^3/s	0.005	0.01	0.015	0.020
Δp, Pa	5800	20,300	42,100	70,800

Verify that these data are slightly outside the range of Fig. 5.10. What is a suitable power-law curve fit for the present data? Use these data to estimate the pressure drop for flow of kerosine at 20°C in a smooth pipe of diameter 5 cm and length 200 m if the flow rate is 50 m^3/h.

P5.64 The natural frequency ω of vibration of a mass M attached to a rod, as in Fig. P5.64, depends only upon M and the stiffness EI and length L of the rod. Tests with a 2-kg mass attached to a 1040 carbon-steel rod of diameter 12 mm and length 40 cm reveal a natural frequency of 0.9 Hz. Use these data to predict the natural frequency of a 1-kg mass attached to a 2024 aluminum-alloy rod of the same size.

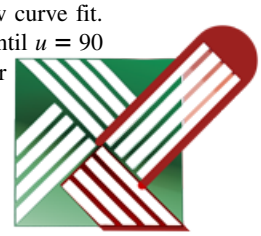


P5.64

P5.65 In turbulent flow near a flat wall, the local velocity u varies only with distance y from the wall, wall shear stress τ_w, and fluid properties ρ and μ. The following data were taken in the University of Rhode Island wind tunnel for airflow, $\rho = 0.0023$ slug/ft^3, $\mu = 3.81$ E-7 slug/(ft · s), and $\tau_w = 0.029$ lbf/ft^2:

y, in	0.021	0.035	0.055	0.080	0.12	0.16
u, ft/s	50.6	54.2	57.6	59.7	63.5	65.9

(*a*) Plot these data in the form of dimensionless u versus dimensionless y, and suggest a suitable power-law curve fit. (*b*) Suppose that the tunnel speed is increased until $u = 90$ ft/s at $y = 0.11$ in. Estimate the new wall shear lbf/ft^2.



ketabline.com Ebook.ketabline.com

P5.66 A torpedo 8 m below the surface in 20°C seawater cavitates at a speed of 21 m/s when atmospheric pressure is 101 kPa. If Reynolds-number and Froude-number effects are negligible, at what speed will it cavitate when running at a depth of 20 m? At what depth should it be to avoid cavitation at 30 m/s?

P5.67 A student needs to measure the drag on a prototype of characteristic dimension d_p moving at velocity U_p in air at standard atmospheric conditions. He constructs a model of characteristic dimension d_m, such that the ratio d_p/d_m is some factor f. He then measures the drag on the model at dynamically similar conditions (also with air at standard atmospheric conditions). The student claims that the drag force on the prototype will be identical to that measured on the model. Is this claim correct? Explain.

P5.68 Consider flow over a very small object in a viscous fluid. Analysis of the equations of motion shows that the inertial terms are much smaller than the viscous and pressure terms. It turns out, then, that fluid density drops out of the equations of motion. Such flows are called *creeping flows*. The only important parameters in the problem are the velocity of motion U, the viscosity of the fluid μ, and the length scale of the body. For three-dimensional bodies, like spheres, creeping flow analysis yields very good results. It is uncertain, however, if such analysis can be applied to two-dimensional bodies such as a circular cylinder, since even though the diameter may be very small, the length of the cylinder is infinite for a two-dimensional flow. Let us see if dimensional analysis can help. (*a*) Using the Buckingham pi theorem, generate an expression for the two-dimensional drag $D_{2\text{-D}}$ as a function of the other parameters in the problem. Use cylinder diameter d as the appropriate length scale. Be careful—the two-dimensional drag has dimensions of force per unit length rather than simply force. (*b*) Is your result physically plausible? If not, explain why not. (*c*) It turns out that fluid density ρ *cannot* be neglected in analysis of creeping flow over two-dimensional bodies. Repeat the dimensional analysis, this time with ρ included as a parameter. Find the nondimensional relationship between the parameters in this problem.

P5.69 A one-sixteenth-scale model of a weir (see Fig. P5.32) has a measured flow rate $Q = 2.1$ ft^3/s when the upstream water height is $H = 6.3$ in. If Q is proportional to weir width b, predict the prototype flow rate when $H_{\text{proto}} = 3.2$ ft.

P5.70 A diamond-shaped body, of characteristic length 9 in, has the following measured drag forces when placed in a wind tunnel at sea-level standard conditions:

V, ft/s	30	38	48	56	61
F, lbf	1.25	1.95	3.02	4.05	4.81

Use these data to predict the drag force of a similar 15-in diamond placed at similar orientation in 20°C water flowing at 2.2 m/s.

P5.71 The pressure drop in a venturi meter (Fig. P3.165) varies only with the fluid density, pipe approach velocity, and diameter ratio of the meter. A model venturi meter tested in water at 20°C shows a 5-kPa drop when the approach velocity is 4 m/s. A geometrically similar prototype meter is used to measure gasoline at 20°C and a flow rate of 9 m^3/min. If the prototype pressure gage is most accurate at 15 kPa, what should the upstream pipe diameter be?

P5.72 A one-fifteenth-scale model of a parachute has a drag of 450 lbf when tested at 20 ft/s in a water tunnel. If Reynolds-number effects are negligible, estimate the terminal fall velocity at 5000-ft standard altitude of a parachutist using the prototype if chute and chutist together weigh 160 lbf. Neglect the drag coefficient of the woman.

P5.73 The yawing moment on a torpedo control surface is tested on a one-eighth-scale model in a water tunnel at 20 m/s, using Reynolds scaling. If the model measured moment is 14 N · m, what will the prototype moment be under similar conditions?

P5.74 A one-tenth-scale model of a supersonic wing tested at 700 m/s in air at 20°C and 1 atm shows a pitching moment of 0.25 kN · m. If Reynolds-number effects are negligible, what will the pitching moment of the prototype wing be if it is flying at the same Mach number at 8-km standard altitude?

P5.75 A one-twelfth-scale model of an airplane is to be tested at 20°C in a pressurized wind tunnel. The prototype is to fly at 240 m/s at 10-km standard altitude. What should the tunnel pressure be in atm to scale both the Mach number and the Reynolds number accurately?

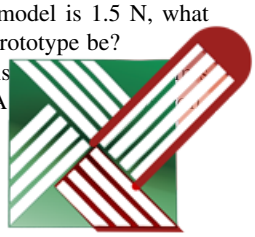
***P5.76** A 2-ft-long model of a ship is tested in a freshwater tow tank. The measured drag may be split into "friction" drag (Reynolds scaling) and "wave" drag (Froude scaling). The model data are as follows:

Tow speed, ft/s	0.8	1.6	2.4	3.2	4.0	4.8
Friction drag, lbf	0.016	0.057	0.122	0.208	0.315	0.441
Wave drag, lbf	0.002	0.021	0.083	0.253	0.509	0.697

The prototype ship is 150 ft long. Estimate its total drag when cruising at 15 kn in seawater at 20°C.

P5.77 A dam spillway is to be tested by using Froude scaling with a one-thirtieth-scale model. The model flow has an average velocity of 0.6 m/s and a volume flow of 0.05 m^3/s. What will the velocity and flow of the prototype be? If the measured force on a certain part of the model is 1.5 N, what will the corresponding force on the prototype be?

P5.78 A prototype spillway has a characteris
and a characteristic length of 10 m. A



ketabline.com Ebook.ketabline.com

structed by using Froude scaling. What is the minimum scale ratio of the model which will ensure that its minimum Weber number is 100? Both flows use water at 20°C.

P5.79 An East Coast estuary has a tidal period of 12.42 h (the semidiurnal lunar tide) and tidal currents of approximately 80 cm/s. If a one-five-hundredth-scale model is constructed with tides driven by a pump and storage apparatus, what should the period of the model tides be and what model current speeds are expected?

P5.80 A prototype ship is 35 m long and designed to cruise at 11 m/s (about 21 kn). Its drag is to be simulated by a 1-m-long model pulled in a tow tank. For Froude scaling find (*a*) the tow speed, (*b*) the ratio of prototype to model drag, and (*c*) the ratio of prototype to model power.

P5.81 An airplane, of overall length 55 ft, is designed to fly at 680 m/s at 8000-m standard altitude. A one-thirtieth-scale model is to be tested in a pressurized helium wind tunnel at 20°C. What is the appropriate tunnel pressure in atm? Even at this (high) pressure, exact dynamic similarity is not achieved. Why?

P5.82 A prototype ship is 400 ft long and has a wetted area of 30,000 ft^2. A one-eightieth-scale model is tested in a tow tank according to Froude scaling at speeds of 1.3, 2.0, and 2.7 kn (1 kn = 1.689 ft/s). The measured friction drag of the model at these speeds is 0.11, 0.24, and 0.41 lbf, respectively. What are the three prototype speeds? What is the estimated prototype friction drag at these speeds if we correct for Reynolds-number discrepancy by extrapolation?

P5.83 A one-fortieth-scale model of a ship's propeller is tested in a tow tank at 1200 r/min and exhibits a power output of 1.4 ft · lbf/s. According to Froude scaling laws, what should the revolutions per minute and horsepower output of the prototype propeller be under dynamically similar conditions?

P5.84 A prototype ocean-platform piling is expected to encounter currents of 150 cm/s and waves of 12-s period and 3-m height. If a one-fifteenth-scale model is tested in a wave channel, what current speed, wave period, and wave height should be encountered by the model?

P5.85 Solve Prob. 5.49, using the modified sphere-drag plot of Fig. 5.11.

P5.86 Solve Prob. 5.49 for glycerin at 20°C, using the modified sphere-drag plot of Fig. 5.11.

P5.87 In Prob. 5.62 it was difficult to solve for Ω because it appeared in both power and flow coefficients. Rescale the problem, using the data of Fig. P5.61, to make a plot of dimensionless power versus dimensionless rotation speed. Enter this plot directly to solve Prob. 5.62 for Ω.

P5.88 Modify Prob. 5.62 as follows: Let $\Omega = 32$ r/s and $Q = 24$ m^3/h for a geometrically similar pump. What is the maximum diameter if the power is not to exceed 340 W? Solve this problem by rescaling the data of Fig. P5.61 to make a plot of dimensionless power versus dimensionless diameter. Enter this plot directly to find the desired diameter.

P5.89 Knowing that Δp is proportional to L, rescale the data of Example 5.7 to plot dimensionless Δp versus dimensionless *diameter*. Use this plot to find the diameter required in the first row of data in Example 5.7 if the pressure drop is increased to 10 kPa for the same flow rate, length, and fluid.

P5.90 Knowing that Δp is proportional to L, rescale the data of Example 5.7 to plot dimensionless Δp versus dimensionless *viscosity*. Use this plot to find the viscosity required in the first row of data in Example 5.7 if the pressure drop is increased to 10 kPa for the same flow rate, length, and density.

P5.91 Develop a plot of dimensionless Δp versus dimensionless viscosity, as described in Prob. 5.90. Suppose that $L = 200$ m, $Q = 60$ m^3/h, and the fluid is kerosine at 20°C. Use your plot to determine the minimum pipe diameter for which the pressure drop is no more than 220 kPa.

Word Problems

W5.1 In 98 percent of data analysis cases, the "reducing factor" j, which lowers the number n of dimensional variables to $n - j$ dimensionless groups, exactly equals the number of relevant dimensions (M, L, T, Θ). In one case (Example 5.5) this was not so. Explain in words why this situation happens.

W5.2 Consider the following equation: **1 dollar bill ≈ 6 in.** Is this relation dimensionally inconsistent? Does it satisfy the PDH? Why?

W5.3 In making a dimensional analysis, what rules do you follow for choosing your scaling variables?

W5.4 In an earlier edition, the writer asked the following question about Fig. 5.1: "Which of the three graphs is a more effective presentation?" Why was this a dumb question?

W5.5 This chapter discusses the difficulty of scaling Mach and Reynolds numbers together (an airplane) and Froude and Reynolds numbers together (a ship). Give an example of a flow which would combine Mach and Froude numbers. Would there be scaling problems for common fluids?

W5.6 What is different about a very *small* model of a weir or dam (Fig. P5.32) which would make the test results difficult to relate to the prototype?

W5.7 What else are you studying this term? Give an example of a popular equation or formula from another course (thermodynamics, strength of materials, etc.) which does not satisfy the principle of dimensional homogeneity. Explain what is wrong and whether it can be modi homogeneous.



ketabline.com Ebook.ketabline.com

W5.8 Some colleges (e.g., Colorado State University) have environmental wind tunnels which can be used to study, e.g., wind flow over city buildings. What details of scaling might be important in such studies?

W5.9 If the model scale ratio is $\alpha = L_m/L_p$, as in Eq. (5.31), and the Weber number is important, how must the model and prototype surface tension be related to α for dynamic similarity?

W5.10 For a typical incompressible velocity potential analysis in Chap. 4 we solve $\nabla^2\phi = 0$, subject to known values of $\partial\phi/\partial n$ on the boundaries. What dimensionless parameters govern this type of motion?

Fundamentals of Engineering Exam Problems

FE5.1 Given the parameters (U, L, g, ρ, μ) which affect a certain liquid flow problem, the ratio $V^2/(Lg)$ is usually known as the
(*a*) velocity head, (*b*) Bernoulli head, (*c*) Froude number, (*d*) kinetic energy, (*e*) impact energy

FE5.2 A ship 150 m long, designed to cruise at 18 kn, is to be tested in a tow tank with a model 3 m long. The appropriate tow velocity is
(*a*) 0.19 m/s, (*b*) 0.35 m/s, (*c*) 1.31 m/s,
(*d*) 2.55 m/s, (*e*) 8.35 m/s

FE5.3 A ship 150 m long, designed to cruise at 18 kn, is to be tested in a tow tank with a model 3 m long. If the model wave drag is 2.2 N, the estimated full-size ship wave drag is
(*a*) 5500 N, (*b*) 8700 N, (*c*) 38,900 N,
(*d*) 61,800 N, (*e*) 275,000 N

FE5.4 A tidal estuary is dominated by the semidiurnal lunar tide, with a period of 12.42 h. If a 1:500 model of the estuary is tested, what should be the model tidal period?
(*a*) 4.0 s, (*b*) 1.5 min, (*c*) 17 min, (*d*) 33 min, (*e*) 64 min

FE5.5 A football, meant to be thrown at 60 mi/h in sea-level air ($\rho = 1.22$ kg/m^3, $\mu = 1.78$ E-5 N $\cdot$ s/m^2), is to be tested using a one-quarter scale model in a water tunnel ($\rho = 998$ kg/m^3, $\mu = 0.0010$ N $\cdot$ s/m^2). For dynamic similarity, what is the proper model water velocity?
(*a*) 7.5 mi/h, (*b*) 15.0 mi/h, (*c*) 15.6 mi/h,
(*d*) 16.5 mi/h, (*e*) 30 mi/h

FE5.6 A football, meant to be thrown at 60 mi/h in sea-level air ($\rho = 1.22$ kg/m^3, $\mu = 1.78$ E-5 N $\cdot$ m^2), is to be tested using a one-quarter scale model in a water tunnel ($\rho = 998$ kg/m^3, $\mu = 0.0010$ N $\cdot$ s/m^2). For dynamic similarity, what is the ratio of prototype force to model force?
(*a*) 3.86:1, (*b*) 16:1, (*c*) 32:1, (*d*) 56:1, (*e*) 64:1

FE5.7 Consider liquid flow of density ρ, viscosity μ, and velocity U over a very small model spillway of length scale L, such that the liquid surface tension coefficient Υ is important. The quantity $\rho U^2L/\Upsilon$ in this case is important and is called the
(*a*) capillary rise, (*b*) Froude number, (*c*) Prandtl number, (*d*) Weber number, (*e*) Bond number

FE5.8 If a stream flowing at velocity U past a body of length L causes a force F on the body which depends only upon U, L, and fluid viscosity μ, then F must be proportional to
(*a*) $\rho UL/\mu$, (*b*) ρU^2L^2, (*c*) $\mu U/L$, (*d*) μUL, (*e*) UL/μ

FE5.9 In supersonic wind tunnel testing, if different gases are used, dynamic similarity requires that the model and prototype have the same Mach number and the same
(*a*) Euler number, (*b*) speed of sound, (*c*) stagnation enthalpy, (*d*) Froude number, (*e*) specific heat ratio

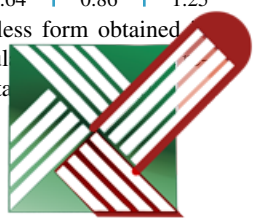
FE5.10 The Reynolds number for a 1-ft-diameter sphere moving at 2.3 mi/h through seawater (specific gravity 1.027, viscosity 1.07 E-3 N $\cdot$ s/m^2) is approximately
(*a*) 300, (*b*) 3000, (*c*) 30,000, (*d*) 300,000, (*e*) 3,000,000

Comprehensive Problems

C5.1 Estimating pipe wall friction is one of the most common tasks in fluids engineering. For long circular rough pipes in turbulent flow, wall shear τ_w is a function of density ρ, viscosity μ, average velocity V, pipe diameter d, and wall roughness height ϵ. Thus, functionally, we can write $\tau_w = \text{fcn}(\rho, \mu, V, d, \epsilon)$. (*a*) Using dimensional analysis, rewrite this function in dimensionless form. (*b*) A certain pipe has $d = 5$ cm and $\epsilon = 0.25$ mm. For flow of water at 20°C, measurements show the following values of wall shear stress:

Q, gal/min	1.5	3.0	6.0	9.0	12.0	14.0
τ_w, Pa	0.05	0.18	0.37	0.64	0.86	1.25

Plot these data using the dimensionless form obtained in part (*a*) and suggest a curve-fit formula which reveal the entire functional relation obta



ketabline.com Ebook.ketabline.com

C5.2 When the fluid exiting a nozzle, as in Fig. P3.49, is a gas, instead of water, compressibility may be important, especially if upstream pressure p_1 is large and exit diameter d_2 is small. In this case, the difference $p_1 - p_2$ is no longer controlling, and the gas mass flow $\dot{m}$ reaches a maximum value which depends upon p_1 and d_2 and also upon the absolute upstream temperature T_1 and the gas constant R. Thus, functionally, $\dot{m} = \text{fcn}(p_1, d_2, T_1, R)$. (*a*) Using dimensional analysis, rewrite this function in dimensionless form. (*b*) A certain pipe has $d_2 = 1$ mm. For flow of air, measurements show the following values of mass flow through the nozzle:

T_1, K	300	300	300	500	800
p_1, kPa	200	250	300	300	300
$\dot{m}$, kg/s	0.037	0.046	0.055	0.043	0.034

Plot these data in the dimensionless form obtained in part (*a*). Does your plot reveal the entire functional relation obtained in part (*a*)?

C5.3 Reconsider the fully developed draining vertical oil-film problem (see Fig. P4.80) as an exercise in dimensional analysis. Let the vertical velocity be a function only of distance from the plate, fluid properties, gravity, and film thickness. That is, $w = \text{fcn}(x, \rho, \mu, g, \delta)$. (*a*) Use the pi theorem to rewrite this function in terms of dimensionless parameters. (*b*) Verify that the exact solution from Prob. 4.80 is consistent with your result in part (*a*).

C5.4 The Taco Inc. model 4013 centrifugal pump has an impeller of diameter $D = 12.95$ in. When pumping 20°C water at $\Omega = 1160$ r/min, the measured flow rate Q and pressure rise Δp are given by the manufacturer as follows:

Q, gal/min	200	300	400	500	600	700
Δp, lb/in^2	36	35	34	32	29	23

(*a*) Assuming that $\Delta p = \text{fcn}(\rho, Q, D, \Omega)$, use the pi theorem to rewrite this function in terms of dimensionless parameters and then plot the given data in dimensionless form. (*b*) It is desired to use the same pump, running at 900 r/min, to pump 20°C gasoline at 400 gal/min. According to your dimensionless correlation, what pressure rise Δp is expected, in lbf/in^2?

Design Projects

D5.1 We are given laboratory data, taken by Prof. Robert Kirchhoff and his students at the University of Massachusetts, for the spin rate of a 2-cup anemometer. The anemometer was made of ping-pong balls ($d = 1.5$ in) split in half, facing in opposite directions, and glued to thin ($\frac{1}{4}$-in) rods pegged to a center axle. (See Fig. P7.91 for a sketch.) There were four rods, of lengths $\ell = 0.212$, 0.322, 0.458, and 0.574 ft. The experimental data, for wind tunnel velocity U and rotation rate Ω, are as follows:

$\ell = 0.212$		$\ell = 0.322$		$\ell = 0.458$		$\ell = 0.574$	
U, ft/s	Ω, r/min	U, ft/s	Ω, r/min	U, ft/s	Ω, r/min	U, ft/s	Ω, r/min
18.95	435.00	18.95	225.00	20.10	140.00	23.21	115.00
22.20	545.00	23.19	290.00	26.77	215.00	27.60	145.00
25.90	650.00	29.15	370.00	31.37	260.00	32.07	175.00
29.94	760.00	32.79	425.00	36.05	295.00	36.05	195.00
38.45	970.00	38.45	495.00	39.03	327.00	39.60	215.00

Assume that the angular velocity Ω of the device is a function of wind speed U, air density ρ and viscosity μ, rod length ℓ, and cup diameter d. For all data, assume air is at 1 atm and 20°C. Define appropriate pi groups for this problem, and plot the data above in this dimensionless manner. Comment on the possible uncertainty of the results.

As a design application, suppose we are to use this anemometer geometry for a large-scale ($d = 30$ cm) airport wind anemometer. If wind speeds vary up to 25 m/s and we desire an average rotation rate $\Omega = 120$ r/min, what should be the proper rod length? What are possible limitations of your design? Predict the expected Ω (in r/min) of your design as affected by wind speeds from 0 to 25 m/s.

D5.2 By analogy with the cylinder-drag data in Fig. 5.3*b*, spheres also show a strong roughness effect on drag, at least in the Reynolds number range 4 E4 $<$ Re$_D$ $<$ 3 E5, which accounts for the dimpling of golf balls to increase their distance traveled. Some experimental data for roughened spheres [43] are given in Fig. D5.2. The figure also shows typical golf-ball data. We see that some roughened spheres are better than golf balls in some regions. For the present study, let us neglect the ball's *spin,* which causes the very important side-force or *Magnus effect* (See Fig. 8.11) and assume that the ball is hit without spin and follows the equations of motion for plane motion (x, z):

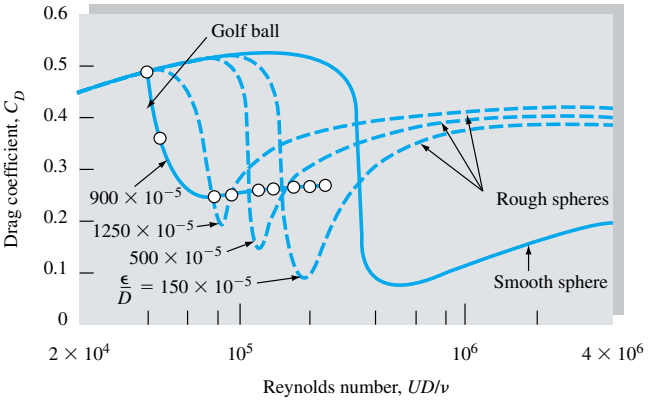
$$m\ddot{x} = -F\cos\theta \qquad m\ddot{z} = -F\sin\theta - W$$

where $F = C_D\frac{\rho}{2}\frac{\pi}{4}D^2(\dot{x}^2 + \dot{z}^2)$ $\theta = \tan$



ketabline.com Ebook.ketabline.com

The ball has a particular $C_D(\mathrm{Re}_D)$ curve from Fig. D5.2 and is struck with an initial velocity V_0 and angle θ_0. Take the ball's average mass to be 46 g and its diameter to be 4.3 cm. Assuming sea-level air and a modest but finite range of initial conditions, integrate the equations of motion to compare the trajectory of "roughened spheres" to actual golf-ball calculations. Can the rough sphere outdrive a normal golf ball for any conditions? What roughness-effect differences occur between a low-impact duffer and, say, Tiger Woods?



D5.2

References

1. P. W. Bridgman, *Dimensional Analysis,* Yale University Press, New Haven, CT, 1922, rev. ed., 1931.
2. A. W. Porter, *The Method of Dimensions,* Methuen, London, 1933.
3. F. M. Lanchester, *The Theory of Dimensions and Its Applications for Engineers,* Crosby-Lockwood, London, 1940.
4. R. Esnault-Pelterie, *L'Analyse dimensionelle,* F. Rouge, Lausanne, Switzerland, 1946.
5. G. W. Stubbings, *Dimensions in Engineering Theory,* Crosby-Lockwood, London, 1948.
6. G. Murphy, *Similitude in Engineering,* Ronald, New York, 1950.
7. H. E. Huntley, *Dimensional Analysis,* Rinehart, New York, 1951.
8. H. L. Langhaar, *Dimensional Analysis and the Theory of Models,* Wiley, New York, 1951.
9. W. J. Duncan, *Physical Similarity and Dimensional Analysis,* Arnold, London, 1953.
10. C. M. Focken, *Dimensional Methods and Their Applications,* Arnold, London, 1953.
11. L. I. Sedov, *Similarity and Dimensional Methods in Mechanics,* Academic, New York, 1959.
12. E. C. Ipsen, *Units, Dimensions, and Dimensionless Numbers,* McGraw-Hill, New York, 1960.
13. E. E. Jupp, *An Introduction to Dimensional Methods,* Cleaver-Hume, London, 1962.
14. R. Pankhurst, *Dimensional Analysis and Scale Factors,* Reinhold, New York, 1964.
15. S. J. Kline, *Similitude and Approximation Theory,* McGraw-Hill, New York, 1965.
16. B. S. Massey, *Units, Dimensional Analysis, and Physical Similarity,* Van Nostrand Reinhold, New York, 1971.
17. J. Zierep, *Similarity Laws and Modeling,* Dekker, New York, 1971.
18. W. E. Baker et al., *Similarity Methods in Engineering Dynamics,* Spartan, Rochelle Park, NJ, 1973.
19. E. S. Taylor, *Dimensional Analysis for Engineers,* Clarendon Press, Oxford, England, 1974.
20. E. de St. Q. Isaacson and M. de St. Q. Isaacson, *Dimensional Methods in Engineering and Physics,* Arnold, London, 1975.
21. P. LeCorbeiller, *Dimensional Analysis,* Irvington, New York, 1966.
22. V. J. Skoglund, *Similitude—Theory and Applications,* International, Scranton, PA, 1967.
23. M. S. Yalin, *Theory of Hydraulic Models,* Macmillan, London, 1971.
24. J. J. Sharp, *Hydraulic Modeling,* Butterworth, London, 1981.
25. G. I. Barenblatt, *Dimensional Analysis,* Gordon and Breach, New York, 1987.
26. R. Esnault-Pelterie, *Dimensional Analysis and Metrology,* F. Rouge, Lausanne, Switzerland, 1950.
27. R. Kurth, *Dimensional Analysis and Group Theory in Astrophysics,* Pergamon, New York, 1972.
28. F. J. de-Jong, *Dimensional Analysis for Economists,* North Holland, Amsterdam, 1967.
29. E. Buckingham, "On Physically Similar Systems: Illustrations of the Use of Dimensional Equations," *Phys. Rev.,* vol. 4, no. 4, 1914, pp. 345–376.
30. "Flow of Fluids through Valves, Fittings, and Pipe," *Crane Co. Tech. Pap.* 410, Chicago, 1957.
31. A. Roshko, "On the Development of Turbulent Wakes from Vortex Streets," *NACA Rep.* 1191, 1954.
32. G. W. Jones, Jr., "Unsteady Lift Forces Generated by Vortex Shedding about a Large, Stationary, Oscillating Cylinder at High Reynolds Numbers," *ASME Symp. Unsteady Flow,* 1968.
33. O. M. Griffin and S. E. Ramberg, "The Vortex Street Wak of Vibrating Cylinders," *J. Fluid Mech.,* pp. 553–576.



ketabline.com Ebook.ketabline.com

34. *Encyclopedia of Science and Technology,* 8th ed., McGraw-Hill, New York, 1997.
35. H. A. Becker, *Dimensionless Parameters,* Halstead Press (Wiley), New York, 1976.
36. D. J. Schuring, *Scale Models in Engineering,* Pergamon Press, New York, 1977.
37. M. Zlokarnik, *Dimensional Analysis and Scale-Up in Chemical Engineering,* Springer-Verlag, New York, 1991.
38. W. G. Jacoby, *Data Theory and Dimensional Analysis,* Sage, Newbury Park, CA, 1991.
39. B. Schepartz, *Dimensional Analysis in the Biomedical Sciences,* Thomas, Springfield, IL, 1980.
40. A. J. Smith, *Dosage and Solution Calculations: The Dimensional Analysis Way,* Mosby, St. Louis, MO, 1989.
41. J. B. Bassingthwaighte et al., *Fractal Physiology,* Oxford Univ. Press, New York, 1994.
42. K. J. Niklas, *Plant Allometry: The Scaling of Form and Process,* Univ. of Chicago Press, Chicago, 1994.
43. R. D. Blevins, *Applied Fluid Dynamics Handbook,* van Nostrand Reinhold, New York, 1984.



ketabline.com Ebook.ketabline.com



Steam pipe bridge in a geothermal power plant. Pipe flows are everywhere, often occurring in groups or networks. They are designed using the principles outlined in this chapter. *(Courtesy of Dr. E. R. Degginger/Color-Pic Inc.)*



ketabline.com Ebook.ketabline.com

Chapter 6
Viscous Flow in Ducts

Motivation. This chapter is completely devoted to an important practical fluids engineering problem: flow in ducts with various velocities, various fluids, and various duct shapes. Piping systems are encountered in almost every engineering design and thus have been studied extensively. There is a small amount of theory plus a large amount of experimentation.

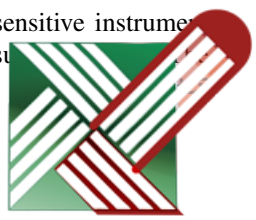
The basic piping problem is this: Given the pipe geometry and its added components (such as fittings, valves, bends, and diffusers) plus the desired flow rate and fluid properties, what pressure drop is needed to drive the flow? Of course, it may be stated in alternate form: Given the pressure drop available from a pump, what flow rate will ensue? The correlations discussed in this chapter are adequate to solve most such piping problems.

6.1 Reynolds-Number Regimes

Now that we have derived and studied the basic flow equations in Chap. 4, you would think that we could just whip off myriad beautiful solutions illustrating the full range of fluid behavior, of course expressing all these educational results in dimensionless form, using our new tool from Chap. 5, dimensional analysis.

The fact of the matter is that no general analysis of fluid motion yet exists. There are several dozen known particular solutions, there are some rather specific digital-computer solutions, and there are a great many experimental data. There is a lot of theory available if we neglect such important effects as viscosity and compressibility (Chap. 8), but there is no general theory and there may never be. The reason is that a profound and vexing change in fluid behavior occurs at moderate Reynolds numbers. The flow ceases being smooth and steady (*laminar*) and becomes fluctuating and agitated (*turbulent*). The changeover is called *transition* to turbulence. In Fig. 5.3*a* we saw that transition on the cylinder and sphere occurred at about $\mathrm{Re} = 3 \times 10^5$, where the sharp drop in the drag coefficient appeared. Transition depends upon many effects, e.g., wall roughness (Fig. 5.3*b*) or fluctuations in the inlet stream, but the primary parameter is the Reynolds number. There are a great many data on transition but only a small amount of theory [1 to 3].

Turbulence can be detected from a measurement by a small, sensitive instrume
such as a hot-wire anemometer (Fig. 6.29*e*) or a piezoelectric pressu



ketabline.com Ebook.ketabline.com

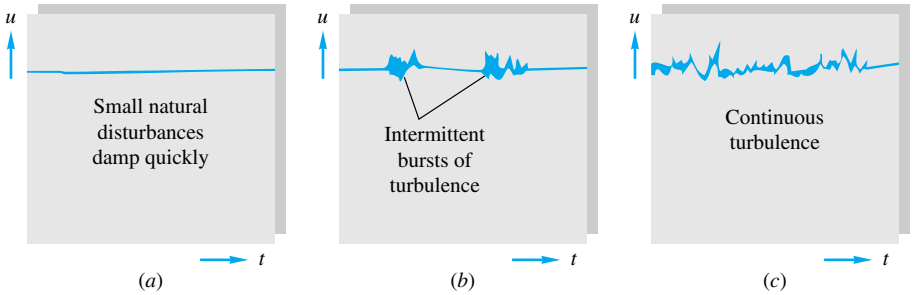


Fig. 6.1 The three regimes of viscous flow: (*a*) laminar flow at low Re; (*b*) transition at intermediate Re; (*c*) turbulent flow at high Re.

flow will appear steady on average but will reveal rapid, random fluctuations if turbulence is present, as sketched in Fig. 6.1. If the flow is laminar, there may be occasional natural disturbances which damp out quickly (Fig. 6.1*a*). If transition is occurring, there will be sharp bursts of turbulent fluctuation (Fig. 6.1*b*) as the increasing Reynolds number causes a breakdown or instability of laminar motion. At sufficiently large Re, the flow will fluctuate continually (Fig. 6.1*c*) and is termed *fully turbulent*. The fluctuations, typically ranging from 1 to 20 percent of the average velocity, are not strictly periodic but are random and encompass a continuous range, or spectrum, of frequencies. In a typical wind-tunnel flow at high Re, the turbulent frequency ranges from 1 to 10,000 Hz, and the wavelength ranges from about 0.01 to 400 cm.

EXAMPLE 6.1

The accepted transition Reynolds number for flow in a circular pipe is $\mathrm{Re}_{d,\mathrm{crit}} \approx 2300$. For flow through a 5-cm-diameter pipe, at what velocity will this occur at 20°C for (*a*) airflow and (*b*) water flow?

Solution

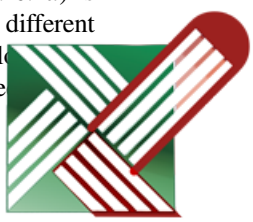
Almost all pipe-flow formulas are based on the *average* velocity $V = Q/A$, not centerline or any other point velocity. Thus transition is specified at $\rho Vd/\mu \approx 2300$. With d known, we introduce the appropriate fluid properties at 20°C from Tables A.3 and A.4:

(*a*) Air: $$\frac{\rho Vd}{\mu} = \frac{(1.205\ \mathrm{kg/m^3})V(0.05\ \mathrm{m})}{1.80\ \text{E-5}\ \mathrm{kg/(m \cdot s)}} = 2300 \quad \text{or} \quad V \approx 0.7\ \frac{\mathrm{m}}{\mathrm{s}}$$

(*b*) Water: $$\frac{\rho Vd}{\mu} = \frac{(998\ \mathrm{kg/m^3})V(0.05\ \mathrm{m})}{0.001\ \mathrm{kg/(m \cdot s)}} = 2300 \quad \text{or} \quad V = 0.046\ \frac{\mathrm{m}}{\mathrm{s}}$$

These are very low velocities, so most engineering air and water pipe flows are turbulent, not laminar. We might expect laminar duct flow with more viscous fluids such as lubricating oils or glycerin.

In free surface flows, turbulence can be observed directly. Figure 6.2 shows liquid flow issuing from the open end of a tube. The low-Reynolds-number jet (Fig. 6.2*a*) is smooth and laminar, with the fast center motion and slower wall flow forming different trajectories joined by a liquid sheet. The higher-Reynolds-number turbulent fl
6.2*b*) is unsteady and irregular but, when averaged over time, is steady and pre



ketabline.com Ebook.ketabline.com

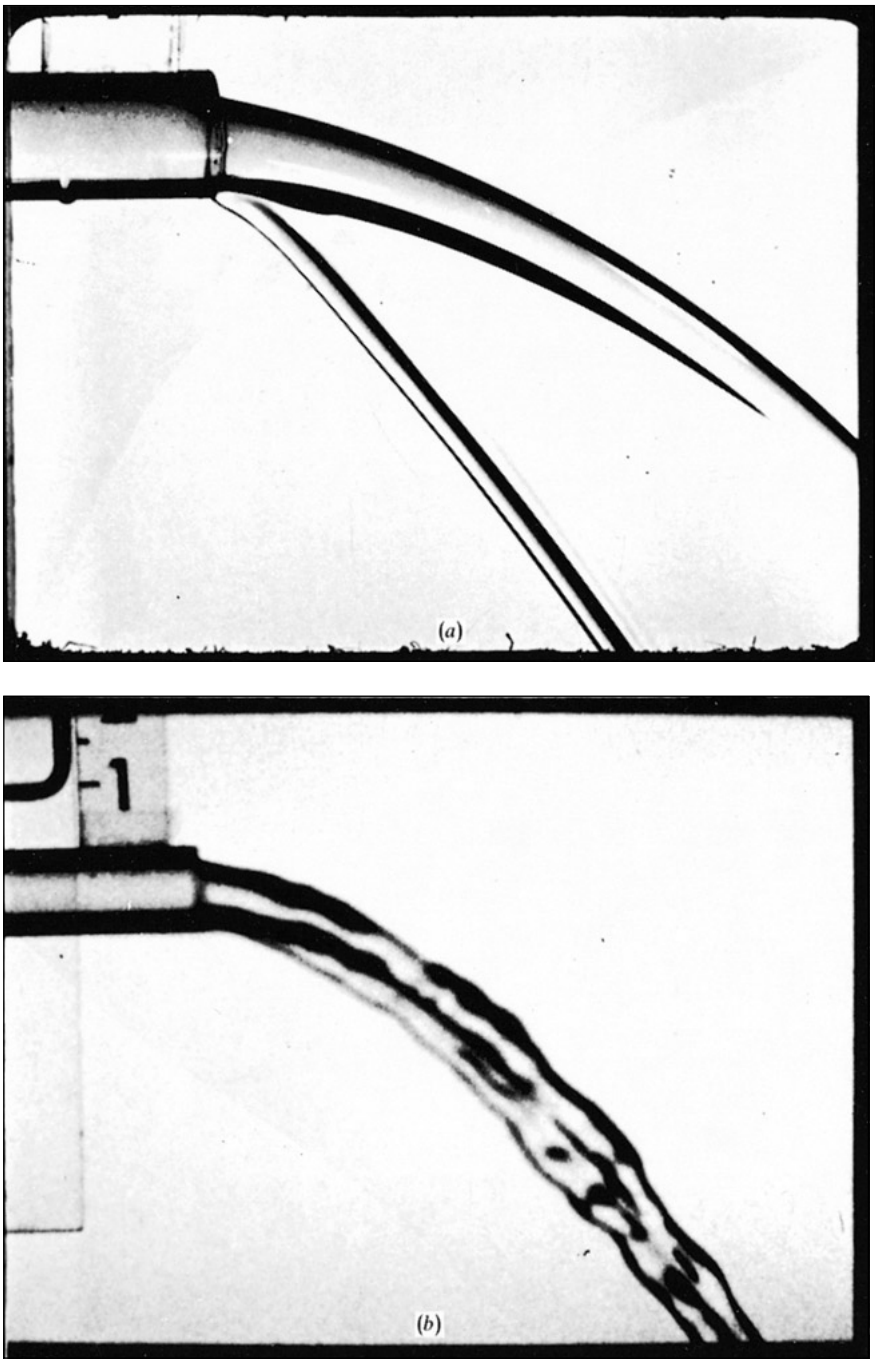


Fig. 6.2 Flow issuing at constant speed from a pipe: (*a*) high-viscosity, low-Reynolds-number, laminar flow; (*b*) low-viscosity, high-Reynolds-number, turbulent flow. *[From* Illustrated Experiments in Fluid Mechanics *(The NCFMF Book of Film Notes), National Committee for Fluid Mechanics Films, Education Development Center, Inc., copyright 1972.]*

How did turbulence form inside the pipe? The laminar parabolic flow profile, whi is similar to Eq. (4.143), became unstable and, at $\mathrm{Re}_d \approx 2300$, beg or "puffs" of intense turbulence. A puff has a fast-moving front and a

ketabline.com Ebook.ketabline.com

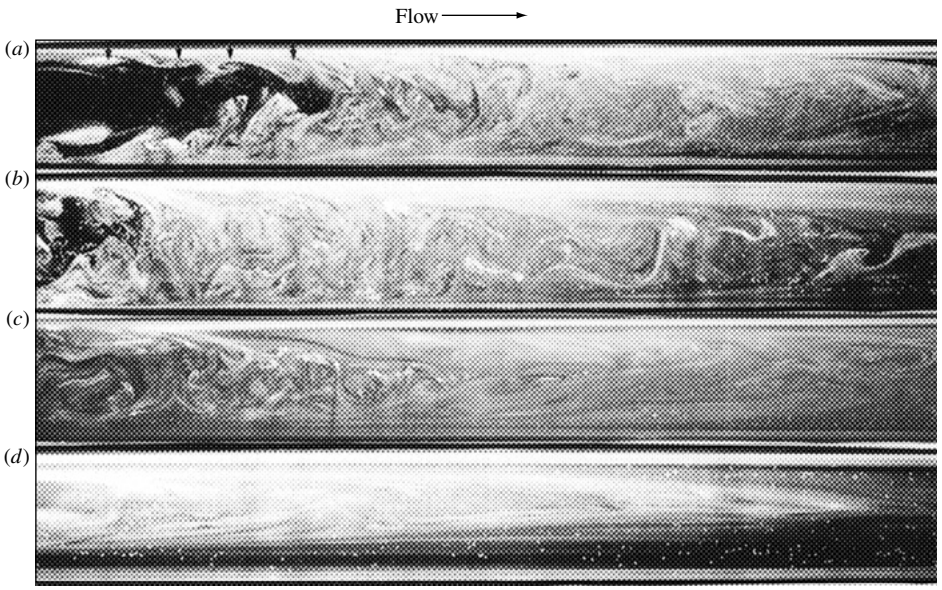


Fig. 6.3 Formation of a turbulent puff in pipe flow: (*a*) and (*b*) near the entrance; (*c*) somewhat downstream; (*d*) far downstream. *(From Ref. 45, courtesy of P. R. Bandyopadhyay.)*

and may be visualized by experimenting with glass tube flow. Figure 6.3 shows a puff as photographed by Bandyopadhyay [45]. Near the entrance (Fig. 6.3*a* and *b*) there is an irregular laminar-turbulent interface, and vortex roll-up is visible. Further downstream (Fig. 6.3*c*) the puff becomes fully turbulent and very active, with helical motions visible. Far downstream (Fig. 6.3*d*), the puff is cone-shaped and less active, with a fuzzy ill-defined interface, sometimes called the "relaminarization" region.

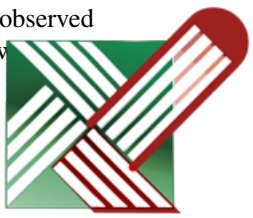
A complete description of the statistical aspects of turbulence is given in Ref. 1, while theory and data on transition effects are given in Refs. 2 and 3. At this introductory level we merely point out that the primary parameter affecting transition is the Reynolds number. If $\mathrm{Re} = UL/\nu$, where U is the average stream velocity and L is the "width," or transverse thickness, of the shear layer, the following approximate ranges occur:

$0 < \mathrm{Re} < 1$:	highly viscous laminar "creeping" motion
$1 < \mathrm{Re} < 100$:	laminar, strong Reynolds-number dependence
$100 < \mathrm{Re} < 10^3$:	laminar, boundary-layer theory useful
$10^3 < \mathrm{Re} < 10^4$:	transition to turbulence
$10^4 < \mathrm{Re} < 10^6$:	turbulent, moderate Reynolds-number dependence
$10^6 < \mathrm{Re} < \infty$:	turbulent, slight Reynolds-number dependence

These are representative ranges which vary somewhat with flow geometry, surface roughness, and the level of fluctuations in the inlet stream. The great majority of our analyses are concerned with laminar flow or with turbulent flow, and one should not normally design a flow operation in the transition region.

Historical Outline

Since turbulent flow is more prevalent than laminar flow, experimenters have observed turbulence for centuries without being aware of the details. Before 1930 flow ments were too insensitive to record rapid fluctuations, and workers simply



ketabline.com Ebook.ketabline.com

mean values of velocity, pressure, force, etc. But turbulence can change the mean values dramatically, e.g., the sharp drop in drag coefficient in Fig. 5.3. A German engineer named G. H. L. Hagen first reported in 1839 that there might be *two* regimes of viscous flow. He measured water flow in long brass pipes and deduced a pressure-drop law

$$\Delta p = (\text{const})\frac{LQ}{R^4} + \text{entrance effect} \tag{6.1}$$

This is exactly our laminar-flow scaling law from Example 5.4, but Hagen did not realize that the constant was proportional to the fluid viscosity.

The formula broke down as Hagen increased Q beyond a certain limit, i.e., past the critical Reynolds number, and he stated in his paper that there must be a second mode of flow characterized by "strong movements of water for which Δp varies as the second power of the discharge. . . ." He admitted that he could not clarify the reasons for the change.

A typical example of Hagen's data is shown in Fig. 6.4. The pressure drop varies linearly with $V = Q/A$ up to about 1.1 ft/s, where there is a sharp change. Above about $V = 2.2$ ft/s the pressure drop is nearly quadratic with V. The actual power $\Delta p \propto V^{1.75}$ seems impossible on dimensional grounds but is easily explained when the dimensionless pipe-flow data (Fig. 5.10) are displayed.

In 1883 Osborne Reynolds, a British engineering professor, showed that the change depended upon the parameter $\rho Vd/\mu$, now named in his honor. By introducing a dye

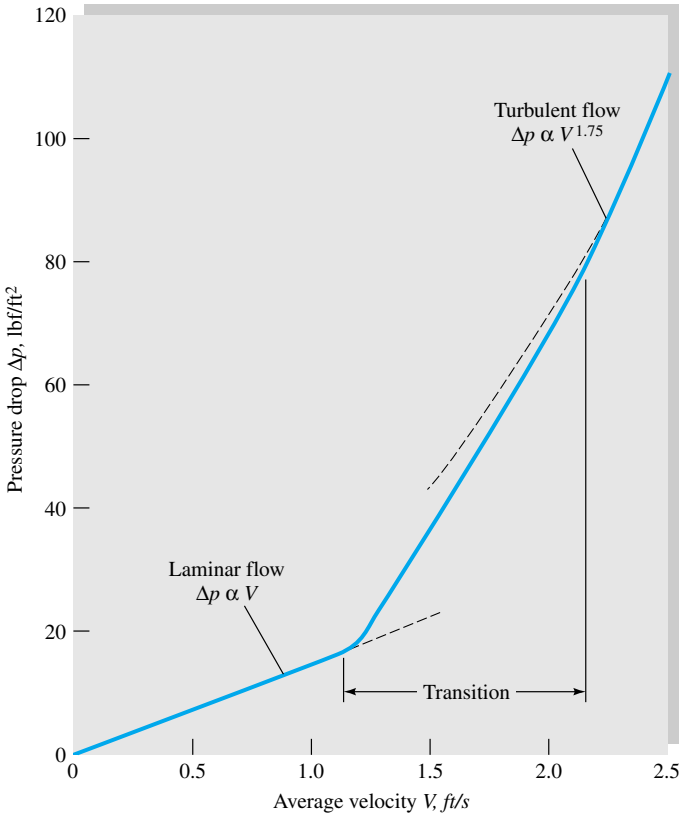


Fig. 6.4 Experimental evidence of transition for water flow in a $\frac{1}{4}$-in smooth pipe 10 ft long.



ketabline.com Ebook.ketabline.com

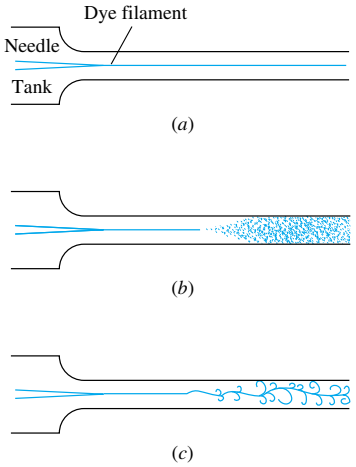


Fig. 6.5 Reynolds' sketches of pipe-flow transition: (*a*) low-speed, laminar flow; (*b*) high-speed, turbulent flow; (*c*) spark photograph of condition (*b*). *(From Ref. 4.)*

streak into a pipe flow, Reynolds could observe transition and turbulence. His sketches of the flow behavior are shown in Fig. 6.5.

If we examine Hagen's data and compute the Reynolds number at $V = 1.1$ ft/s, we obtain $\mathrm{Re}_d = 2100$. The flow became fully turbulent, $V = 2.2$ ft/s, at $\mathrm{Re}_d = 4200$. The accepted design value for pipe-flow transition is now taken to be

$$\mathrm{Re}_{d,\mathrm{crit}} \approx 2300 \tag{6.2}$$

This is accurate for commercial pipes (Fig. 6.13), although with special care in providing a rounded entrance, smooth walls, and a steady inlet stream, $\mathrm{Re}_{d,\mathrm{crit}}$ can be delayed until much higher values.

Transition also occurs in external flows around bodies such as the sphere and cylinder in Fig. 5.3. Ludwig Prandtl, a German engineering professor, showed in 1914 that the thin boundary layer surrounding the body was undergoing transition from laminar to turbulent flow. Thereafter the force coefficient of a body was acknowledged to be a function of the Reynolds number [Eq. (5.2)].

There are now extensive theories and experiments of laminar-flow instability which explain why a flow changes to turbulence. Reference 5 is an advanced textbook on this subject.

Laminar-flow theory is now well developed, and many solutions are known [2, 3], but there are no analyses which can simulate the fine-scale random fluctuations of turbulent flow.[1] Therefore existing turbulent-flow theory is semiempirical, based upon dimensional analysis and physical reasoning; it is concerned with the mean flow properties only and the mean of the fluctuations, not their rapid variations. The turbulent-flow "theory" presented here in Chaps. 6 and 7 is unbelievably crude yet surprisingly effective. We shall attempt a rational approach which places turbulent-flow analysis on a firm physical basis.

6.2 Internal versus External Viscous Flows

Both laminar and turbulent flow may be either internal, i.e., "bounded" by walls, or external and unbounded. This chapter treats internal flows, and Chap. 7 studies external flows.

An internal flow is constrained by the bounding walls, and the viscous effects will grow and meet and permeate the entire flow. Figure 6.6 shows an internal flow in a long duct. There is an *entrance region* where a nearly inviscid upstream flow converges and enters the tube. Viscous boundary layers grow downstream, retarding the axial flow $u(r, x)$ at the wall and thereby accelerating the center-core flow to maintain the incompressible continuity requirement

$$Q = \int u\, dA = \text{const} \tag{6.3}$$

At a finite distance from the entrance, the boundary layers merge and the inviscid core disappears. The tube flow is then entirely viscous, and the axial velocity adjusts slightly further until at $x = L_e$ it no longer changes with x and is said to be *fully developed*, $u \approx u(r)$ only. Downstream of $x = L_e$ the velocity profile is constant, the wall

[1] Reference 32 is a computer model of large-scale turbulent fluctuations.



ketabline.com Ebook.ketabline.com

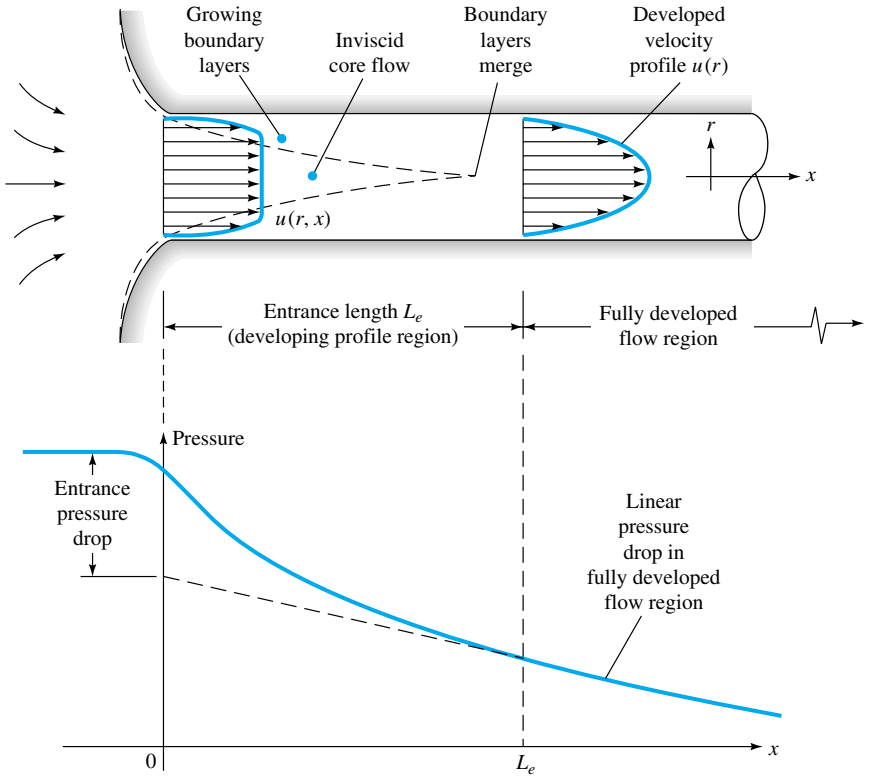


Fig. 6.6 Developing velocity profiles and pressure changes in the entrance of a duct flow.

shear is constant, and the pressure drops linearly with x, for either laminar or turbulent flow. All these details are shown in Fig. 6.6.

Dimensional analysis shows that the Reynolds number is the only parameter affecting entrance length. If

$$L_e = f(d, V, \rho, \mu) \qquad V = \frac{Q}{A}$$

then

$$\frac{L_e}{d} = g\left(\frac{\rho V d}{\mu}\right) = g(\text{Re}) \tag{6.4}$$

For laminar flow [2, 3], the accepted correlation is

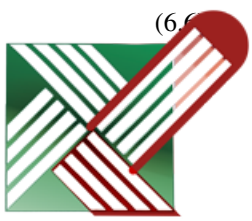
$$\frac{L_e}{d} \approx 0.06\ \text{Re} \qquad \text{laminar} \tag{6.5}$$

The maximum laminar entrance length, at $\text{Re}_{d,\text{crit}} = 2300$, is $L_e = 138d$, which is the longest development length possible.

In turbulent flow the boundary layers grow faster, and L_e is relatively shorter, according to the approximation for smooth walls

$$\frac{L_e}{d} \approx 4.4\ \text{Re}_d^{1/6} \qquad \text{turbulent} \tag{6.6}$$

Some computed turbulent entrance lengths are thus



ketabline.com Ebook.ketabline.com

Re_d	4000	10^4	10^5	10^6	10^7	10^8
L_e/d	18	20	30	44	65	95

Now 44 diameters may seem "long," but typical pipe-flow applications involve an L/d value of 1000 or more, in which case the entrance effect may be neglected and a simple analysis made for fully developed flow (Sec. 6.4). This is possible for both laminar and turbulent flows, including rough walls and noncircular cross sections.

EXAMPLE 6.2

A $\frac{1}{2}$-in-diameter water pipe is 60 ft long and delivers water at 5 gal/min at 20°C. What fraction of this pipe is taken up by the entrance region?

Solution

Convert

$$Q = (5 \text{ gal/min}) \frac{0.00223 \text{ ft}^3/\text{s}}{1 \text{ gal/min}} = 0.0111 \text{ ft}^3/\text{s}$$

The average velocity is

$$V = \frac{Q}{A} = \frac{0.0111 \text{ ft}^3/\text{s}}{(\pi/4)[(\frac{1}{2}/12) \text{ ft}]^2} = 8.17 \text{ ft/s}$$

From Table 1.4 read for water $\nu = 1.01 \times 10^{-6}$ m^2/s $= 1.09 \times 10^{-5}$ ft^2/s. Then the pipe Reynolds number is

$$\mathrm{Re}_d = \frac{Vd}{\nu} = \frac{(8.17 \text{ ft/s})[(\frac{1}{2}/12) \text{ ft}]}{1.09 \times 10^{-5} \text{ ft}^2/\text{s}} = 31{,}300$$

This is greater than 4000; hence the flow is fully turbulent, and Eq. (6.6) applies for entrance length

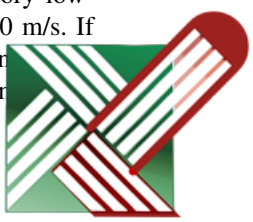
$$\frac{L_e}{d} \approx 4.4 \, \mathrm{Re}_d^{1/6} = (4.4)(31{,}300)^{1/6} = 25$$

The actual pipe has $L/d = (60 \text{ ft})/[(\frac{1}{2}/12) \text{ ft}] = 1440$. Hence the entrance region takes up the fraction

$$\frac{L_e}{L} = \frac{25}{1440} = 0.017 = 1.7\% \qquad \textit{Ans.}$$

This is a very small percentage, so that we can reasonably treat this pipe flow as essentially fully developed.

Shortness can be a virtue in duct flow if one wishes to maintain the inviscid core. For example, a "long" wind tunnel would be ridiculous, since the viscous core would invalidate the purpose of simulating free-flight conditions. A typical laboratory low-speed wind-tunnel test section is 1 m in diameter and 5 m long, with $V = 30$ m/s. If we take $\nu_{\text{air}} = 1.51 \times 10^{-5}$ m^2/s from Table 1.4, then $\mathrm{Re}_d = 1.99 \times 10^6$ and Eq. (6.6), $L_e/d \approx 49$. The test section has $L/d = 5$, which is much shorter than



ketabline.com Ebook.ketabline.com

velopment length. At the end of the section the wall boundary layers are only 10 cm thick, leaving 80 cm of inviscid core suitable for model testing.

An external flow has no restraining walls and is free to expand no matter how thick the viscous layers on the immersed body may become. Thus, far from the body the flow is nearly inviscid, and our analytical technique, treated in Chap. 7, is to patch an inviscid-flow solution onto a viscous boundary-layer solution computed for the wall region. There is no external equivalent of fully developed internal flow.

6.3 Semiempirical Turbulent Shear Correlations

Throughout this chapter we assume constant density and viscosity and no thermal interaction, so that only the continuity and momentum equations are to be solved for velocity and pressure

$$\text{Continuity:} \quad \frac{\partial u}{\partial x} + \frac{\partial v}{\partial y} + \frac{\partial w}{\partial z} = 0$$

$$\text{Momentum:} \quad \rho \frac{d\mathbf{V}}{dt} = -\nabla p + \rho \mathbf{g} + \mu \nabla^2 \mathbf{V} \tag{6.7}$$

subject to no slip at the walls and known inlet and exit conditions. (We shall save our free-surface solutions for Chap. 10.)

Both laminar and turbulent flows satisfy Eqs. (6.7). For laminar flow, where there are no random fluctuations, we go right to the attack and solve them for a variety of geometries [2, 3], leaving many more, of course, for the problems.

Reynolds' Time-Averaging Concept

For turbulent flow, because of the fluctuations, every velocity and pressure term in Eqs. (6.7) is a rapidly varying random function of time and space. At present our mathematics cannot handle such instantaneous fluctuating variables. No single pair of random functions $\mathbf{V}(x, y, z, t)$ and $p(x, y, z, t)$ is known to be a solution to Eqs. (6.7). Moreover, our attention as engineers is toward the average or *mean* values of velocity, pressure, shear stress, etc., in a high-Reynolds-number (turbulent) flow. This approach led Osborne Reynolds in 1895 to rewrite Eqs. (6.7) in terms of mean or time-averaged turbulent variables.

The time mean $\bar{u}$ of a turbulent function $u(x, y, z, t)$ is defined by

$$\bar{u} = \frac{1}{T} \int_0^T u \, dt \tag{6.8}$$

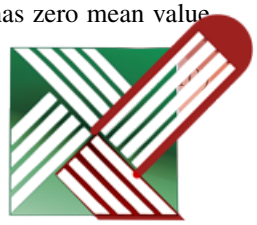
where T is an averaging period taken to be longer than any significant period of the fluctuations themselves. The mean values of turbulent velocity and pressure are illustrated in Fig. 6.7. For turbulent gas and water flows, an averaging period $T \approx 5$ s is usually quite adequate.

The *fluctuation* u' is defined as the deviation of u from its average value

$$u' = u - \bar{u} \tag{6.9}$$

also shown in Fig. 6.7. It follows by definition that a fluctuation has zero mean value

$$\overline{u'} = \frac{1}{T} \int_0^T (u - \bar{u}) \, dt = \bar{u} - \bar{u} = 0$$



ketabline.com Ebook.ketabline.com

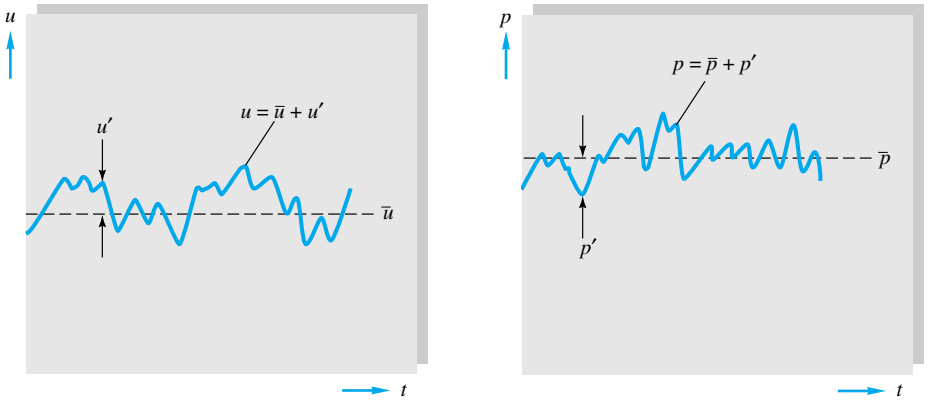


Fig. 6.7 Definition of mean and fluctuating turbulent variables: (*a*) velocity; (*b*) pressure.

However, the mean square of a fluctuation is not zero and is a measure of the *intensity* of the turbulence

$$\overline{u'^2} = \frac{1}{T}\int_0^T u'^2\,dt \neq 0 \tag{6.11}$$

Nor in general are the mean fluctuation products such as $\overline{u'v'}$ and $\overline{u'p'}$ zero in a typical turbulent flow.

Reynolds' idea was to split each property into mean plus fluctuating variables

$$u = \bar{u} + u' \quad v = \bar{v} + v' \quad w = \bar{w} + w' \quad p = \bar{p} + p' \tag{6.12}$$

Substitute these into Eqs. (6.7), and take the time mean of each equation. The continuity relation reduces to

$$\frac{\partial \bar{u}}{\partial x} + \frac{\partial \bar{v}}{\partial y} + \frac{\partial \bar{w}}{\partial z} = 0 \tag{6.13}$$

which is no different from a laminar continuity relation.

However, each component of the momentum equation (6.7*b*), after time averaging, will contain mean values plus three mean products, or *correlations,* of fluctuating velocities. The most important of these is the momentum relation in the mainstream, or x, direction, which takes the form

$$\begin{aligned}\rho\frac{d\bar{u}}{dt} = -\frac{\partial \bar{p}}{\partial x} + \rho g_x + \frac{\partial}{\partial x}\left(\mu\frac{\partial \bar{u}}{\partial x} - \rho\overline{u'^2}\right) \\ + \frac{\partial}{\partial y}\left(\mu\frac{\partial \bar{u}}{\partial y} - \rho\overline{u'v'}\right) + \frac{\partial}{\partial z}\left(\mu\frac{\partial \bar{u}}{\partial z} - \rho\overline{u'w'}\right)\end{aligned} \tag{6.14}$$

The three correlation terms $-\rho\overline{u'^2}$, $-\rho\overline{u'v'}$, and $-\rho\overline{u'w'}$ are called *turbulent stresses* because they have the same dimensions and occur right alongside the newtonian (laminar) stress terms $\mu(\partial\bar{u}/\partial x)$, etc. Actually, they are convective acceleration terms (which is why the density appears), not stresses, but they have the mathematical effect of stress and are so termed almost universally in the literature.

The turbulent stresses are unknown a priori and must be related by experi



ketabline.com Ebook.ketabline.com

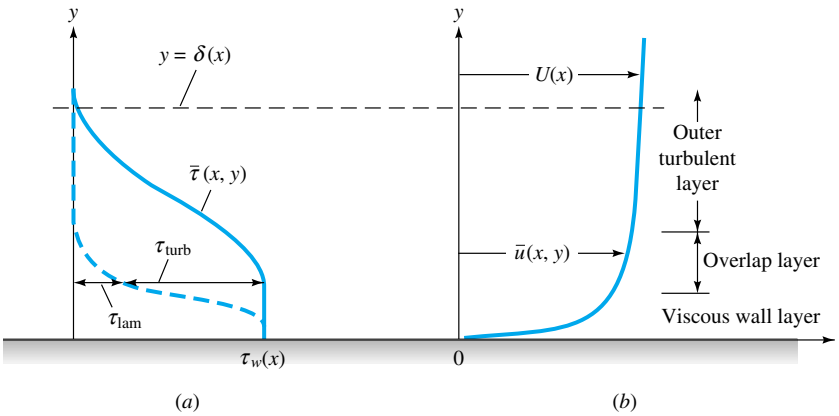


Fig. 6.8 Typical velocity and shear distributions in turbulent flow near a wall: (*a*) shear; (*b*) velocity.

geometry and flow conditions, as detailed in Refs. 1 to 3. Fortunately, in duct and boundary-layer flow, the stress $-\rho\overline{u'v'}$ associated with direction y normal to the wall is dominant, and we can approximate with excellent accuracy a simpler streamwise momentum equation

$$\rho \frac{d\overline{u}}{dt} \approx -\frac{\partial \overline{p}}{\partial x} + \rho g_x + \frac{\partial \tau}{\partial y} \tag{6.15}$$

where

$$\tau = \mu \frac{\partial \overline{u}}{\partial y} - \rho\overline{u'v'} = \tau_{\text{lam}} + \tau_{\text{turb}} \tag{6.16}$$

Figure 6.8 shows the distribution of τ_{lam} and τ_{turb} from typical measurements across a turbulent-shear layer near a wall. Laminar shear is dominant near the wall (the *wall layer*), and turbulent shear dominates in the *outer layer*. There is an intermediate region, called the *overlap layer,* where both laminar and turbulent shear are important. These three regions are labeled in Fig. 6.8.

In the outer layer τ_{turb} is two or three orders of magnitude greater than τ_{lam}, and vice versa in the wall layer. These experimental facts enable us to use a crude but very effective model for the velocity distribution $\overline{u}(y)$ across a turbulent wall layer.

The Logarithmic-Overlap Law

We have seen in Fig. 6.8 that there are three regions in turbulent flow near a wall:

1. Wall layer: Viscous shear dominates.
2. Outer layer: Turbulent shear dominates.
3. Overlap layer: Both types of shear are important.

From now on let us agree to drop the overbar from velocity $\overline{u}$. Let τ_w be the wall shear stress, and let δ and U represent the thickness and velocity at the edge of the outer layer, $y = \delta$.

For the wall layer, Prandtl deduced in 1930 that u must be independent of the shear-layer thickness

$$u = f(\mu, \tau_w, \rho, y) \tag{6.}$$

By dimensional analysis, this is equivalent to



ketabline.com Ebook.ketabline.com

$$u^+ = \frac{u}{u^*} = F\left(\frac{yu^*}{\nu}\right) \qquad u^* = \left(\frac{\tau_w}{\rho}\right)^{1/2} \tag{6.18}$$

Equation (6.18) is called the *law of the wall,* and the quantity u^* is termed the *friction velocity* because it has dimensions $\{LT^{-1}\}$, although it is not actually a flow velocity.

Subsequently, Kármán in 1933 deduced that u in the outer layer is independent of molecular viscosity, but its deviation from the stream velocity U must depend on the layer thickness δ and the other properties

$$(U - u)_{\text{outer}} = g(\delta, \tau_w, \rho, y) \tag{6.19}$$

Again, by dimensional analysis we rewrite this as

$$\frac{U - u}{u^*} = G\left(\frac{y}{\delta}\right) \tag{6.20}$$

where u^* has the same meaning as in Eq. (6.18). Equation (6.20) is called the *velocity-defect law* for the outer layer.

Both the wall law (6.18) and the defect law (6.20) are found to be accurate for a wide variety of experimental turbulent duct and boundary-layer flows [1 to 3]. They are different in form, yet they must overlap smoothly in the intermediate layer. In 1937 C. B. Millikan showed that this can be true only if the overlap-layer velocity varies logarithmically with y:

$$\frac{u}{u^*} = \frac{1}{\kappa} \ln \frac{yu^*}{\nu} + B \qquad \text{overlap layer} \tag{6.21}$$

Over the full range of turbulent smooth wall flows, the dimensionless constants κ and B are found to have the approximate values $\kappa \approx 0.41$ and $B \approx 5.0$. Equation (6.21) is called the *logarithmic-overlap layer.*

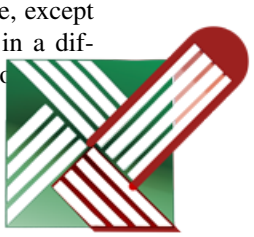
Thus by dimensional reasoning and physical insight we infer that a plot of u versus $\ln y$ in a turbulent-shear layer will show a curved wall region, a curved outer region, and a straight-line logarithmic overlap. Figure 6.9 shows that this is exactly the case. The four outer-law profiles shown all merge smoothly with the logarithmic-overlap law but have different magnitudes because they vary in external pressure gradient. The wall law is unique and follows the linear viscous relation

$$u^+ = \frac{u}{u^*} = \frac{yu^*}{\nu} = y^+ \tag{6.22}$$

from the wall to about $y^+ = 5$, thereafter curving over to merge with the logarithmic law at about $y^+ = 30$.

Believe it or not, Fig. 6.9, which is nothing more than a shrewd correlation of velocity profiles, is the basis for most existing "theory" of turbulent-shear flows. Notice that we have not solved any equations at all but have merely expressed the streamwise velocity in a neat form.

There is serendipity in Fig. 6.9: The logarithmic law (6.21), instead of just being a short overlapping link, actually approximates nearly the entire velocity profile, except for the outer law when the pressure is increasing strongly downstream (as in a diffuser). The inner-wall law typically extends over less than 2 percent of the pr
can be neglected. Thus we can use Eq. (6.21) as an excellent approximation



ketabline.com Ebook.ketabline.com

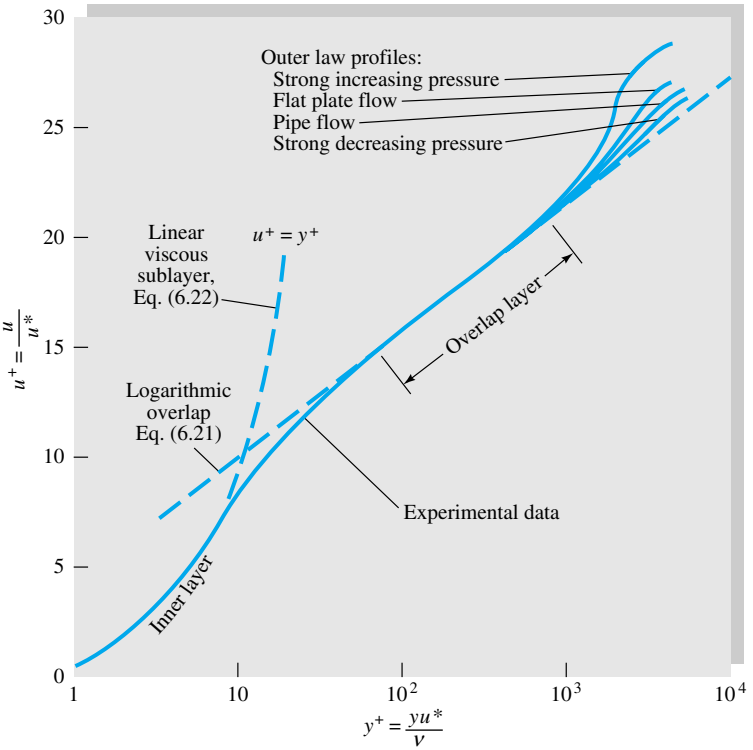


Fig. 6.9 Experimental verification of the inner-, outer-, and overlap-layer laws relating velocity profiles in turbulent wall flow.

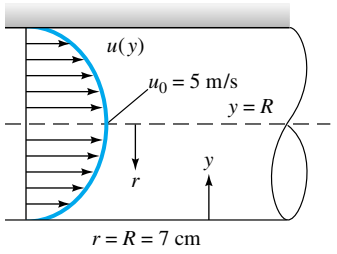
nearly every turbulent-flow problem presented in this and the next chapter. Many additional applications are given in Refs. 2 and 3.

EXAMPLE 6.3

Air at 20°C flows through a 14-cm-diameter tube under fully developed conditions. The centerline velocity is $u_0 = 5$ m/s. Estimate from Fig. 6.9 (*a*) the friction velocity u^*, (*b*) the wall shear stress τ_w, and (*c*) the average velocity $V = Q/A$.

Solution

Part (a)



E6.3

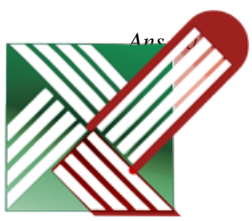
For pipe flow Fig. 6.9 shows that the logarithmic law, Eq. (6.21), is accurate all the way to the center of the tube. From Fig. E6.3 $y = R - r$ should go from the wall to the centerline as shown. At the center $u = u_0$, $y = R$, and Eq. (6.21) becomes

$$\frac{u_0}{u^*} = \frac{1}{0.41} \ln \frac{Ru^*}{\nu} + 5.0 \tag{1}$$

Since we know that $u_0 = 5$ m/s and $R = 0.07$ m, u^* is the only unknown in Eq. (1). Find the solution by trial and error or by EES

$$u^* = 0.228 \text{ m/s} = 22.8 \text{ cm/s}$$

where we have taken $\nu = 1.51 \times 10^{-5}$ m^2/s for air from Table 1.4.



ketabline.com Ebook.ketabline.com

Part (b) Assuming a pressure of 1 atm, we have $\rho = p/(RT) = 1.205$ kg/m^3. Since by definition $u^* = (\tau_w/\rho)^{1/2}$, we compute

$$\tau_w = \rho u^{*2} = (1.205 \text{ kg/m}^3)(0.228 \text{ m/s})^2 = 0.062 \text{ kg/(m} \cdot \text{s}^2) = 0.062 \text{ Pa} \qquad \textit{Ans. (b)}$$

This is a very small shear stress, but it will cause a large pressure drop in a long pipe (170 Pa for every 100 m of pipe).

Part (c) The average velocity V is found by integrating the logarithmic-law velocity distribution

$$V = \frac{Q}{A} = \frac{1}{\pi R^2}\int_0^R u\, 2\pi r\, dr \tag{2}$$

Introducing $u = u^*[(1/\kappa) \ln (yu^*/\nu) + B]$ from Eq. (6.21) and noting that $y = R - r$, we can carry out the integration of Eq. (2), which is rather laborious. The final result is

$$V = 0.835u_0 = 4.17 \text{ m/s} \qquad \textit{Ans. (c)}$$

We shall not bother showing the integration here because it is all worked out and a very neat formula is given in Eqs. (6.49) and (6.59).

Notice that we started from almost nothing (the pipe diameter and the centerline velocity) and found the answers without solving the differential equations of continuity and momentum. We just used the logarithmic law, Eq. (6.21), which makes the differential equations unnecessary for pipe flow. This is a powerful technique, but you should remember that all we are doing is using an experimental velocity correlation to approximate the actual solution to the problem.

We should check the Reynolds number to ensure turbulent flow

$$\text{Re}_d = \frac{Vd}{\nu} = \frac{(4.17 \text{ m/s})(0.14 \text{ m})}{1.51 \times 10^{-5} \text{ m}^2/\text{s}} = 38{,}700$$

Since this is greater than 4000, the flow is definitely turbulent.

6.4 Flow in a Circular Pipe

As our first example of a specific viscous-flow analysis, we take the classic problem of flow in a full pipe, driven by pressure or gravity or both. Figure 6.10 shows the geometry of the pipe of radius R. The x-axis is taken in the flow direction and is inclined to the horizontal at an angle ϕ.

Before proceeding with a solution to the equations of motion, we can learn a lot by making a control-volume analysis of the flow between sections 1 and 2 in Fig. 6.10. The continuity relation, Eq. (3.23), reduces to

$$Q_1 = Q_2 = \text{const}$$

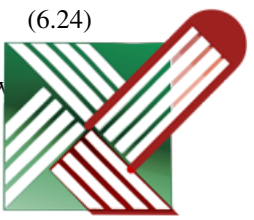
or

$$V_1 = \frac{Q_1}{A_1} = V_2 = \frac{Q_2}{A_2} \tag{6.23}$$

since the pipe is of constant area. The steady-flow energy equation (3.71) reduces to

$$\frac{p_1}{\rho} + \frac{1}{2}\alpha_1 V_1^2 + gz_1 = \frac{p_2}{\rho} + \frac{1}{2}\alpha_2 V_2^2 + gz_2 + gh_f \tag{6.24}$$

since there are no shaft-work or heat-transfer effects. Now assume that the flow



ketabline.com Ebook.ketabline.com

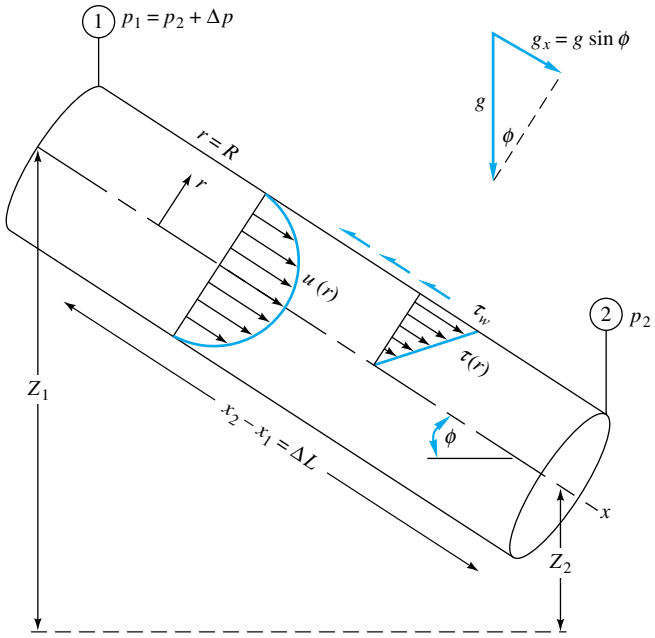


Fig. 6.10 Control volume of steady, fully developed flow between two sections in an inclined pipe.

developed (Fig. 6.6), and correct later for entrance effects. Then the kinetic-energy correction factor $\alpha_1 = \alpha_2$, and since $V_1 = V_2$ from (6.23), Eq. (6.24) now reduces to a simple expression for the friction-head loss h_f

$$h_f = \left(z_1 + \frac{p_1}{\rho g}\right) - \left(z_2 + \frac{p_2}{\rho g}\right) = \Delta\left(z + \frac{p}{\rho g}\right) = \Delta z + \frac{\Delta p}{\rho g} \tag{6.25}$$

The pipe-head loss equals the change in the sum of pressure and gravity head, i.e., the change in height of the hydraulic grade line (HGL). Since the velocity head is constant through the pipe, h_f also equals the height change of the energy grade line (EGL). Recall that the EGL decreases downstream in a flow with losses unless it passes through an energy source, e.g., as a pump or heat exchanger.

Finally apply the momentum relation (3.40) to the control volume in Fig. 6.10, accounting for applied forces due to pressure, gravity, and shear

$$\Delta p\ \pi R^2 + \rho g(\pi R^2)\ \Delta L \sin \phi - \tau_w(2\pi R)\ \Delta L = \dot{m}(V_2 - V_1) = 0 \tag{6.26}$$

This equation relates h_f to the wall shear stress

$$\Delta z + \frac{\Delta p}{\rho g} = h_f = \frac{2\tau_w}{\rho g}\frac{\Delta L}{R} \tag{6.27}$$

where we have substituted $\Delta z = \Delta L \sin \phi$ from Fig. 6.10.

So far we have not assumed either laminar or turbulent flow. If we can correlate τ_w with flow conditions, we have solved the problem of head loss in pipe flow. Functionally, we can assume that

$$\tau_w = F(\rho, V, \mu, d, \epsilon) \tag{6.}$$

where ϵ is the wall-roughness height. Then dimensional analysis te



ketabline.com Ebook.ketabline.com

$$\frac{8\tau_w}{\rho V^2} = f = F\left(\mathrm{Re}_d, \frac{\epsilon}{d}\right) \tag{6.29}$$

The dimensionless parameter f is called the *Darcy friction factor,* after Henry Darcy (1803–1858), a French engineer whose pipe-flow experiments in 1857 first established the effect of roughness on pipe resistance.

Combining Eqs. (6.27) and (6.29), we obtain the desired expression for finding pipe-head loss

$$h_f = f\frac{L}{d}\frac{V^2}{2g} \tag{6.30}$$

This is the *Darcy-Weisbach equation,* valid for duct flows of any cross section and for laminar and turbulent flow. It was proposed by Julius Weisbach, a German professor who in 1850 published the first modern textbook on hydrodynamics.

Our only remaining problem is to find the form of the function F in Eq. (6.29) and plot it in the Moody chart of Fig. 6.13.

Equations of Motion

For either laminar or turbulent flow, the continuity equation in cylindrical coordinates is given by (App. D)

$$\frac{1}{r}\frac{\partial}{\partial r}(rv_r) + \frac{1}{r}\frac{\partial}{\partial \theta}(v_\theta) + \frac{\partial u}{\partial x} = 0 \tag{6.31}$$

We assume that there is no swirl or circumferential variation, $v_\theta = \partial/\partial\theta = 0$, and fully developed flow: $u = u(r)$ only. Then Eq. (6.31) reduces to

$$\frac{1}{r}\frac{\partial}{\partial r}(rv_r) = 0$$

or

$$rv_r = \text{const} \tag{6.32}$$

But at the wall, $r = R$, $v_r = 0$ (no slip); therefore (6.32) implies that $v_r = 0$ everywhere. Thus in fully developed flow there is only one velocity component, $u = u(r)$.

The momentum differential equation in cylindrical coordinates now reduces to

$$\rho u\frac{\partial u}{\partial x} = -\frac{dp}{dx} + \rho g_x + \frac{1}{r}\frac{\partial}{\partial r}(r\tau) \tag{6.33}$$

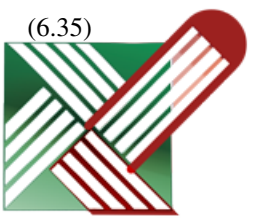
where τ can represent either laminar or turbulent shear. But the left-hand side vanishes because $u = u(r)$ only. Rearrange, noting from Fig. 6.10 that $g_x = g \sin \phi$:

$$\frac{1}{r}\frac{\partial}{\partial r}(r\tau) = \frac{d}{dx}(p - \rho g x \sin\phi) = \frac{d}{dx}(p + \rho g z) \tag{6.34}$$

Since the left-hand side varies only with r and the right-hand side varies only with x, it follows that both sides must be equal to the same constant.[2] Therefore we can integrate Eq. (6.34) to find the shear distribution across the pipe, utilizing the fact that $\tau = 0$ at $r = 0$

$$\tau = \frac{1}{2}r\frac{d}{dx}(p + \rho g z) = (\text{const})(r) \tag{6.35}$$

[2]Ask your instructor to explain this to you if necessary.



ketabline.com Ebook.ketabline.com

Thus the shear varies linearly from the centerline to the wall, for either laminar or turbulent flow. This is also shown in Fig. 6.10. At $r = R$, we have the wall shear

$$\tau_w = \frac{1}{2}R\,\frac{\Delta p + \rho g\,\Delta z}{\Delta L} \tag{6.36}$$

which is identical with our momentum relation (6.27). We can now complete our study of pipe flow by applying either laminar or turbulent assumptions to fill out Eq. (6.35).

Laminar-Flow Solution

Note in Eq. (6.35) that the HGL slope $d(p + \rho gz)/dx$ is *negative* because both pressure and height drop with x. For laminar flow, $\tau = \mu\, du/dr$, which we substitute in Eq. (6.35)

$$\mu\,\frac{du}{dr} = \frac{1}{2}rK \qquad K = \frac{d}{dx}(p + \rho gz) \tag{6.37}$$

Integrate once

$$u = \frac{1}{4}r^2\,\frac{K}{\mu} + C_1 \tag{6.38}$$

The constant C_1 is evaluated from the no-slip condition at the wall: $u = 0$ at $r = R$

$$0 = \frac{1}{4}R^2\,\frac{K}{\mu} + C_1 \tag{6.39}$$

or $C_1 = -\frac{1}{4}R^2K/\mu$. Introduce into Eq. (6.38) to obtain the exact solution for laminar fully developed pipe flow

$$u = \frac{1}{4\mu}\left[-\frac{d}{dx}(p + \rho gz)\right](R^2 - r^2) \tag{6.40}$$

The laminar-flow profile is thus a paraboloid falling to zero at the wall and reaching a maximum at the axis

$$u_{\max} = \frac{R^2}{4\mu}\left[-\frac{d}{dx}(p + \rho gz)\right] \tag{6.41}$$

It resembles the sketch of $u(r)$ given in Fig. 6.10.

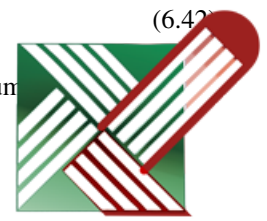
The laminar distribution (6.40) is called *Hagen-Poiseuille flow* to commemorate the experimental work of G. Hagen in 1839 and J. L. Poiseuille in 1940, both of whom established the pressure-drop law, Eq. (6.1). The first theoretical derivation of Eq. (6.40) was given independently by E. Hagenbach and by F. Neumann around 1859.

Other pipe-flow results follow immediately from Eq. (6.40). The volume flow is

$$Q = \int_0^R u\,dA = \int_0^R u_{\max}\left(1 - \frac{r^2}{R^2}\right)2\pi r\,dr$$

$$= \frac{1}{2}u_{\max}\pi R^2 = \frac{\pi R^4}{8\mu}\left[-\frac{d}{dx}(p + \rho gz)\right] \tag{6.42}$$

Thus the average velocity in laminar flow is one-half the maximum



ketabline.com Ebook.ketabline.com

$$V = \frac{Q}{A} = \frac{Q}{\pi R^2} = \frac{1}{2}u_{\max} \tag{6.43}$$

For a horizontal tube ($\Delta z = 0$), Eq. (6.42) is of the form predicted by Hagen's experiment, Eq. (6.1):

$$\Delta p = \frac{8\mu LQ}{\pi R^4} \tag{6.44}$$

The wall shear is computed from the wall velocity gradient

$$\tau_w = \left|\mu \frac{du}{dr}\right|_{r=R} = \frac{2\mu u_{\max}}{R} = \frac{1}{2}R\left|\frac{d}{dx}(p + \rho g z)\right| \tag{6.45}$$

This gives an exact theory for laminar Darcy friction factor

$$f = \frac{8\tau_w}{\rho V^2} = \frac{8(8\mu V/d)}{\rho V^2} = \frac{64\mu}{\rho V d}$$

or

$$f_{\text{lam}} = \frac{64}{\text{Re}_d} \tag{6.46}$$

This is plotted later in the Moody chart (Fig. 6.13). The fact that f drops off with increasing Re_d should not mislead us into thinking that shear decreases with velocity: Eq. (6.45) clearly shows that τ_w is proportional to $u_{\max}$; it is interesting to note that τ_w is independent of density because the fluid acceleration is zero.

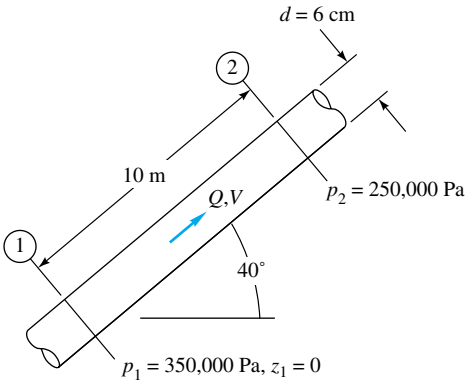
The laminar head loss follows from Eq. (6.30)

$$h_{f,\text{lam}} = \frac{64\mu}{\rho V d}\frac{L}{d}\frac{V^2}{2g} = \frac{32\mu LV}{\rho g d^2} = \frac{128\mu LQ}{\pi \rho g d^4} \tag{6.47}$$

We see that laminar head loss is proportional to V.

EXAMPLE 6.4

An oil with $\rho = 900$ kg/m^3 and $\nu = 0.0002$ m^2/s flows upward through an inclined pipe as shown in Fig. E6.4. The pressure and elevation are known at sections 1 and 2, 10 m apart. Assuming



E6.4

steady laminar flow, (*a*) verify that the flow is up, (*b*) compute h_f between 1 and 2, and (*c*) Q, (*d*) V, and (*e*) Re_d. Is the flow really laminar?



ketabline.com Ebook.ketabline.com

Solution

Part (a) For later use, calculate

$$\mu = \rho\nu = (900 \text{ kg/m}^3)(0.0002 \text{ m}^2/\text{s}) = 0.18 \text{ kg/(m} \cdot \text{s)}$$

$$z_2 = \Delta L \sin 40^\circ = (10 \text{ m})(0.643) = 6.43 \text{ m}$$

The flow goes in the direction of falling HGL; therefore compute the hydraulic grade-line height at each section

$$\text{HGL}_1 = z_1 + \frac{p_1}{\rho g} = 0 + \frac{350{,}000}{900(9.807)} = 39.65 \text{ m}$$

$$\text{HGL}_2 = z_2 + \frac{p_2}{\rho g} = 6.43 + \frac{250{,}000}{900(9.807)} = 34.75 \text{ m}$$

The HGL is lower at section 2; hence the flow is from 1 to 2 as assumed. *Ans. (a)*

Part (b) The head loss is the change in HGL:

$$h_f = \text{HGL}_1 - \text{HGL}_2 = 39.65 \text{ m} - 34.75 \text{ m} = 4.9 \text{ m} \qquad \textit{Ans. (b)}$$

Half the length of the pipe is quite a large head loss.

Part (c) We can compute Q from the various laminar-flow formulas, notably Eq. (6.47)

$$Q = \frac{\pi\rho g d^4 h_f}{128\mu L} = \frac{\pi(900)(9.807)(0.06)^4(4.9)}{128(0.18)(10)} = 0.0076 \text{ m}^3/\text{s} \qquad \textit{Ans. (c)}$$

Part (d) Divide Q by the pipe area to get the average velocity

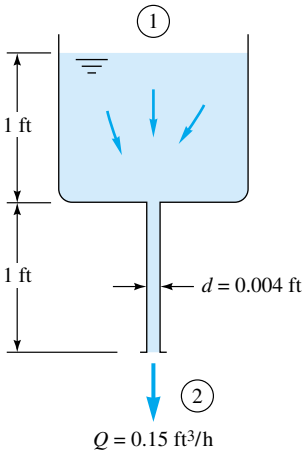
$$V = \frac{Q}{\pi R^2} = \frac{0.0076}{\pi(0.03)^2} = 2.7 \text{ m/s} \qquad \textit{Ans. (d)}$$

Part (e) With V known, the Reynolds number is

$$\text{Re}_d = \frac{Vd}{\nu} = \frac{2.7(0.06)}{0.0002} = 810 \qquad \textit{Ans. (e)}$$

This is well below the transition value $\text{Re}_d = 2300$, and so we are fairly certain the flow is laminar.

Notice that by sticking entirely to consistent SI units (meters, seconds, kilograms, newtons) for all variables we avoid the need for any conversion factors in the calculations.



E6.5

EXAMPLE 6.5

A liquid of specific weight $\rho g = 58$ lb/ft^3 flows by gravity through a 1-ft tank and a 1-ft capillary tube at a rate of 0.15 ft^3/h, as shown in Fig. E6.5. Sections 1 and 2 are at atmospheric pressure. Neglecting entrance effects, compute the viscosity of the liquid.

Solution

Apply the steady-flow energy equation (6.24), including the correction fac



ketabline.com Ebook.ketabline.com

$$\frac{p_1}{\rho g} + \frac{\alpha_1 V_1^2}{2g} + z_1 = \frac{p_2}{\rho g} + \frac{\alpha_2 V_2^2}{2g} + z_2 + h_f$$

The average exit velocity V_2 can be found from the volume flow and the pipe size:

$$V_2 = \frac{Q}{A_2} = \frac{Q}{\pi R^2} = \frac{(0.15/3600)\ \text{ft}^3/\text{s}}{\pi(0.002\ \text{ft})^2} \approx 3.32\ \text{ft/s}$$

Meanwhile $p_1 = p_2 = p_a$, and $V_1 \approx 0$ in the large tank. Therefore, approximately,

$$h_f \approx z_1 - z_2 - \alpha_2 \frac{V_2^2}{2g} = 2.0\ \text{ft} - 2.0\ \frac{(3.32\ \text{ft/s})^2}{2(32.2\ \text{ft/s}^2)} \approx 1.66\ \text{ft}$$

where we have introduced $\alpha_2 = 2.0$ for laminar pipe flow from Eq. (3.72). Note that h_f includes the entire 2-ft drop through the system and not just the 1-ft pipe length.

With the head loss known, the viscosity follows from our laminar-flow formula (6.47):

$$h_f = 1.66\ \text{ft} = \frac{32\mu LV}{\rho g d^2} = \frac{32\mu(1.0\ \text{ft})(3.32\ \text{ft/s})}{(58\ \text{lbf/ft}^3)(0.004\ \text{ft})^2} = 114{,}500\ \mu$$

or

$$\mu = \frac{1.66}{114{,}500} = 1.45\ \text{E-5 slug/(ft} \cdot \text{s)} \qquad \textit{Ans.}$$

Note that L in this formula is the *pipe* length of 1 ft. Finally, check the Reynolds number:

$$\text{Re}_d = \frac{\rho V d}{\mu} = \frac{(58/32.2\ \text{slug/ft}^3)(3.32\ \text{ft/s})(0.004\ \text{ft})}{1.45\ \text{E-5 slug/(ft} \cdot \text{s)}} = 1650 \qquad \text{laminar}$$

Since this is less than 2300, we conclude that the flow is indeed laminar. Actually, for this head loss, there is a *second* (turbulent) solution, as we shall see in Example 6.8.

Turbulent-Flow Solution

For turbulent pipe flow we need not solve a differential equation but instead proceed with the logarithmic law, as in Example 6.3. Assume that Eq. (6.21) correlates the local mean velocity $u(r)$ all the way across the pipe

$$\frac{u(r)}{u^*} \approx \frac{1}{\kappa} \ln \frac{(R - r)u^*}{\nu} + B \tag{6.48}$$

where we have replaced y by $R - r$. Compute the average velocity from this profile

$$V = \frac{Q}{A} = \frac{1}{\pi R^2} \int_0^R u^* \left[\frac{1}{\kappa} \ln \frac{(R - r)u^*}{\nu} + B \right] 2\pi r\, dr$$

$$= \frac{1}{2} u^* \left(\frac{2}{\kappa} \ln \frac{Ru^*}{\nu} + 2B - \frac{3}{\kappa} \right) \tag{6.49}$$

Introducing $\kappa = 0.41$ and $B = 5.0$, we obtain, numerically,

$$\frac{V}{u^*} \approx 2.44 \ln \frac{Ru^*}{\nu} + 1.34 \tag{6.50}$$

This looks only marginally interesting until we realize that V/u^* is directly re the Darcy friction factor



ketabline.com Ebook.ketabline.com

$$\frac{V}{u^*} = \left(\frac{\rho V^2}{\tau_w}\right)^{1/2} = \left(\frac{8}{f}\right)^{1/2} \tag{6.51}$$

Moreover, the argument of the logarithm in (6.50) is equivalent to

$$\frac{Ru^*}{\nu} = \frac{\frac{1}{2}Vd}{\nu}\frac{u^*}{V} = \frac{1}{2}\mathrm{Re}_d\left(\frac{f}{8}\right)^{1/2} \tag{6.52}$$

Introducing (6.52) and (6.51) into Eq. (6.50), changing to a base-10 logarithm, and rearranging, we obtain

$$\frac{1}{f^{1/2}} \approx 1.99 \log (\mathrm{Re}_d f^{1/2}) - 1.02 \tag{6.53}$$

In other words, by simply computing the mean velocity from the logarithmic-law correlation, we obtain a relation between the friction factor and Reynolds number for turbulent pipe flow. Prandtl derived Eq. (6.53) in 1935 and then adjusted the constants slightly to fit friction data better

$$\frac{1}{f^{1/2}} = 2.0 \log (\mathrm{Re}_d f^{1/2}) - 0.8 \tag{6.54}$$

This is the accepted formula for a smooth-walled pipe. Some numerical values may be listed as follows:

Re_d	4000	10^4	10^5	10^6	10^7	10^8
f	0.0399	0.0309	0.0180	0.0116	0.0081	0.0059

Thus f drops by only a factor of 5 over a 10,000-fold increase in Reynolds number. Equation (6.54) is cumbersome to solve if Re_d is known and f is wanted. There are many alternate approximations in the literature from which f can be computed explicitly from Re_d

$$f = \begin{cases} 0.316\ \mathrm{Re}_d^{-1/4} & 4000 < \mathrm{Re}_d < 10^5 \quad \text{H. Blasius (1911)} \\ \left(1.8 \log \dfrac{\mathrm{Re}_d}{6.9}\right)^{-2} & \text{Ref. 9} \end{cases} \tag{6.55}$$

Blasius, a student of Prandtl, presented his formula in the first correlation ever made of pipe friction versus Reynolds number. Although his formula has a limited range, it illustrates what was happening to Hagen's 1839 pressure-drop data. For a horizontal pipe, from Eq. (6.55),

$$h_f = \frac{\Delta p}{\rho g} = f\frac{L}{d}\frac{V^2}{2g} \approx 0.316\left(\frac{\mu}{\rho V d}\right)^{1/4}\frac{L}{d}\frac{V^2}{2g}$$

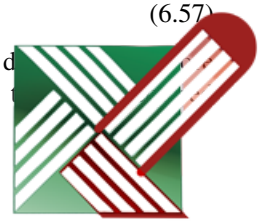
or

$$\Delta p \approx 0.158\, L\rho^{3/4}\mu^{1/4}d^{-5/4}V^{7/4} \tag{6.56}$$

at low turbulent Reynolds numbers. This explains why Hagen's data for pressure drop begin to increase as the 1.75 power of the velocity, in Fig. 6.4. Note that Δp varies only slightly with viscosity, which is characteristic of turbulent flow. Introducing $Q = \frac{1}{4}\pi d^2 V$ into Eq. (6.56), we obtain the alternate form

$$\Delta p \approx 0.241 L\rho^{3/4}\mu^{1/4}d^{-4.75}Q^{1.75} \tag{6.57}$$

For a given flow rate Q, the turbulent pressure drop decreases with d
sharply than the laminar formula (6.47). Thus the quickest way t



ketabline.com Ebook.ketabline.com

pumping pressure is to increase the pipe size, although, of course, the larger pipe is more expensive. Doubling the pipe size decreases Δp by a factor of about 27 for a given Q. Compare Eq. (6.56) with Example 5.7 and Fig. 5.10.

The maximum velocity in turbulent pipe flow is given by Eq. (6.48), evaluated at $r = 0$

$$\frac{u_{\max}}{u^*} \approx \frac{1}{\kappa} \ln \frac{Ru^*}{\nu} + B \tag{6.58}$$

Combining this with Eq. (6.49), we obtain the formula relating mean velocity to maximum velocity

$$\frac{V}{u_{\max}} \approx (1 + 1.33\sqrt{f})^{-1} \tag{6.59}$$

Some numerical values are

Re_d	4000	10^4	10^5	10^6	10^7	10^8
$V/u_{\max}$	0.790	0.811	0.849	0.875	0.893	0.907

The ratio varies with the Reynolds number and is much larger than the value of 0.5 predicted for all laminar pipe flow in Eq. (6.43). Thus a turbulent velocity profile, as shown in Fig. 6.11, is very flat in the center and drops off sharply to zero at the wall.

Effect of Rough Walls

It was not known until experiments in 1800 by Coulomb [6] that surface roughness has an effect on friction resistance. It turns out that the effect is negligible for laminar pipe flow, and all the laminar formulas derived in this section are valid for rough walls also. But turbulent flow is strongly affected by roughness. In Fig. 6.9 the linear viscous sublayer only extends out to $y^+ = yu^*/\nu = 5$. Thus, compared with the diameter, the sublayer thickness y_s is only

$$\frac{y_s}{d} = \frac{5\nu/u^*}{d} = \frac{14.1}{\mathrm{Re}_d f^{1/2}} \tag{6.60}$$

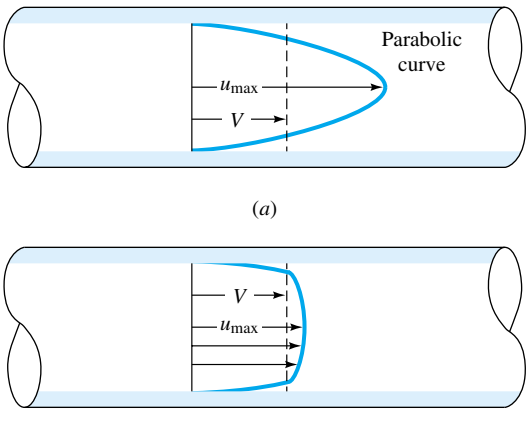


Fig. 6.11 Comparison of laminar and turbulent pipe-flow velocity profiles for the same volume flow: (*a*) laminar flow; (*b*) turbulent flow.



ketabline.com Ebook.ketabline.com

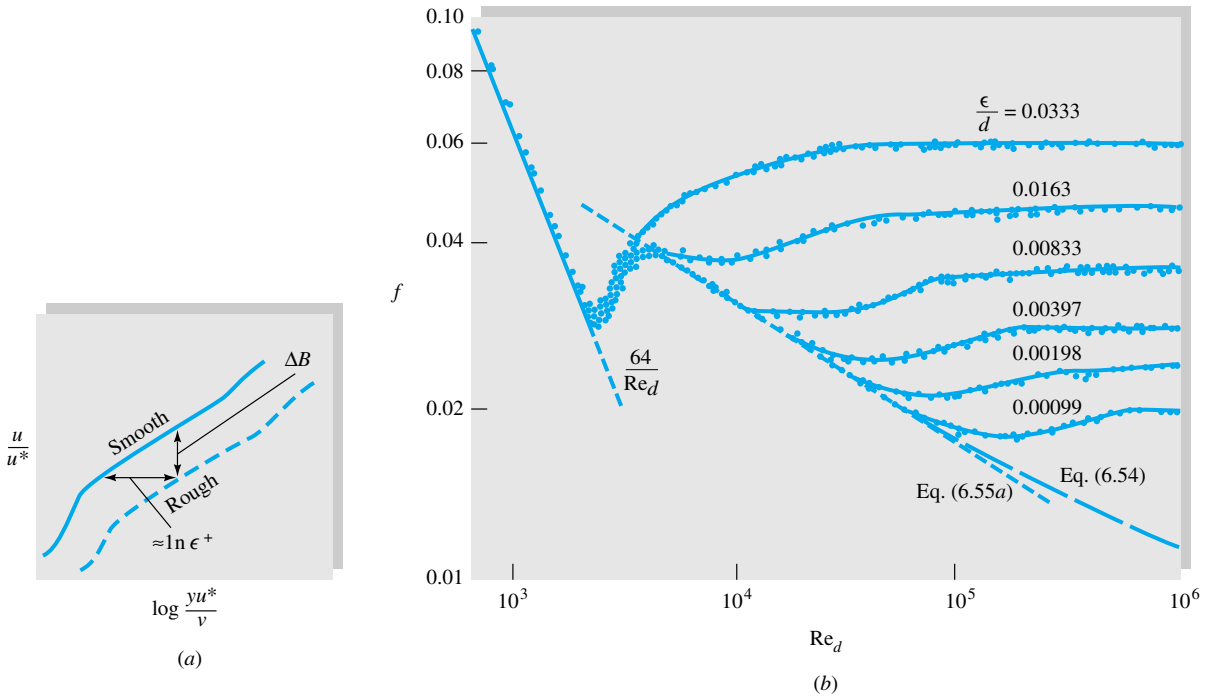


Fig. 6.12 Effect of wall roughness on turbulent pipe flow. (*a*) The logarithmic overlap-velocity profile shifts down and to the right; (*b*) experiments with sand-grain roughness by Nikuradse [7] show a systematic increase of the turbulent friction factor with the roughness ratio.

For example, at $\text{Re}_d = 10^5$, $f = 0.0180$, and $y_s/d = 0.001$, a wall roughness of about $0.001d$ will break up the sublayer and profoundly change the wall law in Fig. 6.9.

Measurements of $u(y)$ in turbulent rough-wall flow by Prandtl's student Nikuradse [7] show, as in Fig. 6.12*a*, that a roughness height ϵ will force the logarithm-law profile outward on the abscissa by an amount approximately equal to $\ln \epsilon^+$, where $\epsilon^+ = \epsilon u^*/\nu$. The slope of the logarithm law remains the same, $1/\kappa$, but the shift outward causes the constant B to be less by an amount $\Delta B \approx (1/\kappa) \ln \epsilon^+$.

Nikuradse [7] simulated roughness by gluing uniform sand grains onto the inner walls of the pipes. He then measured the pressure drops and flow rates and correlated friction factor versus Reynolds number in Fig. 6.12*b*. We see that laminar friction is unaffected, but turbulent friction, after an *onset* point, increases monotonically with the roughness ratio ϵ/d. For any given ϵ/d, the friction factor becomes constant *(fully rough)* at high Reynolds numbers. These points of change are certain values of $\epsilon^+ = \epsilon u^*/\nu$:

$$\frac{\epsilon u^*}{\nu} < 5: \quad \textit{hydraulically smooth} \text{ walls, no effect of roughness on friction}$$

$$5 \leq \frac{\epsilon u^*}{\nu} \leq 70: \quad \textit{transitional} \text{ roughness, moderate Reynolds-number effect}$$

$$\frac{\epsilon u^*}{\nu} > 70: \quad \textit{fully rough} \text{ flow, sublayer totally broken up and friction independent of Reynolds number}$$

For fully rough flow, $\epsilon^+ > 70$, the log-law downshift ΔB in Fig. 6.12*a* is

$$\Delta B \approx \frac{1}{\kappa} \ln \epsilon^+ - 3.5$$



ketabline.com Ebook.ketabline.com

and the logarithm law modified for roughness becomes

$$u^+ = \frac{1}{\kappa} \ln y^+ + B - \Delta B = \frac{1}{\kappa} \ln \frac{y}{\epsilon} + 8.5 \tag{6.62}$$

The viscosity vanishes, and hence fully rough flow is independent of the Reynolds number. If we integrate Eq. (6.62) to obtain the average velocity in the pipe, we obtain

$$\frac{V}{u^*} = 2.44 \ln \frac{d}{\epsilon} + 3.2$$

or

$$\frac{1}{f^{1/2}} = -2.0 \log \frac{\epsilon/d}{3.7} \qquad \text{fully rough flow} \tag{6.63}$$

There is no Reynolds-number effect; hence the head loss varies exactly as the square of the velocity in this case. Some numerical values of friction factor may be listed:

ϵ/d	0.00001	0.0001	0.001	0.01	0.05
f	0.00806	0.0120	0.0196	0.0379	0.0716

The friction factor increases by 9 times as the roughness increases by a factor of 5000. In the transitional-roughness region, sand grains behave somewhat differently from commercially rough pipes, so Fig. 6.12*b* has now been replaced by the Moody chart.

The Moody Chart

In 1939 to cover the transitionally rough range, Colebrook [9] combined the smooth-wall [Eq. (6.54)] and fully rough [Eq. (6.63)] relations into a clever interpolation formula

$$\frac{1}{f^{1/2}} = -2.0 \log \left(\frac{\epsilon/d}{3.7} + \frac{2.51}{\mathrm{Re}_d f^{1/2}} \right) \tag{6.64}$$

This is the accepted design formula for turbulent friction. It was plotted in 1944 by Moody [8] into what is now called the *Moody chart* for pipe friction (Fig. 6.13). The Moody chart is probably the most famous and useful figure in fluid mechanics. It is accurate to $\pm$ 15 percent for design calculations over the full range shown in Fig. 6.13. It can be used for circular and noncircular (Sec. 6.6) pipe flows and for open-channel flows (Chap. 10). The data can even be adapted as an approximation to boundary-layer flows (Chap. 7).

Equation (6.64) is cumbersome to evaluate for f if Re_d is known, although it easily yields to the EES Equation Solver. An alternate explicit formula given by Haaland [33] as

$$\frac{1}{f^{1/2}} \approx -1.8 \log \left[\frac{6.9}{\mathrm{Re}_d} + \left(\frac{\epsilon/d}{3.7} \right)^{1.11} \right] \tag{6.64a}$$

varies less than 2 percent from Eq. (6.64).

The shaded area in the Moody chart indicates the range where transition from laminar to turbulent flow occurs. There are no reliable friction factors in this range, $2000 < \mathrm{Re}_d < 4000$. Notice that the roughness curves are nearly horizontal in the fully rough regime to the right of the dashed line.

From tests with commercial pipes, recommended values for average pipe ro
are listed in Table 6.1.



ketabline.com Ebook.ketabline.com

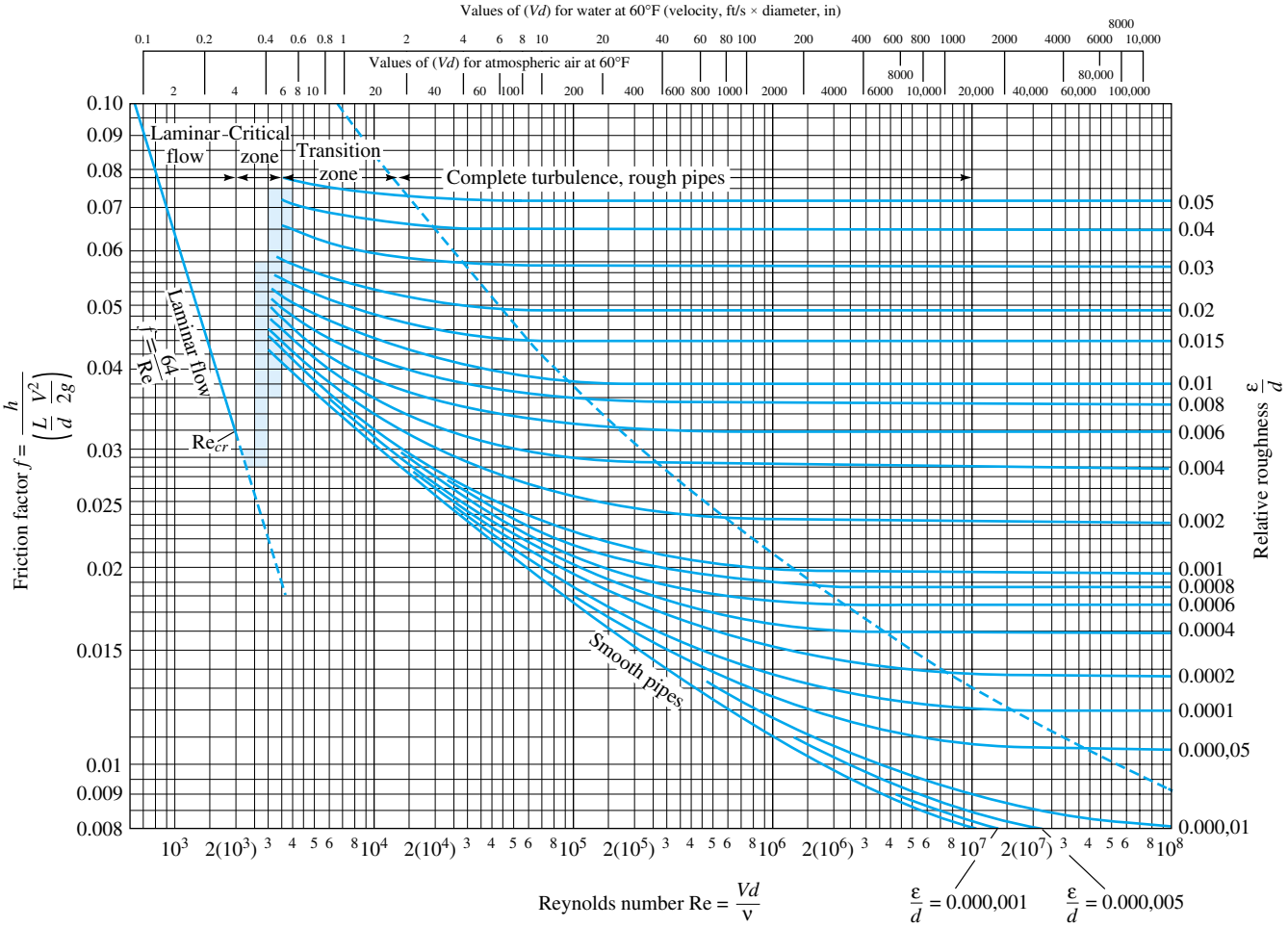


Fig. 6.13 The Moody chart for pipe friction with smooth and rough walls. This chart is identical to Eq. (6.64) for turbulent flow. *(From Ref. 8, by permission of the ASME.)*

Table 6.1 Recommended Roughness Values for Commercial Ducts

Material	Condition	ϵ ft	ϵ mm	Uncertainty, %
Steel	Sheet metal, new	0.00016	0.05	± 60
	Stainless, new	0.000007	0.002	± 50
	Commercial, new	0.00015	0.046	± 30
	Riveted	0.01	3.0	± 70
	Rusted	0.007	2.0	± 50
Iron	Cast, new	0.00085	0.26	± 50
	Wrought, new	0.00015	0.046	± 20
	Galvanized, new	0.0005	0.15	± 40
	Asphalted cast	0.0004	0.12	± 50
Brass	Drawn, new	0.000007	0.002	± 50
Plastic	Drawn tubing	0.000005	0.0015	± 60
Glass	—	Smooth	Smooth	
Concrete	Smoothed	0.00013	0.04	± 60
	Rough	0.007	2.0	± 50
Rubber	Smoothed	0.000033	0.01	± 60
Wood	Stave	0.0016	0.5	

ketabline.com Ebook.ketabline.com

EXAMPLE 6.6[3]

Compute the loss of head and pressure drop in 200 ft of horizontal 6-in-diameter asphalted cast-iron pipe carrying water with a mean velocity of 6 ft/s.

Solution

One can estimate the Reynolds number of water and air from the Moody chart. Look across the top of the chart to V (ft/s) $\times$ d (in) = 36, and then look directly down to the bottom abscissa to find that $\text{Re}_d(\text{water}) \approx 2.7 \times 10^5$. The roughness ratio for asphalted cast iron ($\epsilon = 0.0004$ ft) is

$$\frac{\epsilon}{d} = \frac{0.0004}{\frac{6}{12}} = 0.0008$$

Find the line on the right side for $\epsilon/d = 0.0008$, and follow it to the left until it intersects the vertical line for $\text{Re} = 2.7 \times 10^5$. Read, approximately, $f = 0.02$ [or compute $f = 0.0197$ from Eq. (6.64a)]. Then the head loss is

$$h_f = f\frac{L}{d}\frac{V^2}{2g} = (0.02)\frac{200}{0.5}\frac{(6\text{ ft/s})^2}{2(32.2\text{ ft/s}^2)} = 4.5\text{ ft} \qquad \textit{Ans.}$$

The pressure drop for a horizontal pipe ($z_1 = z_2$) is

$$\Delta p = \rho g h_f = (62.4\text{ lbf/ft}^3)(4.5\text{ ft}) = 280\text{ lbf/ft}^2 \qquad \textit{Ans.}$$

Moody points out that this computation, even for clean new pipe, can be considered accurate only to about $\pm$ 10 percent.

EXAMPLE 6.7

Oil, with $\rho = 900$ kg/m^3 and $\nu = 0.00001$ m^2/s, flows at 0.2 m^3/s through 500 m of 200-mm-diameter cast-iron pipe. Determine (a) the head loss and (b) the pressure drop if the pipe slopes down at 10° in the flow direction.

Solution

First compute the velocity from the known flow rate

$$V = \frac{Q}{\pi R^2} = \frac{0.2\text{ m}^3/\text{s}}{\pi(0.1\text{ m})^2} = 6.4\text{ m/s}$$

Then the Reynolds number is

$$\text{Re}_d = \frac{Vd}{\nu} = \frac{(6.4\text{ m/s})(0.2\text{ m})}{0.00001\text{ m}^2/\text{s}} = 128{,}000$$

From Table 6.1, $\epsilon = 0.26$ mm for cast-iron pipe. Then

$$\frac{\epsilon}{d} = \frac{0.26\text{ mm}}{200\text{ mm}} = 0.0013$$

[3]This example was given by Moody in his 1944 paper [8].



ketabline.com Ebook.ketabline.com

Enter the Moody chart on the right at $\epsilon/d = 0.0013$ (you will have to interpolate), and move to the left to intersect with Re = 128,000. Read $f \approx 0.0225$ [from Eq. (6.64) for these values we could compute $f = 0.0227$]. Then the head loss is

$$h_f = f\frac{L}{d}\frac{V^2}{2g} = (0.0225)\frac{500\text{ m}}{0.2\text{ m}}\frac{(6.4\text{ m/s})^2}{2(9.81\text{ m/s}^2)} = 117\text{ m} \qquad \textit{Ans. (a)}$$

From Eq. (6.25) for the inclined pipe,

$$h_f = \frac{\Delta p}{\rho g} + z_1 - z_2 = \frac{\Delta p}{\rho g} + L\sin 10°$$

or $$\Delta p = \rho g[h_f - (500\text{ m})\sin 10°] = \rho g(117\text{ m} - 87\text{ m})$$

$$= (900\text{ kg/m}^3)(9.81\text{ m/s}^2)(30\text{ m}) = 265{,}000\text{ kg/(m}\cdot\text{s}^2) = 265{,}000\text{ Pa} \qquad \textit{Ans. (b)}$$

EXAMPLE 6.8

Repeat Example 6.5 to see whether there is any possible turbulent-flow solution for a smooth-walled pipe.

Solution

In Example 6.5 we estimated a head loss $h_f \approx 1.66$ ft, assuming laminar exit flow ($\alpha \approx 2.0$). For this condition the friction factor is

$$f = h_f\frac{d}{L}\frac{2g}{V^2} = (1.66\text{ ft})\frac{(0.004\text{ ft})(2)(32.2\text{ ft/s}^2)}{(1.0\text{ ft})(3.32\text{ ft/s})^2} \approx 0.0388$$

For laminar flow, $\text{Re}_d = 64/f = 64/0.0388 \approx 1650$, as we showed in Example 6.5. However, from the Moody chart (Fig. 6.13), we see that $f = 0.0388$ also corresponds to a *turbulent* smooth-wall condition, at $\text{Re}_d \approx 4500$. If the flow actually were turbulent, we should change our kinetic-energy factor to $\alpha \approx 1.06$ [Eq. (3.73)], whence the corrected $h_f \approx 1.82$ ft and $f \approx 0.0425$. With f known, we can estimate the Reynolds number from our formulas:

$$\text{Re}_d \approx 3250 \quad \text{[Eq. (6.54)]} \qquad \text{or} \qquad \text{Re}_d \approx 3400 \quad \text{[Eq. (6.55}b\text{)]}$$

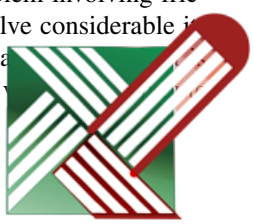
So the flow *might* have been turbulent, in which case the viscosity of the fluid would have been

$$\mu = \frac{\rho V d}{\text{Re}_d} = \frac{1.80(3.32)(0.004)}{3300} = 7.2\times 10^{-6}\text{ slug/(ft}\cdot\text{s)} \qquad \textit{Ans.}$$

This is about 55 percent less than our laminar estimate in Example 6.5. The moral is to keep the capillary-flow Reynolds number below about 1000 to avoid such duplicate solutions.

6.5 Three Types of Pipe-Flow Problems

The Moody chart (Fig. 6.13) can be used to solve almost any problem involving friction losses in long pipe flows. However, many such problems involve considerable i
eration and repeated calculations using the chart because the standa
essentially a *head-loss chart.* One is supposed to know all other



ketabline.com Ebook.ketabline.com

Re_d, enter the chart, find f, and hence compute h_f. This is one of three fundamental problems which are commonly encountered in pipe-flow calculations:

1. Given d, L, and V or Q, ρ, μ, and g, compute the head loss h_f (head-loss problem).
2. Given d, L, h_f, ρ, μ, and g, compute the velocity V or flow rate Q (flow-rate problem).
3. Given Q, L, h_f, ρ, μ, and g, compute the diameter d of the pipe (sizing problem).

Only problem 1 is well suited to the Moody chart. We have to iterate to compute velocity or diameter because both d and V are contained in the ordinate *and* the abscissa of the chart.

There are two alternatives to iteration for problems of type 2 and 3: (*a*) preparation of a suitable new Moody-type chart (see Prob. 6.62 and 6.73); or (*b*) the use of *solver* software, especially the Engineering Equation Solver, known as EES [47], which gives the answer directly if the proper data are entered. Examples 6.9 and 6.11 include the EES approach to these problems.

Type 2 Problem: Find the Flow Rate

Even though velocity (or flow rate) appears in both the ordinate and the abscissa on the Moody chart, iteration for turbulent flow is nevertheless quite fast, because f varies so slowly with Re_d. Alternately, in the spirit of Example 5.7, we could change the scaling variables to (ρ, μ, d) and thus arrive at dimensionless head loss versus dimensionless *velocity*. The result is[4]

$$\zeta = \text{fcn}(\text{Re}_d) \qquad \text{where} \qquad \zeta = \frac{gd^3h_f}{L\nu^2} = \frac{f\,\text{Re}_d^2}{2} \tag{6.65}$$

Example 5.7 did this and offered the simple correlation $\zeta \approx 0.155\ \text{Re}_d^{1.75}$, which is valid for turbulent flow with smooth walls and $\text{Re}_d \leq 1$ E5.

A formula valid for all turbulent pipe flows is found by simply rewriting the Colebrook interpolation, Eq. (6.64), in the form of Eq. (6.65):

$$\text{Re}_d = -(8\zeta)^{1/2} \log\left(\frac{\epsilon/d}{3.7} + \frac{1.775}{\sqrt{\zeta}}\right) \qquad \zeta = \frac{gd^3h_f}{L\nu^2} \tag{6.66}$$

Given ζ, we compute Re_d (and hence velocity) directly. Let us illustrate these two approaches with the following example.

EXAMPLE 6.9

Oil, with $\rho = 950$ kg/m^3 and $\nu = 2$ E-5 m^2/s, flows through a 30-cm-diameter pipe 100 m long with a head loss of 8 m. The roughness ratio is $\epsilon/d = 0.0002$. Find the average velocity and flow rate.

Direct Solution

First calculate the dimensionless head-loss parameter:

$$\zeta = \frac{gd^3h_f}{L\nu^2} = \frac{(9.81\ \text{m/s}^2)(0.3\ \text{m})^3(8.0\ \text{m})}{(100\ \text{m})(2\ \text{E-5}\ \text{m}^2/\text{s})^2} = 5.30\ \text{E7}$$

[4]The parameter ζ was suggested by H. Rouse in 1942.



ketabline.com Ebook.ketabline.com

Now enter Eq. (6.66) to find the Reynolds number:

$$\mathrm{Re}_d = -[8(5.3\ \mathrm{E7})]^{1/2} \log\left(\frac{0.0002}{3.7} + \frac{1.775}{\sqrt{5.3\ \mathrm{E7}}}\right) = 72{,}600$$

The velocity and flow rate follow from the Reynolds number:

$$V = \frac{\nu\,\mathrm{Re}_d}{d} = \frac{(2\ \mathrm{E\text{-}5\ m^2/s})(72{,}600)}{0.3\ \mathrm{m}} \approx 4.84\ \mathrm{m/s}$$

$$Q = V\frac{\pi}{4}d^2 = \left(4.84\frac{\mathrm{m}}{\mathrm{s}}\right)\frac{\pi}{4}(0.3\ \mathrm{m})^2 \approx 0.342\ \mathrm{m^3/s} \qquad \textit{Ans.}$$

No iteration is required, but this idea falters if additional losses are present.

Iterative Solution

By definition, the friction factor is known except for V:

$$f = h_f\frac{d}{L}\frac{2g}{V^2} = (8\ \mathrm{m})\left(\frac{0.3\ \mathrm{m}}{100\ \mathrm{m}}\right)\left[\frac{2(9.81\ \mathrm{m/s^2})}{V^2}\right] \qquad \text{or} \qquad fV^2 \approx 0.471 \qquad \text{(SI units)}$$

To get started, we only need to guess f, compute $V = \sqrt{0.471/f}$, then get Re_d, compute a better f from the Moody chart, and repeat. The process converges fairly rapidly. A good first guess is the "fully rough" value for $\epsilon/d = 0.0002$, or $f \approx 0.014$ from Fig. 6.13. The iteration would be as follows:

Guess $f \approx 0.014$, then $V = \sqrt{0.471/0.014} = 5.80$ m/s and $\mathrm{Re}_d = Vd/\nu \approx 87{,}000$. At $\mathrm{Re}_d = 87{,}000$ and $\epsilon/d = 0.0002$, compute $f_{\text{new}} \approx 0.0195$ [Eq. (6.64)].

New $f \approx 0.0195$, $V = \sqrt{0.481/0.0195} = 4.91$ m/s and $\mathrm{Re}_d = Vd/\nu = 73{,}700$. At $\mathrm{Re}_d = 73{,}700$ and $\epsilon/d = 0.0002$, compute $f_{\text{new}} \approx 0.0201$ [Eq. (6.64)].

Better $f \approx 0.0201$, $V = \sqrt{0.471/0.0201} = 4.84$ m/s and $\mathrm{Re}_d \approx 72{,}600$. At $\mathrm{Re}_d = 72{,}600$ and $\epsilon/d = 0.0002$, compute $f_{\text{new}} \approx 0.0201$ [Eq. (6.64)].

We have converged to three significant figures. Thus our iterative solution is

$$V = 4.84\ \mathrm{m/s}$$

$$Q = V\left(\frac{\pi}{4}\right)d^2 = (4.84)\left(\frac{\pi}{4}\right)(0.3)^2 \approx 0.342\ \mathrm{m^3/s} \qquad \textit{Ans.}$$

The iterative approach is straightforward and not too onerous, so it is routinely used by engineers. Obviously this repetitive procedure is ideal for a personal computer.

Engineering Equation Solver (EES) Solution



In EES, one simply enters the data and the appropriate equations, letting the software do the rest. Correct units must of course be used. For the present example, the data could be entered as SI:

```
rho=950    nu=2E-5    d=0.3    L=100    epsod=0.0002    hf
```

The appropriate equations are the Moody formula (6.64) plus the definitio



ketabline.com Ebook.ketabline.com

ber, volume flow rate as determined from velocity, and the Darcy head-loss formula (6.30):

```
Re = V*d/nu
 Q = V*pi*d^2/4
 f = (-2.0*log10(epsod/3.7 + 2.51/Re/f^0.5))^(-2)
hf = f*L/d*V^2/2/g
```

EES understands that "pi" represents 3.141593. Then hit "SOLVE" from the menu. If errors have been entered, EES will complain that the system cannot be solved and attempt to explain why. Otherwise, the software will iterate, and in this case EES prints the correct solution:

```
Q=0.342    V=4.84    f=0.0201    Re=72585
```

The units are spelled out in a separate list as [m, kg, s, N]. This elegant approach to engineering problem-solving has one drawback, namely, that the user fails to check the solution for engineering viability. For example, are the data typed correctly? Is the Reynolds number turbulent?

EXAMPLE 6.10

Work Moody's problem (Example 6.6) backward, assuming that the head loss of 4.5 ft is known and the velocity (6.0 ft/s) is unknown.

Direct Solution

Find the parameter ζ, and compute the Reynolds number from Eq. (6.66):

$$\zeta = \frac{gd^3h_f}{L\nu^2} = \frac{(32.2\text{ ft/s}^2)(0.5\text{ ft})^3(4.5\text{ ft})}{(200\text{ ft})(1.1\text{ E-5 ft}^2/\text{s})^2} = 7.48\text{ E8}$$

Eq. (6.66): $$\text{Re}_d = -[8(7.48\text{ E8})]^{1/2}\log\left(\frac{0.0008}{3.7} + \frac{1.775}{\sqrt{7.48\text{ E8}}}\right) \approx 274{,}800$$

Then $$V = \nu\frac{\text{Re}_d}{d} = \frac{(1.1\text{ E-5})(274{,}800)}{0.5} \approx 6.05\text{ ft/s} \qquad \textit{Ans.}$$

We did not get 6.0 ft/s exactly because the 4.5-ft head loss was rounded off in Example 6.6.

Iterative Solution

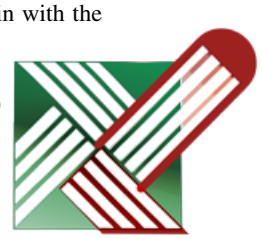
As in Eq. (6.9) the friction factor is related to velocity:

$$f = h_f\frac{d}{L}\frac{2g}{V^2} = (4.5\text{ ft})\left(\frac{0.5\text{ ft}}{200\text{ ft}}\right)\left[\frac{2(32.2\text{ ft/s}^2)}{V^2}\right] \approx \frac{0.7245}{V^2}$$

or $$V = \sqrt{0.7245/f}$$

Knowing $\epsilon/d = 0.0008$, we can guess f and iterate until the velocity converges. Begin with the fully rough estimate $f \approx 0.019$ from Fig. 6.13. The resulting iterates are

$$f_1 = 0.019: \qquad V_1 = \sqrt{0.7245/f_1} = 6.18\text{ ft/s} \qquad \text{Re}_{d_1} = \frac{Vd}{\nu} = 280{,}700$$



ketabline.com Ebook.ketabline.com

$f_2 = 0.0198$: $V_2 = 6.05$ ft/s $\quad \text{Re}_{d_2} = 274{,}900$

$f_3 = 0.01982$: $V_3 = 6.046$ ft/s *Ans.*

The calculation converges rather quickly to the same result as that obtained through direct computation.

Type 3 Problem: Find the Pipe Diameter

The Moody chart is especially awkward for finding the pipe size, since d occurs in all three parameters f, Re_d, and ϵ/d. Further, it depends upon whether we know the velocity or the flow rate. We cannot know both, or else we could immediately compute $d = \sqrt{4Q/(\pi V)}$.

Let us assume that we know the flow rate Q. Note that this requires us to redefine the Reynolds number in terms of Q:

$$\text{Re}_d = \frac{Vd}{\nu} = \frac{4Q}{\pi d \nu} \tag{6.67}$$

Then, if we choose (Q, ρ, μ) as scaling parameters (to eliminate d), we obtain the functional relationship

$$\text{Re}_d = \frac{4Q}{\pi d \nu} = \text{fcn}\left(\frac{gh_f}{L\nu^5}, \frac{\epsilon \nu}{Q}\right) \tag{6.68}$$

and can thus solve d when the right-hand side is known. Unfortunately, the writer knows of no *formula* for this relation, nor is he able to rearrange Eq. (6.64) into the explicit form of Eq. (6.68). One could recalculate and *plot* the relation, and indeed an ingenious "pipe-sizing" plot is given in Ref. 13. Here it seems reasonable to forgo a plot or curve fitted formula and to simply set up the problem as an iteration in terms of the Moody-chart variables. In this case we also have to set up the friction factor in terms of the flow rate:

$$f = h_f \frac{d}{L} \frac{2g}{V^2} = \frac{\pi^2}{8} \frac{gh_f d^5}{LQ^2} \tag{6.69}$$

The following two examples illustrate the iteration.

EXAMPLE 6.11

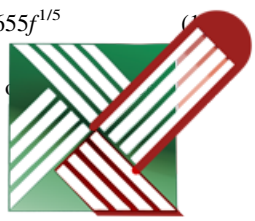
Work Example 6.9 backward, assuming that $Q = 0.342$ m^3/s and $\epsilon = 0.06$ mm are known but that d (30 cm) is unknown. Recall $L = 100$ m, $\rho = 950$ kg/m^3, $\nu = 2$ E-5 m^2/s, and $h_f = 8$ m.

Iterative Solution

First write the diameter in terms of the friction factor:

$$f = \frac{\pi^2}{8} \frac{(9.81 \text{ m/s}^2)(8 \text{ m})d^5}{(100 \text{ m})(0.342 \text{ m}^3/\text{s})^2} = 8.28d^5 \qquad \text{or} \qquad d \approx 0.655 f^{1/5} \quad (1$$

in SI units. Also write the Reynolds number and roughness ratio in terms o



ketabline.com Ebook.ketabline.com

$$\mathrm{Re}_d = \frac{4(0.342\ \mathrm{m^3/s})}{\pi(2\ \text{E-5}\ \mathrm{m^2/s})d} = \frac{21{,}800}{d} \tag{2}$$

$$\frac{\epsilon}{d} = \frac{6\ \text{E-5 m}}{d} \tag{3}$$

Guess f, compute d from (1), then compute Re_d from (2) and ϵ/d from (3), and compute a better f from the Moody chart or Eq. (6.64). Repeat until (fairly rapid) convergence. Having no initial estimate for f, the writer guesses $f \approx 0.03$ (about in the middle of the turbulent portion of the Moody chart). The following calculations result:

$$f \approx 0.03 \qquad d \approx 0.655(0.03)^{1/5} \approx 0.325\ \text{m}$$

$$\mathrm{Re}_d \approx \frac{21{,}800}{0.325} \approx 67{,}000 \qquad \frac{\epsilon}{d} \approx 1.85\ \text{E-4}$$

Eq. (6.54): $f_{\text{new}} \approx 0.0203$ then $d_{\text{new}} \approx 0.301$ m

$$\mathrm{Re}_{d,\text{new}} \approx 72{,}500 \qquad \frac{\epsilon}{d} \approx 2.0\ \text{E-4}$$

Eq. (6.54): $f_{\text{better}} \approx 0.0201$ and $d = 0.300$ m *Ans.*

The procedure has converged to the correct diameter of 30 cm given in Example 6.9.

EES Solution



For an EES solution, enter the data and the appropriate equations. The diameter is unknown. Correct units must of course be used. For the present example, the data should use SI units:

```
rho=950    nu=2E-5    L=100    eps=6E-5    hf=8.0    g=9.81    Q=0.342
```

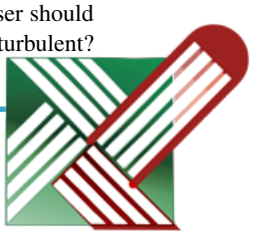
The appropriate equations are the Moody formula, the definition of Reynolds number, volume flow rate as determined from velocity, the Darcy head-loss formula, and the roughness ratio:

```
Re = V*d/nu
Q = V*pi*d^2/4
f = (-2.0*log10(epsod/3.7 + 2.51/Re/f^0.5))^(-2)
hf = f*L/d*V^2/2/g
epsod = eps/d
```

Hit *Solve* from the menu. Unlike Example 6.9, this time EES complains that the system *cannot* be solved and reports "logarithm of a negative number." The reason is that we allowed EES to assume that f could be a negative number. Bring down *Variable Information* from the menu and change the limits of f so that it cannot be negative. EES agrees and iterates to the solution:

```
d = 0.300    V = 4.84    f = 0.0201    Re = 72,585
```

The unit system is spelled out as (m, kg, s, N). As always when using software, the user should check the solution for engineering viability. For example, is the Reynolds number turbulent? (Yes)



ketabline.com Ebook.ketabline.com

EXAMPLE 6.12

Work Moody's problem, Example 6.6, backward to find the unknown (6 in) diameter if the flow rate $Q = 1.18$ ft^3/s is known. Recall $L = 200$ ft, $\epsilon = 0.0004$ ft, and $\nu = 1.1$ E-5 ft^2/s.

Solution

Write f, Re_d, and ϵ/d in terms of the diameter:

$$f = \frac{\pi^2}{8}\frac{gh_f d^5}{LQ^2} = \frac{\pi^2}{8}\frac{(32.2\ \text{ft/s}^2)(4.5\ \text{ft})d^5}{(200\ \text{ft})(1.18\ \text{ft}^3/\text{s})^2} = 0.642d^5 \qquad \text{or} \qquad d \approx 1.093f^{1/5} \tag{1}$$

$$\mathrm{Re}_d = \frac{4(1.18\ \text{ft}^3/\text{s})}{\pi(1.1\text{ E-}5\ \text{ft}^2/\text{s})\,d} = \frac{136{,}600}{d} \tag{2}$$

$$\frac{\epsilon}{d} = \frac{0.0004\ \text{ft}}{d} \tag{3}$$

with everything in BG units, of course. Guess f; compute d from (1), Re_d from (2), and ϵ/d from (3); and then compute a better f from the Moody chart. Repeat until convergence. The writer traditionally guesses an initial $f \approx 0.03$:

$$f \approx 0.03 \qquad d \approx 1.093(0.03)^{1/5} \approx 0.542\ \text{ft}$$

$$\mathrm{Re}_d = \frac{136{,}600}{0.542} \approx 252{,}000 \qquad \frac{\epsilon}{d} \approx 7.38\text{ E-}4$$

$$f_{\text{new}} \approx 0.0196 \qquad d_{\text{new}} \approx 0.498\ \text{ft} \qquad \mathrm{Re}_d \approx 274{,}000 \qquad \frac{\epsilon}{d} \approx 8.03\text{ E-}4$$

$$f_{\text{better}} \approx 0.0198 \qquad d \approx 0.499\ \text{ft} \qquad \textit{Ans.}$$

Convergence is rapid, and the predicted diameter is correct, about 6 in. The slight discrepancy (0.499 rather than 0.500 ft) arises because h_f was rounded to 4.5 ft.

Table 6.2 Nominal and Actual Sizes of Schedule 40 Wrought-Steel Pipe*

Nominal size, in	Actual ID, in
$\frac{1}{8}$	0.269
$\frac{1}{4}$	0.364
$\frac{3}{8}$	0.493
$\frac{1}{2}$	0.622
$\frac{3}{4}$	0.824
1	1.049
$1\frac{1}{2}$	1.610
2	2.067
$2\frac{1}{2}$	2.469
3	3.068

*Nominal size within 1 percent for 4 in or larger.

In discussing pipe-sizing problems, we should remark that commercial pipes are made only in certain sizes. Table 6.2 lists standard water-pipe sizes in the United States. If the sizing calculation gives an intermediate diameter, the next largest pipe size should be selected.

6.6 Flow in Noncircular Ducts[5]

If the duct is noncircular, the analysis of fully developed flow follows that of the circular pipe but is more complicated algebraically. For laminar flow, one can solve the exact equations of continuity and momentum. For turbulent flow, the logarithm-law velocity profile can be used, or (better and simpler) the hydraulic diameter is an excellent approximation.

The Hydraulic Diameter

For a noncircular duct, the control-volume concept of Fig. 6.10 is still valid, but the cross-sectional area A does not equal πR^2 and the cross-sectional perimeter wetted by the shear stress $\mathcal{P}$ does not equal $2\pi R$. The momentum equation (6.26) thus becomes

$$\Delta p\, A + \rho g A\, \Delta L \sin\phi - \bar{\tau}_w \mathcal{P}\, \Delta L = 0$$

[5]This section may be omitted without loss of continuity.



ketabline.com Ebook.ketabline.com

or
$$h_f = \frac{\Delta p}{\rho g} + \Delta z = \frac{\bar{\tau}_w}{\rho g}\frac{\Delta L}{A/\mathcal{P}} \tag{6.70}$$

This is identical to Eq. (6.27) except that (1) the shear stress is an average value integrated around the perimeter and (2) the length scale $A/\mathcal{P}$ takes the place of the pipe radius R. For this reason a noncircular duct is said to have a *hydraulic radius* R_h, defined by

$$R_h = \frac{A}{\mathcal{P}} = \frac{\text{cross-sectional area}}{\text{wetted perimeter}} \tag{6.71}$$

This concept receives constant use in open-channel flow (Chap. 10), where the channel cross section is almost never circular. If, by comparison to Eq. (6.29) for pipe flow, we define the friction factor in terms of average shear

$$f_{\text{NCD}} = \frac{8\bar{\tau}_w}{\rho V^2} \tag{6.72}$$

where NCD stands for noncircular duct and $V = Q/A$ as usual, Eq. (6.70) becomes

$$h_f = f\frac{L}{4R_h}\frac{V^2}{2g} \tag{6.73}$$

This is equivalent to Eq. (6.30) for pipe flow except that d is replaced by $4R_h$. Therefore we customarily define the *hydraulic diameter* as

$$D_h = \frac{4A}{\mathcal{P}} = \frac{4 \times \text{area}}{\text{wetted perimeter}} = 4R_h \tag{6.74}$$

We should stress that the wetted perimeter includes all surfaces acted upon by the shear stress. For example, in a circular annulus, both the outer and the inner perimeter should be added. The fact that D_h equals $4R_h$ is just one of those things: Chalk it up to an engineer's sense of humor. Note that for the degenerate case of a circular pipe, $D_h = 4\pi R^2/(2\pi R) = 2R$, as expected.

We would therefore expect by dimensional analysis that this friction factor f, based upon hydraulic diameter as in Eq. (6.72), would correlate with the Reynolds number and roughness ratio based upon the hydraulic diameter

$$f = F\left(\frac{VD_h}{\nu}, \frac{\epsilon}{D_h}\right) \tag{6.75}$$

and this is the way the data are correlated. But we should not necessarily expect the Moody chart (Fig. 6.13) to hold exactly in terms of this new length scale. And it does not, but it is surprisingly accurate:

$$f \approx \begin{cases} \dfrac{64}{\text{Re}_{D_h}} & \pm 40\% \quad \text{laminar flow} \\ f_{\text{Moody}}\left(\text{Re}_{D_h}, \dfrac{\epsilon}{D_h}\right) & \pm 15\% \quad \text{turbulent flow} \end{cases} \tag{6.76}$$

Now let us look at some particular cases.



ketabline.com Ebook.ketabline.com

Flow between Parallel Plates

As shown in Fig. 6.14, flow between parallel plates a distance h apart is the limiting case of flow through a very wide rectangular channel. For fully developed flow, $u = u(y)$ only, which satisfies continuity identically. The momentum equation in cartesian coordinates reduces to

$$0 = -\frac{dp}{dx} + \rho g_x + \frac{d\tau}{dy} \qquad \tau_{\text{lam}} = \mu \frac{du}{dy} \tag{6.77}$$

subject to no-slip conditions: $u = 0$ at $y = \pm h$. The laminar-flow solution was given as an example in Eq. (4.143). Here we also allow for the possibility of a sloping channel, with a pressure gradient due to gravity. The solution is

$$u = \frac{1}{2\mu}\left[-\frac{d}{dx}(p + \rho g z)\right](h^2 - y^2) \tag{6.78}$$

If the channel has width b, the volume flow is

$$Q = \int_{-h}^{+h} u(y) b \, dy = \frac{bh^3}{3\mu}\left[-\frac{d}{dx}(p + \rho g z)\right]$$

or

$$V = \frac{Q}{bh} = \frac{h^2}{3\mu}\left[-\frac{d}{dx}(p + \rho g z)\right] = \frac{2}{3} u_{\max} \tag{6.79}$$

Note the difference between a parabola [Eq. (6.79)] and a paraboloid [Eq. (6.43)]: the average is two-thirds of the maximum velocity in plane flow and one-half in axisymmetric flow.

The wall shear stress in developed channel flow is a constant:

$$\tau_w = \mu \left|\frac{du}{dy}\right|_{y=+h} = h\left[-\frac{d}{dx}(p + \rho g z)\right] \tag{6.80}$$

This may be nondimensionalized as a friction factor:

$$f = \frac{8\tau_w}{\rho V^2} = \frac{24\mu}{\rho V h} = \frac{24}{\text{Re}_h} \tag{6.81}$$

These are exact analytic laminar-flow results, so there is no reason to resort to the hydraulic-diameter concept. However, if we did use D_h, a discrepancy would arise. The hydraulic diameter of a wide channel is

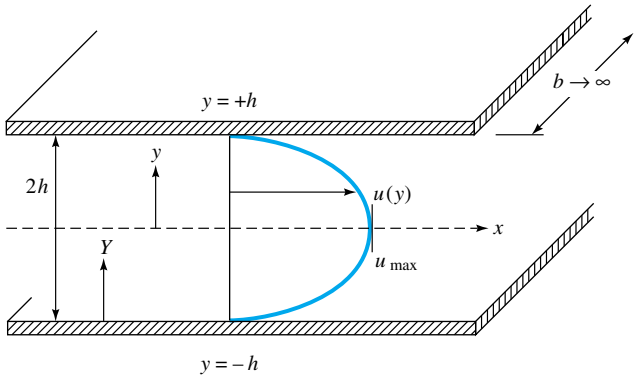


Fig. 6.14 Fully developed flow between parallel plates.



ketabline.com Ebook.ketabline.com

$$D_h = \frac{4A}{\rho} = \lim_{b\to\infty} \frac{4(2bh)}{2b + 4h} = 4h \tag{6.82}$$

or twice the distance between the plates. Substituting into Eq. (6.81), we obtain the interesting result

Parallel plates: $$f_{\text{lam}} = \frac{96\mu}{\rho V(4h)} = \frac{96}{\text{Re}_{D_h}} \tag{6.83}$$

Thus, if we could not work out the laminar theory and chose to use the approximation $f \approx 64/\text{Re}_{D_h}$, we would be 33 percent low. The hydraulic-diameter approximation is relatively crude in laminar flow, as Eq. (6.76) states.

Just as in circular-pipe flow, the laminar solution above becomes unstable at about $\text{Re}_{D_h} \approx 2000$; transition occurs and turbulent flow results.

For turbulent flow between parallel plates, we can again use the logarithm law, Eq. (6.21), as an approximation across the entire channel, using not y but a wall coordinate Y, as shown in Fig. 6.14:

$$\frac{u(Y)}{u^*} \approx \frac{1}{\kappa}\ln\frac{Yu^*}{\nu} + B \qquad 0 < Y < h \tag{6.84}$$

This distribution looks very much like the flat turbulent profile for pipe flow in Fig. 6.11*b*, and the mean velocity is

$$V = \frac{1}{h}\int_0^h u\, dY = u^*\left(\frac{1}{\kappa}\ln\frac{hu^*}{\nu} + B - \frac{1}{\kappa}\right) \tag{6.85}$$

Recalling that $V/u^* = (8/f)^{1/2}$, we see that Eq. (6.85) is equivalent to a parallel-plate friction law. Rearranging and cleaning up the constant terms, we obtain

$$\frac{1}{f^{1/2}} \approx 2.0 \log (\text{Re}_{D_h} f^{1/2}) - 1.19 \tag{6.86}$$

where we have introduced the hydraulic diameter $D_h = 4h$. This is remarkably close to the pipe-friction law, Eq. (6.54). Therefore we conclude that the use of the hydraulic diameter in this turbulent case is quite successful. That turns out to be true for other noncircular turbulent flows also.

Equation (6.86) can be brought into exact agreement with the pipe law by rewriting it in the form

$$\frac{1}{f^{1/2}} = 2.0 \log (0.64\ \text{Re}_{D_h} f^{1/2}) - 0.8 \tag{6.87}$$

Thus the turbulent friction is predicted most accurately when we use an effective diameter D_{eff} equal to 0.64 times the hydraulic diameter. The effect on f itself is much less, about 10 percent at most. We can compare with Eq. (6.83) for laminar flow, which predicted

Parallel plates: $$D_{\text{eff}} = \frac{64}{96}D_h = \frac{2}{3}D_h \tag{6.88}$$

This close resemblance ($0.64D_h$ versus $0.667D_h$) occurs so often in noncircular duct flow that we take it to be a general rule for computing turbulent friction in ducts:

$$D_{\text{eff}} = D_h = \frac{4A}{\mathcal{P}} \quad \text{reasonable accuracy}$$



ketabline.com Ebook.ketabline.com

$$D_{\text{eff}}(\text{laminar theory}) \quad \text{extreme accuracy} \tag{6.89}$$

Jones [10] shows that the effective-laminar-diameter idea collapses all data for rectangular ducts of arbitrary height-to-width ratio onto the Moody chart for pipe flow. We recommend this idea for all noncircular ducts.

EXAMPLE 6.13

Fluid flows at an average velocity of 6 ft/s between horizontal parallel plates a distance of 2.4 in apart. Find the head loss and pressure drop for each 100 ft of length for $\rho = 1.9$ slugs/ft^3 and (*a*) $\nu = 0.00002$ ft^3/s and (*b*) $\nu = 0.002$ ft^3/s. Assume smooth walls.

Solution

Part (a) The viscosity $\mu = \rho\nu = 3.8 \times 10^{-5}$ slug/(ft · s). The spacing is $2h = 2.4$ in $= 0.2$ ft, and $D_h = 4h = 0.4$ ft. The Reynolds number is

$$\text{Re}_{D_h} = \frac{VD_h}{\nu} = \frac{(6.0 \text{ ft/s})(0.4 \text{ ft})}{0.00002 \text{ ft}^2/\text{s}} = 120{,}000$$

The flow is therefore turbulent. For reasonable accuracy, simply look on the Moody chart (Fig. 6.13) for smooth walls

$$f \approx 0.0173 \quad h_f \approx f\frac{L}{D_h}\frac{V^2}{2g} = 0.0173\,\frac{100}{0.4}\,\frac{(6.0)^2}{2(32.2)} \approx 2.42 \text{ ft} \qquad \textit{Ans. (a)}$$

Since there is no change in elevation,

$$\Delta p = \rho g h_f = 1.9(32.2)(2.42) = 148 \text{ lbf/ft}^2 \qquad \textit{Ans. (a)}$$

This is the head loss and pressure drop per 100 ft of channel. For more accuracy, take $D_{\text{eff}} = \frac{2}{3}D_h$ from laminar theory; then

$$\text{Re}_{\text{eff}} = \tfrac{2}{3}(120{,}000) = 80{,}000$$

and from the Moody chart read $f \approx 0.0189$ for smooth walls. Thus a better estimate is

$$h_f = 0.0189\,\frac{100}{0.4}\,\frac{(6.0)^2}{2(32.2)} = 2.64 \text{ ft}$$

and

$$\Delta p = 1.9(32.2)(2.64) = 161 \text{ lbf/ft}^2 \qquad \textit{Better ans. (a)}$$

The more accurate formula predicts friction about 9 percent higher.

Part (b) Compute $\mu = \rho\nu = 0.0038$ slug/(ft · s). The Reynolds number is $6.0(0.4)/0.002 = 1200$; therefore the flow is laminar, since Re is less than 2300.

You could use the laminar-flow friction factor, Eq. (6.83)

$$f_{\text{lam}} = \frac{96}{\text{Re}_{D_h}} = \frac{96}{1200} = 0.08$$

from which

$$h_f = 0.08\,\frac{100}{0.4}\,\frac{(6.0)^2}{2(32.2)} = 11.2 \text{ ft}$$

and

$$\Delta p = 1.9(32.2)(11.2) = 684 \text{ lbf/ft}^2$$



ketabline.com Ebook.ketabline.com

Alternately you can finesse the Reynolds number and go directly to the appropriate laminar-flow formula, Eq. (6.79)

$$V = \frac{h^2}{3\mu}\frac{\Delta p}{L}$$

or $$\Delta p = \frac{3(6.0\text{ ft/s})[0.0038\text{ slug/(ft}\cdot\text{s)}](100\text{ ft})}{(0.1\text{ ft})^2} = 684\text{ slugs/(ft}\cdot\text{s}^2) = 684\text{ lbf/ft}^2$$

and $$h_f = \frac{\Delta p}{\rho g} = \frac{684}{1.9(32.2)} = 11.2\text{ ft}$$

This is one of those—perhaps unexpected—problems where the laminar friction is greater than the turbulent friction.

Flow through a Concentric Annulus

Consider steady axial laminar flow in the annular space between two concentric cylinders, as in Fig. 6.15. There is no slip at the inner ($r = b$) and outer radius ($r = a$). For $u = u(r)$ only, the governing relation is Eq. (6.34)

$$\frac{d}{dr}\left(r\mu\frac{du}{dr}\right) = Kr \qquad K = \frac{d}{dx}(p + \rho gz) \tag{6.90}$$

Integrate this twice

$$u = \frac{1}{4}r^2\frac{K}{\mu} + C_1 \ln r + C_2$$

The constants are found from the two no-slip conditions

$$u(r = a) = 0 = \frac{1}{4}a^2\frac{K}{\mu} + C_1 \ln a + C_2$$

$$u(r = b) = 0 = \frac{1}{4}b^2\frac{K}{\mu} + C_1 \ln b + C_2$$

The final solution for the velocity profile is

$$u = \frac{1}{4\mu}\left[-\frac{d}{dx}(p + \rho gz)\right]\left[a^2 - r^2 + \frac{a^2 - b^2}{\ln (b/a)}\ln\frac{a}{r}\right] \tag{6.91}$$

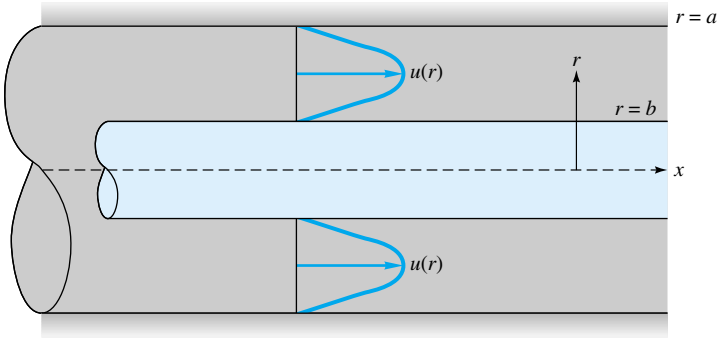


Fig. 6.15 Fully developed flow through a concentric annulus.



ketabline.com Ebook.ketabline.com

The volume flow is given by

$$Q = \int_b^a u 2\pi r \, dr = \frac{\pi}{8\mu}\left[-\frac{d}{dx}(p + \rho g z)\right]\left[a^4 - b^4 - \frac{(a^2 - b^2)^2}{\ln (a/b)}\right] \tag{6.92}$$

The velocity profile $u(r)$ resembles a parabola wrapped around in a circle to form a split doughnut, as in Fig. 6.15. The maximum velocity occurs at the radius

$$r' = \left[\frac{a^2 - b^2}{2 \ln (a/b)}\right]^{1/2} \qquad u = u_{\max} \tag{6.93}$$

This maximum is closer to the inner radius but approaches the midpoint between cylinders as the clearance $a - b$ becomes small. Some numerical values are as follows:

$\frac{b}{a}$	0.01	0.1	0.2	0.5	0.8	0.9	0.99
$\frac{r' - b}{a - b}$	0.323	0.404	0.433	0.471	0.491	0.496	0.499

Also, as the clearance becomes small, the profile approaches a parabolic distribution, as if the flow were between two parallel plates [Eq. (4.143)].

It is confusing to base the friction factor on the wall shear because there are two shear stresses, the inner stress being greater than the outer. It is better to define f with respect to the head loss, as in Eq. (6.73),

$$f = h_f \frac{D_h}{L}\frac{2g}{V^2} \qquad \text{where } V = \frac{Q}{\pi(a^2 - b^2)} \tag{6.94}$$

The hydraulic diameter for an annulus is

$$D_h = \frac{4\pi(a^2 - b^2)}{2\pi(a + b)} = 2(a - b) \tag{6.95}$$

It is twice the clearance, rather like the parallel-plate result of twice the distance between plates [Eq. (6.82)].

Substituting h_f, D_h, and V into Eq. (6.94), we find that the friction factor for laminar flow in a concentric annulus is of the form

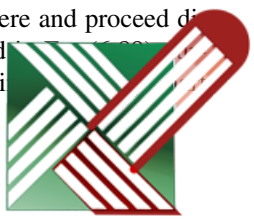
$$f = \frac{64\zeta}{\text{Re}_{D_h}} \qquad \zeta = \frac{(a - b)^2(a^2 - b^2)}{a^4 - b^4 - (a^2 - b^2)^2/\ln (a/b)} \tag{6.96}$$

The dimensionless term ζ is a sort of correction factor for the hydraulic diameter. We could rewrite Eq. (6.96) as

$$\text{Concentric annulus:} \qquad f = \frac{64}{\text{Re}_{\text{eff}}} \qquad \text{Re}_{\text{eff}} = \frac{1}{\zeta}\text{Re}_{D_h} \tag{6.97}$$

Some numerical values of $f\,\text{Re}_{D_h}$ and $D_{\text{eff}}/D_h = 1/\zeta$ are given in Table 6.3.

For turbulent flow through a concentric annulus, the analysis might proceed by patching together two logarithmic-law profiles, one going out from the inner wall to meet the other coming in from the outer wall. We omit such a scheme here and proceed directly to the friction factor. According to the general rule proposed [illegible] bulent friction is predicted with excellent accuracy by replacing d i



ketabline.com Ebook.ketabline.com

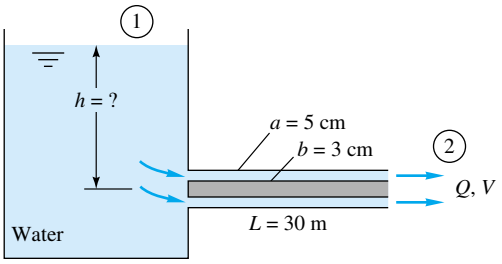
Table 6.3 Laminar Friction Factors for a Concentric Annulus

b/a	$f\,\mathrm{Re}_{D_h}$	$D_{\text{eff}}/D_h = 1/\zeta$
0.0	64.0	1.000
0.00001	70.09	0.913
0.0001	71.78	0.892
0.001	74.68	0.857
0.01	80.11	0.799
0.05	86.27	0.742
0.1	89.37	0.716
0.2	92.35	0.693
0.4	94.71	0.676
0.6	95.59	0.670
0.8	95.92	0.667
1.0	96.0	0.667

by $D_{\text{eff}} = 2(a - b)/\zeta$, with values listed in Table 6.3.[6] This idea includes roughness also (replace ϵ/d in the chart by ϵ/D_{eff}). For a quick design number with about 10 percent accuracy, one can simply use the hydraulic diameter $D_h = 2(a - b)$.

EXAMPLE 6.14

What should the reservoir level h be to maintain a flow of 0.01 m^3/s through the commercial steel annulus 30 m long shown in Fig. E6.14? Neglect entrance effects and take $\rho = 1000$ kg/m^3 and $\nu = 1.02 \times 10^{-6}$ m^2/s for water.



E6.14

Solution

Compute the average velocity and hydraulic diameter

$$V = \frac{Q}{A} = \frac{0.01\ \text{m}^3/\text{s}}{\pi[(0.05\ \text{m})^2 - (0.03\ \text{m})^2]} = 1.99\ \text{m/s}$$

$$D_h = 2(a - b) = 2(0.05 - 0.03)\ \text{m} = 0.04\ \text{m}$$

Apply the steady-flow energy equation between sections 1 and 2:

$$\frac{p_1}{\rho} + \frac{1}{2}V_1^2 + gz_1 = \left(\frac{p_2}{\rho} + \frac{1}{2}V_2^2 + gz_2\right) + gh_f$$

But $p_1 = p_2 = p_a$, $V_1 \approx 0$, and $V_2 = V$ in the pipe. Therefore solve for

$$h_f = f\frac{L}{D_h}\frac{V^2}{2g} = z_1 - z_2 - \frac{V^2}{2g}$$

But $z_1 - z_2 = h$, the desired reservoir height. Thus, finally,

$$h = \frac{V^2}{2g}\left(1 + f\frac{L}{D_h}\right) \tag{1}$$

Since V, L, and D_h are known, our only remaining problem is to compute the annulus friction factor f. For a quick approximation, take $D_{\text{eff}} = D_h = 0.04$ m. Then

$$\mathrm{Re}_{D_h} = \frac{VD_h}{\nu} = \frac{1.99(0.04)}{1.02 \times 10^{-6}} = 78{,}000$$

$$\frac{\epsilon}{D_h} = \frac{0.046\ \text{mm}}{40\ \text{mm}} = 0.00115$$

[6] Jones and Leung [44] show that data for annular flow also satisfy the effective-laminar-diam



ketabline.com Ebook.ketabline.com

where $\epsilon = 0.046$ mm has been read from Table 6.1 for commercial steel surfaces. From the Moody chart, read $f = 0.0232$. Then, from Eq. (1) above,

$$h \approx \frac{(1.99\ \text{m/s})^2}{2(9.81\ \text{m/s}^2)}\left(1 + 0.0232\,\frac{30\ \text{m}}{0.04\ \text{m}}\right) = 3.71\ \text{m} \qquad \textit{Crude ans.}$$

For better accuracy, take $D_{\text{eff}} = D_h/\zeta = 0.670D_h = 2.68$ cm, where the correction factor 0.670 has been read from Table 6.3 for $b/a = \frac{3}{5} = 0.6$. Then the corrected Reynolds number and roughness ratio are

$$\text{Re}_{\text{eff}} = \frac{VD_{\text{eff}}}{\nu} = 52{,}300 \qquad \frac{\epsilon}{D_{\text{eff}}} = 0.00172$$

From the Moody chart, read $f = 0.0257$. Then the improved computation for reservoir height is

$$h = \frac{(1.99\ \text{m/s})^2}{2(9.81\ \text{m/s}^2)}\left(1 + 0.0257\,\frac{30\ \text{m}}{0.04\ \text{m}}\right) = 4.09\ \text{m} \qquad \textit{Better ans.}$$

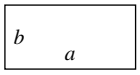
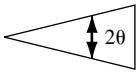
The uncorrected hydraulic-diameter estimate is about 9 percent low. Note that we do *not* replace D_h by D_{eff} in the ratio L/D_h in Eq. (1) since this is implicit in the definition of friction factor.

Other Noncircular Cross Sections

In principle, any duct cross section can be solved analytically for the laminar-flow velocity distribution, volume flow, and friction factor. This is because any cross section can be mapped onto a circle by the methods of complex variables, and other powerful analytical techniques are also available. Many examples are given by White [3, pp. 119–122], Berker [11], and Olson and Wright [12, pp. 315–317]. Reference 34 is devoted entirely to laminar duct flow.

In general, however, most unusual duct sections have strictly academic and not commercial value. We list here only the rectangular and isosceles-triangular sections, in Table 6.4, leaving other cross sections for you to find in the references.

Table 6.4 Laminar Friction Constants $f\text{Re}$ for Rectangular and Triangular Ducts

Rectangular		Isosceles triangle	
			
b/a	$f\text{Re}_{D_h}$	θ, deg	$f\text{Re}_{D_h}$
0.0	96.00	0	48.0
0.05	89.91	10	51.6
0.1	84.68	20	52.9
0.125	82.34	30	53.3
0.167	78.81	40	52.9
0.25	72.93	50	52.0
0.4	65.47	60	51.1
0.5	62.19	70	49.5
0.75	57.89	80	48.3
1.0	56.91	90	48.0

For turbulent flow in a duct of unusual cross section, one should replace d by D_h on the Moody chart if no laminar theory is available. If laminar results are known, such as Table 6.4, replace d by $D_{\text{eff}} = [64/(f\text{Re})]D_h$ for the particular geometry of the duct.

For laminar flow in rectangles and triangles, the wall friction varies greatly, being largest near the midpoints of the sides and zero in the corners. In turbulent flow through the same sections, the shear is nearly constant along the sides, dropping off sharply to zero in the corners. This is because of the phenomenon of turbulent *secondary flow*, in which there are nonzero mean velocities v and w in the plane of the cross section. Some measurements of axial velocity and secondary-flow patterns are shown in Fig. 6.16, as sketched by Nikuradse in his 1926 dissertation. The secondary-flow "cells" drive the mean flow toward the corners, so that the axial-velocity contours are similar to the cross section and the wall shear is nearly constant. This is why the hydraulic-diameter concept is so successful for turbulent flow. Laminar flow in a straight noncircular duct has no secondary flow. An accurate theoretical prediction of turbulent secondary flow has yet to be achieved, although are improving [36].



ketabline.com Ebook.ketabline.com

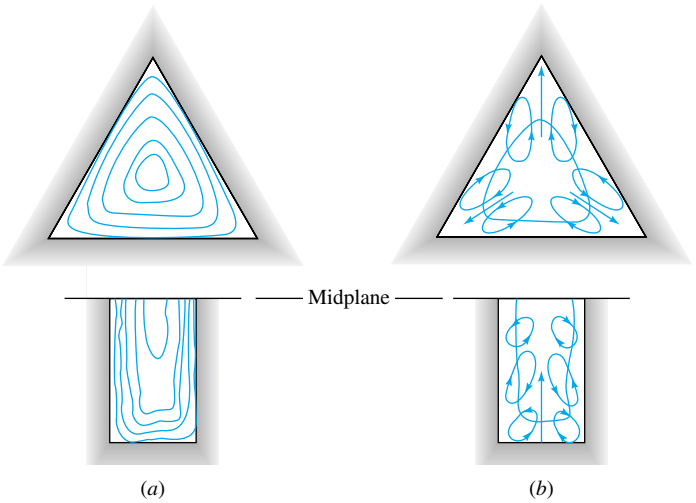


Fig. 6.16 Illustration of secondary turbulent flow in noncircular ducts: (*a*) axial mean-velocity contours; (*b*) secondary-flow cellular motions. *(After J. Nikuradse, dissertation, Göttingen, 1926.)*

EXAMPLE 6.15

Air, with $\rho = 0.00237$ slug/ft^3 and $\nu = 0.000157$ ft^2/s, is forced through a horizontal square 9-by 9-in duct 100 ft long at 25 ft^3/s. Find the pressure drop if $\epsilon = 0.0003$ ft.

Solution

Compute the mean velocity and hydraulic diameter

$$V = \frac{25 \text{ ft}^3/\text{s}}{(0.75 \text{ ft})^2} = 44.4 \text{ ft/s}$$

$$D_h = \frac{4A}{\mathcal{P}} = \frac{4(81 \text{ in}^2)}{36 \text{ in}} = 9 \text{ in} = 0.75 \text{ ft}$$

From Table 6.4, for $b/a = 1.0$, the effective diameter is

$$D_{\text{eff}} = \frac{64}{56.91} D_h = 0.843 \text{ ft}$$

whence

$$\text{Re}_{\text{eff}} = \frac{VD_{\text{eff}}}{\nu} = \frac{44.4(0.843)}{0.000157} = 239{,}000$$

$$\frac{\epsilon}{D_{\text{eff}}} = \frac{0.0003}{0.843} = 0.000356$$

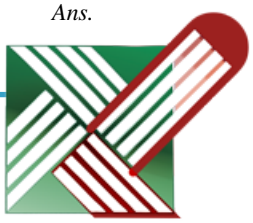
From the Moody chart, read $f = 0.0177$. Then the pressure drop is

$$\Delta p = \rho g h_f = \rho g \left(f \frac{L}{D_h} \frac{V^2}{2g} \right) = 0.00237(32.2)\left[0.0177 \frac{100}{0.75} \frac{44.4^2}{2(32.2)}\right]$$

or

$$\Delta p = 5.5 \text{ lbf/ft}^2 \qquad \textit{Ans.}$$

Pressure drop in air ducts is usually small because of the low density.



ketabline.com Ebook.ketabline.com

6.7 Minor Losses in Pipe Systems[7]

For any pipe system, in addition to the Moody-type friction loss computed for the length of pipe, there are additional so-called *minor losses* due to

1. Pipe entrance or exit
2. Sudden expansion or contraction
3. Bends, elbows, tees, and other fittings
4. Valves, open or partially closed
5. Gradual expansions or contractions

The losses may not be so minor; e.g., a partially closed valve can cause a greater pressure drop than a long pipe.

Since the flow pattern in fittings and valves is quite complex, the theory is very weak. The losses are commonly measured experimentally and correlated with the pipe-flow parameters. The data, especially for valves, are somewhat dependent upon the particular manufacturer's design, so that the values listed here must be taken as average design estimates [15, 16, 35, 43, 46].

The measured minor loss is usually given as a ratio of the head loss $h_m = \Delta p/(\rho g)$ through the device to the velocity head $V^2/(2g)$ of the associated piping system

$$\text{Loss coefficient } K = \frac{h_m}{V^2/(2g)} = \frac{\Delta p}{\frac{1}{2}\rho V^2} \tag{6.98}$$

Although K is dimensionless, it unfortunately is not correlated in the literature with the Reynolds number and roughness ratio but rather simply with the raw size of the pipe in, say, inches. Almost all data are reported for turbulent-flow conditions.

An alternate, and less desirable, procedure is to report the minor loss as if it were an *equivalent length* L_{eq} of pipe, satisfying the Darcy friction-factor relation

$$h_m = f\frac{L_{eq}}{d}\frac{V^2}{2g} = K\frac{V^2}{2g}$$

or

$$L_{eq} = \frac{Kd}{f} \tag{6.99}$$

Although the equivalent length should take some of the variability out of the loss data, it is an artificial concept and will not be pursued here.

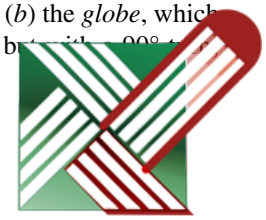
A single pipe system may have many minor losses. Since all are correlated with $V^2/(2g)$, they can be summed into a single total system loss if the pipe has constant diameter

$$\Delta h_{tot} = h_f + \sum h_m = \frac{V^2}{2g}\left(\frac{fL}{d} + \sum K\right) \tag{6.100}$$

Note, however, that we must sum the losses separately if the pipe size changes so that V^2 changes. The length L in Eq. (6.100) is the total length of the pipe axis, including any bends.

There are many different valve designs in commercial use. Figure 6.17 shows five typical designs: (*a*) the *gate*, which slides down across the section; (*b*) the *globe*, which closes a hole in a special insert; (*c*) the *angle*, similar to a globe b[illegible]

[7]This section may be omitted without loss of continuity.



ketabline.com Ebook.ketabline.com

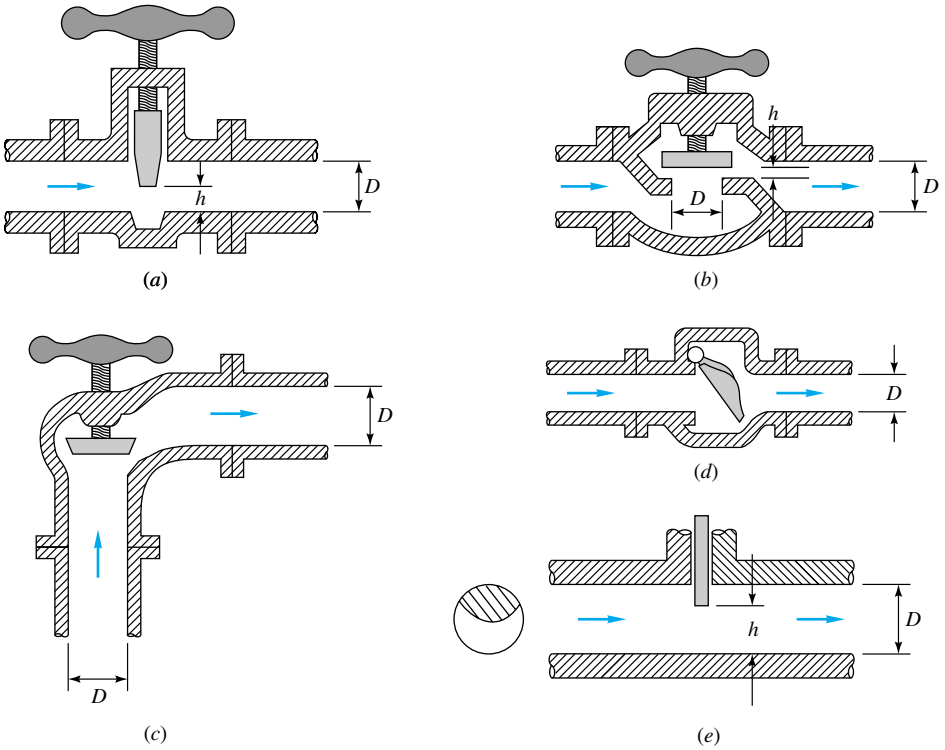


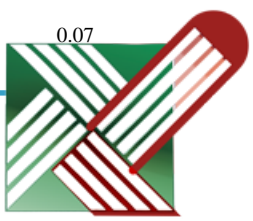
Fig. 6.17 Typical commercial valve geometries: (*a*) gate valve; (*b*) globe valve; (*c*) angle valve; (*d*) swing-check valve; (*e*) disk-type gate valve.

(*d*) the *swing-check* valve, which allows only one-way flow; and (*e*) the *disk*, which closes the section with a circular gate. The globe, with its tortuous flow path, has the highest losses when fully open. Many excellent details about these and other valves are given in the handbook by Lyons [35].

Table 6.5 lists loss coefficients K for four types of valve, three angles of elbow fit-

Table 6.5 Resistance Coefficients $K = h_m/[V^2/(2g)]$ for Open Valves, Elbows, and Tees

	Nominal diameter, in								
	Screwed				Flanged				
	$\frac{1}{2}$	1	2	4	1	2	4	8	20
Valves (fully open):									
Globe	14	8.2	6.9	5.7	13	8.5	6.0	5.8	5.5
Gate	0.30	0.24	0.16	0.11	0.80	0.35	0.16	0.07	0.03
Swing check	5.1	2.9	2.1	2.0	2.0	2.0	2.0	2.0	2.0
Angle	9.0	4.7	2.0	1.0	4.5	2.4	2.0	2.0	2.0
Elbows:									
45° regular	0.39	0.32	0.30	0.29					
45° long radius					0.21	0.20	0.19	0.16	0.14
90° regular	2.0	1.5	0.95	0.64	0.50	0.39	0.30	0.26	0.21
90° long radius	1.0	0.72	0.41	0.23	0.40	0.30	0.19	0.15	0.10
180° regular	2.0	1.5	0.95	0.64	0.41	0.35	0.30	0.25	0.20
180° long radius					0.40	0.30	0.21	0.15	0.10
Tees:									
Line flow	0.90	0.90	0.90	0.90	0.24	0.19	0.14	0.10	0.07
Branch flow	2.4	1.8	1.4	1.1	1.0	0.80	0.64	0.58	



ketabline.com Ebook.ketabline.com

ting, and two tee connections. Fittings may be connected by either internal screws or flanges, hence the two listings. We see that K generally decreases with pipe size, which is consistent with the higher Reynolds number and decreased roughness ratio of large pipes. We stress that Table 6.5 represents losses *averaged among various manufacturers*, so there is an uncertainty as high as ± 50 percent.

In addition, most of the data in Table 6.5 are relatively old [15, 16] and therefore based upon fittings manufactured in the 1950s. Modern forged and molded fittings may yield somewhat different loss factors, often less than listed in Table 6.5. An example, shown in Fig. 6.18*a*, gives very recent data [48] for fairly short (bend-radius/elbow-diameter = 1.2) flanged 90° elbows. The elbow diameter was 1.69 in. Notice first that K is plotted versus Reynolds number, rather than versus the raw (dimensional) pipe diameters in Table 6.5, and therefore Fig. 6.18*a* has more generality. Then notice that the K values of 0.23 ± 0.05 are significantly less than the values for 90° elbows in Table 6.5, indicating smoother walls and/or better design. One may conclude that (1) Table 6.5 data are probably conservative and (2) loss factors are highly dependent upon actual design and manufacturing factors, with Table 6.5 only serving as a rough guide.

The valve losses in Table 6.5 are for the fully open condition. Losses can be much higher for a partially open valve. Figure 6.18*b* gives average losses for three valves as a function of "percentage open," as defined by the opening-distance ratio h/D (see Fig. 6.17 for the geometries). Again we should warn of a possible uncertainty of ± 50 percent. Of all minor losses, valves, because of their complex geometry, are most sensitive to manufacturers' design details. For more accuracy, the particular design and manufacturer should be consulted [35].

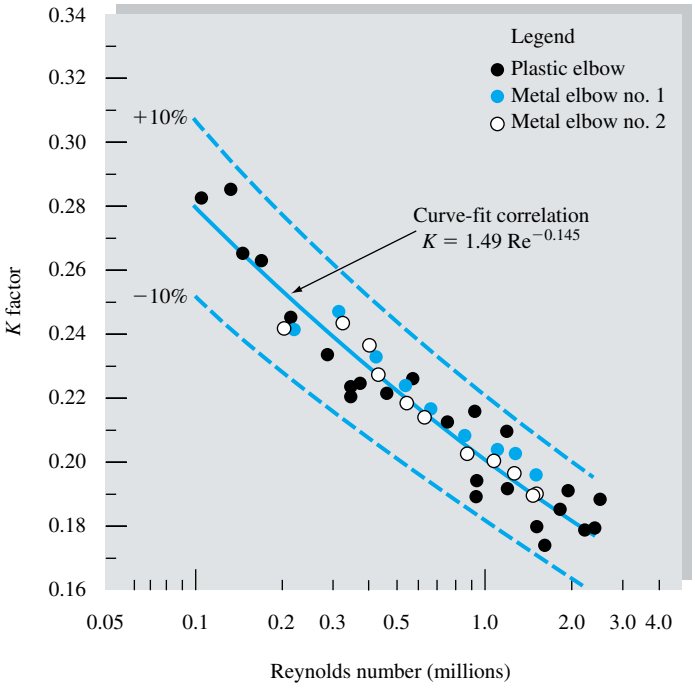


Fig. 6.18a Recent measured loss coefficients for 90° elbows. These values are less than those reported in Table 6.5. *[From Ref. 48, courtesy of R. D. Coffield.]*



ketabline.com Ebook.ketabline.com

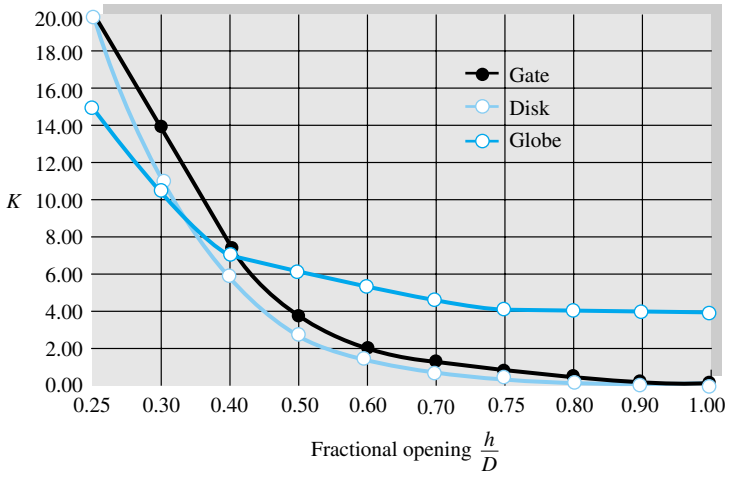
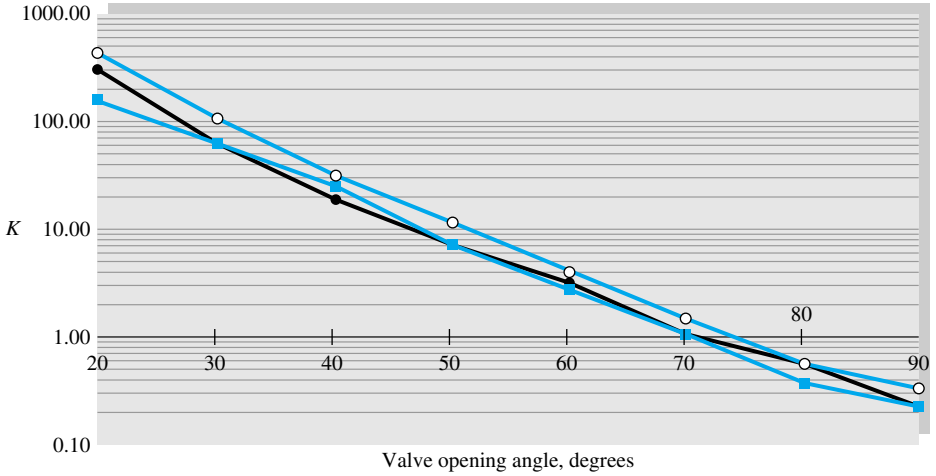


Fig. 6.18b Average-loss coefficients for partially open valves (see sketches in Fig. 6.17).



(*a*)

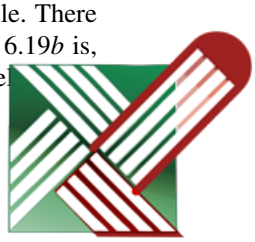


(*b*)

Fig. 6.19 Performance of butterfly valves: (*a*) typical geometry *(courtesy of Grinnell Corp., Cranston, R.I.);* (*b*) loss coefficients for three different manufacturers.

The *butterfly* valve of Fig. 6.19*a* is a stem-mounted disk which, when closed, seats against an O-ring or compliant seal near the pipe surface. A single 90° turn opens the valve completely, hence the design is ideal for controllable quick-opening and quick-closing situations such as occur in fire protection and the electric power industry. However, considerable dynamic torque is needed to close these valves, and losses are high when the valves are nearly closed.

Figure 6.19*b* shows butterfly-valve loss coefficients as a function of the opening angle θ for turbulent-flow conditions ($\theta = 0$ is closed). The losses are huge when the opening is small, and K drops off nearly exponentially with the opening angle. There is a factor of 2 spread among the various manufacturers. Note that K in Fig. 6.19*b* is, as usual, based on the average *pipe* velocity $V = Q/A$, not on the increased ve the flow as it passes through the narrow valve passage.



ketabline.com Ebook.ketabline.com

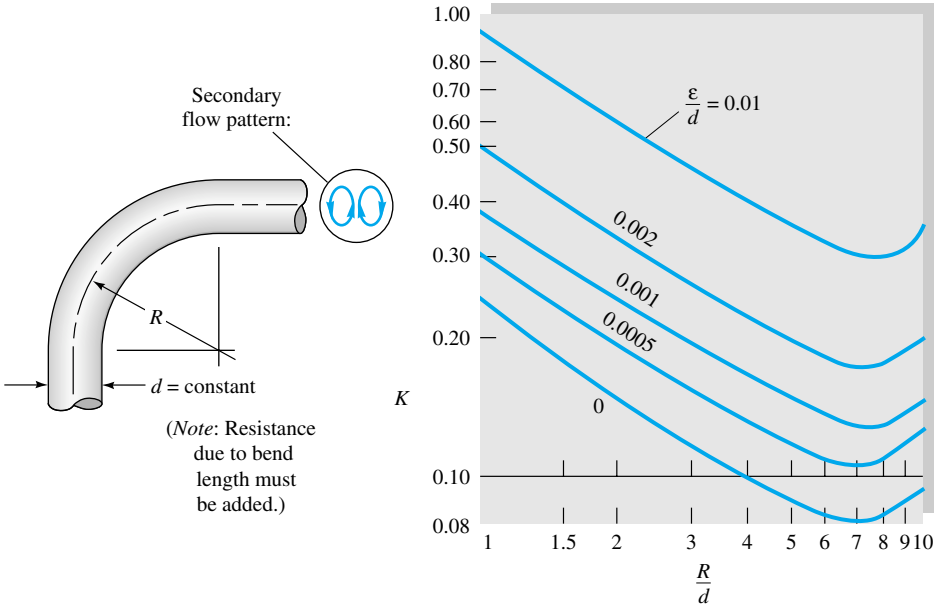


Fig. 6.20 Resistance coefficients for 90° bends.

A bend or curve in a pipe, as in Fig. 6.20, always induces a loss larger than the simple Moody friction loss, due to flow separation at the walls and a swirling secondary flow arising from the centripetal acceleration. The loss coefficients K in Fig. 6.20 are for this additional bend loss. The Moody loss due to the axial length of the bend must be computed separately; i.e., the bend length should be added to the pipe length.

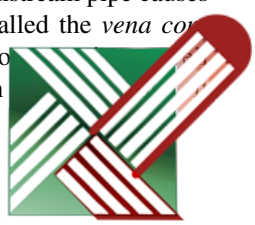
As shown in Fig. 6.21, entrance losses are highly dependent upon entrance geometry, but exit losses are not. Sharp edges or protrusions in the entrance cause large zones of flow separation and large losses. A little rounding goes a long way, and a well-rounded entrance ($r = 0.2d$) has a nearly negligible loss $K = 0.05$. At a submerged exit, on the other hand, the flow simply passes out of the pipe into the large downstream reservoir and loses all its velocity head due to viscous dissipation. Therefore $K = 1.0$ for all *submerged exits,* no matter how well rounded.

If the entrance is from a finite reservoir, it is termed a *sudden contraction* (SC) between two sizes of pipe. If the exit is to finite-sized pipe, it is termed a *sudden expansion* (SE). The losses for both are graphed in Fig. 6.22. For the sudden expansion, the shear stress in the corner separated flow, or deadwater region, is negligible, so that a control-volume analysis between the expansion section and the end of the separation zone gives a theoretical loss

$$K_{SE} = \left(1 - \frac{d^2}{D^2}\right)^2 = \frac{h_m}{V^2/(2g)} \tag{6.101}$$

Note that K is based on the velocity head in the small pipe. Equation (6.101) is in excellent agreement with experiment.

For the sudden contraction, however, flow separation in the downstream pipe causes the main stream to contract through a minimum diameter d_{min}, called the *vena contracta*, as sketched in Fig. 6.22. Because the theory of the vena co
developed, the loss coefficient in the figure for sudden contraction



ketabline.com Ebook.ketabline.com

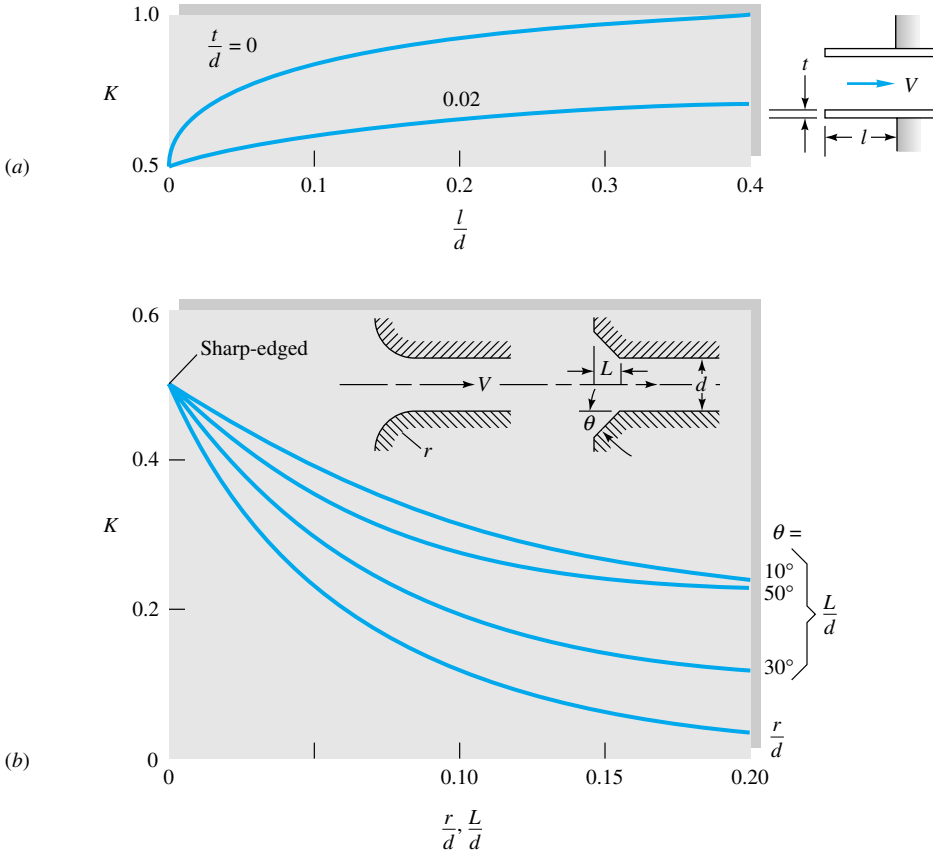


Fig. 6.21 Entrance and exit loss coefficients: (*a*) reentrant inlets; (*b*) rounded and beveled inlets. Exit losses are $K \approx 1.0$ for all shapes of exit (reentrant, sharp, beveled, or rounded). *(From Ref. 37.)*

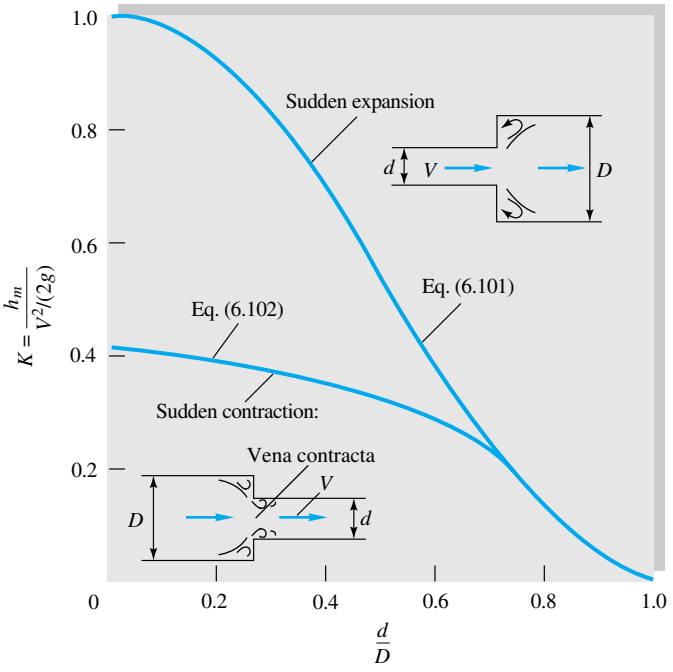


Fig. 6.22 Sudden expansion and contraction losses. Note that the loss is based on velocity head in the small pipe.

ketabline.com Ebook.ketabline.com

fits the empirical formula

$$K_{SC} \approx 0.42\left(1 - \frac{d^2}{D^2}\right) \tag{6.102}$$

up to the value $d/D = 0.76$, above which it merges into the sudden-expansion prediction, Eq. (6.101).

If the expansion or contraction is gradual, the losses are quite different. Figure 6.23 shows the loss through a gradual conical expansion, usually called a *diffuser* [14]. There is a spread in the data, depending upon the boundary-layer conditions in the upstream pipe. A thinner entrance boundary layer, like the entrance profile in Fig. 6.6, gives a smaller loss. Since a diffuser is intendsed to raise the static pressure of the flow, diffuser data list the pressure-recovery coefficient of the flow

$$C_p = \frac{p_2 - p_1}{\frac{1}{2}\rho V_1^2} \tag{6.103}$$

The loss coefficient is related to this parameter by

$$K = \frac{h_m}{V^2/(2g)} = 1 - \frac{d_1^4}{d_2^4} - C_p \tag{6.104}$$

For a given area ratio, the higher the pressure recovery, the lower the loss; hence large C_p means a successful diffuser. From Fig. 6.23 the minimum loss (maximum recovery) occurs for a cone angle 2θ equal to about 5°. Angles smaller than this give a large Moody-type loss because of their excessive length. For cone angles greater than 40 to 60°, the loss is so excessive that it would actually be better to use a sudden expansion.

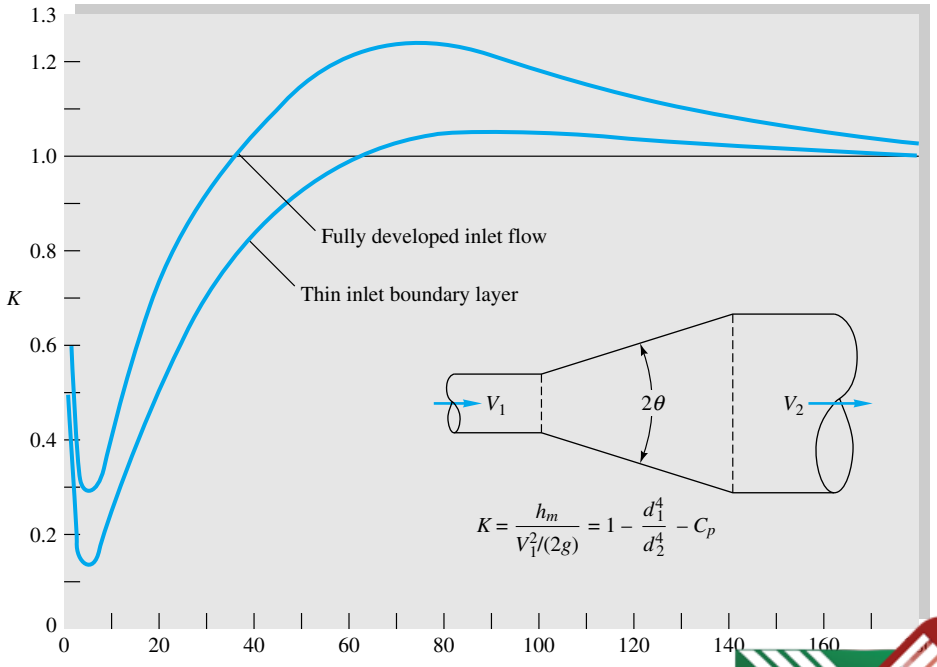


Fig. 6.23 Flow losses in a gradual conical expansion region.

ketabline.com Ebook.ketabline.com

This unexpected effect is due to gross flow separation in a wide-angle diffuser, as we shall see soon when we study boundary layers. Reference 14 has extensive data on diffusers.

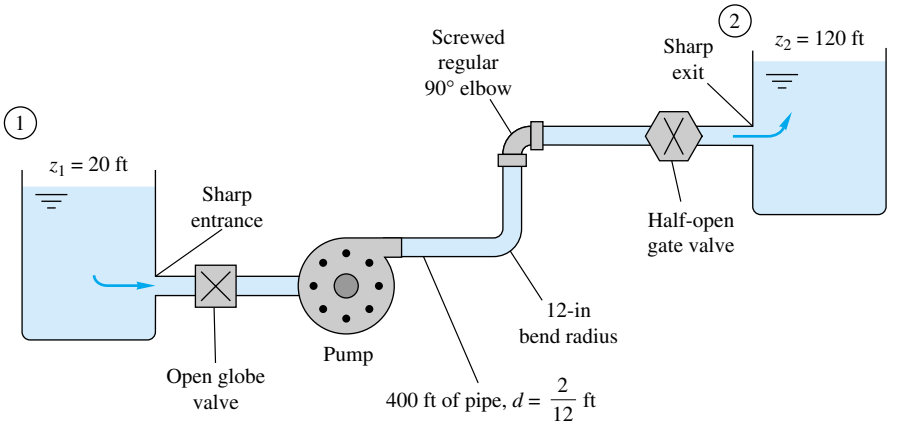
For a gradual *contraction,* the loss is very small, as seen from the following experimental values [15]:

Contraction cone angle 2θ, deg	30	45	60
K for gradual contraction	0.02	0.04	0.07

References 15, 16, 43, and 46 contain additional data on minor losses.

EXAMPLE 6.16

Water, $\rho = 1.94$ slugs/ft^3 and $\nu = 0.000011$ ft^2/s, is pumped between two reservoirs at 0.2 ft^3/s through 400 ft of 2-in-diameter pipe and several minor losses, as shown in Fig. E6.16. The roughness ratio is $\epsilon/d = 0.001$. Compute the pump horsepower required.



E6.16

Solution

Write the steady-flow energy equation between sections 1 and 2, the two reservoir surfaces:

$$\frac{p_1}{\rho g} + \frac{V_1^2}{2g} + z_1 = \left(\frac{p_2}{\rho g} + \frac{V_2^2}{2g} + z_2\right) + h_f + \sum h_m - h_p$$

where h_p is the head increase across the pump. But since $p_1 = p_2$ and $V_1 = V_2 \approx 0$, solve for the pump head

$$h_p = z_2 - z_1 + h_f + \sum h_m = 120 \text{ ft} - 20 \text{ ft} + \frac{V^2}{2g}\left(\frac{fL}{d} + \sum K\right) \tag{1}$$

Now with the flow rate known, calculate

$$V = \frac{Q}{A} = \frac{0.2 \text{ ft}^3/\text{s}}{\frac{1}{4}\pi(\frac{2}{12} \text{ ft})^2} = 9.17 \text{ ft/s}$$

Now list and sum the minor loss coefficients:



ketabline.com Ebook.ketabline.com

Loss	K
Sharp entrance (Fig. 6.21)	0.5
Open globe valve (2 in, Table 6.5)	6.9
12-in bend (Fig. 6.20)	0.15
Regular 90° elbow (Table 6.5)	0.95
Half-closed gate valve (from Fig. 6.18*b*)	2.7
Sharp exit (Fig. 6.21)	1.0
	$\Sigma K = 12.2$

Calculate the Reynolds number and pipe-friction factor

$$\text{Re}_d = \frac{Vd}{\nu} = \frac{9.17(\frac{2}{12})}{0.000011} = 139{,}000$$

For $\epsilon/d = 0.001$, from the Moody chart read $f = 0.0216$. Substitute into Eq. (1)

$$h_p = 100 \text{ ft} + \frac{(9.17 \text{ ft/s})^2}{2(32.2 \text{ ft/s}^2)} \left[\frac{0.0216(400)}{\frac{2}{12}} + 12.2\right]$$

$$= 100 \text{ ft} + 84 \text{ ft} = 184 \text{ ft} \quad \text{pump head}$$

The pump must provide a power to the water of

$$P = \rho g Q h_p = [1.94(32.2) \text{ lbf/ft}^3](0.2 \text{ ft}^3\text{/s})(184 \text{ ft}) = 2300 \text{ ft} \cdot \text{lbf/s}$$

The conversion factor is 1 hp = 550 ft · lbf/s. Therefore

$$P = \frac{2300}{550} = 4.2 \text{ hp} \qquad \textit{Ans.}$$

Allowing for an efficiency of 70 to 80 percent, a pump is needed with an input of about 6 hp.

6.8 Multiple-Pipe Systems[8]

If you can solve the equations for one-pipe systems, you can solve them all; but when systems contain two or more pipes, certain basic rules make the calculations very smooth. Any resemblance between these rules and the rules for handling electric circuits is not coincidental.

Figure 6.24 shows three examples of multiple-pipe systems. The first is a set of three (or more) pipes in series. Rule 1 is that the flow rate is the same in all pipes

$$Q_1 = Q_2 = Q_3 = \text{const}$$

or

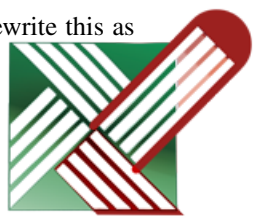
$$V_1 d_1^2 = V_2 d_2^2 = V_3 d_3^2 \tag{6.105}$$

Rule 2 is that the total head loss through the system equals the sum of the head loss in each pipe

$$\Delta h_{A \to B} = \Delta h_1 + \Delta h_2 + \Delta h_3 \tag{6.106}$$

In terms of the friction and minor losses in each pipe, we could rewrite this as

[8]This section may be omitted without loss of continuity.



ketabline.com Ebook.ketabline.com

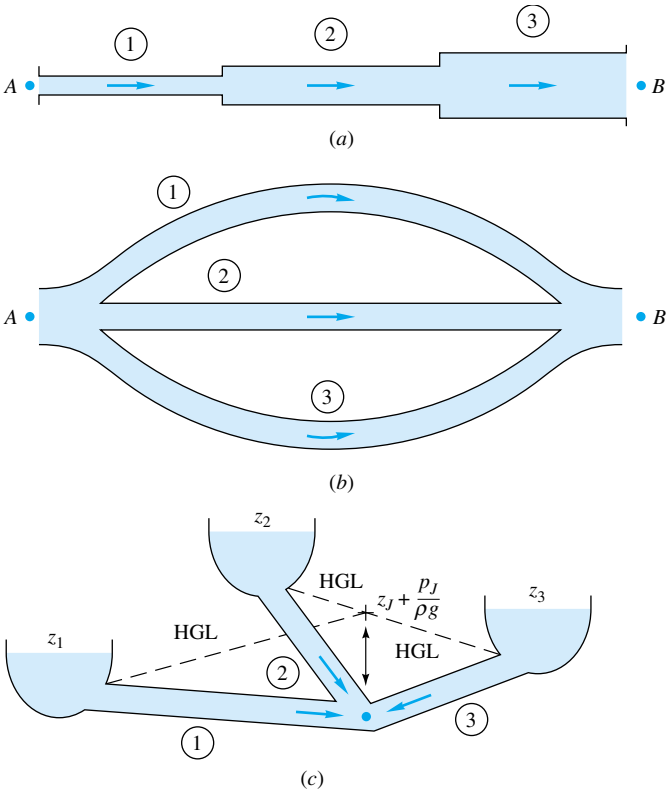


Fig. 6.24 Examples of multiple-pipe systems: (*a*) pipes in series; (*b*) pipes in parallel; (*c*) the three-reservoir junction problem.

$$\Delta h_{A\to B} = \frac{V_1^2}{2g}\left(\frac{f_1 L_1}{d_1} + \sum K_1\right) + \frac{V_2^2}{2g}\left(\frac{f_2 L_2}{d_2} + \sum K_2\right) + \frac{V_3^2}{2g}\left(\frac{f_3 L_3}{d_3} + \sum K_3\right) \tag{6.107}$$

and so on for any number of pipes in the series. Since V_2 and V_3 are proportional to V_1 from Eq. (6.105), Eq. (6.107) is of the form

$$\Delta h_{A\to B} = \frac{V_1^2}{2g}(\alpha_0 + \alpha_1 f_1 + \alpha_2 f_2 + \alpha_3 f_3) \tag{6.108}$$

where the α_i are dimensionless constants. If the flow rate is given, we can evaluate the right-hand side and hence the total head loss. If the head loss is given, a little iteration is needed, since f_1, f_2, and f_3 all depend upon V_1 through the Reynolds number. Begin by calculating f_1, f_2, and f_3, assuming fully rough flow, and the solution for V_1 will converge with one or two iterations. EES is ideal for this purpose.

EXAMPLE 6.17

Given is a three-pipe series system, as in Fig. 6.24*a*. The total pressure drop is $p_A - p_B =$ Pa, and the elevation drop is $z_A - z_B = 5$ m. The pipe data are



ketabline.com Ebook.ketabline.com

Pipe	L, m	d, cm	ϵ, mm	ϵ/d
1	100	8	0.24	0.003
2	150	6	0.12	0.002
3	80	4	0.20	0.005

The fluid is water, $\rho = 1000$ kg/m^3 and $\nu = 1.02 \times 10^{-6}$ m^2/s. Calculate the flow rate Q in m^3/h through the system.

Solution

The total head loss across the system is

$$\Delta h_{A\to B} = \frac{p_A - p_B}{\rho g} + z_A - z_B = \frac{150{,}000}{1000(9.81)} + 5 \text{ m} = 20.3 \text{ m}$$

From the continuity relation (6.105) the velocities are

$$V_2 = \frac{d_1^2}{d_2^2} V_1 = \frac{16}{9} V_1 \qquad V_3 = \frac{d_1^2}{d_3^2} V_1 = 4V_1$$

and

$$\text{Re}_2 = \frac{V_2 d_2}{V_1 d_1} \text{Re}_1 = \frac{4}{3}\text{Re}_1 \qquad \text{Re}_3 = 2\ \text{Re}_1$$

Neglecting minor losses and substituting into Eq. (6.107), we obtain

$$\Delta h_{A\to B} = \frac{V_1^2}{2g}\left[1250 f_1 + 2500\left(\frac{16}{9}\right)^2 f_2 + 2000(4)^2 f_3\right]$$

or

$$20.3 \text{ m} = \frac{V_1^2}{2g}(1250 f_1 + 7900 f_2 + 32{,}000 f_3) \tag{1}$$

This is the form which was hinted at in Eq. (6.108). It seems to be dominated by the third pipe loss $32{,}000 f_3$. Begin by estimating f_1, f_2, and f_3 from the Moody-chart fully rough regime

$$f_1 = 0.0262 \qquad f_2 = 0.0234 \qquad f_3 = 0.0304$$

Substitute in Eq. (1) to find $V_1^2 \approx 2g(20.3)/(33 + 185 + 973)$. The first estimate thus is $V_1 = 0.58$ m/s, from which

$$\text{Re}_1 \approx 45{,}400 \qquad \text{Re}_2 = 60{,}500 \qquad \text{Re}_3 = 90{,}800$$

Hence, from the Moody chart,

$$f_1 = 0.0288 \qquad f_2 = 0.0260 \qquad f_3 = 0.0314$$

Substitution into Eq. (1) gives the better estimate

$$V_1 = 0.565 \text{ m/s} \qquad Q = \tfrac{1}{4}\pi d_1^2 V_1 = 2.84 \times 10^{-3} \text{ m}^3/\text{s}$$

or

$$Q_1 = 10.2 \text{ m}^3/\text{h} \qquad \textit{Ans.}$$

A second iteration gives $Q = 10.22$ m^3/h, a negligible change.

The second multiple-pipe system is the *parallel*-flow case shown
the loss is the same in each pipe, and the total flow is the sum of th



ketabline.com Ebook.ketabline.com

$$\Delta h_{A\to B} = \Delta h_1 = \Delta h_2 = \Delta h_3 \tag{6.109a}$$

$$Q = Q_1 + Q_2 + Q_3 \tag{6.109b}$$

If the total head loss is known, it is straightforward to solve for Q_i in each pipe and sum them, as will be seen in Example 6.18. The reverse problem, of determining ΣQ_i when h_f is known, requires iteration. Each pipe is related to h_f by the Moody relation $h_f = f(L/d)(V^2/2g) = fQ^2/C$, where $C = \pi^2 g d^5/8L$. Thus each pipe has nearly quadratic nonlinear parallel resistance, and head loss is related to total flow rate by

$$h_f = \frac{Q^2}{\left(\sum \sqrt{C_i/f_i}\right)^2} \qquad \text{where } C_i = \frac{\pi^2 g d_i^5}{8L_i} \tag{6.109c}$$

Since the f_i vary with Reynolds number and roughness ratio, one begins Eq. (6.109*c*) by guessing values of f_i (fully rough values are recommended) and calculating a first estimate of h_f. Then each pipe yields a flow-rate estimate $Q_i \approx (C_i h_f/f_i)^{1/2}$ and hence a new Reynolds number and a better estimate of f_i. Then repeat Eq. (6.109*c*) to convergence.

It should be noted that both of these parallel-pipe cases—finding either ΣQ or h_f—are easily solved by EES if reasonable initial guesses are given.

EXAMPLE 6.18

Assume that the same three pipes in Example 6.17 are now in parallel with the same total head loss of 20.3 m. Compute the total flow rate Q, neglecting minor losses.

Solution

From Eq. (6.109*a*) we can solve for each V separately

$$20.3 \text{ m} = \frac{V_1^2}{2g} 1250 f_1 = \frac{V_2^2}{2g} 2500 f_2 = \frac{V_3^2}{2g} 2000 f_3 \tag{1}$$

Guess fully rough flow in pipe 1: $f_1 = 0.0262$, $V_1 = 3.49$ m/s; hence $\text{Re}_1 = V_1 d_1/\nu = 273{,}000$. From the Moody chart read $f_1 = 0.0267$; recompute $V_1 = 3.46$ m/s, $Q_1 = 62.5$ m^3/h. [This problem can also be solved from Eq. (6.66).]

Next guess for pipe 2: $f_2 \approx 0.0234$, $V_2 \approx 2.61$ m/s; then $\text{Re}_2 = 153{,}000$, and hence $f_2 = 0.0246$, $V_2 = 2.55$ m/s, $Q_2 = 25.9$ m^3/h.

Finally guess for pipe 3: $f_3 \approx 0.0304$, $V_3 \approx 2.56$ m/s; then $\text{Re}_3 = 100{,}000$, and hence $f_3 = 0.0313$, $V_3 = 2.52$ m/s, $Q_3 = 11.4$ m^3/h.

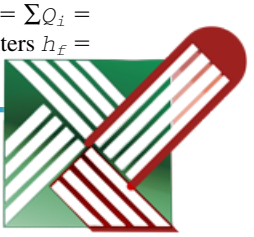
This is satisfactory convergence. The total flow rate is

$$Q = Q_1 + Q_2 + Q_3 = 62.5 + 25.9 + 11.4 = 99.8 \text{ m}^3/\text{h} \qquad \textit{Ans.}$$

These three pipes carry 10 times more flow in parallel than they do in series.



This example is ideal for EES. One enters the pipe data (`L_i, d_i, ε_i`); the fluid properties (`ρ, μ`); the definitions `Q_i = (π/4) d_i^2 V_i`, `Re_i = ρ V_i d_i/μ`, and `h_f = f_i (L_i/d_i) (V_i^2/2g)`; plus the Colebrook formula (6.74) for each friction factor f_i. There is no need to use resistance ideas such as Eq. (6.109*c*). Specify that `f_i > 0` and `Re_i > 4000`. Then, if one enters `Q = ΣQ_i = (99.8/3600) m^3/s`, EES quickly solves for `h_f = 20.3 m`. Conversely, if one enters `h_f = 20.3 m`, EES solves for `Q = 99.8 m^3/h`.



ketabline.com Ebook.ketabline.com

Consider the third example of a *three-reservoir pipe junction,* as in Fig. 6.24*c*. If all flows are considered positive toward the junction, then

$$Q_1 + Q_2 + Q_3 = 0 \tag{6.110}$$

which obviously implies that one or two of the flows must be away from the junction. The pressure must change through each pipe so as to give the same static pressure p_J at the junction. In other words, let the HGL at the junction have the elevation

$$h_J = z_J + \frac{p_J}{\rho g}$$

where p_J is in gage pressure for simplicity. Then the head loss through each, assuming $p_1 = p_2 = p_3 = 0$ (gage) at each reservoir surface, must be such that

$$\begin{aligned} \Delta h_1 &= \frac{V_1^2}{2g}\frac{f_1 L_1}{d_1} = z_1 - h_J \\ \Delta h_2 &= \frac{V_2^2}{2g}\frac{f_2 L_2}{d_2} = z_2 - h_J \\ \Delta h_3 &= \frac{V_3^2}{2g}\frac{f_3 L_3}{d_3} = z_3 - h_J \end{aligned} \tag{6.111}$$

We guess the position h_J and solve Eqs. (6.111) for V_1, V_2, and V_3 and hence Q_1, Q_2, and Q_3, iterating until the flow rates balance at the junction according to Eq. (6.110). If we guess h_J too *high*, the sum $Q_1 + Q_2 + Q_3$ will be *negative* and the remedy is to reduce h_J, and vice versa.

EXAMPLE 6.19

Take the same three pipes as in Example 6.17, and assume that they connect three reservoirs at these surface elevations

$$z_1 = 20 \text{ m} \qquad z_2 = 100 \text{ m} \qquad z_3 = 40 \text{ m}$$

Find the resulting flow rates in each pipe, neglecting minor losses.

Solution

As a first guess, take h_J equal to the middle reservoir height, $z_3 = h_J = 40$ m. This saves one calculation ($Q_3 = 0$) and enables us to get the lay of the land:

Reservoir	h_J, m	$z_i - h_J$, m	f_i	V_i, m/s	Q_i, m³/h	L_i/d_i
1	40	−20	0.0267	−3.43	−62.1	1250
2	40	60	0.0241	4.42	45.0	2500
3	40	0		0	0	2000
					$\sum Q = -17.1$	

Since the sum of the flow rates toward the junction is negative, we guessed h_J to 30 m and repeat:



ketabline.com Ebook.ketabline.com

Reservoir	h_J, m	$z_i - h_J$, m	f_i	V_i, m/s	Q_i, m^3/h
1	30	−10	0.0269	−2.42	−43.7
2	30	70	0.0241	4.78	48.6
3	30	10	0.0317	1.76	8.0
					$\sum Q = 12.9$

This is positive ΣQ, and so we can linearly interpolate to get an accurate guess: $h_J \approx 34.3$ m. Make one final list:

Reservoir	h_J, m	$z_i - h_J$, m	f_i	V_i, m/s	Q_i, m^3/h
1	34.3	−14.3	0.0268	−2.90	−52.4
2	34.3	65.7	0.0241	4.63	47.1
3	34.3	5.7	0.0321	1.32	6.0
					$\sum Q = 0.7$

This is close enough; hence we calculate that the flow rate is 52.4 m^3/h toward reservoir 3, balanced by 47.1 m^3/h away from reservoir 1 and 6.0 m^3/h away from reservoir 3.

One further iteration with this problem would give $h_J = 34.53$ m, resulting in $Q_1 = -52.8$, $Q_2 = 47.0$, and $Q_3 = 5.8$ m^3/h, so that $\Sigma Q = 0$ to three-place accuracy. Pedagogically speaking, we would then be exhausted.

The ultimate case of a multipipe system is the *piping network* illustrated in Fig. 6.25. This might represent a water supply system for an apartment or subdivision or even a city. This network is quite complex algebraically but follows the same basic rules:

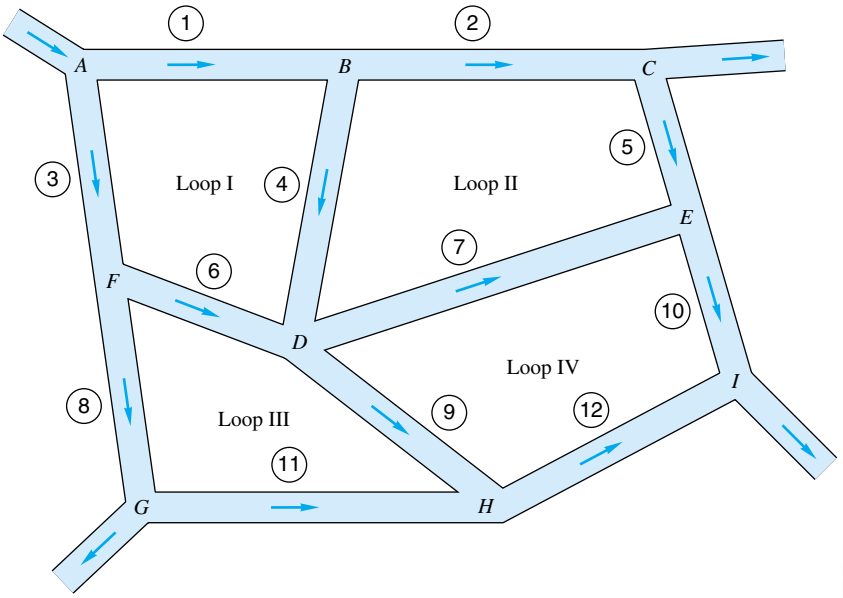


Fig. 6.25 Schematic of a piping network.



ketabline.com Ebook.ketabline.com

1. The net flow into any junction must be zero.
2. The net head loss around any closed loop must be zero. In other words, the HGL at each junction must have one and only one elevation.
3. All head losses must satisfy the Moody and minor-loss friction correlations.

By supplying these rules to each junction and independent loop in the network, one obtains a set of simultaneous equations for the flow rates in each pipe leg and the HGL (or pressure) at each junction. Solution may then be obtained by numerical iteration, as first developed in a hand-calculation technique by Prof. Hardy Cross in 1936 [17]. Computer solution of pipe-network problems is now quite common and covered in at least one specialized text [18]. Solution on microcomputers is also a reality. Some explicit numerical algorithms have been developed by Ormsbee and Wood [19]. Network analysis is quite useful for real water distribution systems if well calibrated with the actual system head-loss data.

6.9 Experimental Duct Flows: Diffuser Performance

The Moody chart is such a great correlation for tubes of any cross section with any roughness or flow rate that we may be deluded into thinking that the world of internal-flow prediction is at our feet. Not so. The theory is reliable only for ducts of constant cross section. As soon as the section varies, we must rely principally upon experiment to determine the flow properties. As mentioned many times before, experiment is a vital part of fluid mechanics.

Literally thousands of papers in the literature report experimental data for specific internal and external viscous flows. We have already seen several examples:

1. Vortex shedding from a cylinder (Fig. 5.2)
2. Drag of a sphere and a cylinder (Fig. 5.3)
3. Hydraulic model of an estuary (Fig. 5.9)
4. Rough-wall pipe flows (Fig. 6.12)
5. Secondary flow in ducts (Fig. 6.16)
6. Minor-duct-loss coefficients (Sec. 6.7)

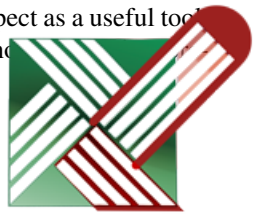
Chapter 7 will treat a great many more external-flow experiments, especially in Sec. 7.5. Here we shall show data for one type of internal flow, the diffuser.

Diffuser Performance

A diffuser, shown in Fig. 6.26*a* and *b*, is an expansion or area increase intended to reduce velocity in order to recover the pressure head of the flow. Rouse and Ince [6] relate that it may have been invented by customers of the early Roman (about 100 A.D.) water supply system, where water flowed continuously and was billed according to pipe size. The ingenious customers discovered that they could increase the flow rate at no extra cost by flaring the outlet section of the pipe.

Engineers have always designed diffusers to increase pressure and reduce kinetic energy of ducted flows, but until about 1950, diffuser design was a combination of art, luck, and vast amounts of empiricism. Small changes in design parameters caused large changes in performance. The Bernoulli equation seemed highly suspect as a useful tool.

Neglecting losses and gravity effects, the incompressible Bernoulli equation predicts that



ketabline.com Ebook.ketabline.com

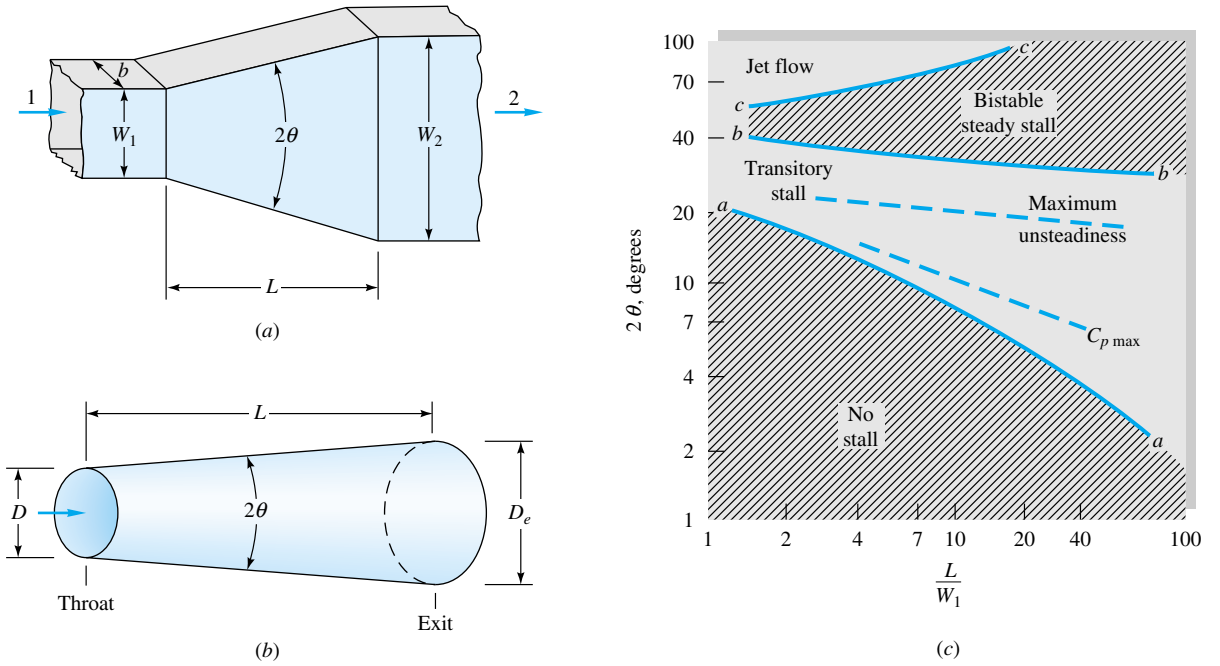


Fig. 6.26 Diffuser geometry and typical flow regimes: (*a*) geometry of a flat-walled diffuser; (*b*) geometry of a conical diffuser; (*c*) flat-diffuser stability map. *(From Ref. 14, by permission of Creare, Inc.)*

$$p + \tfrac{1}{2}\rho V^2 = p_0 = \text{const} \tag{6.112}$$

where p_0 is the stagnation pressure which the fluid would achieve if the fluid were slowed to rest ($V = 0$) without losses.

The basic output of a diffuser is the *pressure-recovery coefficient* C_p, defined as

$$C_p = \frac{p_e - p_t}{p_{0t} - p_t} \tag{6.113}$$

where subscripts e and t mean the exit and the throat (or inlet), respectively. Higher C_p means better performance.

Consider the flat-walled diffuser in Fig. 6.26*a*, where section 1 is the inlet and section 2 the exit. Application of Bernoulli's equation (6.112) to this diffuser predicts that

$$p_{01} = p_1 + \tfrac{1}{2}\rho V_1^2 = p_2 + \tfrac{1}{2}\rho V_2^2 = p_{02}$$

or

$$C_{p,\text{frictionless}} = 1 - \left(\frac{V_2}{V_1}\right)^2 \tag{6.114}$$

Meanwhile, steady one-dimensional continuity would require that

$$Q = V_1 A_1 = V_2 A_2 \tag{6.115}$$

Combining (6.114) and (6.115), we can write the performance in terms of the *area ratio* $\text{AR} = A_2/A_1$, which is a basic parameter in diffuser design:

$$C_{p,\text{frictionless}} = 1 - (\text{AR})^{-2} \tag{6.116}$$

A typical design would have AR = 5:1, for which Eq. (6.116) predicts $C_p = 0.96$, or nearly full recovery. But, in fact, measured values of C_p for this area ratio [14] as high as 0.86 and can be as low as 0.24.



ketabline.com Ebook.ketabline.com

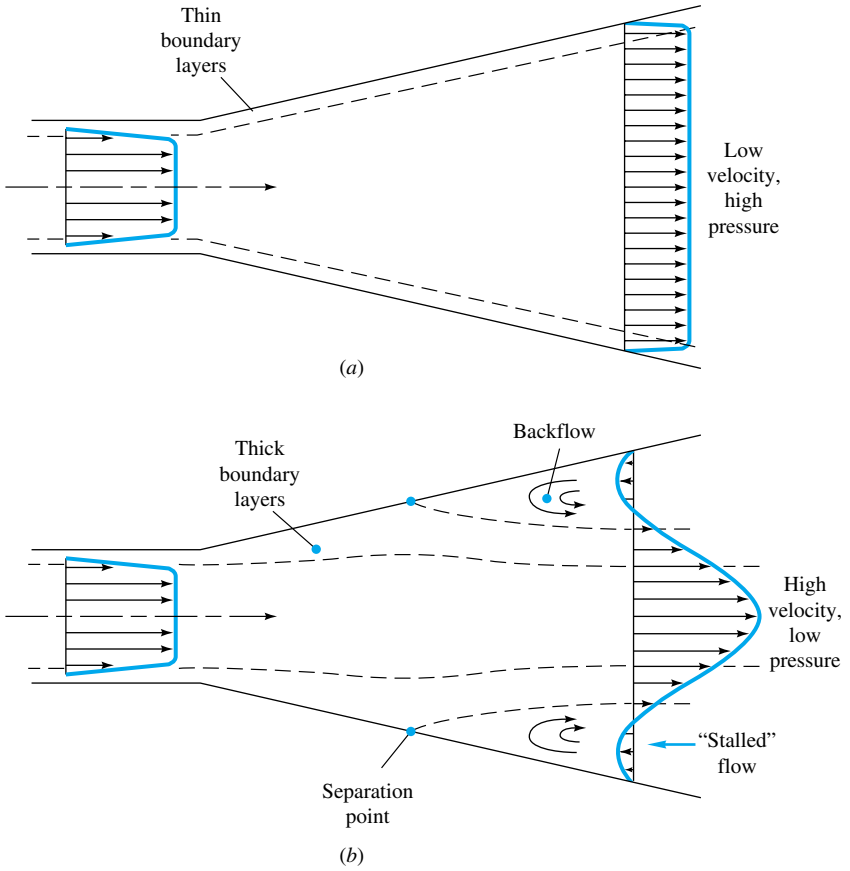


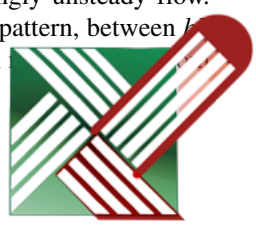
Fig. 6.27 Diffuser performance: (*a*) ideal pattern with good performance; (*b*) actual measured pattern with boundary-layer separation and resultant poor performance.

The basic reason for the discrepancy is flow separation, as sketched in Fig. 6.27. The increasing pressure in the diffuser is an unfavorable gradient (Sec. 7.4), which causes the viscous boundary layers to break away from the walls and greatly reduces the performance. Theories can now predict this behavior (see, e.g., Ref. 20).

As an added complication to boundary-layer separation, the flow patterns in a diffuser are highly variable and were considered mysterious and erratic until 1955, when Kline revealed the structure of these patterns with flow-visualization techniques in a simple water channel.

A complete *stability map* of diffuser flow patterns was published in 1962 by Fox and Kline [21], as shown in Fig. 6.26*c*. There are four basic regions. Below line *aa* there is steady viscous flow, no separation, and moderately good performance. Note that even a very short diffuser will separate, or stall, if its half-angle is greater than 10°.

Between lines *aa* and *bb* is a transitory stall pattern with strongly unsteady flow. Best performance, i.e., highest C_p, occurs in this region. The third pattern, between *bb* and *cc*, is steady bistable stall from one wall only. The stall pattern [illegible] one wall to the other, and performance is poor.



ketabline.com Ebook.ketabline.com

The fourth pattern, above line *cc*, is *jet flow*, where the wall separation is so gross and pervasive that the mainstream ignores the walls and simply passes on through at nearly constant area. Performance is extremely poor in this region.

Dimensional analysis of a flat-walled or conical diffuser shows that C_p should depend upon the following parameters:

1. Any two of the following geometric parameters:
   a. Area ratio AR $= A_2/A_1$ or $(D_e/D)^2$
   b. Divergence angle 2θ
   c. Slenderness L/W_1 or L/D
2. Inlet Reynolds number $\text{Re}_t = V_1W_1/\nu$ or $\text{Re}_t = V_1D/\nu$
3. Inlet Mach number $\text{Ma}_t = V_1/a_1$
4. Inlet boundary-layer *blockage factor* $B_t = A_{\text{BL}}/A_1$, where A_{BL} is the wall area blocked, or displaced, by the retarded boundary-layer flow in the inlet (typically B_t varies from 0.03 to 0.12)

A flat-walled diffuser would require an additional shape parameter to describe its cross section:

5. Aspect ratio AS $= b/W_1$

Even with this formidable list, we have omitted five possible important effects: inlet turbulence, inlet swirl, inlet profile vorticity, superimposed pulsations, and downstream obstruction, all of which occur in practical machinery applications.

The three most important parameters are AR, θ, and B. Typical performance maps for diffusers are shown in Fig. 6.28. For this case of 8 to 9 percent blockage, both the flat-walled and conical types give about the same maximum performance, $C_p = 0.70$, but at different divergence angles (9° flat versus 4.5° conical). Both types fall far short of the Bernoulli estimates of $C_p = 0.93$ (flat) and 0.99 (conical), primarily because of the blockage effect.

From the data of Ref. 14 we can determine that, in general, performance decreases with blockage and is approximately the same for both flat-walled and conical diffusers, as shown in Table 6.6. In all cases, the best conical diffuser is 10 to 80 percent longer than the best flat-walled design. Therefore, if length is limited in the design, the flat-walled design will give the better performance.

The experimental design of a diffuser is an excellent example of a successful attempt to minimize the undesirable effects of adverse pressure gradient and flow separation.

Table 6.6 Maximum Diffuser-Performance Data [14]

Inlet blockage B_t	Flat-walled		Conical	
	$C_{p,\max}$	L/W_1	$C_{p,\max}$	L/d
0.02	0.86	18	0.83	20
0.04	0.80	18	0.78	22
0.06	0.75	19	0.74	24
0.08	0.70	20	0.71	26
0.10	0.66	18	0.68	28
0.12	0.63	16	0.65	30



ketabline.com Ebook.ketabline.com

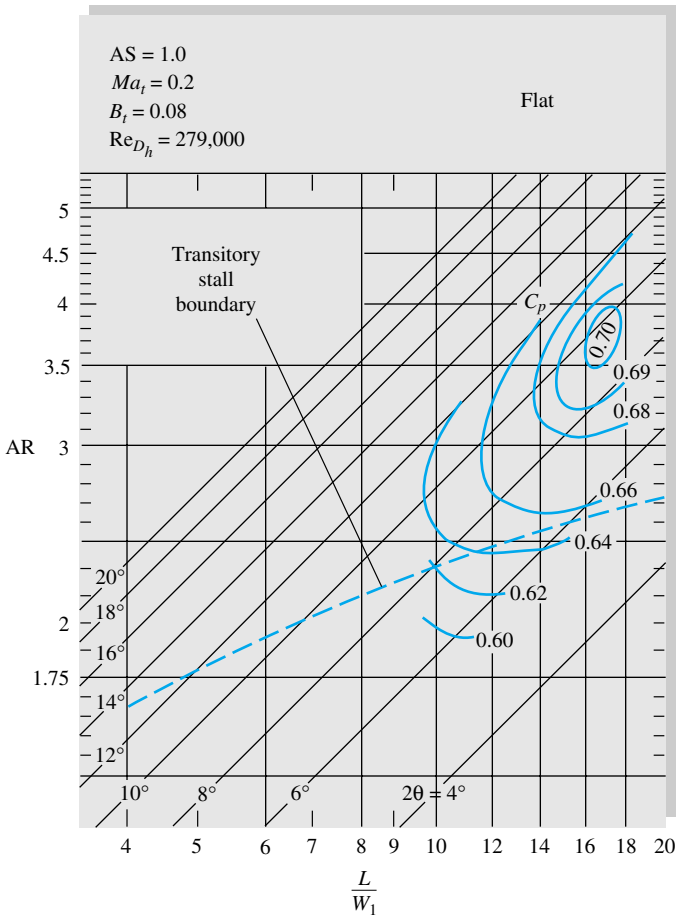


Fig. 6.28a Typical performance maps for flat-wall and conical diffusers at similar operating conditions: (*a*) flat wall. *(From Ref. 14, by permission of Creare, Inc.)*

6.10 Fluid Meters

Almost all practical fluids engineering problems are associated with the need for an accurate flow measurement. There is a need to measure *local* properties (velocity, pressure, temperature, density, viscosity, turbulent intensity), *integrated* properties (mass flow and volume flow), and *global* properties (visualization of the entire flow field). We shall concentrate in this section on velocity and volume-flow measurements.

We have discussed pressure measurement in Sec. 2.10. Measurement of other thermodynamic properties, such as density, temperature, and viscosity, is beyond the scope of this text and is treated in specialized books such as Refs. 22 and 23. Global visualization techniques were discussed in Sec. 1.7 for low-speed flows, and the special optical techniques used in high-speed flows are treated in Ref. 21 of Chap. 1. Flow-measurement schemes suitable for open-channel and other free-surface flows are treated in Chap. 10.

Local-Velocity Measurements

Velocity averaged over a small region, or point, can be measured b
physical principles, listed in order of increasing complexity and so



ketabline.com Ebook.ketabline.com

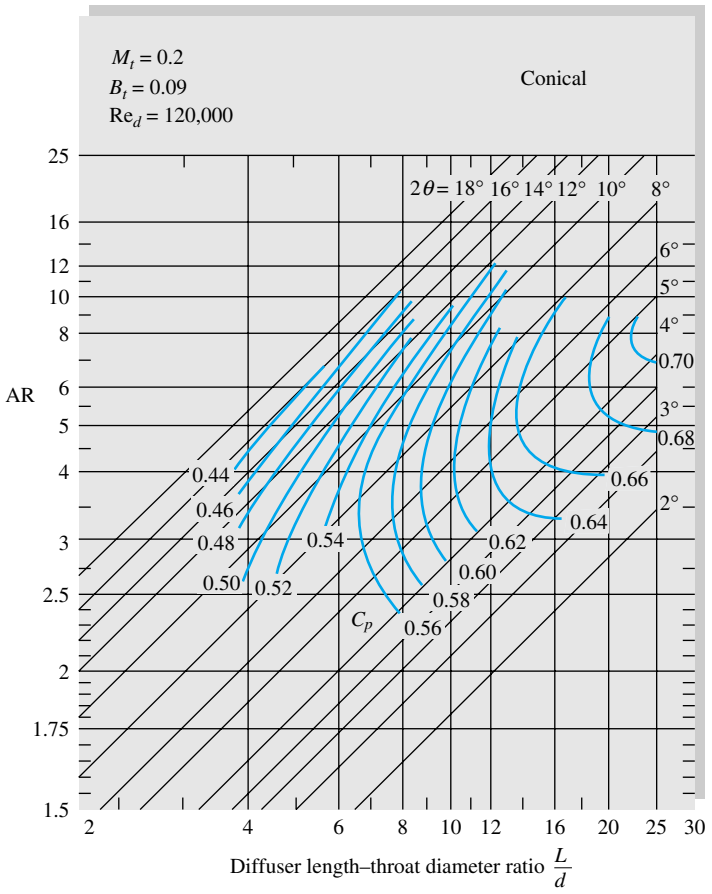
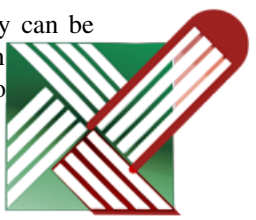


Fig. 6.28b Typical performance maps for flat-wall and conical diffusers at similar operating conditions: (*b*) conical wall. *(From Ref. 14, by permission of Creare, Inc.)*

1. Trajectory of floats or neutrally buoyant particles
2. Rotating mechanical devices
   a. Cup anemometer
   b. Savonius rotor
   c. Propeller meter
   d. Turbine meter
3. Pitot-static tube (Fig. 6.30)
4. Electromagnetic current meter
5. Hot wires and hot films
6. Laser-doppler anemometer (LDA)

Some of these meters are sketched in Fig. 6.29.

Floats or buoyant particles. A simple but effective estimate of flow velocity can be found from visible particles entrained in the flow. Examples include flakes on face of a channel flow, small neutrally buoyant spheres mixed with a liquid, o



ketabline.com Ebook.ketabline.com

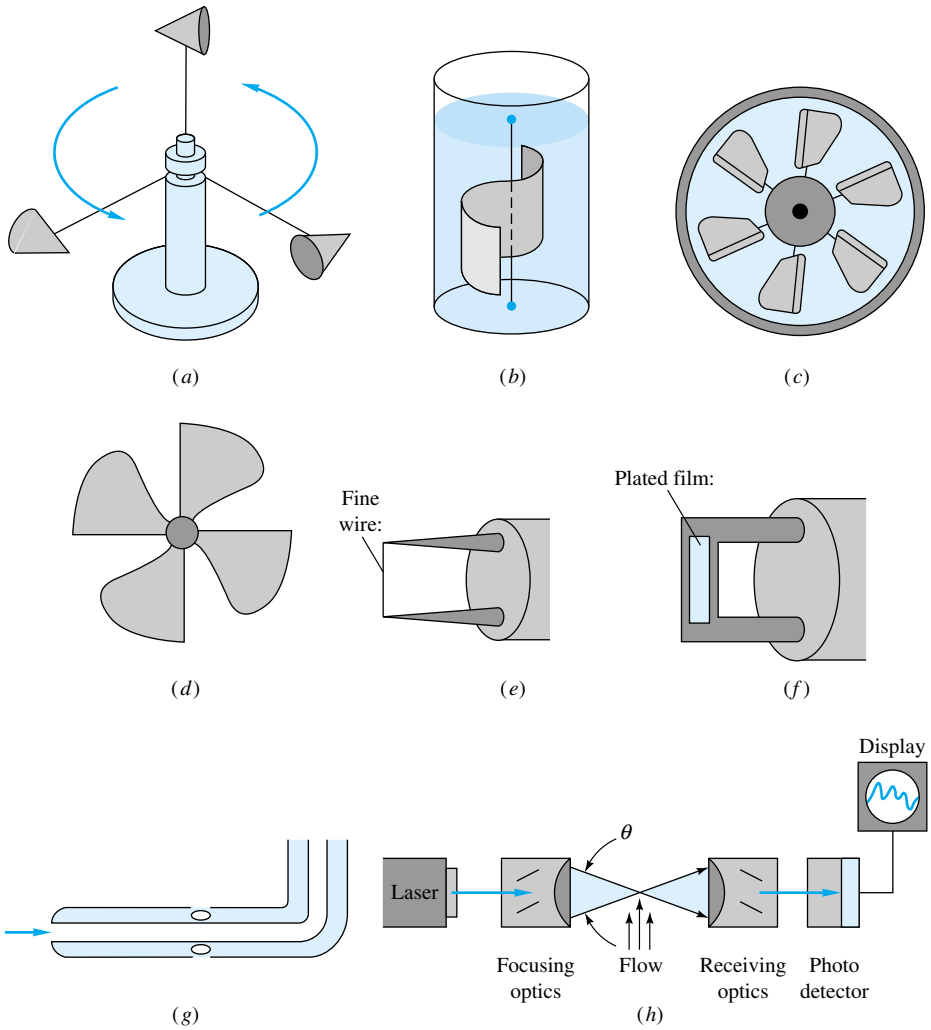
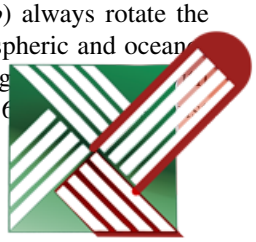


Fig. 6.29 Eight common velocity meters: (*a*) three-cup anemometer; (*b*) Savonius rotor; (*c*) turbine mounted in a duct; (*d*) free-propeller meter; (*e*) hot-wire anemometer; (*f*) hot-film anemometer; (*g*) pitot-static tube; (*h*) laser-doppler anemometer.

gen bubbles. Sometimes gas flows can be estimated from the motion of entrained dust particles. One must establish whether the particle motion truly simulates the fluid motion. Floats are commonly used to track the movement of ocean waters and can be designed to move at the surface, along the bottom, or at any given depth [24]. Many official tidal-current charts [25] were obtained by releasing and timing a floating spar attached to a length of string. One can release whole groups of spars to determine a flow pattern.

Rotating sensors. The rotating devices of Fig. 6.29*a* to *d* can be used in either gases or liquids, and their rotation rate is approximately proportional to the flow velocity. The cup anemometer (Fig. 6.29*a*) and Savonius rotor (Fig. 6.29*b*) always rotate the same way, regardless of flow direction. They are popular in atmospheric and oceanographic applications and can be fitted with a direction vane to align the flow. The ducted-propeller (Fig. 6.29*c*) and free-propeller (Fig. 6



ketabline.com Ebook.ketabline.com

be aligned with the flow parallel to their axis of rotation. They can sense reverse flow because they will then rotate in the opposite direction. All these rotating sensors can be attached to counters or sensed by electromagnetic or slip-ring devices for either a continuous or a digital reading of flow velocity. All have the disadvantage of being relatively large and thus not representing a "point."

Pitot-static tube. A slender tube aligned with the flow (Figs. 6.29*g* and 6.30) can measure local velocity by means of a pressure difference. It has sidewall holes to measure the static pressure p_s in the moving stream and a hole in the front to measure the *stagnation* pressure p_0, where the stream is decelerated to zero velocity. Instead of measuring p_0 or p_s separately, it is customary to measure their difference with, say, a transducer, as in Fig. 6.30.

If $\mathrm{Re}_D > 1000$, where D is the probe diameter, the flow around the probe is nearly frictionless and Bernoulli's relation, Eq. (3.77), applies with good accuracy. For incompressible flow

$$p_s + \tfrac{1}{2}\rho V^2 + \rho g z_s \approx p_0 + \tfrac{1}{2}\rho(0)^2 + \rho g z_0$$

Assuming that the elevation pressure difference $\rho g(z_s - z_0)$ is negligible, this reduces to

$$V \approx \left[2\frac{(p_0 - p_s)}{\rho}\right]^{1/2} \tag{6.117}$$

This is the *Pitot formula,* named after the French engineer who designed the device in 1732.

The primary disadvantage of the pitot tube is that it must be aligned with the flow direction, which may be unknown. For yaw angles greater than 5°, there are substantial errors in both the p_0 and p_s measurements, as shown in Fig. 6.30. The pitot-static tube is useful in liquids and gases; for gases a compressibility correction is necessary if the stream Mach number is high (Chap. 9). Because of the slow response of the fluid-filled tubes leading to the pressure sensors, it is not useful for unsteady-flow measurements. It does resemble a point and can be made small enough to measure, e.g.,

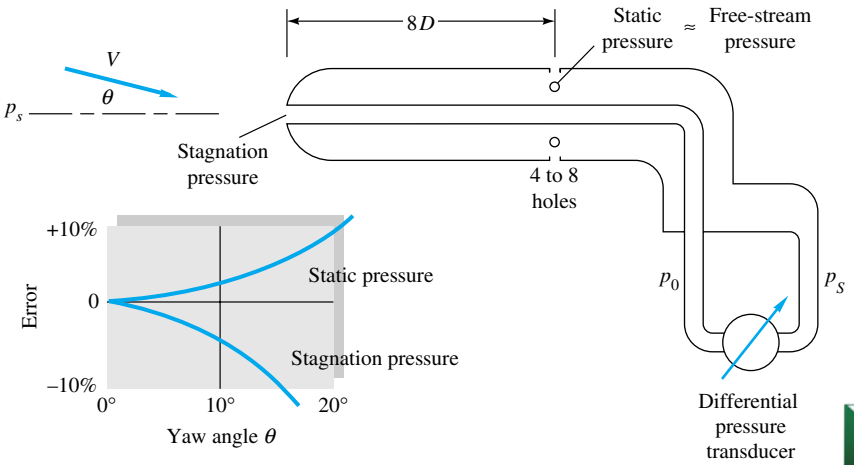


Fig. 6.30 Pitot-static tube for combined measurement of static and stagnation pressure in a moving stream.

ketabline.com Ebook.ketabline.com

blood flow in arteries and veins. It is not suitable for low-velocity measurement in gases because of the small pressure differences developed. For example, if $V = 1$ ft/s in standard air, from Eq. (6.117) we compute $p_0 - p$ equal to only 0.001 lbf/ft^2 (0.048 Pa). This is beyond the resolution of most pressure gages.

Electromagnetic meter. If a magnetic field is applied across a conducting fluid, the fluid motion will induce a voltage across two electrodes placed in or near the flow. The electrodes can be streamlined or built into the wall, and they cause little or no flow resistance. The output is very strong for highly conducting fluids such as liquid metals. Seawater also gives good output, and electromagnetic current meters are in common use in oceanography. Even low-conductivity fresh water can be measured by amplifying the output and insulating the electrodes. Commercial instruments are available for most liquid flows but are relatively costly. Electromagnetic flowmeters are treated in Ref. 26.

Hot-wire anemometer. A very fine wire ($d = 0.01$ mm or less) heated between two small probes, as in Fig. 6.29*e*, is ideally suited to measure rapidly fluctuating flows such as the turbulent boundary layer. The idea dates back to work by L. V. King in 1914 on heat loss from long thin cylinders. If electric power is supplied to heat the cylinder, the loss varies with flow velocity across the cylinder according to *King's law*

$$q = I^2R \approx a + b(\rho V)^n \tag{6.118}$$

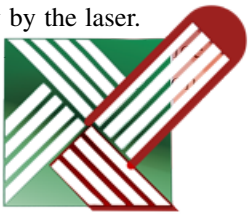
where $n \approx \frac{1}{3}$ at very low Reynolds numbers and equals $\frac{1}{2}$ at high Reynolds numbers. The hot wire normally operates in the high-Reynolds-number range but should be calibrated in each situation to find the best-fit a, b, and n. The wire can be operated either at constant current I, so that resistance R is a measure of V, or at constant resistance R (constant temperature), with I a measure of velocity. In either case, the output is a nonlinear function of V, and the equipment should contain a *linearizer* to produce convenient velocity data. Many varieties of commercial hot-wire equipment are available, as are do-it-yourself designs [27]. Excellent detailed discussions of the hot wire are given in Refs. 1 and 28.

Because of its frailty, the hot wire is not suited to liquid flows, whose high density and entrained sediment will knock the wire right off. A more stable yet quite sensitive alternative for liquid-flow measurement is the hot-film anemometer (Fig. 6.29*f*). A thin metallic film, usually platinum, is plated onto a relatively thick support which can be a wedge, a cone, or a cylinder. The operation is similar to the hot wire. The cone gives best response but is liable to error when the flow is yawed to its axis.

Hot wires can easily be arranged in groups to measure two- and three-dimensional velocity components.

Laser-doppler anemometer. In the LDA a laser beam provides highly focused, coherent monochromatic light which is passed through the flow. When this light is scattered from a moving particle in the flow, a stationary observer can detect a change, or *doppler shift*, in the frequency of the scattered light. The shift Δf is proportional to the velocity of the particle. There is essentially zero disturbance of the flow by the laser.

Figure 6.29*h* shows the popular dual-beam mode of the LDA. splits the laser into two beams, which cross the flow at an angle θ.



ketabline.com Ebook.ketabline.com

which is the measuring volume or resolution of the measurement, resembles an ellipsoid about 0.5 mm wide and 0.1 mm in diameter. Particles passing through this measuring volume scatter the beams; they then pass through receiving optics to a photodetector which converts the light to an electric signal. A signal processor then converts electric frequency to a voltage which can be either displayed or stored. If λ is the wavelength of the laser light, the measured velocity is given by

$$V = \frac{\lambda \, \Delta f}{2 \sin (\theta/2)} \tag{6.119}$$

Multiple components of velocity can be detected by using more than one photodetector and other operating modes. Either liquids or gases can be measured as long as scattering particles are present. In liquids, normal impurities serve as scatterers, but gases may have to be seeded. The particles may be as small as the wavelength of the light. Although the measuring volume is not as small as with a hot wire, the LDA is capable of measuring turbulent fluctuations.

The advantages of the LDA are as follows:

1. No disturbance of the flow
2. High spatial resolution of the flow field
3. Velocity data that are independent of the fluid thermodynamic properties
4. An output voltage that is linear with velocity
5. No need for calibration

The disadvantages are that both the apparatus and the fluid must be transparent to light and that the cost is high (a basic system shown in Fig. 6.29*h* begins at about $50,000).

Once installed, an LDA can map the entire flow field in minutest detail. To truly appreciate the power of the LDA, one should examine, e.g., the amazingly detailed three-dimensional flow profiles measured by Eckardt [29] in a high-speed centrifugal compressor impeller. Extensive discussions of laser velocimetry are given in Refs. 38 and 39.

EXAMPLE 6.20

The pitot-static tube of Fig. 6.30 uses mercury as a manometer fluid. When it is placed in a water flow, the manometer height reading is $h = 8.4$ in. Neglecting yaw and other errors, what is the flow velocity V in ft/s?

Solution

From the two-fluid manometer relation (2.33), with $z_A = z_2$, the pressure difference is related to h by

$$p_0 - p_s = (\gamma_M - \gamma_w)h$$

Taking the specific weights of mercury and water from Table 2.1, we have

$$p_0 - p_s = (846 - 62.4 \text{ lbf/ft}^3) \frac{8.4}{12} \text{ ft} = 549 \text{ lbf/ft}^2$$

The density of water is $62.4/32.2 = 1.94$ slugs/ft^3. Introducing these values into the pi formula (6.117), we obtain



ketabline.com Ebook.ketabline.com

$$V = \left[\frac{2(549 \text{ lbf/ft}^2)}{1.94 \text{ slugs/ft}^3}\right]^{1/2} = 23.8 \text{ ft/s} \qquad \textit{Ans.}$$

Since this is a low-speed flow, no compressibility correction is needed.

Volume-Flow Measurements

It is often desirable to measure the integrated mass, or volume flow, passing through a duct. Accurate measurement of flow is vital in billing customers for a given amount of liquid or gas passing through a duct. The different devices available to make these measurements are discussed in great detail in the ASME text on fluid meters [30]. These devices split into two classes: mechanical instruments and head-loss instruments.

The mechanical instruments measure actual mass or volume of fluid by trapping it and counting it. The various types of measurement are

1. Mass measurement
   a. Weighing tanks
   b. Tilting traps
2. Volume measurement
   a. Volume tanks
   b. Reciprocating pistons
   c. Rotating slotted rings
   d. Nutating disk
   e. Sliding vanes
   f. Gear or lobed impellers
   g. Reciprocating bellows
   h. Sealed-drum compartments

The last three of these are suitable for gas flow measurement.

The head-loss devices obstruct the flow and cause a pressure drop which is a measure of flux:

1. Bernoulli-type devices
   a. Thin-plate orifice
   b. Flow nozzle
   c. Venturi tube
2. Friction-loss devices
   a. Capillary tube
   b. Porous plug

The friction-loss meters cause a large nonrecoverable head loss and obstruct the flow too much to be generally useful.

Six other widely used meters operate on different physical principles:

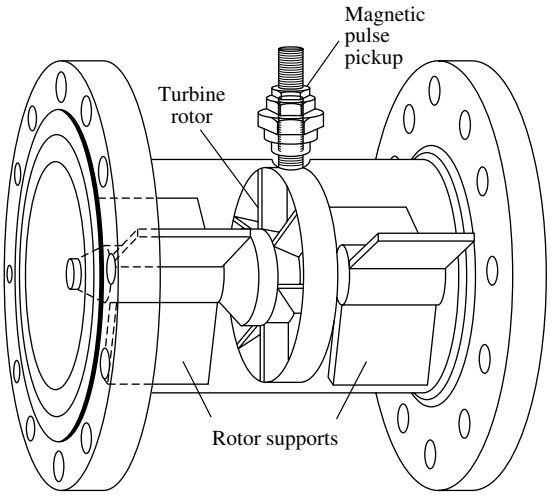
1. Turbine meter
2. Vortex meter
3. Ultrasonic flowmeter
4. Rotameter
5. Coriolis mass flowmeter
6. Laminar flow element



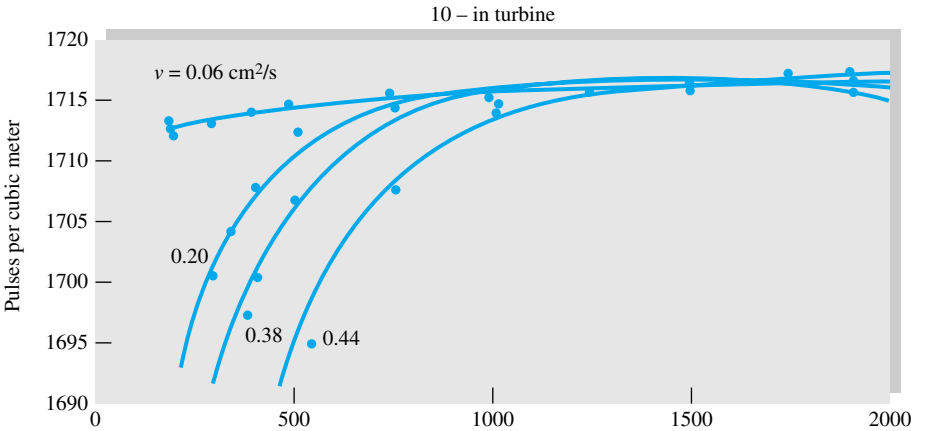
ketabline.com Ebook.ketabline.com

Turbine meter. The turbine meter, sometimes called a *propeller meter*, is a freely rotating propeller which can be installed in a pipeline. A typical design is shown in Fig. 6.31*a*. There are flow straighteners upstream of the rotor, and the rotation is measured by electric or magnetic pickup of pulses caused by passage of a point on the rotor. The rotor rotation is approximately proportional to the volume flow in the pipe.

A major advantage of the turbine meter is that each pulse corresponds to a finite incremental volume of fluid, and the pulses are digital and can be summed easily. Liquid-flow turbine meters have as few as two blades and produce a constant number of pulses per unit fluid volume over a 5 : 1 flow-rate range with ± 0.25 percent accuracy. Gas meters need many blades to produce sufficient torque and are accurate to ± 1 percent.



(*a*)



(*b*)

Fig. 6.31 The turbine meter widely used in the oil, gas, and water supply industries: (*a*) basic design; (*b*) typical calibration curve for a range of crude oils. *(Daniel Industries, Inc., Flow Products Division.)*

ketabline.com Ebook.ketabline.com



Fig. 6.32 A Commercial handheld wind-velocity turbine meter. *(Courtesy of Nielsen-Kellerman Company.)*

Since turbine meters are very individualistic, flow calibration is an absolute necessity. A typical liquid-meter calibration curve is shown in Fig. 6.31*b*. Researchers attempting to establish universal calibration curves have met with little practical success as a result of manufacturing variabilities.

Turbine meters can also be used in unconfined flow situations, such as winds or ocean currents. They can be compact, even microsize with two or three component directions. Figure 6.32 illustrates a handheld wind velocity meter which uses a seven-bladed turbine with a calibrated digital output. The accuracy of this device is quoted at $\pm$ 2 percent.

Vortex flowmeters. Recall from Fig. 5.2 that a bluff body placed in a uniform cross-flow sheds alternating vortices at a nearly uniform Strouhal number $\text{St} = fL/U$, where U is the approach velocity and L is a characteristic body width. Since L and St are constant, this means that the shedding frequency is proportional to velocity

$$f = (\text{const})(U) \tag{6.120}$$

The vortex meter introduces a shedding element across a pipe flow and picks up the shedding frequency downstream with a pressure, ultrasonic, or heat-transfer type of sensor. A typical design is shown in Fig. 6.33.

The advantages of a vortex meter are as follows:

1. Absence of moving parts
2. Accuracy to $\pm$ 1 percent over a wide flow-rate range (up to 100 : 1)
3. Ability to handle very hot or very cold fluids
4. Requirement of only a short pipe length
5. Calibration insensitive to fluid density or viscosity

For further details see Ref. 40.



ketabline.com Ebook.ketabline.com

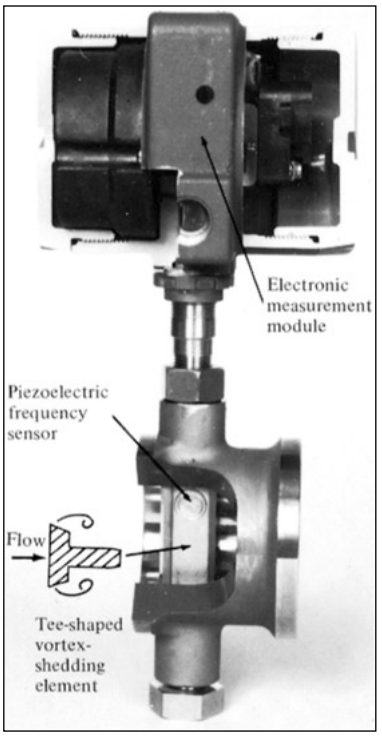
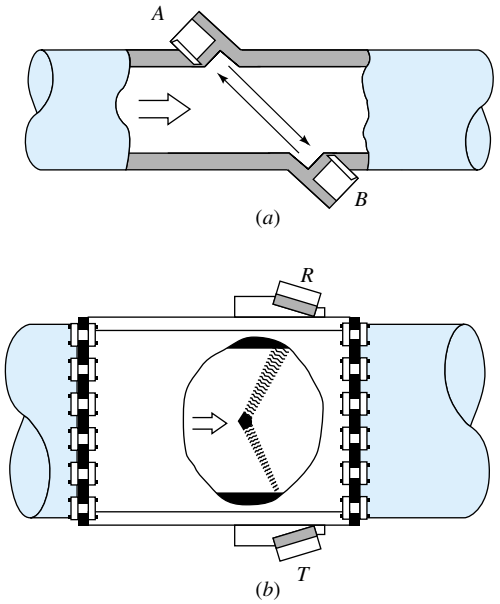


Fig. 6.33 A vortex flowmeter. *(The Foxboro Company.)*





(c)

Fig. 6.34 Ultrasonic flowmeters: (*a*) pulse type; (*b*) doppler-shift type *(from Ref. 41)*; (portable noninvasive installation *(courtesy of Polysonics Inc., Houston, TX).*



ketabline.com Ebook.ketabline.com

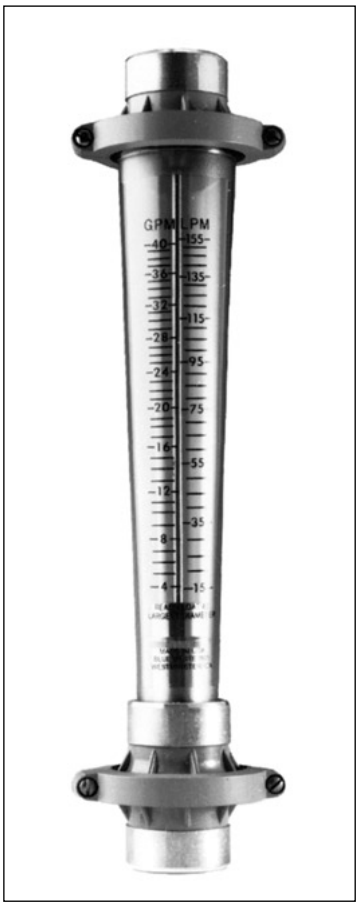


Fig. 6.35 A commercial rotameter. The float rises in the tapered tube to an equilibrium position which is a measure of the fluid-flow rate. *(Courtesy of Blue White Industries, Westminster, CA.)*

Ultrasonic flowmeters. The sound-wave analog of the laser velocimeter of Fig. 6.29*h* is the ultrasonic flowmeter. Two examples are shown in Fig. 6.34. The pulse-type flowmeter is shown in Fig. 6.34*a*. Upstream piezoelectric transducer A is excited with a short sonic pulse which propagates across the flow to downstream transducer B. The arrival at B triggers another pulse to be created at A, resulting in a regular pulse frequency f_A. The same process is duplicated in the reverse direction from B to A, creating frequency f_B. The difference $f_A - f_B$ is proportional to the flow rate. Figure 6.33*b* shows a doppler-type arrangement, where sound waves from transmitter T are scattered by particles or contaminants in the flow to receiver R. Comparison of the two signals reveals a doppler frequency shift which is proportional to the flow rate. Ultrasonic meters are nonintrusive and can be directly attached to pipe flows in the field (Fig. 6.34*c*). Their quoted uncertainty of $\pm$ 1 to 2 percent can rise to $\pm$ 5 percent or more due to irregularities in velocity profile, fluid temperature, or Reynolds number. For further details see Ref. 41.

Rotameter. The variable-area transparent *rotameter* of Fig. 6.35 has a float which, under the action of flow, rises in the vertical tapered tube and takes a certain equilibrium position for any given flow rate. A student exercise for the forces on the float would yield the approximate relation

$$Q = C_d A_a \left(\frac{2W_{\text{net}}}{A_{\text{float}} \rho_{\text{fluid}}} \right)^{1/2} \tag{6.121}$$

where W_{net} is the float's net weight in the fluid, $A_a = A_{\text{tube}} - A_{\text{float}}$ is the annular area between the float and the tube, and C_d is a dimensionless discharge coefficient of order unity, for the annular constricted flow. For slightly tapered tubes, A_a varies nearly linearly with the float position, and the tube may be calibrated and marked with a flow-rate scale, as in Fig. 6.35. The rotameter thus provides a readily visible measure of the flow rate. Capacity may be changed by using different-sized floats. Obviously the tube must be vertical, and the device does not give accurate readings for fluids containing high concentrations of bubbles or particles.

Coriolis mass flowmeter. Most commercial meters measure *volume* flow, with mass flow then computed by multiplying by the nominal fluid density. An attractive modern alternative is a *mass* flowmeter which operates on the principle of the Coriolis acceleration associated with noninertial coordinates [recall Fig. 3.12 and the Coriolis term $2\Omega \times V$ in Eq. (3.48)]. The output of the meter is directly proportional to mass flow.

Figure 6.36 is a schematic of a Coriolis device, to be inserted into a piping system. The flow enters a double-loop, double-tube arrangement which is electromagnetically vibrated at a high natural frequency (amplitude < 1 mm and frequency > 100 Hz). The up flow induces inward loop motion, while the down flow creates outward loop motion, both due to the Coriolis effect. Sensors at both ends register a phase difference which is proportional to mass flow. Quoted accuracy is approximately $\pm$ 0.2 percent of full scale.

Laminar flow element. In many, perhaps most, commercial flowmeters, the flow through the meter is turbulent and the variation of flow rate with pressure drop is nonlinear. In laminar duct flow, however, Q is linearly proportional to Δp, as in Eq. (6.44): $Q = [\pi R^4/(8\mu L)]\, \Delta p$. Thus a *laminar* flow sensing element is attractive since its calibration will be linear. To ensure laminar flow for what otherwise



ketabline.com Ebook.ketabline.com

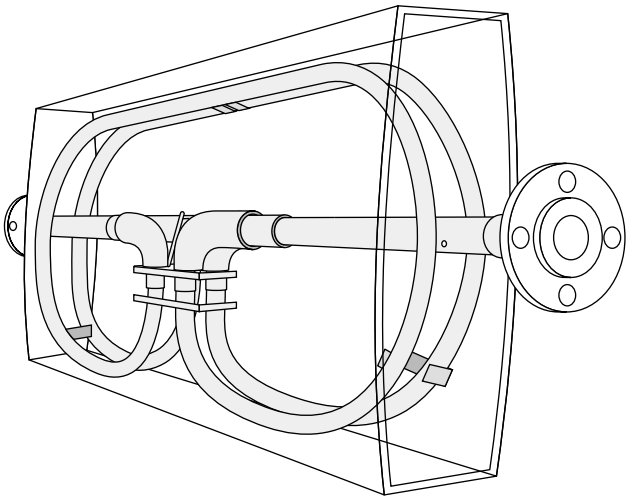


Fig. 6.36 A Coriolis mass flowmeter. *(Courtesy of ABB Instrumentation, Inc.)*

lent condition, all or part of the fluid is directed into small passages, each of which has a low (laminar) Reynolds number. A honeycomb is a popular design.

Figure 6.37 uses axial flow through a narrow annulus to effect laminar flow. The theory again predicts $Q \propto \Delta p$, as in Eq. (6.92). However, the flow is very sensitive to passage size; for example, halving the annulus clearance increases Δp more than eight

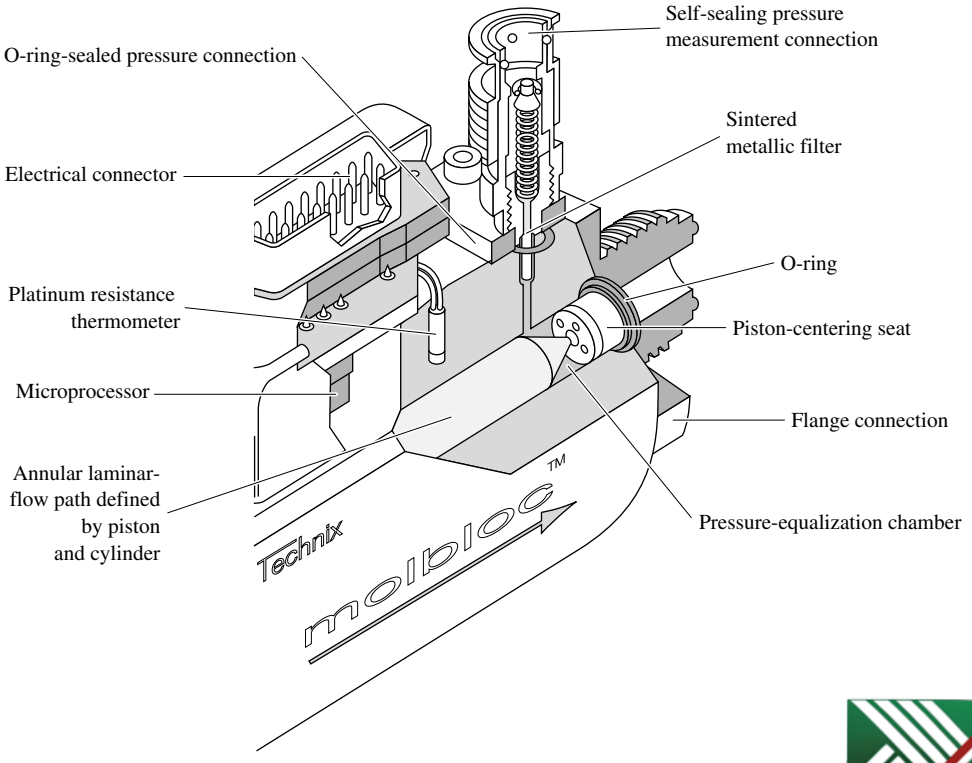


Fig. 6.37 A complete flowmeter system using a laminar-flow element (in this case a narrow annulus). The flow rate is linearly proportional to the pressure drop. *(Courtesy of Martin Girard, DH Instruments, Inc.)*



ketabline.com Ebook.ketabline.com

times. Careful calibration is thus necessary. In Fig. 6.37 the laminar-flow concept has been synthesized into a complete mass-flow system, with temperature control, differential pressure measurement, and a microprocessor all self-contained. The accuracy of this device is rated at ± 0.2 percent.

Bernoulli obstruction theory. Consider the generalized flow obstruction shown in Fig. 6.38. The flow in the basic duct of diameter D is forced through an obstruction of diameter d; the β ratio of the device is a key parameter

$$\beta = \frac{d}{D} \tag{6.122}$$

After leaving the obstruction, the flow may neck down even more through a vena contracta of diameter $D_2 < d$, as shown. Apply the Bernoulli and continuity equations for incompressible steady frictionless flow to estimate the pressure change:

Continuity: $$Q = \frac{\pi}{4}D^2V_1 = \frac{\pi}{4}D_2^2V_2$$

Bernoulli: $$p_0 = p_1 + \tfrac{1}{2}\rho V_1^2 = p_2 + \tfrac{1}{2}\rho V_2^2$$

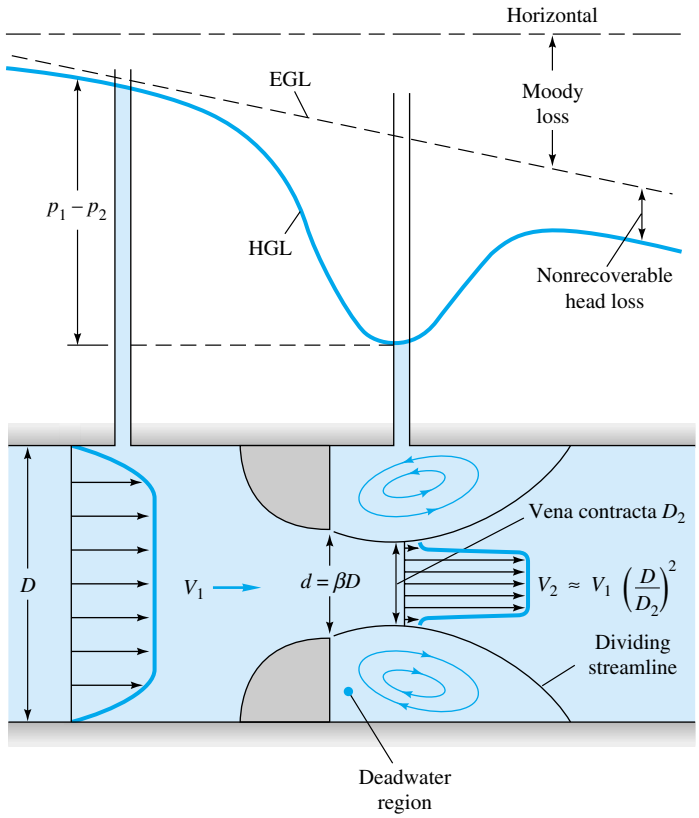


Fig. 6.38 Velocity and pressure change through a generalized Bernoulli obstruction meter.



ketabline.com Ebook.ketabline.com

Eliminating V_1, we solve these for V_2 or Q in terms of the pressure change $p_1 - p_2$:

$$\frac{Q}{A_2} = V_2 \approx \left[\frac{2(p_1 - p_2)}{\rho(1 - D_2^4/D^4)}\right]^{1/2} \tag{6.123}$$

But this is surely inaccurate because we have neglected friction in a duct flow, where we know friction will be very important. Nor do we want to get into the business of measuring vena contracta ratios D_2/d for use in (6.123). Therefore we assume that $D_2/D \approx \beta$ and then calibrate the device to fit the relation

$$Q = A_t V_t = C_d A_t \left[\frac{2(p_1 - p_2)/\rho}{1 - \beta^4}\right]^{1/2} \tag{6.124}$$

where subscript t denotes the throat of the obstruction. The dimensionless *discharge coefficient* C_d accounts for the discrepancies in the approximate analysis. By dimensional analysis for a given design we expect

$$C_d = f(\beta, \mathrm{Re}_D) \quad \text{where} \quad \mathrm{Re}_D = \frac{V_1 D}{\nu} \tag{6.125}$$

The geometric factor involving β in (6.124) is called the *velocity-of-approach factor*

$$E = (1 - \beta^4)^{-1/2} \tag{6.126}$$

One can also group C_d and E in Eq. (6.124) to form the dimensionless *flow coefficient* α

$$\alpha = C_d E = \frac{C_d}{(1 - \beta^4)^{1/2}} \tag{6.127}$$

Thus Eq. (6.124) can be written in the equivalent form

$$Q = \alpha A_t \left[\frac{2(p_1 - p_2)}{\rho}\right]^{1/2} \tag{6.128}$$

Obviously the flow coefficient is correlated in the same manner:

$$\alpha = f(\beta, \mathrm{Re}_D) \tag{6.129}$$

Occasionally one uses the throat Reynolds number instead of the approach Reynolds number

$$\mathrm{Re}_d = \frac{V_t d}{\nu} = \frac{\mathrm{Re}_D}{\beta} \tag{6.130}$$

Since the design parameters are assumed known, the correlation of α from Eq. (6.129) or of C_d from Eq. (6.125) is the desired solution to the fluid-metering problem.

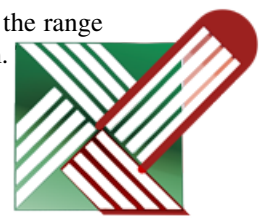
The mass flow is related to Q by

$$\dot{m} = \rho Q \tag{6.131}$$

and is thus correlated by exactly the same formulas.

Figure 6.39 shows the three basic devices recommended for use by the International Organization for Standardization (ISO) [31]: the orifice, nozzle, and venturi tube.

Thin-plate orifice. The thin-plate orifice, Fig. 6.39*b*, can be made with β in the range of 0.2 to 0.8, except that the hole diameter d should not be less than 12.5 mm. sure p_1 and p_2, three types of tappings are commonly used:



ketabline.com Ebook.ketabline.com

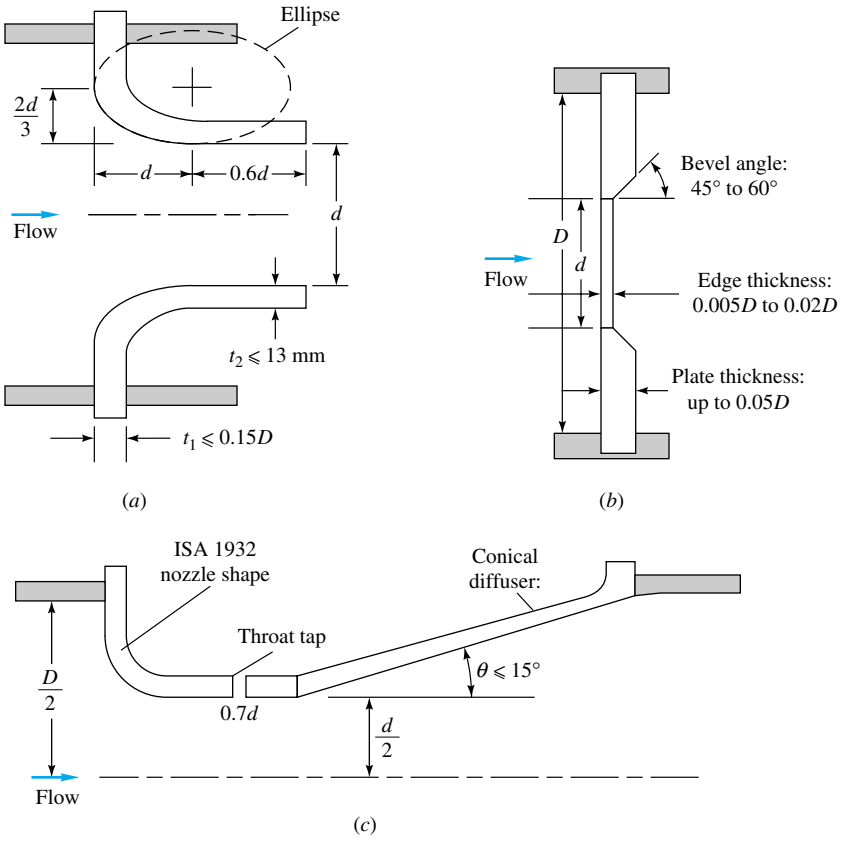


Fig. 6.39 International standard shapes for the three primary Bernoulli obstruction-type meters: (*a*) long radius nozzle; (*b*) thin-plate orifice; (*c*) venturi nozzle. *(From Ref. 31 by permission of the International Organization for Standardization.)*

1. Corner taps where the plate meets the pipe wall
2. D: $\frac{1}{2}D$ taps: pipe-wall taps at D upstream and $\frac{1}{2}D$ downstream
3. Flange taps: 1 in (25 mm) upstream and 1 in (25 mm) downstream of the plate, regardless of the size D

Types 1 and 2 approximate geometric similarity, but since the flange taps 3 do not, they must be correlated separately for every single size of pipe in which a flange-tap plate is used [30, 31].

Figure 6.40 shows the discharge coefficient of an orifice with D: $\frac{1}{2}D$ or type 2 taps in the Reynolds-number range $\mathrm{Re}_D = 10^4$ to 10^7 of normal use. Although detailed charts such as Fig. 6.37 are available for designers [30], the ASME recommends use of the curve-fit formulas developed by the ISO [31]. The basic form of the curve fit is [42]

$$C_d = f(\beta) + 91.71\beta^{2.5}\mathrm{Re}_D^{-0.75} + \frac{0.09\beta^4}{1-\beta^4}F_1 - 0.0337\beta^3 F_2 \qquad (6.132)$$

where $$f(\beta) = 0.5959 + 0.0312\beta^{2.1} - 0.184\beta^8$$

The correlation factors F_1 and F_2 vary with tap position:

Corner taps: $F_1 = 0$ $F_2 = 0$



ketabline.com Ebook.ketabline.com

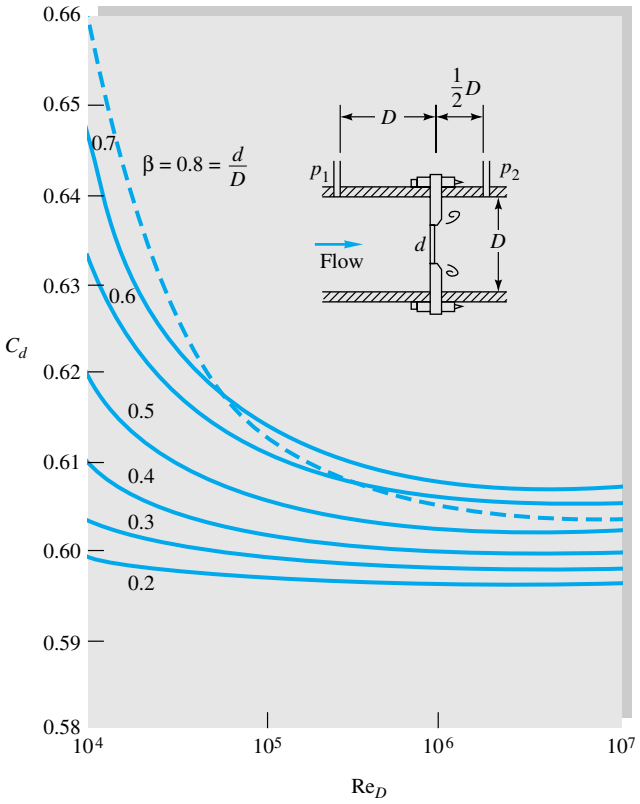


Fig. 6.40 Discharge coefficient for a thin-plate orifice with D: $\frac{1}{2}D$ taps, plotted from Eqs. (6.132) and (6.133*b*).

$$D\text{: } \tfrac{1}{2}D \text{ taps:} \qquad F_1 = 0.4333 \qquad F_2 = 0.47 \tag{6.133b}$$

$$\text{Flange taps:} \qquad F_2 = \frac{1}{D\ (\text{in})} \qquad F_1 = \begin{cases} \dfrac{1}{D\ (\text{in})} & D > 2.3 \text{ in} \\ 0.4333 & 2.0 \le D \le 2.3 \text{ in} \end{cases} \tag{6.133c}$$

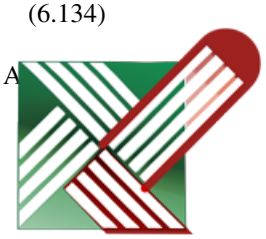
Note that the flange taps (6.133*c*), not being geometrically similar, use raw diameter in inches in the formula. The constants will change if other diameter units are used. We cautioned against such dimensional formulas in Example 1.4 and Eq. (5.17) and give Eq. (6.133*c*) only because flange taps are widely used in the United States.

Flow nozzle. The flow nozzle comes in two types, a long-radius type shown in Fig. 6.39*a* and a short-radius type (not shown) called the ISA 1932 nozzle [30, 31]. The flow nozzle, with its smooth rounded entrance convergence, practically eliminates the vena contracta and gives discharge coefficients near unity. The nonrecoverable loss is still large because there is no diffuser provided for gradual expansion.

The ISO recommended correlation for long-radius-nozzle discharge coefficient is

$$C_d \approx 0.9965 - 0.00653\beta^{1/2}\left(\frac{10^6}{\mathrm{Re}_D}\right)^{1/2} = 0.9965 - 0.00653\left(\frac{10^6}{\mathrm{Re}_d}\right)^{1/2} \tag{6.134}$$

The second form is independent of the β ratio and is plotted in Fig. 6.41. A ISO correlation is recommended for the short-radius ISA 1932 flow nozzle



ketabline.com Ebook.ketabline.com

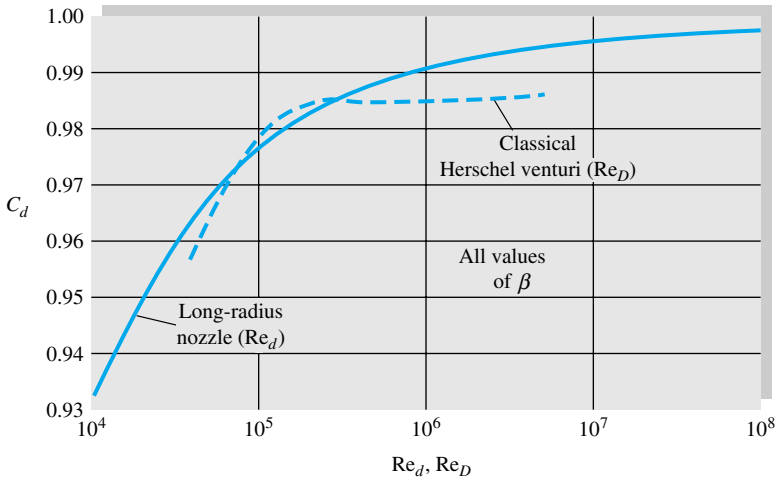


Fig. 6.41 Discharge coefficient for long-radius nozzle and classical Herschel-type venturi.

$$C_d \approx 0.9900 - 0.2262\beta^{4.1} + (0.000215 - 0.001125\beta + 0.00249\beta^{4.7})\left(\frac{10^6}{\mathrm{Re}_D}\right)^{1.15} \quad (6.135)$$

Flow nozzles may have β values between 0.2 and 0.8.

Venturi meter. The third and final type of obstruction meter is the venturi, named in honor of Giovanni Venturi (1746–1822), an Italian physicist who first tested conical expansions and contractions. The original, or *classical*, venturi was invented by a U.S. engineer, Clemens Herschel, in 1898. It consisted of a 21° conical contraction, a straight throat of diameter d and length d, then a 7 to 15° conical expansion. The discharge coefficient is near unity, and the nonrecoverable loss is very small. Herschel venturis are seldom used now.

The modern venturi nozzle, Fig. 6.39*c*, consists of an ISA 1932 nozzle entrance and a conical expansion of half-angle no greater than 15°. It is intended to be operated in a narrow Reynolds-number range of 1.5×10^5 to 2×10^6. Its discharge coefficient, shown in Fig. 6.42, is given by the ISO correlation formula

$$C_d \approx 0.9858 - 0.196\beta^{4.5} \quad (6.136)$$

It is independent of Re_D within the given range. The Herschel venturi discharge varies with Re_D but not with β, as shown in Fig. 6.41. Both have very low net losses.

The choice of meter depends upon the loss and the cost and can be illustrated by the following table:

Type of meter	Net head loss	Cost
Orifice	Large	Small
Nozzle	Medium	Medium
Venturi	Small	Large

As so often happens, the product of inefficiency and initial cost is appr



ketabline.com Ebook.ketabline.com

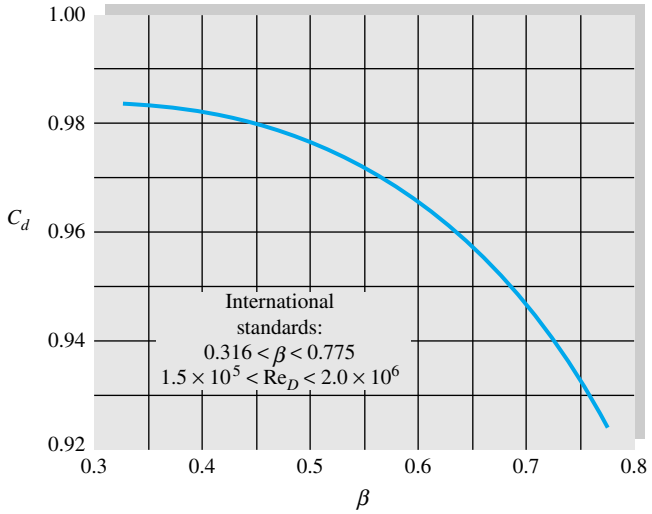


Fig. 6.42 Discharge coefficient for a venturi nozzle.

The average nonrecoverable head losses for the three types of meters, expressed as a fraction of the throat velocity head $V_t^2/(2g)$, are shown in Fig. 6.43. The orifice has the greatest loss and the venturi the least, as discussed. The orifice and nozzle simulate partially closed valves as in Fig. 6.18*b*, while the venturi is a very minor loss. When the loss is given as a fraction of the measured *pressure drop,* the orifice and nozzle have nearly equal losses, as Example 6.21 will illustrate.

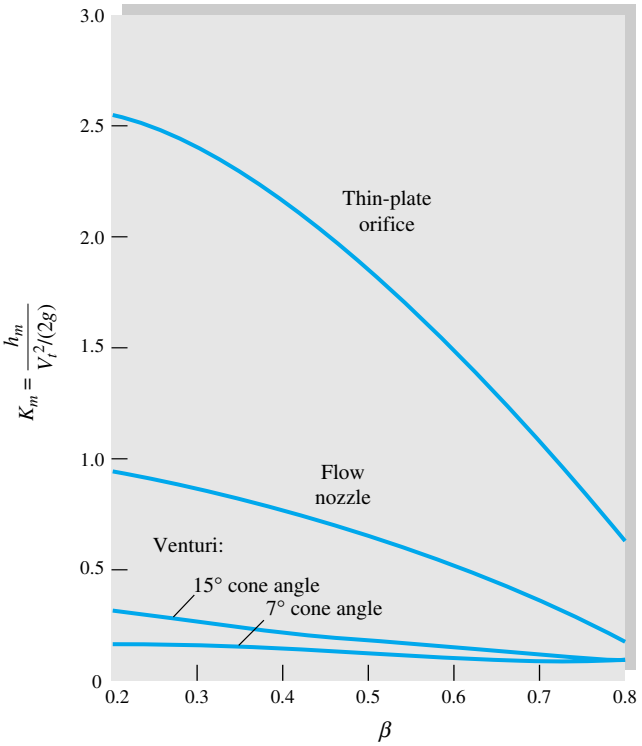


Fig. 6.43 Nonrecoverable head loss in Bernoulli obstruction meters. *(Adapted from Ref. 30.)*



ketabline.com Ebook.ketabline.com

The other types of instruments discussed earlier in this section can also serve as flowmeters if properly constructed. For example, a hot wire mounted in a tube can be calibrated to read volume flow rather than point velocity. Such hot-wire meters are commercially available, as are other meters modified to use velocity instruments. For further details see Ref. 30.

EXAMPLE 6.21

We want to meter the volume flow of water ($\rho = 1000$ kg/m^3, $\nu = 1.02 \times 10^{-6}$ m^2/s) moving through a 200-mm-diameter pipe at an average velocity of 2.0 m/s. If the differential pressure gage selected reads accurately at $p_1 - p_2 = 50{,}000$ Pa, what size meter should be selected for installing (*a*) an orifice with D: $\frac{1}{2}D$ taps, (*b*) a long-radius flow nozzle, or (*c*) a venturi nozzle? What would be the nonrecoverable head loss for each design?

Solution

Here the unknown is the β ratio of the meter. Since the discharge coefficient is a complicated function of β, iteration will be necessary. We are given $D = 0.2$ m and $V_1 = 2.0$ m/s. The pipe-approach Reynolds number is thus

$$\mathrm{Re}_D = \frac{V_1 D}{\nu} = \frac{(2.0)(0.2)}{1.02 \times 10^{-6}} = 392{,}000$$

For all three cases [(*a*) to (*c*)] the generalized formula (6.128) holds:

$$V_t = \frac{V_1}{\beta^2} = \alpha\left[\frac{2(p_1 - p_2)}{\rho}\right]^{1/2} \qquad \alpha = \frac{C_d}{(1 - \beta^4)^{1/2}} \tag{1}$$

where the given data are $V_1 = 2.0$ m/s, $\rho = 1000$ kg/m^3, and $\Delta p = 50{,}000$ Pa. Inserting these known values into Eq. (1) gives a relation between β and α:

$$\frac{2.0}{\beta^2} = \alpha\left[\frac{2(50{,}000)}{1000}\right]^{1/2} \qquad \text{or} \qquad \beta^2 = \frac{0.2}{\alpha} \tag{2}$$

The unknowns are β (or α) and C_d. Parts (*a*) to (*c*) depend upon the particular chart or formula needed for $C_d = \mathrm{fcn}(\mathrm{Re}_D, \beta)$. We can make an initial guess $\beta \approx 0.5$ and iterate to convergence.

Part (a) For the orifice with D: $\frac{1}{2}D$ taps, use Eq. (6.132) or Fig. 6.40. The iterative sequence is

$$\beta_1 \approx 0.5,\ C_{d1} \approx 0.604,\ \alpha_1 \approx 0.624,\ \beta_2 \approx 0.566,\ C_{d2} \approx 0.606,\ \alpha_2 \approx 0.640,\ \beta_3 = \mathbf{0.559}$$

We have converged to three figures. The proper orifice diameter is

$$d = \beta D = \mathbf{112\ mm} \qquad \textit{Ans. (a)}$$

Part (b) For the long-radius flow nozzle, use Eq. (6.134) or Fig. 6.41. The iterative sequence is

$$\beta_1 \approx 0.5,\ C_{d1} \approx 0.9891,\ \alpha_1 \approx 1.022,\ \beta_2 \approx 0.442,\ C_{d2} \approx 0.9896,\ \alpha_2 \approx 1.009,\ \beta_3 = \mathbf{0.445}$$

We have converged to three figures. The proper nozzle diameter is

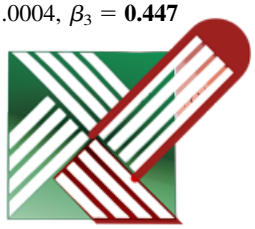
$$d = \beta D = \mathbf{89\ mm} \qquad \textit{Ans. (b)}$$

Part (c) For the venturi nozzle, use Eq. (6.136) or Fig. 6.42. The iterative sequence is

$$\beta_1 \approx 0.5,\ C_{d1} \approx 0.977,\ \alpha_1 \approx 1.009,\ \beta_2 \approx 0.445,\ C_{d2} \approx 0.9807,\ \alpha_2 \approx 1.0004,\ \beta_3 = \mathbf{0.447}$$

We have converged to three figures. The proper venturi diameter is

$$d = \beta D = \mathbf{89\ mm}$$



ketabline.com Ebook.ketabline.com

These meters are of similar size, but their head losses are not the same. From Fig. 6.43 for the three different shapes we may read the three K factors and compute

$$h_{m,\text{orifice}} \approx 3.5 \text{ m} \qquad h_{m,\text{nozzle}} \approx 3.6 \text{ m} \qquad h_{m,\text{venturi}} \approx 0.8 \text{ m}$$

The venturi loss is only about 22 percent of the orifice and nozzle losses.



Solution

The iteration encountered in this example is ideal for the EES. Input the data in SI units:

```
Rho = 1000    Nu = 1.02E-6    D = 0.2    V = 2.0    DeltaP = 50000
```

Then write out the basic formulas for Reynolds number, throat velocity and flow coefficient:

```
Re = V*D/Nu
Vt = V/Beta^2
Alpha = Cd/(1-Beta^4)^0.5
Vt = Alpha*SQRT(2*DeltaP/Rho)
```

Finally, input the proper formula for the discharge coefficient. For example, for the flow nozzle,

```
Cd = 0.9965 - 0.00653*Beta^0.5*(1E6/Re)^0.5
```

When asked to Solve the equation, EES at first complains of dividing by zero. One must then tighten up the Variable Information by not allowing β, α, or C_d to be negative and, in particular, by confining β to its practical range $0.2 < \beta < 0.9$. EES then readily announces correct answers for the flow nozzle:

```
Alpha = 1.0096    Cd = 0.9895    Beta = 0.4451
```

Summary

This chapter is concerned with internal pipe and duct flows, which are probably the most common problems encountered in engineering fluid mechanics. Such flows are very sensitive to the Reynolds number and change from laminar to transitional to turbulent flow as the Reynolds number increases.

The various Reynolds-number regimes are outlined, and a semiempirical approach to turbulent-flow modeling is presented. The chapter then makes a detailed analysis of flow through a straight circular pipe, leading to the famous Moody chart (Fig. 6.13) for the friction factor. Possible uses of the Moody chart are discussed for flow-rate and sizing problems, as well as the application of the Moody chart to noncircular ducts using an equivalent duct "diameter." The addition of minor losses due to valves, elbows, fittings, and other devices is presented in the form of loss coefficients to be incorporated along with Moody-type friction losses. Multiple-pipe systems are discussed briefly and are seen to be quite complex algebraically and appropriate for computer solution.

Diffusers are added to ducts to increase pressure recovery at the exit of a system. Their behavior is presented as experimental data, since the theory of real diffusers is still not well developed. The chapter ends with a discussion of flowmeters, especially the pitot-static tube and the Bernoulli-obstruction type of meter. Flowmeters require careful experimental calibration.



ketabline.com Ebook.ketabline.com

Problems

Most of the problems herein are fairly straightforward. More difficult or open-ended assignments are labeled with an asterisk. Problems labeled with an EES icon will benefit from the use of the Engineering Equation Solver (EES), while problems labeled with a computer disk may require the use of a computer. The standard end-of-chapter problems 6.1 to 6.160 (categorized in the problem list below) are followed by word problems W6.1 to W6.5, fundamentals of engineering exam problems FE6.1 to FE6.15, comprehensive problems C6.1 to C6.5, and design projects D6.1 and D6.2.

Problem distribution

Section	Topic	Problems
6.1	Reynolds-number regimes	6.1–6.7
6.2	Internal and external flow	6.8–6.10
6.3	Turbulent-shear correlations	6.11–6.18
6.4	Laminar pipe flow	6.19–6.41
6.4	Turbulent pipe flow	6.42–6.77
6.5	Flow-rate and pipe-sizing problems	6.78–6.85
6.6	Noncircular ducts	6.86–6.99
6.7	Minor losses	6.100–6.110
6.8	Series and parallel pipe systems	6.111–6.120
6.8	Three-reservoir and pipe-network systems	6.121–6.130
6.9	Diffuser performance	6.131–6.134
6.10	The pitot-static tube	6.135–6.139
6.10	Flowmeters: The orifice plate	6.140–6.148
6.10	Flowmeters: The flow nozzle	6.149–6.153
6.10	Flowmeters: The venturi meter	6.154–6.160

P6.1 In flow past a sphere, the boundary layer becomes turbulent at about $\mathrm{Re}_D \approx 2.5$ E5. To what air speed in mi/h does this correspond for a golf ball whose diameter is 1.6 in? Do the pressure, temperature, and humidity of the air make any difference in your calculation?

P6.2 For a thin wing moving parallel to its chord line, transition to a turbulent boundary layer normally occurs at $\mathrm{Re}_x = 2.8 \times 10^6$, where x is the distance from the leading edge [2, 3]. If the wing is moving at 20 m/s, at what point on the wing will transition occur at 20°C for (*a*) air and (*b*) water?

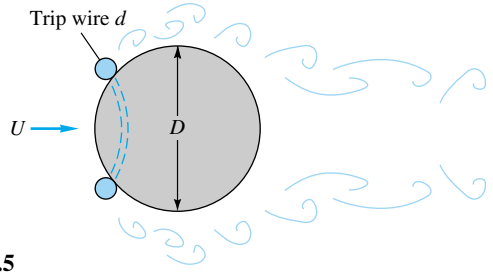
P6.3 If the wing of Prob. 6.2 is tested in a wind or water tunnel, it may undergo transition earlier than $\mathrm{Re}_x = 2.8 \times 10^6$ if the test stream itself contains turbulent fluctuations. A semiempirical correlation for this case [3, p. 383] is

$$\mathrm{Re}_{x_{\mathrm{crit}}}^{1/2} \approx \frac{-1 + (1 + 13.25\zeta^2)^{1/2}}{0.00392\zeta^2}$$

where ζ is the tunnel-turbulence intensity in percent. If $V = 20$ m/s in air at 20°C, use this formula to plot the transition position on the wing versus stream turbulence for ζ between 0 and 2 percent. At what value of ζ is x_{crit} decreased 50 percent from its value at $\zeta = 0$?

P6.4 For flow of SAE 10 oil through a 5-cm-diameter pipe, from Fig. A.1, for what flow rate in m^3/h would we expect transition to turbulence at (*a*) 20°C and (*b*) 100°C?

P6.5 In flow past a body or wall, early transition to turbulence can be induced by placing a trip wire on the wall across the flow, as in Fig. P6.5. If the trip wire in Fig. P6.5 is placed where the local velocity is U, it will trigger turbulence if $Ud/\nu = 850$, where d is the wire diameter [3, p. 386]. If the sphere diameter is 20 cm and transition is observed at $\mathrm{Re}_D = 90{,}000$, what is the diameter of the trip wire in mm?



P6.5

P6.6 A fluid at 20°C flows at 850 cm^3/s through an 8-cm-diameter pipe. Determine whether the flow is laminar or turbulent if the fluid is (*a*) hydrogen, (*b*) air, (*c*) gasoline, (*d*) water, (*e*) mercury, or (*f*) glycerin.

P6.7 Cola, approximated as pure water at 20°C, is to fill an 8-oz container (1 U.S. gal = 128 fl oz) through a 5-mm-diameter tube. Estimate the minimum filling time if the tube flow is to remain laminar. For what cola (water) temperature would this minimum time be 1 min?

P6.8 When water at 20°C is in steady turbulent flow through an 8-cm-diameter pipe, the wall shear stress is 72 Pa. What is the axial pressure gradient $(\partial p/\partial x)$ if the pipe is (*a*) horizontal and (*b*) vertical with the flow up?

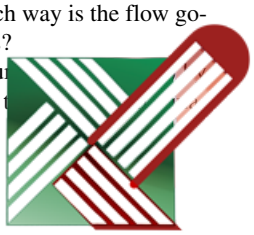
P6.9 A light liquid ($\rho \approx 950$ kg/m^3) flows at an average velocity of 10 m/s through a horizontal smooth tube of diameter 5 cm. The fluid pressure is measured at 1-m intervals along the pipe, as follows:

x, m	0	1	2	3	4	5	6
p, kPa	304	273	255	240	226	213	200

Estimate (*a*) the average wall shear stress, in Pa, and (*b*) the wall shear stress in the fully developed region of the pipe.

P6.10 Water at 20°C flows through an inclined 8-cm-diameter pipe. At sections A and B the following data are taken: $p_A = 186$ kPa, $V_A = 3.2$ m/s, $z_A = 24.5$ m, and $p_B = 260$ kPa, $V_B = 3.2$ m/s, $z_B = 9.1$ m. Which way is the flow going? What is the head loss in meters?

P6.11 Derive the time-averaged x-momentu
direct substitution of Eqs. (6.12) into t



ketabline.com Ebook.ketabline.com

tion (6.7). It is convenient to write the convective acceleration as

$$\frac{du}{dt} = \frac{\partial}{\partial x}(u^2) + \frac{\partial}{\partial y}(uv) + \frac{\partial}{\partial z}(uw)$$

which is valid because of the continuity relation, Eq. (6.7).

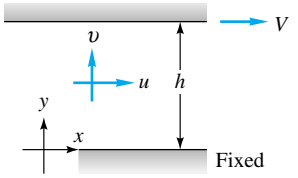
P6.12 By analogy with Eq. (6.14) write the turbulent mean-momentum differential equation for (*a*) the y direction and (*b*) the z direction. How many turbulent stress terms appear in each equation? How many unique turbulent stresses are there for the total of three directions?

P6.13 The following turbulent-flow velocity data $u(y)$, for air at 75°F and 1 atm near a smooth flat wall, were taken in the University of Rhode Island wind tunnel:

y, in	0.025	0.035	0.047	0.055	0.065
u, ft/s	51.2	54.2	56.8	57.6	59.1

Estimate (*a*) the wall shear stress and (*b*) the velocity u at $y = 0.22$ in.

P6.14 Two infinite plates a distance h apart are parallel to the xz plane with the upper plate moving at speed V, as in Fig. P6.14. There is a fluid of viscosity μ and constant pressure between the plates. Neglecting gravity and assuming incompressible turbulent flow $u(y)$ between the plates, use the logarithmic law and appropriate boundary conditions to derive a formula for dimensionless wall shear stress versus dimensionless plate velocity. Sketch a typical shape of the profile $u(y)$.



P6.14

P6.15 Suppose in Fig. P6.14 that $h = 3$ cm, the fluid in water at 20°C, and the flow is turbulent, so that the logarithmic law is valid. If the shear stress in the fluid is 15 Pa, what is V in m/s?

P6.16 By analogy with laminar shear, $\tau = \mu\, du/dy$, T. V. Boussinesq in 1877 postulated that turbulent shear could also be related to the mean-velocity gradient $\tau_{\text{turb}} = \epsilon\, du/dy$, where ϵ is called the *eddy viscosity* and is much larger than μ. If the logarithmic-overlap law, Eq. (6.21), is valid with $\tau \approx \tau_w$, show that $\epsilon \approx \kappa\rho u^* y$.

P6.17 Theodore von Kármán in 1930 theorized that turbulent shear could be represented by $\tau_{\text{turb}} = \epsilon\, du/dy$ where $\epsilon = \rho\kappa^2 y^2 \left|du/dy\right|$ is called the *mixing-length eddy viscosity* and $\kappa \approx 0.41$ is Kármán's dimensionless *mixing-length constant* [2, 3]. Assuming that $\tau_{\text{turb}} \approx \tau_w$ near the wall, show that this expression can be integrated to yield the logarithmic-overlap law, Eq. (6.21).

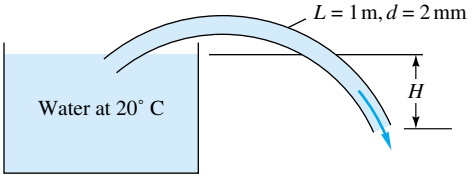
P6.18 Water at 20°C flows in a 9-cm-diameter pipe under fully developed conditions. The centerline velocity is 10 m/s. Compute (*a*) Q, (*b*) V, (*c*) τ_w, and (*d*) Δp for a 100-m pipe length.

In Probs. 6.19 to 6.99, neglect minor losses.

P6.19 A 5-mm-diameter capillary tube is used as a viscometer for oils. When the flow rate is 0.071 m^3/h, the measured pressure drop per unit length is 375 kPa/m. Estimate the viscosity of the fluid. Is the flow laminar? Can you also estimate the density of the fluid?

P6.20 A soda straw is 20 cm long and 2 mm in diameter. It delivers cold cola, approximated as water at 10°C, at a rate of 3 cm^3/s. (*a*) What is the head loss through the straw? What is the axial pressure gradient $\partial p/\partial x$ if the flow is (*b*) vertically up or (*c*) horizontal? Can the human lung deliver this much flow?

P6.21 Water at 20°C is to be siphoned through a tube 1 m long and 2 mm in diameter, as in Fig. P6.21. Is there any height H for which the flow might not be laminar? What is the flow rate if $H = 50$ cm? Neglect the tube curvature.



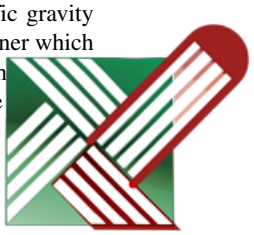
P6.21

P6.22 SAE 30W oil at 20°C flows through a long, horizontal, 12-cm-diameter tube. At section 1, the fluid pressure is 186 kPa. At section 2, which is 6 m further downstream, the pressure is 171 kPa. If the flow is laminar, estimate (*a*) the mass flow in kg/s and (*b*) the Reynolds number.

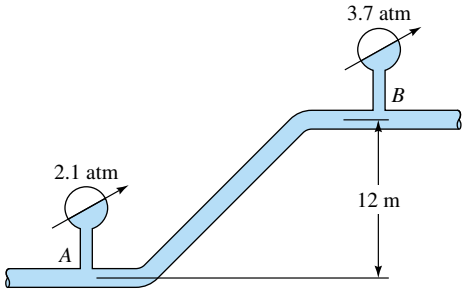
P6.23 Glycerin at 20°C is to be pumped through a horizontal smooth pipe at 3.1 m^3/s. It is desired that (1) the flow be laminar and (2) the pressure drop be no more than 100 Pa/m. What is the minimum pipe diameter allowable?

P6.24 The 6-cm-diameter pipe in Fig. P6.24 contains glycerin at 20°C flowing at a rate of 6 m^3/h. Verify that the flow is laminar. For the pressure measurements shown, is the flow up or down? What is the indicated head loss for these pressures?

P6.25 To determine the viscosity of a liquid of specific gravity 0.95, you fill, to a depth of 12 cm, a large container which drains through a 30-cm-long vertical tube attach bottom. The tube diameter is 2 mm, and the rate



ketabline.com Ebook.ketabline.com

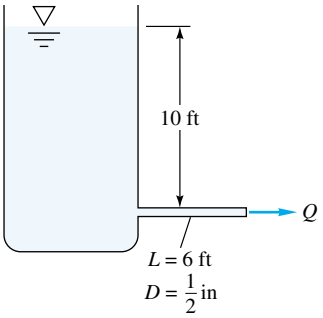


P6.24

ing is found to be 1.9 cm^3/s. What is your estimate of the fluid viscosity? Is the tube flow laminar?

P6.26 Water at 20°C is flowing through a 20-cm-square smooth duct at a (turbulent) Reynolds number of 100,000. For a "laminar flow element" measurement, it is desired to pack the pipe with a honeycomb array of small square passages (see Fig. P6.36 for an example). What passage width h will ensure that the flow in each tube will be laminar (Reynonds number less than 2000)?

P6.27 An oil (SG = 0.9) issues from the pipe in Fig. P6.27 at $Q = 35$ ft^3/h. What is the kinematic viscosity of the oil in ft^3/s? Is the flow laminar?



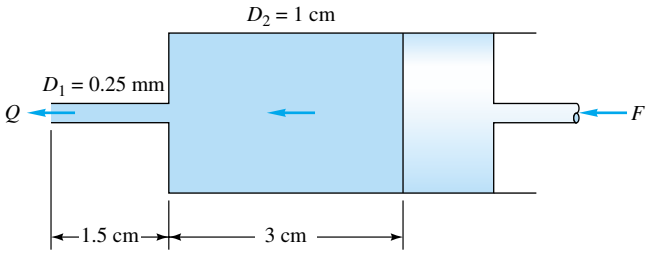
P6.27

P6.28 In Prob. 6.27 what will the flow rate be, in m^3/h, if the fluid is SAE 10 oil at 20°C?

P6.29 Oil, with $\rho = 890$ kg/m^3 and $\mu = 0.06$ kg/(m · s), is to be pumped through 1 km of straight horizontal pipe with a power input of 1 kW. What is the maximum possible mass flow rate, and corresponding pipe diameter, if laminar flow is to be maintained?

P6.30 A steady push on the piston in Fig. P6.30 causes a flow rate $Q = 0.15$ cm^3/s through the needle. The fluid has $\rho = 900$ kg/m^3 and $\mu = 0.002$ kg/(m · s). What force F is required to maintain the flow?

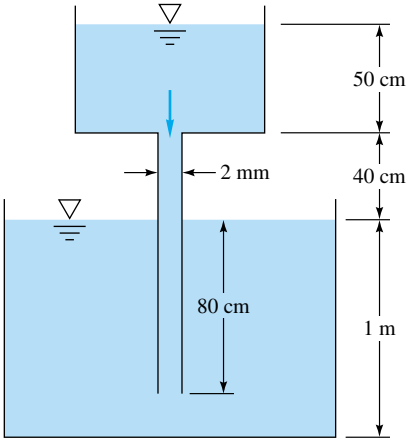
P6.31 SAE 10 oil at 20°C flows in a vertical pipe of diameter 2.5 cm. It is found that the pressure is constant throughout the fluid. What is the oil flow rate in m^3/h? Is the flow up or down?



P6.30

P6.32 SAE 30 oil at 20°C flows at 0.001 m^3/s through 100 m of 1-cm-diameter pipe and then for another 100 m at an increased $d = 2$ cm. The double-pipe system slopes upward at 35° in the flow direction. Estimate (*a*) the total pressure change and (*b*) the power required to drive the flow.

P6.33 For the configuration shown in Fig. P6.33, the fluid is ethyl alcohol at 20°C, and the tanks are very wide. Find the flow rate which occurs in m^3/h. Is the flow laminar?

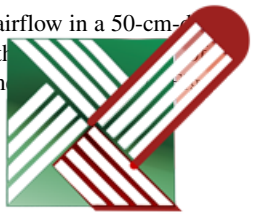


P6.33

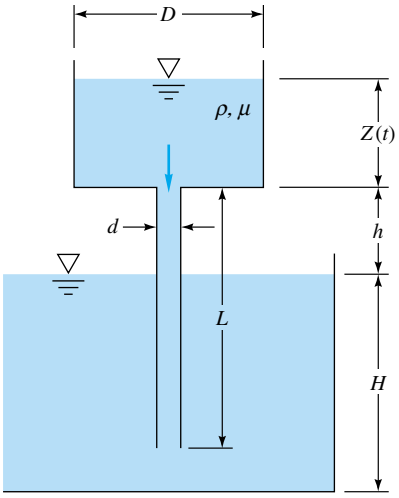
P6.34 For the system in Fig. P6.33, if the fluid has density of 920 kg/m^3 and the flow rate is unknown, for what value of viscosity will the capillary Reynolds number exactly equal the critical value of 2300?

***P6.35** Let us attack Prob. 6.33 in symbolic fashion, using Fig. P6.35. All parameters are constant except the upper tank depth $Z(t)$. Find an expression for the flow rate $Q(t)$ as a function of $Z(t)$. Set up a differential equation, and solve for the time t_0 to drain the upper tank completely. Assume quasi-steady laminar flow.

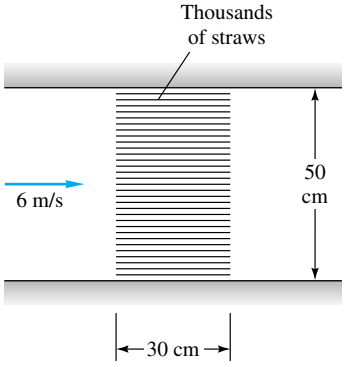
P6.36 For straightening and smoothing an airflow in a 50-cm-diameter duct, the duct is packed with thin straws of length 30 cm and diam



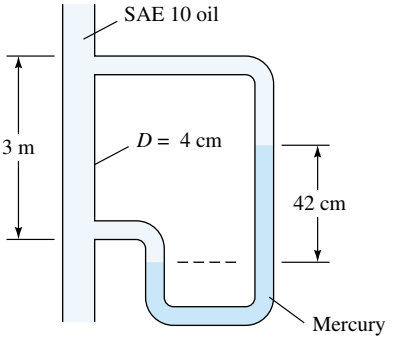
ketabline.com Ebook.ketabline.com



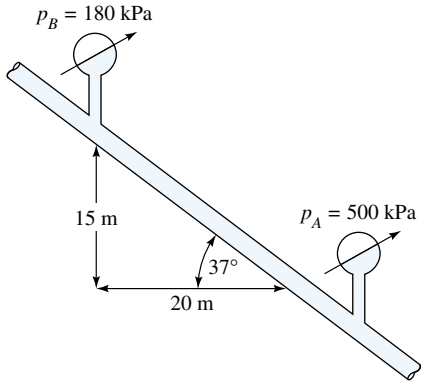
P6.35



P6.36



P6.38



P6.40

P6.36. The inlet flow is air at 110 kPa and 20°C, moving at an average velocity of 6 m/s. Estimate the pressure drop across the honeycomb.

P6.37 Oil, with $\rho = 880$ kg/m^3 and $\mu = 0.08$ kg/(m · s), flows through a pipe with $d = 2$ cm and $L = 12$ m. The wall shear stress is 30 Pa. Estimate (*a*) the Reynolds number, (*b*) the total pressure drop, and (*c*) the power required to drive the fluid.

P6.38 SAE 10 oil at 20°C flows through the 4-cm-diameter vertical pipe of Fig. P6.38. For the mercury manometer reading $h = 42$ cm shown, (*a*) calculate the volume flow rate in m^3/h and (*b*) state the direction of flow.

P6.39 Light oil, $\rho = 880$ kg/m^3 and $\mu = 0.015$ kg/(m · s), flows down a vertical 6-mm-diameter tube due to gravity only. Estimate the volume flow rate in m^3/h if (*a*) $L = 1$ m and (*b*) $L = 2$ m. (*c*) Verify that the flow is laminar.

P6.40 SAE 30 oil at 20°C flows in the 3-cm-diameter pipe in Fig. P6.40, which slopes at 37°. For the pressure measurements shown, determine (*a*) whether the flow is up or down and (*b*) the flow rate in m^3/h.

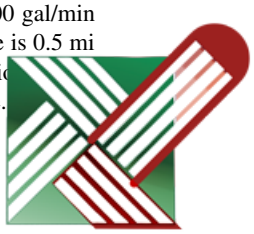
P6.41 In Prob. 6.40 suppose it is desired to add a pump between *A* and *B* to drive the oil upward from *A* to *B* at a rate of 3 kg/s. At 100 percent efficiency, what pump power is required?

***P6.42** It is clear by comparing Figs. 6.12*b* and 6.13 that the effects of sand roughness and commercial (manufactured) roughness are not quite the same. Take the special case of commercial roughness ratio $\epsilon/d = 0.001$ in Fig. 6.13, and replot in the form of the wall-law shift ΔB (Fig. 6.12*a*) versus the logarithm of $\epsilon^+ = \epsilon u^*/\nu$. Compare your plot with Eq. (6.61).

P6.43 Water at 20°C flows for 1 mi through a 3-in-diameter horizontal wrought-iron pipe at 250 gal/min. Estimate the head loss and the pressure drop in this length of pipe.

P6.44 Mercury at 20°C flows through 4 m of 7-mm-diameter glass tubing at an average velocity of 5 m/s. Estimate the head loss in m and the pressure drop in kPa.

P6.45 Oil, SG = 0.88 and $\nu = 4$ E-5 m^2/s, flows at 400 gal/min through a 6-in asphalted cast-iron pipe. The pipe is 0.5 mi long and slopes upward at 8° in the flow direction. Compute the head loss in ft and the pressure change.



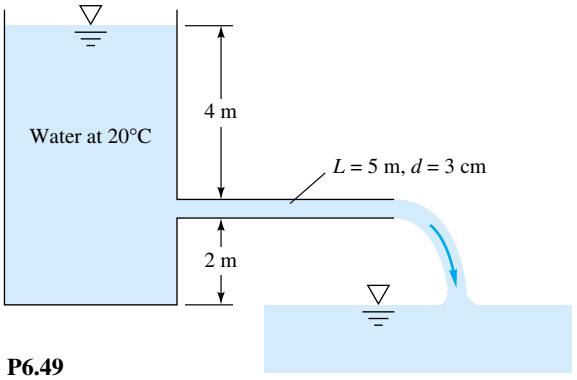
ketabline.com Ebook.ketabline.com

P6.46 Kerosine at 20°C is pumped at 0.15 m^3/s through 20 km of 16-cm-diameter cast-iron horizontal pipe. Compute the input power in kW required if the pumps are 85 percent efficient.

P6.47 Derive Eq. (6.59), showing all steps. The constant 1.33 dates back to Prandtl's work in 1935 and may change slightly to 1.29 in your analysis.

P6.48 Show that if Eq. (6.49) is accurate, the position in a turbulent pipe flow where local velocity u equals average velocity V occurs exactly at $r = 0.777R$, independent of the Reynolds number.

P6.49 The tank-pipe system of Fig. P6.49 is to deliver at least 11 m^3/h of water at 20°C to the reservoir. What is the maximum roughness height ϵ allowable for the pipe?



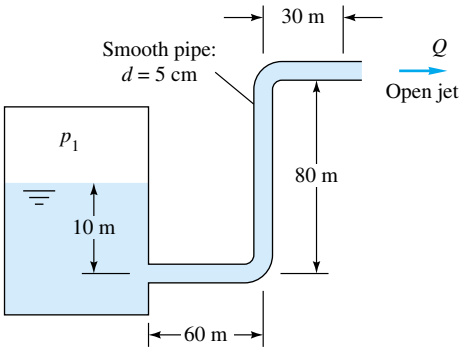
P6.49

P6.50 Ethanol at 20°C flows at 125 U.S. gal/min through a horizontal cast-iron pipe with $L = 12$ m and $d = 5$ cm. Neglecting entrance effects, estimate (*a*) the pressure gradient dp/dx, (*b*) the wall shear stress τ_w, and (*c*) the percent reduction in friction factor if the pipe walls are polished to a smooth surface.

P6.51 The viscous sublayer (Fig. 6.9) is normally less than 1 percent of the pipe diameter and therefore very difficult to probe with a finite-sized instrument. In an effort to generate a thick sublayer for probing, Pennsylvania State University in 1964 built a pipe with a flow of glycerin. Assume a smooth 12-in-diameter pipe with $V = 60$ ft/s and glycerin at 20°C. Compute the sublayer thickness in inches and the pumping horsepower required at 75 percent efficiency if $L = 40$ ft.

P6.52 The pipe flow in Fig. P6.52 is driven by pressurized air in the tank. What gage pressure p_1 is needed to provide a 20°C water flow rate $Q = 60$ m^3/h?

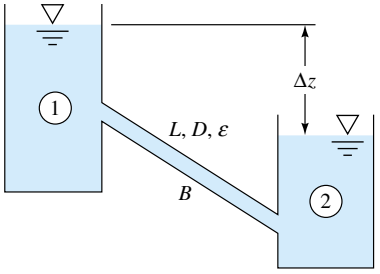
***P6.53** In Fig. P6.52 suppose $P_1 = 700$ kPa and the fluid specific gravity is 0.68. If the flow rate is 27 m^3/h, estimate the viscosity of the fluid. What fluid in Table A.5 is the likely suspect?



P6.52

P6.54 In Fig. P6.52 suppose that the fluid is carbon tetrachloride at 20°C and $p_1 = 1100$ kPa gage. What pipe diameter, in cm, is required to deliver a flow rate of 25 m^3/h?

P6.55 The reservoirs in Fig. P6.55 contain water at 20°C. If the pipe is smooth with $L = 4500$ m and $d = 4$ cm, what will the flow rate in m^3/h be for $\Delta z = 100$ m?



P6.55

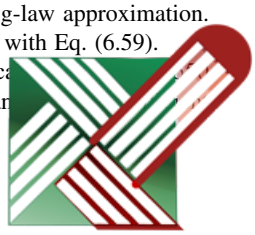
P6.56 Consider a horizontal 4-ft-diameter galvanized-iron pipe simulating the Alaskan pipeline. The oil flow is 70 million U.S. gallons per day, at a density of 910 kg/m^3 and viscosity of 0.01 kg/(m · s) (see Fig. A.1 for SAE 30 oil at 100°C). Each pump along the line raises the oil pressure to 8 MPa, which then drops, due to head loss, to 400-kPa at the entrance to the next pump. Estimate (*a*) the appropriate distance between pumping stations and (*b*) the power required if the pumps are 88 percent efficient.

P6.57 John Laufer (*NACA Tech. Rep.* 1174, 1954) gave velocity data for 20°C airflow in a smooth 24.7-cm-diameter pipe at Re ≈ 5 E5:

u/u_{CL}	1.0	0.997	0.988	0.959	0.908	0.847	0.818	0.771	0.690
r/R	0.0	0.102	0.206	0.412	0.617	0.784	0.846	0.907	0.963

The centerline velocity u_{CL} was 30.5 m/s. Determine (*a*) the average velocity by numerical integration and (*b*) the wall shear stress from the log-law approximation. Compare with the Moody chart and with Eq. (6.59).

P6.58 In Fig. P6.55 assume that the pipe is ca
m, $d = 7$ cm, and $\Delta Z = 100$ m. If ar



ketabline.com Ebook.ketabline.com

pump is placed at point B, what input power is required to deliver 160 m^3/h of water upward from reservoir 2 to 1?

P6.59 The following data were obtained for flow of 20°C water at 20 m^3/h through a badly corroded 5-cm-diameter pipe which slopes downward at an angle of 8°: $p_1 = 420$ kPa, $z_1 = 12$ m, $p_2 = 250$ kPa, $z_2 = 3$ m. Estimate (*a*) the roughness ratio of the pipe and (*b*) the percent change in head loss if the pipe were smooth and the flow rate the same.

P6.60 J. Nikuradse in 1932 suggested that smooth-wall turbulent pipe flow could be approximated by a power-law profile

$$\frac{u}{u_{CL}} \approx \left(\frac{y}{R}\right)^{1/N}$$

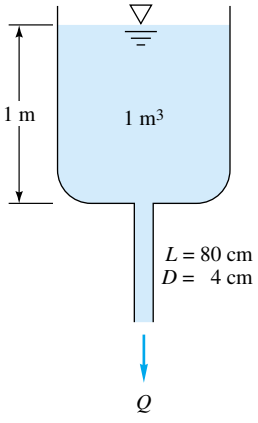
where y is distance from the wall and $N \approx 6$ to 9. Find the best value of N which fits Laufer's data in Prob. 6.57. Then use your formula to estimate the pipe volume flow, and compare with the measured value of 45 ft^3/s.

P6.61 A straight 10-cm commercial-steel pipe is 1 km long and is laid on a constant slope of 5°. Water at 20°C flows downward, due to gravity only. Estimate the flow rate in m^3/h. What happens if the pipe length is 2 km?

P6.62 The Moody chart, Fig. 6.13, is best for finding head loss (or Δp) when Q, V, d, and L are known. It is awkward for the second type of problem, finding Q when h_f or Δp is known (see Example 6.9). Prepare a modified Moody chart whose abscissa is independent of Q and V, using ϵ/d as a parameter, from which one can immediately read the ordinate to find (dimensionless) Q or V. Use your chart to solve Example 6.9.

P6.63 A tank contains 1 m^3 of water at 20°C and has a drawn-capillary outlet tube at the bottom, as in Fig. P6.63. Find the outlet volume flux Q in m^3/h at this instant.

P6.64 For the system in Fig. P6.63, solve for the flow rate in m^3/h if the fluid is SAE 10 oil at 20°C. Is the flow laminar or turbulent?

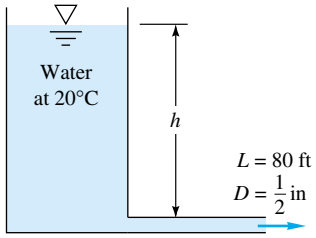


P6.63

P6.65 In Prob. 6.63 the initial flow is turbulent. As the water drains out of the tank, will the flow revert to laminar motion as the tank becomes nearly empty? If so, at what tank depth? Estimate the time, in h, to drain the tank completely.

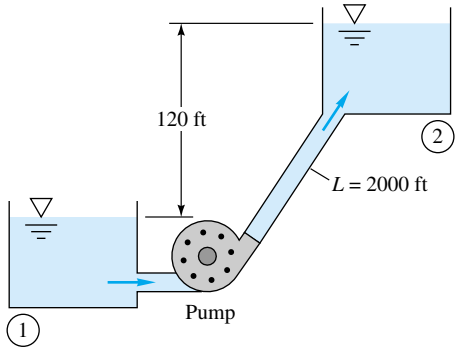
P6.66 Ethyl alcohol at 20°C flows through a 10-cm horizontal drawn tube 100 m long. The fully developed wall shear stress is 14 Pa. Estimate (*a*) the pressure drop, (*b*) the volume flow rate, and (*c*) the velocity u at $r = 1$ cm.

P6.67 What level h must be maintained in Fig. P6.67 to deliver a flow rate of 0.015 ft^3/s through the $\frac{1}{2}$-in commercial-steel pipe?



P6.67

P6.68 Water at 20°C is to be pumped through 2000 ft of pipe from reservoir 1 to 2 at a rate of 3 ft^3/s, as shown in Fig. P6.68. If the pipe is cast iron of diameter 6 in and the pump is 75 percent efficient, what horsepower pump is needed?

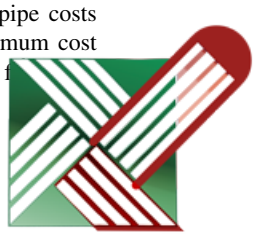


P6.68

P6.69 For Prob. 6.68 suppose the only pump available can deliver 80 hp to the fluid. What is the proper pipe size in inches to maintain the 3 ft^3/s flow rate?

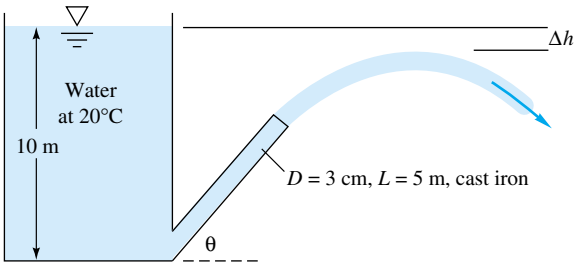
P6.70 In Fig. P6.68 suppose the pipe is 6-in-diameter cast iron and the pump delivers 75 hp to the flow. What flow rate Q ft^3/s results?

P6.71 It is desired to solve Prob. 6.68 for the most economical pump and cast-iron pipe system. If the pump costs $125 per horsepower delivered to the fluid and the pipe costs $7000 per inch of diameter, what are the minimum cost and the pipe and pump size to maintain the 3 f rate? Make some simplifying assumptions.



ketabline.com Ebook.ketabline.com

P6.72 The 5-m-long pipe in Fig. P6.72 may be oriented at any angle θ. If entrance losses are negligible for any θ (pure Moody friction loss), what is the optimum value of θ for which the jet height loss Δh is minimum?



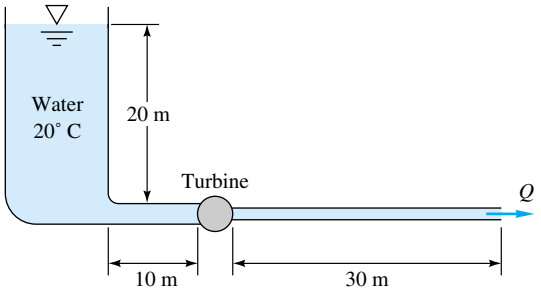
P6.72

P6.73 The Moody chart, Fig. 6.13, is best for finding head loss (or Δp) when Q, V, d, and L are known. It is awkward for the third type of problem, finding d when h_f (or Δp) and Q are known (see Example 6.11). Prepare a modified Moody chart whose abscissa is independent of d, using as a parameter ϵ nondimensionalized without d, from which one can immediately read the (dimensionless) ordinate to find d. Use your chart to solve Example 6.11.

P6.74 In Fig. P6.67 suppose the fluid is gasoline at 20°C and $h = 90$ ft. What commercial-steel pipe diameter is required for the flow rate to be 0.015 ft^3/s?

P6.75 You wish to water your garden with 100 ft of $\frac{5}{8}$-in-diameter hose whose roughness is 0.011 in. What will be the delivery, in ft^3/s, if the gage pressure at the faucet is 60 lbf/in^2? If there is no nozzle (just an open hose exit), what is the maximum horizontal distance the exit jet will carry?

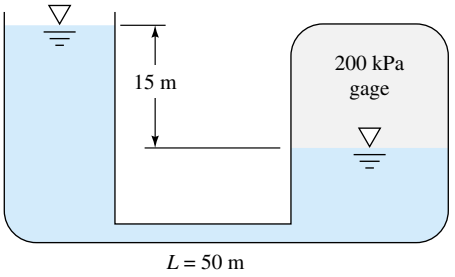
P6.76 The small turbine in Fig. P6.76 extracts 400 W of power from the water flow. Both pipes are wrought iron. Compute the flow rate Q m^3/h. Sketch the EGL and HGL accurately.



P6.76

P6.77 Modify Prob. 6.76 into an economic analysis, as follows. Let the 40 m of wrought-iron pipe have a uniform diameter d. Let the steady water flow available be $Q = 30$ m^3/h. The cost of the turbine is \$4 per watt developed, and the cost of the piping is \$75 per centimeter of diameter. The power generated may be sold for \$0.08 per kilowatthour. Find the proper pipe diameter for minimum *payback time*, i.e., minimum time for which the power sales will equal the initial cost of the system.

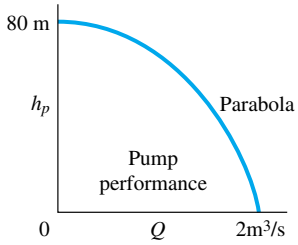
P6.78 In Fig. P6.78 the connecting pipe is commercial steel 6 cm in diameter. Estimate the flow rate, in m^3/h, if the fluid is water at 20°C. Which way is the flow?



P6.78

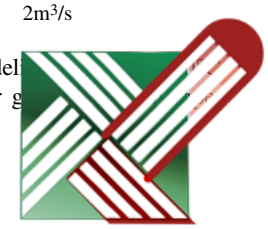
P6.79 A garden hose is to be used as the return line in a waterfall display at a mall. In order to select the proper pump, you need to know the roughness height inside the garden hose. Unfortunately, roughness information is not something supplied by the hose manufacturer. So you devise a simple experiment to measure the roughness. The hose is attached to the drain of an aboveground swimming pool, the surface of which is 3.0 m above the hose outlet. You estimate the minor loss coefficient of the entrance region as 0.5, and the drain valve has a minor loss equivalent length of 200 diameters when fully open. Using a bucket and stopwatch, you open the valve and measure the flow rate to be 2.0×10^{-4} m^3/s for a hose that is 10.0 m long and has an inside diameter of 1.50 cm. Estimate the roughness height in mm inside the hose.

P6.80 The head-versus-flow-rate characteristics of a centrifugal pump are shown in Fig. P6.80. If this pump drives water at 20°C through 120 m of 30-cm-diameter cast-iron pipe, what will be the resulting flow rate, in m^3/s?



P6.80

P6.81 The pump in Fig. P6.80 is used to del
through 350 m of 30-cm-diameter g



ketabline.com Ebook.ketabline.com

Estimate the resulting flow rate, in m^3/s. (Note that the pump head is now in meters of gasoline.)

P6.82 The pump in Fig. P6.80 has its maximum efficiency at a head of 45 m. If it is used to pump ethanol at 20°C through 200 m of commercial-steel pipe, what is the proper pipe diameter for maximum pump efficiency?

P6.83 For the system of Fig. P6.55, let $\Delta z = 80$ m and $L = 185$ m of cast-iron pipe. What is the pipe diameter for which the flow rate will be 7 m^3/h?

P6.84 It is desired to deliver 60 m^3/h of water at 20°C through a horizontal asphalted cast-iron pipe. Estimate the pipe diameter which will cause the pressure drop to be exactly 40 kPa per 100 m of pipe length.

P6.85 The pump of Fig. P6.80 is used to deliver 0.7 m^3/s of methanol at 20°C through 95 m of cast-iron pipe. What is the proper pipe diameter?

P6.86 SAE 10 oil at 20°C flows at an average velocity of 2 m/s between two smooth parallel horizontal plates 3 cm apart. Estimate (*a*) the centerline velocity, (*b*) the head loss per meter, and (*c*) the pressure drop per meter.

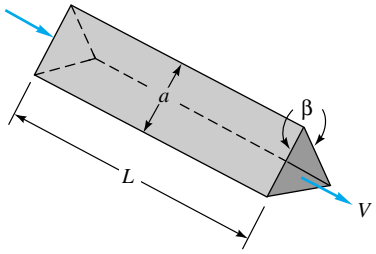
P6.87 A commercial-steel annulus 40 ft long, with $a = 1$ in and $b = \frac{1}{2}$ in, connects two reservoirs which differ in surface height by 20 ft. Compute the flow rate in ft^3/s through the annulus if the fluid is water at 20°C.

P6.88 Show that for laminar flow through an annulus of very small clearance the flow rate Q is approximately proportional to the cube of the clearance $a - b$.

P6.89 An annulus of narrow clearance causes a very large pressure drop and is useful as an accurate measurement of viscosity. If a smooth annulus 1 m long with $a = 50$ mm and $b = 49$ mm carries an oil flow at 0.001 m^3/s, what is the oil viscosity if the pressure drop is 250 kPa?

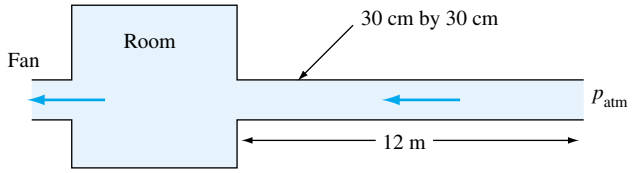
P6.90 A 90-ft-long sheet-steel duct carries air at approximately 20°C and 1 atm. The duct cross section is an equilateral triangle whose side measures 9 in. If a blower can supply 1 hp to the flow, what flow rate, in ft^3/s, will result?

P6.91 Heat exchangers often consist of many triangular passages. Typical is Fig. P6.91, with $L = 60$ cm and an isosceles-triangle cross section of side length $a = 2$ cm and included angle $\beta = 80°$. If the average velocity is $V = 2$ m/s and the fluid is SAE 10 oil at 20°C, estimate the pressure drop.



P6.91

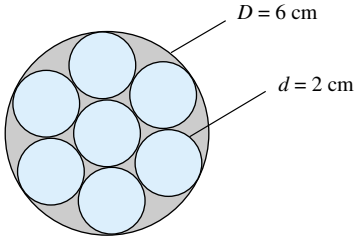
P6.92 A large room uses a fan to draw in atmospheric air at 20°C through a 30-cm by 30-cm commercial-steel duct 12 m long, as in Fig. P6.92. Estimate (*a*) the air flow rate in m^3/h if the room pressure is 10 Pa vacuum and (*b*) the room pressure if the flow rate is 1200 m^3/h. Neglect minor losses.



P6.92

P6.93 Modify Prob. 6.91 so that the angle β is unknown. For SAE 10 oil at 20°C, if the pressure drop is 120 kPa and the flow rate is 4 m^3/h, what is the proper value of the angle β, in degrees?

P6.94 As shown in Fig. P6.94, a multiduct cross section consists of seven 2-cm-diameter smooth thin tubes packed tightly in a hexagonal "bundle" within a single 6-cm-diameter tube. Air, at about 20°C and 1 atm, flows through this system at 150 m^3/h. Estimate the pressure drop per meter.



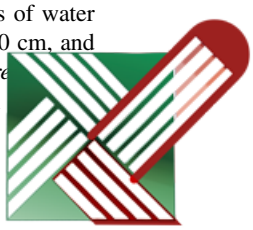
P6.94

P6.95 Modify Prob. 6.94 as follows. Let the seven 2-cm tubes be solid rods, so that the air can only pass through the curved triangular cusped passages. Compute the pressure drop per meter of duct length.

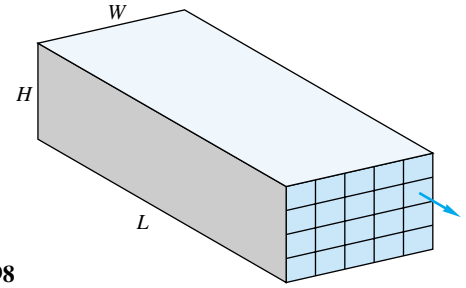
P6.96 Hydrogen, at 20°C and approximately 1 atm, is to be pumped through a smooth rectangular duct 85 m long of aspect ratio 5:1. If the flow rate is 0.7 m^3/s and the pressure drop is 80 Pa, what should the width and height of the duct cross section be?

P6.97 A wind tunnel has a wooden rectangular section 45 cm by 95 cm by 26 m long. It uses sea-level standard air at 31-m/s average velocity. Estimate the pressure drop and the power required if the fan efficiency is 75 percent.

P6.98 A rectangular heat exchanger is to be divided into smaller sections using sheets of commercial steel 0.4 mm thick, as sketched in Fig. P6.98. The flow rate is 20 kg/s of water at 20°C. Basic dimensions are $L = 1$ m, $W = 20$ cm, and $H = 10$ cm. What is the proper number of *square* if the overall pressure drop is to be no more than



ketabline.com Ebook.ketabline.com



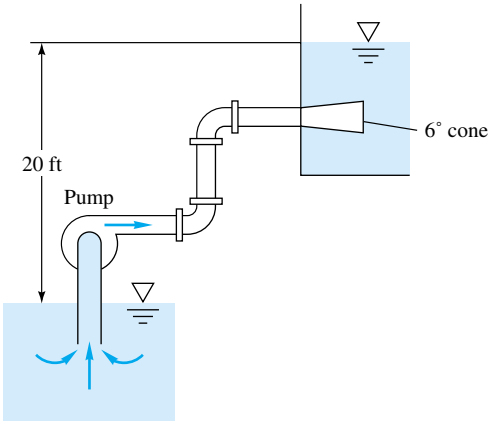
P6.98

P6.99 Air, approximately at sea-level standard conditions, is to be delivered at 3 m^3/s through a horizontal square commercial-steel duct. What are the appropriate duct dimensions if the pressure drop is not to exceed 90 Pa over a 100-m length?

***P6.100** Repeat Prob. 6.92 by including minor losses due to a sharp-edged entrance, the exit into the room, and an open gate valve. If the room pressure is 10 Pa vacuum, by what percentage is the air flow rate decreased from part (*a*) of Prob. 6.92?

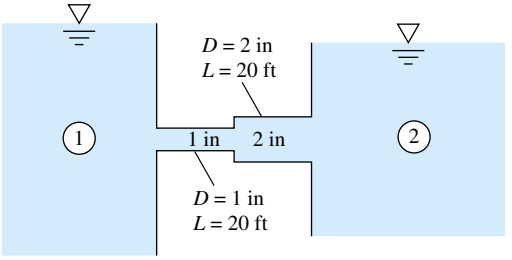
P6.101 Repeat Prob. 6.67 by including losses due to a sharp entrance and a fully open screwed swing-check valve. By what percentage is the required tank level h increased?

***P6.102** A 70 percent efficient pump delivers water at 20°C from one reservoir to another 20 ft higher, as in Fig. P6.102. The piping system consists of 60 ft of galvanized-iron 2-in pipe, a reentrant entrance, two screwed 90° long-radius elbows, a screwed-open gate valve, and a sharp exit. What is the input power required in horsepower with and without a 6° well-designed conical expansion added to the exit? The flow rate is 0.4 ft^3/s.



P6.102

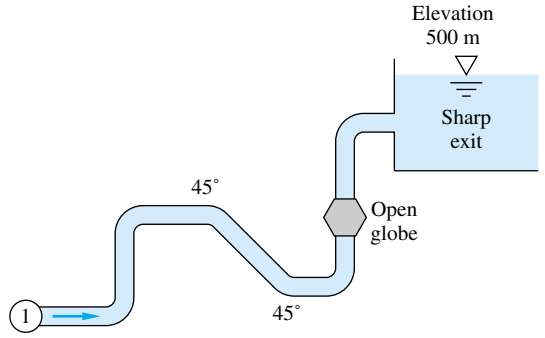
P6.103 The reservoirs in Fig. P6.103 are connected by cast-iron pipes joined abruptly, with sharp-edged entrance and exit. Including minor losses, estimate the flow of water at 20°C if the surface of reservoir 1 is 45 ft higher than that of reservoir 2.



P6.103

***P6.104** Reconsider the air hockey table of Prob. 3.162 but with inclusion of minor losses. The table is 3.0 × 6.0 ft in area, with $\frac{1}{16}$-in-diameter holes spaced every inch in a rectangular grid pattern (2592 holes total). The required jet speed from each hole is estimated to be $V_{jet} = 50$ ft/s. Your job is to select an appropriate blower which will meet the requirements. *Hint:* Assume that the air is stagnant in the large volume of the manifold under the table surface, and assume sharp edge inlets at each hole. (*a*) Estimate the pressure rise (in lb/in^2) required of the blower. (*b*) Compare your answer to the previous calculation in which minor losses were ignored. Are minor losses significant in this application?

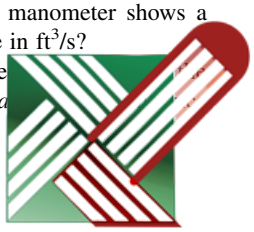
P6.105 The system in Fig. P6.105 consists of 1200 m of 5 cm cast-iron pipe, two 45° and four 90° flanged long-radius elbows, a fully open flanged globe valve, and a sharp exit into a reservoir. If the elevation at point 1 is 400 m, what gage pressure is required at point 1 to deliver 0.005 m^3/s of water at 20°C into the reservoir?



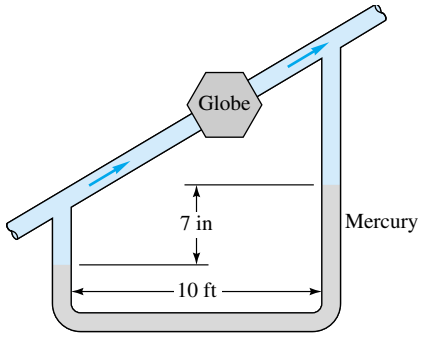
P6.105

P6.106 The water pipe in Fig. P6.106 slopes upward at 30°. The pipe has a 1-in diameter and is smooth. The flanged globe valve is fully open. If the mercury manometer shows a 7-in deflection, what is the flow rate in ft^3/s?

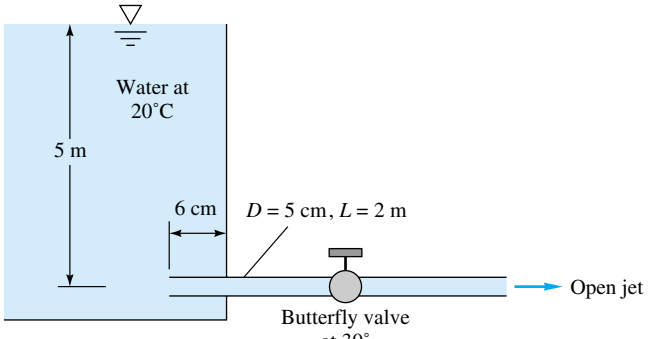
P6.107 In Fig. P6.107 the pipe is galvanize
percentage increase in the flow rate (*a*



ketabline.com Ebook.ketabline.com



P6.106



P6.107

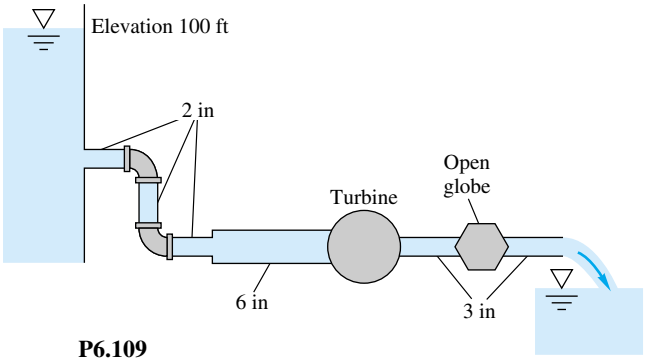
is cut off flush with the wall and (*b*) if the butterfly valve is opened wide.

P6.108 Consider the flow system of Fig. P6.102, including the 6° cone diffuser. Suppose the pump head versus flow rate is approximated by

$$h_p \approx 45 - 125Q^2$$

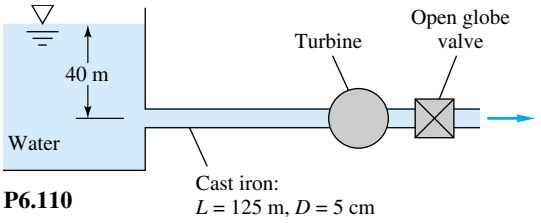
with h_p in ft and Q in ft^3/s. Estimate the resulting flow rate, in ft^3/s.

P6.109 In Fig. P6.109 there are 125 ft of 2-in pipe, 75 ft of 6-in pipe, and 150 ft of 3-in pipe, all cast iron. There are three 90° elbows and an open globe valve, all flanged. If the exit elevation is zero, what horsepower is extracted by the turbine when the flow rate is 0.16 ft^3/s of water at 20°C?



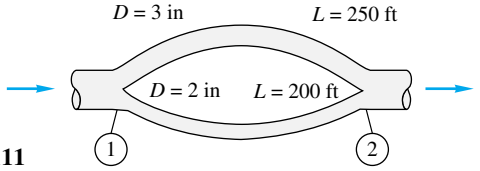
P6.109

P6.110 In Fig. P6.110 the pipe entrance is sharp-edged. If the flow rate is 0.004 m^3/s, what power, in W, is extracted by the turbine?



P6.110

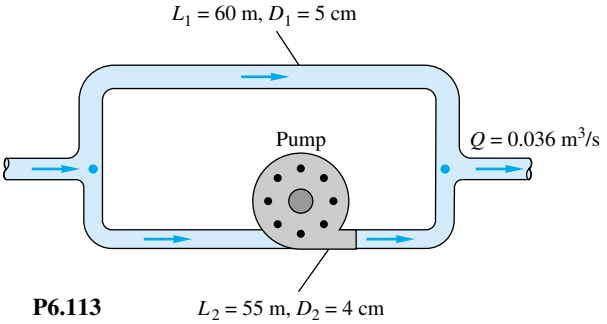
P6.111 For the parallel-pipe system of Fig. P6.111, each pipe is cast iron, and the pressure drop $p_1 - p_2 = 3$ lbf/in^2. Compute the total flow rate between 1 and 2 if the fluid is SAE 10 oil at 20°C.



P6.111

P6.112 If the two pipes in Fig. P6.111 are instead laid in series with the same total pressure drop of 3 lbf/in^2, what will the flow rate be? The fluid is SAE 10 oil at 20°C.

P6.113 The parallel galvanized-iron pipe system of Fig. P6.113 delivers gasoline at 20°C with a total flow rate of 0.036 m^3/s. If the pump is wide open and not running, with a loss coefficient $K = 1.5$, determine (*a*) the flow rate in each pipe and (*b*) the overall pressure drop.



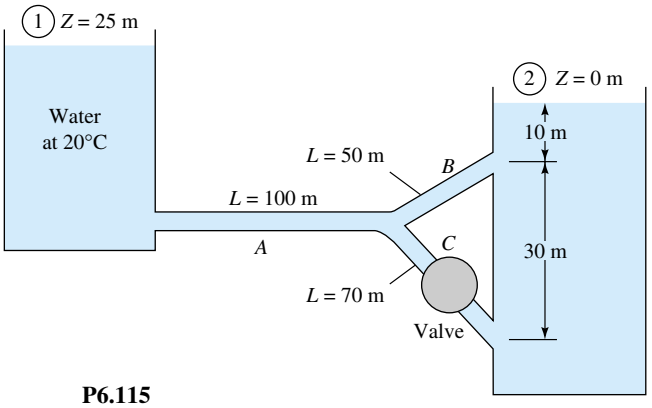
P6.113

P6.114 Modify Prob. 6.113 as follows. Let the pump be running and delivering 45 kW to the flow in pipe 2. The fluid is gasoline at 20°C. Determine (*a*) the flow rate in each pipe and (*b*) the overall pressure drop.

P6.115 In Fig. P6.115 all pipes are 8-cm-diameter cast iron. Determine the flow rate from reservoir 1 if va
(*a*) closed and (*b*) open, $K = 0.5$.

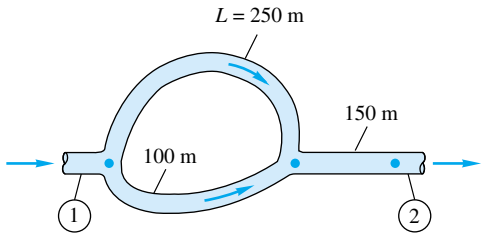


ketabline.com Ebook.ketabline.com



P6.115

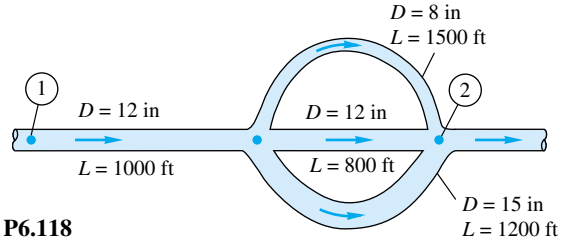
P6.116 For the series-parallel system of Fig. P6.116, all pipes are 8-cm-diameter asphalted cast iron. If the total pressure drop $p_1 - p_2 = 750$ kPa, find the resulting flow rate Q m^3/h for water at 20°C. Neglect minor losses.



P6.116

P6.117 Modify Prob. 6.116 as follows. Let the flow rate be 45 m^3/h of water at 20°C. Determine the overall pressure drop $p_1 - p_2$ in kPa. Neglect minor losses.

P6.118 For the piping system of Fig. P6.118, all pipes are concrete with a roughness of 0.04 in. Neglecting minor losses, compute the overall pressure drop $p_1 - p_2$ in lbf/in^2 if $Q = 20$ ft^3/s. The fluid is water at 20°C.



P6.118

P6.119 Modify Prob. 6.118 as follows. Let the pressure drop $p_1 - p_2$ be 98 lbf/in^2. Neglecting minor losses, determine the flow rate in m^3/h.

P6.120 Three cast-iron pipes are laid in parallel with these dimensions:

Pipe	Length, m	Diameter, cm
1	800	12
2	600	8
3	900	10

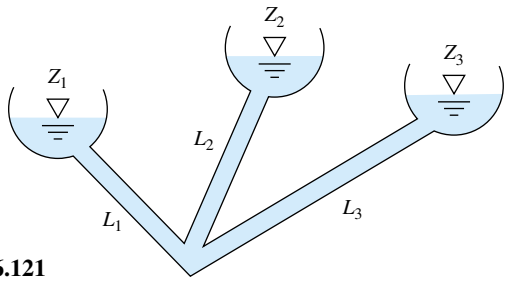
The total flow rate is 200 m^3/h of water at 20°C. Determine (*a*) the flow rate in each pipe and (*b*) the pressure drop across the system.

P6.121 Consider the three-reservoir system of Fig. P6.121 with the following data:

$$L_1 = 95 \text{ m} \quad L_2 = 125 \text{ m} \quad L_3 = 160 \text{ m}$$

$$z_1 = 25 \text{ m} \quad z_2 = 115 \text{ m} \quad z_3 = 85 \text{ m}$$

All pipes are 28-cm-diameter unfinished concrete ($\epsilon = 1$ mm). Compute the steady flow rate in all pipes for water at 20°C.



P6.121

P6.122 Modify Prob. 6.121 as follows. Reduce the diameter to 15 cm (with $\epsilon = 1$ mm), and compute the flow rates for water at 20°C. These flow rates distribute in nearly the same manner as in Prob. 6.121 but are about 5.2 times lower. Can you explain this difference?

P6.123 Modify Prob. 6.121 as follows. All data are the same except that z_3 is unknown. Find the value of z_3 for which the flow rate in pipe 3 is 0.2 m^3/s toward the junction. (This problem requires iteration and is best suited to a digital computer.)

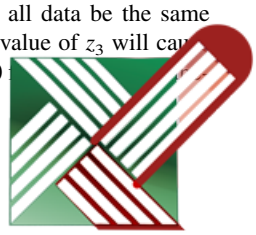
P6.124 The three-reservoir system in Fig. P6.124 delivers water at 20°C. The system data are as follows:

$$D_1 = 8 \text{ in} \quad D_2 = 6 \text{ in} \quad D_3 = 9 \text{ in}$$

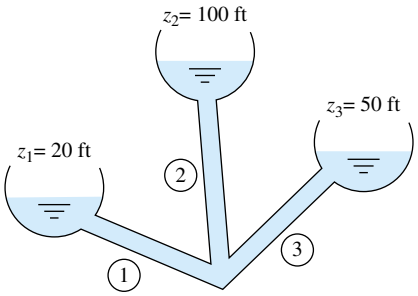
$$L_1 = 1800 \text{ ft} \quad L_2 = 1200 \text{ ft} \quad L_3 = 1600 \text{ ft}$$

All pipes are galvanized iron. Compute the flow rate in all pipes.

P6.125 Modify Prob. 6.124 as follows. Let all data be the same except z_3, which is unknown. What value of z_3 will cau
the flow rate through pipe 3 to be 1.0
tion?



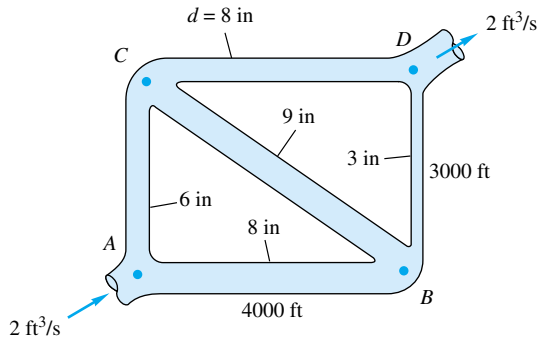
ketabline.com Ebook.ketabline.com



P6.124

P6.126 Modify Prob. 6.124 as follows. Let all data be the same except that pipe 1 is fitted with a butterfly valve (Fig. 6.19*b*). Estimate the proper valve opening angle (in degrees) for the flow rate through pipe 1 to be reduced to 1.5 ft^3/s toward reservoir 1. (This problem requires iteration and is best suited to a digital computer.)

P6.127 In the five-pipe horizontal network of Fig. P6.127, assume that all pipes have a friction factor $f = 0.025$. For the given inlet and exit flow rate of 2 ft^3/s of water at 20°C, determine the flow rate and direction in all pipes. If $p_A =$ 120 lbf/in^2 gage, determine the pressures at points *B*, *C*, and *D*.



P6.127

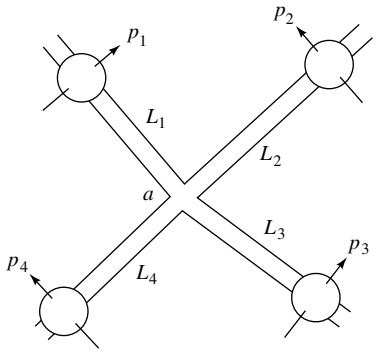
P6.128 Modify Prob. 6.127 as follows. Let the inlet flow rate at *A* and the exit flow at *D* be unknown. Let $p_A - p_B = 100$ lbf/in^2. Compute the flow rate in all five pipes.

P6.129 In Fig. P6.129 all four horizontal cast-iron pipes are 45 m long and 8 cm in diameter and meet at junction *a*, delivering water at 20°C. The pressures are known at four points as shown:

$$p_1 = 950 \text{ kPa} \qquad p_2 = 350 \text{ kPa}$$

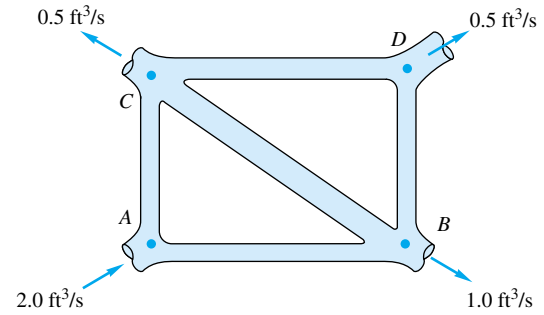
$$p_3 = 675 \text{ kPa} \qquad p_4 = 100 \text{ kPa}$$

Neglecting minor losses, determine the flow rate in each pipe.



P6.129

P6.130 In Fig. P6.130 lengths *AB* and *BD* are 2000 and 1500 ft, respectively. The friction factor is 0.022 everywhere, and $p_A = 90$ lbf/in^2 gage. All pipes have a diameter of 6 in. For water at 20°C, determine the flow rate in all pipes and the pressures at points *B*, *C*, and *D*.



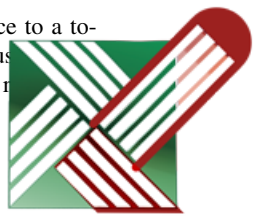
P6.130

P6.131 A water-tunnel test section has a 1-m diameter and flow properties $V = 20$ m/s, $p = 100$ kPa, and $T = 20$°C. The boundary-layer blockage at the end of the section is 9 percent. If a conical diffuser is to be added at the end of the section to achieve maximum pressure recovery, what should its angle, length, exit diameter, and exit pressure be?

P6.132 For Prob. 6.131 suppose we are limited by space to a total diffuser length of 10 m. What should the diffuser angle, exit diameter, and exit pressure be for maximum recovery?

P6.133 A wind-tunnel test section is 3 ft square with flow properties $V = 150$ ft/s, $p = 15$ lbf/in^2 absolute, and $T = 68$°F. Boundary-layer blockage at the end of the test section is 8 percent. Find the angle, length, exit height, and exit pressure of a flat-walled diffuser added onto the section to achieve maximum pressure recovery.

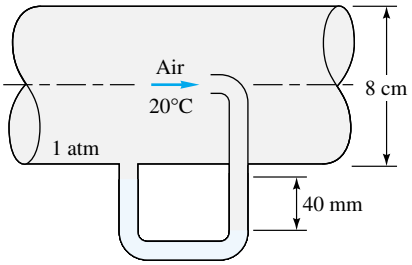
P6.134 For Prob. 6.133 suppose we are limited by space to a total diffuser length of 30 ft. What should the diffus
exit height, and exit pressure be for maximum r



ketabline.com Ebook.ketabline.com

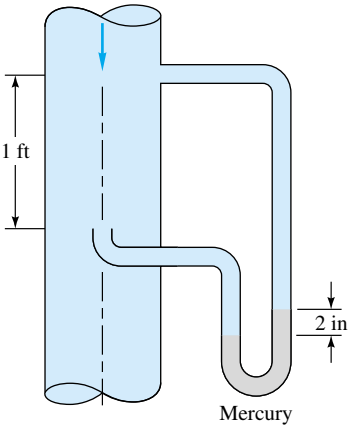
P6.135 A small airplane flying at 5000-m altitude uses a pitot stagnation probe without static holes. The measured stagnation pressure is 56.5 kPa. Estimate the airplane's speed in mi/h and its uncertainty. Is a compressibility correction needed?

P6.136 For the pitot-static pressure arrangement of Fig. P6.136, the manometer fluid is (colored) water at 20°C. Estimate (*a*) the centerline velocity, (*b*) the pipe volume flow, and (*c*) the (smooth) wall shear stress.



P6.136

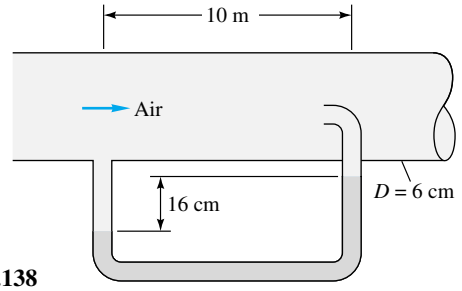
P6.137 For the 20°C water flow of Fig. P6.137, use the pitot-static arrangement to estimate (*a*) the centerline velocity and (*b*) the volume flow in the 5-in-diameter smooth pipe. (*c*) What error in flow rate is caused by neglecting the 1-ft elevation difference?



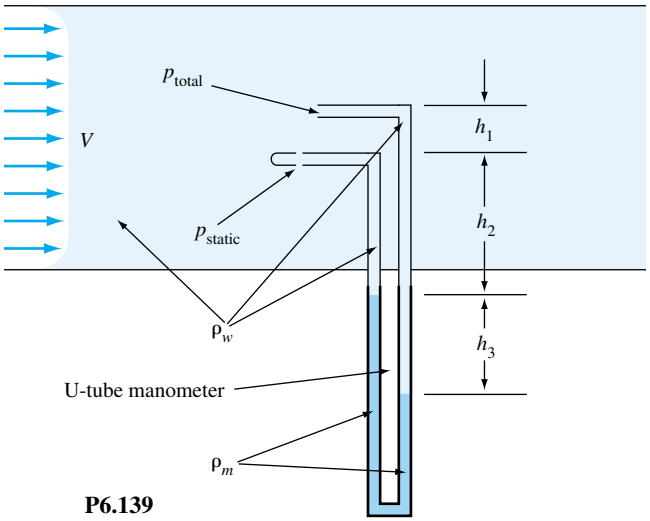
P6.137

P6.138 An engineer who took college fluid mechanics on a pass-fail basis has placed the static pressure hole far upstream of the stagnation probe, as in Fig. P6.138, thus contaminating the pitot measurement ridiculously with pipe friction losses. If the pipe flow is air at 20°C and 1 atm and the manometer fluid is Meriam red oil (SG = 0.827), estimate the air centerline velocity for the given manometer reading of 16 cm. Assume a smooth-walled tube.

P6.139 Professor Walter Tunnel needs to measure the flow velocity in a water tunnel. Due to budgetary restrictions, he cannot afford a pitot-static probe, but instead inserts a total



P6.138



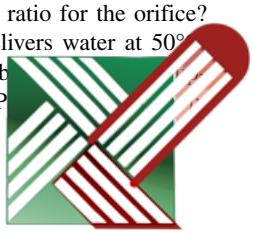
P6.139

head probe and a static pressure probe, as shown in Fig. P6.139, a distance h_1 apart from each other. Both probes are in the main free stream of the water tunnel, unaffected by the thin boundary layers on the sidewalls. The two probes are connected as shown to a U-tube manometer. The densities and vertical distances are shown in Fig. P6.139. (*a*) Write an expression for velocity V in terms of the parameters in the problem. (*b*) Is it critical that distance h_1 be measured accurately? (*c*) How does the expression for velocity V differ from that which would be obtained if a pitot-static probe had been available and used with the same U-tube manometer?

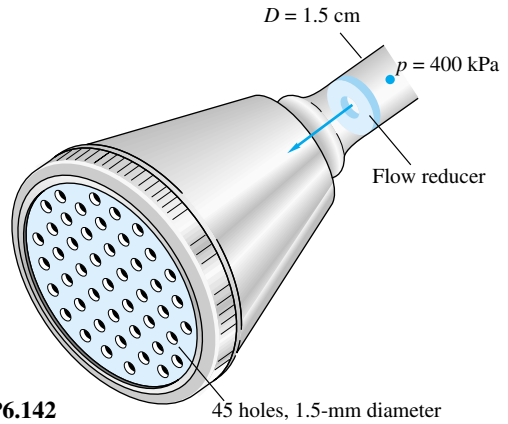
P6.140 Kerosine at 20°C flows at 18 m^3/h in a 5-cm-diameter pipe. If a 2-cm-diameter thin-plate orifice with corner taps is installed, what will the measured pressure drop be, in Pa?

P6.141 Gasoline at 20°C flows at 105 m^3/h in a 10-cm-diameter pipe. We wish to meter the flow with a thin-plate orifice and a differential pressure transducer which reads best at about 55 kPa. What is the proper β ratio for the orifice?

P6.142 The shower head in Fig. P6.142 delivers water at 50°
An orifice-type flow reducer is to b
stream pressure is constant at 400 kP



ketabline.com Ebook.ketabline.com



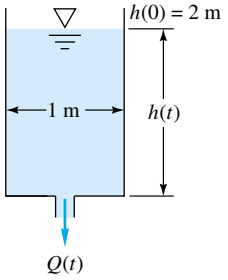
P6.142

gal/min, results without the reducer? What reducer orifice diameter would decrease the flow by 40 percent?

P6.143 A 10-cm-diameter smooth pipe contains an orifice plate with D: $\frac{1}{2}D$ taps and $\beta = 0.5$. The measured orifice pressure drop is 75 kPa for water flow at 20°C. Estimate the flow rate, in m^3/h. What is the nonrecoverable head loss?

P6.144 Accurate solution of Prob. 6.143, using Fig. 6.40, requires iteration because both the ordinate and the abscissa of this figure contain the unknown flow rate Q. In the spirit of Example 5.8, rescale the variables and construct a new plot in which Q may be read directly from the ordinate. Solve Prob. 6.143 with your new chart.

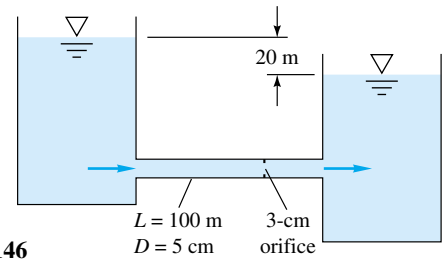
P6.145 The 1-m-diameter tank in Fig. P6.145 is initially filled with gasoline at 20°C. There is a 2-cm-diameter orifice in the bottom. If the orifice is suddenly opened, estimate the time for the fluid level $h(t)$ to drop from 2.0 to 1.6 m.



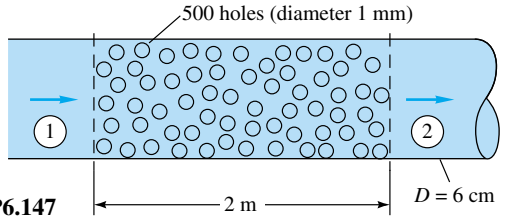
P6.145

P6.146 A pipe connecting two reservoirs, as in Fig. P6.146, contains a thin-plate orifice. For water flow at 20°C, estimate (*a*) the volume flow through the pipe and (*b*) the pressure drop across the orifice plate.

P6.147 Air flows through a 6-cm-diameter smooth pipe which has a 2-m-long perforated section containing 500 holes (diameter 1 mm), as in Fig. P6.147. Pressure outside the pipe is sea-level standard air. If $p_1 = 105$ kPa and $Q_1 = 110$ m^3/h, estimate p_2 and Q_2, assuming that the holes are approximated by thin-plate orifices. *Hint:* A momentum control volume may be very useful.

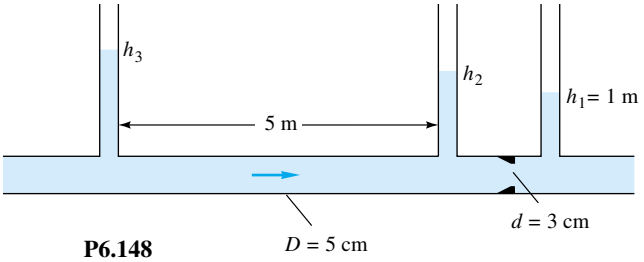


P6.146



P6.147

P6.148 A smooth pipe containing ethanol at 20°C flows at 7 m^3/h through a Bernoulli obstruction, as in Fig. P6.148. Three piezometer tubes are installed, as shown. If the obstruction is a thin-plate orifice, estimate the piezometer levels (*a*) h_2 and (*b*) h_3.



P6.148

P6.149 Repeat Prob. 6.148 if the obstruction is a long-radius flow nozzle.

P6.150 Gasoline at 20°C flows at 0.06 m^3/s through a 15-cm pipe and is metered by a 9-cm long-radius flow nozzle (Fig. 6.39*a*). What is the expected pressure drop across the nozzle?

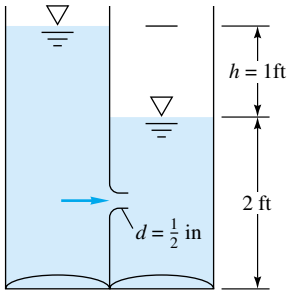
P6.151 Ethyl alcohol at 20°C flowing in a 6-cm-diameter pipe is metered through a 3-cm long-radius flow nozzle. If the measured pressure drop is 45 kPa, what is the estimated volume flow, in m^3/h?

P6.152 Kerosine at 20°C flows at 20 m^3/h in an 8-cm-diameter pipe. The flow is to be metered by an ISA 1932 flow nozzle so that the pressure drop is 7000 Pa. What is t
nozzle diameter?



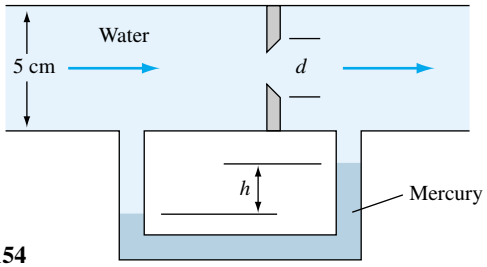
ketabline.com Ebook.ketabline.com

P6.153 Two water tanks, each with base area of 1 ft^2, are connected by a 0.5-in-diameter long-radius nozzle as in Fig. P6.153. If $h = 1$ ft as shown for $t = 0$, estimate the time for $h(t)$ to drop to 0.25 ft.



P6.153

***P6.154** Water at 20°C flows through the orifice in Fig. P6.154, which is monitored by a mercury manometer. If $d = 3$ cm, (*a*) what is h when the flow rate is 20 m^3/h and (*b*) what is Q in m^3/h when $h = 58$ cm?



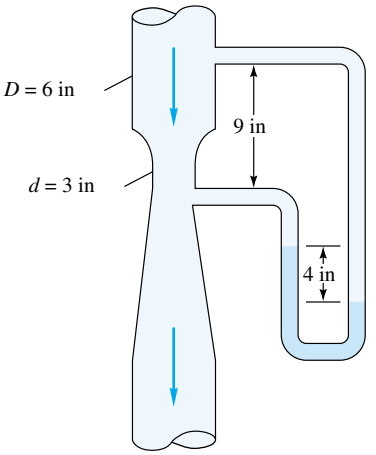
P6.154

P6.155 It is desired to meter a flow of 20°C gasoline in a 12-cm-diameter pipe, using a modern venturi nozzle. In order for international standards to be valid (Fig. 6.42), what is the permissible range of (*a*) flow rates, (*b*) nozzle diameters, and (*c*) pressure drops? (*d*) For the highest pressure-drop condition, would compressibility be a problem?

P6.156 Ethanol at 20°C flows down through a modern venturi nozzle as in Fig. P6.156. If the mercury manometer reading is 4 in, as shown, estimate the flow rate, in gal/min.

P6.157 Modify Prob. 6.156 if the fluid is air at 20°C, entering the venturi at a pressure of 18 lbf/in^2. Should a compressibility correction be used?

P6.158 Water at 20°C flows in a long horizontal commercial-steel 6-cm-diameter pipe which contains a classical Herschel



P6.156

venturi with a 4-cm throat. The venturi is connected to a mercury manometer whose reading is $h = 40$ cm. Estimate (*a*) the flow rate, in m^3/h, and (*b*) the total pressure difference between points 50 cm upstream and 50 cm downstream of the venturi.

P6.159 A modern venturi nozzle is tested in a laboratory flow with water at 20°C. The pipe diameter is 5.5 cm, and the venturi throat diameter is 3.5 cm. The flow rate is measured by a weigh tank and the pressure drop by a water-mercury manometer. The mass flow rate and manometer readings are as follows:

$\dot{m}$, kg/s	0.95	1.98	2.99	5.06	8.15
h, mm	3.7	15.9	36.2	102.4	264.4

Use these data to plot a calibration curve of venturi discharge coefficient versus Reynolds number. Compare with the accepted correlation, Eq. (6.134).

***P6.160** The butterfly-valve losses in Fig. 6.19*b* may be viewed as a type of Bernoulli obstruction device, as in Fig. 6.38. The "throat area" A_t in Eq. (6.125) can be interpreted as the two slivers of opening around the butterfly disk when viewed from upstream. First fit the average loss K_{mean} versus the opening angle in Fig. 6.19*b* to an exponential curve. Then use your curve fit to compute the "discharge coefficient" of a butterfly valve as a function of the opening angle. Plot the results and compare them to those for a typical flowmeter.



ketabline.com Ebook.ketabline.com

Word Problems

W6.1 In fully developed straight-duct flow, the velocity profiles do not change (why?), but the pressure drops along the pipe axis. Thus there is pressure work done on the fluid. If, say, the pipe is insulated from heat loss, where does this energy go? Make a thermodynamic analysis of the pipe flow.

W6.2 From the Moody chart (Fig. 6.13), rough surfaces, such as sand grains or ragged machining, do not affect laminar flow. Can you explain why? They *do* affect turbulent flow. Can you develop, or suggest, an analytical-physical model of turbulent flow near a rough surface which might be used to predict the known increase in pressure drop?

W6.3 Differentiation of the laminar pipe-flow solution, Eq. (6.40), shows that the fluid shear stress $\tau(r)$ varies linearly from zero at the axis to τ_w at the wall. It is claimed that this is also true, at least in the time mean, for fully developed *turbulent* flow. Can you verify this claim analytically?

W6.4 A porous medium consists of many tiny tortuous passages, and Reynolds numbers based on pore size are usually very low, of order unity. In 1856 H. Darcy proposed that the pressure gradient in a porous medium was directly proportional to the volume-averaged velocity $\mathbf{V}$ of the fluid:

$$\nabla p = -\frac{\mu}{K}\mathbf{V}$$

where K is termed the *permeability* of the medium. This is now called *Darcy's law* of porous flow. Can you make a Poiseuille flow model of porous-media flow which verifies Darcy's law? Meanwhile, as the Reynolds number increases, so that $VK^{1/2}/\nu > 1$, the pressure drop becomes nonlinear, as was shown experimentally by P. H. Forscheimer as early as 1782. The flow is still decidedly laminar, yet the pressure gradient is quadratic:

$$\nabla p = -\frac{\mu}{K}\mathbf{V} - C|V|\mathbf{V} \quad \text{Darcy-Forscheimer law}$$

where C is an empirical constant. Can you explain the reason for this nonlinear behavior?

W6.5 One flowmeter device, in wide use in the water supply and gasoline distribution industries, is the *nutating disk*. Look this up in the library, and explain in a brief report how it works and the advantages and disadvantages of typical designs.

Fundamentals of Engineering Exam Problems

FE6.1 In flow through a straight, smooth pipe, the diameter Reynolds number for transition to turbulence is generally taken to be
(*a*) 1500, (*b*) 2100, (*c*) 4000, (*d*) 250,000, (*e*) 500,000

FE6.2 For flow of water at 20°C through a straight, smooth pipe at 0.06 m^3/h, the pipe diameter for which transition to turbulence occurs is approximately
(*a*) 1.0 cm, (*b*) 1.5 cm, (*c*) 2.0 cm, (*d*) 2.5 cm, (*e*) 3.0 cm

FE6.3 For flow of oil [$\mu = 0.1$ kg/(m · s), SG = 0.9] through a long, straight, smooth 5-cm-diameter pipe at 14 m^3/h, the pressure drop per meter is approximately
(*a*) 2200 Pa, (*b*) 2500 Pa, (*c*) 10,000 Pa, (*d*) 160 Pa, (*e*) 2800 Pa

FE6.4 For flow of water at a Reynolds number of 1.03 E6 through a 5-cm-diameter pipe of roughness height 0.5 mm, the approximate Moody friction factor is
(*a*) 0.012, (*b*) 0.018, (*c*) 0.038, (*d*) 0.049, (*e*) 0.102

FE6.5 Minor losses through valves, fittings, bends, contractions, etc., are commonly modeled as proportional to
(*a*) total head, (*b*) static head, (*c*) velocity head, (*d*) pressure drop, (*e*) velocity

FE6.6 A smooth 8-cm-diameter pipe, 200 m long, connects two reservoirs, containing water at 20°C, one of which has a surface elevation of 700 m and the other with its surface elevation at 560 m. If minor losses are neglected, the expected flow rate through the pipe is
(*a*) 0.048 m^3/h, (*b*) 2.87 m^3/h, (*c*) 134 m^3/h, (*d*) 172 m^3/h, (*e*) 385 m^3/h

FE6.7 If, in Prob. FE6.6 the pipe is rough and the actual flow rate is 90 m^3/h, then the expected average roughness height of the pipe is approximately
(*a*) 1.0 mm, (*b*) 1.25 mm, (*c*) 1.5 mm, (*d*) 1.75 mm, (*e*) 2.0 mm

FE6.8 Suppose in Prob. FE6.6 the two reservoirs are connected, not by a pipe, but by a sharp-edged orifice of diameter 8 cm. Then the expected flow rate is approximately
(*a*) 90 m^3/h, (*b*) 579 m^3/h, (*c*) 748 m^3/h, (*d*) 949 m^3/h, (*e*) 1048 m^3/h

FE6.9 Oil [$\mu = 0.1$ kg/(m · s), SG = 0.9] flows through a 50-m-long smooth 8-cm-diameter pipe. The maximum pressure drop for which laminar flow is expected is approximately
(*a*) 30 kPa, (*b*) 40 kPa, (*c*) 50 kPa, (*d*) 60 kPa, (*e*) 70 kPa

FE6.10 Air at 20°C and approximately 1 atm flows through a smooth 30-cm-square duct at 1500 ft^3/min. The expected pressure drop per meter of duct length is
(*a*) 1.0 Pa, (*b*) 2.0 Pa, (*c*) 3.0 Pa, (*d*) 4.0 Pa, (*e*) 5.0 Pa

FE6.11 Water at 20°C flows at 3 m^3/h through a sharp-edged 3-cm-diameter orifice in a 6-cm-diameter pipe. Estimate the expected pressure drop across the orifice.
(*a*) 440 Pa, (*b*) 680 Pa, (*c*) 875 Pa, (*d*) 1750 Pa, (*e*)



ketabline.com Ebook.ketabline.com

FE6.12 Water flows through a straight 10-cm-diameter pipe at a diameter Reynolds number of 250,000. If the pipe roughness is 0.06 mm, what is the approximate Moody friction factor?
(*a*) 0.015, (*b*) 0.017, (*c*) 0.019, (*d*) 0.026, (*e*) 0.032

FE6.13 What is the hydraulic diameter of a rectangular air-ventilation duct whose cross section is 1 m by 25 cm?
(*a*) 25 cm, (*b*) 40 cm, (*c*) 50 cm, (*d*) 75 cm, (*e*) 100 cm

FE6.14 Water at 20°C flows through a pipe at 300 gal/min with a friction head loss of 45 ft. What is the power required to drive this flow?
(*a*) 0.16 kW, (*b*) 1.88 kW, (*c*) 2.54 kW, (*d*) 3.41 kW, (*e*) 4.24 kW

FE6.15 Water at 20°C flows at 200 gal/min through a pipe 150 m long and 8 cm in diameter. If the friction head loss is 12 m, what is the Moody friction factor?
(*a*) 0.010, (*b*) 0.015, (*c*) 0.020, (*d*) 0.025, (*e*) 0.030

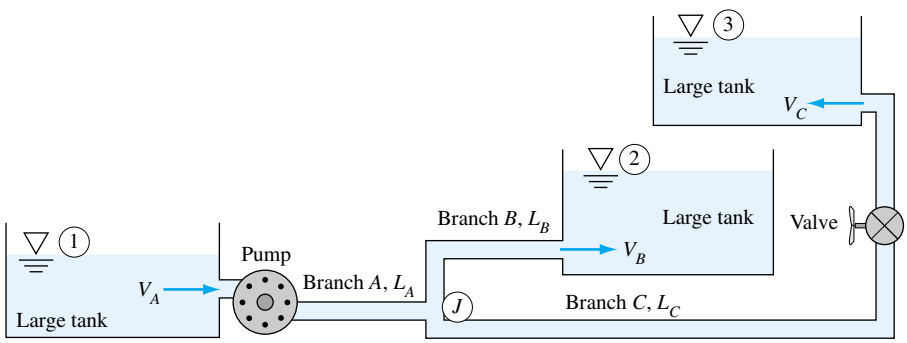
Comprehensive Problems

C6.1 A pitot-static probe will be used to measure the velocity distribution in a water tunnel at 20°C. The two pressure lines from the probe will be connected to a U-tube manometer which uses a liquid of specific gravity 1.7. The maximum velocity expected in the water tunnel is 2.3 m/s. Your job is to select an appropriate U-tube from a manufacturer which supplies manometers of heights 8, 12, 16, 24, and 36 in. The cost increases significantly with manometer height. Which of these should you purchase?

***C6.2** A pump delivers a steady flow of water (ρ, μ) from a large tank to two other higher-elevation tanks, as shown in Fig. C6.2. The same pipe of diameter d and roughness ϵ is used throughout. All minor losses *except through the valve* are neglected, and the partially closed valve has a loss coefficient K_{valve}. Turbulent flow may be assumed with all kinetic energy flux correction coefficients equal to 1.06. The pump net head H is a known function of Q_A and hence also of $V_A = Q_A/A_{pipe}$; for example, $H = a - bV_A^2$, where a and b are constants. Subscript J refers to the junction point at the tee where branch A splits into B and C. Pipe length L_C is much longer than L_B. It is desired to predict the pressure at J, the three pipe velocities and friction factors, and the pump head. Thus there are eight variables: H, V_A, V_B, V_C, f_A, f_B, f_C, p_J. Write down the eight equations needed to resolve this problem, but *do not solve,* since an elaborate iteration procedure, or an equation solver such as EES, would be required.

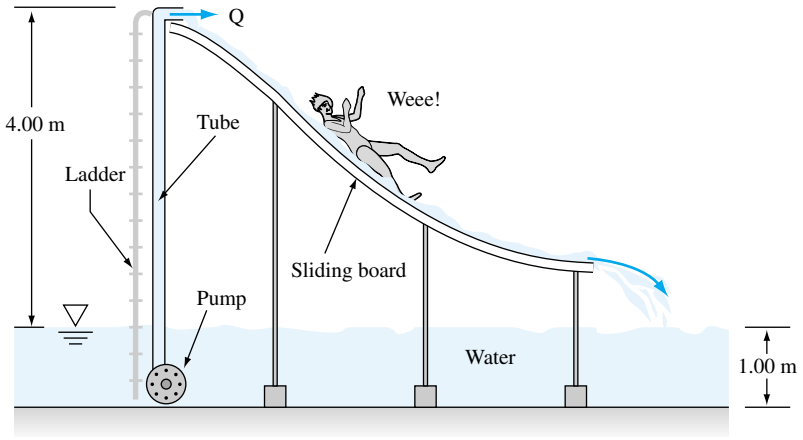
C6.3 A small water slide is to be installed inside a swimming pool. See Fig. C6.3. The slide manufacturer recommends a continuous water flow rate Q of 1.39×10^{-3} m^3/s (about 22 gal/min) down the slide, to ensure that the customers do not burn their bottoms. A pump is to be installed under the slide, with a 5.00-m-long, 4.00-cm-diameter hose supplying swimming pool water for the slide. The pump is 80 percent efficient and will rest fully submerged 1.00 m below the water surface. The roughness inside the hose is about 0.0080 cm. The hose discharges the water at the top of the slide as a free jet open to the atmosphere. The hose outlet is 4.00 m above the water surface. For fully developed turbulent pipe flow, the kinetic energy flux correction factor is about 1.06. Ignore any minor losses here. Assume that $\rho = 998$ kg/m^3 and $\nu = 1.00 \times 10^{-6}$ m^2/s for this water. Find the brake horsepower (i.e., the actual shaft power in watts) required to drive the pump.

C6.2





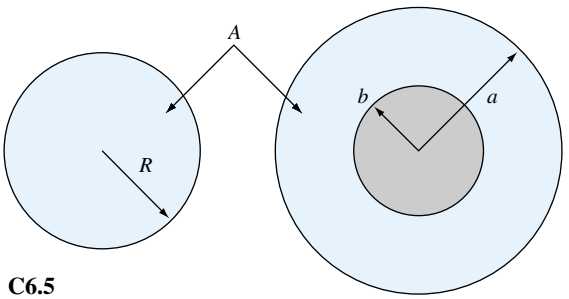
ketabline.com Ebook.ketabline.com



C6.3

***C6.4** Suppose you build a house out in the "boonies" where you need to run a pipe to the nearest water supply, which is fortunately at an elevation of about 1000 m above that of your house. The pipe will be 6.0 km long (the distance to the water supply), and the gage pressure at the water supply is 1000 kPa. You require a minimum of 3.0 gal/min of water when the end of your pipe is open to the atmosphere. To minimize cost, you want to buy the smallest-diameter pipe possible. The pipe you will use is extremely smooth. (*a*) Find the total head loss from the pipe inlet to its exit. Neglect any minor losses due to valves, elbows, entrance lengths, etc., since the length is so long here and major losses dominate. Assume the outlet of the pipe is open to the atmosphere. (*b*) Which is more important in this problem, the head loss due to elevation difference or the head loss due to pressure drop in the pipe? (*c*) Find the minimum required pipe diameter.

C6.5 Water at room temperature flows at the *same* volume flow rate, $Q = 9.4 \times 10^{-4}$ m^3/s, through two ducts, one a round pipe and one an annulus. The cross-sectional area A of the two ducts is identical, and all walls are made of commercial steel. Both ducts are the same length. In the cross sections shown in Fig. C6.5 $R = 15.0$ mm and $a = 25.0$ mm. (*a*) What is the radius b such that the cross-sectional areas of the two ducts are identical? (*b*) Compare the frictional head loss h_f per unit length of pipe for the two cases, assuming fully developed flow. For the annulus, do both a quick estimate (using the hydraulic diameter) and a more accurate estimate (using the effective diameter correction), and compare. (*c*) If the losses are different for the two cases, explain why. Which duct, if any, is more "efficient"?



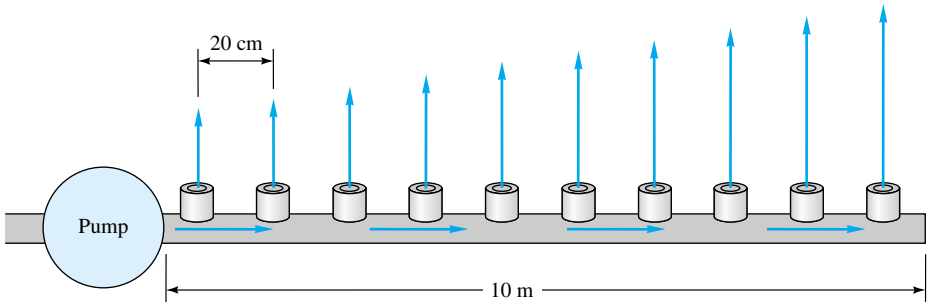
C6.5

Design Projects

D6.1 A hydroponic garden uses the 10-m-long perforated-pipe system in Fig. D6.1 to deliver water at 20°C. The pipe is 5 cm in diameter and contains a circular hole every 20 cm. A pump delivers water at 75 kPa (gage) at the entrance, while the other end of the pipe is closed. If you attempted, e.g., Prob. 3.125, you know that the pressure near the closed end of a perforated "manifold" is surprisingly high, and there will be too much flow through the holes near that end. One remedy is to vary the hole size along the pipe axis. Make a design analysis, perhaps using a personal computer, to pick the optimum hole-size distribution that will make the discharge flow rate as uniform as possible along the pipe axis. You are constrained to pick hole sizes that correspond only to commercial (numbe
ric drill-bit sizes available to the typical machine sh



ketabline.com Ebook.ketabline.com



D6.1

D6.2 It is desired to design a pump-piping system to keep a 1-million-gallon capacity water tank filled. The plan is to use a modified (in size and speed) version of the model 1206 centrifugal pump manufactured by Taco Inc., Cranston, Rhode Island. Test data have been provided to us by Taco Inc. for a small model of this pump: $D = 5.45$ in, $\Omega = 1760$ r/min, tested with water at 20°C:

Q, gal/min	0	5	10	15	20	25	30	35	40	45	50	55	60
H, ft	28	28	29	29	28	28	27	26	25	23	21	18	15
Efficiency, %	0	13	25	35	44	48	51	53	54	55	53	50	45

The tank is to be filled daily with rather chilly (10°C) groundwater from an aquifer, which is 0.8 mi from the tank and 150 ft lower than the tank. Estimated daily water use is 1.5 million gal/day. Filling time should not exceed 8 h per day. The piping system should have four "butterfly" valves with variable openings (see Fig. 6.19), 10 elbows of various angles, and galvanized-iron pipe of a size to be selected in the design. The design should be economical—both in capital costs and operating expense. Taco Inc. has provided the following cost estimates for system components:

Pump and motor	\$3500 plus \$1500 per inch of impeller size
Pump speed	Between 900 and 1800 r/min
Valves	\$300 + \$200 per inch of pipe size
Elbows	\$50 plus \$50 per inch of pipe size
Pipes	\$1 per inch of diameter per foot of length
Electricity cost	10¢ per kilowatthour

Your design task is to select an economical pipe size and pump impeller size and speed for this task, using the pump-test data in nondimensional form (see Prob. 5.61) as design data. Write a brief report (5 to 6 pages) showing your calculations and graphs.

References

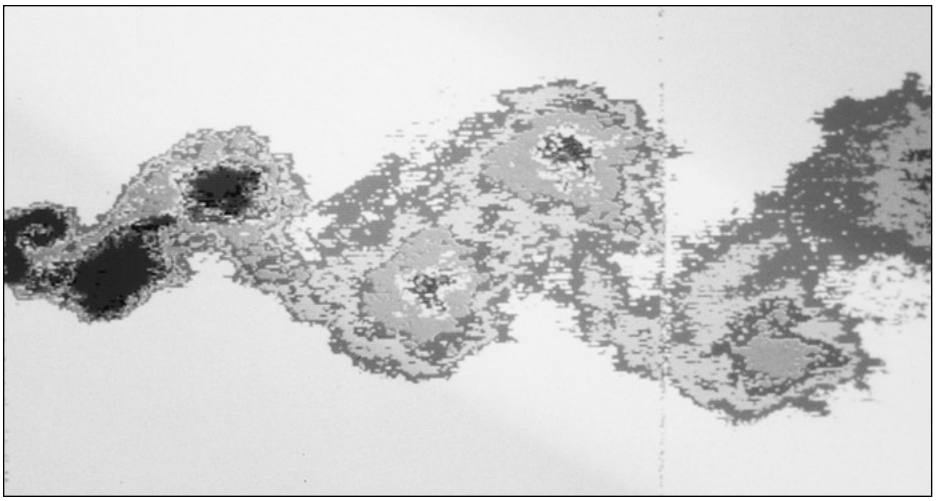
1. J. O. Hinze, *Turbulence,* 2d ed., McGraw-Hill, New York, 1975.
2. H. Schlichting, *Boundary Layer Theory,* 7th ed., McGraw-Hill, New York, 1979.
3. F. M. White, *Viscous Fluid Flow,* 2d ed., McGraw-Hill, New York, 1991.
4. O. Reynolds, "An Experimental Investigation of the Circumstances which Determine Whether the Motion of Water Shall Be Direct or Sinuous and of the Law of Resistance in Parallel Channels," *Phil. Trans. R. Soc.,* vol. 174, 1883, pp. 935–982.
5. P. G. Drazin and W. H. Reid, *Hydrodynamic Stability,* Cambridge University Press, London, 1981.
6. H. Rouse and S. Ince, *History of Hydraulics,* Iowa Institute of Hydraulic Research, State University of Iowa, Iowa City, 1957.
7. J. Nikuradse, "Strömungsgesetze in Rauhen Rohren," *VDI Forschungsh.* 361, 1933; English trans., *NACA Tech. Mem.* 1292.
8. L. F. Moody, "Friction Factors for Pipe Flow," *ASME Trans.,* vol. 66, pp. 671–684, 1944.
9. C. F. Colebrook, "Turbulent Flow in Pipes, with Particular Reference to the Transition between the Smooth and Rough Pipe Laws," *J. Inst. Civ. Eng. Lond.,* vol. 11, 1938–1939, pp. 133–156.
10. O. C. Jones, Jr., "An Improvement in the

ketabline.com Ebook.ketabline.com

bulent Friction in Rectangular Ducts," *J. Fluids Eng.,* June 1976, pp. 173–181.
11. R. Berker, *Handbuch der Physik,* vol. 7, no. 2, pp. 1–384, Springer-Verlag, Berlin, 1963.
12. R. M. Olson and S. J. Wright, *Essentials of Engineering Fluid Mechanics,* 5th ed., Harper & Row, New York, 1990.
13. D. Alciatore and W. S. Janna, "Modified Pipe Friction Diagrams that Eliminate Trial-and-Error Solutions," *Proc. 1st Natl. Fluid Dynamics Congress,* pt. 2, pp. 911–916, AIAA, Washington, DC, 1988.
14. P. W. Runstadler, Jr., et al., "Diffuser Data Book," *Creare Inc. Tech. Note* 186, Hanover, NH, 1975.
15. "Flow of Fluids through Valves, Fittings, and Pipe," *Crane Co. Tech. Pap.* 410, Chicago, 1957.
16. *Pipe Friction Manual,* 3d ed., The Hydraulic Institute, New York, 1961.
17. Hardy Cross, "Analysis of Flow in Networks of Conduits or Conductors," *Univ. Ill. Bull.* 286, November 1936.
18. R. W. Jepson, *Analysis of Flow in Pipe Networks,* Ann Arbor Pub., Ann Arbor, MI, 1976.
19. L. E. Ormsbee and D. J. Wood, "Explicit Pipeline Network Calibration," *J. Water Resources Planning and Management,* vol. 112, no. 2, April 1986, pp. 166–182.
20. J. Bardina et al,. "A Prediction Method for Planar Diffuser Flows," *J. Fluids Eng.,* vol. 103, 1981, pp. 315–321.
21. R. W. Fox and S. J. Kline, "Flow Regime Data and Design Methods for Curved Subsonic Diffusers," *J. Basic Eng*., vol. 84, 1962, pp. 303–312.
22. J. P. Holman, *Experimental Methods for Engineers,* 6th ed., McGraw-Hill, New York, 1993.
23. T. G. Beckwith and R. D. Marangoni, *Mechanical Measurements,* 4th ed., Addison-Wesley, Reading, MA, 1990.
24. B. Warren and C. Wunsch (eds.), *Evolution of Physical Oceanography,* M.I.T. Press, Cambridge, MA, 1981.
25. U.S. Department of Commerce, *Tidal Current Tables,* National Oceanographic and Atmospheric Administration, Washington, DC, 1971.
26. J. A. Shercliff, *Electromagnetic Flow Measurement,* Cambridge University Press, New York, 1962.
27. J. A. Miller, "A Simple Linearized Hot-Wire Anemometer," *J. Fluids Eng.,* December 1976, pp. 749–752.
28. R. J. Goldstein (ed.), *Fluid Mechanics Measurements,* 2d ed., Hemisphere, New York, 1996.
29. D. Eckardt, "Detailed Flow Investigations within a High Speed Centrifugal Compressor Impeller," *J. Fluids Eng.,* September 1976, pp. 390–402.
30. H. S. Bean (ed.), *Fluid Meters: Their Theory and Application,* 6th ed., American Society of Mechanical Engineers, New York, 1971.
31. "Measurement of Fluid Flow by Means of Orifice Plates, Nozzles, and Venturi Tubes Inserted in Circular Cross Section Conduits Running Full," *Int. Organ. Stand. Rep*. DIS-5167, Geneva, April 1976.
32. P. Moin and P. R. Spalart, in *Advances in Turbulence,* W. K. George and R. Arndt (eds.), Hemisphere, New York, 1989, pp. 11–38.
33. S. E. Haaland, "Simple and Explicit Formulas for the Friction Factor in Turbulent Pipe Flow," *J. Fluids Eng.,* March 1983, pp. 89–90.
34. R. K. Shah and A. L. London, *Laminar Flow Forced Convection in Ducts,* Academic, New York, 1979.
35. J. L. Lyons, *Lyons' Valve Designers Handbook,* Van Nostrand Reinhold, New York, 1982.
36. A. O. Demuren and W. Rodi, "Calculations of Turbulence-Driven Secondary Motion in Non-circular Ducts," *J. Fluid Mech.,* vol. 140, 1984, pp. 189– 222.
37. *ASHRAE Handbook of Fundamentals,* chap. 33, ASHRAE, Atlanta, 1981.
38. F. Durst, A. Melling, and J. H. Whitelaw, *Principles and Practice of Laser-Doppler Anemometry,* 2d ed., Academic, New York, 1981.
39. A. Dybbs and B. Ghorashi, *Laser Anemometry: Advances and Applications,* American Society of Mechanical Engineers, New York, 1991.
40. J. G. Kopp, "Vortex Flowmeters," *Meas. Control,* June 1983, pp. 280–284.
41. J. C. Graber, Jr., "Ultrasonic Flow," *Meas. Control,* October 1983, pp. 258–266.
42. ASME Fluid Meters Research Committee, "The ISO-ASME Orifice Coefficient Equation," *Mech. Eng.* July 1981, pp. 44–45.
43. R. D. Blevins, *Applied Fluid Dynamics Handbook,* Van Nostrand Reinhold, New York, 1984.
44. O. C. Jones, Jr., and J. C. M. Leung, "An Improvement in the Calculation of Turbulent Friction in Smooth Concentric Annuli," *J. Fluids Eng.,* December 1981, pp. 615–623.
45. P. R. Bandyopadhyay, "Aspects of the Equilibrium Puff in Transitional Pipe Flow, *J. Fluid Mech.,* vol. 163, 1986, pp. 439–458.
46. I. E. Idelchik, *Handbook of Hydraulic Resistance,* 3d ed., CRC Press, Boca Raton, FL, 1993.
47. Sanford Klein and William Beckman, *Engineering Equation Solver (EES),* University of Wisconsin, Madison, WI, 1997.
48. R. D. Coffield, P. T. McKeown, and R. B. Hammond, "Irrecoverable Pressure Loss Coefficients for Two Elbows in Series with Various Orientation Angles and Separation Distances," *Report WAPD-T-3117,* Bettis Atomic Power Laboratory, West Mifflin, PA, 1997.



ketabline.com Ebook.ketabline.com



The turbulent wake behind a bluff body immersed in a stream flow is a subject of the present chapter. This is a digitized video image showing the distribution of tracer-dye concentration in the wake of the body. Compare with Fig. 5.2a of the text, which is a laminar wake. *(Courtesy of R. Balachandar, by permission of the American Society of Mechanical Engineers.)*



ketabline.com Ebook.ketabline.com

Chapter 7
Flow Past Immersed Bodies

Motivation. This chapter is devoted to "external" flows around bodies immersed in a fluid stream. Such a flow will have viscous (shear and no-slip) effects near the body surfaces and in its wake, but will typically be nearly inviscid far from the body. These are unconfined *boundary-layer* flows.

Chapter 6 considered "internal" flows confined by the walls of a duct. In that case the viscous boundary layers grow from the sidewalls, meet downstream, and fill the entire duct. Viscous shear is the dominant effect. For example, the Moody chart of Fig. 6.13 is essentially a correlation of wall shear stress for long ducts of constant cross section.

External flows are unconfined, free to expand no matter how thick the viscous layers grow. Although boundary-layer theory (Sec. 7.3) is helpful in understanding external flows, complex body geometries usually require experimental data on the forces and moments caused by the flow. Such immersed-body flows are commonly encountered in engineering studies: *aerodynamics* (airplanes, rockets, projectiles), *hydrodynamics* (ships, submarines, torpedos), *transportation* (automobiles, trucks, cycles), *wind engineering* (buildings, bridges, water towers, wind turbines), and *ocean engineering* (buoys, breakwaters, pilings, cables, moored instruments). This chapter provides data and analysis to assist in such studies.

7.1 Reynolds-Number and Geometry Effects

The technique of boundary-layer (BL) analysis can be used to compute viscous effects near solid walls and to "patch" these onto the outer inviscid motion. This patching is more successful as the body Reynolds number becomes larger, as shown in Fig. 7.1.

In Fig. 7.1 a uniform stream U moves parallel to a sharp flat plate of length L. If the Reynolds number UL/ν is low (Fig. 7.1*a*), the viscous region is very broad and extends far ahead and to the sides of the plate. The plate retards the oncoming stream greatly, and small changes in flow parameters cause large changes in the pressure distribution along the plate. Thus, although in principle it should be possible to patch



ketabline.com Ebook.ketabline.com

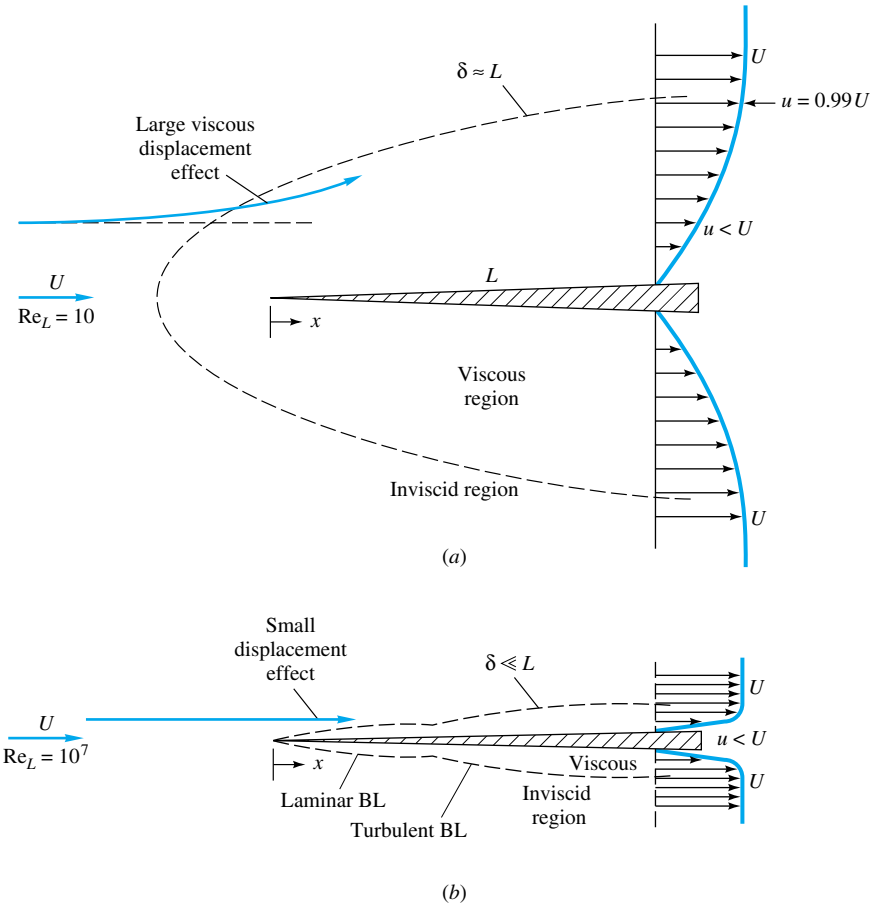
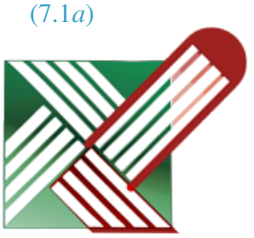


Fig. 7.1 Comparison of flow past a sharp flat plate at low and high Reynolds numbers: (*a*) laminar, low-Re flow; (*b*) high-Re flow.

viscous and inviscid layers in a mathematical analysis, their interaction is strong and nonlinear [1 to 3]. There is no existing simple theory for external-flow analysis at Reynolds numbers from 1 to about 1000. Such thick-shear-layer flows are typically studied by experiment or by numerical modeling of the flow field on a digital computer [4].

A high-Reynolds-number flow (Fig. 7.1*b*) is much more amenable to boundary-layer patching, as first pointed out by Prandtl in 1904. The viscous layers, either laminar or turbulent, are very thin, thinner even than the drawing shows. We define the boundary-layer thickness δ as the locus of points where the velocity u parallel to the plate reaches 99 percent of the external velocity U. As we shall see in Sec. 7.4, the accepted formulas for flat-plate flow are

$$\frac{\delta}{x} \approx \begin{cases} \dfrac{5.0}{\mathrm{Re}_x^{1/2}} & \text{laminar} \\ \dfrac{0.16}{\mathrm{Re}_x^{1/7}} & \text{turbulent} \end{cases} \qquad (7.1a)$$



ketabline.com Ebook.ketabline.com

where $\mathrm{Re}_x = Ux/\nu$ is called the *local Reynolds number* of the flow along the plate surface. The turbulent-flow formula applies for Re_x greater than approximately 10^6.

Some computed values from Eq. (7.1) are

Re_x	10^4	10^5	10^6	10^7	10^8
$(\delta/x)_{\mathrm{lam}}$	0.050	0.016	0.005		
$(\delta/x)_{\mathrm{turb}}$			0.022	0.016	0.011

The blanks indicate that the formula is not applicable. In all cases these boundary layers are so thin that their displacement effect on the outer inviscid layer is negligible. Thus the pressure distribution along the plate can be computed from inviscid theory as if the boundary layer were not even there. This external pressure field then "drives" the boundary-layer flow, acting as a forcing function in the momentum equation along the surface. We shall explain this boundary-layer theory in Secs. 7.4 and 7.5.

For slender bodies, such as plates and airfoils parallel to the oncoming stream, we conclude that this assumption of negligible interaction between the boundary layer and the outer pressure distribution is an excellent approximation.

For a blunt-body flow, however, even at very high Reynolds numbers, there is a discrepancy in the viscous-inviscid patching concept. Figure 7.2 shows two sketches of flow past a two- or three-dimensional blunt body. In the idealized sketch (7.2*a*), there is a thin film of boundary layer about the body and a narrow sheet of viscous wake in the rear. The patching theory would be glorious for this picture, but it is false. In the

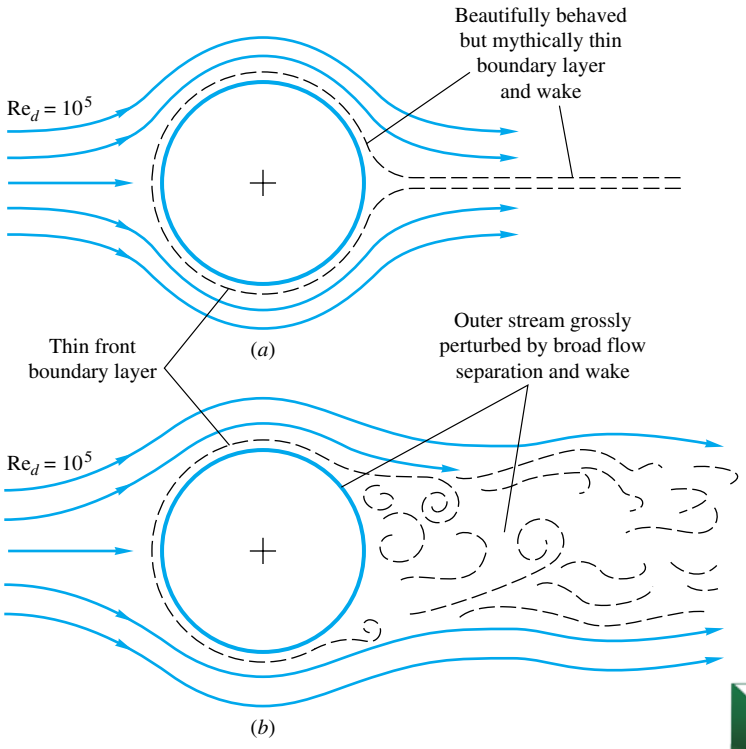


Fig. 7.2 Illustration of the strong interaction between viscous and inviscid regions in the rear of blunt-body flow: (*a*) idealized and definitely false picture of blunt-body flow; (*b*) actual picture of blunt-body flow.



ketabline.com Ebook.ketabline.com

actual flow (Fig. 7.2*b*), the boundary layer is thin on the front, or windward, side of the body, where the pressure decreases along the surface (*favorable* pressure gradient). But in the rear the boundary layer encounters increasing pressure (*adverse* pressure gradient) and breaks off, or separates, into a broad, pulsating wake. (See Fig. 5.2*a* for a photograph of a specific example.) The mainstream is deflected by this wake, so that the external flow is quite different from the prediction from inviscid theory with the addition of a thin boundary layer.

The theory of strong interaction between blunt-body viscous and inviscid layers is not well developed. Flows like that of Fig. 7.2*b* are normally studied experimentally. Reference 5 is an example of efforts to improve the theory of separated-boundary-layer flows. Reference 6 is a textbook devoted to separated flow.

EXAMPLE 7.1

A long, thin flat plate is placed parallel to a 20-ft/s stream of water at 20°C. At what distance x from the leading edge will the boundary-layer thickness be 1 in?

Solution

Since we do not know the Reynolds number, we must guess which of Eqs. (7.1) applies. From Table 1.4 for water, $\nu = 1.09 \times 10^{-5}$ ft^2/s; hence

$$\frac{U}{\nu} = \frac{20 \text{ ft/s}}{1.09 \times 10^{-5} \text{ ft}^2/\text{s}} = 1.84 \times 10^6 \text{ ft}^{-1}$$

With $\delta = 1$ in $= \frac{1}{12}$ ft, try Eq. (7.1*a*):

Laminar flow:
$$\frac{\delta}{x} = \frac{5}{(Ux/\nu)^{1/2}}$$

or
$$x = \frac{\delta^2(U/\nu)}{5^2} = \frac{(\frac{1}{12} \text{ ft})^2(1.84 \times 10^6 \text{ ft}^{-1})}{25} = 511 \text{ ft}$$

Now we can test the Reynolds number to see whether the formula applied:

$$\text{Re}_x = \frac{Ux}{\nu} = \frac{(20 \text{ ft/s})(511 \text{ ft})}{1.09 \times 10^{-5} \text{ ft}^2/\text{s}} = 9.4 \times 10^8$$

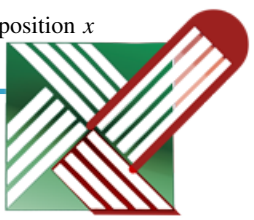
This is impossible since the maximum Re_x for laminar flow past a flat plate is 3×10^6. So we try again with Eq. (7.1*b*):

Turbulent flow:
$$\frac{\delta}{x} = \frac{0.16}{(Ux/\nu)^{1/7}}$$

or
$$x = \left[\frac{\delta(U/\nu)^{1/7}}{0.16}\right]^{7/6} = \left[\frac{(\frac{1}{12} \text{ ft})(1.84 \times 10^6 \text{ ft}^{-1})^{1/7}}{0.16}\right]^{7/6} = (4.09)^{7/6} = 5.17 \text{ ft} \qquad \textit{Ans.}$$

Test
$$\text{Re}_x = \frac{(20 \text{ ft/s})(5.17 \text{ ft})}{1.09 \times 10^{-5} \text{ ft}^2/\text{s}} = 9.5 \times 10^6$$

This is a perfectly proper turbulent-flow condition; hence we have found the correct position x on our second try.



ketabline.com Ebook.ketabline.com

7.2 Momentum-Integral Estimates

When we derived the momentum-integral relation, Eq. (3.37), and applied it to a flat-plate boundary layer in Example 3.11, we promised to consider it further in Chap. 7. Well, here we are! Let us review the problem, using Fig. 7.3.

A shear layer of unknown thickness grows along the sharp flat plate in Fig. 7.3. The no-slip wall condition retards the flow, making it into a rounded profile $u(y)$, which merges into the external velocity U = constant at a "thickness" $y = \delta(x)$. By utilizing the control volume of Fig. 3.11, we found (without making any assumptions about laminar versus turbulent flow) in Example 3.11 that the drag force on the plate is given by the following momentum integral across the exit plane

$$D(x) = \rho b \int_0^{\delta(x)} u(U - u)\, dy \tag{7.2}$$

where b is the plate width into the paper and the integration is carried out along a vertical plane x = constant. You should review the momentum-integral relation (3.37) and its use in Example 3.11.

Kármán's Analysis of the Flat Plate

Equation (7.2) was derived in 1921 by Kármán [7], who wrote it in the convenient form of the *momentum thickness* θ

$$D(x) = \rho b U^2 \theta \qquad \theta = \int_0^{\delta} \frac{u}{U}\left(1 - \frac{u}{U}\right) dy \tag{7.3}$$

Momentum thickness is thus a measure of total plate drag. Kármán then noted that the drag also equals the integrated wall shear stress along the plate

$$D(x) = b \int_0^x \tau_w(x)\, dx$$

or

$$\frac{dD}{dx} = b\tau_w \tag{7.4}$$

Meanwhile, the derivative of Eq. (7.3), with U = constant, is

$$\frac{dD}{dx} = \rho b U^2 \frac{d\theta}{dx}$$

By comparing this with Eq. (7.4) Kármán arrived at what is now called the *momentum-integral relation* for flat-plate boundary-layer flow

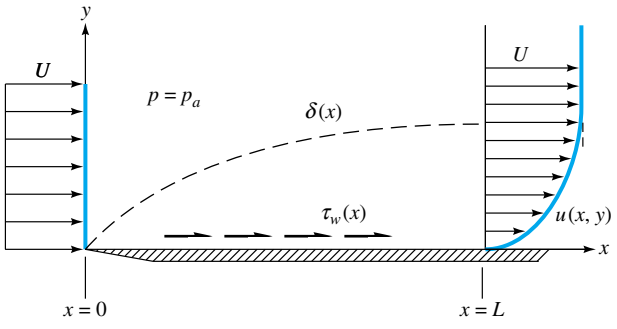


Fig. 7.3 Growth of a boundary layer on a flat plate.



ketabline.com Ebook.ketabline.com

$$\tau_w = \rho U^2 \frac{d\theta}{dx} \tag{7.5}$$

It is valid for either laminar or turbulent flat-plate flow.

To get a numerical result for laminar flow, Kármán assumed that the velocity profiles had an approximately parabolic shape

$$u(x, y) \approx U\left(\frac{2y}{\delta} - \frac{y^2}{\delta^2}\right) \qquad 0 \le y \le \delta(x) \tag{7.6}$$

which makes it possible to estimate both momentum thickness and wall shear

$$\theta = \int_0^\delta \left(\frac{2y}{\delta} - \frac{y^2}{\delta^2}\right)\left(1 - \frac{2y}{\delta} + \frac{y^2}{\delta^2}\right) dy \approx \frac{2}{15}\delta$$
$$\tau_w = \mu \left.\frac{\partial u}{\partial y}\right|_{y=0} \approx \frac{2\mu U}{\delta} \tag{7.7}$$

By substituting (7.7) into (7.5) and rearranging we obtain

$$\delta\, d\delta \approx 15 \frac{\nu}{U} dx \tag{7.8}$$

where $\nu = \mu/\rho$. We can integrate from 0 to x, assuming that $\delta = 0$ at $x = 0$, the leading edge

$$\frac{1}{2}\delta^2 = \frac{15\nu x}{U}$$

or

$$\frac{\delta}{x} \approx 5.5\left(\frac{\nu}{Ux}\right)^{1/2} = \frac{5.5}{\mathrm{Re}_x^{1/2}} \tag{7.9}$$

This is the desired thickness estimate. It is all approximate, of course, part of Kármán's *momentum-integral theory* [7], but it is startlingly accurate, being only 10 percent higher than the known exact solution for laminar flat-plate flow, which we gave as Eq. (7.1*a*).

By combining Eqs. (7.9) and (7.7) we also obtain a shear-stress estimate along the plate

$$c_f = \frac{2\tau_w}{\rho U^2} \approx \left(\frac{\frac{8}{15}}{\mathrm{Re}_x}\right)^{1/2} = \frac{0.73}{\mathrm{Re}_x^{1/2}} \tag{7.10}$$

Again this estimate, in spite of the crudeness of the profile assumption (7.6) is only 10 percent higher than the known exact laminar-plate-flow solution $c_f = 0.664/\mathrm{Re}_x^{1/2}$, treated in Sec. 7.4. The dimensionless quantity c_f, called the *skin-friction coefficient,* is analogous to the friction factor f in ducts.

A boundary layer can be judged as "thin" if, say, the ratio δ/x is less than about 0.1. This occurs at $\delta/x = 0.1 = 5.0/\mathrm{Re}_x^{1/2}$ or at $\mathrm{Re}_x = 2500$. For Re_x less than 2500 we can estimate that boundary-layer theory fails because the thick layer has a significant effect on the outer inviscid flow. The upper limit on Re_x for laminar flow is about 3×10^6, where measurements on a smooth flat plate [8] show that the flow undergoes transition to a turbulent boundary layer. From 3×10^6 upward the turbulent Reynolds num be arbitrarily large, and a practical limit at present is 5×10^9 for oil supertanke



ketabline.com Ebook.ketabline.com

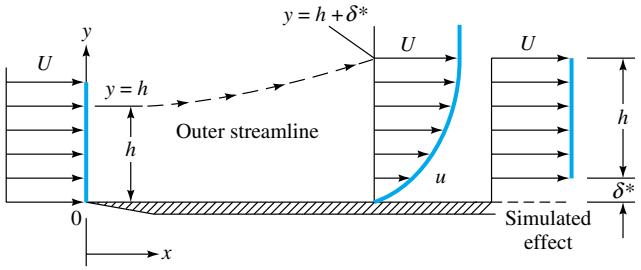


Fig. 7.4 Displacement effect of a boundary layer.

Displacement Thickness

Another interesting effect of a boundary layer is its small but finite displacement of the outer streamlines. As shown in Fig. 7.4, outer streamlines must deflect outward a distance $\delta^*(x)$ to satisfy conservation of mass between the inlet and outlet

$$\int_0^h \rho U b\, dy = \int_0^\delta \rho u b\, dy \qquad \delta = h + \delta^* \tag{7.11}$$

The quantity δ^* is called the *displacement thickness* of the boundary layer. To relate it to $u(y)$, cancel ρ and b from Eq. (7.11), evaluate the left integral, and slyly add and subtract U from the right integrand:

$$Uh = \int_0^\delta (U + u - U)\, dy = U(h + \delta^*) + \int_0^\delta (u - U)\, dy$$

or

$$\delta^* = \int_0^\delta \left(1 - \frac{u}{U}\right) dy \tag{7.12}$$

Thus the ratio of δ^*/δ varies only with the dimensionless velocity-profile shape u/U.

Introducing our profile approximation (7.6) into (7.12), we obtain by integration the approximate result

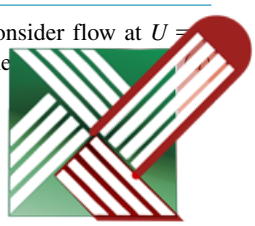
$$\delta^* \approx \frac{1}{3}\,\delta \qquad \frac{\delta^*}{x} \approx \frac{1.83}{\mathrm{Re}_x^{1/2}} \tag{7.13}$$

These estimates are only 6 percent away from the exact solutions for laminar flat-plate flow given in Sec. 7.4: $\delta^* = 0.344\delta = 1.721x/\mathrm{Re}_x^{1/2}$. Since δ^* is much smaller than x for large Re_x and the outer streamline slope V/U is proportional to δ^*, we conclude that the velocity normal to the wall is much smaller than the velocity parallel to the wall. This is a key assumption in boundary-layer theory (Sec. 7.3).

We also conclude from the success of these simple parabolic estimates that Kármán's momentum-integral theory is effective and useful. Many details of this theory are given in Refs. 1 to 3.

EXAMPLE 7.2

Are low-speed, small-scale air and water boundary layers really thin? Consider flow at $U =$ ft/s past a flat plate 1 ft long. Compute the boundary-layer thickness at the (*a*) air and (*b*) water at 20°C.



ketabline.com Ebook.ketabline.com

Solution

Part (a) From Table A.3, $\nu_{air} \approx 1.61$ E-4 ft^2/s. The trailing-edge Reynolds number thus is

$$\mathrm{Re}_L = \frac{UL}{\nu} = \frac{(1 \text{ ft/s})(1 \text{ ft})}{1.61 \text{ E-4 ft}^2/\text{s}} = 6200$$

Since this is less than 10^6, the flow is presumed laminar, and since it is greater than 2500, the boundary layer is reasonably thin. From Eq. (7.1*a*), the predicted laminar thickness is

$$\frac{\delta}{x} \approx \frac{5.0}{\sqrt{6200}} = 0.0634$$

or, at $x = 1$ ft, $\delta = 0.0634$ ft ≈ 0.76 in *Ans. (a)*

Part (b) From Table A.2 $\nu_{water} \approx 1.08$ E-5 ft^2/s. The trailing-edge Reynolds number is

$$\mathrm{Re}_L = \frac{(1 \text{ ft/s})(1 \text{ ft})}{1.08 \text{ E-5 ft}^2/\text{s}} \approx 92{,}600$$

This again satisfies the laminar and thinness conditions. The boundary-layer thickness is

$$\frac{\delta}{x} \approx \frac{5.0}{\sqrt{92{,}600}} = 0.0164$$

or, at $x = 1$ ft, $\delta = 0.0164$ ft ≈ 0.20 in *Ans. (b)*

Thus, even at such low velocities and short lengths, both airflows and water flows satisfy the boundary-layer approximations.

7.3 The Boundary-Layer Equations

In Chaps. 4 and 6 we learned that there are several dozen known analytical laminar-flow solutions [1 to 3]. None are for external flow around immersed bodies, although this is one of the primary applications of fluid mechanics. No exact solutions are known for turbulent flow, whose analysis typically uses empirical modeling laws to relate time-mean variables.

There are presently three techniques used to study external flows: (1) numerical (digital-computer) solutions, (2) experimentation, and (3) boundary-layer theory.

Computational fluid dynamics (CFD) is now well developed and described in advanced texts such as that by Anderson et al. [4]. Thousands of computer solutions and models have been published; execution times, mesh sizes, and graphical presentations are improving each year. Both laminar- and turbulent-flow solutions have been published, and turbulence modeling is a current research topic [9]. Except for a brief discussion of computer analysis in Chap. 8, the topic of CFD is beyond our scope here.

Experimentation is the most common method of studying external flows. Chapter 5 outlined the technique of dimensional analysis, and we shall give many nondimensional experimental data for external flows in Sec. 7.6.

The third tool is boundary-layer theory, first formulated by Ludwig Prandtl in 1904. We shall follow Prandtl's ideas here and make certain order-of-magnitude assumptions to greatly simplify the Navier-Stokes equations (4.38) into boundary-layer e
which are solved relatively easily and patched onto the outer inviscid-flow fie



ketabline.com Ebook.ketabline.com

One of the great achievements of boundary-layer theory is its ability to predict the flow separation illustrated in Fig. 7.2*b*. Before 1904 no one realized that such thin shear layers could cause such a gross effect as flow separation. Unfortunately, even today theory cannot accurately predict the behavior of the separated-flow region and its interaction with the outer layer. This is the weakness of boundary-layer theory, which we hope will be overcome by intensive research into the dynamics of separated flows [6].

Derivation for Two-Dimensional Flow

We consider only steady two-dimensional incompressible viscous flow with the x direction along the wall and y normal to the wall, as in Fig. 7.3.[1] We neglect gravity, which is important only in boundary layers where fluid buoyancy is dominant [2, sec. 4.13]. From Chap. 4, the complete equations of motion consist of continuity and the x- and y-momentum relations

$$\frac{\partial u}{\partial x} + \frac{\partial v}{\partial y} = 0 \tag{7.14a}$$

$$\rho\left(u\frac{\partial u}{\partial x} + v\frac{\partial u}{\partial y}\right) = -\frac{\partial p}{\partial x} + \mu\left(\frac{\partial^2 u}{\partial x^2} + \frac{\partial^2 u}{\partial y^2}\right) \tag{7.14b}$$

$$\rho\left(u\frac{\partial v}{\partial x} + v\frac{\partial v}{\partial y}\right) = -\frac{\partial p}{\partial y} + \mu\left(\frac{\partial^2 v}{\partial x^2} + \frac{\partial^2 v}{\partial y^2}\right) \tag{7.14c}$$

These should be solved for u, v, and p subject to typical no-slip, inlet, and exit boundary conditions, but in fact they are too difficult to handle for most external flows.

In 1904 Prandtl correctly deduced that a shear layer must be very thin if the Reynolds number is large, so that the following approximations apply:

Velocities: $$v \ll u \tag{7.15a}$$

Rates of change: $$\frac{\partial u}{\partial x} \ll \frac{\partial u}{\partial y} \qquad \frac{\partial v}{\partial x} \ll \frac{\partial v}{\partial y} \tag{7.15b}$$

Our discussion of displacement thickness in the previous section was intended to justify these assumptions.

Applying these approximations to Eq. (7.14*c*) results in a powerful simplification

$$\frac{\partial p}{\partial y} \approx 0 \qquad \text{or} \qquad p \approx p(x) \text{ only} \tag{7.16}$$

In other words, the y-momentum equation can be neglected entirely, and the pressure varies only *along* the boundary layer, not through it. The pressure-gradient term in Eq. (7.14*b*) is assumed to be known in advance from Bernoulli's equation applied to the outer inviscid flow

$$\frac{\partial p}{\partial x} = \frac{dp}{dx} = -\rho U\frac{dU}{dx} \tag{7.17}$$

[1] For a curved wall, x can represent the arc length along the wall and y can be everywhere normal to it with negligible change in the boundary-layer equations as long as the radius of curvature is large compared with the boundary-layer thickness [1 to 3].



ketabline.com Ebook.ketabline.com

Presumably we have already made the inviscid analysis and know the distribution of $U(x)$ along the wall (Chap. 8).

Meanwhile, one term in Eq. (7.14*b*) is negligible due to Eqs. (7.15)

$$\frac{\partial^2 u}{\partial x^2} \ll \frac{\partial^2 u}{\partial y^2} \tag{7.18}$$

However, neither term in the continuity relation (7.14*a*) can be neglected—another warning that continuity is always a vital part of any fluid-flow analysis.

The net result is that the three full equations of motion (7.14) are reduced to Prandtl's two boundary-layer equations

Continuity:
$$\frac{\partial u}{\partial x} + \frac{\partial v}{\partial y} = 0 \tag{7.19a}$$

Momentum along wall:
$$u\frac{\partial u}{\partial x} + v\frac{\partial u}{\partial y} \approx U\frac{dU}{dx} + \frac{1}{\rho}\frac{\partial \tau}{\partial y} \tag{7.19b}$$

where
$$\tau = \begin{cases} \mu \dfrac{\partial u}{\partial y} & \text{laminar flow} \\ \mu \dfrac{\partial u}{\partial y} - \rho\overline{u'v'} & \text{turbulent flow} \end{cases}$$

These are to be solved for $u(x, y)$ and $v(x, y)$, with $U(x)$ assumed to be a known function from the outer inviscid-flow analysis. There are two boundary conditions on u and one on v:

At $y = 0$ (wall): $u = v = 0$ (no slip) (7.20*a*)

At $y = \delta(x)$ (outer stream): $u = U(x)$ (patching) (7.20*b*)

Unlike the Navier-Stokes equations (7.14), which are mathematically elliptic and must be solved simultaneously over the entire flow field, the boundary-layer equations (7.19) are mathematically parabolic and are solved by beginning at the leading edge and marching downstream as far as you like, stopping at the separation point or earlier if you prefer.[2]

The boundary-layer equations have been solved for scores of interesting cases of internal and external flow for both laminar and turbulent flow, utilizing the inviscid distribution $U(x)$ appropriate to each flow. Full details of boundary-layer theory and results and comparison with experiment are given in Refs. 1 to 3. Here we shall confine ourselves primarily to flat-plate solutions (Sec. 7.4).

7.4 The Flat-Plate Boundary Layer

The classic and most often used solution of boundary-layer theory is for flat-plate flow, as in Fig. 7.3, which can represent either laminar or turbulent flow.

[2]For further mathematical details, see Ref. 2, sec. 2.8.



ketabline.com Ebook.ketabline.com

Laminar Flow

For laminar flow past the plate, the boundary-layer equations (7.19) can be solved exactly for u and v, assuming that the free-stream velocity U is constant ($dU/dx = 0$). The solution was given by Prandtl's student Blasius, in his 1908 dissertation from Göttingen. With an ingenious coordinate transformation, Blasius showed that the dimensionless velocity profile u/U is a function only of the single composite dimensionless variable $(y)[U/(\nu x)]^{1/2}$:

$$\frac{u}{U} = f'(\eta) \qquad \eta = y\left(\frac{U}{\nu x}\right)^{1/2} \tag{7.21}$$

where the prime denotes differentiation with respect to η. Substitution of (7.21) into the boundary-layer equations (7.19) reduces the problem, after much algebra, to a single third-order nonlinear ordinary differential equation for f

$$f''' + \tfrac{1}{2} f f'' = 0 \tag{7.22}$$

The boundary conditions (7.20) become

At $y = 0$: $$f(0) = f'(0) = 0 \tag{7.23a}$$

As $y \to \infty$: $$f'(\infty) \to 1.0 \tag{7.23b}$$

This is the *Blasius equation,* for which accurate solutions have been obtained only by numerical integration. Some tabulated values of the velocity-profile shape $f'(\eta) = u/U$ are given in Table 7.1.

Since u/U approaches 1.0 only as $y \to \infty$, it is customary to select the boundary-layer thickness δ as that point where $u/U = 0.99$. From the table, this occurs at $\eta \approx 5.0$:

$$\delta_{99\%}\left(\frac{U}{\nu x}\right)^{1/2} \approx 5.0$$

or

$$\frac{\delta}{x} \approx \frac{5.0}{\mathrm{Re}_x^{1/2}} \qquad \text{Blasius (1908)} \tag{7.24}$$

Table 7.1 The Blasius Velocity Profile [1 to 3]

$y[U/(\nu x)]^{1/2}$	u/U	$y[U/(\nu x)]^{1/2}$	u/U
0.0	0.0	2.8	0.81152
0.2	0.06641	3.0	0.84605
0.4	0.13277	3.2	0.87609
0.6	0.19894	3.4	0.90177
0.8	0.26471	3.6	0.92333
1.0	0.32979	3.8	0.94112
1.2	0.39378	4.0	0.95552
1.4	0.45627	4.2	0.96696
1.6	0.51676	4.4	0.97587
1.8	0.57477	4.6	0.98269
2.0	0.62977	4.8	0.98779
2.2	0.68132	5.0	0.99155
2.4	0.72899	∞	1.00000
2.6	0.77246		



ketabline.com Ebook.ketabline.com

With the profile known, Blasius, of course, could also compute the wall shear and displacement thickness

$$c_f = \frac{0.664}{\mathrm{Re}_x^{1/2}} \qquad \frac{\delta^*}{x} = \frac{1.721}{\mathrm{Re}_x^{1/2}} \tag{7.25}$$

Notice how close these are to our integral estimates, Eqs. (7.9), (7.10), and (7.13). When c_f is converted to dimensional form, we have

$$\tau_w(x) = \frac{0.332\rho^{1/2}\mu^{1/2}U^{1.5}}{x^{1/2}}$$

The wall shear drops off with $x^{1/2}$ because of boundary-layer growth and varies as velocity to the 1.5 power. This is in contrast to laminar pipe flow, where $\tau_w \propto U$ and is independent of x.

If $\tau_w(x)$ is substituted into Eq. (7.4), we compute the total drag force

$$D(x) = b\int_0^x \tau_w(x)\,dx = 0.664b\rho^{1/2}\mu^{1/2}U^{1.5}x^{1/2} \tag{7.26}$$

The drag increases only as the square root of the plate length. The nondimensional *drag coefficient* is defined as

$$C_D = \frac{2D(L)}{\rho U^2 bL} = \frac{1.328}{\mathrm{Re}_L^{1/2}} = 2c_f(L) \tag{7.27}$$

Thus, for laminar plate flow, C_D equals twice the value of the skin-friction coefficient at the trailing edge. This is the drag on one side of the plate.

Kármán pointed out that the drag could also be computed from the momentum relation (7.2). In dimensionless form, Eq. (7.2) becomes

$$C_D = \frac{2}{L}\int_0^\delta \frac{u}{U}\left(1 - \frac{u}{U}\right)dy \tag{7.28}$$

This can be rewritten in terms of the momentum thickness at the trailing edge

$$C_D = \frac{2\theta(L)}{L} \tag{7.29}$$

Computation of θ from the profile u/U or from C_D gives

$$\frac{\theta}{x} = \frac{0.664}{\mathrm{Re}_x^{1/2}} \qquad \text{laminar flat plate} \tag{7.30}$$

Since δ is so ill defined, the momentum thickness, being definite, is often used to correlate data taken for a variety of boundary layers under differing conditions. The ratio of displacement to momentum thickness, called the dimensionless-profile *shape factor,* is also useful in integral theories. For laminar flat-plate flow

$$H = \frac{\delta^*}{\theta} = \frac{1.721}{0.664} = 2.59 \tag{7.31}$$

A large shape factor then implies that boundary-layer separation is a
occur.



ketabline.com Ebook.ketabline.com

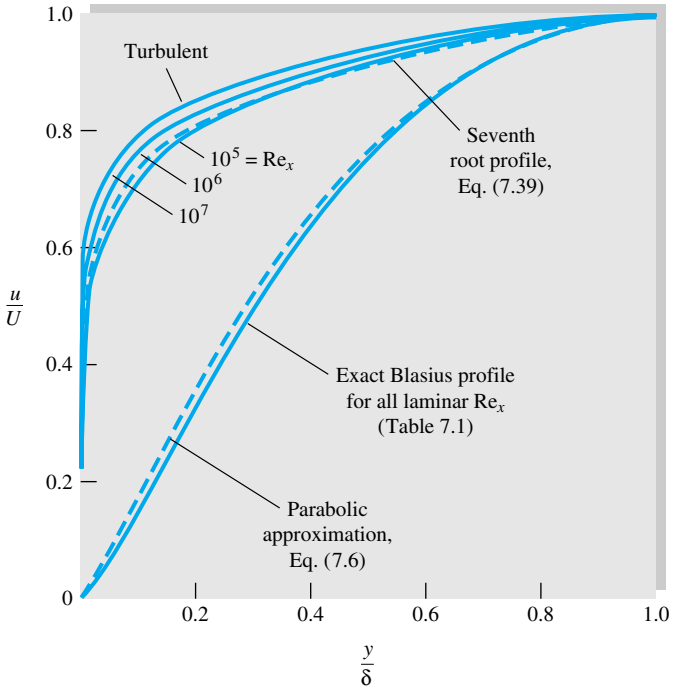


Fig. 7.5 Comparison of dimensionless laminar and turbulent flat-plate velocity profiles.

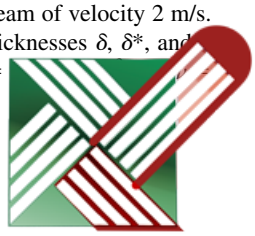
If we plot the Blasius velocity profile from Table 7.1 in the form of u/U versus y/δ, we can see why the simple integral-theory guess, Eq. (7.6), was such a great success. This is done in Fig. 7.5. The simple parabolic approximation is not far from the true Blasius profile; hence its momentum thickness is within 10 percent of the true value. Also shown in Fig. 7.5 are three typical turbulent flat-plate velocity profiles. Notice how strikingly different in shape they are from the laminar profiles. Instead of decreasing monotonically to zero, the turbulent profiles are very flat and then drop off sharply at the wall. As you might guess, they follow the logarithmic-law shape and thus can be analyzed by momentum-integral theory if this shape is properly represented.

Transition to Turbulence

The laminar flat-plate boundary layer eventually becomes turbulent, but there is no unique value for this change to occur. With care in polishing the wall and keeping the free stream quiet, one can delay the transition Reynolds number to $\mathrm{Re}_{x,\mathrm{tr}} \approx 3$ E6 [8]. However, for typical commercial surfaces and gusty free streams, a more realistic value is $\mathrm{Re}_{x,\mathrm{tr}} \approx 5$ E5.

EXAMPLE 7.3

A sharp flat plate with $L = 1$ m and $b = 3$ m is immersed parallel to a stream of velocity 2 m/s. Find the drag on one side of the plate, and at the trailing edge find the thicknesses δ, δ^*, and θ for (*a*) air, $\rho = 1.23$ kg/m^3 and $\nu = 1.46 \times 10^{-5}$ m^2/s, and (*b*) water, $\rho = 999$ kg/m^3 and $\nu = 1.02 \times 10^{-6}$ m^2/s.



ketabline.com Ebook.ketabline.com

Solution

Part (a) The airflow Reynolds number is

$$\frac{VL}{\nu} = \frac{(2.0 \text{ m/s})(1.0 \text{ m})}{1.46 \times 10^{-5} \text{ m}^2/\text{s}} = 137{,}000$$

Since this is less than 3×10^6, we assume that the boundary layer is laminar. From Eq. (7.27), the drag coefficient is

$$C_D = \frac{1.328}{(137{,}000)^{1/2}} = 0.00359$$

Thus the drag on one side in the airflow is

$$D = C_D \tfrac{1}{2}\rho U^2 bL = 0.00359(\tfrac{1}{2})(1.23)(2.0)^2(3.0)(1.0) = 0.0265 \text{ N} \quad \textit{Ans. (a)}$$

The boundary-layer thickness at the end of the plate is

$$\frac{\delta}{L} = \frac{5.0}{\text{Re}_L^{1/2}} = \frac{5.0}{(137{,}000)^{1/2}} = 0.0135$$

or

$$\delta = 0.0135(1.0) = 0.0135 \text{ m} = 13.5 \text{ mm} \quad \textit{Ans. (a)}$$

We find the other two thicknesses simply by ratios:

$$\delta^* = \frac{1.721}{5.0}\,\delta = 4.65 \text{ mm} \qquad \theta = \frac{\delta^*}{2.59} = 1.79 \text{ mm} \quad \textit{Ans. (a)}$$

Notice that no conversion factors are needed with SI units.

Part (b) The water Reynolds number is

$$\text{Re}_L = \frac{2.0(1.0)}{1.02 \times 10^{-6}} = 1.96 \times 10^6$$

This is rather close to the critical value of 3×10^6, so that a rough surface or noisy free stream might trigger transition to turbulence; but let us assume that the flow is laminar. The water drag coefficient is

$$C_D = \frac{1.328}{(1.96 \times 10^6)^{1/2}} = 0.000949$$

and

$$D = 0.000949(\tfrac{1}{2})(1000)(2.0)^2(3.0)(1.0) = 5.70 \text{ N} \quad \textit{Ans. (b)}$$

The drag is 215 times more for water in spite of the higher Reynolds number and lower drag coefficient because water is 57 times more viscous and 813 times denser than air. From Eq. (7.26), in laminar flow, it should have $(57)^{1/2}(813)^{1/2} = 7.53(28.5) = 215$ times more drag.

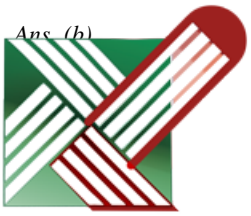
The boundary-layer thickness is given by

$$\frac{\delta}{L} = \frac{5.0}{(1.96 \times 10^6)^{1/2}} = 0.00357$$

or

$$\delta = 0.00357(1000 \text{ mm}) = 3.57 \text{ mm} \quad \textit{Ans. (b)}$$

By scaling down we have



ketabline.com Ebook.ketabline.com

$$\delta^* = \frac{1.721}{5.0}\,\delta = 1.23 \text{ mm} \qquad \theta = \frac{\delta^*}{2.59} = 0.48 \text{ mm} \qquad \textit{Ans. (b)}$$

The water layer is 3.8 times thinner than the air layer, which reflects the square root of the 14.3 ratio of air to water kinematic viscosity.

Turbulent Flow

There is no exact theory for turbulent flat-plate flow, although there are many elegant computer solutions of the boundary-layer equations using various empirical models for the turbulent eddy viscosity [9]. The most widely accepted result is simply an integal analysis similar to our study of the laminar-profile approximation (7.6).

We begin with Eq. (7.5), which is valid for laminar or turbulent flow. We write it here for convenient reference:

$$\tau_w(x) = \rho U^2 \frac{d\theta}{dx} \tag{7.32}$$

From the definition of c_f, Eq. (7.10), this can be rewritten as

$$c_f = 2\frac{d\theta}{dx} \tag{7.33}$$

Now recall from Fig. 7.5 that the turbulent profiles are nowhere near parabolic. Going back to Fig. 6.9, we see that flat-plate flow is very nearly logarithmic, with a slight outer wake and a thin viscous sublayer. Therefore, just as in turbulent pipe flow, we assume that the logarithmic law (6.21) holds all the way across the boundary layer

$$\frac{u}{u^*} \approx \frac{1}{\kappa}\ln\frac{yu^*}{\nu} + B \qquad u^* = \left(\frac{\tau_w}{\rho}\right)^{1/2} \tag{7.34}$$

with, as usual, $\kappa = 0.41$ and $B = 5.0$. At the outer edge of the boundary layer, $y = \delta$ and $u = U$, and Eq. (7.34) becomes

$$\frac{U}{u^*} = \frac{1}{\kappa}\ln\frac{\delta u^*}{\nu} + B \tag{7.35}$$

But the definition of the skin-friction coefficient, Eq. (7.10), is such that the following identities hold:

$$\frac{U}{u^*} \equiv \left(\frac{2}{c_f}\right)^{1/2} \qquad \frac{\delta u^*}{\nu} \equiv \mathrm{Re}_\delta\left(\frac{c_f}{2}\right)^{1/2} \tag{7.36}$$

Therefore Eq. (7.35) is a *skin-friction law* for turbulent flat-plate flow

$$\left(\frac{2}{c_f}\right)^{1/2} \approx 2.44\ln\left[\mathrm{Re}_\delta\left(\frac{c_f}{2}\right)^{1/2}\right] + 5.0 \tag{7.37}$$

It is a complicated law, but we can at least solve for a few values and list them:

Re_δ	10^4	10^5	10^6	10^7
c_f	0.00493	0.00315	0.00217	0.00158



ketabline.com Ebook.ketabline.com

Following a suggestion of Prandtl, we can forget the complex log friction law (7.37) and simply fit the numbers in the table to a power-law approximation

$$c_f \approx 0.02\ \mathrm{Re}_\delta^{-1/6} \tag{7.38}$$

This we shall use as the left-hand side of Eq. (7.33). For the right-hand side, we need an estimate for $\theta(x)$ in terms of $\delta(x)$. If we use the logarithmic-law profile (7.34), we shall be up to our hips in logarithmic integrations for the momentum thickness. Instead we follow another suggestion of Prandtl, who pointed out that the turbulent profiles in Fig. 7.5 can be approximated by a one-seventh-power law

$$\left(\frac{u}{U}\right)_{\text{turb}} \approx \left(\frac{y}{\delta}\right)^{1/7} \tag{7.39}$$

This is shown as a dashed line in Fig. 7.5. It is an excellent fit to the low-Reynolds-number turbulent data, which were all that were available to Prandtl at the time. With this simple approximation, the momentum thickness (7.28) can easily be evaluated:

$$\theta \approx \int_0^\delta \left(\frac{y}{\delta}\right)^{1/7}\left[1 - \left(\frac{y}{\delta}\right)^{1/7}\right] dy = \frac{7}{72}\,\delta \tag{7.40}$$

We accept this result and substitute Eqs. (7.38) and (7.40) into Kármán's momentum law (7.33)

$$c_f = 0.02\ \mathrm{Re}_\delta^{-1/6} = 2\,\frac{d}{dx}\left(\frac{7}{72}\,\delta\right)$$

or

$$\mathrm{Re}_\delta^{-1/6} = 9.72\,\frac{d\delta}{dx} = 9.72\,\frac{d(\mathrm{Re}\delta)}{d(\mathrm{Re}_x)} \tag{7.41}$$

Separate the variables and integrate, assuming $\delta = 0$ at $x = 0$:

$$\mathrm{Re}_\delta \approx 0.16\ \mathrm{Re}_x^{6/7} \qquad \text{or} \qquad \frac{\delta}{x} \approx \frac{0.16}{\mathrm{Re}_x^{1/7}} \tag{7.42}$$

Thus the thickness of a turbulent boundary layer increases as $x^{6/7}$, far more rapidly than the laminar increase $x^{1/2}$. Equation (7.42) is the solution to the problem, because all other parameters are now available. For example, combining Eqs. (7.42) and (7.38), we obtain the friction variation

$$c_f \approx \frac{0.027}{\mathrm{Re}_x^{1/7}} \tag{7.43}$$

Writing this out in dimensional form, we have

$$\tau_{w,\text{turb}} \approx \frac{0.0135\mu^{1/7}\rho^{6/7}U^{13/7}}{x^{1/7}} \tag{7.44}$$

Turbulent plate friction drops slowly with x, increases nearly as ρ and U^2, and is rather insensitive to viscosity.

We can evaluate the drag coefficient from Eq. (7.29)

$$C_D = \frac{0.031}{\mathrm{Re}_L^{1/7}} = \frac{7}{6}\,c_f(L)$$



ketabline.com Ebook.ketabline.com

Then C_D is only 16 percent greater than the trailing-edge skin friction [compare with Eq. (7.27) for laminar flow].

The displacement thickness can be estimated from the one-seventh-power law and Eq. (7.12):

$$\delta^* \approx \int_0^\delta \left[1 - \left(\frac{y}{\delta}\right)^{1/7}\right] dy = \frac{1}{8}\,\delta \tag{7.46}$$

The turbulent flat-plate shape factor is approximately

$$H = \frac{\delta^*}{\theta} = \frac{\frac{1}{8}}{\frac{7}{72}} = 1.3 \tag{7.47}$$

These are the basic results of turbulent flat-plate theory.

Figure 7.6 shows flat-plate drag coefficients for both laminar-and turbulent-flow conditions. The smooth-wall relations (7.27) and (7.45) are shown, along with the effect of wall roughness, which is quite strong. The proper roughness parameter here is x/ϵ or L/ϵ, by analogy with the pipe parameter ϵ/d. In the fully rough regime, C_D is independent of the Reynolds number, so that the drag varies exactly as U^2 and is inde-

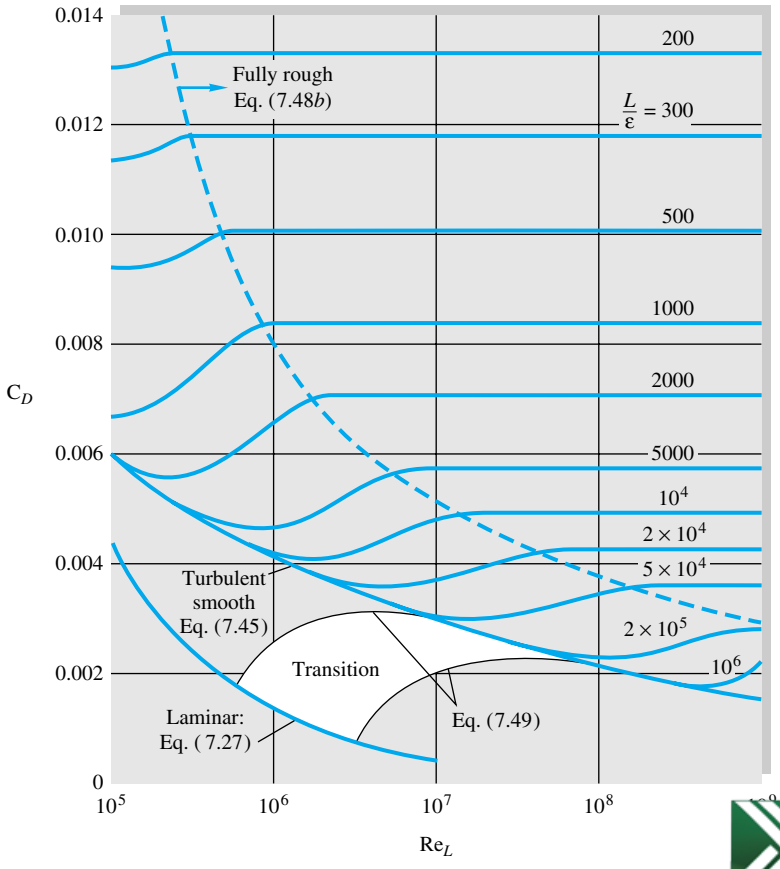


Fig. 7.6 Drag coefficient of laminar and turbulent boundary layers on smooth and rough flat plates. This chart is the flat-plate analog of the Moody diagram of Fig. 6.13.

ketabline.com Ebook.ketabline.com

pendent of μ. Reference 2 presents a theory of rough flat-plate flow, and Ref. 1 gives a curve fit for skin friction and drag in the fully rough regime:

$$c_f \approx \left(2.87 + 1.58 \log \frac{x}{\epsilon}\right)^{-2.5} \tag{7.48a}$$

$$C_D \approx \left(1.89 + 1.62 \log \frac{L}{\epsilon}\right)^{-2.5} \tag{7.48b}$$

Equation (7.48*b*) is plotted to the right of the dashed line in Fig. 7.6. The figure also shows the behavior of the drag coefficient in the transition region $5 \times 10^5 < \mathrm{Re}_L < 8 \times 10^7$, where the laminar drag at the leading edge is an appreciable fraction of the total drag. Schlichting [1] suggests the following curve fits for these transition drag curves depending upon the Reynolds number $\mathrm{Re}_{\mathrm{trans}}$ where transition begins:

$$C_D \approx \begin{cases} \dfrac{0.031}{\mathrm{Re}_L^{1/7}} - \dfrac{1440}{\mathrm{Re}_L} & \mathrm{Re}_{\mathrm{trans}} = 5 \times 10^5 \quad (7.49a) \\ \dfrac{0.031}{\mathrm{Re}_L^{1/7}} - \dfrac{8700}{\mathrm{Re}_L} & \mathrm{Re}_{\mathrm{trans}} = 3 \times 10^6 \quad (7.49b) \end{cases}$$

EXAMPLE 7.4

A hydrofoil 1.2 ft long and 6 ft wide is placed in a water flow of 40 ft/s, with $\rho = 1.99$ slugs/ft^3 and $\nu = 0.000011$ ft^2/s. (*a*) Estimate the boundary-layer thickness at the end of the plate. Estimate the friction drag for (*b*) turbulent smooth-wall flow from the leading edge, (*c*) laminar turbulent flow with $\mathrm{Re}_{\mathrm{trans}} = 5 \times 10^5$, and (*d*) turbulent rough-wall flow with $\epsilon = 0.0004$ ft.

Solution

Part (a) The Reynolds number is

$$\mathrm{Re}_L = \frac{UL}{\nu} = \frac{(40 \text{ ft/s})(1.2 \text{ ft})}{0.000011 \text{ ft}^2/\text{s}} = 4.36 \times 10^6$$

Thus the trailing-edge flow is certainly turbulent. The maximum boundary-layer thickness would occur for turbulent flow starting at the leading edge. From Eq. (7.42),

$$\frac{\delta(L)}{L} = \frac{0.16}{(4.36 \times 10^6)^{1/7}} = 0.018$$

or

$$\delta = 0.018(1.2 \text{ ft}) = 0.0216 \text{ ft} \qquad \textit{Ans. (a)}$$

This is 7.5 times thicker than a fully laminar boundary layer at the same Reynolds number.

Part (b) For fully turbulent smooth-wall flow, the drag coefficient on one side of the plate is, from Eq. (7.45),

$$C_D = \frac{0.031}{(4.36 \times 10^6)^{1/7}} = 0.00349$$



ketabline.com Ebook.ketabline.com

Then the drag on both sides of the foil is approximately

$$D = 2C_D(\tfrac{1}{2}\rho U^2)bL = 2(0.00349)(\tfrac{1}{2})(1.99)(40)^2(6.0)(1.2) = 80 \text{ lb} \qquad \textit{Ans. (b)}$$

Part (c) With a laminar leading edge and $\text{Re}_{\text{trans}} = 5 \times 10^5$, Eq. (7.49*a*) applies:

$$C_D = 0.00349 - \frac{1440}{4.36 \times 10^6} = 0.00316$$

The drag can be recomputed for this lower drag coefficient:

$$D = 2C_D(\tfrac{1}{2}\rho U^2)bL = 72 \text{ lbf} \qquad \textit{Ans. (c)}$$

Part (d) Finally, for the rough wall, we calculate

$$\frac{L}{\epsilon} = \frac{1.2 \text{ ft}}{0.0004 \text{ ft}} = 3000$$

From Fig. 7.6 at $\text{Re}_L = 4.36 \times 10^6$, this condition is just inside the fully rough regime. Equation (7.48*b*) applies:

$$C_D = (1.89 + 1.62 \log 3000)^{-2.5} = 0.00644$$

and the drag estimate is

$$D = 2C_D(\tfrac{1}{2}\rho U^2)bL = 148 \text{ lbf} \qquad \textit{Ans. (d)}$$

This small roughness nearly doubles the drag. It is probable that the total hydrofoil drag is still another factor of 2 larger because of trailing-edge flow-separation effects.

7.5 Boundary Layers with Pressure Gradient[3]

The flat-plate analysis of the previous section should give us a good feeling for the behavior of both laminar and turbulent boundary layers, except for one important effect: flow separation. Prandtl showed that separation like that in Fig. 7.2*b* is caused by excessive momentum loss near the wall in a boundary layer trying to move downstream against increasing pressure, $dp/dx > 0$, which is called an *adverse pressure gradient*. The opposite case of decreasing pressure, $dp/dx < 0$, is called a *favorable gradient,* where flow separation can never occur. In a typical immersed-body flow, e.g., Fig. 7.2*b*, the favorable gradient is on the front of the body and the adverse gradient is in the rear, as discussed in detail in Chap. 8.

We can explain flow separation with a geometric argument about the second derivative of velocity u at the wall. From the momentum equation (7.19*b*) at the wall, where $u = v = 0$, we obtain

$$\left.\frac{\partial \tau}{\partial y}\right|_{\text{wall}} = \mu \left.\frac{\partial^2 u}{\partial y^2}\right|_{\text{wall}} = -\rho U \frac{dU}{dx} = \frac{dp}{dx}$$

or

$$\left.\frac{\partial^2 u}{\partial y^2}\right|_{\text{wall}} = \frac{1}{\mu}\frac{dp}{dx} \qquad (7.50)$$

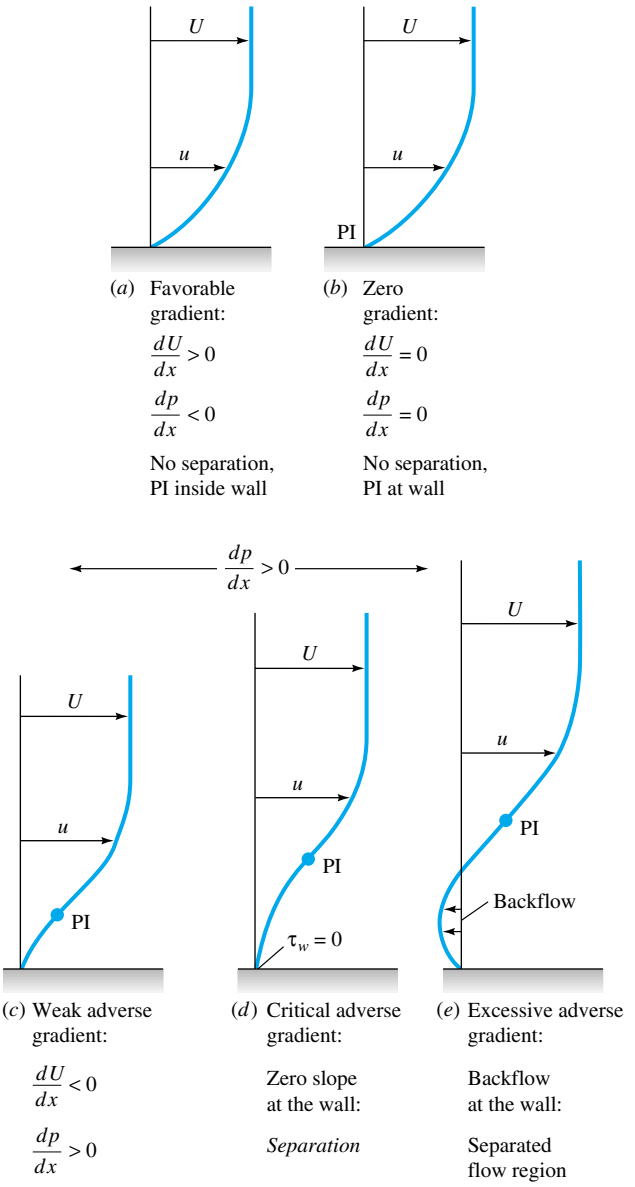
[3]This section may be omitted without loss of continuity.



ketabline.com Ebook.ketabline.com

for either laminar or turbulent flow. Thus in an adverse gradient the second derivative of velocity is positive at the wall; yet it must be negative at the outer layer ($y = \delta$) to merge smoothly with the mainstream flow $U(x)$. It follows that the second derivative must pass through zero somewhere in between, at a point of inflection, and any boundary-layer profile in an adverse gradient must exhibit a characteristic S shape.

Figure 7.7 illustrates the general case. In a favorable gradient (Fig. 7.7*a*) the profile



(*a*) Favorable gradient: $\frac{dU}{dx} > 0$, $\frac{dp}{dx} < 0$. No separation, PI inside wall

(*b*) Zero gradient: $\frac{dU}{dx} = 0$, $\frac{dp}{dx} = 0$. No separation, PI at wall

(*c*) Weak adverse gradient: $\frac{dU}{dx} < 0$, $\frac{dp}{dx} > 0$. No separation, PI in the flow

(*d*) Critical adverse gradient: Zero slope at the wall: *Separation*

(*e*) Excessive adverse gradient: Backflow at the wall: Separated flow region

Fig. 7.7 Effect of pressure gradient on boundary-layer profiles; PI = point of inflection.

ketabline.com Ebook.ketabline.com

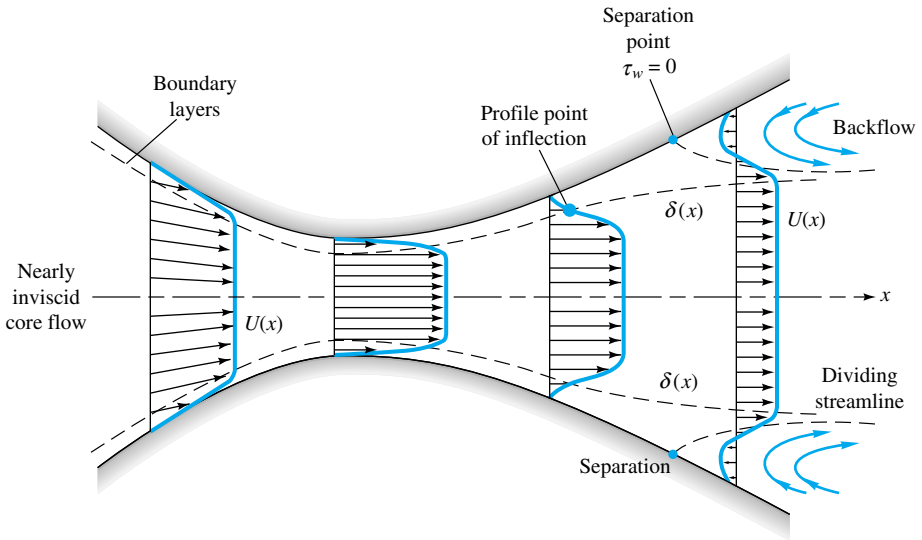
is very rounded, there is no point of inflection, there can be no separation, and laminar profiles of this type are very resistant to a transition to turbulence [1 to 3].

In a zero pressure gradient (Fig. 7.7*b*), e.g., flat-plate flow, the point of inflection is at the wall itself. There can be no separation, and the flow will undergo transition at Re_x no greater than about 3×10^6, as discussed earlier.

In an adverse gradient (Fig. 7.7*c* to *e*), a point of inflection (PI) occurs in the boundary layer, its distance from the wall increasing with the strength of the adverse gradient. For a weak gradient (Fig. 7.7*c*) the flow does not actually separate, but it is vulnerable to transition to turbulence at Re_x as low as 10^5 [1, 2]. At a moderate gradient, a critical condition (Fig. 7.7*d*) is reached where the wall shear is exactly zero ($\partial u/\partial y = 0$). This is defined as the *separation point* ($\tau_w = 0$), because any stronger gradient will actually cause backflow at the wall (Fig. 7.7*e*): the boundary layer thickens greatly, and the main flow breaks away, or separates, from the wall (Fig. 7.2*b*).

The flow profiles of Fig. 7.7 usually occur in sequence as the boundary layer progresses along the wall of a body. For example, in Fig. 7.2*a*, a favorable gradient occurs on the front of the body, zero pressure gradient occurs just upstream of the shoulder, and an adverse gradient occurs successively as we move around the rear of the body.

A second practical example is the flow in a duct consisting of a nozzle, throat, and diffuser, as in Fig. 7.8. The nozzle flow is a favorable gradient and never separates, nor



Nozzle:	*Throat*:	*Diffuser*:
Decreasing pressure and area	Constant pressure and area	Increasing pressure and area
Increasing velocity	Velocity constant	Decreasing velocity
Favorable gradient	Zero gradient	Adverse gradient (boundary layer thickens)

Fig. 7.8 Boundary-layer growth and separation in a nozzle-diffuser configuration.



ketabline.com Ebook.ketabline.com

does the throat flow where the pressure gradient is approximately zero. But the expanding-area diffuser produces low velocity and increasing pressure, an adverse gradient. If the diffuser angle is too large, the adverse gradient is excessive, and the boundary layer will separate at one or both walls, with backflow, increased losses, and poor pressure recovery. In the diffuser literature [10] this condition is called *diffuser stall,* a term used also in airfoil aerodynamics (Sec. 7.6) to denote airfoil boundary-layer separation. Thus the boundary-layer behavior explains why a large-angle diffuser has heavy flow losses (Fig. 6.23) and poor performance (Fig. 6.28).

Presently boundary-layer theory can compute only up to the separation point, after which it is invalid. New techniques are now developed for analyzing the strong interaction effects caused by separated flows [5, 6].

Laminar Integral Theory

Both laminar and turbulent theories can be developed from Kármán's general two-dimensional boundary-layer integral relation [7], which extends Eq. (7.33) to variable $U(x)$

$$\frac{\tau_w}{\rho U^2} = \frac{1}{2} c_f = \frac{d\theta}{dx} + (2 + H)\frac{\theta}{U}\frac{dU}{dx} \tag{7.51}$$

where $\theta(x)$ is the momentum thickness and $H(x) = \delta^*(x)/\theta(x)$ is the shape factor. From Eq. (7.17) negative dU/dx is equivalent to positive dp/dx, that is, an adverse gradient.

We can integrate Eq. (7.51) to determine $\theta(x)$ for a given $U(x)$ if we correlate c_f and H with the momentum thickness. This has been done by examining typical velocity profiles of laminar and turbulent boundary-layer flows for various pressure gradients. Some examples are given in Fig. 7.9, showing that the shape factor H is a good indicator of the pressure gradient. The higher the H, the stronger the adverse gradient, and separation occurs approximately at

$$H \approx \begin{cases} 3.5 & \text{laminar flow} \\ 2.4 & \text{turbulent flow} \end{cases} \tag{7.52}$$

The laminar profiles (Fig. 7.9*a*) clearly exhibit the S shape and a point of inflection with an adverse gradient. But in the turbulent profiles (Fig. 7.9*b*) the points of inflection are typically buried deep within the thin viscous sublayer, which can hardly be seen on the scale of the figure.

There are scores of turbulent theories in the literature, but they are all complicated algebraically and will be omitted here. The reader is referred to advanced texts [1, 2, 9].

For laminar flow, a simple and effective method was developed by Thwaites [11], who found that Eq. (7.51) can be correlated by a single dimensionless momentum-thickness variable λ, defined as

$$\lambda = \frac{\theta^2}{\nu}\frac{dU}{dx} \tag{7.53}$$

Using a straight-line fit to his correlation, Thwaites was able to integrate Eq. (7.51) in closed form, with the result

$$\theta^2 = \theta_0^2\left(\frac{U_0}{U}\right)^6 + \frac{0.45\nu}{U^6}\int_0^x U^5\,dx$$



ketabline.com Ebook.ketabline.com

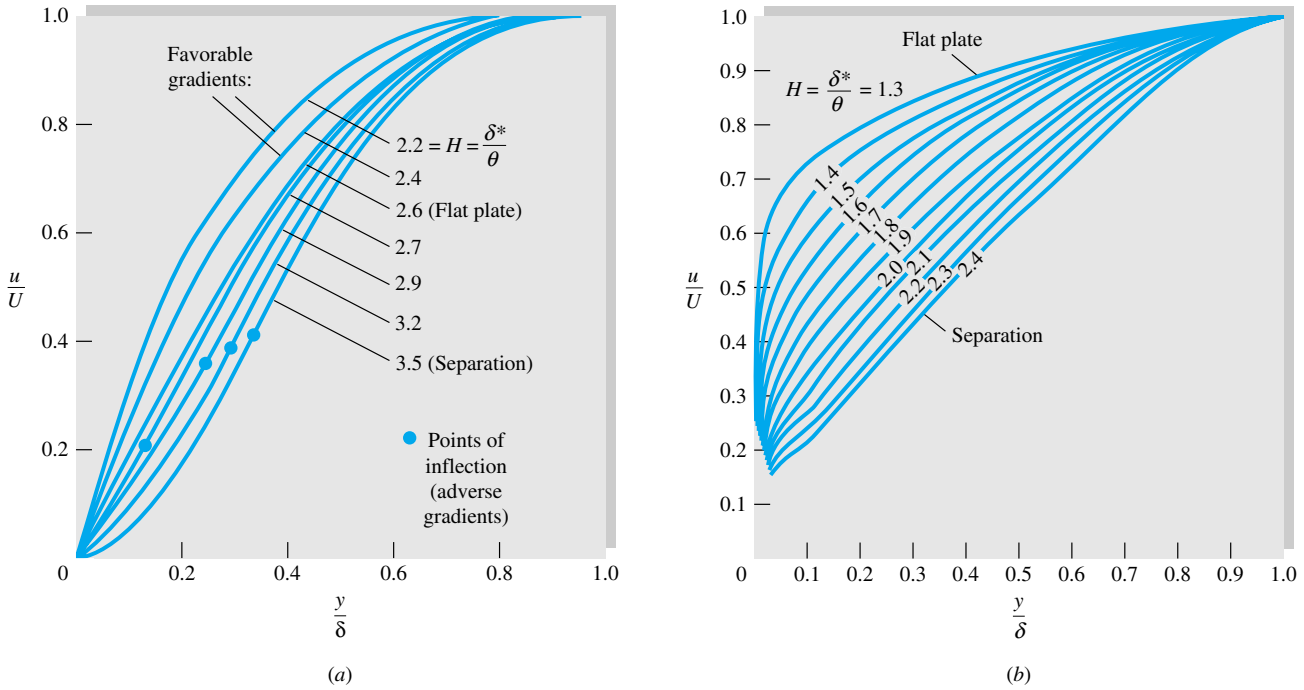


Fig. 7.9 Velocity profiles with pressure gradient: (*a*) laminar flow; (*b*) turbulent flow with adverse gradients.

where θ_0 is the momentum thickness at $x = 0$ (usually taken to be zero). Separation ($c_f = 0$) was found to occur at a particular value of λ

Separation: $$\lambda = -0.09 \tag{7.55}$$

Finally, Thwaites correlated values of the dimensionless shear stress $S = \tau_w\theta/(\mu U)$ with λ, and his graphed result can be curve-fitted as follows:

$$S(\lambda) = \frac{\tau_w \theta}{\mu U} \approx (\lambda + 0.09)^{0.62} \tag{7.56}$$

This parameter is related to the skin friction by the identity

$$S \equiv \tfrac{1}{2} c_f \, \mathrm{Re}_\theta \tag{7.57}$$

Equations (7.54) to (7.56) constitute a complete theory for the laminar boundary layer with variable $U(x)$, with an accuracy of ± 10 percent compared with exact digital-computer solutions of the laminar-boundary-layer equations (7.19). Complete details of Thwaites' and other laminar theories are given in Refs. 2 and 3.

As a demonstration of Thwaites' method, take a flat plate, where U = constant, $\lambda = 0$, and $\theta_0 = 0$. Equation (7.54) integrates to

$$\theta^2 = \frac{0.45\nu x}{U}$$



ketabline.com Ebook.ketabline.com

or
$$\frac{\theta}{x} = \frac{0.671}{\mathrm{Re}_x^{1/2}} \tag{7.58}$$

This is within 1 percent of Blasius' exact solution, Eq. (7.30).

With $\lambda = 0$, Eq. (7.56) predicts the flat-plate shear to be

$$\frac{\tau_w \theta}{\mu U} = (0.09)^{0.62} = 0.225$$

or
$$c_f = \frac{2\tau_w}{\rho U^2} = \frac{0.671}{\mathrm{Re}_x^{1/2}} \tag{7.59}$$

This is also within 1 percent of the Blasius result, Eq. (7.25). However, the general accuracy of this method is poorer than 1 percent because Thwaites actually "tuned" his correlation constants to make them agree with exact flat-plate theory.

We shall not compute any more boundary-layer details here, but as we go along, investigating various immersed-body flows, especially in Chap. 8, we shall use Thwaites' method to make qualitative assessments of the boundary-layer behavior.

EXAMPLE 7.5

In 1938 Howarth proposed a linearly decelerating external-velocity distribution

$$U(x) = U_0\left(1 - \frac{x}{L}\right) \tag{1}$$

as a theoretical model for laminar-boundary-layer study. (*a*) Use Thwaites' method to compute the separation point x_{sep} for $\theta_0 = 0$, and compare with the exact digital-computer solution $x_{\text{sep}}/L = 0.119863$ given by H. Wipperman in 1966. (*b*) Also compute the value of $c_f = 2\tau_w/(\rho U^2)$ at $x/L = 0.1$.

Solution

Part (a) First note that $dU/dx = -U_0/L$ = constant: Velocity decreases, pressure increases, and the pressure gradient is adverse throughout. Now integrate Eq. (7.54)

$$\theta^2 = \frac{0.45\nu}{U_0^6(1 - x/L)^6}\int_0^x U_0^5\left(1 - \frac{x}{L}\right)^5 dx = 0.075\,\frac{\nu L}{U_0}\left[\left(1 - \frac{x}{L}\right)^{-6} - 1\right] \tag{2}$$

Then the dimensionless factor λ is given by

$$\lambda = \frac{\theta^2}{\nu}\frac{dU}{dx} = -\frac{\theta^2 U_0}{\nu L} = -0.075\left[\left(1 - \frac{x}{L}\right)^{-6} - 1\right] \tag{3}$$

From Eq. (7.55) we set this equal to -0.09 for separation

$$\lambda_{\text{sep}} = -0.09 = -0.075\left[\left(1 - \frac{x_{\text{sep}}}{L}\right)^{-6} - 1\right]$$

or
$$\frac{x_{\text{sep}}}{L} = 1 - (2.2)^{-1/6} = 0.123$$



ketabline.com Ebook.ketabline.com

This is less than 3 percent higher than Wipperman's exact solution, and the computational effort is very modest.

Part (b) To compute c_f at $x/L = 0.1$ (just before separation), we first compute λ at this point, using Eq. (3)

$$\lambda(x = 0.1L) = -0.075[(1 - 0.1)^{-6} - 1] = -0.0661$$

Then from Eq. (7.56) the shear parameter is

$$S(x = 0.1L) = (-0.0661 + 0.09)^{0.62} = 0.099 = \tfrac{1}{2}c_f \, \mathrm{Re}_\theta \tag{4}$$

We can compute Re_θ in terms of Re_L from Eq. (2) or (3)

$$\frac{\theta^2}{L^2} = \frac{0.0661}{UL/\nu} = \frac{0.0661}{\mathrm{Re}_L}$$

or

$$\mathrm{Re}_\theta = 0.257 \, \mathrm{Re}_L^{1/2} \qquad \text{at } \frac{x}{L} = 0.1$$

Substitute into Eq. (4):

$$0.099 = \tfrac{1}{2}c_f(0.257 \, \mathrm{Re}_L^{1/2})$$

or

$$c_f = \frac{0.77}{\mathrm{Re}_L^{1/2}} \qquad \mathrm{Re}_L = \frac{UL}{\nu} \qquad \textit{Ans. (b)}$$

We cannot actually compute c_f without the value of, say, U_0L/ν.

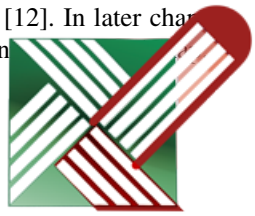
7.6 Experimental External Flows

Boundary-layer theory is very interesting and illuminating and gives us a great qualitative grasp of viscous-flow behavior, but, because of flow separation, the theory does not generally allow a quantitative computation of the complete flow field. In particular, there is at present no satisfactory theory for the forces on an arbitrary body immersed in a stream flowing at an arbitrary Reynolds number. Therefore experimentation is the key to treating external flows.

Literally thousands of papers in the literature report experimental data on specific external viscous flows. This section gives a brief description of the following external-flow problems:

1. Drag of two-and three-dimensional bodies
   - *a*. Blunt bodies
   - *b*. Streamlined shapes
2. Performance of lifting bodies
   - *a*. Airfoils and aircraft
   - *b*. Projectiles and finned bodies
   - *c*. Birds and insects

For further reading see the goldmine of data compiled in Hoerner [12]. In later chapters we shall study data on supersonic airfoils (Chap. 9), open-channel flow (Chap. 10), and turbomachinery performance (Chap. 11).



ketabline.com Ebook.ketabline.com

Drag of Immersed Bodies

Any body of any shape when immersed in a fluid stream will experience forces and moments from the flow. If the body has arbitrary shape and orientation, the flow will exert forces and moments about all three coordinate axes, as shown in Fig. 7.10. It is customary to choose one axis parallel to the free stream and positive downstream. The force on the body along this axis is called *drag,* and the moment about that axis the *rolling moment*. The drag is essentially a flow loss and must be overcome if the body is to move against the stream.

A second and very important force is perpendicular to the drag and usually performs a useful job, such as bearing the weight of the body. It is called the *lift*. The moment about the lift axis is called *yaw*.

The third component, neither a loss nor a gain, is the *side force,* and about this axis is the *pitching moment*. To deal with this three-dimensional force-moment situation is more properly the role of a textbook on aerodynamics [for example, 13]. We shall limit the discussion here to lift and drag.

When the body has symmetry about the lift-drag axis, e.g., airplanes, ships, and cars moving directly into a stream, the side force, yaw, and roll vanish, and the problem reduces to a two-dimensional case: two forces, lift and drag, and one moment, pitch.

A final simplification often occurs when the body has two planes of symmetry, as in Fig. 7.11. A wide variety of shapes such as cylinders, wings, and all bodies of revolution satisfy this requirement. If the free stream is parallel to the intersection of these two planes, called the *principal chord line of the body,* the body experiences drag only, with no lift, side force, or moments.[4] This type of degenerate one-force drag data is what is most commonly reported in the literature, but if the free stream is not parallel to the chord line, the body will have an unsymmetric orientation and all three forces and three moments can arise in principle.

In low-speed flow past geometrically similar bodies with identical orientation and relative roughness, the drag coefficient should be a function of the body Reynolds number

$$C_D = f(\text{Re}) \tag{7.60}$$

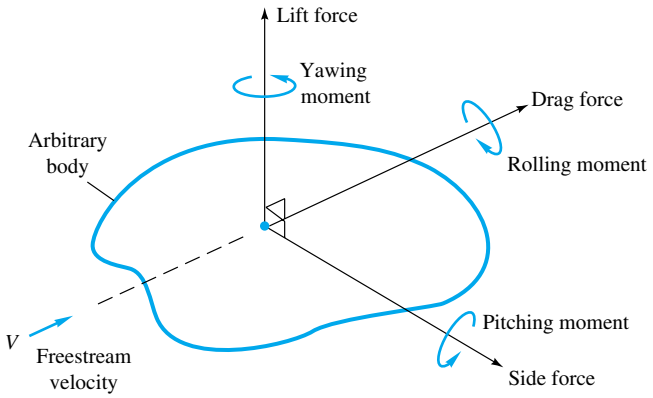


Fig. 7.10 Definition of forces and moments on a body immersed in a uniform flow.

[4]In bodies with shed vortices, such as the cylinder in Fig. 5.2, there may be *oscillating* lift, s and moments, but their mean value is zero.



ketabline.com Ebook.ketabline.com

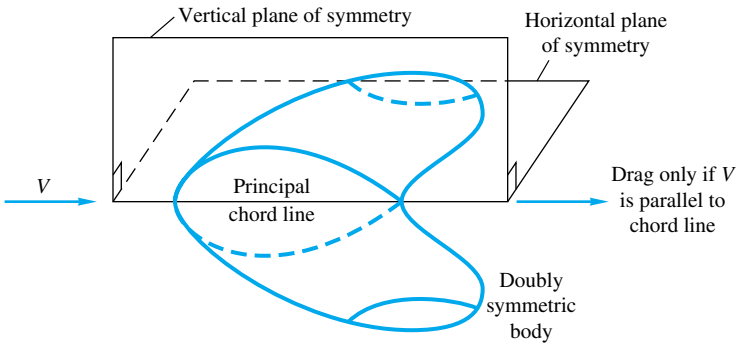


Fig. 7.11 Only the drag force occurs if the flow is parallel to both planes of symmetry.

The Reynolds number is based upon the free-stream velocity V and a characteristic length L of the body, usually the chord or body length parallel to the stream

$$\text{Re} = \frac{VL}{\nu} \tag{7.61}$$

For cylinders, spheres, and disks, the characteristic length is the diameter D.

Characteristic Area

Drag coefficients are defined by using a characteristic area A which may differ depending upon the body shape:

$$C_D = \frac{\text{drag}}{\frac{1}{2}\rho V^2 A} \tag{7.62}$$

The factor $\frac{1}{2}$ is our traditional tribute to Euler and Bernoulli. The area A is usually one of three types:

1. *Frontal area,* the body as seen from the stream; suitable for thick, stubby bodies, such as spheres, cylinders, cars, missiles, projectiles, and torpedoes.
2. *Planform area,* the body area as seen from above; suitable for wide, flat bodies such as wings and hydrofoils.
3. *Wetted area,* customary for surface ships and barges.

In using drag or other fluid-force data, it is important to note what length and area are being used to scale the measured coefficients.

Friction Drag and Pressure Drag

As we have mentioned, the theory of drag is weak and inadequate, except for the flat plate. This is because of flow separation. Boundary-layer theory can predict the separation point but cannot accurately estimate the (usually low) pressure distribution in the separated region. The difference between the high pressure in the front stagnation region and the low pressure in the rear separated region causes a large drag contribution called *pressure drag*. This is added to the integrated shear stress or *friction drag* of the body, which it often exceeds:

$$C_D = C_{D,\text{press}} + C_{D,\text{fric}}$$



ketabline.com Ebook.ketabline.com

The relative contribution of friction and pressure drag depends upon the body's shape, especially its thickness. Figure 7.12 shows drag data for a streamlined cylinder of very large depth into the paper. At zero thickness the body is a flat plate and exhibits 100 percent friction drag. At thickness equal to the chord length, simulating a circular cylinder, the friction drag is only about 3 percent. Friction and pressure drag are about equal at thickness $t/c = 0.25$. Note that C_D in Fig. 7.12*b* looks quite different when based upon frontal area instead of planform area, planform being the usual choice for this body shape. The two curves in Fig. 7.12*b* represent exactly the same drag data.

Figure 7.13 illustrates the dramatic effect of separated flow and the subsequent failure of boundary-layer theory. The theoretical inviscid pressure distribution on a circular cylinder (Chap. 8) is shown as the dashed line in Fig. 7.13*c*:

$$C_p = \frac{p - p_\infty}{\frac{1}{2}\rho V^2} = 1 - 4\sin^2\theta \tag{7.64}$$

where p_∞ and V are the pressure and velocity, respectively, in the free stream. The actual laminar and turbulent boundary-layer pressure distributions in Fig. 7.13*c* are startlingly different from those predicted by theory. Laminar flow is very vulnerable to the adverse gradient on the rear of the cylinder, and separation occurs at $\theta = 82°$, which

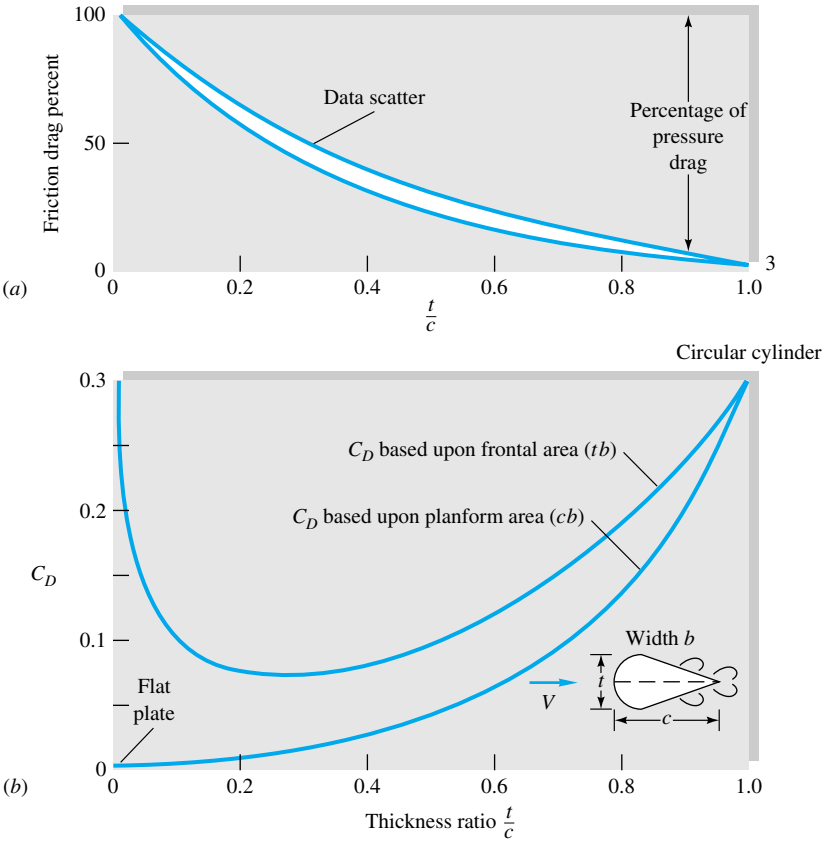


Fig. 7.12 Drag of a streamlined two-dimensional cylinder at $\mathrm{Re}_c = 10^6$: (*a*) effect of thickness ratio on percentage of friction drag; (*b*) total drag versus thickness when based upon two different areas.



ketabline.com Ebook.ketabline.com

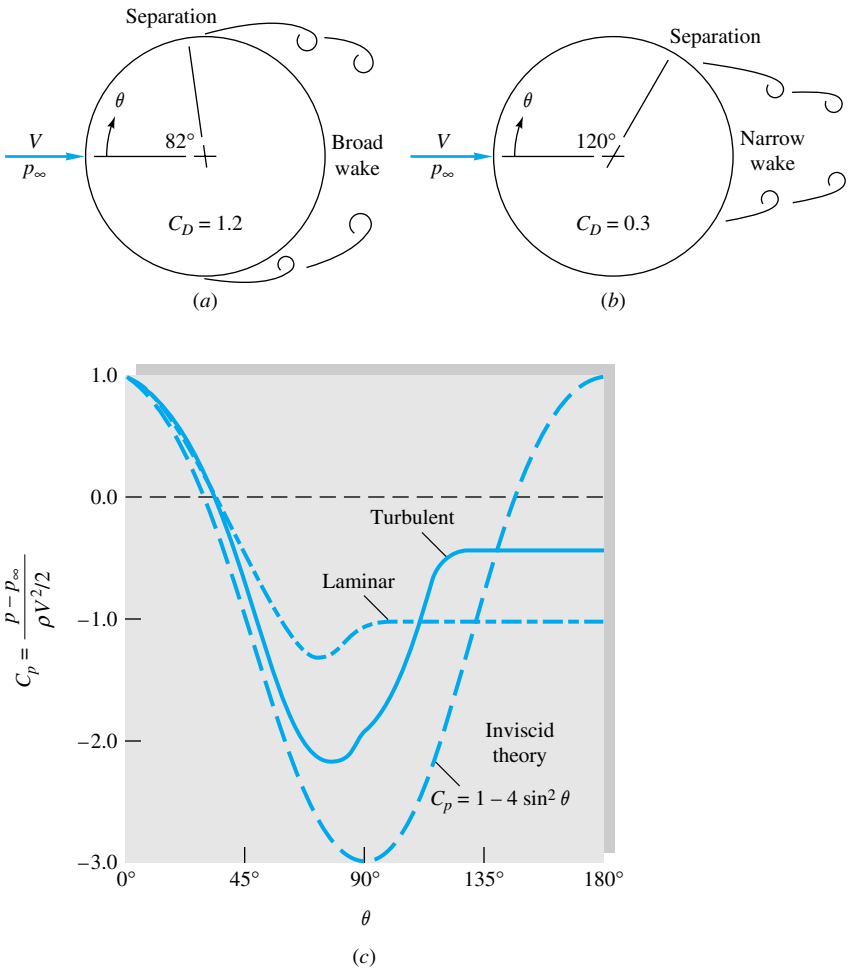


Fig. 7.13 Flow past a circular cylinder: (*a*) laminar separation; (*b*) turbulent separation; (*c*) theoretical and actual surface-pressure distributions.

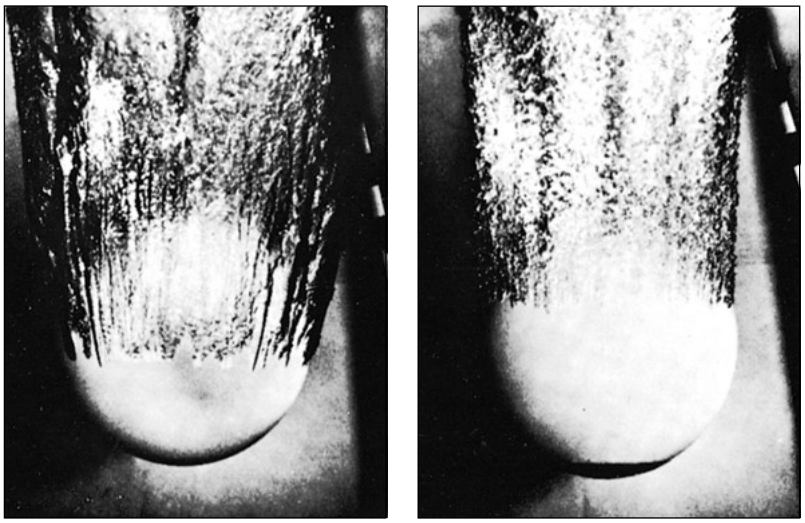
certainly could not have been predicted from inviscid theory. The broad wake and very low pressure in the separated laminar region cause the large drag $C_D = 1.2$.

The turbulent boundary layer in Fig. 7.13*b* is more resistant, and separation is delayed until $\theta = 120°$, with a resulting smaller wake, higher pressure on the rear, and 75 percent less drag, $C_D = 0.3$. This explains the sharp drop in drag at transition in Fig. 5.3.

The same sharp difference between vulnerable laminar separation and resistant turbulent separation can be seen for a sphere in Fig. 7.14. The laminar flow (Fig. 7.14*a*) separates at about 80°, $C_D = 0.5$, while the turbulent flow (Fig. 7.14*b*) separates at 120°, $C_D = 0.2$. Here the Reynolds numbers are exactly the same, and the turbulent boundary layer is induced by a patch of sand roughness at the nose of the ball. Golf balls fly in this range of Reynolds numbers, which is why they are deliberately dimpled − to induce a turbulent boundary layer and lower drag. Again we would find the actual pressure distribution on the sphere to be quite different from inviscid theory.



ketabline.com Ebook.ketabline.com



(*a*) (*b*)

Fig. 7.14 Strong differences in laminar and turbulent separation on an 8.5-in bowling ball entering water at 25 ft/s: (*a*) smooth ball, laminar boundary layer; (*b*) same entry, turbulent flow induced by patch of nose-sand roughness. (*U.S. Navy photograph, Ordnance Test Station, Pasadena Annex.*)

In general, we cannot overstress the importance of body streamlining to reduce drag at Reynolds numbers above about 100. This is illustrated in Fig. 7.15. The rectangular cylinder (Fig. 7.15*a*) has rampant separation at all sharp corners and very high drag. Rounding its nose (Fig. 7.15*b*) reduces drag by about 45 percent, but C_D is still high. Streamlining its rear to a sharp trailing edge (Fig. 7.15*c*) reduces its drag another 85 percent to a practical minimum for the given thickness. As a dramatic contrast, the circular cylinder (Fig. 7.15*d*) has one-eighth the thickness and one-three-hundredth the cross section (*c*) (Fig. 7.15*c*), yet it has the same drag. For high-performance vehicles and other moving bodies, the name of the game is drag reduction, for which intense research continues for both aerodynamic and hydrodynamic applications [20, 39].

The drag of some representative wide-span (nearly two-dimensional) bodies is shown versus the Reynolds number in Fig. 7.16*a*. All bodies have high C_D at very low (*creeping flow*) Re $\leq$ 1.0, while they spread apart at high Reynolds numbers according to

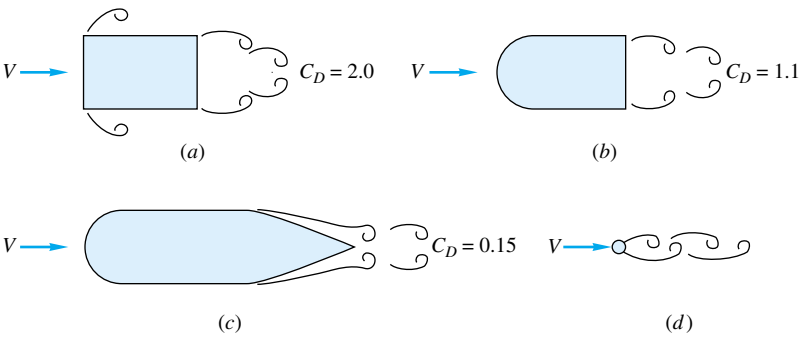


Fig. 7.15 The importance of streamlining in reducing drag of a body (C_D based on frontal area): (*a*) rectangular cylinder; (*b*) rounded nose; (*c*) rounded nose and streamlined sharp trailing edge; (*d*) circular cylinder with the same drag as case (*c*).



ketabline.com Ebook.ketabline.com

their degree of streamlining. All values of C_D are based on the planform area except the plate normal to the flow. The birds and the sailplane are, of course, not very two-dimensional, having only modest span length. Note that birds are not nearly as efficient as modern sailplanes or airfoils [14, 15].

Table 7.2 gives a few data on drag, based on frontal area, of two-dimensional bodies of various cross section, at $\text{Re} \geq 10^4$. The sharp-edged bodies, which tend to cause flow separation regardless of the character of the boundary layer, are insensitive to the Reynolds number. The elliptic cylinders, being smoothly rounded, have the laminar-to-turbulent transition effect of Figs. 7.13 and 7.14 and are therefore quite sensitive to whether the boundary layer is laminar or turbulent.

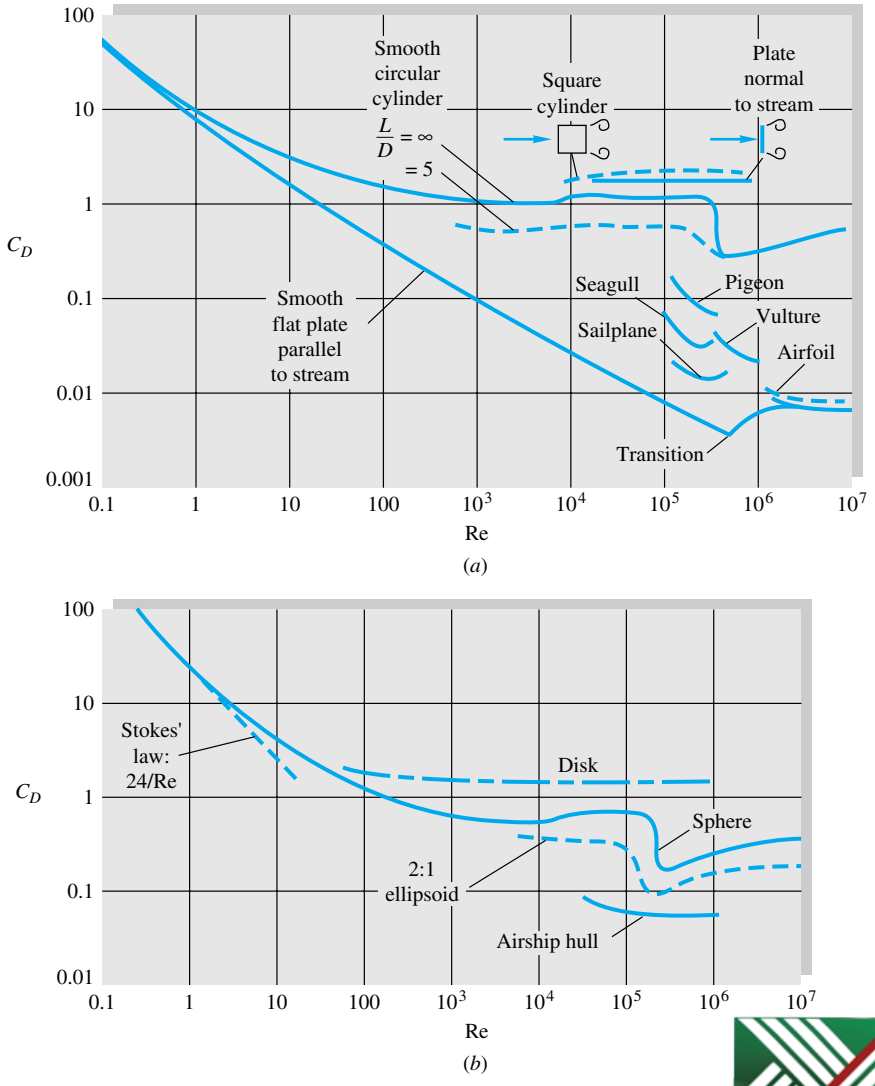
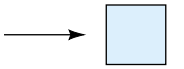
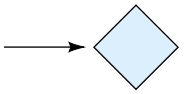
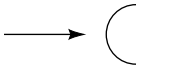
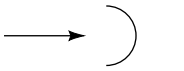
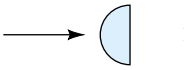
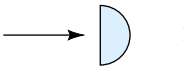
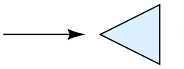
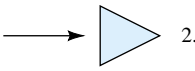
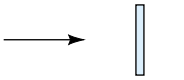
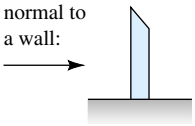
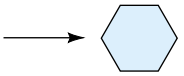
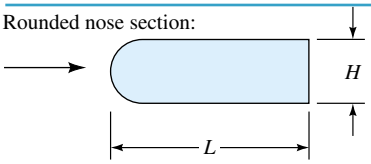
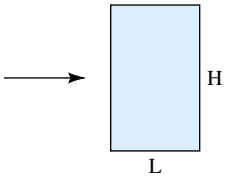


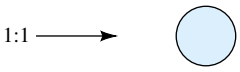
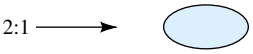
Fig. 7.16 Drag coefficients of smooth bodies at low Mach numbers: (*a*) two-dimensional bodies; (*b*) three-dimensional bodies. Note the Reynolds-number independence of blunt bodies at high Re.

ketabline.com Ebook.ketabline.com

Table 7.2 Drag of Two-Dimensional Bodies at Re $\geq 10^4$

Shape	C_D based on frontal area
Square cylinder: 	2.1
	1.6
Half tube: 	1.2
	2.3
Half-cylinder: 	1.2
	1.7
Equilateral triangle: 	1.6
	2.0
Plate: 	2.0
Thin plate normal to a wall: 	1.4
Hexagon: 	1.0 / 0.7

Shape	C_D based on frontal area
Rounded nose section: 	L/H: 0.5 / 1.0 / 2.0 / 4.0 / 6.0 C_D: 1.16 / 0.90 / 0.70 / 0.68 / 0.64
Flat nose section 	L/H: 0.1 / 0.4 / 0.7 / 1.2 / 2.0 / 2.5 / 3.0 / 6.0 C_D: 1.9 / 2.3 / 2.7 / 2.1 / 1.8 / 1.4 / 1.3 / 0.9

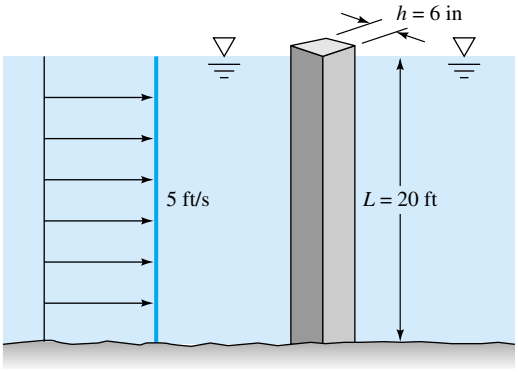
Elliptical cylinder:	Laminar	Turbulent
1:1 	1.2	0.3
2:1 	0.6	0.2
4:1 	0.35	0.15
8:1 	0.25	0.1



ketabline.com Ebook.ketabline.com

EXAMPLE 7.6

A square 6-in piling is acted on by a water flow of 5 ft/s that is 20 ft deep, as shown in Fig. E7.6. Estimate the maximum bending exerted by the flow on the bottom of the piling.



E7.6

Solution

Assume seawater with $\rho = 1.99$ slugs/ft^3 and kinematic viscosity $\nu = 0.000011$ ft^2/s. With a piling width of 0.5 ft, we have

$$\text{Re}_h = \frac{(5 \text{ ft/s})(0.5 \text{ ft})}{0.000011 \text{ ft}^2/\text{s}} = 2.3 \times 10^5$$

This is the range where Table 7.2 applies. The worst case occurs when the flow strikes the flat side of the piling, $C_D \approx 2.1$. The frontal area is $A = Lh = (20 \text{ ft})(0.5 \text{ ft}) = 10 \text{ ft}^2$. The drag is estimated by

$$F = C_D(\tfrac{1}{2}\rho V^2 A) \approx 2.1(\tfrac{1}{2})(1.99 \text{ slugs/ft}^3)(5 \text{ ft/s})^2(10 \text{ ft}^2) = 522 \text{ lbf}$$

If the flow is uniform, the center of this force should be at approximately middepth. Therefore the bottom bending moment is

$$M_0 \approx \frac{FL}{2} = 522(10) = 5220 \text{ ft} \cdot \text{lbf} \qquad \textit{Ans.}$$

According to the flexure formula from strength of materials, the bending stress at the bottom would be

$$S = \frac{M_0 y}{I} = \frac{(5220 \text{ ft} \cdot \text{lb})(0.25 \text{ ft})}{\frac{1}{12}(0.5 \text{ ft})^4} = 251{,}000 \text{ lbf/ft}^2 = 1740 \text{ lbf/in}^2$$

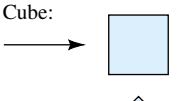
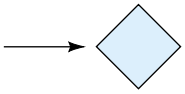
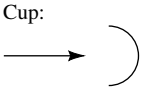
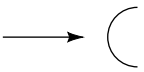
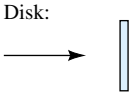
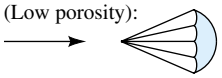
to be multiplied, of course, by the stress-concentration factor due to the built-in end conditions.

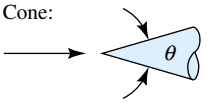
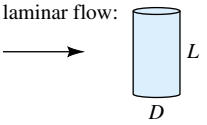
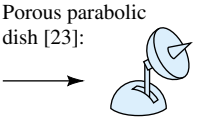
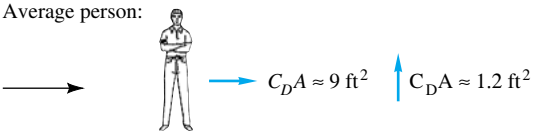
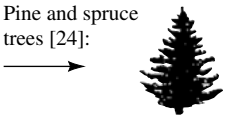
Some drag coefficients of three-dimensional bodies are listed in Table 7.3 and Fig. 7.16*b*. Again we can conclude that sharp edges always cause flow separation and hi drag which is insensitive to the Reynolds number. Rounded bodie have drag which depends upon the point of separation, so that both t

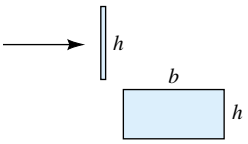


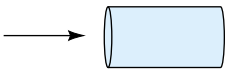
ketabline.com Ebook.ketabline.com

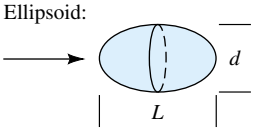
Table 7.3 Drag of Three-Dimensional Bodies at Re $\geq 10^4$

Body	C_D based on frontal area
Cube:	
	1.07
	0.81
Cup:	
	1.4
	0.4
Disk:	
	1.17
Parachute (Low porosity):	
	1.2

Body	C_D based on frontal area
Cone:	
	θ: 10° 20° 30° 40° 60° 75° 90° C_D: 0.30 0.40 0.55 0.65 0.80 1.05 1.15
Short cylinder, laminar flow:	
	L/D: 1 2 3 5 10 20 40 ∞ C_D: 0.64 0.68 0.72 0.74 0.82 0.91 0.98 1.20
Porous parabolic dish [23]:	
	Porosity: 0 0.1 0.2 0.3 0.4 0.5 ← C_D: 1.42 1.33 1.20 1.05 0.95 0.82 → C_D: 0.95 0.92 0.90 0.86 0.83 0.80
Average person:	
	→ $C_DA \approx 9$ ft^2 ↑ $C_DA \approx 1.2$ ft^2
Pine and spruce trees [24]:	
	U, m/s: 10 20 30 40 C_D: 1.2 ± 0.2 1.0 ± 0.2 0.7 ± 0.2 0.5 ± 0.2

Body	Ratio	C_D based on frontal area
Rectangular plate:		
	b/h 1	1.18
	5	1.2
	10	1.3
	20	1.5
	∞	2.0

Body	Ratio	C_D based on frontal area
Flat-faced cylinder:		
	L/d 0.5	1.15
	1	0.90
	2	0.85
	4	0.87
	8	0.99

Body	Ratio	C_D based on frontal area	
		Laminar	Turbulent
Ellipsoid:			
	L/d 0.75	0.5	0.2
	1	0.47	0.2
	2	0.27	0.13
	4	0.25	0.1
	8	0.2	0.08



ketabline.com Ebook.ketabline.com

ber and the character of the boundary layer are important. Body length will generally decrease pressure drag by making the body relatively more slender, but sooner or later the friction drag will catch up. For the flat-faced cylinder in Table 7.3, pressure drag decreases with L/d but friction increases, so that minimum drag occurs at about $L/d = 2$.

Aerodynamic Forces on Road Vehicles

Automobiles and trucks are now the subject of much research on aerodynamic forces, both lift and drag [21]. At least one textbook is devoted to the subject [22]. Consumer, manufacturer, and government interest has cycled between high speed/high horsepower and lower speed/lower drag. Better streamlining of car shapes has resulted over the years in a large decrease in the automobile drag coefficient, as shown in Fig. 7.17*a*. Modern cars have an average drag coefficient of about 0.35, based upon the frontal

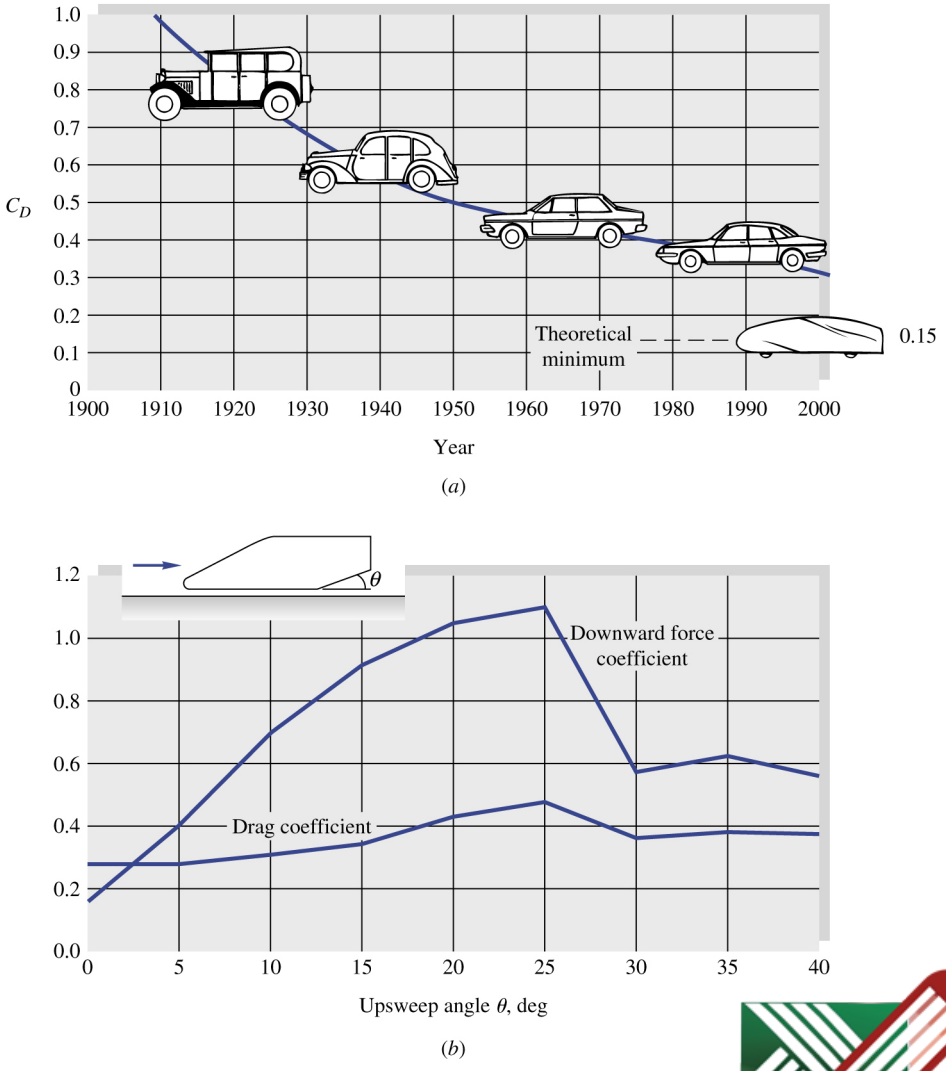


Fig. 7.17 Aerodynamics of automobiles: (*a*) the historical trend for drag coefficients [From Ref. 21]; (*b*) effect of bottom rear upsweep angle on drag and downward lift force [From Ref. 25].

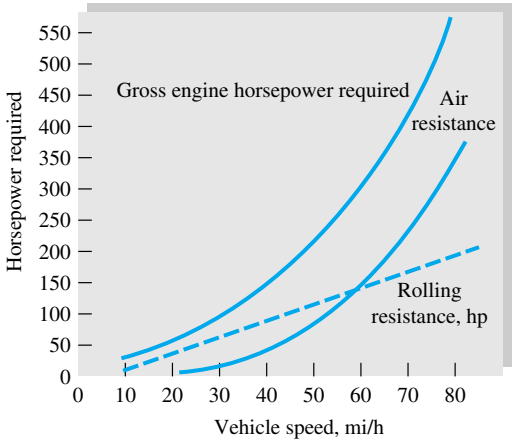
ketabline.com Ebook.ketabline.com

area. Since the frontal area has also decreased sharply, the actual raw drag *force* on cars has dropped even more than indicated in Fig. 7.17*a*. The practical minimum, shown tentatively for the year 2000, is $C_D \approx 0.15$ for a tear-shaped vehicle, which can be achieved any time the public is willing to purchase such a shape. Note that basing C_D on the frontal area is awkward, since one would need an accurate drawing of the automobile to estimate its frontal area. For this reason, some technical articles simply report the raw drag in newtons or pound-force, or the product $C_D A$.

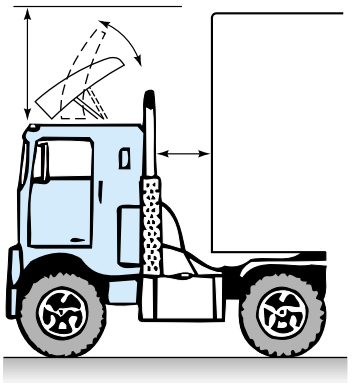
Many companies and laboratories have automotive wind tunnels, some full-scale and/or with moving floors to approximate actual kinematic similarity. The blunt shapes of most automobiles, together with their proximity to the ground, cause a wide variety of flow and geometric effects. Simple changes in part of the shape can have a large influence on aerodynamic forces. Figure 7.17*b* shows force data by Bearman et al. [25] for an idealized smooth automobile shape with upsweep in the rear of the bottom section. We see that by simply adding an upsweep angle of 25°, we can quadruple the downward force, gaining tire traction at the expense of doubling the drag. For this study, the effect of a moving floor was small—about a 10 percent increase in both drag and lift compared to a fixed floor.

It is difficult to quantify the exact effect of geometric changes on automotive forces, since, e.g., changes in a windshield shape might interact with downstream flow over the roof and trunk. Nevertheless, based on correlation of many model and full-scale tests, Ref. 26 proposes a formula for automobile drag which adds separate effects such as front ends, cowls, fenders, windshield, roofs, and rear ends.

Figure 7.18 shows the horsepower required to drive a typical tractor-trailer truck at speeds up to 80 mi/h (117 ft/s or 36 m/s). The rolling resistance increases linearly and the air drag quadratically with speed ($C_D \approx 1.0$). The two are about equally important at 55 mi/h, which is the nominal speed limit in the United States. As shown in Fig. 7.18*b*, air drag can be reduced by attaching a deflector to the top of the tractor. If the angle of the deflector is adjusted to carry the flow smoothly over the top and around the sides of the trailer, the reduction in C_D is about 20 percent. Thus, at 55 mi/h the total resistance is reduced 10 percent, with a corresponding reduction in



(*a*)



(*b*)

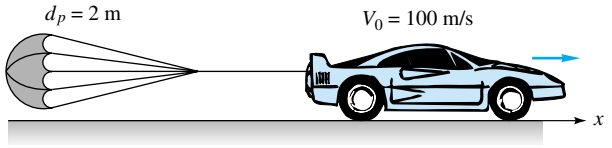
Fig. 7.18 Drag reduction of a tractor-trailer truck: (*a*) horsepower required to overcome resistance; (*b*) deflector added to cab reduces air drag by 20 percent. (*Uniroyal Inc.*)

ketabline.com Ebook.ketabline.com

fuel costs and/or trip time for the trucker. This type of applied fluids engineering can be a large factor in many of the conservation-oriented transportation problems of the future.

EXAMPLE 7.7

A high-speed car with $m = 2000$ kg, $C_D = 0.3$, and $A = 1$ m^2 deploys a 2-m parachute to slow down from an initial velocity of 100 m/s (Fig. E7.7). Assuming constant C_D, brakes free, and no rolling resistance, calculate the distance and velocity of the car after 1, 10, 100, and 1000 s. For air assume $\rho = 1.2$ kg/m^3, and neglect interference between the wake of the car and the parachute.



E7.7

Solution

Newton's law applied in the direction of motion gives

$$F_x = m\frac{dV}{dt} = -F_c - F_p = -\frac{1}{2}\rho V^2(C_{Dc}A_c + C_{Dp}A_p)$$

where subscript c denotes the car and subscript p the parachute. This is of the form

$$\frac{dV}{dt} = -\frac{K}{m}V^2 \qquad K = \sum C_D A\frac{\rho}{2}$$

Separate the variables and integrate

$$\int_{V_0}^{V}\frac{dV}{V^2} = -\frac{K}{m}\int_0^t dt$$

or

$$V_0^{-1} - V^{-1} = -\frac{K}{m}t$$

Rearrange and solve for the velocity V:

$$V = \frac{V_0}{1 + (K/m)V_0 t} \qquad K = \frac{(C_{Dc}A_c + C_{Dp}A_p)\rho}{2} \tag{1}$$

We can integrate this to find the distance traveled:

$$S = \frac{V_0}{\alpha}\ln(1 + \alpha t) \qquad \alpha = \frac{K}{m}V_0 \tag{2}$$

Now work out some numbers. From Table 7.3, $C_{Dp} \approx 1.2$; hence

$$C_{Dc}A_c + C_{Dp}A_p = 0.3(1\text{ m}^2) + 1.2\frac{\pi}{4}(2\text{ m})^2 = 4.07\text{ m}$$



ketabline.com Ebook.ketabline.com

Then $$\frac{K}{m} V_0 = \frac{\frac{1}{2}(4.07\ \text{m}^2)(1.2\ \text{kg/m}^3)(100\ \text{m/s})}{2000\ \text{kg}} = 0.122\ \text{s}^{-1} = \alpha$$

Now make a table of the results for V and S from Eqs. (1) and (2):

t, s	1	10	100	1000
V, m/s	89	45	7.6	0.8
S, m	94	654	2110	3940

Air resistance alone will not stop a body completely. If you don't apply the brakes, you'll be halfway to the Yukon Territory and still going.

Other Methods of Drag Reduction

Sometimes drag is good, for example, when using a parachute. Do not jump out of an airplane holding a flat plate parallel to your motion (see Prob. 7.81). Mostly, though, drag is bad and should be reduced. The classical method of drag reduction is *streamlining* (Figs. 7.15 and 7.18). For example, nose fairings and body panels have produced motorcycles which can travel over 200 mi/h. More recent research has uncovered other methods which hold great promise, especially for turbulent flows.

1. Oil pipelines introduce an *annular core* of water to reduce the pumping power [36]. The low-viscosity water rides the wall and reduces friction up to 60 percent.
2. Turbulent friction in liquid flows is reduced up to 60 percent by dissolving small amounts of a *high-molecular-weight polymer additive* [37]. Without changing pumps, the Trans-Alaska Pipeline System (TAPS) increased oil flow 50 percent by injecting small amounts of polymer dissolved in kerosene.
3. Stream-oriented surface *vee-groove microriblets* reduce turbulent friction up to 8 percent [38]. Riblet heights are of order 1 mm and were used on the Stars and Stripes yacht hull in the Americas Cup races. Riblets are also effective on aircraft skins.
4. Small, near-wall *large-eddy breakup devices* (LEBUs) reduce local turbulent friction up to 10 percent [39]. However, one must add these small structures to the surface.
5. Air *microbubbles* injected at the wall of a water flow create a low-shear bubble blanket [40]. At high void fractions, drag reduction can be 80 percent.
6. Spanwise (transverse) *wall oscillation* may reduce turbulent friction up to 30 percent [41].

Drag reduction is presently an area of intense and fruitful research and applies to many types of airflows and water flows for both vehicles and conduits.

Drag of Surface Ships

The drag data above, such as Tables 7.2 and 7.3, are for bodies "fully immersed" in a free stream, i.e., with no free surface. If, however, the body moves at or near a free liquid surface, *wave-making drag* becomes important and is dependent upon t
Reynolds number and the Froude number. To move through a water surface



ketabline.com Ebook.ketabline.com

must create waves on both sides. This implies putting energy into the water surface and requires a finite drag force to keep the ship moving, even in a frictionless fluid. The total drag of a ship can then be approximated as the sum of friction drag and wave-making drag:

$$F \approx F_{\text{fric}} + F_{\text{wave}} \qquad \text{or} \qquad C_D \approx C_{D,\text{fric}} + C_{D,\text{wave}}$$

The friction drag can be estimated by the (turbulent) flat-plate formula, Eq. (7.45), based on the below-water or *wetted area* of the ship.

Reference 27 is an interesting review of both theory and experiment for wake-making surface ship drag. Generally speaking, the bow of the ship creates a wave system whose wavelength is related to the ship speed but not necessarily to the ship length. If the stern of the ship is a wave *trough,* the ship is essentially climbing uphill and has high wave drag. If the stern is a wave crest, the ship is nearly level and has lower drag. The criterion for these two conditions results in certain approximate Froude numbers [27]:

$$\text{Fr} = \frac{V}{\sqrt{gL}} \approx \frac{0.53}{\sqrt{N}} \qquad \begin{array}{l}\text{high drag if } N = 1, 3, 5, 7, \ldots; \\ \text{low drag if } N = 2, 4, 6, 8, \ldots\end{array} \tag{7.65}$$

where V is the ship's speed, L is the ship's length along the centerline, and N is the number of half-lengths, from bow to stern, of the drag-making wave system. The wave drag will increase with the Froude number and oscillate between lower drag (Fr $\approx$ 0.38, 0.27, 0.22, . . .) and higher drag (Fr $\approx$ 0.53, 0.31, 0.24, . . .) with negligible variation for Fr < 0.2. Thus it is best to design a ship to cruise at $N = 2, 4, 6, 8$. Shaping the bow and stern can further reduce wave-making drag.

Figure 7.19 shows the data of Inui [27] for a model ship. The main hull, curve A, shows peaks and valleys in wave drag at the appropriate Froude numbers > 0.2. Introduction of a *bulb* protrusion on the bow, curve B, greatly reduces the drag. Adding a second bulb to the stern, curve C, is still better, and Inui recommends that the design speed of this two-bulb ship be at $N = 4$, Fr ≈ 0.27, which is a nearly "waveless" condition. In this figure $C_{D,\text{wave}}$ is defined as $2F_{\text{wave}}/(\rho V^2 L^2)$ instead of using the wetted area.

The solid curves in Fig. 7.19 are based on potential-flow theory for the below-water hull shape. Chapter 8 is an introduction to potential-flow theory. Modern digital computers can be programmed for numerical CFD solutions of potential flow over the hulls of ships, submarines, yachts, and sailboats, including boundary-layer effects driven by the potential flow [28]. Thus theoretical prediction of flow past surface ships is now at a fairly high level. See also Ref. 15.

Body Drag at High Mach Numbers

All the data presented above are for nearly incompressible flows, with Mach numbers assumed less than about 0.5. Beyond this value compressibility can be very important, with $C_D = \text{fcn}(\text{Re}, \text{Ma})$. As the stream Mach number increases, at some subsonic value $M_{\text{crit}} < 1$ which depends upon the body's bluntness and thickness, the local velocity at some point near the body surface will become sonic. If Ma increases beyond Ma$_{\text{crit}}$, shock waves form, intensify, and spread, raising surface pressures n[illegible] body and therefore increasing the pressure drag. The effect can be



ketabline.com Ebook.ketabline.com

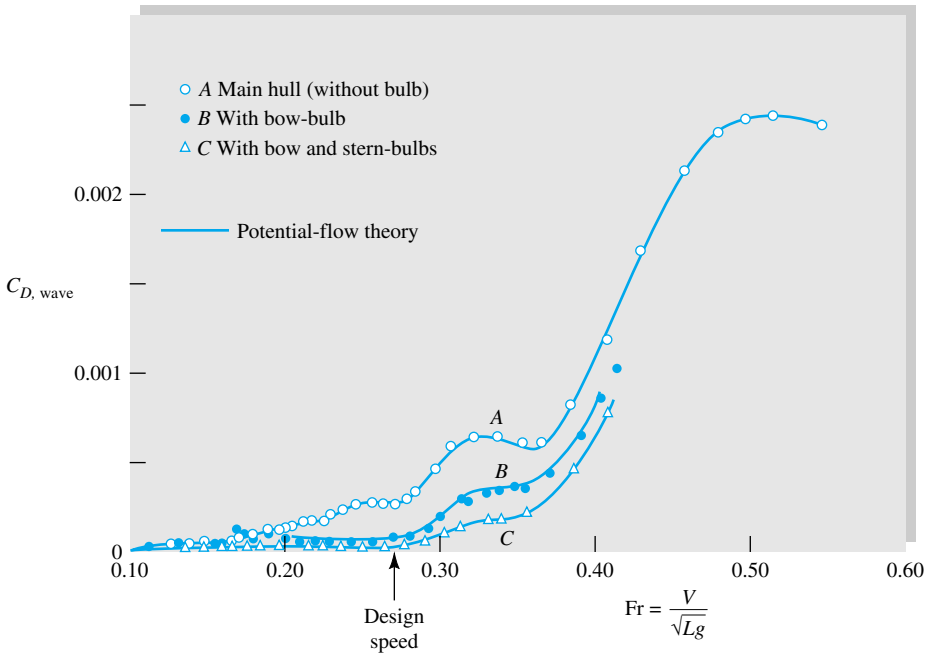


Fig. 7.19 Wave-making drag on a ship model. (*After Inui* [27].) *Note:* The drag coefficient is defined as $C_{DW} = 2F/(\rho V^2 L^2)$.

increasing tenfold, and 70 years ago this sharp increase was called the *sonic barrier,* implying that it could not be surmounted. Of course, it can be—the rise in C_D is finite, as supersonic bullets have proved for centuries.

Figure 7.20 shows the effect of the Mach number on the drag coefficient of various body shapes tested in air.[5] We see that compressibility affects blunt bodies earlier, with Ma_{crit} equal to 0.4 for cylinders, 0.6 for spheres, and 0.7 for airfoils and pointed projectiles. Also the Reynolds number (laminar versus turbulent boundary-layer flow) has a large effect below Ma_{crit} for spheres and cylinders but becomes unimportant above $\text{Ma} \approx 1$. In contrast, the effect of the Reynolds number is small for airfoils and projectiles and is not shown in Fig. 7.20. A general statement might divide Reynolds- and Mach-number effects as follows:

$\text{Ma} \leq 0.4$:	Reynolds number important, Mach number unimportant
$0.4 < \text{Ma} < 1$:	both Reynolds and Mach numbers important
$\text{Ma} > 1.0$:	Reynolds number unimportant, Mach number important

At supersonic speeds, a broad *bow shock wave* forms in front of the body (see Figs. 9.10*b* and 9.19), and the drag is mainly due to high shock-induced pressures on the front. Making the bow a sharp point can sharply reduce the drag (Fig. 9.28) but does not eliminate the bow shock. Chapter 9 gives a brief treatment of compressibility. References 30 and 31 are more advanced textbooks devoted entirely to compressible flow.

[5]There is a slight effect of the specific-heat ratio k which would appear if other gases were te

ketabline.com Ebook.ketabline.com

Biological Drag Reduction

A great deal of engineering effort goes into designing immersed bodies to reduce their drag. Most such effort concentrates on rigid-body shapes. A different process occurs in nature, as organisms adapt to survive high winds or currents, as reported in a series of papers by S. Vogel [33, 34]. A good example is a tree, whose flexible structure allows it to reconfigure in high winds and thus reduce drag and damage. Tree root systems have evolved in several ways to resist wind-induced bending moments, and trunk cross sections have become resistant to bending but relatively easy to twist and reconfigure. We saw this in Table 7.3, where tree drag coefficients [24] reduced by 60 percent as wind velocity increased. The shape of the tree changes to offer less resistance.

The individual branches and leaves of a tree also curl and cluster to reduce drag. Figure 7.21 shows the results of wind tunnel experiments by Vogel [33]. A tulip tree leaf, Fig. 7.21(*a*), broad and open in low wind, curls into a conical low-drag shape as wind increases. A compound black walnut leaf group, Fig. 7.21(*b*), clusters into a low-drag shape at high wind speed. Although drag coefficients were reduced up to 50 percent by flexibility, Vogel points out that rigid structures are sometimes just as effective. An interesting recent symposium [35] was devoted entirely to the solid mechanics and fluid mechanics of biological organisms.

Forces on Lifting Bodies

Lifting bodies (airfoils, hydrofoils, or vanes) are intended to provide a large force normal to the free stream and as little drag as possible. Conventional design practice has evolved a shape not unlike a bird's wing, i.e., relatively thin ($t/c \leq 0/18$) with a rounded leading edge and a sharp trailing edge. A typical shape is sketched in Fig. 7.22.

For our purposes we consider the body to be symmetric, as in Fig. 7.11, with the

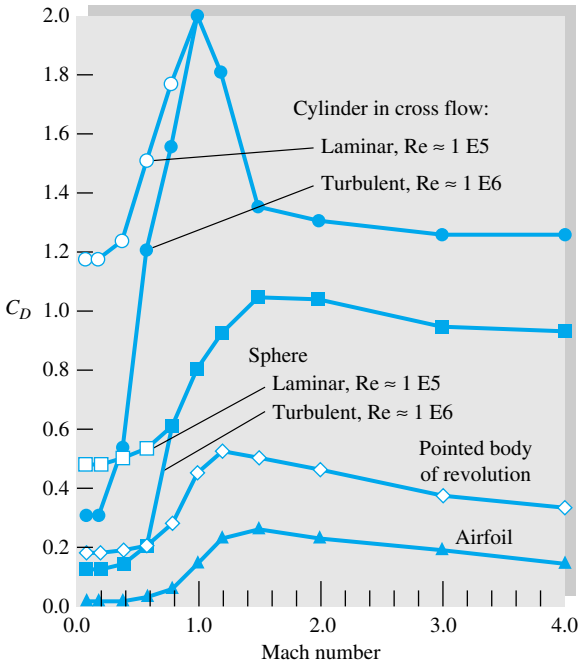


Fig. 7.20 Effect of the Mach number on the drag of various body shapes. (*Data from Refs. 23 and 29.*)



ketabline.com Ebook.ketabline.com

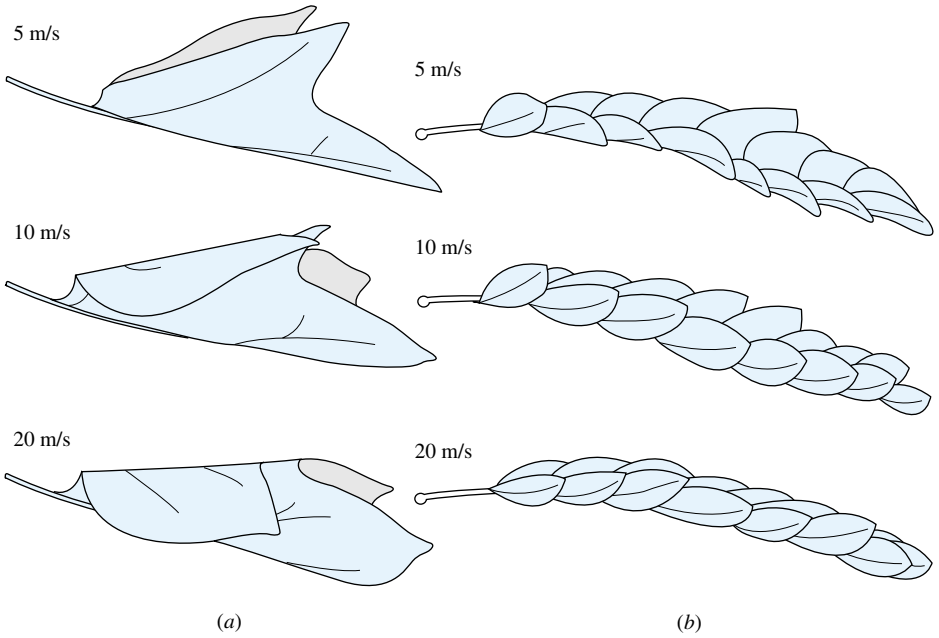


Fig. 7.21 Biological adaptation to wind forces: (*a*) a tulip tree leaf curls into a conical shape at high velocity; (*b*) black walnut leaves cluster into a low-drag shape as wind increases. (*From Vogel, Ref. 33.*)

free-stream velocity in the vertical plane. If the chord line between the leading and trailing edge is not a line of symmetry, the airfoil is said to be *cambered*. The camber line is the line midway between the upper and lower surfaces of the vane.

The angle between the free stream and the chord line is called the *angle of attack* α. The lift L and the drag D vary with this angle. The dimensionless forces are defined with respect to the planform area $A_p = bc$:

Lift coefficient:
$$C_L = \frac{L}{\frac{1}{2}\rho V^2 A_p} \tag{7.66a}$$

Drag coefficient:
$$C_D = \frac{D}{\frac{1}{2}\rho V^2 A_p} \tag{7.66b}$$

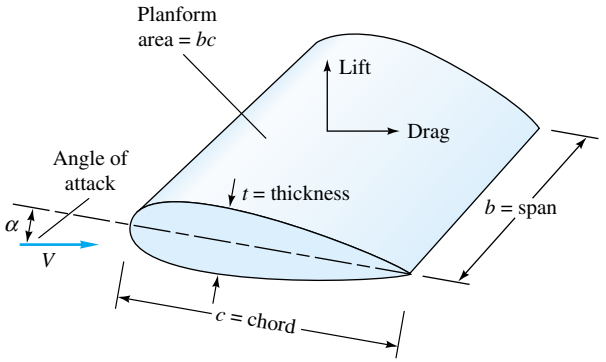


Fig. 7.22 Definition sketch for a lifting vane.



ketabline.com Ebook.ketabline.com

If the chord length is not constant, as in the tapered wings of modern aircraft, $A_p = \int c\, db$.

For low-speed flow with a given roughness ratio, C_L and C_D should vary with α and the chord Reynolds number

$$C_L = f(\alpha, \mathrm{Re}_c) \qquad \text{or} \qquad C_D = f(\alpha, \mathrm{Re}_c)$$

where $\mathrm{Re}_c = Vc/\nu$. The Reynolds numbers are commonly in the turbulent-boundary-layer range and have a modest effect.

The rounded leading edge prevents flow separation there, but the sharp trailing edge causes a separation which generates the lift. Figure 7.23 shows what happens when a flow starts up past a lifting vane or an airfoil.

Just after start-up in Fig. 7.23*a* the streamline motion is irrotational and inviscid. The rear stagnation point, assuming a positive angle of attack, is on the upper surface, and there is no lift; but the flow cannot long negotiate the sharp turn at the trailing edge: it separates, and a *starting vortex* forms in Fig. 7.23*b*. This starting vortex is shed downstream in Fig. 7.23*c* and *d*, and a smooth streamline flow develops over the wing, leaving the foil in a direction approximately parallel to the chord line. Lift at this time is fully developed, and the starting vortex is gone. Should the flow now cease, a *stopping vortex* of opposite (clockwise) sense will form and be shed. During flight, increases or decreases in lift will cause incremental starting or stopping vortices, always with the effect of maintaining a smooth parallel flow at the trailing edge. We pursue this idea mathematically in Chap. 8.

At a low angle of attack, the rear surfaces have an adverse pressure gradient but not enough to cause significant boundary-layer separation. The flow pattern is smooth, as in Fig. 7.23*d*, and drag is small and lift excellent. As the angle of attack is increased, the upper-surface adverse gradient becomes stronger, and generally a *separation bub-*

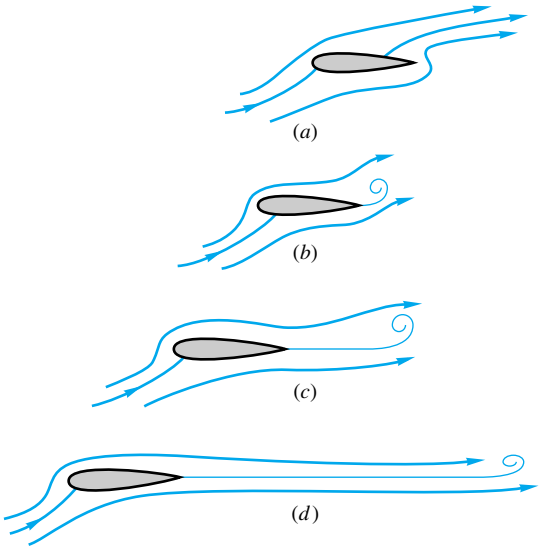


Fig. 7.23 Transient stages in the development of lift: (*a*) start-up: rear stagnation point on the upper surface: no lift; (*b*) sharp trailing edge induces separation, and a starting vortex forms: slight lift; (*c*) starting vortex is shed, and streamlines flow smoothly from trailing edge: lift is now 80 percent developed; (*d*) starting vortex now shed far behind, trailing edge now very smooth: lift fully developed.



ketabline.com Ebook.ketabline.com

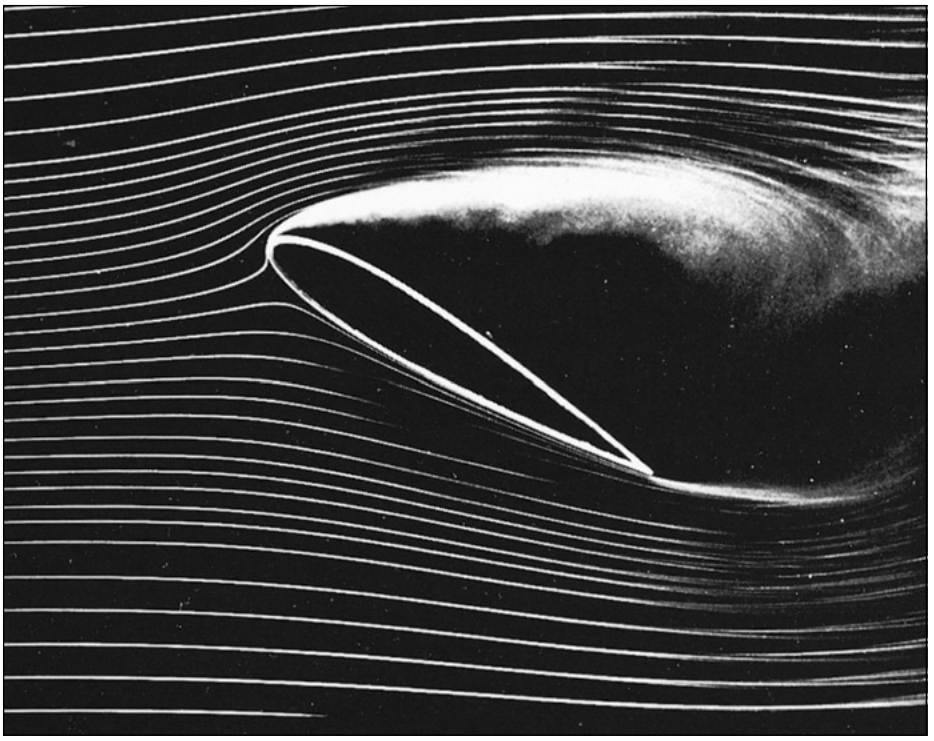


Fig. 7.24 At high angle of attack, smoke-flow visualization shows stalled flow on the upper surface of a lifting vane. *[From Ref. 19,* Illustrated Experiments in Fluid Mechanics (*The NCFMF Book of Film Notes*), *National Committee for Fluid Mechanics Films, Education Development Center, Inc., copyright 1972.]*

ble begins to creep forward on the upper surface.[6] At a certain angle $\alpha = 15$ to $20°$, the flow is separated completely from the upper surface, as in Fig. 7.24. The airfoil is said to be *stalled*: Lift drops off markedly, drag increases markedly, and the foil is no longer flyable.

Early airfoils were thin, modeled after birds' wings. The German engineer Otto Lilienthal (1848–1896) experimented with flat and cambered plates on a rotating arm. He and his brother Gustav flew the world's first glider in 1891. Horatio Frederick Phillips (1845–1912) built the first wind tunnel in 1884 and measured the lift and drag of cambered vanes. The first theory of lift was proposed by Frederick W. Lanchester shortly afterward. Modern airfoil theory dates from 1905, when the Russian hydrodynamicist N. E. Joukowsky (1847–1921) developed a circulation theorem (Chap. 8) for computing airfoil lift for arbitrary camber and thickness. With this basic theory, as extended and developed by Prandtl and Kármán and their students, it is now possible to design a low-speed airfoil to satisfy particular surface-pressure distributions and boundary-layer characteristics. There are whole families of airfoil designs, notably those developed in the United States under the sponsorship of the NACA (now NASA). Extensive theory and data on these airfoils are contained in Ref. 16. We shall discuss this further in Chap. 8.

Figure 7.25 shows the lift and drag on a symmetric airfoil denoted as the NACA 0009 foil, the last digit indicating the thickness of 9 percent. With no flap extended,

[6]For some airfoils the bubble leaps, not creeps, forward, and stall occurs rapidly and dangero



ketabline.com Ebook.ketabline.com

this airfoil, as expected, has zero lift at zero angle of attack. Up to about 12° the lift coefficient increases linearly with a slope of 0.1 per degree, or 6.0 per radian. This is in agreement with the theory outlined in Chap. 8:

$$C_{L,\text{theory}} \approx 2\pi \sin\left(\alpha + \frac{2h}{c}\right) \tag{7.67}$$

where h/c is the maximum camber expressed as a fraction of the chord. The NACA 0009 has zero camber; hence $C_L = 2\pi \sin \alpha \approx 0.11\alpha$, where α is in degrees. This is excellent agreement.

The drag coefficient of the smooth-model airfoils in Fig. 7.25 is as low as 0.005, which is actually lower than both sides of a flat plate in turbulent flow. This is misleading inasmuch as a commercial foil will have roughness effects; e.g., a paint job will double the drag coefficient.

The effect of increasing Reynolds number in Fig. 7.25 is to increase the maximum lift and stall angle (without changing the slope appreciably) and to reduce the drag coefficient. This is a salutary effect, since the prototype will probably be at a higher Reynolds number than the model (10^7 or more).

For takeoff and landing, the lift is greatly increased by deflecting a split flap, as shown in Fig. 7.25. This makes the airfoil unsymmetric (or effectively cambered) and changes the zero-lift point to $\alpha = -12°$. The drag is also greatly increased by the flap, but the reduction in takeoff and landing distance is worth the extra power needed.

A lifting craft cruises at low angle of attack, where the lift is much larger than the drag. Maximum lift-to-drag ratios for the common airfoils lie between 20 and 50.

Some airfoils, such as the NACA 6 series, are shaped to provide favorable gradients over much of the upper surface at low angles. Thus separation is small, and transition to turbulence is delayed; the airfoil retains a good length of laminar flow even

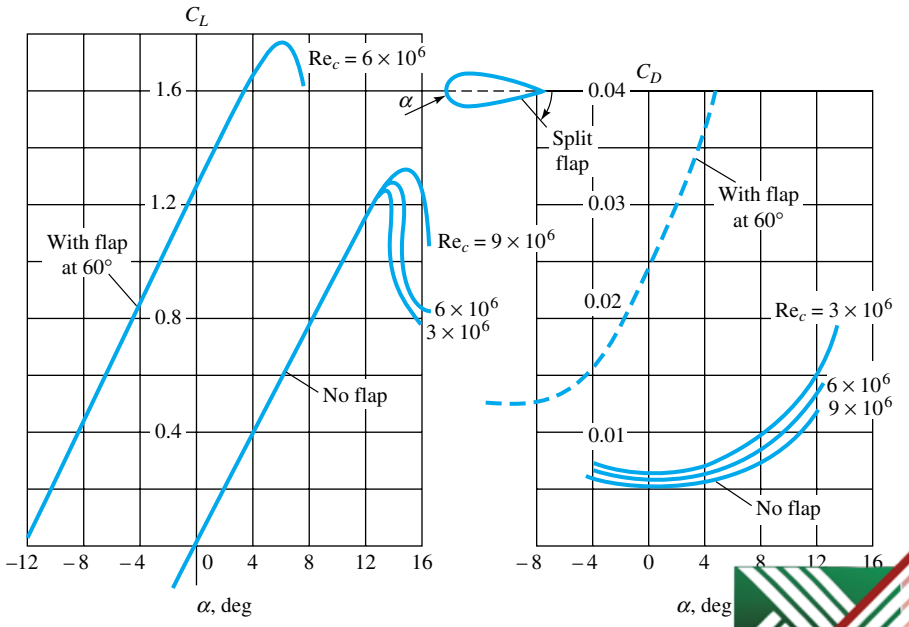


Fig. 7.25 Lift and drag of a symmetric NACA 0009 airfoil of infinite span, including effect of a split-flap deflection. Note that roughness can increase C_D from 100 to 300 percent.

ketabline.com Ebook.ketabline.com

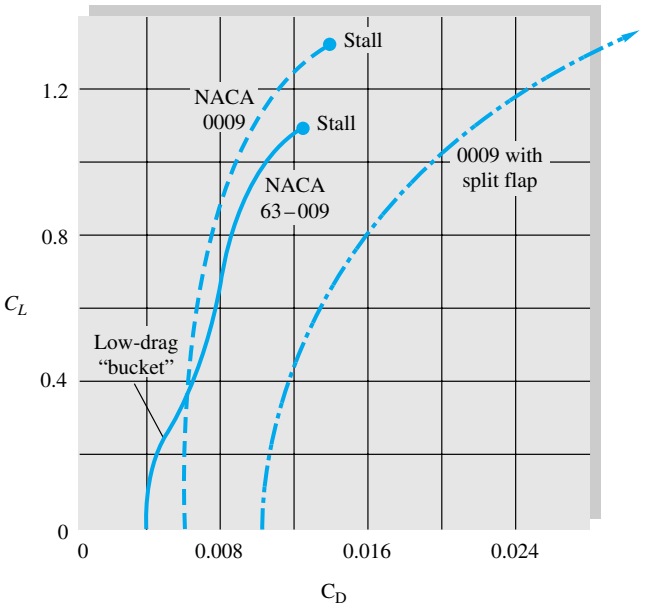


Fig. 7.26 Lift-drag polar plot for standard (0009) and a laminar-flow (63-009) NACA airfoil.

at high Reynolds numbers. The lift-drag polar plot in Fig. 7.26 shows the NACA 0009 data from Fig. 7.25 and a laminar-flow airfoil, NACA 63–009, of the same thickness. The laminar-flow airfoil has a low-drag bucket at small angles but also suffers lower stall angle and lower maximum lift coefficient. The drag is 30 percent less in the bucket, but the bucket disappears if there is significant surface roughness.

All the data in Figs. 7.25 and 7.26 are for infinite span, i.e., a two-dimensional flow pattern about wings without tips. The effect of finite span can be correlated with the dimensionless slenderness, or *aspect ratio,* denoted (AR),

$$\text{AR} = \frac{b^2}{A_p} = \frac{b}{\bar{c}} \tag{7.68}$$

where $\bar{c}$ is the average chord length. Finite-span effects are shown in Fig. 7.27. The lift slope decreases, but the zero-lift angle is the same; and the drag increases, but the zero-lift drag is the same. The theory of finite-span airfoils [16] predicts that the effective angle of attack increases, as in Fig. 7.27, by the amount

$$\Delta\alpha \approx \frac{C_L}{\pi \text{AR}} \tag{7.69}$$

When applied to Eq. (7.67), the finite-span lift becomes

$$C_L \approx \frac{2\pi \sin(\alpha + 2h/c)}{1 + 2/\text{AR}} \tag{7.70}$$

The associated drag increase is $\Delta C_D \approx C_L \sin \Delta\alpha \approx C_L \, \Delta\alpha$, or

$$C_D \approx C_{D\infty} + \frac{C_L^2}{\pi \text{AR}}$$



ketabline.com Ebook.ketabline.com

where $C_{D\infty}$ is the drag of the infinite-span airfoil, as sketched in Fig. 7.25. These correlations are in good agreement with experiments on finite-span wings [16].

The existence of a maximum lift coefficient implies the existence of a minimum speed, or *stall speed,* for a craft whose lift supports its weight

$$L = W = C_{L,\max}(\tfrac{1}{2}\rho V_s^2 A_p)$$

or

$$V_s = \left(\frac{2W}{C_{L,\max}\rho A_p}\right)^{1/2} \tag{7.72}$$

The stall speed of typical aircraft varies between 60 and 200 ft/s, depending upon the weight and value of $C_{L,\max}$. The pilot must hold the speed greater than about $1.2V_s$ to avoid the instability associated with complete stall.

The split flap in Fig. 7.25 is only one of many devices used to secure high lift at low speeds. Figure 7.28a shows six such devices whose lift performance is given in 7.28b along with a standard (A) and laminar-flow (B) airfoil. The double-slotted flap achieves $C_{L,\max} \approx 3.4$, and a combination of this plus a leading-edge slat can achieve $C_{L,\max} \approx 4.0$. These are not scientific curiosities; e.g., the Boeing 727 commercial jet aircraft uses a triple-slotted flap plus a leading-edge slat during landing.

Also shown as C in Fig. 7.28b is the Kline-Fogleman airfoil [17], not yet a reality. The designers are amateur model-plane enthusiasts who did not know that conventional aerodynamic wisdom forbids a sharp leading edge and a step cutout from the trailing edge. The Kline-Fogleman airfoil has relatively high drag but shows an amazing continual increase in lift out to $\alpha = 45°$. In fact, we may fairly say that this airfoil does not stall and provides smooth performance over a tremendous range of flight conditions. No explanation for this behavior has yet been published by any aerodynamicist. This airfoil is under study and may or may not have any commercial value.

Another violation of conventional aerodynamic wisdom is that military aircraft are beginning to fly, briefly, *above the stall point.* Fighter pilots are learning to make quick maneuvers in the stalled region as detailed in Ref. 32. Some planes can even *fly continuously* while stalled—the Grumman X-29 experimental aircraft recently set a record by flying at $\alpha = 67°$.

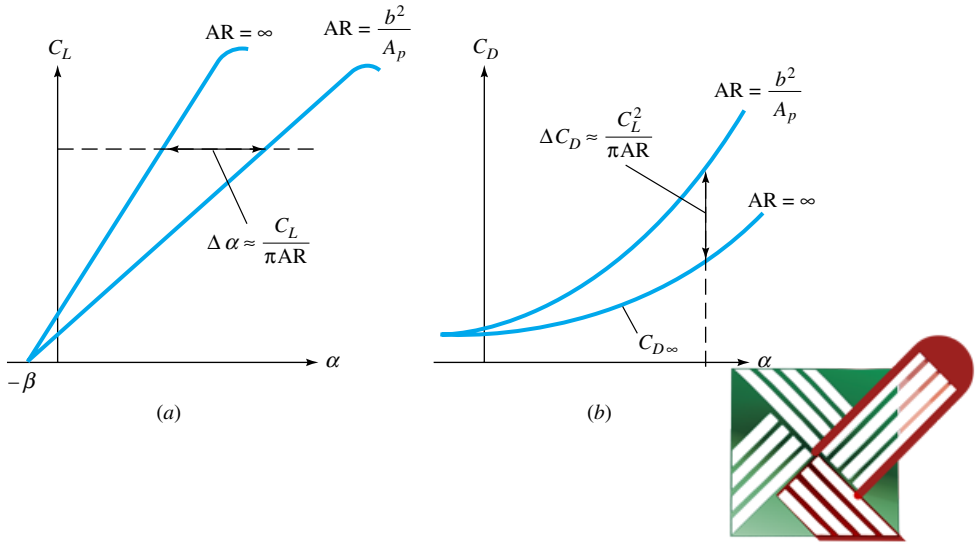


Fig. 7.27 Effect of finite aspect ratio on lift and drag of an airfoil: (*a*) effective angle increase; (*b*) induced drag increase.

ketabline.com Ebook.ketabline.com

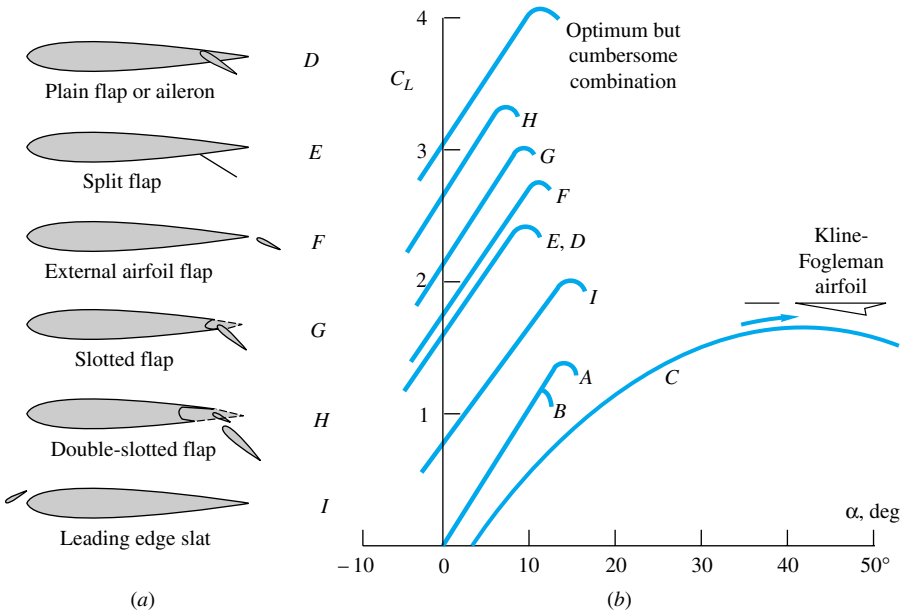


Fig. 7.28 Performance of airfoils with and without high-lift devices: A = NACA 0009; B = NACA 63-009; C = Kline-Fogleman airfoil (*from Ref. 17*); D to I shown in (*a*): (*a*) types of high-lift devices; (*b*) lift coefficients for various devices.

New Aircraft Designs

The Kline-Fogleman airfoil in Fig. 7.28 is a departure from conventional aerodynamics, but there have been other striking departures, as detailed in a recent article [42]. These new aircraft, conceived presently as small models, have a variety of configurations, as shown in Fig. 7.29: ring-wing, cruciform, flying saucer, and flap-wing. A saucer configuration (Fig. 7.29*c*), with a diameter of 40 in, has been successfully flown by radio control, and its inventor, Jack M. Jones, plans for a 20-ft two-passenger version. Another 18-in-span microplane called the Bat (not shown), made by MLB Co., flies for 20 min at 40 mi/h and contains a video camera for surveillance. New engines have been reduced to a 10- by 3-mm size, producing 20 W of power. At the other end of the size spectrum, Boeing and NASA engineers have proposed a jumbo flying-wing jetliner, similar in shape to the stealth bomber, which would carry 800 passengers for a range of 7000 mi.

Further information on the performance of lifting craft can be found in Refs. 12, 13, and 16. We discuss this matter again briefly in Chap. 8.

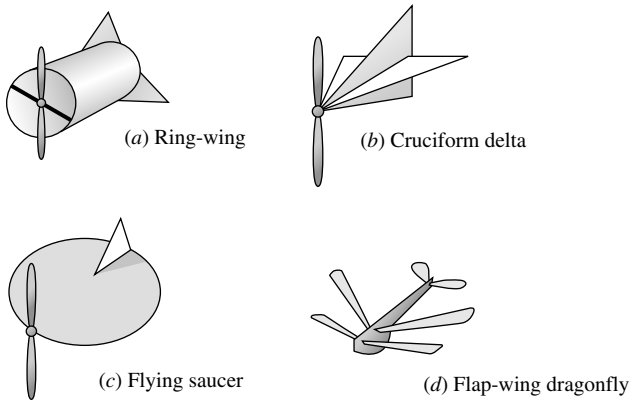


Fig. 7.29 New aircraft designs do not necessarily look like your typical jetliner. *(From Ref. 42.)*



ketabline.com Ebook.ketabline.com

EXAMPLE 7.8

An aircraft weighs 75,000 lb, has a planform area of 2500 ft^2, and can deliver a constant thrust of 12,000 lb. It has an aspect ratio of 7, and $C_{D\infty} \approx 0.02$. Neglecting rolling resistance, estimate the takeoff distance at sea level if takeoff speed equals 1.2 times stall speed. Take $C_{L,\max} = 2.0$.

Solution

The stall speed from Eq. (7.72), with sea-level density $\rho = 0.00237$ slug/ft^3, is

$$V_s = \left(\frac{2W}{C_{L,\max}\rho A_p}\right)^{1/2} = \left[\frac{2(75{,}000)}{2.0(0.00237)(2500)}\right]^{1/2} = 112.5 \text{ ft/s}$$

Hence takeoff speed $V_0 = 1.2V_s = 135$ ft/s. The drag is estimated from Eq. (7.71) for AR = 7 as

$$C_D \approx 0.02 + \frac{C_L^2}{7\pi} = 0.02 + 0.0455C_L^2$$

A force balance in the direction of takeoff gives

$$F_s = m\frac{dV}{dt} = \text{thrust} - \text{drag} = T - kV^2 \qquad k = \tfrac{1}{2}C_D\rho A_p \tag{1}$$

Since we are looking for distance, not time, we introduce $dV/dt = V\,dV/ds$ into Eq. (1), separate variables, and integrate

$$\int_0^{S_0} dS = \frac{m}{2}\int_0^{V_0} \frac{d(V^2)}{T - kV^2} \qquad k \approx \text{const}$$

or

$$S_0 = \frac{m}{2k}\ln\frac{T}{T - kV_0^2} = \frac{m}{2k}\ln\frac{T}{T - D_0} \tag{2}$$

where $D_0 = kV_0^2$ is the takeoff drag. Equation (2) is the desired theoretical relation for takeoff distance. For the particular numerical values, take

$$m = \frac{75{,}000}{32.2} = 2329 \text{ slugs}$$

$$C_{L_0} = \frac{W}{\frac{1}{2}\rho V_0^2 A_p} = \frac{75{,}000}{\frac{1}{2}(0.00237)(135)^2(2500)} = 1.39$$

$$C_{D_0} = 0.02 + 0.0455(C_{L_0})^2 = 0.108$$

$$k \approx \tfrac{1}{2}C_{D_0}\rho A_p = (\tfrac{1}{2})(0.108)(0.00237)(2500) = 0.319 \text{ slug/ft}$$

$$D_0 = kV_0^2 = 5820 \text{ lb}$$

Then Eq. (2) predicts that

$$S_0 = \frac{2329 \text{ slugs}}{2(0.319 \text{ slug/ft})}\ln\frac{12{,}000}{12{,}000 - 5820} = 3650 \ln 1.94 = 2420 \text{ ft} \qquad \textit{Ans.}$$

A more exact analysis accounting for variable k [13] gives the same result.



ketabline.com Ebook.ketabline.com

Summary

This chapter has dealt with viscous effects in external flow past bodies immersed in a stream. When the Reynolds number is large, viscous forces are confined to a thin boundary layer and wake in the vicinity of the body. Flow outside these "shear layers" is essentially inviscid and can be predicted by potential theory and Bernoulli's equation.

The chapter begins with a discussion of the flat-plate boundary layer and the use of momentum-integral estimates to predict the wall shear, friction drag, and thickness of such layers. These approximations suggest how to eliminate certain small terms in the Navier-Stokes equations, resulting in Prandtl's boundary-layer equations for laminar and turbulent flow. Section 7.4 then solves the boundary-layer equations to give very accurate formulas for flat-plate flow at high Reynolds numbers. Rough-wall effects are included, and Sec. 7.5 gives a brief introduction to pressure-gradient effects. An adverse (decelerating) gradient is seen to cause flow separation, where the boundary layer breaks away from the surface and forms a broad, low-pressure wake.

Boundary-layer theory fails in separated flows, which are commonly studied by experiment. Section 7.6 gives data on drag coefficients of various two- and three-dimensional body shapes. The chapter ends with a brief discussion of lift forces generated by lifting bodies such as airfoils and hydrofoils. Airfoils also suffer flow separation or *stall* at high angles of incidence.

Problems

Most of the problems herein are fairly straightforward. More difficult or open-ended assignments are labeled with an asterisk. Problems labeled with an EES icon will benefit from the use of the Engineering Equation Solver (EES), while problems labeled with a computer disk may require the use of a computer. The standard end-of-chapter problems 7.1 to 7.124 (categorized in the problem list below) are followed by word problems W7.1 to W7.12, fundamentals of engineering exam problems FE7.1 to FE7.10, comprehensive problems C7.1 to C7.4, and design project D7.1.

Problem Distribution

Section	Topic	Problems
7.1	Reynolds-number and geometry	7.1–7.5
7.2	Momentum-integral estimates	7.6–7.12
7.3	The boundary-layer equations	7.13–7.15
7.4	Laminar flat-plate flow	7.16–7.29
7.4	Turbulent flat-plate flow	7.30–7.46
7.5	Boundary layers with pressure gradient	7.47–7.52
7.6	Drag of two-dimensional bodies	7.53–7.63
7.6	Drag of three-dimensional bodies	7.64–7.114
7.6	Lifting bodies—airfoils	7.115–7.124

P7.1 For flow at 20 m/s past a thin flat plate, estimate the distances x from the leading edge at which the boundary-layer thickness will be either 1 mm or 10 cm for (*a*) air and (*b*) water at 20°C and 1 atm.

P7.2 Air, equivalent to that at a standard altitude of 4000 m, flows at 450 mi/h past a wing which has a thickness of 18 cm, a chord length of 1.5 m, and a wingspan of 12 m. What is the appropriate value of the Reynolds number for correlating the lift and drag of this wing? Explain your selection.

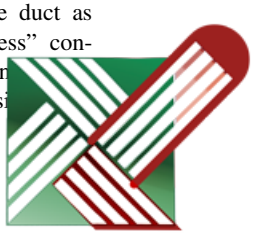
P7.3 Equation (7.1*b*) assumes that the boundary layer on the plate is turbulent from the leading edge onward. Devise a scheme for determining the boundary-layer thickness more accurately when the flow is laminar up to a point $\mathrm{Re}_{x,\mathrm{crit}}$ and turbulent thereafter. Apply this scheme to computation of the boundary-layer thickness at $x = 1.5$ m in 40 m/s flow of air at 20°C and 1 atm past a flat plate. Compare your result with Eq. (7.1*b*). Assume $\mathrm{Re}_{x,\mathrm{crit}} \approx 1.2$ E6.

P7.4 Air at 20°C and 1 atm flows at 15 m/s past a flat plate with $\mathrm{Re}_{x,\mathrm{crit}} \approx 1$ E6. At what point x will the boundary-layer thickness be 8 mm? Why do Eqs. (7.1) seem to fail? Make a sketch illustrating the discrepancy; then use the ideas in Prob. 7.3 to complete this problem correctly.

P7.5 SAE 30 oil at 20°C flows at 1.8 ft^3/s from a reservoir into a 6-in-diameter pipe. Use flat-plate theory to estimate the position x where the pipe-wall boundary layers meet in the center. Compare with Eq. (6.5), and give some explanations for the discrepancy.

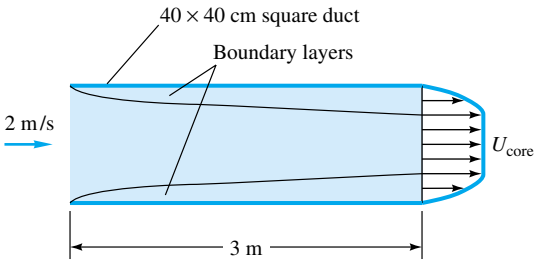
P7.6 For the laminar parabolic boundary-layer profile of Eq. (7.6), compute the shape factor H and compare with the exact Blasius result, Eq. (7.31).

P7.7 Air at 20°C and 1 atm enters a 40-cm-square duct as in Fig. P7.7. Using the "displacement thickness" concept of Fig. 7.4, estimate (*a*) the mean velocity an
mean pressure in the core of the flow at the posi



ketabline.com Ebook.ketabline.com

3 m. (*c*) What is the average gradient, in Pa/m, in this section?



P7.7

P7.8 Air, $\rho = 1.2$ kg/m^3 and $\mu = 1.8$ E-5 kg/(m · s), flows at 10 m/s past a flat plate. At the trailing edge of the plate, the following velocity profile data are measured:

y, mm	0	0.5	1.0	2.0	3.0	4.0	5.0	6.0
u, m/s	0	1.75	3.47	6.58	8.70	9.68	10.0	10.0

If the upper surface has an area of 0.6 m^2, estimate, using momentum concepts, the friction drag, in N, on the upper surface.

P7.9 Repeat the flat-plate momentum analysis of Sec. 7.2 by replacing the parabolic profile, Eq. (7.6), with a more accurate sinusoidal profile:

$$\frac{u}{U} = \sin\frac{\pi y}{2\delta}$$

Compute momentum-integral estimates of c_f, θ/x, δ^*/x, and H.

P7.10 Repeat Prob. 7.9, using the polynomial profile suggested by K. Pohlhausen in 1921:

$$\frac{u}{U} \approx 2\frac{y}{\delta} - 2\frac{y^3}{\delta^3} + \frac{y^4}{\delta^4}$$

Does this profile satisfy the boundary conditions of laminar flat-plate flow?

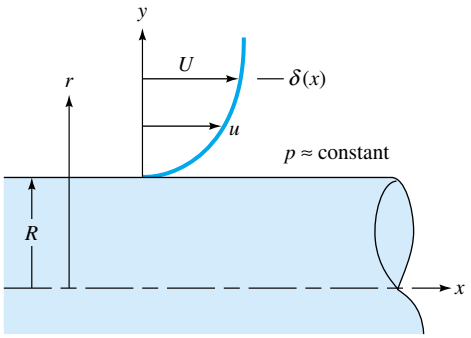
P7.11 Find the correct form for a cubic velocity-profile polynomial

$$u = A + By + Cy^2 + Dy^3$$

to replace Eq. (7.6) in a flat-plate momentum analysis. Find the value of θ/δ for this profile, but do not pursue the analysis further.

P7.12 The velocity profile shape $u/U \approx 1 - \exp(-4.605y/\delta)$ is a smooth curve with $u = 0$ at $y = 0$ and $u = 0.99U$ at $y = \delta$ and thus would seem to be a reasonable substitute for the parabolic flat-plate profile of Eq. (7.3). Yet when this new profile is used in the integral analysis of Sec. 7.3, we get the lousy result $\delta/x \approx 9.2/\mathrm{Re}_x^{1/2}$, which is 80 percent high. What is the reason for the inaccuracy? [*Hint:* The answer lies in evaluating the laminar boundary-layer momentum equation (7.19*b*) at the wall, $y = 0$.]

P7.13 Derive modified forms of the laminar boundary-layer equations (7.19) for the case of axisymmetric flow along the outside of a circular cylinder of constant radius R, as in Fig. P7.13. Consider the two special cases (*a*) $\delta \ll R$ and (*b*) $\delta \approx R$. What are the proper boundary conditions?



P7.13

P7.14 Show that the two-dimensional laminar-flow pattern with $dp/dx = 0$

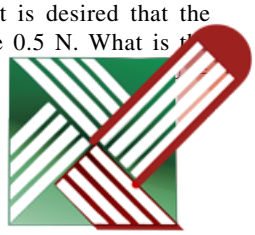
$$u = U_0(1 - e^{Cy}) \qquad v = v_0 < 0$$

is an exact solution to the boundary-layer equations (7.19). Find the value of the constant C in terms of the flow parameters. Are the boundary conditions satisfied? What might this flow represent?

P7.15 Discuss whether fully developed laminar incompressible flow between parallel plates, Eq. (4.143) and Fig. 4.16*b*, represents an exact solution to the boundary-layer equations (7.19) and the boundary conditions (7.20). In what sense, if any, are duct flows also boundary-layer flows?

P7.16 A thin flat plate 55 by 110 cm is immersed in a 6-m/s stream of SAE 10 oil at 20°C. Compute the total friction drag if the stream is parallel to (*a*) the long side and (*b*) the short side.

P7.17 Helium at 20°C and low pressure flows past a thin flat plate 1 m long and 2 m wide. It is desired that the total friction drag of the plate be 0.5 N. What is the appropriate absolute pressure of 35 m/s?

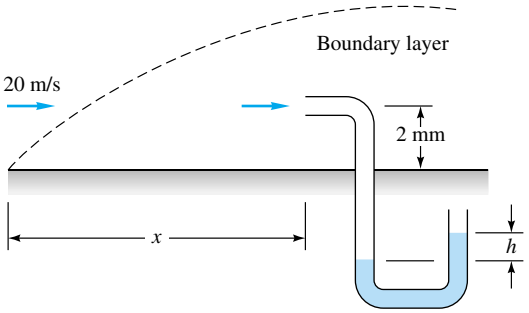


ketabline.com Ebook.ketabline.com

P7.18 In Prob. 7.7, when the duct is perfectly square, the core velocity speeds up. Suppose we wish to hold the core velocity constant by slanting the upper and lower walls while keeping the front and rear walls parallel. What angle of slant will be the best approximation? For this condition, what will be the total friction drag on the duct walls?

P7.19 Program a method of numerical solution of the Blasius flat-plate relation, Eq. (7.22), subject to the conditions in (7.23). You will find that you cannot get started without knowing the initial second derivative $f''(0)$, which lies between 0.2 and 0.5. Devise an iteration scheme which starts at $f''(0) \approx 0.2$ and converges to the correct value. Print out $u/U = f'(\eta)$ and compare with Table 7.1.

P7.20 Air at 20°C and 1 atm flows at 20 m/s past the flat plate in Fig. P7.20. A pitot stagnation tube, placed 2 mm from the wall, develops a manometer head $h = 16$ mm of Meriam red oil, SG = 0.827. Use this information to estimate the downstream position x of the pitot tube. Assume laminar flow.



P7.20

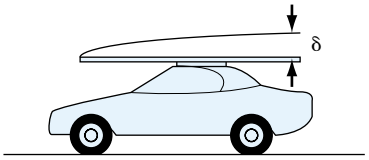
P7.21 For the experimental setup of Fig. P7.20, suppose the stream velocity is unknown and the pitot stagnation tube is traversed across the boundary layer of air at 1 atm and 20°C. The manometer fluid is Meriam red oil, and the following readings are made:

y, mm	0.5	1.0	1.5	2.0	2.5	3.0	3.5	4.0	4.5	5.0
h, mm	1.2	4.6	9.8	15.8	21.2	25.3	27.8	29.0	29.7	29.7

Using these data only (not the Blasius theory) estimate (*a*) the stream velocity, (*b*) the boundary-layer thickness, (*c*) the wall shear stress, and (*d*) the total friction drag between the leading edge and the position of the pitot tube.

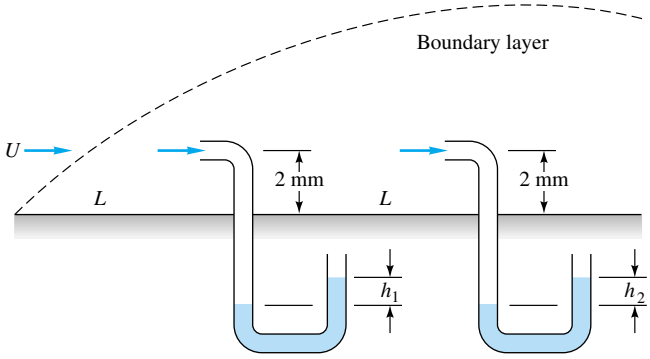
P7.22 For the Blasius flat-plate problem, Eqs. (7.21) to (7.23), does a two-dimensional stream function $\psi(x, y)$ exist? If so, determine the correct *dimensionless* form for ψ, assuming that $\psi = 0$ at the wall, $y = 0$.

P7.23 Suppose you buy a 4- by 8-ft sheet of plywood and put it on your roof rack. (See Fig. P7.23.) You drive home at 35 mi/h. (*a*) Assuming the board is perfectly aligned with the airflow, how thick is the boundary layer at the end of the board? (*b*) Estimate the drag on the sheet of plywood if the boundary layer remains laminar. (*c*) Estimate the drag on the sheet of plywood if the boundary-layer is turbulent (assume the wood is smooth), and compare the result to that of the laminar boundary-layer case.



P7.23

***P7.24** Air at 20°C and 1 atm flows past the flat plate in Fig. P7.24 under laminar conditions. There are two equally spaced pitot stagnation tubes, each placed 2 mm from the wall. The manometer fluid is water at 20°C. If $U = 15$ m/s and $L = 50$ cm, determine the values of the manometer readings h_1 and h_2, in mm.



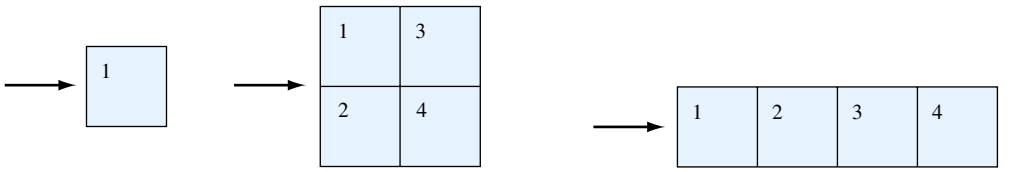
P7.24

P7.25 Modify Prob. 7.24 to the following somewhat more difficult scenario. Let the known data be $U = 15$ m/s and $h_1 = 8$ mm of water. Use this information to determine (*a*) L, in cm, (*b*) h_2, in mm.

P7.26 Consider laminar boundary-layer flow past the square-plate arrangements in Fig. P7.26. Compared to the friction drag of a single plate 1, how much larger is the drag of four plates together as in configurations (*a*) and explain your results.



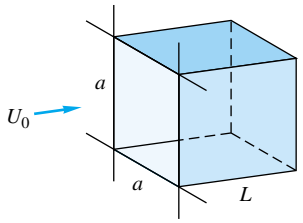
ketabline.com Ebook.ketabline.com



P7.26 (*a*) (*b*)

***P7.27** A thin smooth disk of diameter D is immersed parallel to a uniform stream of velocity U. Assuming laminar flow and using flat-plate theory as a guide, develop an approximate formula for the drag of the disk.

P7.28 Flow straighteners are arrays of narrow ducts placed in wind tunnels to remove swirl and other in-plane secondary velocities. They can be idealized as square boxes constructed by vertical and horizontal plates, as in Fig. P7.28. The cross section is a by a, and the box length is L. Assuming laminar flat-plate flow and an array of $N \times N$ boxes, derive a formula for (*a*) the total drag on the bundle of boxes and (*b*) the effective pressure drop across the bundle.



P7.28

P7.29 Let the flow straighteners in Fig. P7.28 form an array of 20×20 boxes of size $a = 4$ cm and $L = 25$ cm. If the approach velocity is $U_0 = 12$ m/s and the fluid is sea-level standard air, estimate (*a*) the total array drag and (*b*) the pressure drop across the array. Compare with Sec. 6.6.

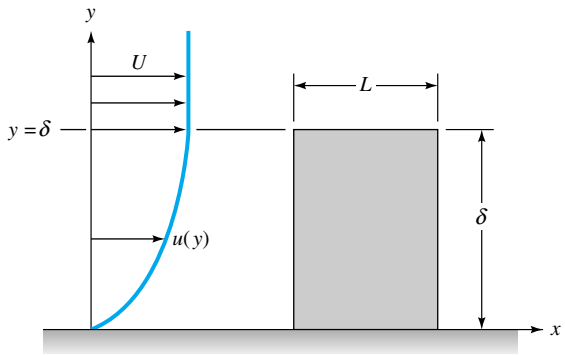
P7.30 Repeat Prob. 7.16 if the fluid is water at 20°C and the plate surface is smooth.

P7.31 Repeat Prob. 7.16 if the fluid is water at 20°C and the plate has an average roughness height of 1.5 mm.

P7.32 A flat plate of length L and height δ is placed at a wall and is parallel to an approaching boundary layer, as in Fig. P7.32. Assume that the flow over the plate is fully turbulent and that the approaching flow is a one-seventh-power law

$$u(y) = U_0\left(\frac{y}{\delta}\right)^{1/7}$$

Using strip theory, derive a formula for the drag coefficient of this plate. Compare this result with the drag of the same plate immersed in a uniform stream U_0.



P7.32

P7.33 An alternate analysis of turbulent flat-plate flow was given by Prandtl in 1927, using a wall shear-stress formula from pipe flow

$$\tau_w = 0.0225\rho U^2\left(\frac{\nu}{U\delta}\right)^{1/4}$$

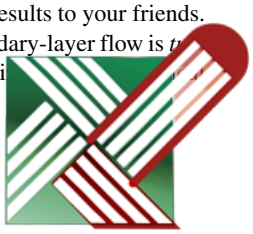
Show that this formula can be combined with Eqs. (7.33) and (7.40) to derive the following relations for turbulent flat-plate flow:

$$\frac{\delta}{x} = \frac{0.37}{\mathrm{Re}_x^{1/5}} \qquad c_f = \frac{0.0577}{\mathrm{Re}_x^{1/5}} \qquad C_D = \frac{0.072}{\mathrm{Re}_L^{1/5}}$$

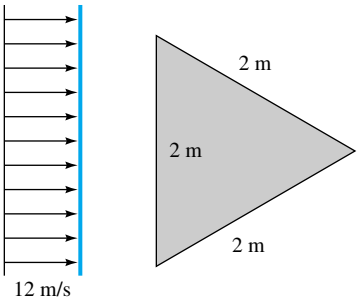
These formulas are limited to Re_x between 5×10^5 and 10^7.

***P7.34** A thin equilateral-triangle plate is immersed parallel to a 12 m/s stream of water at 20°C, as in Fig. P7.34. Assuming $\mathrm{Re}_{tr} = 5 \times 10^5$, estimate the drag of this plate.

P7.35 The solutions to Prob. 7.26 are (*a*) $F = 2.83F_{1\text{-plate}}$ and (*b*) $F = 2.0F_{1\text{-plate}}$. Do not reveal these results to your friends. Repeat Prob. 7.26 assuming the boundary-layer flow is *turbulent*, and comment on the striking i values.



ketabline.com Ebook.ketabline.com



P7.34

P7.36 A ship is 125 m long and has a wetted area of 3500 m^2. Its propellers can deliver a maximum power of 1.1 MW to seawater at 20°C. If all drag is due to friction, estimate the maximum ship speed, in kn.

P7.37 A wind tunnel has a test section 1 m square and 6 m long with air at 20°C moving at an average velocity of 30 m/s. It is planned to slant the walls outward slightly to account for the growing boundary-layer displacement thickness on the four walls, thus keeping the test-section velocity constant. At what angle should they be slanted to keep V constant between $x = 2$ m and $x = 4$ m?

P7.38 Atmospheric boundary layers are very thick but follow formulas very similar to those of flat-plate theory. Consider wind blowing at 10 m/s at a height of 80 m above a smooth beach. Estimate the wind shear stress, in Pa, on the beach if the air is standard sea-level conditions. What will the wind velocity striking your nose be if (*a*) you are standing up and your nose is 170 cm off the ground and (*b*) you are lying on the beach and your nose is 17 cm off the ground?

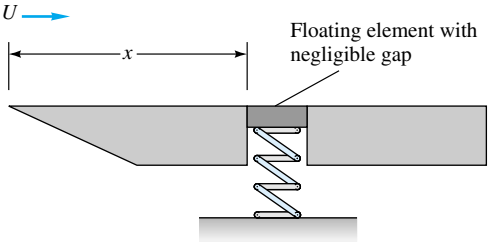
P7.39 A hydrofoil 50 cm long and 4 m wide moves at 28 kn in seawater at 20°C. Using flat-plate theory with $\mathrm{Re}_{tr} = 5$ E5, estimate its drag, in N, for (*a*) a smooth wall and (*b*) a rough wall, $\epsilon = 0.3$ mm.

P7.40 Hoerner [12, p. 3.25] states that the drag coefficient of a flag in winds, based on total wetted area $2bL$, is approximated by $C_D \approx 0.01 + 0.05L/b$, where L is the flag length in the flow direction. Test Reynolds numbers Re_L were 1 E6 or greater. (*a*) Explain why, for $L/b \geq 1$, these drag values are much higher than for a flat plate. Assuming sea-level standard air at 50 mi/h, with area $bL = 4$ m^2, find (*b*) the proper flag dimensions for which the total drag is approximately 400 N.

P7.41 Repeat Prob. 7.20 with the sole change that the pitot probe is now 10 mm from the wall (5 times higher). Show that the flow there cannot possibly be laminar, and use smooth-wall turbulent-flow theory to estimate the position x of the probe, in m.

***P7.42** A four-bladed helicopter rotor rotates at n r/min in air with properties (ρ, μ). Each blade has chord length C and extends from the center of rotation out to radius R (the hub size is neglected). Assuming turbulent flow from the leading edge, develop an analytical estimate for the power P required to drive this rotor.

P7.43 In the flow of air at 20°C and 1 atm past a flat plate in Fig. P7.43, the wall shear is to be determined at position x by a *floating element* (a small area connected to a strain-gage force measurement). At $x = 2$ m, the element indicates a shear stress of 2.1 Pa. Assuming turbulent flow from the leading edge, estimate (*a*) the stream velocity U, (*b*) the boundary-layer thickness δ at the element, and (*c*) the boundary-layer velocity u, in m/s, at 5 mm above the element.



P7.43

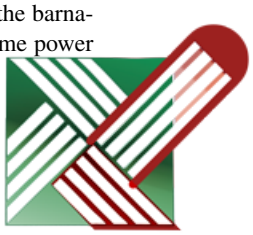
P7.44 Extensive measurements of wall shear stress and local velocity for turbulent airflow on the flat surface of the University of Rhode Island wind tunnel have led to the following proposed correlation:

$$\frac{\rho y^2 \tau_w}{\mu^2} \approx 0.0207 \left(\frac{uy}{\nu}\right)^{1.77}$$

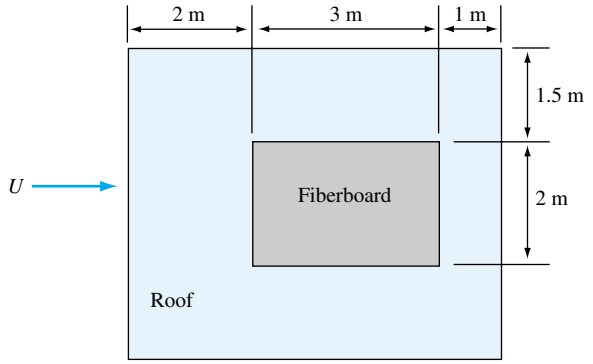
Thus, if y and $u(y)$ are known at a point in a flat-plate boundary layer, the wall shear may be computed directly. If the answer to part (*c*) of Prob. 7.43 is $u \approx 27$ m/s, determine whether the correlation is accurate for this case.

P7.45 A thin sheet of fiberboard weighs 90 N and lies on a rooftop, as shown in Fig. P7.45. Assume ambient air at 20°C and 1 atm. If the coefficient of solid friction between board and roof is $\sigma \approx 0.12$, what wind velocity will generate enough fluid friction to dislodge the board?

P7.46 A ship is 150 m long and has a wetted area of 5000 m^2. If it is encrusted with barnacles, the ship requires 7000 hp to overcome friction drag when moving in seawater at 15 kn and 20°C. What is the average roughness of the barnacles? How fast would the ship move with the same power if the surface were smooth? Neglect wave drag.



ketabline.com Ebook.ketabline.com



P7.45

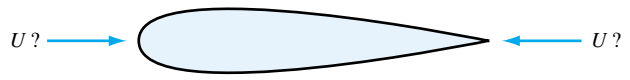
P7.47 As a case similar to Example 7.5, Howarth also proposed the adverse-gradient velocity distribution $U = U_0(1 - x^2/L^2)$ and computed separation at $x_{sep}/L = 0.271$ by a series-expansion method. Compute separation by Thwaites' method and compare.

P7.48 In 1957 H. Görtler proposed the adverse-gradient test cases

$$U = \frac{U_0}{(1 + x/L)^n}$$

and computed separation for laminar flow at $n = 1$ to be $x_{sep}/L = 0.159$. Compare with Thwaites' method, assuming $\theta_0 = 0$.

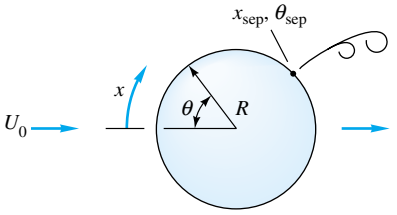
P7.49 Based strictly upon your understanding of flat-plate theory plus adverse and favorable pressure gradients, explain the direction (left or right) for which airflow past the slender airfoil shape in Fig. P7.49 will have lower total (friction + pressure) drag.



P7.49

***P7.50** For flow past a cylinder of radius R as in Fig. P7.50, the theoretical inviscid velocity distribution along the surface is $U = 2U_0 \sin(x/R)$, where U_0 is the oncoming stream velocity and x is the arc length measured from the nose (Chap. 8). Compute the laminar separation point x_{sep} and θ_{sep} by Thwaites' method, and compare with the digital-computer solution $x_{sep}/R = 1.823$ ($\theta_{sep} = 104.5°$) given by R. M. Terrill in 1960.

P7.51 Consider the flat-walled diffuser in Fig. P7.51, which is similar to that of Fig. 6.26*a* with constant width b. If x is measured from the inlet and the wall boundary layers are

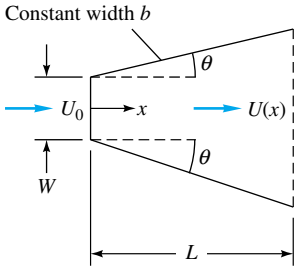


P7.50

thin, show that the core velocity $U(x)$ in the diffuser is given approximately by

$$U = \frac{U_0}{1 + (2x \tan \theta)/W}$$

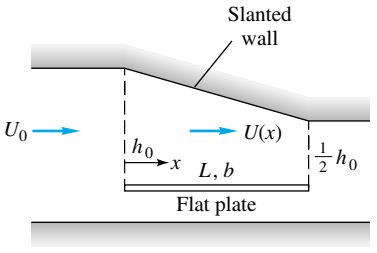
where W is the inlet height. Use this velocity distribution with Thwaites' method to compute the wall angle θ for which laminar separation will occur in the exit plane when diffuser length $L = 2W$. Note that the result is independent of the Reynolds number.



P7.51

***P7.52** In Fig. P7.52 a slanted upper wall creates a favorable pressure gradient on the upper surface of the flat plate. Use Thwaites' theory to estimate

$$C_D = \frac{F}{\frac{1}{2}\rho U_0^2 b L}$$



P7.52



ketabline.com Ebook.ketabline.com

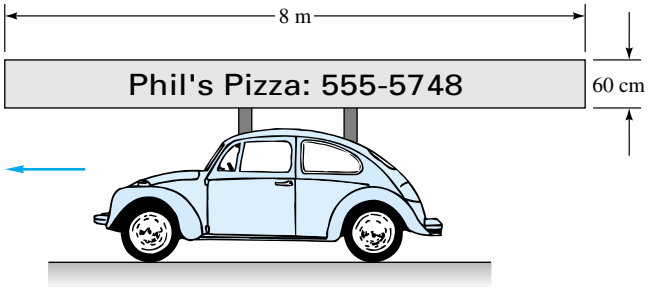
on the upper plate surface if $U_0 L/\nu = 10^5$. Compare with Eq. (7.27).

P7.53 From Table 7.2, the drag coefficient of a wide plate normal to a stream is approximately 2.0. Let the stream conditions be U_∞ and p_∞. If the average pressure on the front of the plate is approximately equal to the free-stream stagnation pressure, what is the average pressure on the rear?

P7.54 A chimney at sea level is 2 m in diameter and 40 m high. When it is subjected to 50 mi/h storm winds, what is the estimated wind-induced bending moment about the bottom of the chimney?

P7.55 A ship tows a submerged cylinder, which is 1.5 m in diameter and 22 m long, at 5 m/s in fresh water at 20°C. Estimate the towing power, in kW, required if the cylinder is (*a*) parallel and (*b*) normal to the tow direction.

P7.56 A delivery vehicle carries a long sign on top, as in Fig. P7.56. If the sign is very thin and the vehicle moves at 55 mi/h, estimate the force on the sign (*a*) with no crosswind and (*b*) with a 10 mi/h crosswind.



P7.56

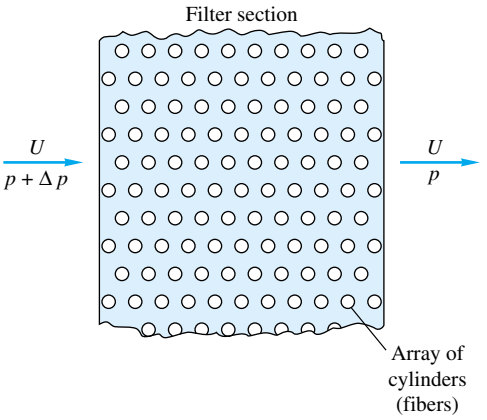
P7.57 The main cross-cable between towers of a coastal suspension bridge is 60 cm in diameter and 90 m long. Estimate the total drag force on this cable in crosswinds of 50 mi/h. Are these laminar-flow conditions?

P7.58 A long cylinder of rectangular cross section, 5 cm high and 30 cm long, is immersed in water at 20°C flowing at 12 m/s parallel to the long side of the rectangle. Estimate the drag force on the cylinder, per unit length, if the rectangle (*a*) has a flat face or (*b*) has a rounded nose.

P7.59 Joe can pedal his bike at 10 m/s on a straight level road with no wind. The rolling resistance of his bike is 0.80 N · s/m, i.e., 0.80 N of force per m/s of speed. The drag area ($C_D A$) of Joe and his bike is 0.422 m^2. Joe's mass is 80 kg and that of the bike is 15 kg. He now encounters a head wind of 5.0 m/s. (*a*) Develop an equation for the speed at which Joe can pedal into the wind. [*Hint:* A cubic equation for V will result.] (*b*) Solve for V, i.e., how fast can Joe ride into the head wind? (*c*) Why is the result not simply $10 - 5.0 = 5.0$ m/s, as one might first suspect?

P7.60 A fishnet consists of 1-mm-diameter strings overlapped and knotted to form 1- by 1-cm squares. Estimate the drag of 1 m^2 of such a net when towed normal to its plane at 3 m/s in 20°C seawater. What horsepower is required to tow 400 ft^2 of this net?

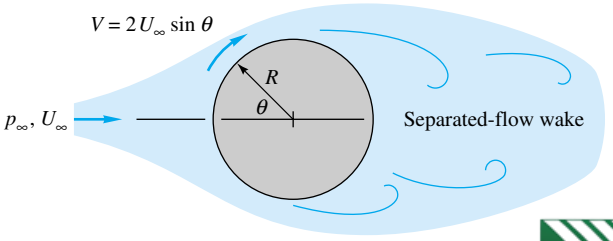
P7.61 A filter may be idealized as an array of cylindrical fibers normal to the flow, as in Fig. P7.61. Assuming that the fibers are uniformly distributed and have drag coefficients given by Fig. 7.16*a*, derive an approximate expression for the pressure drop Δp through a filter of thickness L.



P7.61

P7.62 A sea-level smokestack is 52 m high and has a square cross section. Its supports can withstand a maximum side force of 90 kN. If the stack is to survive 90-mi/h hurricane winds, what is its maximum possible width?

P7.63 The cross section of a cylinder is shown in Fig. P7.63. Assume that on the front surface the velocity is given by potential theory (Sec. 8.4), $V = 2U_\infty \sin\theta$, from which the surface pressure is computed by Bernoulli's equation. In



P7.63



ketabline.com Ebook.ketabline.com

the separated flow on the rear, the pressure is assumed equal to its value at $\theta = 90°$. Compute the theoretical drag coefficient and compare with Table 7.2.

P7.64 A parachutist jumps from a plane, using an 8.5-m-diameter chute in the standard atmosphere. The total mass of the chutist and the chute is 90 kg. Assuming an open chute and quasi-steady motion, estimate the time to fall from 2000- to 1000-m altitude.

P7.65 The drag of a sphere at very low Reynolds numbers $\mathrm{Re}_D \ll 1$ was given analytically by G. G. Stokes in 1851: $F = 3\pi\mu VD$ [2, pp. 175–178]. This formula is an example of Stokes' *law of creeping motion,* where inertia is negligible. Show that the drag coefficient in this region is $C_D = 24/\mathrm{Re}_D$. A 1-mm-diameter sphere falls in 20°C glycerin at 2.5 mm/s. Is this a creeping motion? Compute (*a*) the Reynolds number, (*b*) the drag, and (*c*) the specific gravity of the sphere.

P7.66 A sphere of density ρ_s and diameter D is dropped from rest in a fluid of density ρ and viscosity μ. Assuming a constant drag coefficient C_{d_0}, derive a differential equation for the fall velocity $V(t)$ and show that the solution is

$$V = \left[\frac{4gD(S-1)}{3C_{d_0}}\right]^{1/2} \tanh Ct$$

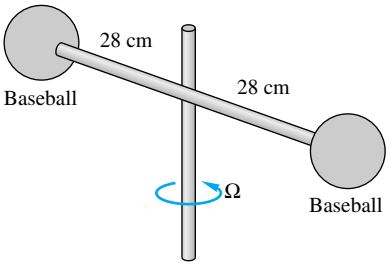
$$C = \left[\frac{3gC_{d_0}(S-1)}{4S^2D}\right]^{1/2}$$

where $S = \rho_s/\rho$ is the specific gravity of the sphere material.

P7.67 Apply the theory of Prob. 7.66 to a steel sphere of diameter 2 cm, dropped from rest in water at 20°C. Estimate the time required for the sphere to reach 99 percent of its terminal (zero-acceleration) velocity.

P7.68 A baseball weighs 145 g and is 7.35 cm in diameter. It is dropped from rest from a 35-m-high tower at approximately sea level. Assuming a laminar-flow drag coefficient, estimate (*a*) its terminal velocity and (*b*) whether it will reach 99 percent of its terminal velocity before it hits the ground.

P7.69 Two baseballs from Prob. 7.68 are connected to a rod 7 mm in diameter and 56 cm long, as in Fig. P7.69. What power, in W, is required to keep the system spinning at 400 r/min? Include the drag of the rod, and assume sea-level standard air.



P7.69

P7.70 A baseball from Prob. 7.68 is batted upward during a game at an angle of 45° and an initial velocity of 98 mi/h. Neglect spin and lift. Estimate the horizontal distance traveled, (*a*) neglecting drag and (*b*) accounting for drag in a numerical (computer) solution with a transition Reynolds number $\mathrm{Re}_{D,\mathrm{crit}} = 2.5$ E5.

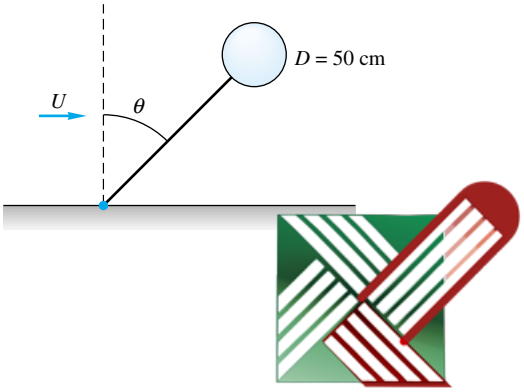
P7.71 A football weighs 0.91 lbf and approximates an ellipsoid 6 in in diameter and 12 in long (Table 7.3). It is thrown upward at a 45° angle with an initial velocity of 80 ft/s. Neglect spin and lift. Assuming turbulent flow, estimate the horizontal distance traveled, (*a*) neglecting drag and (*b*) accounting for drag with a numerical (computer) model.

P7.72 A settling tank for a municipal water supply is 2.5 m deep, and 20°C water flows through continuously at 35 cm/s. Estimate the minimum length of the tank which will ensure that all sediment (SG = 2.55) will fall to the bottom for particle diameters greater than (*a*) 1 mm and (*b*) 100 μm.

P7.73 A balloon is 4 m in diameter and contains helium at 125 kPa and 15°C. Balloon material and payload weigh 200 N, not including the helium. Estimate (*a*) the terminal ascent velocity in sea-level standard air, (*b*) the final standard altitude (neglecting winds) at which the balloon will come to rest, and (*c*) the minimum diameter (<4 m) for which the balloon will just barely begin to rise in sea-level standard air.

P7.74 If $D = 4$ m in Prob. 7.73 and the helium remains at 15°C and 125 kPa, estimate the time required for the balloon to rise through the standard atmosphere from sea level to its equilibrium altitude, which is approximately 4000 m.

P7.75 The helium-filled balloon in Fig. P7.75 is tethered at 20°C and 1 atm with a string of negligible weight and drag. The diameter is 50 cm, and the balloon material weighs 0.2 N,



P7.75

ketabline.com Ebook.ketabline.com

not including the helium. The helium pressure is 120 kPa. Estimate the tilt angle θ if the airstream velocity U is (*a*) 5 m/s or (*b*) 20 m/s.

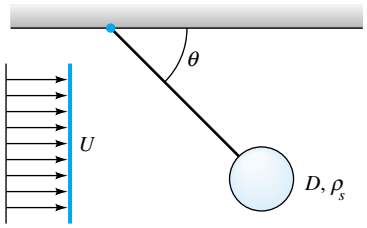
P7.76 Extend Prob. 7.75 to make a smooth plot of tilt angle θ versus stream velocity U in the range $1 < U < 12$ mi/h. (A spreadsheet is recommended for this task.) Comment on the effectiveness of this system as an air-velocity instrument.

P7.77 Modify Prob. 7.75 as follows: Let the fluid be water at 20°C, and let the 50-cm-diameter sphere be solid cork (SG = 0.16). Estimate the tilt angle θ if the water velocity U is 3 m/s.

P7.78 Apply Prob. 7.61 to a filter consisting of 300-μm-diameter fibers packed 250 per square centimeter in the plane of Fig. P7.61. For air at 20°C and 1 atm flowing at 1.5 m/s, estimate the pressure drop if the filter is 5 cm thick.

P7.79 Assume that a radioactive dust particle approximates a sphere of density 2400 kg/m^3. How long, in days, will it take such a particle to settle to sea level from an altitude of 12 km if the particle diameter is (*a*) 1 μm or (*b*) 20 μm?

P7.80 A heavy sphere attached to a string should hang at an angle θ when immersed in a stream of velocity U, as in Fig. P7.80. Derive an expression for θ as a function of the sphere and flow properties. What is θ if the sphere is steel (SG = 7.86) of diameter 3 cm and the flow is sea-level standard air at $U = 40$ m/s? Neglect the string drag.



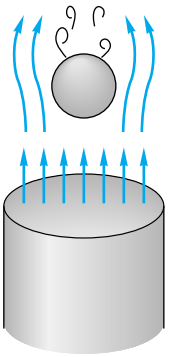
P7.80

P7.81 A typical U.S. Army parachute has a projected diameter of 28 ft. For a payload mass of 80 kg, (*a*) what terminal velocity will result at 1000-m standard altitude? For the same velocity and net payload, what size drag-producing "chute" is required if one uses a square flat plate held (*b*) vertically and (*c*) horizontally? (Neglect the fact that flat shapes are not dynamically stable in free fall.)

P7.82 The average skydiver with parachute unopened weighs 175 lbf and has a drag area $C_DA = 9$ ft^2 spread-eagled and 1.2 ft^2 falling feet first [12, p. 313]. What are the minimum and maximum terminal speeds that can be achieved by a skydiver at 5000-ft standard altitude?

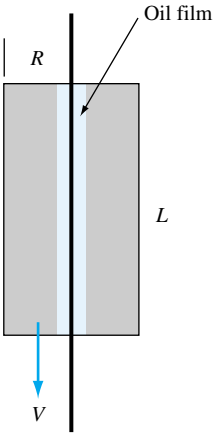
P7.83 A high-speed car has a drag coefficient of 0.3 and a frontal area of 1 m^2. A parachute is to be used to slow this car from 80 to 40 m/s in 8 s. What should the chute diameter be? What distance will be traveled during this deceleration? Take $m = 2000$ kg.

P7.84 A Ping-Pong ball weighs 2.6 g and has a diameter of 3.8 cm. It can be supported by an air jet from a vacuum cleaner outlet, as in Fig. P7.84. For sea-level standard air, what jet velocity is required?



P7.84

***P7.85** An aluminum cylinder (SG = 2.7) slides concentrically down a taut 1-mm-diameter wire as shown in Fig. P7.85. Its length $L = 8$ cm, and its radius $R = 1$ cm. A 2-mm-diameter hole down the cylinder center is lubricated by SAE 30 oil at 20°C. Estimate the terminal fall velocity V of the cylinder if ambient air drag is (*a*) neglected and (*b*) included. Assume air at 1 atm and 20°C.



P7.85

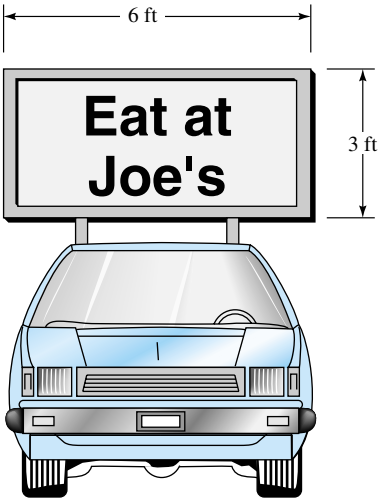


ketabline.com Ebook.ketabline.com

P7.86 Hoerner [Ref. 12, pp. 3–25] states that the drag coefficient of a flag of 2:1 aspect ratio is 0.11 based on planform area. The University of Rhode Island has an aluminum flagpole 25 m high and 14 cm in diameter. It flies equal-sized national and state flags together. If the fracture stress of aluminum is 210 MPa, what is the maximum flag size that can be used yet avoids breaking the flagpole in hurricane (75 mi/h) winds?

P7.87 A tractor-trailer truck has a drag-area $C_DA = 8$ m^2 bare and 6.7 m^2 with an aerodynamic deflector (Fig. 7.18*b*). Its rolling resistance is 50 N for each mile per hour of speed. Calculate the total horsepower required at sea level with and without the deflector if the truck moves at (*a*) 55 mi/h and (*b*) 75 mi/h.

P7.88 A pickup truck has a clean drag-area C_DA of 35 ft^2. Estimate the horsepower required to drive the truck at 55 mi/h (*a*) clean and (*b*) with the 3- by 6-ft sign in Fig. P7.88 installed if the rolling resistance is 150 lbf at sea level.

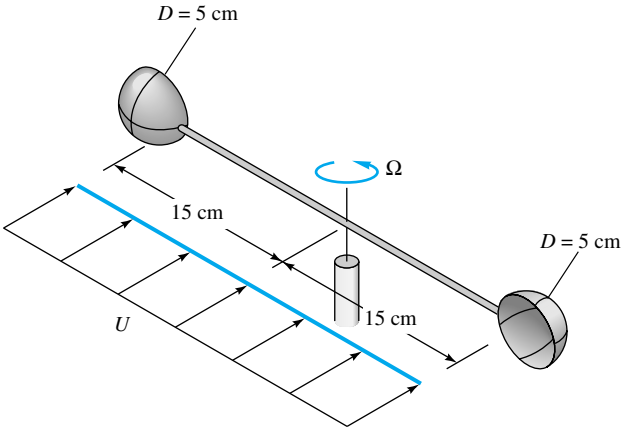


P7.88

P7.89 A water tower is approximated by a 15-m-diameter sphere mounted on a 1-m-diameter rod 20 m long. Estimate the bending moment at the root of the rod due to aerodynamic forces during hurricane winds of 40 m/s.

P7.90 In the great hurricane of 1938, winds of 85 mi/h blew over a boxcar in Providence, Rhode Island. The boxcar was 10 ft high, 40 ft long, and 6 ft wide, with a 3-ft clearance above tracks 4.8 ft apart. What wind speed would topple a boxcar weighing 40,000 lbf?

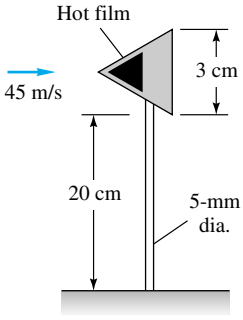
***P7.91** A cup anemometer uses two 5-cm-diameter hollow hemispheres connected to 15-cm rods, as in Fig. P7.91. Rod drag is negligible, and the central bearing has a retarding torque of 0.004 N · m. Making simplifying assumptions to average out the time-varying geometry, estimate and plot the variation of anemometer rotation rate Ω with wind velocity U in the range $0 < U < 25$ m/s for sea-level standard air.



P7.91

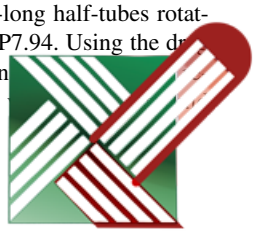
P7.92 A 1500-kg automobile uses its drag area $C_DA = 0.4$ m^2, plus brakes and a parachute, to slow down from 50 m/s. Its brakes apply 5000 N of resistance. Assume sea-level standard air. If the automobile must stop in 8 s, what diameter parachute is appropriate?

P7.93 A hot-film probe is mounted on a cone-and-rod system in a sea-level airstream of 45 m/s, as in Fig. P7.93. Estimate the maximum cone vertex angle allowable if the flow-induced bending moment at the root of the rod is not to exceed 30 N · cm.



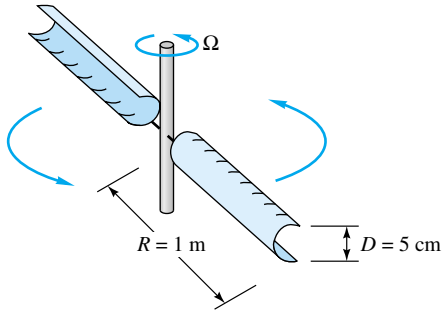
P7.93

P7.94 A rotary mixer consists of two 1-m-long half-tubes rotating around a central arm, as in Fig. P7.94. Using the d
from Table 7.2, derive an expression
quired to drive the mixer at angular



ketabline.com Ebook.ketabline.com

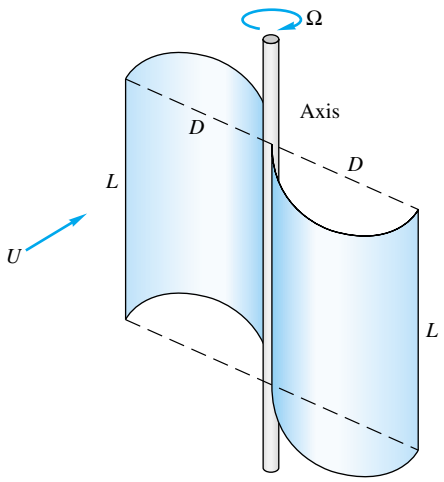
of density ρ. Suppose that the fluid is water at 20°C and the maximum driving power available is 20 kW. What is the maximum rotation speed Ω r/min?



P7.94

P7.95 An airplane weighing 12 kN, with a drag-area $C_D A \approx 5$ m^2, lands at sea level at 55 m/s and deploys a drag parachute 3 m in diameter. No other brakes are applied. (*a*) How long will it take the plane to slow down to 30 m/s? (*b*) How far will it have traveled in that time?

***P7.96** A Savonius rotor (Fig. 6.29*b*) can be approximated by the two open half-tubes in Fig. P7.96 mounted on a central axis. If the drag of each tube is similar to that in Table 7.2, derive an approximate formula for the rotation rate Ω as a function of U, D, L, and the fluid properties (ρ, μ).



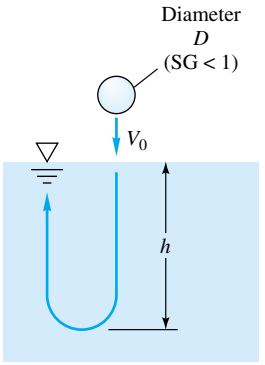
P7.96

P7.97 A simple measurement of automobile drag can be found by an unpowered *coastdown* on a level road with no wind. Assume constant rolling resistance. For an automobile of mass 1500 kg and frontal area 2 m^2, the following velocity-versus-time data are obtained during a coastdown:

t, s	0	10	20	30	40
V, m/s	27.0	24.2	21.8	19.7	17.9

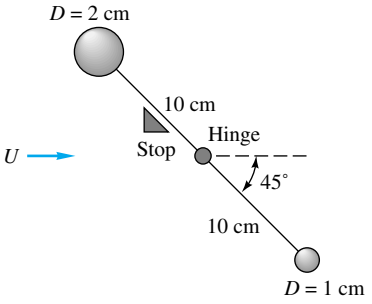
Estimate (*a*) the rolling resistance and (*b*) the drag coefficient. This problem is well suited for digital-computer analysis but can be done by hand also.

***P7.98** A buoyant ball of specific gravity SG < 1 dropped into water at inlet velocity V_0 will penetrate a distance h and then pop out again, as in Fig. P7.98. Make a dynamic analysis of this problem, assuming a constant drag coefficient, and derive an expression for h as a function of the system properties. How far will a 5-cm-diameter ball with SG $= 0.5$ and $C_D \approx 0.47$ penetrate if it enters at 10 m/s?



P7.98

P7.99 Two steel balls (SG $= 7.86$) are connected by a thin hinged rod of negligible weight and drag, as in Fig. P7.99. A stop prevents the rod from rotating counterclockwise. Estimate the sea-level air velocity U for which the rod will first begin to rotate clockwise.



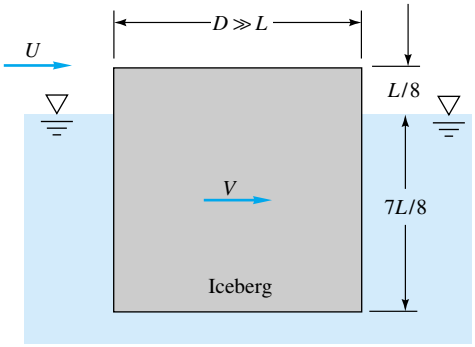
P7.99



ketabline.com Ebook.ketabline.com

P7.100 In creeping motion or *Stokes' flow* at velocity U past a sphere of diameter D, density (fluid inertia) is unimportant and the drag force is $F = 3\pi\mu UD$. This formula is valid if $\text{Re}_D \leq 1.0$ (see Fig. 7.16*b*). (*a*) Verify that Stokes' formula is equivalent to $C_D = 24/\text{Re}_D$. (*b*) Determine the largest diameter raindrop whose terminal fall velocity follows Stokes' formula in sea-level standard air.

P7.101 Icebergs can be driven at substantial speeds by the wind. Let the iceberg be idealized as a large, flat cylinder, $D \gg L$, with one-eighth of its bulk exposed, as in Fig. P7.101. Let the seawater be at rest. If the upper and lower drag forces depend upon relative velocities between the iceberg and the fluid, derive an approximate expression for the steady iceberg speed V when driven by wind velocity U.

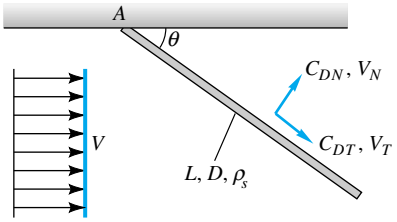


P7.101

P7.102 Sand particles (SG = 2.7), approximately spherical with diameters from 100 to 250 μm, are introduced into an upward-flowing stream of water at 20°C. What is the minimum water velocity which will carry all the sand particles *upward*?

P7.103 When immersed in a uniform stream V, a heavy rod hinged at A will hang at *Pode's angle* θ, after an analysis by L. Pode in 1951 (Fig. P7.103). Assume that the cylinder has normal drag coefficient C_{DN} and tangential coefficient C_{DT} which relate the drag forces to V_N and V_T, respectively. Derive an expression for Pode's angle as a function of the flow and rod parameters. Find θ for a steel rod, $L = 40$ cm, $D = 1$ cm, hanging in sea-level air at $V = 35$ m/s.

P7.104 Suppose that the body in Fig. P7.103 is a thin plate weighing 0.6 N, of length $L = 20$ cm and width $b = 4$ cm into the paper. For sea-level standard air, plot Pode's angle θ versus velocity V in the range $0 < V < 40$ m/s. Would this device make a good air-velocity meter (anemometer)?



P7.103

P7.105 A ship 50 m long, with a wetted area of 800 m^2, has the hull shape tested in Fig. 7.19. There are no bow or stern bulbs. The total propulsive power available is 1 MW. For seawater at 20°C, plot the ship's velocity V kn versus power P for $0 < P < 1$ MW. What is the most efficient setting?

P7.106 A smooth steel 1-cm-diameter sphere ($W \approx 0.04$ N) is fired vertically at sea level at the initial supersonic velocity $V_0 = 1000$ m/s. Its drag coefficient is given by Fig. 7.20. Assuming that the speed of sound is constant at $a \approx 343$ m/s, compute the maximum altitude of the projectile (*a*) by a simple analytical estimate and (*b*) by a digital-computer program.

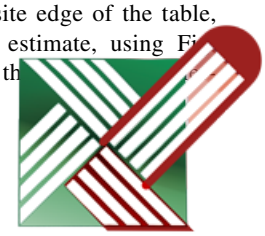
P7.107 Repeat Prob. 7.106 if the body is a 9-mm steel bullet ($W \approx 0.07$ N) which approximates the "pointed body of revolution" in Fig. 7.20.

P7.108 The data in Fig. P7.108 are for the lift and drag of a spinning sphere from Ref. 12, pp. 7–20. Suppose that a tennis ball ($W \approx 0.56$ N, $D \approx 6.35$ cm) is struck at sea level with initial velocity $V_0 = 30$ m/s and "topspin" (front of the ball rotating downward) of 120 r/s. If the initial height of the ball is 1.5 m, estimate the horizontal distance traveled before it strikes the ground.

P7.109 Repeat Prob. 7.108 if the ball is struck with "underspin" (front of the ball rotating upward).

P7.110 A baseball pitcher throws a curveball with an initial velocity of 65 mi/h and a spin of 6500 r/min about a vertical axis. A baseball weighs 0.32 lbf and has a diameter of 2.9 in. Using the data of Fig. P7.108 for turbulent flow, estimate how far such a curveball will have deviated from its straight-line path when it reaches home plate 60.5 ft away.

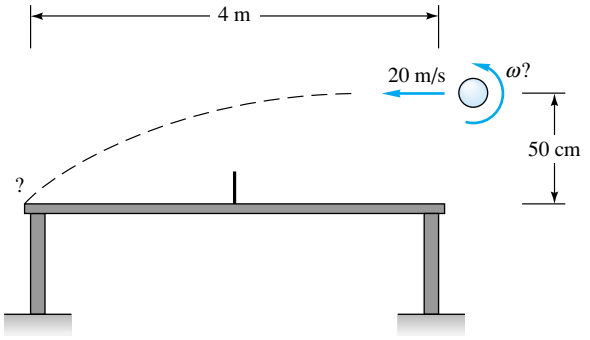
***P7.111** A table tennis ball has a mass of 2.6 g and a diameter of 3.81 cm. It is struck horizontally at an initial velocity of 20 m/s while it is 50 cm above the table, as in Fig. P7.111. For sea-level air, what spin, in r/min, will cause the ball to strike the opposite edge of the table, 4 m away? Make an analytical estimate, using Fi P7.108, and account for the fact th ates during flight.



ketabline.com Ebook.ketabline.com

Figure Unavailable

P7.108



P7.111

P7.112 Repeat Prob. 7.111 by making a detailed digital-computer solution for the flight path of the ball. Use Fig. P7.108 for lift and drag.

P7.113 An automobile has a mass of 1000 kg and a drag-area $C_D A = 0.7$ m^2. The rolling resistance of 70 N is approximately constant. The car is coasting without brakes at 90 km/h as it begins to climb a hill of 10 percent grade (slope $= \tan^{-1} 0.1 = 5.71°$). How far up the hill will the car come to a stop?

***P7.114** Suppose that the car in Prob. 7.113 is placed at the top of the 10 percent grade hill and released from rest to coast down without brakes. What will be its speed, in km/h, after dropping a vertical distance of 20 m?

P7.115 An airplane weighs 180 kN and has a wing area of 160 m^2 and a mean chord of 4 m. The airfoil properties are given by Fig. 7.25. If the airplane cruises at 250 mi/h at 3000-m standard altitude, what propulsive power is required to overcome wing drag?

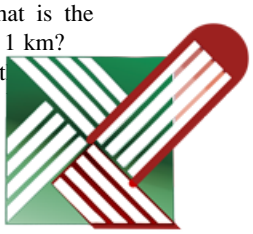
P7.116 The airplane of Prob. 7.115 is designed to land at $V_0 = 1.2V_{stall}$, using a split flap set at 60°. What is the proper landing speed in mi/h? What power is required for takeoff at the same speed?

P7.117 Suppose that the airplane of Prob. 7.115 takes off at sea level without benefit of flaps, with C_L constant so that the takeoff speed is 100 mi/h. Estimate the takeoff distance if the thrust is 10 kN. How much thrust is needed to make the takeoff distance 1250 m?

***P7.118** Suppose that the airplane of Prob. 7.115 is fitted with all the best high-lift devices of Fig. 7.28. What is its minimum stall speed in mi/h? Estimate the stopping distance if the plane lands at $V_0 = 1.25V_{stall}$ with constant $C_L = 3.0$ and $C_D = 0.2$ and the braking force is 20 percent of the weight on the wheels.

P7.119 An airplane has a mass of 5000 kg, a maximum thrust of 7000 N, and a rectangular wing with aspect ratio 6.0. It takes off at sea level with a 60° split flap whose two-dimensional properties are shown in Fig. 7.25. Assume all lift and all drag are due to the wing. What is the proper wing size if the takeoff distance is to be 1 km?

P7.120 Show that if Eqs. (7.70) and (7.71) are valid, t
mum lift-to-drag ratio occurs when $C_D = 2C_{D\infty}$.



ketabline.com Ebook.ketabline.com

$(L/D)_{max}$ and α for a symmetric wing when AR = 5 and $C_{D\infty} = 0.009$?

P7.121 In gliding (unpowered) flight, the lift and drag are in equilibrium with the weight. Show that if there is no wind, the aircraft sinks at an angle

$$\tan\theta \approx \frac{\text{drag}}{\text{lift}}$$

For a sailplane of mass 200 kg, wing area 12 m^2, and aspect ratio 11, with an NACA 0009 airfoil, estimate (*a*) the stall speed, (*b*) the minimum gliding angle, and (*c*) the maximum distance it can glide in still air when it is 1200 m above level ground.

P7.122 A boat of mass 2500 kg has two hydrofoils, each of chord 30 cm and span 1.5 m, with $C_{L,max} = 1.2$ and $C_{D\infty} = 0.08$. Its engine can deliver 130 kW to the water. For seawater at 20°C, estimate (*a*) the minimum speed for which the foils support the boat and (*b*) the maximum speed attainable.

P7.123 In prewar days there was a controversy, perhaps apocryphal, about whether the bumblebee has a legitimate aerodynamic right to fly. The average bumblebee (*Bombus terrestris*) weighs 0.88 g, with a wing span of 1.73 cm and a wing area of 1.26 cm^2. It can indeed fly at 10 m/s. Using fixed-wing theory, what is the lift coefficient of the bee at this speed? Is this reasonable for typical airfoils?

***P7.124** The bumblebee can hover at zero speed by flapping its wings. Using the data of Prob. 7.123, devise a theory for flapping wings where the downstroke approximates a short flat plate normal to the flow (Table 7.3) and the upstroke is feathered at nearly zero drag. How many flaps per second of such a model wing are needed to support the bee's weight? (Actual measurements of bees show a flapping rate of 194 Hz.)

Word Problems

W7.1 How do you *recognize* a boundary layer? Cite some physical properties and some measurements which reveal appropriate characteristics.

W7.2 In Chap. 6 the Reynolds number for transition to turbulence in pipe flow was about $Re_{tr} \approx 2300$, whereas in flat-plate flow $Re_{tr} \approx 1$ E6, nearly three orders of magnitude higher. What accounts for the difference?

W7.3 Without writing any equations, give a verbal description of boundary-layer displacement thickness.

W7.4 Describe, in words only, the basic ideas behind the "boundary-layer approximations."

W7.5 What is an *adverse* pressure gradient? Give three examples of flow regimes where such gradients occur.

W7.6 What is a *favorable* pressure gradient? Give three examples of flow regimes where such gradients occur.

W7.7 The drag of an airfoil (Fig. 7.12) increases considerably if you turn the sharp edge around 180° to face the stream. Can you explain this?

W7.8 In Table 7.3, the drag coefficient of a spruce tree decreases sharply with wind velocity. Can you explain this?

W7.9 Thrust is required to propel an airplane at a finite forward velocity. Does this imply an energy loss to the system? Explain the concepts of thrust and drag in terms of the first law of thermodynamics.

W7.10 How does the concept of *drafting,* in automobile and bicycle racing, apply to the material studied in this chapter?

W7.11 The circular cylinder of Fig. 7.13 is doubly symmetric and therefore should have no lift. Yet a lift sensor would definitely reveal a finite root-mean-square value of lift. Can you explain this behavior?

W7.12 Explain in words why a thrown spinning ball moves in a curved trajectory. Give some physical reasons why a side force is developed in addition to the drag.

Fundamentals of Engineering Exam Problems

FE7.1 A smooth 12-cm-diameter sphere is immersed in a stream of 20°C water moving at 6 m/s. The appropriate Reynolds number of this sphere is approximately
(*a*) 2.3 E5, (*b*) 7.2 E5, (*c*) 2.3 E6, (*d*) 7.2 E6, (*e*) 7.2 E7

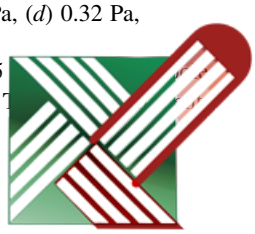
FE7.2 If, in Prob. FE7.1, the drag coefficient based upon frontal area is 0.5, what is the drag force on the sphere?
(*a*) 17 N, (*b*) 51 N, (*c*) 102 N, (*d*) 130 N, (*e*) 203 N

FE7.3 If, in Prob. FE7.1, the drag coefficient based upon frontal area is 0.5, at what terminal velocity will an aluminum sphere (SG = 2.7) fall in still water?
(*a*) 2.3 m/s, (*b*) 2.9 m/s, (*c*) 4.6 m/s, (*d*) 6.5 m/s, (*e*) 8.2 m/s

FE7.4 For flow of sea-level standard air at 4 m/s parallel to a thin flat plate, estimate the boundary-layer thickness at $x = 60$ cm from the leading edge:
(*a*) 1.0 mm, (*b*) 2.6 mm, (*c*) 5.3 mm, (*d*) 7.5 mm, (*e*) 20.2 mm

FE7.5 In Prob. FE7.4, for the same flow conditions, what is the wall shear stress at $x = 60$ cm from the leading edge?
(*a*) 0.053 Pa, (*b*) 0.11 Pa, (*c*) 0.16 Pa, (*d*) 0.32 Pa, (*e*) 0.64 Pa

FE7.6 Wind at 20°C and 1 atm blows at 75
18 m high and 20 cm in diameter. T



ketabline.com Ebook.ketabline.com

based upon frontal area, is 1.15. Estimate the wind-induced bending moment at the base of the pole.
(*a*) 9.7 kN · m, (*b*) 15.2 kN · m, (*c*) 19.4 kN · m, (*d*) 30.5 kN · m, (*e*) 61.0 kN · m

FE7.7 Consider wind at 20°C and 1 atm blowing past a chimney 30 m high and 80 cm in diameter. If the chimney may fracture at a base bending moment of 486 kN · m, and its drag coefficient based upon frontal area is 0.5, what is the approximate maximum allowable wind velocity to avoid fracture?
(*a*) 50 mi/h, (*b*) 75 mi/h, (*c*) 100 mi/h, (*d*) 125 mi/h, (*e*) 150 mi/h

FE7.8 A dust particle of density 2600 kg/m^3, small enough to satisfy Stokes' drag law, settles at 1.5 mm/s in air at 20°C and 1 atm. What is its approximate diameter?
(*a*) 1.8 μm, (*b*) 2.9 μm, (*c*) 4.4 μm, (*d*) 16.8 μm, (*e*) 234 μm

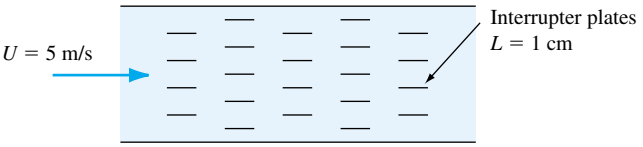
FE7.9 An airplane has a mass of 19,550 kg, a wing span of 20 m, and an average wing chord of 3 m. When flying in air of density 0.5 kg/m^3, its engines provide a thrust of 12 kN against an overall drag coefficient of 0.025. What is its approximate velocity?
(*a*) 250 mi/h, (*b*) 300 mi/h, (*c*) 350 mi/h, (*d*) 400 mi/h, (*e*) 450 mi/h

FE7.10 For the flight conditions of the airplane in Prob. FE7.9 above, what is its approximate lift coefficient?
(*a*) 0.1, (*b*) 0.2, (*c*) 0.3, (*d*) 0.4, (*e*) 0.5

Comprehensive Problems

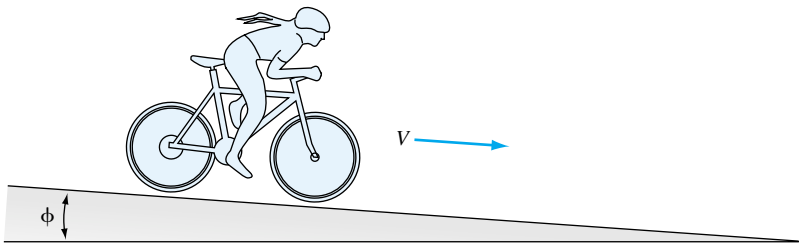
C7.1 Jane wants to estimate the drag coefficient of herself on her bicycle. She measures the projected frontal area to be 0.40 m^2 and the rolling resistance to be 0.80 N · s/m. The mass of the bike is 15 kg, while the mass of Jane is 80 kg. Jane coasts down a long hill which has a constant 4° slope. (See Fig. C7.1.) She reaches a terminal (steady state) speed of 14 m/s down the hill. Estimate the aerodynamic drag coefficient C_D of the rider and bicycle combination.

C7.2 Air at 20°C and 1 atm flows at V_{avg} = 5 m/s between long, smooth parallel heat-exchanger plates 10 cm apart, as in Fig. C7.2. It is proposed to add a number of widely spaced 1-cm-long interrupter plates to increase the heat transfer, as shown. Although the flow in the channel is turbulent, the boundary layers over the interrupter plates are essentially laminar. Assume all plates are 1 m wide into the paper. Find (*a*) the pressure drop in Pa/m without the small plates present. Then find (*b*) the number of small plates per meter of channel length which will cause the pressure drop to rise to 10.0 Pa/m.



C7.2

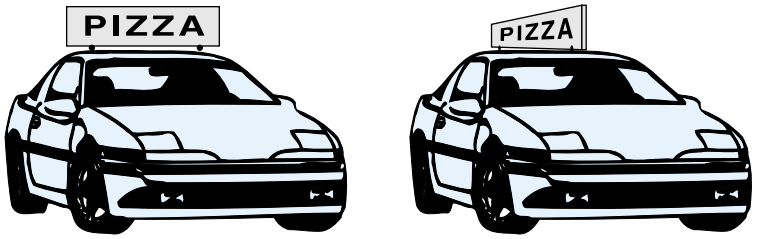
C7.3 A new pizza store is planning to open. They will, of course, offer free delivery, and therefore need a small delivery car with a large sign attached. The sign (a flat plate) is 1.5 ft high and 5 ft long. The boss (having no feel for fluid mechanics) mounts the sign bluntly facing the wind. One of his drivers is taking fluid mechanics and tells his boss he can save lots of money by mounting the sign parallel to the wind. (See Fig. C7.3.) (*a*) Calculate the drag (in lbf) on the *sign alone* at 40 mi/h (58.7 ft/s) in *both orientations*. (*b*) Suppose the car without any sign has a drag coefficient of 0.4 and a frontal area of 40 ft^2. For V = 40 mi/h, calculate the *total* drag of the car-sign combination for both orientations. (*c*) If the car has a rolling resistance of 40 lbf at 40 mi/h, calculate the horsepower required by the engine to drive the car at 40 mi/h in both orientations. (*d*) Finally, if the engine can deliver 10 hp for 1 h on a gallon of gasoline, calculate the fuel efficiency in mi/gal for both orientations at 40 mi/h.



C7.1

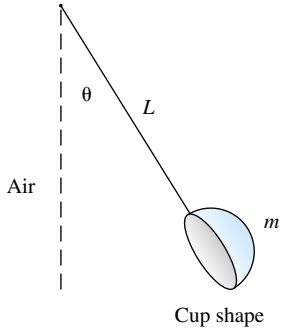


ketabline.com Ebook.ketabline.com



C7.3

C7.4 Consider a pendulum with an unusual bob shape: a hemispherical cup of diameter D whose axis is in the plane of oscillation, as in Fig. C7.4. Neglect the mass and drag of the rod L. (*a*) Set up the differential equation for the oscillation $\theta(t)$, including different cup drag (air density ρ) in each direction, and (*b*) nondimensionalize this equation. (*c*) Determine the natural frequency of oscillation for small $\theta \ll 1$ rad. (*d*) For the special case $L = 1$ m, $D = 10$ cm, $m = 50$ g, and air at 20°C and 1 atm, with $\theta(0) = 30°$, find (numerically) the time required for the oscillation amplitude to drop to 1°.



C7.4

Design Project

D7.1 It is desired to design a cup anemometer for wind speed, similar to Fig. P7.91, with a more sophisticated approach than the "average-torque" method of Prob. 7.91. The design should achieve an approximately linear relation between wind velocity and rotation rate in the range $20 < U < 40$ mi/h, and the anemometer should rotate at about 6 r/s at $U = 30$ mi/h. All specifications—cup diameter D, rod length L, rod diameter d, the bearing type, and all materials—are to be selected through your analysis. Make suitable assumptions about the instantaneous drag of the cups and rods at any given angle $\theta(t)$ of the system. Compute the instantaneous torque $T(t)$, and find and integrate the instantaneous angular acceleration of the device. Develop a complete theory for rotation rate versus wind speed in the range $0 < U < 50$ mi/h. Try to include actual commercial bearing-friction properties.

References

1. H. Schlichting, *Boundary Layer Theory,* 7th ed., McGraw-Hill, New York, 1979.
2. F. M. White, *Viscous Fluid Flow,* 2d ed., McGraw-Hill, New York, 1991.
3. L. Rosenhead (ed.), *Laminar Boundary Layers,* Oxford University Press, London, 1963.
4. D. A. Anderson, J. C. Tannehill, and R. H. Pletcher, *Computational Fluid Mechanics and Heat Transfer,* 2d ed., Hemisphere, New York, 1997.
5. R. H. Pletcher and C. L. Dancey, "A Direct Method of Calculating through Separated Regions in Boundary Layer Flow," *J. Fluids Eng.,* September 1976, pp. 568–572.
6. P. K. Chang, *Control of Flow Separation,* McGraw-Hill, New York, 1976. See also P. K. Chang, *Recent Development in Flow Separation,* Pang Han Pub. Co., Seoul, Korea, 1983.
7. T. von Kármán, "On Laminar and Turbulent Friction," *Z. Angew. Math. Mech.,* vol. 1, 1921, pp. 235–236.
8. G. B. Schubauer and H. K. Skramstad, "Laminar Boundary Layer Oscillations and Stability of Laminar Flow," *Natl. Bur. Stand. Res. Pap.* 1772, April 1943 (see also *J. Aero. Sci.,* vol. 14, 1947, pp. 69–78, and *NACA Rep.* 909, 1947).
9. W. Rodi, *Turbulence Models and Their Application in H draulics,* Brookfield Pub., Brookfield, V

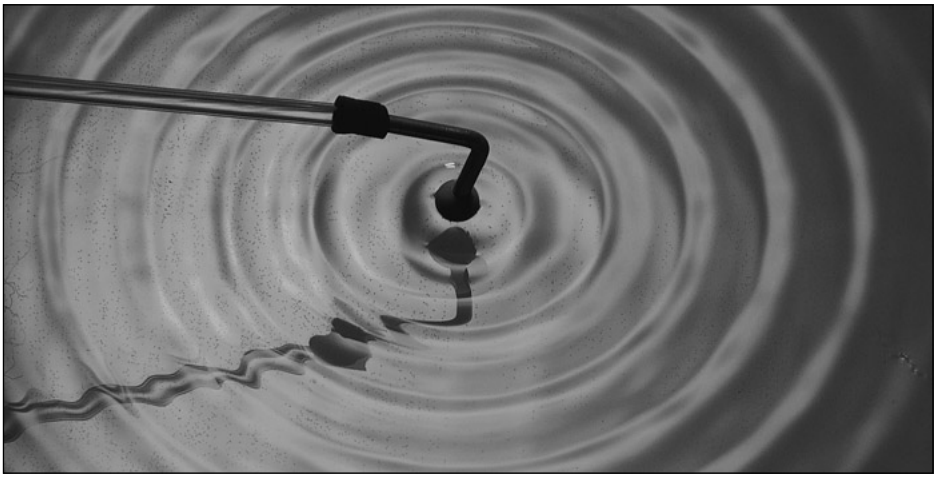


ketabline.com Ebook.ketabline.com

10. P. W. Runstadler, Jr., et al., "Diffuser Data Book," Creare Inc., *Tech. Note* 186, Hanover, NH, May 1975.
11. B. Thwaites, "Approximate Calculation of the Laminar Boundary Layer," *Aeronaut. Q.,* vol. 1, 1949, pp. 245–280.
12. S. F. Hoerner, *Fluid Dynamic Drag,* published by the author, Midland Park, NJ, 1965.
13. J. D. Anderson, *Fundamentals of Aerodynamics,* 2d ed., McGraw-Hill, New York, 1991.
14. V. Tucker and G. C. Parrott, "Aerodynamics of Gliding Flight of Falcons and Other Birds," *J. Exp. Biol.,* vol. 52, 1970, pp. 345–368.
15. Eric Tupper, *Introduction to Naval Architecture,* Butterworth, Boston, 1996.
16. I. H. Abbott and A. E. von Doenhoff, *Theory of Wing Sections,* Dover, New York, 1959.
17. R. L. Kline and F. F. Fogleman, Airfoil for Aircraft, U.S. Patent 3,706,430 Dec. 19, 1972.
18. T. Y. Yu et al. (eds.), *Swimming and Flying in Nature: Proceedings of a Symposium,* Plenum, New York, 1975.
19. National Committee for Fluid Mechanics Films, *Illustrated Experiments in Fluid Mechanics,* M.I.T. Press, Cambridge, MA, 1972.
20. E. M. Uram and H. E. Weber (eds.), "Laminar and Turbulent Boundary Layers," *ASME Symp. Proc.,* vol. I00167, February 1984.
21. G. Sovran, T. Morel, and W. T. Mason, Jr. (eds.), *Aerodynamic Drag Mechanisms of Bluff Bodies and Road Vehicles,* Plenum, New York, 1978.
22. W. H. Hucho, *Aerodynamics of Road Vehicles,* Butterworth, Boston, 1986.
23. R. D. Blevins, *Applied Fluid Dynamics Handbook,* van Nostrand Reinhold, New York, 1984.
24. R. C. Johnson, Jr., G. E. Ramey, and D. S. O'Hagen, "Wind Induced Forces on Trees," *J. Fluids Eng.,* vol. 104, March 1983, pp. 25–30.
25. P. W. Bearman et al., "The Effect of a Moving Floor on Wind-Tunnel Simulation of Road Vehicles," Paper No. 880245, SAE Transactions, *J. Passenger Cars,* vol. 97, sec. 4, 1988, pp. 4.200–4.214.
26. *CRC Handbook of Tables for Applied Engineering Science,* 2d ed., CRC Press, Boca Raton, FL, 1973.
27. T. Inui, "Wavemaking Resistance of Ships," *Trans. Soc. Nav. Arch. Marine Engrs.,* vol. 70, 1962, pp. 283–326.
28. L. Larsson et al., "A Method for Resistance and Flow Prediction in Ship Design," *Trans. Soc. Nav. Arch. Marine Engrs.,* vol. 98, 1990, pp. 495–535.
29. R. L. Street, G. Z. Watters, and J. K. Vennard, *Elementary Fluid Mechanics,* 7th ed., Wiley, New York, 1995.
30. J. D. Anderson, Jr., *Modern Compressible Flow, with Historical Perspective,* 2d ed., McGraw-Hill, New York, 1990.
31. J. D. Anderson, Jr., *Hypersonic and High Temperature Gas Dynamics,* McGraw-Hill, New York, 1989.
32. J. Rom, *High Angle of Attack Aerodynamics: Subsonic, Transonic, and Supersonic Flows,* Springer-Verlag, New York, 1992.
33. S. Vogel, "Drag and Reconfiguration of Broad Leaves in High Winds," *J. Exp. Bot.,* vol. 40, no. 217, August 1989, pp. 941–948.
34. S. Vogel, *Life in Moving Fluids,* Princeton University Press, Princeton, NJ, 1981.
35. J. A. C. Humphrey (ed.), *Proceedings 1st International Symposium on Mechanics of Plants, Animals, and Their Environment,* Engineering Foundation, New York, January 1998.
36. D. D. Joseph, R. Bai, K. P. Chen, and Y. Y. Renardy, "Core-Annular Flows," *Annu. Rev. Fluid Mech.,* vol. 29, 1997, pp. 65–90.
37. J. W. Hoyt and R. H. J. Sellin, "Scale Effects in Polymer Solution Pipe Flow," *Experiments in Fluids,* vol. 15, no. 1, June 1993, pp. 70–74.
38. S. Nakao, "Application of V-shape Riblets to Pipe Flows," *J. Fluids Eng.,* vol. 113, December 1991, pp. 587–590.
39. P. R. Bandyopadhyay, "Review: Mean Flow in Turbulent Boundary Layers Disturbed to Alter Skin Friction," *J. Fluids Eng.,* vol. 108, 1986, pp. 127–140.
40. N. K. Madavan, S. Deutsch, and C. L. Merkle, "Measurements of Local Skin Friction in a Microbubble Modified Turbulent Boundary Layer," *J. Fluid Mech.,* vol. 156, 1985, pp. 237–256.
41. S. M. Trujillo, D. G. Bogard, and K. S. Ball, "Drag Reduction in a Turbulent Boundary Layer by Wall Oscillation," Paper AIAA 97-1870, AIAA Shear Flow Control Conference, Austin, TX, December 1997.
42. J. G. Chandler, "Microplanes," *Popular Science,* January 1998, pp. 54–59.



ketabline.com Ebook.ketabline.com



Cylindrical wave pattern produced in a ripple tank. When not modified by the no-slip condition at solid surfaces, waves are nearly inviscid and well represented by the potential theory of this chapter. *(Courtesy of Dr. E. R. Degginger/Color-Pic Inc.)*



ketabline.com Ebook.ketabline.com

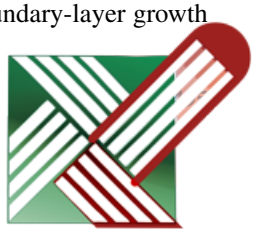
Chapter 8
Potential Flow and Computational Fluid Dynamics

Motivation. The basic partial differential equations of mass, momentum, and energy were discussed in Chap. 4. A few solutions were then given for incompressible *potential* flow in Sec. 4.10 and for incompressible *viscous* flow in Sec. 4.11. The viscous solutions were limited to simple geometries and unidirectional flows, where the difficult nonlinear convective terms were neglected. The potential flows were not limited by such nonlinear terms. Then, in Chap. 7, we found an approximation: patching *boundary-layer flows* onto an outer inviscid flow pattern. For more complicated viscous flows, we found no theory or solutions, just experimental data.

The purposes of the present chapter are (1) to explore more examples of potential theory and (2) to indicate some flows which can be approximated by computational fluid dynamics (CFD). The combination of these two gives us a good picture of incompressible-flow theory and its relation to experiment. One of the most important applications of potential-flow theory is to aerodynamics and marine hydrodynamics. First, however, we will review and extend the concepts of Sec. 4.10.

8.1 Introduction and Review

Figure 8.1 reminds us of the problems to be faced. A free stream approaches two closely spaced bodies, creating an "internal" flow between them and "external" flows above and below them. The fronts of the bodies are regions of favorable gradient (decreasing pressure along the surface), and the boundary layers will be attached and thin: Inviscid theory will give excellent results for the outer flow if $\mathrm{Re} > 10^4$. For the internal flow between bodies, the boundary layers will grow and eventually meet, and the inviscid core vanishes. Inviscid theory works well in a "short" duct $L/D < 10$, such as the nozzle of a wind tunnel. For longer ducts we must estimate boundary-layer growth and be cautious about using inviscid theory.



ketabline.com Ebook.ketabline.com

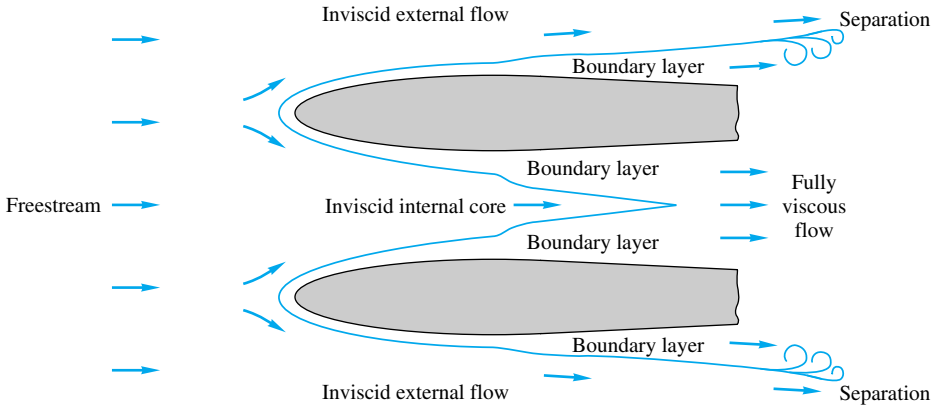


Fig. 8.1 Patching viscous- and inviscid-flow regions. Potential theory in this chapter does not apply to the boundary-layer regions

For the external flows above and below the bodies in Fig. 8.1, inviscid theory should work well for the outer flows, until the surface pressure gradient becomes adverse (increasing pressure) and the boundary layer separates or stalls. After the separation point, boundary-layer theory becomes inaccurate, and the outer flow streamlines are deflected and have a strong interaction with the viscous near-wall regions. The theoretical analysis of separated-flow regions is an active research area at present.

Review of Velocity-Potential Concepts

Recall from Sec. 4.9 that if viscous effects are neglected, low-speed flows are irrotational, $\nabla \times \mathbf{V} = 0$, and the velocity potential ϕ exists, such that

$$\mathbf{V} = \nabla\phi \qquad \text{or} \qquad u = \frac{\partial\phi}{\partial x} \qquad v = \frac{\partial\phi}{\partial y} \qquad w = \frac{\partial\phi}{\partial z} \tag{8.1}$$

The continuity equation (4.73), $\nabla \cdot \mathbf{V} = 0$, reduces to Laplace's equation for ϕ:

$$\nabla^2\phi = \frac{\partial^2\phi}{\partial x^2} + \frac{\partial^2\phi}{\partial y^2} + \frac{\partial^2\phi}{\partial z^2} = 0 \tag{8.2}$$

and the momentum equation (4.74) reduces to Bernoulli's equation:

$$\frac{\partial\phi}{\partial t} + \frac{p}{\rho} + \frac{1}{2}V^2 + gz = \text{const} \qquad \text{where } V = |\nabla\phi| \tag{8.3}$$

Typical boundary conditions are known free-stream conditions

$$\text{Outer boundaries:} \qquad \text{Known } \frac{\partial\phi}{\partial x}, \frac{\partial\phi}{\partial y}, \frac{\partial\phi}{\partial z} \tag{8.4}$$

and no velocity normal to the boundary at the body surface:

$$\text{Solid surfaces:} \qquad \frac{\partial\phi}{\partial n} = 0 \qquad \text{where } n \text{ is perpendicular to body} \tag{8.5}$$

Unlike the no-slip condition in viscous flow, here there is *no* condition on the tangential surface velocity $V_s = \partial\phi/\partial s$, where s is the coordinate along the surface. locity is determined as part of the solution to the problem.



ketabline.com Ebook.ketabline.com

Occasionally the problem involves a free surface, for which the boundary pressure is known and equal to p_a, usually a constant. The Bernoulli equation (8.3) then supplies a relation at the surface between V and the elevation z of the surface. For steady flow, e.g.,

Free surface: $$V^2 = |\nabla\phi|^2 = \text{const} - 2gz_{\text{surf}} \tag{8.6}$$

It should be clear to the reader that this use of Laplace's equation, with known values of the derivative of ϕ along the boundaries, is much easier than a direct attack using the fully viscous Navier-Stokes equations. The analysis of Laplace's equation is very well developed and is termed *potential theory*, with whole books written about the general theory [1] and its application to fluid mechanics [2 to 4]. There are many analytical techniques, including superposition of elementary functions, conformal mapping, numerical finite differences [5], numerical finite elements [6], numerical boundary elements [7], and electric or mechanical analogs [8] now outdated. Having found $\phi(x, y, z, t)$ from such an analysis, we then compute $\mathbf{V}$ by direct differentiation in Eq. (8.1), after which we compute p from Eq. (8.3). The procedure is quite straightforward, and many interesting albeit idealized results can be obtained.

Review of Stream Function Concepts

Recall from Sec. 4.7 that if a flow is described by only two coordinates, the stream function ψ also exists as an alternate approach. For plane incompressible flow in xy coordinates, the correct form is

$$u = \frac{\partial\psi}{\partial y} \qquad v = -\frac{\partial\psi}{\partial x} \tag{8.7}$$

The condition of irrotationality reduces to Laplace's equation for ψ also:

$$2\omega_z = 0 = \frac{\partial v}{\partial x} - \frac{\partial u}{\partial y} = \frac{\partial}{\partial x}\left(-\frac{\partial\psi}{\partial x}\right) - \frac{\partial}{\partial y}\left(\frac{\partial\psi}{\partial y}\right)$$

or $$\frac{\partial^2\psi}{\partial x^2} + \frac{\partial^2\psi}{\partial y^2} = 0 \tag{8.8}$$

The boundary conditions again are known velocity in the stream and no flow through any solid surface:

Free stream: $$\text{Known } \frac{\partial\psi}{\partial x}, \frac{\partial\psi}{\partial y} \tag{8.9a}$$

Solid surface: $$\psi_{\text{body}} = \text{const} \tag{8.9b}$$

Equation (8.9*b*) is particularly interesting because *any* line of constant ψ in a flow can therefore be interpreted as a body shape and may lead to interesting applications.

For the applications in this chapter, we may compute either ϕ or ψ or both, and the solution will be an *orthogonal flow net* as in Fig. 8.2. Once found, either set of lines may be considered the ϕ lines, and the other set will be the ψ lines. They are laplacian and could be useful.



ketabline.com Ebook.ketabline.com

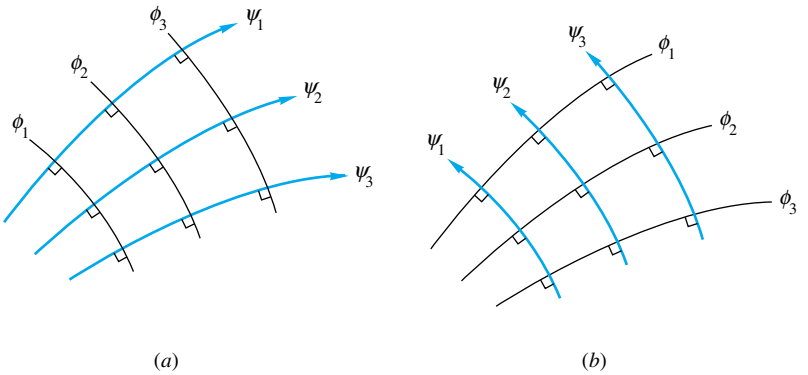


Fig. 8.2 Streamlines and potential lines are orthogonal and may reverse roles if results are useful: (*a*) typical inviscid-flow pattern; (*b*) same as (*a*) with roles reversed.

Plane Polar Coordinates

Many solutions in this chapter are conveniently expressed in polar coordinates (r, θ). Both the velocity components and the differential relations for ϕ and ψ are then changed, as follows:

$$v_r = \frac{\partial \phi}{\partial r} = \frac{1}{r}\frac{\partial \psi}{\partial \theta} \qquad v_\theta = \frac{1}{r}\frac{\partial \phi}{\partial \theta} = -\frac{\partial \psi}{\partial r} \tag{8.10}$$

Laplace's equation takes the form

$$\frac{1}{r}\frac{\partial}{\partial r}\left(r\frac{\partial \phi}{\partial r}\right) + \frac{1}{r^2}\frac{\partial^2 \phi}{\partial \theta^2} = 0 \tag{8.11}$$

Exactly the same equation holds for the polar-coordinate form of $\psi(r, \theta)$.

An intriguing facet of potential flow with no free surface is that the governing equations (8.2) and (8.8) contain no parameters, nor do the boundary conditions. Therefore the solutions are purely geometric, depending only upon the body shape, the free-stream orientation, and—surprisingly—the position of the rear stagnation point.[1] There is no Reynolds, Froude, or Mach number to complicate the dynamic similarity. Inviscid flows are kinematically similar without additional parameters—recall Fig. 5.6*a*.

8.2 Elementary Plane-Flow Solutions

Recall from Sec. 4.10 that we defined three elementary potential flows which are quite useful: (1) uniform stream in the x direction, (2) line source or sink at the origin, and (3) line vortex at the origin. (Recall Fig. 4.12 for these geometries.) Let us review these special cases here:

Uniform stream $\mathbf{i}U$:	$\psi = Uy$	$\phi = Ux$	(8.12*a*)
Line source or sink:	$\psi = m\theta$	$\phi = m \ln r$	(8.12*b*)
Line vortex:	$\psi = -K \ln r$	$\phi = K\theta$	(8.12*c*)

[1] The rear stagnation condition establishes the net amount of "circulation" about the body, gi to a lift force. Otherwise the solution could not be unique. See Sec. 8.4.



ketabline.com Ebook.ketabline.com

The source "strength" m and the vortex "strength" K have the same dimensions, namely, velocity times length, or $\{L^2/T\}$.

If the uniform stream is written in plane polar coordinates, it becomes

$$\text{Uniform stream } \mathbf{i}U: \qquad \psi = Ur \sin\theta \qquad \phi = Ur\cos\theta \tag{8.13}$$

This makes it easier to superimpose, say, a stream and a source or vortex by using the same coordinates. If the uniform stream is moving at angle α with respect to the x-axis, i.e.,

$$u = U\cos\alpha = \frac{\partial\psi}{\partial y} = \frac{\partial\phi}{\partial x} \qquad v = U\sin\alpha = -\frac{\partial\psi}{\partial x} = \frac{\partial\phi}{\partial y}$$

then by integration we obtain the correct functions for flow at an angle:

$$\psi = U(y\cos\alpha - x\sin\alpha) \qquad \phi = U(x\cos\alpha + y\sin\alpha) \tag{8.14}$$

These expressions are useful in airfoil angle-of-attack problems (Sec. 8.7).

Circulation

The line-vortex flow is irrotational everywhere except at the origin, where the vorticity $\nabla \times \mathbf{V}$ is infinite. This means that a certain line integral called the *fluid circulation* Γ does not vanish when taken around a vortex center.

With reference to Fig. 8.3, the circulation is defined as the counterclockwise line integral, around a closed curve C, of arc length ds times the velocity component tangent to the curve

$$\Gamma = \oint_C V\cos\alpha\, ds = \int_C \mathbf{V}\cdot d\mathbf{s} = \int_C (u\,dx + v\,dy + w\,dz) \tag{8.15}$$

From the definition of ϕ, $\mathbf{V}\cdot d\mathbf{s} = \nabla\phi\cdot d\mathbf{s} = d\phi$ for an irrotational flow; hence normally Γ in an irrotational flow would equal the final value of ϕ minus the initial value of ϕ. Since we start and end at the same point, we compute $\Gamma = 0$, but not for vortex flow: With $\phi = K\theta$ from Eq. (8.12c) there is a change in ϕ of amount $2\pi K$ as we make one complete circle:

$$\text{Path enclosing a vortex:} \qquad \Gamma = 2\pi K \tag{8.16}$$

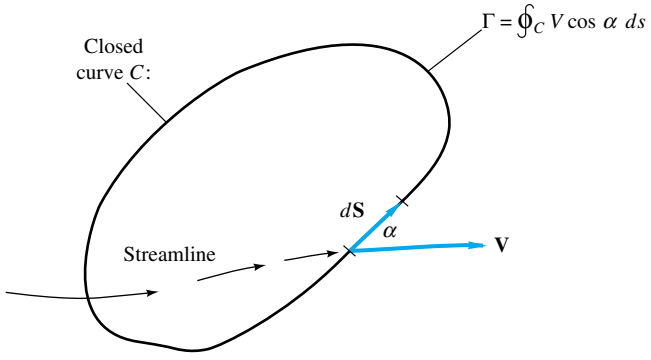


Fig. 8.3 Definition of the fluid circulation Γ.



ketabline.com Ebook.ketabline.com

Alternately the calculation can be made by defining a circular path of radius r around the vortex center, from Eq. (8.15)

$$\Gamma = \int_C v_\theta \, ds = \int_0^{2\pi} \frac{K}{r} \, r \, d\theta = 2\pi K \tag{8.17}$$

In general, Γ denotes the net algebraic strength of all the vortex filaments contained within the closed curve. In the next section we shall see that a region of finite circulation within a flowing stream will be subjected to a lift force proportional to both U_∞ and Γ.

It is easy to show, by using Eq. (8.15), that a source or sink creates no circulation. If there are no vortices present, the circulation will be zero for any path enclosing any number of sources and sinks.

8.3 Superposition of Plane-Flow Solutions

We can now form a variety of interesting potential flows by summing the velocity-potential and stream functions of a uniform stream, source or sink, and vortex. Most of the results are classic, of course, needing only a brief treatment here.

Graphical Method of Superposition

A simple means of accomplishing $\psi_{\text{tot}} = \sum \psi_i$ graphically is to plot the individual stream functions separately and then look at their intersections. The value of ψ_{tot} at each intersection is the sum of the individual values ψ_i which cross there. Connecting intersections with the same value of ψ_{tot} creates the desired superimposed flow streamlines.

A simple example is shown in Fig. 8.4, summing two families of streamlines ψ_a and ψ_b. The individual components are plotted separately, and four typical intersections are shown. Dashed lines are then drawn through intersections representing the same sum of $\psi_a + \psi_b$. These dashed lines are the desired solution. Often this graphical method is a quick means of evaluating the proposed superposition before a full-blown numerical plot routine is executed.

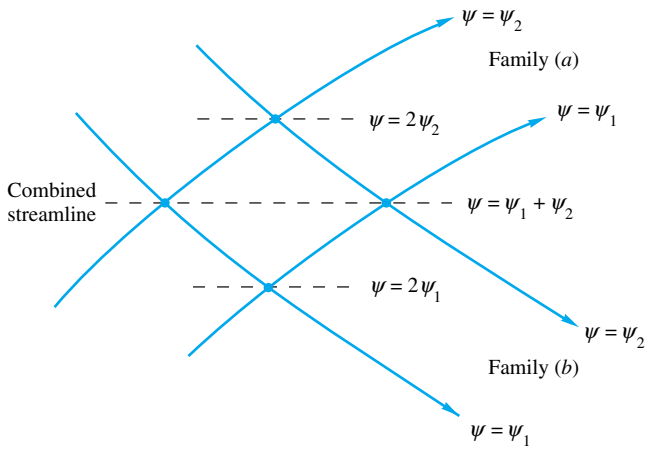


Fig. 8.4 Intersections of elementary streamlines can be joined to form a combined streamline.



ketabline.com Ebook.ketabline.com

Some Examples from Chap. 4

In Sec. 4.10 we discussed a number of superposition examples.

1. Source m at $(-a, 0)$ plus an equal sink at $(\pm a, 0)$, Eq. (4.133), and Fig. 4.13:

$$\psi = -m \tan^{-1} \frac{2ay}{x^2 + y^2 - a^2} \qquad \phi = \frac{1}{2} m \ln \frac{(x+a)^2 + y^2}{(x-a)^2 + y^2} \tag{4.133}$$

   The streamlines and potential lines are two families of orthogonal circles as plotted in Fig. 4.13. They resemble a magnet with poles at $(x, y) = (\pm a, 0)$.

2. Sink m plus a vortex K, both at the origin, Eq. (4.134), and Fig. 4.14:

$$\psi = m\theta - K \ln r \qquad \phi = m \ln r + K\theta \tag{4.134}$$

   The streamlines are logarithmic spirals swirling into the origin, as in Fig. 4.14. They resemble a tornado or a bathtub vortex.

3. Uniform stream $\mathbf{i}U_\infty$ plus a source m at the origin, Eq. (4.135) and Fig. 4.15, the Rankine half-body:

$$\psi = U_\infty r \sin\theta + m\theta \qquad \phi = U_\infty r \cos\theta + m \ln r \tag{4.135}$$

   If the origin contains a source, a plane half-body is formed with its nose to the left, as in Fig. 8.5*a*. If the origin is a *sink*, $m < 0$, the half-body nose is to the right, as in Fig. 8.5*c*. In either case the stagnation point is at a position $a = m/U_\infty$ away from the origin.

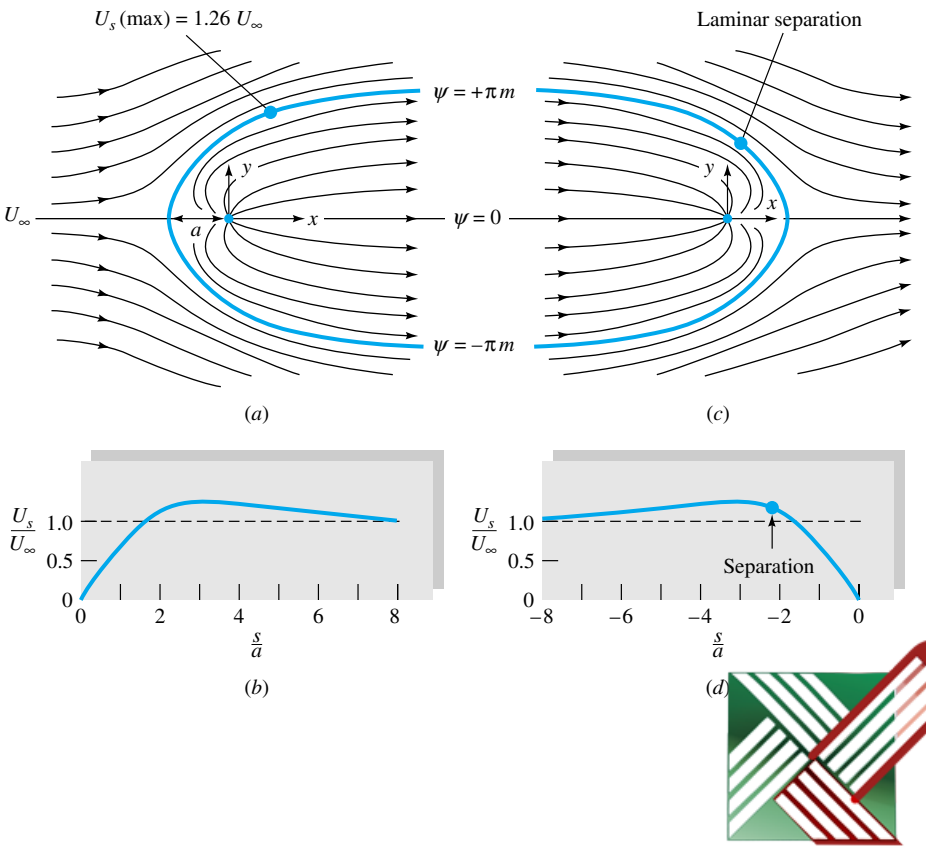


Fig. 8.5 The Rankine half-body; pattern (*c*) is not found in a real fluid because of boundary-layer separation: (*a*) uniform stream plus a source equals a half-body; stagnation point at $x = -a = -m/U_\infty$; (*b*) slight adverse gradient for s/a greater than 3.0: no separation; (*c*) uniform stream plus a sink equals the rear of a half-body; stagnation point at $x = a = m/U_\infty$; (*d*) strong adverse gradient for $s/a > -3.0$: separation.

ketabline.com Ebook.ketabline.com

Boundary-Layer Separation on a Half-Body

Although the inviscid-flow patterns, Fig. 8.5*a* and *c*, are mirror images, their viscous (boundary-layer) behavior is different. The body shape and the velocity along the surface are repeated here from Sec. 4.10:

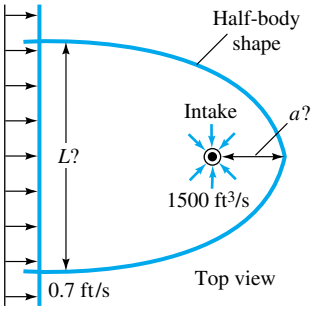
$$V^2 = U_\infty^2\left(1 + \frac{a^2}{r^2} + \frac{2a}{r}\cos\theta\right) \qquad \text{along} \qquad r = \frac{m(\pi - \theta)}{U_\infty \sin\theta} \tag{8.18}$$

The computed surface velocities are plotted along the half-body contours in Fig. 8.5*b* and *d* as a function of arc length *s*/*a* measured from the stagnation point. These plots are also mirror images. However, if the nose is in front, Fig. 8.5*b*, the pressure gradient there is *favorable* (decreasing pressure along the surface). In contrast, the pressure gradient is *adverse* (increasing pressure along the surface) when the nose is in the rear, Fig. 8.5*d*, and boundary-layer separation may occur.

Application to Fig. 8.5*b* of Thwaites' laminar-boundary method from Eqs. (7.54) and (7.56) reveals that separation does not occur on the front nose of the half-body. Therefore Fig. 8.5*a* is a very realistic picture of streamlines past a half-body nose. In contrast, when applied to the tail, Fig. 8.5*c*, Thwaites' method predicts separation at about $s/a \approx -2.2$, or $\theta \approx 110°$. Thus, if a half-body is a solid surface, Fig. 8.5*c* is *not* realistic and a broad separated wake will form. However, if the half-body tail is a *fluid line* separating the sink-directed flow from the outer stream, as in Example 8.1, then Fig. 8.5*c* is quite realistic and useful. Computations for turbulent boundary-layer theory would be similar: separation on the tail, no separation on the nose.

EXAMPLE 8.1

An offshore power plant cooling-water intake sucks in 1500 ft^3/s in water 30 ft deep, as in Fig. E8.1. If the tidal velocity approaching the intake is 0.7 ft/s, (*a*) how far downstream does the intake effect extend and (*b*) how much width L of tidal flow is entrained into the intake?



E8.1

Solution

Recall from Eq. (4.131) that the sink strength m is related to the volume flow Q and the depth b into the paper

$$m = \frac{Q}{2\pi b} = \frac{1500 \text{ ft}^3/\text{s}}{2\pi(30 \text{ ft})} = 7.96 \text{ ft}^2/\text{s}$$

Therefore from Fig. 8.5 the desired lengths a and L are

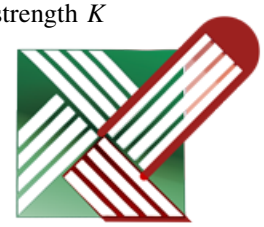
$$a = \frac{m}{U_\infty} = \frac{7.96 \text{ ft}^2/\text{s}}{0.7 \text{ ft/s}} = 11.4 \text{ ft} \qquad \textit{Ans. (a)}$$

$$L = 2\pi a = 2\pi(11.4 \text{ ft}) = 71 \text{ ft} \qquad \textit{Ans. (b)}$$

Flow Past a Vortex

Consider a uniform stream U_∞ in the x direction flowing past a vortex of strength K with center at the origin. By superposition the combined stream function is

$$\psi = \psi_{\text{stream}} + \psi_{\text{vortex}} = U_\infty r \sin\theta - K \ln r$$



ketabline.com Ebook.ketabline.com

The velocity components are given by

$$v_r = \frac{1}{r}\frac{\partial \psi}{\partial \theta} = U_\infty \cos\theta \qquad v_\theta = -\frac{\partial \psi}{\partial r} = -U_\infty \sin\theta + \frac{K}{r} \tag{8.20}$$

The streamlines are plotted in Fig. 8.6 by the graphical method, intersecting the circular streamlines of the vortex with the horizontal lines of the uniform stream.

By setting $v_r = v_\theta = 0$ from (8.20) we find a stagnation point at $\theta = 90°$, $r = a = K/U_\infty$, or $(x, y) = (0, a)$. This is where the counterclockwise vortex velocity K/r exactly cancels the stream velocity U_∞.

Probably the most interesting thing about this example is that there is a nonzero lift force normal to the stream on the surface of any region enclosing the vortex, but we postpone this discussion until the next section.

An Infinite Row of Vortices

Consider an infinite row of vortices of equal strength K and equal spacing a, as in Fig. 8.7*a*. This case is included here to illustrate the interesting concept of a *vortex sheet*.

From Eq. (8.12*c*), the ith vortex in Fig. 8.7*a* has a stream function $\psi_i = -K \ln r_i$, so that the total infinite row has a combined stream function

$$\psi = -K \sum_{i=1}^{\infty} \ln r_i \tag{8.21}$$

It can be shown [2, sec. 4.51] that this infinite sum of logarithms is equivalent to a closed-form function

$$\psi = -\tfrac{1}{2}K \ln \left[\frac{1}{2}\left(\cosh \frac{2\pi y}{a} - \cos \frac{2\pi x}{a} \right) \right] \tag{8.22}$$

Since the proof uses the complex variable $z = x + iy$, $i = (-1)^{1/2}$, we are not going to show the details here.

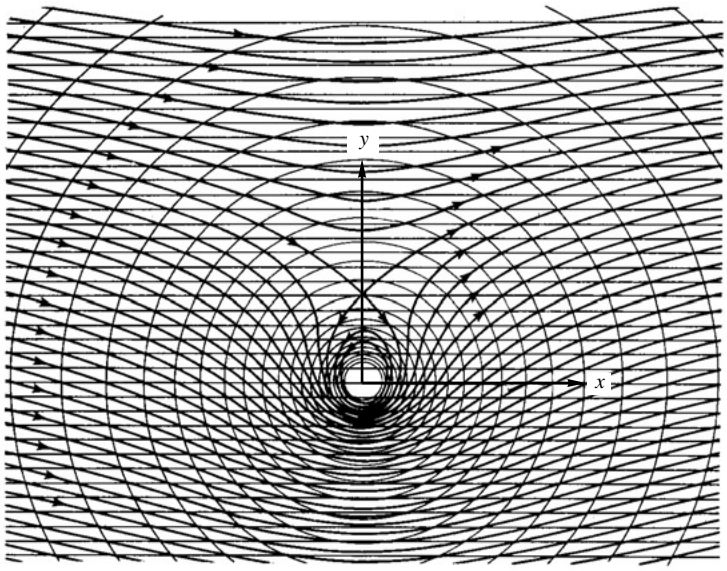


Fig. 8.6 Flow of a uniform stream past a vortex constructed by the graphical method.



ketabline.com Ebook.ketabline.com

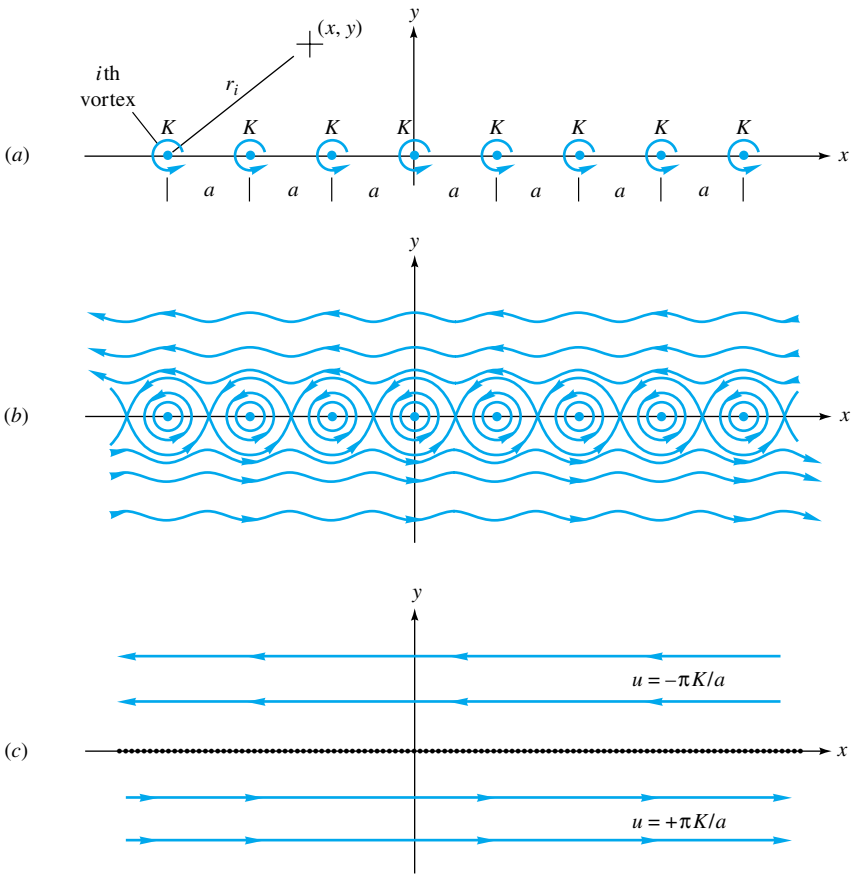


Fig. 8.7 Superposition of vortices: (*a*) an infinite row of equal strength; (*b*) streamline pattern for part (*a*); (*c*) vortex sheet: part (*b*) viewed from afar.

The streamlines from Eq. (8.22) are plotted in Fig. 8.7*b*, showing what is called a *cat's-eye* pattern of enclosed flow cells surrounding the individual vortices. Above the cat's eyes the flow is entirely to the left, and below the cat's eyes the flow is to the right. Moreover, these left and right flows are uniform if $|y| \gg a$, which follows by differentiating Eq. (8.22)

$$u = \frac{\partial \psi}{\partial y}\bigg|_{|y| \gg a} = \pm \frac{\pi K}{a} \tag{8.23}$$

where the plus sign applies below the row and the minus sign above the row. This uniform left and right streaming is sketched in Fig. 8.7*c*. We stress that this effect is induced by the row of vortices: There is no uniform stream approaching the row in this example.

The Vortex Sheet

When Fig. 8.7*b* is viewed from afar, the streaming motion is uniform left ab
uniform right below, as in Fig. 8.7*c*, and the vortices are packed so closely



ketabline.com Ebook.ketabline.com

that they are smudged into a continuous *vortex sheet*. The strength of the sheet is defined as

$$\gamma = \frac{2\pi K}{a} \tag{8.24}$$

and in the general case γ can vary with x. The circulation about any closed curve which encloses a short length dx of the sheet would be, from Eqs. (8.15) and (8.23),

$$d\Gamma = u_l\,dx - u_u\,dx = (u_l - u_u)\,dx = \frac{2\pi K}{a}\,dx = \gamma\,dx \tag{8.25}$$

where the subscripts l and u stand for lower and upper, respectively. Thus the sheet strength $\gamma = d\Gamma/dx$ is the circulation per unit length of the sheet. Thus when a vortex sheet is immersed in a uniform stream, γ is proportional to the lift per unit length of any surface enclosing the sheet.

Note that there is no velocity normal to the sheet at the sheet surface. Therefore a vortex sheet can simulate a thin-body shape, e.g., plate or thin airfoil. This is the basis of the thin-airfoil theory mentioned in Sec. 8.7.

The Doublet

As we move far away from the source-sink pair of Fig. 4.13, the flow pattern begins to resemble a family of circles tangent to the origin, as in Fig. 8.8. This limit of vanishingly small distance a is called a *doublet.* To keep the flow strength large enough to exhibit decent velocities as a becomes small, we specify that the product $2am$ remain constant. Let us call this constant λ. Then the stream function of a doublet is

$$\psi = \lim_{\substack{a\to 0\\ 2am=\lambda}} \left(-m\,\tan^{-1}\frac{2ay}{x^2+y^2-a^2}\right) = -\frac{2amy}{x^2+y^2} = -\frac{\lambda y}{x^2+y^2} \tag{8.26}$$

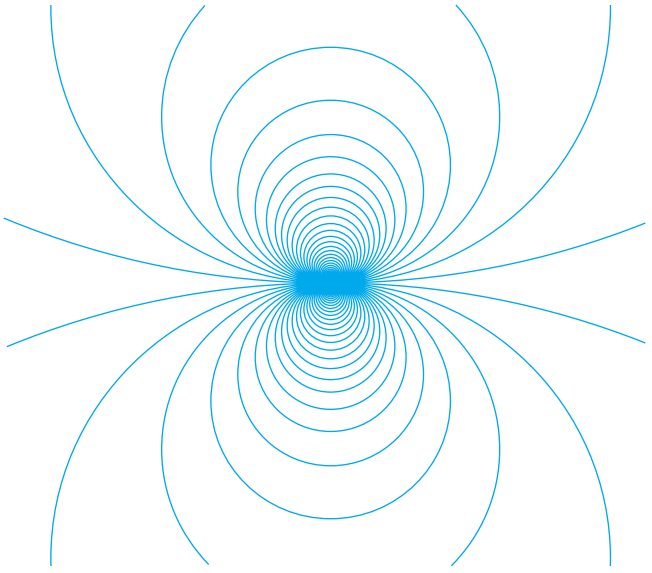


Fig. 8.8 A doublet, or source-sink pair, is the limiting case of Fig. 4.13 viewed from afar. Streamlines are circles tangent to the x-axis at the origin. This figure was prepared using the *contour* feature of MATLAB [34, 35].



ketabline.com Ebook.ketabline.com

We have used the fact that $\tan^{-1}\alpha \approx \alpha$ as α becomes small. The quantity λ is called the *strength* of the doublet.

Equation (8.26) can be rearranged to yield

$$x^2 + \left(y + \frac{\lambda}{2\psi}\right)^2 = \left(\frac{\lambda}{2\psi}\right)^2$$

so that, as advertised, the streamlines are circles tangent to the origin with centers on the y-axis. This pattern is sketched in Fig. 8.8.

Although the author has in the past laboriously sketched streamlines by hand, this is no longer necessary. Figure 8.8 was computer-drawn, using the *contour* feature of the student version of MATLAB [35]. Simply set up a grid of points, spell out the stream function, and call for a contour. For Fig. 8.8, the actual statements were

```
[X,Y] = meshgrid(-1:.02:1);
PSI = -Y./(X.^2 + Y.^2);
contour(X,Y,PSI,100)
```

This would produce 100 contour lines of ψ from Eq. (8.26), with $\lambda = 1$ for convenience. The plot would include grid lines, scale markings, and a surrounding box, and the circles might look a bit elliptical. These blemishes can be eliminated with three statements of cosmetic improvement:

```
axis square
grid off
axis off
```

The final plot, Fig. 8.8, has no markings but the streamlines themselves. MATLAB is thus a recommended tool and, in addition, has scores of other uses. All this chapter's problem assignments which call for "sketch the streamlines/potential lines" can be completed using this contour feature. For further details, consult Ref. 34.

In a similar manner the velocity potential of a doublet is found by taking the limit of Eq. (4.133) as $a \to 0$ and $2am = \lambda$

$$\phi_{\text{doublet}} = \frac{\lambda x}{x^2 + y^2}$$

or

$$\left(x - \frac{\lambda}{2\phi}\right)^2 + y^2 = \left(\frac{\lambda}{2\phi}\right)^2 \tag{8.27}$$

The potential lines are circles tangent to the origin with centers on the x-axis. Simply turn Fig. 8.8 clockwise 90° to visualize the ϕ lines, which are everywhere normal to the streamlines.

The doublet functions can also be written in polar coordinates

$$\psi = -\frac{\lambda \sin\theta}{r} \qquad \phi = \frac{\lambda \cos\theta}{r} \tag{8.28}$$

These forms are convenient for the cylinder flows of the next section.



ketabline.com Ebook.ketabline.com

8.4 Plane Flow Past Closed-Body Shapes

A variety of closed-body external flows can be constructed by superimposing a uniform stream with sources, sinks, and vortices. The body shape will be closed only if the net source outflow equals the net sink inflow.

The Rankine Oval

A cylindrical shape called a *Rankine oval*, which is long compared with its height, is formed by a source-sink pair aligned parallel to a uniform stream, as in Fig. 8.9*a*.

From Eqs. (8.12*a*) and (4.133) the combined stream function is

$$\psi = U_\infty y - m \tan^{-1} \frac{2ay}{x^2 + y^2 - a^2} = U_\infty r \sin \theta + m(\theta_1 - \theta_2) \tag{8.29}$$

When streamlines of constant ψ are plotted from Eq. (8.29), an oval body shape appears, as in Fig. (8.9*b*). The half-length L and half-height h of the oval depend upon the relative strength of source and stream, i.e., the ratio $m/(U_\infty a)$, which equals 1.0 in Fig. 8.9*b*. The circulating streamlines inside the oval are uninteresting and not usually shown. The oval is the line $\psi = 0$.

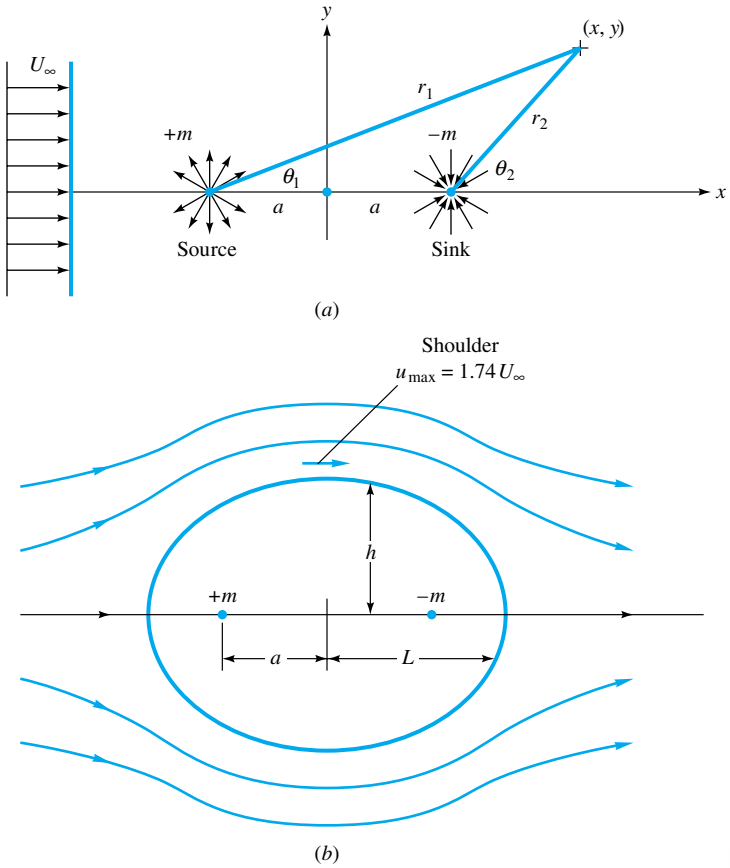


Fig. 8.9 Flow past a Rankine oval: (*a*) uniform stream plus a source-sink pair; (*b*) oval shape and streamlines for $m/(U_\infty a) = 1.0$.



ketabline.com Ebook.ketabline.com

There are stagnation points at the front and rear, $x = \pm L$, and points of maximum velocity and minimum pressure at the shoulders, $y = \pm h$, of the oval. All these parameters are a function of the basic dimensionless parameter $m/(U_\infty a)$, which we can determine from Eq. (8.29):

$$\frac{h}{a} = \cot \frac{h/a}{2m/(U_\infty a)} \qquad \frac{L}{a} = \left(1 + \frac{2m}{U_\infty a}\right)^{1/2}$$
$$\frac{u_{\max}}{U_\infty} = 1 + \frac{2m/(U_\infty a)}{1 + h^2/a^2} \tag{8.30}$$

As we increase $m/(U_\infty a)$ from zero to large values, the oval shape increases in size and thickness from a flat plate of length $2a$ to a huge, nearly circular cylinder. This is shown in Table 8.1. In the limit as $m/(U_\infty a) \to \infty$, $L/h \to 1.0$ and $u_{\max}/U_\infty \to 2.0$, which is equivalent to flow past a circular cylinder.

All the Rankine ovals except very thin ones have a large adverse pressure gradient on their leeward surface. Thus boundary-layer separation will occur in the rear with a broad wake flow, and the inviscid pattern is unrealistic in that region.

Flow Past a Circular Cylinder with Circulation

From Table 8.1 at large source strength the Rankine oval becomes a large circle, much greater in diameter than the source-sink spacing $2a$. Viewed on the scale of the cylinder, this is equivalent to a uniform stream plus a doublet. We also throw in a vortex at the doublet center, which does not change the shape of the cylinder.

Thus the stream function for flow past a circular cylinder with circulation, centered at the origin, is a uniform stream plus a doublet plus a vortex

$$\psi = U_\infty r \sin\theta - \frac{\lambda \sin\theta}{r} - K \ln r + \text{const} \tag{8.31}$$

The doublet strength λ has units of velocity times length squared. For convenience, let $\lambda = U_\infty a^2$, where a is a length, and let the arbitrary constant in Eq. (8.31) equal $K \ln a$. Then the stream function becomes

$$\psi = U_\infty \sin\theta \left(r - \frac{a^2}{r}\right) - K \ln \frac{r}{a} \tag{8.32}$$

The streamlines are plotted in Fig. 8.10 for four different values of the dimensionless vortex strength $K/(U_\infty a)$. For all cases the line $\psi = 0$ corresponds to the circle $r =$

Table 8.1 Rankine-Oval Parameters from Eq. (8.30)

$m/(U_\infty a)$	h/a	L/a	L/h	$u_{\max}/U_\infty$
0.0	0.0	1.0	∞	1.0
0.01	0.031	1.010	32.79	1.020
0.1	0.263	1.095	4.169	1.187
1.0	1.307	1.732	1.326	1.739
10.0	4.435	4.583	1.033	1.968
100.0	14.130	14.177	1.003	1.997
∞	∞	∞	1.000	2.000



ketabline.com Ebook.ketabline.com

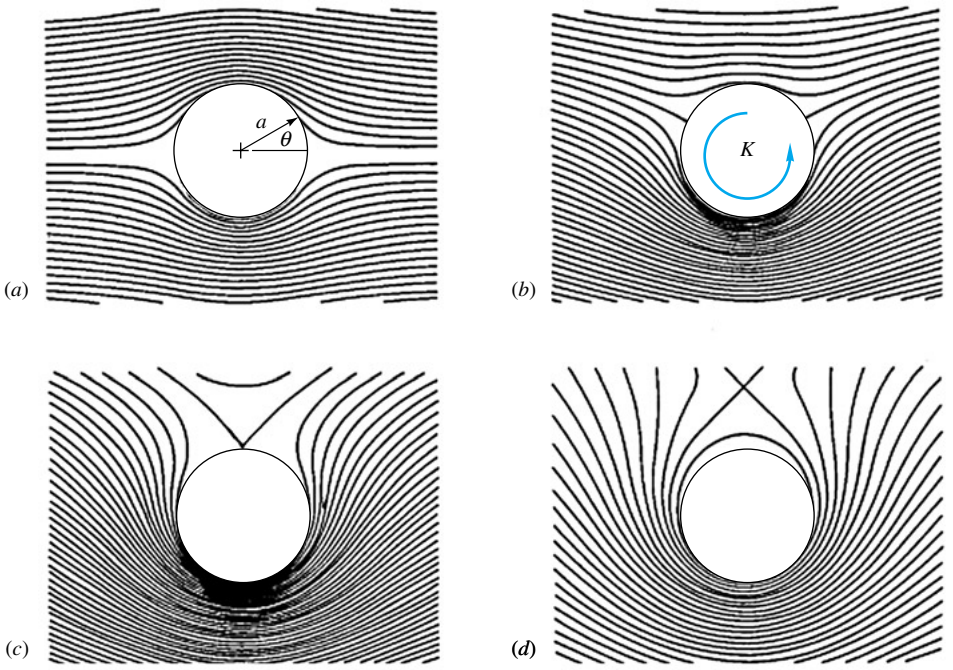


Fig. 8.10 Flow past a circular cylinder with circulation for values of $K/(U_\infty a)$ of (*a*) 0, (*b*) 1.0, (*c*) 2.0, and (*d*) 3.0.

a, that is, the shape of the cylindrical body. As circulation $\Gamma = 2\pi K$ increases, the velocity becomes faster and faster below the cylinder and slower and slower above it. The velocity components in the flow are given by

$$v_r = \frac{1}{r}\frac{\partial \psi}{\partial \theta} = U_\infty \cos\theta\left(1 - \frac{a^2}{r^2}\right)$$
$$v_\theta = -\frac{\partial \psi}{\partial r} = -U_\infty \sin\theta\left(1 + \frac{a^2}{r^2}\right) + \frac{K}{r} \tag{8.33}$$

The velocity at the cylinder surface $r = a$ is purely tangential, as expected

$$v_r(r = a) = 0 \quad v_\theta(r = a) = -2U_\infty \sin\theta + \frac{K}{a} \tag{8.34}$$

For small K, two stagnation points appear on the surface at angles θ_s where $v_\theta = 0$, or, from Eq. (8.34),

$$\sin\theta_s = \frac{K}{2U_\infty a} \tag{8.35}$$

Figure 8.10*a* is for $K = 0$, $\theta_s = 0$ and 180°, or doubly symmetric inviscid flow past a cylinder with no circulation. Figure 8.10*b* is for $K/(U_\infty a) = 1$, $\theta_s = 30$ and 150°, and Fig. 8.10*c* is the limiting case where the two stagnation points meet at the top, $K/(U_\infty a) = 2$, $\theta_s = 90°$.



ketabline.com Ebook.ketabline.com

For $K > 2U_\infty a$, Eq. (8.35) is invalid, and the single stagnation point is above the cylinder, as in Fig. 8.10*d*, at a point $y = h$ given by

$$\frac{h}{a} = \frac{1}{2}\left[\beta + (\beta^2 - 4)^{1/2}\right] \qquad \beta = \frac{K}{U_\infty a} > 2 \tag{8.36}$$

In Fig. 8.10*d*, $K/(U_\infty a) = 3.0$, and $h/a = 2.6$.

The Kutta-Joukowski Lift Theorem

For the cylinder flows of Fig. 8.10*b* to *d* there is a downward force, or negative lift, called the *Magnus effect*, which is proportional to stream velocity and vortex strength. We can see from the streamline pattern that the velocity on the top of the cylinder is less and therefore the pressure higher from Bernoulli's equation; this explains the force. There is no viscous force, of course, because our theory is inviscid.

The surface velocity is given by Eq. (8.34). From Bernoulli's equation (8.4), neglecting gravity, the surface pressure p_s is given by

$$p_\infty + \frac{1}{2}\rho U_\infty^2 = p_s + \frac{1}{2}\rho\left(-2U_\infty \sin\theta + \frac{K}{a}\right)^2$$

or

$$p_s = p_\infty + \tfrac{1}{2}\rho U_\infty^2(1 - 4\sin^2\theta + 4\beta\sin\theta - \beta^2) \tag{8.37}$$

where $\beta = K/(U_\infty a)$ and p_∞ is the free-stream pressure. If b is the cylinder depth into the paper, the drag D is the integral over the surface of the horizontal component of pressure force

$$D = -\int_0^{2\pi} (p_s - p_\infty)\cos\theta\, ba\, d\theta$$

where $p_s - p_\infty$ is substituted from Eq. (8.37). But the integral of cos θ times any power of sin θ over a full cycle 2π is identically zero. Thus we obtain the (perhaps surprising) result

$$D(\text{cylinder with circulation}) = 0 \tag{8.38}$$

This is a special case of d'Alembert's paradox, mentioned in Sec. 1.10:

> According to inviscid theory, the drag of any body of any shape immersed in a uniform stream is identically zero.

D'Alembert published this result in 1752 and pointed out himself that it did not square with the facts for real fluid flows. This unfortunate paradox caused everyone to overreact and reject all inviscid theory until 1904, when Prandtl first pointed out the profound effect of the thin viscous boundary layer on the flow pattern in the rear, as in Fig. 7.2*b*, for example.

The lift force L normal to the stream, taken positive upward, is given by summation of vertical pressure forces

$$L = -\int_0^{2\pi} (p_s - p_\infty)\sin\theta\, ba\, d\theta$$

Since the integral over 2π of any odd power of sin θ is zero, only the third term in the parentheses in Eq. (8.37) contributes to the lift:

$$L = -\frac{1}{2}\rho U_\infty^2 \frac{4K}{aU_\infty} ba \int_0^{2\pi} \sin^2\theta\, d\theta = -\rho U_\infty(2\pi K)b$$



ketabline.com Ebook.ketabline.com

or
$$\frac{L}{b} = -\rho U_\infty \Gamma \tag{8.39}$$

Notice that the lift is independent of the radius a of the cylinder. Actually, though, as we shall see in Sec. 8.7, the circulation Γ depends upon the body size and orientation through a physical requirement.

Equation (8.39) was generalized by W. M. Kutta in 1902 and independently by N. Joukowski in 1906 as follows:

> According to inviscid theory, the lift per unit depth of any cylinder of any shape immersed in a uniform stream equals $\rho u_\infty \Gamma$, where Γ is the total net circulation contained within the body shape. The direction of the lift is 90° from the stream direction, rotating opposite to the circulation.

The problem in airfoil analysis, Sec. 8.7, is thus to determine the circulation Γ as a function of airfoil shape and orientation.

Experimental Lift and Drag of Rotating Cylinders

It is nearly impossible to test Fig. 8.10 by constructing a doublet and vortex with the same center and then letting a stream flow past them. But one physical realization would be a rotating cylinder in a stream. The viscous no-slip condition would cause the fluid in contact with the cylinder to move tangentially at the cylinder peripheral speed $v_\theta = a\omega$. A net circulation Γ would be set up by this no-slip mechanism, but it turns out to be less than 50 percent of the value expected from inviscid theory, primarily because of flow separation behind the cylinder.

Figure 8.11 shows experimental lift and drag coefficients, based on planform area $2ba$, of rotating cylinders. From Eq. (8.38) the theoretical drag is zero, but the actual C_D is quite large, more even than the stationary cylinder of Fig. 5.3. The theoretical lift follows from Eq. (8.39)

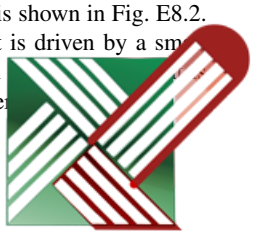
$$C_L = \frac{L}{\frac{1}{2}\rho U_\infty^2 (2ba)} = \frac{2\pi\rho U_\infty K b}{\rho U_\infty^2 ba} = \frac{2\pi v_{\theta s}}{U_\infty} \tag{8.40}$$

where $v_{\theta s} = K/a$ is the peripheral speed of the cylinder.

Figure 8.11 shows that the theoretical lift from Eq. (8.40) is much too high, but the measured lift is quite respectable, much larger in fact than a typical airfoil of the same chord length, e.g., Fig. 7.25. Thus rotating cylinders have practical possibilities. The Flettner rotor ship built in Germany in 1924 employed rotating vertical cylinders which developed a thrust due to any winds blowing past the ship. The Flettner design did not gain any popularity, but such inventions may be more attractive in this era of high energy costs.

EXAMPLE 8.2

The experimental Flettner rotor sailboat at the University of Rhode Island is shown in Fig. E8.2. The rotor is 2.5 ft in diameter and 10 ft long and rotates at 220 r/min. It is driven by a sm lawnmower engine. If the wind is a steady 10 kn and boat relative motion the maximum thrust expected for the rotor? Assume standard air and wate



ketabline.com Ebook.ketabline.com

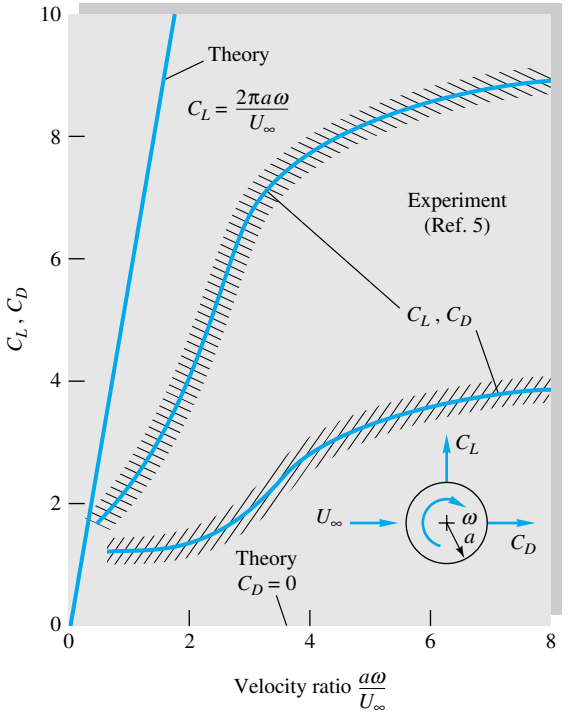


Fig. 8.11 Theoretical and experimental lift and drag of a rotating cylinder. (*From Ref. 22.*)



E8.2 *(Courtesy of R. C. Lessmann, University of Rhode Island.)*

ketabline.com Ebook.ketabline.com

Solution

Convert the rotation rate to $\omega = 2\pi(220)/60 = 23.04$ rad/s. The wind velocity is 10 kn = 16.88 ft/s, so the velocity ratio is

$$\frac{a\omega}{U_\infty} = \frac{(1.25 \text{ ft})(23.04 \text{ rad/s})}{16.88 \text{ ft/s}} = 1.71$$

Entering Fig. 8.11, we read $C_L \approx 3.3$ and $C_D \approx 1.2$. From Table A.6, standard air density is 0.002377 slug/ft^3. Then the estimated rotor lift and drag are

$$L = C_{L\frac{1}{2}}\rho U_\infty^2 2ba = 3.3(\tfrac{1}{2})(0.002377)(16.88)^2(2)(10)(1.25)$$

$$= 27.9 \text{ lbf}$$

$$D = C_{D\frac{1}{2}}\rho U_\infty^2 2ba = L\frac{C_D}{C_L} = 27.9\left(\frac{1.2}{3.3}\right) = 10.2 \text{ lbf}$$

The maximum thrust available is the resultant of these two

$$F = [(27.9)^2 + (10.2)^2]^{1/2} = 29 \text{ lbf} \qquad \textit{Ans.}$$

If aligned along the boat's keel, this thrust will drive the boat at a speed of about 5 kn through the water.

The Kelvin Oval

A family of body shapes taller than they are wide can be formed by letting a uniform stream flow normal to a vortex pair. If U_∞ is to the right, the negative vortex $-K$ is placed at $y = +a$ and the counterclockwise vortex $+K$ placed at $y = -a$, as in Fig. 8.12. The combined stream function is

$$\psi = U_\infty y - \frac{1}{2}K \ln \frac{x^2 + (y+a)^2}{x^2 + (y-a)^2} \tag{8.41}$$

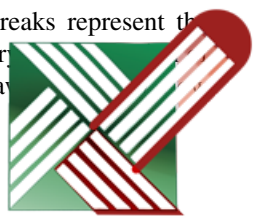
The body shape is the line $\psi = 0$, and some of these shapes are shown in Fig. 8.12. For $K/(U_\infty a) > 10$ the shape is within 1 percent of a Rankine oval (Fig. 8.9) turned 90°, but for small $K/(U_\infty a)$ the waist becomes pinched in, and a figure-eight shape occurs at 0.5. For $K/(U_\infty a) < 0.5$ the stream blasts right between the vortices and isolates two more or less circular body shapes, one surrounding each vortex.

A closed body of practically any shape can be constructed by proper superposition of sources, sinks, and vortices. See the advanced work in Refs. 2 to 4 for further details. A summary of elementary potential flows is given in Table 8.2.

Potential-Flow Analogs

For complicated potential-flow geometries, one can resort to other methods than superposition of sources, sinks, and vortices. There are a variety of devices which simulate solutions to Laplace's equation.

From 1897 to 1900 Hele-Shaw [9] developed a technique whereby laminar flow between very closely spaced parallel plates simulated potential flow when viewed from above the plates. Obstructions simulate body shapes, and dye streaks represent the streamlines. The Hele-Shaw apparatus makes an excellent laboratory potential flow [10, pp. 8–10]. Figure 8.13*a* illustrates Hele-Shaw



ketabline.com Ebook.ketabline.com

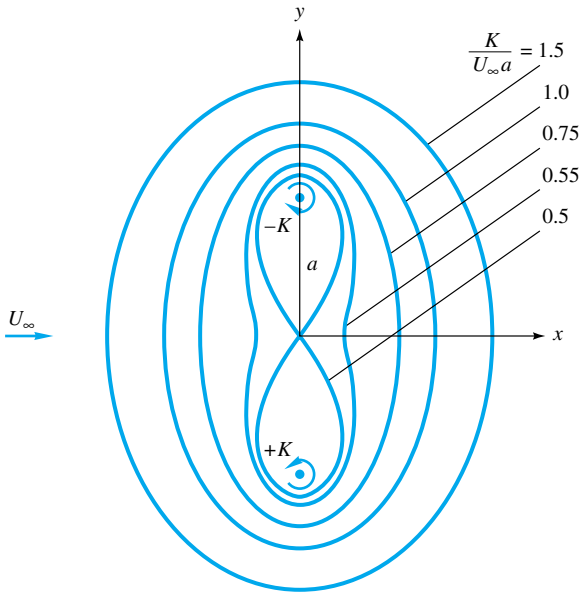


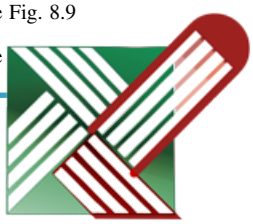
Fig. 8.12 Kelvin-oval body shapes as a function of the vortex-strength parameter $K/(U_\infty a)$; outer streamlines not shown.

through an array of cylinders, a flow pattern that would be difficult to analyze just using Laplace's equation. However beautiful this array pattern may be, it is not a good approximation to real (laminar viscous) array flow. Figure 8.13*b* shows experimental streakline patterns for a similar staggered-array flow at Re $\approx$ 6400. We see that the interacting wakes of the real flow (Fig. 8.13*b*) cause intensive mixing and transverse motion, not the smooth streaming passage of the potential-flow model (Fig. 8.13*a*). The moral is that this is an internal flow with multiple bodies and, therefore, not a good candidate for a realistic potential-flow model.

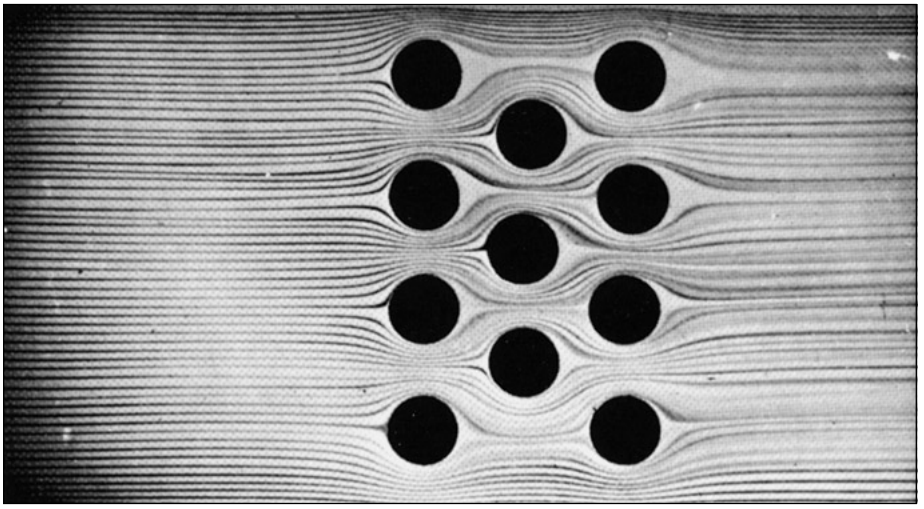
Other flow-mapping techniques are discussed in Ref. 8. Electromagnetic fields also satisfy Laplace's equation, with voltage analogous to velocity potential and current lines analogous to streamlines. At one time commercial analog field plotters were available, using thin conducting paper cut to the shape of the flow geometry. Potential lines (voltage contours) were plotted by probing the paper with a potentiometer pointer.

Table 8.2 Summary of Plane Incompressible Potential Flows

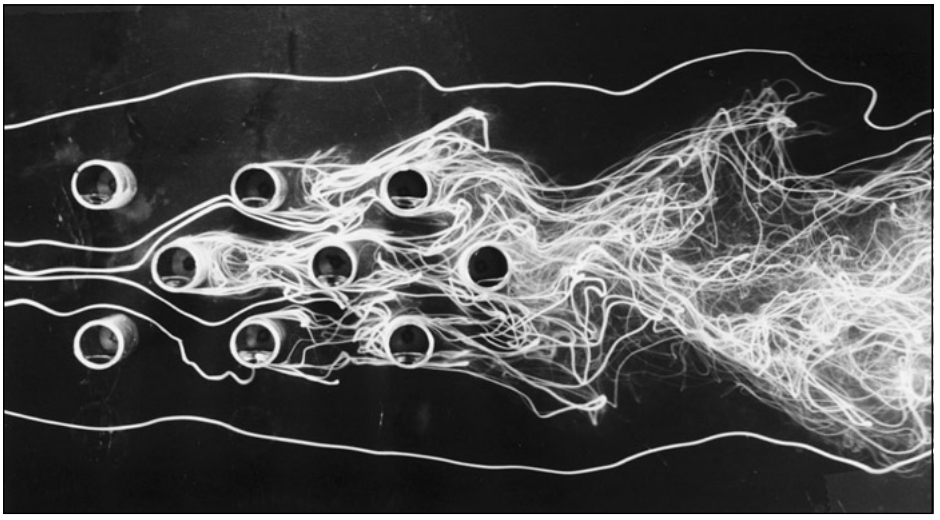
Type of flow	*Potential functions*	*Remarks*
Stream **i***U*	$\psi = Uy \quad \phi = Ux$	See Fig. 4.12a
Line source ($m > 0$) or sink ($m < 0$)	$\psi = m\theta \quad \phi = m \ln r$	See Fig. 4.12*b*
Line vortex	$\psi = -K \ln r \quad \phi = K\theta$	See Fig. 4.12*c*
Half-body	$\psi = Ur \sin\theta + m\theta$	
	$\phi = Ur \cos\theta + m \ln r$	See Fig. 8.5
Doublet	$\psi = \dfrac{-\lambda \sin\theta}{r} \quad \phi = \dfrac{\lambda \cos\theta}{r}$	See Fig. 8.8
Rankine oval	$\psi = Ur \sin\theta + m(\theta_1 - \theta_2)$	See Fig. 8.9
Cylinder with circulation	$\psi = U \sin\theta\left(r - \dfrac{a^2}{r}\right) - K \ln \dfrac{r}{a}$	See



ketabline.com Ebook.ketabline.com



(*a*)



(*b*)

Fig. 8.13 Flow past a staggered array of cylinders: (*a*) potential-flow model using the Hele-Shaw apparatus *(Tecquipment Ltd., Nottingham, England)*; (*b*) experimental streaklines for actual staggered-array flow at $\mathrm{Re}_D \approx 6400$. *(From Ref. 36, courtesy of Jack Hoyt, with the permission of the American Society of Mechanical Engineers.)*

Hand-sketching "curvilinear square" techniques were also popular. The availability and the simplicity of digital-computer potential-flow methods [5 to 7] have made analog models obsolete.

EXAMPLE 8.3

A Kelvin oval from Fig. 8.12 has $K/(U_\infty a) = 1.0$. Compute the velocity at the oval in terms of U_∞.



ketabline.com Ebook.ketabline.com

Solution

We must locate the shoulder $y = h$ from Eq. (8.41) for $\psi = 0$ and then compute the velocity by differentiation. At $\psi = 0$ and $y = h$ and $x = 0$, Eq. (8.41) becomes

$$\frac{h}{a} = \frac{K}{U_\infty a} \ln \frac{h/a + 1}{h/a - 1}$$

With $K/(U_\infty a) = 1.0$ and the initial guess $h/a \approx 1.5$ from Fig. 8.12, we iterate and find the location $h/a = 1.5434$.

By inspection $v = 0$ at the shoulder because the streamline is horizontal. Therefore the shoulder velocity is, from Eq. (8.41),

$$u\Big|_{y=h} = \frac{\partial \psi}{\partial y}\Big|_{y=h} = U_\infty + \frac{K}{h - a} - \frac{K}{h + a}$$

Introducing $K = U_\infty a$ and $h = 1.5434a$, we obtain

$$u_{\text{shoulder}} = U_\infty(1.0 + 1.84 - 0.39) = 2.45U_\infty \qquad \textit{Ans.}$$

Because they are short-waisted compared with a circular cylinder, all the Kelvin ovals have shoulder velocity greater than the cylinder result $2.0U_\infty$ from Eq. (8.34).

8.5 Other Plane Potential Flows[2]

References 2 to 4 treat many other potential flows of interest in addition to the cases presented in Secs. 8.3 and 8.4. In principle, any plane potential flow can be solved by the method of *conformal mapping*, by using the complex variable

$$z = x + iy \qquad i = (-1)^{1/2}$$

It turns out that any arbitrary analytic function of this complex variable z has the remarkable property that both its real and its imaginary parts are solutions of Laplace's equation. If

$$f(z) = f(x + iy) = f_1(x, y) + i\, f_2(x, y)$$

then

$$\frac{\partial^2 f_1}{\partial x^2} + \frac{\partial^2 f_1}{\partial y^2} = 0 = \frac{\partial^2 f_2}{\partial x^2} + \frac{\partial^2 f_2}{\partial y^2} \tag{8.42}$$

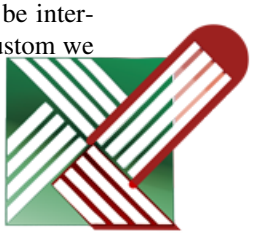
We shall assign the proof of this as a problem. Even more remarkable if you have never seen it before is that lines of constant f_1 will be everywhere perpendicular to lines of constant f_2:

$$\left(\frac{dy}{dx}\right)_{f_1 = C} = -\frac{1}{(dy/dx)_{f_2 = C}} \tag{8.43}$$

We also leave this proof as a problem exercise. This is true for totally arbitrary $f(z)$ as long as this function is analytic; i.e., it must have a unique derivative df/dz at every point in the region.

The net result of Eqs. (8.42) and (8.43) is that the functions f_1 and f_2 can be interpreted to be the potential lines and streamlines of an inviscid flow. By long custom we

[2] This section may be omitted without loss of continuity.



ketabline.com Ebook.ketabline.com

let the real part of $f(z)$ be the velocity potential and the imaginary part be the stream function

$$f(z) = \phi(x, y) + i\psi(x, y) \tag{8.44}$$

We try various functions $f(z)$ and see whether any interesting flow pattern results. Of course, most of them have already been found, and we simply report on them here.

We shall not go into the details, but there are excellent treatments of this complex-variable technique on both an introductory [4, chap. 5; 10, chap. 5] and a more advanced [2, 3,] level. The method is less important now because of the popularity of digital-computer techniques.

As a simple example, consider the linear function

$$f(z) = U_\infty z = U_\infty x + iU_\infty y$$

It follows from Eq. (8.44) that $\phi = U_\infty x$ and $\psi = U_\infty y$, which, we recall from Eq. (8.12*a*), represents a uniform stream in the x direction. Once you get used to the complex variable, the solution practically falls in your lap.

To find the velocities, you may either separate ϕ and ψ from $f(z)$ and differentiate or differentiate f directly

$$\frac{df}{dz} = \frac{\partial \phi}{\partial x} + i\frac{\partial \psi}{\partial x} = -i\frac{\partial \phi}{\partial y} + \frac{\partial \psi}{\partial y} = u - iv \tag{8.45}$$

Thus the real part of df/dz equals $u(x, y)$, and the imaginary part equals $-v(x, y)$. To get a practical result, the derivative df/dz must exist and be unique, hence the requirement that f be an analytic function. For Eq. (8.45), $df/dz = U_\infty = u$, since it is real, and $v = 0$, as expected.

Sometimes it is convenient to use the polar-coordinate form of the complex variable

$$z = x + iy = re^{i\theta} = r\cos\theta + ir\sin\theta$$

where

$$r = (x^2 + y^2)^{1/2} \qquad \theta = \tan^{-1}\frac{y}{x}$$

This form is especially convenient when powers of z occur.

Uniform Stream at an Angle of Attack

All the elementary plane flows of Sec. 8.2 have a complex-variable formulation. The uniform stream U_∞ at an angle of attack α has the complex potential

$$f(z) = U_\infty z e^{-i\alpha} \tag{8.46}$$

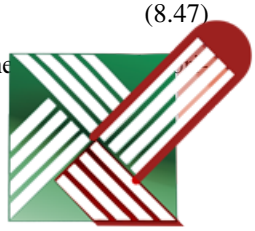
Compare this form with Eq. (8.14).

Line Source at a Point z_0

Consider a line source of strength m placed off the origin at a point $z_0 = x_0 + iy_0$. Its complex potential is

$$f(z) = m\ln(z - z_0) \tag{8.47}$$

This can be compared with Eq. (8.12*b*), which is valid only for the gin. For a line sink, the strength m is negative.



ketabline.com Ebook.ketabline.com

Line Vortex at a Point z_0

If a line vortex of strength K is placed at point z_0, its complex potential is

$$f(z) = -iK \ln (z - z_0) \tag{8.48}$$

to be compared with Eq. (8.12c). Also compare to Eq. (8.47) to see that we reverse the meaning of ϕ and ψ simply by multiplying the complex potential by $-i$.

Flow around a Corner of Arbitrary Angle

Corner flow is an example of a pattern that cannot be conveniently produced by superimposing sources, sinks, and vortices. It has a strikingly simple complex representation

$$f(z) = Az^n = Ar^n e^{in\theta} = Ar^n \cos n\theta + iAr^n \sin n\theta$$

where A and n are constants.

It follows from Eq. (8.44) that for this pattern

$$\phi = Ar^n \cos n\theta \qquad \psi = Ar^n \sin n\theta \tag{8.49}$$

Streamlines from Eq. (8.49) are plotted in Fig. 8.14 for five different values of n. The flow is seen to represent a stream turning through an angle $\beta = \pi/n$. Patterns in Fig. 8.14d and e are not realistic on the downstream side of the corner, where separation will occur due to the adverse pressure gradient and sudden change of direction. In general, separation always occurs downstream of salient, or protruding corners, except in creeping flows at low Reynolds number Re < 1.

Since $360° = 2\pi$ is the largest possible corner, the patterns for $n < \frac{1}{2}$ do not represent corner flow. They are peculiar-looking, and we ask you to plot one as a problem.

If we expand the plot of Fig. 8.14a to c to double size, we can represent stagnation flow toward a corner of angle $2\beta = 2\pi/n$. This is done in Fig. 8.15 for $n = 3$, 2, and

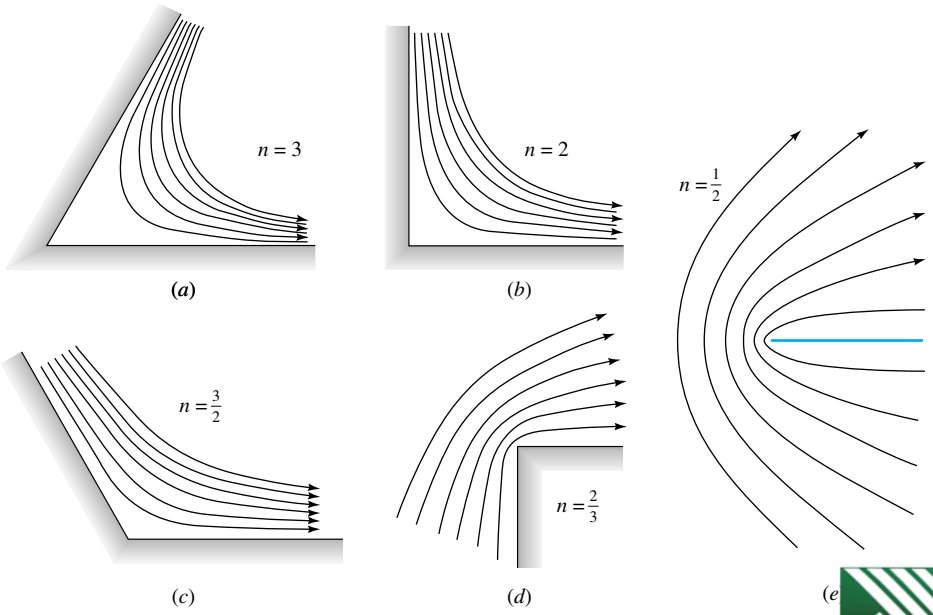


Fig. 8.14 Streamlines for corner flow, Eq. (8.49) for corner angle β of (a) 60°, (b) 90°, (c) 120°, (d) 270°, and (e) 360°.

ketabline.com Ebook.ketabline.com

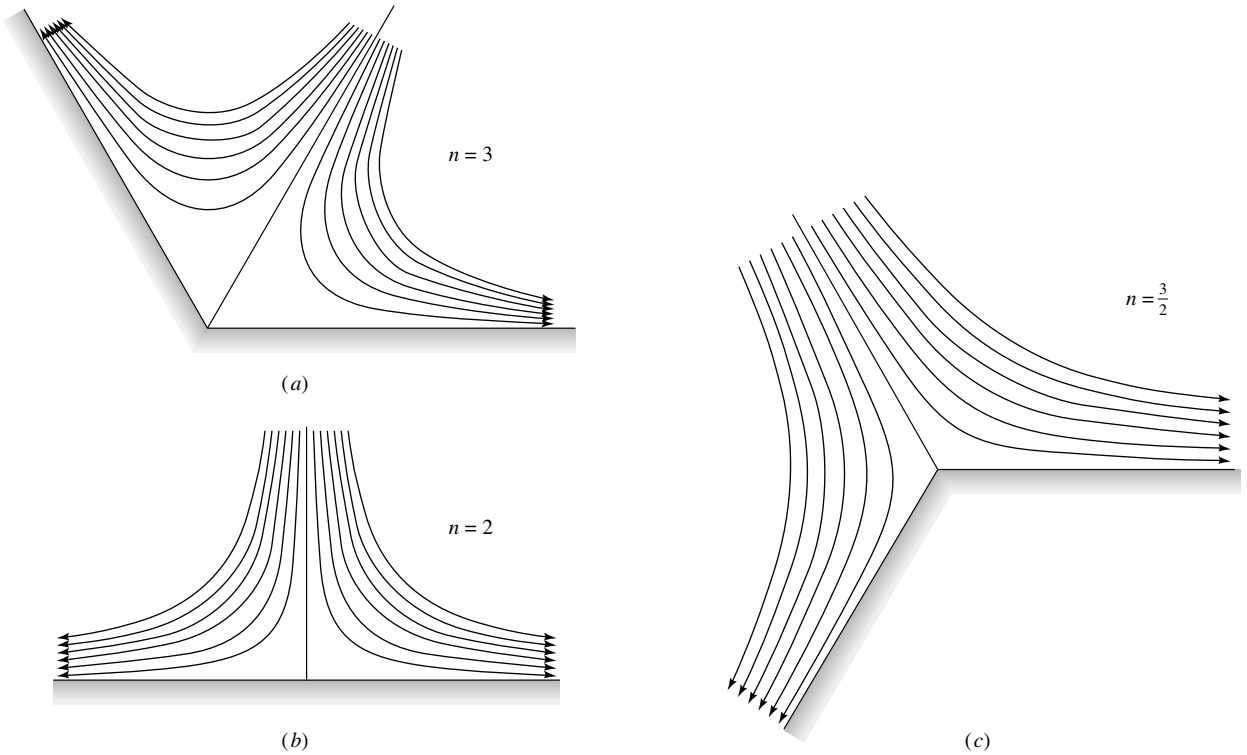


Fig. 8.15 Streamlines for stagnation flow from Eq. (8.49) for corner angle 2β of (*a*) 120°, (*b*) 180°, and (*c*) 240°.

1.5. These are very realistic flows; although they slip at the wall, they can be patched to boundary-layer theories very successfully. We took a brief look at corner flows before, in Examples 4.5 and 4.9 and in Probs. 4.49 to 4.51.

Flow Normal to a Flat Plate

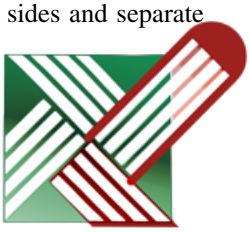
We treat this case separately because the Kelvin ovals of Fig. 8.12 failed to degenerate into a flat plate as K became small. The flat plate normal to a uniform stream is an extreme case worthy of our attention.

Although the result is quite simple, the derivation is very complicated and is given, e.g., in Ref. 2, sec. 9.3. There are three changes of complex variable, or *mappings*, beginning with the basic cylinder-flow solution of Fig. 8.10*a*. First the uniform stream is rotated to be vertical upward, then the cylinder is squeezed down into a plate shape, and finally the free stream is rotated back to the horizontal. The final result for complex potential is

$$f(z) = \phi + i\psi = U_\infty(z^2 + a^2)^{1/2} \tag{8.50}$$

where $2a$ is the height of the plate. To isolate ϕ or ψ, square both sides and separate real and imaginary parts

$$\phi^2 - \psi^2 = U_\infty^2(x^2 - y^2 + a^2) \qquad \phi\psi = U_\infty^2 xy$$



ketabline.com Ebook.ketabline.com

We can solve for ψ to determine the streamlines

$$\psi^4 + \psi^2 U_\infty^2 (x^2 - y^2 + a^2) = U_\infty^4 x^2 y^2 \tag{8.51}$$

Equation (8.51) is plotted in Fig. 8.16*a*, revealing a doubly symmetric pattern of streamlines which approach very closely to the plate and then deflect up and over, with very high velocities and low pressures near the plate tips.

The velocity v_s along the plate surface is found by computing df/dz from Eq. (8.50) and isolating the imaginary part

$$\left.\frac{v_s}{U_\infty}\right|_{\text{plate surface}} = \frac{y/a}{(1 - y^2/a^2)^{1/2}} \tag{8.52}$$

Some values of surface velocity can be tabulated as follows:

y/a	0.0	0.2	0.4	0.6	0.71	0.8	0.9	1.0
v_s/U_∞	0.0	0.204	0.436	0.750	1.00	1.33	2.07	∞

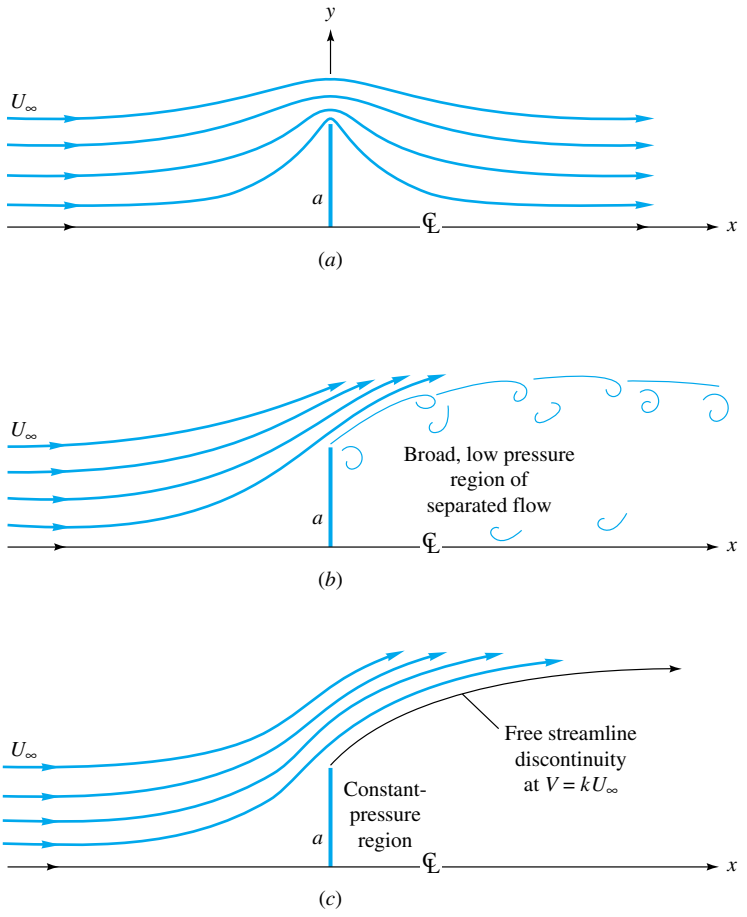


Fig. 8.16 Streamlines in upper half-plane for flow normal to a flat plate of height $2a$: (*a*) continuous potential-flow theory, Eq. (8.51); (*b*) actual measured flow pattern; (*c*) discontinuous potential theory with $k \approx 1.5$.



ketabline.com Ebook.ketabline.com

The origin is a stagnation point; then the velocity grows linearly at first and very rapidly near the tip, with both velocity and acceleration being infinite at the tip.

As you might guess, Fig. 8.16*a* is not realistic. In a real flow the sharp salient edge causes separation, and a broad, low-pressure wake forms in the lee, as in Fig. 8.16*b*. Instead of being zero, the drag coefficient is very large, $C_D \approx 2.0$ from Table 7.2.

A discontinuous-potential-flow theory which accounts for flow separation was devised by Helmholtz in 1868 and Kirchhoff in 1869. This free-streamline solution is shown in Fig. 8.16*c*, with the streamline which breaks away from the tip having a constant velocity $V = kU_\infty$. From Bernoulli's equation the pressure in the dead-water region behind the plate will equal $p_r = p_\infty + \frac{1}{2}\rho U_\infty^2(1 - k^2)$ to match the pressure along the free streamline. For $k = 1.5$ this Helmholtz-Kirchoff theory predicts $p_r = p_\infty - 0.625\rho U_\infty^2$ and an average pressure on the front $p_f = p_\infty + 0.375\rho U_\infty^2$, giving an overall drag coefficient of 2.0, in agreement with experiment. However, the coefficient k is a priori unknown and must be tuned to experimental data, so free-streamline theory can be considered only a qualified success. For further details see Ref. 2, sec. 11.2.

8.6 Images[3]

The previous solutions have all been for unbounded flows, such as a circular cylinder immersed in a broad expanse of uniformly streaming fluid, Fig. 8.10*a*. However, many practical problems involve a nearby rigid boundary constraining the flow, e.g., (1) groundwater flow near the bottom of a dam, (2) an airfoil near the ground, simulating landing or takeoff, or (3) a cylinder mounted in a wind tunnel with narrow walls. In such cases the basic unbounded-potential-flow solutions can be modified for wall effects by the method of *images*.

Consider a line source placed a distance a from a wall, as in Fig. 8.17*a*. To create the desired wall, an image source of identical strength is placed the same distance below the wall. By symmetry the two sources create a plane-surface streamline between them, which is taken to be the wall.

In Fig. 8.17*b* a vortex near a wall requires an image vortex the same distance below but of *opposite* rotation. We have shaded in the wall, but of course the pattern could also be interpreted as the flow near a vortex pair in an unbounded fluid.

In Fig. 8.17*c* an airfoil in a uniform stream near the ground is created by an image airfoil below the ground of opposite circulation and lift. This looks easy, but actually it is not because the airfoils are so close together that they interact and distort each other's shapes. A rule of thumb is that nonnegligible shape distortion occurs if the body shape is within two chord lengths of the wall. To eliminate distortion, a whole series of "corrective" images must be added to the flow to recapture the shape of the original isolated airfoil. Reference 2, sec. 7.75, has a good discussion of this procedure, which usually requires digital-computer summation of the multiple images needed.

Figure 8.17*d* shows a source constrained between two walls. One wall required only one image in Fig. 8.17*a*, but *two* walls require an infinite array of image sources above and below the desired pattern, as shown. Usually computer summation is necessary, but sometimes a closed-form summation can be achieved, as in the infinite vortex row of Eq. (8.22).

[3] This section may be omitted without loss of continuity.



ketabline.com Ebook.ketabline.com

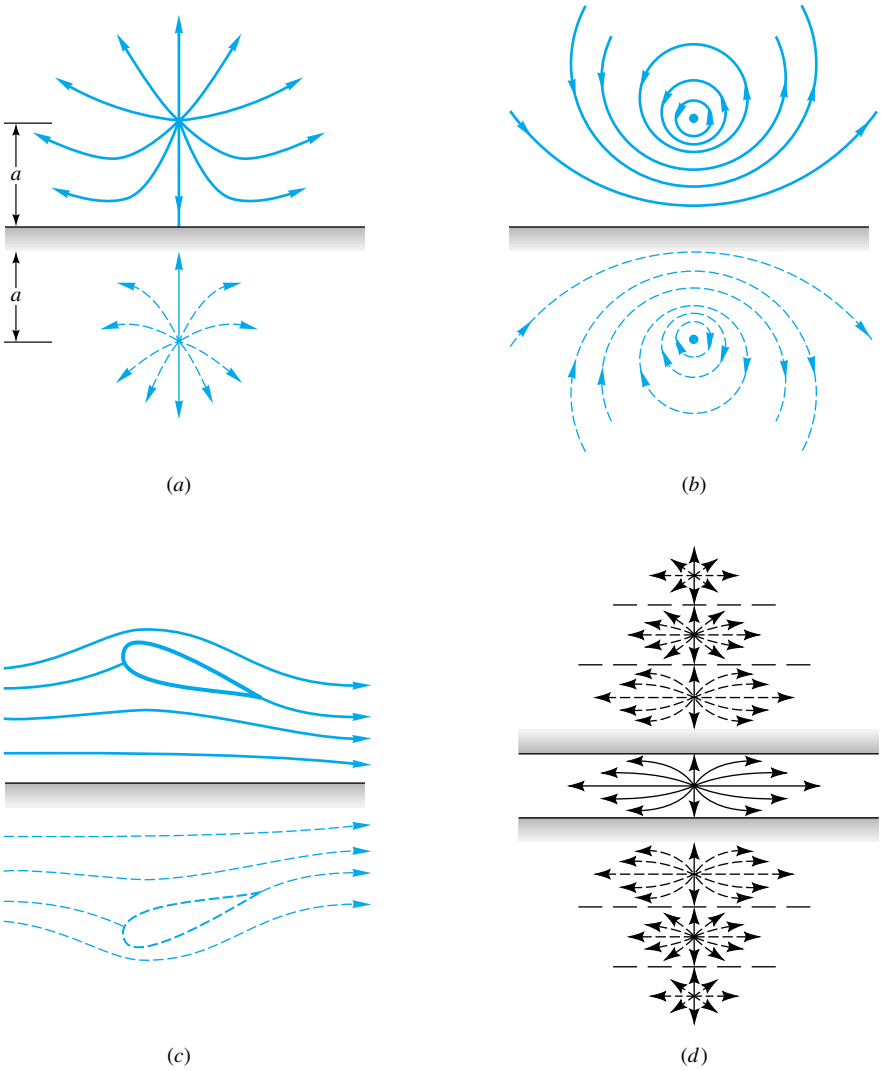


Fig. 8.17 Constraining walls can be created by image flows: (*a*) source near a wall with identical image source; (*b*) vortex near a wall with image vortex of opposite sense; (*c*) airfoil in ground effect with image airfoil of opposite circulation; (*d*) source between two walls requiring an infinite row of images.

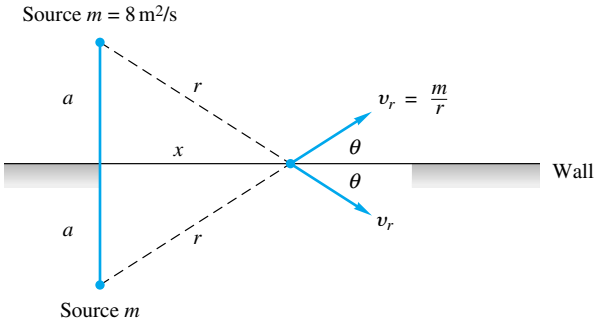
EXAMPLE 8.4

For the source near a wall as in Fig. 8.17*a*, the wall velocity is zero between the sources, rises to a maximum moving out along the wall, and then drops to zero far from the sources. If the source strength is 8 m^2/s, how far from the wall should the source be to ensure that the maximum velocity along the wall will be 5 m/s?

Solution

At any point x along the wall, as in Fig. E8.4, each source induces a radial outward $v_r = m/r$, which has a component $v_r \cos\theta$ along the wall. The total wall velocity is th

ketabline.com Ebook.ketabline.com



E8.4

$$u_{\text{wall}} = 2v_r \cos\,\theta$$

From the geometry of Fig. E8.4, $r = (x^2 + a^2)^{1/2}$ and $\cos\,\theta = x/r$. Then the total wall velocity can be expressed as

$$u = \frac{2mx}{x^2 + a^2}$$

This is zero at $x = 0$ and at $x \to \infty$. To find the maximum velocity, differentiate and set equal to zero

$$\frac{du}{dx} = 0 \quad \text{at} \quad x = a \qquad \text{and} \qquad u_{\text{max}} = \frac{m}{a}$$

We have omitted a bit of algebra in giving these results. For the given source strength and maximum velocity, the proper distance a is

$$a = \frac{m}{u_{\text{max}}} = \frac{8\ \text{m}^2/\text{s}}{5\ \text{m/s}} = 1.625\ \text{m} \qquad \textit{Ans.}$$

For $x > a$, there is an adverse pressure gradient along the wall, and boundary-layer theory should be used to predict separation.

8.7 Airfoil Theory[4]

As mentioned in conjunction with the Kutta-Joukowski lift theorem, Eq. (8.39), the problem in airfoil theory is to determine the net circulation Γ as a function of airfoil shape and free-stream angle of attack α.

The Kutta Condition

Even if the airfoil shape and free-stream angle of attack are specified, the potential-flow-theory solution is nonunique: An infinite family of solutions can be found corresponding to different values of circulation Γ. Four examples of this nonuniqueness were shown for the cylinder flows in Fig. 8.10. The same is true of the airfoil, and Fig. 8.18 shows three mathematically acceptable "solutions" to a given airfoil flow for small (Fig. 8.18*a*), large (Fig. 8.18*b*), and medium (Fig. 8.18*c*) net circulation. You can guess

[4] This section may be omitted without loss of continuity.



ketabline.com Ebook.ketabline.com

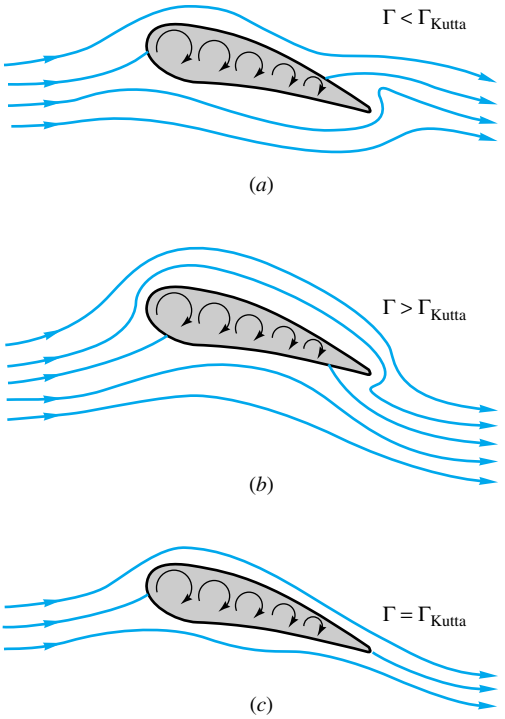


Fig. 8.18 The Kutta condition properly simulates the flow about an airfoil; (*a*) too little circulation, stagnation point on rear upper surface; (*b*) too much, stagnation point on rear lower surface; (*c*) just right, Kutta condition requires smooth flow at trailing edge.

which case best simulates a real airfoil from the earlier discussion of transient-lift development in Fig. 7.23. It is the case (Fig. 8.18*c*) where the upper and lower flows meet and leave the trailing edge smoothly. If the trailing edge is rounded slightly, there will be a stagnation point there. If the trailing edge is sharp, approximating most airfoil designs, the upper- and lower-surface flow velocities will be equal as they meet and leave the airfoil.

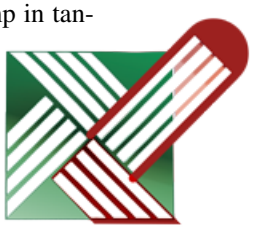
This statement of the physically proper value of Γ is generally attributed to W. M. Kutta, hence the name *Kutta condition*, although some texts give credit to Joukowski and/or Chaplygin. All airfoil theories use the Kutta condition, which is in good agreement with experiment. It turns out that the correct circulation Γ_{Kutta} depends upon flow velocity, angle of attack, and airfoil shape.

Flat-Plate Airfoil Vortex-Sheet Theory

The flat plate is the simplest airfoil, having no thickness or "shape," but even its theory is not so simple. The problem can be solved by a complex-variable mapping [2, p. 480], but here we shall use a vortex-sheet approach. Figure 8.19*a* shows a flat plate of length C simulated by a vortex sheet of variable strength $\gamma(x)$. The free stream U_∞ is at an angle of attack α with respect to the plate chord line.

To make the lift "up" with flow from left to right as shown, we specify here that the circulation is positive clockwise. Recall from Fig. 8.7*c* that there is a jump in tangential velocity across a sheet equal to the local strength

$$u_u - u_l = \gamma(x)$$



ketabline.com Ebook.ketabline.com

If we omit the free stream, the sheet should cause a rightward flow $\delta u = +\frac{1}{2}\gamma$ on the upper surface and an equal and opposite leftward flow on the lower surface, as shown in Fig. 8.19*a*. The Kutta condition for this sharp trailing edge requires that this velocity difference vanish at the trailing edge to keep the exit flow smooth and parallel

$$\gamma(C) = 0 \tag{8.54}$$

The proper solution must satisfy this condition, after which the total lift can be computed by summing the sheet strength over the whole airfoil. From Eq. (8.39) for a foil of depth b

$$L = \rho U_\infty b\Gamma \qquad \Gamma = \int_0^C \gamma(x)\, dx \tag{8.55}$$

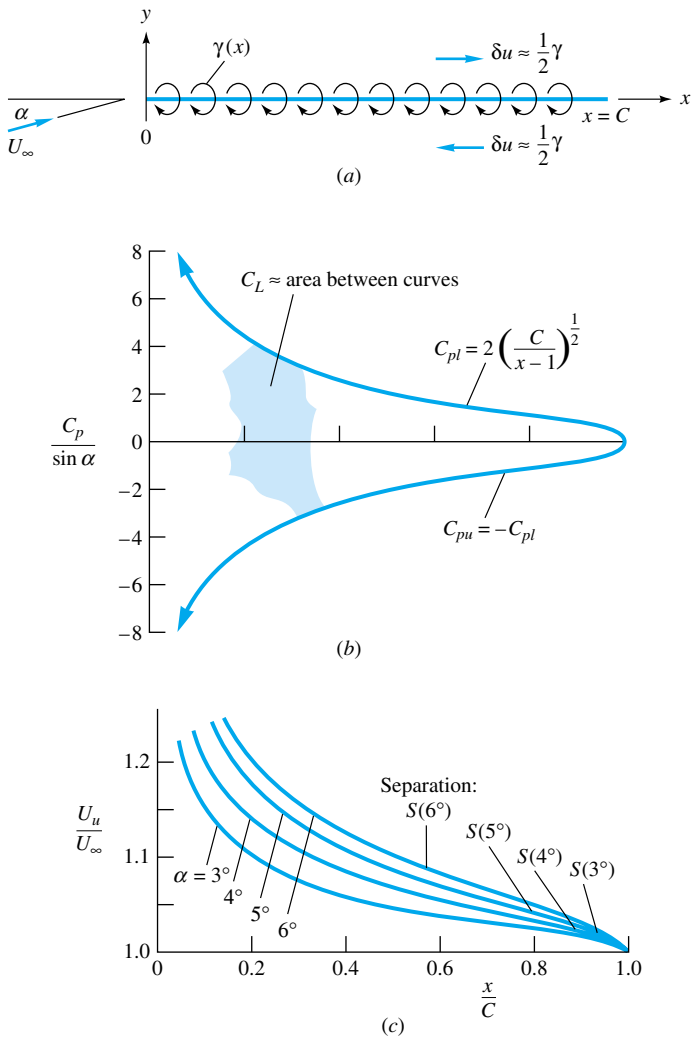


Fig. 8.19 Vortex-sheet solution for the flat-plate airfoil; (*a*) sheet geometry; (*b*) theoretical pressure coefficient on upper and lower surfaces; (*c*) upper-surface velocity with laminar separation points *S*.



ketabline.com Ebook.ketabline.com

An alternate way to compute lift is from the dimensionless pressure coefficient C_p on the upper and lower surfaces

$$C_{p_{u,l}} = \frac{p_{u,l} - p_\infty}{\frac{1}{2}\rho U_\infty^2} = 1 - \frac{U_{u,l}^2}{U_\infty^2} \tag{8.56}$$

where the last expression follows from Bernoulli's equation. The surface velocity squared is given by combining the uniform stream and the vortex-sheet velocity components from Fig. 8.19*a*:

$$\begin{aligned} U_{u,l}^2 &= (U_\infty \cos \alpha \pm \delta u)^2 + (U_\infty \sin \alpha)^2 \\ &= U_\infty^2 \pm 2U_\infty\, \delta u \cos \alpha + \delta u^2 \approx U_\infty^2 \left(1 \pm \frac{2\,\delta u}{U_\infty}\right) \end{aligned} \tag{8.57}$$

where we have made the approximations $\delta u \ll U_\infty$ and cos in the last expression, assuming a small angle of attack. Equations (8.56) and (8.57) combine to the first-order approximation

$$C_{p_{u,l}} = \mp \frac{2\,\delta u}{U_\infty} = \mp \frac{\gamma}{U_\infty} \tag{8.58}$$

The lift force is the integral of the pressure difference over the length of the airfoil, assuming depth b

$$L = \int_0^C (p_l - p_u) b\, dx$$

or

$$C_L = \frac{L}{\frac{1}{2}\rho U_\infty^2 bC} = \int_0^1 (C_{p_l} - C_{p_u}) \frac{dx}{C} = 2\int_0^1 \frac{\gamma}{U_\infty} d\left(\frac{x}{C}\right) \tag{8.59}$$

Equations (8.55) and (8.59) are entirely equivalent within the small-angle approximations.

The sheet strength $\gamma(x)$ is computed from the requirement that the net normal velocity $v(x)$ be zero at the sheet ($y = 0$), since the sheet represents a solid plate or stream surface. Consider a small piece of sheet $\gamma\, dx$ located at position x_0. The velocity v at point x on the sheet is that of an infinitesimal line vortex of strength $d\Gamma = -\gamma\, dx$

$$dv\Big|_x = \frac{d\Gamma}{2\pi r|_{x_0 \to x}} = \frac{-\gamma\, dx}{2\pi(x_0 - x)}$$

The total normal velocity induced by the entire sheet at point x is thus

$$v_{\text{sheet}} = -\int_0^C \frac{-\gamma\, dx}{2\pi(x_0 - x)} \tag{8.60}$$

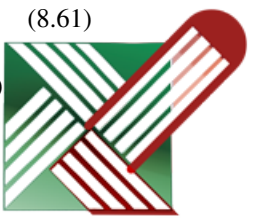
Meanwhile, from Fig. 8.19*a*, the uniform stream induces a constant normal velocity at every point on the sheet given by

$$v_{\text{stream}} = U_\infty \sin \alpha$$

Setting the sum of v_{sheet} and v_{stream} equal to zero gives the integral equation

$$\int_0^C \frac{\gamma\, dx}{x_0 - x} = 2\pi U_\infty \sin \alpha \tag{8.61}$$

to be solved for $\gamma(x)$ subject to the Kutta condition $\gamma(C) = 0$ from Eq. (8.54).



ketabline.com Ebook.ketabline.com

Although Eq. (8.61) is quite formidable (and not only for beginners), in fact it was solved long ago by using integral formulas developed by Poisson in the nineteenth century. The sheet strength which satisfies Eq. (8.61) is

$$\gamma(x) = 2U_\infty \sin\alpha\left(\frac{C}{x} - 1\right)^{1/2} \tag{8.62}$$

From Eq. (8.58) the surface-pressure coefficients are thus

$$C_{p_{u,l}} = \mp 2 \sin\alpha\left(\frac{C}{x} - 1\right)^{1/2} \tag{8.63}$$

Details of the calculations are given in advanced texts [for example, 11, chap. 5].

The pressure coefficients from Eq. (8.63) are plotted in Fig. 8.19*b*, showing that the upper surface has pressure continually increasing with x, that is, an adverse gradient. The upper-surface velocity $U_u \approx U_\infty + \delta u = U_\infty + \frac{1}{2}\gamma$ is plotted in Fig. 8.19*c* for various angles of attack. Above $\alpha = 5°$ the sheet contribution δu is about 20 percent of U_∞ so that the small-disturbance assumption is violated. Figure 8.19*c* also shows separation points computed by Thwaites' laminar-boundary-layer method, Eqs. (7.54) and (7.55). The prediction is that a flat plate would be extensively stalled on the upper surface for $\alpha > 6°$, which is approximately correct.

The lift coefficient of the airfoil is proportional to the area between c_{p_l} and c_{p_u} in Fig. 8.19b, from Eq. (8.59):

$$C_L = 2\int_0^1 \frac{\gamma}{U}\, d\left(\frac{x}{C}\right) = 4 \sin\alpha \int_0^1 \left(\frac{C}{x} - 1\right)^{1/2} d\left(\frac{x}{C}\right) = 2\pi \sin\alpha \approx 2\pi\alpha \tag{8.64}$$

This is a classic result which was alluded to earlier in Eq. (7.70) without proof.

Also of interest is the moment coefficient about the leading edge (LE) of the airfoil, taken as positive counterclockwise

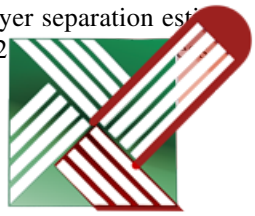
$$C_{M_{\text{LE}}} = \frac{M_{\text{LE}}}{\frac{1}{2}\rho U_\infty^2 b C^2} = \int_0^1 (C_{p_l} - C_{p_u})\frac{x}{C}\, d\left(\frac{x}{C}\right) = \frac{\pi}{2}\sin\alpha = \frac{1}{4}C_L \tag{8.65}$$

Thus the *center of pressure* (CP), or position of the resultant lift force, is at the one-quarter-chord point

$$\left(\frac{x}{C}\right)_{\text{CP}} = \frac{1}{4} \tag{8.66}$$

This theoretical result is independent of the angle of attack.

These results can be compared with experimental results for NACA airfoils in Fig. 8.20). The thinnest NACA airfoil is $t/C = 0.06$, and the thickest is 24 percent, or $t/C = 0.24$. The lift-curve slope $dC_L/d\alpha$ is within 9 percent of the theoretical value of 2π for all the various airfoil families at all thicknesses. Increasing thickness tends to increase both $C_{L,\max}$ and the stall angle. The stall angle at $t/C = 0.06$ is about 8° and would be even less for a flat plate, verifying the boundary-layer separation estimates in Fig. 8.19*c*. Best performance is usually at about the 12 point for any airfoil.



ketabline.com Ebook.ketabline.com

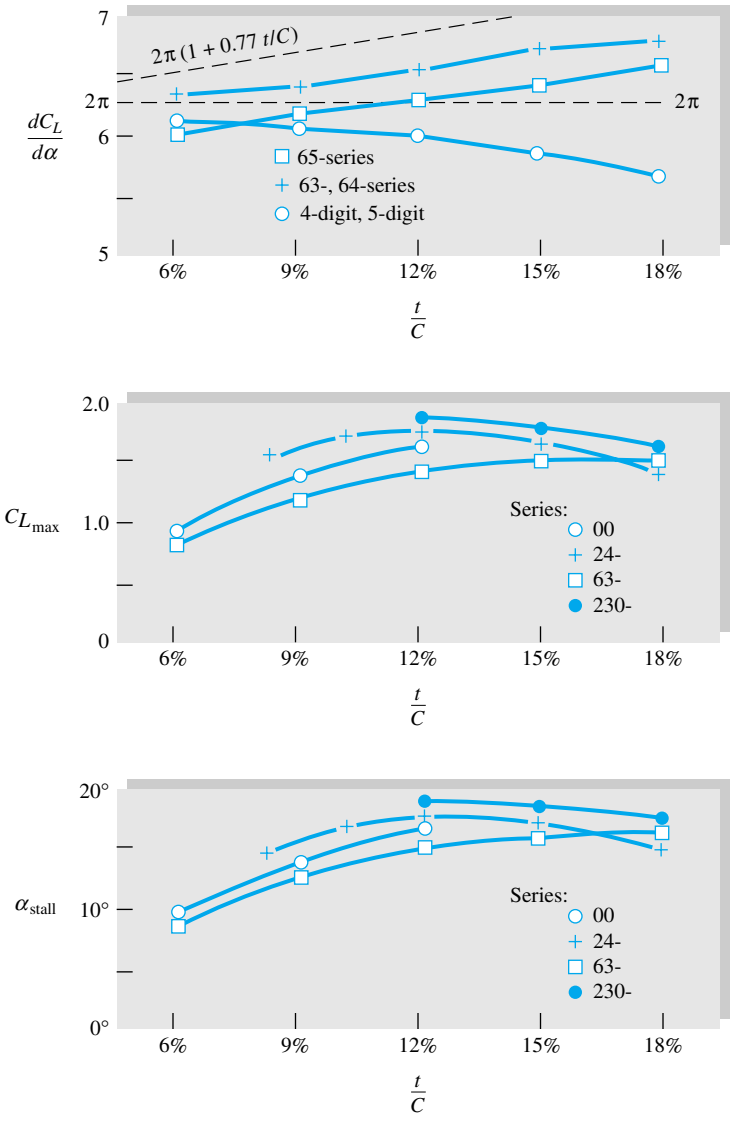


Fig. 8.20 Lift characteristics of smooth NACA airfoils as a function of thickness ratio, for infinite aspect ratio. (*From Ref. 12.*)

Potential Theory for Thick Cambered Airfoils

The theory of thick cambered airfoils is covered in advanced texts [for example, 2 to 4]; Ref. 13 has a thorough and comprehensive review of both inviscid and viscous aspects of airfoil behavior.

Basically the theory uses a complex-variable mapping which transforms the flow about a cylinder with circulation in Fig. 8.10 into flow about a foil shape with circulation. The circulation is then adjusted to match the Kutta condition of smooth exit flow from the trailing edge.

Regardless of the exact airfoil shape, the inviscid mapping theory predicts correct circulation for any thick cambered airfoil is



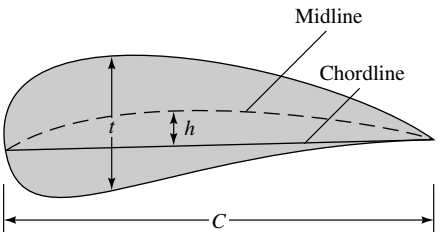
ketabline.com Ebook.ketabline.com

$$\Gamma_{\text{Kutta}} = \pi b C U_\infty \left(1 + 0.77 \frac{t}{C}\right) \sin(\alpha + \beta) \tag{8.67}$$

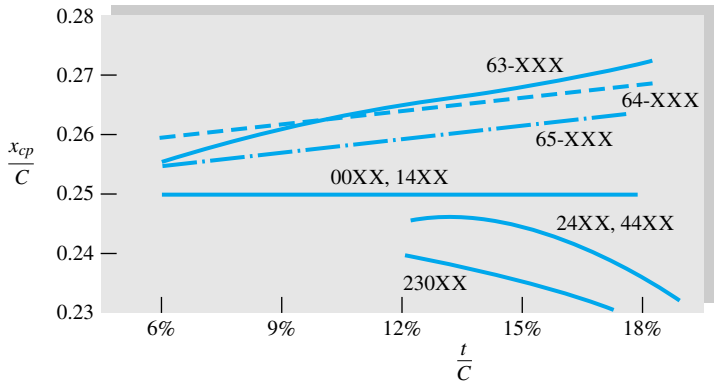
where $\beta = \tan^{-1}(2h/C)$ and h is the maximum camber, or maximum deviation of the airfoil midline from its chord line, as in Fig. 8.21*a*.

The lift coefficient of the infinite-span airfoil is thus

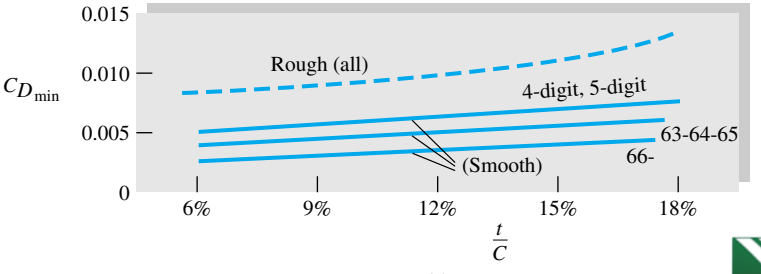
$$C_L = \frac{\rho U_\infty \Gamma}{\frac{1}{2}\rho U_\infty^2 b C} = 2\pi \left(1 + 0.77 \frac{t}{C}\right) \sin(\alpha + \beta) \tag{8.68}$$



(*a*)



(*b*)



(*c*)

Fig. 8.21 Characteristics of NACA airfoils: (*a*) typical thick cambered airfoil; (*b*) center-of-pressure data; and (*c*) minimum drag coefficient.



ketabline.com Ebook.ketabline.com

This reduces to Eq. (8.64) when the thickness and camber are zero. Figure 8.20 shows that the thickness effect $1 + 0.77t/C$ is not verified by experiment. Some airfoils increase lift with thickness, others decrease, and none approach the theory very closely, the primary reason being the boundary-layer growth on the upper surface affecting the airfoil "shape." Thus it is customary to drop the thickness effect from the theory

$$C_L \approx 2\pi \sin(\alpha + \beta) \tag{8.69}$$

The theory correctly predicts that a cambered airfoil will have finite lift at zero angle of attack and zero lift (ZL) at an angle

$$\alpha_{ZL} = -\beta = -\tan^{-1}\frac{2h}{C} \tag{8.70}$$

Equation (8.70) overpredicts the measured zero-lift angle by 1° or so, as shown in Table 8.3. The measured values are essentially independent of thickness. The designation XX in the NACA series indicates the thickness in percent, and the other digits refer to camber and other details. For example, the 2415 airfoil has 2 percent maximum camber (the first digit) occurring at 40 percent chord (the second digit) with 15 percent maximum thickness (the last two digits). The maximum thickness need not occur at the same position as the maximum camber.

Figure 8.21*b* shows the measured position of the center of pressure of the various NACA airfoils, both symmetric and cambered. In all cases x_{CP} is within 0.02 chord length of the theoretical quarter-chord point predicted by Eq. (8.66). The standard cambered airfoils (24, 44, and 230 series) lie slightly forward of $x/C = 0.25$ and the low-drag (60 series) foils slightly aft. The symmetric airfoils are at 0.25.

Figure 8.21*c* shows the minimum drag coefficient of NACA airfoils as a function of thickness. As mentioned earlier in conjunction with Fig. 7.25, these foils when smooth actually have less drag than turbulent flow parallel to a flat plate, especially the low-drag 60 series. However, for standard surface roughness all foils have about the same minimum drag, roughly 30 percent greater than that for a smooth flat plate.

Wings of Finite Span

The results of airfoil theory and experiment in the previous subsection were for two-dimensional, or infinite-span, wings. But all real wings have tips and are therefore of finite span or finite aspect ratio AR, defined by

$$\text{AR} = \frac{b^2}{A_p} = \frac{b}{\overline{C}} \tag{8.71}$$

Table 8.3 Zero-Lift Angle of NACA Airfoils

Airfoil series	Camber h/C, %	Measured α_{ZL}, deg	Theory $-\beta$, deg
24XX	2.0	−2.1	−2.3
44XX	4.0	−4.0	−4.6
230XX	1.8	−1.3	−2.1
63-2XX	2.2	−1.8	−2.5
63-4XX	4.4	−3.1	−5.0
64-1XX	1.1	−0.8	−1.2



ketabline.com Ebook.ketabline.com

where b is the span length from tip to tip and A_p is the planform area of the wing as seen from above. The lift and drag coefficients of a finite-aspect-ratio wing depend strongly upon the aspect ratio and slightly upon the planform shape of the wing.

Vortices cannot end in a fluid; they must either extend to the boundary or form a closed loop. Figure 8.22*a* shows how the vortices which provide the wing circulation bend downstream at finite wing tips and extend far behind the wing to join the starting vortex (Fig. 7.23) downstream. The strongest vortices are shed from the tips, but

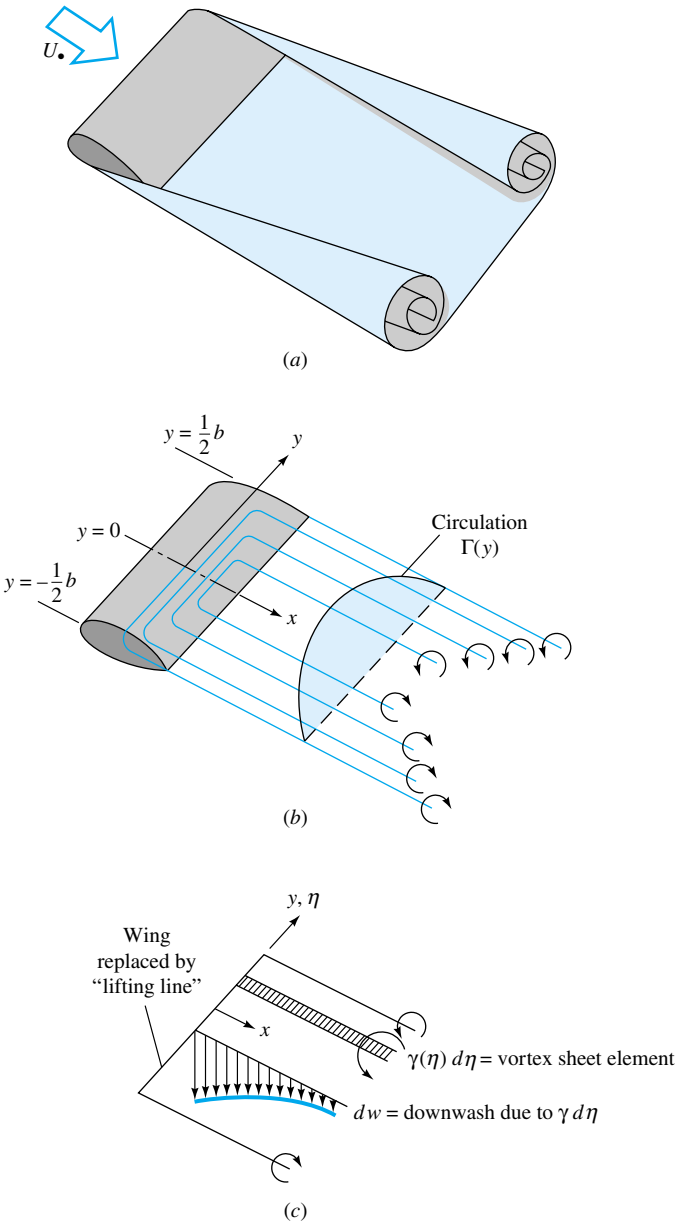


Fig. 8.22 Lifting-line theory for a finite wing: (*a*) actual trailing-vortex system behind a wing; (*b*) simulation by vortex system "bound" to the wing; (*c*) downwash on the wing due to an element of the trailing-vortex system.

ketabline.com Ebook.ketabline.com

some are shed from the body of the wing, as sketched schematically in Fig. 8.22*b*. The effective circulation $\Gamma(y)$ of these trailing shed vortices is zero at the tips and usually a maximum at the center plane, or root, of the wing. In 1918 Prandtl successfully modeled this flow by replacing the wing by a single lifting line and a continuous sheet of semi-infinite trailing vortices of strength $\gamma(y) = d\Gamma/dy$, as in Fig. 8.22*c*. Each elemental piece of trailing sheet $\gamma(\eta)\, d\eta$ induces a downwash, or downward velocity, $dw(y)$, given by

$$dw(y) = \frac{\gamma(\eta)\, d\eta}{4\pi(y - \eta)}$$

at position y on the lifting line. Note the denominator term 4π rather than 2π because the trailing vortex extends only from 0 to ∞ rather than from $-\infty$ to $+\infty$.

The total downwash $w(y)$ induced by the entire trailing vortex system is thus

$$w(y) = \frac{1}{4\pi} \int_{-(1/2)b}^{(1/2)b} \frac{\gamma(\eta)\, d\eta}{y - \eta} \tag{8.72}$$

When the downwash is vectorially added to the approaching free stream U_∞, the effective angle of attack at this section of the wing is reduced to

$$\alpha_{\text{eff}} = \alpha - \alpha_i \qquad \alpha_i = \tan^{-1} \frac{w}{U_\infty} \approx \frac{w}{U_\infty} \tag{8.73}$$

where we have used a small-amplitude approximation $w \ll U_\infty$.

The final step is to assume that the local circulation $\Gamma(y)$ is equal to that of a two-dimensional wing of the same shape and same effective angle of attack. From thin-airfoil theory, Eqs. (8.55) and (8.64), we have the estimate

$$C_L = \frac{\rho U_\infty \Gamma b}{\frac{1}{2}\rho U_\infty^2 b C} \approx 2\pi\alpha_{\text{eff}}$$

or

$$\Gamma \approx \pi C U_\infty \alpha_{\text{ eff}} \tag{8.74}$$

Combining Eqs. (8.72) and (8.74), we obtain Prandtl's lifting-line theory for a finite-span wing

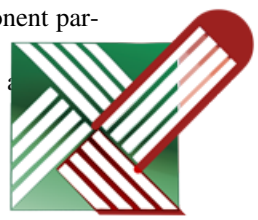
$$\Gamma(y) = \pi C(y) U_\infty \left[\alpha(y) - \frac{1}{4\pi U_\infty} \int_{-(1/2)b}^{(1/2)b} \frac{(d\Gamma/d\eta)\, d\eta}{y - \eta} \right] \tag{8.75}$$

This is an integrodifferential equation to be solved for $\Gamma(y)$ subject to the conditions $\Gamma(\frac{1}{2}b) = \Gamma(-\frac{1}{2}b) = 0$. It is similar to the thin-airfoil integral equation (8.61) and even more formidable. Once it is solved, the total wing lift and induced drag are given by

$$L = \rho U_\infty \int_{-(1/2)b}^{(1/2)b} \Gamma(y)\, dy \qquad D_i = \rho U_\infty \int_{-(1/2)b}^{(1/2)b} \Gamma(y)\alpha_i(y)\, dy \tag{8.76}$$

Here is a case where the drag is not zero in a frictionless theory because the downwash causes the lift to slant backward by angle α_i so that it has a drag component parallel to the free-stream direction, $dD_i = dL \sin \alpha_i \approx dL\alpha_i$.

The complete solution to Eq. (8.75) for arbitrary wing planform $C(y)$ and



ketabline.com Ebook.ketabline.com

twist $\alpha(y)$ is treated in advanced texts [for example, 11]. It turns out that there is a simple representative solution for an untwisted wing of elliptical planform

$$C(y) = C_0\left[1 - \left(\frac{2y}{b}\right)^2\right]^{1/2} \tag{8.77}$$

The area and aspect ratio of this wing are

$$A_p = \int_{-(1/2)b}^{(1/2)b} C\, dy = \frac{1}{4}\,\pi b C_0 \qquad \text{AR} = \frac{4b}{\pi C_0} \tag{8.78}$$

The solution to Eq. (8.75) for this $C(y)$ is an elliptical circulation distribution of exactly similar shape

$$\Gamma(y) = \Gamma_0\left[1 - \left(\frac{2y}{b}\right)^2\right]^{1/2} \tag{8.79}$$

Substituting into Eq. (8.75) and integrating give a relation between Γ_0 and C_0

$$\Gamma_0 = \frac{\pi C_0 U_\infty \alpha}{1 + 2/\text{AR}} \tag{8.80}$$

where α is assumed constant across the untwisted wing.

Substitution into Eq. (8.76) gives the elliptical-wing lift

$$L = \tfrac{1}{4}\pi^2 b C_0 \rho U_\infty^2 \alpha/(1 + 2/\text{AR})$$

or

$$C_L = \frac{2\pi\alpha}{1 + 2/\text{AR}} \tag{8.81}$$

If we generalize this to a thick cambered finite wing of approximately elliptical planform, we obtain

$$C_L = \frac{2\pi \sin(\alpha + \beta)}{1 + 2/\text{AR}} \tag{8.82}$$

This result was given without proof as Eq. (7.70). From Eq. (8.72) the computed downwash for the elliptical wing is constant

$$w(y) = \frac{2U_\infty \alpha}{2 + \text{AR}} = \text{const} \tag{8.83}$$

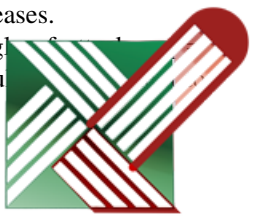
Finally, the induced drag coefficient from Eq. (8.76) is

$$C_{Di} = C_L \frac{w}{U_\infty} = \frac{C_L^2}{\pi\, AR} \tag{8.84}$$

This was given without proof as Eq. (7.71).

Figure 8.23 shows the effectiveness of this theory when tested against a nonelliptical cambered wing by Prandtl in 1921 [14]. Figure 8.23*a* and *b* shows the measured lift curves and drag polars for five different aspect ratios. Note the increase in stall angle and drag and the decrease in lift slope as the aspect ratio decreases.

Figure 8.23*c* shows the lift data replotted against effective angl[illegible] $(\alpha + \beta)/(1 + 2/\text{AR})$, as predicted by Eq. (8.82). These curves shou[illegible]



ketabline.com Ebook.ketabline.com

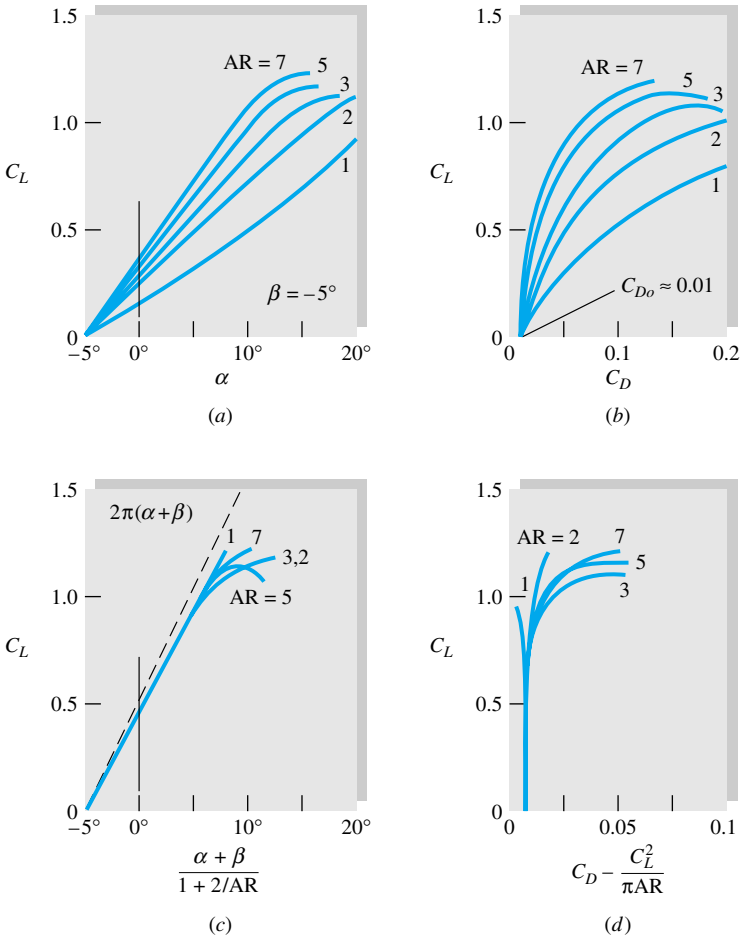


Fig. 8.23 Comparison of theory and experiment for a finite wing: (*a*) measured lift [14]; (*b*) measured drag polar [14]; (*c*) lift reduced to infinite aspect ratio; (*d*) drag polar reduced to infinite aspect ratio.

an infinite-aspect-ratio wing, and they do collapse together except near stall. Their common slope $dC_L/d\alpha$ is about 10 percent less than the theoretical value 2π, but this is consistent with the thickness and shape effects noted in Fig. 8.20.

Figure 8.23*d* shows the drag data replotted with the theoretical induced drag $C_{Di} = C_L^2/(\pi \mathrm{AR})$ subtracted out. Again, except near stall, the data collapse onto a single line of nearly constant infinite-aspect-ratio drag $C_{D0} \approx 0.01$. We conclude that the finite-wing theory is very effective and may be used for design calculations.

8.8 Axisymmetric Potential Flow[5]

The same superposition technique which worked so well for plane flow in Sec. 8.3 is also successful for axisymmetric potential flow. We give some brief examples here.

Most of the basic results carry over from plane to axisymmetric flow with only slight changes owing to the geometric differences. Consider the following related flows:

[5] This section may be omitted without loss of continuity.



ketabline.com Ebook.ketabline.com

Basic plane flow	Counterpart axisymmetric flow
Uniform stream	Uniform stream
Line source or sink	Point source or sink
Line doublet	Point doublet
Line vortex	No counterpart
Rankine half-body cylinder	Rankine half-body of revolution
Rankine-oval cylinder	Rankine oval of revolution
Circular cylinder	Sphere
Symmetric airfoil	Tear-shaped body

Since there is no such thing as a point vortex, we must forgo the pleasure of studying circulation effects in axisymmetric flow. However, as any smoker knows, there is an axisymmetric ring vortex, and there are also ring sources and ring sinks, which we leave to advanced texts [for example, 3].

Spherical Polar Coordinates

Axisymmetric potential flows are conveniently treated in the spherical polar coordinates of Fig. 8.24. There are only two coordinates (r, θ), and flow properties are constant on a circle of radius $r \sin \theta$ about the x-axis.

The equation of continuity for incompressible flow in these coordinates is

$$\frac{\partial}{\partial r}(r^2 v_r \sin \theta) + \frac{\partial}{\partial \theta}(r v_\theta \sin \theta) = 0 \tag{8.85}$$

where v_r and v_θ are radial and tangential velocity as shown. Thus a spherical polar stream function[6] exists such that

$$v_r = -\frac{1}{r^2 \sin \theta}\frac{\partial \psi}{\partial \theta} \qquad v_\theta = \frac{1}{r \sin \theta}\frac{\partial \psi}{\partial r} \tag{8.86}$$

In like manner a velocity potential $\phi(r, \theta)$ exists such that

$$v_r = \frac{\partial \phi}{\partial r} \qquad v_\theta = \frac{1}{r}\frac{\partial \phi}{\partial \theta} \tag{8.87}$$

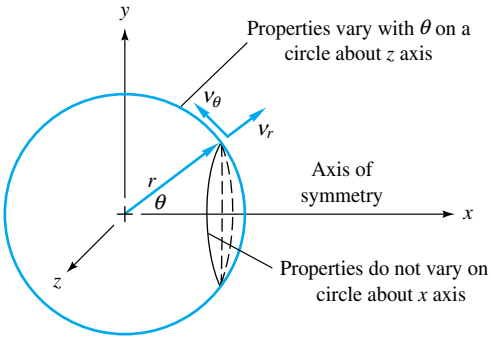


Fig. 8.24 Spherical polar coordinates for axisymmetric flow.

[6] It is often called *Stokes' stream function*, having been used in a paper Stokes w
cous sphere flow.



ketabline.com Ebook.ketabline.com

These formulas serve to deduce the ψ and ϕ functions for various elementary-axisymmetric potential flows.

Uniform Stream in the *x* Direction

A stream U_∞ in the x direction has components

$$v_r = U_\infty \cos\theta \qquad v_\theta = -U_\infty \sin\theta$$

Substitution into Eqs. (8.86) and (8.87) and integrating give

Uniform stream: $$\psi = -\tfrac{1}{2}U_\infty r^2 \sin^2\theta \qquad \phi = U_\infty r \cos\theta \tag{8.88}$$

As usual, arbitrary constants of integration have been neglected.

Point Source or Sink

Consider a volume flux Q issuing from a point source. The flow will spread out radially and at radius r will equal Q divided by the area $4\pi r^2$ of a sphere. Thus

$$v_r = \frac{Q}{4\pi r^2} = \frac{m}{r^2} \qquad v_\theta = 0 \tag{8.89}$$

with $m = Q/(4\pi)$ for convenience. Integrating (8.86) and (8.87) gives

Point source $$\psi = m\cos\theta \qquad \phi = -\frac{m}{r} \tag{8.90}$$

For a point sink, change m to $-m$ in Eq. (8.90).

Point Doublet

Exactly as in Fig. 8.8, place a source at $(x, y) = (-a, 0)$ and an equal sink at $(+a, 0)$, taking the limit as a becomes small with the product $2am = \lambda$ held constant

$$\psi_{\text{doublet}} = \lim_{\substack{a\to 0 \\ 2am\,=\,\lambda}} (m\cos\theta_{\text{source}} - m\cos\theta_{\text{sink}}) = \frac{\lambda \sin^2\theta}{r} \tag{8.91}$$

We leave the proof of this limit as a problem. The point-doublet velocity potential

$$\phi_{\text{doublet}} = \lim_{\substack{a\to 0 \\ 2am\,=\,\lambda}} \left(-\frac{m}{r_{\text{source}}} + \frac{m}{r_{\text{sink}}}\right) = \frac{\lambda\cos\theta}{r^2} \tag{8.92}$$

The streamlines and potential lines are shown in Fig. 8.25. Unlike the plane doublet flow of Fig. 8.8, neither set of lines represents perfect circles.

Uniform Stream plus a Point Source

By combining Eqs. (8.88) and (8.90) we obtain the stream function for a uniform stream plus a point source at the origin

$$\psi = -\tfrac{1}{2}U_\infty r^2 \sin^2\theta + m\cos\theta \tag{8.93}$$

From Eq. (8.86) the velocity components are, by differentiation,

$$v_r = U_\infty \cos\theta + \frac{m}{r^2} \qquad v_\theta = -U_\infty \sin\theta$$



ketabline.com Ebook.ketabline.com

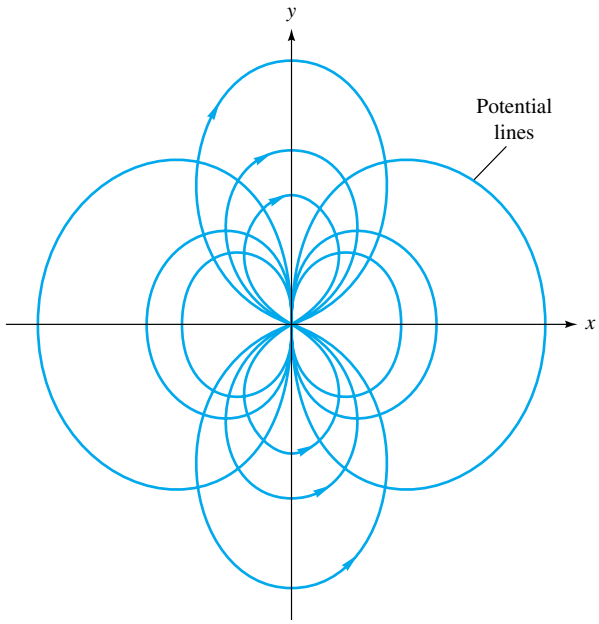


Fig. 8.25 Streamlines and potential lines due to a point doublet at the origin, from Eqs. (8.91) and (8.92).

Setting these equal to zero reveals a stagnation point at $\theta = 180°$ and $r = a = (m/U_\infty)^{1/2}$, as shown in Fig. 8.26. If we let $m = U_\infty a^2$, the stream function can be rewritten as

$$\frac{\psi}{U_\infty a^2} = \cos\theta - \frac{1}{2}\left(\frac{r}{a}\right)^2 \sin^2\theta \tag{8.95}$$

The stream surface which passes through the stagnation point $(r, \theta) = (a, \pi)$ has the value $\psi = -U_\infty a^2$ and forms a half-body of revolution enclosing the point source, as shown in Fig. 8.26. This half-body can be used to simulate a pitot tube. Far downstream the half-body approaches the constant radius $R = 2a$ about the x-axis. The maximum velocity and minimum pressure along the half-body surface occur at $\theta = 70.5°$,

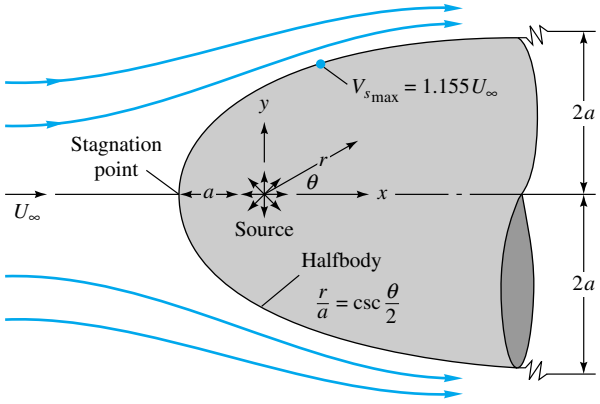


Fig. 8.26 Streamlines for a Rankine half-body of revolution.



ketabline.com Ebook.ketabline.com

$r = a\sqrt{3}$, $V_s = 1.155U_\infty$. Downstream of this point there is an adverse gradient as V_s slowly decelerates to U_∞, but boundary-layer theory indicates no flow separation. Thus Eq. (8.95) is a very realistic simulation of a real half-body flow. But when the uniform stream is added to a sink to form a half-body rear surface, e.g., similar to Fig. 8.5*c*, separation is predicted and the inviscid pattern is not realistic.

Uniform Stream plus a Point Doublet

From Eqs. (8.88) and (8.91), combination of a uniform stream and a point doublet at the origin gives

$$\psi = -\frac{1}{2}U_\infty r^2 \sin^2\theta + \frac{\lambda}{r}\sin^2\theta \tag{8.96}$$

Examination of this relation reveals that the stream surface $\psi = 0$ corresponds to the sphere of radius

$$r = a = \left(\frac{2\lambda}{U_\infty}\right)^{1/3} \tag{8.97}$$

This is exactly analogous to the cylinder flow of Fig. 8.10*a* formed by combining a uniform stream and a line doublet.

Letting $\lambda = \frac{1}{2}U_\infty a^3$ for convenience, we rewrite Eq. (8.96) as

$$\frac{\psi}{\frac{1}{2}U_\infty a^2} = -\sin^2\theta\left(\frac{r^2}{a^2} - \frac{a}{r}\right) \tag{8.98}$$

The streamlines for this sphere flow are plotted in Fig. 8.27. By differentiation from Eq. (8.86) the velocity components are

$$v_r = U_\infty \cos\theta\left(1 - \frac{a^3}{r^3}\right) \qquad v_\theta = -\frac{1}{2}U_\infty \sin\theta\left(2 + \frac{a^3}{r^3}\right) \tag{8.99}$$

We see that the radial velocity vanishes at the sphere surface $r = a$, as expected. There is a stagnation point at the front (a, π) and the rear $(a, 0)$ of the sphere. The maximum

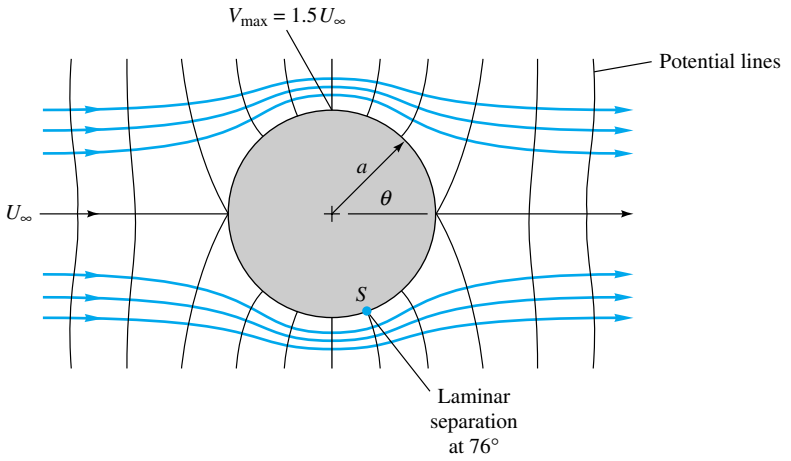


Fig. 8.27 Streamlines and potential lines for inviscid flow past a sphere.



ketabline.com Ebook.ketabline.com

velocity occurs at the shoulder $(a, \pm\frac{1}{2}\pi)$, where $v_r = 0$ and $v_\theta = -1.5U_\infty$. The surface-velocity distribution is

$$V_s = -v_\theta|_{r=a} = \tfrac{3}{2}U_\infty \sin\theta \tag{8.100}$$

Note the similarity to the cylinder surface velocity equal to $2U_\infty \sin\theta$ from Eq. (8.34) with zero circulation.

Equation (8.100) predicts, as expected, an adverse pressure gradient on the rear ($\theta < 90°$) of the sphere. If we use this distribution with laminar-boundary-layer theory [for example, 15, p. 298], separation is computed to occur at about $\theta = 76°$, so that in the actual flow pattern of Fig. 7.14 a broad wake forms in the rear. This wake interacts with the free stream and causes Eq. (8.100) to be inaccurate even in the front of the sphere. The measured maximum surface velocity is equal only to about $1.3U_\infty$ and occurs at about $\theta = 107°$ (see Ref. 15, sec. 4.10.4, for further details).

The Concept of Hydrodynamic Mass

When a body moves through a fluid, it must push a finite mass of fluid out of the way. If the body is accelerated, the surrounding fluid must also be accelerated. The body behaves as if it were heavier by an amount called the *hydrodynamic mass* (also called the *added* or *virtual mass*) of the fluid. If the instantaneous body velocity is $\mathbf{U}(t)$, the summation of forces must include this effect

$$\Sigma\,\mathbf{F} = (m + m_h)\frac{d\mathbf{U}}{dt} \tag{8.101}$$

where m_h, the hydrodynamic mass, is a function of body shape, the direction of motion, and (to a lesser extent) flow parameters such as the Reynolds number.

According to potential theory [2, sec. 6.4; 3, sec. 9.22], m_h depends only on the shape and direction of motion and can be computed by summing the total kinetic energy of the fluid relative to the body and setting this equal to an equivalent body energy

$$\mathrm{KE}_{\mathrm{fluid}} = \int \tfrac{1}{2}dm\, V_{\mathrm{rel}}^2 = \tfrac{1}{2}m_h U^2 \tag{8.102}$$

The integration of fluid kinetic energy can also be accomplished by a body-surface integral involving the velocity potential [16, sec. 11].

Consider the previous example of a sphere immersed in a uniform stream. By subtracting out the stream velocity we can replot the flow as in Fig. 8.28, showing the streamlines relative to the moving sphere. Note the similarity to the doublet flow in Fig. 8.25. The relative-velocity components are found by subtracting U from Eqs. (8.99)

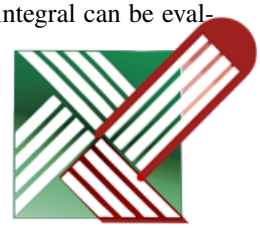
$$v_r = -\frac{Ua^3 \cos\theta}{r^3} \qquad v_\theta = -\frac{Ua^3 \sin\theta}{2r^3}$$

The element of fluid mass, in spherical polar coordinates, is

$$dm = \rho(2\pi r \sin\theta)r\, dr\, d\theta$$

When dm and $V_{\mathrm{rel}}^2 = v_r^2 + v_\theta^2$ are substituted into Eq. (8.102), the integral can be evaluated

$$\mathrm{KE}_{\mathrm{fluid}} = \tfrac{1}{3}\rho\pi a^3 U^2$$



ketabline.com Ebook.ketabline.com

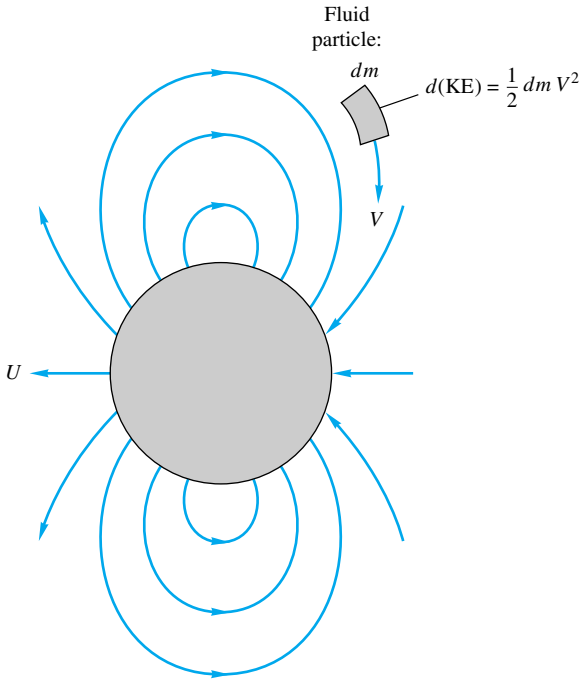


Fig. 8.28 Potential-flow streamlines relative to a moving sphere. Compare with Figs. 8.25 and 8.27.

or
$$m_h(\text{sphere}) = \tfrac{2}{3}\rho\pi a^3 \tag{8.103}$$

Thus, according to potential theory, the hydrodynamic mass of a sphere equals one-half of its displaced mass, independent of the direction of motion.

A similar result for a cylinder moving normal to its axis can be computed from Eqs. (8.33) after subtracting out the stream velocity. The result is

$$m_h(\text{cylinder}) = \rho\pi a^2 L \tag{8.104}$$

for a cylinder of length L, assuming two-dimensional motion. The cylinder's hydrodynamic mass equals its displaced mass.

Tables of hydrodynamic mass for various body shapes and directions of motion are given by Patton [17]. See also Ref. 21.

8.9 Numerical Analysis

When potential flow involves complicated geometries or unusual stream conditions, the classical superposition scheme of Secs. 8.3 and 8.4 becomes less attractive. Conformal mapping of body shapes, by using the complex-variable technique of Sec. 8.5, is no longer popular. Numerical analysis is the appropriate modern approach, and at least three different approaches are in use:

1. The finite-element method (FEM) [6, 19]
2. The finite-difference method (FDM) [5, 20]
3. *a.* Integral methods with distributed singularities [18]
   b. The boundary-element method [7]



ketabline.com Ebook.ketabline.com

Methods 3*a* and 3*b* are closely related, having first been developed on an ad hoc basis by aerodynamicists in the 1960s [18] and then generalized into a multipurpose applied-mechanics technique in the 1970s [7].

Methods 1 (or FEM) and 2 (or FDM), though strikingly different in concept, are comparable in scope, mesh size, and general accuracy. We concentrate here on the latter method for illustration purposes.

The Finite-Element Method

The finite-element method [19] is applicable to all types of linear and nonlinear partial differential equations in physics and engineering. The computational domain is divided into small regions, usually triangular or quadrilateral. These regions are delineated with a finite number of *nodes* where the field variables—temperature, velocity, pressure, stream function, etc.—are to be calculated. The solution in each region is approximated by an algebraic combination of local nodal values. Then the approximate functions are integrated over the region, and their error is minimized, often by using a weighting function. This process yields a set of N algebraic equations for the N unknown nodal values. The nodal equations are solved simultaneously, by matrix inversion or iteration. For further details see Ref. 6 or 19.

The Finite-Difference Method

Although textbooks on numerical analysis [5, 20] apply finite-difference techniques to many different problems, here we concentrate on potential flow. The idea of FDM is to approximate the partial derivatives in a physical equation by "differences" between nodel values spaced a finite distance apart—a sort of numerical calculus. The basic partial differential equation is thus replaced by a set of algebraic equations for the nodal values. For potential (inviscid) flow, these algebraic equations are linear, but they are generally nonlinear for viscous flows. The solution for nodal values is obtained by iteration or matrix inversion. Nodal spacings need not be equal.

Here we illustrate the two-dimensional Laplace equation, choosing for convenience the stream-function form

$$\frac{\partial^2 \psi}{\partial x^2} + \frac{\partial^2 \psi}{\partial y^2} = 0 \tag{8.105}$$

subject to known values of ψ along any body surface and known values of $\partial\psi/\partial x$ and $\partial\psi/\partial y$ in the free stream.

Our finite-difference technique divides the flow field into equally spaced nodes, as shown in Fig. 8.29. To economize on the use of parentheses or functional notation, subscripts i and j denote the position of an arbitrary, equally spaced node, and $\psi_{i,j}$ denotes the value of the stream function at that node

$$\psi_{i,j} = \psi(x_0 + i\,\Delta x,\, y_0 + j\,\Delta y)$$

Thus, $\psi_{i+1,j}$ is just to the right of $\psi_{i,j}$, and $\psi_{i,j+1}$ is just above.

An algebraic approximation for the derivative $\partial\psi/\partial x$ is

$$\frac{\partial \psi}{\partial x} \approx \frac{\psi(x + \Delta x,\, y) - \psi(x,\, y)}{\Delta x}$$



ketabline.com Ebook.ketabline.com

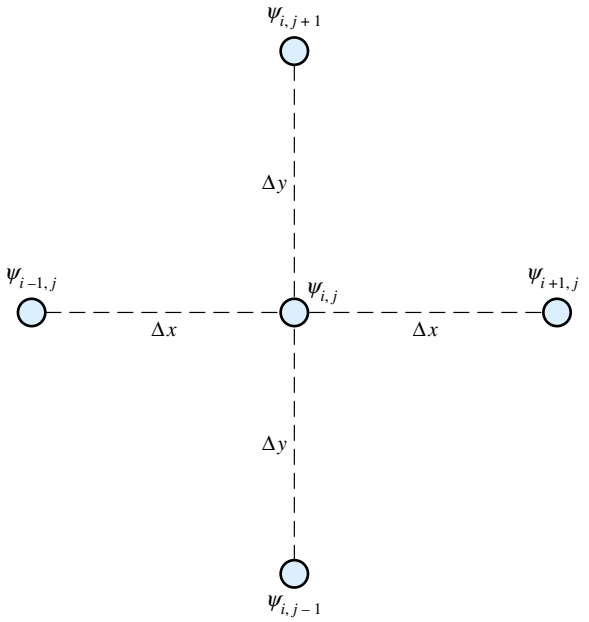


Fig. 8.29 Definition sketch for a two-dimensional rectangular finite-difference grid.

A similar approximation for the second derivative is

$$\frac{\partial^2 \psi}{\partial x^2} \approx \frac{1}{\Delta x}\left[\frac{\psi(x+\Delta x, y) - \psi(x, y)}{\Delta x} - \frac{\psi(x, y) - \psi(x-\Delta x, y)}{\Delta x}\right]$$

The subscript notation makes these expressions more compact

$$\begin{aligned} \frac{\partial \psi}{\partial x} &\approx \frac{1}{\Delta x}(\psi_{i+1,j} - \psi_{i,j}) \\ \frac{\partial^2 \psi}{\partial x^2} &\approx \frac{1}{\Delta x^2}(\psi_{i+1,j} - 2\psi_{i,j} + \psi_{i-1,j}) \end{aligned} \tag{8.106}$$

These formulas are exact in the calculus limit as $\Delta x \to 0$, but in numerical analysis we keep Δx and Δy finite, hence the term *finite differences*.

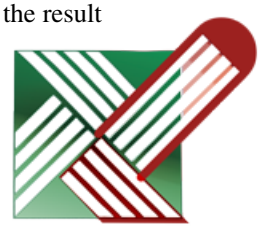
In an exactly similar manner we can derive the equivalent difference expressions for the y direction

$$\begin{aligned} \frac{\partial \psi}{\partial y} &\approx \frac{1}{\Delta y}(\psi_{i,j+1} - \psi_{i,j}) \\ \frac{\partial^2 \psi}{\partial y^2} &\approx \frac{1}{\Delta y^2}(\psi_{i,j+1} - 2\psi_{i,j} + \psi_{i,j-1}) \end{aligned} \tag{8.107}$$

The use of subscript notation allows these expressions to be programmed directly into a scientific computer language such as BASIC or FORTRAN.

When (8.106) and (8.107) are substituted into Laplace's equation (8.105), the result is the algebraic formula

$$2(1+\beta)\psi_{i,j} \approx \psi_{i-1,j} + \psi_{i+1,j} + \beta(\psi_{i,j-1} + \psi_{i,j+1})$$



ketabline.com Ebook.ketabline.com

where $\beta = (\Delta x/\Delta y)^2$ depends upon the mesh size selected. This finite-difference model of Laplace's equation states that every nodal stream-function value $\psi_{i,j}$ is a linear combination of its four nearest neighbors.

The most commonly programmed case is a square mesh ($\beta = 1$), for which Eq. (8.108) reduces to

$$\psi_{i,j} \approx \tfrac{1}{4}(\psi_{i,j+1} + \psi_{i,j-1} + \psi_{i+1,j} + \psi_{i-1,j}) \tag{8.109}$$

Thus, for a square mesh, each nodal value equals the arithmetic average of the four neighbors shown in Fig. 8.29. The formula is easily remembered and easily programmed. If P(I, J) is a subscripted variable stream function, the BASIC or FORTRAN statement of (8.109) is

$$\text{P(I, J)} = 0.25 * (\text{P(I, J + 1)} + \text{P(I, J - 1)} + \text{P(I + 1, J)} + \text{P(I - 1, J)}) \tag{8.110}$$

This is applied in iterative fashion sweeping over each of the internal nodes (I, J), with known values of P specified at each of the surrounding boundary nodes. Any initial guesses can be specified for the internal nodes P(I, J), and the iteration process will converge to the final algebraic solution in a finite number of sweeps. The numerical error, compared with the exact solution of Laplace's equation, is proportional to the square of the mesh size.

Convergence can be speeded up by the *successive overrelaxation* (SOR) method, discussed by Patankar [5]. The modified SOR form of the iteration is

$$\begin{aligned}\text{P(I, J)} = {} & \text{P(I, J)} + 0.25 * \text{A} * (\text{P(I, J + 1)} + \text{P(I, J - 1)} \\ & + \text{P(I + 1, J)} + \text{P(I - 1, J)} - 4 * \text{P(I, J)})\end{aligned} \tag{8.111}$$

The recommended value of the SOR convergence factor A is about 1.7. Note that the value $A = 1.0$ reduces Eq. (8.111) to (8.110).

Let us illustrate the finite-difference method with an example.

EXAMPLE 8.5

Make a numerical analysis, using $\Delta x = \Delta y = 0.2$ m, of potential flow in the duct expansion shown in Fig. 8.30. The flow enters at a uniform 10 m/s, where the duct width is 1 m, and is assumed to leave at a uniform velocity of 5 m/s, where the duct width is 2 m. There is a straight section 1 m long, a 45° expansion section, and a final straight section 1 m long.

Solution

Using the mesh shown in Fig. 8.30 results in 45 boundary nodes and 91 internal nodes, with i varying from 1 to 16 and j varying from 1 to 11. The internal points are modeled by Eq. (8.110). For convenience, let the stream function be zero along the lower wall. Then since the volume flow is (10 m/s)(1 m) = 10 m^2/s per unit depth, the stream function must equal 10 m^2/s along the upper wall. Over the entrance and exit planes, the stream function must vary linearly to give uniform velocities:

Inlet:	ψ(1, J) = 2 * (J − 6)	for J = 7 to 10
Exit:	ψ(16, J) = J − 1	for J = 2 to 10



ketabline.com Ebook.ketabline.com

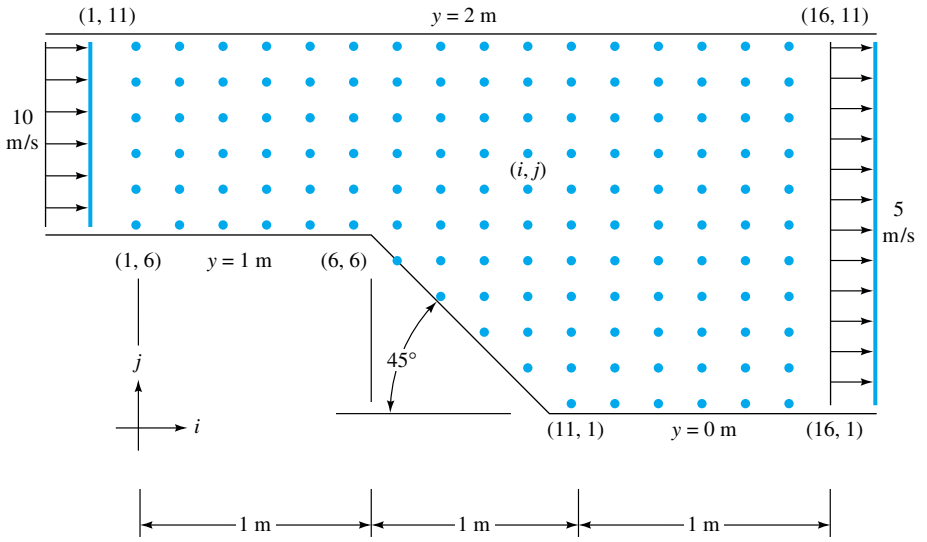


Fig. 8.30 Numerical model of potential flow through a two-dimensional 45° expansion. The nodal points shown are 20 cm apart. There are 45 boundary nodes and 91 internal nodes.

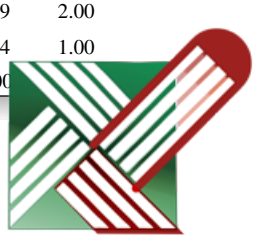
All these boundary values must be input to the program and are shown printed in Fig. 8.31.

Initial guesses are stored for the internal points, say, zero or an average value of 5.0 m^2/s. The program then starts at any convenient point, such as the upper left (2, 10), and evaluates Eq. (8.110) at every internal point, repeating this sweep iteratively until there are no further changes (within some selected maximum change) in the nodal values. The results are the finite-difference simulation of this potential flow for this mesh size; they are shown printed in Fig. 8.31 to three-digit accuracy. The reader should test a few nodes in Fig. 8.31 to verify that Eq. (8.110) is satisfied everywhere. The numerical accuracy of these printed values is difficult to estimate, since there is no known exact solution to this problem. In practice, one would keep decreasing the mesh size to see whether there were any significant changes in nodal values.

This problem is well within the capability of a small personal computer. The values shown in Fig. 8.31 were obtained after 100 iterations, or 6 min of execution time, on a Macintosh SE personal computer, using BASIC.

ψ = 10.00	10.00	10.00	10.00	10.00	10.00	10.00	10.00	10.00	10.00	10.00	10.00	10.00	10.00	10.00	10.00
8.00	8.02	8.04	8.07	8.12	8.20	8.30	8.41	8.52	8.62	8.71	8.79	8.85	8.91	8.95	9.00
6.00	6.03	6.06	6.12	6.22	6.37	6.58	6.82	7.05	7.26	7.44	7.59	7.71	7.82	7.91	8.00
4.00	4.03	4.07	4.13	4.26	4.48	4.84	5.24	5.61	5.93	6.19	6.41	6.59	6.74	6.88	7.00
2.00	2.02	2.05	2.09	2.20	2.44	3.08	3.69	4.22	4.65	5.00	5.28	5.50	5.69	5.85	6.00
ψ = 0.00	0.00	0.00	0.00	0.00	0.00	1.33	2.22	2.92	3.45	3.87	4.19	4.45	4.66	4.84	5.00
						0.00	1.00	1.77	2.37	2.83	3.18	3.45	3.66	3.84	4.00
							0.00	0.80	1.42	1.90	2.24	2.50	2.70	2.86	3.00
								0.00	0.63	1.09	1.40	1.61	1.77	1.89	2.00
									0.00	0.44	0.66	0.79	0.87	0.94	1.00
										0.00	0.00	0.00	0.00	0.00	

Fig. 8.31 Stream-function nodal values for the potential flow of Fig. 8.30. Boundary values are known inputs. Internal nodes are solutions to Eq. (8.110).



ketabline.com Ebook.ketabline.com

Although Fig. 8.31 is the computer solution to the problem, these numbers must be manipulated to yield practical engineering results. For example, one can interpolate these numbers to sketch various streamlines of the flow. This is done in Fig. 8.32*a*. We see that the streamlines are curved both upstream and downstream of the corner regions, especially near the lower wall. This indicates that the flow is not one-dimensional.

The velocities at any point in the flow can be computed from finite-difference formulas such as Eqs. (8.106) and (8.107). For example, at the point (I, J) = (3, 6), from Eq. (8.107), the horizontal velocity is approximately

$$u(3, 6) \approx \frac{\psi(3, 7) - \psi(3, 6)}{\Delta y} = \frac{2.09 - 0.00}{0.2} = 10.45 \text{ m/s}$$

and the vertical velocity is zero from Eq. (8.106). Directly above this on the upper wall, we estimate

$$u(3, 11) \approx \frac{\psi(3, 11) - \psi(3,10)}{\Delta y} = \frac{10.00 - 8.07}{0.2} = 9.65 \text{ m/s}$$

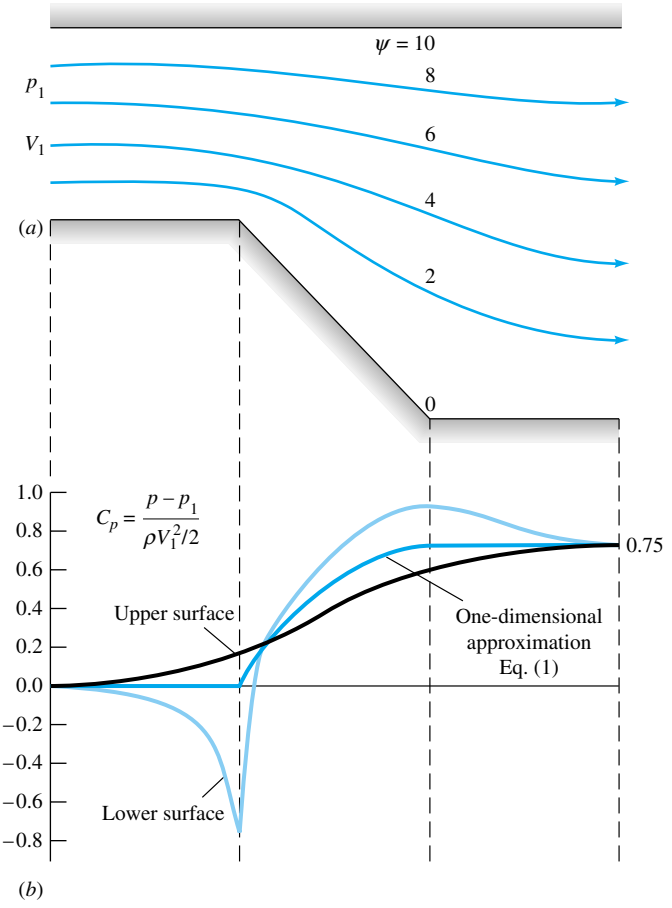


Fig. 8.32 Useful results computed from Fig. 8.31: (*a*) streamlines of the flow; (*b*) pressure-coefficient distribution along each wall.



ketabline.com Ebook.ketabline.com

The flow is not truly one-dimensional in the entrance duct. The lower wall, which contains the diverging section, accelerates the fluid, while the flat upper wall is actually decelerating the fluid.

Another output function, useful in making boundary-layer analyses of the wall regions, is the pressure distribution along the walls. If p_1 and V_1 are the pressure and velocity at the entrance (I = 1), conditions at any other point are computed from Bernoulli's equation (8.3), neglecting gravity

$$p + \tfrac{1}{2}\rho V^2 = p_1 + \tfrac{1}{2}\rho V_1^2$$

which can be rewritten as a dimensionless pressure coefficient

$$C_p = \frac{p - p_1}{\frac{1}{2}\rho V_1^2} = 1 - \left(\frac{V}{V_1}\right)^2$$

This determines p after V is computed from the stream-function differences in Fig. 8.31.

Figure 8.32*b* shows the computed wall-pressure distributions as compared with the one-dimensional continuity approximation $V_1 A_1 \approx V(x)A(x)$, or

$$C_p(\text{one-dim}) \approx 1 - \left(\frac{A_1}{A}\right)^2 \tag{1}$$

The one-dimensional approximation, which is rather crude for this large (45°) expansion, lies between the upper and lower wall pressures. One-dimensional theory would be much more accurate for a 10° expansion.

Analyzing Fig. 8.32*b*, we predict that boundary-layer separation will probably occur on the lower wall between the corners, where pressure is strongly rising (highly adverse gradient). Therefore potential theory is probably not too realistic for this flow, where viscous effects are strong. (Recall Figs. 6.27 and 7.8.)

Potential theory is *reversible*; i.e., when we reverse the flow arrows in Fig. 8.32*a*, then Fig. 8.32*b* is still valid and would represent a 45° *contraction* flow. The pressure would fall on both walls (no separation) from $x = 3$ m to $x = 1$ m. Between $x = 1$ m and $x = 0$, the pressure rises on the lower surface, indicating possible separation, probably just downstream of the corner.

This example should give the reader an idea of the usefulness and generality of numerical analysis of fluid flows.

The Boundary-Element Method

A relatively new technique for numerical solution of partial differential equations is the *boundary-element method* (BEM). Reference 7 is an introductory textbook outlining the concepts of BEM, including FORTRAN programs for potential theory and elastostatics. There are no interior elements. Rather, all nodes are placed on the boundary of the domain, as in Fig. 8.33. The "element" is a small piece of the boundary surrounding the node. The "strength" of the element can be either constant or variable.

For plane potential flow, the method takes advantage of the particular solution

$$\psi^* = \frac{1}{2\pi} \ln \frac{1}{r} \tag{8.112}$$

which satisfies Laplace's equation, $\nabla^2 \psi = 0$. Each element i is assumed to have a different strength ψ_i. Then r represents the distance from that element to any other point in the flow field. Summing all these elemental effects, with proper boundary conditions, will give the total solution to the potential-flow problem.

At each element of the boundary, we typically know either the value of ψ or the value of $\partial\psi/\partial n$, where n is normal to the boundary. (Mixed combinations o



ketabline.com Ebook.ketabline.com

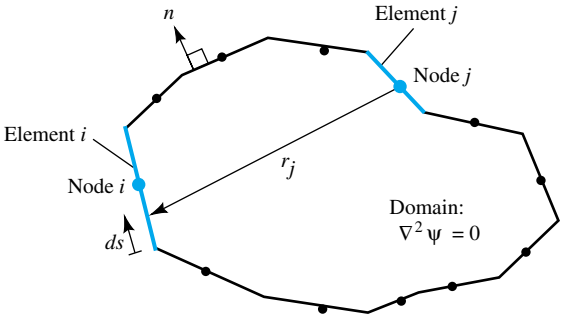


Fig. 8.33 Boundary elements of constant strength in plane potential flow.

$\partial\psi/\partial n$ are also possible but are not discussed here.) The correct strengths ψ_i are such that these boundary conditions are satisfied at every element. Summing these effects over N elements requires integration by parts plus a careful evaluation of the (singular) effect of element i upon itself. The mathematical details are given in Ref. 7. The result is a set of N algebraic equations for the unknown boundary values. In the case of elements of constant strength, the final expression is

$$\frac{1}{2}\psi_i + \sum_{j=1}^{N} \psi_j \left(\int_j \frac{\partial \psi^*}{\partial n}\, ds \right) = \sum_{j=1}^{N} \left(\frac{\partial \psi}{\partial n} \right)_j \left(\int_j \psi^*\, ds \right) \qquad i = 1 \text{ to } N \qquad (8.113)$$

The integrals, which involve the logarithmic particular solution ψ^* from Eq. (8.112), are evaluated numerically for each element. Reference 7 recommends − and gives a program for − gaussian quadrature formulas.

Equations (8.113) contain $2N$ element values, ψ_i and $(\partial\psi/\partial n)_i$, of which N are known from the given boundary conditions. The remaining N are solved simultaneously from Eqs. (8.113). Generally this completes the analysis − only the boundary solution is computed, and interior points are not studied. In most cases, the boundary velocity and pressure are all that is needed.

We illustrated the method with stream function ψ. Naturally the entire technique also applies to velocity potential ϕ, if we are given proper conditions on ϕ or $\partial\phi/\partial n$ at each boundary element. The method is readily extended to three dimensions [7].

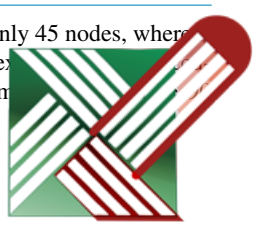
Reference 7 gives a complete FORTRAN listing for solving Eqs. (8.113) numerically for constant, linear, and quadratic element strength variations. We now use their constant-element-strength program, POCONBE [7], to take an alternate look at Example 8.5, which used the finite-difference method.

EXAMPLE 8.6

Solve the duct expansion problem, Example 8.5, using boundary elements. Use the same grid spacing $\Delta x = \Delta y = 0.2$ m for the element sizes.

Solution

The boundary nodes are equally spaced, as shown in Fig. 8.34. There are only 45 nodes, where there were 91 interior points for the FDM solution of Example 8.5. We ex racy for 50 percent fewer nodes. (Had we reduced the grid size to 0.1 m



ketabline.com Ebook.ketabline.com

nodes as opposed to 406 interior points − a savings of 78 percent.) The program POCONBE [7] asks you to input the location of these 45 nodes. The stream-function values are known all around the boundary: ψ equals 0 on the bottom and 10.0 on the top and is linearly increasing from 0 to 10.0 at entrance and exit. These values of ψ, shown on the outside in Fig. 8.34, are inputted into the program.

Once the input of nodes and element values is complete, the program immediately computes and displays or stores the 45 unknowns, which in this case are the values of $\partial\psi/\partial n$ all around the boundary. These values are shown on the inside of the top and bottom surfaces in Fig. 8.34 and represent the local surface velocity near each element, in m/s. The values of $\partial\psi/\partial n$ at entrance and exit, which are small fractions representing vertical velocity components, are not shown here.

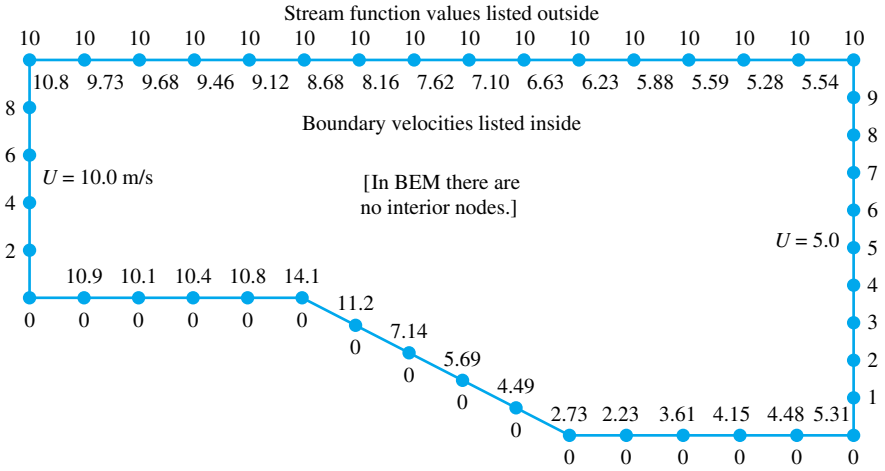


Fig. 8.34 Boundary elements corresponding to the same grid size as Fig. 8.31. Nodal values of stream function and computed surface velocity are shown.

The reader may verify that use of the surface velocities in Fig. 8.34 to compute surface pressure coefficients, as in Example 8.5, leads to curves very similar to those shown in Fig. 8.32. The BEM approach, using the same boundary nodes, has accuracy comparable to that for an FDM computation. For further details see Ref. 7.

Viscous-Flow Computer Models

Our previous finite-difference model of Laplace's equation, e.g., Eq. (8.109), was very well behaved and converged nicely with or without overrelaxation. Much more care is needed to model the full Navier-Stokes equations. The challenges are quite different, and they have been met to a large extent, so there are now many textbooks [20, 23 to 27] on (fully viscous) *computational fluid dynamics* (CFD). This is not a textbook on CFD, but we will address some of the issues in this section.

One-Dimensional Unsteady Flow

We begin with a simplified problem, showing that even a single viscous term introduces new effects and possible instabilities. Recall (or review) Prob. 4.85, where a wall moves and drives a viscous fluid parallel to itself. Gravity is neglected. Let the wall be the plane $y = 0$, moving at a speed $U_0(t)$, as in Fig. 8.35. A uniform vertical spacing Δy, has nodes n at which the local velocity u_n^j is to be calculated, w

ketabline.com Ebook.ketabline.com

perscript j denotes the time-step $j\Delta t$. The wall is $n = 1$. If $u = u(y, t)$ only and $v = w = 0$, continuity, $\nabla \cdot \mathbf{V} = 0$, is satisfied and we need only solve the x-momentum Navier-Stokes equation:

$$\frac{\partial u}{\partial t} = \nu \frac{\partial^2 u}{\partial y^2} \tag{8.114}$$

where $\nu = \mu/\rho$. Utilizing the same finite-difference approximations as in Eq. (8.106), we may model Eq. (8.114) algebraically as a forward time difference and a central spatial difference:

$$\frac{u_n^{j+1} - u_n^j}{\Delta t} \approx \nu \frac{u_{n+1}^j - 2u_n^j + u_{n-1}^j}{\Delta y^2}$$

Rearrange and find that we can solve explicitly for u_n at the next time-step $j + 1$:

$$u_n^{j+1} \approx (1 - 2\sigma)\, u_n^j + \sigma\,(u_{n-1}^j + u_{n+1}^j) \qquad \sigma = \frac{\nu \Delta t}{\Delta y^2} \tag{8.115}$$

Thus u at node n at the next time-step $j + 1$ is a weighted average of three previous values, similar to the "four-nearest-neighbors" average in the laplacian model of Eq. (8.109). Since the new velocity is calculated immediately, Eq. (8.115) is called an *explicit* model. It differs from the well-behaved laplacian model, however, because it may be *unstable*. The weighting coefficients in Eq. (8.115) must all be positive to avoid divergence. Now σ is positive, but $(1 - 2\sigma)$ may not be. Therefore, our explicit viscous flow model has a stability requirement:

$$\sigma = \frac{\nu \Delta t}{\Delta y^2} \leq \frac{1}{2} \tag{8.116}$$

Normally one would first set up the mesh size Δy in Fig. 8.35, after which Eq. (8.116) would limit the time-step Δt. The solutions for nodal values would then be stable, but not necessarily that accurate. The mesh sizes Δy and Δt could be reduced to increase accuracy, similar to the case of the potential-flow laplacian model (8.109).

For example, to solve Prob. 4.85 numerically, one sets up a mesh with plenty of nodes (30 or more Δy within the expected viscous layer); selects Δt according to Eq.

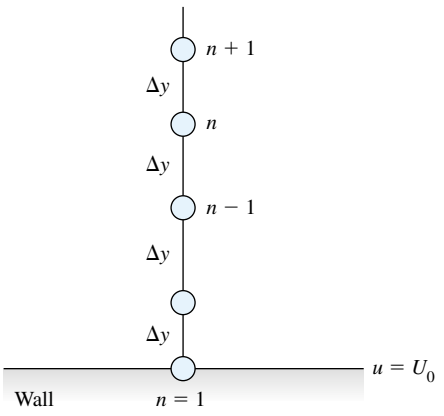


Fig. 8.35 An equally spaced finite-difference mesh for one-dimensional viscous flow [Eq. (8.114)].



ketabline.com Ebook.ketabline.com

(8.116); and sets two boundary conditions for all j: $u_1 = U_0 \sin \omega t$[†] and $u_N = 0$, where N is the outermost node. For initial conditions, perhaps assume the fluid initially at rest: $u_n^1 = 0$ for $2 \leq n \leq N - 1$. Sweeping the nodes $2 \leq n \leq N - 1$ using Eq. (8.115) (an Excel spreadsheet is excellent for this), one generates numerical values of u_n^j for as long as one desires. After an initial transient, the final "steady" fluid oscillation will approach the classical solution in viscous-flow textbooks [15]. Try Prob. 8.115 to demonstrate this.

An Alternate Implicit Approach

In many finite-difference problems, a stability limitation such as Eq. (8.116) requires an extremely small time-step. To allow larger steps, one can recast the model in an implicit fashion by evaluating the second-derivative model in Eq. (8.114) at the *next* time-step:

$$\frac{u_n^{j+1} - u_n^j}{\Delta t} \approx \nu \frac{u_{n+1}^{j+1} - 2u_n^{j+1} + u_{n-1}^{j+1}}{\Delta y^2}$$

This rearrangement is unconditionally stable for any σ, but now we have *three* unknowns:

$$-\sigma u_{n-1}^{j+1} + (1 + 2\sigma)u_n^{j+1} - \sigma u_{n+1}^{j+1} \approx u_n^j \tag{8.117}$$

This is an *implicit* model, meaning that one must solve a large system of algebraic equations for the new nodal values at time $j + 1$. Fortunately, the system is narrowly banded, with the unknowns confined to the principal diagonal and its two nearest diagonals. In other words, the coefficient matrix of Eq. (8.117) is *tridiagonal*, a happy event. A direct method, called the *tridiagonal matrix algorithm* (TDMA), is available and explained in most CFD texts [20, 23 to 27]. Appendix A of Ref. 20 includes a complete program for solving the TDMA. If you have not learned the TDMA yet, Eq. (8.117) converges satisfactorily by rearrangement and iteration:

$$u_n^{j+1} \approx \frac{u_n^j + \sigma (u_{n-1}^{j+1} + u_{n+1}^{j+1})}{1 + 2\sigma} \tag{8.118}$$

At each time-step $j + 1$, sweep the nodes $2 \leq n \leq N - 1$ over and over, using Eq. (8.118), until the nodal values have converged. This implicit method is stable for any σ, however large. To ensure accuracy, though, one should keep Δt and Δy small compared to the basic time and length scales of the problem. This author's habit is to keep Δt and Δy small enough that nodal values change no more than 10 percent from one (n, j) to the next.

EXAMPLE 8.7

SAE 30 oil at 20°C is at rest near a wall when the wall suddenly begins moving at a constant 1 m/s. Using the explicit model of Eq. (8.114), estimate the oil velocity at $y = 3$ cm after 1 second of wall motion.

[†]Finite differences are not analytical; one must set U_0 and ω equal to numerical values.



ketabline.com Ebook.ketabline.com

Solution

For SAE 30 oil, from Table A-3, $\nu = 0.29/891 = 3.25$ E-4 m^2/s. For convenience in putting a node exactly at $y = 3$ cm, choose $\Delta y = 0.01$ m. The stability limit (8.116) is $\nu\Delta t/\Delta y^2 < 0.5$, or $\Delta t < 0.154$ s. Again for convenience, to hit $t = 1$ s on the nose, choose $\Delta t = 0.1$ s, or $\sigma = 0.3255$ and $(1 - 2\sigma) = 0.3491$. Then our explicit algebraic model (8.115) for this problem is

$$u_n^{j+1} \approx 0.3491\ u_n^j + 0.3255(u_{n-1}^j + u_{n-1}^j) \tag{1}$$

We apply this relation from $n = 2$ out to at least $n = N = 15$, to make sure that the desired value of u at $n = 3$ is accurate. The wall no-slip boundary requires $u_1^j = 1.0$ m/s = constant for all j. The outer boundary condition is $u_N = 0$. The initial conditions are $u_n^1 = 0$ for $n \geq 2$. We then apply Eq. (1) repeatedly for $n \geq 2$ until we reach $j = 11$, which corresponds to $t = 1$ s. This is easily programmed on a spreadsheet such as Excel. Here we print out only $j = 1$, 6, and 11 as follows:

j	t	u_1	u_2	u_3	u_4	u_5	u_6	u_7	u_8	u_9	u_{10}	u_{11}
1	0.000	1.000	0.000	0.000	0.000	0.000	0.000	0.000	0.000	0.000	0.000	0.000
6	0.500	1.000	0.601	0.290	0.107	0.027	0.004	0.000	0.000	0.000	0.000	0.000
11	1.000	1.000	0.704	0.446	**0.250**	0.123	0.052	0.018	0.005	0.001	0.000	0.000

Note: Units for t and u's are s and m/s, respectively.

Our numerical estimate is $u_4^{11} = u(3\text{ cm}, 1\text{ s}) \approx 0.250$ m/s, which is about 4 percent high—this problem has a known exact solution, $u = 0.241$ m/s [15]. We could improve the accuracy indefinitely by decreasing Δy and Δt.

Steady Two-Dimensional Laminar Flow

The previous example, unsteady one-dimensional flow, had only one viscous term and no convective accelerations. Let us look briefly at incompressible two-dimensional steady flow, which has four of each type of term, plus a nontrivial continuity equation:

Continuity:
$$\frac{\partial u}{\partial x} + \frac{\partial v}{\partial y} = 0 \tag{8.119a}$$

x momentum:
$$u\frac{\partial u}{\partial x} + v\frac{\partial u}{\partial y} = -\frac{1}{\rho}\frac{\partial p}{\partial x} + \nu\left(\frac{\partial^2 u}{\partial x^2} + \frac{\partial^2 u}{\partial y^2}\right) \tag{8.119b}$$

y momentum
$$u\frac{\partial v}{\partial x} + v\frac{\partial v}{\partial y} = -\frac{1}{\rho}\frac{\partial p}{\partial y} + \nu\left(\frac{\partial^2 v}{\partial x^2} + \frac{\partial^2 v}{\partial y^2}\right) \tag{8.119c}$$

These equations, to be solved for (u, v, p) as functions of (x, y), are familiar to us from analytical solutions in Chaps. 4 and 6. However, to a numerical analyst, they are odd, because there is no *pressure equation*, that is, a differential equation for which the dominant derivatives involve p. This situation has led to several different "pressure-adjustment" schemes in the literature [20, 23 to 27], most of which manipulate the continuity equation to insert a pressure correction.

A second difficulty in Eq. (8.119*b* and *c*) is the presence of no
accelerations such as $u(\partial u/\partial x)$, which create asymmetry in viscou



ketabline.com Ebook.ketabline.com

tempts, which modeled such terms with a central difference, led to numerical instability. The remedy is to relate convection finite differences solely to the *upwind* flow entering the cell, ignoring the downwind cell. For example, the derivative $\partial u/\partial x$ could be modeled, for a given cell, as $(u_{\text{upwind}} - u_{\text{cell}})/\Delta x$. Such improvements have made fully viscous CFD an effective tool, with various commercial user-friendly codes available. For details beyond our scope, see Refs. 20 and 23 to 27.

Mesh generation and gridding have also become quite refined in modern CFD. Figure 8.36 illustrates a CFD solution of two-dimensional flow past an NACA 66(MOD) hydrofoil [28]. The gridding in Fig. 8.36*a* is of the C type, which wraps around the leading edge and trails off behind the foil, thus capturing the important near-wall and wake details without wasting nodes in front or to the sides. The grid size is 262 by 91.

The CFD model for this hydrofoil flow is also quite sophisticated: a full Navier-Stokes solver with turbulence modeling [29] and allowance for cavitation bubble formation when surface pressures drop below the local vapor pressure. Figure 8.36*b* compares computed and experimental surface pressure coefficients for an angle of attack of 1°. The dimensionless pressure coefficient is defined as $C_p = (p_{\text{surface}} - p_\infty)/(\rho V_\infty^2/2)$. The agreement is excellent, as indeed it is also for cases where the hydrofoil cavitates [28]. Clearly, when properly implemented for the proper flow cases, CFD can be an extremely effective tool for engineers.

Commercial CFD Codes

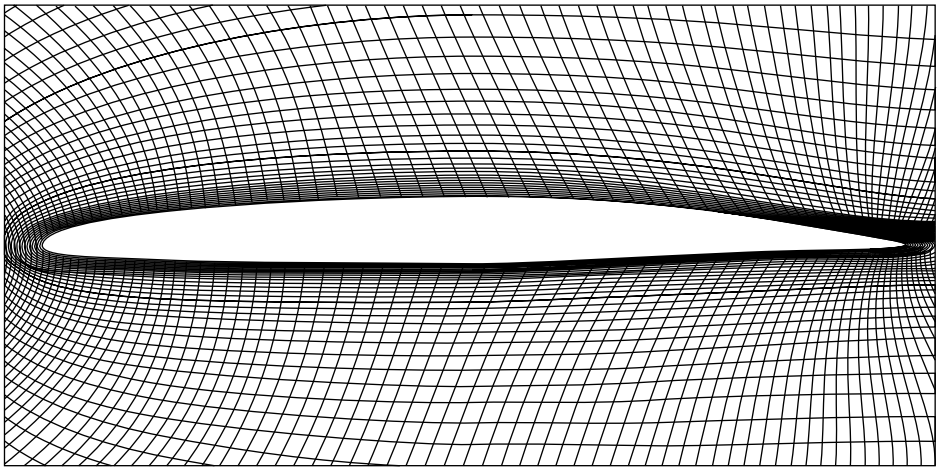
The coming of the third millennium has seen an enormous emphasis on computer applications in nearly every field, fluid mechanics being a prime example. It is now possible, at least for moderately complex geometries and flow patterns, to model on a digital computer, approximately, the equations of motion of fluid flow, with dedicated CFD textbooks available [20, 23 to 27]. The flow region is broken into a fine grid of elements and nodes, which algebraically simulate the basic partial differential equations of flow. While simple two-dimensional flow simulations have long been reported and can be programmed as student exercises, three-dimensional flows, involving thousands or even millions of grid points, are now solvable with the modern supercomputer.

Although elementary computer modeling was treated briefly here, the general topic of CFD is essentially for advanced study or professional practice. The big change over the past decade is that engineers, rather than laboriously programming CFD problems themselves, can now take advantage of any of several commercial CFD codes. These are extensive software packages which allow engineers to construct a geometry and boundary conditions to simulate a given viscous-flow problem. The software then grids the flow region and attempts to compute flow properties at each grid element. The convenience is great; the danger is also great. That is, computations are not merely automatic, like when using a hand calculator, but rather require care and concern from the user. Convergence and accuracy are real problems for the modeler. Use of the codes requires some art and experience. In particular, when the flow Reynolds number, $\text{Re} = \rho VL/\mu$, goes from moderate (laminar flow) to high (turbulent flow), the accuracy of the simulation is no longer assured in any real sense. The reason is that turbulent flows are not completely resolved by the full equations of motion, and one resorts to using approximate turbulence models.

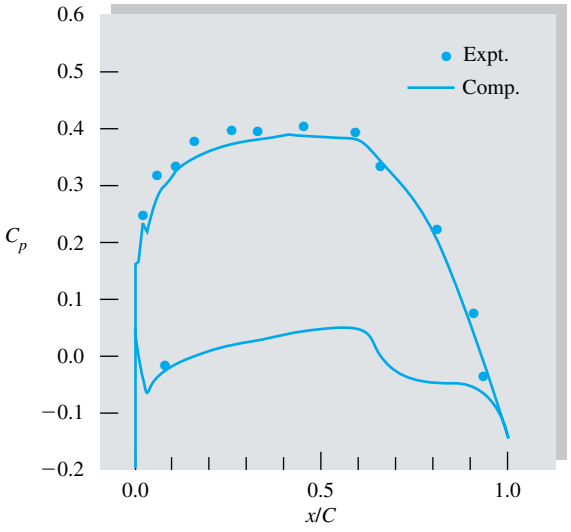
Turbulence models [29] are developed for particular geometries and flow co
and may be inaccurate or unrealistic for others. This is discussed by Freitas [3



ketabline.com Ebook.ketabline.com



(*a*)

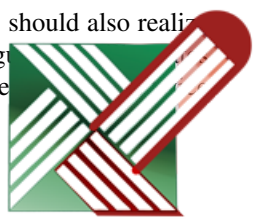


(*b*)

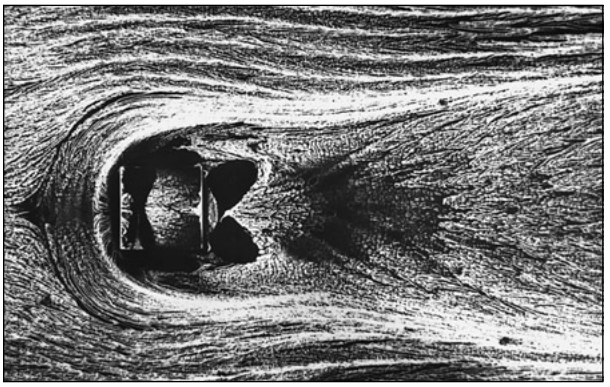
Fig. 8.36 CFD results for water flow past an NASA 66(MOD) hydrofoil [*from Ref 28, with permission of the American Society of Mechanical Engineers*]: (*a*) C gridding, 262 by 91 nodes; (*b*) surface pressures at $\alpha = 1°$.

compared eight different commercial-code calculations (FLOW-3D, FLOTRAN, STAR-CD, N3S, CFD-ACE, FLUENT, CFDS-FLOW3D, and NISA/3D-FLUID) with experimental results for five benchmark flow experiments. Calculations were made by the vendors themselves. Freitas concludes that commercial codes, though promising in general, can be inaccurate for certain laminar- and turbulent-flow situations. Further research is recommended before engineers can truly rely upon such software to give generally accurate fluid-flow predictions.

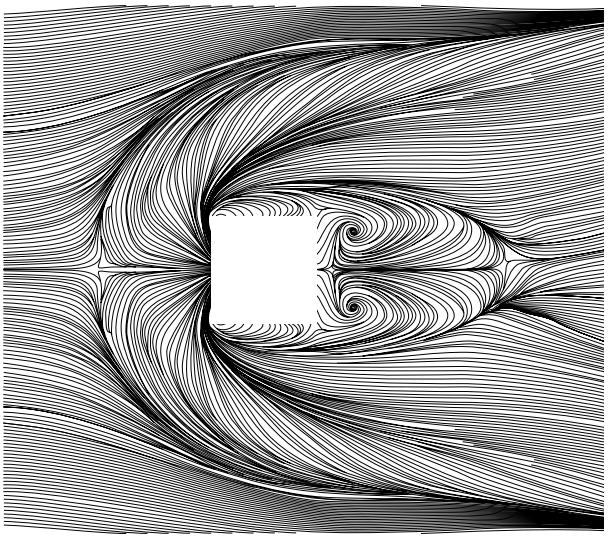
In spite of the above warning to treat CFD codes with care, one should also realize that the results of a given CFD simulation can be spectacular. Figure turbulent flow past a cube mounted on the floor of a channel whose



ketabline.com Ebook.ketabline.com



(*a*)



(*b*)



(*c*)

Fig. 8.37 Flow over a surface-mounted cube creates a complex and perhaps unexpected pattern: (*a*) experimental oil-streak visualization of surface flow at Re = 40,000 (based on cube height) (*from Ref. 31, courtesy of Robert Martinuzzi, with the permission of the American Society of Mechanical Engineers*); (*b*) computational large-eddy simulation of the surface flow in (*a*) (*from Ref. 32, courtesy of Kishan Shah, Stanford University*); and (*c*) a side view of the flow in (*a*) visualized by smoke generation and a laser light sheet (*from Ref. 31, courtesy of Robert Martinuzzi, with the permission of the American Society of Mechanical Engineers*).



ketabline.com Ebook.ketabline.com

the cube height. Compare Fig. 8.37*a*, a top view of the experimental surface flow [31] as visualized by oil streaks, with Fig. 8.37*b*, a CFD supercomputer result using the method of large-eddy simulation [32, 33]. The agreement is remarkable. The C-shaped flow pattern in front of the cube is caused by formation of a horseshoe vortex, as seen in a side view of the experiment [31] in Fig. 8.37*c*. Horseshoe vortices commonly result when surface shear flows meet an obstacle. We conclude that CFD has a tremendous potential for flow prediction.

Summary

This chapter has analyzed a highly idealized but very useful type of flow: inviscid, incompressible, irrotational flow, for which Laplace's equation holds for the velocity potential (8.1) and for the plane stream function (8.7). The mathematics is well developed, and solutions of potential flows can be obtained for practically any body shape.

Some solution techniques outlined here are (1) superposition of elementary line or point solutions in both plane and axisymmetric flow, (2) the analytic functions of a complex variable, (3) use of variable-strength vortex sheets, and (4) numerical analysis on a digital computer. Potential theory is especially useful and accurate for thin bodies such as airfoils. The only requirement is that the boundary layer be thin, i.e., that the Reynolds number be large.

For blunt bodies or highly divergent flows, potential theory serves as a first approximation, to be used as input to a boundary-layer analysis. The reader should consult the advanced texts [for example, 2 to 4, 10 to 13] for further applications of potential theory. Section 8.9 discusses computational methods for viscous (nonpotential) flows.

Problems

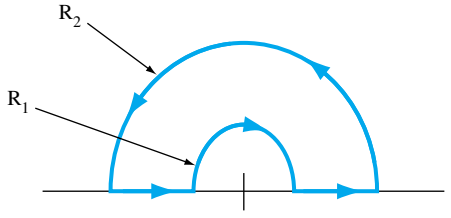
Most of the problems herein are fairly straightforward. More difficult or open-ended assignments are labeled with an asterisk. Problems labeled with an EES icon will benefit from the use of the Engineering Equation Solver (EES), while problems labeled with a computer disk may require the use of a computer. The standard end-of-chapter problems 8.1 to 8.115 (categorized in the problem list below) are followed by word problems W8.1 to W8.7, comprehensive problems C8.1 to C8.3, and design projects D8.1 to D8.3.

Problem Distribution

Section	Topic	Problems
8.1	Introduction and review	8.1–8.7
8.2	Elementary plane-flow solutions	8.8–8.17
8.3	Superposition of plane flows	8.18–8.34
8.4	Plane flow past closed-body shapes	8.35–8.59
8.5	The complex potential	8.60–8.71
8.6	Images	8.72–8.79
8.7	Airfoil theory: Two-dimensional	8.80–8.84
8.7	Airfoil theory: Finite-span wings	8.85–8.90
8.8	Axisymmetric potential flow	8.91–8.103
8.8	Hydrodynamic mass	8.104–8.105
8.9	Numerical methods	8.106–8.115

P8.1 Prove that the streamlines $\psi(r, \theta)$ in polar coordinates from Eqs. (8.10) are orthogonal to the potential lines $\phi(r, \theta)$.

P8.2 The steady plane flow in Fig. P8.2 has the polar velocity components $v_\theta = \Omega r$ and $v_r = 0$. Determine the circulation Γ around the path shown.

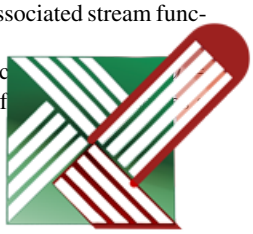


P8.2

P8.3 Using cartesian coordinates, show that each velocity component (u, v, w) of a potential flow satisfies Laplace's equation separately.

P8.4 Is the function $1/r$ a legitimate velocity potential in plane polar coordinates? If so, what is the associated stream function $\psi(r, \theta)$?

P8.5 Consider the two-dimensional veloc
$-By$, $v = Bx$, where B is a constant. If



ketabline.com Ebook.ketabline.com

stream function, find its form. If it has a velocity potential, find that also. Compute the local angular velocity of the flow, if any, and describe what the flow might represent.

P8.6 An incompressible flow has the velocity potential $\phi = 2Bxy$, where B is a constant. Find the stream function of this flow, sketch a few streamlines, and interpret the pattern.

P8.7 Consider a flow with constant density and viscosity. If the flow possesses a velocity potential as defined by Eq. (8.1), show that it exactly satisfies the full Navier-Stokes equations (4.38). If this is so, why for inviscid theory do we back away from the full Navier-Stokes equations?

P8.8 For the velocity distribution of Prob. 8.5, evaluate the circulation Γ around the rectangular closed curve defined by $(x, y) = (1, 1)$, $(3, 1)$, $(3, 2)$, and $(1, 2)$. Interpret your result, especially vis-à-vis the velocity potential.

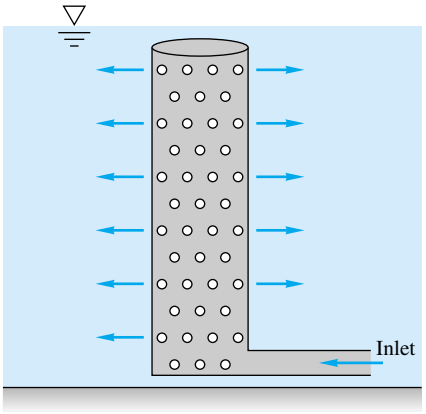
P8.9 Consider the two-dimensional flow $u = -Ax$, $v = Ay$, where A is a constant. Evaluate the circulation Γ around the rectangular closed curve defined by $(x, y) = (1, 1)$, $(4, 1)$, $(4, 3)$, and $(1, 3)$. Interpret your result, especially vis-à-vis the velocity potential.

P8.10 A mathematical relation sometimes used in fluid mechanics is the theorem of Stokes [1]

$$\oint_C \mathbf{V} \cdot d\mathbf{s} = \int_A \int (\nabla \times \mathbf{V}) \cdot \mathbf{n}\, dA$$

where A is any surface and C is the curve enclosing that surface. The vector $d\mathbf{s}$ is the differential arc length along C, and $\mathbf{n}$ is the unit outward normal vector to A. How does this relation simplify for irrotational flow, and how does the resulting line integral relate to velocity potential?

P8.11 A power plant discharges cooling water through the manifold in Fig. P8.11, which is 55 cm in diameter and 8 m high and is perforated with 25,000 holes 1 cm in diameter. Does this manifold simulate a line source? If so, what is the equivalent source strength m?



P8.11

P8.12 Consider the flow due to a vortex of strength K at the origin. Evaluate the circulation from Eq. (8.15) about the clockwise path from $(r, \theta) = (a, 0)$ to $(2a, 0)$ to $(2a, 3\pi/2)$ to $(a, 3\pi/2)$ and back to $(a, 0)$. Interpret the result.

P8.13 A well-known exact solution to the Navier-Stokes equations (4.38) is the unsteady circulating motion [15]

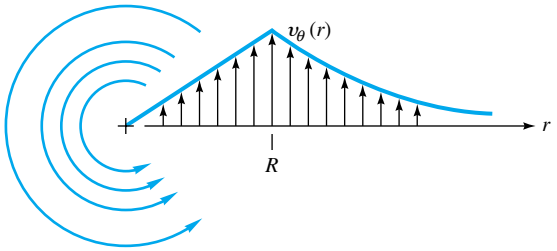
$$v_\theta = \frac{K}{2\pi r}\left[1 - \exp\left(-\frac{r^2}{4\nu t}\right)\right] \qquad v_r = v_z = 0$$

where K is a constant and ν is the kinematic viscosity. Does this flow have a polar-coordinate stream function and/or velocity potential? Explain. Evaluate the circulation Γ for this motion, plot it versus r for a given finite time, and interpret compared to ordinary line vortex motion.

P8.14 A tornado may be modeled as the circulating flow shown in Fig. P8.14, with $v_r = v_z = 0$ and $v_\theta(r)$ such that

$$v_\theta = \begin{cases} \omega r & r \le R \\ \dfrac{\omega R^2}{r} & r > R \end{cases}$$

Determine whether this flow pattern is irrotational in either the inner or outer region. Using the r-momentum equation (D.5) of App. D, determine the pressure distribution $p(r)$ in the tornado, assuming $p = p_\infty$ as $r \to \infty$. Find the location and magnitude of the lowest pressure.

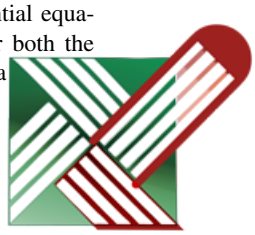


P8.14

P8.15 Evaluate Prob. 8.14 for the particular case of a small-scale tornado, $R = 100$ m, $v_{\theta,\max} = 65$ m/s, with sea-level conditions at $r = \infty$. Plot $p(r)$ out to $r = 400$ m.

P8.16 Consider inviscid stagnation flow, $\psi = Kxy$ (see Fig. 8.15*b*) superimposed with a source at the origin of strength m. Plot the resulting streamlines in the upper half plane, using the length scale $a = (m/K)^{1/2}$. Give a physical interpretation of the flow pattern.

P8.17 Examine the flow of Fig. 8.30 as an *analytical* (not a numerical) problem. Give the appropriate differential equation and the complete boundary conditions for both the stream function and the velocity potential. Is a series solution possible?



ketabline.com Ebook.ketabline.com

P8.18 Plot the streamlines and potential lines of the flow due to a line source of strength m at $(a, 0)$ plus a source $3m$ at $(-a, 0)$. What is the flow pattern viewed from afar?

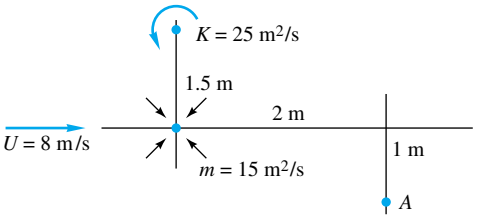
P8.19 Plot the streamlines and potential lines of the flow due to a line source of strength $3m$ at $(a, 0)$ plus a sink $-m$ at $(-a, 0)$. What is the pattern viewed from afar?

P8.20 Plot the streamlines of the flow due to a line vortex $+K$ at $(0, +a)$ and a vortex $-K$ at $(0, -a)$. What is the pattern viewed from afar?

P8.21 Plot the streamlines of the flow due to a line vortex $+K$ at $(+a, 0)$ and a vortex $-2K$ at $(-a, 0)$. What is the pattern viewed from afar?

P8.22 Plot the streamlines of a uniform stream $\mathbf{V} = \boldsymbol{i}U$ plus a clockwise line vortex $-K$ located at the origin. Are there any stagnation points?

P8.23 Find the resultant velocity vector induced at point A in Fig. P8.23 by the uniform stream, vortex, and line source.



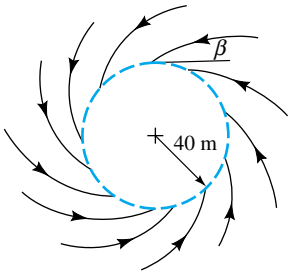
P8.23

P8.24 Line sources of equal strength $m = Ua$, where U is a reference velocity, are placed at $(x, y) = (0, a)$ and $(0, -a)$. Sketch the stream and potential lines in the upper half plane. Is $y = 0$ a "wall"? If so, sketch the pressure coefficient

$$C_p = \frac{p - p_0}{\frac{1}{2}\rho U^2}$$

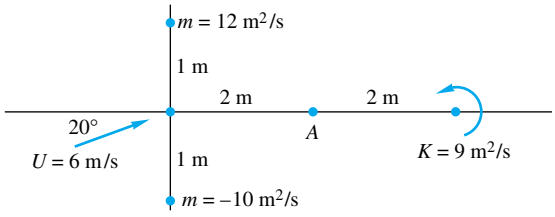
along the wall, where p_0 is the pressure at $(0, 0)$. Find the minimum pressure point and indicate where flow separation might occur in the boundary layer.

P8.25 Let the vortex/sink flow of Eq. (4.134) simulate a tornado as in Fig. P8.25. Suppose that the circulation about the tornado is $\Gamma = 8500$ m^2/s and that the pressure at $r = 40$ m is 2200 Pa less than the far-field pressure. Assuming inviscid flow at sea-level density, estimate (a) the appropriate sink strength $-m$, (b) the pressure at $r = 15$ m, and (c) the angle β at which the streamlines cross the circle at $r = 40$ m (see Fig. P8.25).



P8.25

P8.26 Find the resultant velocity vector induced at point A in Fig. P8.26 by the uniform stream, line source, line sink, and vortex.



P8.26

P8.27 A counterclockwise line vortex of strength $3K$ at $(x, y) = (0, a)$ is combined with a clockwise vortex K at $(0, -a)$. Plot the streamline and potential-line pattern, and find the point of minimum velocity between the two vortices.

P8.28 Sources of equal strength m are placed at the four symmetric positions $(x, y) = (a, a)$, $(-a, a)$, $(-a, -a)$, and $(a, -a)$. Sketch the streamline and potential-line patterns. Do any plane "walls" appear?

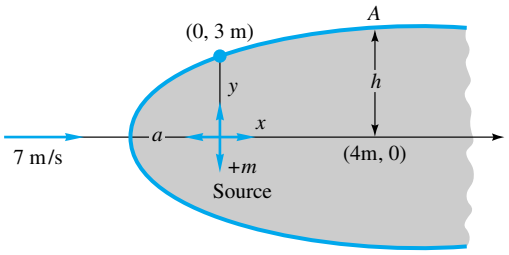
P8.29 A uniform water stream, $U_\infty = 20$ m/s and $\rho = 998$ kg/m^3, combines with a source at the origin to form a half-body. At $(x, y) = (0, 1.2$ m$)$, the pressure is 12.5 kPa less than p_∞. (a) Is this point outside the body? Estimate (b) the appropriate source strength m and (c) the pressure at the nose of the body.

P8.30 Suppose that the total discharge from the manifold in Fig. P8.11 is 450 m^3/s and that there is a uniform ocean current of 60 cm/s to the right. Sketch the flow pattern from above, showing the dimensions and the region where the cooling-water discharge is confined.

P8.31 A Rankine half-body is formed as shown in Fig. P8.31. For the stream velocity and body dimension shown, compute (a) the source strength m in m
a, (c) the distance h, and (d) the tota



ketabline.com Ebook.ketabline.com



P8.31

P8.32 Sketch the streamlines, especially the body shape, due to equal line sources $+m$ at $(-a, 0)$ and $(+a, 0)$ plus a uniform stream $U_\infty = ma$.

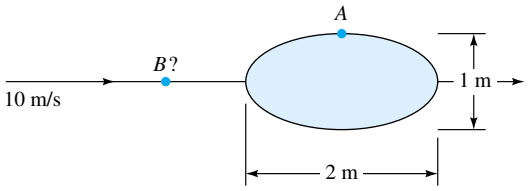
P8.33 Sketch the streamlines, especially the body shape, due to equal line sources $+m$ at $(0, +a)$ and $(0, -a)$ plus a uniform stream $U_\infty = ma$.

P8.34 Consider three equally spaced sources of strength m placed at $(x, y) = (0, +a)$, $(0, 0)$, and $(0, -a)$. Sketch the resulting streamlines, noting the position of any stagnation points. What would the pattern look like from afar?

P8.35 Consider three equal sources m in a triangular configuration: one at $(a/2, 0)$, one at $(-a/2, 0)$, and one at $(0, a)$. Plot the streamlines for this flow. Are there any stagnation points? *Hint*: Try the MATLAB contour command [34].

P8.36 When a line source-sink pair with $m = 2$ m^2/s is combined with a uniform stream, it forms a Rankine oval whose minimum dimension is 40 cm. If $a = 15$ cm, what are the stream velocity and the velocity at the shoulder? What is the maximum dimension?

P8.37 A Rankine oval 2 m long and 1 m high is immersed in a stream $U_\infty = 10$ m/s, as in Fig. P8.37. Estimate (a) the velocity at point A and (b) the location of point B where a particle approaching the stagnation point achieves its maximum deceleration.



P8.37

P8.38 A uniform stream U in the x direction combines with a source m at $(a, 0)$ and a sink $-m$ at $(-a, 0)$. Plot the resulting streamlines and note any stagnation points.

P8.39 Sketch the streamlines of a uniform stream U_∞ past a line source-sink pair aligned vertically with the source at $+a$ and the sink at $-a$ on the y-axis. Does a closed-body shape form?

P8.40 Consider a uniform stream U_∞ plus line sources $+m$ at $(x, y) = (+a, 0)$ and $(-a, 0)$ and a single line sink $-2m$ at the origin. Does a closed-body shape appear? If so, plot its shape for $m/(U_\infty a)$ equal to (a) 1.0 and (b) 5.0.

P8.41 A Kelvin oval is formed by a line-vortex pair with $K = 9$ m^2/s, $a = 1$ m, and $U = 10$ m/s. What are the height, width, and shoulder velocity of this oval?

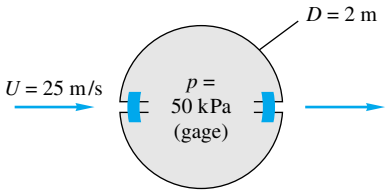
P8.42 For what value of $K/(U_\infty a)$ does the velocity at the shoulder of a Kelvin oval equal $4U_\infty$? What is the height h/a of this oval?

P8.43 Consider water at 20°C flowing at 6 m/s past a 1-m-diameter circular cylinder. What doublet strength λ in m^3/s is required to simulate this flow? If the stream pressure is 200 kPa, use inviscid theory to estimate the surface pressure at θ equal to (a) 180°, (b) 135°, and (c) 90°.

P8.44 Suppose that circulation is added to the cylinder flow of Prob. 8.43 sufficient to place the stagnation points at θ equal to 50° and 130°. What is the required vortex strength K in m^2/s? Compute the resulting pressure and surface velocity at (a) the stagnation points and (b) the upper and lower shoulders. What will the lift per meter of cylinder width be?

P8.45 What circulation K must be added to the cylinder flow in Prob. 8.43 to place the stagnation point exactly at the upper shoulder? What will the velocity and pressure at the lower shoulder be then? What value of K causes the lower shoulder pressure to be 10 kPa?

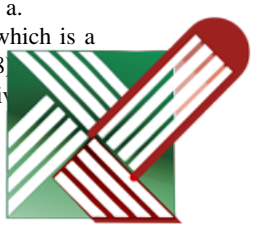
P8.46 A cylinder is formed by bolting two semicylindrical channels together on the inside, as shown in Fig. P8.46. There are 10 bolts per meter of width on each side, and the inside pressure is 50 kPa (gage). Using potential theory for the outside pressure, compute the tension force in each bolt if the fluid outside is sea-level air.



P8.46

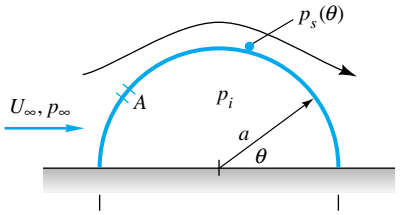
P8.47 A circular cylinder is fitted with two surface-mounted pressure sensors, to measure p_a at $\theta = 180°$ and p_b at $\theta = 105°$. The intention is to use the cylinder as a stream velocimeter. Using inviscid theory, derive a formula for estimating U_∞ in terms of p_a, p_b, ρ, and the cylinder radius a.

***P8.48** Wind at U_∞ and p_∞ flows past a Quonset hut which is a half-cylinder of radius a and length L (Fig. P8.48). Internal pressure is p_i. Using inviscid theory, deri



ketabline.com Ebook.ketabline.com

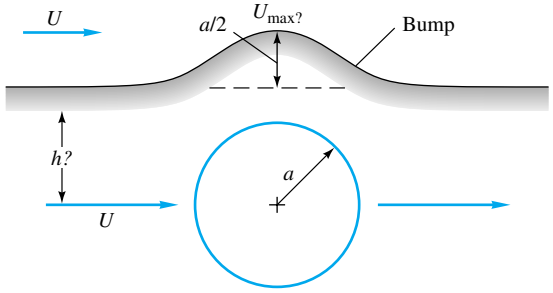
pression for the upward force on the hut due to the difference between p_i and p_s.



P8.48

P8.49 In strong winds the force in Prob. 8.48 can be quite large. Suppose that a hole is introduced in the hut roof at point A to make p_i equal to the surface pressure there. At what angle θ should hole A be placed to make the net wind force zero?

P8.50 It is desired to simulate flow past a two-dimensional ridge or bump by using a streamline which passes above the flow over a cylinder, as in Fig. P8.50. The bump is to be $a/2$ high, where a is the cylinder radius. What is the elevation h of this streamline? What is U_{max} on the bump compared with stream velocity U?



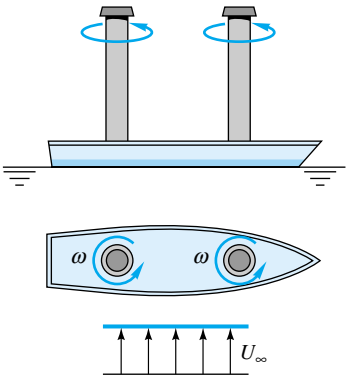
P8.50

P8.51 Modify Prob. 8.50 as follows. Let the bump be such that $U_{max} = 1.5U$. Find (*a*) the upstream elevation h and (*b*) the height of the bump.

P8.52 The Flettner rotor sailboat in Fig. E8.2 has a water drag coefficient of 0.006 based on a wetted area of 45 ft^2. If the rotor spins at 220 r/min, find the maximum boat velocity that can be achieved in a 15-mi/h wind. What is the optimum angle between the boat and the wind?

P8.53 Modify Prob. 8.52 as follows. For the same sailboat data, find the wind velocity, in mi/h, which will drive the boat at an optimum speed of 10 kn parallel to its keel.

P8.54 The original Flettner rotor ship was approximately 100 ft long, displaced 800 tons, and had a wetted area of 3500 ft^2. As sketched in Fig. P8.54, it had two rotors 50 ft high and 9 ft in diameter rotating at 750 r/min, which is far outside the range of Fig. 8.11. The measured lift and drag coefficients for each rotor were about 10 and 4, respectively. If the ship is moored and subjected to a crosswind of 25 ft/s, as in Fig. P8.54, what will the wind force parallel and normal to the ship centerline be? Estimate the power required to drive the rotors.



P8.54

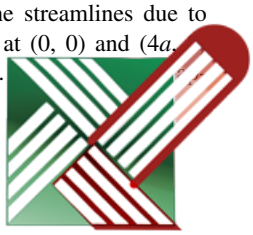
P8.55 Assume that the Flettner rotorship of Fig. P8.54 has a water resistance coefficient of 0.005. How fast will the ship sail in seawater at 20°C in a 20-ft/s wind if the keel aligns itself with the resultant force on the rotors? *Hint:* This is a problem in relative velocities.

P8.56 The measured drag coefficient of a cylinder in crossflow, based on frontal area DL, is approximately 1.0 for the laminar-boundary-layer range (see Fig. 7.16*a*). Boundary-layer separation occurs near the shoulder (see Fig. 7.13*a*). This suggests an analytical model: the standard inviscid-flow solution on the front of the cylinder and constant pressure (equal to the shoulder value) on the rear. Use this model to predict the drag coefficient and comment on the results with reference to Fig. 7.13*c*.

P8.57 In principle, it is possible to use rotating cylinders as aircraft wings. Consider a cylinder 30 cm in diameter, rotating at 2400 r/min. It is to lift a 55-kN airplane cruising at 100 m/s. What should the cylinder length be? How much power is required to maintain this speed? Neglect end effects on the rotating wing.

P8.58 Plot the streamlines due to the combined flow of a line sink $-m$ at the origin plus line sources $+m$ at (a, 0) and ($4a$, 0). *Hint:* A cylinder of radius $2a$ will appear.

P8.59 By analogy with Prob. 8.58 plot the streamlines due to counterclockwise line vortices $+K$ at (0, 0) and ($4a$, plus a clockwise vortex $-K$ at (a, 0). pears.



ketabline.com Ebook.ketabline.com

P8.60 One of the corner-flow patterns of Fig. 8.15 is given by the cartesian stream function $\psi = A(3yx^2 - y^3)$. Which one? Can the correspondence be proved from Eq. (8.49)?

P8.61 Plot the streamlines of Eq. (8.49) in the upper right quadrant for $n = 4$. How does the velocity increase with x outward along the x-axis from the origin? For what corner angle and value of n would this increase be linear in x? For what corner angle and n would the increase be as x^5?

P8.62 Combine stagnation flow, Fig. 8.14*b*, with a source at the origin:

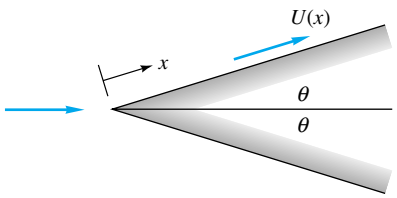
$$f(z) = Az^2 + m \ln z$$

Plot the streamlines for $m = AL^2$, where L is a length scale. Interpret.

P8.63 The superposition in Prob. 8.62 leads to stagnation flow near a curved bump, in contrast to the flat wall of Fig. 8.14*b*. Determine the maximum height H of the bump as a function of the constants A and m.

P8.64 Determine qualitatively from boundary-layer theory (Chap. 7) whether any of the three stagnation-flow patterns of Fig. 8.15 can suffer flow separation along the walls.

P8.65 Potential flow past a wedge of half-angle θ leads to an important application of laminar-boundary-layer theory called the *Falkner-Skan flows* [15, pp. 242–247]. Let x denote distance along the wedge wall, as in Fig. P8.65, and let $\theta = 10°$. Use Eq. (8.49) to find the variation of surface velocity $U(x)$ along the wall. Is the pressure gradient adverse or favorable?



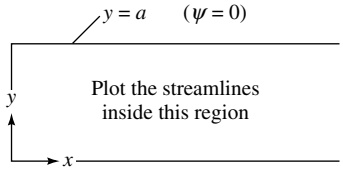
P8.65

***P8.66** The inviscid velocity along the wedge in Prob. 8.65 has the analytic form $U(x) = Cx^m$, where $m = n - 1$ and n is the exponent in Eq. (8.49). Show that, for any C and n, computation of the boundary layer by Thwaites' method, Eqs. (7.53) and (7.54), leads to a unique value of the Thwaites parameter λ. Thus wedge flows are called *similar* [15, p. 244].

P8.67 Investigate the complex potential function $f(z) = U_\infty(z + a^2/z)$ and interpret the flow pattern.

P8.68 Investigate the complex potential function $f(z) = U_\infty z + m \ln [(z + a)/(z - a)]$ and interpret the flow pattern.

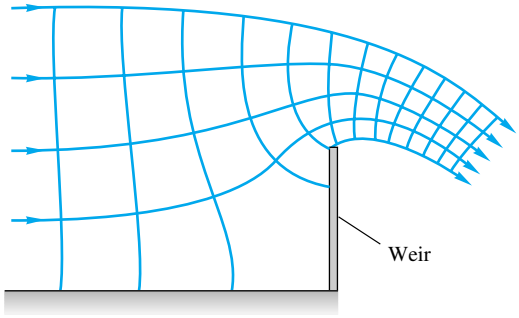
P8.69 Investigate the complex potential $f(z) = A \cosh [\pi(z/a)]$, and plot the streamlines inside the region shown in Fig. P8.69. What hyphenated word (originally French) might describe such a flow pattern?



P8.69

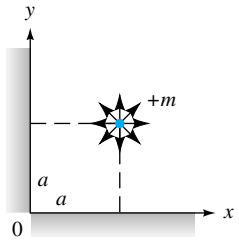
P8.70 Show that the complex potential $f = U_\infty\{z + \frac{1}{4}a \coth [\pi(z/a)]\}$ represents flow past an oval shape placed midway between two parallel walls $y = \pm\frac{1}{2}a$. What is a practical application?

P8.71 Figure P8.71 shows the streamlines and potential lines of flow over a thin-plate weir as computed by the complex potential method. Compare qualitatively with Fig. 10.16*a*. State the proper boundary conditions at all boundaries. The velocity potential has equally spaced values. Why do the flow-net "squares" become smaller in the overflow jet?



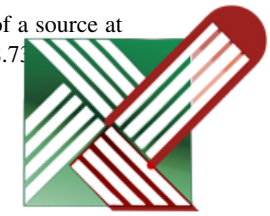
P8.71

P8.72 Use the method of images to construct the flow pattern for a source + m near two walls, as shown in Fig. P8.72. Sketch the velocity distribution along the lower wall ($y = 0$). Is there any danger of flow separation along this wall?

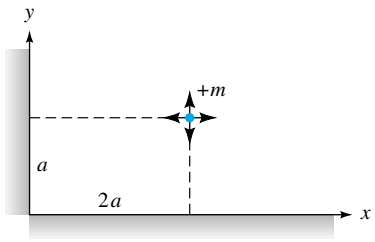


P8.72

P8.73 Set up an image system to compute the flow of a source at unequal distances from two walls, as in Fig. P8.7
point of maximum velocity on the y-axis.

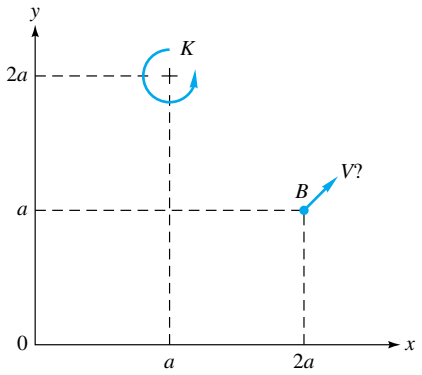


ketabline.com Ebook.ketabline.com



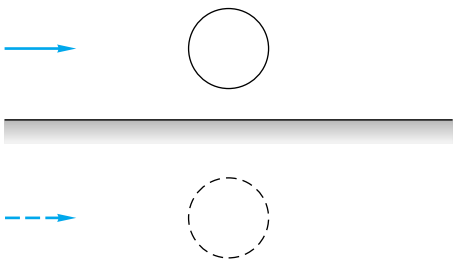
P8.73

P8.74 A positive line vortex K is trapped in a corner, as in Fig. P8.74. Compute the total induced velocity vector at point B, $(x, y) = (2a, a)$, and compare with the induced velocity when no walls are present.



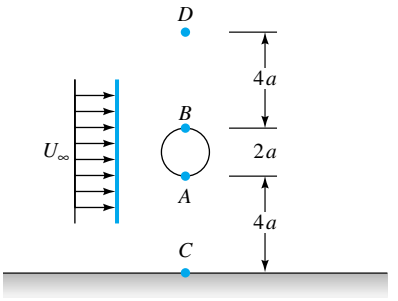
P8.74

P8.75 The flow past a cylinder very near a wall might be simulated by doublet images, as in Fig. P8.75. Explain why the result is not very successful and the cylinder shape becomes badly distorted.



P8.75

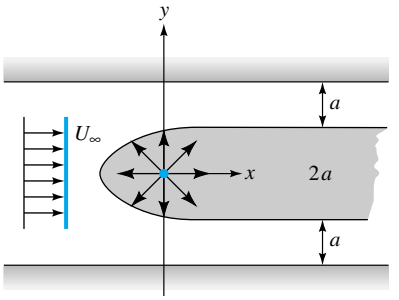
P8.76 Use the method of images to approximate the flow pattern past a cylinder a distance $4a$ from a single wall, as in Fig. P8.76. To illustrate the effect of the wall, compute the velocities at corresponding points A, B and C, D, comparing with a cylinder flow in an infinite expanse of fluid.



P8.76

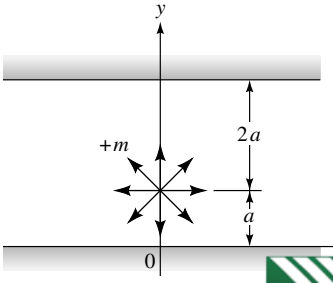
P8.77 Discuss how the flow pattern of Prob. 8.58 might be interpreted to be an image-system construction for circular walls. Why are there two images instead of one?

***P8.78** Indicate the system of images needed to construct the flow of a uniform stream past a Rankine half-body constrained between two parallel walls, as in Fig. P8.78. For the particular dimensions shown in this figure, estimate the position of the nose of the resulting half-body.

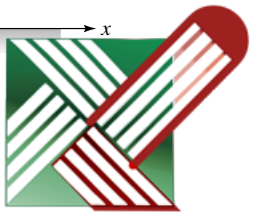


P8.78

P8.79 Explain the system of images needed to simulate the flow of a line source placed unsymmetrically between two parallel walls as in Fig. P8.79. Compute the velocity on the lower wall at $x = a$. How many images are needed to estimate this velocity within 1 percent?



P8.79



ketabline.com Ebook.ketabline.com

***P8.80** The beautiful expression for lift of a two-dimensional airfoil, Eq. (8.69), arose from applying the Joukowski transformation, $\zeta = z + a^2/z$, where $z = x + iy$ and $\zeta = \eta + i\beta$. The constant a is a length scale. The theory transforms a certain circle in the z plane into an airfoil in the ζ plane. Taking $a = 1$ unit for convenience, show that (*a*) a circle with center at the origin and radius > 1 will become an ellipse in the ζ plane and (*b*) a circle with center at $x = -\epsilon \ll 1$, $y = 0$, and radius $(1 + \epsilon)$ will become an airfoil shape in the ζ plane. *Hint*: The Excel spreadsheet is excellent for solving this problem.

P8.81 A two-dimensional airfoil has 2 percent camber and 10 percent thickness. If $C = 1.75$ m, estimate its lift per meter when immersed in 20°C water at $\alpha = 6°$ and $U = 18$ m/s.

P8.82 The ultralight plane *Gossamer Condor* in 1977 was the first to complete the Kremer Prize figure-eight course under human power. Its wingspan was 29 m, with $C_{av} = 2.3$ m and a total mass of 95 kg. The drag coefficient was approximately 0.05. The pilot was able to deliver $\frac{1}{4}$ hp to propel the plane. Assuming two-dimensional flow at sea level, estimate (*a*) the cruise speed attained, (*b*) the lift coefficient, and (*c*) the horsepower required to achieve a speed of 15 kn.

P8.83 Two-dimensional lift-drag data for the NACA 2412 airfoil with 2 percent camber (from Ref. 12) may be curve-fitted accurately as follows:

$$C_L \approx 0.178 + 0.109\alpha - 0.00109\alpha^2$$

$$C_D \approx 0.0089 + 1.97\text{ E-}4\ \alpha + 8.45\text{ E-}5\ \alpha^2 - 1.35\text{ E-}5\ \alpha^3 + 9.92\text{ E-}7\ \alpha^4$$

with α in degrees in the range $-4° < \alpha < +10°$. Compare (*a*) the lift-curve slope and (*b*) the angle of zero lift with theory, Eq. (8.69). (*c*) Prepare a polar lift-drag plot and compare with Fig. 7.26.

P8.84  Reference 12 contains inviscid-theory calculations for the upper and lower surface velocity distributions $V(x)$ over an airfoil, where x is the chordwise coordinate. A typical result for small angle of attack is as follows:

x/c	*V/U∞(upper)*	*V/U∞(lower)*
0.0	0.0	0.0
0.025	0.97	0.82
0.05	1.23	0.98
0.1	1.28	1.05
0.2	1.29	1.13
0.3	1.29	1.16
0.4	1.24	1.16
0.6	1.14	1.08
0.8	0.99	0.95
1.0	0.82	0.82

Use these data, plus Bernoulli's equation, to estimate (*a*) the lift coefficient and (*b*) the angle of attack if the airfoil is symmetric.

P8.85 A wing of 2 percent camber, 5-in chord, and 30-in span is tested at a certain angle of attack in a wind tunnel with sea-level standard air at 200 ft/s and is found to have lift of 30 lbf and drag of 1.5 lbf. Estimate from wing theory (*a*) the angle of attack, (*b*) the minimum drag of the wing and the angle of attack at which it occurs, and (*c*) the maximum lift-to-drag ratio.

P8.86 An airplane has a mass of 20,000 kg and flies at 175 m/s at 5000-m standard altitude. Its rectangular wing has a 3-m chord and a symmetric airfoil at 2.5° angle of attack. Estimate (*a*) the wing span, (*b*) the aspect ratio, and (*c*) the induced drag.

P8.87 A freshwater boat of mass 400 kg is supported by a rectangular hydrofoil of aspect ratio 8, 2 percent camber, and 12 percent thickness. If the boat travels at 8 m/s and $\alpha = 3.5°$, estimate (*a*) the chord length, (*b*) the power required if $C_{D_\infty} = 0.01$, and (*c*) the top speed if the boat is refitted with an engine which delivers 50 hp to the water.

P8.88  The Boeing 727 airplane has a gross weight of 125,000 lbf, a wing area of 1200 ft^2, and an aspect ratio of 6. It is fitted with two turbofan engines and cruises at 532 mi/h at 30,000-ft standard altitude. Assume for this problem that its airfoil is the NACA 2412 section described in Prob. 8.83. If we neglect all drag except the wing, what thrust is required from each engine for these conditions?

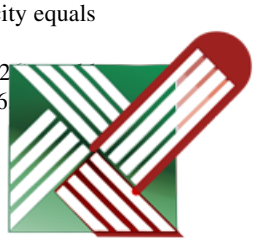
P8.89 The Beechcraft T-34C aircraft has a gross weight of 5500 lbf and a wing area of 60 ft^2 and flies at 322 mi/h at 10,000-ft standard altitude. It is driven by a propeller which delivers 300 hp to the air. Assume for this problem that its airfoil is the NACA 2412 section described in Prob. 8.83, and neglect all drag except the wing. What is the appropriate aspect ratio for the wing?

P8.90 When moving at 15 m/s in seawater at its maximum lift-to-drag ratio of 18:1, a symmetric hydrofoil, of plan area 3 m^2, develops a lift of 120 kN. Estimate from wing theory (*a*) the aspect ratio and (*b*) the angle of attack in degrees.

P8.91 If $\phi(r, \theta)$ in axisymmetric flow is defined by Eq. (8.85) and the coordinates are given in Fig. 8.24, determine what partial differential equation is satisfied by ϕ.

P8.92 A point source with volume flow $Q = 30$ m^3/s is immersed in a uniform stream of speed 4 m/s. A Rankine half-body of revolution results. Compute (*a*) the distance from source to the stagnation point and (*b*) the two points (r, θ) on the body surface where the local velocity equals 4.5 m/s.

P8.93 The Rankine half-body of revolution (Fig. 8.2 simulate the shape of a pitot-static tube (Fig. 6

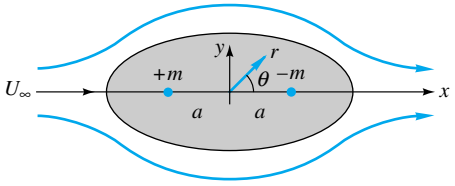


ketabline.com Ebook.ketabline.com

cording to inviscid theory, how far downstream from the nose should the static pressure holes be placed so that the local velocity is within ±0.5 percent of U_∞? Compare your answer with the recommendation $x \approx 8D$ in Fig. 6.30.

P8.94 Determine whether the Stokes streamlines from Eq. (8.86) are everywhere orthogonal to the Stokes potential lines from Eq. (8.87), as is the case for cartesian and plane polar coordinates.

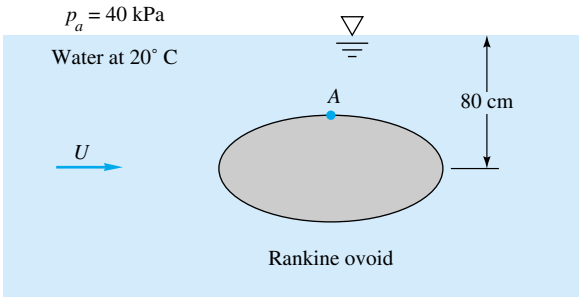
P8.95 Show that the-axisymmetric potential flow formed by superposition of a point source $+m$ at $(x, y) = (-a, 0)$, a point sink $-m$ at $(+a, 0)$, and a stream U_∞ in the x direction forms a Rankine body of revolution as in Fig. P8.95. Find analytic expressions for determining the length $2L$ and maximum diameter $2R$ of the body in terms of m, U_∞, and a.



P8.95

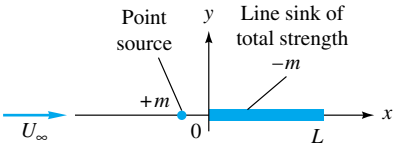
P8.96 Suppose that a sphere with a single stagnation hole is to be used as a velocimeter. The pressure at this hole is used to compute the stream velocity, but there are errors if the hole is not perfectly aligned with the oncoming stream. Using inviscid incompressible theory, plot the percent error in stream velocity estimate as a function of misalignment angle ϕ. At what angle is the error 10 percent?

P8.97 The Rankine body of revolution in Fig. P8.97 is 60 cm long and 30 cm in diameter. When it is immersed in the low-pressure water tunnel as shown, cavitation may appear at point A. Compute the stream velocity U, neglecting surface wave formation, for which cavitation occurs.



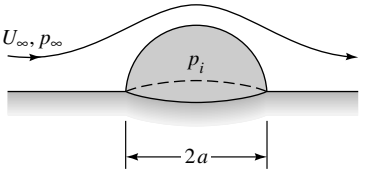
P8.97

P8.98 We have studied the point source (sink) and the line source (sink) of infinite depth into the paper. Does it make any sense to define a finite-length line sink (source) as in Fig. P8.98? If so, how would you establish the mathematical properties of such a finite line sink? When combined with a uniform stream and a point source of equivalent strength as in Fig. P8.98, should a closed-body shape be formed? Make a guess and sketch some of these possible shapes for various values of the dimensionless parameter $m/(U_\infty L^2)$.



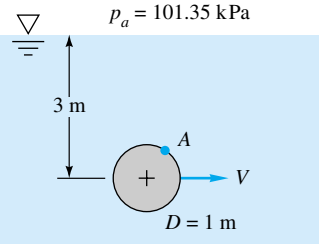
P8.98

***P8.99** Consider air flowing past a hemisphere resting on a flat surface, as in Fig. P8.99. If the internal pressure is p_i, find an expression for the pressure force on the hemisphere. By analogy with Prob. 8.49, at what point A on the hemisphere should a hole be cut so that the pressure force will be zero according to inviscid theory?



P8.99

P8.100 A 1-m-diameter sphere is being towed at speed V in fresh water at 20°C as shown in Fig. P8.100. Assuming inviscid theory with an undistorted free surface, estimate the speed V in m/s at which cavitation will first appear on the sphere surface. Where will cavitation appear? For this condition, what will be the pressure at point A on the sphere which is 45° up from the direction of travel?



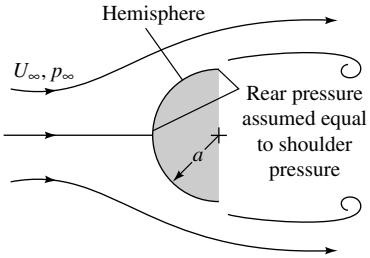
P8.100

P8.101 Normally by its very nature inviscid theory is incapable predicting body drag, but by analogy can analyze flow approaching a he



ketabline.com Ebook.ketabline.com

P8.101. Assume that the flow on the front follows inviscid sphere theory, Eq. (8.96), and the pressure in the rear equals the shoulder pressure. Compute the drag coefficient and compare with experiment (Table 7.3). What are the defects and limitations of this analysis?

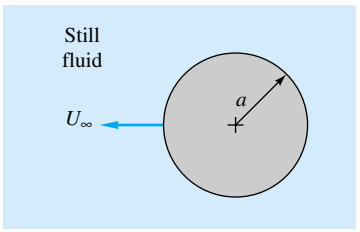


P8.101

P8.102 A golf ball weighs 0.102 lbf and has a diameter of 1.7 in. A professional golfer strikes the ball at an initial velocity of 250 ft/s, an upward angle of 20°, and a backspin (front of the ball rotating upward). Assume that the lift coefficient on the ball (based on frontal area) follows Fig. P7.108. If the ground is level and drag is neglected, make a simple analysis to predict the impact point (*a*) without spin and (*b*) with backspin of 7500 r/min.

P8.103 Modify Prob. 8.102 as follows. Golf balls are dimpled, not smooth, and have higher lift and lower drag ($C_L \approx 0.2$ and $C_D \approx 0.3$ for typical backspin). Using these values, make a computer analysis of the ball trajectory for the initial conditions of Prob. 8.102. If time permits, investigate the effect of initial angle for the range $10° < \theta_0 < 50°$.

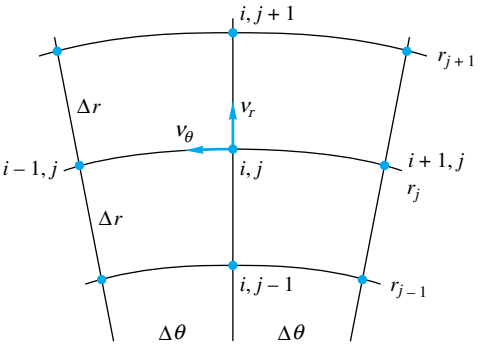
P8.104 Consider a cylinder of radius a moving at speed U_∞ through a still fluid, as in Fig. P8.104. Plot the streamlines relative to the cylinder by modifying Eq. (8.32) to give the relative flow with $K = 0$. Integrate to find the total relative kinetic energy, and verify the hydrodynamic mass of a cylinder from Eq. (8.104).



P8.104

***P8.105** In Table 7.2 the drag coefficient of a 4:1 elliptical cylinder in laminar-boundary-layer flow is 0.35. According to Patton [17], the hydrodynamic mass of this cylinder is $\pi\rho hb/4$, where b is width into the paper and h is the maximum thickness. Use these results to derive a formula from the time history $U(t)$ of the cylinder if it is accelerated from rest in a still fluid by the sudden application of a constant force F.

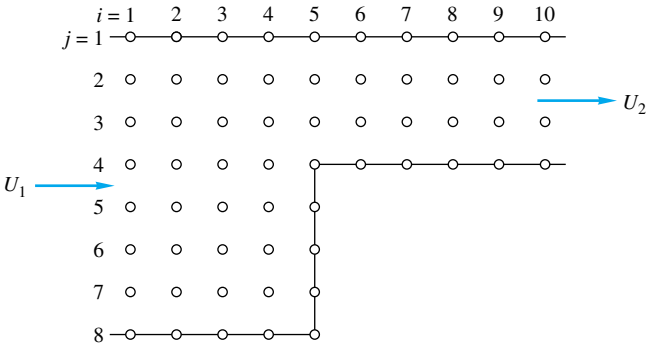
P8.106 Laplace's equation in plane polar coordinates, Eq. (8.11), is complicated by the variable radius. Consider the finite-difference mesh in Fig. P8.106, with nodes (i, j) equally spaced $\Delta\theta$ and Δr apart. Derive a finite-difference model for Eq. (8.11) similar to the cartesian expression (8.109).



P8.106

P8.107 Set up the numerical problem of Fig. 8.30 for an expansion of 30°. A new grid system and a nonsquare mesh may be needed. Give the proper nodal equation and boundary conditions. If possible, program this 30° expansion and solve on a digital computer.

P8.108 Consider two-dimensional potential flow into a step contraction as in Fig. P8.108. The inlet velocity $U_1 = 7$ m/s, and the outlet velocity U_2 is uniform. The nodes (i, j) are labeled in the figure. Set up the complete finite-difference algebraic relations for all nodes. Solve, if possible, on a digital computer and plot the streamlines in the flow.

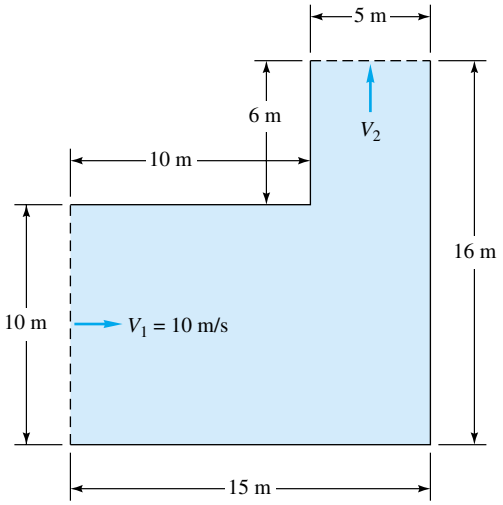


P8.108



ketabline.com Ebook.ketabline.com

P8.109 Consider inviscid flow through a two-dimensional 90° bend with a contraction, as in Fig. P8.109. Assume uniform flow at the entrance and exit. Make a finite-difference computer analysis for small grid size (at least 150 nodes), determine the dimensionless pressure distribution along the walls, and sketch the streamlines. (You may use either square or rectangular grids.)



P8.109

P8.110 For fully developed laminar incompressible flow through a straight noncircular duct, as in Sec. 6.6, the Navier-Stokes equations (4.38) reduce to

$$\frac{\partial^2 u}{\partial y^2} + \frac{\partial^2 u}{\partial z^2} = \frac{1}{\mu}\frac{dp}{dx} = \text{const} < 0$$

where (y, z) is the plane of the duct cross section and x is along the duct-axis. Gravity is neglected. Using a nonsquare rectangular grid $(\Delta x, \Delta y)$, develop a finite-difference model for this equation, and indicate how it may be applied to solve for flow in a rectangular duct of side lengths a and b.

P8.111 Solve Prob. 8.110 numerically for a rectangular duct of side length b by $2b$, using at least 100 nodal points. Evaluate the volume flow rate and the friction factor, and compare with the results in Table 6.4:

$$Q \approx 0.1143\,\frac{b^4}{\mu}\left(-\frac{dp}{dx}\right) \qquad f\,\mathrm{Re}_{D_h} \approx 62.19$$

where $D_h = 4A/P = 4b/3$ for this case. Comment on the possible truncation errors of your model.

P8.112 In his CFD textbook, Patankar [5] replaces the left-hand sides of Eq. (8.119*b* and *c*) with the following two expressions, respectively:

$$\frac{\partial}{\partial x}(u^2) + \frac{\partial}{\partial y}(vu) \qquad \text{and} \qquad \frac{\partial}{\partial x}(uv) + \frac{\partial}{\partial y}(v^2)$$

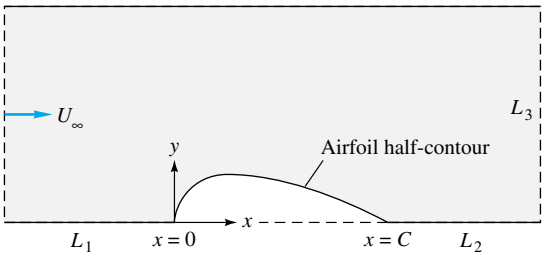
Are these equivalent expressions, or are they merely simplified approximations? Either way, why might these forms be better for finite-difference purposes?

P8.113 Repeat Example 8.7 using the implicit method of Eq. (8.118). Take $\Delta t = 0.2$ s and $\Delta y = 0.01$ m, which ensures that an explicit model would diverge. Compare your accuracy with Example 8.7.

P8.114 If your institution has an online potential-flow boundary-element computer code, consider flow past a symmetric airfoil, as in Fig. P8.114. The basic shape of an NACA symmetric airfoil is defined by the function [12]

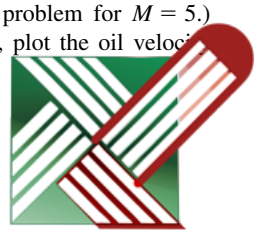
$$\frac{2y}{t_{\max}} \approx 1.4845\zeta^{1/2} - 0.63\zeta - 1.758\zeta^2 + 1.4215\zeta^3 - 0.5075\zeta^4$$

where $\zeta = x/C$ and the maximum thickness $t_{\max}$ occurs at $\zeta = 0.3$. Use this shape as part of the lower boundary for zero angle of attack. Let the thickness be fairly large, say, $t_{\max} = 0.12$, 0.15, or 0.18. Choose a generous number of nodes (≥60), and calculate and plot the velocity distribution V/U_∞ along the airfoil surface. Compare with the theoretical results in Ref. 12 for NACA 0012, 0015, or 0018 airfoils. If time permits, investigate the effect of the boundary lengths L_1, L_2, and L_3, which can initially be set equal to the chord length C.



P8.114

P8.115 Use the explicit method of Eq. (8.115) to solve Prob. 4.85 numerically for SAE 30 oil at 20°C with $U_0 = 1$ m/s and $\omega = M$ rad/s, where M is the number of letters in your surname. (This author will solve the problem for $M = 5$.) When steady oscillation is reached, plot the oil velocity versus time at $y = 2$ cm.



ketabline.com Ebook.ketabline.com

Word Problems

W8.1 What simplifications have been made, in the potential-flow theory of this chapter, which result in the elimination of the Reynolds number, Froude number, and Mach number as important parameters?

W8.2 In this chapter we superimpose many basic solutions, a concept associated with *linear* equations. Yet Bernoulli's equation (8.3) is *nonlinear*, being proportional to the square of the velocity. How, then, do we justify the use of superposition in inviscid-flow analysis?

W8.3 Give a physical explanation of circulation Γ as it relates to the lift force on an immersed body. If the line integral defined by Eq. (8.15) is zero, it means that the integrand is a perfect differential—but of what variable?

W8.4 Give a simple proof of Eq. (8.42), namely, that both the real and imaginary parts of a function $f(z)$ are laplacian if $z = x + iy$. What is the secret of this remarkable behavior?

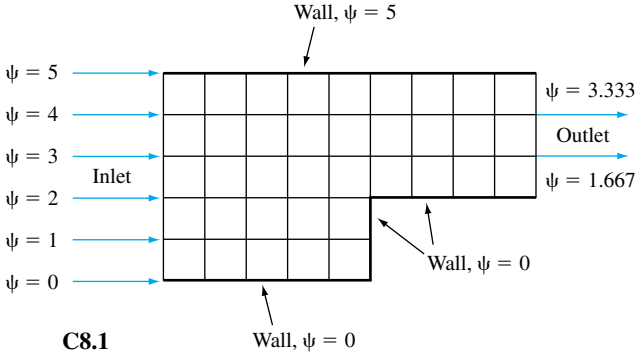
W8.5 Figure 8.14 contains five body corners. Without carrying out any calculations, explain physically what the value of the inviscid fluid velocity must be at each of these five corners. Is any flow separation expected?

W8.6 Explain the Kutta condition physically. Why is it necessary?

W8.7 We have briefly outlined finite-difference and boundary-element methods for potential flow but have neglected the *finite-element* technique. Do some reading and write a brief essay on the use of the finite-element method for potential-flow problems.

Comprehensive Problems

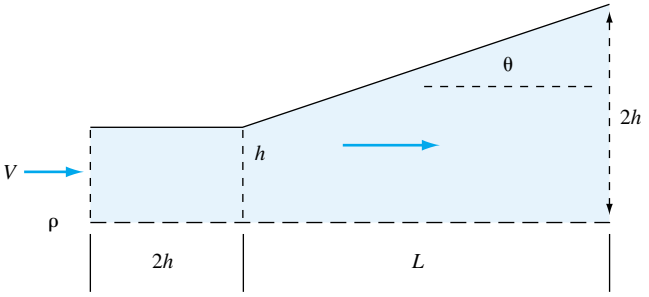
C8.1 Did you know that you can solve simple fluid mechanics problems with Microsoft Excel? The successive relaxation technique for solving the Laplace equation for potential-flow problems is easily set up on a spreadsheet, since the stream function at each interior cell is simply the average of its four neighbors. As an example, solve for the irrotational potential flow through a contraction, as given in Fig. C8.1. *Note:* To avoid the "circular reference" error, you must turn on the iteration option. Use the help index for more information. For full credit, attach a printout of your spreadsheet, with stream function converged and the value of the stream function at each node displayed to four digits of accuracy.



C8.1

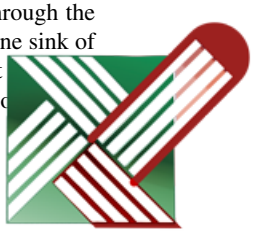
C8.2 Use an explicit method, similar to but not identical to Eq. (8.115), to solve the case of SAE 30 oil at 20°C starting from rest near a *fixed* wall. Far from the wall, the oil accelerates linearly, that is, $u_\infty = u_N = at$, where $a = 9$ m/s^2. At $t = 1$ s, determine (*a*) the oil velocity at $y = 1$ cm and (*b*) the instantaneous boundary-layer thickness (where $u \approx 0.99\ u_\infty$). *Hint*: There is a nonzero pressure gradient in the outer (nearly shear-free) stream, $n = N$, which must be included in Eq. (8.114) and your explicit model.

C8.3 Consider plane inviscid flow through a symmetric diffuser, as in Fig. C8.3. Only the upper half is shown. The flow is to expand from inlet half-width h to exit half-width $2h$, as shown. The expansion angle θ is 18.5° ($L \approx 3h$). Set up a nonsquare potential-flow mesh for this problem, and calculate and plot (*a*) the velocity distribution and (*b*) the pressure coefficient along the centerline. Assume uniform inlet and exit flows.



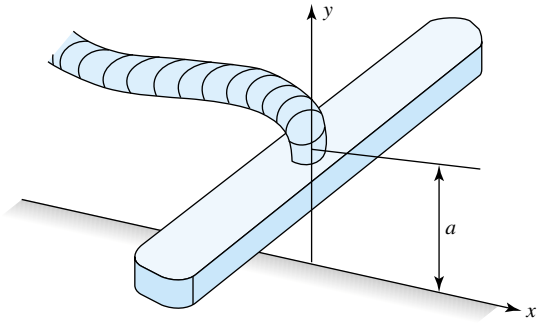
C8.3

C8.4 Use potential flow to approximate the flow of air being sucked up into a vacuum cleaner through a two-dimensional slit attachment, as in Fig. C8.4. In the x-y plane through the centerline of the attachment, model the flow as a line sink of strength $(-m)$, with its axis in the z-direction at
above the floor. (*a*) Sketch the streamlines and lo



ketabline.com Ebook.ketabline.com

stagnation points in the flow. (*b*) Find the magnitude of velocity $V(x)$ along the floor in terms of the parameters a and m. (*c*) Let the pressure far away be p_∞, where velocity is zero. Define a velocity scale $U = m/a$. Determine the variation of dimensionless pressure coefficient, $C_p = (p - p_\infty)/(\rho U^2/2)$, along the floor. (*d*) The vacuum cleaner is most effective where C_p is a minimum, that is, where velocity is maximum. Find the locations of minimum pressure coefficient along the x-axis. (*e*) At which points along the x-axis do you expect the vacuum cleaner to work most effectively? Is it best at $x = 0$ directly beneath the slit, or at some other x location along the floor? Conduct a scientific experiment at home with a vacuum cleaner and some small pieces of dust or dirt to test your prediction. Report your results and discuss the agreement with prediction. Give reasons for any disagreements.



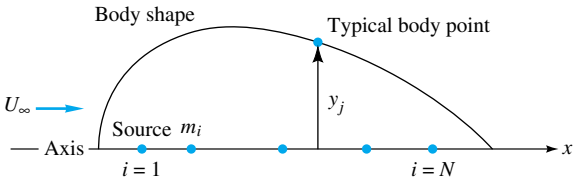
C8.4

C8.5 Consider a three-dimensional, incompressible, irrotational flow. Use the following two methods to prove that the viscous term in the Navier-Stokes equation is identically zero: (*a*) using vector notation; and (*b*) expanding out the scalar terms and substituting terms from the definition of irrotationality.

Design Projects

D8.1 In 1927, Theodore von Kármán developed a scheme to use a uniform stream, plus a row of sources and sinks, to generate an arbitrary closed-body shape. A schematic of the idea is sketched in Fig. D8.1. The body is symmetric and at zero angle of attack. A total of N sources and sinks are distributed along the axis within the body, with strengths m_i at positions x_i, for $i = 1$ to N. The object is to find the correct distribution of strengths which approximates a given body shape $y(x)$ at a finite number of surface locations and then to compute the approximate surface velocity and pressure. The technique should work for either two-dimensional bodies (distributed line sources) or bodies of revolution (distributed point sources).

For our body shape let us select the NACA 0018 airfoil, given by the formula in Prob. 8.114 with $t_{max} = 0.18$. Develop the ideas stated above into N simultaneous algebraic equations which can be used to solve for the N unknown line source/sink strengths. Then program your equations for a computer, with $N \geq 20$; solve for m_i; compute the surface velocities; and compare with the theoretical velocities for this shape in Ref. 12. Your goal should be to achieve accuracy within ± 1 percent of the classical results. If necessary, you should adjust N and the locations of the sources.



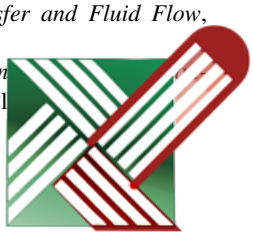
D8.1

D8.2 Modify Prob. D8.1 to solve for the point-source distribution which approximates an "0018" body-of-revolution shape. Since no theoretical results are published, simply make sure that your results converge to ± 1 percent.

D8.3 Consider water at 20°C flowing at 12 m/s in a water channel. A Rankine oval cylinder, 40 cm long, is to be placed parallel to the flow, where the water static pressure is 120 kPa. The oval's thickness is a design parameter. Prepare a plot of the minimum pressure on the oval's surface as a function of body thickness. Especially note the thicknesses where (*a*) the local pressure is 50 kPa and (*b*) cavitation first occurs on the surface.

References

1. O. D. Kellogg, *Foundations of Potential Theory*, Dover, New York, 1969.
2. J. M. Robertson, *Hydrodynamics in Theory and Application*, Prentice-Hall, Englewood Cliffs, NJ, 1965.
3. L. M. Milne-Thomson, *Theoretical Hydrodynamics*, 4th ed., Macmillan, New York, 1960.
4. I. G. Currie, *Fundamental Mechanics of Fluids*, 2d ed., McGraw-Hill, New York, 1993.
5. S. V. Patankar, *Numerical Heat Transfer and Fluid Flow*, McGraw-Hill, New York, 1980.
6. G. F. Carey and J. T. Oden, *Finite Elem ics*, vol. 6, Prentice-Hall, Englewood Cl

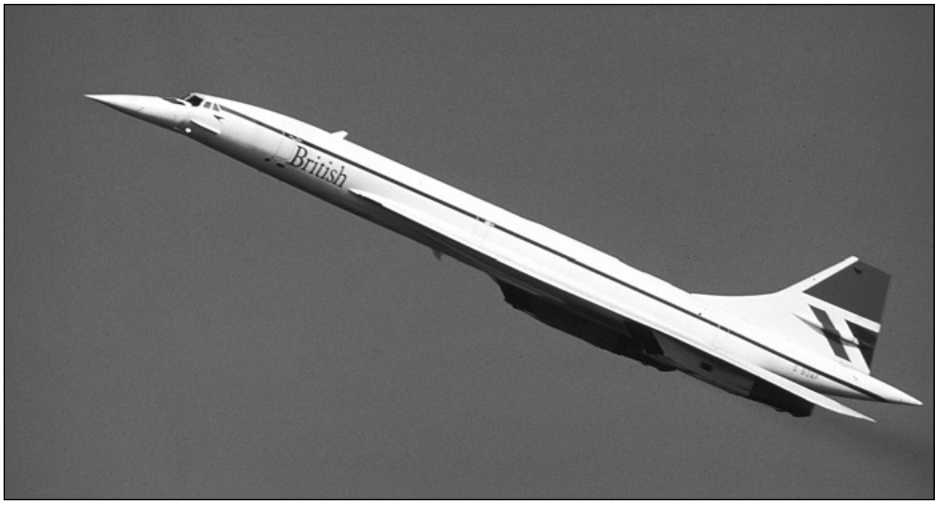


ketabline.com Ebook.ketabline.com

7. C. A. Brebbia and J. Dominquez, *Boundary Elements—An Introductory Course*, 2d ed., Computational Mechanics Publications, Southampton, England, and McGraw-Hill, New York, 1991.
8. A. D. Moore, "Fields from Fluid Flow Mappers," *J. Appl. Phys.,* vol. 20, 1949, pp. 790–804.
9. H. J. S. Hele-Shaw, "Investigation of the Nature of the Surface Resistance of Water and of Streamline Motion under Certain Experimental Conditions," *Trans. Inst. Nav. Archit.*, vol. 40, 1898, p. 25.
10. R. H. F. Pao, *Fluid Dynamics*, Merrill, Columbus, OH, 1967.
11. A. M. Kuethe and C.-Y. Chow, *Foundations of Aerodynamics*, 5th ed., Wiley, New York, 1997.
12. I. H. Abbott and A. E. von Doenhoff, *Theory of Wing Sections*, Dover, New York, 1959.
13. B. Thwaites (ed.), *Incompressible Aerodynamics*, Clarendon Press, Oxford, England, 1960.
14. L. Prandtl, "Applications of Modern Hydrodynamics to Aeronautics," *NACA Rep. 116*, 1921.
15. F. M. White, *Viscous Fluid Flow*, 2d ed., McGraw-Hill, New York, 1991.
16. C. S. Yih, *Fluid Mechanics*, McGraw-Hill, New York, 1969.
17. K. T. Patton, "Tables of Hydrodynamic Mass Factors for Translational Motion," *ASME Winter Annual Meeting*, Paper 65-WA/UNT-2, 1965.
18. J. L. Hess and A. M. O. Smith, "Calculation of Nonlifting Potential Flow about Arbitrary Three-Dimensional Bodies," *J. Ship Res.*, vol. 8, 1964, pp. 22–44.
19. K. H. Huebner, *The Finite Element Method for Engineers*, 3d ed., Wiley, New York, 1994.
20. J. C. Tannehill, D. A. Anderson, and R. H. Pletcher, *Computational Fluid Mechanics and Heat Transfer*, 2d ed., Taylor and Francis, Bristol, PA, 1997.
21. J. N. Newman, *Marine Hydrodynamics*, M.I.T. Press, Cambridge, MA, 1977.
22. H. Rouse, *Elementary Mechanics of Fluids*, Dover, New York, 1978.
23. J. H. Ferziger and M. Peric, *Computational Methods for Fluid Dynamics*, Springer-Verlag, New York, 1996.
24. C. Hirsch, *Numerical Computation of Internal and External Flows*, 2 vols., Wiley, New York, 1990.
25. K. A. Hoffmann and S. T. Chiang, *CFD for Engineers*, 2 vols., Engineering Education System, New York, 1993.
26. J. D. Anderson, *Computational Fluid Dynamics: The Basics with Applications*, McGraw-Hill, New York, 1995.
27. C. A. J. Fletcher, *Computational Techniques for Fluid Dynamics*, 2 vols., Springer Verlag, New York, 1997.
28. M. Deshpande, J. Feng, and C. L. Merkle, "Numerical Modeling of the Thermodynamic Effects of Cavitation," *J. Fluids Eng.*, June 1997, pp. 420–427.
29. P. A. Libby, *An Introduction to Turbulence,* Taylor and Francis, Bristol, PA, 1996.
30. C. J. Freitas, "Perspective: Selected Benchmarks from Commercial CFD Codes," *J. Fluids Eng.*, vol. 117, June 1995, pp. 208–218.
31. R. Martinuzzi and C. Tropea, "The Flow Around Surface-Mounted, Prismatic Obstacles in a Fully Developed Channel Flow," *J. Fluids Eng.*, vol. 115, March 1993, pp. 85–92.
32. K. B. Shah and J. H. Ferziger, "Large Eddy Simulations of Flow Past a Cubic Obstacle," *Thermosciences Division Report,* Dept. of Mechanical Engineering, Stanford University, Stanford, CA, 1996.
33. B. Galperin and S. A. Orszag (eds.), *Large Eddy Simulation of Complex Engineering and Geophysical Flows*, Cambridge University Press, New York, 1993.
34. W. J. Palm, *Introduction to MATLAB for Engineers*, McGraw-Hill, New York, 1998.
35. D. Hanselman and B. Littlefield, *The Student Edition of MATLAB*, Prentice-Hall, Upper Saddle River, NJ, 1997.
36. J. W. Hoyt and R. H. J. Sellin, "Flow Over Tube Banks—A Visualization Study," *J. Fluids Eng.*, vol. 119, June 1997, pp. 480–483.



ketabline.com Ebook.ketabline.com



The Concorde 264 supersonic airliner. Flying more than twice as fast as the speed of sound, as discussed in the present chapter, the Concorde is a milestone in commercial aviation. However, this great technical achievement is accompanied by high expense for the traveller. *(Courtesy of Don Riepe/Peter Arnold, Inc.)*



ketabline.com Ebook.ketabline.com

Chapter 9
Compressible Flow

Motivation. All eight of our previous chapters have been concerned with "low-speed" or "incompressible" flow, i.e., where the fluid velocity is much less than its speed of sound. In fact, we did not even develop an expression for the speed of sound of a fluid. That is done in this chapter.

When a fluid moves at speeds comparable to its speed of sound, density changes become significant and the flow is termed *compressible*. Such flows are difficult to obtain in liquids, since high pressures of order 1000 atm are needed to generate sonic velocities. In gases, however, a pressure ratio of only 2:1 will likely cause sonic flow. Thus compressible gas flow is quite common, and this subject is often called *gas dynamics*.

Probably the two most important and distinctive effects of compressibility on flow are (1) *choking*, wherein the duct flow rate is sharply limited by the sonic condition, and (2) *shock waves*, which are nearly discontinuous property changes in a supersonic flow. The purpose of this chapter is to explain such striking phenomena and to familiarize the reader with engineering calculations of compressible flow.

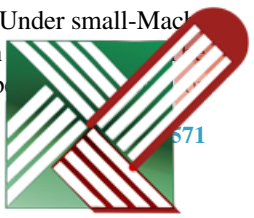
Speaking of calculations, the present chapter is made to order for the Engineering Equation Solver (EES) in App. E. Compressible-flow analysis is filled with scores of complicated algebraic equations, most of which are very difficult to manipulate or invert. Consequently, for nearly a century, compressible-flow textbooks have relied upon extensive tables of Mach number relations (see App. B) for numerical work. With EES, however, any set of equations in this chapter can be typed out and solved for any variable—see part (*b*) of Example 9.13 for an especially intricate example. With such a tool, App. B serves only as a backup and indeed may soon vanish from textbooks.

9.1 Introduction

We took a brief look in Chap. 4 [Eqs. (4.13) to (4.17)] to see when we might safely neglect the compressibility inherent in every real fluid. We found that the proper criterion for a nearly incompressible flow was a small Mach number

$$\text{Ma} = \frac{V}{a} \ll 1$$

where V is the flow velocity and a is the speed of sound of the fluid. Under small-Mach-number conditions, changes in fluid density are everywhere small in [illegible] energy equation becomes uncoupled, and temperature effects can b[illegible]



ketabline.com Ebook.ketabline.com

put aside for later study. The equation of state degenerates into the simple statement that density is nearly constant. This means that an incompressible flow requires only a momentum and continuity analysis, as we showed with many examples in Chaps. 7 and 8.

This chapter treats compressible flows, which have Mach numbers greater than about 0.3 and thus exhibit nonnegligible density changes. If the density change is significant, it follows from the equation of state that the temperature and pressure changes are also substantial. Large temperature changes imply that the energy equation can no longer be neglected. Therefore the work is doubled from two basic equations to four

1. Continuity equation
2. Momentum equation
3. Energy equation
4. Equation of state

to be solved simultaneously for four unknowns: pressure, density, temperature, and flow velocity (p, ρ, T, V). Thus the general theory of compressible flow is quite complicated, and we try here to make further simplifications, especially by assuming a reversible adiabatic or *isentropic* flow.

The Mach Number

The Mach number is the dominant parameter in compressible-flow analysis, with different effects depending upon its magnitude. Aerodynamicists especially make a distinction between the various ranges of Mach number, and the following rough classifications are commonly used:

$\text{Ma} < 0.3$:	*incompressible flow*, where density effects are negligible.
$0.3 < \text{Ma} < 0.8$:	*subsonic flow*, where density effects are important but no shock waves appear.
$0.8 < \text{Ma} < 1.2$:	*transonic flow*, where shock waves first appear, dividing subsonic and supersonic regions of the flow. Powered flight in the transonic region is difficult because of the mixed character of the flow field.
$1.2 < \text{Ma} < 3.0$:	*supersonic flow*, where shock waves are present but there are no subsonic regions.
$3.0 < \text{Ma}$:	*hypersonic flow* [13], where shock waves and other flow changes are especially strong.

The numerical values listed above are only rough guides. These five categories of flow are appropriate to external high-speed aerodynamics. For internal (duct) flows, the most important question is simply whether the flow is subsonic ($\text{Ma} < 1$) or supersonic ($\text{Ma} > 1$), because the effect of area changes reverses, as we show in Sec. 9.4. Since supersonic-flow effects may go against intuition, you should study these differences carefully.

The Specific-Heat Ratio

In addition to geometry and Mach number, compressible-flow calculations also depend upon a second dimensionless parameter, the *specific-heat ratio* of the gas:

$$k = \frac{c_p}{c_v}$$



ketabline.com Ebook.ketabline.com

Earlier, in Chaps. 1 and 4, we used the same symbol k to denote the thermal conductivity of a fluid. We apologize for the duplication; thermal conductivity does not appear in these later chapters of the text.

Recall from Fig. 1.3 that k for the common gases decreases slowly with temperature and lies between 1.0 and 1.7. Variations in k have only a slight effect upon compressible-flow computations, and air, $k \approx 1.40$, is the dominant fluid of interest. Therefore, although we assign some problems involving, e.g., steam and CO_2 and helium, the compressible-flow tables in App. B are based solely upon the single value $k = 1.40$ for air.

This text contains only a single chapter on compressible flow, but, as usual, whole books have been written on the subject. References 1 to 6, 26, 29, and 33 are introductory, fairly elementary treatments, while Refs. 7 to 14, 27 to 28, 31 to 32, and 35 are advanced. From time to time we shall defer some specialized topic to these texts.

We note in passing that there are at least two flow patterns which depend strongly upon very small density differences, acoustics, and natural convection. Acoustics [9, 14] is the study of sound-wave propagation, which is accompanied by extremely small changes in density, pressure, and temperature. Natural convection is the gentle circulating pattern set up by buoyancy forces in a fluid stratified by uneven heating or uneven concentration of dissolved materials. Here we are concerned only with steady compressible flow where the fluid velocity is of magnitude comparable to that of the speed of sound.

The Perfect Gas

In principle, compressible-flow calculations can be made for any fluid equation of state, and we shall assign problems involving the steam tables [15], the gas tables [16], and liquids [Eq. (1.19)]. But in fact most elementary treatments are confined to the perfect gas with constant specific heats

$$p = \rho RT \qquad R = c_p - c_v = \text{const} \qquad k = \frac{c_p}{c_v} = \text{const} \tag{9.2}$$

For all real gases, c_p, c_v, and k vary with temperature but only moderately; for example, c_p of air increases 30 percent as temperature increases from 0 to 5000°F. Since we rarely deal with such large temperature changes, it is quite reasonable to assume constant specific heats.

Recall from Sec. 1.6 that the gas constant is related to a universal constant Λ divided by the gas molecular weight

$$R_{\text{gas}} = \frac{\Lambda}{M_{\text{gas}}} \tag{9.3}$$

where $$\Lambda = 49{,}720 \text{ ft}^2/(\text{s}^2 \cdot {}^\circ\text{R}) = 8314 \text{ m}^2/(\text{s}^2 \cdot \text{K})$$

For air, $M = 28.97$, and we shall adopt the following property values for air throughout this chapter:

$$R = 1717 \text{ ft}^2/(\text{s}^2 \cdot {}^\circ\text{R}) = 287 \text{ m}^2/(\text{s}^2 \cdot \text{K}) \qquad k = 1.400$$

$$c_v = \frac{R}{k-1} = 4293 \text{ ft}^2/(\text{s}^2 \cdot {}^\circ\text{R}) = 718 \text{ m}^2/(\text{s}^2 \cdot \text{K}) \tag{9.4}$$

$$c_p = \frac{kR}{k-1} = 6010 \text{ ft}^2/(\text{s}^2 \cdot {}^\circ\text{R}) = 1005 \text{ m}^2/(\text{s}^2 \cdot \text{K})$$



ketabline.com Ebook.ketabline.com

Experimental values of k for eight common gases were shown in Fig. 1.3. From this figure and the molecular weight, the other properties can be computed, as in Eqs. (9.4).

The changes in the internal energy $\hat{u}$ and enthalpy h of a perfect gas are computed for constant specific heats as

$$\hat{u}_2 - \hat{u}_1 = c_v(T_2 - T_1) \qquad h_2 - h_1 = c_p(T_2 - T_1) \tag{9.5}$$

For variable specific heats one must integrate $\hat{u} = \int c_v\, dT$ and $h = \int c_p\, dT$ or use the gas tables [16]. Most modern thermodynamics texts now contain software for evaluating properties of nonideal gases [17].

Isentropic Process

The isentropic approximation is common in compressible-flow theory. We compute the entropy change from the first and second laws of thermodynamics for a pure substance [17 or 18]

$$T\, ds = dh - \frac{dp}{\rho} \tag{9.6}$$

Introducing $dh = c_p\, dT$ for a perfect gas and solving for ds, we substitute $\rho T = p/R$ from the perfect-gas law and obtain

$$\int_1^2 ds = \int_1^2 c_p \frac{dT}{T} - R\int_1^2 \frac{dp}{p} \tag{9.7}$$

If c_p is variable, the gas tables will be needed, but for constant c_p we obtain the analytic results

$$s_2 - s_1 = c_p \ln\frac{T_2}{T_1} - R\ln\frac{p_2}{p_1} = c_v \ln\frac{T_2}{T_1} - R\ln\frac{\rho_2}{\rho_1} \tag{9.8}$$

Equations (9.8) are used to compute the entropy change across a shock wave (Sec. 9.5), which is an irreversible process.

For isentropic flow, we set $s_2 = s_1$ and obtain the interesting power-law relations for an isentropic perfect gas

$$\frac{p_2}{p_1} = \left(\frac{T_2}{T_1}\right)^{k/(k-1)} = \left(\frac{\rho_2}{\rho_1}\right)^k \tag{9.9}$$

These relations are used in Sec. 9.3.

EXAMPLE 9.1

Argon flows through a tube such that its initial condition is $p_1 = 1.7$ MPa and $\rho_1 = 18$ kg/m^3 and its final condition is $p_2 = 248$ kPa and $T_2 = 400$ K. Estimate (*a*) the initial temperature, (*b*) the final density, (*c*) the change in enthalpy, and (*d*) the change in entropy of the gas.

Solution

From Table A.4 for argon, $R = 208$ m^2/(s$^2 \cdot$ K) and $k = 1.67$. Therefore estimate its spe
at constant pressure from Eq. (9.4):



ketabline.com Ebook.ketabline.com

$$c_p = \frac{kR}{k-1} = \frac{1.67(208)}{1.67-1} \approx 519 \text{ m}^2/(\text{s}^2 \cdot \text{K})$$

The initial temperature and final density are estimated from the ideal gas law, Eq. (9.2):

$$T_1 = \frac{p_1}{\rho_1 R} = \frac{1.7 \text{ E6 N/m}^2}{(18 \text{ kg/m}^3)[208 \text{ m}^2/(\text{s}^2 \cdot \text{K})]} = 454 \text{ K} \qquad \textit{Ans. (a)}$$

$$\rho_2 = \frac{p_2}{T_2 R} = \frac{248 \text{ E3 N/m}^2}{(400 \text{ K})[208 \text{ m}^2/(\text{s}^2 \cdot \text{K})]} = 2.98 \text{ kg/m}^3 \qquad \textit{Ans. (b)}$$

From Eq. (9.5) the enthalpy change is

$$h_2 - h_1 = c_p(T_2 - T_1) = 519(400 - 454) \approx -28{,}000 \text{ J/kg (or m}^2/\text{s}^2) \qquad \textit{Ans. (c)}$$

The argon temperature and enthalpy decrease as we move down the tube. Actually, there may not be any external cooling; i.e., the fluid enthalpy may be converted by friction to increased kinetic energy (Sec. 9.7).

Finally, the entropy change is computed from Eq. (9.8):

$$\begin{aligned} s_2 - s_1 &= c_p \ln \frac{T_2}{T_1} - R \ln \frac{p_2}{p_1} \\ &= 519 \ln \frac{400}{454} - 208 \ln \frac{0.248 \text{ E6}}{1.7 \text{ E6}} \\ &= -66 + 400 \approx 334 \text{ m}^2/(\text{s}^2 \cdot \text{K}) \end{aligned} \qquad \textit{Ans. (d)}$$

The fluid entropy has increased. If there is no heat transfer, this indicates an irreversible process. Note that entropy has the same units as the gas constant and specific heat.

This problem is not just arbitrary numbers. It correctly simulates the behavior of argon moving subsonically through a tube with large frictional effects (Sec. 9.7).

9.2 The Speed of Sound

The so-called speed of sound is the rate of propagation of a pressure pulse of infinitesimal strength through a still fluid. It is a thermodynamic property of a fluid. Let us analyze it by first considering a pulse of finite strength, as in Fig. 9.1. In Fig. 9.1*a* the pulse, or pressure wave, moves at speed C toward the still fluid (p, ρ, T, $V = 0$) at the left, leaving behind at the right a fluid of increased properties ($p + \Delta p$, $\rho + \Delta\rho$, $T + \Delta T$) and a fluid velocity ΔV toward the left following the wave but much slower. We can determine these effects by making a control-volume analysis across the wave. To avoid the unsteady terms which would be necessary in Fig. 9.1*a*, we adopt instead the control volume of Fig. 9.1*b*, which moves at wave speed C to the left. The wave appears fixed from this viewpoint, and the fluid appears to have velocity C on the left and $C - \Delta V$ on the right. The thermodynamic properties p, ρ, and T are not affected by this change of viewpoint.

The flow in Fig. 9.1*b* is steady and one-dimensional across the wave. The continuity equation is thus, from Eq. (3.24),

$$\rho AC = (\rho + \Delta\rho)(A)(C - \Delta V)$$

or

$$\Delta V = C \frac{\Delta\rho}{\rho + \Delta\rho}$$



ketabline.com Ebook.ketabline.com

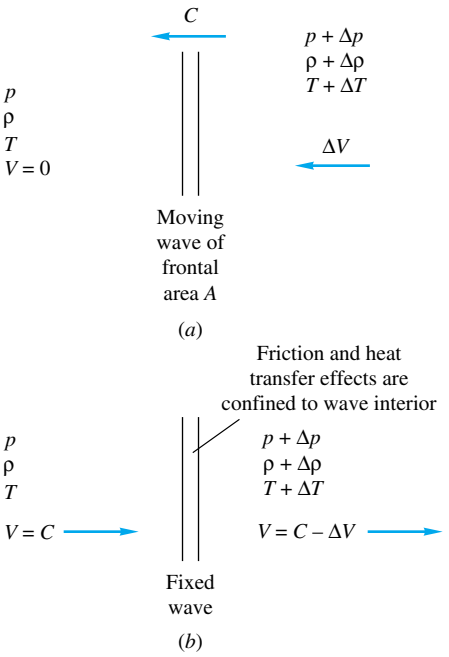


Fig. 9.1 Control-volume analysis of a finite-strength pressure wave: (*a*) control volume fixed to still fluid at left; (*b*) control volume moving left at wave speed *C*.

This proves our contention that the induced fluid velocity on the right is much smaller than the wave speed C. In the limit of infinitesimal wave strength (sound wave) this speed is itself infinitesimal.

Notice that there are no velocity gradients on either side of the wave. Therefore, even if fluid viscosity is large, frictional effects are confined to the interior of the wave. Advanced texts [for example, 14] show that the thickness of pressure waves in gases is of order 10^{-6} ft at atmospheric pressure. Thus we can safely neglect friction and apply the one-dimensional momentum equation (3.40) across the wave

$$\sum F_{\text{right}} = \dot{m}(V_{\text{out}} - V_{\text{in}})$$

or

$$pA - (p + \Delta p)A = (\rho AC)(C - \Delta V - C) \tag{9.11}$$

Again the area cancels, and we can solve for the pressure change

$$\Delta p = \rho C\, \Delta V \tag{9.12}$$

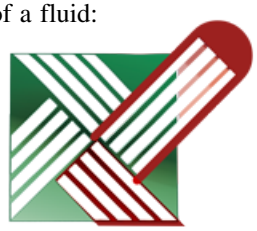
If the wave strength is very small, the pressure change is small.

Finally combine Eqs. (9.10) and (9.12) to give an expression for the wave speed

$$C^2 = \frac{\Delta p}{\Delta \rho}\left(1 + \frac{\Delta \rho}{\rho}\right) \tag{9.13}$$

The larger the strength $\Delta\rho/\rho$ of the wave, the faster the wave speed; i.e., powerful explosion waves move much more quickly than sound waves. In the limit of infinitesimal strength $\Delta\rho \to 0$, we have what is defined to be the speed of sound a of a fluid:

$$a^2 = \frac{\partial p}{\partial \rho}$$



ketabline.com Ebook.ketabline.com

Table 9.1 Sound Speed of Various Materials at 60°F (15.5°C) and 1 atm

Material	a, ft/s	a, m/s
Gases:		
H_2	4,246	1,294
He	3,281	1,000
Air	1,117	340
Ar	1,040	317
CO_2	873	266
CH_4	607	185
$^{238}UF_6$	297	91
Liquids:		
Glycerin	6,100	1,860
Water	4,890	1,490
Mercury	4,760	1,450
Ethyl alcohol	3,940	1,200
Solids:*		
Aluminum	16,900	5,150
Steel	16,600	5,060
Hickory	13,200	4,020
Ice	10,500	3,200

*Plane waves. Solids also have a *shear-wave speed.*

But the evaluation of the derivative requires knowledge of the thermodynamic process undergone by the fluid as the wave passes. Sir Isaac Newton in 1686 made a famous error by deriving a formula for sound speed which was equivalent to assuming an isothermal process, the result being 20 percent low for air, for example. He rationalized the discrepancy as being due to the "crassitude" (dust particles, etc.) in the air; the error is certainly understandable when we reflect that it was made 180 years before the proper basis was laid for the second law of thermodynamics.

We now see that the correct process must be *adiabatic* because there are no temperature gradients except inside the wave itself. For vanishing-strength sound waves we therefore have an infinitesimal adiabatic or isentropic process. The correct expression for the sound speed is

$$a = \left(\frac{\partial p}{\partial \rho} \bigg|_s \right)^{1/2} = \left(k \frac{\partial p}{\partial \rho} \bigg|_T \right)^{1/2} \tag{9.15}$$

for any fluid, gas or liquid. Even a solid has a sound speed.

For a perfect gas, From Eq. (9.2) or (9.9), we deduce that the speed of sound is

$$a = \left(\frac{kp}{\rho} \right)^{1/2} = (kRT)^{1/2} \tag{9.16}$$

The speed of sound increases as the square root of the absolute temperature. For air, with $k = 1.4$ and $R = 1717$, an easily memorized dimensional formula is

$$\begin{aligned} a \text{ (ft/s)} &\approx 49[T \text{ (°R)}]^{1/2} \\ a \text{ (m/s)} &\approx 20[T \text{ (K)}]^{1/2} \end{aligned} \tag{9.17}$$

At sea-level standard temperature, 60°F = 520°R, $a = 1117$ ft/s. This decreases in the upper atmosphere, which is cooler; at 50,000-ft standard altitude, $T = -69.7$°F = 389.9°R and $a = 49(389.9)^{1/2} = 968$ ft/s, or 13 percent less.

Some representative values of sound speed in various materials are given in Table 9.1. For liquids and solids it is common to define the *bulk modulus* K of the material

$$K = -\mathcal{V} \frac{\partial p}{\partial \mathcal{V}} \bigg|_s = \rho \frac{\partial p}{\partial \rho} \bigg|_s \tag{9.18}$$

For example, at standard conditions, the bulk modulus of carbon tetrachloride is 163,000 lbf/in^2 absolute, and its density is 3.09 slugs/ft^3. Its speed of sound is therefore $[163{,}000(144)/3.09]^{1/2} = 2756$ ft/s, or 840 m/s. Steel has a bulk modulus of about 29×10^6 lbf/in^2 absolute and water about 320×10^3 lbf/in^2 absolute, or 90 times less.

For solids, it is sometimes assumed that the bulk modulus is approximately equivalent to Young's modulus of elasticity E, but in fact their ratio depends upon Poisson's ratio σ

$$\frac{E}{K} = 3(1 - 2\sigma) \tag{9.19}$$

The two are equal for $\sigma = \frac{1}{3}$, which is approximately the case for m
als such as steel and aluminum.



ketabline.com Ebook.ketabline.com

EXAMPLE 9.2

Estimate the speed of sound of carbon monoxide at 200-kPa pressure and 300°C in m/s.

Solution

From Table A.4, for CO, the molecular weight is 28.01 and $k \approx 1.40$. Thus from Eq. (9.3) $R_{CO} = 8314/28.01 = 297\ \text{m}^2/(\text{s}^2 \cdot \text{K})$, and the given temperature is 300°C + 273 = 573 K. Thus from Eq. (9.16) we estimate

$$a_{CO} = (kRT)^{1/2} = [1.40(297)(573)]^{1/2} = 488\ \text{m/s} \qquad \textit{Ans.}$$

9.3 Adiabatic and Isentropic Steady Flow

As mentioned in Sec. 9.1, the isentropic approximation greatly simplifies a compressible-flow calculation. So does the assumption of adiabatic flow, even if nonisentropic.

Consider high-speed flow of a gas past an insulated wall, as in Fig. 9.2. There is no shaft work delivered to any part of the fluid. Therefore every streamtube in the flow satisfies the steady-flow energy equation in the form of Eq. (3.66)

$$h_1 + \tfrac{1}{2}V_1^2 + gz_1 = h_2 + \tfrac{1}{2}V_2^2 + gz_2 - q + w_v \tag{9.20}$$

where point 1 is upstream of point 2. You may wish to review the details of Eq. (3.66) and its development. We saw in Example 3.16 that potential-energy changes of a gas are extremely small compared with kinetic-energy and enthalpy terms. We shall neglect the terms gz_1 and gz_2 in all gas-dynamic analyses.

Inside the thermal and velocity boundary layers in Fig. 9.2 the heat-transfer and viscous-work terms q and w_v are not zero. But outside the boundary layer q and w_v are zero by definition, so that the outer flow satisfies the simple relation

$$h_1 + \tfrac{1}{2}V_1^2 = h_2 + \tfrac{1}{2}V_2^2 = \text{const} \tag{9.21}$$

The constant in Eq. (9.21) is equal to the maximum enthalpy which the fluid would achieve if brought to rest adiabatically. We call this value h_0, the *stagnation enthalpy* of the flow. Thus we rewrite Eq. (9.21) in the form

$$h + \tfrac{1}{2}V^2 = h_0 = \text{const} \tag{9.22}$$

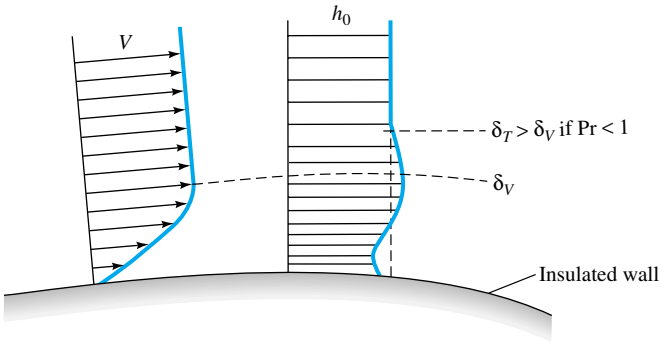


Fig. 9.2 Velocity and stagnation-enthalpy distributions near an insulated wall in a typical high-speed gas flow.



ketabline.com Ebook.ketabline.com

This should hold for steady adiabatic flow of any compressible fluid outside the boundary layer. The wall in Fig. 9.2 could be either the surface of an immersed body or the wall of a duct. We have shown the details of Fig. 9.2; typically the thermal-layer thickness δ_T is greater than the velocity-layer thickness δ_V because most gases have a dimensionless Prandtl number Pr less than unity (see, e.g., Ref. 19, sec. 4-3.2). Note that the stagnation enthalpy varies inside the thermal boundary layer, but its average value is the same as that at the outer layer due to the insulated wall.

For nonperfect gases we may have to use the steam tables [15] or the gas tables [16] to implement Eq. (9.22). But for a perfect gas $h = c_pT$, and Eq. (9.22) becomes

$$c_pT + \tfrac{1}{2}V^2 = c_pT_0 \tag{9.23}$$

This establishes the stagnation temperature T_0 of an adiabatic perfect-gas flow, i.e., the temperature it achieves when decelerated to rest adiabatically.

An alternate interpretation of Eq. (9.22) occurs when the enthalpy and temperature drop to (absolute) zero, so that the velocity achieves a maximum value

$$V_{\max} = (2h_0)^{1/2} = (2c_pT_0)^{1/2} \tag{9.24}$$

No higher flow velocity can occur unless additional energy is added to the fluid through shaft work or heat transfer (Sec. 9.8).

Mach-Number Relations

The dimensionless form of Eq. (9.23) brings in the Mach number Ma as a parameter, by using Eq. (9.16) for the speed of sound of a perfect gas. Divide through by c_pT to obtain

$$1 + \frac{V^2}{2c_pT} = \frac{T_0}{T} \tag{9.25}$$

But, from the perfect-gas law, $c_pT = [kR/(k-1)]T = a^2/(k-1)$, so that Eq. (9.25) becomes

$$1 + \frac{(k-1)V^2}{2a^2} = \frac{T_0}{T}$$

or

$$\frac{T_0}{T} = 1 + \frac{k-1}{2}\,\mathrm{Ma}^2 \qquad \mathrm{Ma} = \frac{V}{a} \tag{9.26}$$

This relation is plotted in Fig. 9.3 versus the Mach number for $k = 1.4$. At Ma = 5 the temperature has dropped to $\frac{1}{6}T_0$.

Since $a \propto T^{1/2}$, the ratio a_0/a is the square root of (9.26)

$$\frac{a_0}{a} = \left(\frac{T_0}{T}\right)^{1/2} = \left[1 + \frac{1}{2}(k-1)\mathrm{Ma}^2\right]^{1/2} \tag{9.27}$$

Equation (9.27) is also plotted in Fig. 9.3. At Ma = 5 the speed of sound has dropped to 41 percent of the stagnation value.

Isentropic Pressure and Density Relations

Note that Eqs. (9.26) and (9.27) require only adiabatic flow and hol
ence of irreversibilities such as friction losses or shock waves.



ketabline.com Ebook.ketabline.com

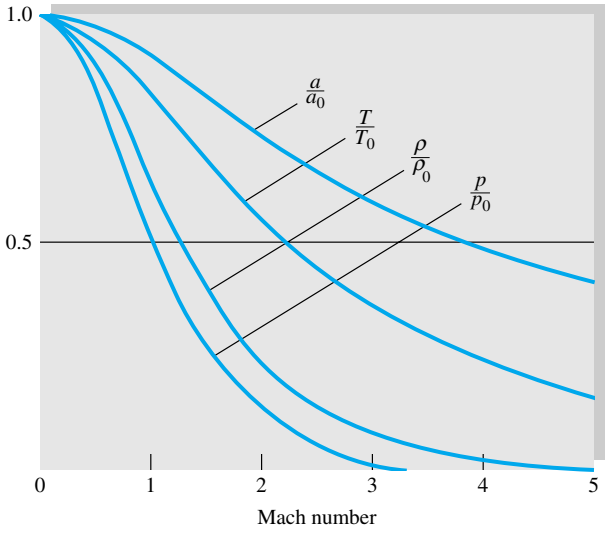


Fig. 9.3 Adiabatic $(T/T_0$ and $a/a_0)$ and isentropic $(p/p_0$ and $\rho/\rho_0)$ properties versus Mach number for $k = 1.4$.

If the flow is also *isentropic*, then for a perfect gas the pressure and density ratios can be computed from Eq. (9.9) as a power of the temperature ratio

$$\frac{p_0}{p} = \left(\frac{T_0}{T}\right)^{k/(k-1)} = \left[1 + \frac{1}{2}(k-1)\,\mathrm{Ma}^2\right]^{k/(k-1)} \tag{9.28a}$$

$$\frac{\rho_0}{\rho} = \left(\frac{T_0}{T}\right)^{1/(k-1)} = \left[1 + \frac{1}{2}(k-1)\,\mathrm{Ma}^2\right]^{1/(k-1)} \tag{9.28b}$$

These relations are also plotted in Fig. 9.3; at Ma = 5 the density is 1.13 percent of its stagnation value, and the pressure is only 0.19 percent of stagnation pressure.

The quantities p_0 and ρ_0 are the isentropic stagnation pressure and density, respectively, i.e., the pressure and density which the flow would achieve if brought isentropically to rest. In an adiabatic nonisentropic flow p_0 and ρ_0 retain their local meaning, but they vary throughout the flow as the entropy changes due to friction or shock waves. The quantities h_0, T_0, and a_0 are constant in an adiabatic nonisentropic flow (see Sec. 9.7 for further details).

Relationship to Bernoulli's Equation

The isentropic assumptions (9.28) are effective, but are they realistic? Yes. To see why, differentiate Eq. (9.22)

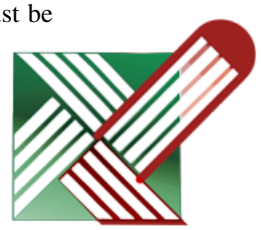
Adiabatic: $$dh + V\,dV = 0 \tag{9.29}$$

Meanwhile, from Eq. (9.6), if $ds = 0$ (isentropic process),

$$dh = \frac{dp}{\rho} \tag{9.30}$$

Combining (9.29) and (9.30), we find that an isentropic streamtube flow must be

$$\frac{dp}{\rho} + V\,dV = 0$$



ketabline.com Ebook.ketabline.com

But this is exactly the Bernoulli relation, Eq. (3.75), for steady frictionless flow with negligible gravity terms. Thus we see that the isentropic-flow assumption is equivalent to use of the Bernoulli or streamline form of the frictionless momentum equation.

Critical Values at the Sonic Point

The stagnation values (a_0, T_0, p_0, ρ_0) are useful reference conditions in a compressible flow, but of comparable usefulness are the conditions where the flow is sonic, Ma = 1.0. These sonic, or *critical*, properties are denoted by asterisks: p^*, ρ^*, a^*, and T^*. They are certain ratios of the stagnation properties as given by Eqs. (9.26) to (9.28) when Ma = 1.0; for $k = 1.4$

$$\frac{p^*}{p_0} = \left(\frac{2}{k+1}\right)^{k/(k-1)} = 0.5283 \qquad \frac{\rho^*}{\rho_0} = \left(\frac{2}{k+1}\right)^{1/(k-1)} = 0.6339$$
$$\frac{T^*}{T_0} = \frac{2}{k+1} = 0.8333 \qquad \frac{a^*}{a_0} = \left(\frac{2}{k+1}\right)^{1/2} = 0.9129 \tag{9.32}$$

In all isentropic flow, all critical properties are constant; in adiabatic nonisentropic flow, a^* and T^* are constant, but p^* and ρ^* may vary.

The critical velocity V^* equals the sonic sound speed a^* by definition and is often used as a reference velocity in isentropic or adiabatic flow

$$V^* = a^* = (kRT^*)^{1/2} = \left(\frac{2k}{k+1}RT_0\right)^{1/2} \tag{9.33}$$

The usefulness of these critical values will become clearer as we study compressible duct flow with friction or heat transfer later in this chapter.

Some Useful Numbers for Air

Since the great bulk of our practical calculations are for air, $k = 1.4$, the stagnation-property ratios p/p_0, etc., from Eqs. (9.26) to (9.28), are tabulated for this value in Table B.1. The increments in Mach number are rather coarse in this table because the values are only meant as a guide; these equations are now a trivial matter to manipulate on a hand calculator. Thirty years ago every text had extensive compressible-flow tables with Mach-number spacings of about 0.01, so that accurate values could be interpolated.

For $k = 1.4$, the following numerical versions of the isentropic and adiabatic flow formulas are obtained:

$$\frac{T_0}{T} = 1 + 0.2\,\mathrm{Ma}^2 \qquad \frac{\rho_0}{\rho} = (1 + 0.2\,\mathrm{Ma}^2)^{2.5}$$
$$\frac{p_0}{p} = (1 + 0.2\,\mathrm{Ma}^2)^{3.5} \tag{9.34}$$

Or, if we are given the properties, it is equally easy to solve for the Mach number (again with $k = 1.4$)

$$\mathrm{Ma}^2 = 5\left(\frac{T_0}{T} - 1\right) = 5\left[\left(\frac{\rho_0}{\rho}\right)^{2/5} - 1\right] = 5\left[\left(\frac{p_0}{p}\right)^{2/7} - 1\right] \tag{9.35}$$

Note that these isentropic-flow formulas serve as the equivalent of the frictionless adiabatic momentum and energy equations. They relate velocity to phy
a perfect gas, but they are *not* the "solution" to a gas-dynamics prob



ketabline.com Ebook.ketabline.com

solution is not obtained until the continuity equation has also been satisfied, for either one-dimensional (Sec. 9.4) or multidimensional (Sec. 9.9) flow.

One final note: These isentropic-ratio–versus–Mach-number formulas are seductive, tempting one to solve all problems by jumping right into the tables. Actually, many problems involving (dimensional) velocity and temperature can be solved more easily from the original raw dimensional energy equation (9.23) plus the perfect-gas law (9.2), as the next example will illustrate.

EXAMPLE 9.3

Air flows adiabatically through a duct. At point 1 the velocity is 240 m/s, with $T_1 = 320$ K and $p_1 = 170$ kPa. Compute (*a*) T_0, (*b*) p_{01}, (*c*) ρ_0, (*d*) Ma, (*e*) V_{max}, and (*f*) V^*. At point 2 further downstream $V_2 = 290$ m/s and $p_2 = 135$ kPa. (*g*) What is the stagnation pressure p_{02}?

Solution

For air take $k = 1.4$, $c_p = 1005$ m^2/(s$^2 \cdot$ K), and $R = 287$ m^2/(s$^2 \cdot$ K). With V_1 and T_1 known, we can compute T_{01} from Eq. (9.23) without using the Mach number:

$$T_{01} = T_1 + \frac{V_1^2}{2c_p} = 320 + \frac{(240\text{ m/s})^2}{2[1005\text{ m}^2/(\text{s}^2 \cdot \text{K})]} = 320 + 29 = 349\text{ K} \qquad \textit{Ans. (a)}$$

Then compute Ma_1 from the known temperature ratio, using Eq. (9.35):

$$\text{Ma}_1^2 = 5\left(\frac{349}{320} - 1\right) = 0.453 \qquad \text{Ma}_1 = 0.67 \qquad \textit{Ans. (d)}$$

Alternately compute $a_1 = \sqrt{kRT_1} = 359$ m/s, whence $\text{Ma}_1 = V_1/a_1 = 240/359 = 0.67$. The stagnation pressure at section 1 follows from Eq. (9.34):

$$p_{01} = p_1(1 + 0.2\ \text{Ma}_1^2)^{3.5} = (170\text{ kPa})[1 + 0.2(0.67)^2]^{3.5} = 230\text{ kPa} \qquad \textit{Ans. (b)}$$

We need the density from the perfect-gas law before we can compute the stagnation density:

$$\rho_1 = \frac{p_1}{RT_1} = \frac{170{,}000}{(287)(320)} = 1.85\text{ kg/m}^3$$

whence $$\rho_{01} = \rho_1(1 + 0.2\ \text{Ma}_1^2)^{2.5} = (1.85)[1 + 0.2(0.67)^2]^{2.5} = 2.29\text{ kg/m}^3 \qquad \textit{Ans. (c)}$$

Alternately, we could have gone directly to $\rho_0 = p_0/(RT_0) = (230\text{ E3})/[(287)(349)] = 2.29$ kg/m^3. Meanwhile, the maximum velocity follows from Eq. (9.24):

$$V_{max} = (2c_pT_0)^{1/2} = [2(1005)(349)]^{1/2} = 838\text{ m/s} \qquad \textit{Ans. (e)}$$

and the sonic velocity from Eq. (9.33) is

$$V^* = \left(\frac{2k}{k+1}RT_0\right)^{1/2} = \left[\frac{2(1.4)}{1.4+1}(287)(349)\right]^{1/2} = 342\text{ m/s} \qquad \textit{Ans. (f)}$$

At point 2, the temperature is not given, but since we know the flow is adiabatic, the stagnation temperature is constant: $T_{02} = T_{01} = 349$ K. Thus, from Eq. (9.23),

$$T_2 = T_{02} - \frac{V_2^2}{2c_p} = 349 - \frac{(290)^2}{2(1005)} = 307\text{ K}$$

Then, although the flow itself is not isentropic, the local stagnation pressure is comput*local* isentropic condition



ketabline.com Ebook.ketabline.com

$$p_{02} = p_2\left(\frac{T_{02}}{T_2}\right)^{k/(k-1)} = (135)\left(\frac{349}{307}\right)^{3.5} = 211 \text{ kPa} \qquad \textit{Ans. (g)}$$

This is 8 percent less than the upstream stagnation pressure p_{01}. Notice that, in this last part, we took advantage of the given information (T_{02}, p_2, V_2) to obtain p_{02} in an efficient manner. You may verify by comparison that approaching this part through the (unknown) Mach number Ma_2 is more laborious.

9.4 Isentropic Flow with Area Changes

By combining the isentropic- and/or adiabatic-flow relations with the equation of continuity we can study practical compressible-flow problems. This section treats the one-dimensional flow approximation.

Figure 9.4 illustrates the one-dimensional flow assumption. A real flow, Fig. 9.4*a*, has no slip at the walls and a velocity profile $V(x, y)$ which varies across the duct section (compare with Fig. 7.8). If, however, the area change is small and the wall radius of curvature large

$$\frac{dh}{dx} \ll 1 \qquad h(x) \ll R(x) \tag{9.36}$$

then the flow is approximately one-dimensional, as in Fig. 9.4*b*, with $V \approx V(x)$ reacting to area change $A(x)$. Compressible-flow nozzles and diffusers do not always satisfy conditions (9.36), but we use the one-dimensional theory anyway because of its simplicity.

For steady one-dimensional flow the equation of continuity is, from Eq. (3.24),

$$\rho(x)V(x)A(x) = \dot{m} = \text{const} \tag{9.37}$$

Before applying this to duct theory, we can learn a lot from the differential form of Eq. (9.37)

$$\frac{d\rho}{\rho} + \frac{dV}{V} + \frac{dA}{A} = 0 \tag{9.38}$$

The differential forms of the frictionless momentum equation (9.31) and the sound-speed relation (9.15) are recalled here for convenience:

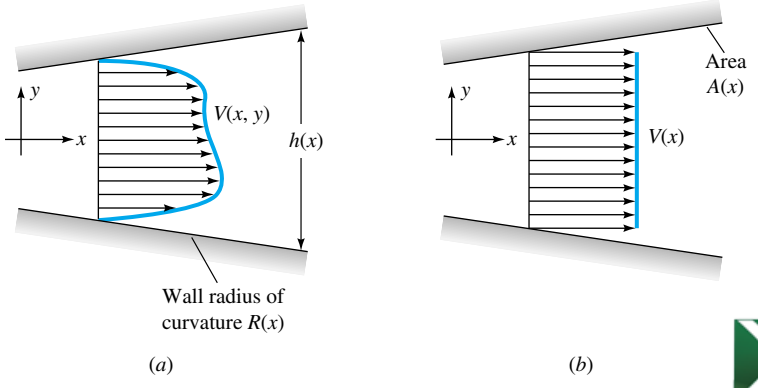


Fig. 9.4 Compressible flow through a duct: (*a*) real-fluid velocity profile; (*b*) one-dimensional approximation.



ketabline.com Ebook.ketabline.com

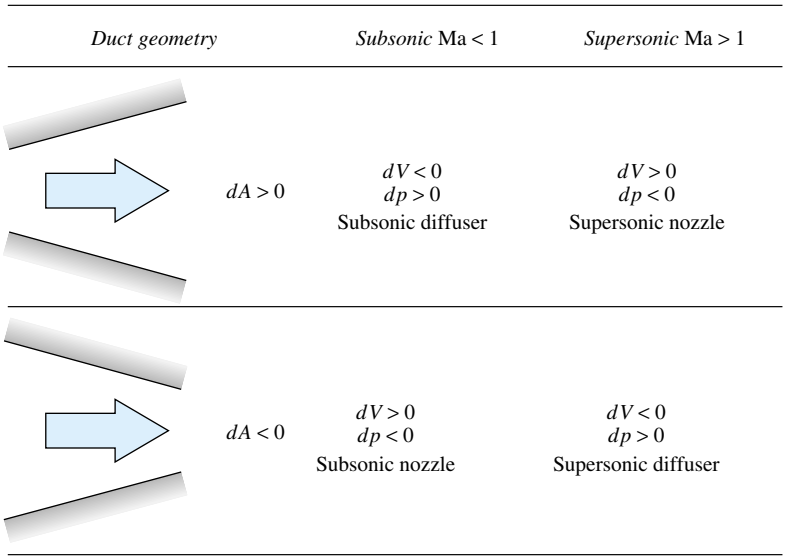


Fig. 9.5 Effect of Mach number on property changes with area change in duct flow.

$$\text{Momentum} \qquad \frac{dp}{\rho} + V\,dV = 0$$
$$\text{Sound speed:} \qquad dp = a^2\,d\rho \tag{9.39}$$

Now eliminate dp and $d\rho$ between Eqs. (9.38) and (9.39) to obtain the following relation between velocity change and area change in isentropic duct flow:

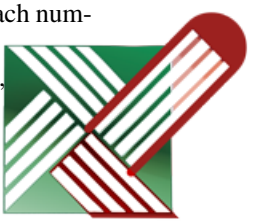
$$\frac{dV}{V} = \frac{dA}{A}\frac{1}{\text{Ma}^2 - 1} = -\frac{dp}{\rho V^2} \tag{9.40}$$

Inspection of this equation, without actually solving it, reveals a fascinating aspect of compressible flow: Property changes are of opposite sign for subsonic and supersonic flow because of the term $\text{Ma}^2 - 1$. There are four combinations of area change and Mach number, summarized in Fig. 9.5.

From earlier chapters we are used to subsonic behavior ($\text{Ma} < 1$): When area increases, velocity decreases and pressure increases, which is denoted a subsonic diffuser. But in supersonic flow ($\text{Ma} > 1$), the velocity actually increases when the area increases, a supersonic nozzle. The same opposing behavior occurs for an area decrease, which speeds up a subsonic flow and slows down a supersonic flow.

What about the sonic point $\text{Ma} = 1$? Since infinite acceleration is physically impossible, Eq. (9.40) indicates that dV can be finite only when $dA = 0$, that is, a minimum area (throat) or a maximum area (bulge). In Fig. 9.6 we patch together a throat section and a bulge section, using the rules from Fig. 9.5. The throat or converging-diverging section can smoothly accelerate a subsonic flow through sonic to supersonic flow, as in Fig. 9.6*a*. This is the only way a supersonic flow can be created by expanding the gas from a stagnant reservoir. The bulge section fails; the bulge Mach number moves away from a sonic condition rather than toward it.

Although supersonic flow downstream of a nozzle requires a sonic throat,



ketabline.com Ebook.ketabline.com

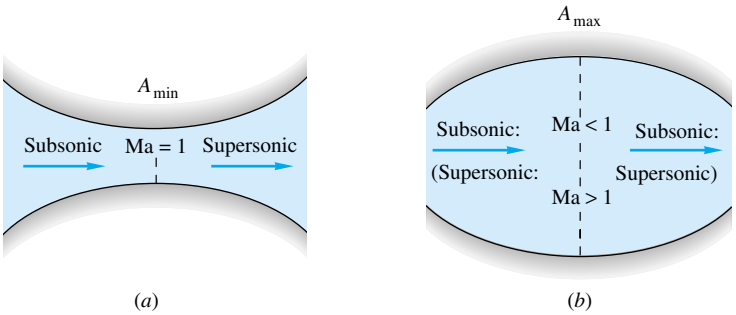


Fig. 9.6 From Eq. (9.40), in flow through a throat (*a*) the fluid can accelerate smoothly through sonic and supersonic flow. In flow through the bulge (*b*) the flow at the bulge cannot be sonic on physical grounds.

posite is not true: A compressible gas can pass through a throat section without becoming sonic.

Perfect-Gas Relations

We can use the perfect-gas and isentropic-flow relations to convert the continuity relation (9.37) into an algebraic expression involving only area and Mach number, as follows. Equate the mass flow at any section to the mass flow under sonic conditions (which may not actually occur in the duct)

$$\rho VA = \rho^* V^* A^*$$

or

$$\frac{A}{A^*} = \frac{\rho^*}{\rho}\frac{V^*}{V} \tag{9.41}$$

Both the terms on the right are functions only of Mach number for isentropic flow. From Eqs. (9.28) and (9.32)

$$\frac{\rho^*}{\rho} = \frac{\rho^*}{\rho_0}\frac{\rho_0}{\rho} = \left\{\frac{2}{k+1}\left[1 + \frac{1}{2}(k-1)\,\mathrm{Ma}^2\right]\right\}^{1/(k-1)} \tag{9.42}$$

From Eqs. (9.26) and (9.32) we obtain

$$\frac{V^*}{V} = \frac{(kRT^*)^{1/2}}{V} = \frac{(kRT)^{1/2}}{V}\left(\frac{T^*}{T_0}\right)^{1/2}\left(\frac{T_0}{T}\right)^{1/2}$$

$$= \frac{1}{\mathrm{Ma}}\left\{\frac{2}{k+1}\left[1 + \frac{1}{2}(k-1)\,\mathrm{Ma}^2\right]\right\}^{1/2} \tag{9.43}$$

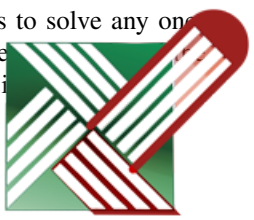
Combining Eqs. (9.41) to (9.43), we get the desired result

$$\frac{A}{A^*} = \frac{1}{\mathrm{Ma}}\left[\frac{1 + \frac{1}{2}(k-1)\,\mathrm{Ma}^2}{\frac{1}{2}(k+1)}\right]^{(1/2)(k+1)/(k-1)} \tag{9.44}$$

For $k = 1.4$, Eq. (9.44) takes the numerical form

$$\frac{A}{A^*} = \frac{1}{\mathrm{Ma}}\frac{(1 + 0.2\,\mathrm{Ma}^2)^3}{1.728} \tag{9.45}$$

which is plotted in Fig. 9.7. Equations (9.45) and (9.34) enable us to solve any one-dimensional isentropic-airflow problem given, say, the shape of the [illegible] stagnation conditions and assuming that there are no shock waves i[illegible]



ketabline.com Ebook.ketabline.com

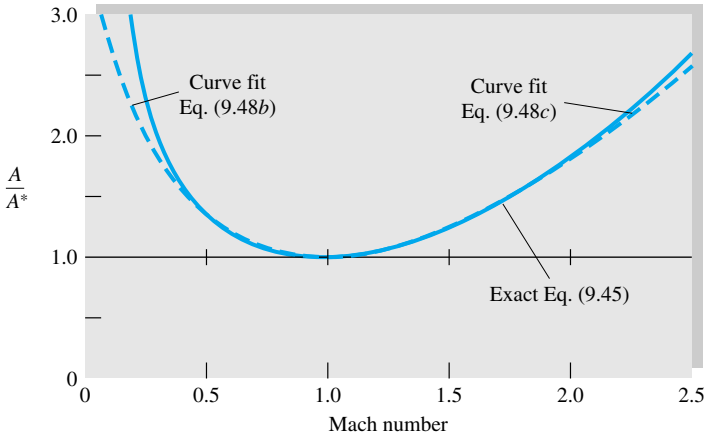


Fig. 9.7 Area ratio versus Mach number for isentropic flow of a perfect gas with $k = 1.4$.

Figure 9.7 shows that the minimum area which can occur in a given isentropic duct flow is the sonic, or critical, throat area. All other duct sections must have A greater than A^*. In many flows a critical sonic throat is not actually present, and the flow in the duct is either entirely subsonic or, more rarely, entirely supersonic.

Choking

From Eq. (9.41) the inverse ratio A^*/A equals $\rho V/(\rho^* V^*)$, the mass flow per unit area at any section compared with the critical mass flow per unit area. From Fig. 9.7 this inverse ratio rises from zero at Ma = 0 to unity at Ma = 1 and back down to zero at large Ma. Thus, for given stagnation conditions, the maximum possible mass flow passes through a duct when its throat is at the critical or sonic condition. The duct is then said to be *choked* and can carry no additional mass flow unless the throat is widened. If the throat is constricted further, the mass flow through the duct must decrease.

From Eqs. (9.32) and (9.33) the maximum mass flow is

$$\dot{m}_{\max} = \rho^* A^* V^* = \rho_0 \left(\frac{2}{k+1}\right)^{1/(k-1)} A^* \left(\frac{2k}{k+1} RT_0\right)^{1/2}$$

$$= k^{1/2} \left(\frac{2}{k+1}\right)^{(1/2)(k+1)/(k-1)} A^* \rho_0 (RT_0)^{1/2} \qquad (9.46a)$$

For $k = 1.4$ this reduces to

$$\dot{m}_{\max} = 0.6847 A^* \rho_0 (RT_0)^{1/2} = \frac{0.6847 p_0 A^*}{(RT_0)^{1/2}} \qquad (9.46b)$$

For isentropic flow through a duct, the maximum mass flow possible is proportional to the throat area and stagnation pressure and inversely proportional to the square root of the stagnation temperature. These are somewhat abstract facts, so let us illustrate with some examples.

The Local Mass-Flow Function

Equation (9.46) gives the *maximum* mass flow, which occurs at the choking c
(sonic exit). It can be modified to predict the actual (nonmaximum) mass flo



ketabline.com Ebook.ketabline.com

section where local area A and pressure p are known.[1] The algebra is convoluted, so here we give only the final result, expressed in dimensionless form:

$$\text{Mass-flow function} = \frac{\dot{m}}{A}\frac{\sqrt{RT_0}}{p_0} = \sqrt{\frac{2k}{k-1}\left(\frac{p}{p_0}\right)^{2/k}\left[1-\left(\frac{p}{p_0}\right)^{(k-1)/k}\right]} \tag{9.47}$$

We stress that p and A in this relation are the *local* values at position x. As p/p_0 falls, this function rises rapidly and then levels out at the maximum of Eq. (9.46). A few values may be tabulated here for $k = 1.4$:

p/p_0	1.0	0.98	0.95	0.9	0.8	0.7	0.6	≤0.5283
Function	0.0	0.1978	0.3076	0.4226	0.5607	0.6383	0.6769	**0.6847**

Equation (9.47) is handy if stagnation conditions are known and the flow is not choked.

The only cumbersome algebra in these problems is the inversion of Eq. (9.45) to compute the Mach number when A/A^* is known. If available, EES is ideal for this situation and will yield Ma in a flash. In the absence of EES, the following curve-fitted formulas are suggested; given A/A^*, they estimate the Mach number within ±2 percent for $k = 1.4$ if you stay within the ranges listed for each formula:

$$\text{Ma} \approx \begin{cases} \dfrac{1 + 0.27(A/A^*)^{-2}}{1.728A/A^*} & 1.34 < \dfrac{A}{A^*} < \infty \quad (9.48a) \\ 1 - 0.88\left(\ln\dfrac{A}{A^*}\right)^{0.45} & 1.0 < \dfrac{A}{A^*} < 1.34 \quad (9.48b) \end{cases} \text{ subsonic flow}$$

$$\text{Ma} \approx \begin{cases} 1 + 1.2\left(\dfrac{A}{A^*} - 1\right)^{1/2} & 1.0 < \dfrac{A}{A^*} < 2.9 \quad (9.48c) \\ \left[216\dfrac{A}{A^*} - 254\left(\dfrac{A}{A^*}\right)^{2/3}\right]^{1/5} & 2.9 < \dfrac{A}{A^*} < \infty \quad (9.48d) \end{cases} \text{ supersonic flow}$$

Formulas (9.48*a*) and (9.48*d*) are asymptotically correct as $A/A^* \to \infty$, while (9.48*b*) and (9.48*c*) are just curve fits. However, formulas (9.48*b*) and (9.48*c*) are seen in Fig. 9.7 to be accurate within their recommended ranges.

Note that two solutions are possible for a given A/A^*, one subsonic and one supersonic. The proper solution cannot be selected without further information, e.g., known pressure or temperature at the given duct section.

EXAMPLE 9.4

Air flows isentropically through a duct. At section 1 the area is 0.05 m^2 and $V_1 = 180$ m/s, $p_1 = 500$ kPa, and $T_1 = 470$ K. Compute (*a*) T_0, (*b*) Ma_1, (*c*) p_0, and (*d*) both A^* and $\dot{m}$. If at section 2 the area is 0.036 m^2, compute Ma_2 and p_2 if the flow is (*e*) subsonic or (*f*) supersonic. Assume $k = 1.4$.

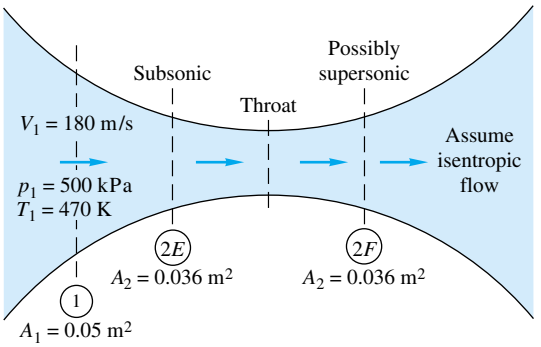
Solution

Part (a) A general sketch of the problem is shown in Fig. E9.4. With V_1 and T_1 known, the energy equation (9.23) gives

[1] The author is indebted to Georges Aigret, of Chimay, Belgium, for suggesting t



ketabline.com Ebook.ketabline.com



E9.4

$$T_0 = T_1 + \frac{V_1^2}{2c_p} = 470 + \frac{(180)^2}{2(1005)} = 486 \text{ K} \qquad \textit{Ans. (a)}$$

Part (b) The local sound speed $a_1 = \sqrt{kRT_1} = [(1.4)(287)(470)]^{1/2} = 435$ m/s. Hence

$$\text{Ma}_1 = \frac{V_1}{a_1} = \frac{180}{435} = 0.414 \qquad \textit{Ans. (b)}$$

Part (c) With Ma_1 known, the stagnation pressure follows from Eq. (9.34):

$$p_0 = p_1(1 + 0.2\ \text{Ma}_1^2)^{3.5} = (500 \text{ kPa})[1 + 0.2(0.414)^2]^{3.5} = 563 \text{ kPa} \qquad \textit{Ans. (c)}$$

Part (d) Similarly, from Eq. (9.45), the critical sonic-throat area is

$$\frac{A_1}{A^*} = \frac{(1 + 0.2\ \text{Ma}_1^2)^3}{1.728\ \text{Ma}_1} = \frac{[1 + 0.2(0.414)^2]^3}{1.728(0.414)} = 1.547$$

or

$$A^* = \frac{A_1}{1.547} = \frac{0.05 \text{ m}^2}{1.547} = 0.0323 \text{ m}^2 \qquad \textit{Ans. (d)}$$

This throat must *actually be present* in the duct if the flow is to become supersonic.

We now know A^*. So to compute the mass flow we can use Eq. (9.46), which remains valid, based on the numerical value of A^*, whether or not a throat actually exists:

$$\dot{m} = 0.6847 \frac{p_0 A^*}{\sqrt{RT_0}} = 0.6847 \frac{(563{,}000)(0.0323)}{\sqrt{(287)(486)}} = 33.4 \text{ kg/s} \qquad \textit{Ans. (d)}$$

Or we could fare equally well with our new "local mass flow" formula, Eq. (9.47), using, say, the pressure and area at section 1. Given $p_1/p_0 = 500/563 = 0.889$, Eq. (9.47) yields

$$\dot{m}\frac{\sqrt{287(486)}}{563{,}000(0.05)} = \sqrt{\frac{2(1.4)}{0.4}(0.889)^{2/1.4}[1 - (0.889)^{0.4/1.4}]} = 0.447 \qquad \dot{m} = 33.4 \frac{\text{kg}}{\text{s}} \quad \textit{Ans. (d)}$$



Part (e) Assume *subsonic* flow corresponds to section 2*E* in Fig. E9.4. The duct contracts to an area ratio $A_2/A^* = 0.036/0.0323 = 1.115$, which we find on the left side of Fig. 9.7 or the subsonic part of Table B.1. Neither the figure nor the table is that accurate. There are two accurate options. First, Eq. (9.48*b*) gives the estimate $\text{Ma}_2 \approx 1 - 0.88 \ln (1.115)^{0.45} \approx 0.676$ (error less than 0.5 percent). Second, EES (App. E) will give an arbitrarily accurate solution with only three statements (in SI units):

```
A2 = 0.036
Astar = 0.0323
A2/Astar = (1+0.2*Ma2^2)^3/1.2^3/Ma2
```



ketabline.com Ebook.ketabline.com

Specify that you want a *subsonic* solution (e.g., limit $\text{Ma}_2 < 1$), and EES reports

$$\texttt{Ma}_2 = \textbf{0.6758} \qquad \textit{Ans. (e)}$$

[Ask for a supersonic solution and you receive $\texttt{Ma}_2 = \texttt{1.4001}$, which is the answer to part (*f*).] The pressure is given by the isentropic relation

$$p_2 = \frac{p_0}{[1 + 0.2(0.676)^2]^{3.5}} = \frac{563 \text{ kPa}}{1.358} \approx 415 \text{ kPa} \qquad \textit{Ans. (e)}$$

Part (*e*) does *not* require a throat, sonic or otherwise; the flow could simply be contracting subsonically from A_1 to A_2.



Part (f) This time assume *supersonic* flow, corresponding to section 2*F* in Fig. E9.4. Again the area ratio is $A_2/A^* = 0.036/0.0323 = 1.115$, and we look on the *right* side of Fig. 9.7 or the supersonic part of Table B.1—the latter can be read quite accurately as $\text{Ma}_2 \approx 1.40$. Again there are two other accurate options. First, Eq. (9.48*c*) gives the curve-fit estimate $\text{Ma}_2 \approx 1 + 1.2(1.115 - 1)1^{1/2} \approx 1.407$, only 0.5 percent high. Second, EES will give a very accurate solution with the same three statements from part (*e*). Specify that you want a *supersonic* solution (e.g., limit $\text{Ma}_2 > 1$), and EES reports

$$\texttt{Ma}_2 = \textbf{1.4001} \qquad \textit{Ans. (f)}$$

Again the pressure is given by the isentropic relation at the new Mach number:

$$p_2 = \frac{p_0}{[1 + 0.2(1.4001)^2]^{3.5}} = \frac{563 \text{ kPa}}{3.183} = 177 \text{ kPa} \qquad \textit{Ans. (f)}$$

Note that the supersonic-flow pressure level is much less than p_2 in part (*e*), and a sonic throat *must* have occurred between sections 1 and 2F.

EXAMPLE 9.5

It is desired to expand air from $p_0 = 200$ kPa and $T_0 = 500$ K through a throat to an exit Mach number of 2.5. If the desired mass flow is 3 kg/s, compute (*a*) the throat area and the exit (*b*) pressure, (*c*) temperature, (*d*) velocity, and (*e*) area, assuming isentropic flow, with $k = 1.4$.

Solution

The throat area follows from Eq. (9.47), because the throat flow must be sonic to produce a supersonic exit:

$$A^* = \frac{\dot{m}(RT_0)^{1/2}}{0.6847 p_0} = \frac{3.0[287(500)]^{1/2}}{0.6847(200{,}000)} = 0.00830 \text{ m}^2 = \frac{1}{4}\pi D^{*2}$$

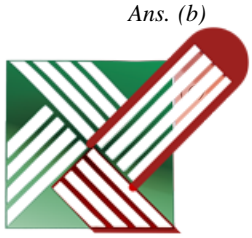
or

$$D_{\text{throat}} = 10.3 \text{ cm} \qquad \textit{Ans. (a)}$$

With the exit Mach number known, the isentropic-flow relations give the pressure and temperature:

$$p_e = \frac{p_0}{[1 + 0.2(2.5)^2]^{3.5}} = \frac{200{,}000}{17.08} = 11{,}700 \text{ Pa} \qquad \textit{Ans. (b)}$$

$$T_e = \frac{T_0}{1 + 0.2(2.5)^2} = \frac{500}{2.25} = 222 \text{ K}$$



ketabline.com Ebook.ketabline.com

The exit velocity follows from the known Mach number and temperature

$$V_e = \text{Ma}_e\,(kRT_e)^{1/2} = 2.5[1.4(287)(222)]^{1/2} = 2.5(299\text{ m/s}) = 747\text{ m/s} \qquad \textit{Ans. (d)}$$

The exit area follows from the known throat area and exit Mach number and Eq. (9.45):

$$\frac{A_e}{A^*} = \frac{[1 + 0.2(2.5)^2]^3}{1.728(2.5)} = 2.64$$

or $$A_e = 2.64A^* = 2.64(0.0083\text{ m}^2) = 0.0219\text{ m}^2 = \tfrac{1}{4}\pi D_e^2$$

or $$D_e = 16.7\text{ cm} \qquad \textit{Ans. (e)}$$

One point might be noted: The computation of the throat area A^* did not depend in any way on the numerical value of the exit Mach number. The exit was supersonic; therefore the throat is sonic and choked, and no further information is needed.

9.5 The Normal-Shock Wave

A common irreversibility occurring in supersonic internal or external flows is the normal-shock wave sketched in Fig. 9.8. Except at near-vacuum pressures such shock waves are very thin (a few micrometers thick) and approximate a discontinuous change in flow properties. We select a control volume just before and after the wave, as in Fig. 9.8.

The analysis is identical to that of Fig. 9.1; i.e., a shock wave is a fixed strong pressure wave. To compute all property changes rather than just the wave speed, we use all our basic one-dimensional steady-flow relations, letting section 1 be upstream and section 2 be downstream:

$$\rho_1 V_1 = \rho_2 V_2 = G = \text{const} \qquad (9.49a)$$

$$p_1 - p_2 = \rho_2 V_2^2 - \rho_1 V_1^2 \qquad (9.49b)$$

Energy: $$h_1 + \tfrac{1}{2}V_1^2 = h_2 + \tfrac{1}{2}V_2^2 = h_0 = \text{const} \qquad (9.49c)$$

Perfect gas: $$\frac{p_1}{\rho_1 T_1} = \frac{p_2}{\rho_2 T_2} \qquad (9.49d)$$

Constant c_p: $$h = c_p T \qquad k = \text{const} \qquad (9.49e)$$

Note that we have canceled out the areas $A_1 \approx A_2$, which is justified even in a variable duct section because of the thinness of the wave. The first successful analyses of these normal-shock relations are credited to W. J. M. Rankine (1870) and A. Hugoniot (1887), hence the modern term *Rankine-Hugoniot relations*. If we assume that the upstream conditions (p_1, V_1, ρ_1, h_1, T_1) are known, Eqs. (9.49) are five algebraic relations in the five unknowns (p_2, V_2, ρ_2, h_2, T_2). Because of the velocity-squared term, two solutions are found, and the correct one is determined from the second law of thermodynamics, which requires that $s_2 > s_1$.

The velocities V_1 and V_2 can be eliminated from Eqs. (9.49*a*) to (9.49*c*) to obtain the Rankine-Hugoniot relation

$$h_2 - h_1 = \frac{1}{2}(p_2 - p_1)\left(\frac{1}{\rho_2} + \frac{1}{\rho_1}\right)$$



ketabline.com Ebook.ketabline.com

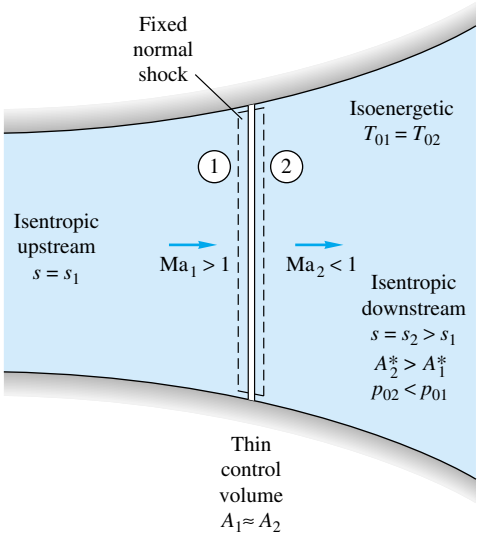


Fig. 9.8 Flow through a fixed normal-shock wave.

This contains only thermodynamic properties and is independent of the equation of state. Introducing the perfect-gas law $h = c_pT = kp/[(k-1)\rho]$, we can rewrite this as

$$\frac{\rho_2}{\rho_1} = \frac{1 + \beta p_2/p_1}{\beta + p_2/p_1} \qquad \beta = \frac{k+1}{k-1} \tag{9.51}$$

We can compare this with the isentropic-flow relation for a very weak pressure wave in a perfect gas

$$\frac{\rho_2}{\rho_1} = \left(\frac{p_2}{p_1}\right)^{1/k} \tag{9.52}$$

Also, the actual change in entropy across the shock can be computed from the perfect-gas relation

$$\frac{s_2 - s_1}{c_v} = \ln\left[\frac{p_2}{p_1}\left(\frac{\rho_1}{\rho_2}\right)^k\right] \tag{9.53}$$

Assuming a given wave strength p_2/p_1, we can compute the density ratio and the entropy change and list them as follows for $k = 1.4$:

$\frac{p_2}{p_1}$	ρ_2/ρ_1		$\frac{s_2 - s_1}{c_v}$
	Eq. (9.51)	Isentropic	
0.5	0.6154	0.6095	−0.0134
0.9	0.9275	0.9275	−0.00005
1.0	1.0	1.0	0.0
1.1	1.00704	1.00705	0.00004
1.5	1.3333	1.3359	0.0027
2.0	1.6250	1.6407	0.0134



ketabline.com Ebook.ketabline.com

We see that the entropy change is negative if the pressure decreases across the shock, which violates the second law. Thus a rarefaction shock is impossible in a perfect gas.[2] We see also that weak-shock waves ($p_2/p_1 \leq 2.0$) are very nearly isentropic.

Mach-Number Relations

For a perfect gas all the property ratios across the normal shock are unique functions of k and the upstream Mach number Ma_1. For example, if we eliminate ρ_2 and V_2 from Eqs. (9.49*a*) to (9.49*c*) and introduce $h = kp/[(k-1)\rho]$, we obtain

$$\frac{p_2}{p_1} = \frac{1}{k+1}\left[\frac{2\rho_1 V_1^2}{p_1} - (k-1)\right] \tag{9.54}$$

But for a perfect gas $\rho_1 V_1^2/p_1 = kV_1^2/(kRT_1) = k\,\text{Ma}_1^2$, so that Eq. (9.54) is equivalent to

$$\frac{p_2}{p_1} = \frac{1}{k+1}\left[2k\,\text{Ma}_1^2 - (k-1)\right] \tag{9.55}$$

From this equation we see that, for any k, $p_2 > p_1$ only if $\text{Ma}_1 > 1.0$. Thus for flow through a normal-shock wave, the upstream Mach number must be supersonic to satisfy the second law of thermodynamics.

What about the downstream Mach number? From the perfect-gas identity $\rho V^2 = kp\,\text{Ma}^2$, we can rewrite Eq. (9.49*b*) as

$$\frac{p_2}{p_1} = \frac{1 + k\,\text{Ma}_1^2}{1 + k\,\text{Ma}_2^2} \tag{9.56}$$

which relates the pressure ratio to both Mach numbers. By equating Eqs. (9.55) and (9.56) we can solve for

$$\text{Ma}_2^2 = \frac{(k-1)\,\text{Ma}_1^2 + 2}{2k\,\text{Ma}_1^2 - (k-1)} \tag{9.57}$$

Since Ma_1 must be supersonic, this equation predicts for all $k > 1$ that Ma_2 must be subsonic. Thus a normal-shock wave decelerates a flow almost discontinuously from supersonic to subsonic conditions.

Further manipulation of the basic relations (9.49) for a perfect gas gives additional equations relating the change in properties across a normal-shock wave in a perfect gas

$$\frac{\rho_2}{\rho_1} = \frac{(k+1)\,\text{Ma}_1^2}{(k-1)\,\text{Ma}_1^2 + 2} = \frac{V_1}{V_2}$$

$$\frac{T_2}{T_1} = [2 + (k-1)\,\text{Ma}_1^2]\,\frac{2k\,\text{Ma}_1^2 - (k-1)}{(k+1)^2\,\text{Ma}_1^2} \tag{9.58}$$

$$T_{02} = T_{01}$$

$$\frac{p_{02}}{p_{01}} = \frac{\rho_{02}}{\rho_{01}} = \left[\frac{(k+1)\,\text{Ma}_1^2}{2 + (k-1)\,\text{Ma}_1^2}\right]^{k/(k-1)}\left[\frac{k+1}{2k\,\text{Ma}_1^2 - (k-1)}\right]^{1/(k-1)}$$

Of additional interest is the fact that the critical, or sonic, throat area A^* in a duct increases across a normal shock

[2] This is true also for most real gases; see Ref. 14, sec. 7.3.



ketabline.com Ebook.ketabline.com

$$\frac{A_2^*}{A_1^*} = \frac{\text{Ma}_2}{\text{Ma}_1}\left[\frac{2 + (k-1)\,\text{Ma}_1^2}{2 + (k-1)\,\text{Ma}_2^2}\right]^{(1/2)(k+1)/(k-1)} \tag{9.59}$$

All these relations are given in Table B.2 and plotted versus upstream Mach number Ma_1 in Fig. 9.9 for $k = 1.4$. We see that pressure increases greatly while temperature and density increase moderately. The effective throat area A^* increases slowly at first and then rapidly. The failure of students to account for this change in A^* is a common source of error in shock calculations.

The stagnation temperature remains the same, but the stagnation pressure and density decrease in the same ratio; i.e., the flow across the shock is adiabatic but nonisentropic. Other basic principles governing the behavior of shock waves can be summarized as follows:

1. The upstream flow is supersonic, and the downstream flow is subsonic.
2. For perfect gases (and also for real fluids except under bizarre thermodynamic conditions) rarefaction shocks are impossible, and only a compression shock can exist.
3. The entropy increases across a shock with consequent decreases in stagnation pressure and stagnation density and an increase in the effective sonic-throat area.
4. Weak shock waves are very nearly isentropic.

Normal-shock waves form in ducts under transient conditions, e.g., shock tubes, and in steady flow for certain ranges of the downstream pressure. Figure 9.10*a* shows a normal shock in a supersonic nozzle. Flow is from left to right. The oblique wave pattern to the left is formed by roughness elements on the nozzle walls and indicates that the upstream flow is supersonic. Note the absence of these Mach waves (see Sec. 9.10) in the subsonic flow downstream.

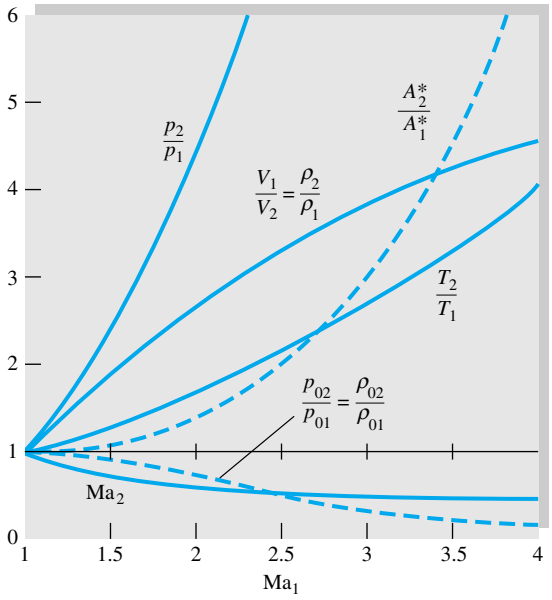
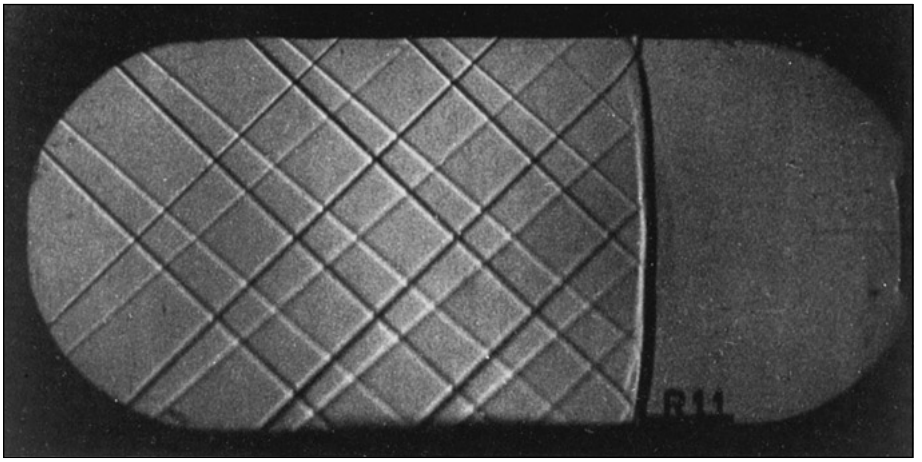


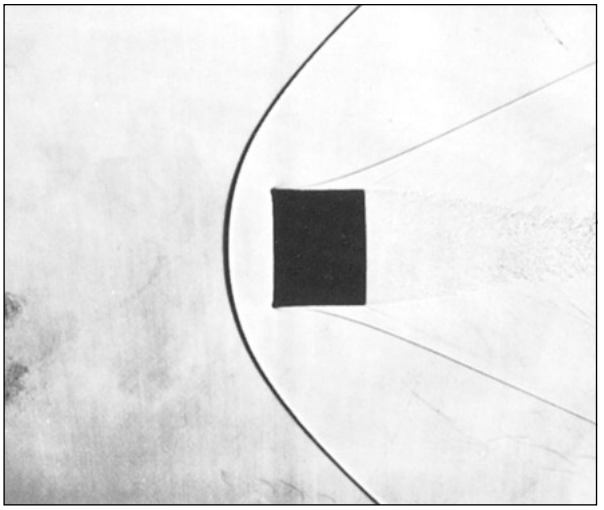
Fig. 9.9 Change in flow properties across a normal-shock wave for $k = 1.4$.



ketabline.com Ebook.ketabline.com



(*a*)

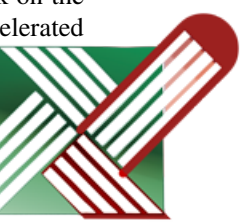


(*b*)

Fig. 9.10 Normal shocks form in both internal and external flows: (*a*) Normal shock in a duct; note the Mach-wave pattern to the left (upstream), indicating supersonic flow. *(Courtesy of U.S. Air Force Arnold Engineering Development Center.)* (*b*) Supersonic flow past a blunt body creates a normal shock at the nose; the apparent shock thickness and body-corner curvature are optical distortions. *(Courtesy of U.S. Army Ballistic Research Laboratory, Aberdeen Proving Ground.)*

Normal-shock waves occur not only in supersonic duct flows but also in a variety of supersonic external flows. An example is the supersonic flow past a blunt body shown in Fig. 9.10*b*. The bow shock is curved, with a portion in front of the body which is essentially normal to the oncoming flow. This normal portion of the bow shock satisfies the property-change conditions just as outlined in this section. The flow inside the shock near the body nose is thus subsonic and at relatively high temperature $T_2 > T_1$, and convective heat transfer is especially high in this region.

Each nonnormal portion of the bow shock in Fig. 9.10*b* satisfies the oblique-shock relations to be outlined in Sec. 9.9. Note also the oblique recompression shock on the sides of the body. What has happened is that the subsonic nose flow has accelerated around the corners back to supersonic flow at low pressure, which must th through the second shock to match the higher downstream pressure condition



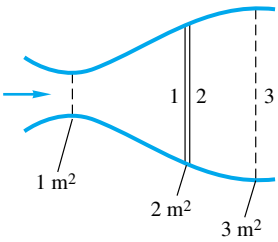
ketabline.com Ebook.ketabline.com

Note the fine-grained turbulent wake structure in the rear of the body in Fig. 9.10*b*. The turbulent boundary layer along the sides of the body is also clearly visible.

The analysis of a complex multidimensional supersonic flow such as in Fig. 9.10 is beyond the scope of this book. For further information see, e.g., Ref. 14, chap. 9, or Ref. 8, chap. 16.

Moving Normal Shocks

The preceding analysis of the fixed shock applies equally well to the moving shock if we reverse the transformation used in Fig. 9.1. To make the upstream conditions simulate a still fluid, we move the shock of Fig. 9.8 to the left at speed V_1; that is, we fix our coordinates to a control volume moving with the shock. The downstream flow then appears to move to the left at a slower speed $V_1 - V_2$ following the shock. The thermodynamic properties are not changed by this transformation, so that all our Eqs. (9.50) to (9.59) are still valid.



E9.6

EXAMPLE 9.6

Air flows from a reservoir where $p = 300$ kPa and $T = 500$ K through a throat to section 1 in Fig. E9.6, where there is a normal-shock wave. Compute (*a*) p_1, (*b*) p_2, (*c*) p_{02}, (*d*) A_2^*, (*e*) p_{03}, (*f*) A_3^*, (*g*) p_3, (*h*) T_{03}, and (*i*) T_3.

Solution

The reservoir conditions are the stagnation properties, which, for assumed one-dimensional adiabatic frictionless flow, hold through the throat up to section 1

$$p_{01} = 300 \text{ kPa} \qquad T_{01} = 500 \text{ K}$$

A shock wave cannot exist unless Ma_1 is supersonic; therefore the flow must have accelerated through a throat which is sonic

$$A_t = A_1^* = 1 \text{ m}^2$$

We can now find the Mach number Ma_1 from the known isentropic area ratio

$$\frac{A_1}{A_1^*} = \frac{2 \text{ m}^2}{1 \text{ m}^2} = 2.0$$

From Eq. (9.48*c*)

$$\text{Ma}_1 \approx 1 + 1.2(2.0 - 1)^{1/2} = 2.20$$

Further iteration with Eq. (9.45) would give $\text{Ma}_1 = 2.1972$, showing that Eq. (9.48*c*) gives satisfactory accuracy. The pressure p_1 follows from the isentropic relation (9.28) (or Table B.1)

$$\frac{p_{01}}{p_1} = [1 + 0.2(2.20)^2]^{3.5} = 10.7$$

or

$$p_1 = \frac{300 \text{ kPa}}{10.7} = 28.06 \text{ kPa}$$



ketabline.com Ebook.ketabline.com

The pressure p_2 is now obtained from Ma_1 and the normal-shock relation (9.55) or Table B.2

$$\frac{p_2}{p_1} = \frac{1}{2.4}[2.8(2.20)^2 - 0.4] = 5.48$$

or $$p_2 = 5.48(28.06) = 154 \text{ kPa} \qquad \textit{Ans. (b)}$$

In similar manner, for $\text{Ma}_1 = 2.20$, $p_{02}/p_{01} = 0.628$ from Eq. (9.58) and $A_2^*/A_1^* = 1.592$ from Eq. (9.59), or we can read Table B.2 for these values. Thus

$$p_{02} = 0.628(300 \text{ kPa}) = 188 \text{ kPa} \qquad \textit{Ans. (c)}$$

$$A_2^* = 1.592(1 \text{ m}^2) = 1.592 \text{ m}^2 \qquad \textit{Ans. (d)}$$

The flow from section 2 to 3 is isentropic (but at higher entropy than the flow upstream of the shock). Thus

$$p_{03} = p_{02} = 188 \text{ kPa} \qquad \textit{Ans. (e)}$$

$$A_3^* = A_2^* = 1.592 \text{ m}^2 \qquad \textit{Ans. (f)}$$

Knowing A_3^*, we can now compute p_3 by finding Ma_3 and without bothering to find Ma_2 (which happens to equal 0.547). The area ratio at section 3 is

$$\frac{A_3}{A_3^*} = \frac{3 \text{ m}^2}{1.592 \text{ m}^2} = 1.884$$

Then, since Ma_3 is known to be subsonic because it is downstream of a normal shock, we use Eq. (9.48*a*) to estimate

$$\text{Ma}_3 \approx \frac{1 + 0.27/(1.884)^2}{1.728(1.884)} = 0.330$$

The pressure p_3 then follows from the isentropic relation (9.28) or Table B.1

$$\frac{p_{03}}{p_3} = [1 + 0.2(0.330)^2]^{3.5} = 1.078$$

or $$p_3 = \frac{188 \text{ kPa}}{1.078} = 174 \text{ kPa} \qquad \textit{Ans. (g)}$$

Meanwhile, the flow is adiabatic throughout the duct; thus

$$T_{01} = T_{02} = T_{03} = 500 \text{ K} \qquad \textit{Ans. (h)}$$

Therefore, finally, from the adiabatic relation (9.26)

$$\frac{T_{03}}{T_3} = 1 + 0.2(0.330)^2 = 1.022$$

or $$T_3 = \frac{500 \text{ K}}{1.022} = 489 \text{ K} \qquad \textit{Ans. (i)}$$

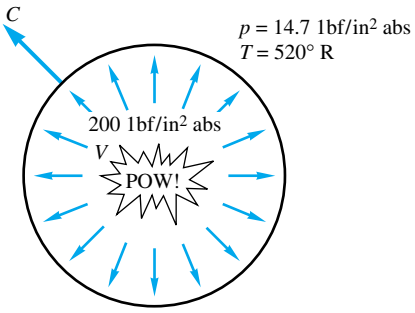
Notice that this type of duct-flow problem, with or without a shock wave, requires straightforward application of algebraic perfect-gas relations coupled with a little thought given to which formula is appropriate for the particular situation.



ketabline.com Ebook.ketabline.com

EXAMPLE 9.7

An explosion in air, $k = 1.4$, creates a spherical shock wave propagating radially into still air at standard conditions. At the instant shown in Fig. E9.7, the pressure just inside the shock is 200 lbf/in^2 absolute. Estimate (*a*) the shock speed C and (*b*) the air velocity V just inside the shock.



E9.7

Solution

Part (a) In spite of the spherical geometry the flow across the shock moves normal to the spherical wavefront; hence the normal-shock relations (9.50) to (9.59) apply. Fixing our control volume to the moving shock, we find that the proper conditions to use in Fig. 9.8 are

$$C = V_1 \qquad p_1 = 14.7 \text{ lbf/in}^2 \text{ absolute} \qquad T_1 = 520°\text{R}$$

$$V = V_1 - V_2 \qquad p_2 = 200 \text{ lbf/in}^2 \text{ absolute}$$

The speed of sound outside the shock is $a_1 \approx 49T_1^{1/2} = 1117$ ft/s. We can find Ma_1 from the known pressure ratio across the shock

$$\frac{p_2}{p_1} = \frac{200 \text{ lbf/in}^2 \text{ absolute}}{14.7 \text{ lbf/in}^2 \text{ absolute}} = 13.61$$

From Eq. (9.55) or Table B.2

$$13.61 = \frac{1}{2.4}(2.8\,\text{Ma}_1^2 - 0.4) \qquad \text{or} \qquad \text{Ma}_1 = 3.436$$

Then, by definition of the Mach number,

$$C = V_1 = \text{Ma}_1\, a_1 = 3.436(1117 \text{ ft/s}) = 3840 \text{ ft/s} \qquad \textit{Ans. (a)}$$

Part (b) To find V_2, we need the temperature or sound speed inside the shock. Since Ma_1 is known, from Eq. (9.58) or Table B.2 for $\text{Ma}_1 = 3.436$ we compute $T_2/T_1 = 3.228$. Then

$$T_2 = 3.228T_1 = 3.228(520°\text{R}) = 1679°\text{R}$$

At such a high temperature we should account for non-perfect-gas effects or at least use the gas tables [16], but we won't. Here just estimate from the perfect-gas energy equation (9.23) that

$$V_2^2 = 2c_p(T_1 - T_2) + V_1^2 = 2(6010)(520 - 1679) + (3840)^2 = 815{,}000$$

or

$$V_2 \approx 903 \text{ ft/s}$$

Notice that we did this without bothering to compute Ma_2, which equals 0.4
2000 ft/s.



ketabline.com Ebook.ketabline.com

Finally, the air velocity behind the shock is

$$V = V_1 - V_2 = 3840 - 903 \approx 2940 \text{ ft/s} \qquad \textit{Ans. (b)}$$

Thus a powerful explosion creates a brief but intense blast wind as it passes.[3]

9.6 Operation of Converging and Diverging Nozzles

By combining the isentropic-flow and normal-shock relations plus the concept of sonic throat choking, we can outline the characteristics of converging and diverging nozzles.

Converging Nozzle

First consider the converging nozzle sketched in Fig. 9.11*a*. There is an upstream reservoir at stagnation pressure p_0. The flow is induced by lowering the downstream outside, or *back*, pressure p_b below p_0, resulting in the sequence of states *a* to *e* shown in Fig. 9.11*b* and *c*.

For a moderate drop in p_b to states *a* and *b*, the throat pressure is higher than the critical value p^* which would make the throat sonic. The flow in the nozzle is subsonic throughout, and the jet exit pressure p_e equals the back pressure p_b. The mass flow is predicted by subsonic isentropic theory and is less than the critical value $\dot{m}_{\max}$, as shown in Fig. 9.11*c*.

For condition *c*, the back pressure exactly equals the critical pressure p^* of the throat. The throat becomes sonic, the jet exit flow is sonic, $p_e = p_b$, and the mass flow equals its maximum value from Eq. (9.46). The flow upstream of the throat is subsonic everywhere and predicted by isentropic theory based on the local area ratio $A(x)/A^*$ and Table B.1.

Finally, if p_b is lowered further to conditions *d* or *e* below p^*, the nozzle cannot respond further because it is choked at its maximum throat mass flow. The throat remains sonic with $p_e = p^*$, and the nozzle-pressure distribution is the same as in state *c*, as sketched in Fig. 9.11*b*. The exit jet expands supersonically so that the jet pressure can be reduced from p^* down to p_b. The jet structure is complex and multidimensional and is not shown here. Being supersonic, the jet cannot send any signal upstream to influence the choked flow conditions in the nozzle.

If the stagnation plenum chamber is large or supplemented by a compressor, and if the discharge chamber is larger or supplemented by a vacuum pump, the converging-nozzle flow will be steady or nearly so. Otherwise the nozzle will be blowing down, with p_0 decreasing and p_b increasing, and the flow states will be changing from, say, state *e* backward to state *a*. Blowdown calculations are usually made by a quasi-steady analysis based on isentropic steady-flow theory for the instantaneous pressures $p_0(t)$ and $p_b(t)$.

EXAMPLE 9.8

A converging nozzle has a throat area of 6 cm^2 and stagnation air conditions of 120 kPa and 400 K. Compute the exit pressure and mass flow if the back pressure is (*a*) 90 kPa and (*b*) 45 kPa. Assume $k = 1.4$.

[3] This is the principle of the *shock-tube wind tunnel*, in which a controlled explosion creates flow at very high Mach number, with data taken by fast-response instruments. See, e.g., Ref. 5, s



ketabline.com Ebook.ketabline.com

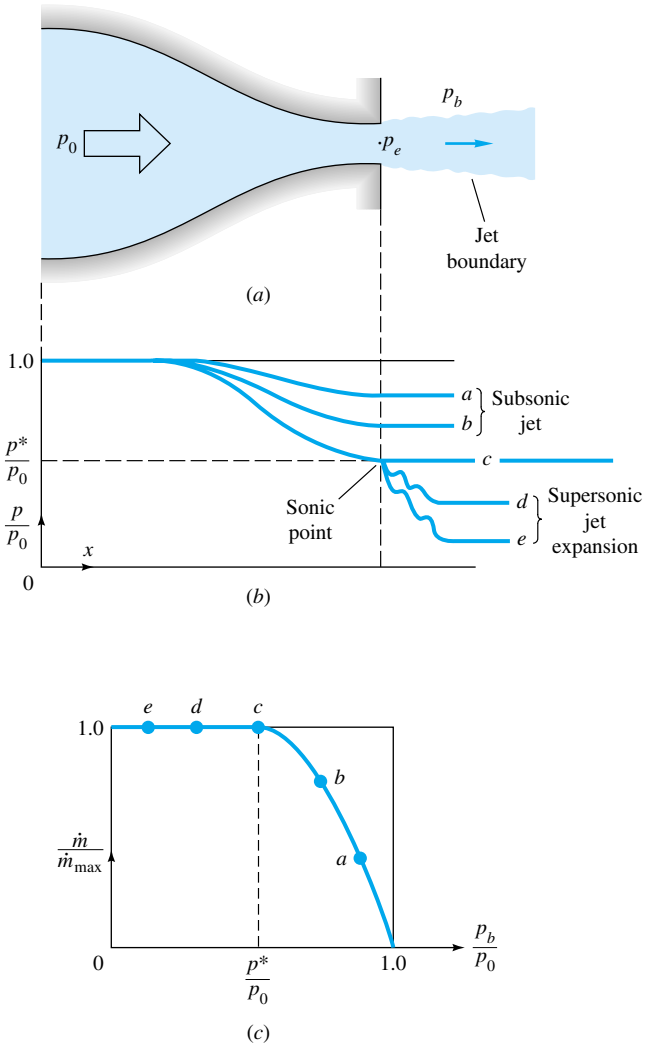


Fig. 9.11 Operation of a converging nozzle: (*a*) nozzle geometry showing characteristic pressures; (*b*) pressure distribution caused by various back pressures; (*c*) mass flow versus back pressure.

Solution

From Eq. (9.32) for $k = 1.4$ the critical (sonic) throat pressure is

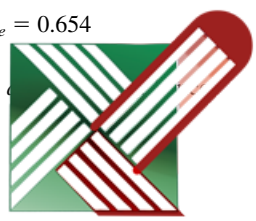
$$\frac{p^*}{p_0} = 0.5283 \qquad \text{or} \qquad p^* = (0.5283)(120 \text{ kPa}) = 63.4 \text{ kPa}$$

If the back pressure is less than this amount, the nozzle flow is choked.

Part (a) For $p_b = 90$ kPa $> p^*$, the flow is subsonic, not choked. The exit pressure is $p_e = p_b$. The throat Mach number is found from the isentropic relation (9.35) or Table B.1:

$$\text{Ma}_e^2 = 5\left[\left(\frac{p_0}{p_e}\right)^{2/7} - 1\right] = 5\left[\left(\frac{120}{90}\right)^{2/7} - 1\right] = 0.4283 \qquad \text{Ma}_e = 0.654$$

To find the mass flow, we could proceed with a serial attack on Ma_e, T_e, ρ



ketabline.com Ebook.ketabline.com

to compute $\rho_e A_e V_e$. However, since the local pressure is known, this part is ideally suited for the dimensionless mass-flow function in Eq. (9.47). With $p_e/p_0 = 90/120 = 0.75$, compute

$$\frac{\dot{m}\sqrt{RT_0}}{Ap_0} = \sqrt{\frac{2(1.4)}{0.4}(0.75)^{2/1.4}[1 - (0.75)^{0.4/1.4}]} = 0.6052$$

hence $$\dot{m} = 0.6052\frac{(0.0006)(120{,}000)}{\sqrt{287(400)}} = 0.129 \text{ kg/s} \qquad \textit{Ans. (a)}$$

for $$p_e = p_b = 90 \text{ kPa} \qquad \textit{Ans. (a)}$$

Part (b) For $p_b = 45$ kPa $< p^*$, the flow is choked, similar to condition *d* in Fig. 9.11*b*. The exit pressure is sonic:

$$p_e = p^* = 63.4 \text{ kPa} \qquad \textit{Ans. (b)}$$

The (choked) mass flow is a maximum from Eq. (9.46*b*):

$$\dot{m} = \dot{m}_{\max} = \frac{0.6847 p_0 A_e}{(RT_0)^{1/2}} = \frac{0.6847(120{,}000)(0.0006)}{[287(400)]^{1/2}} = 0.145 \text{ kg/s} \qquad \textit{Ans. (b)}$$

Any back pressure less than 63.4 kPa would cause this same choked mass flow. Note that the 50 percent increase in exit Mach number, from 0.654 to 1.0, has increased the mass flow only 12 percent, from 0.128 to 0.145 kg/s.

Converging-Diverging Nozzle

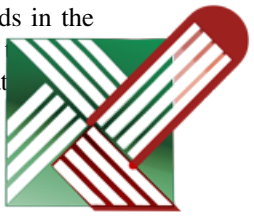
Now consider the converging-diverging nozzle sketched in Fig. 9.12*a*. If the back pressure p_b is low enough, there will be supersonic flow in the diverging portion and a variety of shock-wave conditions may occur, which are sketched in Fig. 9.12*b*. Let the back pressure be gradually decreased.

For curves *A* and *B* in Fig. 9.12*b* the back pressure is not low enough to induce sonic flow in the throat, and the flow in the nozzle is subsonic throughout. The pressure distribution is computed from subsonic isentropic area-change relations, e.g., Table B.1. The exit pressure $p_e = p_b$, and the jet is subsonic.

For curve *C* the area ratio A_e/A_t exactly equals the critical ratio A_e/A^* for a subsonic Ma_e in Table B.1. The throat becomes sonic, and the mass flux reaches a maximum in Fig. 9.12*c*. The remainder of the nozzle flow is subsonic, including the exit jet, and $p_e = p_b$.

Now jump for a moment to curve *H*. Here p_b is such that p_b/p_0 exactly corresponds to the critical-area ratio A_e/A^* for a *supersonic* Ma_e in Table B.1. The diverging flow is entirely supersonic, including the jet flow, and $p_e = p_b$. This is called the *design pressure ratio* of the nozzle and is the back pressure suitable for operating a supersonic wind tunnel or an efficient rocket exhaust.

Now back up and suppose that p_b lies between curves *C* and *H*, which is impossible according to purely isentropic-flow calculations. Then back pressures *D* to *F* occur in Fig. 9.12*b*. The throat remains choked at the sonic value, and we can match $p_e = p_b$ by placing a normal shock at just the right place in the diverging section to cause a *subsonic-diffuser* flow back to the back-pressure condition. The mass flow remains at maximum in Fig. 9.12*c*. At back pressure *F* the required normal shock stands in the duct exit. At back pressure *G* no single normal shock can do the job, and so it compresses outside the exit in a complex series of oblique shocks until it mat



ketabline.com Ebook.ketabline.com

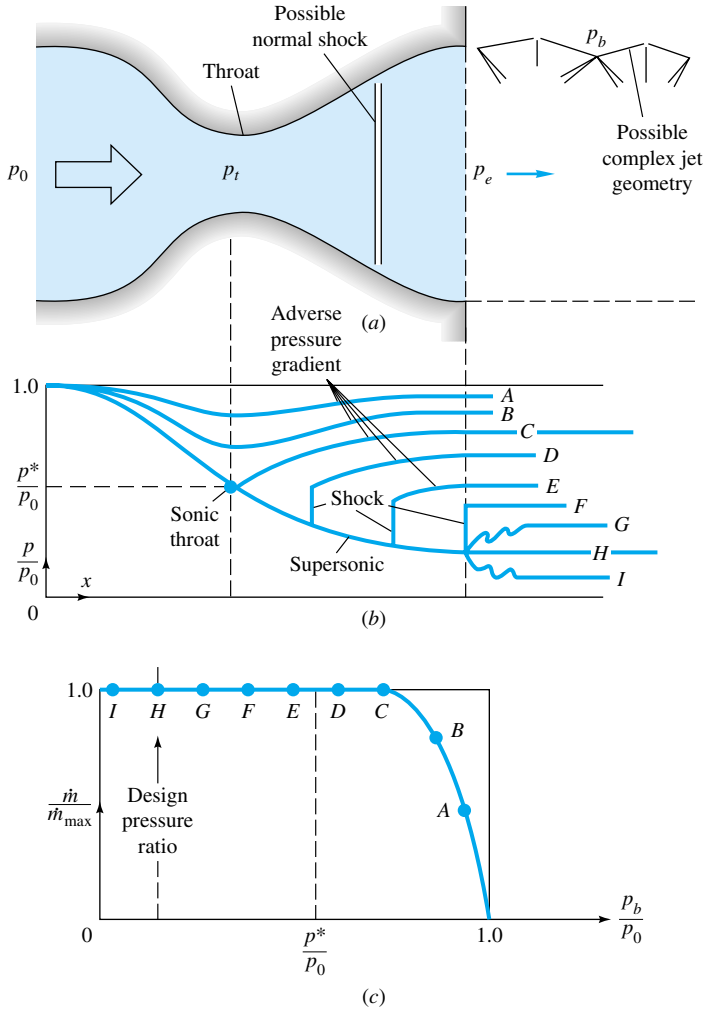
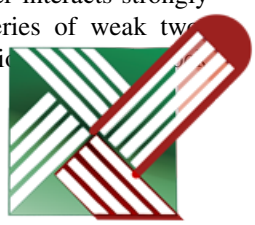


Fig. 9.12 Operation of a converging-diverging nozzle: (*a*) nozzle geometry with possible flow configurations; (*b*) pressure distribution caused by various back pressures; (*c*) mass flow versus back pressure.

Finally, at back pressure I, p_b is lower than the design pressure H, but the nozzle is choked and cannot respond. The exit flow expands in a complex series of supersonic wave motions until it matches the low back pressure. See, e.g., Ref. 9, sec. 5.4, for further details of these off-design jet-flow configurations.

Note that for p_b less than back pressure C, there is supersonic flow in the nozzle and the throat can receive no signal from the exit behavior. The flow remains choked, and the throat has no idea what the exit conditions are.

Note also that the normal shock-patching idea is idealized. Downstream of the shock the nozzle flow has an adverse pressure gradient, usually leading to wall boundary-layer separation. Blockage by the greatly thickened separated layer interacts strongly with the core flow (recall Fig. 6.27) and usually induces a series of weak two-dimensional compression shocks rather than a single one-dimensional (see, e.g., Ref. 14, pp. 292 and 293, for further details).



ketabline.com Ebook.ketabline.com

EXAMPLE 9.9

A converging-diverging nozzle (Fig. 9.12*a*) has a throat area of 0.002 m^2 and an exit area of 0.008 m^2. Air stagnation conditions are $p_0 = 1000$ kPa and $T_0 = 500$ K. Compute the exit pressure and mass flow for (*a*) design condition and the exit pressure and mass flow if (*b*) $p_b \approx 300$ kPa and (*c*) $p_b \approx 900$ kPa. Assume $k = 1.4$.

Solution

Part (a) The design condition corresponds to supersonic isentropic flow at the given area ratio $A_e/A_t = 0.008/0.002 = 4.0$. We can find the design Mach number either by iteration of the area-ratio formula (9.45), using EES, or by the curve fit (9.48*d*)

$$\mathrm{Ma}_{e,\mathrm{design}} \approx [216(4.0) - 254(4.0)^{2/3}]^{1/5} \approx 2.95 \qquad (\text{exact} = 2.9402)$$

The accuracy of the curve fit is seen to be satisfactory. The design pressure ratio follows from Eq. (9.34)

$$\frac{p_0}{p_e} = [1 + 0.2(2.95)^2]^{3.5} = 34.1$$

or

$$p_{e,\mathrm{design}} = \frac{1000 \text{ kPa}}{34.1} = 29.3 \text{ kPa} \qquad \textit{Ans. (a)}$$

Since the throat is clearly sonic at design conditions, Eq. (9.46*b*) applies

$$\dot{m}_{\mathrm{design}} = \dot{m}_{\max} = \frac{0.6847 p_0 A_t}{(RT_0)^{1/2}} = \frac{0.6847(10^6 \text{ Pa})(0.002 \text{ m}^2)}{[287(500)]^{1/2}} \qquad \textit{Ans. (a)}$$

$$= 3.61 \text{ kg/s}$$

Part (b) For $p_b = 300$ kPa we are definitely far below the subsonic isentropic condition *C* in Fig. 9.12*b*, but we may even be below condition *F* with a normal shock in the exit, i.e., in condition *G*, where oblique shocks occur outside the exit plane. If it is condition *G*, then $p_e = p_{e,\mathrm{design}} = 29.3$ kPa because no shock has yet occurred. To find out, compute condition *F* by assuming an exit normal shock with $\mathrm{Ma}_1 = 2.95$, that is, the design Mach number just upstream of the shock. From Eq. (9.55)

$$\frac{p_2}{p_1} = \frac{1}{2.4}[2.8(2.95)^2 - 0.4] = 9.99$$

or

$$p_2 = 9.99 p_1 = 9.99 p_{e,\mathrm{design}} = 293 \text{ kPa}$$

Since this is less than the given $p_b = 300$ kPa, there is a normal shock just upstream of the exit plane (condition *E*). The exit flow is subsonic and equals the back pressure

$$p_e = p_b = 300 \text{ kPa} \qquad \textit{Ans. (b)}$$

Also

$$\dot{m} = \dot{m}_{\max} = 3.61 \text{ kg/s} \qquad \textit{Ans. (b)}$$

The throat is still sonic and choked at its maximum mass flow.

Part (c) Finally, for $p_b = 900$ kPa, which is up near condition *C*, we compute Ma_e and p_e for condition *C* as a comparison. Again $A_e/A_t = 4.0$ for this condition, with a subsonic Ma_e estimated from the curve-fitted Eq. (9.48*a*):

$$\mathrm{Ma}_e(C) \approx \frac{1 + 0.27/(4.0)^2}{1.728(4.0)} = 0.147 \qquad (\text{exact} = 0.14655)$$



ketabline.com Ebook.ketabline.com

Then the isentropic exit-pressure ratio for this condition is

$$\frac{p_0}{p_e} = [1 + 0.2(0.147)^2]^{3.5} = 1.0152$$

or

$$p_e = \frac{1000}{1.0152} = 985 \text{ kPa}$$

The given back pressure of 900 kPa is less than this value, corresponding roughly to condition *D* in Fig. 9.12*b*. Thus for this case there is a normal shock just downstream of the throat, and the throat is choked

$$p_e = p_b = 900 \text{ kPa} \qquad \dot{m} = \dot{m}_{\max} = 3.61 \text{ kg/s} \qquad \textit{Ans. (c)}$$

For this large exit-area ratio, the exit pressure would have to be larger than 985 kPa to cause a subsonic flow in the throat and a mass flow less than maximum.

9.7 Compressible Duct Flow with Friction[4]

Section 9.4 showed the effect of area change on a compressible flow while neglecting friction and heat transfer. We could now add friction and heat transfer to the area change and consider coupled effects, which is done in advanced texts [for example, 8, chap. 8]. Instead, as an elementary introduction, this section treats only the effect of friction, neglecting area change and heat transfer. The basic assumptions are

1. Steady one-dimensional adiabatic flow
2. Perfect gas with constant specific heats
3. Constant-area straight duct
4. Negligible shaft-work and potential-energy changes
5. Wall shear stress correlated by a Darcy friction factor

In effect, we are studying a Moody-type pipe-friction problem but with large changes in kinetic energy, enthalpy, and pressure in the flow.

Consider the elemental duct control volume of area A and length dx in Fig. 9.13. The area is constant, but other flow properties (p, ρ, T, h, V) may vary with x. Appli-

[4] This section may be omitted without loss of continuity.

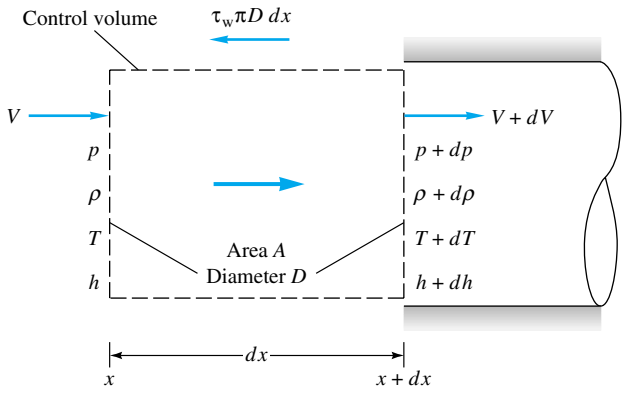


Fig. 9.13 Elemental control volume for flow in a constant-area duct with friction.



ketabline.com Ebook.ketabline.com

cation of the three conservation laws to this control volume gives three differential equations

Continuity: $$\rho V = \frac{\dot{m}}{A} = G = \text{const}$$

or $$\frac{d\rho}{\rho} + \frac{dV}{V} = 0 \tag{9.60a}$$

x momentum: $$pA - (p + dp)A - \tau_w \pi D\, dx = \dot{m}(V + dV - V)$$

or $$dp + \frac{4\tau_w dx}{D} + \rho V\, dV = 0 \tag{9.60b}$$

Energy: $$h + \tfrac{1}{2}V^2 = h_0 = c_p T_0 = c_p T + \tfrac{1}{2}V^2$$

or $$c_p\, dT + V\, dV = 0 \tag{9.60c}$$

Since these three equations have five unknowns—p, ρ, T, V, and τ_w—we need two additional relations. One is the perfect-gas law

$$p = \rho RT \qquad \text{or} \qquad \frac{dp}{p} = \frac{d\rho}{\rho} + \frac{dT}{T} \tag{9.61}$$

To eliminate τ_w as an unknown, it is assumed that wall shear is correlated by a local Darcy friction factor f

$$\tau_w = \tfrac{1}{8} f\rho V^2 = \tfrac{1}{8} fkp\ \text{Ma}^2 \tag{9.62}$$

where the last form follows from the perfect-gas speed-of-sound expression $a^2 = kp/\rho$. In practice, f can be related to the local Reynolds number and wall roughness from, say, the Moody chart, Fig. 6.13.

Equations (9.60) and (9.61) are first-order differential equations and can be integrated, by using friction-factor data, from any inlet section 1, where p_1, T_1, V_1, etc., are known, to determine $p(x)$, $T(x)$, etc., along the duct. It is practically impossible to eliminate all but one variable to give, say, a single differential equation for $p(x)$, but all equations can be written in terms of the Mach number $\text{Ma}(x)$ and the friction factor, by using the definition of Mach number

$$V^2 = \text{Ma}^2\, kRT$$

or $$\frac{2\, dV}{V} = \frac{2\, d\,\text{Ma}}{\text{Ma}} + \frac{dT}{T} \tag{9.63}$$

Adiabatic Flow

By eliminating variables between Eqs. (9.60) to (9.63), we obtain the working relations

$$\frac{dp}{p} = -k\,\text{Ma}^2 \frac{1 + (k-1)\,\text{Ma}^2}{2(1 - \text{Ma}^2)} f\frac{dx}{D} \tag{9.64a}$$

$$\frac{d\rho}{\rho} = -\frac{k\,\text{Ma}^2}{2(1 - \text{Ma}^2)} f\frac{dx}{D} = -\frac{dV}{V}$$



ketabline.com Ebook.ketabline.com

$$\frac{dp_0}{p_0} = \frac{d\rho_0}{\rho_0} = -\frac{1}{2}\,k\,\mathrm{Ma}^2\,f\,\frac{dx}{D} \tag{9.64c}$$

$$\frac{dT}{T} = -\frac{k(k-1)\,\mathrm{Ma}^4}{2(1-\mathrm{Ma}^2)}\,f\,\frac{dx}{D} \tag{9.64d}$$

$$\frac{d\,\mathrm{Ma}^2}{\mathrm{Ma}^2} = k\,\mathrm{Ma}^2\,\frac{1+\frac{1}{2}(k-1)\,\mathrm{Ma}^2}{1-\mathrm{Ma}^2}\,f\,\frac{dx}{D} \tag{9.64e}$$

All these except dp_0/p_0 have the factor $1 - \mathrm{Ma}^2$ in the denominator, so that, like the area-change formulas in Fig. 9.5, subsonic and supersonic flow have opposite effects:

Property	Subsonic	Supersonic
p	Decreases	Increases
ρ	Decreases	Increases
V	Increases	Decreases
p_0, ρ_0	Decreases	Decreases
T	Decreases	Increases
Ma	Increases	Decreases
Entropy	Increases	Increases

We have added to the list above that entropy must increase along the duct for either subsonic or supersonic flow as a consequence of the second law for adiabatic flow. For the same reason, stagnation pressure and density must both decrease.

The key parameter above is the Mach number. Whether the inlet flow is subsonic or supersonic, the duct Mach number always tends downstream toward $\mathrm{Ma} = 1$ because this is the path along which the entropy increases. If the pressure and density are computed from Eqs. (9.64*a*) and (9.64*b*) and the entropy from Eq. (9.53), the result can be plotted in Fig. 9.14 versus Mach number for $k = 1.4$. The maximum entropy occurs at $\mathrm{Ma} = 1$, so that the second law requires that the duct-flow properties continually approach the sonic point. Since p_0 and ρ_0 continually decrease along the duct due to the frictional (nonisentropic) losses, they are not useful as reference properties. Instead, the sonic properties p^*, ρ^*, T^*, p_0^*, and ρ_0^* are the appropriate constant reference quantities in adiabatic duct flow. The theory then computes the ratios p/p^*, T/T^*, etc., as a function of local Mach number and the integrated friction effect.

To derive working formulas, we first attack Eq. (9.64*e*), which relates the Mach number to friction. Separate the variables and integrate:

$$\int_0^{L^*} f\,\frac{dx}{D} = \int_{\mathrm{Ma}^2}^{1.0} \frac{1-\mathrm{Ma}^2}{k\,\mathrm{Ma}^4[1+\frac{1}{2}(k-1)\,\mathrm{Ma}^2]}\,d\,\mathrm{Ma}^2 \tag{9.65}$$

The upper limit is the sonic point, whether or not it is actually reached in the duct flow. The lower limit is arbitrarily placed at the position $x = 0$, where the Mach number is Ma. The result of the integration is

$$\frac{\bar{f}L^*}{D} = \frac{1-\mathrm{Ma}^2}{k\,\mathrm{Ma}^2} + \frac{k+1}{2k}\ln\frac{(k+1)\,\mathrm{Ma}^2}{2+(k-1)\,\mathrm{Ma}^2} \tag{9.66}$$

where $\bar{f}$ is the average friction factor between 0 and L^*. In practice, ways assumed, and no attempt is made to account for the slight ch



ketabline.com Ebook.ketabline.com

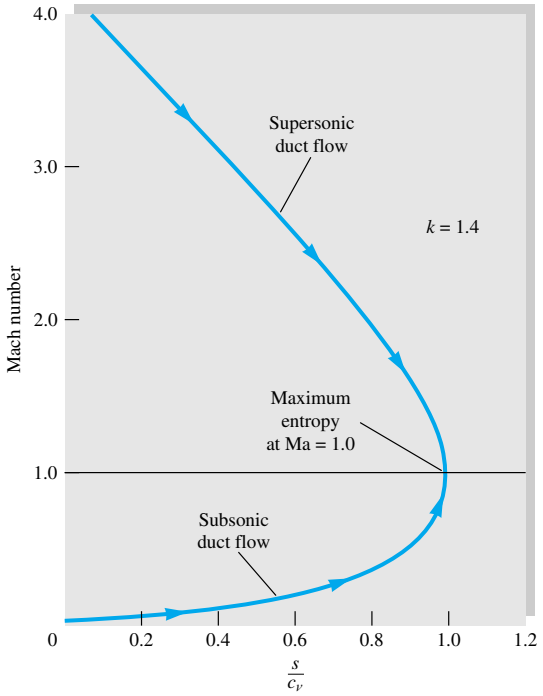


Fig. 9.14 Adiabatic frictional flow in a constant-area duct always approaches Ma = 1 to satisfy the second law of thermodynamics. The computed curve is independent of the value of the friction factor.

number along the duct. For noncircular ducts, D is replaced by the hydraulic diameter $D_h = (4 \times \text{area})/\text{perimeter}$ as in Eq. (6.74).

Equation (9.66) is tabulated versus Mach number in Table B.3. The length L^* is the length of duct required to develop a duct flow from Mach number Ma to the sonic point. Many problems involve short ducts which never become sonic, for which the solution uses the differences in the tabulated "maximum," or sonic, length. For example, the length ΔL required to develop from Ma_1 to Ma_2 is given by

$$\bar{f}\,\frac{\Delta L}{D} = \left(\frac{\bar{f}L^*}{D}\right)_1 - \left(\frac{\bar{f}L^*}{D}\right)_2 \tag{9.67}$$

This avoids the need for separate tabulations for short ducts.

It is recommended that the friction factor $\bar{f}$ be estimated from the Moody chart (Fig. 6.13) for the average Reynolds number and wall-roughness ratio of the duct. Available data [20] on duct friction for compressible flow show good agreement with the Moody chart for subsonic flow, but the measured data in supersonic duct flow are up to 50 percent less than the equivalent Moody friction factor.

EXAMPLE 9.10

Air flows subsonically in an adiabatic 2-cm-diameter duct. The average friction factor is 0.024. What length of duct is necessary to accelerate the flow from $\text{Ma}_1 = 0.1$ to $\text{Ma}_2 = 0.5$? ditional length will accelerate it to $\text{Ma}_3 = 1.0$? Assume $k = 1.4$.



ketabline.com Ebook.ketabline.com

Solution

Equation (9.67) applies, with values of $\bar{f}L^*/D$ computed from Eq. (9.66) or read from Table B.3:

$$\bar{f}\frac{\Delta L}{D} = \frac{0.024\ \Delta L}{0.02\ \text{m}} = \left(\frac{\bar{f}L^*}{D}\right)_{\text{Ma}=0.1} - \left(\frac{\bar{f}L^*}{D}\right)_{\text{Ma}=0.5}$$

$$= 66.9216 - 1.0691 = 65.8525$$

Thus
$$\Delta L = \frac{65.8525(0.02\ \text{m})}{0.024} = 55\ \text{m} \qquad \textit{Ans. (a)}$$

The additional length $\Delta L'$ to go from Ma = 0.5 to Ma = 1.0 is taken directly from Table B.2

$$f\frac{\Delta L'}{D} = \left(\frac{fL^*}{D}\right)_{\text{Ma}=0.5} = 1.0691$$

or
$$\Delta L' = L^*_{\text{Ma}=0.5} = \frac{1.0691(0.02\ \text{m})}{0.024} = 0.9\ \text{m} \qquad \textit{Ans. (b)}$$

This is typical of these calculations: It takes 55 m to accelerate up to Ma = 0.5 and then only 0.9 m more to get all the way up to the sonic point.

Formulas for other flow properties along the duct can be derived from Eqs. (9.64). Equation (9.64*e*) can be used to eliminate $f\,dx/D$ from each of the other relations, giving, for example, dp/p as a function only of Ma and $d\ \text{Ma}^2/\text{Ma}^2$. For convenience in tabulating the results, each expression is then integrated all the way from (p, Ma) to the sonic point (p^*, 1.0). The integrated results are

$$\frac{p}{p^*} = \frac{1}{\text{Ma}}\left[\frac{k+1}{2+(k-1)\ \text{Ma}^2}\right]^{1/2} \tag{9.68a}$$

$$\frac{\rho}{\rho^*} = \frac{V^*}{V} = \frac{1}{\text{Ma}}\left[\frac{2+(k-1)\ \text{Ma}^2}{k+1}\right]^{1/2} \tag{9.68b}$$

$$\frac{T}{T^*} = \frac{a^2}{a^{*2}} = \frac{k+1}{2+(k-1)\ \text{Ma}^2} \tag{9.68c}$$

$$\frac{p_0}{p_0^*} = \frac{\rho_0}{\rho_0^*} = \frac{1}{\text{Ma}}\left[\frac{2+(k-1)\ \text{Ma}^2}{k+1}\right]^{(1/2)(k+1)/(k-1)} \tag{9.68d}$$

All these ratios are also tabulated in Table B.3. For finding changes between points Ma_1 and Ma_2 which are not sonic, products of these ratios are used. For example,

$$\frac{p_2}{p_1} = \frac{p_2}{p^*}\frac{p^*}{p_1} \tag{9.69}$$

since p^* is a constant reference value for the flow.

EXAMPLE 9.11

For the duct flow of Example 9.10 assume that, at $\text{Ma}_1 = 0.1$, we have p_1
450 K. At section 2 farther downstream, $\text{Ma}_2 = 0.5$. Compute (*a*) p_2, (*b*) T_2



ketabline.com Ebook.ketabline.com

Solution

As preliminary information we can compute V_1 and p_{01} from the given data:

$$V_1 = \text{Ma}_1\, a_1 = 0.1[(1.4)(287)(450)]^{1/2} = 0.1(425 \text{ m/s}) = 42.5 \text{ m/s}$$

$$p_{01} = p_1(1 + 0.2\,\text{Ma}_1^2)^{3.5} = (600 \text{ kPa})[1 + 0.2(0.1)^2]^{3.5} = 604 \text{ kPa}$$

Now enter Table B.3 or Eqs. (9.68) to find the following property ratios:

Section	Ma	p/p^*	T/T^*	V/V^*	p_0/p_0^*
1	0.1	10.9435	1.1976	0.1094	5.8218
2	0.5	2.1381	1.1429	0.5345	1.3399

Use these ratios to compute all properties downstream:

$$p_2 = p_1 \frac{p_2/p^*}{p_1/p^*} = (600 \text{ kPa}) \frac{2.1381}{10.9435} = 117 \text{ kPa} \qquad \textit{Ans. (a)}$$

$$T_2 = T_1 \frac{T_2/T^*}{T_1/T^*} = (450 \text{ K}) \frac{1.1429}{1.1976} = 429 \text{ K} \qquad \textit{Ans. (b)}$$

$$V_2 = V_1 \frac{V_2/V^*}{V_1/V^*} = (42.5 \text{ m/s}) \frac{0.5345}{0.1094} = 208 \frac{\text{m}}{\text{s}} \qquad \textit{Ans. (c)}$$

$$p_{02} = p_{01} \frac{p_{02}/p_0^*}{p_{01}/p_0^*} = (604 \text{ kPa}) \frac{1.3399}{5.8218} = 139 \text{ kPa} \qquad \textit{Ans. (d)}$$

Note the 77 percent reduction in stagnation pressure due to friction. The formulas are seductive, so check your work by other means. For example, check $p_{02} = p_2(1 + 0.2\,\text{Ma}_2^2)^{3.5}$.

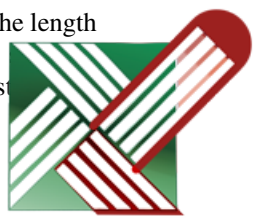
Choking due to Friction

The theory here predicts that for adiabatic frictional flow in a constant-area duct, no matter what the inlet Mach number Ma_1 is, the flow downstream tends toward the sonic point. There is a certain duct length $L^*(\text{Ma}_1)$ for which the exit Mach number will be exactly unity. The duct is then choked.

But what if the actual length L is greater than the predicted "maximum" length L^*? Then the flow conditions must change, and there are two classifications.

Subsonic inlet. If $L > L^*(\text{Ma}_1)$, the flow slows down until an inlet Mach number Ma_2 is reached such that $L = L^*(\text{Ma}_2)$. The exit flow is sonic, and the mass flow has been reduced by *frictional choking*. Further increases in duct length will continue to decrease the inlet Ma and mass flow.

Supersonic inlet. From Table B.3 we see that friction has a very large effect on supersonic duct flow. Even an infinite inlet Mach number will be reduced to sonic conditions in only 41 diameters for $\bar{f} = 0.02$. Some typical numerical values are shown in Fig. 9.15, assuming an inlet Ma = 3.0 and $\bar{f} = 0.02$. For this condition $L^* = 26$ diameters. If L is increased beyond $26D$, the flow will not choke but a normal shock will form at just the right place for the subsequent subsonic frictional flow to become sonic exactly at the exit. Figure 9.15 shows two examples, for $L/D = 40$ and 53. As the length increases, the required normal shock moves upstream until, for Fig. 9.15, the
at the inlet for $L/D = 63$. Further increase in L causes the shock to move ups



ketabline.com Ebook.ketabline.com

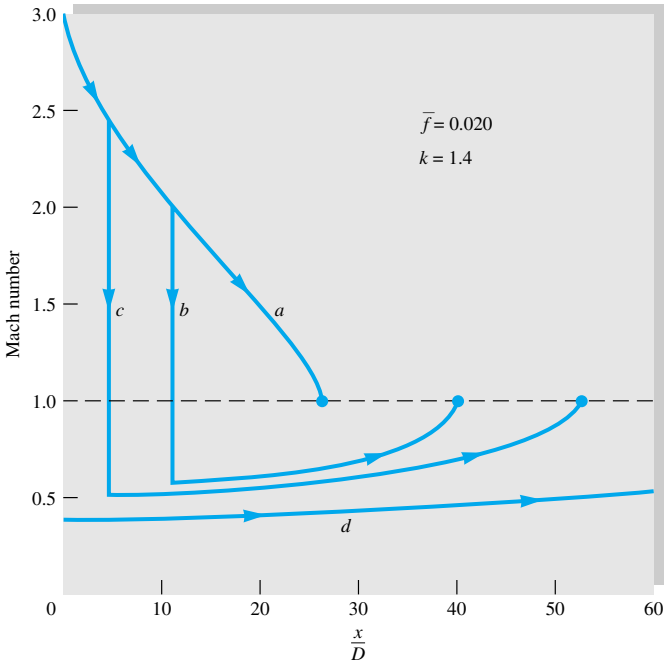


Fig. 9.15 Behavior of duct flow with a nominal supersonic inlet condition Ma = 3.0: (*a*) $L/D \leq 26$, flow is supersonic throughout duct; (*b*) $L/D = 40 > L^*/D$, normal shock at Ma = 2.0 with subsonic flow then accelerating to sonic exit point; (*c*) $L/D = 53$, shock must now occur at Ma = 2.5; (*d*) $L/D > 63$, flow must be entirely subsonic and choked at exit.

the inlet into the supersonic nozzle feeding the duct. Yet the mass flow is still the same as for the very short duct, because presumably the feed nozzle still has a sonic throat. Eventually, a very long duct will cause the feed-nozzle throat to become choked, thus reducing the duct mass flow. Thus supersonic friction changes the flow pattern if $L > L^*$ but does not choke the flow until L is much larger than L^*.

EXAMPLE 9.12

Air enters a 3-cm-diameter duct at $p_0 = 200$ kPa, $T_0 = 500$ K, and $V_1 = 100$ m/s. The friction factor is 0.02. Compute (*a*) the maximum duct length for these conditions, (*b*) the mass flow if the duct length is 15 m, and (*c*) the reduced mass flow if $L = 30$ m.

Solution

Part (a) First compute

$$T_1 = T_0 - \frac{\frac{1}{2}V_1^2}{c_p} = 500 - \frac{\frac{1}{2}(100 \text{ m/s})^2}{1005 \text{ m}^2/(\text{s}^2 \cdot \text{K})} = 500 - 5 = 495 \text{ K}$$

$$a_1 = (kRT_1)^{1/2} \approx 20(495)^{1/2} = 445 \text{ m/s}$$

Thus

$$\text{Ma}_1 = \frac{V_1}{a_1} = \frac{100}{445} = 0.225$$

For this Ma_1, from Eq. (9.66) or interpolation in Table B.3,

$$\frac{\bar{f}L^*}{D} = 11.0$$



ketabline.com Ebook.ketabline.com

The maximum duct length possible for these inlet conditions is

$$L^* = \frac{(\bar{f}L^*/D)D}{\bar{f}} = \frac{11.0(0.03\text{ m})}{0.02} = 16.5\text{ m} \qquad \textit{Ans. (a)}$$

Part (b) The given $L = 15$ m is less than L^*, and so the duct is not choked and the mass flow follows from inlet conditions

$$\rho_{01} = \frac{p_{01}}{RT_0} = \frac{200{,}000\text{ Pa}}{287(500\text{ K})} = 1.394\text{ kg/m}^3$$

$$\rho_1 = \frac{\rho_{01}}{[1 + 0.2(0.225)^2]^{2.5}} = \frac{1.394}{1.0255} = 1.359\text{ kg/m}^3$$

whence

$$\dot{m} = \rho_1 A V_1 = (1.359\text{ kg/m}^3)\left[\frac{\pi}{4}(0.03\text{ m})^2\right](100\text{ m/s})$$

$$= 0.0961\text{ kg/s} \qquad \textit{Ans. (b)}$$

Part (c) Since $L = 30$ m is greater than L^*, the duct must choke back until $L = L^*$, corresponding to a lower inlet Ma_1:

$$L^* = L = 30\text{ m}$$

$$\frac{\bar{f}L^*}{D} = \frac{0.02(30\text{ m})}{0.03\text{ m}} = 20.0$$



It is difficult to interpolate for $fL/D = 20$ in Table B.3 and impossible to invert Eq. (9.66) for the Mach number without laborious iteration. But it is a breeze for EES to solve Eq. (9.66) for the Mach number, using the following three statements:

```
k = 1.4
fLD = 20
fLD = (1 - Ma^2)/k/Ma^2 + (k + 1)/2/k*LN((k + 1)*Ma^2/(2 + (k - 1)*Ma^2))
```

Simply specify $\text{Ma} < 1$ in the Variable Information menu and EES cheerfully reports

$$\text{Ma}_{\text{choked}} = 0.174 \quad (23\ \text{percent less})$$

$$T_{1,\text{new}} = \frac{T_0}{1 + 0.2(0.174)^2} = 497\ \text{K}$$

$$a_{1,\text{new}} \approx 20(497\ \text{K})^{1/2} = 446\ \text{m/s}$$

$$V_{1,\text{new}} = \text{Ma}_1\, a_1 = 0.174(446) = 77.6\ \text{m/s}$$

$$\rho_{1,\text{new}} = \frac{\rho_{01}}{[1 + 0.2(0.174)^2]^{2.5}} = 1.373\ \text{kg/m}^3$$

$$\dot{m}_{\text{new}} = \rho_1 A V_1 = 1.373\left[\frac{\pi}{4}(0.03)^2\right](77.6)$$

$$= 0.0753\ \text{kg/s} \quad (22\ \text{percent less}) \qquad \textit{Ans. (c)}$$

Isothermal Flow with Friction

The adiabatic frictional-flow assumption is appropriate to high-speed flow ducts. For flow in long ducts, e.g., natural-gas pipelines, the gas state more clo



ketabline.com Ebook.ketabline.com

proximates an isothermal flow. The analysis is the same except that the isoenergetic energy equation (9.60*c*) is replaced by the simple relation

$$T = \text{const} \qquad dT = 0 \tag{9.70}$$

Again it is possible to write all property changes in terms of the Mach number. Integration of the Mach-number–friction relation yields

$$\frac{\bar{f}L_{\max}}{D} = \frac{1 - k\,\text{Ma}^2}{k\,\text{Ma}^2} + \ln\,(k\,\text{Ma}^2) \tag{9.71}$$

which is the isothermal analog of Eq. (9.66) for adiabatic flow.

This friction relation has the interesting result that $L_{\max}$ becomes zero not at the sonic point but at $\text{Ma}_{\text{crit}} = 1/k^{1/2} = 0.845$ if $k = 1.4$. The inlet flow, whether subsonic or supersonic, tends downstream toward this limiting Mach number $1/k^{1/2}$. If the tube length L is greater than $L_{\max}$ from Eq. (9.71), a subsonic flow will choke back to a smaller Ma_1 and mass flow and a supersonic flow will experience a normal-shock adjustment similar to Fig. 9.15.

The exit isothermal choked flow is not sonic, and so the use of the asterisk is inappropriate. Let p', ρ', and V' represent properties at the choking point $L = L_{\max}$. Then the isothermal analysis leads to the following Mach-number relations for the flow properties:

$$\frac{p}{p'} = \frac{1}{\text{Ma}\,k^{1/2}} \qquad \frac{V}{V'} = \frac{\rho'}{\rho} = \text{Ma}\,k^{1/2} \tag{9.72}$$

The complete analysis and some examples are given in advanced texts [for example, 8, sec. 6.4].

Mass Flow for a Given Pressure Drop

An interesting by-product of the isothermal analysis is an explicit relation between the pressure drop and duct mass flow. This is a common problem which requires numerical iteration for adiabatic flow, as outlined below. In isothermal flow, we may substitute $dV/V = -dp/p$ and $V^2 = G^2/[p/(RT)]^2$ in Eq. (9.63) to obtain

$$\frac{2p\,dp}{G^2RT} + f\frac{dx}{D} - \frac{2\,dp}{p} = 0$$

Since G^2RT is constant for isothermal flow, this may be integrated in closed form between $(x, p) = (0, p_1)$ and (L, p_2):

$$G^2 = \left(\frac{\dot{m}}{A}\right)^2 = \frac{p_1^2 - p_2^2}{RT[\bar{f}L/D + 2\ln\,(p_1/p_2)]} \tag{9.73}$$

Thus mass flow follows directly from the known end pressures, without any use of Mach numbers or tables.

The writer does not know of any direct analogy to Eq. (9.73) for adiabatic flow. However, a useful adiabatic relation, involving velocities instead of pressures, is derived in several textbooks [5, p. 212; 34, p. 418]:

$$V_1^2 = \frac{a_0^2[1 - (V_1/V_2)^2]}{k\bar{f}L/D + (k+1)\ln\,(V_2/V_1)}$$



ketabline.com Ebook.ketabline.com

where $a_0 = (kRT_0)^{1/2}$ is the stagnation speed of sound, constant for adiabatic flow. We assign the proof of this as a problem exercise. This may be combined with continuity for constant duct area $V_1/V_2 = \rho_2/\rho_1$, plus the following combination of adiabatic energy and the perfect-gas relation:

$$\frac{V_1}{V_2} = \frac{p_2}{p_1}\frac{T_1}{T_2} = \frac{p_2}{p_1}\left[\frac{2a_0^2 - (k-1)V_1^2}{2a_0^2 - (k-1)V_2^2}\right] \tag{9.75}$$

If we are given the end pressures, neither V_1 nor V_2 will likely be known in advance. Here, if EES is not available, we suggest only the following simple procedure. Begin with $a_0 \approx a_1$ and the bracketed term in Eq. (9.75) approximately equal to 1.0. Solve Eq. (9.75) for a first estimate of V_1/V_2, and use this value in Eq. (9.74) to get a better estimate of V_1. Use V_1 to improve your estimate of a_0, and repeat the procedure. The process should converge in a few iterations.

Equations (9.73) and (9.74) have one flaw: With the Mach number eliminated, the frictional choking phenomenon is not directly evident. Therefore, assuming a subsonic inlet flow, one should check the exit Mach number Ma_2 to ensure that it is not greater than $1/k^{1/2}$ for isothermal flow or greater than 1.0 for adiabatic flow. We illustrate both adiabatic and isothermal flow with the following example.

EXAMPLE 9.13

Air enters a pipe of 1-cm diameter and 1.2-m length at $p_1 = 220$ kPa and $T_1 = 300$ K. If $\bar{f} = 0.025$ and the exit pressure is $p_2 = 140$ kPa, estimate the mass flow for (*a*) isothermal flow and (*b*) adiabatic flow.

Solution

Part (a) For isothermal flow Eq. (9.73) applies without iteration:

$$\frac{\bar{f}L}{D} + 2\ln\frac{p_1}{p_2} = \frac{(0.025)(1.2\text{ m})}{0.01\text{ m}} + 2\ln\frac{220}{140} = 3.904$$

$$G^2 = \frac{(220{,}000\text{ Pa})^2 - (140{,}000\text{ Pa})^2}{[287\text{ m}^2/(\text{s}^2\cdot\text{K})](300\text{ K})(3.904)} = 85{,}700 \qquad \text{or} \qquad G = 293\text{ kg/(s}\cdot\text{m}^2)$$

Since $A = (\pi/4)(0.01\text{ m})^2 = 7.85\text{ E-5 m}^2$, the isothermal mass flow estimate is

$$\dot{m} = GA = (293)(7.85\text{ E-5}) \approx 0.0230\text{ kg/s} \qquad \textit{Ans. (a)}$$

Check that the exit Mach number is not choked:

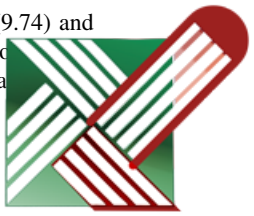
$$\rho_2 = \frac{p_2}{RT} = \frac{140{,}000}{(287)(300)} = 1.626\text{ kg/m}^3 \qquad V_2 = \frac{G}{\rho_2} = \frac{293}{1.626} = 180\text{ m/s}$$

or

$$\mathrm{Ma}_2 = \frac{V_2}{\sqrt{kRT}} = \frac{180}{[1.4(287)(300)]^{1/2}} = \frac{180}{347} \approx 0.52$$

This is well below choking, and the isothermal solution is accurate.

Part (b) For adiabatic flow, we can iterate by hand, in the time-honored fashion, using Eqs. (9.74) and (9.75) plus the definition of stagnation speed of sound. A few years ago the author wo
done just that, laboriously. However, EES makes handwork and manipulation of equa



ketabline.com Ebook.ketabline.com

necessary, although careful programming and good guesses are required. If we ignore superfluous output such as T_2 and V_2, 13 statements are appropriate. First, spell out the given physical properties (in SI units):

```
k = 1.4
P1 = 220000
P2 = 140000
T1 = 300
```

Next, apply the adiabatic friction relations, Eqs. (9.66) and (9.67), to both points 1 and 2:

```
fLD1 = (1 - Ma1^2)/k/Ma1^2+(k+1)/2/k*LN((k+1)*Ma1^2/(2+(k-1)*Ma1^2))
fLD2 = (1 - Ma2^2)/k/Ma2^2+(k+1)/2/k*LN((k+1)*Ma2^2/(2+(k-1)*Ma2^2))
DeltafLD = 0.025*1.2/0.01
fLD1 = fLD2 + DeltafLD
```

Then apply the pressure-ratio formula (9.68*a*) to both points 1 and 2:

```
P1/Pstar = ((k+1)/(2+(k-1)*Ma1^2))^0.5/Ma1
P2/Pstar = ((k+1)/(2+(k-1)*Ma2^2))^0.5/Ma2
```

These are *adiabatic* relations, so we need not further spell out quantities such as T_0 or a_0 unless we want them as additional output.

The above 10 statements are a closed algebraic system, and EES will solve them for Ma_1 and Ma_2. However, the problem asks for mass flow, so we complete the system:

```
V1 = Ma1*sqrt(1.4*287*T1)
Rho1 = P1/287/T1
Mdot = Rho1*(pi/4*0.01^2)*V1
```

If we apply no constraints, EES reports "cannot solve", because its default allows all variables to lie between $-\infty$ and $+\infty$. So we enter Variable Information and constrain Ma_1 and Ma_2 to lie between 0 and 1 (subsonic flow). EES still complains that it "cannot solve" but hints that "better guesses are needed". Indeed, the default guesses for EES variables are normally 1.0, too large for the Mach numbers. Guess the Mach numbers equal to 0.8 or even 0.5, and EES still complains, for a subtle reason: Since $f\Delta L/D = 0.025(1.2/0.01) = 3.0$, Ma_1 can be no larger than 0.36 (see Table B.3). Finally, then, we guess Ma_1 and $\text{Ma}_2 = 0.3$ or 0.4, and EES happily reports the solution:

$$\text{Ma}_1 = 0.3343 \qquad \text{Ma}_2 = 0.5175 \qquad \frac{fL}{D_1} = 3.935 \qquad \frac{fL}{D_2} = 0.9348$$

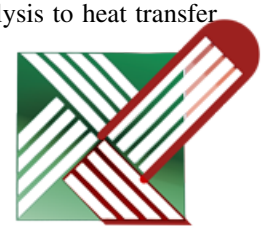
$$p^* = 67{,}892 \text{ Pa} \qquad \dot{m} = \mathbf{0.0233 \text{ kg/s}} \qquad \textit{Ans. (b)}$$

Though the programming is complicated, the EES approach is superior to hand iteration and, of course, we can save this program for use again with new data.

9.8 Frictionless Duct Flow with Heat Transfer[5]

Heat addition or removal has an interesting effect on a compressible flow. Advanced texts [for example, 8, chap. 8] consider the combined effect of heat transfer coupled with friction and area change in a duct. Here we confine the analysis to heat transfer with no friction in a constant-area duct.

[5] This section may be omitted without loss of continuity.



ketabline.com Ebook.ketabline.com

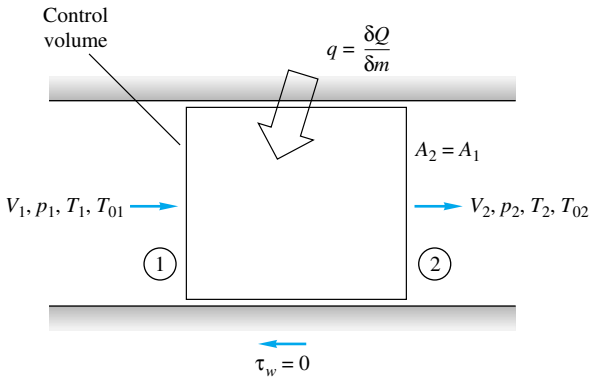


Fig. 9.16 Elemental control volume for frictionless flow in a constant-area duct with heat transfer. The length of the element is indeterminate in this simplified theory.

Consider the elemental duct control volume in Fig. 9.16. Between sections 1 and 2 an amount of heat δQ is added (or removed) to each incremental mass δm passing through. With no friction or area change, the control-volume conservation relations are quite simple:

Continuity: $$\rho_1 V_1 = \rho_2 V_2 = G = \text{const} \tag{9.76a}$$

x momentum: $$p_1 - p_2 = G(V_2 - V_1) \tag{9.76b}$$

Energy: $$\dot{Q} = \dot{m}(h_2 + \tfrac{1}{2}V_2^2 - h_1 - \tfrac{1}{2}V_1^2)$$

or $$q = \frac{\dot{Q}}{\dot{m}} = \frac{\delta Q}{\delta m} = h_{02} - h_{01} \tag{9.76c}$$

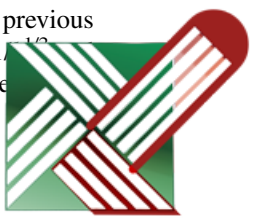
The heat transfer results in a change in stagnation enthalpy of the flow. We shall not specify exactly how the heat is transferred—combustion, nuclear reaction, evaporation, condensation, or wall heat exchange—but simply that it happened in amount q between 1 and 2. We remark, however, that wall heat exchange is not a good candidate for the theory because wall convection is inevitably coupled with wall friction, which we neglected.

To complete the analysis, we use the perfect-gas and Mach-number relations

$$\frac{p_2}{\rho_2 T_2} = \frac{p_1}{\rho_1 T_1} \qquad h_{02} - h_{01} = c_p(T_{02} - T_{01})$$
$$\frac{V_2}{V_1} = \frac{\text{Ma}_2\, a_2}{\text{Ma}_1\, a_1} = \frac{\text{Ma}_2}{\text{Ma}_1}\left(\frac{T_2}{T_1}\right)^{1/2} \tag{9.77}$$

For a given heat transfer $q = \delta Q/\delta m$ or, equivalently, a given change $h_{02} - h_{01}$, Eqs. (9.76) and (9.77) can be solved algebraically for the property ratios p_2/p_1, Ma_2/Ma_1, etc., between inlet and outlet. Note that because the heat transfer allows the entropy to either increase or decrease, the second law imposes no restrictions on these solutions.

Before writing down these property-ratio functions, we illustrate the effect of heat transfer in Fig. 9.17, which shows T_0 and T versus Mach number in the duct. Heating increases T_0, and cooling decreases it. The maximum possible T_0 occurs at $\text{Ma} = 1.0$, and we see that heating, whether the inlet is subsonic or supersonic, drives the duct Mach number toward unity. This is analogous to the effect of friction in the previous section. The temperature of a perfect gas increases from $\text{Ma} = 0$ up to $\text{Ma} = 1/\sqrt{\gamma}$, then decreases. Thus there is a peculiar—or at least unexpected—region whe



ketabline.com Ebook.ketabline.com

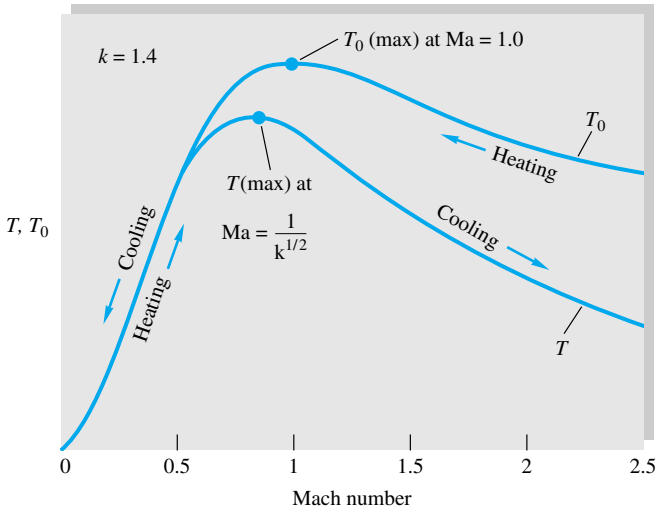


Fig. 9.17 Effect of heat transfer on Mach number.

ing (increasing T_0) actually decreases the gas temperature, the difference being reflected in a large increase of the gas kinetic energy. For $k = 1.4$ this peculiar area lies between Ma = 0.845 and Ma = 1.0 (interesting but not very useful information).

The complete list of the effects of simple T_0 change on duct-flow properties is as follows:

	Heating		Cooling	
	Subsonic	Supersonic	Subsonic	Supersonic
T_0	Increases	Increases	Decreases	Decreases
Ma	Increases	Decreases	Decreases	Increases
p	Decreases	Increases	Increases	Decreases
ρ	Decreases	Increases	Increases	Decreases
V	Increases	Decreases	Decreases	Increases
p_0	Decreases	Decreases	Increases	Increases
s	Increases	Increases	Decreases	Decreases
T	*	Increases	†	Decreases

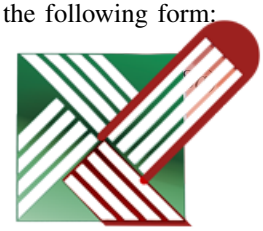
*Increases up to Ma = $1/k^{1/2}$ and decreases thereafter.
†Decreases up to Ma = $1/k^{1/2}$ and increases thereafter.

Probably the most significant item on this list is the stagnation pressure p_0, which always decreases during heating whether the flow is subsonic or supersonic. Thus heating does increase the Mach number of a flow but entails a loss in effective pressure recovery.

Mach-Number Relations

Equations (9.76) and (9.77) can be rearranged in terms of the Mach number and the results tabulated. For convenience, we specify that the outlet section is sonic, Ma = 1, with reference properties T_0^*, T^*, p^*, ρ^*, V^*, and p_0^*. The inlet is assumed to be at arbitrary Mach number Ma. Equations (9.76) and (9.77) then take the following form:

$$\frac{T_0}{T_0^*} = \frac{(k+1)\,\mathrm{Ma}^2\,[2+(k-1)\,\mathrm{Ma}^2]}{(1+k\,\mathrm{Ma}^2)^2}$$



ketabline.com Ebook.ketabline.com

$$\frac{T}{T^*} = \frac{(k+1)^2\,\mathrm{Ma}^2}{(1+k\,\mathrm{Ma}^2)^2} \tag{9.78b}$$

$$\frac{p}{p^*} = \frac{k+1}{1+k\,\mathrm{Ma}^2} \tag{9.78c}$$

$$\frac{V}{V^*} = \frac{\rho^*}{\rho} = \frac{(k+1)\,\mathrm{Ma}^2}{1+k\,\mathrm{Ma}^2} \tag{9.78d}$$

$$\frac{p_0}{p_0^*} = \frac{k+1}{1+k\,\mathrm{Ma}^2}\left[\frac{2+(k-1)\,\mathrm{Ma}^2}{k+1}\right]^{k/(k-1)} \tag{9.78e}$$

These formulas are all tabulated versus Mach number in Table B.4. The tables are very convenient if inlet properties Ma_1, V_1, etc., are given but are somewhat cumbersome if the given information centers on T_{01} and T_{02}. Let us illustrate with an example.

EXAMPLE 9.14

A fuel-air mixture, approximated as air with $k = 1.4$, enters a duct combustion chamber at $V_1 = 75$ m/s, $p_1 = 150$ kPa, and $T_1 = 300$ K. The heat addition by combustion is 900 kJ/kg of mixture. Compute (*a*) the exit properties V_2, p_2, and T_2 and (*b*) the total heat addition which would have caused a sonic exit flow.

Solution

Part (a) First compute $T_{01} = T_1 + V_1^2/(2c_p) = 300 + (75)^2/[2(1005)] = 303$ K. Then compute the change in stagnation temperature of the gas:

$$q = c_p(T_{02} - T_{01})$$

or

$$T_{02} = T_{01} + \frac{q}{c_p} = 303\text{ K} + \frac{900{,}000\text{ J/kg}}{1005\text{ J/(kg}\cdot\text{K)}} = 1199\text{ K}$$

We have enough information to compute the initial Mach number:

$$a_1 = \sqrt{kRT_1} = [1.4(287)(300)]^{1/2} = 347\text{ m/s} \qquad \mathrm{Ma}_1 = \frac{V_1}{a_1} = \frac{75}{347} = 0.216$$

For this Mach number, use Eq. (9.78*a*) or Table B.4 to find the sonic value T^*_0:

$$\text{At } \mathrm{Ma}_1 = 0.216\text{:} \qquad \frac{T_{01}}{T_0^*} \approx 0.1992 \qquad \text{or} \qquad T_0^* = \frac{303\text{ K}}{0.1992} \approx 1521\text{ K}$$

Then the stagnation temperature ratio at section 2 is $T_{02}/T_0^* = 1199/1521 = 0.788$, which corresponds in Table B.4 to a Mach number $\mathrm{Ma}_2 \approx 0.573$.

Now use Table B.4 at Ma_1 and Ma_2 to tabulate the desired property ratios.

Section	Ma	V/V^*	p/p^*	T/T^*
1	0.216	0.1051	2.2528	0.2368
2	0.573	0.5398	1.6442	0.8876



ketabline.com Ebook.ketabline.com

The exit properties are computed by using these ratios to find state 2 from state 1:

$$V_2 = V_1 \frac{V_2/V^*}{V_1/V^*} = (75 \text{ m/s}) \frac{0.5398}{0.1051} = 385 \text{ m/s} \qquad \textit{Ans. (a)}$$

$$p_2 = p_1 \frac{p_2/p^*}{p_1/p^*} = (150 \text{ kPa}) \frac{1.6442}{2.2528} = 109 \text{ kPa} \qquad \textit{Ans. (a)}$$

$$T_2 = T_1 \frac{T_2/T^*}{T_1/T^*} = (300 \text{ K}) \frac{0.8876}{0.2368} = 1124 \text{ K} \qquad \textit{Ans. (a)}$$

Part (b) The maximum allowable heat addition would drive the exit Mach number to unity:

$$T_{02} = T_0^* = 1521 \text{ K}$$

$$q_{\max} = c_p(T_0^* - T_{01}) = [1005 \text{ J/(kg} \cdot \text{K)}](1521 - 303 \text{ K}) \approx 1.22 \text{ E6 J/kg} \qquad \textit{Ans. (b)}$$

Choking Effects due to Simple Heating

Equation (9.78*a*) and Table B.4 indicate that the maximum possible stagnation temperature in simple heating corresponds to T_0^*, or the sonic exit Mach number. Thus, for given inlet conditions, only a certain maximum amount of heat can be added to the flow, for example, 1.22 MJ/kg in Example 9.14. For a subsonic inlet there is no theoretical limit on heat addition: The flow chokes more and more as we add more heat, with the inlet velocity approaching zero. For supersonic flow, even if Ma_1 is infinite, there is a finite ratio $T_{01}/T_0^* = 0.4898$ for $k = 1.4$. Thus if heat is added without limit to a supersonic flow, a normal-shock-wave adjustment is required to accommodate the required property changes.

In subsonic flow there is no theoretical limit to the amount of cooling allowed: The exit flow just becomes slower and slower, and the temperature approaches zero. In supersonic flow only a finite amount of cooling can be allowed before the exit flow approaches infinite Mach number, with $T_{02}/T_0^* = 0.4898$ and the exit temperature equal to zero. There are very few practical applications for supersonic cooling.

EXAMPLE 9.15

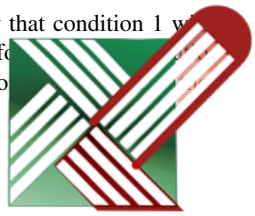
What happens to the inlet flow in Example 9.14 if the heat addition is increased to 1400 kJ/kg and the inlet pressure and stagnation temperature are fixed? What will be the subsequent decrease in mass flow?

Solution

For $q = 1400$ kJ/kg, the exit will be choked at the stagnation temperature

$$T_0^* = T_{01} + \frac{q}{c_p} = 303 + \frac{1.4 \text{ E6 J/kg}}{1005 \text{ J/(kg} \cdot \text{K)}} \approx 1696 \text{ K}$$

This is higher than the value $T_0^* = 1521$ K in Example 9.14, so we know that condition 1 w
have to choke down to a lower Mach number. The proper value is f
$T_{01}/T_0^* = 303/1696 = 0.1787$. From Table B.4 or Eq. (9.78*a*) for this co



ketabline.com Ebook.ketabline.com

new, lowered entrance Mach number: $\text{Ma}_{1,\text{new}} \approx 0.203$. With T_{01} and p_1 known, the other inlet properties follow from this Mach number:

$$T_1 = \frac{T_{01}}{1 + 0.2\ \text{Ma}_1^2} = \frac{303}{1 + 0.2(0.203)^2} = 301\ \text{K}$$

$$a_1 = \sqrt{kRT_1} = [1.4(287)(301)]^{1/2} = 348\ \text{m/s}$$

$$V_1 = \text{Ma}_1\, a_1 = (0.202)(348\ \text{m/s}) = 70\ \text{m/s}$$

$$\rho_1 = \frac{p_1}{RT_1} = \frac{150{,}000}{(287)(301)} = 1.74\ \text{kg/m}^3$$

Finally, the new lowered mass flow per unit area is

$$\frac{\dot{m}_{\text{new}}}{A} = \rho_1 V_1 = (1.74\ \text{kg/m}^3)(70\ \text{m/s}) = 122\ \text{kg/(s} \cdot \text{m}^2)$$

This is 7 percent less than in Example 9.14, due to choking by excess heat addition.

Relationship to the Normal-Shock Wave

The normal-shock-wave relations of Sec. 9.5 actually lurk within the simple heating relations as a special case. From Table B.4 or Fig. 9.17 we see that for a given stagnation temperature less than T_0^* there are two flow states which satisfy the simple heating relations, one subsonic and the other supersonic. These two states have (1) the same value of T_0, (2) the same mass flow per unit area, and (3) the same value of $p + \rho V^2$. Therefore these two states are exactly equivalent to the conditions on each side of a normal-shock wave. The second law would again require that the upstream flow Ma_1 be supersonic.

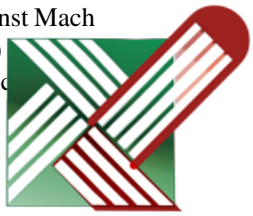
To illustrate this point, take $\text{Ma}_1 = 3.0$ and from Table B.4 read $T_{01}/T_0^* = 0.6540$ and $p_1/p^* = 0.1765$. Now, for the same value $T_{02}/T_0^* = 0.6540$, use Table B.4 or Eq. (9.78*a*) to compute $\text{Ma}_2 = 0.4752$ and $p_2/p^* = 1.8235$. The value of Ma_2 is exactly what we read in the shock table, Table B.2, as the downstream Mach number when $\text{Ma}_1 = 3.0$. The pressure ratio for these two states is $p_2/p_1 = (p_2/p^*)/(p_1/p^*) = 1.8235/0.1765 = 10.33$, which again is just what we read in Table B.2 for $\text{Ma}_1 = 3.0$. This illustration is meant only to show the physical background of the simple heating relations; it would be silly to make a practice of computing normal-shock waves in this manner.

9.9 Two-Dimensional Supersonic Flow

Up to this point we have considered only one-dimensional compressible-flow theories. This illustrated many important effects, but a one-dimensional world completely loses sight of the wave motions which are so characteristic of supersonic flow. The only "wave motion" we could muster in a one-dimensional theory was the normal-shock wave, which amounted only to a flow discontinuity in the duct.

Mach Waves

When we add a second dimension to the flow, wave motions immediately become apparent if the flow is supersonic. Figure 9.18 shows a celebrated graphical construction which appears in every fluid-mechanics textbook and was first presented by Ernst Mach in 1887. The figure shows the pattern of pressure disturbances (sound waves) by a small particle moving at speed U through a still fluid whose sound veloc



ketabline.com Ebook.ketabline.com

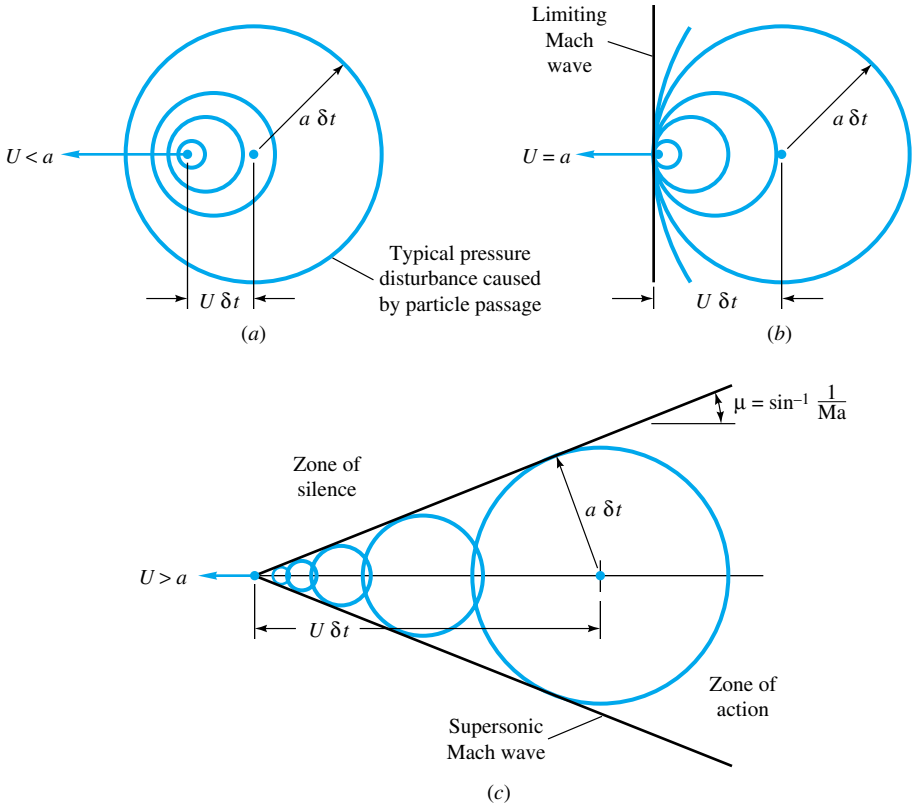


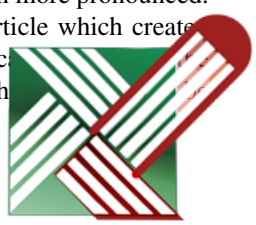
Fig. 9.18 Wave patterns set up by a particle moving at speed U into still fluid of sound velocity a: (a) subsonic, (b) sonic, and (c) supersonic motion.

As the particle moves, it continually crashes against fluid particles and sends out spherical sound waves emanating from every point along its path. A few of these spherical disturbance fronts are shown in Fig. 9.18. The behavior of these fronts is quite different according to whether the particle speed is subsonic or supersonic.

In Fig. 9.18a, the particle moves subsonically, $U < a$, $\mathrm{Ma} = U/a < 1$. The spherical disturbances move out in all directions and do not catch up with one another. They move well out in front of the particle also, because they travel a distance $a\ \delta t$ during the time interval δt in which the particle has moved only $U\ \delta t$. Therefore a subsonic body motion makes its presence felt everywhere in the flow field: You can "hear" or "feel" the pressure rise of an oncoming body before it reaches you. This is apparently why that pigeon in the road, without turning around to look at you, takes to the air and avoids being hit by your car.

At sonic speed, $U = a$, Fig. 9.18b, the pressure disturbances move at exactly the speed of the particle and thus pile up on the left at the position of the particle into a sort of "front locus," which is now called a *Mach wave*, after Ernst Mach. No disturbance reaches beyond the particle. If you are stationed to the left of the particle, you cannot "hear" the oncoming motion. If the particle blew its horn, you couldn't hear that either: A sonic car can sneak up on a pigeon.

In supersonic motion, $U > a$, the lack of advance warning is even more pronounced. The disturbance spheres cannot catch up with the fast-moving particle which create them. They all trail behind the particle and are tangent to a conic *Mach cone.* From the geometry of Fig. 9.18c the angle of the Mach



ketabline.com Ebook.ketabline.com

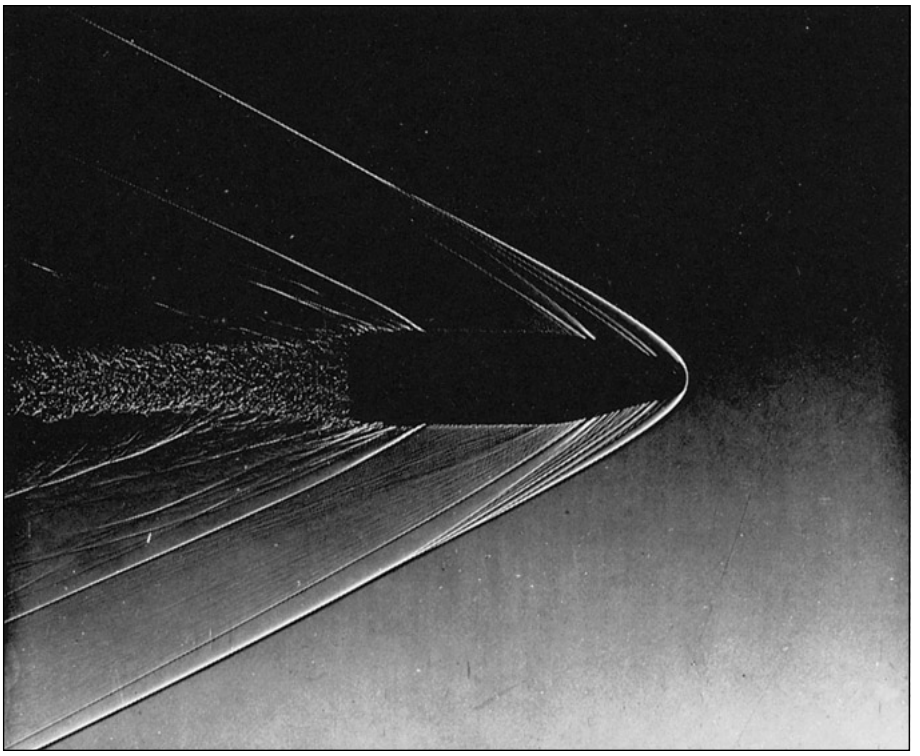


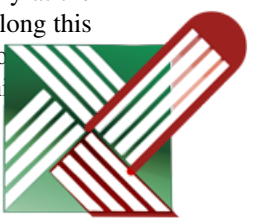
Fig. 9.19 Supersonic wave pattern emanating from a projectile moving at Ma $\approx$ 2.0. The heavy lines are oblique-shock waves and the light lines Mach waves (*Courtesy of U.S. Army Ballistic Research Laboratory, Aberdeen Proving Ground.*)

$$\mu = \sin^{-1}\frac{a}{U}\frac{\delta t}{\delta t} = \sin^{-1}\frac{a}{U} = \sin^{-1}\frac{1}{\text{Ma}} \tag{9.79}$$

The higher the particle Mach number, the more slender the Mach cone; for example, μ is 30° at Ma = 2.0 and 11.5° at Ma = 5.0. For the limiting case of sonic flow, Ma = 1, μ = 90°; the Mach cone becomes a plane front moving with the particle, in agreement with Fig. 9.18*b*.

You cannot "hear" the disturbance caused by the supersonic particle in Fig. 9.18*c* until you are in the *zone of action* inside the Mach cone. No warning can reach your ears if you are in the *zone of silence* outside the cone. Thus an observer on the ground beneath a supersonic airplane does not hear the *sonic boom* of the passing cone until the plane is well past.

The Mach wave need not be a cone: Similar waves are formed by a small disturbance of any shape moving supersonically with respect to the ambient fluid. For example, the "particle" in Fig. 9.18*c* could be the leading edge of a sharp flat plate, which would form a Mach wedge of exactly the same angle μ. Mach waves are formed by small roughnesses or boundary-layer irregularities in a supersonic wind tunnel or at the surface of a supersonic body. Look again at Fig. 9.10: Mach waves are clearly visible along the body surface downstream of the recompression shock, especially at the rear corner. Their angle is about 30°, indicating a Mach number of about 2.0 along this surface. A more complicated system of Mach waves emanates from the supersc
jectile in Fig. 9.19. The Mach angles change, indicating a variable superson



ketabline.com Ebook.ketabline.com

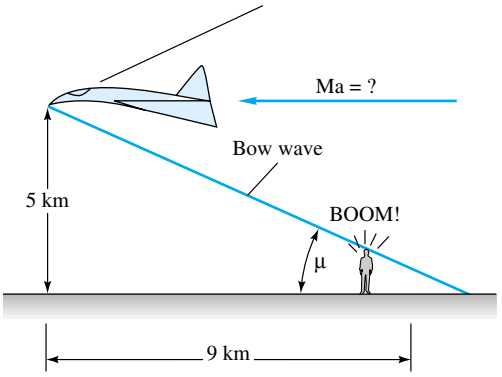
number along the body surface. There are also several stronger oblique-shock waves formed along the surface.

EXAMPLE 9.16

An observer on the ground does not hear the sonic boom caused by an airplane moving at 5-km altitude until it is 9 km past her. What is the approximate Mach number of the plane? Assume a small disturbance and neglect the variation of sound speed with altitude.

Solution

A finite disturbance like an airplane will create a finite-strength oblique-shock wave whose angle will be somewhat larger than the Mach-wave angle μ and will curve downward due to the variation in atmospheric sound speed. If we neglect these effects, the altitude and distance are a measure of μ, as seen in Fig. E9.16. Thus



E9.16

$$\tan \mu = \frac{5 \text{ km}}{9 \text{ km}} = 0.5556 \qquad \text{or} \qquad \mu = 29.05°$$

Hence, from Eq. (9.79),

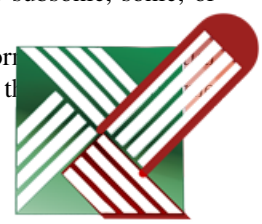
$$\text{Ma} = \csc \mu = 2.06 \qquad \textit{Ans.}$$

The Oblique-Shock Wave

Figures 9.10 and 9.19 and our earlier discussion all indicate that a shock wave can form at an oblique angle to the oncoming supersonic stream. Such a wave will deflect the stream through an angle θ, unlike the normal-shock wave, for which the downstream flow is in the same direction. In essence, an oblique shock is caused by the necessity for a supersonic stream to turn through such an angle. Examples could be a finite wedge at the leading edge of a body and a ramp in the wall of a supersonic wind tunnel.

The flow geometry of an oblique shock is shown in Fig. 9.20. As for the normal shock of Fig. 9.8, state 1 denotes the upstream conditions and state 2 is downstream. The shock angle has an arbitrary value β, and the downstream flow V_2 turns at an angle θ which is a function of β and state 1 conditions. The upstream flow is always supersonic, but the downstream Mach number $\text{Ma}_2 = V_2/a_2$ may be subsonic, sonic, or supersonic, depending upon the conditions.

It is convenient to analyze the flow by breaking it up into nor components with respect to the wave, as shown in Fig. 9.20. For a t



ketabline.com Ebook.ketabline.com

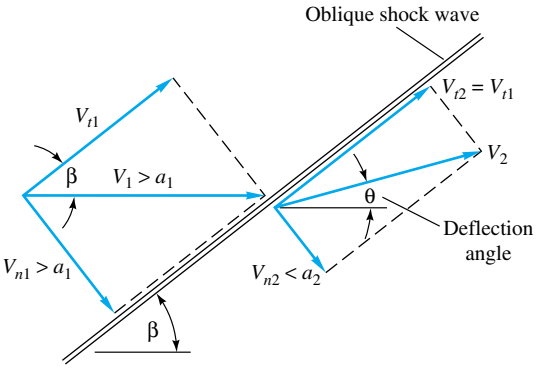


Fig. 9.20 Geometry of flow through an oblique-shock wave.

just encompassing the wave, we can then derive the following integral relations, canceling out $A_1 = A_2$ on each side of the wave:

Continuity: $$\rho_1 V_{n1} = \rho_2 V_{n2} \tag{9.80a}$$

Normal momentum: $$p_1 - p_2 = \rho_2 V_{n2}^2 - \rho_1 V_{n1}^2 \tag{9.80b}$$

Tangential momentum: $$0 = \rho_1 V_{n1}(V_{t2} - V_{t1}) \tag{9.80c}$$

Energy: $$h_1 + \tfrac{1}{2}V_{n1}^2 + \tfrac{1}{2}V_{t1}^2 = h_2 + \tfrac{1}{2}V_{n2}^2 + \tfrac{1}{2}V_{t2}^2 = h_0 \tag{9.80d}$$

We see from Eq. (9.80*c*) that there is no change in tangential velocity across an oblique shock

$$V_{t2} = V_{t1} = V_t = \text{const} \tag{9.81}$$

Thus tangential velocity has as its only effect the addition of a constant kinetic energy $\frac{1}{2}V_t^2$ to each side of the energy equation (9.80*d*). We conclude that Eqs. (9.80) are identical to the normal-shock relations (9.49), with V_1 and V_2 replaced by the normal components V_{n1} and V_{n2}. All the various relations from Sec. 9.5 can be used to compute properties of an oblique-shock wave. The trick is to use the "normal" Mach numbers in place of Ma_1 and Ma_2:

$$\begin{aligned} \text{Ma}_{n1} &= \frac{V_{n1}}{a_1} = \text{Ma}_1 \sin \beta \\ \text{Ma}_{n2} &= \frac{V_{n2}}{a_2} = \text{Ma}_2 \sin (\beta - \theta) \end{aligned} \tag{9.82}$$

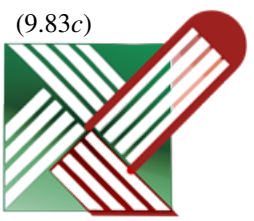
Then, for a perfect gas with constant specific heats, the property ratios across the oblique shock are the analogs of Eqs. (9.55) to (9.58) with Ma_1 replaced by Ma_{n1}:

$$\frac{p_2}{p_1} = \frac{1}{k+1}\left[2k\,\text{Ma}_1^2 \sin^2 \beta - (k-1)\right] \tag{9.83a}$$

$$\frac{\rho_2}{\rho_1} = \frac{\tan \beta}{\tan (\beta - \theta)} = \frac{(k+1)\,\text{Ma}_1^2 \sin^2 \beta}{(k-1)\,\text{Ma}_1^2 \sin^2 \beta + 2} = \frac{V_{n1}}{V_{n2}} \tag{9.83b}$$

$$\frac{T_2}{T_1} = \left[2 + (k-1)\,\text{Ma}_1^2 \sin^2 \beta\right] \frac{2k\,\text{Ma}_1^2 \sin^2 \beta - (k-1)}{(k+1)^2\,\text{Ma}_1^2 \sin^2 \beta} \tag{9.83c}$$

$$T_{02} = T_{01}$$



ketabline.com Ebook.ketabline.com

$$\frac{p_{02}}{p_{01}} = \left[\frac{(k+1)\,\mathrm{Ma}_1^2 \sin^2\beta}{2 + (k-1)\,\mathrm{Ma}_1^2 \sin^2\beta}\right]^{k/(k-1)} \left[\frac{k+1}{2k\,\mathrm{Ma}_1^2 \sin^2\beta - (k-1)}\right]^{1/(k-1)} \tag{9.83e}$$

$$\mathrm{Ma}_{n2}^2 = \frac{(k-1)\,\mathrm{Ma}_{n1}^2 + 2}{2k\,\mathrm{Ma}_{n1}^2 - (k-1)} \tag{9.83f}$$

All these are tabulated in the normal-shock Table B.2. If you wondered why that table listed the Mach numbers as Ma_{n1} and Ma_{n2}, it should be clear now that the table is also valid for the oblique-shock wave.

Thinking all this over, we realize by hindsight that an oblique-shock wave is the flow pattern one would observe by running along a normal-shock wave (Fig. 9.8) at a constant tangential speed V_t. Thus the normal and oblique shocks are related by a galilean, or inertial, velocity transformation and therefore satisfy the same basic equations.

If we continue with this run-along-the-shock analogy, we find that the deflection angle θ increases with speed V_t up to a maximum and then decreases. From the geometry of Fig. 9.20 the deflection angle is given by

$$\theta = \tan^{-1}\frac{V_t}{V_{n2}} - \tan^{-1}\frac{V_t}{V_{n1}} \tag{9.84}$$

If we differentiate θ with respect to V_t and set the result equal to zero, we find that the maximum deflection occurs when $V_t/V_{n1} = (V_{n2}/V_{n1})^{1/2}$. We can substitute this back into Eq. (9.84) to compute

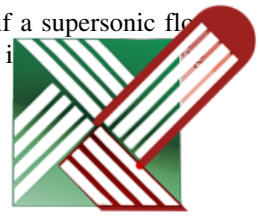
$$\theta_{\max} = \tan^{-1} r^{1/2} - \tan^{-1} r^{-1/2} \qquad r = \frac{V_{n1}}{V_{n2}} \tag{9.85}$$

For example, if $\mathrm{Ma}_{n1} = 3.0$, from Table B.2 we find that $V_{n1}/V_{n2} = 3.8571$, the square root of which is 1.9640. Then Eq. (9.85) predicts a maximum deflection of $\tan^{-1} 1.9640 - \tan^{-1}(1/1.9640) = 36.03°$. The deflection is quite limited even for infinite Ma_{n1}: From Table B.2 for this case $V_{n1}/V_{n2} = 6.0$, and we compute from Eq. (9.85) that $\theta_{\max} = 45.58°$.

This limited-deflection idea and other facts become more evident if we plot some of the solutions of Eqs. (9.83). For given values of V_1 and a_1, assuming as usual that $k = 1.4$, we can plot all possible solutions for V_2 downstream of the shock. Figure 9.21 does this in velocity-component coordinates V_x and V_y, with x parallel to V_1. Such a plot is called a *hodograph*. The heavy dark line which looks like a fat airfoil is the locus, or *shock polar*, of all physically possible solutions for the given Ma_1. The two dashed-line fishtails are solutions which increase V_2; they are physically impossible because they violate the second law.

Examining the shock polar in Fig. 9.21, we see that a given deflection line of small angle θ crosses the polar at two possible solutions: the *strong* shock, which greatly decelerates the flow, and the *weak* shock, which causes a much milder deceleration. The flow downstream of the strong shock is always subsonic, while that of the weak shock is usually supersonic but occasionally subsonic if the deflection is large. Both types of shock occur in practice. The weak shock is more prevalent, but the strong shock will occur if there is a blockage or high-pressure condition downstream.

Since the shock polar is only of finite size, there is a maximum deflection $\theta_{\max}$, shown in Fig. 9.21, which just grazes the upper edge of the polar curve. This verifies the kinematic discussion which led to Eq. (9.85). What happens if a supersonic flo is forced to deflect through an angle greater than $\theta_{\max}$? The answer i 9.22 for flow past a wedge-shaped body.



ketabline.com Ebook.ketabline.com

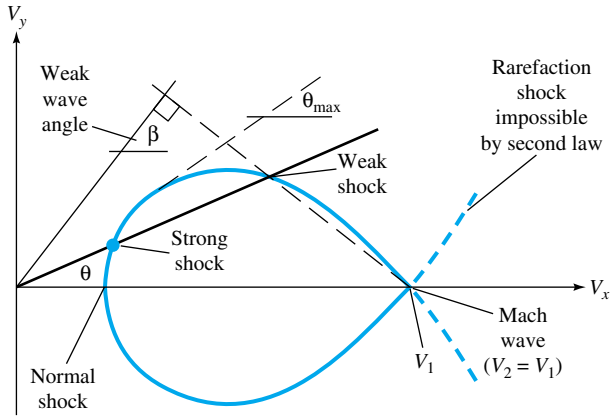


Fig. 9.21 The oblique-shock polar hodograph, showing double solutions (strong and weak) for small deflection angle and no solutions at all for large deflection.

In Fig. 9.22*a* the wedge half-angle θ is less than θ_{max}, and thus an oblique shock forms at the nose of wave angle β just sufficient to cause the oncoming supersonic stream to deflect through the wedge angle θ. Except for the usually small effect of boundary-layer growth (see, e.g., Ref. 19, sec. 7–5.2), the Mach number Ma_2 is constant along the wedge surface and is given by the solution of Eqs. (9.83). The pressure, density, and temperature along the surface are also nearly constant, as predicted by Eqs. (9.83). When the flow reaches the corner of the wedge, it expands to higher Mach number and forms a wake (not shown) similar to that in Fig. 9.10.

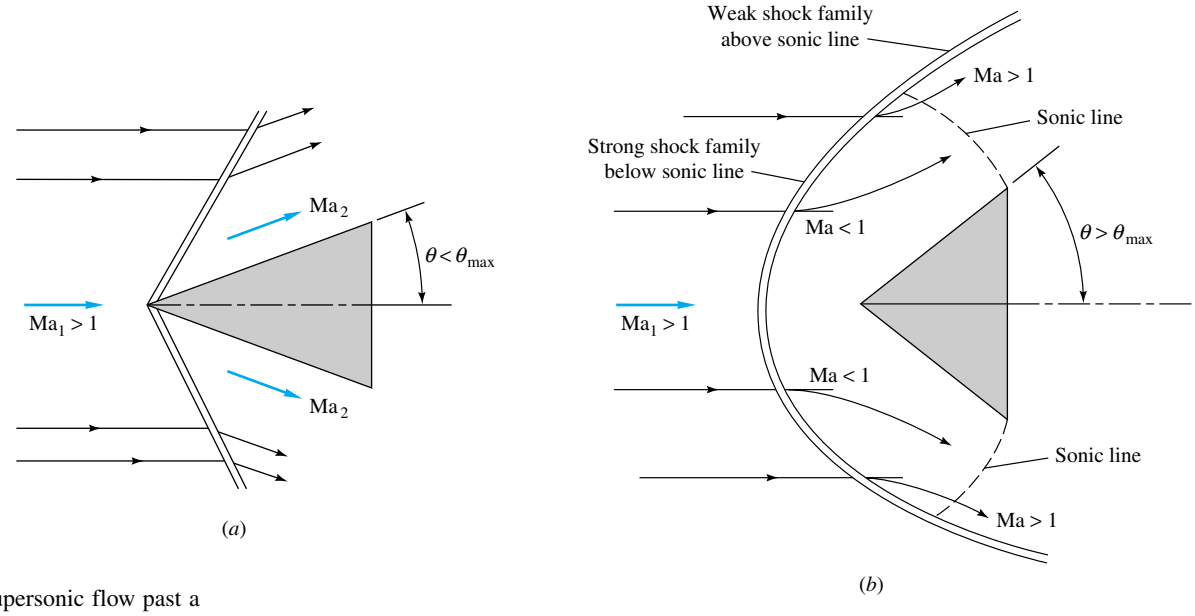


Fig. 9.22 Supersonic flow past a wedge: (*a*) small wedge angle, attached oblique shock forms; (*b*) large wedge angle, attached shock not possible, broad curved detached shock forms.

In Fig. 9.22*b* the wedge half-angle is greater than θ_{max}, and an attached oblique shock is impossible. The flow cannot deflect at once through the entire angle θ_{max}, yet somehow the flow must get around the wedge. A detached curve shock wave f front of the body, discontinuously deflecting the flow through angles smaller th

ketabline.com Ebook.ketabline.com

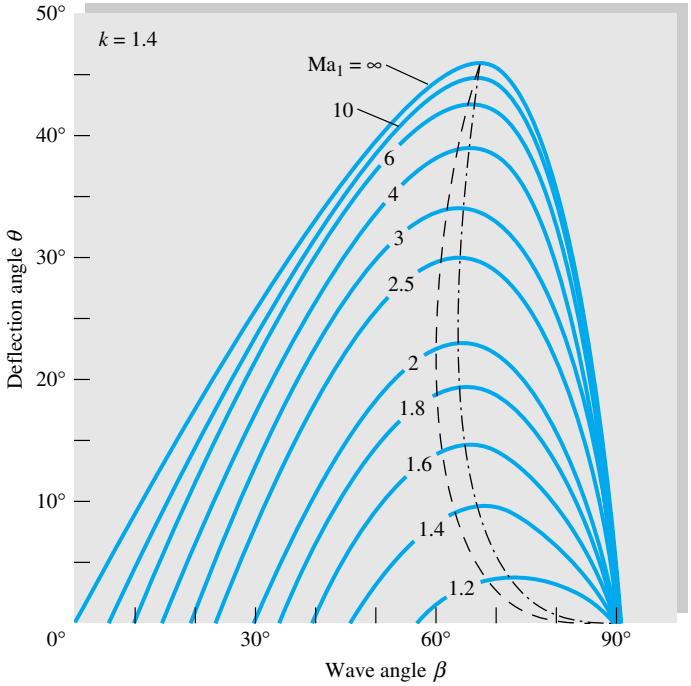


Fig. 9.23 Oblique-shock deflection versus wave angle for various upstream Mach numbers, $k = 1.4$: dash-dot curve, locus of θ_{max}, divides strong (right) from weak (left) shocks; dashed curve, locus of sonic points, divides subsonic Ma_2 (right) from supersonic Ma_2 (left).

The flow then curves, expands, and deflects subsonically around the wedge, becoming sonic and then supersonic as it passes the corner region. The flow just inside each point on the curved shock exactly satisfies the oblique-shock relations (9.83) for that particular value of β and the given Ma_1. Every condition along the curved shock is a point on the shock polar of Fig. 9.21. Points near the front of the wedge are in the strong-shock family, and points aft of the sonic line are in the weak-shock family. The analysis of detached shock waves is extremely complex, and experimentation is usually needed, e.g., the shadowgraph optical technique of Fig. 9.10.

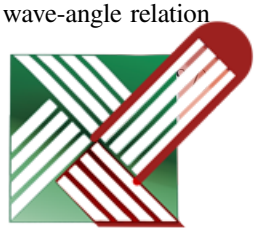
The complete family of oblique-shock solutions can be plotted or computed from Eqs. (9.83). For a given k, the wave angle β varies with Ma_1 and θ, from Eq. (9.83*b*). By using a trigonometric identity for tan $(\beta - \theta)$ this can be rewritten in the more convenient form

$$\tan\,\theta = \frac{2\,\cot\,\beta\,(Ma_1^2\,\sin^2\,\beta - 1)}{Ma_1^2\,(k + \cos\,2\beta) + 2} \tag{9.86}$$

All possible solutions of Eq. (9.86) for $k = 1.4$ are shown in Fig. 9.23. For deflections $\theta < \theta_{max}$ there are two solutions: a weak shock (small β) and a strong shock (large β), as expected. All points along the dash-dot line for θ_{max} satisfy Eq. (9.85). A dashed line has been added to show where Ma_2 is exactly sonic. We see that there is a narrow region near maximum deflection where the weak-shock downstream flow is subsonic.

For zero deflections ($\theta = 0$) the weak-shock family satisfies the wave-angle relation

$$\beta = \mu = \sin^{-1}\frac{1}{Ma_1}$$



ketabline.com Ebook.ketabline.com

Thus weak shocks of vanishing deflection are equivalent to Mach waves. Meanwhile the strong shocks all converge at zero deflection to the normal-shock condition $\beta = 90°$.

Two additional oblique-shock charts are given in App. B, where Fig. B.1 gives the downstream Mach number Ma_2 and Fig. B.2 the pressure ratio p_2/p_1, each plotted as a function of Ma_1 and θ. Additional graphs, tables, and computer programs are given in Refs. 24 and 25.

Very Weak Shock Waves

For any finite θ the wave angle β for a weak shock is greater than the Mach angle μ. For small θ Eq. (9.86) can be expanded in a power series in tan θ with the following linearized result for the wave angle:

$$\sin \beta = \sin \mu + \frac{k+1}{4 \cos \mu} \tan \theta + \cdots + \mathcal{O}(\tan^2 \theta) + \cdots \tag{9.88}$$

For Ma_1 between 1.4 and 20.0 and deflections less than 6° this relation predicts β to within 1° for a weak shock. For larger deflections it can be used as a useful initial guess for iterative solution of Eq. (9.86).

Other property changes across the oblique shock can also be expanded in a power series for small deflection angles. Of particular interest is the pressure change from Eq. (9.83*a*), for which the linearized result for a weak shock is

$$\frac{p_2 - p_1}{p_1} = \frac{k\,\text{Ma}_1^2}{(\text{Ma}_1^2 - 1)^{1/2}} \tan \theta + \cdots + \mathcal{O}(\tan^2 \theta) + \cdots \tag{9.89}$$

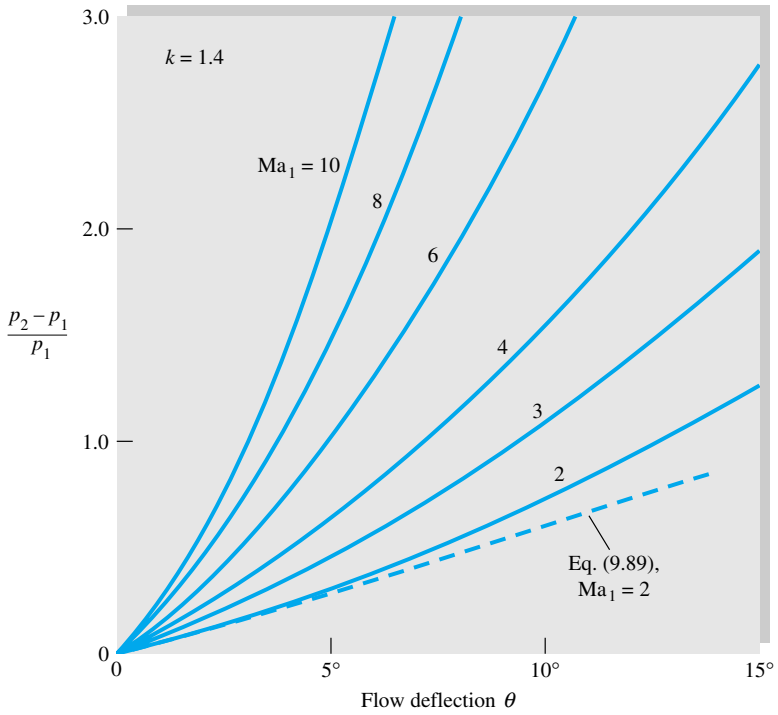


Fig. 9.24 Pressure jump across a weak oblique-shock wave from Eq. (9.83*a*) for $k = 1.4$. For very small deflections Eq. (9.89) applies.



ketabline.com Ebook.ketabline.com

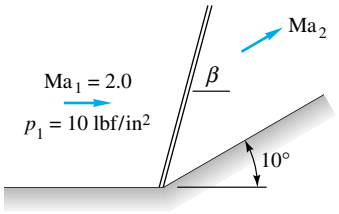
The differential form of this relation is used in the next section to develop a theory for supersonic expansion turns. Figure 9.24 shows the exact weak-shock pressure jump computed from Eq. (9.83*a*). At very small deflections the curves are linear with slopes given by Eq. (9.89).

Finally, it is educational to examine the entropy change across a very weak shock. Using the same power-series expansion technique, we can obtain the following result for small flow deflections:

$$\frac{s_2 - s_1}{c_p} = \frac{(k^2 - 1)\text{Ma}_1^6}{12(\text{Ma}_1^2 - 1)^{3/2}} \tan^3 \theta + \cdots + \mathbb{O}(\tan^4 \theta) + \cdots \tag{9.90}$$

The entropy change is cubic in the deflection angle θ. Thus weak shock waves are very nearly isentropic, a fact which is also used in the next section.

EXAMPLE 9.17



E9.17

Air at Ma = 2.0 and $p = 10$ lbf/in^2 absolute is forced to turn through 10° by a ramp at the body surface. A weak oblique shock forms as in Fig. E9.17. For $k = 1.4$ compute from exact oblique-shock theory (*a*) the wave angle β, (*b*) Ma_2, and (*c*) p_2. Also use the linearized theory to estimate (*d*) β and (*e*) p_2.

Solution

With $\text{Ma}_1 = 2.0$ and $\theta = 10°$ known, we can estimate $\beta \approx 40° \pm 2°$ from Fig. 9.23. For more (hand calculated) accuracy, we have to solve Eq. (9.86) by iteration. Or we can program Eq. (9.86) in EES with six statements (in SI units, with angles in degrees):

```
Ma = 2.0
k = 1.4
Theta = 10
Num = 2*(Ma^2*SIN(Beta)^2 - 1)/TAN(Beta)
Denom = Ma^2*(k + COS(2*Beta)) + 2
Theta = ARCTAN(Num/Denom)
```

Specify that Beta > 0 and EES promptly reports an accurate result:

$$\beta = 39.32° \qquad \textit{Ans. (a)}$$

The normal Mach number upstream is thus

$$\text{Ma}_{n1} = \text{Ma}_1 \sin \beta = 2.0 \sin 39.32° = 1.267$$

With Ma_{n1} we can use the normal-shock relations (Table B.2) or Fig. 9.9 or Eqs. (9.56) to (9.58) to compute

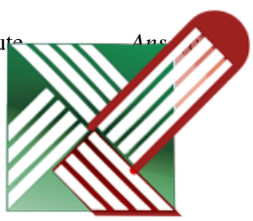
$$\text{Ma}_{n2} = 0.8031 \qquad \frac{p_2}{p_1} = 1.707$$

Thus the downstream Mach number and pressure are

$$\text{Ma}_2 = \frac{\text{Ma}_{n2}}{\sin(\beta - \theta)} = \frac{0.8031}{\sin(39.32° - 10°)} = 1.64 \qquad \textit{Ans. (b)}$$

$$p_2 = (10 \text{ lbf/in}^2 \text{ absolute})(1.707) = 17.07 \text{ lbf/in}^2 \text{ absolute} \qquad \textit{Ans.}$$

Notice that the computed pressure ratio agrees with Figs. 9.24 and B.2.



ketabline.com Ebook.ketabline.com

For the linearized theory the Mach angle is $\mu = \sin^{-1}(1/2.0) = 30°$. Equation (9.88) then estimates that

$$\sin\beta \approx \sin 30° + \frac{2.4 \tan 10°}{4 \cos 30°} = 0.622$$

or $$\beta \approx 38.5° \qquad \textit{Ans. (d)}$$

Equation (9.89) estimates that

$$\frac{p_2}{p_1} \approx 1 + \frac{1.4(2)^2 \tan 10°}{(2^2 - 1)^{1/2}} = 1.57$$

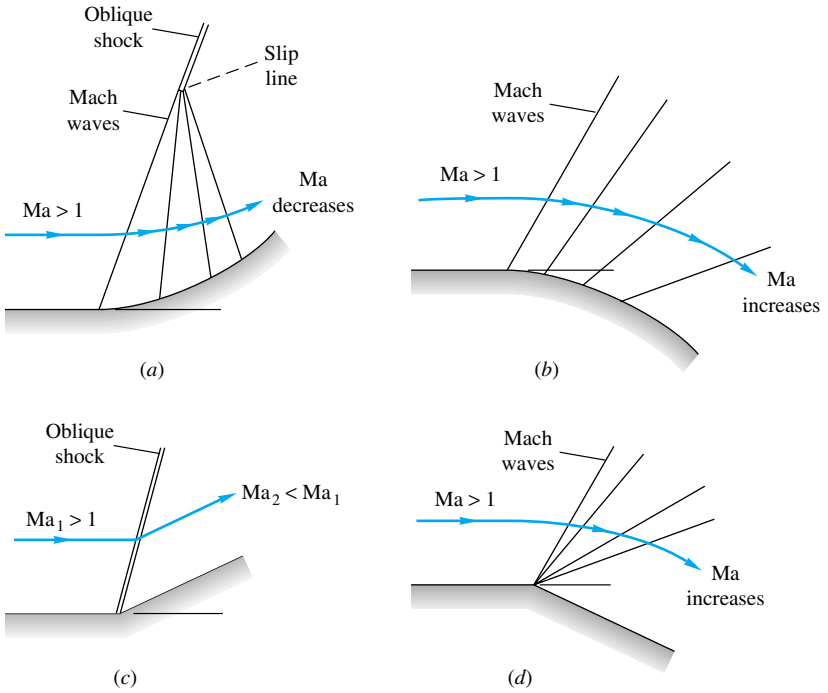
or $$p_2 \approx 1.57(10 \text{ lbf/in}^2 \text{ absolute}) \approx 15.7 \text{ lbf/in}^2 \text{ absolute} \qquad \textit{Ans. (e)}$$

These are reasonable estimates in spite of the fact that 10° is really not a "small" flow deflection.

9.10 Prandtl-Meyer Expansion Waves

The oblique-shock solution of Sec. 9.9 is for a finite compressive deflection θ which obstructs a supersonic flow and thus decreases its Mach number and velocity. The present section treats gradual changes in flow angle which are primarily *expansive*; i.e., they widen the flow area and increase the Mach number and velocity. The property changes accumulate in infinitesimal increments, and the linearized relations (9.88) and (9.89) are used. The local flow deflections are infinitesimal, so that the flow is nearly isentropic according to Eq. (9.90).

Figure 9.25 shows four examples, one of which (Fig. 9.25*c*) fails the test for gradual changes. The gradual compression of Fig. 9.25*a* is essentially isentropic, with a



9.25 Some examples of supersonic expansion and compression: (*a*) gradual isentropic compression on a concave surface, Mach waves coalesce farther out to form oblique shock; (*b*) gradual isentropic expansion on convex surface, Mach waves diverge; (*c*) sudden compression, nonisentropic shock forms; (*d*) sudden expansion, centered isentropic fan of Mach waves forms.



ketabline.com Ebook.ketabline.com

smooth increase in pressure along the surface, but the Mach angle decreases along the surface and the waves tend to coalesce farther out into an oblique-shock wave. The gradual expansion of Fig. 9.25*b* causes a smooth isentropic increase of Mach number and velocity along the surface, with diverging Mach waves formed.

The sudden compression of Fig. 9.25*c* cannot be accomplished by Mach waves: An oblique shock forms, and the flow is nonisentropic. This could be what you would see if you looked at Fig. 9.25*a* from far away. Finally, the sudden expansion of Fig. 9.25*d* is isentropic and forms a fan of centered Mach waves emanating from the corner. Note that the flow on any streamline passing through the fan changes smoothly to higher Mach number and velocity. In the limit as we near the corner the flow expands almost discontinuously at the surface. The cases in Fig. 9.25*a*, *b*, and *d* can all be handled by the Prandtl-Meyer supersonic-wave theory of this section, first formulated by Ludwig Prandtl and his student Theodor Meyer in 1907 to 1908.

Note that none of this discussion makes sense if the upstream Mach number is subsonic, since Mach wave and shock wave patterns cannot exist in subsonic flow.

The Prandtl-Meyer Perfect-Gas Function

Consider a small, nearly infinitesimal flow deflection $d\theta$ such as occurs between the first two Mach waves in Fig. 9.25*a*. From Eqs. (9.88) and (9.89) we have, in the limit,

$$\beta \approx \mu = \sin^{-1} \frac{1}{\text{Ma}} \tag{9.91a}$$

$$\frac{dp}{p} \approx \frac{k\ \text{Ma}^2}{(\text{Ma}^2 - 1)^{1/2}}\, d\theta \tag{9.91b}$$

Since the flow is nearly isentropic, we have the frictionless differential momentum equation for a perfect gas

$$dp = -\rho V\, dV = -kp\ \text{Ma}^2 \frac{dV}{V} \tag{9.92}$$

Combining Eqs. (9.91*a*) and (9.92) to eliminate dp, we obtain a relation between turning angle and velocity change

$$d\theta = -(\text{Ma}^2 - 1)^{1/2} \frac{dV}{V} \tag{9.93}$$

This can be integrated into a functional relation for finite turning angles if we can relate V to Ma. We do this from the definition of Mach number

$$V = \text{Ma}\ a$$

or

$$\frac{dV}{V} = \frac{d\ \text{Ma}}{\text{Ma}} + \frac{da}{a} \tag{9.94}$$

Finally, we can eliminate da/a because the flow is isentropic and hence a_0 is constant for a perfect gas

$$a = a_0[1 + \tfrac{1}{2}(k - 1)\ \text{Ma}^2]^{-1/2}$$

or

$$\frac{da}{a} = \frac{-\tfrac{1}{2}(k - 1)\ \text{Ma}\ d\ \text{Ma}}{1 + \tfrac{1}{2}(k - 1)\ \text{Ma}^2}$$



ketabline.com Ebook.ketabline.com

Eliminating dV/V and da/a from Eqs. (9.93) to (9.95), we obtain a relation solely between turning angle and Mach number

$$d\theta = -\frac{(\mathrm{Ma}^2 - 1)^{1/2}}{1 + \frac{1}{2}(k-1)\,\mathrm{Ma}^2}\,\frac{d\,\mathrm{Ma}}{\mathrm{Ma}} \tag{9.96}$$

Before integrating this expression, we note that the primary application is to expansions, i.e., increasing Ma and decreasing θ. Therefore, for convenience, we define the Prandtl-Meyer angle $\omega(\mathrm{Ma})$ which increases when θ decreases and is zero at the sonic point

$$d\omega = -d\theta \qquad \omega = 0 \quad \text{at} \quad \mathrm{Ma} = 1 \tag{9.97}$$

Thus we integrate Eq. (9.96) from the sonic point to any value of Ma

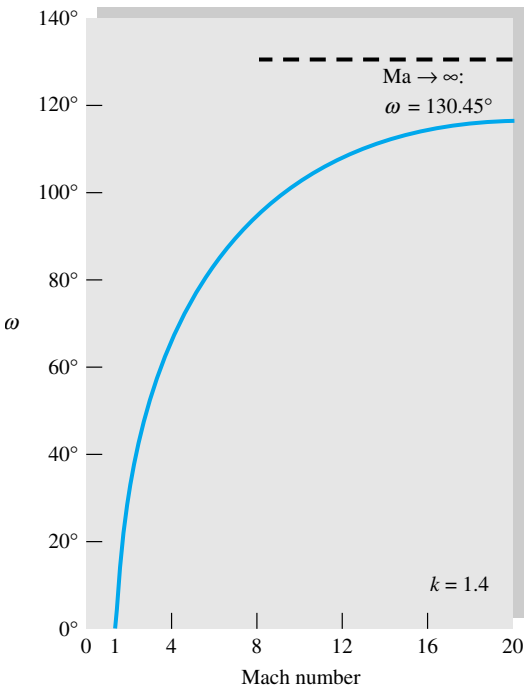
$$\int_0^{\omega} d\omega = \int_1^{\mathrm{Ma}} \frac{(\mathrm{Ma}^2 - 1)^{1/2}}{1 + \frac{1}{2}(k-1)\,\mathrm{Ma}^2}\,\frac{d\,\mathrm{Ma}}{\mathrm{Ma}} \tag{9.98}$$

The integrals are evaluated in closed form, with the result, in radians,

$$\omega(\mathrm{Ma}) = K^{1/2}\tan^{-1}\left(\frac{\mathrm{Ma}^2 - 1}{K}\right)^{1/2} - \tan^{-1}(\mathrm{Ma}^2 - 1)^{1/2} \tag{9.99}$$

where $$K = \frac{k+1}{k-1}$$

This is the *Prandtl-Meyer supersonic expansion function*, which is plotted in Fig. 9.26



Fig,. 9.26 The Prandtl-Meyer supersonic expansion from Eq. (9.99) for $k = 1.4$.



ketabline.com Ebook.ketabline.com

and tabulated in Table B.5 for $k = 1.4$, $K = 6$. The angle ω changes rapidly at first and then levels off at high Mach number to a limiting value as Ma $\rightarrow \infty$:

$$\omega_{\max} = \frac{\pi}{2}(K^{1/2} - 1) = 130.45^\circ \qquad \text{if} \qquad k = 1.4 \tag{9.100}$$

Thus a supersonic flow can expand only through a finite turning angle before it reaches infinite Mach number, maximum velocity, and zero temperature.

Gradual expansion or compression between finite Mach numbers Ma_1 and Ma_2, neither of which is unity, is computed by relating the turning angle $\Delta\omega$ to the difference in Prandtl-Meyer angles for the two conditions

$$\Delta\omega_{1\rightarrow 2} = \omega(\text{Ma}_2) - \omega(\text{Ma}_1) \tag{9.101}$$

The change $\Delta\omega$ may be either positive (expansion) or negative (compression) as long as the end conditions lie in the supersonic range. Let us illustrate with an example.



EXAMPLE 9.18

Air ($k = 1.4$) flows at $\text{Ma}_1 = 3.0$ and $p_1 = 200$ kPa. Compute the final downstream Mach number and pressure for (*a*) an expansion turn of 20° and (*b*) a gradual compression turn of 20°.

Solution

Part (a) The isentropic stagnation pressure is

$$p_0 = p_1[1 + 0.2(3.0)^2]^{3.5} = 7347 \text{ kPa}$$

and this will be the same at the downstream point. For $\text{Ma}_1 = 3.0$ we find from Table B.5 or Eq. (9.99) that $\omega_1 = 49.757^\circ$. The flow expands to a new condition such that

$$\omega_2 = \omega_1 + \Delta\omega = 49.757^\circ + 20^\circ = 69.757^\circ$$



Linear interpolation in Table B.5 is quite accurate, yielding $\text{Ma}_2 \approx 4.32$. Inversion of Eq. (9.99), to find Ma when ω is given, is impossible without iteration. Once again, our friend EES easily handles Eq. (9.99) with four statements (angles specified in degrees):

```
k = 1.4
C = ((k+1)/(k - 1))^0.5
Omega = 69.757
Omega = C*ARCTAN((Ma^2-1)^0.5/C) - ARCTAN((Ma^2-1)^0.5)
```

Specify that Ma > 1, and EES readily reports an accurate result:[6]

$$\text{Ma}_2 = 4.32 \qquad \textit{Ans. (a)}$$

The isentropic pressure at this new condition is

$$p_2 = \frac{p_0}{[1 + 0.2(4.32)^2]^{3.5}} = \frac{7347}{230.1} = 31.9 \text{ kPa} \qquad \textit{Ans. (a)}$$

[6]The author saves these little programs for further use, giving them names such



ketabline.com Ebook.ketabline.com

Part (b) The flow compresses to a lower Prandtl-Meyer angle

$$\omega_2 = 49.757^\circ - 20^\circ = 29.757^\circ$$

Again from Eq. (9.99), Table B.5, or EES we compute that

$$\text{Ma}_2 = 2.125 \qquad \textit{Ans. (b)}$$

$$p_2 = \frac{p_0}{[1 + 0.2(2.125)^2]^{3.5}} = \frac{7347}{9.51} = 773 \text{ kPa} \qquad \textit{Ans. (b)}$$

Similarly, density and temperature changes are computed by noticing that T_0 and ρ_0 are constant for isentropic flow.

Application to Supersonic Airfoils

The oblique-shock and Prandtl-Meyer expansion theories can be used to patch together a number of interesting and practical supersonic flow fields. This marriage, called *shock expansion theory*, is limited by two conditions: (1) Except in rare instances the flow must be supersonic throughout, and (2) the wave pattern must not suffer interference from waves formed in other parts of the flow field.

A very successful application of shock expansion theory is to supersonic airfoils. Figure 9.27 shows two examples, a flat plate and a diamond-shaped foil. In contrast to subsonic-flow designs (Fig. 8.21), these airfoils must have sharp leading edges, which form attached oblique shocks or expansion fans. Rounded supersonic leading edges would cause detached bow shocks, as in Fig. 9.19 or 9.22*b*, greatly increasing the drag and lowering the lift.

In applying shock expansion theory, one examines each surface turning angle to see whether it is an expansion ("opening up") or compression (obstruction) to the surface flow. Figure 9.27*a* shows a flat-plate foil at an angle of attack. There is a leading-edge shock on the lower edge with flow deflection $\theta = \alpha$, while the upper edge has an expansion fan with increasing Prandtl-Meyer angle $\Delta\omega = \alpha$. We compute p_3 with expansion theory and p_2 with oblique-shock theory. The force on the plate is thus $F = (p_2 - p_3)Cb$, where C is the chord length and b the span width (assuming no wingtip effects). This force is normal to the plate, and thus the lift force normal to the stream is $L = F\cos\alpha$, and the drag parallel to the stream is $D = F\sin\alpha$. The dimensionless coefficients C_L and C_D have the same definitions as in low-speed flow, Eq. (7.66), except that the perfect-gas-law identity $\frac{1}{2}\rho V^2 \equiv \frac{1}{2}kp\ \text{Ma}^2$ is very useful here

$$C_L = \frac{L}{\frac{1}{2}kp_\infty\ \text{Ma}_\infty^2\ bC} \qquad C_D = \frac{D}{\frac{1}{2}kp_\infty\ \text{Ma}_\infty^2\ bC} \tag{9.102}$$

The typical supersonic lift coefficient is much smaller than the subsonic value $C_L \approx 2\pi\alpha$, but the lift can be very large because of the large value of $\frac{1}{2}\rho V^2$ at supersonic speeds.

At the trailing edge in Fig. 9.27*a*, a shock and fan appear in reversed positions and bend the two flows back so that they are parallel in the wake and have the same pressure. They do not have quite the same velocity because of the unequal shock strengths on the upper and lower surfaces; hence a vortex sheet trails behind the wing very interesting, but in the theory you ignore the trailing-edge pattern entirely.



ketabline.com Ebook.ketabline.com

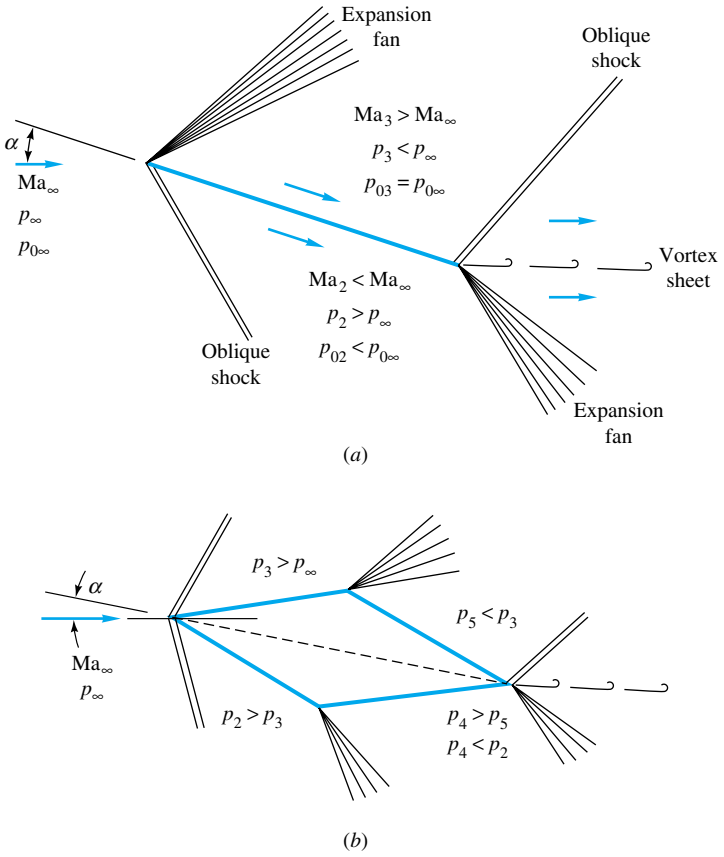


Fig. 9.27 Supersonic airfoils: (*a*) flat plate, higher pressure on lower surface, drag due to small downstream component of net pressure force; (*b*) diamond foil, higher pressures on both lower surfaces, additional drag due to body thickness.

does not affect the surface pressures: The supersonic surface flow cannot "hear" the wake disturbances.

The diamond foil in Fig. 9.27*b* adds two more wave patterns to the flow. At this particular α less than the diamond half-angle, there are leading-edge shocks on both surfaces, the upper shock being much weaker. Then there are expansion fans on each shoulder of the diamond: The Prandtl-Meyer angle change $\Delta\omega$ equals the sum of the leading-edge and trailing-edge diamond half-angles. Finally, the trailing-edge pattern is similar to that of the flat plate (9.27*a*) and can be ignored in the calculation. Both lower-surface pressures p_2 and p_4 are greater than their upper counterparts, and the lift is nearly that of the flat plate. There is an additional drag due to thickness, because p_4 and p_5 on the trailing surfaces are lower than their counterparts p_2 and p_3. The diamond drag is greater than the flat-plate drag, but this must be endured in practice to achieve a wing structure strong enough to hold these forces.

The theory sketched in Fig. 9.27 is in good agreement with measured supersonic lift and drag as long as the Reynolds number is not too small (thick boundary layers) and the Mach number not too large (hypersonic flow). It turns out that for large Re_C and moderate supersonic Ma_∞ the boundary layers are thin and separation seldom o
curs, so that the shock expansion theory, although frictionless, is qu
us look now at an example.



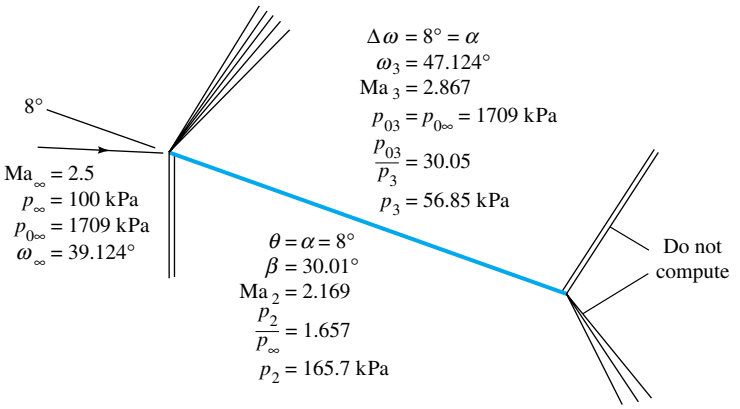
ketabline.com Ebook.ketabline.com

EXAMPLE 9.19

A flat-plate airfoil with $C = 2$ m is immersed at $\alpha = 8°$ in a stream with $\text{Ma}_\infty = 2.5$ and $p_\infty = 100$ kPa. Compute (*a*) C_L and (*b*) C_D, and compare with low-speed airfoils. Compute (*c*) lift and (*d*) drag in newtons per unit span width.

Solution

Instead of using a lot of space outlining the detailed oblique-shock and Prandtl-Meyer expansion computations, we list all pertinent results in Fig. E9.19 on the upper and lower surfaces. Using the theories of Secs. 9.9 and 9.10, you should verify every single one of the calculations in Fig. E9.19 to make sure that all details of shock expansion theory are well understood.



E9.19

The important final results are p_2 and p_3, from which the total force per unit width on the plate is

$$F = (p_2 - p_3)bC = (165.7 - 56.85)(\text{kPa})(1\text{ m})(2\text{ m}) = 218\text{ kN}$$

The lift and drag per meter width are thus

$$L = F\cos 8° = 216\text{ kN} \qquad \textit{Ans. (c)}$$

$$D = F\sin 8° = 30\text{ kN} \qquad \textit{Ans. (d)}$$

These are very large forces for only 2 m^2 of wing area.

From Eq. (9.102) the lift coefficient is

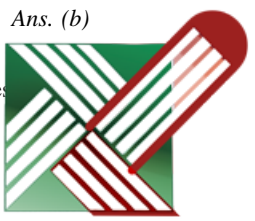
$$C_L = \frac{216\text{ kN}}{\frac{1}{2}(1.4)(100\text{ kPa})(2.5)^2(2\text{ m}^2)} = 0.246 \qquad \textit{Ans. (a)}$$

The comparable low-speed coefficient from Eq. (8.64) is $C_L = 2\pi\sin 8° = 0.874$, which is 3.5 times larger.

From Eq. (9.102) the drag coefficient is

$$C_D = \frac{30\text{ kN}}{\frac{1}{2}(1.4)(100\text{ kPa})(2.5)^2(2\text{ m}^2)} = 0.035 \qquad \textit{Ans. (b)}$$

From Fig. 7.25 for the NACA 0009 airfoil C_D at $\alpha = 8°$ is about 0.009, or about 4 times



ketabline.com Ebook.ketabline.com

Notice that this supersonic theory predicts a finite drag in spite of assuming frictionless flow with infinite wing aspect ratio. This is called *wave drag*, and we see that the d'Alembert paradox of zero body drag does not occur in supersonic flow.

Thin-Airfoil Theory

In spite of the simplicity of the flat-plate geometry, the calculations in Example 9.19 were laborious. In 1925 Ackeret [21] developed simple yet effective expressions for the lift, drag, and center of pressure of supersonic airfoils, assuming small thickness and angle of attack.

The theory is based on the linearized expression (9.89), where $\tan\theta \approx$ surface deflection relative to the free stream and condition 1 is the free stream, $\text{Ma}_1 = \text{Ma}_\infty$. For the flat-plate airfoil, the total force F is based on

$$\frac{p_2 - p_3}{p_\infty} = \frac{p_2 - p_\infty}{p_\infty} - \frac{p_3 - p_\infty}{p_\infty}$$

$$= \frac{k\,\text{Ma}_\infty^2}{(\text{Ma}_\infty^2 - 1)^{1/2}}\,[\alpha - (-\alpha)] \tag{9.103}$$

Substitution into Eq. (9.102) gives the linearized lift coefficient for a supersonic flat-plate airfoil

$$C_L \approx \frac{(p_2 - p_3)bC}{\frac{1}{2}kp_\infty\,\text{Ma}_\infty^2\,bC} \approx \frac{4\alpha}{(\text{Ma}_\infty^2 - 1)^{1/2}} \tag{9.104}$$

Computations for diamond and other finite-thickness airfoils show no first-order effect of thickness on lift. Therefore Eq. (9.104) is valid for any sharp-edged supersonic thin airfoil at a small angle of attack.

The flat-plate drag coefficient is

$$C_D = C_L \tan\alpha \approx C_L\alpha \approx \frac{4\alpha^2}{(\text{Ma}_\infty^2 - 1)^{1/2}} \tag{9.105}$$

However, the thicker airfoils have additional thickness drag. Let the chord line of the airfoil be the x-axis, and let the upper-surface shape be denoted by $y_u(x)$ and the lower profile by $y_l(x)$. Then the complete Ackeret drag theory (see, e.g., Ref. 8, sec. 14.6, for details) shows that the additional drag depends on the mean square of the slopes of the upper and lower surfaces, defined by

$$\overline{y'^2} = \frac{1}{C}\int_0^C \left(\frac{dy}{dx}\right)^2 dx \tag{9.106}$$

The final expression for drag [8, p. 442] is

$$C_D \approx \frac{4}{(\text{Ma}_\infty^2 - 1)^{1/2}}\left[\alpha^2 + \frac{1}{2}\left(\overline{y_u'^2} + \overline{y_l'^2}\right)\right] \tag{9.107}$$

These are all in reasonable agreement with more exact computations, and their extrem
simplicity makes them attractive alternatives to the laborious but a
pansion theory. Consider the following example.



ketabline.com Ebook.ketabline.com

EXAMPLE 9.20

Repeat parts (*a*) and (*b*) of Example 9.19, using the linearized Ackeret theory.

Solution

From Eqs. (9.104) and (9.105) we have, for $\text{Ma}_\infty = 2.5$ and $\alpha = 8° = 0.1396$ rad,

$$C_L \approx \frac{4(0.1396)}{(2.5^2 - 1)^{1/2}} = 0.244 \qquad C_D = \frac{4(0.1396)^2}{(2.5^2 - 1)^{1/2}} = 0.034 \qquad \textit{Ans.}$$

These are less than 3 percent lower than the more exact computations of Example 9.19.

A further result of the Ackeret linearized theory is an expression for the position x_{CP} of the center of pressure (CP) of the force distribution on the wing:

$$\frac{x_{\text{CP}}}{C} = 0.5 + \frac{S_u - S_l}{2\alpha C^2} \tag{9.108}$$

where S_u is the cross-sectional area between the upper surface and the chord and S_l is the area between the chord and the lower surface. For a symmetric airfoil ($S_l = S_u$) we obtain x_{CP} at the half-chord point, in contrast with the low-speed airfoil result of Eq. (8.66), where x_{CP} is at the quarter-chord.

The difference in difficulty between the simple Ackeret theory and shock expansion theory is even greater for a thick airfoil, as the following example shows.

EXAMPLE 9.21

By analogy with Example 9.19 analyze a diamond, or double-wedge, airfoil of 2° half-angle and $C = 2$ m at $\alpha = 8°$ and $\text{Ma}_\infty = 2.5$. Compute C_L and C_D by (*a*) shock expansion theory and (*b*) Ackeret theory. Pinpoint the difference from Example 9.19.

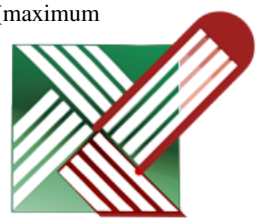
Solution

Part (a) Again we omit the details of shock expansion theory and simply list the properties computed on each of the four airfoil surfaces in Fig. E9.21. Assume $p_\infty = 100$ kPa. There are both a force F normal to the chord line and a force P parallel to the chord. For the normal force the pressure difference on the front half is $p_2 - p_3 = 186.4 - 65.9 = 120.5$ kPa, and on the rear half it is $p_4 - p_5 = 146.9 - 48.1 = 98.1$ kPa. The average pressure difference is $\frac{1}{2}(120.5 + 98.1) = 109.3$ kPa, so that the normal force is

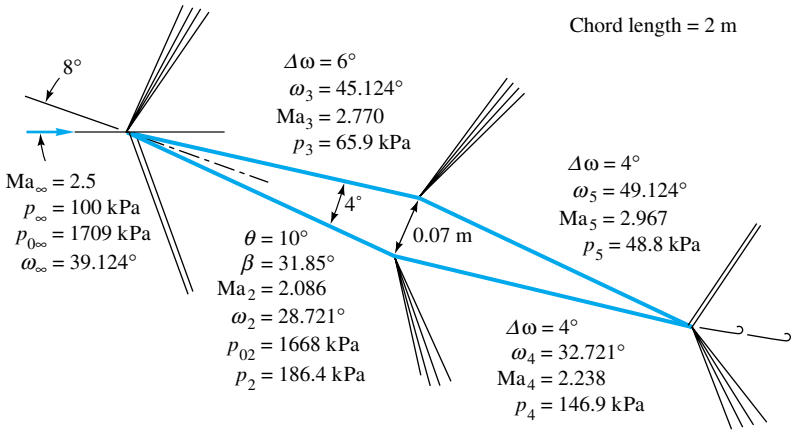
$$F = (109.3 \text{ kPa})(2 \text{ m}^2) = 218.6 \text{ kN}$$

For the chordwise force P the pressure difference on the top half is $p_3 - p_5 = 65.9 - 48.8 = 17.1$ kPa, and on the bottom half it is $p_2 - p_4 = 186.4 - 146.9 = 39.5$ kPa. The average difference is $\frac{1}{2}(17.1 + 39.5) = 28.3$ kPa, which when multiplied by the frontal area (maximum thickness times 1-m width) gives

$$P = (28.3 \text{ kPa})(0.07 \text{ m})(1 \text{ m}) = 2.0 \text{ kN}$$



ketabline.com Ebook.ketabline.com



E9.21

Both F and P have components in the lift and drag directions. The lift force normal to the free stream is

$$L = F\cos 8° - P\sin 8° = 216.2 \text{ kN}$$

and

$$D = F\sin 8° + P\cos 8° = 32.4 \text{ kN}$$

For computing the coefficients, the denominator of Eq. (9.102) is the same as in Example 9.19: $\frac{1}{2}kp_\infty \text{Ma}_\infty^2\, bC = \frac{1}{2}(1.4)(100 \text{ kPa})(2.5)^2(2 \text{ m}^2) = 875$ kN. Thus, finally, shock expansion theory predicts

$$C_L = \frac{216.2 \text{ kN}}{875 \text{ kN}} = 0.247 \qquad C_D = \frac{32.4 \text{ kN}}{875 \text{ kN}} = 0.0370 \qquad \textit{Ans. (a)}$$

Part (b) Meanwhile, by Ackeret theory, C_L is the same as in Example 9.20:

$$C_L = \frac{4(0.1396)}{(2.5^2 - 1)^{1/2}} = 0.244 \qquad \textit{Ans. (b)}$$

This is 1 percent less than the shock expansion result above. For the drag we need the mean-square slopes from Eq. (9.106)

$$\overline{y_u'^2} = \overline{y_l'^2} = \tan^2 2° = 0.00122$$

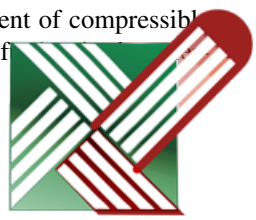
Then Eq. (9.107) predicts the linearized result

$$C_D = \frac{4}{(2.5^2 - 1)^{1/2}}\left[(0.1396)^2 + \tfrac{1}{2}(0.00122 + 0.00122)\right] = 0.0362 \qquad \textit{Ans. (b)}$$

This is 2 percent lower than shock expansion theory predicts. We could judge Ackeret theory to be "satisfactory." Ackeret theory predicts $p_2 = 167$ kPa (-11 percent), $p_3 = 60$ kPa (-9 percent), $p_4 = 140$ kPa (-5 percent), and $p_5 = 33$ kPa (-6 percent).

Three-Dimensional Supersonic Flow

We have gone about as far as we can go in an introductory treatment of compressibl flow. Of course, there is much more, and you are invited to study f ences at the end of the chapter.



ketabline.com Ebook.ketabline.com

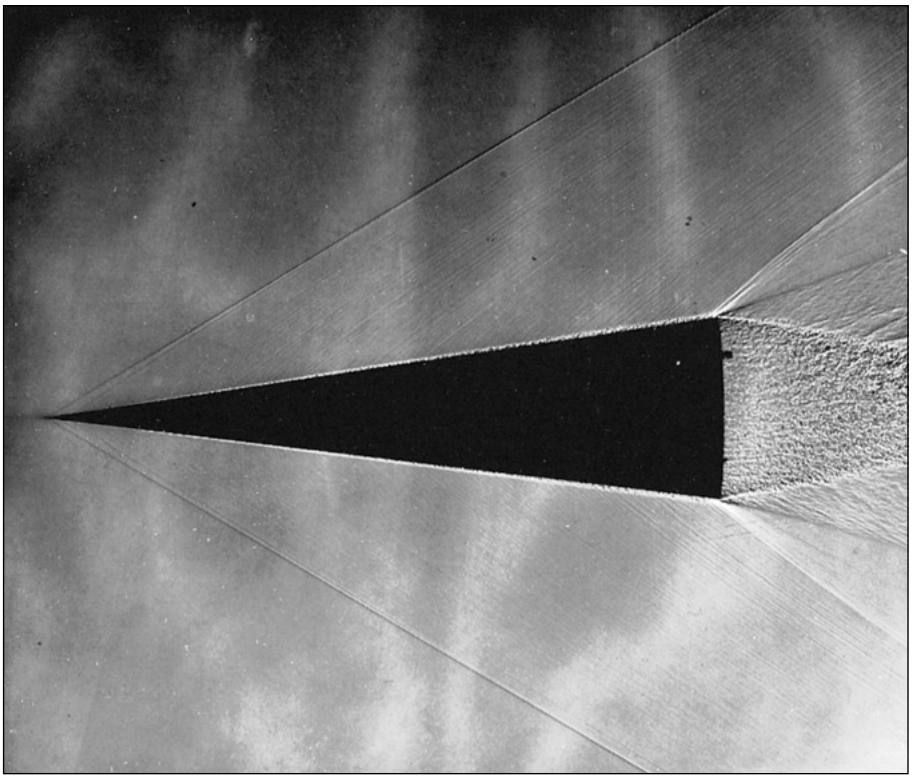
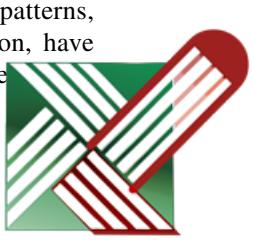


Fig. 9.28 Shadowgraph of flow past an 8° half-angle cone at $Ma_\infty = 2.0$. The turbulent boundary layer is clearly visible. The Mach lines curve slightly, and the Mach number varies from 1.98 just inside the shock to 1.90 at the surface. *(Courtesy of U.S. Army Ballistic Research Center, Aberdeen Proving Ground.)*

Three-dimensional supersonic flows are highly complex, especially if they concern blunt bodies, which therefore contain embedded regions of subsonic and transonic flow, e.g., Fig. 9.10. Some flows, however, yield to accurate theoretical treatment such as flow past a cone at zero incidence, as shown in Fig. 9.28. The exact theory of cone flow is discussed in advanced texts [for example, 8, chap. 17], and extensive tables of such solutions have been published [22, 23]. There are similarities between cone flow and the wedge flows illustrated in Fig. 9.22: an attached oblique shock, a thin turbulent boundary layer, and an expansion fan at the rear corner. However, the conical shock deflects the flow through an angle less than the cone half-angle, unlike the wedge shock. As in the wedge flow, there is a maximum cone angle above which the shock must detach, as in Fig. 9.22*b*. For $k = 1.4$ and $Ma_\infty = \infty$, the maximum cone half-angle for an attached shock is about 57°, compared with the maximum wedge angle of 45.6° (see Ref. 23).

For more complicated body shapes one usually resorts to experimentation in a supersonic wind tunnel. Figure 9.29 shows a wind-tunnel study of supersonic flow past a model of an interceptor aircraft. The many junctions and wingtips and shape changes make theoretical analysis very difficult. Here the surface-flow patterns, which indicate boundary-layer development and regions of flow separation, have been visualized by the smearing of oil drops placed on the model surface be
test.



ketabline.com Ebook.ketabline.com

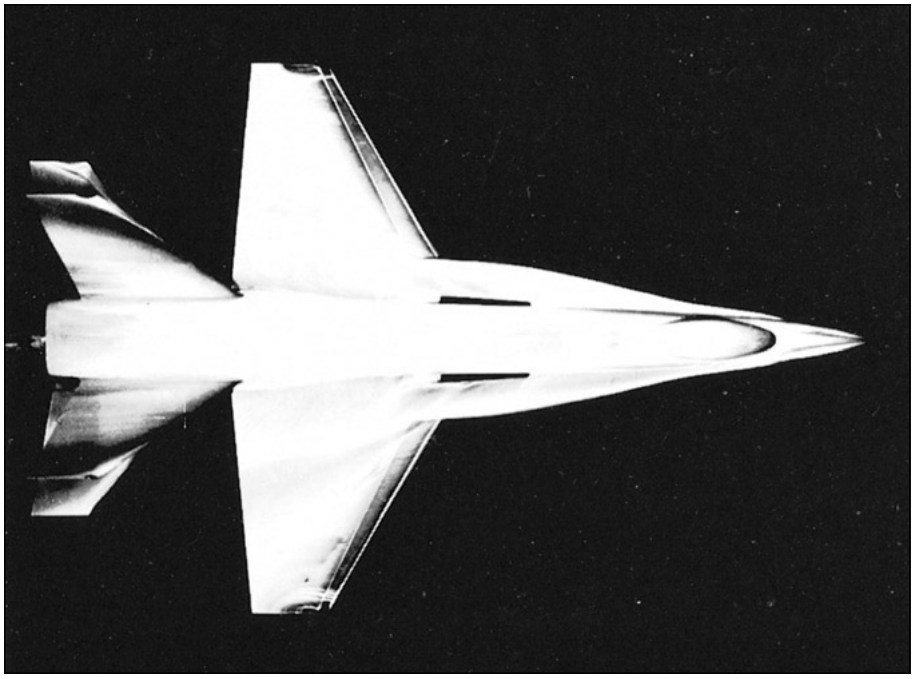


Fig. 9.29 Wind-tunnel test of the Cobra P-530 supersonic interceptor. The surface flow patterns are visualized by the smearing of oil droplets. *(Courtesy of Northrop Corp.)*

As we shall see in the next chapter, there is an interesting analogy between gas-dynamic shock waves and the surface water waves which form in an open-channel flow. Chapter 11 of Ref. 14 explains how a water channel can be used in an inexpensive simulation of supersonic-flow experiments.

Reusable Hypersonic Launch Vehicles

Having achieved reliable supersonic flight with both military and commercial aircraft, the next step is probably to develop a hypersonic vehicle that can achieve orbit, yet be retrieved. Presently the United States employs the Space Shuttle, where only the manned vehicle is retrieved, the very expensive giant rocket boosters being lost. In 1996, NASA selected Lockheed-Martin to develop the X-33, the first smaller-scale step toward a retrievable single-stage-to-orbit (SSTO) vehicle, to be called the VentureStar [36].

The X-33, shown in an artist's rendering in Fig. 9.30, will be 20 m long, about half the size of the VentureStar, and it will be *suborbital*. It will take off vertically, rise to a height of 73 km, and coast back to earth at a steep (stressful) angle. Such a flight will test many new plans for the VentureStar [37], such as metallic tiles, titanium components, graphite composite fuel tanks, high-voltage control actuators, and Rocketdyne's novel "aerospike" rocket nozzles. If successful, the VentureSt is planned as a standard reusable, low-cost orbital vehicle. Ve 39 m long and weigh 9.7 MN, of which 88 percent (965 tons!)



ketabline.com Ebook.ketabline.com

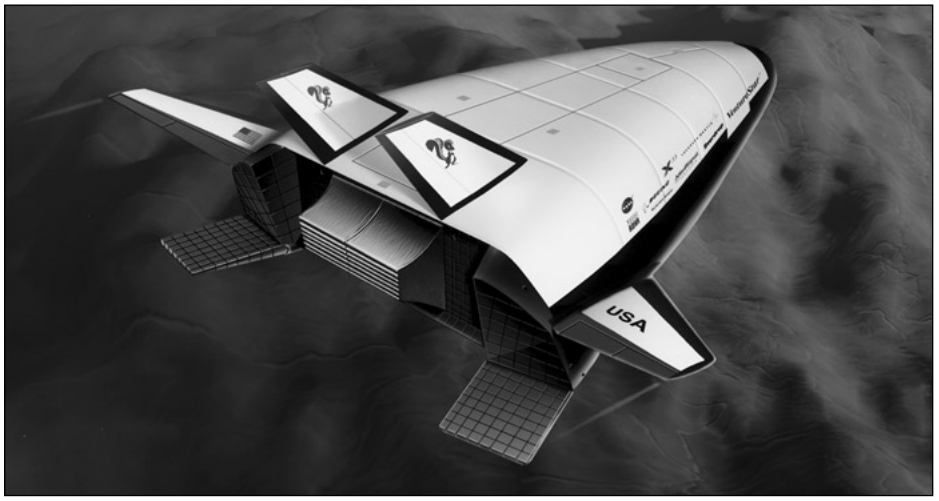


Fig. 9.30 The X-33 is a half-size suborbital test version of the VentureStar, which is planned as an orbital, low-cost retrievable space vehicle. It takes off vertically but then uses its lifting shape to glide back to earth and land horizontally [36, 37]. *(Courtesy of Lockheed Martin Corp.)*

and only 2.7 percent (260 kN) will be payload. The dream is that the X-33 and VentureStar and their progeny will lead to an era of routine, low-cost space travel appropriate to the new millennium.

Summary

This chapter is a brief introduction to a very broad subject, compressible flow, sometimes called *gas dynamics*. The primary parameter is the Mach number Ma = V/a, which is large and causes the fluid density to vary significantly. This means that the continuity and momentum equations must be coupled to the energy relation and the equation of state to solve for the four unknowns (p, ρ, T, $\mathbf{V}$).

The chapter reviews the thermodynamic properties of an ideal gas and derives a formula for the speed of sound of a fluid. The analysis is then simplified to one-dimensional steady adiabatic flow without shaft work, for which the stagnation enthalpy of the gas is constant. A further simplification to isentropic flow enables formulas to be derived for high-speed gas flow in a variable-area duct. This reveals the phenomenon of sonic-flow *choking* (maximum mass flow) in the throat of a nozzle. At supersonic velocities there is the possibility of a normal-shock wave, where the gas discontinuously reverts to subsonic conditions. The normal shock explains the effect of back pressure on the performance of converging-diverging nozzles.

To illustrate nonisentropic flow conditions, there is a brief study of constant-area duct flow with friction and with heat transfer, both of which lead to choking of the exit flow.

The chapter ends with a discussion of two-dimensional supersonic flow, where oblique-shock waves and Prandtl-Meyer (isentropic) expansion waves appear. With a proper combination of shocks and expansions one can analyze supersonic foils.



ketabline.com Ebook.ketabline.com

Problems

Most of the problems herein are fairly straightforward. More difficult or open-ended assignments are labeled with an asterisk. Problems labeled with an EES icon will benefit from the use of the Engineering Equations Solver (EES), while problems labeled with a computer icon may require the use of a computer. The standard end-of-chapter problems 9.1 to 9.157 (categorized in the problem list below) are followed by word problems W9.1 to W9.8, fundamentals of engineering exam problems FE9.1 to FE9.10, comprehensive problems C9.1 to C9.3, and design projects D9.1 and D9.2.

Problem distribution

Section	Topic	Problems
9.1	Introduction	9.1–9.9
9.2	The speed of sound	9.10–9.18
9.3	Adiabatic and isentropic flow	9.19–9.33
9.4	Isentropic flow with area changes	9.34–9.53
9.5	The normal-shock wave	9.54–9.62
9.6	Converging and diverging nozzles	9.63–9.85
9.7	Duct flow with friction	9.86–9.107
9.8	Frictionless duct flow with heat transfer	9.108–9.115
9.9	Mach waves	9.116–9.121
9.9	The oblique-shock wave	9.122–9.139
9.10	Prandtl-Meyer expansion waves	9.140–9.147
9.10	Supersonic airfoils	9.148–9.157

P9.1 An ideal gas flows adiabatically through a duct. At section 1, $p_1 = 140$ kPa, $T_1 = 260°C$, and $V_1 = 75$ m/s. Farther downstream, $p_2 = 30$ kPa and $T_2 = 207°C$. Calculate V_2 in m/s and $s_2 - s_1$ in J/(kg · K) if the gas is (*a*) air, $k = 1.4$, and (*b*) argon, $k = 1.67$.

P9.2 Solve Prob. 9.1 if the gas is steam. Use two approaches: (*a*) an ideal gas from Table A.4 and (*b*) real gas data from the steam tables [15].

P9.3 If 8 kg of oxygen in a closed tank at 200°C and 300 kPa is heated until the pressure rises to 400 kPa, calculate (*a*) the new temperature, (*b*) the total heat transfer, and (*c*) the change in entropy.

P9.4 Compressibility effects become important when the Mach number exceeds approximately 0.3. How fast can a two-dimensional cylinder travel in sea-level standard air before compressibility becomes important *somewhere* in its vicinity?

P9.5 Steam enters a nozzle at 377°C, 1.6 MPa, and a steady speed of 200 m/s and accelerates isentropically until it exits at saturation conditions. Estimate the exit velocity and temperature.

P9.6 Is it possible for the steam in Prob. 9.5 to continue accelerating until it exits with a moisture content of 12 percent? If so, estimate the new exit velocity and temperature.

P9.7 Carbon dioxide ($k = 1.28$) enters a constant-area duct at 400°F, 100 lbf/in^2 absolute, and 500 ft/s. Farther downstream the properties are $V_2 = 1000$ ft/s and $T_2 = 900°F$. Compute (*a*) p_2, (*b*) the heat added between sections, (*c*) the entropy change between sections, and (*d*) the mass flow per unit area. *Hint:* This problem requires the continuity equation.

P9.8 Atmospheric air at 20°C enters and fills an insulated tank which is initially evacuated. Using a control-volume analysis from Eq. (3.63), compute the tank air temperature when it is full.

P9.9 Liquid hydrogen and oxygen are burned in a combustion chamber and fed through a rocket nozzle which exhausts at $V_{exit} = 1600$ m/s to an ambient pressure of 54 kPa. The nozzle exit diameter is 45 cm, and the jet exit density is 0.15 kg/m^3. If the exhaust gas has a molecular weight of 18, estimate (*a*) the exit gas temperature, (*b*) the mass flow, and (*c*) the thrust developed by the rocket.

P9.10 A certain aircraft flies at the same Mach number regardless of its altitude. Compared to its speed at 12,000-m standard altitude, it flies 127 km/h faster at sea level. Determine its Mach number.

P9.11 At 300°C and 1 atm, estimate the speed of sound of (*a*) nitrogen, (*b*) hydrogen, (*c*) helium, (*d*) steam, and (*e*) $^{238}UF_6$ ($k \approx 1.06$).

P9.12 Assume that water follows Eq. (1.19) with $n \approx 7$ and $B \approx 3000$. Compute the bulk modulus (in kPa) and the speed of sound (in m/s) at (*a*) 1 atm and (*b*) 1100 atm (the deepest part of the ocean). (*c*) Compute the speed of sound at 20°C and 9000 atm and compare with the measured value of 2650 m/s (A. H. Smith and A. W. Lawson, *J. Chem. Phys.,* vol. 22, 1954, p. 351).

P9.13 From Prob. 1.33, mercury data fit Eq. (1.19) with $n \approx 6$ and $B \approx 41{,}000$. Estimate (*a*) the bulk modulus and (*b*) the speed of sound of mercury at 2500 atm and compare with Table 9.1.

P9.14 Assume steady adiabatic flow of a perfect gas. Show that the energy equation (9.21), when plotted as speed of sound versus velocity, forms an ellipse. Sketch this ellipse; label the intercepts and the regions of subsonic, sonic, and supersonic flow; and determine the ratio of the major and minor axes.

P9.15 A weak pressure wave (sound wave) with a pressure change $\Delta p = 40$ Pa propagates through air at 20°C and 1 atm. Estimate (*a*) the density change, (*b*) the temperature change, and (*c*) the velocity change across the wave.

P9.16 A weak pressure pulse Δp propagates through still air. Discuss the type of reflected pulse which occurs and the boundary conditions which must be



ketabline.com Ebook.ketabline.com

wave strikes normal to, and is reflected from, (*a*) a solid wall and (*b*) a free liquid surface.

P9.17 A submarine at a depth of 800 m sends a sonar signal and receives the reflected wave back from a similar submerged object in 15 s. Using Prob. 9.12 as a guide, estimate the distance to the other object.

***P9.18** The properties of a dense gas (high pressure and low temperature) are often approximated by van der Waals' equation of state [17, 18]:

$$p = \frac{\rho RT}{1 - b_1\rho} - a_1\rho^2$$

where constants a_1 and b_1 can be found from the critical temperature and pressure

$$a_1 = \frac{27R^2T_c^2}{64p_c} = 9.0 \times 10^5 \text{ lbf} \cdot \text{ft}^4/\text{slug}^2$$

for air, and

$$b_1 = \frac{RT_c}{8p_c} = 0.65 \text{ ft}^3/\text{slug}$$

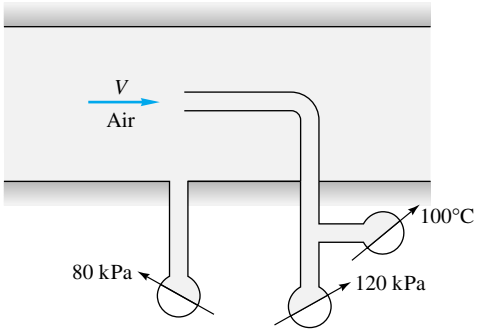
for air. Find an analytic expression for the speed of sound of a van der Waals gas. Assuming $k = 1.4$, compute the speed of sound of air in ft/s at −100°F and 20 atm for (*a*) a perfect gas and (*b*) a van der Waals gas. What percentage higher density does the van der Waals relation predict?

P9.19 The Concorde aircraft flies at Ma ≈ 2.3 at 11-km standard altitude. Estimate the temperature in °C at the front stagnation point. At what Mach number would it have a front stagnation-point temperature of 450°C?

P9.20 A gas flows at $V = 200$ m/s, $p = 125$ kPa, and $T = 200$°C. For (*a*) air and (*b*) helium, compute the maximum pressure and the maximum velocity attainable by expansion or compression.

P9.21 Air expands isentropically through a duct from $p_1 = 125$ kPa and $T_1 = 100$°C to $p_2 = 80$ kPa and $V_2 = 325$ m/s. Compute (*a*) T_2, (*b*) Ma_2, (*c*) T_0, (*d*) p_0, (*e*) V_1, and (f) Ma_1.

P9.22 Given the pitot stagnation temperature and pressure and the static-pressure measurements in Fig. P9.22, estimate the air velocity V, assuming (*a*) incompressible flow and (*b*) compressible flow.



P9.22

P9.23 A large rocket engine delivers hydrogen at 1500°C and 3 MPa, $k = 1.41$, $R = 4124$ J/(kg·K), to a nozzle which exits with gas pressure equal to the ambient pressure of 54 kPa. Assuming isentropic flow, if the rocket thrust is 2 MN, what is (*a*) the exit velocity and (*b*) the mass flow of hydrogen?

P9.24 For low-speed (nearly incompressible) gas flow, the stagnation pressure can be computed from Bernoulli's equation

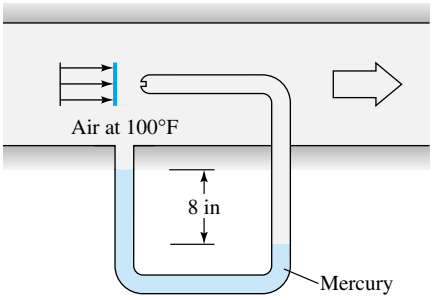
$$p_0 = p + \frac{1}{2}\rho V^2$$

(*a*) For higher subsonic speeds, show that the isentropic relation (9.28*a*) can be expanded in a power series as follows:

$$p_0 \approx p + \frac{1}{2}\rho V^2\left(1 + \frac{1}{4}\text{Ma}^2 + \frac{2-k}{24}\text{Ma}^4 + \cdots\right)$$

(*b*) Suppose that a pitot-static tube in air measures the pressure difference $p_0 - p$ and uses the Bernoulli relation, with stagnation density, to estimate the gas velocity. At what Mach number will the error be 4 percent?

P9.25 If it is known that the air velocity in the duct is 750 ft/s, use the mercury-manometer measurement in Fig. P9.25 to estimate the static pressure in the duct in lbf/in^2 absolute.



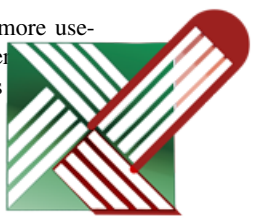
P9.25

P9.26 Show that for isentropic flow of a perfect gas if a pitot-static probe measures p_0, p, and T_0, the gas velocity can be calculated from

$$V^2 = 2c_pT_0\left[1 - \left(\frac{p}{p_0}\right)^{(k-1)/k}\right]$$

What would be a source of error if a shock wave were formed in front of the probe?

P9.27 In many problems the sonic (*) properties are more useful reference values than the stagnation proper
isentropic flow of a perfect gas, derive relations



ketabline.com Ebook.ketabline.com

T/T^*, and ρ/ρ^* as functions of the Mach number. Let us help by giving the density-ratio formula:

$$\frac{\rho}{\rho^*} = \left[\frac{k+1}{2+(k-1)\,\mathrm{Ma}^2}\right]^{1/(k-1)}$$

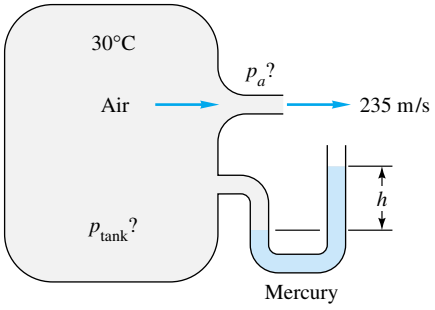
P9.28 A large vacuum tank, held at 60 kPa absolute, sucks sea-level standard air through a converging nozzle whose throat diameter is 3 cm. Estimate (*a*) the mass-flow rate through the nozzle and (*b*) the Mach number at the throat.

P9.29 Steam from a large tank, where $T = 400°C$ and $p = 1$ MPa, expands isentropically through a nozzle until, at a section of 2-cm diameter, the pressure is 500 kPa. Using the steam tables [15], estimate (*a*) the temperature, (*b*) the velocity, and (*c*) the mass flow at this section. Is the flow subsonic?

P9.30 Air flows in a duct of diameter 5 cm. At one section, $T_0 = 300°C$, $p = 120$ kPa, and $\dot{m} = 0.4$ kg/s. Estimate, at this section, (*a*) V, (*b*) Ma, and (*c*) ρ_0.

P9.31 Air flows adiabatically through a duct. At one section $V_1 = 400$ ft/s, $T_1 = 200°F$, and $p_1 = 35$ lbf/in^2 absolute, while farther downstream $V_2 = 1100$ ft/s and $p_2 = 18$ lbf/in^2 absolute. Compute (*a*) Ma_2, (*b*) $U_{\max}$, and (*c*) p_{02}/p_{01}.

P9.32 The large compressed-air tank in Fig. P9.32 exhausts from a nozzle at an exit velocity of 235 m/s. The mercury manometer reads $h = 30$ cm. Assuming isentropic flow, compute the pressure (*a*) in the tank and (*b*) in the atmosphere. (*c*) What is the exit Mach number?



P9.32

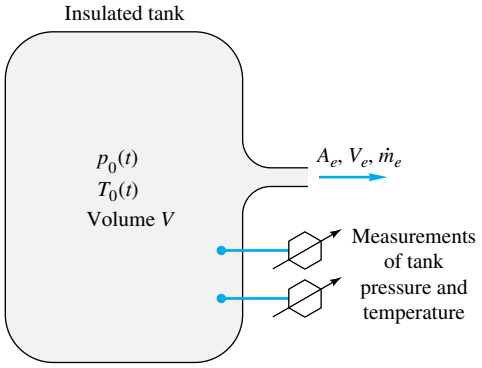
P9.33 Air flows isentropically from a reservoir, where $p = 300$ kPa and $T = 500$ K, to section 1 in a duct, where $A_1 = 0.2$ m^2 and $V_1 = 550$ m/s. Compute (*a*) Ma_1, (*b*) T_1, (*c*) p_1, (*d*) $\dot{m}$, and (*e*) A^*. Is the flow choked?

P9.34 Steam in a tank at 450°F and 100 lbf/in^2 absolute exhausts through a converging nozzle of 0.1-in^2 throat area to a 1-atm environment. Compute the initial mass flow (*a*) for an ideal gas and (*b*) from the steam tables [15].

P9.35 Helium, at $T_0 = 400$ K, enters a nozzle isentropically. At section 1, where $A_1 = 0.1$ m^2, a pitot-static arrangement (see Fig. P9.25) measures stagnation pressure of 150 kPa and static pressure of 123 kPa. Estimate (*a*) Ma_1, (*b*) mass flow $\dot{m}$, (*c*) T_1, and (*d*) A^*.

P9.36 An air tank of volume 1.5 m^3 is initially at 800 kPa and 20°C. At $t = 0$, it begins exhausting through a converging nozzle to sea-level conditions. The throat area is 0.75 cm^2. Estimate (*a*) the initial mass flow in kg/s, (*b*) the time required to blow down to 500 kPa, and (*c*) the time at which the nozzle ceases being choked.

P9.37 Make an exact control-volume analysis of the blowdown process in Fig. P9.37, assuming an insulated tank with negligible kinetic and potential energy within. Assume critical flow at the exit, and show that both p_0 and T_0 decrease during blowdown. Set up first-order differential equations for $p_0(t)$ and $T_0(t)$, and reduce and solve as far as you can.



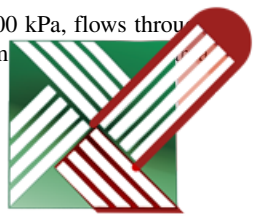
P9.37

P9.38 Prob. 9.37 makes an ideal senior project or combined laboratory and computer problem, as described in Ref. 30, sec. 8.6. In Bober and Kenyon's lab experiment, the tank had a volume of 0.0352 ft^3 and was initially filled with air at 50 lb/in^2 gage and 72°F. Atmospheric pressure was 14.5 lb/in^2 absolute, and the nozzle exit diameter was 0.05 in. After 2 s of blowdown, the measured tank pressure was 20 lb/in^2 gage and the tank temperature was −5°F. Compare these values with the theoretical analysis of Prob. 9.37.

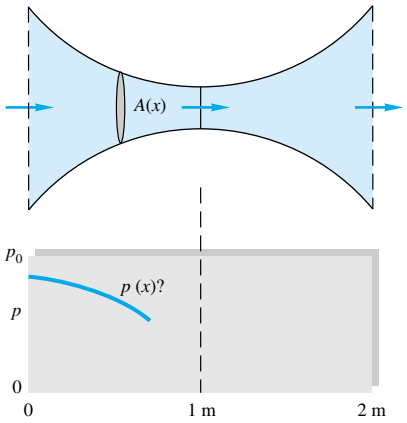
P9.39 Consider isentropic flow in a channel of varying area, from section 1 to section 2. We know that $\mathrm{Ma}_1 = 2.0$ and desire that the velocity ratio V_2/V_1 be 1.2. Estimate (*a*) Ma_2 and (*b*) A_2/A_1. (*c*) Sketch what this channel looks like. For example, does it converge or diverge? Is there a throat?

P9.40 Air, with stagnation conditions of 800 kPa and 100°C, expands isentropically to a section of a duct where $A_1 = 20$ cm^2 and $p_1 = 47$ kPa. Compute (*a*) Ma_1, (*b*) the throat area, and (*c*) $\dot{m}$. At section 2 between the throat and section 1, the area is 9 cm^2. (*d*) Estimate the Mach number at section 2.

P9.41 Air, with a stagnation pressure of 100 kPa, flows through the nozzle in Fig. P9.41, which is 2 m variation approximated by



ketabline.com Ebook.ketabline.com



P9.41

$$A \approx 20 - 20x + 10x^2$$

with A in cm^2 and x in m. It is desired to plot the complete family of isentropic pressures $p(x)$ in this nozzle, for the range of inlet pressures $1 < p(0) < 100$ kPa. Indicate those inlet pressures which are not physically possible and discuss briefly. If your computer has an online graphics routine, plot at least 15 pressure profiles; otherwise just hit the highlights and explain.

P9.42 A bicycle tire is filled with air at an absolute pressure of 169.12 kPa, and the temperature inside is 30.0°C. Suppose the valve breaks, and air starts to exhaust out of the tire into the atmosphere ($p_a = 100$ kPa absolute and $T_a = 20.0$°C). The valve exit is 2.00 mm in diameter and is the smallest cross-sectional area of the entire system. Frictional losses can be ignored here, i.e., one-dimensional isentropic flow is a reasonable assumption. (*a*) Find the Mach number, velocity, and temperature at the exit plane of the valve (initially). (*b*) Find the initial mass-flow rate out of the tire. (*c*) Estimate the velocity at the exit plane using the incompressible Bernoulli equation. How well does this estimate agree with the "exact" answer of part (*a*)? Explain.

P9.43 Air flows isentropically through a duct with $T_0 = 300$°C. At two sections with identical areas of 25 cm^2, the pressures are $p_1 = 120$ kPa and $p_2 = 60$ kPa. Determine (*a*) the mass flow, (*b*) the throat area, and (*c*) Ma_2.

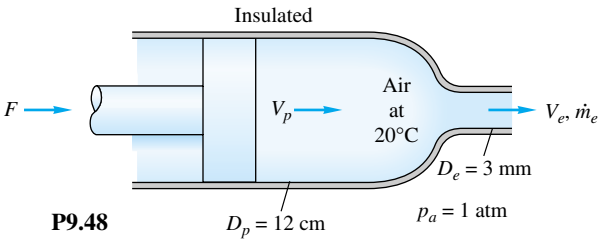
P9.44 In Prob. 3.34 we knew nothing about compressible flow at the time, so we merely assumed exit conditions p_2 and T_2 and computed V_2 as an application of the continuity equation. Suppose that the throat diameter is 3 in. For the given stagnation conditions in the rocket chamber in Fig. P3.34 and assuming $k = 1.4$ and a molecular weight of 26, compute the actual exit velocity, pressure, and temperature according to one-dimensional theory. If $p_a = 14.7$ lbf/in^2 absolute, compute the thrust from the analysis of Prob. 3.68. This thrust is entirely independent of the stagnation temperature (check this by changing T_0 to 2000°R if you like). Why?

P9.45 At a point upstream of the throat of a converging-diverging nozzle the properties are $V_1 = 200$ m/s, $T_1 = 300$ K, and $p_1 = 125$ kPa. If the exit flow is supersonic, compute, from isentropic theory, (*a*) $\dot{m}$ and (*b*) A_1. The throat area is 35 cm^2.

P9.46 If the author did not falter, the results of Prob. 9.43 are (*a*) 0.671 kg/s, (*b*) 23.3 cm^2, and (*c*) 1.32. Do not tell your friends who are still working on Prob. 9.43. Consider a control volume which encloses the nozzle between these two 25-cm^2 sections. If the pressure outside the duct is 1 atm, determine the total force acting on this section of nozzle.

P9.47 In wind-tunnel testing near Mach 1, a small area decrease caused by model blockage can be important. Suppose the test section area is 1 m^2, with unblocked test conditions $\text{Ma} = 1.10$ and $T = 20$°C. What model area will first cause the test section to choke? If the model cross section is 0.004 m^2 (0.4 percent blockage), what percentage change in test-section velocity results?

P9.48 A force $F = 1100$ N pushes a piston of diameter 12 cm through an insulated cylinder containing air at 20°C, as in Fig. P9.48. The exit diameter is 3 mm, and $p_a = 1$ atm. Estimate (*a*) V_e, (*b*) V_p, and (*c*) $\dot{m}_e$.

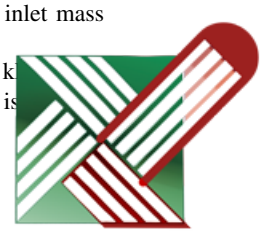


P9.48

P9.49 Air expands through a nozzle and exits supersonically. The throat area is 10 cm^2, and the throat pressure is 100 kPa. Find the pressure on either side of the throat where the duct area is 24 cm^2.

P9.50 Argon expands isentropically in a converging nozzle whose entrance conditions are $D_1 = 10$ cm, $p_1 = 150$ kPa, $T_1 = 100$°C, and $\dot{m} = 1$ kg/s. The flow discharges smoothly to an ambient pressure of 101 kPa. (*a*) What is the exit diameter of the nozzle? (*b*) How much further can the ambient pressure be reduced before it affects the inlet mass flow?

P9.51 Air, at stagnation conditions of 500 K and 200 k
through a nozzle. At section 1, where the area is

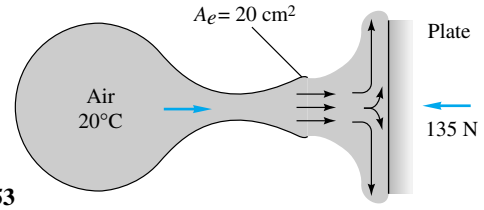


ketabline.com Ebook.ketabline.com

the density is 0.32 kg/m^3. Assuming isentropic flow, (*a*) find the mass flow. (*b*) Is the flow choked? If so, estimate A^*. Also estimate (*c*) p_1 and (*d*) Ma_1.

P9.52 A converging-diverging nozzle exits smoothly to sea-level standard atmosphere. It is supplied by a 40-m^3 tank initially at 800 kPa and 100°C. Assuming isentropic flow in the nozzle, estimate (*a*) the throat area and (*b*) the tank pressure after 10 s of operation. The exit area is 10 cm^2.

P9.53 Air flows steadily from a reservoir at 20°C through a nozzle of exit area 20 cm^2 and strikes a vertical plate as in Fig. P9.53. The flow is subsonic throughout. A force of 135 N is required to hold the plate stationary. Compute (*a*) V_e, (*b*) Ma_e, and (*c*) p_0 if $p_a = 101$ kPa.



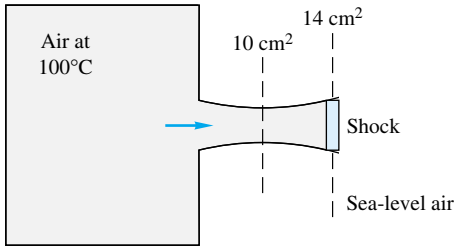
P9.53

P9.54 For flow of air through a normal shock the upstream conditions are $V_1 = 600$ m/s, $T_{01} = 500$ K, and $p_{01} = 700$ kPa. Compute the downstream conditions Ma_2, V_2, T_2, p_2, and p_{02}.

P9.55 Air, supplied by a reservoir at 450 kPa, flows through a converging-diverging nozzle whose throat area is 12 cm^2. A normal shock stands where $A_1 = 20$ cm^2. (*a*) Compute the pressure just downstream of this shock. Still farther downstream, at $A_3 = 30$ cm^2, estimate (*b*) p_3, (*c*) A_3^*, and (*d*) Ma_3.

P9.56 Air from a reservoir at 20°C and 500 kPa flows through a duct and forms a normal shock downstream of a throat of area 10 cm^2. By an odd coincidence it is found that the stagnation pressure downstream of this shock exactly equals the throat pressure. What is the area where the shock wave stands?

P9.57 Air flows from a tank through a nozzle into the standard atmosphere, as in Fig. P9.57. A normal shock stands in the exit of the nozzle, as shown. Estimate (*a*) the pressure in the tank and (*b*) the mass flow.



P9.57

P9.58 Argon (Table A.4) approaches a normal shock with $V_1 = 700$ m/s, $p_1 = 125$ kPa, and $T_1 = 350$ K. Estimate (*a*) V_2 and (*b*) p_2. (*c*) What pressure p_2 would result if the same velocity change V_1 to V_2 were accomplished isentropically?

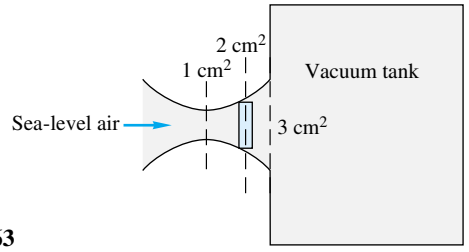
P9.59 Air, at stagnation conditions of 450 K and 250 kPa, flows through a nozzle. At section 1, where the area is 15 cm^2, there is a normal shock wave. If the mass flow is 0.4 kg/s, estimate (*a*) the Mach number and (*b*) the stagnation pressure just downstream of the shock.

P9.60 When a pitot tube such as in Fig. 6.30 is placed in a supersonic flow, a normal shock will stand in front of the probe. Suppose the probe reads $p_0 = 190$ kPa and $p = 150$ kPa. If the stagnation temperature is 400 K, estimate the (supersonic) Mach number and velocity upstream of the shock.

P9.61 Repeat Prob. 9.56 except this time let the odd coincidence be that the *static* pressure downstream of the shock exactly equals the throat pressure. What is the area where the shock stands?

P9.62 An atomic explosion propagates into still air at 14.7 lbf/in^2 absolute and 520°R. The pressure just inside the shock is 5000 lbf/in^2 absolute. Assuming $k = 1.4$, what are the speed C of the shock and the velocity V just inside the shock?

P9.63 Sea-level standard air is sucked into a vacuum tank through a nozzle, as in Fig. P9.63. A normal shock stands where the nozzle area is 2 cm^2, as shown. Estimate (*a*) the pressure in the tank and (*b*) the mass flow.

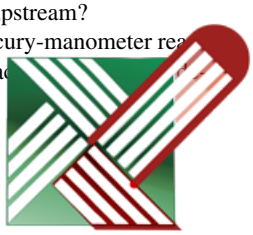


P9.63

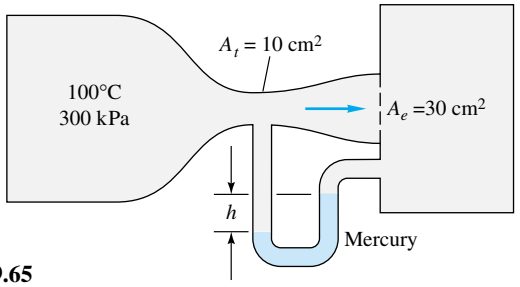
P9.64 Air in a large tank at 100°C and 150 kPa exhausts to the atmosphere through a converging nozzle with a 5-cm^2 throat area. Compute the exit mass flow if the atmospheric pressure is (*a*) 100 kPa, (*b*) 60 kPa, and (*c*) 30 kPa.

P9.65 Air flows through a converging-diverging nozzle between two large reservoirs, as shown in Fig. P9.65. A mercury manometer between the throat and the downstream reservoir reads $h = 15$ cm. Estimate the downstream reservoir pressure. Is there a normal shock in the flow? If so, does it stand in the exit plane or farther upstream?

P9.66 In Prob. 9.65 what would be the mercury-manometer rea ing h if the nozzle were operating exac sign conditions?



ketabline.com Ebook.ketabline.com



P9.65

P9.67 In Prob. 9.65 estimate the complete range of manometer readings h for which the flow through the nozzle is entirely isentropic, except possibly in the exit plane.

P9.68 Air in a tank at 120 kPa and 300 K exhausts to the atmosphere through a 5-cm^2-throat converging nozzle at a rate of 0.12 kg/s. What is the atmospheric pressure? What is the maximum mass flow possible at low atmospheric pressure?

P9.69 With reference to Prob. 3.68, show that the thrust of a rocket engine exhausting into a vacuum is given by

$$F = \frac{p_0 A_e (1 + k\,\mathrm{Ma}_e^2)}{\left(1 + \dfrac{k-1}{2}\,\mathrm{Ma}_e^2\right)^{k/(k-1)}}$$

where A_e = exit area
Ma_e = exit Mach number
p_0 = stagnation pressure in combustion chamber

Note that stagnation temperature does not enter into the thrust.

P9.70 Air, at stagnation temperature 100°C, expands isentropically through a nozzle of 6-cm^2 throat area and 18-cm^2 exit area. The mass flow is at its maximum value of 0.5 kg/s. Estimate the exit pressure for (*a*) subsonic and (*b*) supersonic exit flow.

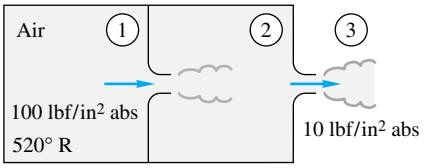
P9.71 For the nozzle of Prob. 9.70, allowing for nonisentropic flow, what is the range of exit tank pressures p_b for which (*a*) the diverging nozzle flow is fully supersonic, (*b*) the exit flow is subsonic, (*c*) the mass flow is independent of p_b, (*d*) the exit plane pressure p_e is independent of p_b, and (*e*) $p_e < p_b$?

P9.72 Suppose the nozzle flow of Prob. 9.70 is not isentropic but instead has a normal shock at the position where area is 15 cm^2. Compute the resulting mass flow, exit pressure, and exit Mach number.

P9.73 Air flows isentropically in a converging-diverging nozzle with a throat area of 3 cm^2. At section 1, the pressure is 101 kPa, the temperature is 300 K, and the velocity is 868 m/s. (*a*) Is the nozzle choked? Determine (*b*) A_1 and (*c*) the mass flow. Suppose, without changing stagnation conditions or A_1, the (flexible) throat is reduced to 2 cm^2. Assuming shock-free flow, will there be any change in the gas properties at section 1? If so, compute new p_1, V_1, and T_1 and explain.

P9.74 The perfect-gas assumption leads smoothly to Mach-number relations which are very convenient (and tabulated). This is not so for a real gas such as steam. To illustrate, let steam at $T_0 = 500°\mathrm{C}$ and $p_0 = 2$ MPa expand isentropically through a converging nozzle whose exit area is 10 cm^2. Using the steam tables, find (*a*) the exit pressure and (*b*) the mass flow when the flow is sonic, or choked. What complicates the analysis?

***P9.75** A double-tank system in Fig. P9.75 has two identical converging nozzles of 1-in^2 throat area. Tank 1 is very large, and tank 2 is small enough to be in steady-flow equilibrium with the jet from tank 1. Nozzle flow is isentropic, but entropy changes between 1 and 3 due to jet dissipation in tank 2. Compute the mass flow. (If you give up, Ref. 14, pp. 288–290, has a good discussion.)

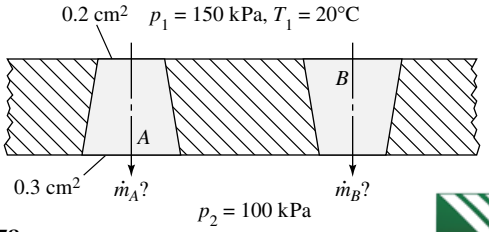


P9.75

P9.76 A large reservoir at 20°C and 800 kPa is used to fill a small insulated tank through a converging-diverging nozzle with 1-cm^2 throat area and 1.66-cm^2 exit area. The small tank has a volume of 1 m^3 and is initially at 20°C and 100 kPa. Estimate the elapsed time when (*a*) shock waves begin to appear inside the nozzle and (*b*) the mass flow begins to drop below its maximum value.

P9.77 A perfect gas (not air) expands isentropically through a supersonic nozzle with an exit area 5 times its throat area. The exit Mach number is 3.8. What is the specific-heat ratio of the gas? What might this gas be? If $p_0 = 300$ kPa, what is the exit pressure of the gas?

P9.78 The orientation of a hole can make a difference. Consider holes *A* and *B* in Fig. P9.78, which are identical but reversed. For the given air properties on either side, compute the mass flow through each hole and explain why they are different.



P9.78

ketabline.com Ebook.ketabline.com

P9.79 Air with $p_0 = 300$ kPa and $T_0 = 500$ K flows through a converging-diverging nozzle with throat area of 1 cm^2 and exit area of 3 cm^2 into a receiver tank. The mass flow is 195.2 kg/h. For what range of receiver pressure is this mass flow possible?

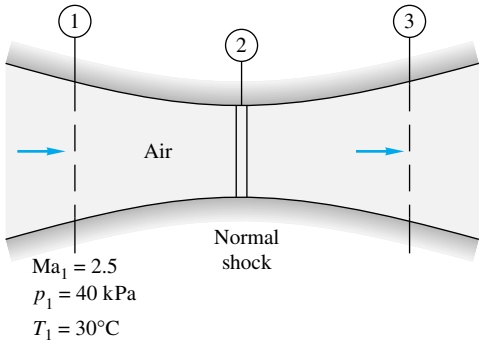
P9.80 A sea-level automobile tire is initially at 32 lbf/in^2 gage pressure and 75°F. When it is punctured with a hole which resembles a converging nozzle, its pressure drops to 15 lbf/in^2 gage in 12 min. Estimate the size of the hole, in thousandths of an inch. The tire volume is 2.5 ft^2.

P9.81 Helium, in a large tank at 100°C and 400 kPa, discharges to a receiver through a converging-diverging nozzle designed to exit at Ma = 2.5 with exit area 1.2 cm^2. Compute (*a*) the receiver pressure and (*b*) the mass flow at design conditions. (*c*) Also estimate the range of receiver pressures for which mass flow will be a maximum.

P9.82 Air at 500 K flows through a converging-diverging nozzle with throat area of 1 cm^2 and exit area of 2.7 cm^2. When the mass flow is 182.2 kg/h, a pitot-static probe placed in the exit plane reads $p_0 = 250.6$ kPa and $p = 240.1$ kPa. Estimate the exit velocity. Is there a normal shock wave in the duct? If so, compute the Mach number just downstream of this shock.

P9.83 When operating at design conditions (smooth exit to sea-level pressure), a rocket engine has a thrust of 1 million lbf. The chamber pressure and temperature are 600 lbf/in^2 absolute and 4000°R, respectively. The exhaust gases approximate $k = 1.38$ with a molecular weight of 26. Estimate (*a*) the exit Mach number and (*b*) the throat diameter.

P9.84 Air flows through a duct as in Fig. P9.84, where $A_1 = 24$ cm^2, $A_2 = 18$ cm^2, and $A_3 = 32$ cm^2. A normal shock stands at section 2. Compute (*a*) the mass flow, (*b*) the Mach number, and (*c*) the stagnation pressure at section 3.



P9.84

P9.85 A large tank delivers air through a nozzle of 1-cm^2 throat area and 2.7-cm^2 exit area. When the receiver pressure is 125 kPa, a normal shock stands in the exit plane. Estimate (*a*) the throat pressure and (*b*) the stagnation pressure in the upstream supply tank.

P9.86 Air enters a 3-cm-diameter pipe 15 m long at $V_1 = 73$ m/s, $p_1 = 550$ kPa, and $T_1 = 60$°C. The friction factor is 0.018. Compute V_2, p_2, T_2, and p_{02} at the end of the pipe. How much additional pipe length would cause the exit flow to be sonic?

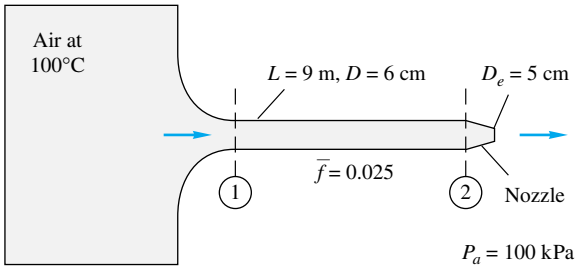
P9.87 Air enters a duct of $L/D = 40$ at $V_1 = 170$ m/s and $T_1 = 300$ K. The flow at the exit is choked. What is the average friction factor in the duct for adiabatic flow?

P9.88 Air enters a 5- by 5-cm square duct at $V_1 = 900$ m/s and $T_1 = 300$ K. The friction factor is 0.02. For what length duct will the flow exactly decelerate to Ma = 1.0? If the duct length is 2 m, will there be a normal shock in the duct? If so, at what Mach number will it occur?

P9.89 Air flows adiabatically in a 5-cm-diameter tube with $f \approx 0.025$. At section 1, $V_1 = 75$ m/s, $T_1 = 350$ K, and $p_1 = 300$ kPa. How much further down the tube will (*a*) the pressure be 156 kPa, (*b*) the temperature be 343 K, and (*c*) the flow reach the choking point?

P9.90 Air, supplied at $p_0 = 700$ kPa and $T_0 = 330$ K, flows through a converging nozzle into a pipe of 2.5-cm diameter which exits to a near vacuum. If $\bar{f} = 0.022$, what will be the mass flow through the pipe if its length is (*a*) 0 m, (*b*) 1 m, and (*c*) 10 m?

P9.91 Air flows steadily from a tank through the pipe in Fig. P9.91. There is a converging nozzle on the end. If the mass flow is 3 kg/s and the nozzle is choked, estimate (*a*) the Mach number at section 1 and (*b*) the pressure inside the tank.

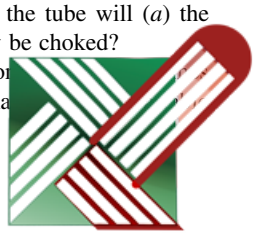


P9.91

P9.92 Modify Prob. 9.91 as follows. Let the pressure in the tank be 700 kPa, and let the nozzle be choked. Determine (*a*) Ma$_2$ and (*b*) the mass flow.

P9.93 Air flows adiabatically in a 3-cm-diameter duct. The average friction factor is 0.015. If, at the entrance, $V = 950$ m/s and $T = 250$ K, how far down the tube will (*a*) the Mach number be 1.8 or (*b*) the flow be choked?

P9.94 Compressible pipe flow with friction constant stagnation enthalpy and ma



ketabline.com Ebook.ketabline.com

momentum. Such a flow is often called *Fanno flow*, and a line representing all possible property changes on a temperature-entropy chart is called a *Fanno line*. Assuming a perfect gas with $k = 1.4$ and the data of Prob. 9.86, draw a Fanno curve of the flow for a range of velocities from very low (Ma $\ll 1$) to very high (Ma $\gg 1$). Comment on the meaning of the maximum-entropy point on this curve.

P9.95 Helium (Table A.4) enters a 5-cm-diameter pipe at $p_1 = 550$ kPa, $V_1 = 312$ m/s, and $T_1 = 40°C$. The friction factor is 0.025. If the flow is choked, determine (*a*) the length of the duct and (*b*) the exit pressure.

P9.96 Derive and verify the adiabatic-pipe-flow velocity relation of Eq. (9.74), which is usually written in the form

$$\frac{\bar{f}L}{D} + \frac{k+1}{k}\ln\frac{V_2}{V_1} = \frac{a_0^2}{k}\left(\frac{1}{V_1^2} - \frac{1}{V_2^2}\right)$$

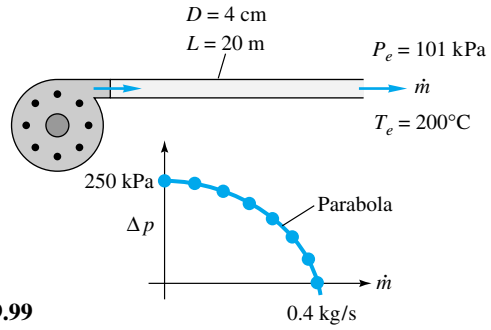
P9.97 By making a few algebraic substitutions, show that Eq. (9.74), or the relation in Prob. 9.96, may be written in the density form

$$\rho_1^2 = \rho_2^2 + \rho^{*2}\left(\frac{2k}{k+1}\frac{\bar{f}L}{D} + 2\ln\frac{\rho_1}{\rho_2}\right)$$

Why is this formula awkward if one is trying to solve for the mass flow when the pressures are given at sections 1 and 2?

P9.98 Compressible *laminar* flow, $f \approx 64/\text{Re}$, may occur in capillary tubes. Consider air, at stagnation conditions of 100°C and 200 kPa, entering a tube 3 cm long and 0.1 mm in diameter. If the receiver pressure is near vacuum, estimate (*a*) the average Reynolds number, (*b*) the Mach number at the entrance, and (*c*) the mass flow in kg/h.

P9.99 A compressor forces air through a smooth pipe 20 m long and 4 cm in diameter, as in Fig. P9.99. The air leaves at 101 kPa and 200°C. The compressor data for pressure rise versus mass flow are shown in the figure. Using the Moody chart to estimate $\bar{f}$, compute the resulting mass flow.

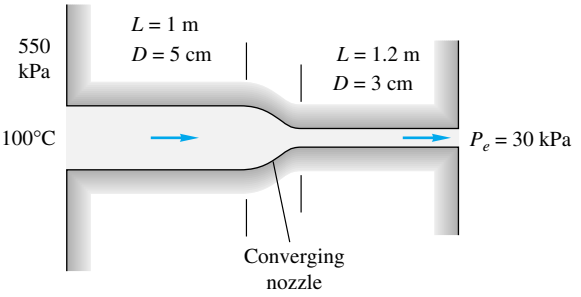


P9.99

P9.100 Modify Prob. 9.99 as follows. Find the length of 4-cm-diameter pipe for which the pump pressure rise will be exactly 200 kPa.

P9.101 How do the compressible-pipe-flow formulas behave for small pressure drops? Let air at 20°C enter a tube of diameter 1 cm and length 3 m. If $\bar{f} = 0.028$ with $p_1 = 102$ kPa and $p_2 = 100$ kPa, estimate the mass flow in kg/h for (*a*) isothermal flow, (*b*) adiabatic flow, and (*c*) incompressible flow (Chap. 6) at the entrance density.

P9.102 Air at 550 kPa and 100°C enters a smooth 1-m-long pipe and then passes through a second smooth pipe to a 30-kPa reservoir, as in Fig. P9.102. Using the Moody chart to compute $\bar{f}$, estimate the mass flow through this system. Is the flow choked?



P9.102

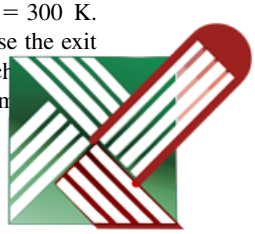
P9.103 Natural gas, with $k \approx 1.3$ and a molecular weight of 16, is to be pumped through 100 km of 81-cm-diameter pipeline. The downstream pressure is 150 kPa. If the gas enters at 60°C, the mass flow is 20 kg/s, and $\bar{f} = 0.024$, estimate the required entrance pressure for (*a*) isothermal flow and (*b*) adiabatic flow.

P9.104 A tank of oxygen (Table A.4) at 20°C is to supply an astronaut through an umbilical tube 12 m long and 2 cm in diameter. The exit pressure in the tube is 40 kPa. If the desired mass flow is 90 kg/h and $\bar{f} = 0.025$, what should be the pressure in the tank?

P9.105 Air enters a 5-cm-diameter pipe at $p_1 = 200$ kPa and $T_1 = 350$ K. The downstream receiver pressure is 74 kPa. The friction factor is 0.02. If the exit is choked, what is (*a*) the length of the pipe and (*b*) the mass flow? (*c*) If p_1, T_1, and p_{receiver} stay the same, what pipe length will cause the mass flow to increase by 50 percent over (*b*)? *Hint*: In part (*c*) the exit pressure does not equal the receiver pressure.

P9.106 Air at 300 K flows through a duct 50 m long with $\bar{f} = 0.019$. What is the minimum duct diameter which can carry the flow without choking if the entrance velocity is (*a*) 50 m/s, (*b*) 150 m/s, and (*c*) 420 m/s?

P9.107 A fuel-air mixture, assumed equivalent to air, enters a duct combustion chamber at $V_1 = 104$ m/s and $T_1 = 300$ K. What amount of heat addition in kJ/kg will cause the exit flow to be choked? What will be the exit Mach and temperature if 504 kJ/kg is added during com



ketabline.com Ebook.ketabline.com

P9.108 What happens to the inlet flow of Prob. 9.107 if the combustion yields 1500 kJ/kg heat addition and p_{01} and T_{01} remain the same? How much is the mass flow reduced?

P9.109 A jet engine at 7000-m altitude takes in 45 kg/s of air and adds 550 kJ/kg in the combustion chamber. The chamber cross section is 0.5 m^2, and the air enters the chamber at 80 kPa and 5°C. After combustion the air expands through an isentropic converging nozzle to exit at atmospheric pressure. Estimate (*a*) the nozzle throat diameter, (*b*) the nozzle exit velocity, and (*c*) the thrust produced by the engine.

P9.110 Compressible pipe flow with heat addition, Sec. 9.8, assumes constant momentum ($p + \rho V^2$) and constant mass flow but variable stagnation enthalpy. Such a flow is often called *Rayleigh flow*, and a line representing all possible property changes on a temperature-entropy chart is called a *Rayleigh line*. Assuming air passing through the flow state $p_1 = 548$ kPa, $T_1 = 588$ K, $V_1 = 266$ m/s, and $A = 1$ m^2, draw a Rayleigh curve of the flow for a range of velocities from very low ($\text{Ma} \ll 1$) to very high ($\text{Ma} \gg 1$). Comment on the meaning of the maximum-entropy point on this curve.

P9.111 Add to your Rayleigh line of Prob. 9.110 a Fanno line (see Prob. 9.94) for stagnation enthalpy equal to the value associated with state 1 in Prob. 9.110. The two curves will intersect at state 1, which is subsonic, and at a certain state 2, which is supersonic. Interpret these two states vis-à-vis Table B.2.

P9.112 Air enters a duct subsonically at section 1 at 1.2 kg/s. When 650 kW of heat is added, the flow chokes at the exit at $p_2 = 95$ kPa and $T_2 = 700$ K. Assuming frictionless heat addition, estimate (*a*) the velocity and (*b*) the stagnation pressure at section 1.

P9.113 Air enters a constant-area duct at $p_1 = 90$ kPa, $V_1 = 520$ m/s, and $T_1 = 558$°C. It is then cooled with negligible friction until it exits at $p_2 = 160$ kPa. Estimate (*a*) V_2, (*b*) T_2, and (*c*) the total amount of cooling in kJ/kg.

P9.114 We have simplified things here by separating friction (Sec. 9.7) from heat addition (Sec. 9.8). Actually, they often occur together, and their effects must be evaluated simultaneously. Show that, for flow with friction *and* heat transfer in a constant-diameter pipe, the continuity, momentum, and energy equations may be combined into the following differential equation for Mach-number changes:

$$\frac{d\,\text{Ma}^2}{\text{Ma}^2} = \frac{1 + k\,\text{Ma}^2}{1 - \text{Ma}^2}\frac{dQ}{c_pT} + \frac{k\,\text{Ma}^2\,[2 + (k-1)\,\text{Ma}^2]}{2(1 - \text{Ma}^2)}\frac{f\,dx}{D}$$

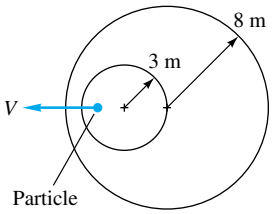
where dQ is the heat added. A complete derivation, including many additional combined effects such as area change and mass addition, is given in chap. 8 of Ref. 8.

P9.115 Air flows subsonically in a duct with negligible friction. When heat is added in the amount of 948 kJ/kg, the pressure drops from $p_1 = 200$ to $p_2 = 106$ kPa. Estimate (*a*) Ma_1, (*b*) T_1, and (*c*) V_1, assuming $T_{01} = 305$ K.

P9.116 An observer at sea level does not hear an aircraft flying at 12,000-ft standard altitude until it is 5 (statute) mi past her. Estimate the aircraft speed in ft/s.

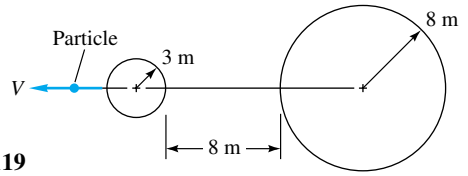
P9.117 An observer at sea level does not hear an aircraft flying at 6000-m standard altitude until 15 s after it has passed overhead. Estimate the aircraft speed in m/s.

P9.118 A particle moving at uniform velocity in sea-level standard air creates the two disturbance spheres shown in Fig. P9.118. Compute the particle velocity and Mach number.



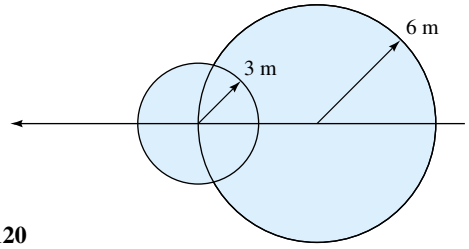
P9.118

P9.119 The particle in Fig. P9.119 is moving supersonically in sea-level standard air. From the two given disturbance spheres, compute the particle Mach number, velocity, and Mach angle.



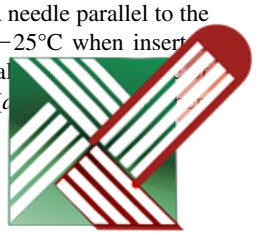
P9.119

P9.120 The particle in Fig. P9.120 is moving in sea-level standard air. From the two disturbance spheres shown, estimate (*a*) the position of the particle at this instant and (*b*) the temperature in °C at the front stagnation point of the particle.



P9.120

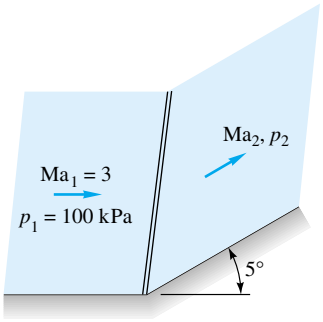
P9.121 A thermistor probe, in the shape of a needle parallel to the flow, reads a static temperature of −25°C when inserted into a supersonic airstream. A conical half-angle 17° is created. Estimate (*a*



ketabline.com Ebook.ketabline.com

(b) the velocity, and (c) the stagnation temperature of the stream.

P9.122 Supersonic air takes a 5° compression turn, as in Fig. P9.122. Compute the downstream pressure and Mach number and the wave angle, and compare with small-disturbance theory.



P9.122

P9.123 Modify Prob. 9.122 as follows. Let the 5° total turn be in the form of five separate compression turns of 1° each. Compute the final Mach number and pressure, and compare the pressure with an isentropic expansion to the same final Mach number.

P9.124 Determine the validity of the following alternate relation for the pressure ratio across an oblique shock wave:

$$\frac{p_2}{p_1} = \frac{\cot\theta \sin 2\beta - \cos 2\beta + k}{\cot\theta \sin 2\beta - \cos 2\beta - k}$$

If necessary, your proof (or disproof) may be somewhat tentative and heuristic.

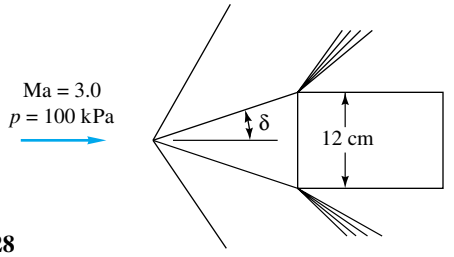
P9.125 Show that, as the upstream Mach number approaches infinity, the Mach number downstream of an attached oblique-shock wave will have the value

$$\text{Ma}_2 \approx \sqrt{\frac{k-1}{2k \sin^2(\beta - \theta)}}$$

P9.126 Consider airflow at Ma$_1$ = 2.2. Calculate, to two decimal places, (a) the deflection angle for which the downstream flow is sonic and (b) the maximum deflection angle.

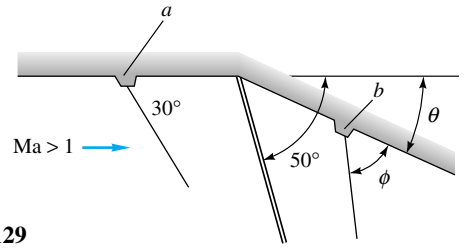
P9.127 Do the Mach waves upstream of an oblique-shock wave intersect with the shock? Assuming supersonic downstream flow, do the downstream Mach waves intersect the shock? Show that for small deflections the shock-wave angle β lies halfway between μ_1 and $\mu_2 + \theta$ for any Mach number.

P9.128 Air flows past a two-dimensional wedge-nosed body as in Fig. P9.128. Determine the wedge half-angle δ for which the horizontal component of the total pressure force on the nose is 35 kN/m of depth into the paper.



P9.128

P9.129 Air flows at supersonic speed toward a compression ramp, as in Fig. P9.129. A scratch on the wall at point a creates a wave of 30° angle, while the oblique shock created has a 50° angle. What is (a) the ramp angle θ and (b) the wave angle ϕ caused by a scratch at b?

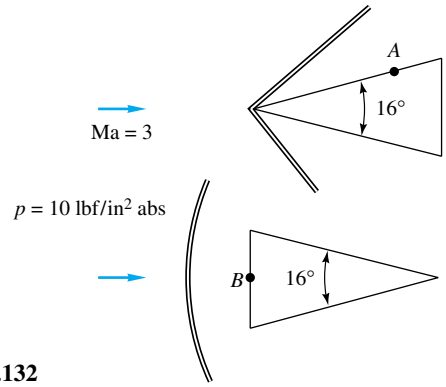


P9.129

P9.130 Modify Prob. 9.129 as follows. If the wave angle ϕ is 42°, determine (a) the shock-wave angle and (b) the deflection angle.

P9.131 In Fig. P9.128, assume that the approach stream temperature is 20°C. For what wedge half-angle δ will the stream temperature along the wedge surface be 200°C?

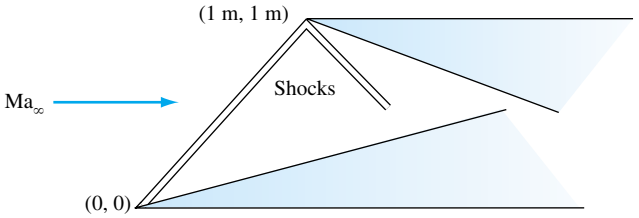
P9.132 Air flows at Ma = 3 and p = 10 lbf/in^2 absolute toward a wedge of 16° angle at zero incidence in Fig. P9.132. If the pointed edge is forward, what will be the pressure at point A? If the blunt edge is forward, what will be the pressure at point B?



P9.132

P9.133 Air flows supersonically toward the double-wedg
in Fig. P9.133. The (x, y) coordinates of the tips a

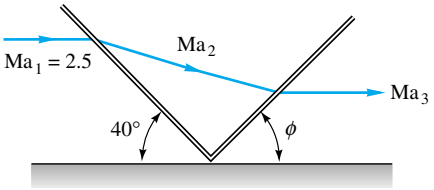
ketabline.com Ebook.ketabline.com



P9.133

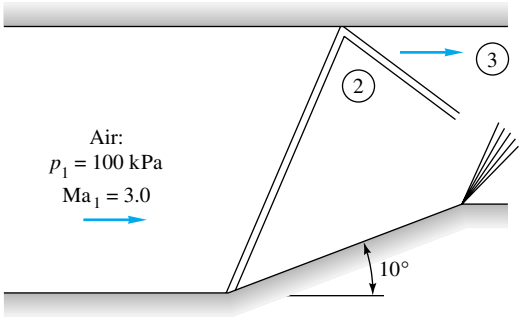
The shock wave of the forward wedge strikes the tip of the aft wedge. Both wedges have 15° deflection angles. What is the free-stream Mach number?

P9.134 When an oblique shock strikes a solid wall, it reflects as a shock of sufficient strength to cause the exit flow Ma_3 to be parallel to the wall, as in Fig. P9.134. For airflow with $Ma_1 = 2.5$ and $p_1 = 100$ kPa, compute Ma_3, p_3, and the angle ϕ.



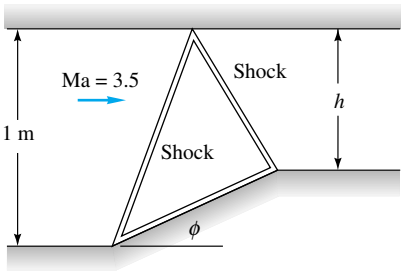
P9.134

P9.135 A bend in the bottom of a supersonic duct flow induces a shock wave which reflects from the upper wall, as in Fig. P9.135. Compute the Mach number and pressure in region 3.



P9.135

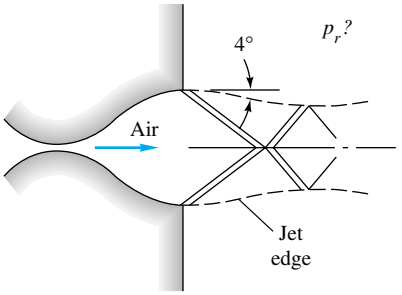
P9.136 Figure P9.136 is a special application of Prob. 9.135. With careful design, one can orient the bend on the lower wall so that the reflected wave is exactly canceled by the return bend, as shown. This is a method of reducing the Mach number in a channel (a supersonic diffuser). If the bend angle is $\phi = 10°$, find (*a*) the downstream width h and (*b*) the downstream Mach number. Assume a weak shock wave.



P9.136

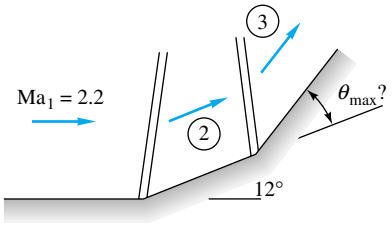
P9.137 Generalize Prob. 9.136 into a computer study as follows. Assuming weak shocks, find and plot all combinations of ϕ and h in Fig. P9.136 for which the canceled or "swallowed" reflected shock is possible.

P9.138 The supersonic nozzle of Fig. P9.138 is overexpanded (case *G* of Fig. 9.12) with $A_e/A_t = 3.0$ and a stagnation pressure of 350 kPa. If the jet edge makes a 4° angle with the nozzle centerline, what is the back pressure p_r in kPa?



P9.138

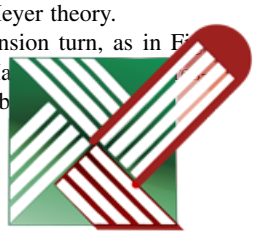
P9.139 Airflow at Ma = 2.2 takes a compression turn of 12° and then another turn of angle θ in Fig. P9.139. What is the maximum value of θ for the second shock to be attached? Will the two shocks intersect for any θ less than θ_{max}?



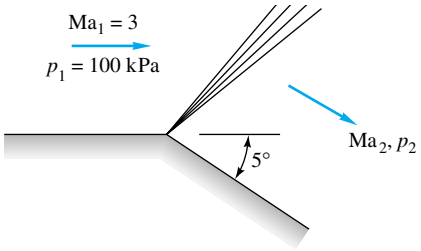
P9.139

P9.140 The solution to Prob. 9.122 is $Ma_2 = 2.750$, and $p_2 = 145.5$ kPa. Compare these results with an isentropic compression turn of 5°, using Prandtl-Meyer theory.

P9.141 Supersonic airflow takes a 5° expansion turn, as in Fi
P9.141. Compute the downstream Ma
sure, and compare with small-disturb



ketabline.com Ebook.ketabline.com

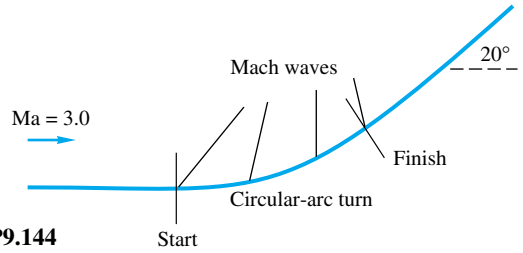


P9.141

P9.142 A supersonic airflow at $Ma_1 = 3.2$ and $p_1 = 50$ kPa undergoes a compression shock followed by an isentropic expansion turn. The flow deflection is 30° for each turn. Compute Ma_2 and p_2 if (*a*) the shock is followed by the expansion and (*b*) the expansion is followed by the shock.

P9.143 Airflow at $Ma_1 = 3.2$ passes through a 25° oblique-shock deflection. What isentropic expansion turn is required to bring the flow back to (*a*) Ma_1 and (*b*) p_1?

P9.144 Consider a smooth isentropic compression turn of 20°, as shown in Fig. P9.144. The Mach waves thus generated will form a converging fan. Sketch this fan as accurately as possible, using at least five equally spaced waves, and demonstrate how the fan indicates the probable formation of an oblique-shock wave.



P9.144

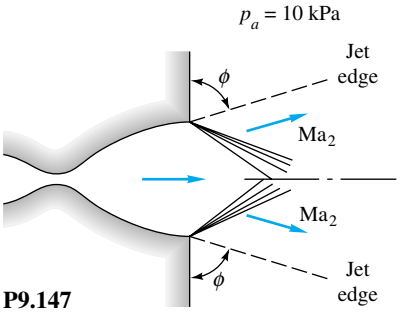
P9.145 Air at $Ma_1 = 2.0$ and $p_1 = 100$ kPa undergoes an isentropic expansion to a downstream pressure of 50 kPa. What is the desired turn angle in degrees?

P9.146 Helium, at 20°C and $V_1 = 2010$ m/s, undergoes a Prandtl-Meyer expansion until the temperature is −50°C. Estimate the turn angle in degrees.

P9.147 A converging-diverging nozzle with a 4:1 exit-area ratio and $p_0 = 500$ kPa operates in an underexpanded condition (case *I* of Fig. 9.12*b*) as in Fig. P9.147. The receiver pressure is $p_a = 10$ kPa, which is less than the exit pressure, so that expansion waves form outside the exit. For the given conditions, what will the Mach number Ma_2 and the angle ϕ of the edge of the jet be? Assume $k = 1.4$ as usual.

P9.148 Repeat Example 9.19 for an angle of attack of 6°. Is the lift coefficient linear with angle α in this range of $0° \le \alpha \le 8°$? Is the drag coefficient parabolic with α in this range?

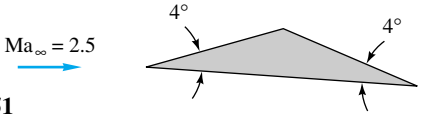
P9.149 Repeat Example 9.21 for an angle of attack of 2°. Is the lift coefficient linear with angle α in this range of $0° \le \alpha \le 8°$? Why does the drag coefficient not have the simple parabolic form $C_D \approx K\alpha^2$ in this range?



P9.147

P9.150 A flat-plate airfoil with $C = 1.2$ m is to have a lift of 30 kN/m when flying at 5000-m standard altitude with $U_\infty = 641$ m/s. Using Ackeret theory, estimate (*a*) the angle of attack and (*b*) the drag force in N/m.

P9.151 Air flows at Ma = 2.5 past a half-wedge airfoil whose angles are 4°, as in Fig. P9.151. Compute the lift and drag coefficient at α equal to (*a*) 0° and (*b*) 6°.



P9.151

P9.152 A supersonic airfoil has a parabolic symmetric shape for upper and lower surfaces

$$y_{u,l} = \pm 2t\left(\frac{x}{C} - \frac{x^2}{C^2}\right)$$

such that the maximum thickness is t at $x = \frac{1}{2}C$. Compute the drag coefficient at zero incidence by Ackeret theory, and compare with a symmetric double wedge of the same thickness.

P9.153 A supersonic transport has a mass of 65 Mg and cruises at 11-km standard altitude at a Mach number of 2.25. If the angle of attack is 2° and its wings can be approximated by flat plates, estimate (*a*) the required wing area in m^2 and (*b*) the thrust required in N.

P9.154 A symmetric supersonic airfoil has its upper and lower surfaces defined by a sine-wave shape:

$$y = \frac{t}{2}\sin\frac{\pi x}{C}$$

where t is the maximum thickness, which occurs at $x = C/2$. Use Ackeret theory to derive an expression for the drag coefficient at zero angle of attack. Compare your result with Ackeret theory for a symmetric double-wedge airfoil of the same thickness.

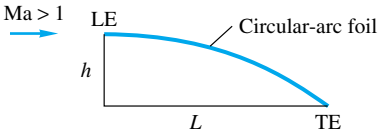
P9.155 For the sine-wave airfoil shape of Prob. 9.154, wit
2.5, $k = 1.4$, $t/C = 0.1$, and $\alpha = 0°$, plot (with



ketabline.com Ebook.ketabline.com

puting the overall forces) the pressure distribution $p(x)/p_\infty$ along the upper surface for (*a*) Ackeret theory and (*b*) an oblique shock plus a continuous Prandtl-Meyer expansion.

P9.156 A thin circular-arc airfoil is shown in Fig. P9.156. The leading edge is parallel to the free stream. Using linearized (small-turning-angle) supersonic-flow theory, derive a formula for the lift and drag coefficient for this orientation, and compare with Ackeret-theory results for an angle of attack $\alpha = \tan^{-1}(h/L)$.



P9.156

P9.157 Prove from Ackeret theory that for a given supersonic airfoil shape with sharp leading and trailing edges and a given thickness, the minimum-thickness drag occurs for a symmetric double-wedge shape.

Word Problems

W9.1 Notice from Table 9.1 that (*a*) water and mercury and (*b*) aluminum and steel have nearly the same speeds of sound, yet the second of the two materials is much denser. Can you account for this oddity? Can molecular theory explain it?

W9.2 When an object approaches you at Ma = 0.8, you can hear it, according to Fig. 9.18*a*. But would there be a Doppler shift? For example, would a musical tone seem to you to have a higher or a lower pitch?

W9.3 The subject of this chapter is commonly called *gas dynamics*. But can liquids not perform in this manner? Using water as an example, make a rule-of-thumb estimate of the pressure level needed to drive a water flow at velocities comparable to the sound speed.

W9.4 Suppose a gas is driven at compressible subsonic speeds by a large pressure drop, p_1 to p_2. Describe its behavior on an appropriately labeled Mollier chart for (*a*) frictionless flow in a converging nozzle and (*b*) flow with friction in a long duct.

W9.5 Describe physically what the "speed of sound" represents. What kind of pressure changes occur in air sound waves during ordinary conversation?

W9.6 Give a physical description of the phenomenon of choking in a converging-nozzle gas flow. Could choking happen even if wall friction were not negligible?

W9.7 Shock waves are treated as discontinuities here, but they actually have a very small finite thickness. After giving it some thought, sketch your idea of the distribution of gas velocity, pressure, temperature, and entropy through the inside of a shock wave.

W9.8 Describe how an observer, running along a normal-shock wave at finite speed V, will see what appears to be an oblique-shock wave. Is there any limit to the running speed?

Fundamentals of Engineering Exam Problems

One-dimensional compressible-flow problems have become quite popular on the FE Exam, especially in the afternoon sessions. In the following problems, assume one-dimensional flow of ideal air, $R = 287$ J/(kg·K) and $k = 1.4$.

FE9.1 For steady isentropic flow, if the absolute temperature increases 50 percent, by what ratio does the static pressure increase?
(*a*) 1.12, (*b*) 1.22, (*c*) 2.25, (*d*) 2.76, (*e*) 4.13

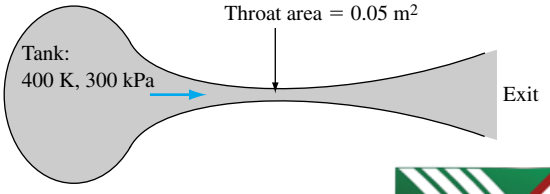
FE9.2 For steady isentropic flow, if the density doubles, by what ratio does the static pressure increase?
(*a*) 1.22, (*b*) 1.32, (*c*) 1.44, (*d*) 2.64, (*e*) 5.66

FE9.3 A large tank, at 500 K and 200 kPa, supplies isentropic airflow to a nozzle. At section 1, the pressure is only 120 kPa. What is the Mach number at this section?
(*a*) 0.63, (*b*) 0.78, (*c*) 0.89, (*d*) 1.00, (*e*) 1.83

FE9.4 In Prob. FE9.3 what is the temperature at section 1?
(*a*) 300 K, (*b*) 408 K, (*c*) 417 K, (*d*) 432 K, (*e*) 500 K

FE9.5 In Prob. FE9.3, if the area at section 1 is 0.15 m^2, what is the mass flow?
(*a*) 38.1 kg/s, (*b*) 53.6 kg/s, (*c*) 57.8 kg/s, (*d*) 67.8 kg/s, (*e*) 77.2 kg/s

FE9.6 For steady isentropic flow, what is the maximum possible mass flow through the duct in Fig. FE9.6?
(*a*) 9.5 kg/s, (*b*) 15.1 kg/s, (*c*) 26.2 kg/s, (*d*) 30.3 kg/s, (*e*) 52.4 kg/s



FE9.6



ketabline.com Ebook.ketabline.com

FE9.7 If the exit Mach number in Fig. FE9.6 is 2.2, what is the exit area?
(*a*) 0.10 m^2, (*b*) 0.12 m^2, (*c*) 0.15 m^2, (*d*) 0.18 m^2, (*e*) 0.22 m^2

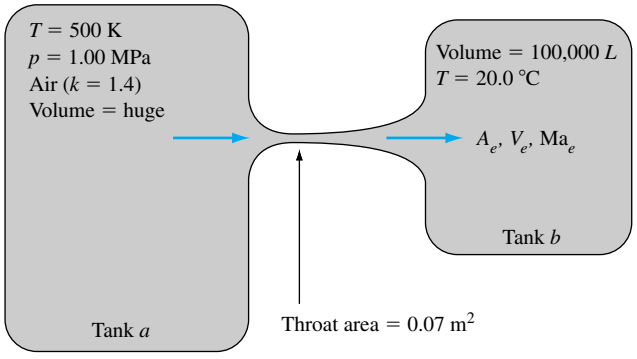
FE9.8 If there are no shock waves and the pressure at one duct section in Fig. FE9.6 is 55.5 kPa, what is the velocity at that section?
(*a*) 166 m/s, (*b*) 232 m/s, (*c*) 554 m/s, (*d*) 706 m/s, (*e*) 774 m/s

FE9.9 If, in Fig. FE9.6, there is a normal shock wave at a section where the area is 0.07 m^2, what is the air density just upstream of that shock?
(*a*) 0.48 kg/m^3, (*b*) 0.78 kg/m^3, (*c*) 1.35 kg/m^3, (*d*) 1.61 kg/m^3, (*e*) 2.61 kg/m^3

FE9.10 In Prob. FE9.9, what is the Mach number just downstream of the shock wave?
(*a*) 0.42, (*b*) 0.55, (*c*) 0.63, (*d*) 1.00, (*e*) 1.76

Comprehensive Problems

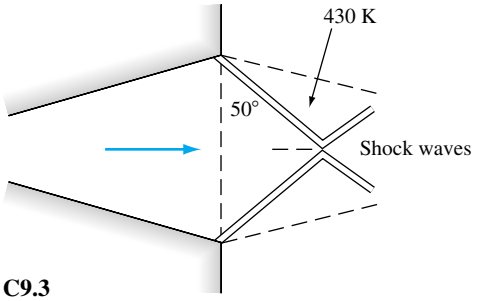
C9.1 The converging-diverging nozzle sketched in Fig. C9.1 is designed to have a Mach number of 2.00 at the exit plane (assuming the flow remains nearly isentropic). The flow travels from tank *a* to tank *b,* where tank *a* is much larger than tank *b.* (*a*) Find the area at the exit A_e and the back pressure p_b which will allow the system to operate at design conditions. (*b*) As time goes on, the back pressure will grow, since the second tank slowly fills up with more air. Since tank *a* is huge, the flow in the nozzle will remain the same, however, until a normal shock wave appears at the exit plane. At what back pressure will this occur? (*c*) If tank *b* is held at constant temperature, $T = 20°C$, estimate how long it will take for the flow to go from design conditions to the condition of part (*b*), i.e., with a shock wave at the exit plane.



C9.1

C9.2 Two large air tanks, one at 400 K and 300 kPa and the other at 300 K and 100 kPa, are connected by a straight tube 6 m long and 5 cm in diameter. The average friction factor is 0.0225. Assuming adiabatic flow, estimate the mass flow through the tube.

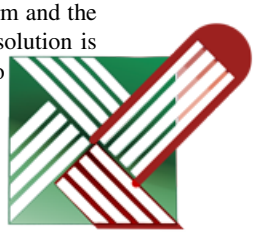
***C9.3** Figure C9.3 shows the exit of a converging-diverging nozzle, where an oblique-shock pattern is formed. In the exit plane, which has an area of 15 cm^2, the air pressure is 16 kPa and the temperature is 250 K. Just outside the exit shock, which makes an angle of 50° with the exit plane, the temperature is 430 K. Estimate (*a*) the mass flow, (*b*) the throat area, (*c*) the turning angle of the exit flow, and, in the tank supplying the air, (*d*) the pressure and (*e*) the temperature.



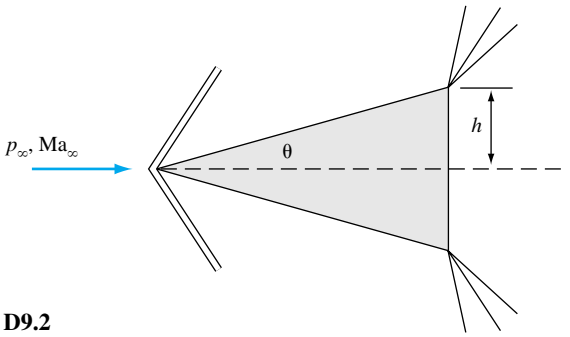
C9.3

Design Projects

D9.1 It is desired to select a rectangular wing for a fighter aircraft. The plane must be able (*a*) to take off and land on a 4500-ft-long sea-level runway and (*b*) to cruise supersonically at Ma = 2.3 at 28,000-ft altitude. For simplicity, assume a wing with zero sweepback. Let the aircraft maximum weight equal (30 + *n*)(1000) lbf, where *n* is the number of letters in your surname. Let the available sea-level maximum thrust be one-third of the maximum weight, decreasing at altitude proportional to ambient density. Making suitable assumptions about the effect of finite aspect ratio on wing lift and drag for both subsonic and supersonic flight, select a wing of minimum area sufficient to perform these takeoff/landing and cruise requirements. Some thought should be given to analyzing the wingtips and wing roots in supersonic flight, where Mach cones form and the flow is not two-dimensional. If no satisfactory solution is possible, gradually increase the available thrust to to an acceptable design.



ketabline.com Ebook.ketabline.com



D9.2

D9.2 Consider supersonic flow of air at sea-level conditions past a wedge of half-angle θ, as shown in Fig. D9.2. Assume that the pressure on the back of the wedge equals the fluid pressure as it exits the Prandtl-Meyer fan. (*a*) Suppose $\text{Ma}_\infty = 3.0$. For what angle θ will the supersonic wave-drag coefficient C_D, based on frontal area, be exactly 0.5? (*b*) Suppose that $\theta = 20°$. Is there a free-stream Mach number for which the wave-drag coefficient C_D, based on frontal area, will be exactly 0.5? (*c*) Investigate the percent increase in C_D from (*a*) and (*b*) due to including boundary-layer friction drag in the calculation.

References

1. A. Y. Pope, *Aerodynamics of Supersonic Flight*, 2d ed., Pitman, New York, 1958.
2. A. B. Cambel and B. H. Jennings, *Gas Dynamics*, McGraw-Hill, New York, 1958.
3. F. Cheers, *Elements of Compressible Flow*, Wiley, New York, 1963.
4. J. E. John, *Gas Dynamics*, 2d ed., Allyn & Bacon, Boston, 1984.
5. A. J. Chapman and W. F. Walker, *Introductory Gas Dynamics*, Holt, New York, 1971.
6. B. W. Imrie, *Compressible Fluid Flow*, Halstead, New York, 1974.
7. R. Courant and K. O. Friedrichs, *Supersonic Flow and Shock Waves*, Interscience, New York, 1948; reprinted by Springer-Verlag, New York, 1977.
8. A. H. Shapiro, *The Dynamics and Thermodynamics of Compressible Fluid Flow*, Ronald, New York, 1953.
9. H. W. Liepmann and A. Roshko, *Elements of Gas Dynamics*, Wiley, New York, 1957.
10. R. von Mises, *Mathematical Theory of Compressible Fluid Flow*, Academic, New York, 1958.
11. J. A. Owczarek, *Gas Dynamics*, International Textbook, Scranton, PA, 1964.
12. W. G. Vincenti and C. Kruger, *Introduction to Physical Gas Dynamics*, Wiley, New York, 1965.
13. J. D. Anderson, *Hypersonic and High-Temperature Gas Dynamics*, McGraw-Hill, New York, 1989.
14. P. A. Thompson, *Compressible Fluid Dynamics*, McGraw-Hill, New York, 1972.
15. J. H. Keenan et al., *Steam Tables: SI Version*, 2 vols., Wiley, New York, 1985.
16. J. H. Keenan et al., *Gas Tables*, 2d ed., Wiley-Interscience, New York, 1983.
17. Y. A. Cengel and M. A. Boles, *Thermodynamics: An Engineering Approach*, 3d ed., McGraw-Hill, New York, 1998.
18. K. Wark, *Thermodynamics*, 6th ed., McGraw-Hill, New York, 1999.
19. F. M. White, *Viscous Fluid Flow*, 2d ed., McGraw-Hill, New York, 1991.
20. J. H. Keenan and E. P. Neumann, "Measurements of Friction in a Pipe for Subsonic and Supersonic Flow of Air," *J. Appl. Mech.,* vol. 13, no. 2, 1946, p. A-91.
21. J. Ackeret, "Air Forces on Airfoils Moving Faster than Sound Velocity," *NACA Tech. Mem.* 317, 1925.
22. Z. Kopal, "Tables of Supersonic Flow around Cones," *M.I.T. Center Anal. Tech. Rep.* 1, 1947 (see also *Tech. Rep.* 3 and 5, 1947).
23. J. L. Sims, *Tables for Supersonic Flow around Right Circular Cones at Zero Angle of Attack*, NASA SP-3004, 1964 (see also NASA SP-3007).
24. J. Palmer et al., *Compressible Flow Tables for Engineers: With Appropriate Computer Programs*, Scholium Intl., Port Washington, NY, 1989.
25. S. M. Yahya (ed.), *Gas Tables for Compressible Flow Calculations*, Wiley Eastern, New Delhi, India, 1985.
26. S. M. Yahya, *Fundamentals of Compressible Flow*, Wiley Eastern, New Delhi, India, 1982.
27. S. Schreier, *Compressible Flow*, Wiley, New York, 1982.
28. M. A. Saad, *Compressible Fluid Flow*, 2d ed., Prentice-Hall, Englewood Cliffs, NJ, 1992.
29. A. Y. Pope and K. L. Goin, *High Speed Wind Tunnel Testing*, Wiley, New York, 1965.
30. W. Bober and R. A. Kenyon, *Fluid Mechanics*, Wiley, New York, 1980.
31. J. D. Anderson, *Modern Compressible F*
Perspective, 2d ed., McGraw-Hill, New

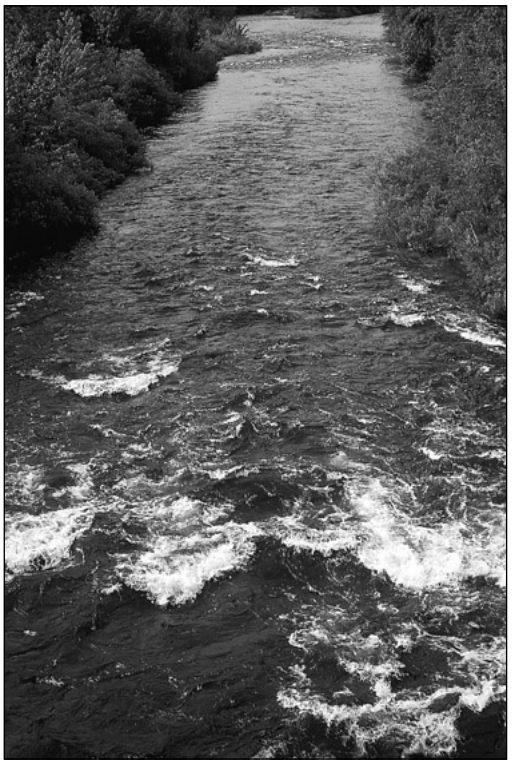


ketabline.com Ebook.ketabline.com

32. M. J. Zucrow and J. D. Hoffman, *Gas Dynamics*, Wiley, New York, 1976.
33. Z. Husain, *Gas Dynamics through Problems*, Halsted Press, New York, 1989.
34. J. E. Plapp, *Engineering Fluid Mechanics*, Prentice-Hall, Englewood Cliffs, NJ, 1968.
35. P. H. Oosthuizen and W. E. Carscallen, *Compressible Fluid Flow*, McGraw-Hill, New York, 1997.
36. M. H. Kaplan, "The Reusable Launch Vehicle: Is the Stage Set*?" Launchspace Magazine*, March 1997, pp. 26–30.
37. T. K. Mattingly, "A Simpler Ride into Space," *Scientific American*, October 1997, pp. 120–125.



ketabline.com Ebook.ketabline.com



The Lehigh River, White Haven, Pennsylvania. Open channel flows are everywhere, often rough and turbulent, as in this photo. They are analyzed by the methods of the present chapter. *(Courtesy of Dr. E. R. Degginger/Color-Pic Inc.)*



ketabline.com Ebook.ketabline.com

Chapter 10
Open-Channel Flow

Motivation. The duct flows of Chap. 6 were driven by a pressure difference between the ends of the duct. Such channels are closed and full of fluid, either gas or liquid. By contrast, an *open-channel flow* is liquid only and is *not* full; i.e., there is always a free surface exposed to ambient pressure. The basic balance of forces is between gravity (fluid weight) and friction.

Practical open-channel problems almost always concern *water* as the relevant fluid. The flow is generally turbulent, due to its large scale and small kinematic viscosity, and is three-dimensional, sometimes unsteady, and often surprisingly complex due to geometric effects. This chapter presents some simple engineering theories and correlations for steady flow in straight channels of simple geometry. Many of the concepts from steady duct flow—hydraulic diameter, friction factor, head losses—apply also to open channels.

10.1 Introduction

Simply stated, open-channel flow is the flow of a liquid in a conduit with a free surface. There are many practical examples, both artificial (flumes, spillways, canals, weirs, drainage ditches, culverts) and natural (streams, rivers, estuaries, floodplains). This chapter introduces the elementary analysis of such flows, which are dominated by the effects of gravity.

The presence of the free surface, which is essentially at atmospheric pressure, both helps and hurts the analysis. It helps because the pressure can be taken constant along the free surface, which therefore is equivalent to the *hydraulic grade line* (HGL) of the flow. Unlike flow in closed ducts, the pressure gradient is not a direct factor in open-channel flow, where the balance of forces is confined to gravity and friction.[1] But the free surface complicates the analysis because its shape is a priori unknown: The depth profile changes with conditions and must be computed as part of the problem, especially in unsteady problems involving wave motion.

Before proceeding, we remark, as usual, that whole books have been written on open-channel hydraulics [1 to 4]. There are also specialized texts devoted to wave motion [5 to 7] and to engineering aspects of coastal free-surface flows [8, 9]. This chapter is only an introduction to broader and more detailed treatments.

[1]Surface tension is rarely important because open channels are normally quite large and have a very large Weber number.



ketabline.com Ebook.ketabline.com

The One-Dimensional Approximation

An open channel always has two sides and a bottom, where the flow satisfies the no-slip condition. Therefore even a straight channel has a three-dimensional velocity distribution. Some measurements of straight-channel velocity contours are shown in Fig. 10.1. The profiles are quite complex, with maximum velocity typically occurring in the midplane about 20 percent below the surface. In very broad shallow channels the maximum velocity is near the surface, and the velocity profile is nearly logarithmic from the bottom to the free surface, as in Eq. (6.84). In noncircular channels there are also secondary motions similar to Fig. 6.16 for closed-duct flows. If the channel curves or meanders, the secondary motion intensifies due to centrifugal effects, with high velocity occurring near the outer radius of the bend. Curved natural channels are subject to strong bottom erosion and deposition effects.

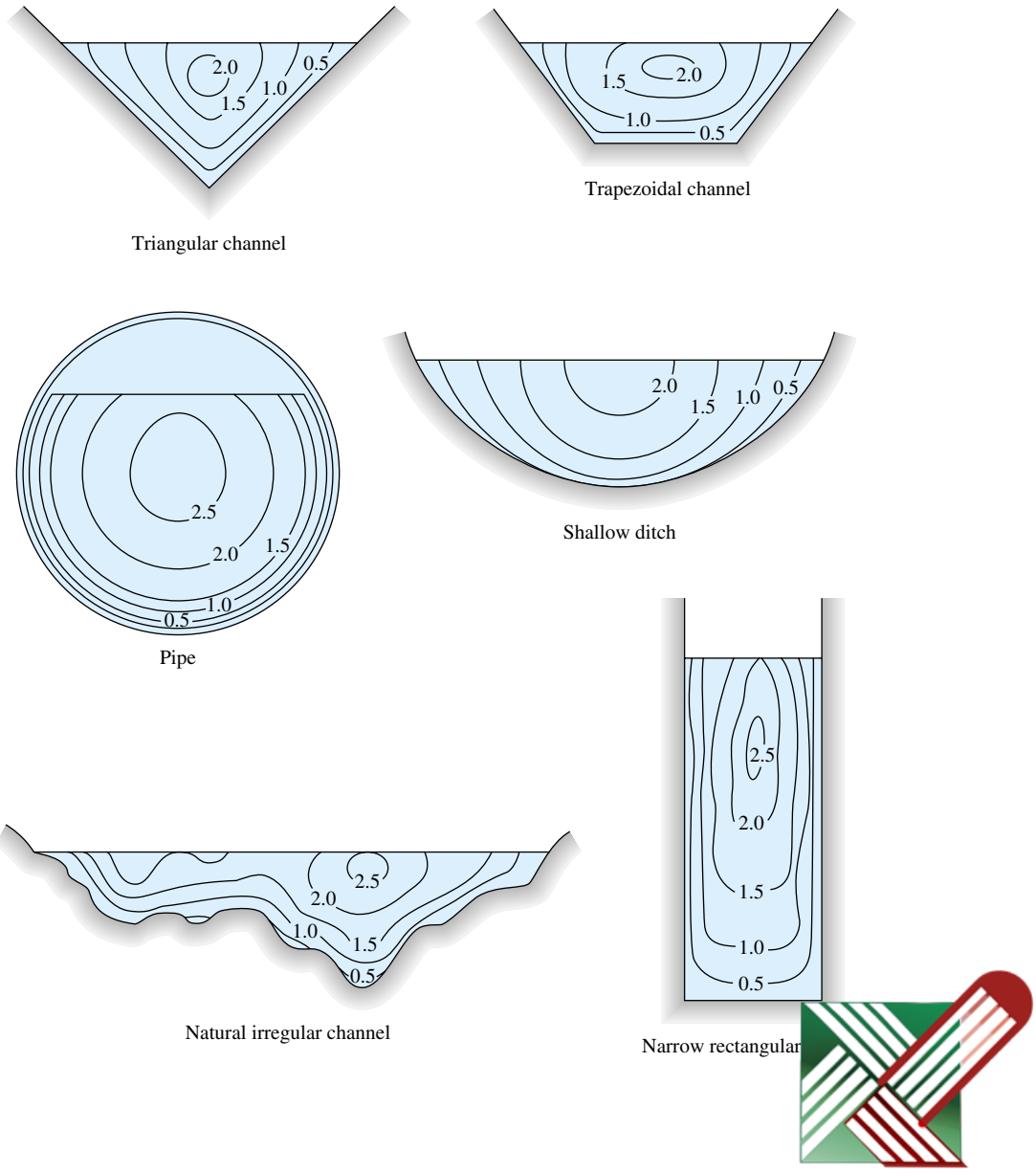


Fig. 10.1 Measured isovelocity contours in typical straight open-channel flows. *(From Ref. 3.)*

ketabline.com Ebook.ketabline.com

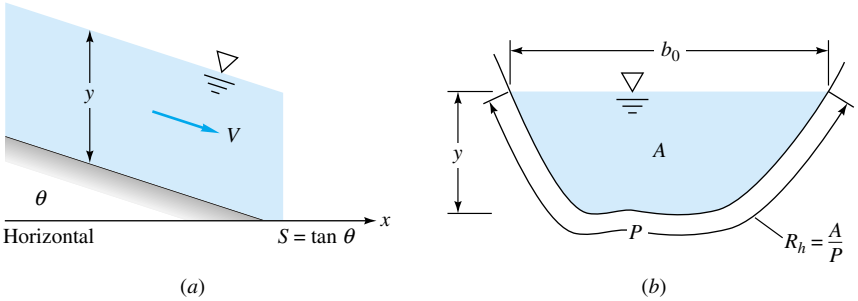


Fig. 10.2 Geometry and notation for open-channel flow: (*a*) side view; (*b*) cross section. All these parameters are constant in uniform flow.

With the advent of the supercomputer, it is possible to make numerical simulations of complex flow patterns such as in Fig. 10.1 [23]. However, the practical engineering approach, used here, is to make a one-dimensional-flow approximation, as in Fig. 10.2. Since the liquid density is nearly constant, the steady-flow continuity equation reduces to constant-volume flow Q along the channel

$$Q = V(x)A(x) = \text{const} \tag{10.1}$$

where V is average velocity and A the local cross-sectional area, as sketched in Fig. 10.2.

A second one-dimensional relation between velocity and channel geometry is the energy equation, including friction losses. If points 1 (upstream) and 2 (downstream) are on the free surface, $p_1 = p_2 = p_a$, and we have, for steady flow,

$$\frac{V_1^2}{2g} + z_1 = \frac{V_2^2}{2g} + z_2 + h_f \tag{10.2}$$

where z denotes the total elevation of the free surface, which includes the water depth y (see Fig. 10.2*a*) plus the height of the (sloping) bottom. The friction head loss h_f is analogous to head loss in duct flow from Eq. (6.30):

$$h_f \approx f \frac{x_2 - x_1}{D_h} \frac{V_{\text{av}}^2}{2g} \qquad D_h = \text{hydraulic diameter} = \frac{4A}{P} \tag{10.3}$$

where f is the average friction factor (Fig. 6.13) between sections 1 and 2. Since channels are irregular in shape, their "size" is taken to be the hydraulic diameter, with P the *wetted* perimeter—see Fig. 10.2*b*. Actually, open-channel formulas typically use the hydraulic *radius*

$$R_h = \frac{1}{4} D_h = \frac{A}{P} \tag{10.4}$$

The local Reynolds number of the channel would be $\text{Re} = VD_h/\nu$, which is usually highly turbulent (>1 E5). The only commonly occurring laminar channel flows are the thin sheets which form as rainwater drains from crowned streets and airport runways.

The wetted perimeter P (see Fig. 10.2*b*) includes the sides and bottom of the channel but not the free surface and, of course, not the parts of the sides above the water level. For example, if a rectangular channel is b wide and h high and contains water to depth y, its wetted perimeter is

$$P = b + 2y \tag{10.}$$

not $2b + 2h$.



ketabline.com Ebook.ketabline.com

Although the Moody chart (Fig. 6.13) would give a good estimate of the friction factor in channel flow, in practice it is seldom used. An alternate correlation due to Robert Manning, discussed in Sec. 10.2, is the formula of choice in open-channel hydraulics.

Flow Classification by Depth Variation

The most common method of classifying open-channel flows is by the rate of change of the free-surface depth. The simplest and most widely analyzed case is *uniform flow,* where the depth (hence the velocity in steady flow) remains constant. Uniform-flow conditions are approximated by long straight runs of constant-slope and constant-area channel. A channel in uniform flow is said to be moving at its *normal depth* y_n, which is an important design parameter.

If the channel slope or cross section changes or there is an obstruction in the flow, then the depth changes and the flow is said to be *varied*. The flow is *gradually varying* if the one-dimensional approximation is valid and *rapidly varying* if not. Some examples of this method of classification are shown in Fig. 10.3. The classes can be summarized as follows:

1. Uniform flow (constant depth and slope)
2. Varied flow
   a. Gradually varied (one-dimensional)
   b. Rapidly varied (multidimensional)

Typically uniform flow is separated from rapidly varying flow by a region of gradually varied flow. Gradually varied flow can be analyzed by a first-order differential equation (Sec. 10.6), but rapidly varying flow usually requires experimentation or three-dimensional potential theory.

Flow Classification by Froude Number: Surface Wave Speed

A second and very interesting classification is by dimensionless Froude number, which for a rectangular or very wide channel takes the form $\text{Fr} = V/(gy)^{1/2}$, where y is the

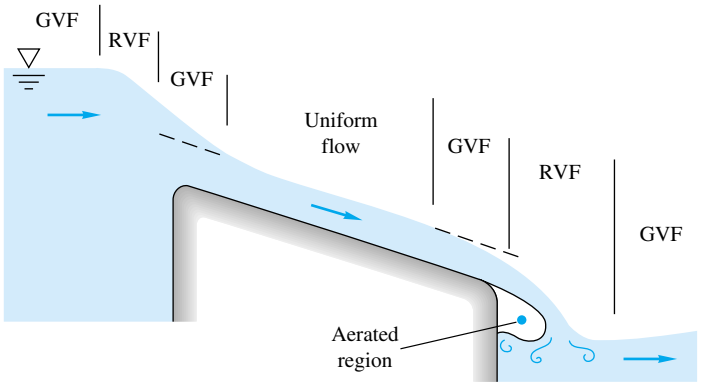


Fig. 10.3 Open-channel flow classified by regions of rapidly varying flow (RVF), gradually varying flow (GVF), and uniform-flow depth profiles.



ketabline.com Ebook.ketabline.com

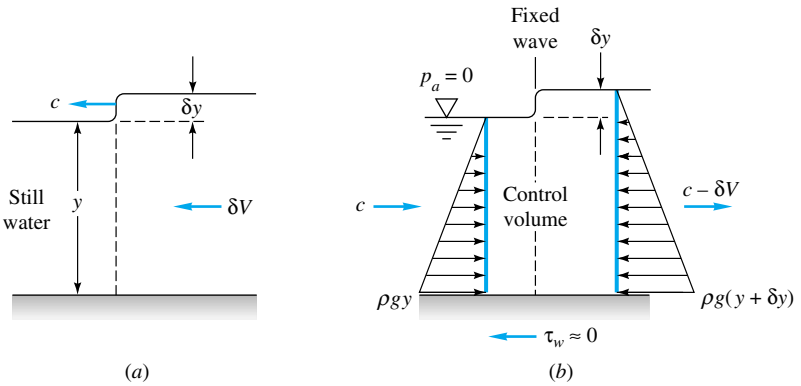


Fig. 10.4 Analysis of a small surface wave propagating into still shallow water; (*a*) moving wave, nonsteady frame; (*b*) fixed wave, inertial frame of reference.

water depth. The three flow regimes are

$$\begin{aligned} \text{Fr} &< 1.0 \quad \text{subcritical flow} \\ \text{Fr} &= 1.0 \quad \text{critical flow} \\ \text{Fr} &> 1.0 \quad \text{supercritical flow} \end{aligned} \tag{10.6}$$

The Froude number for irregular channels is defined in Sec. 10.4. As mentioned in Sec. 9.10, there is a strong analogy here with the three compressible-flow regimes of the Mach number: subsonic (Ma $<$ 1), sonic (Ma $=$ 1), and supersonic (Ma $>$ 1). We shall pursue the analogy in Sec. 10.4.

The Froude-number denominator $(gy)^{1/2}$ is the speed of an infinitesimal shallow-water surface wave. We can derive this with reference to Fig. 10.4*a*, which shows a wave of height δy propagating at speed c into still liquid. To achieve a steady-flow inertial frame of reference, we fix the coordinates on the wave as in Fig. 10.4*b*, so that the still water moves to the right at velocity c. Figure 10.4 is exactly analogous to Fig. 9.1, which analyzed the speed of sound in a fluid.

For the control volume of Fig. 10.4*b*, the one-dimensional continuity relation is, for channel width b,

$$\rho c y b = \rho(c - \delta V)(y + \delta y)b$$

or

$$\delta V = c\,\frac{\delta y}{y + \delta y} \tag{10.7}$$

This is analogous to Eq. (9.10); the velocity change δV induced by a surface wave is small if the wave is "weak," $\delta y \ll y$. If we neglect bottom friction in the short distance across the wave in Fig. 10.4*b*, the momentum relation is a balance between the net hydrostatic pressure force and momentum

$$-\tfrac{1}{2}\rho g b[(y + \delta y)^2 - y^2] = \rho c b y(c - \delta V - c)$$

or

$$g\left(1 + \frac{\frac{1}{2}\,\delta y}{y}\right)\delta y = c\;\delta V \tag{10.}$$



ketabline.com Ebook.ketabline.com

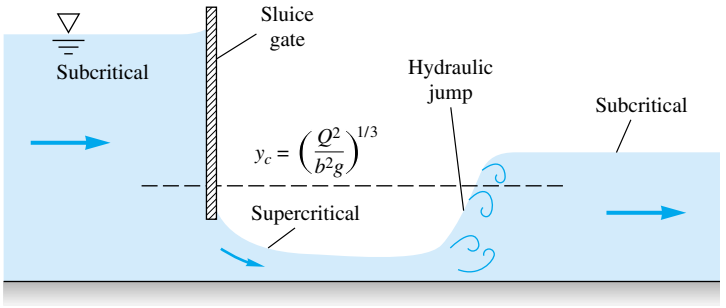


Fig. 10.5 Flow under a sluice gate accelerates from subcritical to critical to supercritical flow and then jumps back to subcritical flow.

This is analogous to Eq. (9.12). By eliminating δV between Eqs. (10.7) and (10.8) we obtain the desired expression for wave propagation speed

$$c^2 = gy\left(1 + \frac{\delta y}{y}\right)\left(1 + \frac{\frac{1}{2}\,\delta y}{y}\right) \tag{10.9}$$

The "stronger" the wave height δy, the faster the wave speed c, by analogy with Eq. (9.13). In the limit of an infinitesimal wave height $\delta y \to 0$, the speed becomes

$$c_0^2 = gy \tag{10.10}$$

This is the surface-wave equivalent of fluid sound speed a, and thus the Froude number in channel flow $\mathrm{Fr} = V/c_0$ is the analog of the Mach number.

As in gas dynamics, a channel flow can accelerate from subcritical to critical to supercritical flow and then return to subcritical flow through a sort of normal shock called a *hydraulic jump* (Sec. 10.5). This is illustrated in Fig. 10.5. The flow upstream of the sluice gate is subcritical. It then accelerates to critical and supercritical flow as it passes under the gate, which serves as a sort of "nozzle." Further downstream the flow "shocks" back to subcritical flow because the downstream "receiver" height is too high to maintain supercritical flow. Note the similarity with the nozzle gas flows of Fig. 9.12.

The critical depth $y_c = [Q^2/(b^2 g)]^{1/3}$ is sketched as a dashed line in Fig. 10.5 for reference. Like the normal depth y_n, y_c is an important parameter in characterizing open-channel flow (see Sec. 10.4).

An excellent discussion of the various regimes of open-channel flow is given in Ref. 10.

10.2 Uniform Flow; the Chézy Formula

Uniform flow can occur in long straight runs of constant slope and constant channel cross section. The water depth is constant at $y = y_n$, and the velocity is constant at $V = V_0$. Let the slope be $S_0 = \tan\theta$, where θ is the angle the bottom makes with the horizontal, considered positive for downhill flow. Then Eq. (10.2), with $V_1 = V_2 = V_0$, becomes

$$h_f = z_1 - z_2 = S_0 L \tag{10.11}$$

where L is the horizontal distance between sections 1 and 2. The head loss thus balances the loss in height of the channel. The flow is essentially fully developed, so that the Darcy-Weisbach relation, Eq. (6.30), holds

$$h_f = f\frac{L}{D_h}\frac{V_0^2}{2g} \qquad D_h = 4R_h$$



ketabline.com Ebook.ketabline.com

with $D_h = 4A/P$ used to accommodate noncircular channels. The geometry and notation for open-channel flow analysis are shown in Fig. 10.2.

By combining Eqs. (10.11) and (10.12) we obtain an expression for flow velocity in uniform channel flow

$$V_0 = \left(\frac{8g}{f}\right)^{1/2} R_h^{1/2} S_0^{1/2} \tag{10.13}$$

For a given channel shape and bottom roughness, the quantity $(8g/f)^{1/2}$ is constant and can be denoted by C. Equation (10.13) becomes

$$V_0 = C(R_h S_0)^{1/2} \qquad Q = CA(R_h S_0)^{1/2} \tag{10.14}$$

These are called the *Chézy formulas,* first developed by the French engineer Antoine Chézy in conjunction with his experiments on the Seine River and the Courpalet Canal in 1769. The quantity C, called the *Chézy coefficient,* varies from about 60 $ft^{1/2}/s$ for small rough channels to 160 $ft^{1/2}/s$ for large smooth channels (30 to 90 $m^{1/2}/s$ in SI units).

Over the past century a great deal of hydraulics research [11] has been devoted to the correlation of the Chézy coefficient with the roughness, shape, and slope of various open channels. Correlations are due to Ganguillet and Kutter in 1869, Manning in 1889, Bazin in 1897, and Powell in 1950 [11]. All these formulations are discussed in delicious detail in Ref. 3, chap. 5. Here we confine our treatment to Manning's correlation, the most popular.

The Manning Roughness Correlation

The most fundamentally sound approach to the Chézy formula is to use Eq. (10.13) with f estimated from the Moody friction-factor chart, Fig. 6.13. Indeed, the open channel research establishment [17] strongly recommends use of the friction factor in all calculations. Since typical channels are large and rough, we would generally use the fully rough turbulent-flow limit of Eq. (6.64):

$$f \approx \left(2.0 \log \frac{14.8R_h}{\epsilon}\right)^{-2} \tag{10.15a}$$

A special case, for rocky channel beds, is recommended in Ref. 2:

$$f \approx \left[1.2 + 2.03 \log\left(\frac{R_h}{d_{84\%}}\right)\right]^{-2} \tag{10.15b}$$

where $d_{84\%}$ is the size for which 84 percent of the rocks are smaller (the largest rocks dominate the friction in the channel). Note that $d_{84\%}$ and ϵ are *not* equal, ϵ being an overall average size. In spite of the attractiveness of this friction-factor approach, most engineers prefer to use a simple (dimensional) correlation published in 1891 by Robert Manning [12], an Irish engineer. In tests with real channels, Manning found that the Chézy coefficient C increased approximately as the sixth root of the channel size. He proposed the simple formula

$$C = \left(\frac{8g}{f}\right)^{1/2} \approx \alpha \frac{R_h^{1/6}}{n} \tag{10.16}$$

where n is a roughness parameter. Since the formula is clearly not d
sistent, it requires a conversion factor α which changes with the sy



ketabline.com Ebook.ketabline.com

$$\alpha = 1.0 \quad \text{SI units} \qquad \alpha = 1.486 \quad \text{BG units} \tag{10.17}$$

Recall that we warned about this awkwardness in Example 1.4. You may verify that α is the cube root of the conversion factor between the meter and your chosen length scale: In BG units, $\alpha = (3.2808 \text{ ft/m})^{1/3} = 1.486$.*

The Manning formula for uniform-flow velocity is thus

$$V_0 \text{ (m/s)} \approx \frac{1.0}{n} [R_h \text{ (m)}]^{2/3} S_0^{1/2}$$
$$V_0 \text{ (ft/s)} \approx \frac{1.486}{n} [R_h \text{ (ft)}]^{2/3} S_0^{1/2} \tag{10.18}$$

The channel slope S_0 is dimensionless, and n is taken to be the same in both systems. The volume flow rate simply multiplies this result by the area:

Uniform flow: $$Q = V_0 A \approx \frac{\alpha}{n} A R_h^{2/3} S_0^{1/2} \tag{10.19}$$

Experimental values of n (and the corresponding roughness height) are listed in Table 10.1 for various channel surfaces. There is a factor-of-15 variation from a smooth glass surface ($n \approx 0.01$) to a tree-lined floodplain ($n \approx 0.15$). Due to the irregularity of typical channel shapes and roughness, the scatter bands in Table 10.1 should be taken seriously.

Since Manning's sixth-root size variation is not exact, real channels can have a variable n depending upon the water depth. The Mississippi River near Memphis, Tennessee, has $n \approx 0.032$ at 40-ft flood depth, 0.030 at normal 20-ft depth, and 0.040 at 5-ft low-stage depth. Seasonal vegetative growth and factors such as bottom erosion can also affect the value of n.

EXAMPLE 10.1

A finished-concrete 8-ft-wide rectangular channel has a bed slope of 0.5° and a water depth of 4 ft. Predict the uniform flow rate in ft^3/s.

Solution

Part (a) From Table 10.1, for finished concrete, $n \approx 0.012$. The slope $S_0 = \tan 0.5° = 0.00873$. For depth $y = 4$ ft and width $b = 8$ ft, the geometric properties are

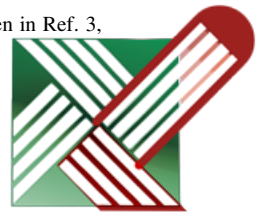
$$A = by = (8 \text{ ft})(4 \text{ ft}) = 32 \text{ ft}^2 \qquad P = b + 2y = 8 + 2(4) = 16 \text{ ft}$$

$$R_h = \frac{A}{P} = \frac{32 \text{ ft}^2}{16 \text{ ft}} = 2.0 \text{ ft} \qquad D_h = 4R_h = 8.0 \text{ ft}$$

From Manning's formula (10.19) in BG units, the estimated flow rate is

$$Q \approx \frac{1.486}{n} A R_h^{2/3} S_0^{1/2} = \frac{1.486}{0.012} (32 \text{ ft}^2)(2.0 \text{ ft})^{2/3}(0.00873)^{1/2} \approx 590 \text{ ft}^3\text{/s} \qquad \textit{Ans.}$$

*An interesting discussion of the history and "dimensionality" of Manning's formula is given in Ref. 3, pp. 98–99.



ketabline.com Ebook.ketabline.com

Table 10.1 Experimental Values of Manning's n Factor*

	n	Average roughness height ϵ ft	Average roughness height ϵ mm
Artificial lined channels:			
Glass	0.010 ± 0.002	0.0011	0.3
Brass	0.011 ± 0.002	0.0019	0.6
Steel, smooth	0.012 ± 0.002	0.0032	1.0
Painted	0.014 ± 0.003	0.0080	2.4
Riveted	0.015 ± 0.002	0.012	3.7
Cast iron	0.013 ± 0.003	0.0051	1.6
Cement, finished	0.012 ± 0.002	0.0032	1.0
Unfinished	0.014 ± 0.002	0.0080	2.4
Planed wood	0.012 ± 0.002	0.0032	1.0
Clay tile	0.014 ± 0.003	0.0080	2.4
Brickwork	0.015 ± 0.002	0.012	3.7
Asphalt	0.016 ± 0.003	0.018	5.4
Corrugated metal	0.022 ± 0.005	0.12	37
Rubble masonry	0.025 ± 0.005	0.26	80
Excavated earth channels:			
Clean	0.022 ± 0.004	0.12	37
Gravelly	0.025 ± 0.005	0.26	80
Weedy	0.030 ± 0.005	0.8	240
Stony, cobbles	0.035 ± 0.010	1.5	500
Natural channels:			
Clean and straight	0.030 ± 0.005	0.8	240
Sluggish, deep pools	0.040 ± 0.010	3	900
Major rivers	0.035 ± 0.010	1.5	500
Floodplains:			
Pasture, farmland	0.035 ± 0.010	1.5	500
Light brush	0.05 ± 0.02	6	2000
Heavy brush	0.075 ± 0.025	15	5000
Trees	0.15 ± 0.05	?	?

*A more complete list is given in Ref. 3, pp. 110–113.

Considering the uncertainty in n (±17 percent), it would be more realistic to report this estimate as $Q \approx 600 \pm 100$ ft^3/s. An alternate estimate, using the Moody formula (10.15) with $\epsilon = 0.0032$ ft from Table 10.1, would give $Q \approx 540$ ft^3/s.

Normal-Depth Estimates

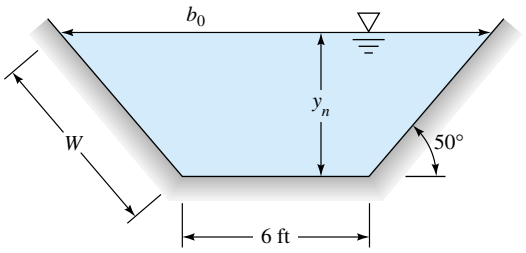
With water depth y known, the computation of Q in Example 10.1 was quite straightforward. However, if Q is given, the computation of the normal depth y_n may require iteration or trial and error. Since the normal depth is a characteristic flow parameter, this is an important type of problem.

EXAMPLE 10.2

The asphalt-lined trapezoidal channel in Fig. E10.2 carries 300 ft^3/s of water under uniform-flo conditions when $S = 0.0015$. What is the normal depth y_n?



ketabline.com Ebook.ketabline.com



E10.2

Solution

From Table 10.1, for asphalt, $n \approx 0.016$. The area and hydraulic radius are functions of y_n, which is unknown

$$b_0 = 6 \text{ ft} + 2y_n \cot 50° \qquad A = \tfrac{1}{2}(6 + b_0)y_n = 6y_n + y_n^2 \cot 50°$$

$$P = 6 + 2W = 6 + 2y_n \csc 50°$$

From Manning's formula (10.19) with a known $Q = 300$ ft^3/s, we have

$$300 = \frac{1.49}{0.016}(6y_n + y_n^2 \cot 50°)\left(\frac{6y_n + y_n^2 \cot 50°}{6 + 2y_n \csc 50°}\right)^{2/3}(0.0015)^{1/2}$$

or

$$(6y_n + y_n^2 \cot 50°)^{5/3} = 83.2(6 + 2y_n \csc 50°)^{2/3}$$

One can iterate this formula laboriously and eventually find $y_n \approx 4.6$ ft. However, it is a perfect candidate for EES. Instead of manipulating and programming the final formula, one might simply evaluate each separate part of the Chézy equation (in English units, with angles in degrees):

```
P = 6 + 2*yn/sin(50)
A = 6*yn + yn^2/tan(50)
Rh = A/P
300 = 1.49/0.016*A*Rh^(2/3)*0.0015^0.5
```

Hit Solve from the menu bar and EES complains of "negative numbers to a power". Go back to Variable Information on the menu bar and make sure that y_n is positive. EES then immediately solves for

$P = 17.95$ $\quad A = 45.04$ $\quad R_h = 2.509$ $\quad \mathbf{y_n = 4.577 \text{ ft}}$ *Ans.*

Generally, EES is ideal for open-channel-flow problems where the depth is unknown.

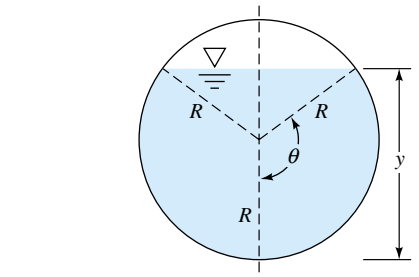
Uniform Flow in a Partly Full Circular Pipe

Consider the partially full pipe of Fig. 10.6*a* in uniform flow. The maximum velocity and flow rate actually occur before the pipe is completely full. In terms of the pipe radius R and the angle θ up to the free surface, the geometric properties are

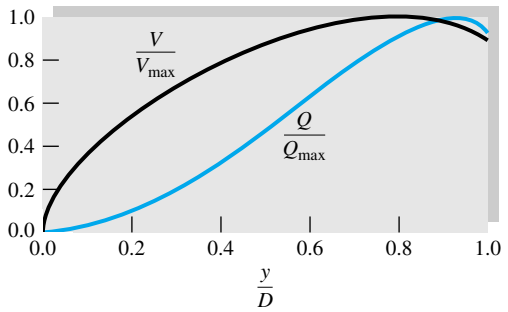
$$A = R^2\left(\theta - \frac{\sin 2\theta}{2}\right) \qquad P = 2R\theta \qquad R_h = \frac{R}{2}\left(1 - \frac{\sin 2\theta}{2\theta}\right)$$



ketabline.com Ebook.ketabline.com



(*a*)



(*b*)

Fig. 10.6 Uniform flow in a partly full circular channel: (*a*) geometry; (*b*) velocity and flow rate versus depth.

The Manning formulas (10.19) predict a uniform flow as follows:

$$V_0 \approx \frac{\alpha}{n}\left[\frac{R}{2}\left(1 - \frac{\sin 2\theta}{2\theta}\right)\right]^{2/3} S_0^{1/2} \qquad Q = V_0 R^2\left(\theta - \frac{\sin 2\theta}{2}\right) \tag{10.20}$$

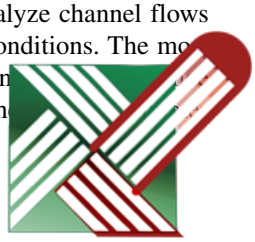
For a given n and slope S_0, we may plot these two relations versus θ in Fig. 10.6*b*. There are two different maxima, as follows:

$$V_{\max} = 0.718\,\frac{\alpha}{n}\,R^{2/3}S_0^{1/2} \qquad \text{at} \quad \theta = 128.73° \quad \text{and} \quad y = 0.813D$$
$$Q_{\max} = 2.129\,\frac{\alpha}{n}\,R^{8/3}S_0^{1/2} \qquad \text{at} \quad \theta = 151.21° \quad \text{and} \quad y = 0.938D \tag{10.21}$$

As shown in Fig. 10.6*b*, the maximum velocity is 14 percent more than the velocity when running full, and similarly the maximum discharge is 8 percent more. Since real pipes running nearly full tend to have somewhat unstable flow, these differences are not that significant.

10.3 Efficient Uniform-Flow Channels

The simplicity of Manning's formulation (10.19) enables us to analyze channel flows to determine the most efficient low-resistance sections for given conditions. The mo common problem is that of maximizing R_h for a given flow area an $R_h = A/P$, maximizing R_h for given A is the same as minimizing th



ketabline.com Ebook.ketabline.com

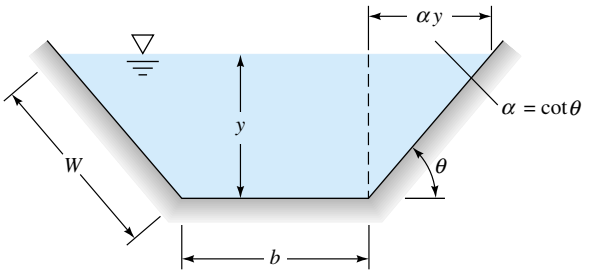


Fig. 10.7 Geometry of a trapezoidal channel section.

P. There is no general solution for arbitrary cross sections, but an analysis of the trapezoid section will show the basic results.

Consider the generalized trapezoid of angle θ in Fig. 10.7. For a given side angle θ, the flow area is

$$A = by + \alpha y^2 \qquad \alpha = \cot\theta \tag{10.22}$$

The wetted perimeter is

$$P = b + 2W = b + 2y(1 + \alpha^2)^{1/2} \tag{10.23}$$

Eliminating b between (10.22) and (10.23) gives

$$P = \frac{A}{y} - \alpha y + 2y(1 + \alpha^2)^{1/2} \tag{10.24}$$

To minimize P, evaluate dP/dy for constant A and α and set equal to zero. The result is

$$A = y^2[2(1 + \alpha^2)^{1/2} - \alpha] \qquad P = 4y(1 + \alpha^2)^{1/2} - 2\alpha y \qquad R_h = \tfrac{1}{2}y \tag{10.25}$$

The last result is very interesting: For any angle θ, the most efficient cross section for uniform flow occurs when the hydraulic radius is half the depth.

Since a rectangle is a trapezoid with $\alpha = 0$, the most efficient rectangular section is such that

$$A = 2y^2 \qquad P = 4y \qquad R_h = \tfrac{1}{2}y \qquad b = 2y \tag{10.26}$$

To find the correct depth y, these relations must be solved in conjunction with Manning's flow-rate formula (10.19) for the given discharge Q.

Best Trapezoid Angle

Equations (10.25) are valid for any value of α. What is the best value of α for a given depth and area? To answer this question, evaluate $dP/d\alpha$ from Eq. (10.24) with A and y held constant. The result is

$$2\alpha = (1 + \alpha^2)^{1/2} \qquad \alpha = \cot\theta = \frac{1}{3^{1/2}}$$

or

$$\theta = 60^\circ \tag{10.27}$$

Thus the very best trapezoid section is half a hexagon.

Similar calculations with a circular channel section running partially full sh
efficiency for a semicircle, $y = \frac{1}{2}D$. In fact, the semicircle is the best of all



ketabline.com Ebook.ketabline.com

channel sections (minimum wetted perimeter for a given flow area). The percentage improvement over, say, half a hexagon is very slight, however.

EXAMPLE 10.3

What are the best dimensions for a rectangular brick channel designed to carry 5 m^3/s of water in uniform flow with $S_0 = 0.001$?

Solution

From Eq. (10.26), $A = 2y^2$ and $R_h = \frac{1}{2}y$. Manning's formula (10.19) in SI units gives, with $n \approx 0.015$ from Table 10.1,

$$Q = \frac{1.0}{n} AR_h^{2/3} S_0^{1/2} \qquad \text{or} \qquad 5\ \text{m}^3/\text{s} = \frac{1.0}{0.015}(2y^2)\left(\frac{1}{2}y\right)^{2/3}(0.001)^{1/2}$$

which can be solved for

$$y^{8/3} = 1.882\ \text{m}^{8/3}$$

$$y = 1.27\ \text{m} \qquad \textit{Ans.}$$

The proper area and width are

$$A = 2y^2 = 3.21\ \text{m}^2 \qquad b = \frac{A}{y} = 2.53\ \text{m} \qquad \textit{Ans.}$$

It is constructive to see what flow rate a half-hexagon and semicircle would carry for the same area of 3.214 m^2.

For the half-hexagon (HH), with $\alpha = 1/3^{1/2} = 0.577$, Eq. (10.25) predicts

$$A = y_{\text{HH}}^2[2(1 + 0.577^2)^{1/2} - 0.577] = 1.732y_{\text{HH}}^2 = 3.214$$

or $y_{\text{HH}} = 1.362$ m, whence $R_h = \frac{1}{2}y = 0.681$ m. The half-hexagon flow rate is thus

$$Q = \frac{1.0}{0.015}(3.214)(0.681)^{2/3}(0.001)^{1/2} = 5.25\ \text{m}^3/\text{s}$$

or about 5 percent more than that for the rectangle.

For a semicircle, $A = 3.214\ \text{m}^2 = \pi D^2/8$, or $D = 2.861$ m, whence $P = \frac{1}{2}\pi D = 4.494$ m and $R_h = A/P = 3.214/4.484 = 0.715$ m. The semicircle flow rate will thus be

$$Q = \frac{1.0}{0.015}(3.214)(0.715)^{2/3}(0.001)^{1/2} = 5.42\ \text{m}^3/\text{s}$$

or about 8 percent more than that of the rectangle and 3 percent more than that of the half-hexagon.

10.4 Specific Energy; Critical Depth

As suggested by Bakhmeteff [13] in 1911, the specific energy E is a useful parameter in channel flow

$$E = y + \frac{V^2}{2g}$$



ketabline.com Ebook.ketabline.com

where y is the water depth. It is seen from Fig. 10.8*a* that E is the height of the *energy grade line* (EGL) above the channel bottom. For a given flow rate, there are usually two states possible for the same specific energy.

Rectangular Channels

Consider the possible states at a given location. Let $q = Q/b = Vy$ be the discharge per unit width of a rectangular channel. Then, with q constant, Eq. (10.28) becomes

$$E = y + \frac{q^2}{2gy^2} \qquad q = \frac{Q}{b} \tag{10.29}$$

Figure 10.8*b* is a plot of y versus E for constant q from Eq. (10.29). There is a minimum value of E at a certain value of y called the *critical depth*. By setting $dE/dy = 0$ at constant q, we find that $E_{\min}$ occurs at

$$y = y_c = \left(\frac{q^2}{g}\right)^{1/3} = \left(\frac{Q^2}{b^2 g}\right)^{1/3} \tag{10.30}$$

The associated minimum energy is

$$E_{\min} = E(y_c) = \tfrac{3}{2} y_c \tag{10.31}$$

The depth y_c corresponds to channel velocity equal to the shallow-water wave propagation speed C_0 from Eq. (10.10). To see this, rewrite Eq. (10.30) as

$$q^2 = g y_c^3 = (g y_c) y_c^2 = V_c^2 y_c^2 \tag{10.32}$$

By comparison it follows that the critical channel velocity is

$$V_c = (g y_c)^{1/2} = C_0 \qquad \text{Fr} = 1 \tag{10.33}$$

For $E < E_{\min}$ no solution exists in Fig. 10.8*b*, and thus such a flow is impossible physically. For $E > E_{\min}$ two solutions are possible: (1) large depth with $V < V_c$, called *subcritical,* and (2) small depth with $V > V_c$, called *supercritical*. In subcritical flow, disturbances can propagate upstream because wave speed $C_0 > V$. In supercritical flow, waves are swept downstream: Upstream is a zone of silence, and a small obstruction in the flow will create a wedge-shaped wave exactly analogous to the Mach waves in

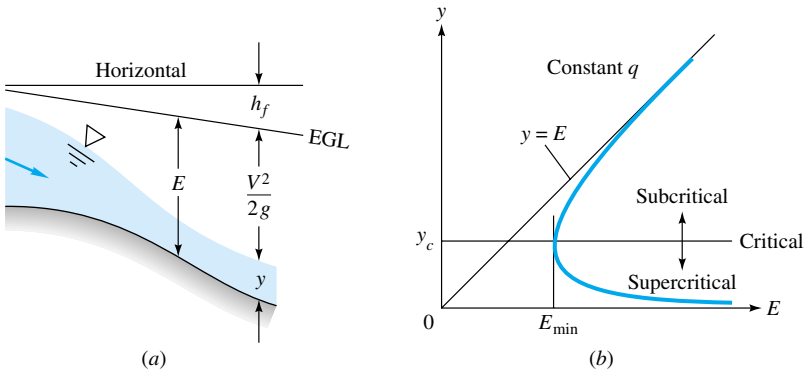


Fig. 10.8 Specific-energy considerations: (*a*) illustration sketch; (*b*) depth versus E from Eq. (10.29), showing minimum specific energy occurring at critical depth.



ketabline.com Ebook.ketabline.com

Fig. 9.18*c*.[2] The angle of these waves must be

$$\mu = \sin^{-1}\frac{c_0}{V} = \sin^{-1}\frac{(gy)^{1/2}}{V} \tag{10.34}$$

The wave angle and the depth can thus be used as a simple measurement of supercritical-flow velocity.

Note from Fig. 10.8*b* that small changes in E near $E_{\min}$ cause a large change in the depth y, by analogy with small changes in duct area near the sonic point in Fig. 9.7. Thus critical flow is neutrally stable and is often accompanied by waves and undulations in the free surface. Channel designers should avoid long runs of near-critical flow.

EXAMPLE 10.4

A wide rectangular clean-earth channel has a flow rate $q = 50$ ft^3/(s · ft). (*a*) What is the critical depth? (*b*) What type of flow exists if $y = 3$ ft?

Solution

Part (a) From Table 10.1, $n \approx 0.022$ and $\epsilon \approx 0.12$ ft. The critical depth follows from Eq. (10.30):

$$y_c = \left(\frac{q^2}{g}\right)^{1/3} = \left(\frac{50^2}{32.2}\right)^{1/3} = 4.27 \text{ ft} \qquad \textit{Ans. (a)}$$

Part (b) If the actual depth is 3 ft, which is less than y_c, the flow must be *supercritical*. *Ans. (b)*

Nonrectangular Channels

If the channel width varies with y, the specific energy must be written in the form

$$E = y + \frac{Q^2}{2gA^2} \tag{10.35}$$

The critical point of minimum energy occurs where $dE/dy = 0$ at constant Q. Since $A = A(y)$, Eq. (10.35) yields, for $E = E_{\min}$,

$$\frac{dA}{dy} = \frac{gA^3}{Q^2} \tag{10.36}$$

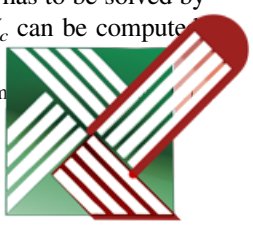
But $dA = b_0\,dy$, where b_0 is the channel width at the free surface. Therefore Eq. (10.36) is equivalent to

$$A_c = \left(\frac{b_0 Q^2}{g}\right)^{1/3} \tag{10.37a}$$

$$V_c = \frac{Q}{A_c} = \left(\frac{gA_c}{b_0}\right)^{1/2} \tag{10.37b}$$

For a given channel shape $A(y)$ and $b_0(y)$ and a given Q, Eq. (10.37) has to be solved by trial and error or by EES to find the critical area A_c, from which V_c can be computed.

[2]This is the basis of the water-channel analogy for supersonic gas-dynamics experim



ketabline.com Ebook.ketabline.com

By comparing the actual depth and velocity with the critical values, we can determine the local flow condition

$$y > y_c,\ V < V_c: \quad \text{subcritical flow (Fr} < 1)$$
$$y < y_c,\ V > V_c: \quad \text{supercritical flow (Fr} > 1)$$

Critical Uniform Flow: The Critical Slope

If a critical channel flow is also moving uniformly (at constant depth), it must correspond to a *critical slope* S_c, with $y_n = y_c$. This condition is analyzed by equating Eq. (10.37*a*) to the Chézy (or Manning) formula:

$$Q^2 = \frac{gA_c^3}{b_0} = C^2A_c^2R_hS_c = \frac{\alpha^2}{n^2}A_c^2R_h^{4/3}S_c$$

or

$$S_c = \frac{n^2gA_c}{\alpha^2 b_0 R_{hc}^{4/3}} = \frac{n^2g}{\alpha^2 R_{hc}^{1/3}}\frac{P}{b_0} = \frac{f}{8}\frac{P}{b_0} \tag{10.38}$$

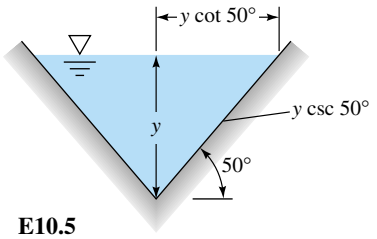
where α^2 equals 1.0 for SI units and 2.208 for BG units. Equation (10.38) is valid for any channel shape. For a wide rectangular channel, $b_0 \gg y_c$, the formula reduces to

Wide rectangular channel: $$S_c \approx \frac{n^2g}{\alpha^2 y_c^{1/3}} \approx \frac{f}{8}$$

This is a special case, a reference point. In most channel flows $y_n \neq y_c$. For fully rough turbulent flow, the critical slope varies between 0.002 and 0.008.

EXAMPLE 10.5

Part (a) The 50° triangular channel in Fig. E10.5 has a flow rate $Q = 16$ m^3/s. Compute (*a*) y_c, (*b*) V_c, and (*c*) S_c if $n = 0.018$.



E10.5

Solution

This is an easy cross section because all geometric quantities can be written directly in terms of depth y

$$P = 2y\csc 50° \qquad A = y^2\cot 50°$$
$$R_h = \tfrac{1}{2}y\cos 50° \qquad b_0 = 2y\cot 50° \tag{1}$$

The critical-flow condition satisfies Eq. (10.37*a*)

$$gA_c^3 = b_0Q^2$$

or

$$g(y_c^2\cot 50°)^3 = (2y_c\cot 50°)Q^2$$

$$y_c = \left(\frac{2Q^2}{g\cot^2 50°}\right)^{1/5} = \left[\frac{2(16)^2}{9.81(0.839)^2}\right]^{1/5} = 2.37 \text{ m} \qquad \textit{Ans. (a)}$$

Part (b) With y_c known, from Eqs. (1) we compute $P_c = 6.18$ m, $R_{hc} = 0.760$ m, $A_c = 4.70$ m^2, and $b_{0c} = 3.97$ m. The critical velocity from Eq. (10.37*b*) is

$$V_c = \frac{Q}{A} = \frac{16 \text{ m}^3/\text{s}}{4.70 \text{ m}^2} = 3.41 \text{ m/s}$$



ketabline.com Ebook.ketabline.com

Part (c) With $n = 0.018$, we compute from Eq. (10.38) a critical slope

$$S_c = \frac{gn^2P}{\alpha^2 R_h^{1/3} b_0} = \frac{9.81(0.018)^2(6.18)}{1.0(0.760)^{1/3}(3.97)} = 0.00542 \qquad \textit{Ans. (c)}$$

Frictionless Flow over a Bump

A rough analogy to compressible gas flow in a nozzle (Fig. 9.12) is open-channel flow over a bump, as in Fig. 10.9*a*. The behavior of the free surface is sharply different according to whether the approach flow is subcritical or supercritical. The height of the bump also can change the character of the results. For frictionless two-dimensional flow, sections 1 and 2 in Fig. 10.9*a* are related by continuity and momentum:

$$V_1 y_1 = V_2 y_2 \qquad \frac{V_1^2}{2g} + y_1 = \frac{V_2^2}{2g} + y_2 + \Delta h$$

Eliminating V_2 between these two gives a cubic polynomial equation for the water depth y_2 over the bump:

$$y_2^3 - E_2 y_2^2 + \frac{V_1^2 y_1^2}{2g} = 0 \qquad \text{where } E_2 = \frac{V_1^2}{2g} + y_1 - \Delta h \tag{10.39}$$

This equation has one negative and two positive solutions if Δh is not too large. Its behavior is illustrated in Fig. 10.9*b* and depends upon whether condition 1 is on the upper or lower leg of the energy curve. The specific energy E_2 is exactly Δh less than the approach energy E_1, and point 2 will lie on the same leg of the curve as E_1. A sub-

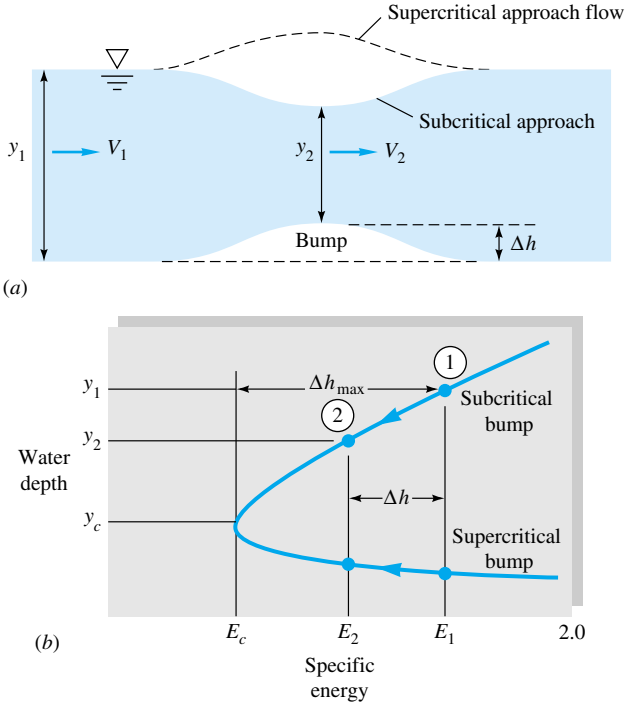


Fig. 10.9 Frictionless two-dimensional flow over a bump: (*a*) definition sketch showing Froude-number dependence; (*b*) specific-energy plot showing bump size and water depths.

ketabline.com Ebook.ketabline.com

critical approach, $\mathrm{Fr}_1 < 1$, will cause the water level to decrease at the bump. Supercritical approach flow, $\mathrm{Fr}_1 > 1$, causes a water-level increase over the bump.

If the bump height reaches $\Delta h_{\max} = E_1 - E_c$, as illustrated in Fig. 10.9*b*, the flow at the crest will be exactly critical (Fr = 1). If $\Delta h > \Delta h_{\max}$, there are no physically correct solutions to Eq. (10.39). That is, a bump too large will "choke" the channel and cause frictional effects, typically a hydraulic jump (Sec. 10.5).

These bump arguments are reversed if the channel has a *depression* ($\Delta h < 0$): Subcritical approach flow will cause a water-level rise and supercritical flow a fall in depth. Point 2 will be $|\Delta h|$ to the right of point 1, and critical flow cannot occur.

EXAMPLE 10.6

Water flow in a wide channel approaches a 10-cm-high bump at 1.5 m/s and a depth of 1 m. Estimate (*a*) the water depth y_2 over the bump and (*b*) the bump height which will cause the crest flow to be critical.

Solution

Part (a) First check the approach Froude number, assuming $C_0 = \sqrt{gy}$:

$$\mathrm{Fr}_1 = \frac{V_1}{\sqrt{gy_1}} = \frac{1.5 \text{ m/s}}{\sqrt{(9.81 \text{ m/s}^2)(1.0 \text{ m})}} = 0.479 \qquad \text{(subcritical)}$$

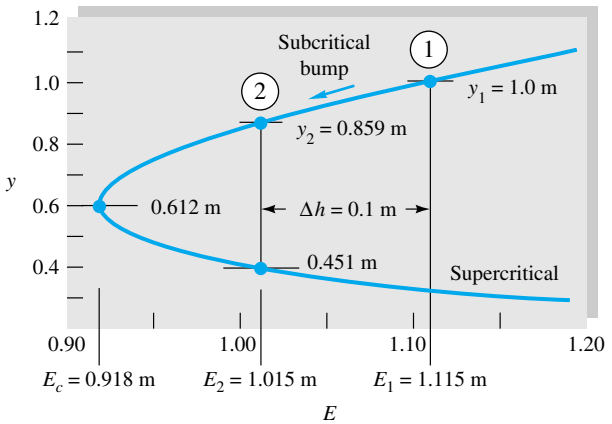
For subcritical approach flow, if Δh is not too large, we expect a depression in the water level over the bump and a higher subcritical Froude number at the crest. With $\Delta h = 0.1$ m, the specific-energy levels must be

$$E_1 = \frac{V_1^2}{2g} + y_1 = \frac{(1.5)^2}{2(9.81)} + 1.0 = 1.115 \qquad E_2 = E_1 - \Delta h = 1.015 \text{ m}$$

This physical situation is shown on a specific-energy plot in Fig. E10.6. With y_1 in meters, Eq. (10.39) takes on the numerical values

$$y_2^3 - 1.015y_2^2 + 0.115 = 0$$

There are three real roots: $y_2 = +0.859$ m, $+0.451$ m, and -0.296 m. The third (negative) solution is physically impossible. The second (smaller) solution is the *supercritical* condition for



E10.6

ketabline.com Ebook.ketabline.com

E_2 and is not possible for this subcritical bump. The first solution is correct:

$$y_2(\text{subcritical}) \approx 0.859 \text{ m} \qquad \textit{Ans. (a)}$$

The surface level has dropped by $y_1 - y_2 - \Delta h = 1.0 - 0.859 - 0.1 = 0.041$ m. The crest velocity is $V_2 = V_1 y_1 / y_2 = 1.745$ m/s. The Froude number at the crest is $\text{Fr}_2 = 0.601$. Flow downstream of the bump is subcritical. These flow conditions are shown in Fig. E10.6.

Part (b) For critical flow in a wide channel, with $q = Vy = 1.5$ m^2/s, from Eq. (10.31),

$$E_{2,\min} = E_c = \frac{3}{2} y_c = \frac{3}{2}\left(\frac{q^2}{g}\right)^{1/3} = \frac{3}{2}\left[\frac{(1.5 \text{ m}^2/\text{s})^2}{9.81 \text{ m/s}^2}\right]^{1/3} = 0.918 \text{ m}$$

Therefore the maximum height for frictionless flow over this particular bump is

$$\Delta h_{\max} = E_1 - E_{2,\min} = 1.115 - 0.918 = 0.197 \text{ m} \qquad \textit{Ans. (b)}$$

For this bump, the solution of Eq. (10.39) is $y_2 = y_c = 0.612$ m, and the Froude number is unity at the crest. At critical flow the surface level has dropped by $y_1 - y_2 - \Delta h = 0.191$ m.

Flow under a Sluice Gate

A sluice gate is a bottom opening in a wall, as sketched in Fig. 10.10*a*, commonly used in control of rivers and channel flows. If the flow is allowed free discharge through the gap, as in Fig. 10.10*a*, the flow smoothly accelerates from subcritical (upstream) to critical (near the gap) to supercritical (downstream). The gate is then analogous to a converging-diverging nozzle in gas dynamics, as in Fig. 9.12, operating at its *design condition* (similar to point H in Fig. 9.12*b*).

For free discharge, friction may be neglected, and since there is no bump ($\Delta h = 0$), Eq. (10.39) applies with $E_1 = E_2$:

$$y_2^3 - \left(\frac{V_1^2}{2g} + y_1\right) y_2^2 + \frac{V_1^2 y_1^2}{2g} = 0 \qquad (10.40)$$

Given subcritical upstream flow (V_1, y_1), this cubic equation has only one positive real solution: supercritical flow at the same specific energy, as in Fig. 10.10*b*. The flow rate varies with the ratio y_2/y_1; we ask, as a problem exercise, to show that the flow rate is a maximum when $y_2/y_1 = \frac{2}{3}$.

The free discharge, Fig. 10.10*a*, contracts to a depth y_2 about 40 percent less than the gate's gap height, as shown. This is similar to a free *orifice* discharge, as in Fig. 6.38. If H is the height of the gate gap and b is the gap width into the paper, we can approximate the flow rate by orifice theory:

$$Q = C_d H b \sqrt{2 g y_1} \qquad \text{where} \qquad C_d \approx \frac{0.61}{\sqrt{1 + 0.61 H/y_1}} \qquad (10.41)$$

in the range $H/y_1 < 0.5$. Thus a continuous variation in flow rate is accomplished by raising the gate.

If the tailwater is high, as in Fig. 10.10*c*, free discharge is not possible. The sluice gate is said to be *drowned* or partially drowned. There will be energy dissipation in the exit flow, probably in the form of a drowned hydraulic jump, and the downstream flow will return to subcritical. Equations (10.40) and (10.41) do not apply, and experimental discharge correlations are necessary [2, 15



ketabline.com Ebook.ketabline.com

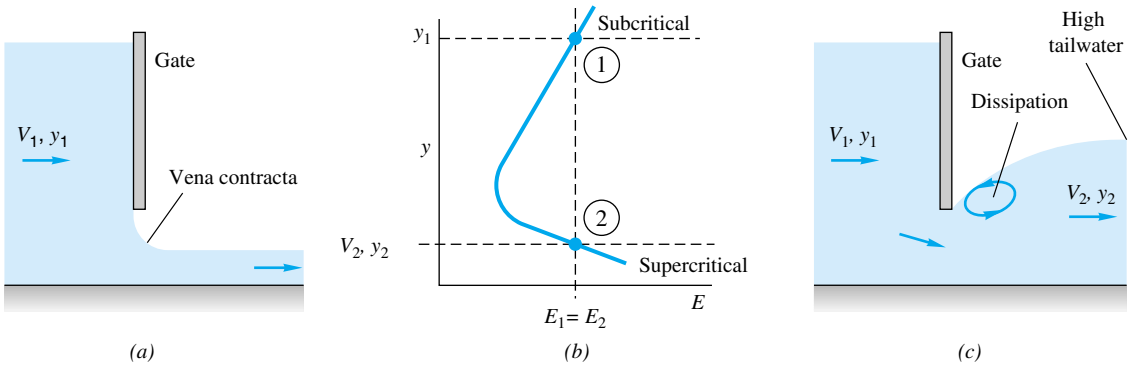


Fig. 10.10 Flow under a sluice gate passes through critical flow: (*a*) free discharge with vena contracta; (*b*) specific energy for free discharge; (*c*) dissipative flow under a drowned gate.

10.5 The Hydraulic Jump

In open-channel flow a supercritical flow can change quickly back to a subcritical flow by passing through a hydraulic jump, as in Fig. 10.5. The upstream flow is fast and shallow, and the downstream flow is slow and deep, analogous to the normal-shock wave of Fig. 9.8. Unlike the infinitesimally thin normal shock, the hydraulic jump is quite thick, ranging in length from 4 to 6 times the downstream depth y_2 [16].

Being extremely turbulent and agitated, the hydraulic jump is a very effective energy dissipator and is a feature of stilling-basin and spillway applications [16]. Figure 10.11 shows the jump formed at the bottom of a dam spillway in a model test. It is very important that such jumps be located on specially designed aprons; otherwise the channel bottom will be badly scoured by the agitation. Jumps also mix fluids very effectively and have application to sewage and water treatment designs.

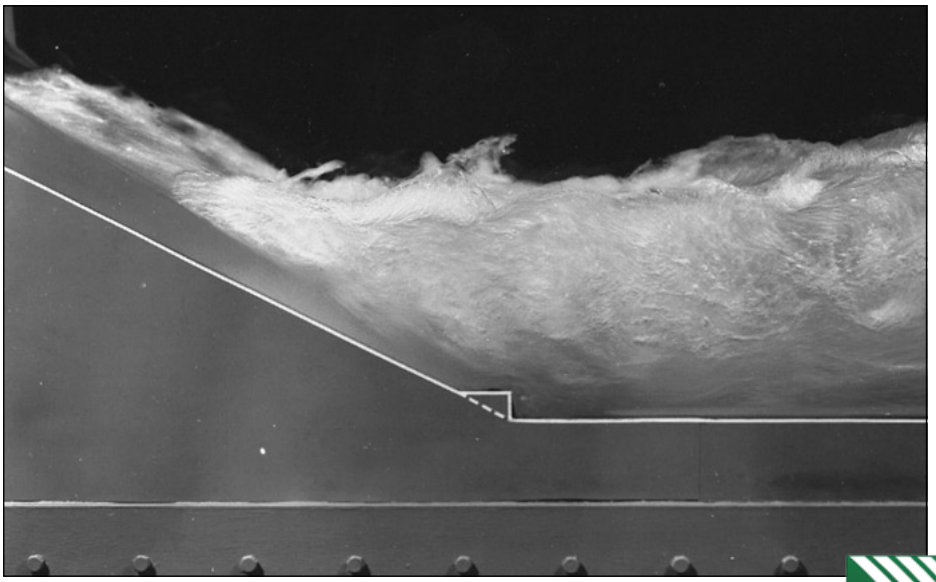


Fig. 10.11 Hydraulic jump formed on a spillway model for the Karnafuli Dam in East Pakistan. *(Courtesy of the St. Anthony Falls Hydraulic Laboratory, University of Minnesota.)*



ketabline.com Ebook.ketabline.com

Classification

The principal parameter affecting hydraulic-jump performance is the upstream Froude number $\mathrm{Fr}_1 = V_1/(gy_1)^{1/2}$. The Reynolds number and channel geometry have only a secondary effect. As detailed in Ref. 16, the following ranges of operation can be outlined, as illustrated in Fig. 10.12:

$\mathrm{Fr}_1 < 1.0$:	Jump impossible, violates second law of thermodynamics.
$\mathrm{Fr}_1 = 1.0$ to 1.7:	Standing-wave, or *undular, jump* about $4y_2$ long; low dissipation, less than 5 percent.
$\mathrm{Fr}_1 = 1.7$ to 2.5:	Smooth surface rise with small rollers, known as a *weak jump*; dissipation 5 to 15 percent.

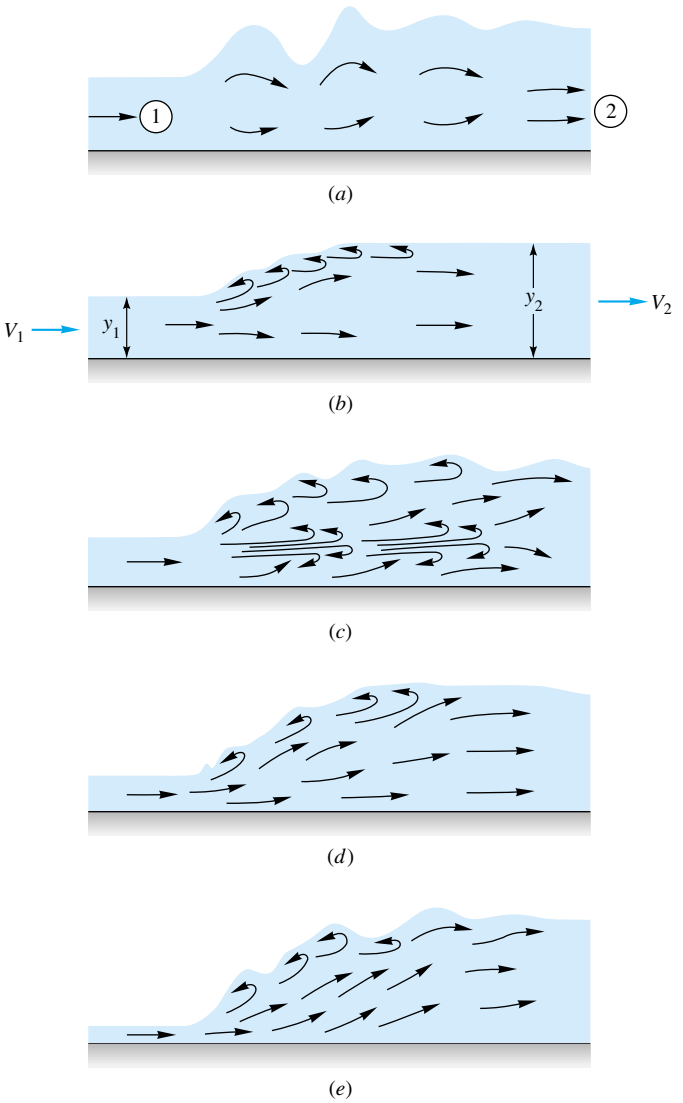


Fig. 10.12 Classification of hydraulic jumps: (*a*) Fr = 1.0 to 1.7: undular jumps; (*b*) Fr = 1.7 to 2.5: weak jump; (*c*) Fr = 2.5 to 4.5: oscillating jump; (*d*) Fr = 4.5 to 9.0: steady jump; (*e*) Fr > 9.0: strong jump. *(Adapted from Ref. 16.)*



ketabline.com Ebook.ketabline.com

$Fr_1 = 2.5$ to 4.5:	Unstable, *oscillating jump*; each irregular pulsation creates a large wave which can travel downstream for miles, damaging earth banks and other structures. Not recommended for design conditions. Dissipation 15 to 45 percent.
$Fr_1 = 4.5$ to 9.0:	Stable, well-balanced, *steady jump*; best performance and action, insensitive to downstream conditions. Best design range. Dissipation 45 to 70 percent.
$Fr_1 > 9.0$:	Rough, somewhat intermittent *strong jump*, but good performance. Dissipation 70 to 85 percent.

Further details can be found in Ref. 16 and Ref. 3, chap. 15.

Theory for a Horizontal Jump

A jump which occurs on a steep channel slope can be affected by the difference in water-weight components along the flow. The effect is small, however, so that the classic theory assumes that the jump occurs on a horizontal bottom.

You will be pleased to know that we have already analyzed this problem in Sec. 10.1. A hydraulic jump is exactly equivalent to the strong fixed wave in Fig. 10.4*b*, where the change in depth δy is not neglected. If V_1 and y_1 upstream are known, V_2 and y_2 are computed by applying continuity and momentum across the wave, as in Eqs. (10.7) and (10.8). Equation (10.9) is therefore the correct solution for a jump if we interpret C and y in Fig. 10.4*b* as upstream conditions V_1 and y_1, with $C - \delta V$ and $y + \delta y$ being the downstream conditions V_2 and y_2, as in Fig. 10.12*b*. Equation (10.9) becomes

$$V_1^2 = \tfrac{1}{2} g y_1 \eta(\eta + 1) \tag{10.42}$$

where $\eta = y_2/y_1$. Introducing the Froude number $Fr_1 = V_1/(gy_1)^{1/2}$ and solving this quadratic equation for η, we obtain

$$\frac{2y_2}{y_1} = -1 + (1 + 8\,Fr_1^2)^{1/2} \tag{10.43}$$

With y_2 thus known, V_2 follows from the wide-channel continuity relation

$$V_2 = \frac{V_1 y_1}{y_2} \tag{10.44}$$

Finally, we can evaluate the dissipation head loss across the jump from the steady-flow energy equation

$$h_f = E_1 - E_2 = \left(y_1 + \frac{V_1^2}{2g}\right) - \left(y_2 + \frac{V_2^2}{2g}\right)$$

Introducing y_2 and V_2 from Eqs. (10.43) and (10.44), we find after considerable algebraic manipulation that

$$h_f = \frac{(y_2 - y_1)^3}{4y_1 y_2} \tag{10.45}$$

Equation (10.45) shows that the dissipation loss is positive only if $y_2 > y_1$, wh requirement of the second law of thermodynamics. Equation (10.43) then requ



ketabline.com Ebook.ketabline.com

$\text{Fr}_1 > 1.0$; that is, the upstream flow must be supercritical. Finally, Eq. (10.44) shows that $V_2 < V_1$ and the downstream flow is subcritical. All these results agree with our previous experience analyzing the normal-shock wave.

The present theory is for hydraulic jumps in wide horizontal channels. For the theory of prismatic or sloping channels see advanced texts [for example, 3, chaps. 15 and 16].

EXAMPLE 10.7

Water flows in a wide channel at $q = 10\ \text{m}^3/(\text{s} \cdot \text{m})$ and $y_1 = 1.25$ m. If the flow undergoes a hydraulic jump, compute (*a*) y_2, (*b*) V_2, (*c*) Fr_2, (*d*) h_f, (*e*) the percentage dissipation, (*f*) the power dissipated per unit width, and (*g*) the temperature rise due to dissipation if $c_p = 4200\ \text{J/(kg} \cdot \text{K)}$.

Solution

Part (a) The upstream velocity is

$$V_1 = \frac{q}{y_1} = \frac{10\ \text{m}^3/(\text{s} \cdot \text{m})}{1.25\ \text{m}} = 8.0\ \text{m/s}$$

The upstream Froude number is therefore

$$\text{Fr}_1 = \frac{V_1}{(gy_1)^{1/2}} = \frac{8.0}{[9.81(1.25)]^{1/2}} = 2.285$$

From Fig. 10.12 this is a weak jump. The depth y_2 is obtained from Eq. (10.43):

$$\frac{2y_2}{y_1} = -1 + [1 + 8(2.285)^2]^{1/2} = 5.54$$

or

$$y_2 = \tfrac{1}{2}y_1(5.54) = \tfrac{1}{2}(1.25)(5.54) = 3.46\ \text{m} \qquad \textit{Ans. (a)}$$

Part (b) From Eq. (10.44) the downstream velocity is

$$V_2 = \frac{V_1 y_1}{y_2} = \frac{8.0(1.25)}{3.46} = 2.89\ \text{m/s} \qquad \textit{Ans. (b)}$$

Part (c) The downstream Froude number is

$$\text{Fr}_2 = \frac{V_2}{(gy_2)^{1/2}} = \frac{2.89}{[9.81(3.46)]^{1/2}} = 0.496 \qquad \textit{Ans. (c)}$$

Part (d) As expected, Fr_2 is subcritical. From Eq. (10.45) the dissipation loss is

$$h_f = \frac{(3.46 - 1.25)^3}{4(3.46)(1.25)} = 0.625\ \text{m} \qquad \textit{Ans. (d)}$$

Part (e) The percentage dissipation relates h_f to upstream energy

$$E_1 = y_1 + \frac{V_1^2}{2g} = 1.25 + \frac{(8.0)^2}{2(9.81)} = 4.51\ \text{m}$$

Hence

$$\text{Percentage loss} = (100)\frac{h_f}{E_1} = \frac{100(0.625)}{4.51} = 14\ \text{percen}$$



ketabline.com Ebook.ketabline.com

Part (f) The power dissipated per unit width is

$$\text{Power} = \rho g q h_f = (9800\ \text{N/m}^3)[10\ \text{m}^3/(\text{s}\cdot\text{m})](0.625\ \text{m})$$

$$= 61.3\ \text{kW/m} \qquad \textit{Ans. (f)}$$

Part (g) Finally the mass flow rate is $\dot{m} = \rho q = (1000\ \text{kg/m}^3)[10\ \text{m}^3/(\text{s}\cdot\text{m})] = 10{,}000\ \text{kg/(s}\cdot\text{m})$, and the temperature rise from the steady-flow energy equation is

$$\text{Power dissipated} = \dot{m} c_p\, \Delta T$$

or

$$61{,}300\ \text{W/m} = [10{,}000\ \text{kg/(s}\cdot\text{m})][4200\ \text{J/(kg}\cdot\text{K})]\ \Delta T$$

from which

$$\Delta T = 0.0015\ \text{K} \qquad \textit{Ans. (g)}$$

The dissipation is large, but the temperature rise is negligible.

10.6 Gradually Varied Flow[3]

In practical channel flows both the bottom slope and the water depth change with position, as in Fig. 10.3. An approximate analysis is possible if the flow is gradually varied, e.g., if the slopes are small and changes not too sudden. The basic assumptions are

1. Slowly changing bottom slope
2. Slowly changing water depth (no hydraulic jumps)
3. Slowly changing cross section
4. One-dimensional velocity distribution
5. Pressure distribution approximately hydrostatic

The flow then satisfies the continuity relation (10.1) plus the energy equation with bottom friction losses included. The two unknowns for steady flow are velocity $V(x)$ and water depth $y(x)$, where x is distance along the channel.

Basic Differential Equation

Consider the length of channel dx illustrated in Fig. 10.13. All the terms which enter the steady-flow energy equation are shown, and the balance between x and $x + dx$ is

$$\frac{V^2}{2g} + y + S_0\, dx = S\, dx + \frac{V^2}{2g} + d\left(\frac{V^2}{2g}\right) + y + dy$$

or

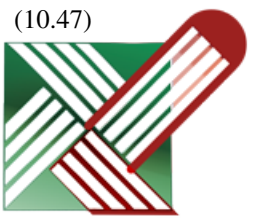
$$\frac{dy}{dx} + \frac{d}{dx}\left(\frac{V^2}{2g}\right) = S_0 - S \tag{10.46}$$

where S_0 is the slope of the channel bottom (positive as shown in Fig. 10.13) and S is the slope of the EGL (which drops due to wall friction losses).

To eliminate the velocity derivative, differentiate the continuity relation

$$\frac{dQ}{dx} = 0 = A\frac{dV}{dx} + V\frac{dA}{dx} \tag{10.47}$$

[3]This section may be omitted without loss of continuity.



ketabline.com Ebook.ketabline.com

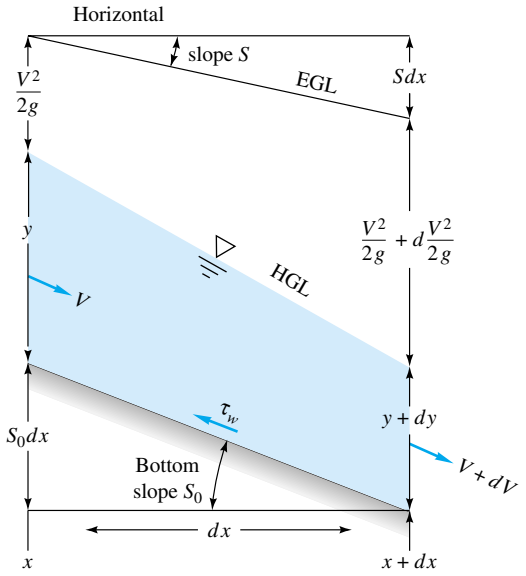


Fig. 10.13 Energy balance between two sections in a gradually varied open-channel flow.

But $dA = b_0\,dy$, where b_0 is the channel width at the surface. Eliminating dV/dx between Eqs. (10.46) and (10.47), we obtain

$$\frac{dy}{dx}\left(1 - \frac{V^2 b_0}{gA}\right) = S_0 - S \tag{10.48}$$

Finally, recall from Eq. (10.37) that $V^2 b_0/(gA)$ is the square of the Froude number of the local channel flow. The final desired form of the gradually varied flow equation is

$$\frac{dy}{dx} = \frac{S_0 - S}{1 - \mathrm{Fr}^2} \tag{10.49}$$

This equation changes sign according as the Froude number is subcritical or supercritical and is analogous to the one-dimensional gas-dynamic area-change formula (9.40).

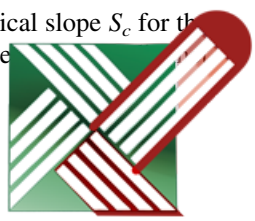
The numerator of Eq. (10.49) changes sign according as S_0 is greater or less than S, which is the slope equivalent to uniform flow at the same discharge Q

$$S = S_{0n} = \frac{f}{D_h}\frac{V^2}{2g} = \frac{V^2}{R_h C^2} = \frac{n^2 V^2}{\alpha^2 R_h^{4/3}} \tag{10.50}$$

where C is the Chézy coefficient. The behavior of Eq. (10.49) thus depends upon the relative magnitude of the local bottom slope $S_0(x)$, compared with (1) uniform flow, $y = y_n$, and (2) critical flow, $y = y_c$. As in Eq. (10.38), the dimensional parameter α^2 equals 1.0 for SI units and 2.208 for BG units.

Classification of Solutions

It is customary to compare the actual channel slope S_0 with the critical slope S_c for the same Q from Eq. (10.38). There are five classes for S_0, giving rise to three types of solution curves, all of which are illustrated in Fig. 10.14:



ketabline.com Ebook.ketabline.com

Slope class	Slope notation	Depth class	Solution curves
$S_0 > S_c$	Steep	$y_c > y_n$	S-1, S-2, S-3
$S_0 = S_c$	Critical	$y_c = y_n$	C-1, C-3
$S_0 < S_c$	Mild	$y_c < y_n$	M-1, M-2, M-3
$S_0 = 0$	Horizontal	$y_n = \infty$	H-2, H-3
$S_0 < 0$	Adverse	y_n = imaginary	A-2, A-3

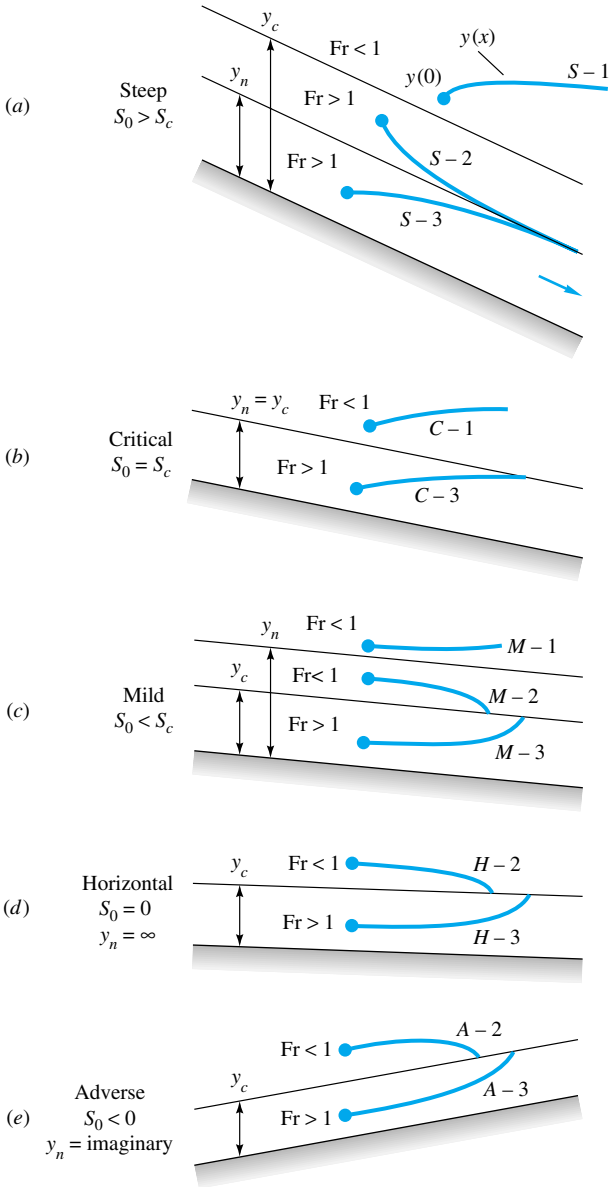


Fig. 10.14 Gradually varied flow for five classes of channel slope, showing the twelve basic solution curves.



ketabline.com Ebook.ketabline.com

The solution letters S, C, M, H, and A obviously denote the names of the five types of slope. The numbers 1, 2, 3 relate to the position of the initial point on the solution curve with respect to the normal depth y_n and the critical depth y_c. In type 1 solutions, the initial point is above both y_n and y_c, and in all cases the water-depth solution $y(x)$ becomes even deeper and farther away from y_n and y_c. In type 2 solutions, the initial point lies between y_n and y_c, and if there is no change in S_0 or roughness, the solution tends asymptotically toward the lower of y_n or y_c. In type 3 cases, the initial point lies below both y_n and y_c, and the solution curve tends asymptotically toward the lower of these.

Figure 10.14 shows the basic character of the local solutions, but in practice, of course, S_0 varies with x and the overall solution patches together the various cases to form a continuous depth profile $y(x)$ compatible with a given initial condition and a given discharge Q. There is a fine discussion of various composite solutions in Ref. 3, chap. 9; see also Ref. 18, sec. 12.7.

Numerical Solution

The basic relation for gradually varied flow, Eq. (10.49), is a first-order ordinary differential equation which can be easily solved numerically. For a given constant-volume flow rate Q, it may be written in the form

$$\frac{dy}{dx} = \frac{S_0 - n^2Q^2/(\alpha^2A^2R_h^{4/3})}{1 - Q^2b_0/(gA^3)} \tag{10.51}$$

subject to an initial condition $y = y_0$ at $x = x_0$. It is assumed that the bottom slope $S_0(x)$ and the cross-sectional shape parameters (b_0, P, A) are known everywhere along the channel. Then one may solve Eq. (10.51) for local water depth $y(x)$ by any standard numerical method. The author uses an Excel spreadsheet for a personal computer. Step sizes Δx may be selected so that each change Δy is limited to no greater than, say, 1 percent. The solution curves are generally well behaved unless there are discontinuous changes in channel parameters. Note that if one approaches the critical depth y_c, the denominator of Eq. (10.51) approaches zero, so small step sizes are required. It helps physically to know what type solution curve (M-1, S-2, etc.) you are proceeding along, but this is not mathematically necessary.

EXAMPLE 10.8

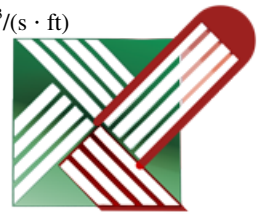
Let us extend the data of Example 10.4 to compute a portion of the profile shape. Given is a wide channel with $n = 0.022$, $S_0 = 0.0048$, and $q = 50\ \text{ft}^3/(\text{s} \cdot \text{ft})$. If $y_0 = 3$ ft at $x = 0$, how far along the channel $x = L$ does it take the depth to rise to $y_L = 4$ ft? Is the 4-ft depth position upstream or downstream in Fig. E10.8*a*?

Solution

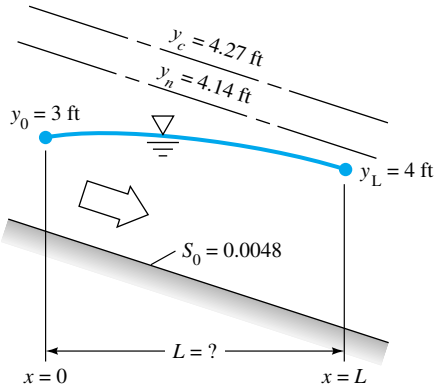
In Example 10.4 we computed $y_c = 4.27$ ft. Since our initial depth $y = 3$ ft is less than y_c, we know the flow is supercritical. Let us also compute the normal depth for the given slope S_0 by setting $q = 50\ \text{ft}^3/(\text{s} \cdot \text{ft})$ in the Chézy formula (10.19) with $R_h = y_n$:

$$q = \frac{\alpha}{n} AR_h^{2/3}S_0^{1/2} = \frac{1.486}{0.022}\,[y_n(1\ \text{ft})]y_n^{2/3}(0.0048)^{1/2} = 50\ \text{ft}^3/(\text{s} \cdot \text{ft})$$

Solve for: $y_n \approx 4.14$ ft



ketabline.com Ebook.ketabline.com



E10.8a

Thus both $y(0) = 3$ ft and $y(L) = 4$ ft are less than y_n, which is less than y_c, so we *must* be on an S-3 curve, as in Fig. 10.14*a*. For a wide channel, Eq. (10.51) reduces to

$$\frac{dy}{dx} = \frac{S_0 - n^2q^2/(\alpha^2 y^{10/3})}{1 - q^2/(gy^3)}$$

$$\approx \frac{0.0048 - (0.022)^2(50)^2/(2.208y^{10/3})}{1 - (50)^2/(32.2y^3)} \qquad \text{with } y(0) = 3 \text{ ft}$$

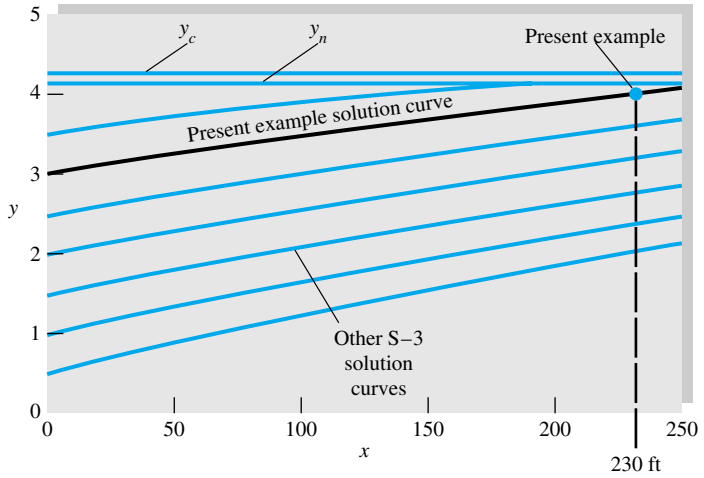
The initial slope is $y'(0) \approx 0.00494$, and a step size $\Delta x = 5$ ft would cause a change $\Delta y \approx (0.00494)(5 \text{ ft}) \approx 0.025$ ft, less than 1 percent. We therefore integrate numerically with $\Delta x = 5$ ft to determine when the depth $y = 4$ ft is achieved. Tabulate some values:

x, ft	0	50	100	150	200	230
y, ft	3.00	3.25	3.48	3.70	3.90	4.00

The water depth, still supercritical, reaches $y = 4$ ft at

$$x \approx 230 \text{ ft downstream} \qquad \textit{Ans.}$$

We verify from Fig. 10.14*a* that water depth does increase downstream on an S-3 curve. The solution curve $y(x)$ is shown as the bold line in Fig. E10.8*b*.



E10.8b



ketabline.com Ebook.ketabline.com

For little extra effort we can investigate the entire family of S-3 solution curves for this problem. Figure E10.8*b* also shows what happens if the initial depth is varied from 0.5 to 3.5 ft in increments of 0.5 ft. All S-3 solutions smoothly rise and asymptotically approach the uniform-flow condition $y = y_n = 4.14$ ft.

Some Illustrative Composite-Flow Profiles

The solution curves in Fig. 10.14 are somewhat simplistic, since they postulate constant bottom slopes. In practice, channel slopes can vary greatly, $S_0 = S_0(x)$, and the solution curves can cross between two regimes. Other parameter changes, such as $A(x)$, $b_0(x)$, and $n(x)$, can cause interesting composite-flow profiles. Some examples are shown in Fig. 10.15.

Figure 10.15*a* shows a change from a mild slope to a steep slope in a constant-width channel. The initial M-2 curve must change to an S-2 curve farther down the steep slope. The only way this can happen physically is for the solution curve to pass smoothly through the critical depth, as shown. The critical point is mathematically *singular* [3, sec. 9.6], and the flow near this point is generally *rapidly,* not gradually, varied. The flow pattern, accelerating from subcritical to supercritical, is similar to a converging-diverging nozzle in gas dynamics. Other scenarios for Fig. 10.15*a* are impossible. For example, the upstream curve cannot be M-1, for the break in slope would cause an S-1 curve which would move away from uniform steep flow.

Figure 10.15*b* shows a mild slope which becomes even milder. The water depth moves smoothly along an M-1 curve to the new (higher) uniform flow. There is no singular point, so gradually varied theory is adequate.

Figure 10.15*c* illustrates a steep slope which becomes less steep. The depth will change smoothly along an S-3 curve to approach the new (higher) uniform flow. There is no singular point. Compare with Fig. 10.15*b*.

Figure 10.15*d* shows a steep slope which changes to mild. It is generally impossible to revert back smoothly from supercritical to subcritical flow without dissipation. A hydraulic jump will form whose position depends upon downstream conditions. Two cases are illustrated: (1) a jump to an S-1 curve to reach a high downstream normal depth and (2) a change to an M-3 curve and then a jump to a lower downstream depth.

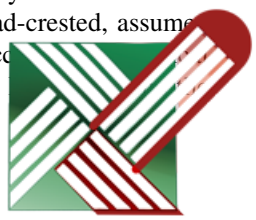
Figure 10.15*e* illustrates a *free overfall* with a mild slope. This acts as a *control section* to the upstream flow, which then forms an M-2 curve and accelerates to critical flow near the overfall. The falling stream will be supercritical. The overfall "controls" the water depths upstream and can serve as an initial condition for computation of $y(x)$. This is the type of flow which occurs in a weir or waterfall, Sec. 10.7.

The examples in Fig. 10.15 show that changing conditions in open-channel flow can result in complex flow patterns. Many more examples of composite-flow profiles are given in Refs. 1, 3, and 18.

10.7 Flow Measurement and Control by Weirs

A *weir,* of which the ordinary dam is an example, is a channel obstruction over which the flow must deflect. For simple geometries the channel discharge Q correlates with gravity and with the blockage height H to which the upstream flow is backed up above the weir elevation (see Fig. 10.16). Thus a weir is a simple but effective open-channel flowmeter. We used a weir as an example of dimensional analysis in Prob. 5.32.

Figure 10.16 shows two common weirs, sharp-crested and broad-crested, assume to be very wide. In both cases the flow upstream is subcritical, acc near the top of the weir, and spills over into a supercritical *nappe*.



ketabline.com Ebook.ketabline.com

discharge q per unit width is proportional to $g^{1/2}H^{3/2}$ but with somewhat different coefficients. The short-crested (or thin-plate) weir nappe should be *ventilated* to the atmosphere; i.e., it should spring clear of the weir crest. Unventilated or drowned nappes are more difficult to correlate and depend upon tailwater conditions. (The spillway of Fig. 10.11 is a sort of unventilated weir.)

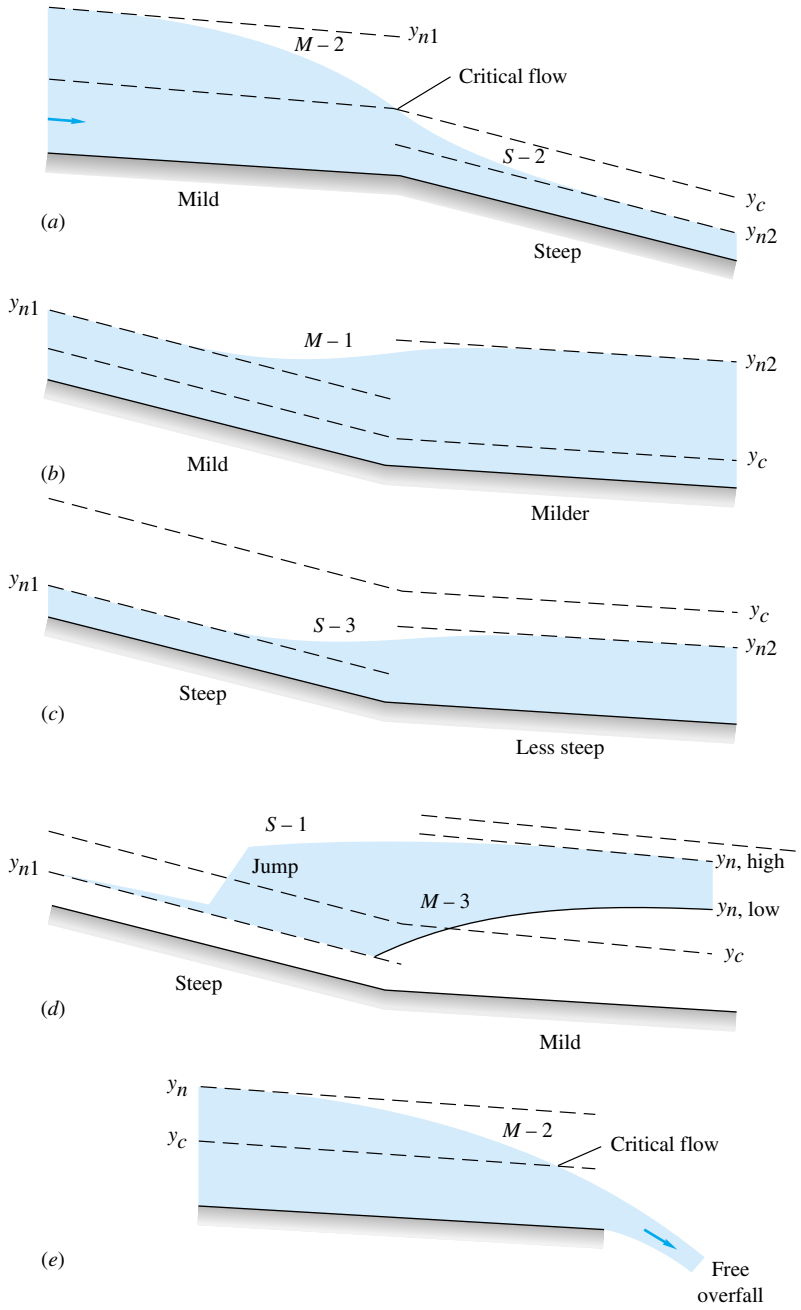
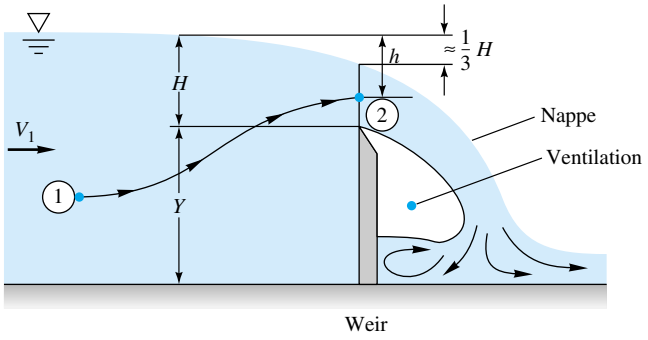
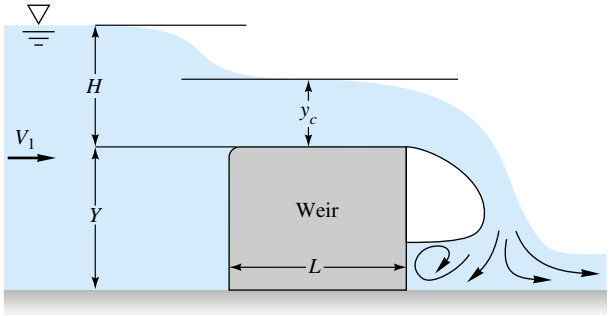


Fig. 10.15 Some examples of composite-flow profiles.

ketabline.com Ebook.ketabline.com



(*a*)



(*b*)

Fig. 10.16 Flow over wide, well-ventilated weirs: (*a*) sharp-crested; (*b*) broad-crested.

A very complete discussion of weirs, including other designs such as the polygonal "Crump" weir and various contracting flumes, is given in the text by Ackers et al. [19]. See Prob. 10.122.

Analysis of Sharp-Crested Weirs

It is possible to analyze weir flow by inviscid potential theory with an unknown (but solvable) free surface, as in Fig. P8.71. Here, however, we simply use one-dimensional-flow theory plus dimensional analysis to develop suitable weir flow-rate correlations.

A very early theoretical approach is credited to J. Weisbach in 1855. The velocity head at any point 2 above the weir crest is assumed to equal the total head upstream; i.e., Bernoulli's equation is used with no losses:

$$\frac{V_2^2}{2g} + H - h \approx \frac{V_1^2}{2g} + H \qquad \text{or} \qquad V_2(h) \approx \sqrt{2gh + V_1^2}$$

where h is the vertical distance down to point 2, as shown in Fig. 10.16*a*. If we accept for the moment, without proof, that the flow over the crest draws down to $h_{\min} \approx H/3$, the volume flow $q = Q/b$ over the crest is approximately

$$q = \int_{\text{crest}} V_2\, dh \approx \int_{H/3}^{H} (2gh + V_1^2)^{1/2}\, dh$$

$$= \frac{2}{3}\sqrt{2g}\left[\left(H + \frac{V_1^2}{2g}\right)^{3/2} - \left(\frac{H}{3} + \frac{V_1^2}{2g}\right)^{3/2}\right]$$



ketabline.com Ebook.ketabline.com

Normally the upstream velocity head $V_1^2/(2g)$ is neglected, so this expression reduces to

Sharp-crested theory: $$q \approx 0.81(\tfrac{2}{3})(2g)^{1/2}H^{3/2} \tag{10.53}$$

This formula is functionally correct, but the coefficient 0.81 is too high and should be replaced by an experimentally determined discharge coefficient.

Analysis of Broad-Crested Weirs

The broad-crested weir of Fig. 10.16*b* can be analyzed more accurately because it creates a short run of nearly one-dimensional critical flow, as shown. Bernoulli's equation from upstream to the weir crest yields

$$\frac{V_1^2}{2g} + Y + H \approx \frac{V_c^2}{2g} + Y + y_c$$

If the crest is very wide into the paper, $V_c^2 = gy_c$ from Eq. (10.33). Thus we can solve for

$$y_c \approx \frac{2H}{3} + \frac{V_1^2}{3g} \approx \frac{2H}{3}$$

This result was used without proof to derive Eq. (10.53). Finally, the flow rate follows from wide-channel critical flow, Eq. (10.32):

Broad-crested theory: $$q = \sqrt{gy_c^3} \approx \frac{1}{\sqrt{3}}\left(\frac{2}{3}\right)\sqrt{2g}\left(H + \frac{V_1^2}{2g}\right)^{3/2} \tag{10.54}$$

Again we may usually neglect the upstream velocity head $V_1^2/(2g)$. The coefficient $1/\sqrt{3} \approx 0.577$ is about right, but experimental data are preferred.

Experimental Weir Discharge Coefficients

Theoretical weir-flow formulas may be modified experimentally as follows. Eliminate the numerical coefficients $\frac{2}{3}$ and $\sqrt{2}$, for which there is much sentimental attachment in the literature, and reduce the formula to

$$Q_{\text{weir}} = C_d b\sqrt{g}\left(H + \frac{V_1^2}{2g}\right)^{3/2} \approx C_d b\sqrt{g}H^{3/2} \tag{10.55}$$

where b is the crest width and C_d is a dimensionless, experimentally determined *weir discharge coefficient* which may vary with the weir geometry, Reynolds number, and Weber number. Many data for many different weirs have been reported in the literature, as detailed in Ref. 19.

An accurate (± 2 percent) composite correlation for wide ventilated sharp crests is recommended as follows [19]:

Wide sharp-crested weir: $$C_d \approx 0.564 + 0.0846\frac{H}{Y} \qquad \text{for} \qquad \frac{H}{Y} \leq 2 \tag{10.56}$$

The Reynolds numbers V_1H/ν for these data varied from 1 E4 to 2 E6, but the formula should apply to higher Re, such as large dams on rivers.

The broad-crested weir of Fig. 10.16*b* is considerably more sensitive to geometric parameters, including the surface roughness ϵ of the crest. If the leading-edge nose is rounded, $R/L \geq 0.05$, available data [19, chap. 7] may be correlated as follows:

Round-nosed broad-crested weir: $$C_d \approx 0.544\left(1 - \frac{\delta^*/L}{H/L}\right)^{3/2}$$



ketabline.com Ebook.ketabline.com

where $$\frac{\delta^*}{L} \approx 0.001 + 0.2\sqrt{\epsilon/L}$$

The chief effect is due to turbulent boundary-layer displacement-thickness growth δ^* on the crest as compared to upstream head H. The formula is limited to $H/L < 0.7$, $\epsilon/L \leq 0.002$, and $V_1 H/\nu > 3$ E5. If the nose is round, there is no significant effect of weir height Y, at least if $H/Y < 2.4$.

If the broad-crested weir has a sharp leading edge, thus commonly called a *rectangular* weir, the discharge may depend upon the weir height Y. However, in a certain range of weir height and length, C_d is nearly constant:

Sharp-nosed broad-crested weir:
$$C_d \approx 0.462 \quad \text{for} \quad 0.08 < \frac{H}{L} < 0.33 \quad 0.22 < \frac{H}{Y} < 0.56 \tag{10.58}$$

Surface roughness is not a significant factor here. For $H/L < 0.08$ there is large scatter (± 10 percent) in the data. For $H/L > 0.33$ and $H/Y > 0.56$, C_d increases up to 10 percent due to each parameter, and complex charts are needed for the discharge coefficient [19, chap. 6].

EXAMPLE 10.9

A weir in a horizontal channel is 1 m high and 4 m wide. The water depth upstream is 1.6 m. Estimate the discharge if the weir is (*a*) sharp-crested and (*b*) round-nosed with an unfinished cement broad crest 1.2 m long. Neglect $V_1^2/(2g)$.

Solution

Part (a) We are given $Y = 1$ m and $H + Y \approx 1.6$ m, hence $H \approx 0.6$ m. Since $H \ll b$, we assume that the weir is "wide." For a sharp crest, Eq. (10.56) applies:

$$C_d \approx 0.564 + 0.0846 \frac{0.6 \text{ m}}{1 \text{ m}} \approx 0.615$$

Then the discharge is given by the basic correlation, Eq. (10.55):

$$Q = C_d b \sqrt{g} H^{3/2} = (0.615)(4 \text{ m})\sqrt{(9.81 \text{ m/s}^2)}(0.6 \text{ m})^{3/2} \approx 3.58 \text{ m}^3/\text{s} \qquad \textit{Ans. (a)}$$

We check that $H/Y = 0.6 < 2.0$ for Eq. (10.56) to be valid. From continuity, $V_1 = Q/(by_1) = 3.58/[(4.0)(1.6)] = 0.56$ m/s, giving a Reynolds number $V_1 H/\nu \approx 3.4$ E5.

Part (b) For a round-nosed broad-crested weir, Eq. (10.57) applies. For an unfinished cement surface, read $\epsilon \approx 2.4$ mm from Table 10.1. Then the displacement thickness is

$$\frac{\delta^*}{L} \approx 0.001 + 0.2\sqrt{\epsilon/L} = 0.001 + 0.2\left(\frac{0.0024 \text{ m}}{1.2 \text{ m}}\right)^{1/2} \approx 0.00994$$

Then Eq. (10.57) predicts the discharge coefficient:

$$C_d \approx 0.544\left(1 - \frac{0.00994}{0.6 \text{ m}/1.2 \text{ m}}\right)^{3/2} \approx 0.528$$



ketabline.com Ebook.ketabline.com

The estimated flow rate is thus

$$Q = C_d b\sqrt{g}H^{3/2} = 0.528(4\text{ m})\sqrt{(9.81\text{ m}^2/\text{s})}(0.6\text{ m})^{3/2} \approx 3.07\text{ m}^3/\text{s} \qquad \textit{Ans. (b)}$$

Check that $H/L = 0.5 < 0.7$ as required. The approach Reynolds number is $V_1 H/\nu \approx 2.9$ E5, just barely below the recommended limit in Eq. (10.57).

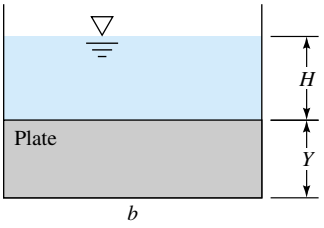
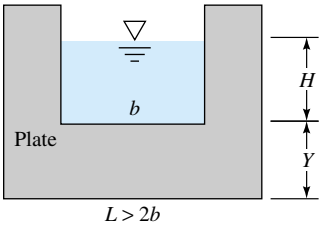
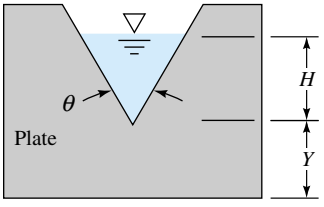
Since $V_1 \approx 0.5$ m/s, $V_1^2/(2g) \approx 0.012$ m, so the error in taking total head equal to 0.6 m is about 2 percent. We could correct this for upstream velocity head if desired.

Other Thin-Plate Weir Designs

Weirs are often used for flow measurement and control of artificial channels. The two most common shapes are a rectangle and a V notch, as shown in Table 10.2. All should be fully ventilated and not drowned.

Table 10.2*a* shows a full-width rectangle, which will have slight end-boundary-layer effects but no end contractions. For a thin-plate design, the top is approximately sharp-crested, and Eq. (10.56) should give adequate accuracy, as shown in the table. Since the overfall spans the entire channel, artificial ventilation may be needed, such as holes in the channel walls.

Table 10.2 Thin-Plate Weirs for Flow Measurement

Thin-plate weir	Flow-rate correlation
 (*a*) Full-width rectangle.	$Q \approx \left(0.564 + 0.0846\,\frac{H}{Y}\right) b g^{1/2} H^{3/2}$
 (*b*) Rectangle with side contractions.	$Q \approx 0.581(b - 0.1H) g^{1/2} H^{3/2} \qquad H < 0.5Y$
 (*c*) V notch.	$Q \approx 0.44 \tan\frac{\theta}{2}\, g^{1/2} H^{5/2} \qquad 20° < \theta < 100°$



ketabline.com Ebook.ketabline.com

Table 10.2*b* shows a partial-width rectangle, $b < L$, which will cause the sides of the overfall to contract inward and reduce the flow rate. An adequate contraction correction [19, 20] is to reduce the effective weir width by $0.1H$, as shown in the table. It seems, however, that this type of weir is rather sensitive to small effects, such as plate thickness and sidewall boundary-layer growth. Small heads ($H < 75$ mm) and small slot widths ($b < 30$ cm) are not recommended. See Refs. 19 and 20 for further details.

The V notch, in Table 10.2*c*, is intrinsically interesting in that its overfall has only one length scale, H—there is no separate "width." The discharge will thus be proportional to $H^{5/2}$, rather than a power of $\frac{3}{2}$. Application of Bernoulli's equation to the triangular opening, in the spirit of Eq. (10.52), leads to the following ideal flow rate for a V notch:

$$\text{V notch:} \qquad Q_{\text{ideal}} = \frac{8\sqrt{2}}{15} \tan\frac{\theta}{2}\, g^{1/2} H^{5/2} \tag{10.59}$$

where θ is the total included angle of the notch. The actual measured flow is about 40 percent less than this, due to contraction similar to a thin-plate orifice. In terms of an experimental discharge coefficient, the recommended formula is

$$Q_{\text{V notch}} \approx C_d \tan\frac{\theta}{2}\, g^{1/2} H^{5/2} \qquad C_d \approx 0.44 \qquad \text{for} \qquad 20^\circ < \theta < 100^\circ \tag{10.60}$$

for heads $H > 50$ mm. For smaller heads, both Reynolds-number and Weber-number effects may be important, and a recommended correction [19] is

$$\text{Low heads, } H < 50 \text{ mm:} \qquad C_{d,\,\text{V notch}} \approx 0.44 + \frac{0.9}{(\text{Re We})^{1/6}} \tag{10.61}$$

where $\text{Re} = \rho g^{1/2} H^{3/2}/\mu$ and $\text{We} = \rho g H^2/\Upsilon$, with Υ being the coefficient of surface tension. Liquids other than water may be used with this formula, as long as $\text{Re} > 300/\tan(\theta/2)^{3/4}$ and $\text{We} > 300$.

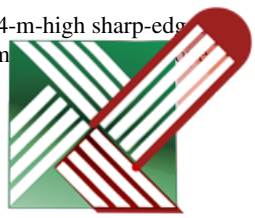
A number of other thin-plate weir designs—trapezoidal, parabolic, circular arc, and U-shaped—are discussed in Ref. 21, which also contains considerable data on broad-crested weirs.

Backwater Curves

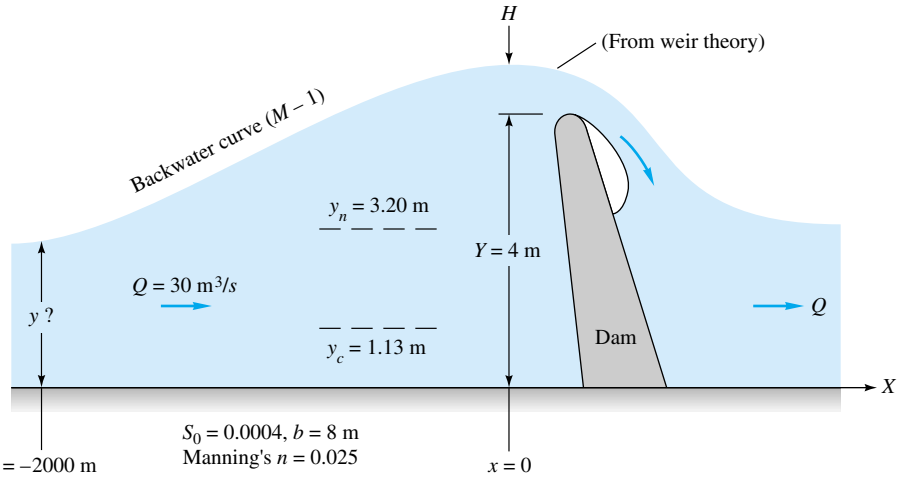
A weir is a flow barrier which not only alters the local flow over the weir but also modifies the flow-depth distribution far upstream. Any strong barrier in an open-channel flow creates a *backwater curve,* which can be computed by the gradually varied flow theory of Sec. 10.6. If Q is known, the weir formula, Eq. (10.55), determines H and hence the water depth just upstream of the weir, $y = H + Y$, where Y is the weir height. We then compute $y(x)$ upstream of the weir from Eq. (10.51), following in this case an M-1 curve (Fig. 10.14*c*). Such a barrier, where the water depth correlates with the flow rate, is called a channel *control point*. These are the starting points for numerical analysis of floodwater profiles in rivers as studied, e.g., by the U.S. Army Corps of Engineers [22].

EXAMPLE 10.10

A rectangular channel 8 m wide, with a flow rate of 30 m^3/s, encounters a 4-m-high sharp-edg
dam, as shown in Fig. E10.10*a*. Determine the water depth 2 km upstream
is $S_0 = 0.0004$ and $n = 0.025$.



ketabline.com Ebook.ketabline.com



E10.10a

Solution

First determine the head H produced by the dam, using sharp-crested full-width weir theory, Eq. (10.56):

$$Q = 30\ \text{m}^3/\text{s} = C_d b g^{1/2} H^{3/2} = \left(0.564 + 0.0846\,\frac{H}{4\ \text{m}}\right)(8\ \text{m})(9.81\ \text{m/s}^2)^{1/2} H^{3/2}$$

Since the term $0.0846H/4$ in parentheses is small, we may proceed by iteration or EES to the solution $H \approx 1.59$ m. Then our initial condition at $x = 0$, just upstream of the dam, is $y(0) = Y + H = 4 + 1.59 = 5.59$ m. Compare this to the critical depth from Eq. (10.30):

$$y_c = \left(\frac{Q^2}{b^2 g}\right)^{1/3} = \left[\frac{(30\ \text{m}^3/\text{s})^2}{(8\ \text{m})^2(9.81\ \text{m/s}^2)}\right]^{1/3} = 1.13\ \text{m}$$

Since $y(0)$ is greater than y_c, the flow upstream is subcritical. Finally, for reference purposes, estimate the normal depth from the Chézy equation (10.19):

$$Q = 30\ \text{m}^3/\text{s} = \frac{\alpha}{n} b y R_h^{2/3} S_0^{1/2} = \frac{1.0}{0.025}(8\ \text{m}) y_n \left(\frac{8y_n}{8 + 2y_n}\right)^{2/3} (0.0004)^{1/2}$$

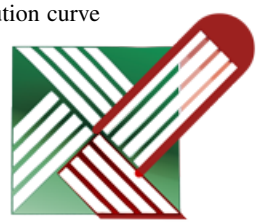
By trial and error or EES solve for $y_n \approx 3.20$ m. If there are no changes in channel width or slope, the water depth far upstream of the dam will approach this value. All these reference values $y(0)$, y_c, and y_n are shown in Fig. E10.10*b*.

Since $y(0) > y_n > y_c$, the solution will be an M-1 curve as computed from gradually varied theory, Eq. (10.51), for a rectangular channel with the given input data:

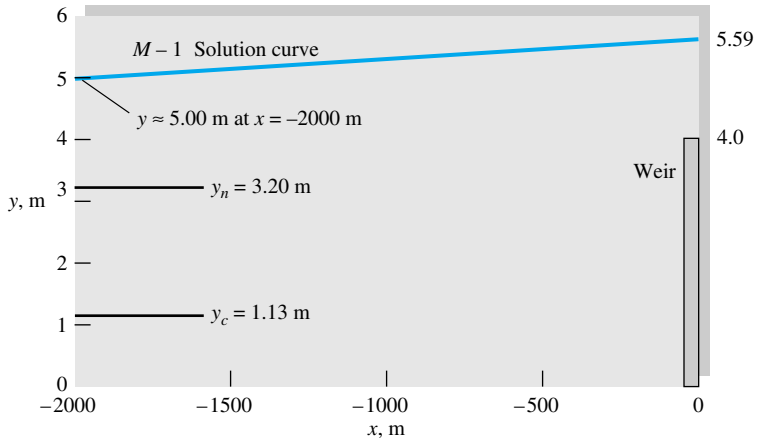
$$\frac{dy}{dx} \approx \frac{S_0 - n^2 Q^2/(\alpha^2 A^2 R_h^{4/3})}{1 - Q^2 b_0/(gA^3)} \qquad \alpha = 1.0 \qquad A = 8y \qquad n = 0.025 \qquad R_h = \frac{8y}{8 + 2y} \qquad b_0 = 8$$

Beginning with $y = 5.59$ m at $x = 0$, we integrate backward to $x = -2000$ m. For the Runge-Kutta method, four-figure accuracy is achieved for $\Delta x = -100$ m. The complete solution curve is shown in Fig. E10.10*b*. The desired solution value is

At $x = -2000$ m: $y \approx 5.00$ m



ketabline.com Ebook.ketabline.com



E10.10b

Thus, even 2 km upstream, the dam has produced a "backwater" which is 1.8 m above the normal depth which would occur without a dam. For this example, a near-normal depth of, say, 10 cm greater than y_n, or $y \approx 3.3$ m, would not be achieved until $x = -13{,}400$ m. Backwater curves are quite far-reaching upstream, especially in flood stages.

Summary

This chapter is an introduction to open-channel flow analysis, limited to steady, one-dimensional-flow conditions. The basic analysis combines the continuity equation with the extended Bernoulli equation including friction losses.

Open-channel flows are classified either by depth variation or by Froude number, the latter being analogous to the Mach number in compressible duct flow (Chap. 9). Flow at constant slope and depth is called uniform flow and satisfies the classical Chézy equation (10.19). Straight prismatic channels can be optimized to find the cross section which gives maximum flow rate with minimum friction losses. As the slope and flow velocity increase, the channel reaches a *critical* condition of Froude number unity, where velocity equals the speed of a small-amplitude surface wave in the channel. Every channel has a critical slope which varies with the flow rate and roughness. If the flow becomes supercritical (Fr $>$ 1), it may undergo a hydraulic jump to a greater depth and lower (subcritical) velocity, analogous to a normal-shock wave.

The analysis of gradually varied flow leads to a differential equation (10.51) which can be solved by numerical methods. The chapter ends with a discussion of the flow over a dam or weir, where the total flow rate can be correlated with upstream water depth.

Problems

Most of the problems herein are fairly straightforward. More difficult or open-ended assignments are labeled with an asterisk. Problems labeled with an EES icon will benefit from the use of the Engineering Equations Solver (EES), while problems labeled with a computer icon may require the use of a computer. The standard end-of-chapter problems 10.1 to 10.128 (categorized in the problem list below) are followed by word problems W10.1 to W10.13, fundamentals of engineering exam problems FE10.1 to FE10.[illegible], comprehensive problems C10.1 to C10.3, and D10.1 and D10.2.



ketabline.com Ebook.ketabline.com

Problem distribution

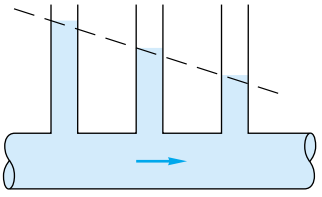
Section	Topic	Problems
10.1	Introduction: Froude number, wave speed	10.1–10.10
10.2	Uniform flow: The Chézy formula	10.11–10.36
10.3	Efficient uniform-flow channels	10.37–10.46
10.4	Specific energy: Critical depth	10.47–10.58
10.4	Flow over a bump	10.59–10.68
10.4	Sluice-gate flow	10.69–10.78
10.5	The hydraulic jump	10.79–10.96
10.6	Gradually varied flow	10.97–10.112
10.7	Weirs and flumes	10.113–10.123
10.7	Backwater curves	10.124–10.128

P10.1 The formula for shallow-water wave propagation speed, Eq. (10.9) or (10.10), is independent of the physical properties of the liquid, i.e., density, viscosity, or surface tension. Does this mean that waves propagate at the same speed in water, mercury, gasoline, and glycerin? Explain.

P10.2 A shallow-water wave 1 cm high propagates into still water of depth 1.1 m. Compute (*a*) the wave speed c and (*b*) the induced velocity δV.

P10.3 Narragansett Bay is approximately 21 (statute) mi long and has an average depth of 42 ft. Tidal charts for the area indicate a time delay of 30 min between high tide at the mouth of the bay (Newport, Rhode Island) and its head (Providence, Rhode Island). Is this delay correlated with the propagation of a shallow-water tidal-crest wave through the bay? Explain.

P10.4 The water-channel flow in Fig. P10.4 has a free surface in three places. Does it qualify as an open-channel flow? Explain. What does the dashed line represent?

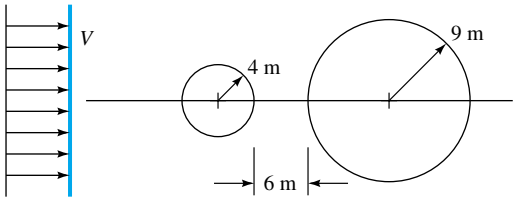


P10.4

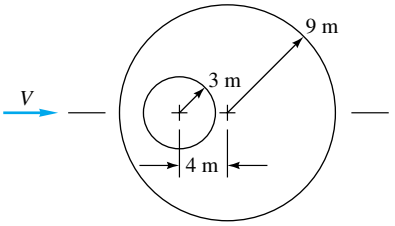
P10.5 Water flows rapidly in a channel 15 cm deep. Piercing the surface with a pencil point creates a wedgelike downstream wave of included angle 35°. Estimate the velocity V of the water.

P10.6 Pebbles dropped successively at the same point, into a water channel flow of depth 42 cm, create two circular ripples, as in Fig. P10.6. From this information estimate (*a*) the Froude number and (*b*) the stream velocity.

P10.7 Pebbles dropped successively at the same point, into a water channel flow of depth 65 cm, create two circular ripples, as in Fig. P10.7. From this information estimate (*a*) the Froude number and (*b*) the stream velocity.



P10.6



P10.7

P10.8 An earthquake near the Kenai Peninsula, Alaska, creates a single "tidal" wave (called a *tsunami*) which propagates south across the Pacific Ocean. If the average ocean depth is 4 km and seawater density is 1025 kg/m^3, estimate the time of arrival of this tsunami in Hilo, Hawaii.

P10.9 Equation (10.10) is for a single disturbance wave. For *periodic* small-amplitude surface waves of wavelength λ and period T, inviscid theory [5 to 9] predicts a wave propagation speed

$$c_0^2 = \frac{g\lambda}{2\pi}\tanh\frac{2\pi y}{\lambda}$$

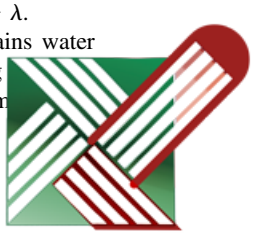
where y is the water depth and surface tension is neglected. (*a*) Determine if this expression is affected by the Reynolds number, Froude number, or Weber number. Derive the limiting values of this expression for (*b*) $y \ll \lambda$ and (*c*) $y \gg \lambda$. (*d*) Also for what ratio y/λ is the wave speed within 1 percent of limit (*c*)?

P10.10 If surface tension Υ is included in the analysis of Prob. 10.9, the resulting wave speed is [5 to 9]

$$c_0^2 = \left(\frac{g\lambda}{2\pi} + \frac{2\pi\Upsilon}{\rho\lambda}\right)\tanh\frac{2\pi y}{\lambda}$$

(*a*) Determine if this expression is affected by the Reynolds number, Froude number, or Weber number. Derive the limiting values of this expression for (*b*) $y \ll \lambda$ and (*c*) $y \gg \lambda$. (*d*) Finally determine the wavelength λ_{crit} for a minimum value of c_0, assuming that $y \gg \lambda$.

P10.11 A rectangular channel is 2 m wide and contains water 3 m deep. If the slope is 0.85° and the lining is galvanized metal, estimate the discharge for uniform



ketabline.com Ebook.ketabline.com

P10.12 (*a*) For laminar draining of a wide thin sheet of water on pavement sloped at angle θ, as in Fig. P4.36, show that the flow rate is given by

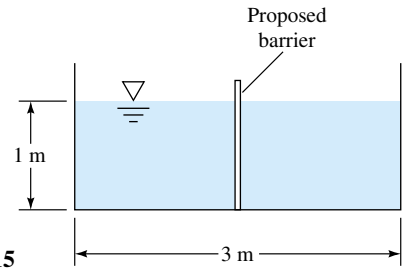
$$Q = \frac{\rho g b h^3 \sin\theta}{3\mu}$$

where b is the sheet width and h its depth. (*b*) By (somewhat laborious) comparison with Eq. (10.13), show that this expression is compatible with a friction factor $f = 24/\text{Re}$, where $\text{Re} = V_{av}h/\nu$.

P10.13 The laminar-draining flow from Prob. 10.12 may undergo transition to turbulence if $\text{Re} > 500$. If the pavement slope is 0.0045, what is the maximum sheet thickness, in mm, for which laminar flow is ensured?

P10.14 The Chézy formula (10.18) is independent of fluid density and viscosity. Does this mean that water, mercury, alcohol, and SAE 30 oil will all flow down a given open channel at the same rate? Explain.

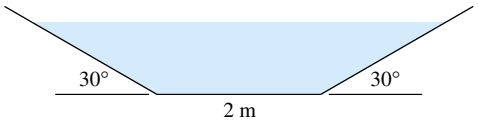
P10.15 The finished-concrete channel of Fig. P10.15 is designed for a flow rate of 6 m^3/s at a normal depth of 1 m. Determine (*a*) the design slope of the channel and (*b*) the percentage of reduction in flow if the surface is asphalt.



P10.15

P10.16 In Prob. 10.15, for finished concrete, determine the percentage of reduction in flow if the channel is divided in the center by the proposed barrier in Fig. P10.15. How does your estimate change if all surfaces are clay tile?

P10.17 The trapezoidal channel of Fig. P10.17 is made of brickwork and slopes at 1:500. Determine the flow rate if the normal depth is 80 cm.



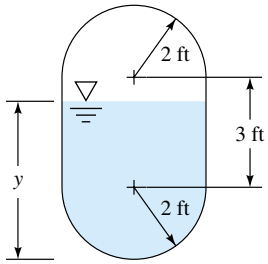
P10.17

P10.18 Modify Prob. 10.17 as follows. Determine the normal depth for which the flow rate will be 8 m^3/s.

P10.19 Modify Prob. 10.17 as follows. Let the surface be clean earth, which erodes if V exceeds 1.5 m/s. What is the maximum depth to avoid erosion?

P10.20 A circular corrugated-metal storm drain is flowing half full over a slope 4 ft/mi. Estimate the normal discharge if the drain diameter is 8 ft.

***P10.21** A sewer pipe has the shape of Fig. P10.21 and is constructed of unfinished concrete. The slope is 3 ft/mi. Plot the normal flow rate as a function of depth over the full range $0 < y < 7$ ft, and determine the maximum discharge and maximum velocity.



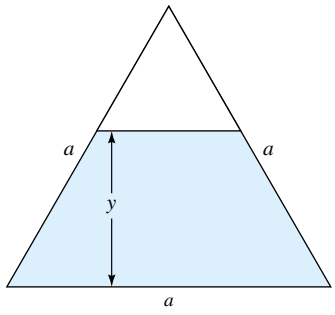
P10.21

P10.22 A trapezoidal aqueduct (Fig. 10.7) has $b = 5$ m and $\theta = 40°$ and carries a normal flow of 60 m^3/s of water when $y = 3.2$ m. For clay tile surfaces, estimate the required elevation drop in m/km.

P10.23 For the aqueduct of Prob. 10.22, if the slope is 0.0004 and the discharge is 40 m^3/s, use the Moody-chart formulation (10.15*a*) to estimate the normal depth.

P10.24 A riveted-steel channel slopes at 1:500 and has a V shape with an included angle of 80°. Find the normal depth if the flow rate is 900 m^3/h.

***P10.25** The equilateral-triangle channel in Fig. P10.25 has constant slope S_0 and constant Manning factor n. Find Q_{max} and V_{max}. Then, by analogy with Fig. 10.6*b*, plot the ratios Q/Q_{max} and V/V_{max} as a function of y/a for the complete range $0 < y/a < 0.866$.



P10.25

P10.26 Water flows in a 6-m-wide rectangular channel lined with rocks whose dominant size is 20 cm. The channel slope is 0.003. Assuming uniform flow and the rock-friction correlation of Eq. (10.15*b*), estimate (*a*) the depth if the flow rate is 2 m and (*b*) the depth

ketabline.com Ebook.ketabline.com

15 m^3/s. (*c*) In part (*a*) what is the equivalent value of Manning's roughness factor n for the same flow rate? Does your result agree with Table 10.1?

P10.27 A circular unfinished-cement water channel has a slope of 1:600 and a diameter of 5 ft. Estimate the normal discharge in gal/min for which the average wall shear stress is 0.15 lbf/ft^2, and compare your result to the maximum possible discharge for this channel.

P10.28 Show that, for any straight prismatic channel in uniform flow, the average wall shear stress is given by

$$\tau_{av} \approx \rho g R_h S_0$$

If you happen to spot this result early, you can use it in solving Prob. 10.27.

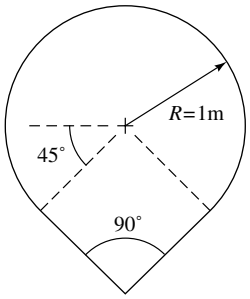
P10.29 Suppose that the trapezoidal channel of Fig. P10.17 contains sand and silt which we wish not to erode. According to an empirical correlation by A. Shields in 1936, the average wall shear stress τ_{crit} required to erode sand particles of diameter d_p is approximated by

$$\frac{\tau_{crit}}{(\rho_s - \rho)g\, d_p} \approx 0.5$$

where $\rho_s \approx 2400$ kg/m^3 is the density of sand. If the slope of the channel in Fig. P10.17 is 1:900 and $n \approx 0.014$, determine the maximum water depth to keep from eroding particles of 1-mm diameter.

P10.30 A clay tile V-shaped channel, with an included angle of 90°, is 1 km long and is laid out on a 1:400 slope. When running at a depth of 2 m, the upstream end is suddenly closed while the lower end continues to drain. Assuming quasi-steady normal discharge, find the time for the channel depth to drop to 20 cm.

P10.31 A storm drain has the cross section shown in Fig. P10.31 and is laid on a slope of 1.5 m/km. If it is constructed of brickwork, find the normal discharge when it is exactly half full of water.



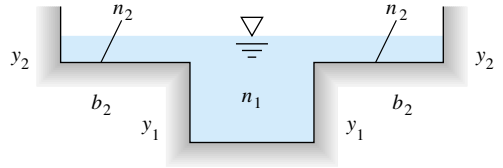
P10.31

P10.32 A 2-m-diameter clay tile sewer pipe runs half full on a slope of 0.25°. Compute the normal flow rate in gal/min.

P10.33 Five of the sewer pipes from Prob. 10.32 empty into a single asphalt pipe, also laid out at 0.25°. If the large pipe is also to run half full, what should be its diameter?

P10.34 A brick rectangular channel with $S_0 = 0.002$ is designed to carry 230 ft^3/s of water in uniform flow. There is an argument over whether the channel width should be 4 or 8 ft. Which design needs fewer bricks? By what percentage?

P10.35 In flood stage a natural channel often consists of a deep main channel plus two floodplains, as in Fig. P10.35. The floodplains are often shallow and rough. If the channel has the same slope everywhere, how would you analyze this situation for the discharge? Suppose that $y_1 = 20$ ft, $y_2 = 5$ ft, $b_1 = 40$ ft, $b_2 = 100$ ft, $n_1 = 0.020$, $n_2 = 0.040$, with a slope of 0.0002. Estimate the discharge in ft^3/s.



P10.35

P10.36 The Blackstone River in northern Rhode Island normally flows at about 25 m^3/s and resembles Fig. P10.35 with a clean-earth center channel, $b_1 \approx 20$ m and $y_1 \approx 3$ m. The bed slope is about 2 ft/mi. The sides are heavy brush with $b_2 \approx 150$ m. During hurricane Carol in 1955, a record flow rate of 1000 m^3/s was estimated. Use this information to estimate the maximum flood depth y_2 during this event.

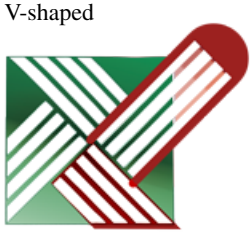
P10.37 The answer to Prob. 10.34 is that the 8-ft width is 29 percent more efficient than the 4-ft width and is almost optimum. Verify this result, using the "best-efficiency" concepts of Sec. 10.3.

P10.38 A rectangular channel has $b = 3$ m and $y = 1$ m. If n and S_0 are the same, what is the diameter of a semicircular channel that will have the same discharge? Compare the two wetted perimeters.

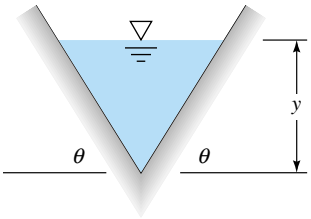
P10.39 A trapezoidal channel has $n = 0.022$ and $S_0 = 0.0003$ and is made in the shape of a half-hexagon for maximum efficiency. What should the length of the side of the hexagon be if the channel is to carry 225 ft^3/s of water? What is the discharge of a semicircular channel of the same cross-sectional area and the same S_0 and n?

P10.40 Using the geometry of Fig. 10.6*a*, prove that the most efficient circular open channel (maximum hydraulic radius for a given flow area) is a semicircle.

P10.41 Determine the most efficient value of θ for the V-shaped channel of Fig. P10.41.



ketabline.com Ebook.ketabline.com



P10.41

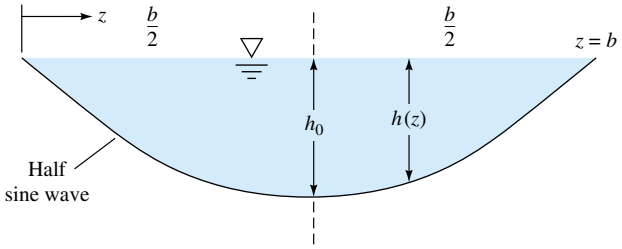
P10.42 Suppose that the side angles of the trapezoidal channel in Prob. 10.39 are reduced to 15° to avoid earth slides. If the bottom flat width is 8 ft, (*a*) determine the normal depth and (*b*) compare the resulting wetted perimeter with the solution $P = 24.1$ ft from Prob. 10.39. (Do not reveal this answer to friends still struggling with Prob. 10.39.)

P10.43 What are the most efficient dimensions for a riveted-steel rectangular channel to carry 4.8 m^3/s at a slope of 1:900?

P10.44 What are the most efficient dimensions for a half-hexagon cast-iron channel to carry 15,000 gal/min on a slope of 0.16°?

P10.45 What is the most efficient depth for an asphalt trapezoidal channel, with sides sloping at 45°, to carry 3 m^3/s on a slope of 0.0008?

P10.46 It is suggested that a channel which affords minimum erosion has a half-sine-wave shape, as in Fig. P10.46. The local depth takes the form $h(z) = h_0 \sin(\pi z/b)$. For uniform-flow conditions, determine the most efficient ratio h_0/b for this channel shape.



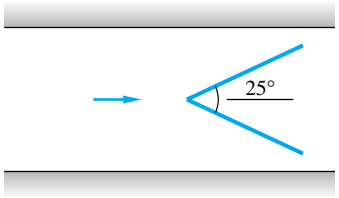
P10.46

P10.47 Replot Fig. 10.8*b* in the form of q versus y for constant E. Does the maximum q occur at the critical depth?

P10.48 A wide, clean-earth river has a flow rate $q = 150$ $ft^3/(s \cdot ft)$. What is the critical depth? If the actual depth is 12 ft, what is the Froude number of the river? Compute the critical slope by (*a*) Manning's formula and (*b*) the Moody chart.

P10.49 Find the critical depth of the brick channel in Prob. 10.34 for both the 4- and 8-ft widths. Are the normal flows sub- or supercritical?

P10.50 A pencil point piercing the surface of a rectangular channel flow creates a wedgelike 25° half-angle wave, as in Fig. P10.50. If the channel surface is painted steel and the depth is 35 cm, determine (*a*) the Froude number, (*b*) the critical depth, and (*c*) the critical slope for uniform flow.



P10.50

P10.51 Modify Prob. 10.50 as follows. Let the water be flowing in an unfinished-cement half-full circular channel of diameter 60 cm. Determine (*a*) the Froude number, (*b*) the flow velocity, and (*c*) the critical slope.

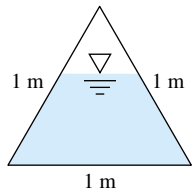
P10.52 Water flows full in an asphalt half-hexagon channel of bottom width W. The flow rate is 12 m^3/s. Estimate W if the Froude number is exactly 0.60.

P10.53 For the river flow of Prob. 10.48, find the depth y_2 which has the same specific energy as the given depth $y_1 = 12$ ft. These are called *conjugate depths*. What is Fr_2?

P10.54 A clay tile V-shaped channel has an included angle of 70° and carries 8.5 m^3/s. Compute (*a*) the critical depth, (*b*) the critical velocity, and (*c*) the critical slope for uniform flow.

P10.55 A trapezoidal channel resembles Fig. 10.7 with $b = 1$ m and $\theta = 50°$. The water depth is 2 m, and the flow rate is 32 m^3/s. If you stick your fingernail in the surface, as in Fig. P10.50, what half-angle wave might appear?

P10.56 A riveted-steel triangular duct flows partly full as in Fig. P10.56. If the critical depth is 50 cm, compute (*a*) the critical flow rate and (*b*) the critical slope.

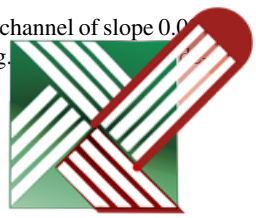


P10.56

P10.57 For the triangular duct of Prob. 10.56, if the critical flow rate is 1.0 m^3/s, compute (*a*) the critical depth and (*b*) the critical slope.

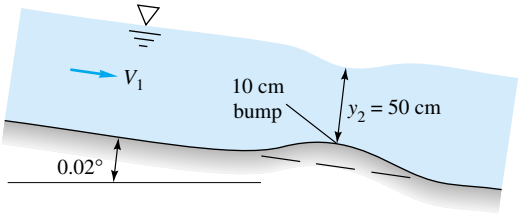
P10.58 A circular corrugated-metal channel is half full and in uniform flow at a slope $S_0 = 0.0037$. Estimate the Froude number of the flow.

P10.59 Uniform water flow in a wide brick channel of slope 0.0 moves over a 10-cm bump as in Fig.



ketabline.com Ebook.ketabline.com

pression in the water surface results. If the minimum water depth over the bump is 50 cm, compute (*a*) the velocity over the bump and (*b*) the flow rate per meter of width.



P10.59

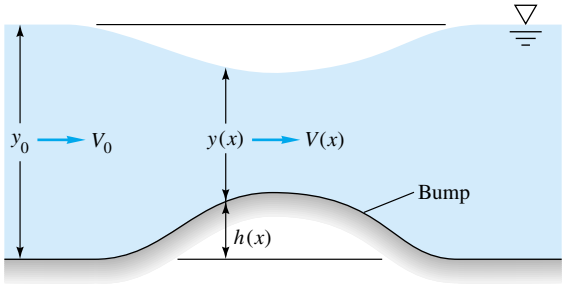
P10.60 Modify Prob. 10.59 as follows. Again assuming uniform subcritical approach flow (V_1, y_1), find (*a*) the flow rate and (*b*) y_2 for which the Froude number Fr_2 at the crest of the bump is exactly 0.8.

P10.61 Modify Prob. 10.59 as follows. Again assuming uniform subcritical approach flow (V_1, y_1), find (*a*) the flow rate and (*b*) y_2 for which the flow at the crest of the bump is exactly critical ($\text{Fr}_2 = 1.0$).

P10.62 Consider the flow in a wide channel over a bump, as in Fig. P10.62. One can estimate the water-depth change or *transition* with frictionless flow. Use continuity and the Bernoulli equation to show that

$$\frac{dy}{dx} = -\frac{dh/dx}{1 - V^2/(gy)}$$

Is the drawdown of the water surface realistic in Fig. P10.62? Explain under what conditions the surface might rise above its upstream position y_0.



P10.62

P10.63 In Fig. P10.62 let $V_0 = 1$ m/s and $y_0 = 1$ m. If the maximum bump height is 15 cm, estimate (*a*) the Froude number over the top of the bump and (*b*) the maximum depression in the water surface.

P10.64 In Fig. P10.62 let $V_0 = 1$ m/s and $y_0 = 1$ m. If the flow over the top of the bump is exactly critical ($\text{Fr} = 1.0$), determine the bump height $h_{\max}$.

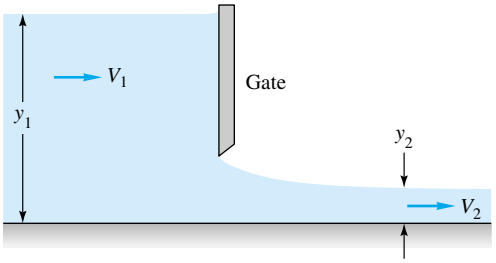
P10.65 Program and solve the differential equation of "frictionless flow over a bump," from Prob. 10.62, for entrance conditions $V_0 = 1$ m/s and $y_0 = 1$ m. Let the bump have the convenient shape $h = 0.5h_{\max}[1 - \cos(2\pi x/L)]$, which simulates Fig. P10.62. Let $L = 3$ m, and generate a numerical solution for $y(x)$ in the bump region $0 < x < L$. If you have time for only one case, use $h_{\max} = 15$ cm (Prob. 10.63), for which the maximum Froude number is 0.425. If more time is available, it is instructive to examine a complete family of surface profiles for $h_{\max} \approx 1$ cm up to 35 cm (which is the solution of Prob. 10.64).

P10.66 In Fig. P10.62 let $V_0 = 6$ m/s and $y_0 = 1$ m. If the maximum bump height is 35 cm, estimate (*a*) the Froude number over the top of the bump and (*b*) the maximum increase in the water-surface level.

P10.67 In Fig. P10.62 let $V_0 = 6$ m/s and $y_0 = 1$ m. If the flow over the top of the bump is exactly critical ($\text{Fr} = 1.0$), determine the bump height $h_{\max}$.

P10.68 Modify Prob. 10.65 to have a supercritical approach condition $V_0 = 6$ m/s and $y_0 = 1$ m. If you have time for only one case, use $h_{\max} = 35$ cm (Prob. 10.66), for which the maximum Froude number is 1.47. If more time is available, it is instructive to examine a complete family of surface profiles for 1 cm $< h_{\max} <$ 52 cm (which is the solution to Prob. 10.67).

***P10.69** Given is the flow of a channel of large width b under a sluice gate, as in Fig. P10.69. Assuming frictionless steady flow with negligible upstream kinetic energy, derive a formula for the dimensionless flow ratio $Q^2/(y_1^3 b^2 g)$ as a function of the ratio y_2/y_1. Show by differentiation that the maximum flow rate occurs at $y_2 = 2y_1/3$.

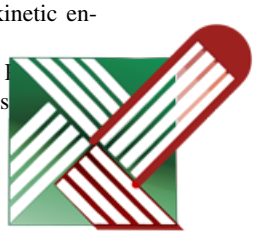


P10.69

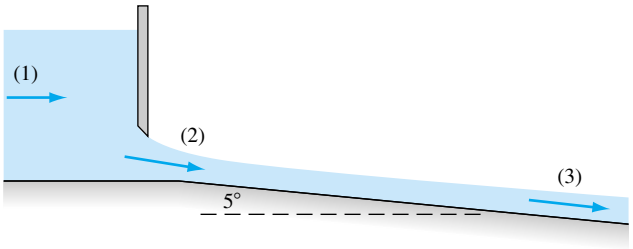
P10.70 In Fig. P10.69 let $y_1 = 90$ cm and $V_1 = 65$ cm/s. Estimate (*a*) y_2, (*b*) Fr_2, and (*c*) the flow rate per unit width.

P10.71 In Fig. P10.69 let $y_1 = 95$ cm and $y_2 = 50$ cm. Estimate the flow rate per unit width if the upstream kinetic energy is (*a*) neglected and (*b*) included.

***P10.72** Water approaches the wide sluice gate of Fig. I
$V_1 = 0.2$ m/s and $y_1 = 1$ m. Accounting for ups



ketabline.com Ebook.ketabline.com



P10.72

netic energy, estimate at the outlet, section 2, the (*a*) depth, (*b*) velocity, and (*c*) Froude number.

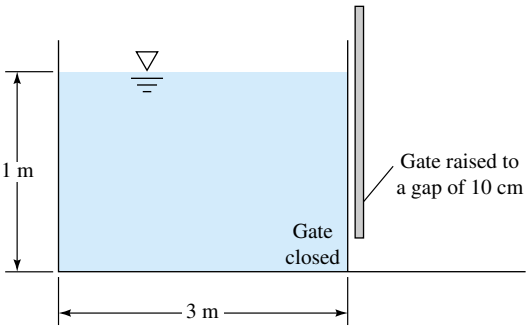
P10.73 In Fig. P10.69 suppose that $y_1 = 1.2$ m and the gate is raised so that its gap is 15 cm. Estimate the resulting flow rate per unit width.

P10.74 With respect to Fig. P10.69, show that, for frictionless flow, the upstream velocity may be related to the water levels by

$$V_1 = \sqrt{\frac{2g(y_1 - y_2)}{K^2 - 1}}$$

where $K = y_1/y_2$.

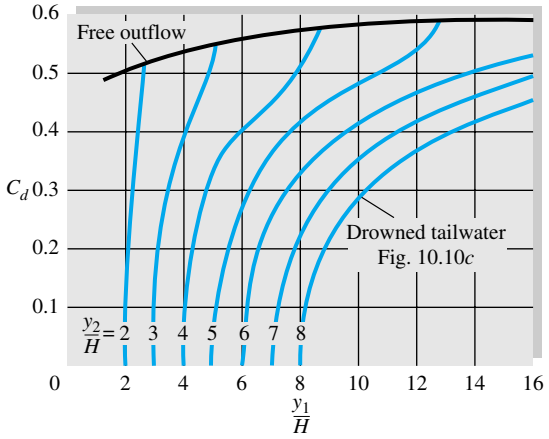
P10.75 A tank of water 1 m deep, 3 m long, and 4 m wide into the paper has a closed sluice gate on the right side, as in Fig. P10.75. At $t = 0$ the gate is opened to a gap of 10 cm. Assuming quasi-steady sluice-gate theory, estimate the time required for the water level to drop to 50 cm. Assume free outflow.



P10.75

P10.76 In Prob. 10.75 estimate what gap height would cause the tank level to drop from 1 m to 50 cm in exactly 1 min. Assume free outflow.

***P10.77** Equation (10.41) for the discharge coefficient is for free (nearly frictionless) outflow. If the outlet is *drowned,* as in Fig. 10.10*c*, there is dissipation and C_d drops sharply. Figure P10.77 shows data from Ref. 3 on drowned vertical sluice gates. Use this chart to repeat Prob. 10.73, and plot the estimated flow rate versus y_2 in the range $0 < y_2 < 110$ cm.



P10.77 *(From Ref. 3, p. 509.)*

P10.78 Repeat Prob. 10.75 if the gate is drowned at $y_2 = 40$ cm.

P10.79 Show that the Froude number downstream of a hydraulic jump will be given by

$$\mathrm{Fr}_2 = 8^{1/2}\,\mathrm{Fr}_1/[(1 + 8\,\mathrm{Fr}_1^2)^{1/2} - 1]^{3/2}$$

Does the formula remain correct if we reverse subscripts 1 and 2? Why?

P10.80 EES Water, flowing horizontally in a wide channel of depth 30 cm, undergoes a hydraulic jump whose energy dissipation is 71 percent. Estimate (*a*) the downstream depth and (*b*) the volume flow rate per meter of width.

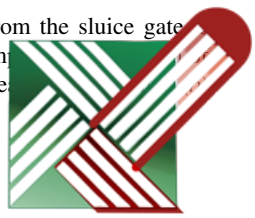
P10.81 Water flows in a wide channel at $q = 25$ ft^3/(s · ft), $y_1 = 1$ ft, and then undergoes a hydraulic jump. Compute y_2, V_2, Fr_2, h_f, the percentage dissipation, and the horsepower dissipated per unit width. What is the critical depth?

P10.82 The flow downstream of a wide hydraulic jump is 7 m deep and has a velocity of 2.2 m/s. Estimate the upstream (*a*) depth and (*b*) velocity and (*c*) the critical depth of the flow.

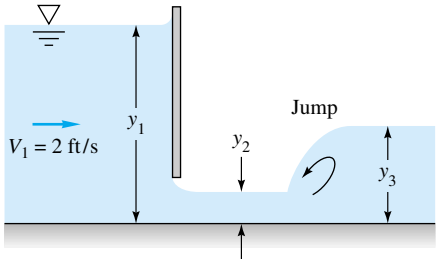
P10.83 A wide-channel flow undergoes a hydraulic jump from 40 to 140 cm. Estimate (*a*) V_1, (*b*) V_2, (*c*) the critical depth, in cm, and (*d*) the percentage of dissipation.

***P10.84** Consider the flow under the sluice gate of Fig. P10.84. If $y_1 = 10$ ft and all losses are neglected except the dissipation in the jump, calculate y_2 and y_3 and the percentage of dissipation, and sketch the flow to scale with the EGL included. The channel is horizontal and wide.

P10.85 In Prob. 10.72 the exit velocity from the sluice gate is 4.33 m/s. If there is a hydraulic jump, section 2, determine the downstre



ketabline.com Ebook.ketabline.com



P10.84

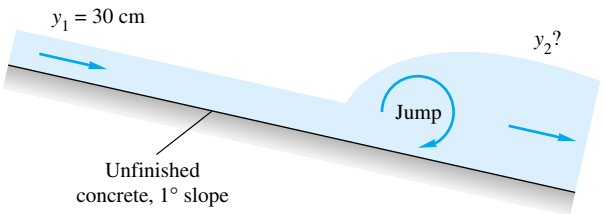
depth, (*c*) Froude number, and (*d*) percent dissipation. Neglect the effect of the nonhorizontal bottom (see Prob. 10.91).

P10.86 A *bore* is a hydraulic jump which propagates upstream into a still or slower-moving fluid, as in Fig. 10.4*a*. Suppose that the still water is 2 m deep and the water behind the bore is 3 m deep. Estimate (*a*) the propagation speed of the bore and (*b*) the induced water velocity.

P10.87 A *tidal bore* may occur when the ocean tide enters an estuary against an oncoming river discharge, such as on the Severn River in England. Suppose that the tidal bore is 10 ft deep and propagates at 13 mi/h upstream into a river which is 7 ft deep. Estimate the river current in kn.

P10.88 At one point in a rectangular channel 7 ft wide, the depth is 2 ft and the flow rate is 200 ft^3/s. If a hydraulic jump occurs nearby, determine (*a*) whether it is upstream or downstream of this point and (*b*) the percentage of dissipation in the jump.

P10.89 Water 30 cm deep is in uniform flow down a 1° unfinished-concrete slope when a hydraulic jump occurs, as in Fig. P10.89. If the channel is very wide, estimate the water depth y_2 downstream of the jump.



P10.89

P10.90 Modify Prob. 10.89 as follows. Suppose that $y_2 = 1$ m and $y_1 = 30$ cm but the channel slope is not equal to 1°. Determine the proper slope for this condition.

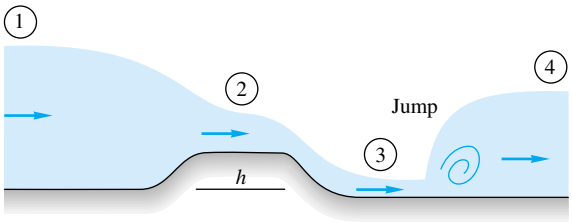
***P10.91** No doubt you used the horizontal-jump formula (10.43) to solve Probs. 10.89 and 10.90, which is reasonable since the slope is so small. However, Chow [3, p. 425] points out that hydraulic jumps are *higher* on sloped channels, due to "the weight of the fluid in the jump." Make a control-volume sketch of a sloping jump to show why this is so. The sloped-jump chart given in Chow's figure 15-20 may be approximated by the following curve fit:

$$\frac{2y_2}{y_1} \approx [(1 + 8\,\mathrm{Fr}_1^2)^{1/2} - 1]e^{3.5S_0}$$

where $0 < S_0 < 0.3$ are the channel slopes for which data are available. Use this correlation to modify your solution to Prob. 10.89. If time permits, make a graph of y_2/y_1 (≤ 20) versus Fr_1 (≤ 15) for various S_0 (≤ 0.3).

P10.92 At the bottom of an 80-ft-wide spillway is a horizontal hydraulic jump with water depths 1 ft upstream and 10 ft downstream. Estimate (*a*) the flow rate and (*b*) the horsepower dissipated.

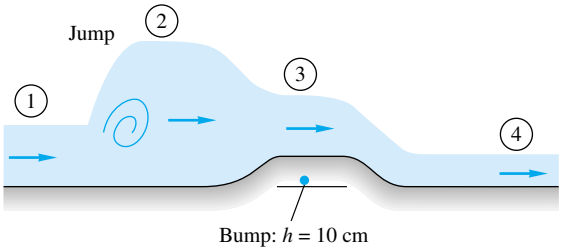
P10.93 Water in a horizontal channel accelerates smoothly over a bump and then undergoes a hydraulic jump, as in Fig. P10.93. If $y_1 = 1$ m and $y_3 = 40$ cm, estimate (*a*) V_1, (*b*) V_3, (*c*) y_4, and (*d*) the bump height h.



P10.93

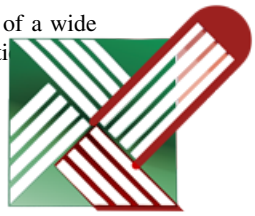
P10.94 Modify Prob. 10.93 as follows. Let the bump height be 20 cm and the subcritical approach velocity be $V_1 = 1.5$ m/s. Determine (*a*) y_2, (*b*) the supercritical flow V_3, and (*c*) y_4.

P10.95 A 10-cm-high bump in a wide horizontal water channel creates a hydraulic jump just upstream and the flow pattern in Fig. P10.95. Neglecting losses except in the jump, for the case $y_3 = 30$ cm, estimate (*a*) V_4, (*b*) y_4, (*c*) V_1, and (*d*) y_1.



P10.95

P10.96 Show that the Froude numbers on either side of a wide hydraulic jump are related by the simple relati
$\mathrm{Fr}_1(y_1/y_2)^{3/2}$.



ketabline.com Ebook.ketabline.com

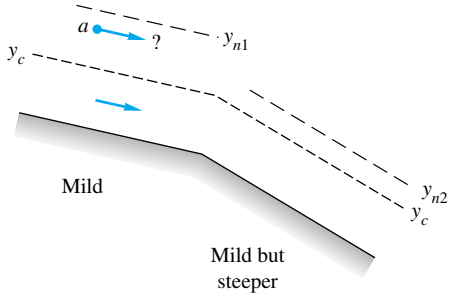
P10.97 A brickwork rectangular channel 4 m wide is flowing at 8.0 m^3/s on a slope of 0.1°. Is this a mild, critical, or steep slope? What type of gradually varied solution curve are we on if the local water depth is (*a*) 1 m, (*b*) 1.5 m, and (*c*) 2 m?

P10.98 A gravelly earth wide channel is flowing at 10 m^3/s per meter of width on a slope of 0.75°. Is this a mild, critical, or steep slope? What type of gradually varied solution curve are we on if the local water depth is (*a*) 1 m, (*b*) 2 m, and (*c*) 3 m?

P10.99 A clay tile V-shaped channel of included angle 60° is flowing at 1.98 m^3/s on a slope of 0.33°. Is this a mild, critical, or steep slope? What type of gradually varied solution curve are we on if the local water depth is (*a*) 1 m, (*b*) 2 m, and (*c*) 3 m?

P10.100 If bottom friction is included in the sluice-gate flow of Prob. 10.84, the depths (y_1, y_2, y_3) will vary with x. Sketch the type and shape of gradually varied solution curve in each region (1, 2, 3), and show the regions of rapidly varied flow.

P10.101 Consider the gradual change from the profile beginning at point *a* in Fig. P10.101 on a mild slope S_{01} to a mild but steeper slope S_{02} downstream. Sketch and label the curve $y(x)$ expected.



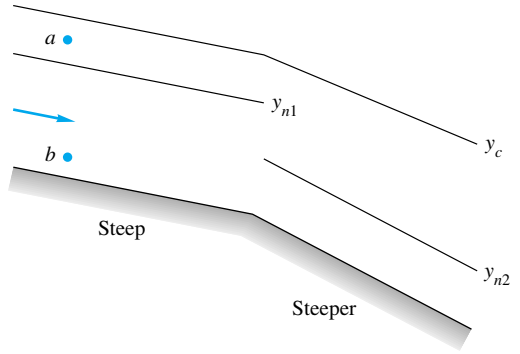
P10.101

***P10.102** The wide-channel flow in Fig. P10.102 changes from a steep slope to one even steeper. Beginning at points *a* and *b*, sketch and label the water-surface profiles which are expected for gradually varied flow.

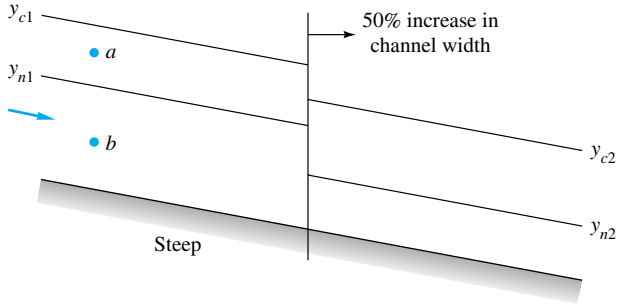
P10.103 A circular painted-steel channel is running half full at 1 m^3/s and is laid out on a slope of 5 m/km. Is this a mild or steep slope, of type 1, 2, or 3? Take $R = 50$ cm.

P10.104 The rectangular-channel flow in Fig. P10.104 expands to a cross section 50 percent wider. Beginning at points *a* and *b*, sketch and label the water-surface profiles which are expected for gradually varied flow.

P10.105 In Prob. 10.84 the frictionless solution is $y_2 = 0.82$ ft, which we denote as $x = 0$ just downstream of the gate. If the channel is horizontal with $n = 0.018$ and there is no hydraulic jump, compute from gradually varied theory the downstream distance where $y = 2.0$ ft.

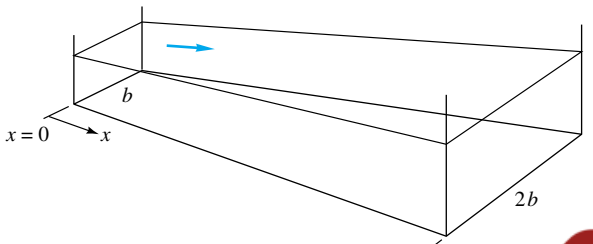


P10.102

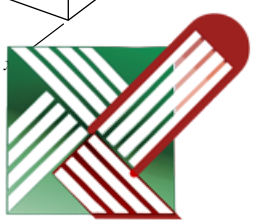


P10.104

P10.106 A rectangular channel with $n = 0.018$ and a constant slope of 0.0025 increases its width linearly from b to $2b$ over a distance L, as in Fig. P10.106. (*a*) Determine the variation $y(x)$ along the channel if $b = 4$ m, $L = 250$ m, the initial depth is $y(0) = 1.05$ m, and the flow rate is 7 m^3/s. (*b*) Then, if your computer program is running well, determine the initial depth $y(0)$ for which the exit flow will be exactly critical.



P10.106

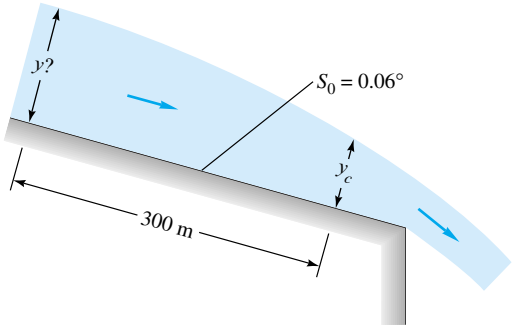


ketabline.com Ebook.ketabline.com

P10.107 A clean-earth wide-channel flow is flowing up an adverse slope with $S_0 = -0.002$. If the flow rate is $q = 4.5$ m^3/(s · m), use gradually varied theory to compute the distance for the depth to drop from 3.0 to 2.0 m.

P10.108 Illustrate Prob. 10.104 with a numerical example. Let the channel be rectangular with a width $b_1 = 10$ m for $0 < x < 100$ m, expanding to $b_2 = 15$ m for $100 < x < 250$ m. The flow rate is 27 m^3/s, and $n = 0.012$. Compute the water depth at $x = 250$ m for initial depth $y(0)$ equal to (*a*) 75 cm and (*b*) 5 cm. Compare your results with the discussion in Prob. 10.104. Let $S_0 = 0.005$.

P10.109 Figure P10.109 illustrates a free overfall or *dropdown* flow pattern, where a channel flow accelerates down a slope and falls freely over an abrupt edge. As shown, the flow reaches critical just before the overfall. Between y_c and the edge the flow is rapidly varied and does not satisfy gradually varied theory. Suppose that the flow rate is $q = 1.3$ m^3/(s · m) and the surface is unfinished cement. Use Eq. (10.51) to estimate the water depth 300 m upstream as shown.

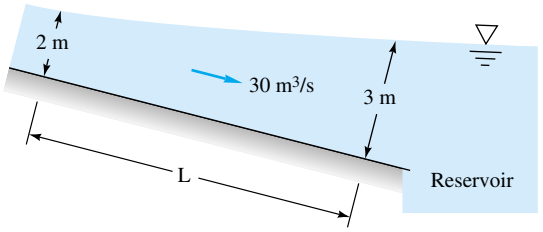


P10.109

P10.110 We assumed frictionless flow in solving the bump case, Prob. 10.65, for which $V_2 = 1.21$ m/s and $y_2 = 0.826$ m over the crest when $h_{max} = 15$ cm, $V_1 = 1$ m/s, and $y_1 = 1$ m. However, if the bump is long and rough, friction may be important. Repeat Prob. 10.65 for the same bump shape, $h = 0.5h_{max}[1 - \cos(2\pi x/L)]$, to compute conditions (*a*) at the crest and (*b*) at the end of the bump, $x = L$. Let $h_{max} = 15$ cm and $L = 100$ m, and assume a clean-earth surface.

P10.111 Modify Prob. 10.110 as follows. Keep all other data the same, and find the bump length L for which the flow first becomes critical somewhere along the bump surface.

P10.112 The clean-earth channel in Fig. P10.112 is 6 m wide and slopes at 0.3°. Water flows at 30 m^3/s in the channel and enters a reservoir so that the channel depth is 3 m just before the entry. Assuming gradually varied flow, how far is the distance L to a point in the channel where $y = 2$ m? What type of curve is the water surface?

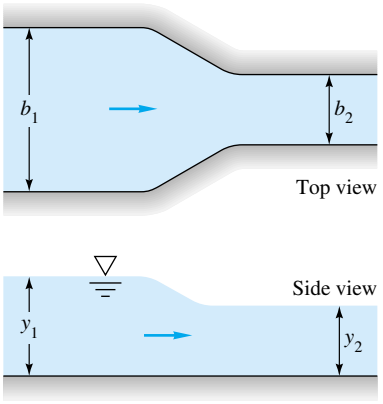


P10.112

P10.113 Figure P10.113 shows a channel contraction section often called a *venturi flume* [19, p. 167], because measurements of y_1 and y_2 can be used to meter the flow rate. Show that if losses are neglected and the flow is one-dimensional and subcritical, the flow rate is given by

$$Q = \left[\frac{2g(y_1 - y_2)}{1/(b_2^2y_2^2) - 1/(b_1^2y_1^2)}\right]^{1/2}$$

Apply this to the special case $b_1 = 3$ m, $b_2 = 2$ m, and $y_1 = 1.9$ m. (*a*) Find the flow rate if $y_2 = 1.5$ m. (*b*) Also find the depth y_2 for which the flow becomes critical in the throat.



P10.113

P10.114 Investigate the possibility of *choking* in the venturi flume of Fig. P10.113. Let $b_1 = 4$ ft, $b_2 = 3$ ft, and $y_1 = 2$ ft. Compute the values of y_2 and V_1 for a flow rate of (*a*) 30 ft^3/s and (*b*) 35 ft^3/s. Explain your vexation.

P10.115 Gradually varied theory, Eq. (10.49), neglects the effect of *width* changes, db/dx, assuming that they are small. But they are not small for a short, sharp contraction such as the venturi flume in Fig. P10.113. Show that, for a rectangular section with $b = b(x)$, Eq. (10.49) should be modified as follows:

$$\frac{dy}{dx} \approx \frac{S_0 - S + [V^2/(gb)](db/dx)}{1 - \text{Fr}^2}$$



ketabline.com Ebook.ketabline.com

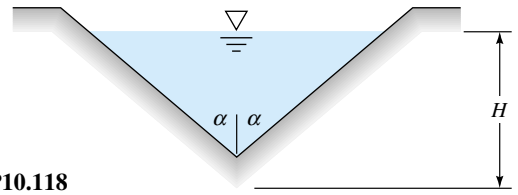
Investigate a criterion for reducing this relation to Eq. (10.49).

P10.116 Investigate the possibility of *frictional effects* in the venturi flume of Prob. 10.113, part (*a*), for which the frictionless solution is $Q = 9.88$ m^3/s. Let the contraction be 3 m long and the measurements of y_1 and y_2 be at positions 3 m upstream and 3 m downstream of the contraction, respectively. Use the modified gradually varied theory of Prob. 10.115, with $n = 0.018$ to estimate the flow rate.

P10.117 A full-width weir in a horizontal channel is 5 m wide and 80 cm high. The upstream depth is 1.5 m. Estimate the flow rate for (*a*) a sharp-crested weir and (*b*) a round-nosed broad-crested weir.

***P10.118** Using a Bernoulli-type analysis similar to Fig. 10.16*a*, show that the theoretical discharge of the V-shaped weir in Fig. P10.118 is given by

$$Q = 0.7542 g^{1/2} \tan \alpha \, H^{5/2}$$



***P10.118**

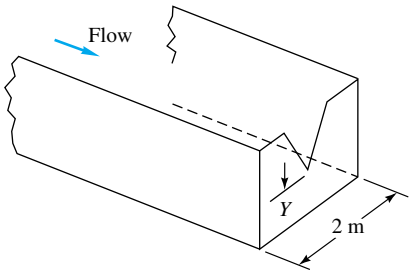
P10.119 Data by A. T. Lenz for water at 20°C (reported in Ref. 19) show a significant increase of discharge coefficient of V-notch weirs (Fig. P10.118) at low heads. For $\alpha = 20°$, some measured values are as follows:

H, ft	0.2	0.4	0.6	0.8	1.0
C_d	0.499	0.470	0.461	0.456	0.452

Determine if these data can be correlated with the Reynolds and Weber numbers vis-à-vis Eq. (10.61). If not, suggest another correlation.

P10.120 The rectangular channel in Fig. P10.120 contains a V-notch weir as shown. The intent is to meter flow rates between 2.0 and 6.0 m^3/s with an upstream hook gage set to measure water depths between 2.0 and 2.75 m. What are the most appropriate values for the notch height Y and the notch half-angle α?

P10.121 Water flow in a rectangular channel is to be metered by a thin-plate weir with side contractions, as in Table 10.1*b*, with $L = 6$ ft and $Y = 1$ ft. It is desired to measure flow rates between 1500 and 3000 gal/min with only a 6-in change in upstream water depth. What is the most appropriate length for the weir width b?



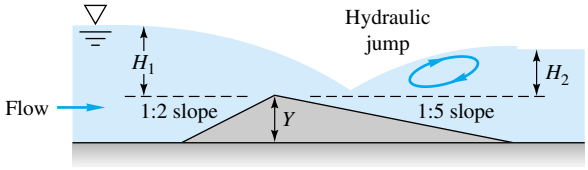
P10.120

P10.122 In 1952 E. S Crump developed the triangular weir shape shown in Fig. P10.122 [19, chap. 4]. The front slope is 1:2 to avoid sediment deposition, and the rear slope is 1:5 to maintain a stable tailwater flow. The beauty of the design is that it has a unique discharge correlation up to near-drowning conditions, $H_2/H_1 \leq 0.75$:

$$Q = C_d b g^{1/2} \left(H_1 + \frac{V_1^2}{2g} - k_h \right)^{3/2}$$

where $C_d \approx 0.63$ and $k_h \approx 0.3$ mm

The term k_h is a low-head loss factor. Suppose that the weir is 3 m wide and has a crest height $Y = 50$ cm. If the water depth upstream is 65 cm, estimate the flow rate in gal/min.



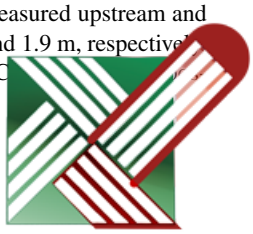
P10.122 The Crump weir [19, chap. 4]

***P10.123** The Crump weir calibration in Prob. 10.122 is for *modular* flow, i.e., when the flow rate is independent of downstream tailwater. When the weir becomes drowned, the flow rate decreases by the following factor:

$$Q = Q_{\text{mod}} f$$

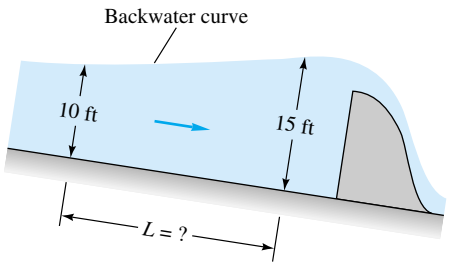
where $$f \approx 1.035 \left[0.817 - \left(\frac{H_2^*}{H_1^*} \right)^4 \right]^{0.0647}$$

for $0.70 \leq H_2^*/H_1^* \leq 0.93$, where H^* denotes $H_1 + V_1^2/(2g) - k_h$ for brevity. The weir is then *double-gaged* to measure both H_1 and H_2. Suppose that the weir crest is 1 m high and 2 m wide. If the measured upstream and downstream water depths are 2.0 and 1.9 m, respectively, estimate the flow rate in gal/min. C sible uncertainty of your estimate.



ketabline.com Ebook.ketabline.com

P10.124 Water flows at 600 ft^3/s in a rectangular channel 22 ft wide with $n \approx 0.024$ and a slope of 0.1°. A dam increases the depth to 15 ft, as in Fig. P10.124. Using gradually varied theory, estimate the distance L upstream at which the water depth will be 10 ft. What type of solution curve are we on? What should be the water depth asymptotically far upstream?



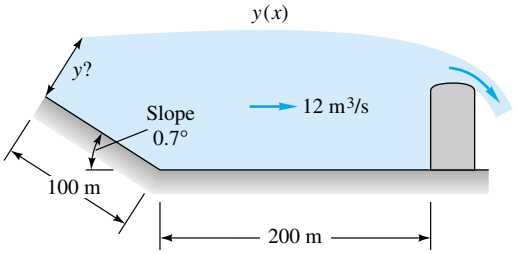
P10.124

P10.125 The Tupperware dam on the Blackstone River is 12 ft high, 100 ft wide, and sharp-edged. It creates a backwater similar to Fig. P10.124. Assume that the river is a weedy-earth rectangular channel 100 ft wide with a flow rate of 800 ft^3/s. Estimate the water-depth 2 mi upstream of the dam if $S_0 = 0.001$.

P10.126 Suppose that the rectangular channel of Fig. P10.120 is made of riveted steel and carries a flow of 8 m^3/s on a slope of 0.15°. If the V-notch weir has $\alpha = 30°$ and $Y = 50$ cm, estimate, from gradually varied theory, the water depth 100 m upstream.

P10.127 A horizontal gravelly earth channel 2 m wide contains a full-width Crump weir (Fig. P10.122) 1 m high. If the weir is not drowned, estimate, from gradually varied theory, the flow rate for which the water depth 100 m upstream will be 2 m.

P10.128 A rectangular channel 4 m wide is blocked by a broad-crested weir 2 m high, as in Fig. P10.128. The channel is horizontal for 200 m upstream and then slopes at 0.7° as shown. The flow rate is 12 m^3/s, and $n = 0.03$. Compute the water depth y at 300 m upstream from gradually varied theory.



P10.128

Word Problems

W10.1 Free-surface problems are driven by gravity. Why do so many of the formulas in this chapter contain the *square root* of the acceleration of gravity?

W10.2 Explain why the flow under a sluice gate, Fig. 10.10, either is or is not analogous to compressible gas flow through a converging-diverging nozzle, Fig. 9.12.

W10.3 In uniform open-channel flow, what is the balance of forces? Can you use such a force balance to derive the Chézy equation (10.13)?

W10.4 A shallow-water wave propagates at the speed $c_0 \approx (gy)^{1/2}$. What makes it propagate? That is, what is the balance of forces in such wave motion? In which direction does such a wave propagate?

W10.5 Why is the Manning friction correlation, Eq. (10.16), used almost universally by hydraulics engineers, instead of the Moody friction factor?

W10.6 During horizontal channel flow over a bump, is the specific energy constant? Explain.

W10.7 Cite some similarities, and perhaps some dissimilarities, between a hydraulic jump and a gas-dynamic normal-shock wave.

W10.8 Give three examples of rapidly varied flow. For each case, cite reasons why it does not satisfy one or more of the five basic assumptions of gradually varied flow theory.

W10.9 Is a free overfall, Fig. 10.15*e*, similar to a weir? Could it be calibrated versus flow rate in the same manner as a weir? Explain.

W10.10 Cite some similarities, and perhaps some dissimilarities, between a weir and a Bernoulli obstruction flowmeter from Sec. 6.7.

W10.11 Is a bump, Fig. 10.9*a*, similar to a weir? If not, when does a bump become large enough, or sharp enough, to be a weir?

W10.12 After doing some reading and/or thinking, explain the design and operation of a *long-throated flume*.

W10.13 Describe the design and operation of a *critical-depth flume*. What are its advantages compared to the venturi flume of Prob. 10.113?



ketabline.com Ebook.ketabline.com

Fundamentals of Engineering Exam Problems

The FE Exam is fairly light on open-channel problems in the general (morning) session, but it plays a big part in the specialized civil engineering (afternoon) exam.

FE10.1 Consider a rectangular channel 3 m wide laid on a 1° slope. If the water depth is 2 m, the hydraulic radius is (*a*) 0.43 m, (*b*) 0.6 m, (*c*) 0.86 m, (*d*) 1.0 m, (*e*) 1.2 m

FE10.2 For the channel of Prob. FE10.1, the most efficient water depth (best flow for a given slope and resistance) is (*a*) 1 m, (*b*) 1.5 m, (*c*) 2 m, (*d*) 2.5 m, (*e*) 3 m

FE10.3 If the channel of Prob. FE10.1 is built of rubble cement (Manning's $n \approx 0.020$), what is the uniform-flow rate when the water depth is 2 m?
(*a*) 6 m^3/s, (*b*) 18 m^3/s, (*c*) 36 m^3/s, (*d*) 40 m^3/s, (*e*) 53 m^3/s

FE10.4 For the channel of Prob. FE10.1, if the water depth is 2 m and the uniform-flow rate is 24 m^3/s, what is the approximate value of Manning's roughness factor n?
(*a*) 0.015, (*b*) 0.020, (*c*) 0.025, (*d*) 0.030, (*e*) 0.035

FE10.5 For the channel of Prob. FE10.1, if Manning's roughness factor $n \approx 0.020$ and $Q \approx 29$ m^3/s, what is the normal depth y_n?
(*a*) 1 m, (*b*) 1.5 m, (*c*) 2 m, (*d*) 2.5 m, (*e*) 3 m

FE10.6 For the channel of Prob. FE10.1, if $Q \approx 24$ m^3/s, what is the critical depth y_c?
(*a*) 1.0 m, (*b*) 1.26 m, (*c*) 1.5 m, (*d*) 1.87 m, (*e*) 2.0 m

FE10.7 For the channel of Prob. FE10.1, if $Q \approx 24$ m^3/s and the depth is 2 m, what is the Froude number of the flow?
(*a*) 0.50, (*b*) 0.77, (*c*) 0.90, (*d*) 1.00, (*e*) 1.11

Comprehensive Problems

C10.1 February 1998 saw the failure of the earthen dam impounding California Jim's Pond in southern Rhode Island. The resulting flood raised temporary havoc in the nearby village of Peace Dale. The pond is 17 acres in area and 15 ft deep and was full from heavy rains. The breach in the dam was 22 ft wide and 15 ft deep. Estimate the time required for the pond to drain to a depth of 2 ft.

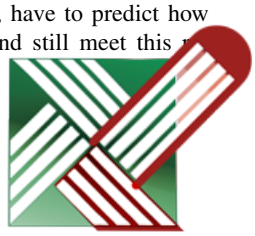
C10.2 A circular, unfinished concrete drainpipe is laid on a slope of 0.0025 and is planned to carry from 50 to 300 ft^3/s of runoff water. Design constraints are that (1) the water depth should be no more than three-fourths of the diameter and (2) the flow should always be subcritical. What is the appropriate pipe diameter to satisfy these requirements? If no commercial pipe is exactly this calculated size, should you buy the next smallest or the next largest pipe?

C10.3 Extend Prob. 10.72, whose solution was $V_2 \approx 4.33$ m/s. Use gradually varied theory to estimate the water depth 10 m downstream at section (3) for (*a*) the 5° unfinished-concrete slope shown in Fig. P10.72. (*b*) Repeat your calculation for an *upward* (adverse) slope of 5°. (*c*) When you find that part (*b*) is impossible with gradually varied theory, explain why and repeat for an adverse slope of 1°.

Design Projects

D10.1 A straight weedy-earth channel has the trapezoidal shape of Fig. 10.7, with $b = 4$ m and $\theta = 35°$. The channel has a constant bottom slope of 0.001. The flow rate varies seasonally from 5 up to 10 m^3/s. It is desired to place a sharp-edged weir across the channel so that the water depth 1 km upstream remains at 2.0 m ± 10 percent throughout the year. Investigate the possibility of accomplishing this with a full-width weir; if successful, determine the proper weir height Y. If unsuccessful, try other alternatives, such as (*a*) a full-width broad crested weir or (*b*) a weir with side contractions or (*c*) a V-notch weir. Whatever your final design, cite the seasonal variation of normal depths and critical depths for comparison with the desired year-round depth of 2 m.

D10.2 The Caroselli Dam on the Pawcatuck River is 10 ft high, 90 ft wide, and sharp edged. The Coakley Company uses this head to generate hydropower electricity and wants *more* head. They ask the town for permission to raise the dam higher. The river above the dam may be approximated as rectangular, 90 ft wide, sloping upstream at 12 ft per statute mile, and with a stony, cobbled bed. The average flow rate is 400 ft^3/s, with a 30-year predicted flood rate of 1200 ft^3/s. The river sides are steep until 1 mi upstream, where there are low-lying residences. The town council agrees the dam may be heightened if the new river level near these houses, during the 30-year flood, is no more than 3 ft higher than the present level during average-flow conditions. You, as project engineer, have to predict how high the dam crest can be raised and still meet this requirement.



ketabline.com Ebook.ketabline.com

References

1. R. H. French, *Open-Channel Hydraulics,* McGraw-Hill, New York, 1985.
2. M. H. Chaudhry, *Open Channel Flow,* Prentice-Hall, Upper Saddle River, NJ, 1993.
3. Ven Te Chow, *Open Channel Hydraulics,* McGraw-Hill, New York, 1959.
4. F. M. Henderson, *Open Channel Flow,* Macmillan, New York, 1966.
5. B. Kinsman, *Wind Waves: Their Generation and Propagation on the Ocean Surface,* Prentice-Hall, Englewood Cliffs, NJ, 1964; Dover, New York, 1984.
6. M. J. Lighthill, *Waves in Fluids,* Cambridge University Press, London, 1978.
7. C. C. Mei, *The Applied Dynamics of Ocean Surface Waves,* Wiley, New York, 1983.
8. A. T. Ippen, *Estuary and Coastline Hydrodynamics,* McGraw-Hill, New York, 1966.
9. R. M. Sorenson, *Basic Coastal Engineering,* Wiley, New York, 1978.
10. J. M. Robertson and H. Rouse, "The Four Regimes of Open Channel Flow," *Civ. Eng.,* vol. 11, no. 3, March 1941, pp. 169–171.
11. R. W. Powell, "Resistance to Flow in Rough Channels," *Trans. Am. Geophys. Union,* vol. 31, no. 4, August 1950, pp. 575–582.
12. R. Manning, "On the Flow of Water in Open Channels and Pipes," *Trans. I.C.E. Ireland,* vol. 20, 1891, pp. 161–207.
13. B. A. Bakhmeteff, *Hydraulics of Open Channels,* McGraw-Hill, New York, 1932.
14. P. A. Thompson, *Compressible-Fluid Dynamics,* McGraw-Hill, New York, 1972.
15. E. F. Brater, *Handbook of Hydraulics,* 6th ed., McGraw-Hill, New York, 1976.
16. U.S. Bureau of Reclamation, "Research Studies on Stilling Basins, Energy Dissipators, and Associated Appurtenances," *Hydraulic Lab. Rep.* Hyd-399, June 1, 1955.
17. "Friction Factors in Open Channels, Report of the Committee on Hydromechanics," *ASCE J. Hydraul. Div.,* March 1963, pp. 97–143.
18. R. M. Olson and S. J. Wright, *Essentials of Engineering Fluid Mechanics,* 5th ed., Harper & Row, New York, 1990.
19. P. Ackers et al., *Weirs and Flumes for Flow Measurement,* Wiley, New York, 1978.
20. M. G. Bos, J. A. Replogle, and A. J. Clemmens, *Flow Measuring Flumes for Open Channel Systems,* Wiley, New York, 1984.
21. M. G. Bos, *Long-Throated Flumes and Broad-Crested Weirs,* Martinus Nijhoff (Kluwer), Dordrecht, The Netherlands, 1985.
22. U.S. Army Corps of Engineers, *HEC-2 Water Surface Profiles,* Hydrologic Engineering Center, 609 Second Street, Davis, CA.
23. W. Rodi, *Turbulence Models and Their Application in Hydraulics,* Brookfield Publishing, Brookfield, VT, 1984.



ketabline.com Ebook.ketabline.com



Wind-energy generator farm, Altamont Pass, California. Windmills have been used for power for more than two thousand years. These multi-bladed horizontal-axis wind turbines (HAWT's) are among the most efficient of windpower designs, as discussed in this chapter. *(Courtesy of Kevin Schafer/Peter Arnold, Inc.)*



ketabline.com Ebook.ketabline.com

Chapter 11
Turbomachinery

Motivation. The most common practical engineering application for fluid mechanics is the design of fluid machinery. The most numerous types are machines which *add* energy to the fluid (the pump family), but also important are those which *extract* energy (turbines). Both types are usually connected to a rotating shaft, hence the name *turbomachinery*.

The purpose of this chapter is to make elementary engineering estimates of the performance of fluid machines. The emphasis will be upon nearly incompressible flow, i.e., liquids or low-velocity gases. Basic flow principles are discussed, but not the detailed construction of the machine.

11.1 Introduction and Classification

Turbomachines divide naturally into those which add energy (pumps) and those which extract energy (turbines). The prefix *turbo-* is a Latin word meaning "spin" or "whirl," appropriate for rotating devices.

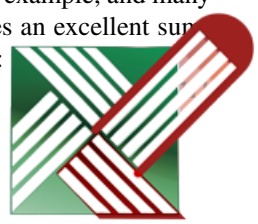
The pump is the oldest fluid-energy-transfer device known. At least two designs date before Christ: (1) the undershot-bucket waterwheels, or *norias*, used in Asia and Africa (1000 B.C.) and (2) Archimedes' screw pump (250 B.C.), still being manufactured today to handle solid-liquid mixtures. Paddlewheel turbines were used by the Romans in 70 B.C., and Babylonian windmills date back to 700 B.C. [1].

Machines which deliver liquids are simply called *pumps*, but if gases are involved, three different terms are in use, depending upon the pressure rise achieved. If the pressure rise is very small (a few inches of water), a gas pump is called a *fan*; up to 1 atm, it is usually called a *blower*; and above 1 atm it is commonly termed a *compressor*.

Classification of Pumps

There are two basic types of pumps: positive-displacement and dynamic or momentum-change pumps. There are several billion of each type in use in the world today.

Positive-displacement pumps (PDPs) force the fluid along by volume changes. A cavity opens, and the fluid is admitted through an inlet. The cavity then closes, and the fluid is squeezed through an outlet. The mammalian heart is a good example, and many mechanical designs are in wide use. The text by Warring [14] gives an excellent summary of PDPs. A brief classification of PDP designs is as follows:



ketabline.com Ebook.ketabline.com

A. Reciprocating
   1. Piston or plunger
   2. Diaphragm

B. Rotary
   1. Single rotor
      a. Sliding vane
      b. Flexible tube or lining
      c. Screw
      d. Peristaltic (wave contraction)
   2. Multiple rotors
      a. Gear
      b. Lobe
      c. Screw
      d. Circumferential piston

All PDPs deliver a pulsating or periodic flow as the cavity volume opens, traps, and squeezes the fluid. Their great advantage is the delivery of any fluid regardless of its viscosity.

Figure 11.1 shows schematics of the operating principles of seven of these PDPs. It is rare for such devices to be run backward, so to speak, as turbines or energy extractors, the steam engine (reciprocating piston) being a classic exception.

Since PDPs compress mechanically against a cavity filled with liquid, a common feature is that they develop immense pressures if the outlet is shut down for any reason. Sturdy construction is required, and complete shutoff would cause damage if pressure-relief valves were not used.

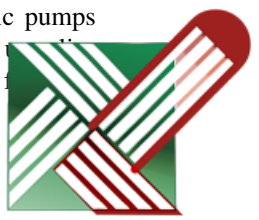
Dynamic pumps simply add momentum to the fluid by means of fast-moving blades or vanes or certain special designs. There is no closed volume: The fluid increases momentum while moving through open passages and then converts its high velocity to a pressure increase by exiting into a diffuser section. Dynamic pumps can be classified as follows:

A. Rotary
   1. Centrifugal or radial exit flow
   2. Axial flow
   3. Mixed flow (between radial and axial)

B. Special designs
   1. Jet pump or ejector (see Fig. P3.36)
   2. Electromagnetic pumps for liquid metals
   3. Fluid-actuated: gas-lift or hydraulic-ram

We shall concentrate in this chapter on the rotary designs, sometimes called *rotodynamic pumps*. Other designs of both PDP and dynamic pumps are discussed in specialized texts [for example, 11, 14, 31].

Dynamic pumps generally provide a higher flow rate than PDPs and a much steadier discharge but are ineffective in handling high-viscosity liquids. Dynamic pumps also generally need *priming*; i.e., if they are filled with gas, they cannot suck [illegible] uid from below into their inlet. The PDP, on the other hand, is self-priming [illegible]



ketabline.com Ebook.ketabline.com

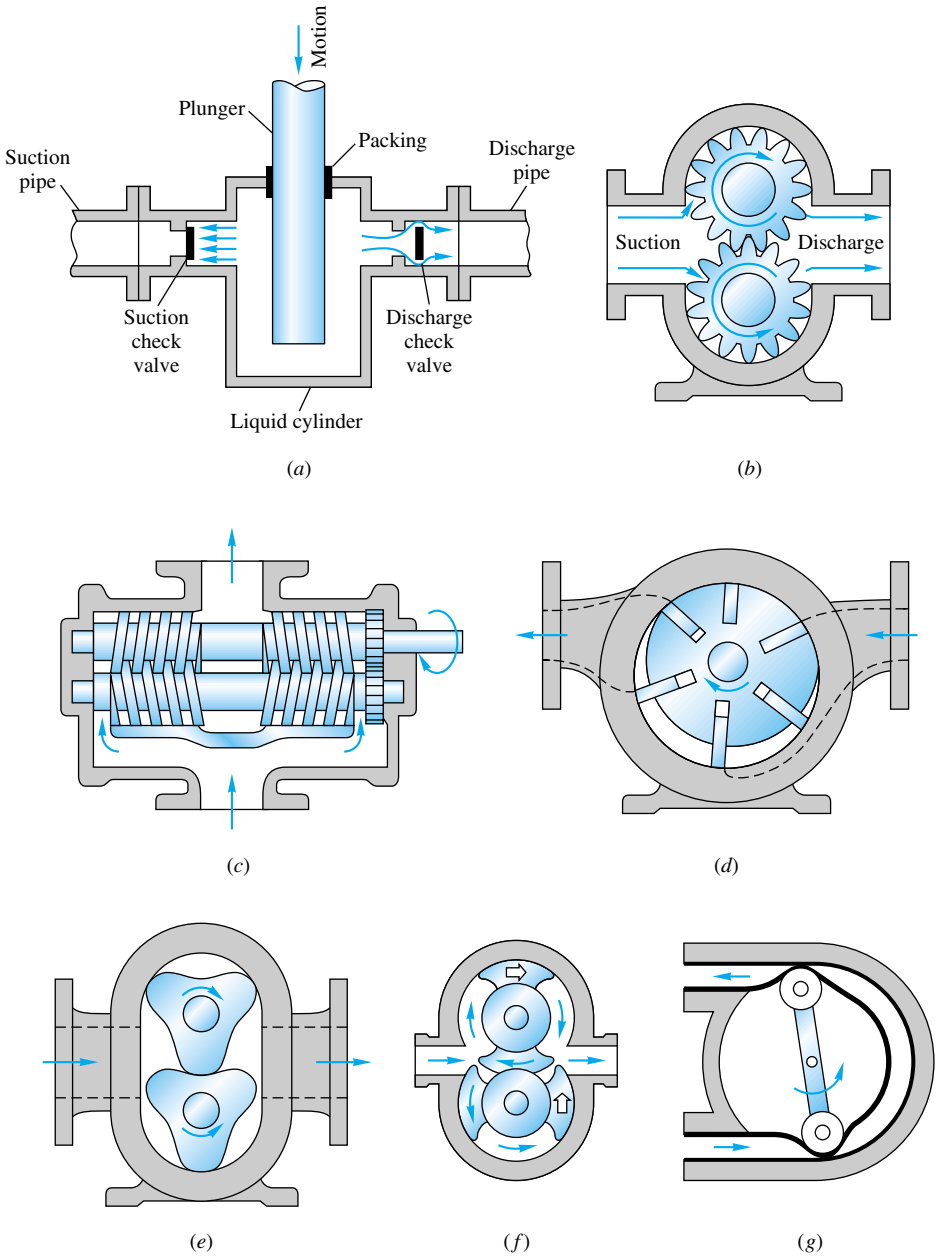


Fig. 11.1 Schematic design of positive-displacement pumps: (*a*) reciprocating piston or plunger, (*b*) external gear pump, (*c*) double-screw pump, (*d*) sliding vane, (*e*) three-lobe pump, (*f*) double circumferential piston, (*g*) flexible-tube squeegee.

applications. A dynamic pump can provide very high flow rates (up to 300,000 gal/min) but usually with moderate pressure rises (a few atmospheres). In contrast, a PDP can operate up to very high pressures (300 atm) but typically produces low flow rates (100 gal/min).

The relative *performance* (Δp versus Q) is quite different for the t
as shown in Fig. 11.2. At constant shaft rotation speed, the PDP pr

ketabline.com Ebook.ketabline.com

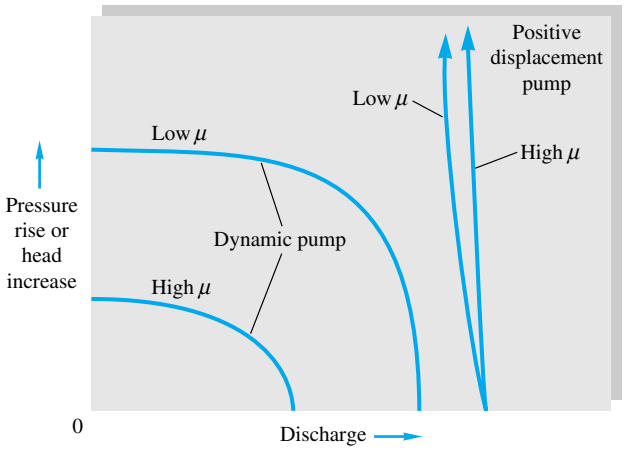


Fig. 11.2 Comparison of performance curves of typical dynamic and positive-displacement pumps at constant speed.

stant flow rate and virtually unlimited pressure rise, with little effect of viscosity. The flow rate of a PDP cannot be varied except by changing the displacement or the speed. The reliable constant-speed discharge from PDPs has led to their wide use in metering flows [35].

The dynamic pump, by contrast in Fig. 11.2, provides a continuous constant-speed variation of performance, from near-maximum Δp at zero flow (shutoff conditions) to zero Δp at maximum flow rate. High-viscosity fluids sharply degrade the performance of a dynamic pump.

As usual—and for the last time in this text—we remind the reader that this is merely an introductory chapter. Many books are devoted solely to turbomachines: generalized treatments [2 to 7], texts specializing in pumps [8 to 16], fans [17 to 20], compressors [21 to 23], turbines [24 to 28], and PDPs [35 to 38]. There are several useful handbooks [29 to 32], and at least two elementary textbooks [33, 34] have a comprehensive discussion of turbomachines. The reader is referred to these sources for further details.

11.2 The Centrifugal Pump

Let us begin our brief look at rotodynamic machines by examining the characteristics of the centrifugal pump. As sketched in Fig. 11.3, this pump consists of an impeller rotating within a casing. Fluid enters axially through the *eye* of the casing, is caught

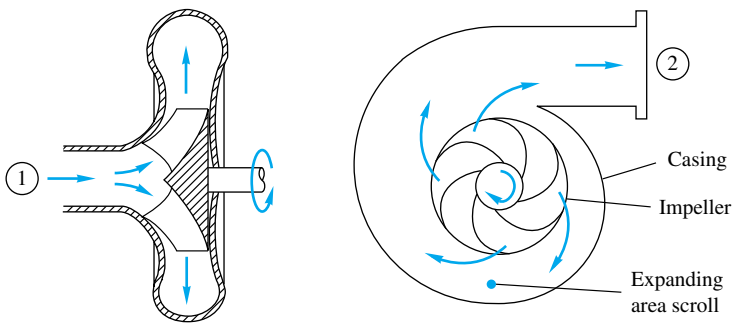


Fig. 11.3 Cutaway schematic of a typical centrifugal pump.



ketabline.com Ebook.ketabline.com

up in the impeller blades, and is whirled tangentially and radially outward until it leaves through all circumferential parts of the impeller into the diffuser part of the casing. The fluid gains both velocity and pressure while passing through the impeller. The doughnut-shaped diffuser, or *scroll*, section of the casing decelerates the flow and further increases the pressure.

The impeller blades are usually *backward-curved*, as in Fig. 11.3, but there are also radial and forward-curved blade designs, which slightly change the output pressure. The blades may be *open*, i.e., separated from the front casing only by a narrow clearance, or *closed*, i.e., shrouded from the casing on both sides by an impeller wall. The diffuser may be *vaneless*, as in Fig. 11.3, or fitted with fixed vanes to help guide the flow toward the exit.

Basic Output Parameters

Assuming steady flow, the pump basically increases the Bernoulli head of the flow between point 1, the eye, and point 2, the exit. From Eq. (3.67), neglecting viscous work and heat transfer, this change is denoted by H:

$$H = \left(\frac{p}{\rho g} + \frac{V^2}{2g} + z\right)_2 - \left(\frac{p}{\rho g} + \frac{V^2}{2g} + z\right)_1 = h_s - h_f \tag{11.1}$$

where h_s is the pump head supplied and h_f the losses. The net head H is a primary output parameter for any turbomachine. Since Eq. (11.1) is for incompressible flow, it must be modified for gas compressors with large density changes.

Usually V_2 and V_1 are about the same, $z_2 - z_1$ is no more than a meter or so, and the net pump head is essentially equal to the change in pressure head

$$H \approx \frac{p_2 - p_1}{\rho g} = \frac{\Delta p}{\rho g} \tag{11.2}$$

The power delivered to the fluid simply equals the specific weight times the discharge times the net head change

$$P_w = \rho g Q H \tag{11.3}$$

This is traditionally called the *water horsepower*. The power required to drive the pump is the *brake horsepower*[1]

$$\text{bhp} = \omega T \tag{11.4}$$

where ω is the shaft angular velocity and T the shaft torque. If there were no losses, P_w and brake horsepower would be equal, but of course P_w is actually less, and the *efficiency* η of the pump is defined as

$$\eta = \frac{P_w}{\text{bhp}} = \frac{\rho g Q H}{\omega T} \tag{11.5}$$

The chief aim of the pump designer is to make η as high as possible over as broad a range of discharge Q as possible.

[1] Conversion factors may be needed: 1 hp = 550 ft · lbf/s = 746 W.



ketabline.com Ebook.ketabline.com

The efficiency is basically composed of three parts: volumetric, hydraulic, and mechanical. The *volumetric efficiency* is

$$\eta_v = \frac{Q}{Q + Q_L} \tag{11.6}$$

where Q_L is the loss of fluid due to leakage in the impeller-casing clearances. The *hydraulic efficiency* is

$$\eta_h = 1 - \frac{h_f}{h_s} \tag{11.7}$$

where h_f has three parts: (1) *shock* loss at the eye due to imperfect match between inlet flow and the blade entrances, (2) *friction* losses in the blade passages, and (3) *circulation* loss due to imperfect match at the exit side of the blades.

Finally, the *mechanical efficiency* is

$$\eta_m = 1 - \frac{P_f}{\text{bhp}} \tag{11.8}$$

where P_f is the power loss due to mechanical friction in the bearings, packing glands, and other contact points in the machine.

By definition, the total efficiency is simply the product of its three parts

$$\eta \equiv \eta_v \eta_h \eta_m \tag{11.9}$$

The designer has to work in all three areas to improve the pump.

Elementary Pump Theory

You may have thought that Eqs. (11.1) to (11.9) were formulas from pump *theory*. Not so; they are merely definitions of performance parameters and cannot be used in any predictive mode. To actually *predict* the head, power, efficiency, and flow rate of a pump, two theoretical approaches are possible: (1) simple one-dimensional-flow formulas and (2) complex digital-computer models which account for viscosity and three-dimensionality. Many of the best design improvements still come from testing and experience, and pump research remains a very active field [39]. The last 10 years have seen considerable advances in *computational fluid-dynamics* (CFD) modeling of flow in turbomachines [42], and at least eight commercial turbulent-flow three-dimensional CFD codes are now available.

To construct an elementary theory of pump performance, we assume one-dimensional flow and combine idealized fluid-velocity vectors through the impeller with the angular-momentum theorem for a control volume, Eq. (3.55).

The idealized velocity diagrams are shown in Fig. 11.4. The fluid is assumed to enter the impeller at $r = r_1$ with velocity component w_1 tangent to the blade angle β_1 plus circumferential speed $u_1 = \omega r_1$ matching the tip speed of the impeller. Its absolute entrance velocity is thus the vector sum of w_1 and u_1, shown as V_1. Similarly, the flow exits at $r = r_2$ with component w_2 parallel to the blade angle β_2 plus tip speed $u_2 = \omega r_2$, with resultant velocity V_2.

We applied the angular-momentum theorem to a turbomachine in Example 3.14 (Fig. 3.13) and arrived at a result for the applied torque T

$$T = \rho Q(r_2 V_{t2} - r_1 V_{t1})$$



ketabline.com Ebook.ketabline.com

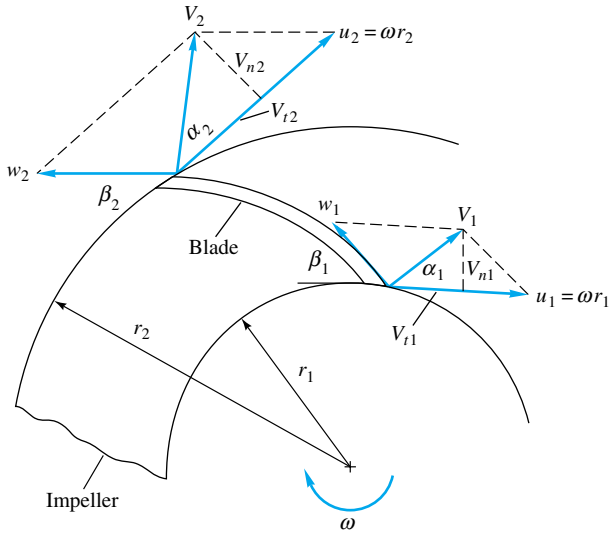


Fig. 11.4 Inlet and exit velocity diagrams for an idealized pump impeller.

where V_{t1} and V_{t2} are the absolute circumferential velocity components of the flow. The power delivered to the fluid is thus

$$P_w = \omega T = \rho Q(u_2 V_{t2} - u_1 V_{t1})$$

or

$$H = \frac{P_w}{\rho g Q} = \frac{1}{g}(u_2 V_{t2} - u_1 V_{t1}) \tag{11.11}$$

These are the *Euler turbomachine equations*, showing that the torque, power, and ideal head are functions only of the rotor-tip velocities $u_{1,2}$ and the absolute fluid tangential velocities $V_{t1,2}$, independent of the axial velocities (if any) through the machine.

Additional insight is gained by rewriting these relations in another form. From the geometry of Fig. 11.4

$$V^2 = u^2 + w^2 - 2uw\cos\beta \qquad w\cos\beta = u - V_t$$

or

$$uV_t = \tfrac{1}{2}(V^2 + u^2 - w^2) \tag{11.12}$$

Substituting this into Eq. (11.11) gives

$$H = \frac{1}{2g}[(V_2^2 - V_1^2) + (u_2^2 - u_1^2) - (w_2^2 - w_1^2)] \tag{11.13}$$

Thus the ideal head relates to the absolute plus the relative kinetic-energy change of the fluid minus the rotor-tip kinetic-energy change. Finally, substituting for H from its definition in Eq. (11.1) and rearranging, we obtain the classic relation

$$\frac{p}{\rho g} + z + \frac{w^2}{2g} - \frac{r^2\omega^2}{2g} = \text{const} \tag{11.14}$$

This is the *Bernoulli equation in rotating coordinates* and applies three-dimensional ideal incompressible flow.



ketabline.com Ebook.ketabline.com

For a centrifugal pump, the power can be related to the radial velocity $V_n = V_t \tan \alpha$ and the continuity relation

$$P_w = \rho Q(u_2 V_{n2} \cot \alpha_2 - u_1 V_{n1} \cot \alpha_1) \tag{11.15}$$

where

$$V_{n2} = \frac{Q}{2\pi r_2 b_2} \qquad \text{and} \qquad V_{n1} = \frac{Q}{2\pi r_1 b_1}$$

and where b_1 and b_2 are the blade widths at inlet and exit. With the pump parameters r_1, r_2, β_1, β_2, and ω known, Eqs. (11.11) or Eq. (11.15) is used to compute idealized power and head versus discharge. The "design" flow rate Q^* is commonly estimated by assuming that the flow enters exactly normal to the impeller

$$\alpha_1 = 90° \qquad V_{n1} = V_1 \tag{11.16}$$

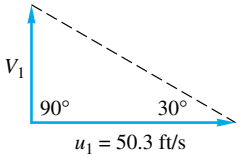
We can expect this simple analysis to yield estimates within ±25 percent for the head, water horsepower, and discharge of a pump. Let us illustrate with an example.

EXAMPLE 11.1

Given are the following data for a commercial centrifugal water pump: $r_1 = 4$ in, $r_2 = 7$ in, $\beta_1 = 30°$, $\beta_2 = 20°$, speed = 1440 r/min. Estimate (*a*) the design-point discharge, (*b*) the water horsepower, and (*c*) the head if $b_1 = b_2 = 1.75$ in.

Solution

Part (a) The angular velocity is $\omega = 2\pi$ r/s $= 2\pi(1440/60) = 150.8$ rad/s. Thus the tip speeds are $u_1 = \omega r_1 = 150.8(4/12) = 50.3$ ft/s and $u_2 = \omega r_2 = 150.8(7/12) = 88.0$ ft/s. From the inlet-velocity diagram, Fig. E11.1*a*, with $\alpha_1 = 90°$ for design point, we compute



E11.1a

$$V_{n1} = u_1 \tan 30° = 29.0 \text{ ft/s}$$

whence the discharge is

$$Q = 2\pi r_1 b_1 V_{n1} = (2\pi)\left(\frac{4}{12}\right)\left(\frac{1.75}{12}\right)(29.0)$$

$$= (8.87 \text{ ft}^3\text{/s})(60 \text{ s/min})\left(\frac{1728}{231} \text{ gal/ft}^3\right)$$

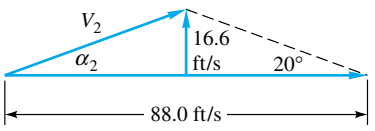
$$= 3980 \text{ gal/min} \qquad \textit{Ans. (a)}$$

(The actual pump produces about 3500 gal/min.)

Part (b) The outlet radial velocity follows from Q

$$V_{n2} = \frac{Q}{2\pi r_2 b_2} = \frac{8.87}{2\pi(\frac{7}{12})(1.75/12)} = 16.6 \text{ ft/s}$$

This enables us to construct the outlet-velocity diagram as in Fig. E11.1*b*, given $\beta_2 = 20°$. The tangential component is



E11.1b

$$V_{t2} = u_2 - V_{n2} \cot \beta_2 = 88.0 - 16.6 \cot 20° = 42.4 \text{ ft/s}$$

$$\alpha_2 = \tan^{-1} \frac{16.6}{42.4} = 21.4°$$



ketabline.com Ebook.ketabline.com

The power is then computed from Eq. (11.11) with $V_{t1} = 0$ at the design point

$$P_w = \rho Q u_2 V_{t2} = (1.94 \text{ slugs/ft}^3)(8.87 \text{ ft}^3\text{/s})(88.0 \text{ ft/s})(42.4 \text{ ft/s})$$

$$= \frac{64{,}100 \text{ ft} \cdot \text{lbf/s}}{550} = 117 \text{ hp} \qquad \textit{Ans. (b)}$$

(The actual pump delivers about 125 water horsepower, requiring 147 bhp at 85 percent efficiency.)

Part (c) Finally, the head is estimated from Eq. (11.11)

$$H \approx \frac{P_w}{\rho g Q} = \frac{64{,}100 \text{ ft} \cdot \text{lbf/s}}{(62.4 \text{ lbf/ft}^3)(8.87 \text{ ft}^3\text{/s})} = 116 \text{ ft} \qquad \textit{Ans. (c)}$$

(The actual pump develops about 140-ft head.) Improved methods for obtaining closer estimates are given in advanced references [for example, 6, 8, and 31].

Effect of Blade Angle on Pump Head

The simple theory above can be used to predict an important blade-angle effect. If we neglect inlet angular momentum, the theoretical water horsepower is

$$P_w = \rho Q u_2 V_{t2} \tag{11.17}$$

where $$V_{t2} = u_2 - V_{n2} \cot \beta_2 \qquad V_{n2} = \frac{Q}{2\pi r_2 b_2}$$

Then the theoretical head from Eq. (11.11) becomes

$$H \approx \frac{u_2^2}{g} - \frac{u_2 \cot \beta_2}{2\pi r_2 b_2 g} Q \tag{11.18}$$

The head varies linearly with discharge Q, having a shutoff value u_2^2/g, where u_2 is the exit blade-tip speed. The slope is negative if $\beta_2 < 90°$ (backward-curved blades) and positive for $\beta_2 > 90°$ (forward-curved blades). This effect is shown in Fig. 11.5 and is accurate only at low flow rates.

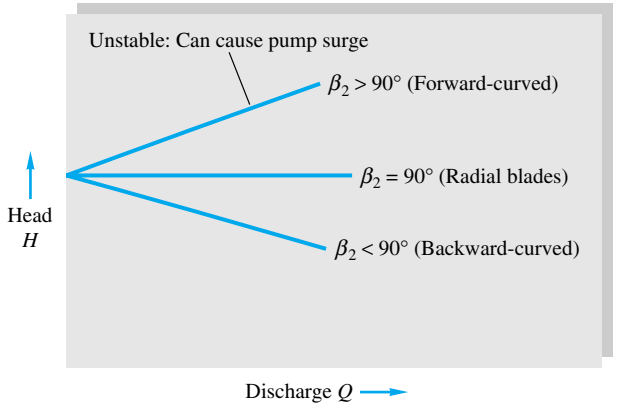


Fig. 11.5 Theoretical effect of blade exit angle on pump head versus discharge.



ketabline.com Ebook.ketabline.com

The measured shutoff head of centrifugal pumps is only about 60 percent of the theoretical value $H_0 = \omega^2 r_2^2 / g$. With the advent of the laser-doppler anemometer, researchers can now make detailed three-dimensional flow measurements inside pumps and can even animate the data into a movie [40].

The positive-slope condition in Fig. 11.5 can be unstable and can cause pump *surge*, an oscillatory condition where the pump "hunts" for the proper operating point. Surge may cause only rough operation in a liquid pump, but it can be a major problem in gas-compressor operation. For this reason a backward-curved or radial blade design is generally preferred. A survey of the problem of pump stability is given by Greitzer [41].

11.3 Pump Performance Curves and Similarity Rules

Since the theory of the previous section is rather qualitative, the only solid indicator of a pump's performance lies in extensive testing. For the moment let us discuss the centrifugal pump in particular. The general principles and the presentation of data are exactly the same for mixed-flow and axial-flow pumps and compressors.

Performance charts are almost always plotted for constant shaft-rotation speed n (in r/min usually). The basic independent variable is taken to be discharge Q (in gal/min usually for liquids and ft^3/min for gases). The dependent variables, or "output," are taken to be head H (pressure rise Δp for gases), brake horsepower (bhp), and efficiency η.

Figure 11.6 shows typical performance curves for a centrifugal pump. The head is approximately constant at low discharge and then drops to zero at $Q = Q_{max}$. At this speed and impeller size, the pump cannot deliver any more fluid than Q_{max}. The positive-slope part of the head is shown dashed; as mentioned earlier, this region can be unstable and can cause hunting for the operating point.

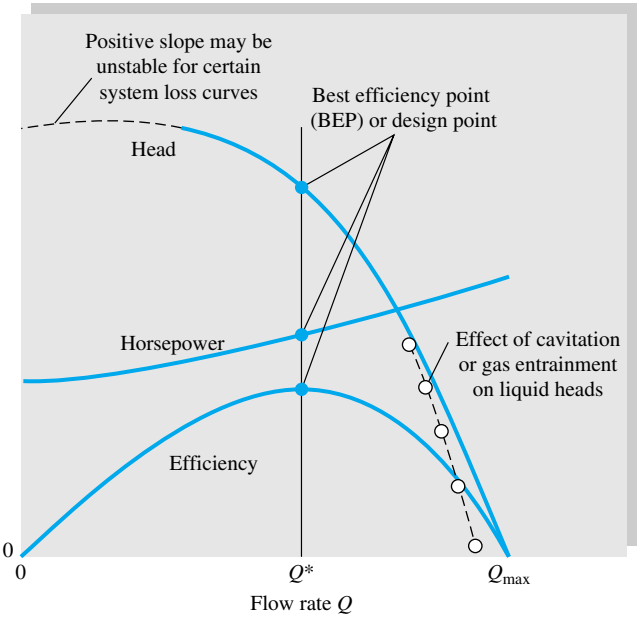


Fig. 11.6 Typical centrifugal pump performance curves at constant impeller-rotation speed. The units are arbitrary.



ketabline.com Ebook.ketabline.com

The efficiency η is always zero at no flow and at Q_{max}, and it reaches a maximum, perhaps 80 to 90 percent, at about $0.6Q_{max}$. This is the *design flow rate* Q^* or *best efficiency point* (BEP), $\eta = \eta_{max}$. The head and horsepower at BEP will be termed H^* and P^* (or bhp*), respectively. It is desirable that the efficiency curve be flat near η_{max}, so that a wide range of efficient operation is achieved. However, some designs simply do not achieve flat efficiency curves. Note that η is not independent of H and P but rather is calculated from the relation in Eq. (11.5), $\eta = \rho gQH/P$.

As shown in Fig. 11.6, the horsepower required to drive the pump typically rises monotonically with the flow rate. Sometimes there is a large power rise beyond the BEP, especially for radial-tipped and forward-curved blades. This is considered undesirable because a much larger motor is then needed to provide high flow rates. Backward-curved blades typically have their horsepower level off above BEP ("nonoverloading" type of curve).

Measured Performance Curves

Figure 11.7 shows actual performance data for a commercial centrifugal pump. Figure 11.7*a* is for a basic casing size with three different impeller diameters. The head curves $H(Q)$ are shown, but the horsepower and efficiency curves have to be inferred from the contour plots. Maximum discharges are not shown, being far outside the normal operating range near the BEP. Everything is plotted raw, of course [feet, horsepower, gallons per minute (1 U.S. gal = 231 in^3)] since it is to be used directly by designers. Figure 11.7*b* is the same pump design with a 20 percent larger casing, a lower speed, and three larger impeller diameters. Comparing the two pumps may be a little confusing: The larger pump produces exactly the same discharge but only half the horsepower and half the head. This will be readily understood from the scaling or similarity laws we are about to formulate.

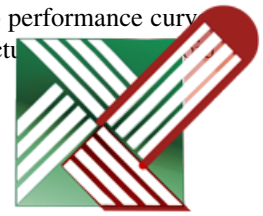
A point often overlooked is that raw curves like Fig. 11.7 are strictly applicable to a fluid of a certain density and viscosity, in this case water. If the pump were used to deliver, say, mercury, the brake horsepower would be about 13 times higher while Q, H, and η would be about the same. But in that case H should be interpreted as feet of *mercury*, not feet of water. If the pump were used for SAE 30 oil, *all* data would change (brake horsepower, Q, H, and η) due to the large change in viscosity (Reynolds number). Again this should become clear with the similarity rules.

Net Positive-Suction Head

In the top of Fig. 11.7 is plotted the *net positive-suction head* (NPSH), which is the head required at the pump inlet to keep the liquid from cavitating or boiling. The pump inlet or suction side is the low-pressure point where cavitation will first occur. The NPSH is defined as

$$\text{NPSH} = \frac{p_i}{\rho g} + \frac{V_i^2}{2g} - \frac{p_v}{\rho g} \tag{11.19}$$

where p_i and V_i are the pressure and velocity at the pump inlet and p_v is the vapor pressure of the liquid. Given the left-hand side, NPSH, from the pump performance curv we must ensure that the right-hand side is equal or greater in the actu cavitation.



ketabline.com Ebook.ketabline.com

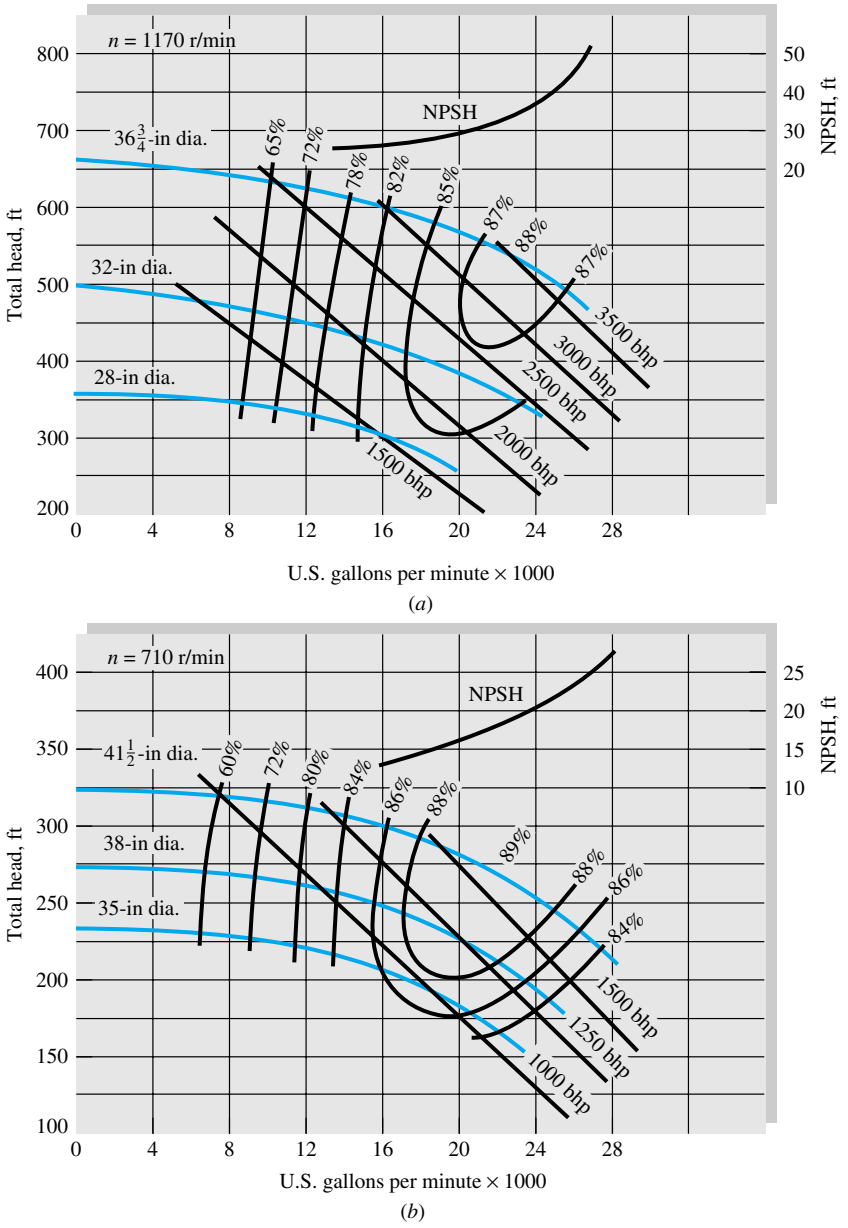
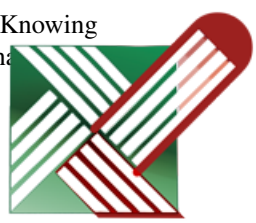


Fig. 11.7 Measured-performance curves for two models of a centrifugal water pump: (*a*) basic casing with three impeller sizes; (*b*) 20 percent larger casing with three larger impellers at slower speed. *(Courtesy of Ingersoll-Rand Corporation, Cameron Pump Division.)*

If the pump inlet is placed at a height Z_i above a reservoir whose free surface is at pressure p_a, we can use Bernoulli's equation to rewrite NPSH as

$$\text{NPSH} = \frac{p_a}{\rho g} - Z_i - h_{fi} - \frac{p_v}{\rho g} \tag{11.20}$$

where h_{fi} is the friction-head loss between the reservoir and the pump inlet. Knowing p_a and h_{fi}, we can set the pump at a height Z_i which will keep the right-ha
greater than the "required" NPSH plotted in Fig. 11.7.



ketabline.com Ebook.ketabline.com

If cavitation does occur, there will be pump noise and vibration, pitting damage to the impeller, and a sharp dropoff in pump head and discharge. In some liquids this deterioration starts before actual boiling, as dissolved gases and light hydrocarbons are liberated.

Deviations from Ideal Pump Theory

The actual pump head data in Fig. 11.7 differ considerably from ideal theory, Eq. (11.18). Take, e.g., the 36.75-in-diameter pump at 1170 r/min in Fig. 11.7*a*. The theoretical shutoff head is

$$H_0(\text{ideal}) = \frac{\omega^2 r_2^2}{g} = \frac{[1170(2\pi/60)\ \text{rad/s}]^2[(36.75/2)/(12)\ \text{ft}]^2}{32.2\ \text{ft/s}^2} = 1093\ \text{ft}$$

From Fig. 11.7*a*, at $Q = 0$, we read the actual shutoff head to be only 670 ft, or 61 percent of the theoretical value. This is a sharp dropoff and is indicative of nonrecoverable losses of three types:

1. *Impeller recirculation loss,* significant only at low flow rates
2. *Friction losses* on the blade and passage surfaces, which increase monotonically with the flow rate
3. *"Shock" loss* due to mismatch between the blade angles and the inlet flow direction, especially significant at high flow rates

These are complicated three-dimensional-flow effects and hence are difficult to predict. Although, as mentioned, numerical (CFD) techniques are becoming more important [42], modern performance prediction is still a blend of experience, empirical correlations, idealized theory, and CFD modifications [45].

EXAMPLE 11.2

The 32-in pump of Fig. 11.7*a* is to pump 24,000 gal/min of water at 1170 r/min from a reservoir whose surface is at 14.7 lbf/in^2 absolute. If head loss from reservoir to pump inlet is 6 ft, where should the pump inlet be placed to avoid cavitation for water at (*a*) 60°F, $p_v = 0.26$ lbf/in^2 absolute, SG = 1.0 and (*b*) 200°F, $p_v = 11.52$ lbf/in^2 absolute, SG = 0.9635?

Solution

Part (a) For either case read from Fig. 11.7*a* at 24,000 gal/min that the required NPSH is 40 ft. For this case $\rho g = 62.4$ lbf/ft^3. From Eq. (11.20) it is necessary that

$$\text{NPSH} \le \frac{p_a - p_v}{\rho g} - Z_i - h_{fi}$$

or

$$40\ \text{ft} \le \frac{(14.7 - 0.26)(144)}{62.4} - Z_i - 6.0$$

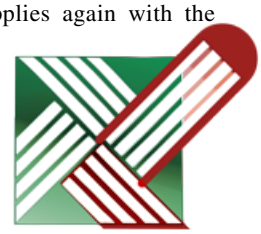
or

$$Z_i \le 27.3 - 40 = -12.7\ \text{ft} \qquad \textit{Ans. (a)}$$

The pump must be placed at least 12.7 ft *below* the reservoir surface to avoid cavitation.

Part (b) For this case $\rho g = 62.4(0.9635) = 60.1$ lbf/ft^3. Equation (11.20) applies again with the higher p_v

$$40\ \text{ft} \le \frac{(14.7 - 11.52)(144)}{60.1} - Z_i - 6.0$$



ketabline.com Ebook.ketabline.com

or $$Z_i \leq 1.6 - 40 = -38.4 \text{ ft} \qquad \textit{Ans. (b)}$$

The pump must now be placed at least 38.4 ft below the reservoir surface. These are unusually stringent conditions because a large, high-discharge pump requires a large NPSH.

Dimensionless Pump Performance

For a given pump design, the output variables H and brake horsepower should be dependent upon discharge Q, impeller diameter D, and shaft speed n, at least. Other possible parameters are the fluid density ρ, viscosity μ, and surface roughness ϵ. Thus the performance curves in Fig. 11.7 are equivalent to the following assumed functional relations:[2]

$$gH = f_1(Q, D, n, \rho, \mu, \epsilon) \qquad \text{bhp} = f_2(Q, D, n, \rho, \mu, \epsilon) \tag{11.21}$$

This is a straightforward application of dimensional-analysis principles from Chap. 5. As a matter of fact, it was given as an exercise (Prob. 5.20). For each function in Eq. (11.21) there are seven variables and three primary dimensions (M, L, and T); hence we expect $7 - 3 = 4$ dimensionless pis, and that is what we get. You can verify as an exercise that appropriate dimensionless forms for Eqs. (11.21) are

$$\frac{gH}{n^2D^2} = g_1\left(\frac{Q}{nD^3}, \frac{\rho nD^2}{\mu}, \frac{\epsilon}{D}\right)$$
$$\frac{\text{bhp}}{\rho n^3D^5} = g_2\left(\frac{Q}{nD^3}, \frac{\rho nD^2}{\mu}, \frac{\epsilon}{D}\right) \tag{11.22}$$

The quantities $\rho nD^2/\mu$ and ϵ/D are recognized as the Reynolds number and roughness ratio, respectively. Three new pump parameters have arisen:

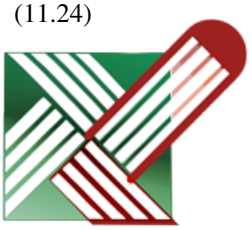
$$\text{Capacity coefficient } C_Q = \frac{Q}{nD^3}$$
$$\text{Head coefficient } C_H = \frac{gH}{n^2D^2} \tag{11.23}$$
$$\text{Power coefficient } C_P = \frac{\text{bhp}}{\rho n^3D^5}$$

Note that only the power coefficient contains fluid density, the parameters C_Q and C_H being kinematic types.

Figure 11.7 gives no warning of viscous or roughness effects. The Reynolds numbers are from 0.8 to 1.5×10^7, or fully turbulent flow in all passages probably. The roughness is not given and varies greatly among commercial pumps. But at such high Reynolds numbers we expect more or less the same percentage effect on all these pumps. Therefore it is common to assume that the Reynolds number and the roughness ratio have a constant effect, so that Eqs. (11.23) reduce to, approximately,

$$C_H \approx C_H(C_Q) \qquad C_P \approx C_P(C_Q) \tag{11.24}$$

[2] We adopt gH as a variable instead of H for dimensional reasons.



ketabline.com Ebook.ketabline.com

For geometrically similar pumps, we expect head and power coefficients to be (nearly) unique functions of the capacity coefficient. We have to watch out that the pumps are geometrically similar or nearly so because (1) manufacturers put different-sized impellers in the same casing, thus violating geometric similarity, and (2) large pumps have smaller ratios of roughness and clearances to impeller diameter than small pumps. In addition, the more viscous liquids will have significant Reynolds-number effects; e.g., a factor-of-3 or more viscosity increase causes a clearly visible effect on C_H and C_P.

The efficiency η is already dimensionless and is uniquely related to the other three. It varies with C_Q also

$$\eta \equiv \frac{C_H C_Q}{C_P} = \eta(C_Q) \tag{11.25}$$

We can test Eqs. (11.24) and (11.25) from the data of Fig. 11.7. The impeller diameters of 32 and 38 in are approximately 20 percent different in size, and so their ratio of impeller to casing size is the same. The parameters C_Q, C_H, and C_P are computed with n in r/s, Q in ft^3/s (gal/min $\times$ 2.23 $\times$ 10^{-3}), H and D in ft, g = 32.2 ft/s^2, and brake horsepower in horsepower times 550 ft $\cdot$ lbf/(s $\cdot$ hp). The nondimensional data are then plotted in Fig. 11.8. A dimensionless suction-head coefficient is also defined

$$C_{HS} = \frac{g(\text{NPSH})}{n^2 D^2} = C_{HS}(C_Q) \tag{11.26}$$

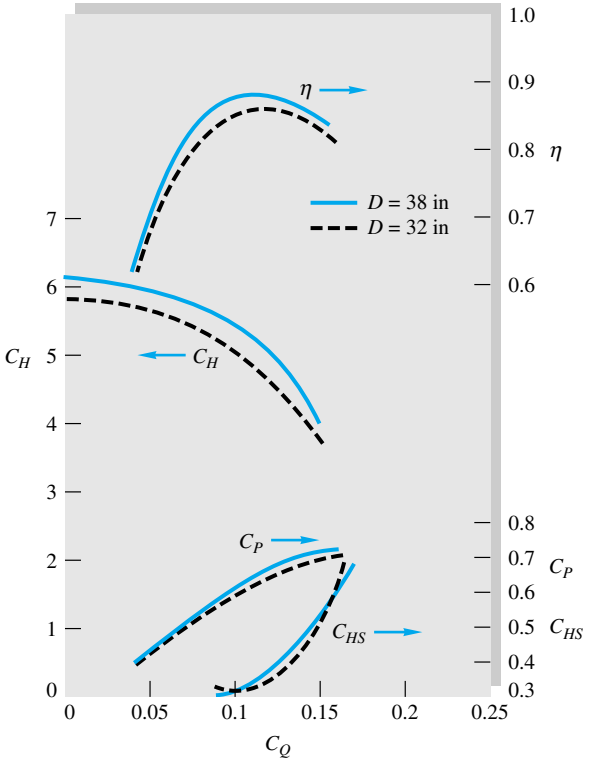


Fig. 11.8 Nondimensional plot of the pump performance data from Fig. 11.7. These numbers are not representative of other pump designs.



ketabline.com Ebook.ketabline.com

The coefficients C_P and C_{HS} are seen to correlate almost perfectly into a single function of C_Q, while η and C_H data deviate by a few percent. The last two parameters are more sensitive to slight discrepancies in model similarity; since the larger pump has smaller roughness and clearance ratios and a 40 percent larger Reynolds number, it develops slightly more head and is more efficient. The overall effect is a resounding victory for dimensional analysis.

The best-efficiency point in Fig. 11.8 is approximately

$$\eta_{\max} \approx 0.88: \qquad C_{Q^*} \approx 0.115 \qquad C_{P^*} \approx 0.65 \qquad C_{H^*} \approx 5.0 \qquad C_{HS^*} \approx 0.37 \tag{11.27}$$

These values can be used to estimate the BEP performance of any size pump in this geometrically similar family. In like manner, the shutoff head is $C_H(0) \approx 6.0$, and by extrapolation the shutoff power is $C_P(0) \approx 0.25$ and the maximum discharge is $C_{Q,\max} \approx 0.23$. Note, however, that Fig. 11.8 gives no reliable information about, say, the 28- or 35-in impellers in Fig. 11.7, which have a different impeller-to-casing-size ratio and thus must be correlated separately.

By comparing values of n^2D^2, nD^3, and n^3D^5 for two pumps in Fig. 11.7 we can see readily why the large pump had the same discharge but less power and head:

	D, ft	n, r/s	Discharge nD^3, ft^3/s	Head n^2D^2/g, ft	Power $\rho n^3D^5/550$, hp
Fig. 11.7*a*	32/12	1170/60	370	84	3527
Fig. 11.7*b*	38/12	710/60	376	44	1861
Ratio	—	—	1.02	0.52	0.53

Discharge goes as nD^3, which is about the same for both pumps. Head goes as n^2D^2 and power as n^3D^5 for the same ρ (water), and these are about half as much for the larger pump. The NPSH goes as n^2D^2 and is also half as much for the 38-in pump.

EXAMPLE 11.3

A pump from the family of Fig. 11.8 has $D = 21$ in and $n = 1500$ r/min. Estimate (*a*) discharge, (*b*) head, (*c*) pressure rise, and (*d*) brake horsepower of this pump for water at 60°F and best efficiency.

Solution

Part (a) In BG units take $D = 21/12 = 1.75$ ft and $n = 1500/60 = 25$ r/s. At 60°F, ρ of water is 1.94 slugs/ft^3. The BEP parameters are known from Fig. 11.8 or Eqs. (11.27). The BEP discharge is thus

$$Q^* = C_{Q^*}nD^3 = 0.115(25)(1.75)^3 = (15.4 \text{ ft}^3/\text{s})(448.8) = 6900 \text{ gal/min} \qquad \textit{Ans. (a)}$$

Part (b) Similarly, the BEP head is

$$H^* = \frac{C_{H^*}n^2D^2}{g} = \frac{5.0(25)^2(1.75)^2}{32.2} = 300\text{-ft water}$$



ketabline.com Ebook.ketabline.com

Part (c) Since we are not given elevation or velocity-head changes across the pump, we neglect them and estimate

$$\Delta p \approx \rho g H = 1.94(32.2)(300) = 18{,}600 \text{ lbf/ft}^2 = 129 \text{ lbf/in}^2 \qquad \textit{Ans. (c)}$$

Part (d) Finally, the BEP power is

$$P^* = C_{P*}\rho n^3 D^5 = 0.65(1.94)(25)^3(1.75)^5$$

$$= \frac{323{,}000 \text{ ft} \cdot \text{lbf/s}}{550} = 590 \text{ hp} \qquad \textit{Ans. (d)}$$

EXAMPLE 11.4

We want to build a pump from the family of Fig. 11.8, which delivers 3000 gal/min water at 1200 r/min at best efficiency. Estimate (*a*) the impeller diameter, (*b*) the maximum discharge, (*c*) the shutoff head, and (*d*) the NPSH at best efficiency.

Solution

Part (a) 3000 gal/min = 6.68 ft^3/s and 1200 r/min = 20 r/s. At BEP we have

$$Q^* = C_{Q*}nD^3 = 6.68 \text{ ft}^3/\text{s} = (0.115)(20)D^3$$

or

$$D = \left[\frac{6.68}{0.115(20)}\right]^{1/3} = 1.43 \text{ ft} = 17.1 \text{ in} \qquad \textit{Ans. (a)}$$

Part (b) The maximum Q is related to Q^* by a ratio of capacity coefficients

$$Q_{\max} = \frac{Q^* C_{Q,\max}}{C_{Q^*}} \approx \frac{3000(0.23)}{0.115} = 6000 \text{ gal/min} \qquad \textit{Ans. (b)}$$

Part (c) From Fig. 11.8 we estimated the shutoff head coefficient to be 6.0. Thus

$$H(0) \approx \frac{C_H(0)n^2D^2}{g} = \frac{6.0(20)^2(1.43)^2}{32.2} = 152 \text{ ft} \qquad \textit{Ans. (c)}$$

Part (d) Finally, from Eq. (11.27), the NPSH at BEP is approximately

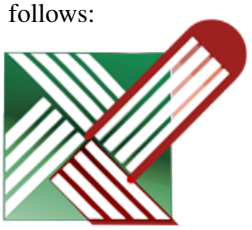
$$\text{NPSH}^* = \frac{C_{HS*}n^2D^2}{g} = \frac{0.37(20)^2(1.43)^2}{32.2} = 9.4 \text{ ft} \qquad \textit{Ans. (d)}$$

Since this a small pump, it will be less efficient than the pumps in Fig. 11.8, probably about 85 percent maximum.

Similarity Rules

The success of Fig. 11.8 in correlating pump data leads to simple rules for comparing pump performance. If pump 1 and pump 2 are from the same geometric family and are operating at homologous points (the same dimensionless position on a chart such as Fig. 11.8), their flow rates, heads, and powers will be related as follows:

$$\frac{Q_2}{Q_1} = \frac{n_2}{n_1}\left(\frac{D_2}{D_1}\right)^3 \qquad \frac{H_2}{H_1} = \left(\frac{n_2}{n_1}\right)^2\left(\frac{D_2}{D_1}\right)^2$$



ketabline.com Ebook.ketabline.com

$$\frac{P_2}{P_1} = \frac{\rho_2}{\rho_1}\left(\frac{n_2}{n_1}\right)^3\left(\frac{D_2}{D_1}\right)^5 \tag{11.28}$$

These are the *similarity rules*, which can be used to estimate the effect of changing the fluid, speed, or size on any dynamic turbomachine—pump or turbine—within a geometrically similar family. A graphic display of these rules is given in Fig. 11.9, showing the effect of speed and diameter changes on pump performance. In Fig. 11.9*a* the size is held constant and the speed is varied 20 percent, while Fig. 11.9*b* shows a 20 percent size change at constant speed. The curves are plotted to scale but with arbitrary units. The speed effect (Fig. 11.9*a*) is substantial, but the size effect (Fig. 11.9*b*) is even more dramatic, especially for power, which varies as D^5. Generally we see that a given pump family can be adjusted in size and speed to fit a variety of system characteristics.

Strictly speaking, we would expect for perfect similarity that $\eta_1 = \eta_2$, but we have seen that larger pumps are more efficient, having a higher Reynolds number and lower roughness and clearance ratios. Two empirical correlations are recommended for maximum efficiency. One, developed by Moody [43] for turbines but also used for pumps, is a size effect. The other, suggested by Anderson [44] from thousands of pump tests, is a flow-rate effect:

Size changes [43]:
$$\frac{1-\eta_2}{1-\eta_1} \approx \left(\frac{D_1}{D_2}\right)^{1/4} \tag{11.29a}$$

Flow-rate changes [44]:
$$\frac{0.94-\eta_2}{0.94-\eta_1} \approx \left(\frac{Q_1}{Q_2}\right)^{0.32} \tag{11.29b}$$

Anderson's formula (11.29*b*) makes the practical observation that even an infinitely large pump will have losses. He thus proposes a maximum possible efficiency of 94 percent, rather than 100 percent. Anderson recommends that the same formula be used

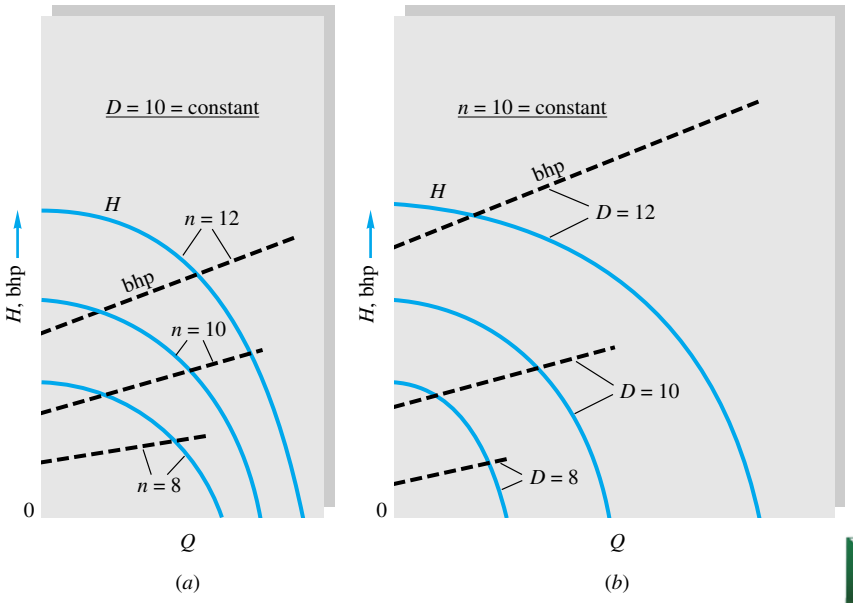


Fig. 11.9 Effect of changes in size and speed on homologous pump performance: (*a*) 20 percent change in speed at constant size; (*b*) 20 percent change in size at constant speed.



ketabline.com Ebook.ketabline.com

for turbines if the constant 0.94 is replaced by 0.95. The formulas in Eq. (11.29) assume the same value of surface roughness for both machines—one could micropolish a small pump and achieve the efficiency of a larger machine.

Effect of Viscosity

Centrifugal pumps are often used to pump oils and other viscous liquids up to 1000 times the viscosity of water. But the Reynolds numbers become low turbulent or even laminar, with a strong effect on performance. Figure 11.10 shows typical test curves of head and brake horsepower versus discharge. High viscosity causes a dramatic drop in head and discharge and increases in power requirements. The efficiency also drops substantially according to the following typical results:

μ/μ_{water}	1.0	10.0	100	1000
η_{max}, %	85	76	52	11

Beyond about $300\mu_{water}$ the deterioration in performance is so great that a positive-displacement pump is recommended.

11.4 Mixed- and Axial-Flow Pumps: The Specific Speed

We have seen from the previous section that the modern centrifugal pump is a formidable device, able to deliver very high heads and reasonable flow rates with excellent efficiency. It can match many system requirements. But basically the centrifugal pump is a high-head, low-flow machine, whereas there are many applications requiring low head and high discharge. To see that the centrifugal design is not convenient for such systems, consider the following example.

EXAMPLE 11.5

We want to use a centrifugal pump from the family of Fig. 11.8 to deliver 100,000 gal/min of water at 60°F with a head of 25 ft. What should be (*a*) the pump size and speed and (*b*) brake horsepower, assuming operation at best efficiency?

Solution

Part (a) Enter the known head and discharge into the BEP parameters from Eq. (11.27):

$$H^* = 25 \text{ ft} = \frac{C_{H^*} n^2 D^2}{g} = \frac{5.0 n^2 D^2}{32.2}$$

$$Q^* = 100{,}000 \text{ gal/min} = 222.8 \text{ ft}^3/\text{s} = C_{Q^*} n D^3 = 0.115 n D^3$$

The two unknowns are n and D. Solve simultaneously for

$$D = 12.4 \text{ ft} \qquad n = 1.03 \text{ r/s} = 62 \text{ r/min} \qquad \textit{Ans. (a)}$$



If you wish to avoid algebraic manipulation, simply program the above two simultaneous equations in EES, using English units:

```
25 = 5.0*n^2*D^2/32.2
222.8 = 0.115*n*D^3
```



ketabline.com Ebook.ketabline.com

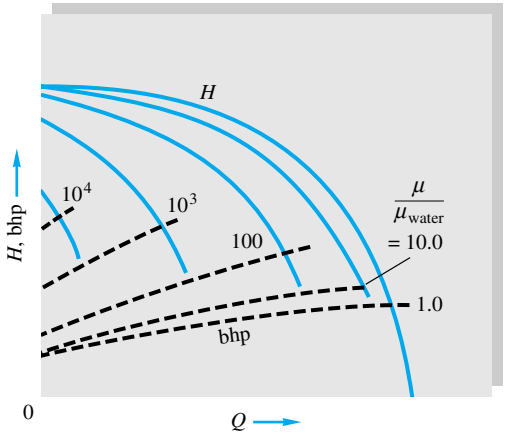


Fig. 11.10 Effect of viscosity on centrifugal pump performance.

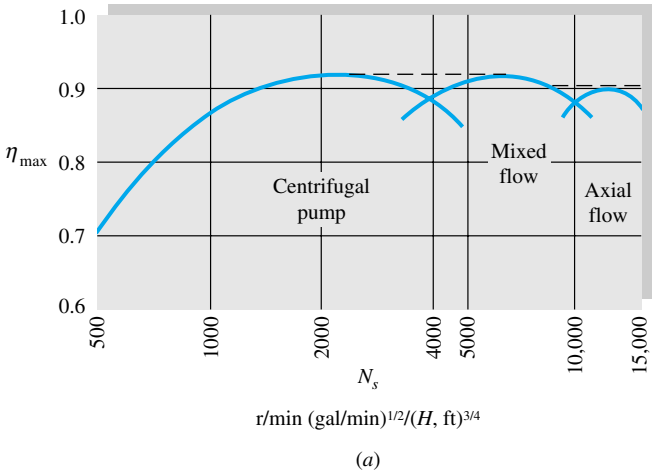


Fig. 11.11 (*a*) Optimum efficiency and (*b*) vane design of dynamic-pump families as a function of specific speed.

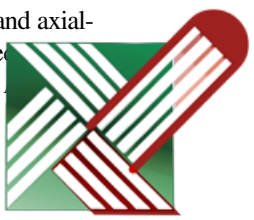
Specify in Variable Information that n and D are positive, and EES promptly returns the correct solution: `D = 12.36 ft` and `n = 1.027 r/s`.

Part (b) The most efficient horsepower is then, from Eq. (11.27),

$$\text{bhp}^* \approx C_{P^*}\rho n^3 D^5 = \frac{0.65(1.94)(1.03)^3(12.4)^5}{550} = 720 \text{ hp} \qquad \textit{Ans. (b)}$$

The solution to Example 11.5 is mathematically correct but results in a grotesque pump: an impeller more than 12 ft in diameter, rotating so slowly one can visualize oxen walking in a circle turning the shaft.

There are other dynamic-pump designs which do provide low head and high discharge. For example, there is a type of 38-in, 710 r/min pump, e.g., with the same input parameters as Fig. 11.7*b*, which will deliver the 25-ft head and 100,000 gal/min flow rate called for in Example 11.5. This is done by allowing the flow to pass through the impeller with an axial-flow component and less centrifugal component. The passages can be opened up to the increased flow rate with very little size increase, but the drop in radial outlet velocity decreases the head produced. These are the mixed-flow (part radial, part axial) and axial-flow (propeller-type) families of dynamic pump. Some vane designs are sketched in Fig. 11.11, which introduces an interesting new "design" parameter, the specific speed N_s.



ketabline.com Ebook.ketabline.com

The Specific Speed

Most pump applications involve a known head and discharge for the particular system, plus a speed range dictated by electric motor speeds or cavitation requirements. The designer then selects the best size and shape (centrifugal, mixed, axial) for the pump. To help this selection, we need a dimensionless parameter involving speed, discharge, and head but not size. This is accomplished by eliminating the diameter between C_Q and C_H, applying the result only to the BEP. This ratio is called the *specific speed* and has both a dimensionless form and a somewhat lazy, practical form:

Rigorous form:
$$N_s' = \frac{C_{Q^*}^{1/2}}{C_{H^*}^{3/4}} = \frac{n(Q^*)^{1/2}}{(gH^*)^{3/4}} \tag{11.30a}$$

Lazy but common:
$$N_s = \frac{(\text{r/min})(\text{gal/min})^{1/2}}{[H\ (\text{ft})]^{3/4}} \tag{11.30b}$$

In other words, practicing engineers do not bother to change n to revolutions per second or Q^* to cubic feet per second or to include gravity with head, although the latter would be necessary for, say, a pump on the moon. The conversion factor is

$$N_s = 17{,}182 N_s'$$

Note that N_s is applied only to BEP; thus a single number characterizes an entire family of pumps. For example, the family of Fig. 11.8 has $N_s' \approx (0.115)^{1/2}/(5.0)^{3/4} = 0.1014$, $N_s = 1740$, regardless of size or speed.

It turns out that the specific speed is directly related to the most efficient pump design, as shown in Fig. 11.11. Low N_s means low Q and high H, hence a centrifugal pump, and large N_s implies an axial pump. The centrifugal pump is best for N_s between 500 and 4000, the mixed-flow pump for N_s between 4000 and 10,000, and the axial-flow pump for N_s above 10,000. Note the changes in impeller shape as N_s increases.

Suction Specific Speed

If we use NPSH rather than H in Eq. (11.30), the result is called *suction specific speed*

Rigorous:
$$N_{ss}' = \frac{nQ^{1/2}}{(g\ \text{NPSH})^{3/4}} \tag{11.31a}$$

Lazy:
$$N_{ss} = \frac{(\text{r/min})(\text{gal/min})^{1/2}}{[\text{NPSH (ft)}]^{3/4}} \tag{11.31b}$$

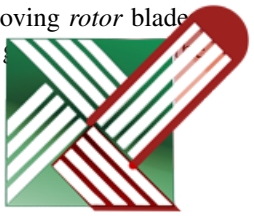
where NPSH denotes the available suction head of the system. Data from Wislicenus [4] show that a given pump is in danger of inlet cavitation if

$$N_{ss}' \geq 0.47 \qquad N_{ss} \geq 8100$$

In the absence of test data, this relation can be used, given n and Q, to estimate the minimum required NPSH.

Axial-Flow Pump Theory

A multistage axial-flow geometry is shown in Fig. 11.12*a*. The fluid essentially passes almost axially through alternate rows of fixed *stator* blades and moving *rotor* blade The incompressible-flow assumption is frequently used even for pressure rise per stage is usually small.



ketabline.com Ebook.ketabline.com

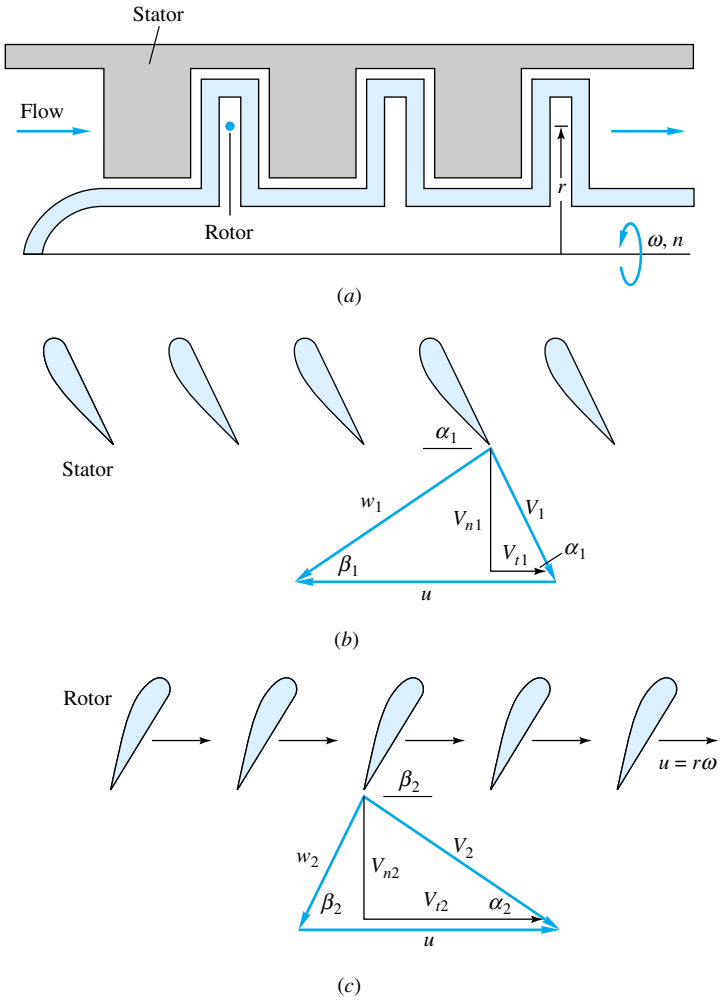


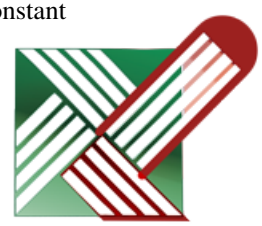
Fig. 11.12 Analysis of an axial-flow pump: (*a*) basic geometry; (*b*) stator blades and exit-velocity diagram; (*c*) rotor blades and exit-velocity diagram.

The simplified vector-diagram analysis assumes that the flow is one-dimensional and leaves each blade row at a relative velocity exactly parallel to the exit blade angle. Figure 11.12*b* shows the stator blades and their exit-velocity diagram. Since the stator is fixed, ideally the absolute velocity V_1 is parallel to the trailing edge of the blade. After vectorially subtracting the rotor tangential velocity u from V_1, we obtain the velocity w_1 relative to the rotor, which ideally should be parallel to the rotor leading edge.

Figure 11.12*c* shows the rotor blades and their exit-velocity diagram. Here the relative velocity w_2 is parallel to the blade trailing edge, while the absolute velocity V_2 should be designed to enter smoothly the next row of stator blades.

The theoretical power and head are given by Euler's turbine relation (11.11). Since there is no radial flow, the inlet and exit rotor speeds are equal, $u_1 = u_2$, and one-dimensional continuity requires that the axial-velocity component remain constant

$$V_{n1} = V_{n2} = V_n = \frac{Q}{A} = \text{const}$$



ketabline.com Ebook.ketabline.com

From the geometry of the velocity diagrams, the normal velocity (or volume flow) can be directly related to the blade rotational speed u:

$$u = \omega r_{av} = V_{n1}(\tan \alpha_1 + \tan \beta_1) = V_{n2}(\tan \alpha_2 + \tan \beta_2) \tag{11.32}$$

Thus the flow rate can be predicted from the rotational speed and the blade angles. Meanwhile, since $V_{t1} = V_{n1} \cot \alpha_1$ and $V_{t2} = u - V_{n2} \cot \beta_2$, Euler's relation (11.11) for the pump head becomes

$$gH = uV_n(\cot \alpha_2 - \cot \alpha_1)$$

$$= u^2 - uV_n(\cot \alpha_1 + \cot \beta_2) \tag{11.33}$$

the preferred form because it relates to the blade angles α_1 and β_2. The shutoff or no-flow head is seen to be $H_0 = u^2/g$, just as in Eq. (11.18) for a centrifugal pump. The blade-angle parameter $\cot \alpha_1 + \cot \beta_2$ can be designed to be negative, zero, or positive, corresponding to a rising, flat, or falling head curve, as in Fig. 11.5.

Strictly speaking, Eq. (11.33) applies only to a single streamtube of radius r, but it is a good approximation for very short blades if r denotes the average radius. For long blades it is customary to sum Eq. (11.33) in radial strips over the blade area. Such complexity may not be warranted since theory, being idealized, neglects losses and usually predicts the head and power larger than those in actual pump performance.

Performance of an Axial-Flow Pump

At high specific speeds, the most efficient choice is an axial-flow, or propeller, pump, which develops high flow rate and low head. A typical dimensionless chart for a propeller pump is shown in Fig. 11.13. Note, as expected, the higher C_Q and lower C_H compared with Fig. 11.8. The head curve drops sharply with discharge, so that a large system-head change will cause a mild flow change. The power curve drops with head also, which means a possible overloading condition if the system discharge should sud-

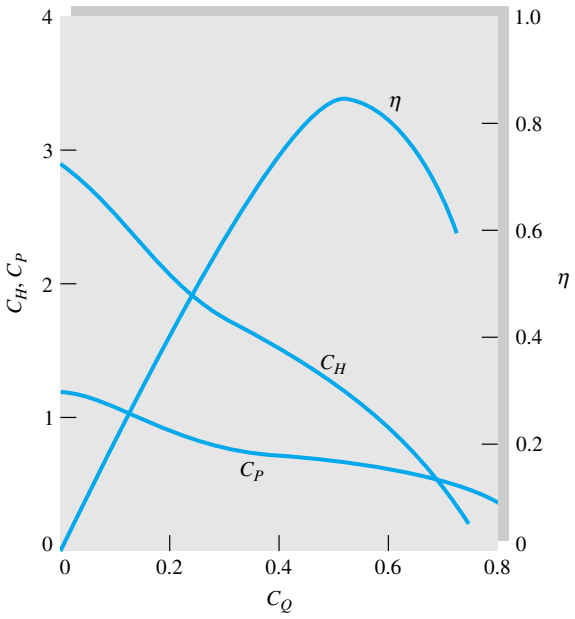


Fig. 11.13 Dimensionless performance curves for a typical axial-flow pump, $N_s = 12{,}000$. Constructed from data given by Stepanoff [8] for a 14-in pump at 690 r/min.



ketabline.com Ebook.ketabline.com

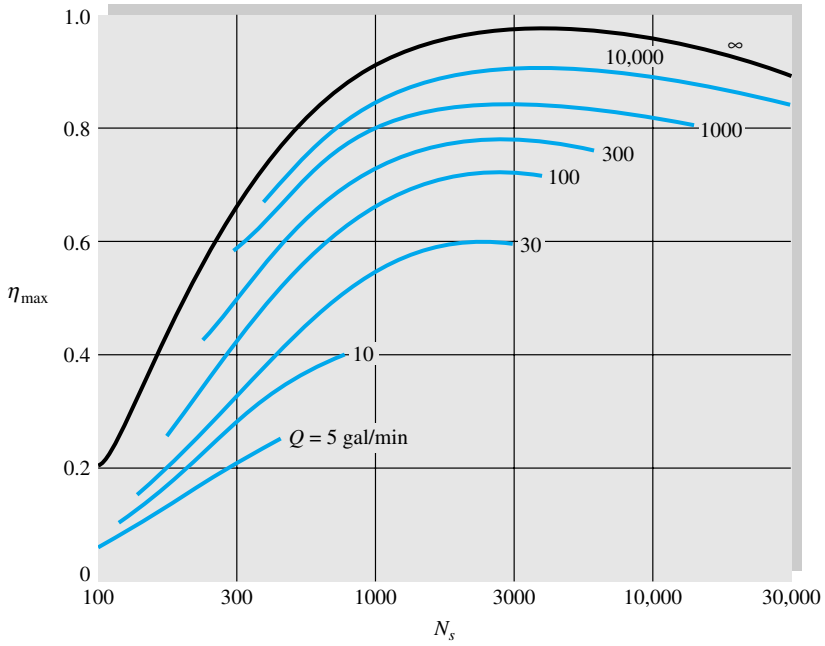


Fig. 11.14 Optimum efficiency of pumps versus capacity and specific speed. *(Adapted from Refs. 4 and 31.)*

denly decrease. Finally, the efficiency curve is rather narrow and triangular, as opposed to the broad, parabolic-shaped centrifugal pump efficiency (Fig. 11.8).

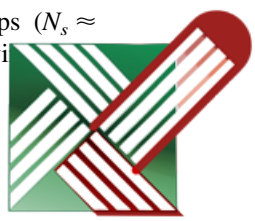
By inspection of Fig. 11.13, $C_{Q*} \approx 0.55$, $C_{H*} \approx 1.07$, $C_{P*} \approx 0.70$, and $\eta_{max} \approx 0.84$. From this we compute $N_s' \approx (0.55)^{1/2}/(1.07)^{3/4} = 0.705$, $N_s = 12{,}000$. The relatively low efficiency is due to small pump size: $d = 14$ in, $n = 690$ r/min, $Q^* = 4400$ gal/min.

A repetition of Example 11.5 using Fig. 11.13 would show that this propeller pump family can provide a 25-ft head and 100,000 gal/min discharge if $D = 46$ in and $n = 430$ r/min, with bhp = 750; this is a much more reasonable design solution, with improvements still possible at larger-N_s conditions.

Pump Performance versus Specific Speed

Specific speed is such an effective parameter that it is used as an indicator of both performance and efficiency. Figure 11.14 shows a correlation of the optimum efficiency of a pump as a function of the specific speed and capacity. Because the dimensional parameter Q is a rough measure of both size and Reynolds number, η increases with Q. When this type of correlation was first published by Wislicenus [4] in 1947, it became known as *the* pump curve, a challenge to all manufacturers. We can check that the pumps of Figs. 11.7 and 11.13 fit the correlation very well.

Figure 11.15 shows the effect of specific speed on the shape of the pump performance curves, normalized with respect to the BEP point. The numerical values shown are representative but somewhat qualitative. The high-specific-speed pumps ($N_s \approx$ 10,000) have head and power curves which drop sharply with discharge, implyi load or start-up problems at low flow. Their efficiency curve is very narrow.



ketabline.com Ebook.ketabline.com

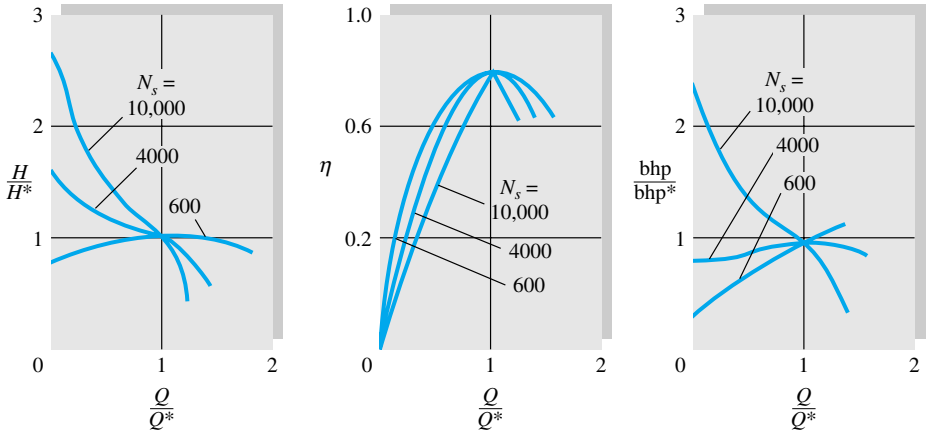


Fig. 11.15 Effect of specific speed on pump performance curves.

A low-specific-speed pump ($N_s = 600$) has a broad efficiency curve, a rising power curve, and a head curve which "droops" at shutoff, implying possible surge or hunting problems.

Computational Fluid Dynamics

The design of turbomachinery has traditionally been highly experimental, with simple theories, such as in Sec. 11.2, only able to predict trends. Dimensionless correlations, such as Fig. 11.15, are useful but require extensive experimentation. Consider that flow in a pump is three-dimensional; unsteady (both periodic and turbulent); and involves flow separation, recirculation in the impeller, unsteady blade wakes passing through the diffuser, and blade roots, tips, and clearances. It is no wonder that one-dimensional theory cannot give firm quantitative predictions.

Modern computer analysis can give realistic results and is becoming a useful tool for turbomachinery designers. A good example is Ref. 56, reporting combined experimental and computational results for a centrifugal pump diffuser. A photograph of the device is shown in Fig. 11.16*a*. It is made of clear Perspex, so that laser measurements of particle tracking velocimetry (LPTV) and doppler anemometry (LDA) could be taken throughout the system. The data were compared with a CFD simulation of the impeller and diffuser, using the grids shown in Fig. 11.16*b*. The computations used a turbulence formulation called the k-ϵ model, popular in commercial CFD codes (see Sec. 8.9). Results were good but not excellent. The CFD model predicted velocity and pressure data adequately up until flow separation, after which it was only qualitative. Clearly, CFD is developing a significant role in turbomachinery design.

11.5 Matching Pumps to System Characteristics

The ultimate test of a pump is its match with the operating-system characteristics. Physically, the system head must match the head produced by the pump, and this intersection should occur in the region of best efficiency.

The system head will probably contain a static-elevation change $z_2 - z_1$ plus friction losses in pipes and fittings

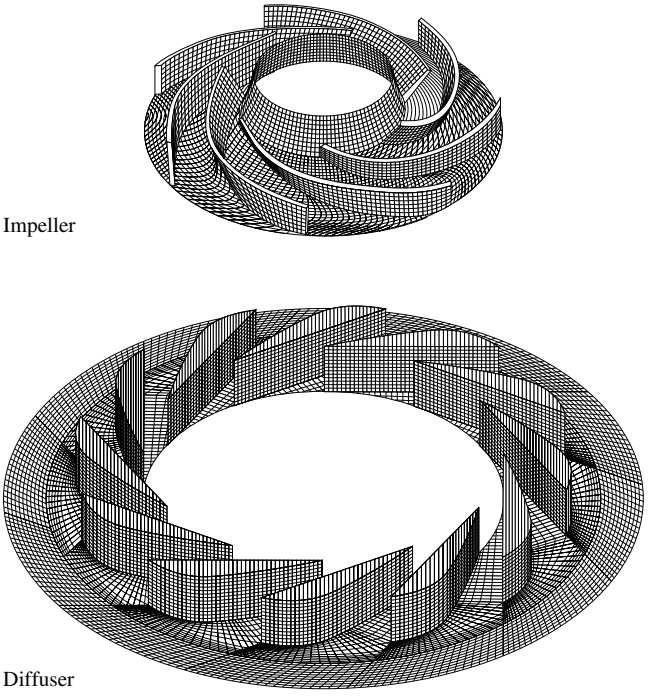
$$H_{\text{sys}} = (z_2 - z_1) + \frac{V^2}{2g}\left(\sum\frac{fL}{D} + \sum K\right)$$



ketabline.com Ebook.ketabline.com



(*a*)



(*b*)

Fig. 11.16 Turbomachinery design now involves both experimentation and computational fluid dynamics (CFD): (*a*) a centrifugal impeller and diffuser *(Courtesy of K. Eisele and Z. Zhang, Sulzer Innotec Ltd.)*; (*b*) a three-dimensional CFD model grid for this system. *(From Ref. 56 by permission of the American Society of Mechanical Engineers.)*

where ΣK denotes minor losses and V is the flow velocity in the principal pipe. Since V is proportional to the pump discharge Q, Eq. (11.34) represents a system-head curve $H_s(Q)$. Three examples are shown in Fig. 11.17: a static head $H_s = a$, static head plus laminar friction $H_s = a + bQ$, and static head plus turbulent friction $H_s = a$ The intersection of the system curve with the pump performance curve $H(Q)$

ketabline.com Ebook.ketabline.com

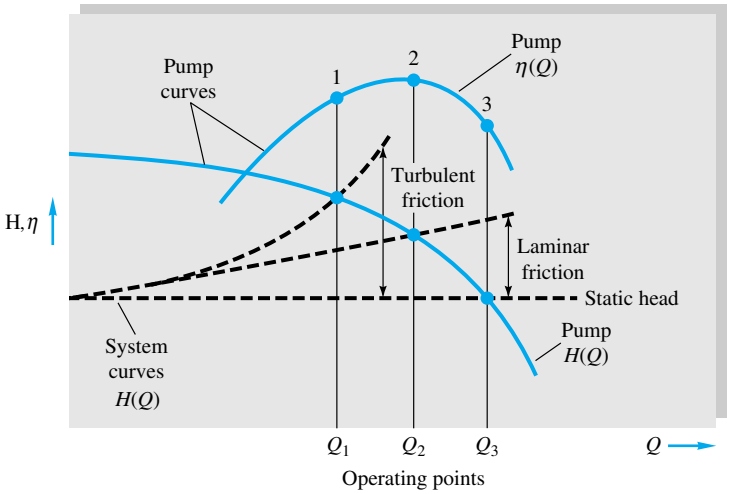


Fig. 11.17 Illustration of pump operating points for three types of system-head curves.

the operating point. In Fig. 11.17 the laminar-friction operating point is at maximum efficiency while the turbulent and static curves are off design. This may be unavoidable if system variables change, but the pump should be changed in size or speed if its operating point is consistently off design. Of course, a perfect match may not be possible because commercial pumps have only certain discrete sizes and speeds. Let us illustrate these concepts with an example.

EXAMPLE 11.6

We want to use the 32-in pump of Fig. 11.7*a* at 1170 r/min to pump water at 60°F from one reservoir to another 120 ft higher through 1500 ft of 16-in-ID pipe with friction factor $f = 0.030$. (*a*) What will the operating point and efficiency be? (*b*) To what speed should the pump be changed to operate at the BEP?

Solution

Part (a) For reservoirs the initial and final velocities are zero; thus the system head is

$$H_s = z_2 - z_1 + \frac{V^2}{2g}\frac{fL}{D} = 120 \text{ ft} + \frac{V^2}{2g}\frac{0.030(1500 \text{ ft})}{\frac{16}{12} \text{ ft}}$$

From continuity in the pipe, $V = Q/A = Q/[\frac{1}{4}\pi(\frac{16}{12} \text{ ft})^2]$, and so we substitute for V above to get

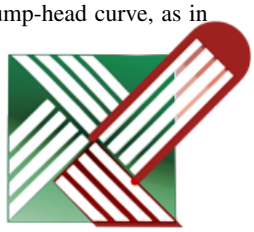
$$H_s = 120 + 0.269Q^2 \qquad Q \text{ in ft}^3/\text{s} \tag{1}$$

Since Fig. 11.7*a* uses thousands of gallons per minute for the abscissa, we convert Q in Eq. (1) to this unit:

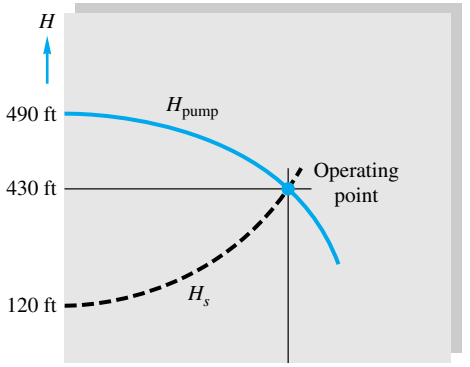
$$H_s = 120 + 1.335Q^2 \qquad Q \text{ in } 10^3 \text{ gal/min} \tag{2}$$

We can plot Eq. (2) on Fig. 11.7*a* and see where it intersects the 32-in pump-head curve, as in Fig. E11.6. A graphical solution gives approximately

$$H \approx 430 \text{ ft} \qquad Q \approx 15{,}000 \text{ gal/min}$$



ketabline.com Ebook.ketabline.com



E11.6

The efficiency is about 82 percent, slightly off design.

An analytic solution is possible if we fit the pump-head curve to a parabola, which is very accurate

$$H_{pump} \approx 490 - 0.26Q^2 \qquad Q \text{ in } 10^3 \text{ gal/min} \tag{3}$$

Equations (2) and (3) must match at the operating point:

$$490 - 0.26Q^2 = 120 + 1.335Q^2$$

or

$$Q^2 = \frac{490 - 120}{0.26 + 1.335} = 232$$

$$Q = 15.2 \times 10^3 \text{ gal/min} = 15{,}200 \text{ gal/min} \qquad \textit{Ans. (a)}$$

$$H = 490 - 0.26(15.2)^2 = 430 \text{ ft} \qquad \textit{Ans. (a)}$$

Part (b) To move the operating point to BEP, we change n, which changes both $Q \propto n$ and $H \propto n^2$. From Fig. 11.7*a*, at BEP, $H^* \approx 386$ ft; thus for any n, $H^* = 386(n/1170)^2$. Also read $Q^* \approx 20 \times 10^3$ gal/min; thus for any n, $Q^* = 20(n/1170)$. Match H^* to the system characteristics, Eq. (2),

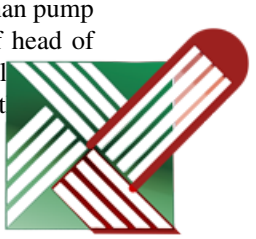
$$H^* = 386\left(\frac{n}{1170}\right)^2 \approx 120 + 1.335\left(20\,\frac{n}{1170}\right)^2 \qquad \textit{Ans. (b)}$$

which gives $n^2 < 0$. Thus it is impossible to operate at maximum efficiency with this particular system and pump.

Pumps Combined in Parallel

If a pump provides the right head but too little discharge, a possible remedy is to combine two similar pumps in parallel, i.e., sharing the same suction and inlet conditions. A parallel arrangement is also used if delivery demand varies, so that one pump is used at low flow and the second pump is started up for higher discharges. Both pumps should have check valves to avoid backflow when one is shut down.

The two pumps in parallel need not be identical. Physically, their flow rates will sum for the same head, as illustrated in Fig. 11.18. If pump A has more head than pump B, pump B cannot be added in until the operating head is below the shutoff head of pump B. Since the system curve rises with Q, the combined delivery Q_{A+B} wil
than the separate operating discharges $Q_A + Q_B$ but certainly greater than eit



ketabline.com Ebook.ketabline.com

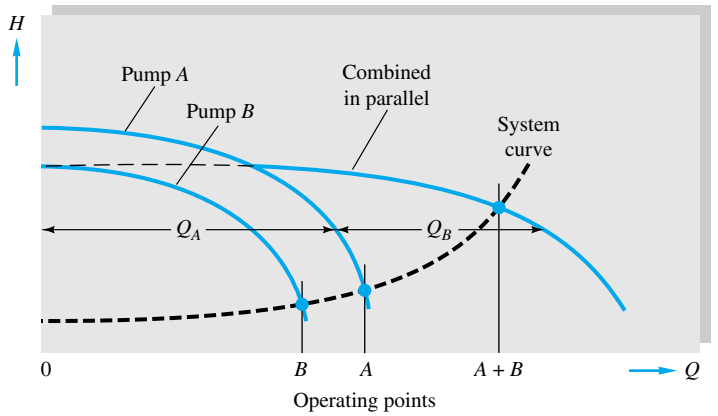


Fig. 11.18 Performance and operating points of two pumps operating singly and combined in parallel.

For a very flat (static) curve two similar pumps in parallel will deliver nearly twice the flow. The combined brake horsepower is found by adding brake horsepower for each of pumps A and B at the same head as the operating point. The combined efficiency equals $\rho g(Q_{A+B})(H_{A+B})/(550\ \text{bhp}_{A+B})$.

If pumps A and B are not identical, as in Fig. 11.18, pump B should not be run and cannot even be started up if the operating point is above its shutoff head.

Pumps Combined in Series

If a pump provides the right discharge but too little head, consider adding a similar pump in series, with the output of pump B fed directly into the suction side of pump A. As sketched in Fig. 11.19, the physical principle for summing in series is that the two heads add at the same flow rate to give the combined-performance curve. The two

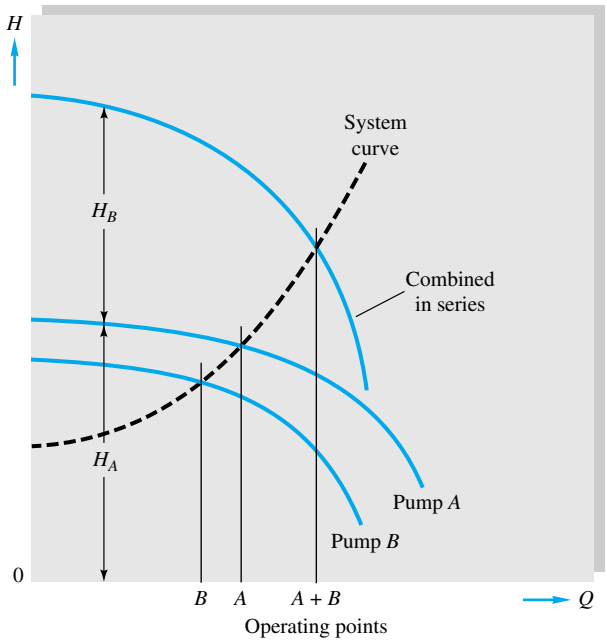


Fig. 11.19 Performance of two pumps combined in series.



ketabline.com Ebook.ketabline.com

need not be identical at all, since they merely handle the same discharge; they may even have different speeds, although normally both are driven by the same shaft.

The need for a series arrangement implies that the system curve is steep, i.e., requires higher head than either pump A or B can provide. The combined operating-point head will be more than either A or B separately but not as great as their sum. The combined power is the sum of brake horsepower for A and B at the operating point flow rate. The combined efficiency is

$$\frac{\rho g(Q_{A+B})(H_{A+B})}{550 \text{ bhp}_{A+B}}$$

similar to parallel pumps.

Whether pumps are used in series or in parallel, the arrangement will be uneconomical unless both pumps are operating near their best efficiency.

Multistage Pumps

For very high heads in continuous operation, the solution is a multistage pump, with the exit of one impeller feeding directly into the eye of the next. Centrifugal, mixed-flow, and axial-flow pumps have all been grouped in as many as 50 stages, with heads up to 8000 ft of water and pressure rises up to 5000 lbf/in^2 absolute. Figure 11.20 shows a section of a seven-stage centrifugal propane compressor which develops 300 lbf/in^2 rise at 40,000 ft^3/min and 35,000 bhp.

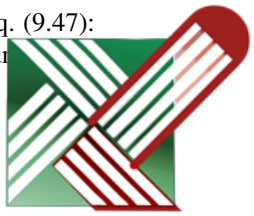
Compressors

Most of the discussion in this chapter concerns incompressible flow, that is, negligible change in fluid density. Even the pump of Fig. 11.7, which can produce 600 ft of head at 1170 r/min, will only increase standard air pressure by 46 lbf/ft^2, about a 2 percent change in density. The picture changes at higher speeds, $\Delta p \propto n^2$, and multiple stages, where very large changes in pressure and density are achieved. Such devices are called *compressors*, as in Fig. 11.20. The concept of static head, $H = \Delta p/\rho g$, becomes inappropriate, since ρ varies. Compressor performance is measured by (1) the pressure ratio across the stage p_2/p_1 and (2) the change in stagnation enthalpy $(h_{02} - h_{01})$, where $h_0 = h + \frac{1}{2}V^2$ (see Sec. 9.3). Combining m stages in series results in $p_{\text{final}}/p_{\text{initial}} \approx (p_2/p_1)^m$. As density increases, less area is needed: note the decrease in impeller size from right to left in Fig. 11.20. Compressors may be either of the centrifugal or axial-flow type [21 to 23].

Compressor efficiency, from inlet condition 1 to final outlet f, is defined by the change in gas enthalpy, assuming an adiabatic process:

$$\eta_{\text{comp}} = \frac{h_f - h_{01}}{h_{0f} - h_{01}} \approx \frac{T_f - T_{01}}{T_{0f} - T_{01}}$$

Compressor efficiencies are similar to hydraulic machines ($\eta_{\max} \approx 70$ to 80 percent), but the mass-flow range is more limited: on the low side by compressor *surge*, where blade stall and vibration occur, and on the high side by *choking* (Sec. 9.4), where the Mach number reaches 1.0 somewhere in the system. Compressor mass flow is normally plotted using the same type of dimensionless function formulated in Eq. (9.47): $\dot{m}(RT_0)^{1/2}/(D^2 p_0)$, which will reach a maximum when choking occurs. For fu
tails, see Refs. 21 to 23.



ketabline.com Ebook.ketabline.com

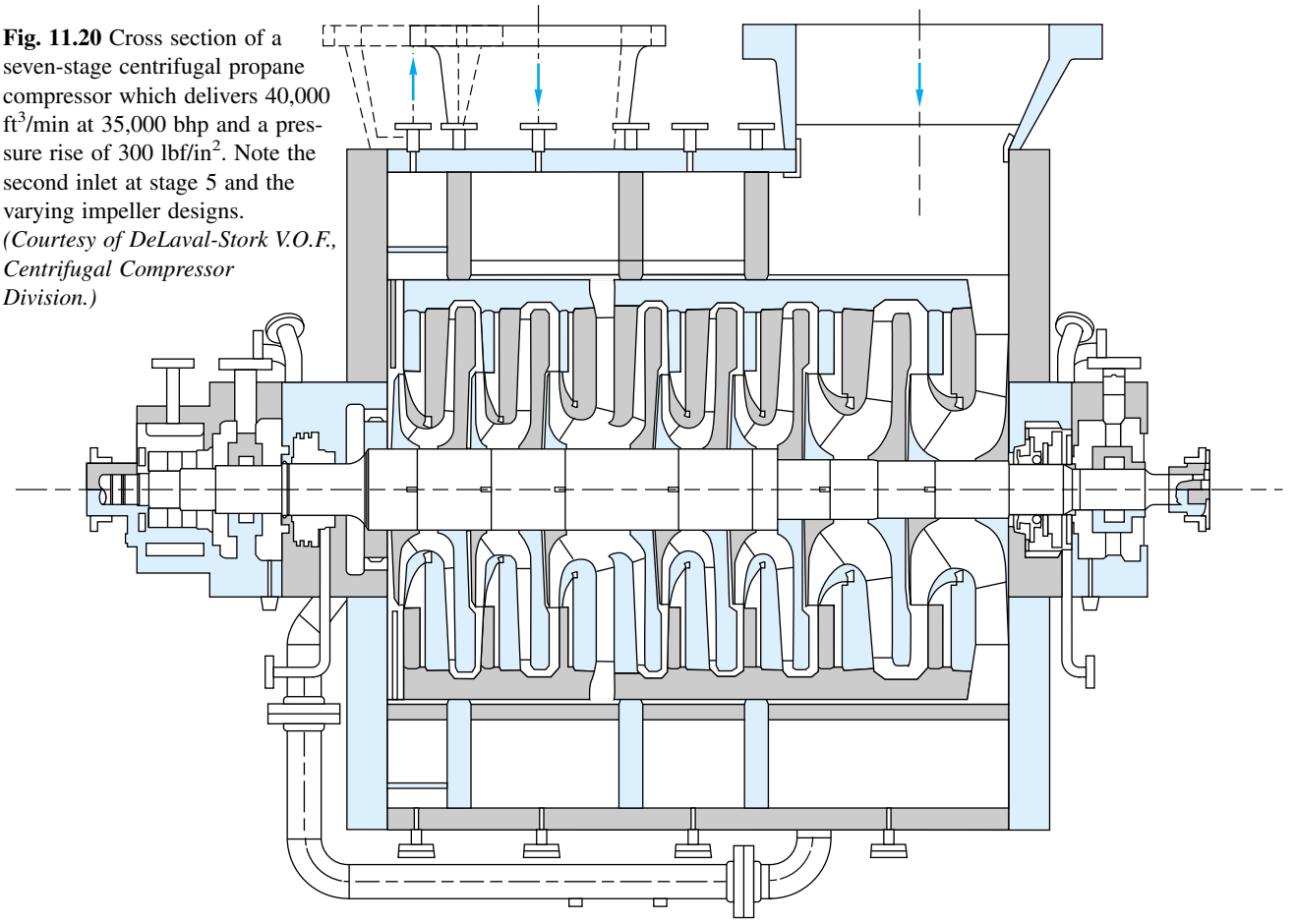


Fig. 11.20 Cross section of a seven-stage centrifugal propane compressor which delivers 40,000 ft^3/min at 35,000 bhp and a pressure rise of 300 lbf/in^2. Note the second inlet at stage 5 and the varying impeller designs. *(Courtesy of DeLaval-Stork V.O.F., Centrifugal Compressor Division.)*

EXAMPLE 11.7

Investigate extending Example 11.6 by using two 32-in pumps in parallel to deliver more flow. Is this efficient?

Solution

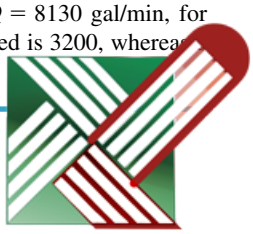
Since the pumps are identical, each delivers $\frac{1}{2}Q$ at the same 1170 r/min speed. The system curve is the same, and the balance-of-head relation becomes

$$H = 490 - 0.26(\tfrac{1}{2}Q)^2 = 120 + 1.335Q^2$$

or

$$Q^2 = \frac{490 - 120}{1.335 + 0.065} \qquad Q = 16{,}300 \text{ gal/min} \qquad \textit{Ans.}$$

This is only 7 percent more than a single pump. Each pump delivers $\frac{1}{2}Q = 8130$ gal/min, for which the efficiency is only 60 percent. The total brake horsepower required is 3200, whereas a single pump used only 2000 bhp. This is a poor design.



ketabline.com Ebook.ketabline.com

EXAMPLE 11.8

Suppose the elevation change in Example 11.6 is raised from 120 to 500 ft, greater than a single 32-in pump can supply. Investigate using 32-in pumps in series at 1170 r/min.

Solution

Since the pumps are identical, the total head is twice as much and the constant 120 in the system-head curve is replaced by 500. The balance of heads becomes

$$H = 2(490 - 0.26Q^2) = 500 + 1.335Q^2$$

or

$$Q^2 = \frac{980 - 500}{1.335 + 0.52} \qquad Q = 16.1 \times 10^3 \text{ gal/min} \qquad \textit{Ans.}$$

The operating head is $500 + 1.335(16.1)^2 = 845$ ft, or 97 percent more than that for a single pump in Example 11.5. Each pump is operating at 16.1×10^3 gal/min, which from Fig. 11.7*a* is 83 percent efficient, a pretty good match to the system. To pump at this operating point requires 4100 bhp, or about 2050 bhp for each pump.

11.6 Turbines

A turbine extracts energy from a fluid which possesses high head, but it is fatuous to say a turbine is a pump run backward. Basically there are two types, reaction and impulse, the difference lying in the manner of head conversion. In the reaction turbine, the fluid fills the blade passages, and the head change or pressure drop occurs within the impeller. Reaction designs are of the radial-flow, mixed-flow, and axial-flow types and are essentially dynamic devices designed to admit the high-energy fluid and extract its momentum. An impulse turbine first converts the high head through a nozzle into a high-velocity jet, which then strikes the blades at one position as they pass by. The impeller passages are not fluid-filled, and the jet flow past the blades is essentially at constant pressure. Reaction turbines are smaller because fluid fills all the blades at one time.

Reaction Turbines

Reaction turbines are low-head, high-flow devices. The flow is opposite that in a pump, entering at the larger-diameter section and discharging through the eye after giving up most of its energy to the impeller. Early designs were very inefficient because they lacked stationary guide vanes at the entrance to direct the flow smoothly into the impeller passages. The first efficient inward-flow turbine was built in 1849 by James B. Francis, a U.S. engineer, and all radial- or mixed-flow designs are now called *Francis turbines*. At still lower heads, a turbine can be designed more compactly with purely axial flow and is termed a *propeller turbine*. The propeller may be either fixed-blade or adjustable (Kaplan type), the latter being complicated mechanically but much more efficient at low-power settings. Figure 11.21 shows sketches of runner designs for Francis radial, Francis mixed-flow, and propeller-type turbines.

Idealized Radial Turbine Theory

The Euler turbomachine formulas (11.11) also apply to energy-extracting machines if we reverse the flow direction and reshape the blades. Figure 11.22 shows a radial turbine runner. Again assume one-dimensional frictionless flow through the blades. Adjustable inlet guide vanes are absolutely necessary for good efficiency. They b
inlet flow to the blades at angle α_2 and absolute velocity V_2 for minimum "sh



ketabline.com Ebook.ketabline.com

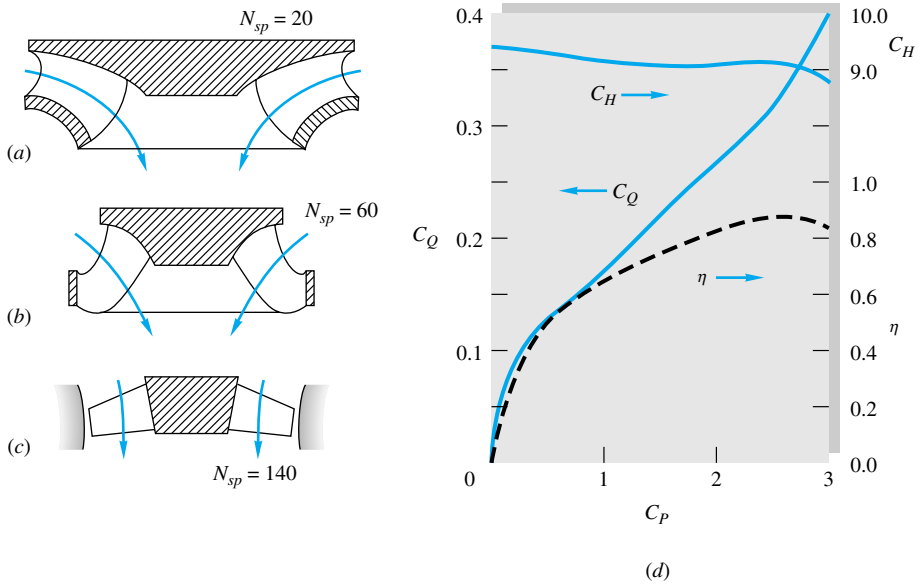


Fig. 11.21 Reaction turbines: (*a*) Francis, radial type; (*b*) Francis mixed-flow; (*c*) propeller axial-flow; (*d*) performance curves for a Francis turbine, $n = 600$ r/min, $D = 2.25$ ft, $N_{sp} = 29$.

directional-mismatch loss. After vectorially adding in the runner tip speed $u_2 = \omega r_2$, the outer blade angle should be set at angle β_2 to accommodate the relative velocity w_2, as shown in the figure. (See Fig. 11.4 for the analogous radial-pump velocity diagrams.)

Application of the angular-momentum control-volume theorem, Eq. (3.55), to Fig. 11.22 (see Example 3.14 for a similar case) yields an idealized formula for the power P extracted by the runner:

$$P = \omega T = \rho\omega Q(r_2 V_{t2} - r_1 V_{t1}) = \rho Q(u_2 V_2 \cos \alpha_2 - u_1 V_1 \cos \alpha_1) \quad (11.35)$$

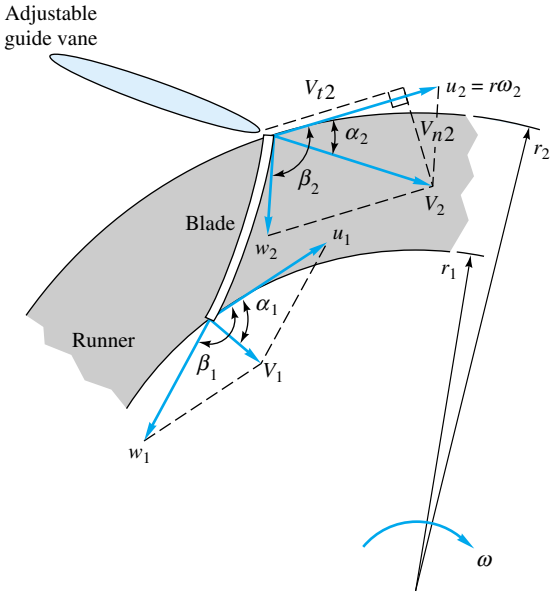


Fig. 11.22 Inlet- and outlet-velocity diagrams for an idealized radial-flow reaction turbine runner.



ketabline.com Ebook.ketabline.com

where V_{t2} and V_{t1} are the absolute inlet and outlet circumferential velocity components of the flow. Note that Eq. (11.35) is identical to Eq. (11.11) for a radial pump, except that the blade shapes are different.

The absolute inlet normal velocity $V_{n2} = V_2 \sin \alpha_2$ is proportional to the flow rate Q. If the flow rate changes and the runner speed u_2 is constant, the vanes must be adjusted to a new angle α_2 so that w_2 still follows the blade surface. Thus adjustable inlet vanes are very important to avoid shock loss.

Power Specific Speed

Turbine parameters are similar to those of a pump, but the dependent variable is the output brake horsepower, which depends upon the inlet flow rate Q, available head H, impeller speed n, and diameter D. The efficiency is the output brake horsepower divided by the available water horsepower ρgQH. The dimensionless forms are C_Q, C_H, and C_P, defined just as for a pump, Eqs. (11.23). If we neglect Reynolds-number and roughness effects, the functional relationships are written with C_P as the independent variable:

$$C_H = C_H(C_P) \qquad C_Q = C_Q(C_P) \qquad \eta = \frac{\text{bhp}}{\rho g Q H} = \eta(C_P) \tag{11.36}$$

Figure 11.21*d* shows typical performance curves for a small Francis radial turbine. The maximum efficiency point is called the *normal power*, and the values for this particular turbine are

$$\eta_{\max} = 0.89 \qquad C_{P*} = 2.70 \qquad C_{Q*} = 0.34 \qquad C_{H*} = 9.03$$

A parameter which compares the output power with the available head, independent of size, is found by eliminating the diameter between C_H and C_P. It is called the *power specific speed:*

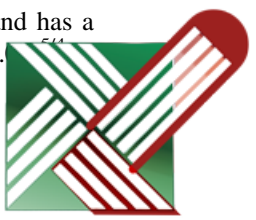
Rigorous form:
$$N'_{sp} = \frac{C_P^{*1/2}}{C_H^{*5/4}} = \frac{n(\text{bhp})^{1/2}}{\rho^{1/2}(gH)^{5/4}} \tag{11.37a}$$

Lazy but common:
$$N_{sp} = \frac{(\text{r/min})(\text{bhp})^{1/2}}{[H\ (\text{ft})]^{5/4}} \tag{11.37b}$$

For water, $\rho = 1.94$ slugs/ft^3 and $N_{sp} = 273.3 N'_{sp}$. The various turbine designs divide up nicely according to the range of power specific speed, as follows:

Turbine type	N_{sp} range	C_H range
Impulse	1–10	15–50
Francis	10–110	5–25
Propeller:		
Water	100–250	1–4
Gas, steam	25–300	10–80

Note that N_{sp}, like N_s for pumps, is defined only with respect to the BEP and has a single value for a given turbine family. In Fig. 11.21*d*, $N_{sp} = 273.3(2.70)^{1/2}/(9.$ 29, regardless of size.



ketabline.com Ebook.ketabline.com

Like pumps, turbines of large size are generally more efficient, and Eqs. (11.29) can be used as an estimate when data are lacking.

The design of a complete large-scale power-generating turbine system is a major engineering project, involving inlet and outlet ducts, trash racks, guide vanes, wicket gates, spiral cases, generator with cooling coils, bearings and transmission gears, runner blades, draft tubes, and automatic controls. Some typical large-scale reaction turbine designs are shown in Fig. 11.23. The reversible pump-and-turbine design of Fig. 11.23*d* requires special care for adjustable guide vanes to be efficient for flow in either direction.

The largest (1000-MW) hydropower designs are awesome when viewed on a human scale, as shown in Fig. 11.24. The economic advantages of small-scale model testing are evident from this photograph of the Francis turbine units at Grand Coulee Dam.

Impulse Turbines

For high head and relatively low power, i.e., low N_{sp}, not only would a reaction turbine require too high a speed but also the high pressure in the runner would require a massive casing thickness. The impulse turbine of Fig. 11.25 is ideal for this situation. Since N_{sp} is low, n will be low and the high pressure is confined to the small nozzle, which converts the head to an atmospheric pressure jet of high velocity V_j. The jet strikes the buckets and imparts a momentum change similar to that in our control-volume analysis for a moving vane in Example 3.10 or Prob. 3.51. The buckets have an elliptical split-cup shape, as in Fig. 11.25*b*. They are named *Pelton wheels*, after Lester A. Pelton (1829–1908), who produced the first efficient design.

From Example 3.10 the force and power delivered to a Pelton wheel are theoretically

$$\begin{aligned} F &= \rho Q(V_j - u)(1 - \cos\beta) \\ P &= Fu = \rho Qu(V_j - u)(1 - \cos\beta) \end{aligned} \tag{11.38}$$

where $u = 2\pi nr$ is the bucket linear velocity and r is the *pitch radius*, or distance to the jet centerline. A bucket angle $\beta = 180°$ gives maximum power but is physically impractical. In practice, $\beta \approx 165°$, or $1 - \cos\beta \approx 1.966$ or only 2 percent less than maximum power.

From Eq. (11.38) the theoretical power of an impulse turbine is parabolic in bucket speed u and is maximum when $dP/du = 0$, or

$$u^* = 2\pi n^* r = \tfrac{1}{2}V_j \tag{11.39}$$

For a perfect nozzle, the entire available head would be converted to jet velocity $V_j = (2gH)^{1/2}$. Actually, since there are 2 to 8 percent nozzle losses, a velocity coefficient C_v is used

$$V_j = C_v(2gH)^{1/2} \qquad 0.92 \le C_v \le 0.98 \tag{11.40}$$

By combining Eqs. (11.36) and (11.40), the theoretical impulse turbine efficiency becomes

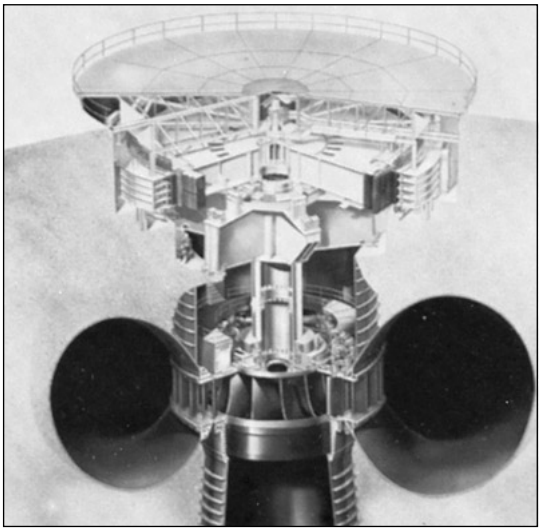
$$\eta = 2(1 - \cos\beta)\phi(C_v - \phi) \tag{11.41}$$

where $$\phi = \frac{u}{(2gH)^{1/2}} = \text{peripheral-velocity factor}$$

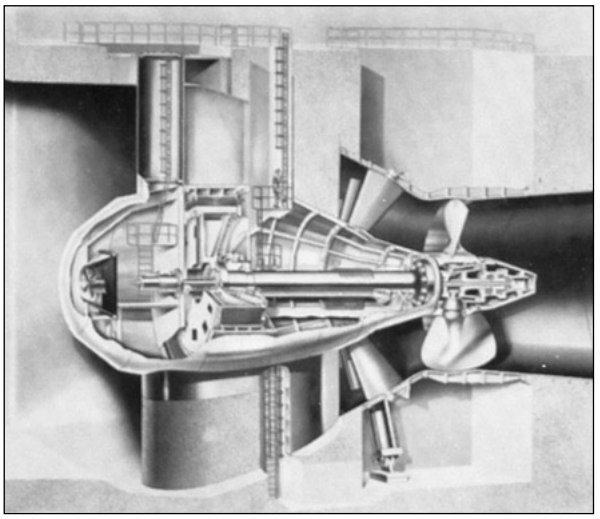
Maximum efficiency occurs at $\phi = \frac{1}{2}C_v \approx 0.47$.



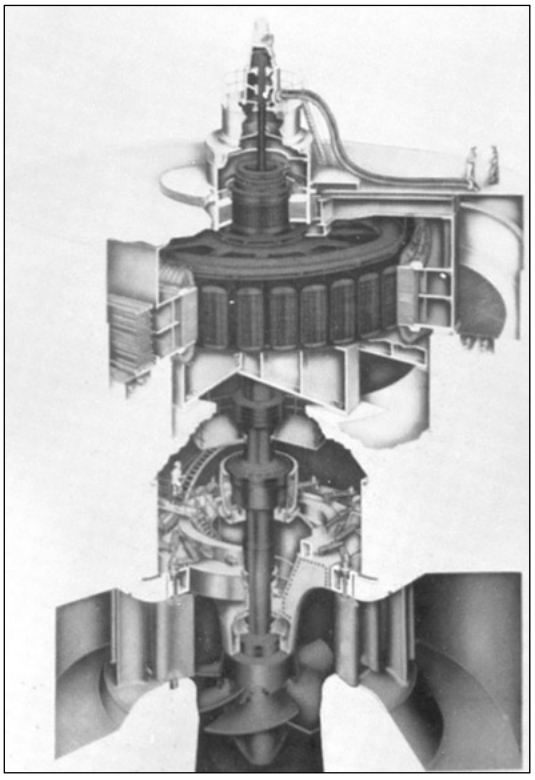
ketabline.com Ebook.ketabline.com



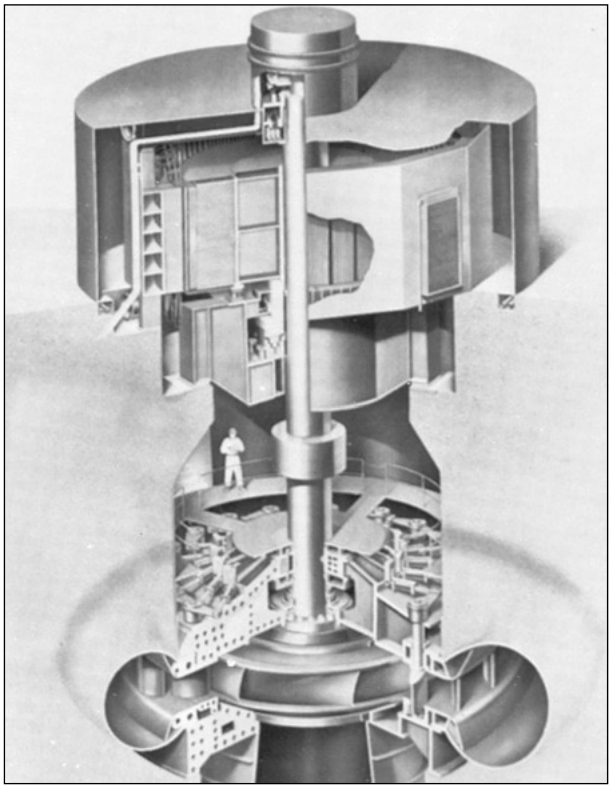
(*a*)



(*c*)



(*b*)



(*d*)

Fig. 11.23 Large-scale turbine designs depend upon available head and flow rate and operating conditions: (*a*) Francis (radial); (*b*) Kaplan (propeller); (*c*) bulb mounting with propeller runner; (*d*) reversible pump turbine with radial runner. *(Courtesy of Allis-Chalmers Fluid Products Company.)*



ketabline.com Ebook.ketabline.com

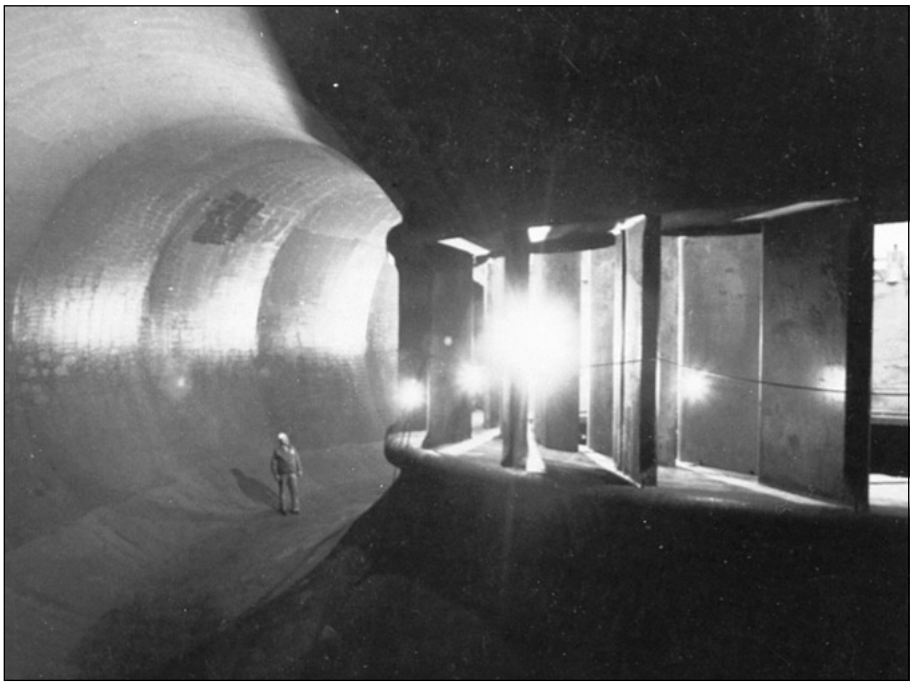


Fig. 11.24 Interior view of the 1.1-million hp (820-MW) turbine units on the Grand Coulee Dam of the Columbia River, showing the spiral case, the outer fixed vanes ("stay ring"), and the inner adjustable vanes ("wicket gates"). *(Courtesy of Allis-Chalmers Fluid Products Company.)*

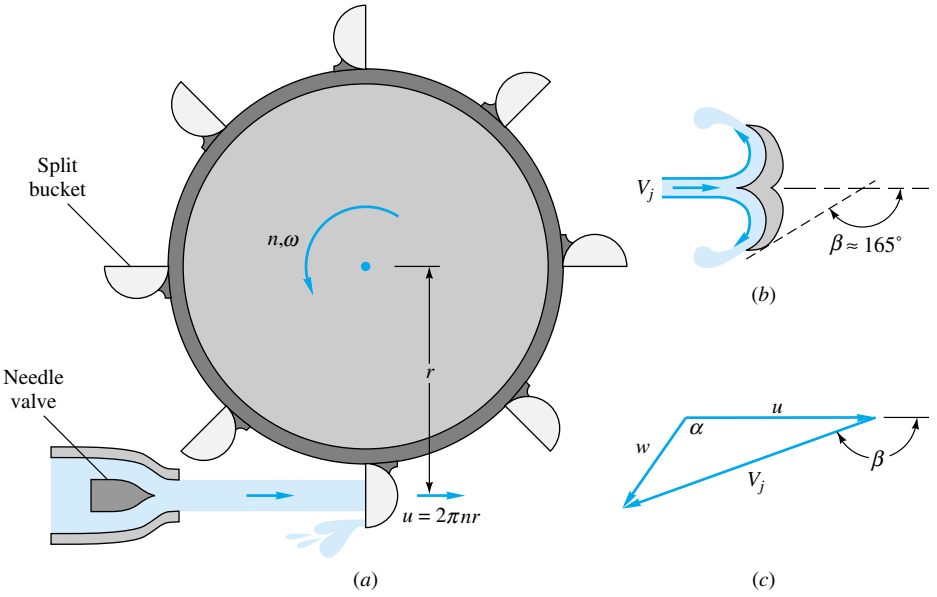


Fig. 11.25 Impulse turbine: (*a*) side view of wheel and jet; (*b*) top view of bucket; (*c*) typical velocity diagram.

Figure 11.26 shows Eq. (11.41) plotted for an ideal turbine ($\beta = 180°$, $C_v = 1.0$) and for typical working conditions ($\beta = 160°$, $C_v = 0.94$). The latter case predic $\eta_{max} = 85$ percent at $\phi = 0.47$, but the actual data for a 24-in Pel somewhat less efficient due to windage, mechanical friction, backspla

ketabline.com Ebook.ketabline.com

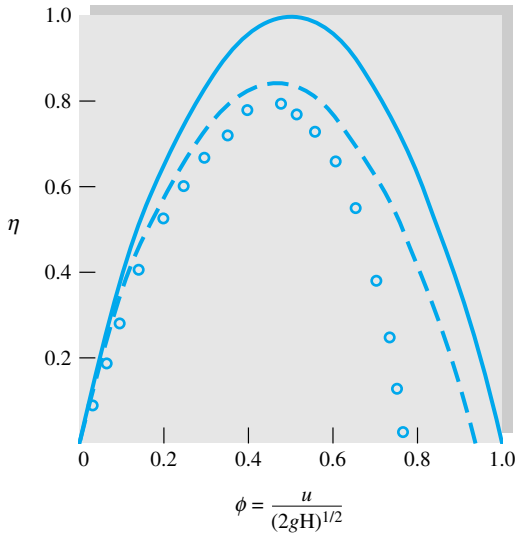


Fig. 11.26 Efficiency of an impulse turbine calculated from Eq. (11.41): solid curve = ideal, $\beta = 180°$, $C_v = 1.0$; dashed curve = actual, $\beta = 160°$, $C_v = 0.94$; open circles = data, Pelton wheel, diameter = 2 ft.

form bucket flow. For this test $\eta_{max} = 80$ percent, and, generally speaking, an impulse turbine is not quite as efficient as the Francis or propeller turbines at their BEPs.

Figure 11.27 shows the optimum efficiency of the three turbine types, and the importance of the power specific speed N_{sp} as a selection tool for the designer. These efficiencies are optimum and are obtained in careful design of large machines.

The water power available to a turbine may vary due to either net-head or flow-rate changes, both of which are common in field installations such as hydroelectric plants. The demand for turbine power also varies from light to heavy, and the operating response is a change in the flow rate by adjustment of a gate valve or needle valve (Fig. 11.25*a*). As shown in Fig. 11.28, all three turbine types achieve fairly uniform efficiency as a function of the level of power being extracted. Especially effective is the adjustable-blade (Kaplan-type) propeller turbine, while the poorest is a fixed-blade propeller. The term *rated power* in Fig. 11.28 is the largest power delivery guaranteed by the manufacturer, as opposed to *normal power*, which is delivered at maximum efficiency.

For further details of design and operation of turbomachinery, the readable and interesting treatment in Ref. 33 is especially recommended. The feasibility of microhydropower is discussed in [26]. See also Refs. 27 and 28.

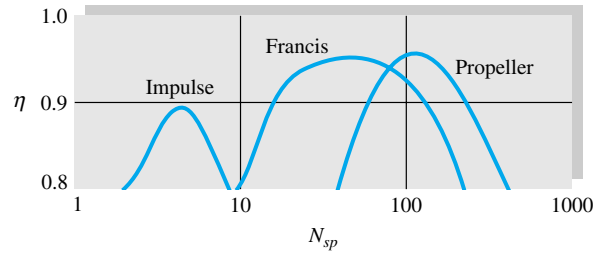


Fig. 11.27 Optimum efficiency of turbine designs.



ketabline.com Ebook.ketabline.com

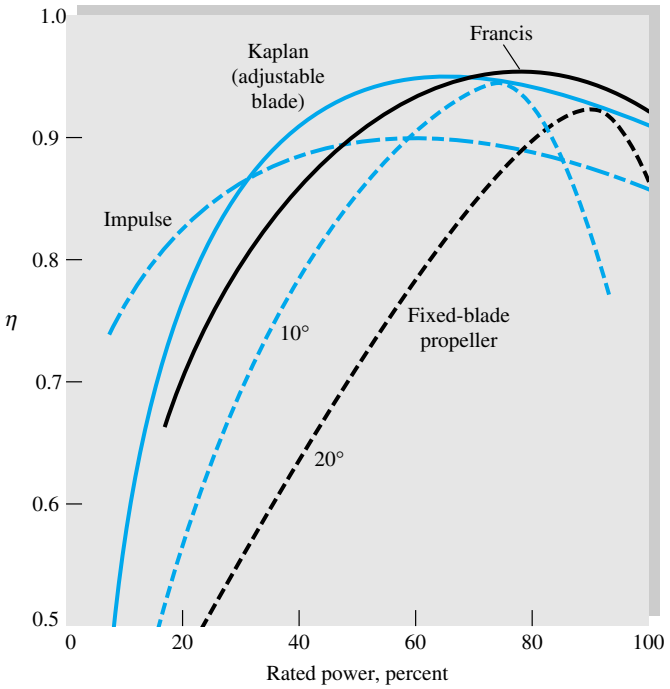


Fig. 11.28 Efficiency versus power level for various turbine designs at constant speed and head.

EXAMPLE 11.9

Investigate the possibility of using (*a*) a Pelton wheel similar to Fig. 11.26 or (*b*) the Francis turbine family of Fig. 11.21*d* to deliver 30,000 bhp from a net head of 1200 ft.

Solution

Part (a) From Fig. 11.27, the most efficient Pelton wheel occurs at about

$$N_{sp} \approx 4.5 = \frac{(\text{r/min})(30{,}000\ \text{bhp})^{1/2}}{(1200\ \text{ft})^{1.25}}$$

or

$$n = 183\ \text{r/min} = 3.06\ \text{r/s}$$

From Fig. 11.26 the best operating point is

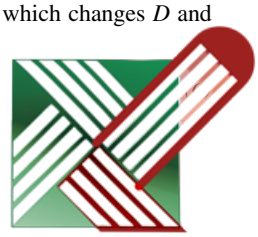
$$\phi \approx 0.47 = \frac{\pi D(3.06\ \text{r/s})}{[2(32.2)(1200)]^{1/2}}$$

or

$$D = 13.6\ \text{ft} \qquad \textit{Ans. (a)}$$

This Pelton wheel is perhaps a little slow and a trifle large. You could reduce D and increase n by increasing N_{sp} to, say, 6 or 7 and accepting the slight reduction in efficiency. Or you could use a double-hung, two-wheel configuration, each delivering 15,000 bhp, which changes D and n by the factor $2^{1/2}$:

Double wheel: $n = (183)2^{1/2} = 260$ r/min $\qquad D = \dfrac{13.6}{2^{1/2}} = 9.6$ ft



ketabline.com Ebook.ketabline.com

Part (b) The Francis wheel of Fig. 11.21*d* must have

$$N_{sp} = 29 = \frac{(\text{r/min})(30{,}000\ \text{bhp})^{1/2}}{(1200\ \text{ft})^{1.25}}$$

or $$n = 1183\ \text{r/min} = 19.7\ \text{r/s}$$

Then the optimum power coefficient is

$$C_{P*} = 2.70 = \frac{P}{\rho n^3 D^5} = \frac{30{,}000(550)}{(1.94)(19.7)^3 D^5}$$

or $$D^5 = 412 \qquad D = 3.33\ \text{ft} = 40\ \text{in} \qquad \textit{Ans. (b)}$$

This is a faster speed than normal practice, and the casing would have to withstand 1200 ft of water or about 520 lbf/in^2 internal pressure, but the 40-in size is extremely attractive. Francis turbines are now being operated at heads up to 1500 ft.

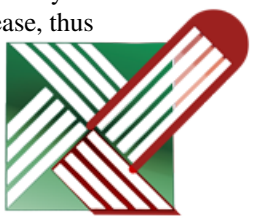
Wind Turbines

Wind energy has long been used as a source of mechanical power. The familiar four-bladed windmills of Holland, England, and the Greek islands have been used for centuries to pump water, grind grain, and saw wood. Modern research concentrates on the ability of wind turbines to generate electric power. Koeppl [47] stresses the potential for propeller-type machines. Spera [49] gives a detailed discussion of the technical and economic feasibility of large-scale electric power generation by wind. See also Refs. 46, 48, and 50 to 52.

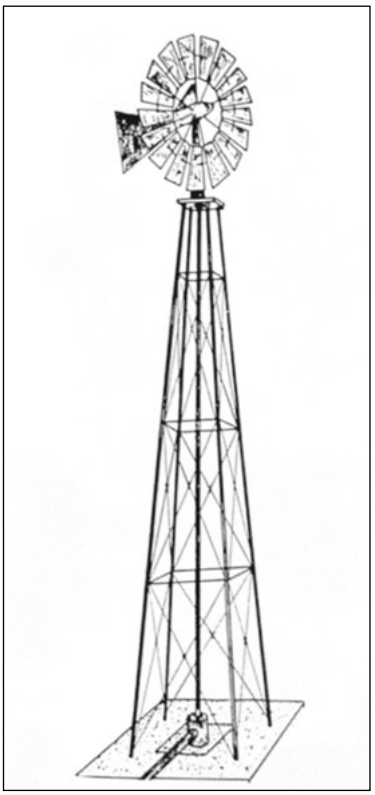
Some examples of wind turbine designs are shown in Fig. 11.29. The familiar American multiblade farm windmill (Fig. 11.29*a*) is of low efficiency, but thousands are in use as a rugged, reliable, and inexpensive way to pump water. A more efficient design is the propeller mill in Fig. 11.29*b*, similar to the pioneering Smith-Putnam 1250-kW two-bladed system which operated on Grampa's Knob, 12 mi west of Rutland, Vermont, from 1941 to 1945. The Smith-Putnam design broke because of inadequate blade strength, but it withstood winds up to 115 mi/h and its efficiency was amply demonstrated [47].

The Dutch, American multiblade, and propeller mills are examples of *horizontal-axis wind turbines* (HAWTs), which are efficient but somewhat awkward in that they require extensive bracing and gear systems when combined with an electric generator. Thus a competing family of *vertical-axis wind turbines* (VAWTs) has been proposed which simplifies gearing and strength requirements. Figure 11.29*c* shows the "egg-beater" VAWT invented by G. J. M. Darrieus in 1925, now used in several government-sponsored demonstration systems. To minimize centrifugal stresses, the twisted blades of the Darrieus turbine follow a *troposkien* curve formed by a chain anchored at two points on a spinning vertical rod.

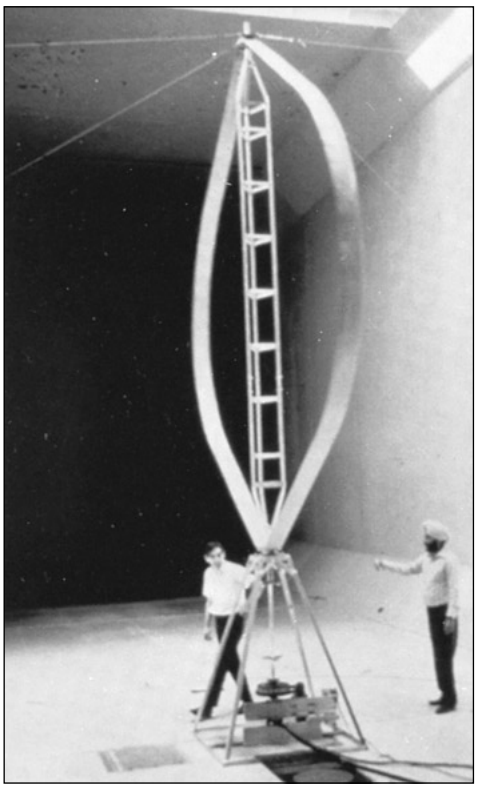
An alternative VAWT, simpler to construct than the troposkien, is the straight-bladed Darrieus-type turbine in Fig. 11.29*d*. This design, proposed by Reading University in England, has blades which pivot due to centrifugal action as wind speeds increase, thus limiting bending stresses.



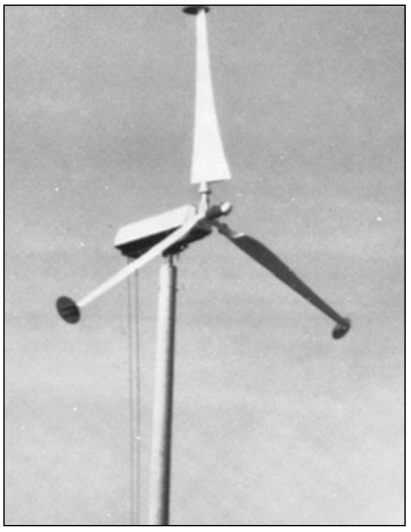
ketabline.com Ebook.ketabline.com



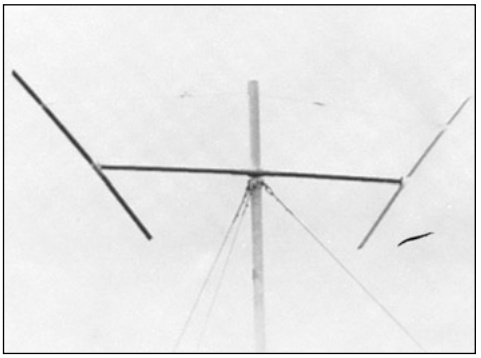
(*a*)



(*c*)



(*b*)



(*d*)

Fig. 11.29 Wind turbine designs: (*a*) the American multiblade farm HAWT; (*b*) propeller HAWT *(Courtesy of Grumman Aerospace Corp.)*; (*c*) the Darrieus VAWT *(Courtesy of National Research Council, Canada)*; (*d*) modified straight-blade Darrieus VAWT *(Courtesy of Reading University—Nat'l Wind Power Ltd.)*.



ketabline.com Ebook.ketabline.com

Idealized Wind Turbine Theory

The ideal, frictionless efficiency of a propeller windmill was predicted by A. Betz in 1920, using the simulation shown in Fig. 11.30. The propeller is represented by an *actuator disk* which creates across the propeller plane a pressure discontinuity of area A and local velocity V. The wind is represented by a streamtube of approach velocity V_1 and a slower downstream wake velocity V_2. The pressure rises to p_b just before the disk and drops to p_a just after, returning to free-stream pressure in the far wake. To hold the propeller rigid when it is extracting energy from the wind, there must be a leftward force F on its support, as shown.

A control-volume–horizontal-momentum relation applied between sections 1 and 2 gives

$$\sum F_x = -F = \dot{m}(V_2 - V_1)$$

A similar relation for a control volume just before and after the disk gives

$$\sum F_x = -F + (p_b - p_a)A = \dot{m}(V_a - V_b) = 0$$

Equating these two yields the propeller force

$$F = (p_b - p_a)A = \dot{m}(V_1 - V_2) \tag{11.42}$$

Assuming ideal flow, the pressures can be found by applying the incompressible Bernoulli relation up to the disk

From 1 to b: $$p_\infty + \tfrac{1}{2}\rho V_1^2 = p_b + \tfrac{1}{2}\rho V^2$$

From a to 2: $$p_a + \tfrac{1}{2}\rho V^2 = p_\infty + \tfrac{1}{2}\rho V_2^2$$

Subtracting these and noting that $\dot{m} = \rho AV$ through the propeller, we can substitute for $p_b - p_a$ in Eq. (11.42) to obtain

$$p_b - p_a = \tfrac{1}{2}\rho(V_1^2 - V_2^2) = \rho V(V_1 - V_2)$$

or $$V = \tfrac{1}{2}(V_1 + V_2) \tag{11.43}$$

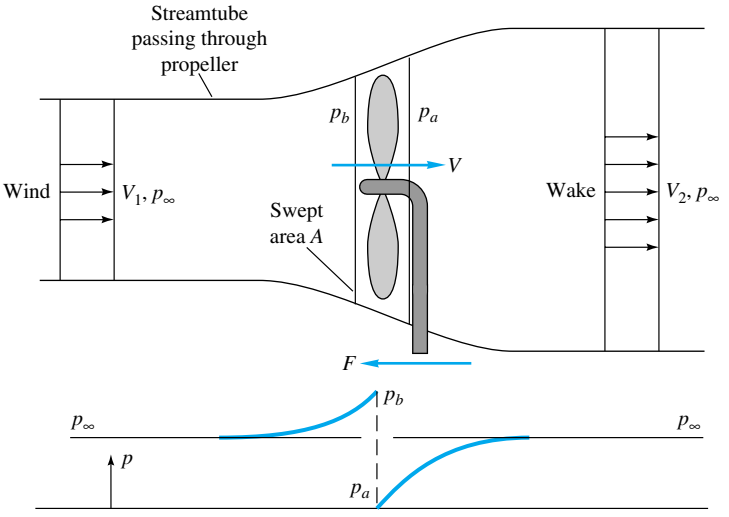


Fig. 11.30 Idealized actuator-disk and streamtube analysis of flow through a windmill.



ketabline.com Ebook.ketabline.com

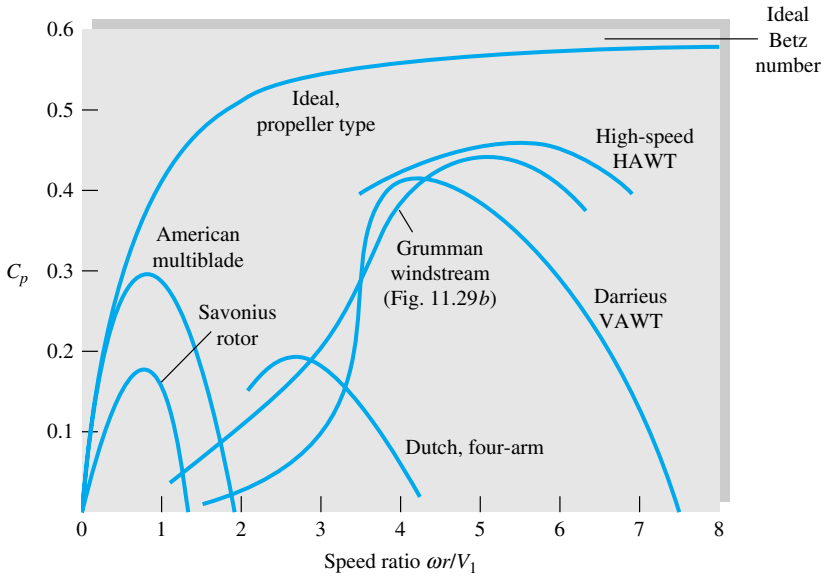


Fig. 11.31 Estimated performance of various wind turbine designs as a function of blade-tip speed ratio. *(From Ref. 53.)*

Continuity and momentum thus require that the velocity V through the disk equal the average of the wind and far-wake speeds.

Finally, the power extracted by the disk can be written in terms of V_1 and V_2 by combining Eqs. (11.42) and (11.43)

$$P = FV = \rho AV^2(V_1 - V_2) = \tfrac{1}{4}\rho A(V_1^2 - V_2^2)(V_1 + V_2) \tag{11.44}$$

For a given wind speed V_1, we can find the maximum possible power by differentiating P with respect to V_2 and setting equal to zero. The result is

$$P = P_{\max} = \tfrac{8}{27}\rho AV_1^3 \qquad \text{at } V_2 = \tfrac{1}{3}V_1 \tag{11.45}$$

which corresponds to $V = 2V_1/3$ through the disk.

The maximum available power to the propeller is the mass flow through the propeller times the total kinetic energy of the wind

$$P_{\text{avail}} = \tfrac{1}{2}\dot{m}V_1^2 = \tfrac{1}{2}\rho AV_1^3$$

Thus the maximum possible efficiency of an ideal frictionless wind turbine is usually stated in terms of the *power coefficient*

$$C_P = \frac{P}{\tfrac{1}{2}\rho AV_1^3} \tag{11.46}$$

Equation (11.45) states that the total power coefficient is

$$C_{p,\max} = \tfrac{16}{27} = 0.593 \tag{11.47}$$

This is called the *Betz number* and serves as an ideal with which to compare the actual performance of real windmills.

Figure 11.31 shows the measured power coefficients of various designs. The independent variable is not V_2/V_1 (which is artificial and



ketabline.com Ebook.ketabline.com

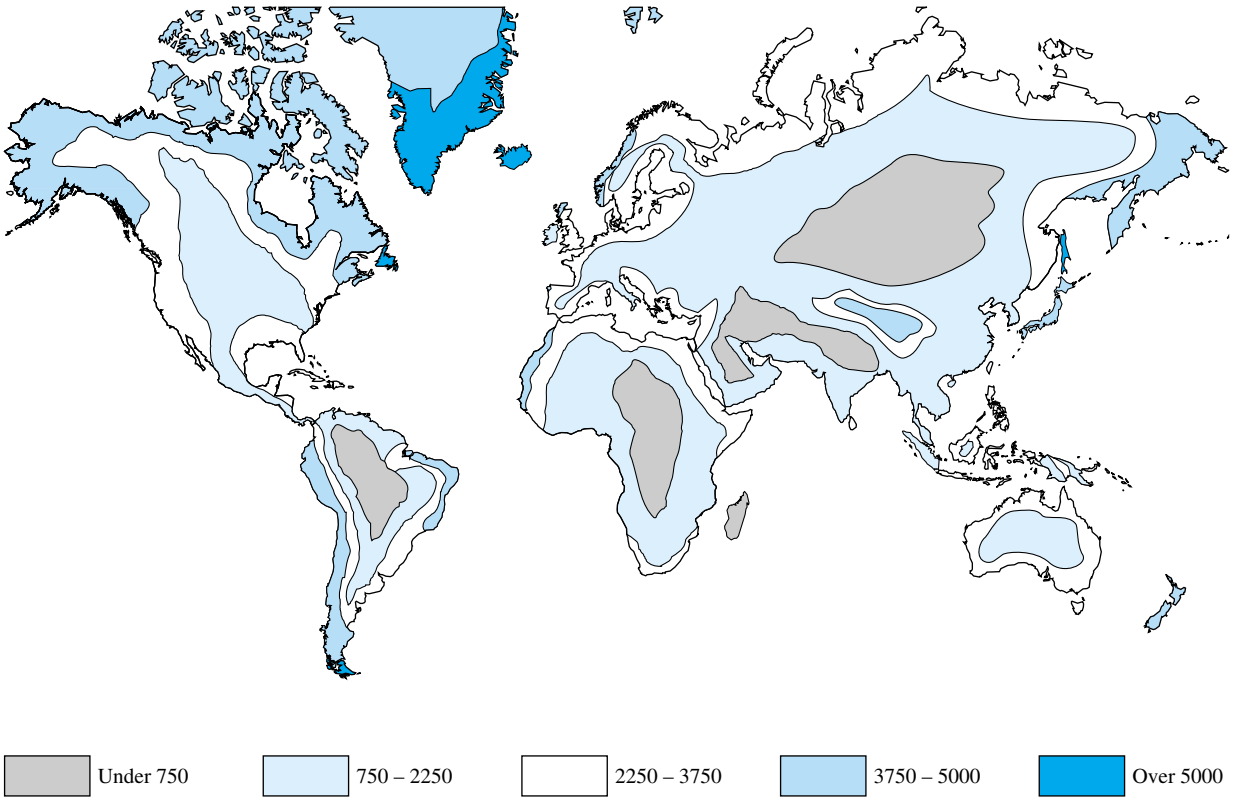


Fig. 11.32 World availability of land-based wind energy: estimated annual electric output in kWh/kW of a wind turbine rated at 11.2 m/s (25 mi/h). *(From Ref. 54.)*

the ideal theory) but the ratio of blade-tip speed ωr to wind speed. Note that the tip can move much faster than the wind, a fact disturbing to the laity but familiar to engineers in the behavior of iceboats and sailing vessels. The Darrieus has the many advantages of a vertical axis but has little torque at low speeds and also rotates more slowly at maximum power than a propeller, thus requiring a higher gear ratio for the generator. The Savonius rotor (Fig. 6.29*b*) has been suggested as a VAWT design because it produces power at very low wind speeds, but it is inefficient and susceptible to storm damage because it cannot be feathered in high winds.

As shown in Fig. 11.32, there are many areas of the world where wind energy is an attractive alternative. Greenland, Newfoundland, Argentina, Chile, New Zealand, Iceland, Ireland, and the United Kingdom have the highest prevailing winds, but Australia, e.g., with only moderate winds, has the potential to generate half its electricity with wind turbines [53]. In addition, since the ocean is generally even windier than the land, there are many island areas of high potential for wind power. There have also been proposals [47] for ocean-based floating windmill farms. The inexhaustible availability of the winds, coupled with improved low-cost turbine designs, indicates a bri ture for this alternative.



ketabline.com Ebook.ketabline.com

Summary

Turbomachinery design is perhaps the most practical and most active application of the principles of fluid mechanics. There are billions of pumps and turbines in use in the world, and thousands of companies are seeking improvements. This chapter discusses both positive-displacement devices and, more extensively, rotodynamic machines. With the centrifugal pump as an example, the basic concepts of torque, power, head, flow rate, and efficiency are developed for a turbomachine. Nondimensionalization leads to the pump similarity rules and some typical dimensionless performance curves for axial and centrifugal machines. The single most useful pump parameter is found to be the specific speed, which delineates the type of design needed. An interesting design application is the theory of pumps combined in series and in parallel.

Turbines extract energy from flowing fluids and are of two types: impulse turbines, which convert the momentum of a high-speed stream, and reaction turbines, where the pressure drop occurs within the blade passages in an internal flow. By analogy with pumps, the power specific speed is important for turbines and is used to classify them into impulse, Francis, and propeller-type designs. A special case of reaction turbine with unconfined flow is the wind turbine. Several types of windmills are discussed and their relative performances compared.

Problems

Most of the problems herein are fairly straightforward. More difficult or open-ended assignments are labeled with an asterisk. Problems labeled with an EES icon will benefit from the use of the Engineering Equations Solver (EES), while problems labeled with a computer icon may require the use of a computer. The standard end-of-chapter problems 11.1 to 11.103 (categorized in the problem list below) are followed by word problems W11.1 to W11.10, comprehensive problems C11.1 to C11.3, and design project D11.1.

Problem distribution

Section	Topic	Problems
11.1	Introduction and classification	11.1–11.14
11.2	Centrifugal pump theory	11.15–11.21
11.3	Pump performance and similarity rules	11.22–11.41
11.3	Net positive-suction head	11.42–11.44
11.4	Specific speed: Mixed- and axial-flow pumps	11.45–11.62
11.5	Matching pumps to system characteristics	11.63–11.73
11.5	Pumps in parallel or series	11.74–11.81
11.5	Pump instability	11.82–11.83
11.6	Reaction and impulse turbines	11.84–11.99
11.6	Wind turbines	11.100–11.103

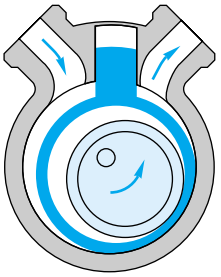
P11.1 Describe the geometry and operation of a peristaltic positive-displacement pump which occurs in nature.

P11.2 What would be the technical classification of the following turbomachines: (*a*) a household fan, (*b*) a windmill, (*c*) an aircraft propeller, (*d*) a fuel pump in a car, (*e*) an eductor, (*f*) a fluid-coupling transmission, and (*g*) a power plant steam turbine?

P11.3 A PDP can deliver almost any fluid, but there is always a limiting very high viscosity for which performance will deteriorate. Can you explain the probable reason?

P11.4 Figure 11.2*c* shows a double-screw pump. Sketch a single-screw pump and explain its operation. How did Archimedes' screw pump operate?

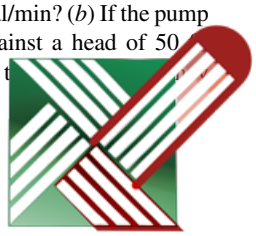
P11.5 What type of pump is shown in Fig. P11.5? How does it operate?



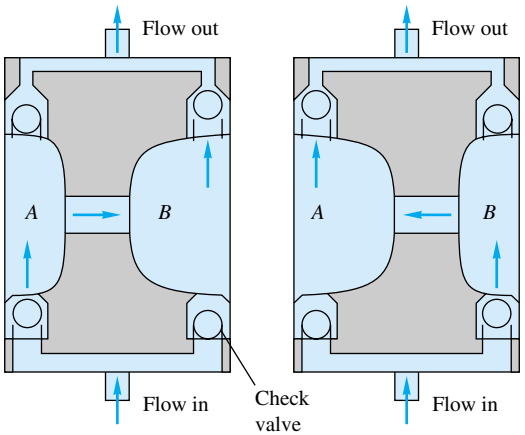
P11.5

P11.6 Figure P11.6 shows two points a half-period apart in the operation of a pump. What type of pump is this? How does it work? Sketch your best guess of flow rate versus time for a few cycles.

P11.7 A piston PDP has a 5-in diameter and a 2-in stroke and operates at 750 r/min with 92 percent volumetric efficiency. (*a*) What is its delivery, in gal/min? (*b*) If the pump delivers SAE 10W oil at 20°C against a head of 50 [illegible] what horsepower is required when t[illegible] is 84 percent?



ketabline.com Ebook.ketabline.com



P11.6

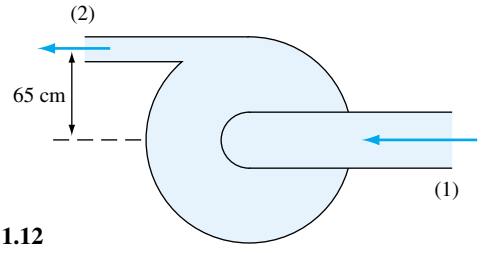
P11.8 A centrifugal pump delivers 550 gal/min of water at 20°C when the brake horsepower is 22 and the efficiency is 71 percent. (*a*) Estimate the head rise in ft and the pressure rise in lbf/in^2. (*b*) Also estimate the head rise and horsepower if instead the delivery is 550 gal/min of gasoline at 20°C.

P11.9 Figure P11.9 shows the measured performance of the Vickers model PVQ40 piston pump when delivering SAE 10W oil at 180°F ($\rho \approx 910$ kg/m^3). Make some general observations about these data vis-à-vis Fig. 11.2 and your intuition about the behavior of piston pumps.

P11.10 Suppose that the piston pump of Fig. P11.9 is used to deliver 15 gal/min of water at 20°C using 20 brake horsepower. Neglecting Reynolds-number effects, use the figure to estimate (*a*) the speed in r/min and (*b*) the pressure rise in lbf/in^2.

P11.11 A pump delivers 1500 L/min of water at 20°C against a pressure rise of 270 kPa. Kinetic- and potential-energy changes are negligible. If the driving motor supplies 9 kW, what is the overall efficiency?

P11.12 In a test of the centrifugal pump shown in Fig. P11.12, the following data are taken: $p_1 = 100$ mmHg (vacuum) and $p_2 = 500$ mmHg (gage). The pipe diameters are $D_1 = 12$ cm and $D_2 = 5$ cm. The flow rate is 180 gal/min of light oil (SG = 0.91). Estimate (*a*) the head developed, in meters; and (*b*) the input power required at 75 percent efficiency.

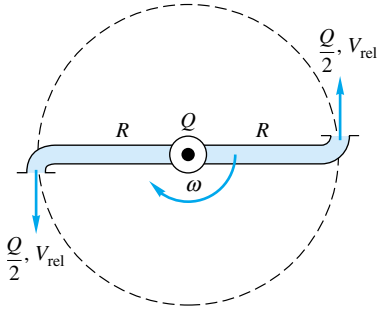


P11.12

P11.13 A 20-hp pump delivers 400 gal/min of gasoline at 20°C with 75 percent efficiency. What head and pressure rise result across the pump?

P11.14 A pump delivers gasoline at 20°C and 12 m^3/h. At the inlet $p_1 = 100$ kPa, $z_1 = 1$ m, and $V_1 = 2$ m/s. At the exit $p_2 = 500$ kPa, $z_2 = 4$ m, and $V_2 = 3$ m/s. How much power is required if the motor efficiency is 75 percent?

P11.15 A lawn sprinkler can be used as a simple turbine. As shown in Fig. P11.15, flow enters normal to the paper in the center and splits evenly into $Q/2$ and V_{rel} leaving each nozzle. The arms rotate at angular velocity ω and do work on a shaft. Draw the velocity diagram for this turbine. Neglecting friction, find an expression for the power delivered to the shaft. Find the rotation rate for which the power is a maximum.

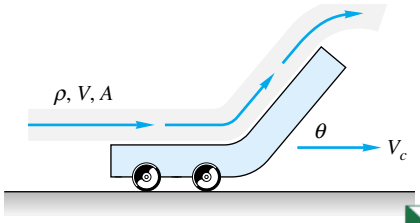


P11.15

P11.16 For the "sprinkler turbine" of Fig. P11.15, let $R = 18$ cm, with total flow rate of 14 m^3/h of water at 20°C. If the nozzle exit diameter is 8 mm, estimate (*a*) the maximum power delivered in W and (*b*) the appropriate rotation rate in r/min.

P11.17 A centrifugal pump has $d_1 = 7$ in, $d_2 = 13$ in, $b_1 = 4$ in, $b_2 = 3$ in, $\beta_1 = 25°$, and $\beta_2 = 40°$ and rotates at 1160 r/min. If the fluid is gasoline at 20°C and the flow enters the blades radially, estimate the theoretical (*a*) flow rate in gal/min, (*b*) horsepower, and (*c*) head in ft.

P11.18 A jet of velocity V strikes a vane which moves to the right at speed V_c, as in Fig. P11.18. The vane has a turning angle θ.



P11.18



ketabline.com Ebook.ketabline.com

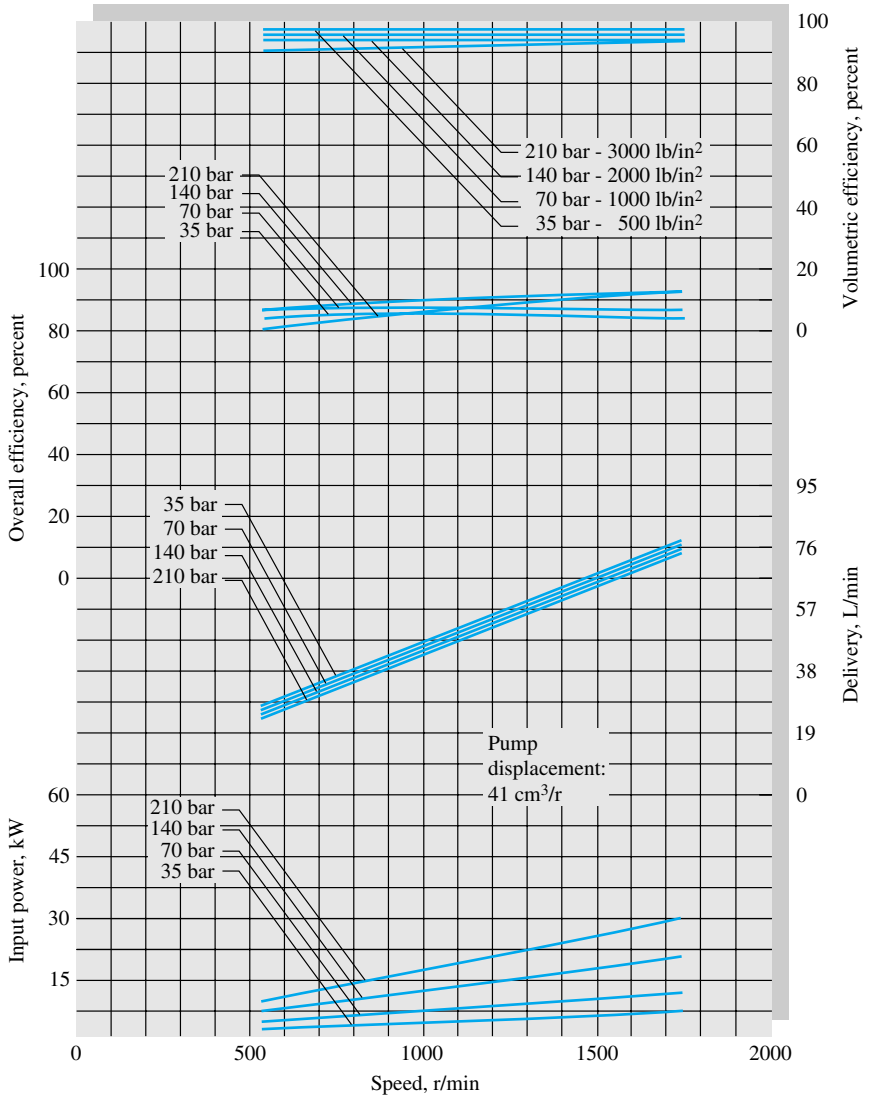


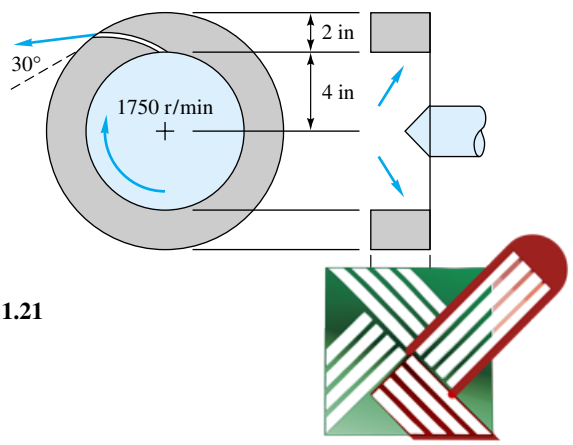
Fig. P11.9 Performance of the model PVQ40 piston pump delivering SAE 10W oil at 180°F. *(Courtesy of Vickers Inc., PDN/PACE Division.)*

Derive an expression for the power delivered to the vane by the jet. For what vane speed is the power maximum?

P11.19 A centrifugal pump has $r_2 = 9$ in, $b_2 = 2$ in, and $\beta_2 = 35°$ and rotates at 1060 r/min. If it generates a head of 180 ft, determine the theoretical (*a*) flow rate in gal/min and (*b*) horsepower. Assume near-radial entry flow.

P11.20 Suppose that Prob. 11.19 is reversed into a statement of the theoretical power $P_w \approx 153$ hp. Can you then compute the theoretical (*a*) flow rate and (*b*) head? Explain and resolve the difficulty which arises.

P11.21 The centrifugal pump of Fig. P11.21 develops a flow rate of 4200 gal/min of gasoline at 20°C with near-radial absolute



P11.21

ketabline.com Ebook.ketabline.com

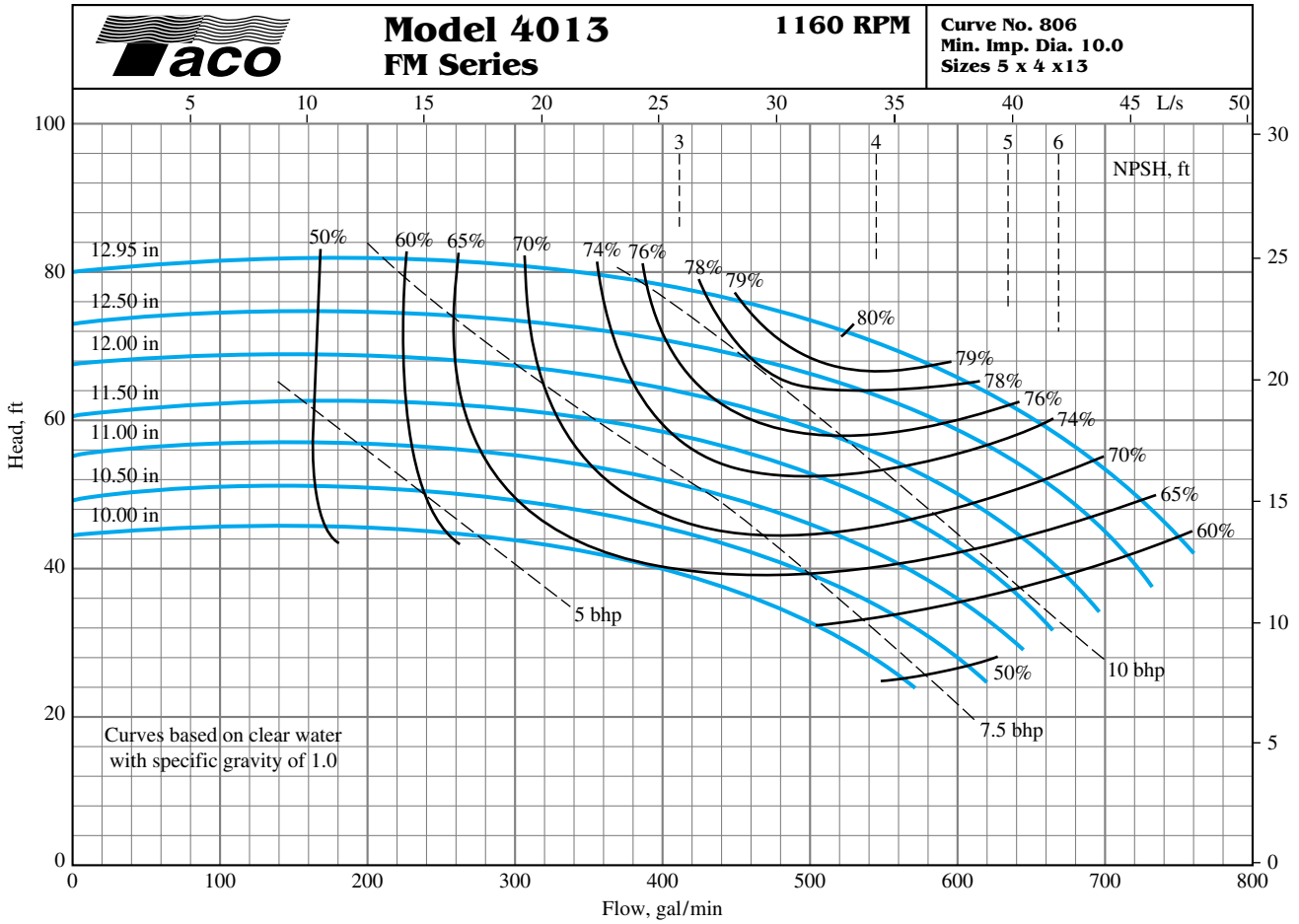


Fig. P11.24 Performance data for a centrifugal pump. *(Courtesy of Taco, Inc., Cranston, Rhode Island.)*

inflow. Estimate the theoretical (*a*) horsepower, (*b*) head rise, and (*c*) appropriate blade angle at the inner radius.

P11.22 A 37-cm-diameter centrifugal pump, running at 2140 r/min with water at 20°C, produces the following performance data:

Q, m^3/s	0.0	0.05	0.10	0.15	0.20	0.25	0.30
H, m	105	104	102	100	95	85	67
P, kW	100	115	135	171	202	228	249

(*a*) Determine the best efficiency point. (*b*) Plot C_H versus C_Q. (*c*) If we desire to use this same pump family to deliver 7000 gal/min of kerosine at 20°C at an input power of 400 kW, what pump speed (in r/min) and impeller size (in cm) are needed? What head will be developed?

P11.23 If the 38-in-diameter pump of Fig. 11.7*b* is used to deliver 20°C kerosine at 850 r/min and 22,000 gal/min, what (*a*) head and (*b*) brake horsepower will result?

P11.24 Figure P11.24 shows performance data for the Taco, Inc., model 4013 pump. Compute the ratios of measured shutoff head to the ideal value U^2/g for all seven impeller sizes. Determine the average and standard deviation of this ratio and compare it to the average for the six impellers in Fig. 11.7.

P11.25 At what speed in r/min should the 35-in-diameter pump of Fig. 11.7*b* be run to produce a head of 400 ft at a discharge of 20,000 gal/min? What brake horsepower will be required? *Hint:* Fit $H(Q)$ to a formula.

P11.26 Determine if the seven Taco, Inc., pump size[illegible] P11.24 can be collapsed into a single dimension[illegible]



ketabline.com Ebook.ketabline.com

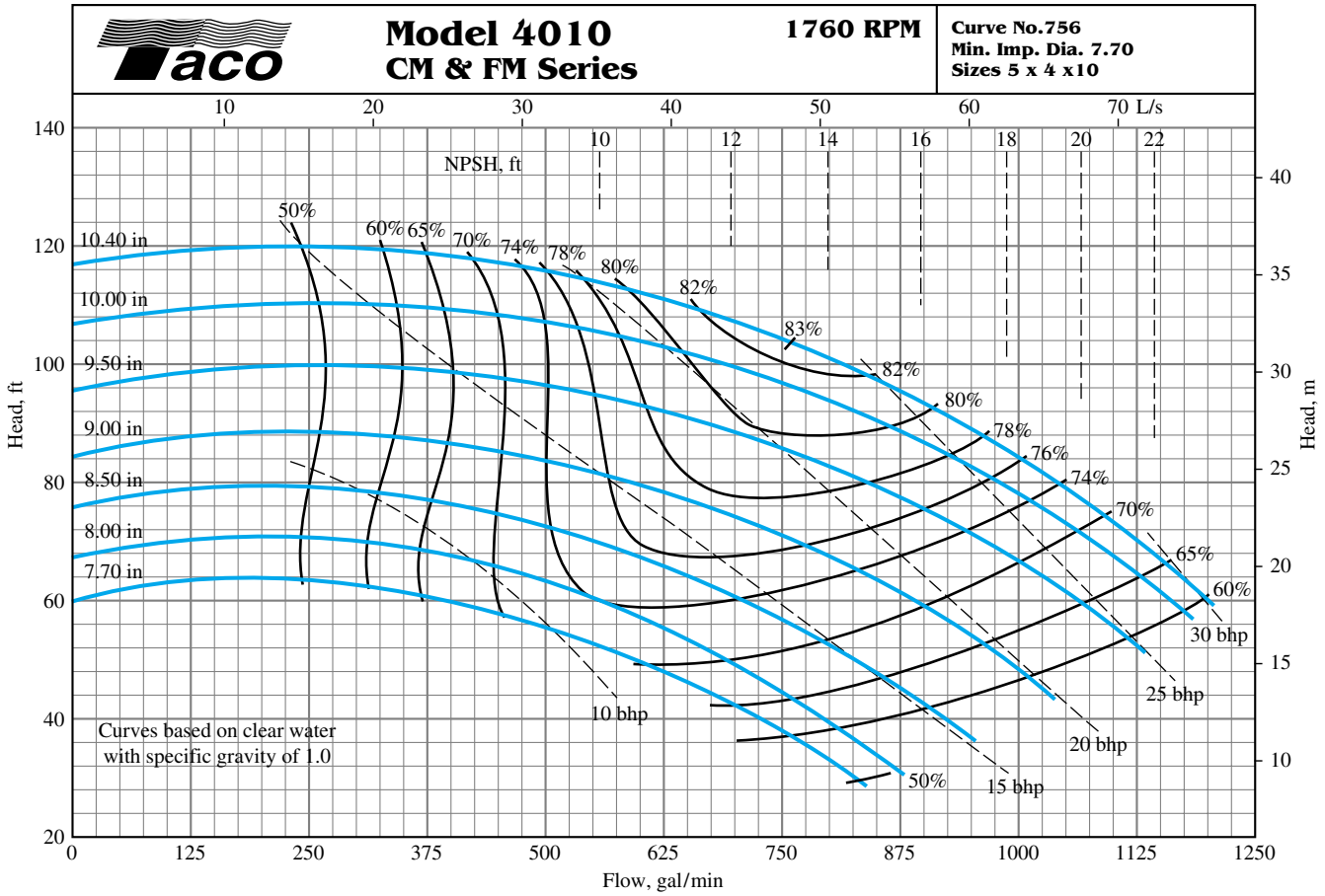


Fig. P11.31 Performance data for a family of centrifugal pump impellers. *(Courtesy of Taco, Inc., Cranston, Rhode Island.)*

of C_H, C_P, and η versus C_Q, as in Fig. 11.8. Comment on the results.

P11.27 The 12-in pump of Fig. P11.24 is to be scaled up in size to provide a head of 90 ft and a flow rate of 1000 gal/min at BEP. Determine the correct (*a*) impeller diameter, (*b*) speed in r/min, and (*c*) horsepower required.

P11.28 Tests by the Byron Jackson Co. of a 14.62-in-diameter centrifugal water pump at 2134 r/min yield the following data:

Q, ft^3/s	0	2	4	6	8	10
H, ft	340	340	340	330	300	220
bhp	135	160	205	255	330	330

What is the BEP? What is the specific speed? Estimate the maximum discharge possible.

P11.29 If the scaling laws are applied to the pump of Prob. 11.28 for the same impeller diameter, determine (*a*) the speed for which the shutoff head will be 280 ft, (*b*) the speed for which the BEP flow rate will be 8.0 ft^3/s, and (*c*) the speed for which the BEP conditions will require 80 hp.

P11.30 A pump from the same family as Prob. 11.28 is built with $D = 18$ in and a BEP power of 250 hp for *gasoline* (not water). Using the scaling laws, estimate the resulting (*a*) speed in r/min, (*b*) flow rate at BEP, and (*c*) shutoff head.

P11.31 Figure P11.31 shows performance data for the Taco, Inc., model 4010 pump. Compute the ratios of measured shutoff head to the ideal value U^2/g for all seven impeller sizes. Determine the average and standard deviation of this ratio, and compare it to the average of 0.58 ± 0.0 for the seven impellers in Fig. P11.2 results.

ketabline.com Ebook.ketabline.com

P11.32 Determine if the seven Taco, Inc., impeller sizes in Fig. P11.31 can be collapsed into a single dimensionless chart of C_H, C_P, and η versus C_Q, as in Fig. 11.8. Comment on the results.

P11.33 Clearly the maximum efficiencies of the pumps in Figs. P11.24 and P11.31 decrease with impeller size. Compare η_{max} for these two pump families with both the Moody and the Anderson correlations, Eqs. (11.29). Use the central impeller size as a comparison point.

P11.34 You are asked to consider a pump geometrically similar to the 9-in-diameter pump of Fig. P11.31 to deliver 1200 gal/min at 1500 r/min. Determine the appropriate (*a*) impeller diameter, (*b*) BEP horsepower, (*c*) shutoff head, and (*d*) maximum efficiency. The fluid is kerosine, not water.

P11.35 An 18-in-diameter centrifugal pump, running at 880 r/min with water at 20°C, generates the following performance data:

Q, gal/min	0.0	2000	4000	6000	8000	10,000
H, ft	92	89	84	78	68	50
P, hp	100	112	130	143	156	163

Determine (*a*) the BEP, (*b*) the maximum efficiency, and (*c*) the specific speed. (*d*) Plot the required input power versus the flow rate.

P11.36 Plot the dimensionless performance curves for the pump of Prob. 11.35 and compare with Fig. 11.8. Find the appropriate diameter in inches and speed in r/min for a geometrically similar pump to deliver 400 gal/min against a head of 200 ft. What brake horsepower would be required?

P11.37 The efficiency of a centrifugal pump can be approximated by the curve fit $\eta \approx aQ - bQ^3$, where a and b are constants. For this approximation, (*a*) what is the ratio of Q^* at BEP to Q_{max}? If the maximum efficiency is 88 percent, what is the efficiency at (*b*) $\frac{1}{3}Q_{max}$ and (*c*) $\frac{4}{3}Q^*$?

P11.38 A 6.85-in pump, running at 3500 r/min, has the following measured performance for water at 20°C:

Q, gal/min	50	100	150	200	250	300	350	400	450
H, ft	201	200	198	194	189	181	169	156	139
η, %	29	50	64	72	77	80	81	79	74

(*a*) Estimate the horsepower at BEP. If this pump is rescaled in water to provide 20 bhp at 3000 r/min, determine the appropriate (*b*) impeller diameter, (*c*) flow rate, and (*d*) efficiency for this new condition.

P11.39 The Allis-Chalmers D30LR centrifugal compressor delivers 33,000 ft^3/min of SO_2 with a pressure change from 14.0 to 18.0 lbf/in^2 absolute using an 800-hp motor at 3550 r/min. What is the overall efficiency? What will the flow rate and Δp be at 3000 r/min? Estimate the diameter of the impeller.

P11.40 The specific speed N_s, as defined by Eqs. (11.30), does not contain the impeller diameter. How then should we size the pump for a given N_s? Logan [7] suggests a parameter called the *specific diameter* D_s, which is a dimensionless combination of Q, gH, and D. (*a*) If D_s is proportional to D, determine its form. (*b*) What is the relationship, if any, of D_s to C_{Q^*}, C_{H^*}, and C_{P^*}? (*c*) Estimate D_s for the two pumps of Figs. 11.8 and 11.13.

P11.41 It is desired to build a centrifugal pump geometrically similar to that of Prob. 11.28 to deliver 6500 gal/min of gasoline at 20°C at 1060 r/min. Estimate the resulting (*a*) impeller diameter, (*b*) head, (*c*) brake horsepower, and (*d*) maximum efficiency.

P11.42 An 8-in model pump delivering 180°F water at 800 gal/min and 2400 r/min begins to cavitate when the inlet pressure and velocity are 12 lbf/in^2 absolute and 20 ft/s, respectively. Find the required NPSH of a prototype which is 4 times larger and runs at 1000 r/min.

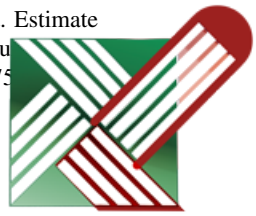
P11.43 The 28-in-diameter pump in Fig. 11.7*a* at 1170 r/min is used to pump water at 20°C through a piping system at 14,000 gal/min. (*a*) Determine the required brake horsepower. The average friction factor is 0.018. (*b*) If there is 65 ft of 12-in-diameter pipe upstream of the pump, how far below the surface should the pump inlet be placed to avoid cavitation?

P11.44 The pump of Prob. 11.28 is scaled up to an 18-in diameter, operating in water at best efficiency at 1760 r/min. The measured NPSH is 16 ft, and the friction loss between the inlet and the pump is 22 ft. Will it be sufficient to avoid cavitation if the pump inlet is placed 9 ft below the surface of a sea-level reservoir?

P11.45 Determine the specific speeds of the seven Taco, Inc., pump impellers in Fig. P11.24. Are they appropriate for centrifugal designs? Are they approximately equal within experimental uncertainty? If not, why not?

P11.46 The answer to Prob. 11.40 is that the dimensionless "specific diameter" takes the form $D_s = D(gH^*)^{1/4}/Q^{*1/2}$, evaluated at the BEP. Data collected by the author for 30 different pumps indicate, in Fig. P11.46, that D_s correlates well with specific speed N_s. Use this figure to estimate the appropriate impeller diameter for a pump which delivers 20,000 gal/min of water and a head of 400 ft when running at 1200 r/min. Suggest a curve-fit formula to the data. *Hint*: Use a hyperbolic formula.

P11.47 A typical household basement sump pump provides a discharge of 5 gal/min against a head of 15 ft. Estimate (*a*) the maximum efficiency and (*b*) the minimu
power required to drive such a pump at 17



ketabline.com Ebook.ketabline.com

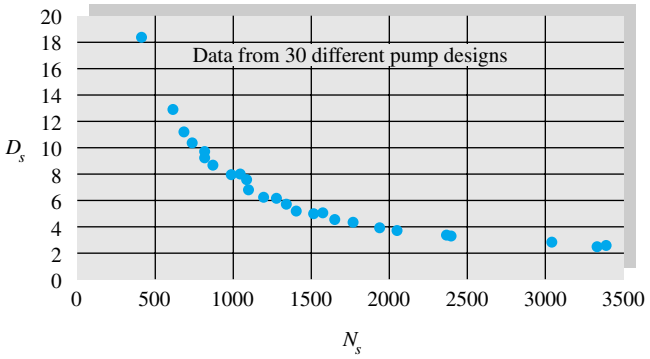


Fig. P11.46 Specific diameter at BEP for 30 commercial pumps.

P11.48 Compute the specific speeds for the pumps in Probs. 11.28, 11.35, and 11.38 plus the median sizes in Figs. P11.24 and P11.31. Then determine if their maximum efficiencies match the values predicted in Fig. 11.14.

P11.49 Data collected by the author for flow coefficient at BEP for 30 different pumps are plotted versus specific speed in Fig. P11.49. Determine if the values of C_Q^* for the five pumps in Prob. 11.48 also fit on this correlation. If so, suggest a curve-fitted formula for the data.

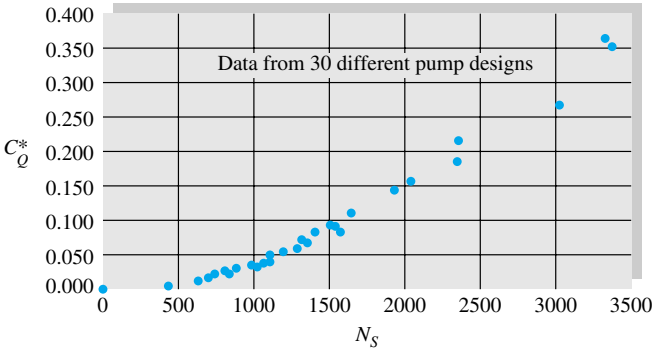


Fig. P11.49 Flow coefficient at BEP for 30 commercial pumps.

P11.50 Data collected by the author for power coefficient at BEP for 30 different pumps are plotted versus specific speed in Fig. P11.50. Determine if the values of C_P^* for the five pumps in Prob. 11.48 also fit on this correlation. If so, suggest a curve-fitted formula for the data.

P11.51 An axial-flow pump delivers 40 ft^3/s of air which enters at 20°C and 1 atm. The flow passage has a 10-in outer radius and an 8-in inner radius. Blade angles are $\alpha_1 = 60°$ and $\beta_2 = 70°$, and the rotor runs at 1800 r/min. For the first stage compute (*a*) the head rise and (*b*) the power required.

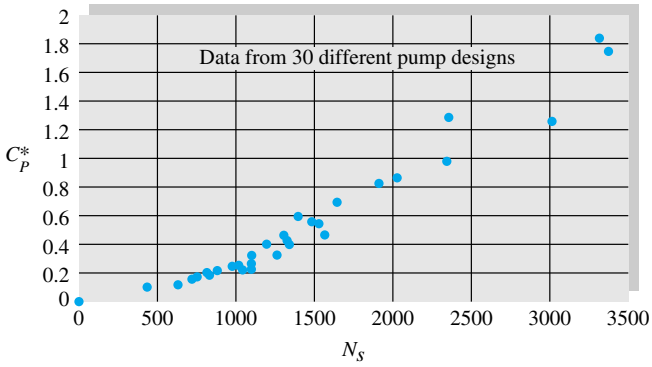


Fig. P11.50 Power coefficient at BEP for 30 commercial pumps.

P11.52 An axial-flow fan operates in sea-level air at 1200 r/min and has a blade-tip diameter of 1 m and a root diameter of 80 cm. The inlet angles are $\alpha_1 = 55°$ and $\beta_1 = 30°$, while at the outlet $\beta_2 = 60°$. Estimate the theoretical values of the (*a*) flow rate, (*b*) horsepower, and (*c*) outlet angle α_2.

P11.53 If the axial-flow pump of Fig. 11.13 is used to deliver 70,000 gal/min of 20°C water at 1170 r/min, estimate (*a*) the proper impeller diameter, (*b*) the shutoff head, (*c*) the shutoff horsepower, and (*d*) Δp at best efficiency.

P11.54 The Colorado River Aqueduct uses Worthington Corp. pumps which deliver 200 ft^3/s at 450 r/min against a head of 440 ft. What types of pump are these? Estimate the impeller diameter.

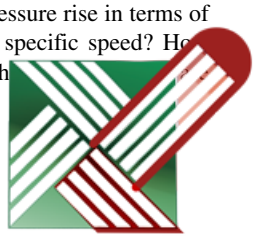
P11.55 We want to pump 70°C water at 20,000 gal/min and 1800 r/min. Estimate the type of pump, the horsepower required, and the impeller diameter if the required pressure rise for one stage is (*a*) 170 kPa and (*b*) 1350 kPa.

P11.56 A pump is needed to deliver 40,000 gal/min of gasoline at 20°C against a head of 90 ft. Find the impeller size, speed, and brake horsepower needed to use the pump families of (*a*) Fig. 11.8 and (*b*) Fig. 11.13. Which is the better design?

P11.57 Performance data for a 21-in-diameter air blower running at 3550 r/min are as follows:

Δp, inH_2O	29	30	28	21	10
Q, ft^3/min	500	1000	2000	3000	4000
bhp	6	8	12	18	25

Note the fictitious expression of pressure rise in terms of water rather than air. What is the specific speed? How does the performance compare with C_Q^*, C_H^*, and C_P^*?



ketabline.com Ebook.ketabline.com

P11.58 The Worthington Corp. model A-12251 water pump, operating at maximum efficiency, produces 53 ft of head at 3500 r/min, 1.1 bhp at 3200 r/min, and 60 gal/min at 2940 r/min. What type of pump is this? What is its efficiency, and how does this compare with Fig. 11.14? Estimate the impeller diameter.

P11.59 Suppose it is desired to deliver 700 ft^3/min of propane gas (molecular weight = 44.06) at 1 atm and 20°C with a single-stage pressure rise of 8.0 inH_2O. Determine the appropriate size and speed for using the pump families of (*a*) Prob. 11.57 and (*b*) Fig. 11.13. Which is the better design?

P11.60 A 45-hp pump is desired to generate a head of 200 ft when running at BEP with 20°C gasoline at 1200 r/min. Using the correlations in Figs. P11.49 and P11.50, determine the appropriate (*a*) specific speed, (*b*) flow rate, and (*c*) impeller diameter.

P11.61 A mine ventilation fan, running at 295 r/min, delivers 500 m^3/s of sea-level air with a pressure rise of 1100 Pa. Is this fan axial, centrifugal, or mixed? Estimate its diameter in ft. If the flow rate is increased 50 percent for the same diameter, by what percentage will the pressure rise change?

P11.62 The actual mine ventilation fan discussed in Prob. 11.61 had a diameter of 20 ft [20, p. 339]. What would be the proper diameter for the pump family of Fig. 11.14 to provide 500 m^3/s at 295 r/min and BEP? What would be the resulting pressure rise in Pa?

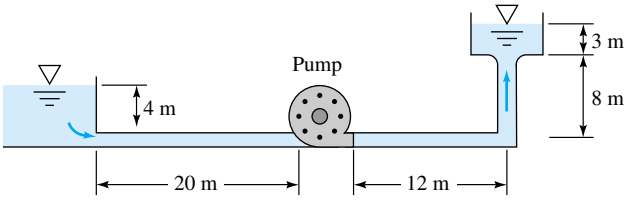
P11.63 The 36.75-in pump in Fig. 11.7*a* at 1170 r/min is used to pump water at 60°F from a reservoir through 1000 ft of 12-in-ID galvanized-iron pipe to a point 200 ft above the reservoir surface. What flow rate and brake horsepower will result? If there is 40 ft of pipe upstream of the pump, how far below the surface should the pump inlet be placed to avoid cavitation?

P11.64 In Prob. 11.63 the operating point is off design at an efficiency of only 77 percent. Is it possible, with the similarity rules, to change the pump rotation speed to deliver the water near BEP? Explain your results.

P11.65 The 38-in pump of Fig. 11.7*a* is used in series to lift 20°C water 3000 ft through 4000 ft of 18-in-ID cast-iron pipe. For most efficient operation, how many pumps in series are needed if the rotation speed is (*a*) 710 r/min and (*b*) 1200 r/min?

P11.66 It is proposed to run the pump of Prob. 11.35 at 880 r/min to pump water at 20°C through the system in Fig. P11.66. The pipe is 20-cm-diameter commercial steel. What flow rate in ft^3/min will result? Is this an efficient application?

P11.67 The pump of Prob. 11.35, running at 880 r/min, is to pump water at 20°C through 75 m of horizontal galvanized-iron pipe. All other system losses are neglected.



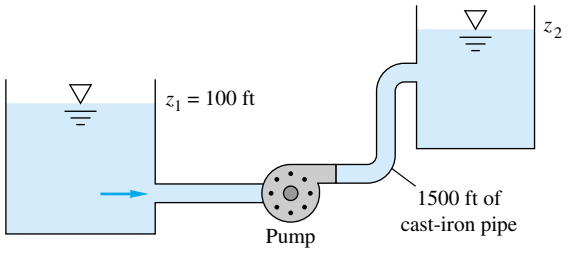
P11.66

Determine the flow rate and input power for (*a*) pipe diameter = 20 cm and (*b*) the pipe diameter found to yield maximum pump efficiency.

P11.68 A 24-in pump is homologous to the 32-in pump in Fig. 11.7*a*. At 1400 r/min this pump delivers 12,000 gal/min of water from one reservoir through a long pipe to another 50 ft higher. What will the flow rate be if the pump speed is increased to 1750 r/min? Assume no change in pipe friction factor or efficiency.

P11.69 The pump of Prob. 11.38, running at 3500 r/min, is used to deliver water at 20°C through 600 ft of cast-iron pipe to an elevation 100 ft higher. Determine (*a*) the proper pipe diameter for BEP operation and (*b*) the flow rate which results if the pipe diameter is 3 in.

P11.70 The pump of Prob. 11.28, operating at 2134 r/min, is used with 20°C water in the system of Fig. P11.70. (*a*) If it is operating at BEP, what is the proper elevation z_2? (*b*) If z_2 = 225 ft, what is the flow rate if d = 8 in.?

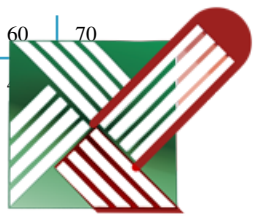


P11.70

P11.71 The pump of Prob. 11.38, running at 3500 r/min, delivers water at 20°C through 7200 ft of horizontal 5-in-diameter commercial-steel pipe. There are a sharp entrance, sharp exit, four 90° elbows, and a gate valve. Estimate (*a*) the flow rate if the valve is wide open and (*b*) the valve closing percentage which causes the pump to operate at BEP. (*c*) If the latter condition holds continuously for 1 year, estimate the energy cost at 10 ¢/kWh.

P11.72 Performance data for a small commercial pump are as follows:

Q, gal/min	0	10	20	30	40	50	60	70
H, ft	75	75	74	72	68	62		



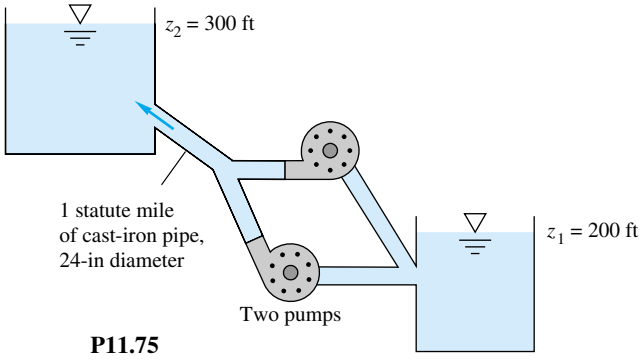
ketabline.com Ebook.ketabline.com

This pump supplies 20°C water to a horizontal $\frac{5}{8}$-in-diameter garden hose ($\epsilon \approx 0.01$ in) which is 50 ft long. Estimate (*a*) the flow rate and (*b*) the hose diameter which would cause the pump to operate at BEP.

P11.73 The piston pump of Fig. P11.9 is run at 1500 r/min to deliver SAE 10W oil through 100 m of vertical 2-cm-diameter wrought-iron pipe. If other system losses are neglected, estimate (*a*) the flow rate, (*b*) the pressure rise, and (*c*) the power required.

P11.74 The 32-in pump in Fig. 11.7*a* is used at 1170 r/min in a system whose head curve is H_s (ft) = 100 + 1.5Q^2, with Q in thousands of gallons of water per minute. Find the discharge and brake horsepower required for (*a*) one pump, (*b*) two pumps in parallel, and (*c*) two pumps in series. Which configuration is best?

P11.75 Two 35-in pumps from Fig. 11.7*b* are installed in parallel for the system of Fig. P11.75. Neglect minor losses. For water at 20°C, estimate the flow rate and power required if (*a*) both pumps are running and (*b*) one pump is shut off and isolated.



P11.75

P11.76 Two 32-in pumps from Fig. 11.7*a* are combined in parallel to deliver water at 60°F through 1500 ft of horizontal pipe. If $f = 0.025$, what pipe diameter will ensure a flow rate of 35,000 gal/min for n = 1170 r/min?

P11.77 Two pumps of the type tested in Prob. 11.22 are to be used at 2140 r/min to pump water at 20°C vertically upward through 100 m of commercial-steel pipe. Should they be in series or in parallel? What is the proper pipe diameter for most efficient operation?

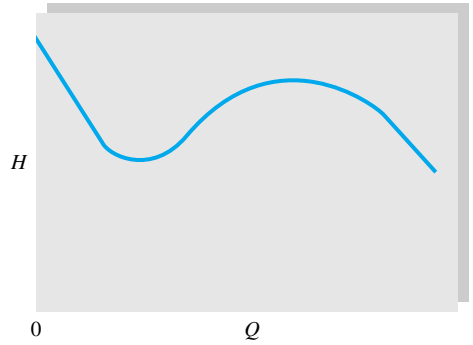
P11.78 Suppose that the two pumps in Fig. P11.75 are modified to be in series, still at 710 r/min. What pipe diameter is required for BEP operation?

P11.79 Two 32-in pumps from Fig. 11.7*a* are to be used in series at 1170 r/min to lift water through 500 ft of vertical cast-iron pipe. What should the pipe diameter be for most efficient operation? Neglect minor losses.

P11.80 It is proposed to use one 32- and one 28-in pump from Fig. 11.7*a* in parallel to deliver water at 60°F. The system-head curve is $H_s = 50 + 0.3Q^2$, with Q in thousands of gallons per minute. What will the head and delivery be if both pumps run at 1170 r/min? If the 28-in pump is reduced below 1170 r/min, at what speed will it cease to deliver?

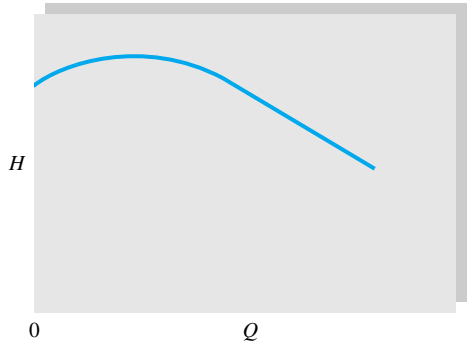
P11.81 Reconsider the system of Fig. P6.68. Use the Byron Jackson pump of Prob. 11.28 running at 2134 r/min, no scaling, to drive the flow. Determine the resulting flow rate between the reservoirs. What is the pump efficiency?

P11.82 The S-shaped head-versus-flow curve in Fig. P11.82 occurs in some axial-flow pumps. Explain how a fairly flat system-loss curve might cause instabilities in the operation of the pump. How might we avoid instability?



P11.82

P11.83 The low-shutoff head-versus-flow curve in Fig. P11.83 occurs in some centrifugal pumps. Explain how a fairly flat system-loss curve might cause instabilities in the operation of the pump. What additional vexation occurs when two of these pumps are in parallel? How might we avoid instability?



P11.83

P11.84 Turbines are to be installed where t
and the flow rate 250,000 gal/min. D



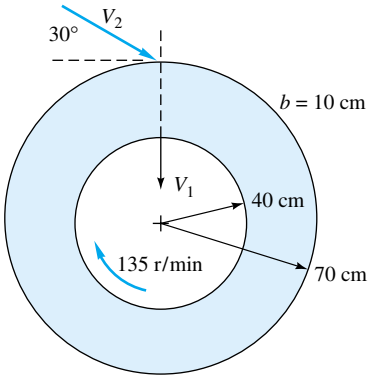
ketabline.com Ebook.ketabline.com

ber, and size of turbine which might be selected if the generator selected is (*a*) 48-pole, 60-cycle ($n = 150$ r/min) and (*b*) 8-pole ($n = 900$ r/min). Why are at least two turbines desirable from a planning point of view?

P11.85 Turbines at the Conowingo Plant on the Susquehanna River each develop 54,000 bhp at 82 r/min under a head of 89 ft. What type of turbines are these? Estimate the flow rate and impeller diameter.

P11.86 The Tupperware hydroelectric plant on the Blackstone River has four 36-in-diameter turbines, each providing 447 kW at 200 r/min and 205 ft^3/s for a head of 30 ft. What type of turbines are these? How does their performance compare with Fig. 11.21?

P11.87 An idealized radial turbine is shown in Fig. P11.87. The absolute flow enters at 30° and leaves radially inward. The flow rate is 3.5 m^3/s of water at 20°C. The blade thickness is constant at 10 cm. Compute the theoretical power developed at 100 percent efficiency.



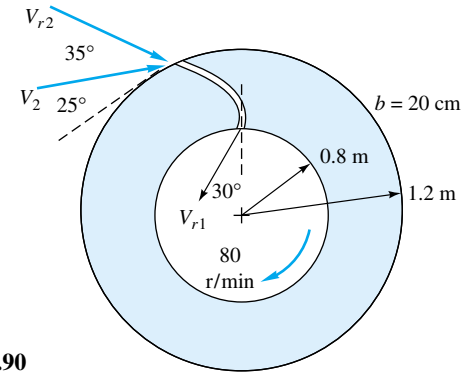
P11.87

P11.88 A certain turbine in Switzerland delivers 25,000 bhp at 500 r/min under a net head of 5330 ft. What type of turbine is this? Estimate the approximate discharge and size.

P11.89 A Pelton wheel of 12-ft pitch diameter operates under a net head of 2000 ft. Estimate the speed, power output, and flow rate for best efficiency if the nozzle exit diameter is 4 in.

P11.90 An idealized radial turbine is shown in Fig. P11.90. The absolute flow enters at 25° with the blade angles as shown. The flow rate is 8 m^3/s of water at 20°C. The blade thickness is constant at 20 cm. Compute the theoretical power developed at 100 percent efficiency.

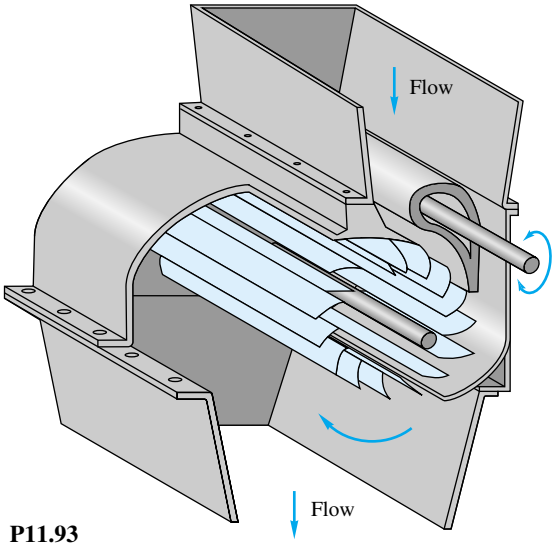
P11.91 The flow through an axial-flow *turbine* can be idealized by modifying the stator-rotor diagrams of Fig. 11.12 for energy absorption. Sketch a suitable blade and flow arrangement and the associated velocity vector diagrams. For further details see chap. 8 of Ref. 25.



P11.90

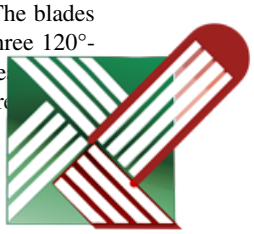
P11.92 At a proposed turbine installation the available head is 800 ft, and the water flow rate is 40,000 gal/min. Discuss the size, speed, and number of turbines which might be suitable for this purpose while using (*a*) a Pelton wheel and (*b*) a Francis wheel.

P11.93 Figure P11.93 shows a cutaway of a *cross-flow* or "Banki" turbine [55], which resembles a squirrel cage with slotted curved blades. The flow enters at about 2 o'clock, passes through the center and then again through the blades, leaving at about 8 o'clock. Report to the class on the operation and advantages of this design, including idealized velocity vector diagrams.



P11.93

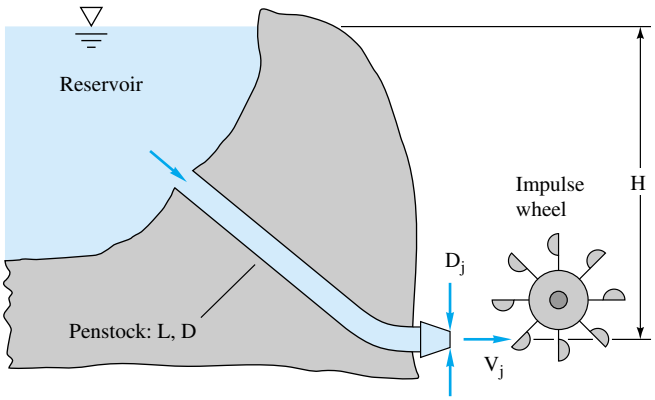
P11.94 A simple cross-flow turbine, Fig. P11.93, was constructed and tested at the University of Rhode Island. The blades were made of PVC pipe cut lengthwise into three 120°-arc pieces. When it was tested in water at a he
ft and a flow rate of 630 gal/min, the measur



ketabline.com Ebook.ketabline.com

output was 0.6 hp. Estimate (*a*) the efficiency and (*b*) the power specific speed if $n = 200$ rev/min.

P11.95 One can make a theoretical estimate of the proper diameter for a penstock in an impulse turbine installation, as in Fig. P11.95. Let L and H be known, and let the turbine performance be idealized by Eqs. (11.38) and (11.39). Account for friction loss h_f in the penstock, but neglect minor losses. Show that (*a*) the maximum power is generated when $h_f = H/3$, (*b*) the optimum jet velocity is $(4gH/3)^{1/2}$, and (*c*) the best nozzle diameter is $D_j = [D^5/(2\ fL)]^{1/4}$, where f is the pipe-friction factor.



P11.95

P11.96 Apply the results of Prob. 11.95 to determining the optimum (*a*) penstock diameter and (*b*) nozzle diameter for the data of Prob. 11.92 with a commercial-steel penstock of length 1500 ft.

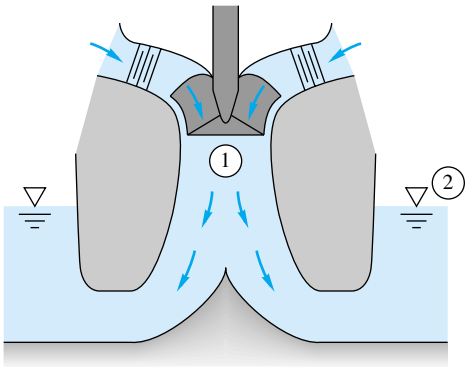
P11.97 Consider the following nonoptimum version of Prob. 11.95: $H = 450$ m, $L = 5$ km, $D = 1.2$ m, $D_j = 20$ cm. The penstock is concrete, $\epsilon = 1$ mm. The impulse wheel diameter is 3.2 m. Estimate (*a*) the power generated by the wheel at 80 percent efficiency and (*b*) the best speed of the wheel in r/min. Neglect minor losses.

P11.98 Francis and Kaplan turbines are often provided with *draft tubes*, which lead the exit flow into the tailwater region, as in Fig. P11.98. Explain at least two advantages in using a draft tube.

P11.99 Turbines can also cavitate when the pressure at point 1 in Fig. P11.98 drops too low. With NPSH defined by Eq. (11.20), the empirical criterion given by Wislicenus [4] for cavitation is

$$N_{ss} = \frac{(\text{r/min})(\text{gal/min})^{1/2}}{[\text{NPSH (ft)}]^{3/4}} \geq 11{,}000$$

Use this criterion to compute how high $z_1 - z_2$, the impeller eye in Fig. P11.98, can be placed for a Francis turbine with a head of 300 ft, $N_{sp} = 40$, and $p_a = 14$ lbf/in^2 absolute before cavitation occurs in 60°F water.



P11.98

P11.100 One of the largest wind generators in operation today is the ERDA/NASA two-blade propeller HAWT in Sandusky, Ohio. The blades are 125 ft in diameter and reach maximum power in 19 mi/h winds. For this condition estimate (*a*) the power generated in kW, (*b*) the rotor speed in r/min, and (*c*) the velocity V_2 behind the rotor.

P11.101 A Darrieus VAWT in operation in Lumsden, Saskatchewan, that is 32 ft high and 20 ft in diameter sweeps out an area of 432 ft^2. Estimate (*a*) the maximum power and (*b*) the rotor speed if it is operating in 16 mi/h winds.

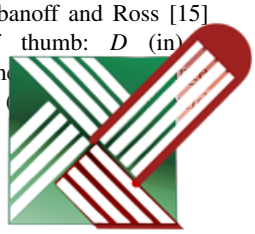
P11.102 An American 6-ft diameter multiblade HAWT is used to pump water to a height of 10 ft through 3-in-diameter cast-iron pipe. If the winds are 12 mi/h, estimate the rate of water flow in gal/min.

P11.103 A very large Darrieus VAWT was constructed by the U.S. Department of Energy near Sandia, New Mexico. It is 60 ft high and 30 ft in diameter, with a swept area of 1200 ft^2. If the turbine is constrained to rotate at 90 r/min, use Fig. 11.31 to plot the predicted power output in kW versus wind speed in the range $V = 5$ to 40 mi/h.

Word Problems

W11.1 We know that an enclosed rotating bladed impeller will impart energy to a fluid, usually in the form of a pressure rise, but how does it actually happen? Discuss, with sketches, the physical mechanisms through which an impeller actually transfers energy to a fluid.

W11.2 Dynamic pumps (as opposed to PDPs) have difficulty moving highly viscous fluids. Lobanoff and Ross [15] suggest the following rule of thumb: D (in) $0.015\nu/\nu_{water}$, where D is the diam pipe. For example, SAE 30W oil (



ketabline.com Ebook.ketabline.com

require at least a 4.5-in outlet. Can you explain some reasons for this limitation?

W11.3 The concept of NPSH dictates that liquid dynamic pumps should generally be immersed below the surface. Can you explain this? What is the effect of increasing the liquid temperature?

W11.4 For nondimensional fan performance, Wallis [20] suggests that the head coefficient should be replaced by FTP/($\rho n^2 D^2$), where FTP is the fan total pressure change. Explain the usefulness of this modification.

W11.5 Performance data for centrifugal pumps, even if well scaled geometrically, show a decrease in efficiency with decreasing impeller size. Discuss some physical reasons why this is so.

W11.6 Consider a dimensionless pump performance chart such as Fig. 11.8. What additional dimensionless parameters might modify or even destroy the similarity indicated in such data?

W11.7 One parameter not discussed in this text is the *number of blades* on an impeller. Do some reading on this subject, and report to the class about its effect on pump performance.

W11.8 Explain why some pump performance curves may lead to unstable operating conditions.

W11.9 Why are Francis and Kaplan turbines generally considered unsuitable for hydropower sites where the available head exceeds 1000 ft?

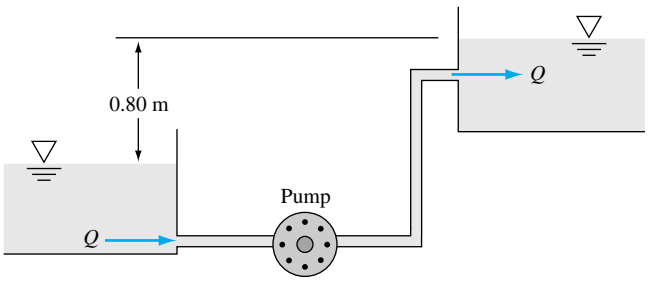
W11.10 Do some reading on the performance of the *free propeller* that is used on small, low-speed aircraft. What dimensionless parameters are typically reported for the data? How do the performance and efficiency compare with those for the axial-flow pump?

Comprehensive Problems

C11.1 The net head of a little aquarium pump is given by the manufacturer as a function of volume flow rate as listed below:

Q, m^3/s	H, mH_2O
0	1.10
1.0 E-6	1.00
2.0 E-6	0.80
3.0 E-6	0.60
4.0 E-6	0.35
5.0 E-6	0.0

What is the maximum achievable flow rate if you use this pump to pump water from the lower reservoir to the upper reservoir as shown in Fig. C11.1? *Note*: The tubing is smooth with an inner diameter of 5.0 mm and a total length of 29.8 m. The water is at room temperature and pressure. Minor losses in the system can be neglected.



C11.1

C11.2 Reconsider Prob. 6.68 as an exercise in pump selection. Select an impeller size and rotational speed from the Byron Jackson pump family of Prob. 11.28 which will deliver a flow rate of 3 ft^3/s to the system of Fig. P6.68 at minimum input power. Calculate the horsepower required.

C11.3 Reconsider Prob. 6.77 as an exercise in turbine selection. Select an impeller size and rotational speed from the Francis turbine family of Fig. 11.21*d* which will deliver maximum power generated by the turbine. Calculate the turbine power output and remark on the practicality of your design.

C11.4 A pump provides a net head H which is dependent on the volume flow rate Q, as follows: $H = a - bQ^2$, where a = 80 m and b = 20 s^2/m^5. The pump delivers water at 20°C through a horizontal 30-cm-diameter cast-iron pipe which is 120 m long. The pressures at the inlet and exit of the system are the same. Neglecting minor losses, calculate the expected volume flow rate in gal/min.

C11.5 In Prob. 11.23, estimate the efficiency of the pump in two ways: (*a*) Read it directly from Fig. 11.7*b* (for the dynamically similar water pump); and (*b*) Calculate it from Eq. (11.5) for the actual kerosene flow. Compare your results and discuss any discrepancies.



ketabline.com Ebook.ketabline.com

Design Project

D11.1 To save on electricity costs, a town water supply system uses gravity-driven flow from five large storage tanks during the day and then refills these tanks from 10 p.m. to 6 a.m. at a cheaper night rate of 7 ¢/kWh. The total resupply needed each night varies from 5 E5 to 2 E6 gal, with no more than 5 E5 gallons to any one tank. Tank elevations vary from 40 to 100 ft. A single constant-speed pump, drawing from a large groundwater aquifer and valved into five different cast-iron tank supply lines, does this job. Distances from the pump to the five tanks vary more or less evenly from 1 to 3 mi. Each line averages one elbow every 100 ft and has four butterfly valves which can be controlled at any desirable angle. Select a suitable pump family from one of the six data sets in this chapter: Figs. 11.8, P11.24, and P11.31 plus Probs. 11.28, 11.35, and 11.38. Assume ideal similarity (no Reynolds-number or pump roughness effects). The goal is to determine pump and pipeline sizes which achieve minimum total cost over a 5-year period. Some suggested cost data are

1. Pump and motor: $2500 plus $1500 per inch of pipe size
2. Valves: $100 plus $100 per inch of pipe size
3. Pipelines: 50¢ per inch of diameter per foot of length

Since the flow and elevation parameters vary considerably, a random daily variation within the specified ranges might give a realistic approach.

References

1. D. G. Wilson, "Turbomachinery—From Paddle Wheels to Turbojets," *Mech. Eng.,* vol. 104, Oct. 1982, pp. 28–40.
2. D. Japikse and N. C. Baines, *Introduction to Turbomachinery*, Oxford University Press, New York, 1995.
3. D. W. Childs, *Turbomachinery Rotordynamics: Phenomena, Modeling, and Analysis*, Wiley, New York, 1993.
4. G. F. Wislicenus, *Fluid Mechanics of Turbomachinery,* 2d ed., McGraw-Hill, New York, 1965.
5. S. L. Dixon, *Fluid Mechanics and Thermodynamics of Turbomachinery*, 2d ed., Butterworth, London, 1998.
6. R. I. Lewis, *Turbomachinery Performance Analysis*, Wiley, New York, 1996.
7. E. S. Logan, Jr., *Turbomachinery: Basic Theory and Applications*, 2d ed., Marcel Dekker, New York, 1993.
8. A. J. Stepanoff, *Centrifugal and Axial Flow Pumps,* 2d ed., Wiley, New York, 1957.
9. J. W. Dufour and W. E. Nelson, *Centrifugal Pump Sourcebook*, McGraw-Hill, New York, 1992.
10. Sam Yedidiah, *Centrifugal Pump User's Guidebook: Problems and Solutions*, Chapman and Hall, New York, 1996.
11. T. G. Hicks and T. W. Edwards, *Pump Application Engineering,* McGraw-Hill, New York, 1971.
12. *Pump Selector for Industry,* Worthington Pump, Mountainside, NJ, 1977.
13. R. Walker, *Pump Selection,* 2d ed., Butterworth, London, 1979.
14. R. H. Warring, *Pumps: Selection, Systems, and Applications,* 2d ed., Gulf Pub., Houston, TX, 1984.
15. V. L. Lobanoff and R. R. Ross, *Centrifugal Pumps, Design and Application,* Gulf Pub., Houston, TX, 1985.
16. H. L. Stewart, *Pumps,* 5th ed. Macmillan, New York, 1991.
17. A. B. McKenzie, *Axial Flow Fans and Compressors: Aerodynamic Design and Performance*, Ashgate Publishing, Brookfield, VT, 1997.
18. W. C. Osborne, *Fans,* 2d ed., Pergamon, London, 1977.
19. R. Jorgensen (ed.), *Fan Engineering,* Buffalo Forge, Buffalo, NY, 1983.
20. R. A. Wallis, *Axial Flow Fans and Ducts,* Wiley, New York, 1983.
21. H. P. Bloch, *A Practical Guide to Compressor Technology*, McGraw-Hill, New York, 1996.
22. H. Cohen et al., *Gas Turbine Theory*, Longman, London, 1996.
23. N. A. Cumpsty, *Compressor Aerodynamics,* Longmans, London, 1989.
24. G. C. Oates, *Aerothermodynamics of Gas Turbine and Rocket Propulsion*, 3d ed., AIAA, Washington, DC, 1998.
25. W. W. Bathe, *Fundamentals of Gas Turbines,* 2d ed., Wiley, New York, 1995.
26. J. Tong (ed.), *Mini-Hydropower*, Wiley, New York, 1997.
27. C. C. Warnick, *Hydropower Engineering,* Prentice-Hall, Englewood Cliffs, NJ, 1984.
28. J. J. Fritz, *Small and Mini Hydropower Systems,* McGraw-Hill, New York, 1984.
29. N. P. Cheremisinoff and P. N. Cheremisinoff, *Pumps/Compressors/Fans: Pocket Handbook*, Technomic Publishing, Lancaster, PA, 1989.
30. Hydraulic Institute, *Hydraulic Institute Standards for Centrifugal, Rotating, and Reciprocal Pumps,* New York, 1983.
31. I. J. Karassik, W. C. Krutzsch, W. H. Fraser, and J. P. Messina, *Pump Handbook,* 2d ed., McGraw-Hill, New York, 1985.
32. J. S. Gulliver and R. E. A. Arndt, *Hydr*
Handbook, McGraw-Hill, New York, 19



ketabline.com Ebook.ketabline.com

33. R. L. Daugherty, J. B. Franzini, and E. J. Finnemore, *Fluid Mechanics and Engineering Applications,* 8th ed., McGraw-Hill, New York, 1985.
34. R. H. Sabersky, A. J. Acosta, and E. G. Hauptmann, *Fluid Flow: A First Course in Fluid Mechanics,* 3d ed., Macmillan, New York, 1989.
35. J. P. Poynton, *Metering Pumps,* Marcel-Dekker, New York, 1983.
36. R. P. Lambeck, *Hydraulic Pumps and Motors: Selection and Application for Hydraulic Power Control Systems,* Marcel Dekker, New York, 1983.
37. T. L. Henshaw, *Reciprocating Pumps,* Van Nostrand Reinhold, New York, 1987.
38. J. E. Miller, *The Reciprocating Pump: Theory, Design and Use,* Wiley, NewYork, 1987.
39. D. G. Wilson, *The Design of High-Efficiency Turbomachinery and Gas Turbines*, 2d ed., Prentice-Hall, Upper Saddle River, N.J., 1998.
40. M. C. Roco, P. Hamelin, T. Cader, and G. Davidson, "Animation of LDV Measurements in a Centrifugal Pump," in *Fluid Machinery Forum—1990,* U.S. Rohatgi (ed.), FED, vol. 96, American Society of Mechanical Engineers, New York, 1990.
41. E. M. Greitzer, "The Stability of Pumping Systems: The 1980 Freeman Scholar Lecture," *J. Fluids Eng.,* vol. 103, June 1981, pp. 193–242.
42. B. Lakshminarayana, *Fluid Dynamics and Heat Transfer in Turbomachinery*, Wiley, New York, 1995.
43. L. F. Moody, "The Propeller Type Turbine," *ASCE Trans.,* vol. 89, 1926, p. 628.
44. H. H. Anderson, "Prediction of Head, Quantity, and Efficiency in Pumps—The Area-Ratio Principle," in *Performance Prediction of Centrifugal Pumps and Compressors,* vol. I00127, ASME Symp., New York, 1980, pp. 201–211.
45. B. Lakshminarayana and P. Runstadler, Jr. (eds.), "Measurement Methods in Rotating Components of Turbomachinery," *ASME Symp. Proc., New Orleans,* vol. I00130, 1980.
46. M. Murakami, K. Kikuyama, and B. Asakura, "Velocity and Pressure Distributions in the Impeller Passages of Centrifugal Pumps," *J. Fluids Eng.*, vol. 102, December 1980, pp. 420–426.
47. G. W. Koeppl, *Putnam's Power from the Wind,* 2d ed., Van Nostrand Reinhold, New York, 1982.
48. R. L. Hills, *Power from Wind: A History of Windmill Technology*, Cambridge Univ. Press, Cambridge, 1996.
49. D. A. Spera, *Wind Turbine Technology: Fundamental Concepts of Wind Turbine Engineering*, ASME Press, New York, 1994.
50. A. J. Wortman, *Introduction to Wind Turbine Engineering,* Butterworth, Woburn, Mass., 1983.
51. F. R. Eldridge, *Wind Machines,* 2d ed., Van Nostrand Reinhold, New York, 1980.
52. D. M. Eggleston and F. S. Stoddard, *Wind Turbine Engineering Design,* Van Nostrand, New York, 1987.
53. M. L. Robinson, "The Darrieus Wind Turbine for Electrical Power Generation," *Aeronaut. J.,* June 1981, pp. 244–255.
54. D. F. Warne and P. G. Calnan, "Generation of Electricity from the Wind," *IEE Rev.,* vol. 124, no. 11R, November 1977, pp. 963–985.
55. L. A. Haimerl, "The Crossflow Turbine," *Waterpower,* January 1960, pp. 5–13; see also *ASME Symp. Small Hydropower Fluid Mach.,* vol. 1, 1980, and vol. 2, 1982.
56. K. Eisele et al., "Flow Analysis in a Pump Diffuser: Part 1, Measurements; Part 2, CFD," *J. Fluids Eng,*, vol. 119, December 1997, pp. 968–984.



ketabline.com Ebook.ketabline.com

Appendix A
Physical Properties of Fluids

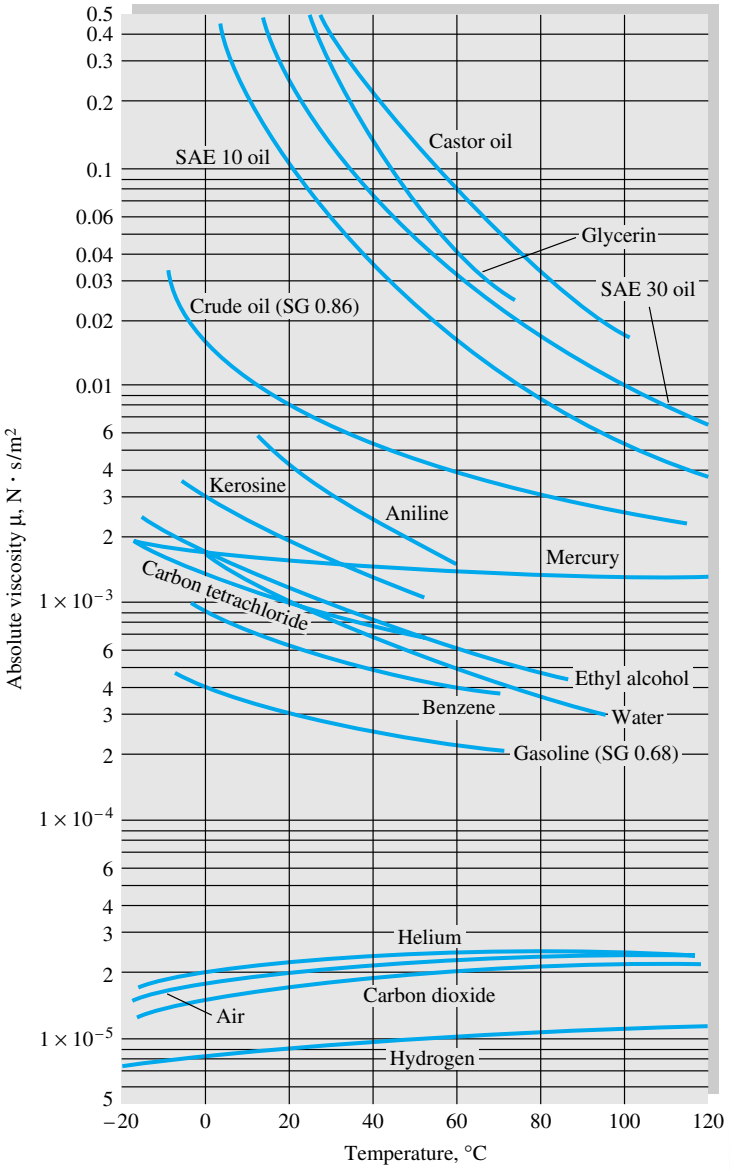


Fig. A.1 Absolute viscosity of common fluids at 1 atm.

ketabline.com Ebook.ketabline.com

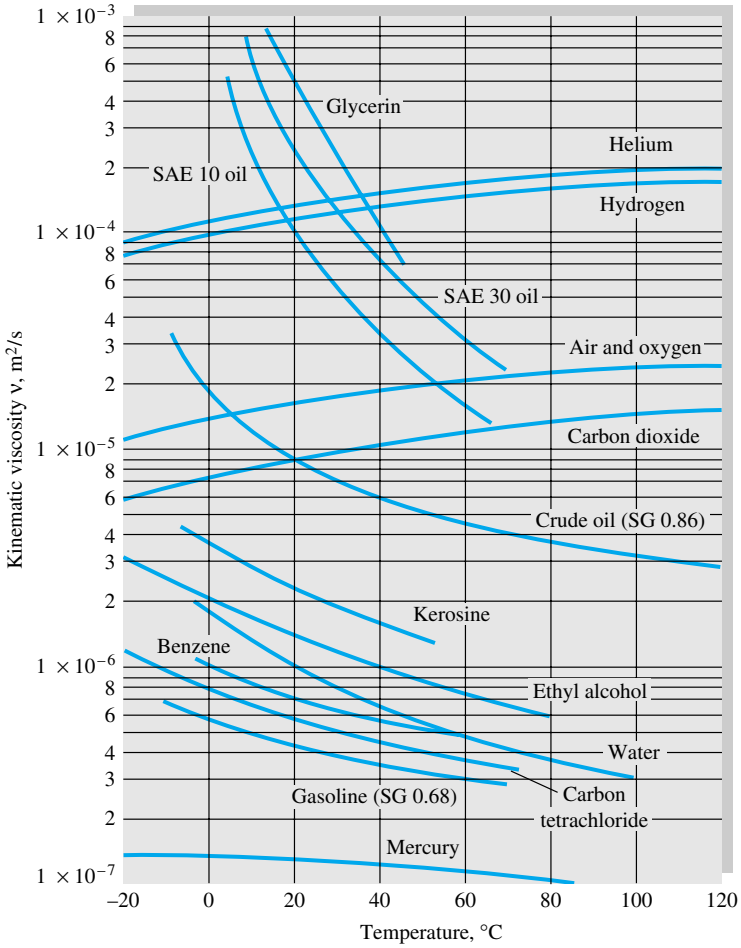


Fig. A.2 Kinematic viscosity of common fluids at 1 atm.



ketabline.com Ebook.ketabline.com

Table A.1 Viscosity and Density of Water at 1 atm

T, °C	ρ, kg/m^3	μ, N · s/m^2	ν, m^2/s	T, °F	ρ, slug/ft^3	μ, lb · s/ft^2	ν, ft^2/s
0	1000	1.788 E-3	1.788 E-6	32	1.940	3.73 E-5	1.925 E-5
10	1000	1.307 E-3	1.307 E-6	50	1.940	2.73 E-5	1.407 E-5
20	998	1.003 E-3	1.005 E-6	68	1.937	2.09 E-5	1.082 E-5
30	996	0.799 E-3	0.802 E-6	86	1.932	1.67 E-5	0.864 E-5
40	992	0.657 E-3	0.662 E-6	104	1.925	1.37 E-5	0.713 E-5
50	988	0.548 E-3	0.555 E-6	122	1.917	1.14 E-5	0.597 E-5
60	983	0.467 E-3	0.475 E-6	140	1.908	0.975 E-5	0.511 E-5
70	978	0.405 E-3	0.414 E-6	158	1.897	0.846 E-5	0.446 E-5
80	972	0.355 E-3	0.365 E-6	176	1.886	0.741 E-5	0.393 E-5
90	965	0.316 E-3	0.327 E-6	194	1.873	0.660 E-5	0.352 E-5
100	958	0.283 E-3	0.295 E-6	212	1.859	0.591 E-5	0.318 E-5

Suggested curve fits for water in the range $0 \le T \le 100$°C:

$$\rho(\text{kg/m}^3) \approx 1000 - 0.0178\,|\,T°\text{C} - 4°\text{C}\,|^{1.7} \pm 0.2\%$$

$$\ln \frac{\mu}{\mu_0} \approx -1.704 - 5.306z + 7.003z^2$$

$$z = \frac{273\ \text{K}}{T\ \text{K}} \qquad \mu_0 = 1.788\ \text{E-3 kg/(m} \cdot \text{s)}$$

Table A.2 Viscosity and Density of Air at 1 atm

T, °C	ρ, kg/m^3	μ, N · s/m^2	ν, m^2/s	T, °F	ρ, slug/ft^3	μ, lb · s/ft^2	ν, ft^2/s
−40	1.52	1.51 E-5	0.99 E-5	−40	2.94 E-3	3.16 E-7	1.07 E-4
0	1.29	1.71 E-5	1.33 E-5	32	2.51 E-3	3.58 E-7	1.43 E-4
20	1.20	1.80 E-5	1.50 E-5	68	2.34 E-3	3.76 E-7	1.61 E-4
50	1.09	1.95 E-5	1.79 E-5	122	2.12 E-3	4.08 E-7	1.93 E-4
100	0.946	2.17 E-5	2.30 E-5	212	1.84 E-3	4.54 E-7	2.47 E-4
150	0.835	2.38 E-5	2.85 E-5	302	1.62 E-3	4.97 E-7	3.07 E-4
200	0.746	2.57 E-5	3.45 E-5	392	1.45 E-3	5.37 E-7	3.71 E-4
250	0.675	2.75 E-5	4.08 E-5	482	1.31 E-3	5.75 E-7	4.39 E-4
300	0.616	2.93 E-5	4.75 E-5	572	1.20 E-3	6.11 E-7	5.12 E-4
400	0.525	3.25 E-5	6.20 E-5	752	1.02 E-3	6.79 E-7	6.67 E-4
500	0.457	3.55 E-5	7.77 E-5	932	0.89 E-3	7.41 E-7	8.37 E-4

Suggested curve fits for air:

$$\rho = \frac{p}{RT} \qquad R_{\text{air}} \approx 287\ \text{J/(kg} \cdot \text{K)}$$

Power law: $$\frac{\mu}{\mu_0} \approx \left(\frac{T}{T_0}\right)^{0.7}$$

Sutherland law: $$\frac{\mu}{\mu_0} \approx \left(\frac{T}{T_0}\right)^{3/2}\left(\frac{T_0 + S}{T + S}\right) \qquad S_{\text{air}} \approx 110.4\ \text{K}$$

with $T_0 = 273$ K, $\mu_0 = 1.71$ E-5 kg/(m · s), and T in kelvins.



ketabline.com Ebook.ketabline.com

Table A.3 Properties of Common Liquids at 1 atm and 20°C (68°F)

Liquid	ρ, kg/m^3	μ, kg/(m · s)	Y, N/m*	p_v, N/m^2	Bulk modulus, N/m^2	Viscosity parameter $C^\dagger$
Ammonia	608	2.20 E-4	2.13 E-2	9.10 E+5	—	1.05
Benzene	881	6.51 E-4	2.88 E-2	1.01 E+4	1.4 E+9	4.34
Carbon tetrachloride	1,590	9.67 E-4	2.70 E-2	1.20 E+4	9.65 E+8	4.45
Ethanol	789	1.20 E-3	2.28 E-2	5.7 E+3	9.0 E+8	5.72
Ethylene glycol	1,117	2.14 E-2	4.84 E-2	1.2 E+1	—	11.7
Freon 12	1,327	2.62 E-4	—	—	—	1.76
Gasoline	680	2.92 E-4	2.16 E-2	5.51 E+4	9.58 E+8	3.68
Glycerin	1,260	1.49	6.33 E-2	1.4 E-2	4.34 E+9	28.0
Kerosine	804	1.92 E-3	2.8 E-2	3.11 E+3	1.6 E+9	5.56
Mercury	13,550	1.56 E-3	4.84 E-1	1.1 E-3	2.55 E+10	1.07
Methanol	791	5.98 E-4	2.25 E-2	1.34 E+4	8.3 E+8	4.63
SAE 10W oil	870	1.04 E-1‡	3.6 E-2	—	1.31 E+9	15.7
SAE 10W30 oil	876	1.7 E-1‡	—	—	—	14.0
SAE 30W oil	891	2.9 E-1‡	3.5 E-2	—	1.38 E+9	18.3
SAE 50W oil	902	8.6 E-1‡	—	—	—	20.2
Water	998	1.00 E-3	7.28 E-2	2.34 E+3	2.19 E+9	Table A.1
Seawater (30%)	1,025	1.07 E-3	7.28 E-2	2.34 E+3	2.33 E+9	7.28

*In contact with air.
†The viscosity-temperature variation of these liquids may be fitted to the empirical expression

$$\frac{\mu}{\mu_{20^\circ C}} \approx \exp\left[C\left(\frac{293\ \text{K}}{T\ \text{K}} - 1\right)\right]$$

with accuracy of ±6 percent in the range $0 \le T \le 100^\circ$C.
‡Representative values. The SAE oil classifications allow a viscosity variation of up to ±50 percent, especially at lower temperatures.

Table A.4 Properties of Common Gases at 1 atm and 20°C (68°F)

Gas	Molecular weight	R, m^2/(s^2 · K)	ρg, N/m^3	μ, N · s/m^2	Specific-heat ratio	Power-law exponent $n^\dagger$
H_2	2.016	4124	0.822	9.05 E-6	1.41	0.68
He	4.003	2077	1.63	1.97 E-5	1.66	0.67
H_2O	18.02	461	7.35	1.02 E-5	1.33	1.15
Ar	39.944	208	16.3	2.24 E-5	1.67	0.72
Dry air	28.96	287	11.8	1.80 E-5	1.40	0.67
CO_2	44.01	189	17.9	1.48 E-5	1.30	0.79
CO	28.01	297	11.4	1.82 E-5	1.40	0.71
N_2	28.02	297	11.4	1.76 E-5	1.40	0.67
O_2	32.00	260	13.1	2.00 E-5	1.40	0.69
NO	30.01	277	12.1	1.90 E-5	1.40	0.78
N_2O	44.02	189	17.9	1.45 E-5	1.31	0.89
Cl_2	70.91	117	28.9	1.03 E-5	1.34	1.00
CH_4	16.04	518	6.54	1.34 E-5	1.32	0.87

†The power-law curve fit, Eq. (1.27), $\mu/\mu_{293\text{K}} \approx (T/293)^n$, fits these gases to within ±4 percent in the range $250 \le T \le 1000$ K. The temperature must be in kelvins.



ketabline.com Ebook.ketabline.com

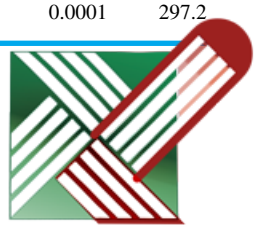
Table A.5 Surface Tension, Vapor Pressure, and Sound Speed of Water

T, °C	Y, N/m	p_v, kPa	a, m/s
0	0.0756	0.611	1402
10	0.0742	1.227	1447
20	0.0728	2.337	1482
30	0.0712	4.242	1509
40	0.0696	7.375	1529
50	0.0679	12.34	1542
60	0.0662	19.92	1551
70	0.0644	31.16	1553
80	0.0626	47.35	1554
90	0.0608	70.11	1550
100	0.0589	101.3	1543
120	0.0550	198.5	1518
140	0.0509	361.3	1483
160	0.0466	617.8	1440
180	0.0422	1,002	1389
200	0.0377	1,554	1334
220	0.0331	2,318	1268
240	0.0284	3,344	1192
260	0.0237	4,688	1110
280	0.0190	6,412	1022
300	0.0144	8,581	920
320	0.0099	11,274	800
340	0.0056	14,586	630
360	0.0019	18,651	370
374*	0.0*	22,090*	0*

*Critical point.

Table A.6 Properties of the Standard Atmosphere

z, m	T, K	p, Pa	ρ, kg/m^3	a, m/s
−500	291.41	107,508	1.2854	342.2
0	288.16	101,350	1.2255	340.3
500	284.91	95,480	1.1677	338.4
1,000	281.66	89,889	1.1120	336.5
1,500	278.41	84,565	1.0583	334.5
2,000	275.16	79,500	1.0067	332.6
2,500	271.91	74,684	0.9570	330.6
3,000	268.66	70,107	0.9092	328.6
3,500	265.41	65,759	0.8633	326.6
4,000	262.16	61,633	0.8191	324.6
4,500	258.91	57,718	0.7768	322.6
5,000	255.66	54,008	0.7361	320.6
5,500	252.41	50,493	0.6970	318.5
6,000	249.16	47,166	0.6596	316.5
6,500	245.91	44,018	0.6237	314.4
7,000	242.66	41,043	0.5893	312.3
7,500	239.41	38,233	0.5564	310.2
8,000	236.16	35,581	0.5250	308.1
8,500	232.91	33,080	0.4949	306.0
9,000	229.66	30,723	0.4661	303.8
9,500	226.41	28,504	0.4387	301.7
10,000	223.16	26,416	0.4125	299.5
10,500	219.91	24,455	0.3875	297.3
11,000	216.66	22,612	0.3637	295.1
11,500	216.66	20,897	0.3361	295.1
12,000	216.66	19,312	0.3106	295.1
12,500	216.66	17,847	0.2870	295.1
13,000	216.66	16,494	0.2652	295.1
13,500	216.66	15,243	0.2451	295.1
14,000	216.66	14,087	0.2265	295.1
14,500	216.66	13,018	0.2094	295.1
15,000	216.66	12,031	0.1935	295.1
15,500	216.66	11,118	0.1788	295.1
16,000	216.66	10,275	0.1652	295.1
16,500	216.66	9,496	0.1527	295.1
17,000	216.66	8,775	0.1411	295.1
17,500	216.66	8,110	0.1304	295.1
18,000	216.66	7,495	0.1205	295.1
18,500	216.66	6,926	0.1114	295.1
19,000	216.66	6,401	0.1029	295.1
19,500	216.66	5,915	0.0951	295.1
20,000	216.66	5,467	0.0879	295.1
22,000	218.6	4,048	0.0645	296.4
24,000	220.6	2,972	0.0469	297.8
26,000	222.5	2,189	0.0343	299.1
28,000	224.5	1,616	0.0251	300.4
30,000	226.5	1,197	0.0184	301.7
40,000	250.4	287	0.0040	317.2
50,000	270.7	80	0.0010	329.9
60,000	255.7	22	0.0003	320.6
70,000	219.7	6	0.0001	297.2

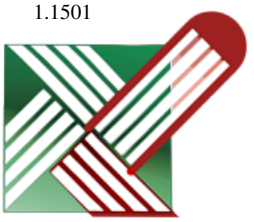


ketabline.com Ebook.ketabline.com

Appendix B
Compressible-Flow Tables

Table B.1
Isentropic Flow of a Perfect Gas, $k = 1.4$

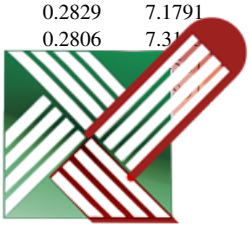
Ma	p/p_0	ρ/ρ_0	T/T_0	A/A^*
0.0	1.0	1.0	1.0	∞
0.02	0.9997	0.9998	0.9999	28.9421
0.04	0.9989	0.9992	0.9997	14.4815
0.06	0.9975	0.9982	0.9993	9.6659
0.08	0.9955	0.9968	0.9987	7.2616
0.1	0.9930	0.9950	0.9980	5.8218
0.12	0.9900	0.9928	0.9971	4.8643
0.14	0.9864	0.9903	0.9961	4.1824
0.16	0.9823	0.9873	0.9949	3.6727
0.18	0.9776	0.9840	0.9936	3.2779
0.2	0.9725	0.9803	0.9921	2.9635
0.22	0.9668	0.9762	0.9904	2.7076
0.24	0.9607	0.9718	0.9886	2.4956
0.26	0.9541	0.9670	0.9867	2.3173
0.28	0.9470	0.9619	0.9846	2.1656
0.3	0.9395	0.9564	0.9823	2.0351
0.32	0.9315	0.9506	0.9799	1.9219
0.34	0.9231	0.9445	0.9774	1.8229
0.36	0.9143	0.9380	0.9747	1.7358
0.38	0.9052	0.9313	0.9719	1.6587
0.4	0.8956	0.9243	0.9690	1.5901
0.42	0.8857	0.9170	0.9659	1.5289
0.44	0.8755	0.9094	0.9627	1.4740
0.46	0.8650	0.9016	0.9594	1.4246
0.48	0.8541	0.8935	0.9559	1.3801
0.5	0.8430	0.8852	0.9524	1.3398
0.52	0.8317	0.8766	0.9487	1.3034
0.54	0.8201	0.8679	0.9449	1.2703
0.56	0.8082	0.8589	0.9410	1.2403
0.58	0.7962	0.8498	0.9370	1.2130
0.6	0.7840	0.8405	0.9328	1.1882
0.62	0.7716	0.8310	0.9286	1.1656
0.64	0.7591	0.8213	0.9243	1.1451
0.66	0.7465	0.8115	0.9199	1.1265
0.68	0.7338	0.8016	0.9153	1.1097
0.7	0.7209	0.7916	0.9107	1.0944
0.72	0.7080	0.7814	0.9061	1.0806
0.74	0.6951	0.7712	0.9013	1.0681
0.76	0.6821	0.7609	0.8964	1.0570
0.78	0.6690	0.7505	0.8915	1.0471
0.8	0.6560	0.7400	0.8865	1.0382
0.82	0.6430	0.7295	0.8815	1.0305
0.84	0.6300	0.7189	0.8763	1.0237
0.86	0.6170	0.7083	0.8711	1.0179
0.88	0.6041	0.6977	0.8659	1.0129
0.9	0.5913	0.6870	0.8606	1.0089
0.92	0.5785	0.6764	0.8552	1.0056
0.94	0.5658	0.6658	0.8498	1.0031
0.96	0.5532	0.6551	0.8444	1.0014
0.98	0.5407	0.6445	0.8389	1.0003
1.0	0.5283	0.6339	0.8333	1.0000
1.02	0.5160	0.6234	0.8278	1.0003
1.04	0.5039	0.6129	0.8222	1.0013
1.06	0.4919	0.6024	0.8165	1.0029
1.08	0.4800	0.5920	0.8108	1.0051
1.1	0.4684	0.5817	0.8052	1.0079
1.12	0.4568	0.5714	0.7994	1.0113
1.14	0.4455	0.5612	0.7937	1.0153
1.16	0.4343	0.5511	0.7879	1.0198
1.18	0.4232	0.5411	0.7822	1.0248
1.2	0.4124	0.5311	0.7764	1.0304
1.22	0.4017	0.5213	0.7706	1.0366
1.24	0.3912	0.5115	0.7648	1.0432
1.26	0.3809	0.5019	0.7590	1.0504
1.28	0.3708	0.4923	0.7532	1.0581
1.3	0.3609	0.4829	0.7474	1.0663
1.32	0.3512	0.4736	0.7416	1.0750
1.34	0.3417	0.4644	0.7358	1.0842
1.36	0.3323	0.4553	0.7300	1.0940
1.38	0.3232	0.4463	0.7242	1.1042
1.4	0.3142	0.4374	0.7184	1.1149
1.42	0.3055	0.4287	0.7126	1.1262
1.44	0.2969	0.4201	0.7069	1.1379
1.46	0.2886	0.4116	0.7011	1.1501



ketabline.com Ebook.ketabline.com

Table B.1 (*Cont.*) Isentropic Flow of a Perfect Gas, $k = 1.4$

Ma	p/p_0	ρ/ρ_0	T/T_0	A/A^*
1.48	0.2804	0.4032	0.6954	1.1629
1.5	0.2724	0.3950	0.6897	1.1762
1.52	0.2646	0.3869	0.6840	1.1899
1.54	0.2570	0.3789	0.6783	1.2042
1.56	0.2496	0.3710	0.6726	1.2190
1.58	0.2423	0.3633	0.6670	1.2344
1.6	0.2353	0.3557	0.6614	1.2502
1.62	0.2284	0.3483	0.6558	1.2666
1.64	0.2217	0.3409	0.6502	1.2836
1.66	0.2151	0.3337	0.6447	1.3010
1.68	0.2088	0.3266	0.6392	1.3190
1.7	0.2026	0.3197	0.6337	1.3376
1.72	0.1966	0.3129	0.6283	1.3567
1.74	0.1907	0.3062	0.6229	1.3764
1.76	0.1850	0.2996	0.6175	1.3967
1.78	0.1794	0.2931	0.6121	1.4175
1.8	0.1740	0.2868	0.6068	1.4390
1.82	0.1688	0.2806	0.6015	1.4610
1.84	0.1637	0.2745	0.5963	1.4836
1.86	0.1587	0.2686	0.5910	1.5069
1.88	0.1539	0.2627	0.5859	1.5308
1.9	0.1492	0.2570	0.5807	1.5553
1.92	0.1447	0.2514	0.5756	1.5804
1.94	0.1403	0.2459	0.5705	1.6062
1.96	0.1360	0.2405	0.5655	1.6326
1.98	0.1318	0.2352	0.5605	1.6597
2.0	0.1278	0.2300	0.5556	1.6875
2.02	0.1239	0.2250	0.5506	1.7160
2.04	0.1201	0.2200	0.5458	1.7451
2.06	0.1164	0.2152	0.5409	1.7750
2.08	0.1128	0.2104	0.5361	1.8056
2.1	0.1094	0.2058	0.5313	1.8369
2.12	0.1060	0.2013	0.5266	1.8690
2.14	0.1027	0.1968	0.5219	1.9018
2.16	0.0996	0.1925	0.5173	1.9354
2.18	0.0965	0.1882	0.5127	1.9698
2.2	0.0935	0.1841	0.5081	2.0050
2.22	0.0906	0.1800	0.5036	2.0409
2.24	0.0878	0.1760	0.4991	2.0777
2.26	0.0851	0.1721	0.4947	2.1153
2.28	0.0825	0.1683	0.4903	2.1538
2.3	0.0800	0.1646	0.4859	2.1931
2.32	0.0775	0.1609	0.4816	2.2333
2.34	0.0751	0.1574	0.4773	2.2744
2.36	0.0728	0.1539	0.4731	2.3164
2.38	0.0706	0.1505	0.4688	2.3593
2.4	0.0684	0.1472	0.4647	2.4031
2.42	0.0663	0.1439	0.4606	2.4479
2.44	0.0643	0.1408	0.4565	2.4936
2.46	0.0623	0.1377	0.4524	2.5403
2.48	0.0604	0.1346	0.4484	2.5880
2.5	0.0585	0.1317	0.4444	2.6367
2.52	0.0567	0.1288	0.4405	2.6865
2.54	0.0550	0.1260	0.4366	2.7372
2.56	0.0533	0.1232	0.4328	2.7891
2.58	0.0517	0.1205	0.4289	2.8420
2.6	0.0501	0.1179	0.4252	2.8960
2.62	0.0486	0.1153	0.4214	2.9511
2.64	0.0471	0.1128	0.4177	3.0073
2.66	0.0457	0.1103	0.4141	3.0647
2.68	0.0443	0.1079	0.4104	3.1233
2.7	0.0430	0.1056	0.4068	3.1830
2.72	0.0417	0.1033	0.4033	3.2440
2.74	0.0404	0.1010	0.3998	3.3061
2.76	0.0392	0.0989	0.3963	3.3695
2.78	0.0380	0.0967	0.3928	3.4342
2.8	0.0368	0.0946	0.3894	3.5001
2.82	0.0357	0.0926	0.3860	3.5674
2.84	0.0347	0.0906	0.3827	3.6359
2.86	0.0336	0.0886	0.3794	3.7058
2.88	0.0326	0.0867	0.3761	3.7771
2.9	0.0317	0.0849	0.3729	3.8498
2.92	0.0307	0.0831	0.3696	3.9238
2.94	0.0298	0.0813	0.3665	3.9993
2.96	0.0289	0.0796	0.3633	4.0763
2.98	0.0281	0.0779	0.3602	4.1547
3.0	0.0272	0.0762	0.3571	4.2346
3.02	0.0264	0.0746	0.3541	4.3160
3.04	0.0256	0.0730	0.3511	4.3990
3.06	0.0249	0.0715	0.3481	4.4835
3.08	0.0242	0.0700	0.3452	4.5696
3.1	0.0234	0.0685	0.3422	4.6573
3.12	0.0228	0.0671	0.3393	4.7467
3.14	0.0221	0.0657	0.3365	4.8377
3.16	0.0215	0.0643	0.3337	4.9304
3.18	0.0208	0.0630	0.3309	5.0248
3.2	0.0202	0.0617	0.3281	5.1210
3.22	0.0196	0.0604	0.3253	5.2189
3.24	0.0191	0.0591	0.3226	5.3186
3.26	0.0185	0.0579	0.3199	5.4201
3.28	0.0180	0.0567	0.3173	5.5234
3.3	0.0175	0.0555	0.3147	5.6286
3.32	0.0170	0.0544	0.3121	5.7358
3.34	0.0165	0.0533	0.3095	5.8448
3.36	0.0160	0.0522	0.3069	5.9558
3.38	0.0156	0.0511	0.3044	6.0687
3.4	0.0151	0.0501	0.3019	6.1837
3.42	0.0147	0.0491	0.2995	6.3007
3.44	0.0143	0.0481	0.2970	6.4198
3.46	0.0139	0.0471	0.2946	6.5409
3.48	0.0135	0.0462	0.2922	6.6642
3.5	0.0131	0.0452	0.2899	6.7896
3.52	0.0127	0.0443	0.2875	6.9172
3.54	0.0124	0.0434	0.2852	7.0471
3.56	0.0120	0.0426	0.2829	7.1791
3.58	0.0117	0.0417	0.2806	7.31
3.6	0.0114	0.0409		
3.62	0.0111	0.0401		



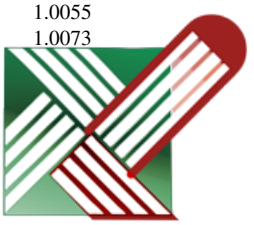
ketabline.com Ebook.ketabline.com

Table B.1 (*Cont.*) Isentropic Flow of a Perfect Gas, $k = 1.4$

Ma	p/p_0	ρ/ρ_0	T/T_0	A/A^*	Ma	p/p_0	ρ/ρ_0	T/T_0	A/A^*
3.64	0.0108	0.0393	0.2740	7.7305	4.34	0.0042	0.0202	0.2098	14.4456
3.66	0.0105	0.0385	0.2718	7.8742	4.36	0.0041	0.0198	0.2083	14.6965
3.68	0.0102	0.0378	0.2697	8.0204	4.38	0.0040	0.0194	0.2067	14.9513
3.7	0.0099	0.0370	0.2675	8.1691	4.4	0.0039	0.0191	0.2053	15.2099
3.72	0.0096	0.0363	0.2654	8.3202	4.42	0.0038	0.0187	0.2038	15.4724
3.74	0.0094	0.0356	0.2633	8.4739	4.44	0.0037	0.0184	0.2023	15.7388
3.76	0.0091	0.0349	0.2613	8.6302	4.46	0.0036	0.0181	0.2009	16.0092
3.78	0.0089	0.0342	0.2592	8.7891	4.48	0.0035	0.0178	0.1994	16.2837
3.8	0.0086	0.0335	0.2572	8.9506	4.5	0.0035	0.0174	0.1980	16.5622
3.82	0.0084	0.0329	0.2552	9.1148	4.52	0.0034	0.0171	0.1966	16.8449
3.84	0.0082	0.0323	0.2532	9.2817	4.54	0.0033	0.0168	0.1952	17.1317
3.86	0.0080	0.0316	0.2513	9.4513	4.56	0.0032	0.0165	0.1938	17.4228
3.88	0.0077	0.0310	0.2493	9.6237	4.58	0.0031	0.0163	0.1925	17.7181
3.9	0.0075	0.0304	0.2474	9.7990	4.6	0.0031	0.0160	0.1911	18.0178
3.92	0.0073	0.0299	0.2455	9.9771	4.62	0.0030	0.0157	0.1898	18.3218
3.94	0.0071	0.0293	0.2436	10.1581	4.64	0.0029	0.0154	0.1885	18.6303
3.96	0.0069	0.0287	0.2418	10.3420	4.66	0.0028	0.0152	0.1872	18.9433
3.98	0.0068	0.0282	0.2399	10.5289	4.68	0.0028	0.0149	0.1859	19.2608
4.0	0.0066	0.0277	0.2381	10.7188	4.7	0.0027	0.0146	0.1846	19.5828
4.02	0.0064	0.0271	0.2363	10.9117	4.72	0.0026	0.0144	0.1833	19.9095
4.04	0.0062	0.0266	0.2345	11.1077	4.74	0.0026	0.0141	0.1820	20.2409
4.06	0.0061	0.0261	0.2327	11.3068	4.76	0.0025	0.0139	0.1808	20.5770
4.08	0.0059	0.0256	0.2310	11.5091	4.78	0.0025	0.0137	0.1795	20.9179
4.1	0.0058	0.0252	0.2293	11.7147	4.8	0.0024	0.0134	0.1783	21.2637
4.12	0.0056	0.0247	0.2275	11.9234	4.82	0.0023	0.0132	0.1771	21.6144
4.14	0.0055	0.0242	0.2258	12.1354	4.84	0.0023	0.0130	0.1759	21.9700
4.16	0.0053	0.0238	0.2242	12.3508	4.86	0.0022	0.0128	0.1747	22.3306
4.18	0.0052	0.0234	0.2225	12.5695	4.88	0.0022	0.0125	0.1735	22.6963
4.2	0.0051	0.0229	0.2208	12.7916	4.9	0.0021	0.0123	0.1724	23.0671
4.22	0.0049	0.0225	0.2192	13.0172	4.92	0.0021	0.0121	0.1712	23.4431
4.24	0.0048	0.0221	0.2176	13.2463	4.94	0.0020	0.0119	0.1700	23.8243
4.26	0.0047	0.0217	0.2160	13.4789	4.96	0.0020	0.0117	0.1689	24.2109
4.28	0.0046	0.0213	0.2144	13.7151	4.98	0.0019	0.0115	0.1678	24.6027
4.3	0.0044	0.0209	0.2129	13.9549	5.0	0.0019	0.0113	0.1667	25.0000
4.32	0.0043	0.0205	0.2113	14.1984					

Table B.2 Normal-Shock Relations for a Perfect Gas, $k = 1.4$

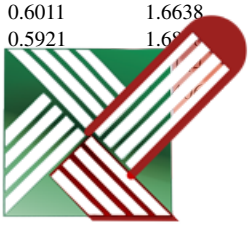
Ma_{n1}	Ma_{n2}	p_2/p_1	$V_1/V_2 = \rho_2/\rho_1$	T_2/T_1	p_{02}/p_{01}	A_2^*/A_1^*
1.0	1.0000	1.0000	1.0000	1.0000	1.0000	1.0000
1.02	0.9805	1.0471	1.0334	1.0132	1.0000	1.0000
1.04	0.9620	1.0952	1.0671	1.0263	0.9999	1.0001
1.06	0.9444	1.1442	1.1009	1.0393	0.9998	1.0002
1.08	0.9277	1.1941	1.1349	1.0522	0.9994	1.0006
1.1	0.9118	1.2450	1.1691	1.0649	0.9989	1.0011
1.12	0.8966	1.2968	1.2034	1.0776	0.9982	1.0018
1.14	0.8820	1.3495	1.2378	1.0903	0.9973	1.0027
1.16	0.8682	1.4032	1.2723	1.1029	0.9961	1.0040
1.18	0.8549	1.4578	1.3069	1.1154	0.9946	1.0055
1.2	0.8422	1.5133	1.3416	1.1280	0.9928	1.0073
1.22	0.8300	1.5698	1.3764	1.1405	0.9907	
1.24	0.8183	1.6272	1.4112	1.1531	0.9884	



ketabline.com Ebook.ketabline.com

Table B.2 (*Cont.*) Normal-Shock Relations for a Perfect Gas, $k = 1.4$

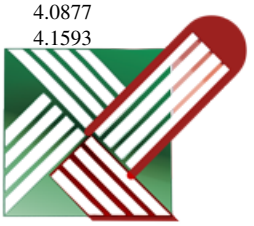
Ma_{n1}	Ma_{n2}	p_2/p_1	$V_1/V_2 = \rho_2/\rho_1$	T_2/T_1	p_{02}/p_{01}	A_2^*/A_1^*
1.26	0.8071	1.6855	1.4460	1.1657	0.9857	1.0145
1.28	0.7963	1.7448	1.4808	1.1783	0.9827	1.0176
1.3	0.7860	1.8050	1.5157	1.1909	0.9794	1.0211
1.32	0.7760	1.8661	1.5505	1.2035	0.9758	1.0249
1.34	0.7664	1.9282	1.5854	1.2162	0.9718	1.0290
1.36	0.7572	1.9912	1.6202	1.2290	0.9676	1.0335
1.38	0.7483	2.0551	1.6549	1.2418	0.9630	1.0384
1.4	0.7397	2.1200	1.6897	1.2547	0.9582	1.0436
1.42	0.7314	2.1858	1.7243	1.2676	0.9531	1.0492
1.44	0.7235	2.2525	1.7589	1.2807	0.9476	1.0552
1.46	0.7157	2.3202	1.7934	1.2938	0.9420	1.0616
1.48	0.7083	2.3888	1.8278	1.3069	0.9360	1.0684
1.5	0.7011	2.4583	1.8621	1.3202	0.9298	1.0755
1.52	0.6941	2.5288	1.8963	1.3336	0.9233	1.0830
1.54	0.6874	2.6002	1.9303	1.3470	0.9166	1.0910
1.56	0.6809	2.6725	1.9643	1.3606	0.9097	1.0993
1.58	0.6746	2.7458	1.9981	1.3742	0.9026	1.1080
1.6	0.6684	2.8200	2.0317	1.3880	0.8952	1.1171
1.62	0.6625	2.8951	2.0653	1.4018	0.8877	1.1266
1.64	0.6568	2.9712	2.0986	1.4158	0.8799	1.1365
1.66	0.6512	3.0482	2.1318	1.4299	0.8720	1.1468
1.68	0.6458	3.1261	2.1649	1.4440	0.8639	1.1575
1.7	0.6405	3.2050	2.1977	1.4583	0.8557	1.1686
1.72	0.6355	3.2848	2.2304	1.4727	0.8474	1.1801
1.74	0.6305	3.3655	2.2629	1.4873	0.8389	1.1921
1.76	0.6257	3.4472	2.2952	1.5019	0.8302	1.2045
1.78	0.6210	3.5298	2.3273	1.5167	0.8215	1.2173
1.8	0.6165	3.6133	2.3592	1.5316	0.8127	1.2305
1.82	0.6121	3.6978	2.3909	1.5466	0.8038	1.2441
1.84	0.6078	3.7832	2.4224	1.5617	0.7948	1.2582
1.86	0.6036	3.8695	2.4537	1.5770	0.7857	1.2728
1.88	0.5996	3.9568	2.4848	1.5924	0.7765	1.2877
1.9	0.5956	4.0450	2.5157	1.6079	0.7674	1.3032
1.92	0.5918	4.1341	2.5463	1.6236	0.7581	1.3191
1.94	0.5880	4.2242	2.5767	1.6394	0.7488	1.3354
1.96	0.5844	4.3152	2.6069	1.6553	0.7395	1.3522
1.98	0.5808	4.4071	2.6369	1.6713	0.7302	1.3695
2.0	0.5774	4.5000	2.6667	1.6875	0.7209	1.3872
2.02	0.5740	4.5938	2.6962	1.7038	0.7115	1.4054
2.04	0.5707	4.6885	2.7255	1.7203	0.7022	1.4241
2.06	0.5675	4.7842	2.7545	1.7369	0.6928	1.4433
2.08	0.5643	4.8808	2.7833	1.7536	0.6835	1.4630
2.1	0.5613	4.9783	2.8119	1.7705	0.6742	1.4832
2.12	0.5583	5.0768	2.8402	1.7875	0.6649	1.5039
2.14	0.5554	5.1762	2.8683	1.8046	0.6557	1.5252
2.16	0.5525	5.2765	2.8962	1.8219	0.6464	1.5469
2.18	0.5498	5.3778	2.9238	1.8393	0.6373	1.5692
2.2	0.5471	5.4800	2.9512	1.8569	0.6281	1.5920
2.22	0.5444	5.5831	2.9784	1.8746	0.6191	1.6154
2.24	0.5418	5.6872	3.0053	1.8924	0.6100	1.6393
2.26	0.5393	5.7922	3.0319	1.9104	0.6011	1.6638
2.28	0.5368	5.8981	3.0584	1.9285	0.5921	1.68
2.3	0.5344	6.0050	3.0845	1.9468		
2.32	0.5321	6.1128	3.1105	1.9652		



ketabline.com Ebook.ketabline.com

Table B.2 (*Cont.*) Normal-Shock Relations for a Perfect Gas, $k = 1.4$

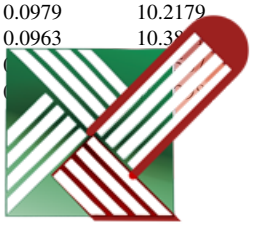
Ma_{n1}	Ma_{n2}	p_2/p_1	$V_1/V_2 = \rho_2/\rho_1$	T_2/T_1	p_{02}/p_{01}	A_2^*/A_1^*
2.34	0.5297	6.2215	3.1362	1.9838	0.5658	1.7674
2.36	0.5275	6.3312	3.1617	2.0025	0.5572	1.7948
2.38	0.5253	6.4418	3.1869	2.0213	0.5486	1.8228
2.4	0.5231	6.5533	3.2119	2.0403	0.5401	1.8514
2.42	0.5210	6.6658	3.2367	2.0595	0.5317	1.8806
2.44	0.5189	6.7792	3.2612	2.0788	0.5234	1.9105
2.46	0.5169	6.8935	3.2855	2.0982	0.5152	1.9410
2.48	0.5149	7.0088	3.3095	2.1178	0.5071	1.9721
2.5	0.5130	7.1250	3.3333	2.1375	0.4990	2.0039
2.52	0.5111	7.2421	3.3569	2.1574	0.4911	2.0364
2.54	0.5092	7.3602	3.3803	2.1774	0.4832	2.0696
2.56	0.5074	7.4792	3.4034	2.1976	0.4754	2.1035
2.58	0.5056	7.5991	3.4263	2.2179	0.4677	2.1381
2.6	0.5039	7.7200	3.4490	2.2383	0.4601	2.1733
2.62	0.5022	7.8418	3.4714	2.2590	0.4526	2.2093
2.64	0.5005	7.9645	3.4937	2.2797	0.4452	2.2461
2.66	0.4988	8.0882	3.5157	2.3006	0.4379	2.2835
2.68	0.4972	8.2128	3.5374	2.3217	0.4307	2.3218
2.7	0.4956	8.3383	3.5590	2.3429	0.4236	2.3608
2.72	0.4941	8.4648	3.5803	2.3642	0.4166	2.4005
2.74	0.4926	8.5922	3.6015	2.3858	0.4097	2.4411
2.76	0.4911	8.7205	3.6224	2.4074	0.4028	2.4825
2.78	0.4896	8.8498	3.6431	2.4292	0.3961	2.5246
2.8	0.4882	8.9800	2.6636	2.4512	0.3895	2.5676
2.82	0.4868	9.1111	3.6838	2.4733	0.3829	2.6115
2.84	0.4854	9.2432	3.7039	2.4955	0.3765	2.6561
2.86	0.4840	9.3762	3.7238	2.5179	0.3701	2.7017
2.88	0.4827	9.5101	3.7434	2.5405	0.3639	2.7481
2.9	0.4814	9.6450	3.7629	2.5632	0.3577	2.7954
2.92	0.4801	9.7808	3.7821	2.5861	0.3517	2.8436
2.94	0.4788	9.9175	3.8012	2.6091	0.3457	2.8927
2.96	0.4776	10.0552	3.8200	2.6322	0.3398	2.9427
2.98	0.4764	10.1938	3.8387	2.6555	0.3340	2.9937
3.0	0.4752	10.3333	3.8571	2.6790	0.3283	3.0456
3.02	0.4740	10.4738	3.8754	2.7026	0.3227	3.0985
3.04	0.4729	10.6152	3.8935	2.7264	0.3172	3.1523
3.06	0.4717	10.7575	3.9114	2.7503	0.3118	3.2072
3.08	0.4706	10.9008	3.9291	2.7744	0.3065	3.2630
3.1	0.4695	11.0450	3.9466	2.7986	0.3012	3.3199
3.12	0.4685	11.1901	3.9639	2.8230	0.2960	3.3778
3.14	0.4674	11.3362	3.9811	2.8475	0.2910	3.4368
3.16	0.4664	11.4832	3.9981	2.8722	0.2860	3.4969
3.18	0.4654	11.6311	4.0149	2.8970	0.2811	3.5580
3.2	0.4643	11.7800	4.0315	2.9220	0.2762	3.6202
3.22	0.4634	11.9298	4.0479	2.9471	0.2715	3.6835
3.24	0.4624	12.0805	4.0642	2.9724	0.2668	3.7480
3.26	0.4614	12.2322	4.0803	2.9979	0.2622	3.8136
3.28	0.4605	12.3848	4.0963	3.0234	0.2577	3.8803
3.3	0.4596	12.5383	4.1120	3.0492	0.2533	3.9483
3.32	0.4587	12.6928	4.1276	3.0751	0.2489	4.0174
3.34	0.4578	12.8482	4.1431	3.1011	0.2446	4.0877
3.36	0.4569	13.0045	4.1583	3.1273	0.2404	4.1593
3.38	0.4560	13.1618	4.1734	3.1537	0.2363	
3.4	0.4552	13.3200	4.1884	3.1802	0.2322	



ketabline.com Ebook.ketabline.com

Table B.2 (*Cont.*) Normal-Shock Relations for a Perfect Gas, $k = 1.4$

Ma_{n1}	Ma_{n2}	p_2/p_1	$V_1/V_2 = \rho_2/\rho_1$	T_2/T_1	p_{02}/p_{01}	A_2^*/A_1^*
3.42	0.4544	13.4791	4.2032	3.2069	0.2282	4.3815
3.44	0.4535	13.6392	4.2178	3.2337	0.2243	4.4581
3.46	0.4527	13.8002	4.2323	3.2607	0.2205	4.5361
3.48	0.4519	13.9621	4.2467	3.2878	0.2167	4.6154
3.5	0.4512	14.1250	4.2609	3.3151	0.2129	4.6960
3.52	0.4504	14.2888	4.2749	3.3425	0.2093	4.7780
3.54	0.4496	14.4535	4.2888	3.3701	0.2057	4.8614
3.56	0.4489	14.6192	4.3026	3.3978	0.2022	4.9461
3.58	0.4481	14.7858	4.3162	3.4257	0.1987	5.0324
3.6	0.4474	14.9533	4.3296	3.4537	0.1953	5.1200
3.62	0.4467	15.1218	4.3429	3.4819	0.1920	5.2091
3.64	0.4460	15.2912	4.3561	3.5103	0.1887	5.2997
3.66	0.4453	15.4615	4.3692	3.5388	0.1855	5.3918
3.68	0.4446	15.6328	4.3821	3.5674	0.1823	5.4854
3.7	0.4439	15.8050	4.3949	3.5962	0.1792	5.5806
3.72	0.4433	15.9781	4.4075	3.6252	0.1761	5.6773
3.74	0.4426	16.1522	4.4200	3.6543	0.1731	5.7756
3.76	0.4420	16.3272	4.4324	3.6836	0.1702	5.8755
3.78	0.4414	16.5031	4.4447	3.7130	0.1673	5.9770
3.8	0.4407	16.6800	4.4568	3.7426	0.1645	6.0801
3.82	0.4401	16.8578	4.4688	3.7723	0.1617	6.1849
3.84	0.4395	17.0365	4.4807	3.8022	0.1589	6.2915
3.86	0.4389	17.2162	4.4924	3.8323	0.1563	6.3997
3.88	0.4383	17.3968	4.5041	3.8625	0.1536	6.5096
3.9	0.4377	17.5783	4.4156	3.8928	0.1510	6.6213
3.92	0.4372	17.7608	4.5270	3.9233	0.1485	6.7348
3.94	0.4366	17.9442	4.5383	3.9540	0.1460	6.8501
3.96	0.4360	18.1285	4.5494	3.9848	0.1435	6.9672
3.98	0.4355	18.3138	4.5605	4.0158	0.1411	7.0861
4.0	0.4350	18.5000	4.5714	4.0469	0.1388	7.2069
4.02	0.4344	18.6871	4.5823	4.0781	0.1364	7.3296
4.04	0.4339	18.8752	4.5930	4.1096	0.1342	7.4542
4.06	0.4334	19.0642	4.6036	4.1412	0.1319	7.5807
4.08	0.4329	19.2541	4.6141	4.1729	0.1297	7.7092
4.1	0.4324	19.4450	4.6245	4.2048	0.1276	7.8397
4.12	0.4319	19.6368	4.6348	4.2368	0.1254	7.9722
4.14	0.4314	19.8295	4.6450	4.2690	0.1234	8.1067
4.16	0.4309	20.0232	4.6550	4.3014	0.1213	8.2433
4.18	0.4304	20.2178	4.6650	4.3339	0.1193	8.3819
4.2	0.4299	20.4133	4.6749	4.3666	0.1173	8.5227
4.22	0.4295	20.6098	4.6847	4.3994	0.1154	8.6656
4.24	0.4290	20.8072	4.6944	4.4324	0.1135	8.8107
4.26	0.4286	21.0055	4.7040	4.4655	0.1116	8.9579
4.28	0.4281	21.2048	4.7135	4.4988	0.1098	9.1074
4.3	0.4277	21.4050	4.7229	4.5322	0.1080	9.2591
4.32	0.4272	21.6061	4.7322	4.5658	0.1062	9.4131
4.34	0.4268	21.8082	4.7414	4.5995	0.1045	9.5694
4.36	0.4264	22.0112	4.7505	4.6334	0.1028	9.7280
4.38	0.4260	22.2151	4.7595	4.6675	0.1011	9.8889
4.4	0.4255	22.4200	4.7685	4.7017	0.0995	10.0522
4.42	0.4251	22.6258	4.7773	4.7361	0.0979	10.2179
4.44	0.4247	22.8325	4.7861	4.7706	0.0963	10.39
4.46	0.4243	23.0402	4.7948	4.8053		
4.48	0.4239	23.2488	4.8034	4.8401		



ketabline.com Ebook.ketabline.com

Table B.2 (*Cont.*) Normal-Shock Relations for a Perfect Gas, $k = 1.4$

Ma_{n1}	Ma_{n2}	p_2/p_1	$V_1/V_2 = \rho_2/\rho_1$	T_2/T_1	p_{02}/p_{01}	A_2^*/A_1^*
4.5	0.4236	23.4583	4.8119	4.8751	0.0917	10.9054
4.52	0.4232	23.6688	4.8203	4.9102	0.0902	11.0835
4.54	0.4228	23.8802	4.8287	4.9455	0.0888	11.2643
4.56	0.4224	24.0925	4.8369	4.9810	0.0874	11.4476
4.58	0.4220	24.3058	4.8451	5.0166	0.0860	11.6336
4.6	0.4217	24.5200	4.8532	5.0523	0.0846	11.8222
4.62	0.4213	24.7351	4.8612	5.0882	0.0832	12.0136
4.64	0.4210	24.9512	4.8692	5.1243	0.0819	12.2076
4.66	0.4206	25.1682	4.8771	5.1605	0.0806	12.4044
4.68	0.4203	25.3861	4.8849	5.1969	0.0793	12.6040
4.7	0.4199	25.6050	4.8926	5.2334	0.0781	12.8065
4.72	0.4196	25.8248	4.9002	5.2701	0.0769	13.0117
4.74	0.4192	26.0455	4.9078	5.3070	0.0756	13.2199
4.76	0.4189	26.2672	4.9153	5.3440	0.0745	13.4310
4.78	0.4186	26.4898	4.9227	5.3811	0.0733	13.6450
4.8	0.4183	26.7133	4.9301	5.4184	0.0721	13.8620
4.82	0.4179	26.9378	4.9374	5.4559	0.0710	14.0820
4.84	0.4176	27.1632	4.9446	5.4935	0.0699	14.3050
4.86	0.4173	27.3895	4.9518	5.5313	0.0688	14.5312
4.88	0.4170	27.6168	4.9589	5.5692	0.0677	14.7604
4.9	0.4167	27.8450	4.9659	5.6073	0.0667	14.9928
4.92	0.4164	28.0741	4.9728	5.6455	0.0657	15.2284
4.94	0.4161	28.3042	4.9797	5.6839	0.0647	15.4672
4.96	0.4158	28.5352	4.9865	5.7224	0.0637	15.7902
4.98	0.4155	28.7671	4.9933	5.7611	0.0627	15.9545
5.0	0.4152	29.0000	5.0000	5.8000	0.0617	16.2032

Table B.3 Adiabatic Frictional Flow in a Constant-Area Duct for $k = 1.4$

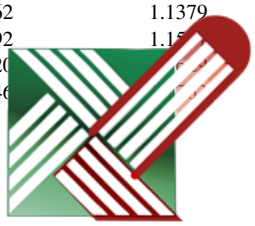
Ma	$\bar{f}L^*/D$	p/p^*	T/T^*	$\rho^*/\rho = V/V^*$	p_0/p_0^*
0.0	∞	∞	1.2000	0.0	∞
0.02	1778.4500	54.7701	1.1999	0.0219	28.9421
0.04	440.3520	27.3817	1.1996	0.0438	14.4815
0.06	193.0310	18.2508	1.1991	0.0657	9.6659
0.08	106.7180	13.6843	1.1985	0.0876	7.2616
0.1	66.9216	10.9435	1.1976	0.1094	5.8218
0.12	45.4080	9.1156	1.1966	0.1313	4.8643
0.14	32.5113	7.8093	1.1953	0.1531	4.1824
0.16	24.1978	6.8291	1.1939	0.1748	3.6727
0.18	18.5427	6.0662	1.1923	0.1965	3.2779
0.2	14.5333	5.4554	1.1905	0.2182	2.9635
0.22	11.5961	4.9554	1.1885	0.2398	2.7076
0.24	9.3865	4.5383	1.1863	0.2614	2.4956
0.26	7.6876	4.1851	1.1840	0.2829	2.3173
0.28	6.3572	3.8820	1.1815	0.3043	2.1656
0.3	5.2993	3.6191	1.1788	0.3257	2.0351
0.32	4.4467	3.3887	1.1759	0.3470	1.9219
0.34	3.7520	3.1853	1.1729	0.3682	1.8229
0.36	3.1801	3.0042	1.1697	0.3893	1.7358
0.38	2.7054	2.8420	1.1663	0.4104	1.6587
0.4	2.3085	2.6958	1.1628	0.4313	
0.42	1.9744	2.5634	1.1591	0.4522	



ketabline.com Ebook.ketabline.com

Table B.3 (*Cont.*) Adiabatic Frictional Flow in a Constant-Area Duct for $k = 1.4$

Ma	$\bar{f}L^*/D$	p/p^*	T/T^*	$\rho^*/\rho = V/V^*$	p_0/p_0^*
0.44	1.6915	2.4428	1.1553	0.4729	1.4740
0.46	1.4509	2.3326	1.1513	0.4936	1.4246
0.48	1.2453	2.2313	1.1471	0.5141	1.3801
0.5	1.0691	2.1381	1.1429	0.5345	1.3398
0.52	0.9174	2.0519	1.1384	0.5548	1.3034
0.54	0.7866	1.9719	1.1339	0.5750	1.2703
0.56	0.6736	1.8975	1.1292	0.5951	1.2403
0.58	0.5757	1.8282	1.1244	0.6150	1.2130
0.6	0.4908	1.7634	1.1194	0.6348	1.1882
0.62	0.4172	1.7026	1.1143	0.6545	1.1656
0.64	0.3533	1.6456	1.1091	0.6740	1.1451
0.66	0.2979	1.5919	1.1038	0.6934	1.1265
0.68	0.2498	1.5413	1.0984	0.7127	1.1097
0.7	0.2081	1.4935	1.0929	0.7318	1.0944
0.72	0.1721	1.4482	1.0873	0.7508	1.0806
0.74	0.1411	1.4054	1.0815	0.7696	1.0681
0.76	0.1145	1.3647	1.0757	0.7883	1.0570
0.78	0.0917	1.3261	1.0698	0.8068	1.0471
0.8	0.0723	1.2893	1.0638	0.8251	1.0382
0.82	0.0559	1.2542	1.0578	0.8433	1.0305
0.84	0.0423	1.2208	1.0516	0.8614	1.0237
0.86	0.0310	1.1889	1.0454	0.8793	1.0179
0.88	0.0218	1.1583	1.0391	0.8970	1.0129
0.9	0.0145	1.1291	1.0327	0.9146	1.0089
0.92	0.0089	1.1011	1.0263	0.9320	1.0056
0.94	0.0048	1.0743	1.0198	0.9493	1.0031
0.96	0.0021	1.0485	1.0132	0.9663	1.0014
0.98	0.0005	1.0238	1.0066	0.9833	1.0003
1.0	0.0000	1.0000	1.0000	1.0000	1.0000
1.02	0.0005	0.9771	0.9933	1.0166	1.0003
1.04	0.0018	0.9551	0.9866	1.0330	1.0013
1.06	0.0038	0.9338	0.9798	1.0492	1.0029
1.08	0.0066	0.9133	0.9730	1.0653	1.0051
1.1	0.0099	0.8936	0.9662	1.0812	1.0079
1.12	0.0138	0.8745	0.9593	1.0970	1.0113
1.14	0.0182	0.8561	0.9524	1.1126	1.0153
1.16	0.0230	0.8383	0.9455	1.1280	1.0198
1.18	0.0281	0.8210	0.9386	1.1432	1.0248
1.2	0.0336	0.8044	0.9317	1.1583	1.0304
1.22	0.0394	0.7882	0.9247	1.1732	1.0366
1.24	0.0455	0.7726	0.9178	1.1879	1.0432
1.26	0.0517	0.7574	0.9108	1.2025	1.0504
1.28	0.0582	0.7427	0.9038	1.2169	1.0581
1.3	0.0648	0.7285	0.8969	1.2311	1.0663
1.32	0.0716	0.7147	0.8899	1.2452	1.0750
1.34	0.0785	0.7012	0.8829	1.2591	1.0842
1.36	0.0855	0.6882	0.8760	1.2729	1.0940
1.38	0.0926	0.6755	0.8690	1.2864	1.1042
1.4	0.0997	0.6632	0.8621	1.2999	1.1149
1.42	0.1069	0.6512	0.8551	1.3131	1.1262
1.44	0.1142	0.6396	0.8482	1.3262	1.1379
1.46	0.1215	0.6282	0.8413	1.3392	1.15
1.48	0.1288	0.6172	0.8344	1.3520	
1.5	0.1361	0.6065	0.8276	1.3646	



ketabline.com Ebook.ketabline.com

Table B.3 (*Cont.*) Adiabatic Frictional Flow in a Constant-Area Duct for $k = 1.4$

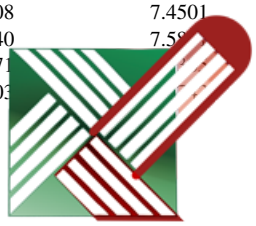
Ma	$\bar{f}L^*/D$	p/p^*	T/T^*	$\rho^*/\rho = V/V^*$	p_0/p_0^*
1.52	0.1433	0.5960	0.8207	1.3770	1.1899
1.54	0.1506	0.5858	0.8139	1.3894	1.2042
1.56	0.1579	0.5759	0.8071	1.4015	1.2190
1.58	0.1651	0.5662	0.8004	1.4135	1.2344
1.6	0.1724	0.5568	0.7937	1.4254	1.2502
1.62	0.1795	0.5476	0.7869	1.4371	1.2666
1.64	0.1867	0.5386	0.7803	1.4487	1.2836
1.66	0.1938	0.5299	0.7736	1.4601	1.3010
1.68	0.2008	0.5213	0.7670	1.4713	1.3190
1.7	0.2078	0.5130	0.7605	1.4825	1.3376
1.72	0.2147	0.5048	0.7539	1.4935	1.3567
1.74	0.2216	0.4969	0.7474	1.5043	1.3764
1.76	0.2284	0.4891	0.7410	1.5150	1.3967
1.78	0.2352	0.4815	0.7345	1.5256	1.4175
1.8	0.2419	0.4741	0.7282	1.5360	1.4390
1.82	0.2485	0.4668	0.7218	1.5463	1.4610
1.84	0.2551	0.4597	0.7155	1.5564	1.4836
1.86	0.2616	0.4528	0.7093	1.5664	1.5069
1.88	0.2680	0.4460	0.7030	1.5763	1.5308
1.9	0.2743	0.4394	0.6969	1.5861	1.5553
1.92	0.2806	0.4329	0.6907	1.5957	1.5804
1.94	0.2868	0.4265	0.6847	1.6052	1.6062
1.96	0.2929	0.4203	0.6786	1.6146	1.6326
1.98	0.2990	0.4142	0.6726	1.6239	1.6597
2.0	0.3050	0.4082	0.6667	1.6330	1.6875
2.02	0.3109	0.4024	0.6608	1.6420	1.7160
2.04	0.3168	0.3967	0.6549	1.6509	1.7451
2.06	0.3225	0.3911	0.6491	1.6597	1.7750
2.08	0.3282	0.3856	0.6433	1.6683	1.8056
2.1	0.3339	0.3802	0.6376	1.6769	1.8369
2.12	0.3394	0.3750	0.6320	1.6853	1.8690
2.14	0.3449	0.3698	0.6263	1.6936	1.9018
2.16	0.3503	0.3648	0.6208	1.7018	1.9354
2.18	0.3556	0.3598	0.6152	1.7099	1.9698
2.2	0.3609	0.3549	0.6098	1.7179	2.0050
2.22	0.3661	0.3502	0.6043	1.7258	2.0409
2.24	0.3712	0.3455	0.5989	1.7336	2.0777
2.26	0.3763	0.3409	0.5936	1.7412	2.1153
2.28	0.3813	0.3364	0.5883	1.7488	2.1538
2.3	0.3862	0.3320	0.5831	1.7563	2.1931
2.32	0.3911	0.3277	0.5779	1.7637	2.2333
2.34	0.3959	0.3234	0.5728	1.7709	2.2744
2.36	0.4006	0.3193	0.5677	1.7781	2.3164
2.38	0.4053	0.3152	0.5626	1.7852	2.3593
2.4	0.4099	0.3111	0.5576	1.7922	2.4031
2.42	0.4144	0.3072	0.5527	1.7991	2.4479
2.44	0.4189	0.3033	0.5478	1.8059	2.4936
2.46	0.4233	0.2995	0.5429	1.8126	2.5403
2.48	0.4277	0.2958	0.5381	1.8192	2.5880
2.5	0.4320	0.2921	0.5333	1.8257	2.6367
2.52	0.4362	0.2885	0.5286	1.8322	2.6865
2.54	0.4404	0.2850	0.5239	1.8386	2.7372
2.56	0.4445	0.2815	0.5193	1.8448	
2.58	0.4486	0.2781	0.5147	1.8510	



ketabline.com Ebook.ketabline.com

Table B.3 (*Cont.*) Adiabatic Frictional Flow in a Constant-Area Duct for $k = 1.4$

Ma	$\bar{f}L^*/D$	p/p^*	T/T^*	$\rho^*/\rho = V/V^*$	p_0/p_0^*
2.6	0.4526	0.2747	0.5102	1.8571	2.8960
2.62	0.4565	0.2714	0.5057	1.8632	2.9511
2.64	0.4604	0.2682	0.5013	1.8691	3.0073
2.66	0.4643	0.2650	0.4969	1.8750	3.0647
2.68	0.4681	0.2619	0.4925	1.8808	3.1233
2.7	0.4718	0.2588	0.4882	1.8865	3.1830
2.72	0.4755	0.2558	0.4839	1.8922	3.2440
2.74	0.4791	0.2528	0.4797	1.8978	3.3061
2.76	0.4827	0.2498	0.4755	1.9033	3.3695
2.78	0.4863	0.2470	0.4714	1.9087	3.4342
2.8	0.4898	0.2441	0.4673	1.9140	3.5001
2.82	0.4932	0.2414	0.4632	1.9193	3.5674
2.84	0.4966	0.2386	0.4592	1.9246	3.6359
2.86	0.5000	0.2359	0.4552	1.9297	3.7058
2.88	0.5033	0.2333	0.4513	1.9348	3.7771
2.9	0.5065	0.2307	0.4474	1.9398	3.8498
2.92	0.5097	0.2281	0.4436	1.9448	3.9238
2.94	0.5129	0.2256	0.4398	1.9497	3.9993
2.96	0.5160	0.2231	0.4360	1.9545	4.0763
2.98	0.5191	0.2206	0.4323	1.9593	4.1547
3.0	0.5222	0.2182	0.4286	1.9640	4.2346
3.02	0.5252	0.2158	0.4249	1.9686	4.3160
3.04	0.5281	0.2135	0.4213	1.9732	4.3989
3.06	0.5310	0.2112	0.4177	1.9777	4.4835
3.08	0.5339	0.2090	0.4142	1.9822	4.5696
3.1	0.5368	0.2067	0.4107	1.9866	4.6573
3.12	0.5396	0.2045	0.4072	1.9910	4.7467
3.14	0.5424	0.2024	0.4038	1.9953	4.8377
3.16	0.5451	0.2002	0.4004	1.9995	4.9304
3.18	0.5478	0.1981	0.3970	2.0037	5.0248
3.2	0.5504	0.1961	0.3937	2.0079	5.1210
3.22	0.5531	0.1940	0.3904	2.0120	5.2189
3.24	0.5557	0.1920	0.3872	2.0160	5.3186
3.26	0.5582	0.1901	0.3839	2.0200	5.4201
3.28	0.5607	0.1881	0.3807	2.0239	5.5234
3.3	0.5632	0.1862	0.3776	2.0278	5.6286
3.32	0.5657	0.1843	0.3745	2.0317	5.7358
3.34	0.5681	0.1825	0.3714	2.0355	5.8448
3.36	0.5705	0.1806	0.3683	2.0392	5.9558
3.38	0.5729	0.1788	0.3653	2.0429	6.0687
3.4	0.5752	0.1770	0.3623	2.0466	6.1837
3.42	0.5775	0.1753	0.3594	2.0502	6.3007
3.44	0.5798	0.1736	0.3564	2.0537	6.4198
3.46	0.5820	0.1718	0.3535	2.0573	6.5409
3.48	0.5842	0.1702	0.3507	2.0607	6.6642
3.5	0.5864	0.1685	0.3478	2.0642	6.7896
3.52	0.5886	0.1669	0.3450	2.0676	6.9172
3.54	0.5907	0.1653	0.3422	2.0709	7.0471
3.56	0.5928	0.1637	0.3395	2.0743	7.1791
3.58	0.5949	0.1621	0.3368	2.0775	7.3135
3.6	0.5970	0.1616	0.3341	2.0808	7.4501
3.62	0.5990	0.1590	0.3314	2.0840	7.5
3.64	0.6010	0.1575	0.3288	2.087	
3.66	0.6030	0.1560	0.3262	2.090	



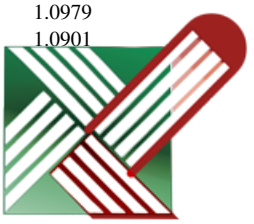
ketabline.com Ebook.ketabline.com

Table B.3 (*Cont.*) Adiabatic Frictional Flow in a Constant-Area Duct for $k = 1.4$

Ma	$\bar{f}L^*/D$	p/p^*	T/T^*	$\rho^*/\rho = V/V^*$	p_0/p_0^*
3.68	0.6049	0.1546	0.3236	2.0933	8.0204
3.7	0.6068	0.1531	0.3210	2.0964	8.1691
3.72	0.6087	0.1517	0.3185	2.0994	8.3202
3.74	0.6106	0.1503	0.3160	2.1024	8.4739
3.76	0.6125	0.1489	0.3135	2.1053	8.6302
3.78	0.6143	0.1475	0.3111	2.1082	8.7891
3.8	0.6161	0.1462	0.3086	2.1111	8.9506
3.82	0.6179	0.1449	0.3062	2.1140	9.1148
3.84	0.6197	0.1436	0.3039	2.1168	9.2817
3.86	0.6214	0.1423	0.3015	2.1195	9.4513
3.88	0.6231	0.1410	0.2992	2.1223	9.6237
3.9	0.6248	0.1397	0.2969	2.1250	9.7990
3.92	0.6265	0.1385	0.2946	2.1277	9.9771
3.94	0.6282	0.1372	0.2923	2.1303	10.1581
3.96	0.6298	0.1360	0.2901	2.1329	10.3420
3.98	0.6315	0.1348	0.2879	2.1355	10.5289
4.0	0.6331	0.1336	0.2857	2.1381	10.7188

Table B.4 Frictionless Duct Flow with Heat Transfer for $k = 1.4$

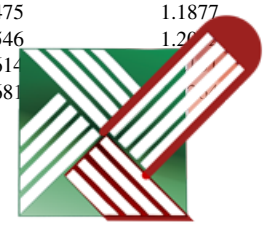
Ma	T_0/T_0^*	p/p^*	T/T^*	$\rho^*/\rho = V/V^*$	p_0/p_0^*
0.0	0.0	2.4000	0.0	0.0	1.2679
0.02	0.0019	2.3987	0.0023	0.0010	1.2675
0.04	0.0076	2.3946	0.0092	0.0038	1.2665
0.06	0.0171	2.3800	0.0205	0.0086	1.2647
0.08	0.0302	2.3787	0.0362	0.0152	1.2623
0.1	0.0468	2.3669	0.0560	0.0237	1.2591
0.12	0.0666	2.3526	0.0797	0.0339	1.2554
0.14	0.0895	2.3359	0.1069	0.0458	1.2510
0.16	0.1151	2.3170	0.1374	0.0593	1.2461
0.18	0.1432	2.2959	0.1708	0.0744	1.2406
0.2	0.1736	2.2727	0.2066	0.0909	1.2346
0.22	0.2057	2.2477	0.2445	0.1088	1.2281
0.24	0.2395	2.2209	0.2841	0.1279	1.2213
0.26	0.2745	2.1925	0.3250	0.1482	1.2140
0.28	0.3104	2.1626	0.3667	0.1696	1.2064
0.3	0.3469	2.1314	0.4089	0.1918	1.1985
0.32	0.3837	2.0991	0.4512	0.2149	1.1904
0.34	0.4206	2.0657	0.4933	0.2388	1.1822
0.36	0.4572	2.0314	0.5348	0.2633	1.1737
0.38	0.4935	1.9964	0.5755	0.2883	1.1652
0.4	0.5290	1.9608	0.6151	0.3137	1.1566
0.42	0.5638	1.9247	0.6535	0.3395	1.1480
0.44	0.5975	1.8882	0.6903	0.3656	1.1394
0.46	0.6301	1.8515	0.7254	0.3918	1.1308
0.48	0.6614	1.8147	0.7587	0.4181	1.1224
0.5	0.6914	1.7778	0.7901	0.4444	1.1141
0.52	0.7199	1.7409	0.8196	0.4708	1.1059
0.54	0.7470	1.7043	0.8469	0.4970	1.0979
0.56	0.7725	1.6678	0.8723	0.5230	1.0901
0.58	0.7965	1.6316	0.8955	0.5489	
0.6	0.8189	1.5957	0.9167	0.5745	



ketabline.com Ebook.ketabline.com

Table B.4 (*Cont.*) Frictionless Duct Flow with Heat Transfer for $k = 1.4$

Ma	T_0/T_0^*	p/p^*	T/T^*	$\rho^*/\rho = V/V^*$	p_0/p_0^*
0.62	0.8398	1.5603	0.9358	0.5998	1.0682
0.64	0.8592	1.5253	0.9530	0.6248	1.0615
0.66	0.8771	1.4908	0.9682	0.6494	1.0550
0.68	0.8935	1.4569	0.9814	0.6737	1.0489
0.7	0.9085	1.4235	0.9929	0.6975	1.0431
0.72	0.9221	1.3907	1.0026	0.7209	1.0376
0.74	0.9344	1.3585	1.0106	0.7439	1.0325
0.76	0.9455	1.3270	1.0171	0.7665	1.0278
0.78	0.9553	1.2961	1.0220	0.7885	1.0234
0.8	0.9639	1.2658	1.0255	0.8101	1.0193
0.82	0.9715	1.2362	1.0276	0.8313	1.0157
0.84	0.9781	1.2073	1.0285	0.8519	1.0124
0.86	0.9836	1.1791	1.0283	0.8721	1.0095
0.88	0.9883	1.1515	1.0269	0.8918	1.0070
0.9	0.9921	1.1246	1.0245	0.9110	1.0049
0.92	0.9951	1.0984	1.0212	0.9297	1.0031
0.94	0.9973	1.0728	1.0170	0.9480	1.0017
0.96	0.9988	1.0479	1.0121	0.9658	1.0008
0.98	0.9997	1.0236	1.0064	0.9831	1.0002
1.0	1.0000	1.0000	1.0000	1.0000	1.0000
1.02	0.9997	0.9770	0.9930	1.0164	1.0002
1.04	0.9989	0.9546	0.9855	1.0325	1.0008
1.06	0.9977	0.9327	0.9776	1.0480	1.0017
1.08	0.9960	0.9115	0.9691	1.0632	1.0031
1.1	0.9939	0.8909	0.9603	1.0780	1.0049
1.12	0.9915	0.8708	0.9512	1.0923	1.0070
1.14	0.9887	0.8512	0.9417	1.1063	1.0095
1.16	0.9856	0.8322	0.9320	1.1198	1.0124
1.18	0.9823	0.8137	0.9220	1.1330	1.0157
1.2	0.9787	0.7958	0.9118	1.1459	1.0194
1.22	0.9749	0.7783	0.9015	1.1584	1.0235
1.24	0.9709	0.7613	0.8911	1.1705	1.0279
1.26	0.9668	0.7447	0.8805	1.1823	1.0328
1.28	0.9624	0.7287	0.8699	1.1938	1.0380
1.3	0.9580	0.7130	0.8592	1.2050	1.0437
1.32	0.9534	0.6978	0.8484	1.2159	1.0497
1.34	0.9487	0.6830	0.8377	1.2264	1.0561
1.36	0.9440	0.6686	0.8269	1.2367	1.0629
1.38	0.9391	0.6546	0.8161	1.2467	1.0701
1.4	0.9343	0.6410	0.8054	1.2564	1.0777
1.42	0.9293	0.6278	0.7947	1.2659	1.0856
1.44	0.9243	0.6149	0.7840	1.2751	1.0940
1.46	0.9193	0.6024	0.7735	1.2840	1.1028
1.48	0.9143	0.5902	0.7629	1.2927	1.1120
1.5	0.9093	0.5783	0.7525	1.3012	1.1215
1.52	0.9042	0.5668	0.7422	1.3095	1.1315
1.54	0.8992	0.5555	0.7319	1.3175	1.1419
1.56	0.8942	0.5446	0.7217	1.3253	1.1527
1.58	0.8892	0.5339	0.7117	1.3329	1.1640
1.6	0.8842	0.5236	0.7017	1.3403	1.1756
1.62	0.8792	0.5135	0.6919	1.3475	1.1877
1.64	0.8743	0.5036	0.6822	1.3546	1.20
1.66	0.8694	0.4940	0.6726	1.3614	
1.68	0.8645	0.4847	0.6631	1.3681	



ketabline.com Ebook.ketabline.com

Table B.4 (*Cont.*) Frictionless Duct Flow with Heat Transfer for $k = 1.4$

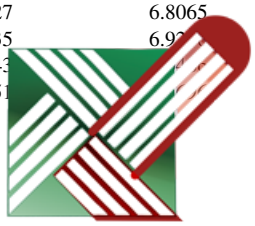
Ma	T_0/T_0^*	p/p^*	T/T^*	$\rho^*/\rho = V/V^*$	p_0/p_0^*
1.7	0.8597	0.4756	0.6538	1.3746	1.2402
1.72	0.8549	0.4668	0.6445	1.3809	1.2545
1.74	0.8502	0.4581	0.6355	1.3870	1.2692
1.76	0.8455	0.4497	0.6265	1.3931	1.2843
1.78	0.8409	0.4415	0.6176	1.3989	1.2999
1.8	0.8363	0.4335	0.6089	1.4046	1.3159
1.82	0.8317	0.4257	0.6004	1.4102	1.3324
1.84	0.8273	0.4181	0.5919	1.4156	1.3494
1.86	0.8228	0.4107	0.5836	1.4209	1.3669
1.88	0.8185	0.4035	0.5754	1.4261	1.3849
1.9	0.8141	0.3964	0.5673	1.4311	1.4033
1.92	0.8099	0.3895	0.5594	1.4360	1.4222
1.94	0.8057	0.3828	0.5516	1.4408	1.4417
1.96	0.8015	0.3763	0.5439	1.4455	1.4616
1.98	0.7974	0.3699	0.5364	1.4501	1.4821
2.0	0.7934	0.3636	0.5289	1.4545	1.5031
2.02	0.7894	0.3575	0.5216	1.4589	1.5246
2.04	0.7855	0.3516	0.5144	1.4632	1.5467
2.06	0.7816	0.3458	0.5074	1.4673	1.5693
2.08	0.7778	0.3401	0.5004	1.4714	1.5924
2.1	0.7741	0.3345	0.4936	1.4753	1.6162
2.12	0.7704	0.3291	0.4868	1.4792	1.6404
2.14	0.7667	0.3238	0.4802	1.4830	1.6653
2.16	0.7631	0.3186	0.4737	1.4867	1.6908
2.18	0.7596	0.3136	0.4673	1.4903	1.7168
2.2	0.7561	0.3086	0.4611	1.4938	1.7434
2.22	0.7527	0.3038	0.4549	1.4973	1.7707
2.24	0.7493	0.2991	0.4488	1.5007	1.7986
2.26	0.7460	0.2945	0.4428	1.5040	1.8271
2.28	0.7428	0.2899	0.4370	1.5072	1.8562
2.3	0.7395	0.2855	0.4312	1.5104	1.8860
2.32	0.7364	0.2812	0.4256	1.5134	1.9165
2.34	0.7333	0.2769	0.4200	1.5165	1.9476
2.36	0.7302	0.2728	0.4145	1.5194	1.9794
2.38	0.7272	0.2688	0.4091	1.5223	2.0119
2.4	0.7242	0.2648	0.4038	1.5252	2.0451
2.42	0.7213	0.2609	0.3986	1.5279	2.0789
2.44	0.7184	0.2571	0.3935	1.5306	2.1136
2.46	0.7156	0.2534	0.3885	1.5333	2.1489
2.48	0.7128	0.2497	0.3836	1.5359	2.1850
2.5	0.7101	0.2462	0.3787	1.5385	2.2218
2.52	0.7074	0.2427	0.3739	1.5410	2.2594
2.54	0.7047	0.2392	0.3692	1.5434	2.2978
2.56	0.7021	0.2359	0.3646	1.5458	2.3370
2.58	0.6995	0.2326	0.3601	1.5482	2.3770
2.6	0.6970	0.2294	0.3556	1.5505	2.4177
2.62	0.6945	0.2262	0.3512	1.5527	2.4593
2.64	0.6921	0.2231	0.3469	1.5549	2.5018
2.66	0.6896	0.2201	0.3427	1.5571	2.5451
2.68	0.6873	0.2171	0.3385	1.5592	2.5892
2.7	0.6849	0.2142	0.3344	1.5613	2.6343
2.72	0.6826	0.2113	0.3304	1.5634	2.6802
2.74	0.6804	0.2085	0.3264	1.5654	
2.76	0.6781	0.2058	0.3225	1.5673	



ketabline.com Ebook.ketabline.com

Table B.4 (*Cont.*) Frictionless Duct Flow with Heat Transfer for $k = 1.4$

Ma	T_0/T_0^*	p/p^*	T/T^*	$\rho^*/\rho = V/V^*$	p_0/p_0^*
2.78	0.6761	0.2030	0.3186	1.5693	2.8235
2.8	0.6738	0.2004	0.3149	1.5711	2.8731
2.82	0.6717	0.1978	0.3111	1.5730	2.9237
2.84	0.6696	0.1953	0.3075	1.5748	2.9752
2.86	0.6675	0.1927	0.3039	1.5766	3.0278
2.88	0.6655	0.1903	0.3004	1.5784	3.0813
2.9	0.6635	0.1879	0.2969	1.5801	3.1359
2.92	0.6615	0.1855	0.2934	1.5818	3.1914
2.94	0.6596	0.1832	0.2901	1.5834	3.2481
2.96	0.6577	0.1809	0.2868	1.5851	3.3058
2.98	0.6558	0.1787	0.2835	1.5867	3.3646
3.0	0.6540	0.1765	0.2803	1.5882	3.4245
3.02	0.6522	0.1743	0.2771	1.5898	3.4854
3.04	0.6504	0.1722	0.2740	1.5913	3.5476
3.06	0.6486	0.1701	0.2709	1.5928	3.6108
3.08	0.6469	0.1681	0.2679	1.5942	3.6752
3.1	0.6452	0.1660	0.2650	1.5957	3.7408
3.12	0.6435	0.1641	0.2620	1.5971	3.8076
3.14	0.6418	0.1621	0.2592	1.5985	3.8756
3.16	0.6402	0.1602	0.2563	1.5998	3.9449
3.18	0.6386	0.1583	0.2535	1.6012	4.0154
3.2	0.6370	0.1565	0.2508	1.6025	4.0871
3.22	0.6354	0.1547	0.2481	1.6038	4.1602
3.24	0.6339	0.1529	0.2454	1.6051	4.2345
3.26	0.6324	0.1511	0.2428	1.6063	4.3101
3.28	0.6309	0.1494	0.2402	1.6076	4.3871
3.3	0.6294	0.1477	0.2377	1.6088	4.4655
3.32	0.6280	0.1461	0.2352	1.6100	4.5452
3.34	0.6265	0.1444	0.2327	1.6111	4.6263
3.36	0.6251	0.1428	0.2303	1.6123	4.7089
3.38	0.6237	0.1412	0.2279	1.6134	4.7929
3.4	0.6224	0.1397	0.2255	1.6145	4.8783
3.42	0.6210	0.1381	0.2232	1.6156	4.9652
3.44	0.6197	0.1366	0.2209	1.6167	5.0536
3.46	0.6184	0.1351	0.2186	1.6178	5.1435
3.48	0.6171	0.1337	0.2164	1.6188	5.2350
3.5	0.6158	0.1322	0.2142	1.6198	5.3280
3.52	0.6145	0.1308	0.2120	1.6208	5.4226
3.54	0.6133	0.1294	0.2099	1.6218	5.5188
3.56	0.6121	0.1280	0.2078	1.6228	5.6167
3.58	0.6109	0.1267	0.2057	1.6238	5.7162
3.6	0.6097	0.1254	0.2037	1.6247	5.8173
3.62	0.6085	0.1241	0.2017	1.6257	5.9201
3.64	0.6074	0.1228	0.1997	1.6266	6.0247
3.66	0.6062	0.1215	0.1977	1.6275	6.1310
3.68	0.6051	0.1202	0.1958	1.6284	6.2390
3.7	0.6040	0.1190	0.1939	1.6293	6.3488
3.72	0.6029	0.1178	0.1920	1.6301	6.4605
3.74	0.6018	0.1166	0.1902	1.6310	6.5739
3.76	0.6008	0.1154	0.1884	1.6318	6.6893
3.78	0.5997	0.1143	0.1866	1.6327	6.8065
3.8	0.5987	0.1131	0.1848	1.6335	6.9
3.82	0.5977	0.1120	0.1830	1.6343	
3.84	0.5967	0.1109	0.1813	1.6351	



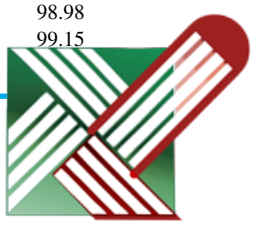
ketabline.com Ebook.ketabline.com

Table B.4 (*Cont.*) Frictionless Duct Flow with Heat Transfer for $k = 1.4$

Ma	T_0/T_0^*	p/p^*	T/T^*	$\rho^*/\rho = V/V^*$	p_0/p_0^*
3.86	0.5957	0.1098	0.1796	1.6359	7.2945
3.88	0.5947	0.1087	0.1779	1.6366	7.4215
3.9	0.5937	0.1077	0.1763	1.6374	7.5505
3.92	0.5928	0.1066	0.1746	1.6381	7.6816
3.94	0.5918	0.1056	0.1730	1.6389	7.8147
3.96	0.5909	0.1046	0.1714	1.6396	7.9499
3.98	0.5900	0.1036	0.1699	1.6403	8.0873
4.0	0.5891	0.1026	0.1683	1.6410	8.2269

Table B.5 Prandtl-Meyer Supersonic Expansion Function for $k = 1.4$

Ma	ω, deg	Ma	ω, deg	Ma	ω, deg	Ma	ω, deg
1.00	0.0						
1.05	0.49	3.05	50.71	5.05	77.38	7.05	91.23
1.10	1.34	3.10	51.65	5.10	77.84	7.10	91.49
1.15	2.38	3.15	52.57	5.15	78.29	7.15	91.75
1.20	3.56	3.20	53.47	5.20	78.73	7.20	92.00
1.25	4.83	3.25	54.35	5.25	79.17	7.25	92.24
1.30	6.17	3.30	55.22	5.30	79.60	7.30	92.49
1.35	7.56	3.35	56.07	5.35	80.02	7.35	92.73
1.40	8.99	3.40	56.91	5.40	80.43	7.40	92.97
1.45	10.44	3.45	57.73	5.45	80.84	7.45	93.21
1.50	11.91	3.50	58.53	5.50	81.24	7.50	93.44
1.55	13.38	3.55	59.32	5.55	81.64	7.55	93.67
1.60	14.86	3.60	60.09	5.60	82.03	7.60	93.90
1.65	16.34	3.65	60.85	5.65	82.42	7.65	94.12
1.70	17.81	3.70	61.60	5.70	82.80	7.70	94.34
1.75	19.27	3.75	62.33	5.75	83.17	7.75	94.56
1.80	20.73	3.80	63.04	5.80	83.54	7.80	94.78
1.85	22.16	3.85	63.75	5.85	83.90	7.85	95.00
1.90	23.59	3.90	64.44	5.90	84.26	7.90	95.21
1.95	24.99	3.95	65.12	5.95	84.61	7.95	95.42
2.00	26.38	4.00	65.78	6.00	84.96	8.00	95.62
2.05	27.75	4.05	66.44	6.05	85.30	8.05	95.83
2.10	29.10	4.10	67.08	6.10	85.63	8.10	96.03
2.15	30.43	4.15	67.71	6.15	85.97	8.15	96.23
2.20	31.73	4.20	68.33	6.20	86.29	8.20	96.43
2.25	33.02	4.25	68.94	6.25	86.62	8.25	96.63
2.30	34.28	4.30	69.54	6.30	86.94	8.30	96.82
2.35	35.53	4.35	70.13	6.35	87.25	8.35	97.01
2.40	36.75	4.40	70.71	6.40	87.56	8.40	97.20
2.45	37.95	4.45	71.27	6.45	87.87	8.45	97.39
2.50	39.12	4.50	71.83	6.50	88.17	8.50	97.57
2.55	40.28	4.55	72.38	6.55	88.47	8.55	97.76
2.60	41.41	4.60	72.92	6.60	88.76	8.60	97.94
2.65	42.53	4.65	73.45	6.65	89.05	8.65	98.12
2.70	43.62	4.70	73.97	6.70	89.33	8.70	98.29
2.75	44.69	4.75	74.48	6.75	89.62	8.75	98.47
2.80	45.75	4.80	74.99	6.80	89.90	8.80	98.64
2.85	46.78	4.85	75.48	6.85	90.17	8.85	98.81
2.90	47.79	4.90	75.97	6.90	90.44	8.90	98.98
2.95	48.78	4.95	76.45	6.95	90.71	8.95	99.15
3.00	49.76	5.00	76.92	7.00	90.97	9.00	



ketabline.com Ebook.ketabline.com

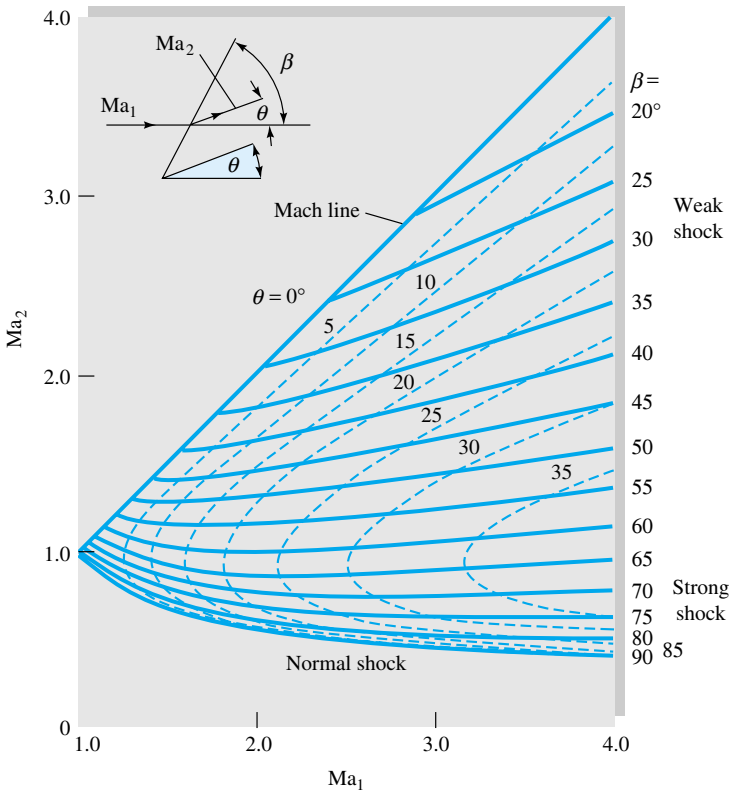


Fig. B.1 Mach number downstream of an oblique shock for $k = 1.4$.

ketabline.com Ebook.ketabline.com

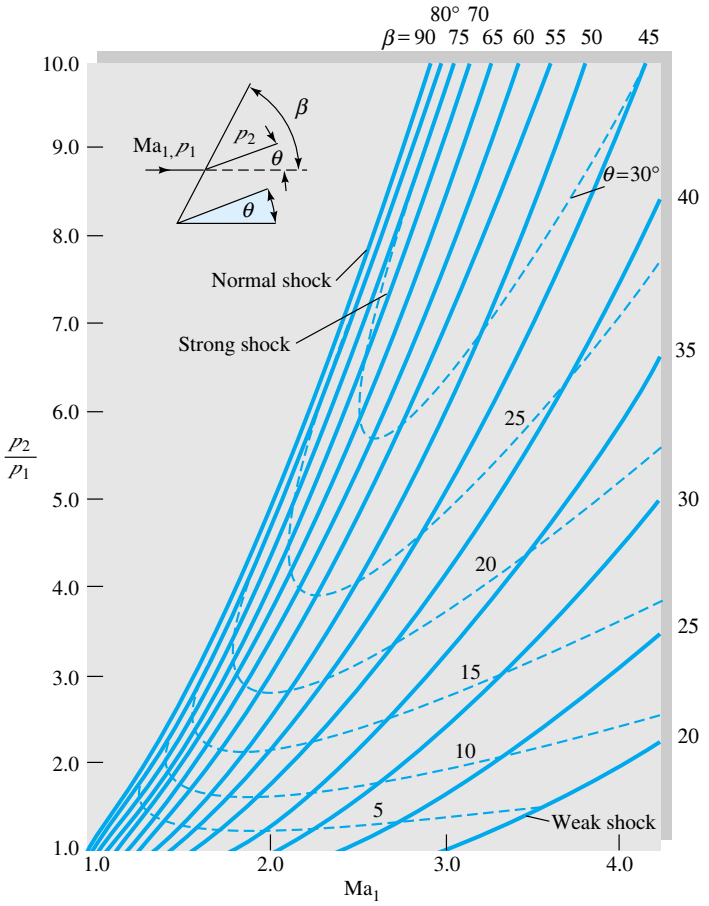


Fig. B.2 Pressure ratio downstream of an oblique shock for $k = 1.4$.



ketabline.com Ebook.ketabline.com

Appendix C
Conversion Factors

During this period of transition there is a constant need for conversions between BG and SI units (see Table 1.2). Some additional conversions are given here. Conversion factors are given inside the front cover.

Length	Volume
1 ft = 12 in = 0.3048 m 1 mi = 5280 ft = 1609.344 m 1 nautical mile (nmi) = 6076 ft = 1852 m 1 yd = 3 ft = 0.9144 m 1 angstrom (Å) = 1.0 E-10 m	1 ft^3 = 0.028317 m^3 1 U.S. gal = 231 in^3 = 0.0037854 m^3 1 L = 0.001 m^3 = 0.035315 ft^3 1 U.S. fluid ounce = 2.9574 E-5 m^3 1 U.S. quart (qt) = 9.4635 E-4 m^3
Mass	**Area**
1 slug = 32.174 lbm = 14.594 kg 1 lbm = 0.4536 kg 1 short ton = 2000 lbm = 907.185 kg 1 tonne = 1000 kg	1 ft^2 = 0.092903 m^2 1 mi^2 = 2.78784 E7 ft^2 = 2.59 E6 m^2 1 acre = 43,560 ft^2 = 4046.9 m^2 1 hectare (ha) = 10,000 m^2
Velocity	**Acceleration**
1 ft/s = 0.3048 m/s 1 mi/h = 1.466666 ft/s = 0.44704 m/s 1 kn = 1 nmi/h = 1.6878 ft/s = 0.5144 m/s	1 ft/s^2 = 0.3048 m/s^2
Mass flow	**Volume flow**
1 slug/s = 14.594 kg/s 1 lbm/s = 0.4536 kg/s	1 gal/min = 0.002228 ft^3/s = 0.06309 L/s 1 × 10^6 gal/day = 1.5472 ft^3/s = 0.04381 m^3/s
Pressure	**Force**
1 lbf/ft^2 = 47.88 Pa 1 lbf/in^2 = 144 lbf/ft^2 = 6895 Pa 1 atm = 2116.2 lbf/ft^2 = 14.696 lbf/in^2 = 101,325 Pa 1 inHg (at 20°C) = 3375 Pa 1 bar = 1.0 E5 Pa	1 lbf = 4.448222 N = 16 oz 1 kgf = 2.2046 lbf = 9.80665 N 1 U.S. (short) ton = 2000 lbf 1 dyne = 1.0 E-5 N 1 ounce (avoirdupois) (oz) = 0.27801 N



ketabline.com Ebook.ketabline.com

Energy	Power
1 ft · lbf = 1.35582 J 1 Btu = 252 cal = 1055.056 J = 778.17 ft · lbf 1 kilowatt hour (kWh) = 3.6 E6 J	1 hp = 550 ft · lbf/s = 745.7 W 1 ft · lbf/s = 1.3558 W
Specific weight	**Density**
1 lbf/ft^3 = 157.09 N/m^3	1 slug/ft^3 = 515.38 kg/m^3 1 lbm/ft^3 = 16.0185 kg/m^3 1 g/cm^3 = 1000 kg/m^3
Viscosity	**Kinematic viscosity**
1 slug/(ft · s) = 47.88 kg/(m · s) 1 poise (P) = 1 g/(cm · s) = 0.1 kg/(m · s)	1 ft^2/h = 0.000025806 m^2/s 1 stokes (St) = 1 cm^2/s = 0.0001 m^2/s

Temperature scale readings

$T_F = \frac{9}{5}T_C + 32$ $T_C = \frac{5}{9}(T_F - 32)$ $T_R = T_F + 459.69$ $T_K = T_C + 273.16$

where subscripts F, C, R, and K refer to readings on the Fahrenheit, Celsius, Kelvin, and Rankine scales, respectively

Specific heat or gas constant*	Thermal conductivity*
1 ft · lbf/(slug · °R) = 0.16723 N · m/(kg · K) 1 Btu/(lb · °R) = 4186.8 J/(kg · K)	1 Btu/(h · ft · °R) = 1.7307 W/(m · K)

*Although the absolute (Kelvin) and Celsius temperature scales have different starting points, the intervals are the same size: 1 kelvin = 1 Celsius degree. The same holds true for the nonmetric absolute (Rankine) and Fahrenheit scales: 1 Rankine degree = 1 Fahrenheit degree. It is customary to express temperature differences in absolute-temperature units.



ketabline.com Ebook.ketabline.com

Appendix D
Equations of Motion in Cylindrical Coordinates

The equations of motion of an incompressible newtonian fluid with constant μ, k, and c_p are given here in cylindrical coordinates (r, θ, z), which are related to cartesian coordinates (x, y, z) as in Fig. 4.2:

$$x = r\cos\theta \qquad y = r\sin\theta \qquad z = z \tag{D.1}$$

The velocity components are v_r, v_θ, and v_z. The equations are:

Continuity:

$$\frac{1}{r}\frac{\partial}{\partial r}(rv_r) + \frac{1}{r}\frac{\partial}{\partial\theta}(v_\theta) + \frac{\partial}{\partial z}(v_z) = 0 \tag{D.2}$$

Convective time derivative:

$$\mathbf{V}\cdot\nabla = v_r\frac{\partial}{\partial r} + \frac{1}{r}v_\theta\frac{\partial}{\partial\theta} + v_z\frac{\partial}{\partial z} \tag{D.3}$$

Laplacian operator:

$$\nabla^2 = \frac{1}{r}\frac{\partial}{\partial r}\left(r\frac{\partial}{\partial r}\right) + \frac{1}{r^2}\frac{\partial^2}{\partial\theta^2} + \frac{\partial^2}{\partial z^2} \tag{D.4}$$

The r-momentum equation:

$$\frac{\partial v_r}{\partial t} + (\mathbf{V}\cdot\nabla)v_r - \frac{1}{r}v_\theta^2 = -\frac{1}{\rho}\frac{\partial p}{\partial r} + g_r + \nu\left(\nabla^2 v_r - \frac{v_r}{r^2} - \frac{2}{r^2}\frac{\partial v_\theta}{\partial\theta}\right) \tag{D.5}$$

The θ-momentum equation:

$$\frac{\partial v_\theta}{\partial t} + (\mathbf{V}\cdot\nabla)v_\theta + \frac{1}{r}v_r v_\theta = -\frac{1}{\rho r}\frac{\partial p}{\partial\theta} + g_\theta + \nu\left(\nabla^2 v_\theta - \frac{v_\theta}{r^2} + \frac{2}{r^2}\frac{\partial v_r}{\partial\theta}\right) \tag{D.6}$$

The z-momentum equation:

$$\frac{\partial v_z}{\partial t} + (\mathbf{V}\cdot\nabla)v_z = -\frac{1}{\rho}\frac{\partial p}{\partial z} + g_z + \nu\nabla^2 v_z \tag{D}$$



ketabline.com Ebook.ketabline.com

The energy equation:

$$\rho c_p\left[\frac{\partial T}{\partial t} + (\mathbf{V}\cdot\nabla)T\right] = k\nabla^2 T + \mu[2(\epsilon_{rr}^2 + \epsilon_{\theta\theta}^2 + \epsilon_{zz}^2) + \epsilon_{\theta z}^2 + \epsilon_{rz}^2 + \epsilon_{r\theta}^2] \quad \text{(D.8)}$$

where

$$\epsilon_{rr} = \frac{\partial v_r}{\partial r} \qquad \epsilon_{\theta\theta} = \frac{1}{r}\left(\frac{\partial v_\theta}{\partial \theta} + v_r\right)$$

$$\epsilon_{zz} = \frac{\partial v_z}{\partial z} \qquad \epsilon_{\theta z} = \frac{1}{r}\frac{\partial v_z}{\partial \theta} + \frac{\partial v_\theta}{\partial z} \quad \text{(D.9)}$$

$$\epsilon_{rz} = \frac{\partial v_r}{\partial z} + \frac{\partial v_z}{\partial r} \qquad \epsilon_{r\theta} = \frac{1}{r}\left(\frac{\partial v_r}{\partial \theta} - v_\theta\right) + \frac{\partial v_\theta}{\partial r}$$

Viscous stress components:

$$\tau_{rr} = 2\mu\epsilon_{rr} \qquad \tau_{\theta\theta} = 2\mu\epsilon_{\theta\theta} \qquad \tau_{zz} = 2\mu\epsilon_{zz}$$
$$\tau_{r\theta} = \mu\epsilon_{r\theta} \qquad \tau_{\theta z} = \mu\epsilon_{\theta z} \qquad \tau_{rz} = \mu\epsilon_{rz} \quad \text{(D.10)}$$

Angular-velocity components:

$$\omega_r = \frac{1}{r}\frac{\partial v_z}{\partial \theta} - \frac{\partial v_\theta}{\partial z}$$

$$\omega_\theta = \frac{\partial v_r}{\partial z} - \frac{\partial v_z}{\partial r} \quad \text{(D.11)}$$

$$\omega_z = \frac{1}{r}\frac{\partial}{\partial r}(rv_\theta) - \frac{1}{r}\frac{\partial v_r}{\partial \theta}$$



ketabline.com Ebook.ketabline.com

Appendix E
Introduction to EES

Overview

EES (pronounced "ease") is an acronym for Engineering Equation Solver. The basic function provided by EES is the numerical solution of nonlinear algebraic and differential equations. In addition, EES provides built-in thermodynamic and transport property functions for many fluids, including water, dry and moist air, refrigerants, and combustion gases. Additional property data can be added by the user. The combination of equation solving capability and engineering property data makes EES a very powerful tool.

A license for EES is provided to departments of educational institutions which adopt this text by WCB/McGraw-Hill. If you need more information, contact your local WCB/McGraw-Hill representative, call 1-800-338-3987, or visit our website at www.mhhe.com. A commercial version of EES can be obtained from:

F-Chart Software
4406 Fox Bluff Rd
Middleton, WI 53562
Phone: (608)836-8531
Fax: (608)836-8536

Background Information

The EES program is probably installed on your departmental computer. In addition, the license agreement for EES allows students and faculty in a participating educational department to copy the program for educational use on their personal computer systems. Ask your instructor for details.

To start EES from the Windows File Manager or Explorer, double-click on the EES program icon or on any file created by EES. You can also start EES from the **Windows Run** command in the **Start** menu. EES begins by displaying a dialog window which shows registration information, the version number, and other information. Click the OK button to dismiss the dialog window.

Detailed help is available at any point in EES. Pressing the F1 key will bring up a Help window relating to the foremost window. (See Fig. E.1.) Clicking the Conten



ketabline.com Ebook.ketabline.com

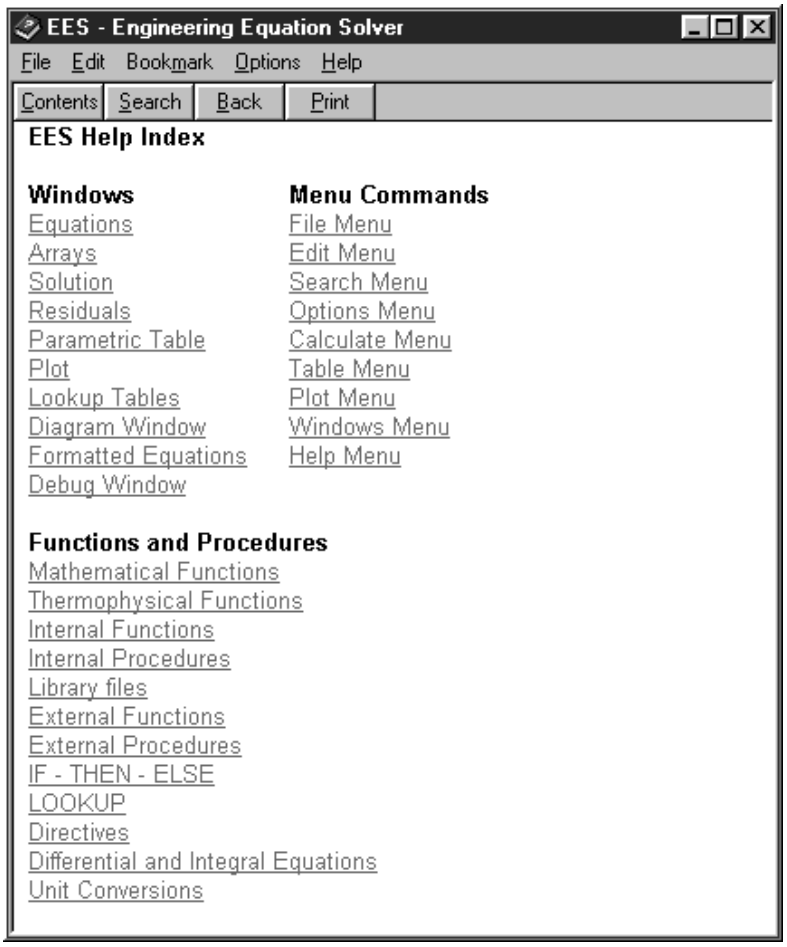


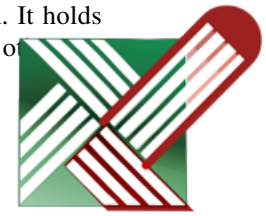
Fig. E.1 EES Help index.

button will present the Help index shown below. Clicking on an underlined word (shown in green on color monitors) will provide help relating to that subject.

EES commands are distributed among nine pull-down menus as shown below. Many of the commands are accessible with the speed button palette that appears below the menu bar. A brief summary of their functions follows. (A tenth pull-down menu, which is made visible with the **Load Textbook** command described below, provides access to problems from this text.)



The **System** menu appears above the **File** menu. The **System** menu is not part of EES but rather is a feature of the Windows operating system. It holds commands which allow window moving, resizing, and switching to o plications.



ketabline.com Ebook.ketabline.com

The **File** menu provides commands for loading, merging, and saving work files; libraries; and printing. The **Load Textbook** command in this menu reads the problem disk developed for this text and creates a new menu to the right of the **Help** menu for easy access to EES problems accompanying this text.

The **Edit** menu provides the editing commands to cut, copy, and paste information.

The **Search** menu provides **Find** and **Replace** commands for use in the Equations window.

The **Options** menu provides commands for setting the guess values and bounds of variables, the unit system, default information, and program preferences. A command is also provided for displaying information on built-in and user-supplied functions.

The **Calculate** menu contains the commands to check, format, and solve the equation set.

The **Tables** menu contains commands to set up and alter the contents of the parametric and lookup tables and to do linear regression on the data in these tables. The parametric table, which is similar to a spreadsheet, allows the equation set to be solved repeatedly while varying the values of one or more variables. The lookup table holds user-supplied data which can be interpolated and used in the solution of the equation set.

The **Plot** menu provides commands to modify an existing plot or prepare a new plot of data in the parametric, lookup, or array tables. Curve-fitting capability is also provided.

The **Windows** menu provides a convenient method of bringing any of the EES windows to the front or to organize the windows.

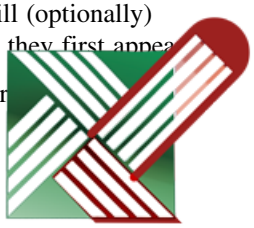
The **Help** menu provides commands for accessing the on-line help documentation.

A basic capability provided by EES is the solution of a set of nonlinear algebraic equations. To demonstrate this capability, start EES and enter this simple example problem in the Equations window.



Text is entered in the same manner as for any word processor. Formatting rules are as follows:

1. Uppercase and lowercase letters are not distinguished. EES will (optionally) change the case of all variables to match the manner in which they first appea
2. Blank lines and spaces may be entered as desired since they ar



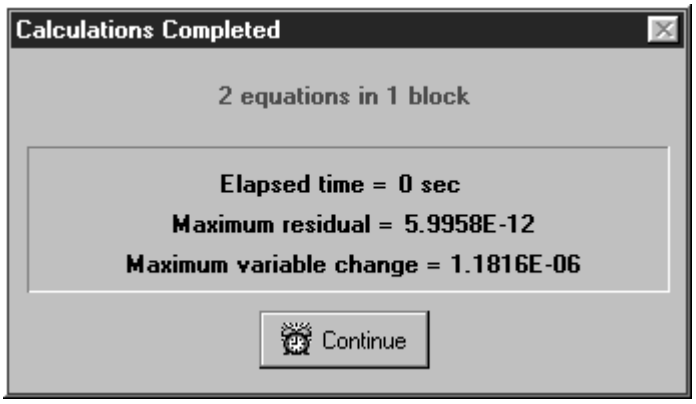
ketabline.com Ebook.ketabline.com

3. Comments must be enclosed within braces { } or within quotation marks " ". Comments may span as many lines as needed. Comments within braces may be nested, in which case only the outermost set of braces is recognized. Comments within quotes will also be displayed in the Formatted Equations window.
4. Variable names must start with a letter and consist of any keyboard characters except ( ) ' | */ + − ^ { } : " or ;. Array variables are identified with square braces around the array index or indices, e.g., X[5,3]. The maximum variable length is 30 characters.
5. Multiple equations may be entered on one line if they are separated by a semicolon (;). The maximum line length is 255 characters.
6. The caret symbol (^) or ** is used to indicate raising to a power.
7. The order in which the equations are entered does not matter.
8. The position of knowns and unknowns in the equation does not matter.

If you wish, you may view the equations in mathematical notation by selecting the **Formatted Equations** command from the **Windows** menu.



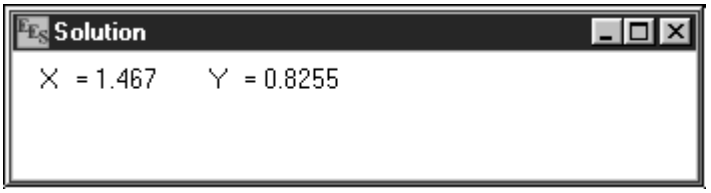
Select the **Solve** command from the **Calculate** menu. A Dialog window will appear indicating the progress of the solution. When the calculations are completed, the button will change from Abort to Continue.



Click the Continue button. The solution to this equation set will then be displ



ketabline.com Ebook.ketabline.com



A Pipe Friction Example Problem

Let us now solve Prob. 6.55 from the text, for a cast-iron pipe, to illustrate the capabilities of the EES program. This problem, without EES, would require iteration for Reynolds number, velocity, and friction factor, a daunting task. State the problem:

6.55 Reservoirs 1 and 2 contain water at 20°C. The pipe is cast iron, with $L = 4500$ m and $D = 4$ cm. What will be the flow rate in m^3/h if $\Delta z = 100$ m?

This is a representative problem in pipe flow (see Fig. E.2), and, being water in a reasonably large (noncapillary) pipe, it will probably be turbulent (Re > 4000). The steady-flow energy equation (3.71) may be written between the surfaces of reservoirs 1 and 2:

$$\frac{p_1}{\rho g} + \frac{V_1^2}{2g} + z_1 = \frac{p_2}{\rho g} + \frac{V_2^2}{2g} + z_2 + h_f \qquad \text{where} \qquad h_f = f\frac{L}{D}\frac{V_{\text{pipe}}^2}{2g}$$

Since $p_1 = p_2 = p_{\text{atm}}$ and $V_1 \approx V_2 \approx 0$, this relation simplifies to

$$\Delta z = f\frac{L}{D}\frac{V^2}{2g} \tag{1}$$

where $V = Q/A$ is the velocity in the pipe. The friction factor f is a function of Reynolds number and pipe roughness ratio, if the flow is turbulent, from Eq. (6.64):

$$\frac{1}{f^{1/2}} = -2.0\log_{10}\left(\frac{\epsilon/D}{3.7} + \frac{2.51}{\text{Re}\,f^{1/2}}\right) \qquad \text{if Re} > 4000 \tag{2}$$

Finally, we need the definitions of Reynolds number and volume flow rate:

$$\text{Re} = \frac{\rho VD}{\mu} \tag{3}$$

and

$$Q = V\frac{\pi}{4}D^2 \tag{4}$$

where ρ and μ are the fluid density and viscosity, respectively.

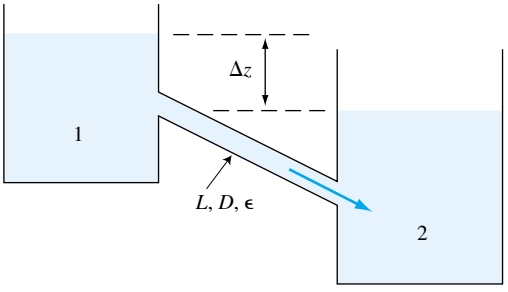


Fig. E.2 Sketch of the flow system.



ketabline.com Ebook.ketabline.com

There are a total of 11 variables involved in this problem: (L, D, Δz, ϵ, g, μ, ρ, V, Re, f, Q). Of these, seven can be specified at the start (L, D, Δz, ϵ, g, μ, ρ), while four (V, Re, f, Q) must be calculated from relations (1) to (4) above. These four equations in four unknowns are well posed and solvable but only by laborious iteration, exactly what EES is designed to do.

Start EES or select the **New** command from the **File** menu if you have already been using the program. A blank Equations window will appear. Our recommendation is to always set the unit system immediately: Select **Unit System** from the **Options** menu (Fig. E.3). We select *SI* and *Mass* units and trig *Degrees,* although we do not actually have trigonometric functions this time. We select *kPa* for pressure and *Celsius* for temperature, which will be handy for using the EES built-in physical properties of water.

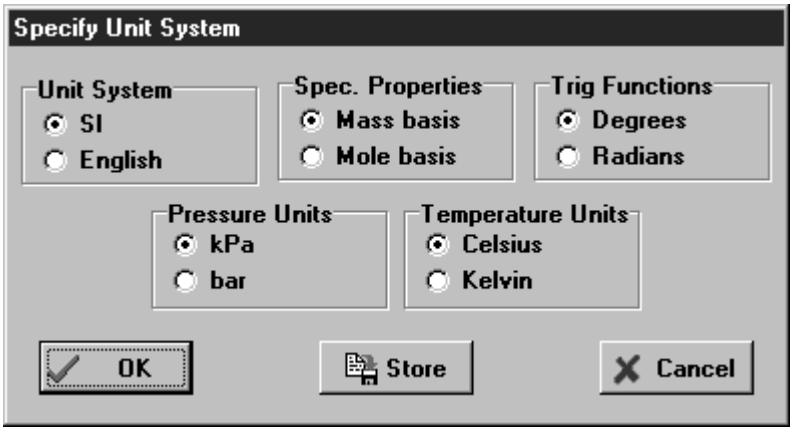


Fig. E.3 Unit Selection dialog window.

Now, onto the blank screen, enter the equations for this problem (Fig. E.4), of which five are known input values, two are property evaluations, and four are the relations (1) to (4) from above.

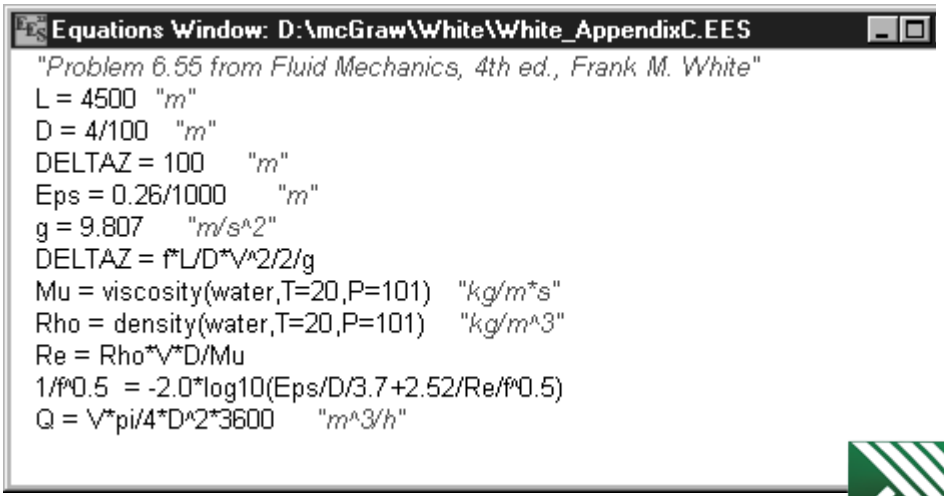


Fig. E.4 Equations window.



ketabline.com Ebook.ketabline.com

There are several things to notice in Fig. E.4. First, quantities in quotes, such as "m," are for the user's benefit and ignored by EES. Second, we changed *Eps* and *D* to meters right away, to keep the SI units consistent. Third, we called on EES to input the viscosity and density of water at 20°C and 1 atm, a procedure well explained in the **Help** menu. For example, **viscosity(water,T=20,P=101)** meets the EES requirement that temperature (T) and pressure (P) should be input in °C and kPa—EES will then evaluate μ in kg/(m · s). Finally, note that EES recognizes **pi** to be 3.141593.

In Fig. E.4 we used only one built-in function, **log10.** There are many such functions, found by scrolling down the **Function Information** command in the **Options** menu.

Having entered the equations, check the syntax by using the **Check/Format** command in the **Calculate** menu. If you did well, EES will report that the 11 equations in 11 unknowns look OK. If not, EES will guess at what might be wrong. If OK, why not go for it? Hit the **Solve** command in the **Options** menu. EES reports "logarithm of a negative number—try setting limits on the variables". We might have known. Go to the **Variable Information** command in the **Options** menu. A box, listing the 11 variables, will appear (Fig. E.5). All default EES "guesses" are unity; all default limits are $-\infty$ to $+\infty$, which is too broad a range. Enter (as already shown in Fig. E.5) guesses for $f = 0.02$ and Re = 10,000, while $V = 1$ and $Q = 1$ seem adequate, and other variables are fixed. Make sure that *f*, Re, *V*, and *Q* cannot be negative. The "display" columns normally say "A", automatic, satisfactory for most variables. We have changed "A" to "F" (fixed decimal) for *Q* and *V* to make sure they are displayed to four decimal places. The "units" column is normally blank—type in the correct units and they will be displayed in the solution.

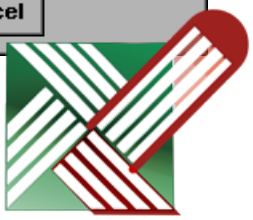
Our guesses and limits are excellent, and the **Solve** command now iterates and reports success: "max residual = 2E-10", a negligible error. (The default runs for 100

Variable Information

Variable	Guess	Lower	Upper	Display			Units
D	0.04	*-infinity*	*infinity*	A	3	N	m
DELTAZ	500	*-infinity*	*infinity*	A	3	N	m
Eps	0.00026	*-infinity*	*infinity*	A	3	N	m
f	0.02	0.0000E+00	infinity	A	3	N	
g	9.807	*-infinity*	*infinity*	A	3	N	m/s^2
L	4500	*-infinity*	*infinity*	A	3	N	m
Mu	0.001001	*-infinity*	*infinity*	A	3	N	kg/m*s
Q	1.0000	0.0000E+00	infinity	F	4	N	m^3/h
Re	10000	0.0000E+00	infinity	A	3	N	
Rho	999.6	*-infinity*	*infinity*	A	3	N	kg/m^3
V	1.0000	0.0000E+00	infinity	F	4	N	m/s

OK Print Update Cancel

Fig. E.5 Variable Information window with units and guess values entered.



ketabline.com Ebook.ketabline.com

iterations, which can be modified by the **Stop Criteria** command in the **Options** menu.) Hit **Continue,** and the complete solution is displayed for all variables (Fig. E.6).

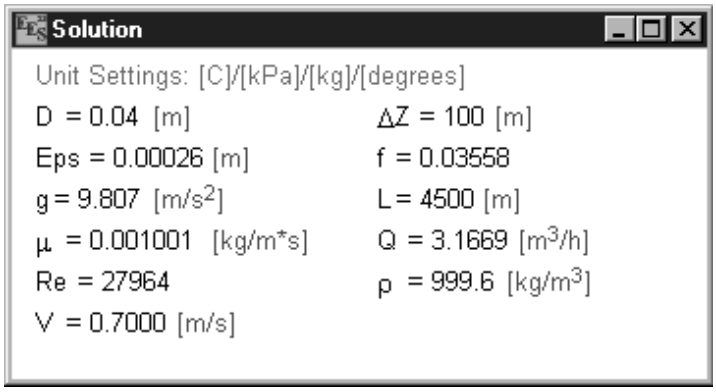


Fig. E.6 The Solutions window for Prob. 6.55.

This is the correct solution to Prob. 6.55: this cast-iron pipe, when subjected to a 100-m elevation difference, will deliver $Q = 3.17$ m^3/h of water. EES did all the iteration.

Parametric Studies with Tabular Input

One of the most useful features of EES is its ability to provide parametric studies. For example, suppose we wished to know how varying Δz changed the flow rate Q. First comment out the equation that reads DELTAZ = 100 by enclosing it within braces. (If you select the equation and press the right mouse button, EES will automatically enter the braces.) Select the **New Parametric Table** command in the **Options** menu. A dialog will be displayed (Fig. E.7) listing all the variables in the problem. Highlight what you wish to vary: Δz. Also highlight variables to be calculated and tabulated: V, Q, Re, and f.

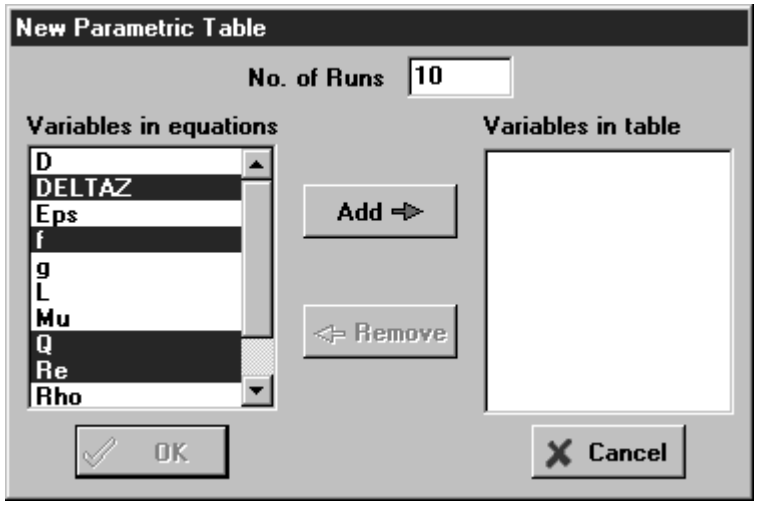
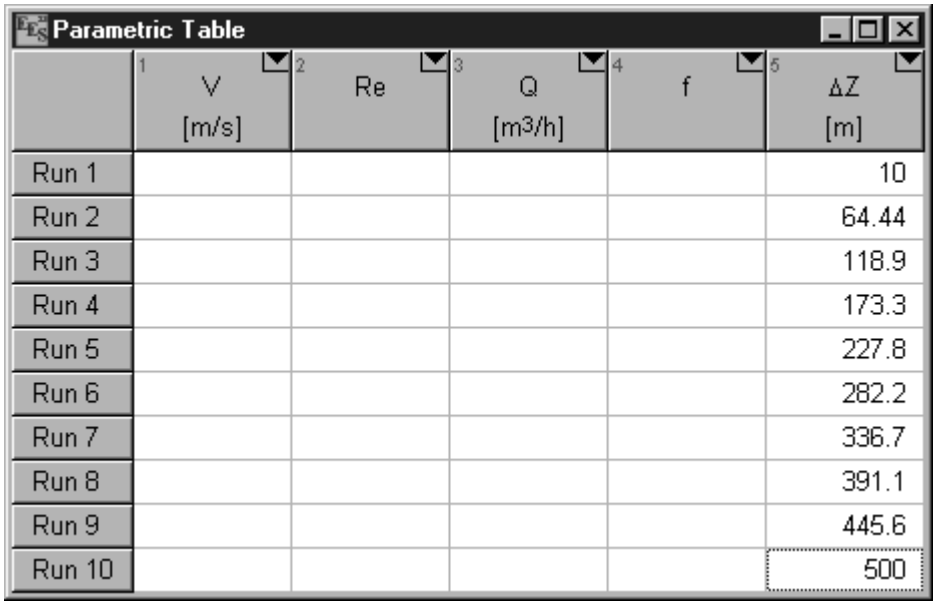


Fig. E.7 New Parametric Table window showing selected variables (V is not shown).



ketabline.com Ebook.ketabline.com

Click the **OK** button and the new table will be displays (Fig. E.8). Enter 10 values of Δz that cover the range of interest—we have selected the linear range $10 < \Delta z < 500$ m.



Parametric Table

	1 V [m/s]	2 Re	3 Q [m3/h]	4 f	5 ΔZ [m]
Run 1					10
Run 2					64.44
Run 3					118.9
Run 4					173.3
Run 5					227.8
Run 6					282.2
Run 7					336.7
Run 8					391.1
Run 9					445.6
Run 10					500

Fig. E.8 Parametric Table window.

Clearly the parametric table operates much like a spreadsheet. Select **Solve Table** from the **Calculate** menu, and the Solve Table dialog window will appear (Fig. E.9). These are satisfactory default values; the author has changed nothing. Hit the **OK** button and the calculations will be made and the entire parametric table filled out, as in Fig. E.10.

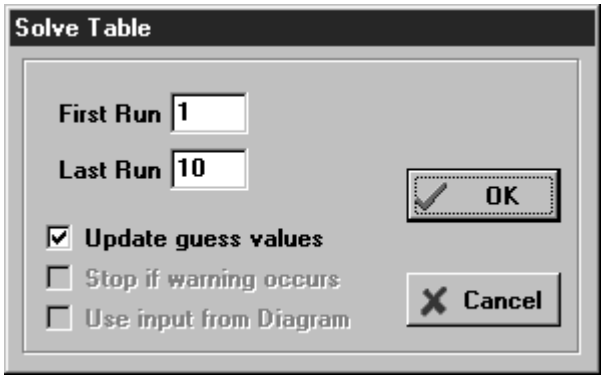


Fig. E.9 Solve Table Dialog.

The flow rates can be seen in Fig. E.10, but as always, in the author's experience, a plot is more illuminating. Select **New Plot window** from the **Plot** menu. The New Plot window dialog (Fig. E.11) will appear. Choose Δz as the x-axis and Q as the y-axis. We added grid lines. Click the OK button, and the desired plot will appear in the Plot window (Fig. E.12). We see a nonlinear relationship, roughly a square-root type, and learn that flow rate Q is not linearly proportional to head difference Δz.

The plot appearance in Fig. E.12 can be modified in several ways. Right-click the mouse in the plot rectangle to see some of these options.



ketabline.com Ebook.ketabline.com

Parametric Table

	1 V [m/s]	2 Re	3 Q [m3/h]	4 f	5 ΔZ [m]
Run 1	0.2076	8292	0.9391	0.04046	10
Run 2	0.5573	22261	2.5209	0.03618	64.44
Run 3	0.7655	30580	3.4631	0.03537	118.9
Run 4	0.9296	37135	4.2054	0.03497	173.3
Run 5	1.0695	42722	4.8382	0.03472	227.8
Run 6	1.1935	47675	5.3991	0.03455	282.2
Run 7	1.3060	52170	5.9081	0.03441	336.7
Run 8	1.4098	56316	6.3776	0.03431	391.1
Run 9	1.5065	60182	6.8154	0.03423	445.6
Run 10	1.5976	63818	7.2272	0.03416	500

Fig. E.10 Parametric Table window after calculations are completed.

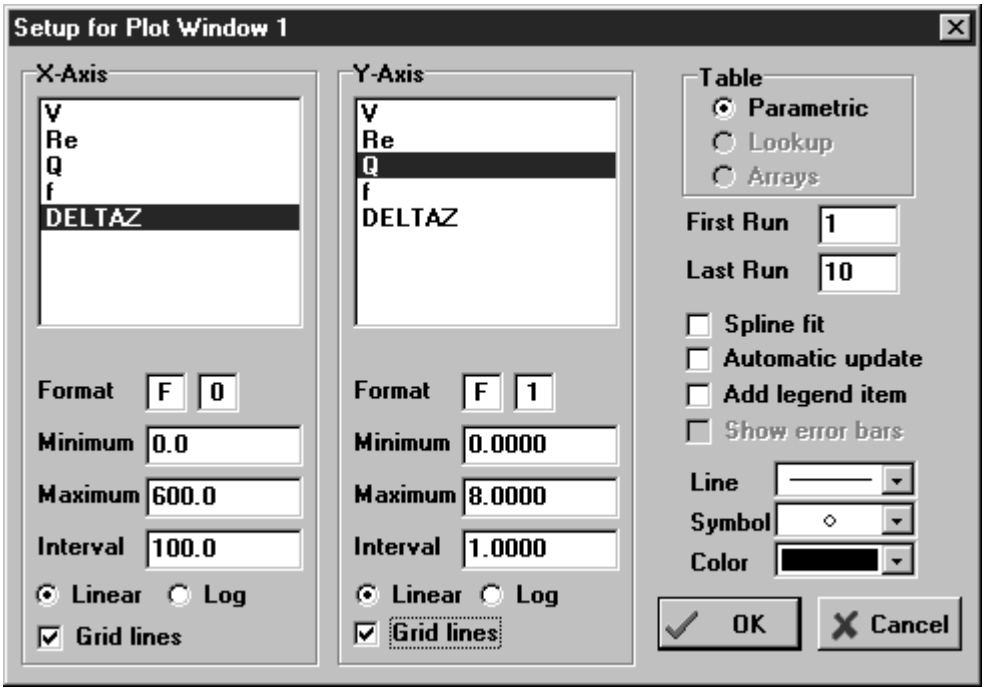


Fig. E.11 New Plot Setup dialog window.



ketabline.com Ebook.ketabline.com

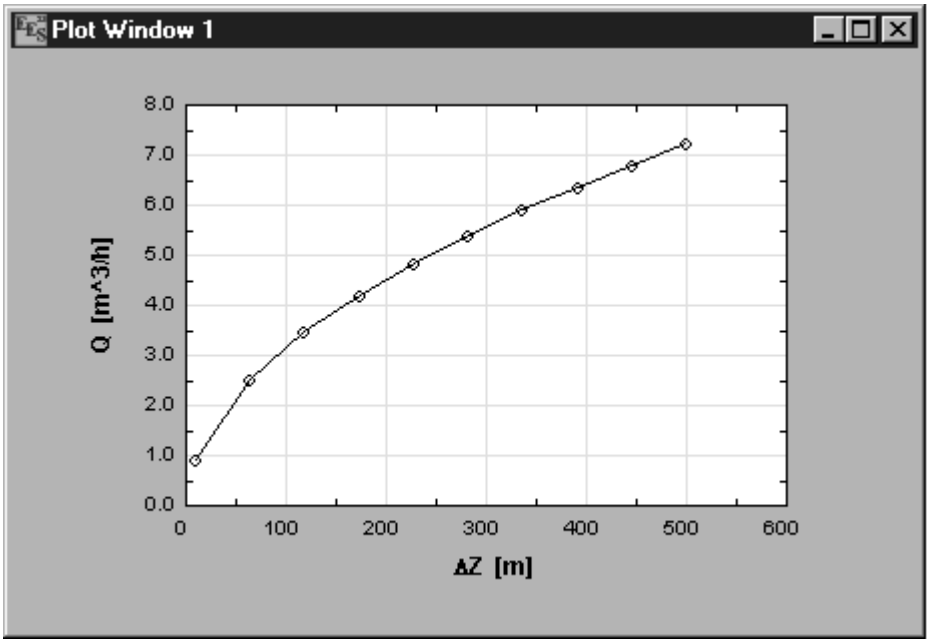


Fig. E.12 Plot window for flow rate versus elevation difference.

Loading a Textbook File

A problems disk developed for EES has been included with this textbook. Place the disk in the disk drive, and then select the **Load Textbook** command in the **File** menu. Use the **Windows Open File** command to open the textbook problem index file which, for this book, is named WHITE.TXB. A new menu called **Fluid Mechanics** will appear to the right of the **Help** menu. This menu will provide access to all the EES problem solutions developed for this book organized by chapter. As an example, select Chap. 6 from the **Fluid Mechanics** menu. A dialog window will appear listing the problems in Chap. 6. Select Problem 6.55—Flow Between Reservoirs. This problem is a modification (smooth instead of cast-iron pipe) of the problem you just entered. It provides a diagram window in which you can enter Δz. Enter other values, and then select the **Solve** command in the **Calculate** menu to see their effect on the flow rate.

At this point, you should explore. Try whatever you wish. You can't hurt anything. The on-line help (invoked by pressing F1) will provide details for the **EES** commands. EES is a powerful tool that you will find very useful in your studies.



ketabline.com Ebook.ketabline.com

Answers to Selected Problems

Chapter 1

1.2 1.3 E44 molecules
1.4 1.63 slug/ft^3, 839 kg/m^3
1.6 (*a*) $\{L^2/T^2\}$; (*b*) $\{M/T\}$
1.8 $\sigma \approx 1.00\ My/I$
1.10 Yes, all terms are $\{ML/T^2\}$
1.12 $\{B\} = \{L^{-1}\}$
1.14 $Q = \text{Const}\ B\ g^{1/2}H^{3/2}$
1.16 All terms are $\{ML^{-2}T^{-2}\}$
1.18 $V = V_0e^{-mt/K}$
1.20 $z_{\max} = 64.2$ m at $t = 3.36$ s
1.22 (*a*) $-0.372U_\infty^2/R$; (*b*) $x = -1.291\ R$
1.24 $e = 221{,}000$ J/kg
1.26 $W_{\text{air}} = 0.71$ lbf
1.28 $\rho_{\text{wet}} = 1.10$ kg/m^3, $\rho_{\text{dry}} = 1.13$ kg/m^3
1.30 $W_{1\text{-}2} = 21$ ft · lbf
1.32 (*a*) 76 kN; (*b*) 501 kN
1.34 1300 atm
1.36 (*a*) $B_{N_2O} = 1.33$ E5 Pa; (*b*) $B_{\text{water}} = 2.13$ E9 Pa
1.38 $\tau = 1380$ Pa, $\text{Re}_L = 28$
1.40 $A = 0.0016$ kg/(m · s), $B = 1903$ K
1.42 $\mu/\mu_{200\text{K}} \approx (T\ \text{K}/200\ \text{K})^{0.68}$
1.44 Data 50 percent higher; Andrade fit varies ±50 percent
1.46 $V \approx 15$ m/s
1.48 $F \approx (\mu_1/h_1 + \mu_2/h_2)AV$
1.50 $\mu \approx M(r_o - r_i)/(2\pi\Omega r_i^3 L)$
1.52 $P \approx 73$ W
1.54 $M \approx \pi\mu\Omega R^4/h$
1.56 $\mu = 3M \sin\theta/(2\pi\Omega R^3)$
1.58 $\mu = 0.040$ kg/(m · s), last 2 points are *turbulent* flow
1.60 $\mu = 0.88 \pm 0.023$ kg/(m · s)
1.62 28,500 Pa
1.64 (*a*) −0.023 m; (*b*) + 0.069 m
1.66 $F = 0.014$ N
1.68 $h = (\Upsilon/\rho g)^{1/2} \cot\theta$
1.70 $h = 2\Upsilon \cos\theta/(\rho gW)$
1.72 $z \approx 4800$ m
1.74 Cavitation occurs for both (*a*) and (*b*)
1.76 $z \approx 7500$ m
1.78 (*a*) 25°C; (*b*) 4°C
1.80 $x^2y - y^3/3 = \text{constant}$
1.82 $y = x \tan\theta + \text{constant}$
1.84 $x = x_0\{\ln(y/y_0) + \ln^2(y/y_0)\}$

Chapter 2

2.2 $\sigma_{xy} = -289$ lb/ft^2, $\tau_{AA} = -577$ lb/ft^2
2.4 $x = \text{Const}\ e^{-2Cz/B}$
2.6 (*a*) 30.3 ft; (*b*) 30.0 in; (*c*) 10.35 m; (*d*) 13,100 mm
2.8 DALR = 9.77°C/km
2.10 10,500 Pa
2.12 8.0 cm
2.14 74,450 Pa with air; 75,420 Pa without air
2.16 (*a*) 21,526 cm^3; (*b*) 137 kPa
2.18 1.56
2.20 14 lbf
2.22 0.94 cm
2.24 $p_{\text{sealevel}} \approx 117$ kPa, $m_{\text{exact}} = 5.3$ E18 kg
2.26 (*a*) 2580 m; (*b*) 5410 m
2.28 4400 ± 400 ft
2.30 101,100 Pa
2.32 22.6 cm
2.34 $\Delta p = \Delta h[\gamma_{\text{water}}(1 + d^2/D^2) - \gamma_{\text{oil}}(1 - d^2/D^2)]$
2.36 25°
2.38 (*a*) $p_{1,\text{gage}} = (\rho_m - \rho_a)gh - (\rho_t - \rho_a)g\text{H}$
2.40 21.3 cm
2.42 $p_A - p_B = (\rho_2 - \rho_1)gh$
2.44 (*a*) 171 lb/ft^2; (*b*) 392 lb/ft^2; manometer reads friction loss



ketabline.com Ebook.ketabline.com

2.46 1.45
2.48 $F = 39700$ N
2.50 (*a*) 524 kN; (*b*) 350 kN; (*c*) 100 kN
2.52 0.96
2.54 879 kg/m^3
2.56 16.08 ft
2.58 0.40 m
2.60 $F_{net} = 23{,}940$ N at 1.07 m above B
2.62 10.6 ft
2.64 1.35 m
2.66 $F = 1.18$ E9 N, $M_C = 3.13$ E9 N · m counterclockwise, no tipping
2.68 18,040 N
2.70 4490 lbf at 1.44 ft to right and 1.67 ft up from point B
2.72 33,500 N
2.74 $F = ba^2\rho_0\{(a^2/g)[\exp(gh/a^2) - 1] - h\}$
2.76 $P = (\gamma/24)h^2b(3 + \csc^2\theta)$
2.78 $P = \pi\gamma R^3/4$
2.80 (*a*) 58,800 Pa; (*b*) 0.44 m
2.82 $F_H = 97.9$ MN, $F_V = 153.8$ MN
2.84 $F_H = 4895$ N, $F_V = 7343$ N
2.86 $F_H = 0$, $F_V = 6800$ lbf
2.88 $F_H = 176$ kN, $F_V = 31.9$ kN, yes
2.90 467 lbf
2.92 $F_{\text{one bolt}} \approx 11{,}300$ N
2.94 $C_x = 2996$ lb, $C_z = 313$ lbf
2.96 (*a*) 940 kN; (*b*) 1074 kN; (*c*) 1427 kN
2.98 $F_H = 7987$ lbf, $F_V = 2280$ lbf
2.100 $F_H = 0$, $F_V = 297$ kN
2.102 124 kN
2.104 5.0 N
2.106 4310 N/m^3
2.108 12.6 N
2.110 $h \approx$ (*a*) 7.05 mm; (*b*) 7.00 mm
2.112 (*a*) 39 N; (*b*) 0.64
2.114 0.636
2.116 19100 N/m^3
2.118 (*a*) draft = 7.24 in; (*b*) 25 lbf
2.120 34.3°
2.122 $a/b \approx 0.834$
2.124 6850 m
2.126 $h/H = Z - (Z^2 - 1 + \beta)^{1/2}$, $\beta = d/H$, $Z = (2 + \lambda - \beta)/2$, $\lambda = p_a/(\rho gH)$
2.128 Yes, stable if $S > 0.789$
2.130 Slightly unstable, MG = −0.007 m
2.132 Stable if $R/h > 3.31$
2.134 (*a*) unstable; (*b*) stable
2.136 $MG = L^2/(3\pi R) - 4R/(3\pi) > 0$ if $L > 2R$
2.138 2.77 in deep; volume = 10.8 fluid ounces
2.140 $a_x =$ (*a*) −1.96 m/s^2 (deceleration); (*b*) −5.69 m/s^2 (deceleration)
2.142 (*a*) 16.3 cm; (*b*) 15.7 N
2.144 (*a*) $a_x \approx 319$ m/s^2; (*b*) no effect, $p_A = p_B$
2.146 Leans to the right at $\theta = 27°$
2.148 Leans to the left at $\theta = 27°$
2.150 5.5 cm; linear scale OK
2.152 (*a*) 224 r/min; (*b*) 275 r/min
2.154 (*a*) both are paraboloids; (*b*) $p_B = 2550$ Pa (gage)
2.157 77 r/min, minimum pressure halfway between B and C
2.158 10.57 r/min

Chapter 3

3.2 **r** = position vector from point O
3.6 $Q = (2b/3)(2g)^{1/2}[(h + L)^{3/2} - (h - L)^{3/2}]$
3.8 $Q = K$ per unit depth
3.10 $(\pi/3)R^2\rho U_0 c_p T_w$
3.12 (*a*) 44 m^3/h; (*b*) 9.6 m/s
3.14 $dh/dt = (Q_1 + Q_2 - Q_3)/(\pi d^2/4)$
3.16 $Q_{top} = 3U_0 b\delta/8$
3.18 (*b*) $Q = 16bhu_{max}/9$
3.20 (*a*) 7.97 mL/s; (*b*) 1.27 cm/s
3.22 (*a*) 0.06 kg/s; (*b*) 1060 m/s; (*c*) 3.4
3.24 $h = [3Kt^2d^2/(8\tan^2\theta)]^{1/3}$
3.26 $Q = 2U_0bh/3$
3.28 $t = \pi(1 - 1/\sqrt{3})h_0^{1/2}/(2CA\sqrt{2g})$
3.30 (*a*) $dh/dt = Q/(2hb \cot 20°)$
3.32 $V_{hole} = 6.1$ m/s
3.34 $V_2 = 4660$ ft/s
3.36 $U_3 = 6.33$ m/s
3.38 $V = V_0 r/(2h)$
3.40 500 N to the left
3.42 $F = (p_1 - p_a)A_1 - \rho_1 A_1 V_1^2[(D_1/D_2)^2 - 1]$
3.44 $F = \rho U^2 Lb/3$
3.46 $\alpha = (1 + \cos\theta)/2$
3.48 $V_0 \approx 2.27$ m/s
3.50 102 kN
3.52 $F = \rho WhV_1^2[1/(1 - \sin\theta) - 1]$ to the left
3.54 163 N
3.56 2.45 N/m
3.58 40 N
3.60 2100 N
3.62 3100 N
3.64 980 N
3.66 8800 N
3.70 91 lbf
3.72 Drag ≈ 4260 N
3.74 $F_x = 0$, $F_y = -17$ N, $F_z = 126$ N
3.76 77 m/s
3.80 $F = (\rho/2)gb(h_1^2 - h_2^2) - \rho h_1 bV_1^2(h_1/h_2 - 1)$
3.82 25 m/s
3.84 23 N
3.86 274 kPa



ketabline.com Ebook.ketabline.com

3.88 $V = \zeta + [\zeta^2 + 2V_j]^{1/2}$, $\zeta = \rho Q/2k$
3.90 $dV/dt = g$
3.92 $dV/dt = gh/(L + h)$
3.94 $h = 0$ at $t \approx 70$ s
3.96 $d^2Z/dt^2 + 2gZ/L = 0$
3.100 (*a*) 507 m/s and 1393 m; (*b*) 14.5 km
3.102 $h_2/h_1 = -\frac{1}{2} + \frac{1}{2}[1 + 8V_1^2/(gh_1)]^{1/2}$
3.104 $\Omega = (-V_e/R) \ln (1 - \dot{m}t/M_0)$
3.106 $\Omega_{\text{final}} = 75$ rad/s
3.108 (*a*) $V = V_0/(1 + CV_0t/M)$, $C = \rho bh(1 - \cos\theta)$
3.110 (*a*) 0.113 ft · lbf; (*b*) 250 r/min
3.112 $T = \dot{m}R_0^2\Omega$
3.114 (*a*) 414 r/min; (*b*) 317 r/min
3.116 $P = \rho Q r_2 \omega[r_2\omega - Q \cot\theta_2/(2\pi r_2 b_2)]$
3.118 $P = \rho Q u V_n(\cot\alpha_1 + \cot\alpha_2)$
3.120 (*a*) 22 ft/s; (*b*) 110 ft/s; (*c*) 710 hp
3.122 $L = -h_1 (\cot\theta)/2$
3.124 41 r/min
3.126 −15.5 kW (work done *on* the fluid)
3.128 1.07 m^3/s
3.130 34 kW
3.134 4500 hp
3.136 5.6 m^3/h
3.138 $\mu = \pi\rho g d^4(H + \bar{L})/(128\bar{L}Q) - \alpha_2\rho Q/(16\pi\bar{L})$
3.140 1640 hp
3.142 (*a*) 1150 gal/min; (*b*) 67 hp
3.144 26 kW
3.146 $h = 3.6$ ft
3.148 $h_f = 0.21$ m
3.152 (*a*) 85.9°; (*b*) 55.4°
3.154 $h = 0.133$ m
3.156 (*a*) 102 kPa; (*b*) 88 mi/h
3.158 (*a*) 169.4 kPa; (*b*) 209 m^3/h
3.160 (*a*) 31 m^3/s; (*b*) 54 kW
3.162 $Q = 166$ ft^3/min, $\Delta p = 0.0204$ lbf/in^2
3.164 (*a*) 5.25 kg/s; (*b*) 2.9 cm
3.166 (*a*) 60 mi/h; (*b*) 1 atm
3.168 $h = 1.08$ ft
3.170 $h = 1.76$ m
3.172 $D = 0.132$ ft
3.174 (*a*) 5.61 ft/s; (*b*) further constriction *reduces* V_2
3.176 (*a*) 9.3 m/s; (*b*) 68 kN/m
3.178 $h_2 = 2.03$ ft (subcritical) or 0.74 ft (supercritical)
3.180 $V = V_f \tanh(V_f t/2L)$, $V_f = (2gh)^{1/2}$
3.182 $kp/[(k - 1)\rho] + V^2/2 + gz =$ constant

Chapter 4

4.2 (*a*) $du/dt = (2V_0^2/L)(1 + 2x/L)$
4.4 At (2, 1), $dT/dt = 125$ units
4.6 (*a*) $6V_0^2/L$; (*b*) $L \ln 3/(2V_0)$
4.8 (*a*) 0.0196 V^2/L; (*b*) at $t = 1.05\ L/U$
4.12 If $v_\theta = v_\phi = 0$, $v_r = r^{-2}$ fcn (θ, ϕ)
4.14 $v_\theta =$ fcn(r) only
4.16 $v = y^2 - 3x^2y +$ fcn(x, z)
4.18 $\rho = \rho_0 L_0/(L_0 - Vt)$
4.20 $v = v_0 =$ const, $\{K\} = \{L/T\}$, $\{a\} = \{L^{-1}\}$
4.22 $\rho_{x=L} = 1.82$ kg/m^3
4.28 Exact solution for any a or b
4.30 $p =$ const $- (\rho K^2/2)(x^2 + y^2)$
4.32 $f_1 = C_1 r$; $f_2 = C_2/r$
4.34 $p = p(0) - 4\mu u_{\max} z/R^2$
4.36 $C = \rho g \sin\theta/(2\mu)$
4.38 $C_z = \tau_{yx} - \tau_{xy}$
4.42 $T_{\text{mean}} \approx (\int uT\, dy)/(\int u\, dy)$
4.48 $\psi = Kxy +$ const
4.50 Inviscid flow around a 180° turn
4.52 $\psi = -4Q\theta/(\pi b)$
4.54 $Q = ULb$
4.60 Irrotational, $z_0 = H - \omega^2R^2/(2g)$
4.62 $\psi = Vy^2/(2h) +$ const
4.66 $\psi = -K \sin\theta/r$
4.68 $\psi = m \tan^{-1}[2xy/(x^2 - y^2 + a^2)]$
4.70 $\phi = \lambda \cos\theta/r^2$, $\lambda = 2am$
4.72 (*a*) 8.8m; (*b*) 55 m
4.74 $\psi = Uy + K \ln r$
4.76 (*a*) 0.106 m from A; (*b*) 0.333 m above the wall
4.78 (*a*) $V_{\text{wall,max}} = m/\bar{L}$; (*b*) $p_{\min}$ at $x = \bar{L}$
4.80 (*a*) $w = (\rho g/2\mu)(2\delta x - x^2)$
4.82 Obsessive result: $v_\theta = \Omega R^2/r$
4.84 $v_z = (\rho g b^2/2\mu) \ln(r/a) - (\rho g/4\mu)(r^2 - a^2)$
4.86 $Q = 0.0031$ m^3/(s · m)
4.88 $v_z = U \ln(r/b)/[\ln(a/b)]$
4.90 $F \approx 3.34$ N

Chapter 5

5.2 1.21 m
5.4 $V = 1.55$ m/s, $F = 1.3$ N
5.6 $F \approx 450$ N
5.10 (*a*) $\{ML^{-2}T^{-2}\}$; (*b*) $\{MLT^{-2}\}$
5.14 $\delta/x = fcn\ (\rho Ux/\mu)$
5.16 Stanton number $= h/(\rho V c_p)$
5.18 $Q\mu/[(\Delta p/L)b^4] =$ const
5.20 $P/(\rho\Omega^3D^5) =$ fcn$[Q/(\Omega D^3), \rho\Omega D^2/\mu]$
5.22 $\Omega D/V =$ fcn$(N, H/L)$
5.24 $F/(\rho V^2L^2) =$ fcn$(\alpha, \rho VL/\mu, L/D, V/a)$
5.26 (*a*) indeterminate; (*b*) $T = 2.75$ s
5.28 $\delta/L =$ fcn$[L/D, \rho VD/\mu, E/(\rho V^2)]$
5.30 $hL/k =$ fcn$(\rho UL/\mu, \mu c_p/k)$
5.32 $Q/(bg^{1/2}H^{3/2}) =$ const
5.34 $k_{\text{hydrogen}} \approx 0.182$ W/(m · K)



ketabline.com Ebook.ketabline.com

5.36 (*a*) $Q_{loss}R/(A\Delta T)$ = constant
5.38 d/D = fcn($\rho UD/\mu$, $\rho U^2D/Y$)
5.40 h/L = fcn($\rho gL^2/Y$, α, θ)
5.44 (*a*) $\{\sigma\} = \{L^2\}$
5.48 $F \approx 0.17$ N; (doubling U quadruples F)
5.50 (*a*) $F/(\mu UL)$ = constant
5.52 $U \approx 5$ ft/s, $F \approx 0.003$ lbf/ft
5.54 Power ≈ 7 hp
5.56 $V \approx 128$ ft/s = 87 mi/h
5.58 $V \approx 2.8$ m/s
5.60 Prototype power ≈ 157 hp
5.62 $\Omega_{max} \approx 26.5$ r/s; $\Delta p \approx 22{,}300$ Pa
5.64 $\omega_{aluminum} = 0.77$ Hz
5.66 (*a*) $V = 27$ m/s; (*b*) $z = 27$ m
5.68 (*a*) $F/(\mu U)$ = constant; (*b*) No, not plausible
5.70 $F = 87$ lbf
5.72 $V = 25$ ft/s
5.74 Prototype moment = 88 kN · m
5.76 Drag = 107,000 lbf
5.78 Weber no. ≈ 100 if $L_m/L_p = 0.0090$
5.80 (*a*) 1.86 m/s; (*b*) 42,900; (*c*) 254,000
5.82 Speeds: 19.6, 30.2, and 40.8 ft/s;
Drags: 14,600; 31,800; and 54,600 lbf
5.84 $V_m = 39$ cm/s; $T_m = 3.1$ s; $H_m = 0.20$ m
5.88 At 340 W, $D = 0.109$ m
5.90 $\Delta pD/(\rho V^2L) = 0.155(\rho VD/\mu)^{-1/4}$

Chapter 6

6.2 (*a*) $x = 2.1$ m; (*b*) $x = 0.14$ m
6.4 (*a*) 39 m^3/h; (*b*) 1.3 m^3/h
6.6 (*a*) laminar; (*b*) laminar
6.8 (*a*) −3600 Pa/m; (*b*) −13,400 Pa/m
6.10 (*a*) from *A* to *B*; (*b*) $h_f = 7.8$ m
6.18 (*a*) 0.054 m^3/s; (*b*) 8.5 m/s; (*c*) 122 Pa; (*d*) 542 kPa
6.20 (*a*) 0.204 m; (*b*) −19,800 Pa/m; (*c*) −9980 Pa/m
6.22 (*a*) 39 kg/s; (*b*) 1430
6.24 Head loss ≈ 25 m
6.26 4 mm
6.28 $Q \approx 0.31$ m^3/h
6.30 $F = 4$ N
6.32 (*a*) 127 MPa; (*b*) 127 kW
6.34 $\mu = 0.000823$ kg/(m · s)
6.36 $\Delta p \approx 65$ Pa
6.38 (*a*) 19.3 m^3/h; (*b*) flow is *up*
6.40 (*a*) flow is up; (*b*) 1.86 m^3/h
6.44 $h_f \approx 10.5$ m, $\Delta p \approx 1.4$ MPa
6.46 Input power ≈ 11.2 MW
6.48 $r/R = 1 - e^{-3/2}$
6.50 (*a*) −4000 Pa/m; (*b*) 50 Pa; (*c*) 46 percent
6.52 $p_1 = 2.38$ MPa
6.54 $D \approx 0.118$ m
6.56 (*a*) 188 km; (*b*) 27 MW
6.58 Power ≈ 870 kW
6.64 $Q = 19.6$ m^3/h (laminar, Re = 1450)
6.66 (*a*) 56 kPa; (*b*) 85 m^3/h; (*c*) $u = 3.3$ m/s at $r = 1$ cm
6.68 Power = 204 hp
6.70 $Q = 2.21$ ft^3/s
6.72 Optimum $\theta = 90°$ (0.7 m rise)
6.74 $D = 0.52$ in
6.76 $Q = 15$ m^3/h
6.78 $Q = 25$ m^3/h (to the left)
6.80 $Q = 0.905$ m^3/s
6.82 $D = 0.394$ m
6.84 $D \approx 0.104$ m
6.86 (*a*) 3.0 m/s; (*b*) 0.325 m/m; (*c*) 2770 Pa/m
6.90 $Q = 19.6$ ft^3/s
6.92 (*a*) 1530 m^3/h; (*b*) 6.5 Pa (vacuum)
6.94 260 Pa/m
6.96 Cross section 0.106 m by 0.531 m
6.98 Approximately 128 squares
6.102 (*a*) 5.55 hp; (*b*) 5.31 hp with 6° cone
6.104 $\Delta p = 0.0305$ lbf/in^2
6.106 $Q = 0.0296$ ft^3/s
6.108 $Q = 0.22$ ft^3/s
6.110 840 W
6.112 $Q = 0.0151$ ft^3/s
6.114 (*a*) $Q_1 = 0.0167$ m^3/s, $Q_2 = 0.0193$ m^3/s, $\Delta p = 774$ kPa
6.116 $Q = 0.027$ m^3/s
6.118 $\Delta p = 131$ lbf/in^2
6.120 $Q_1 = 0.0109$ m^3/s, $Q_2 = 0.0264$ m^3/s, $Q_3 = 0.0183$ m^3/s
6.122 Increased ϵ/d and L/d are the causes
6.124 $Q_1 = -2.09$ ft^3/s, $Q_2 = 1.61$ ft^3/s, $Q_3 = 0.49$ ft^3/s
6.126 $\theta_{opening} = 35°$
6.128 $Q_{AB} = 3.47$, $Q_{BC} = 2.90$, $Q_{BD} = 0.58$, $Q_{CD} = 5.28$, $Q_{AC} = 2.38$ ft^3/s (all)
6.130 $Q_{AB} = 0.95$, $Q_{BC} = 0.24$, $Q_{BD} = 0.19$, $Q_{CD} = 0.31$, $Q_{AC} = 1.05$ ft^3/s (all)
6.132 $2\theta = 6°$, $D_e = 2.0$ m, $p_e = 224$ kPa
6.134 $2\theta = 10°$, $W_e = 8.4$ ft, $p_e = 2180$ lbf/ft^2
6.136 (*a*) 25.5 m/s, (*b*) 0.109 m^3/s, (*c*) 1.23 Pa
6.138 46.7 m/s
6.140 $\Delta p = 273$ kPa
6.142 $Q = 18.6$ gal/min, $d_{reducer} = 0.84$ cm
6.144 $Q = 54$ m^3/h
6.146 (*a*) 0.00653 m^3/s; (*b*) 100 kPa
6.148 (*a*) 1.58 m; (*b*) 1.7 m
6.150 $\Delta p = 27$ kPa
6.152 $D = 4.12$ cm
6.154 $h = 59$ cm



ketabline.com Ebook.ketabline.com

6.156 $Q = 0.924$ ft^3/s
6.158 (*a*) 49 m^3/h; (*b*) 6200 Pa

Chapter 7

7.2 $\text{Re}_c = 1.5$ E7
7.4 $d = 8$ mm lies in the transition region
7.6 $H = 2.5$ (versus 2.59 for Blasius)
7.8 Approximately 0.08 N
7.12 Does not satisfy $\partial^2 u/\partial y^2 = 0$ at $y = 0$
7.14 $C = \rho v_0/\mu = \text{const} < 0$ (wall suction)
7.16 (*a*) F = 181 N; (*b*) 256 N
7.18 $\theta \approx 0.16°$; $F_{\text{drag}} \approx 0.024$ N
7.20 $x \approx 0.91$ m
7.22 $\psi = (\nu x \text{U})^{1/2} f(\eta)$
7.24 $h_1 = 9.2$ mm; $h_2 = 5.5$ mm
7.26 $F_a = 2.83\ F_1$, $F_b = 2.0\ F_1$
7.28 (*a*) $F_{\text{drag}} = 2.66\ N^2(\rho\mu L)^{1/2}U^{3/2}a$
7.30 (*a*) $F = 72$ N; (*b*) 79 N
7.32 $F = 0.0245\ \rho\nu^{1/7}\ L^{6/7}\ U_0{}^{13/7}\ \delta$
7.34 $F = 725$ N
7.36 7.2 m/s = 14 kn
7.38 (*a*) 7.6 m/s; (*b*) 6.2 m/s
7.40 $L = 3.53$ m, $b = 1.13$ m
7.42 $P_{4\text{ blades}} \approx 0.032\mu^{1/7}(\rho\text{C})^{6/7}\ \Omega^{20/7}\ R^{27/7}$
7.44 Accurate to about ±6 percent
7.46 $\epsilon \approx 9$ mm, $U = 11.2$ m/s = 22 kn
7.48 Separation at $x/L = 0.158$ (1 percent error)
7.50 Separation at $x/R = 1.80$ rad = 103.1°
7.52 $C_D\ (\text{Re}_{\bar{L}})^{1/2} \approx 2.67$ (by numerical integration)
7.54 Moment ≈ 200,000 N · m
7.56 (*a*) 10 N; (*b*) 80 N
7.58 (*a*) 3200 N/m; (*b*) 2300 N/m
7.60 Tow power = 140 hp
7.62 Square side length ≈ 0.83 m
7.64 $\Delta t_{1000-2000\text{m}} = 202$ s
7.68 (*a*) 34 m/s; (*b*) no, only 67 percent of terminal velocity at impact
7.70 (*a*) 642 ft; (*b*) 425 ft
7.72 (*a*) $L = 6.3$ m; (*b*) 120 m
7.78 $\Delta p = 100$ Pa
7.80 $\theta = 72°$
7.82 $V_{\text{min}} = 138$ ft/s; (*b*) $V_{\text{max}} = 377$ ft/s
7.84 $V = 9$ m/s
7.86 Approximately 3.05 m by 6.1 m
7.88 (*a*) 62 hp; (*b*) 86 hp
7.90 $V_{\text{overturn}} \approx 145$ ft/s = 99 mi/h
7.94 Torque $\approx (C_D/4)\rho\Omega^2 D R^4$, $\Omega_{\text{max}} = 85$ r/min
7.96 $\Omega_{\text{avg}} \approx 0.21\ U/D$
7.98 (*b*) $h \approx 0.18$ m
7.100 (*b*) $D_{\text{max}} = 78\ \mu$m
7.106 (*a*) 300 m; (*b*) 380 m
7.108 $\Delta x_{\text{ball}} \approx 13$ m
7.110 $\Delta y \approx 1.9$ ft
7.114 $V_{\text{final}} \approx 18.3$ m/s = 66 km/h
7.116 (*a*) 87 mi/h; (*b*) 680 hp
7.118 (*a*) 21 m/s; (*b*) 360 m
7.120 $(L/D)_{\text{max}} = 21$; $\alpha = 4.8°$
7.122 (*a*) 6.7 m/s; (*b*) 13.5 m/s = 26 kn
7.124 $\Omega_{\text{crude theory}} \approx 340$ r/s

Chapter 8

8.2 $\Gamma = \pi\Omega(R_2^2 - R_1^2)$
8.4 No, $1/r$ is not a proper two-dimensional potential
8.6 $\psi = B(y^2 - x^2)$
8.8 $\Gamma = 4B$
8.12 $\Gamma = 0$
8.14 Irrotational outer, rotational inner; minimum $p = p_\infty - \rho\omega^2 R^2$ at $r = 0$
8.18 From afar: a single source $4m$
8.20 Vortex near a wall (see Fig. 8.17*b*)
8.22 Same as Fig. 8.6 except upside down
8.24 $C_p = -\{2(x/a)/[1 + (x/a)^2]\}^2$, $C_{p,\text{min}} = -1.0$ at $x = a$
8.26 $V_{\text{resultant}} = 9.4$ m/s at $\theta = 47°$
8.28 Creates a source in a square corner
8.34 Two stagnation points, at $x = \pm a/\sqrt{3}$
8.36 $U_\infty = 12.9$ m/s, $2L = 53$ cm, $V_{\text{max}} = 22.5$ m/s
8.42 $K/(U_\infty a) = 0.396$, $h/a = 1.124$
8.44 $K = 4.6$ m^2/s; (*a*) 218 kPa; (*b*) 214 kPa at upper shoulder, −6 kPa at lower shoulder (cavitation)
8.46 $F_{\text{1-bolt}} = 5000$ N
8.50 $h = 3a/2$, $U_{\text{max}} = 5U/4$
8.52 $V_{\text{boat}} = 10.2$ ft/s with wind at 44°
8.54 $F_{\text{parallel}} = 6700$ lbf, $F_{\text{normal}} = 2700$ lbf, power ≈ 560 hp (very approximate)
8.56 $C_D \approx 2.67$ (too high, incorrect p_{rear})
8.60 This is Fig. 8.15*a*, flow in a 60° corner
8.62 Stagnation flow near a "bump"
8.64 All favorable gradients: no separation
8.66 $\lambda = 0.45m/(5m + 1)$ if $U = Cx^m$
8.68 Flow past a Rankine oval
8.70 Applied to wind-tunnel "blockage"
8.72 Adverse gradient for $x > a$
8.74 $V_{B,\text{total}} = (8K\mathbf{i} + 4K\mathbf{j})/(15a)$
8.78 Need an infinite array of images
8.82 (*a*) 4.5 m/s; (*b*) 1.13; (*c*) 1.26 hp
8.84 (*a*) 0.21; (*b*) 1.9°
8.86 (*a*) 26 m; (*b*) 8.7; (*c*) 1600 N
8.88 $\text{Thrust}_{\text{1-engine}} \approx 2900$ lbf
8.90 (*a*) 4.0; (*b*) 4.8°
8.92 (*a*) 0.77 m; (*b*) $V = 4.5$ m/s at $(r, \theta) = (1.81, 51°)$ and $(1.11, 88°)$
8.94 Yes, they are orthogonal



ketabline.com Ebook.ketabline.com

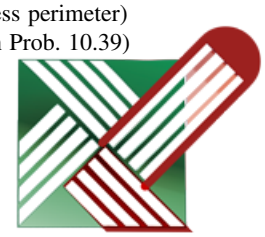
8.98 Yes, a closed teardrop shape appears
8.100 $V = 14.1$ m/s, $p_A = 115$ kPa
8.102 (*a*) 1250 ft; (*b*) 1570 ft (crudely)

Chapter 9

9.2 (*a*) $V_2 = 450$ m/s, $\Delta s = 515$ J/(kg · K); (*b*) $V_2 = 453$ m/s, $\Delta s = 512$ J/(kg · K)
9.4 About 50 m/s
9.6 Exit at about $T_2 \approx 54°C$ and $V_2 \approx 1445$ m/s
9.8 410 K
9.10 Ma = 0.78
9.12 (*a*) 2.13 E9 Pa and 1460 m/s; (*b*) 2.91 E9 Pa and 1670 m/s; (*c*) 2645 m/s
9.18 (*a*) 930 ft/s; (*b*) 878 ft/s
9.20 (*a*) air: 144 kPa and 995 m/s; (*b*) helium: 128 kPa and 2230 m/s
9.22 (*a*) 267 m/s; (*b*) 286 m/s
9.24 (*b*) at Ma ≈ 0.576
9.28 (*a*) 0.17 kg/s; (*b*) 0.90
9.30 (*a*) 262 m/s; (*b*) 0.563; (*c*) 0.905 kg/m^3
9.32 (*a*) 141 kPa; (*b*) 101 kPa; (*c*) 0.706
9.34 (*a*) 0.00424 slug/s; (*b*) 0.00427 slug/s
9.40 (*a*) 2.50; (*b*) 7.6 cm^2; (*c*) 1.27 kg/s; (*d*) $\text{Ma}_2 = 1.50$
9.42 (*a*) Ma = 0.90, $T = 260$ K, $V = 291$ m/s
9.44 $V_e = 5680$ ft/s, $p_e = 15.7$ psia, $T_e = 1587°$R, thrust = 4000 lbf
9.46 $R_x = -8$ N (to the left)
9.48 (*a*) 313 m/s; (*b*) 0.124 m/s; (*c*) 0.00331 kg/s
9.50 (*a*) $D_{\text{exit}} = 5.8$ cm
9.52 (*a*) 5.9 cm^2; (*b*) 773 kPa
9.54 $\text{Ma}_2 = 0.648$, $V_2 = 279$ m/s, $T_2 = 461°$K, $p_2 = 458$ kPa, $p_{02} = 607$ kPa
9.56 At about $A_1 \approx 24.7$ cm^2
9.58 (*a*) 306 m/s; (*b*) 599 kPa; (*c*) 498 kPa
9.60 Upstream: Ma = 1.92, $V = 585$ m/s
9.62 $C = 19{,}100$ ft/s, $V_{\text{inside}} = 15{,}900$ ft/s
9.64 (*a*) 0.150 kg/s; (*b*, *c*) 0.157 kg/s
9.66 $h = 1.09$ m
9.68 $p_{\text{atm}} = 92.6$ kPa; max flow = 0.140 kg/s
9.70 (*a*) 388 kPa; (*b*) 19 kPa
9.72 Mass flow = 0.5 kg/s, $p_e = 185$ kPa, $\text{Ma}_e = 0.407$
9.74 (*a*) 1.096 MPa; (*b*) 2.24 kg/s
9.76 $\Delta t_{\text{shocks}} \approx 23$ s; $\Delta t_{\text{choking-stops}} \approx 39$ s
9.78 Case *A*: 0.0071 kg/s; *B*: 0.0068 kg/s
9.80 $A^* = 2.4$ E-6 ft^2 or $D_{\text{hole}} = 0.021$ in
9.82 $V_e = 110$ m/s, $\text{Ma}_e = 0.67$ (yes)
9.84 (*a*) 0.96 kg/s; (*b*) 0.27; (*c*) 435 kPa
9.86 $V_2 = 107$ m/s, $p_2 = 371$ kPa, $T_2 = 330$ K, $p_{02} = 394$ kPa
9.88 $L = 2$ m, yes, a shock at $\text{Ma}_2 = 2.14$
9.90 (*a*) 0.764 kg/s; (*b*) 0.590 kg/s; (*c*) 0.314 kg/s
9.92 (*a*) 0.45; (*b*) 2.04 kg/s
9.98 (*a*) 430; (*b*) 0.12; (*c*) 0.00243 kg/h
9.100 $L_{\text{pipe}} = 69$ m
9.102 Flow is choked at 0.69 kg/s
9.104 $p_{\text{tank}} = 99$ kPa
9.106 (*a*) 0.031 m; (*b*) 0.53 m; (*c*) 26 m
9.108 Mass flow drops by about 32 percent
9.112 (*a*) 105 m/s; (*b*) 215 kPa
9.116 $V_{\text{plane}} \approx 2640$ ft/s
9.118 $V = 204$ m/s, Ma = 0.6
9.120 *P* is 3 m ahead of the small circle, Ma = 2.0, $T_{\text{stag}} = 518$ K
9.122 $\beta = 23.13°$, $\text{Ma}_2 = 2.75$, $p_2 = 145$ kPa
9.126 (*a*) 25.9°; (*b*) 26.1°
9.128 $\delta_{\text{wedge}} \approx 15.5°$
9.130 (*a*) 57.87°; (*b*) 21.82°
9.132 (*a*) $p_A = 18.0$ psia; (*b*) $p_B = 121$ psia
9.134 $\text{Ma}_3 = 1.02$, $p_3 = 727$ kPa, $\phi = 42.8°$
9.136 (*a*) $h = 0.40$ m; (*b*) $\text{Ma}_3 = 2.43$
9.138 $p_r = 21.7$ kPa
9.140 $\text{Ma}_2 = 2.75$, $p_2 = 145$ kPa
9.142 (*a*) $\text{Ma}_2 = 2.641$, $p_2 = 60.3$ kPa; (*b*) $\text{Ma}_2 = 2.299$, $p_2 = 24.1$ kPa
9.146 $\Delta\theta = 9.47°$ (helium)
9.148 $C_L = 0.184$ (approximately linear), $C_D = 0.0193$ (approximately parabolic)
9.150 (*a*) $\alpha = 4.10°$; (*b*) drag = 2150 N/m
9.152 Parabolic shape has 33 percent more drag

Chapter 10

10.2 (*a*) $C = 3.31$ m/s; (*b*) $\delta V = 0.030$ m/s
10.4 These are piezometer tubes (no flow)
10.6 (*a*) Fr = 3.8; (*b*) $V_{\text{current}} = 7.7$ m/s
10.8 $\Delta t_{\text{travel}} = 6.3$ h
10.10 $\lambda_{\text{crit}} = 2\pi(\text{Y}/\rho g)^{1/2}$
10.14 Flow must be fully rough turbulent (high Re) for Chézy to be valid
10.16 20 percent less flow, independent of *n*
10.18 $y_n = 0.993$ m
10.20 $Q = 74$ ft^3/s
10.22 $S_0 = 0.00038$ (or 0.38 m/km)
10.24 $y_n = 0.56$ m
10.26 (*a*) 17.8 m^3/s; (*b*) 1.79 m
10.30 $\Delta t \approx 32$ min
10.32 74,000 gal/min
10.34 If $b = 4$ ft, $y = 9.31$ ft, $P = 22.62$ ft; if $b = 8$ ft, $y = 4.07$ ft, $P = 16.14$ ft
10.36 $y_2 = 3.6$ m
10.38 $D_{\text{semicircle}} = 2.67$ m (16 percent less perimeter)
10.42 $P = 41.3$ ft (71 percent more than Prob. 10.39)
10.44 Hexagon side length $b = 2.12$ ft
10.46 Best $h_0/b = 0.53 \pm 0.03$



ketabline.com Ebook.ketabline.com

10.48 (*a*) 0.00634; (*b*) 0.00637
10.50 (*a*) 2.37; (*b*) 0.62 m; (*c*) 0.0026
10.52 $W = 2.06$ m
10.54 (*a*) 1.98 m; (*b*) 3.11 m/s; (*c*) 0.00405
10.56 (*a*) 1.02 m^3/s; (*b*) 0.0205
10.58 $Fr = 0.628R^{1/6}$, R in meters
10.60 (*a*) 0.052 $m^3/(m \cdot s)$; (*b*) 0.0765 m
10.64 $h_{max} \approx 0.35$ m
10.66 (*a*) 1.47; (*b*) $y_2 = 1.19$ m
10.70 (*a*) 0.15 m; (*b*) 3.2; (*c*) 0.59 $m^3/(s \cdot m)$
10.72 (*a*) 0.046 m; (*b*) 4.33 m/s; (*c*) 6.43
10.76 $H \approx 0.011$ m
10.78 $\Delta t \approx 8.6$ s (crude analysis)
10.80 (*a*) 3.83 m; (*b*) 4.83 $m^3/(s \cdot m)$
10.82 (*a*) 0.88 m; (*b*) 17.6 m/s; (*c*) 2.89 m
10.84 $y_2 = 0.82$ ft; $y_3 = 5.11$ ft; 47 percent
10.86 (*a*) 6.07 m/s; (*b*) $\Delta V = 2.03$ m/s
10.88 (*a*) downstream; (*b*) 5.7 percent
10.90 0.0207 (or 1.19°)
10.92 (*a*) 3370 ft^3/s; (*b*) 7000 hp
10.94 (*a*) 0.61 m; (*b*) 3.74 m/s; (*c*) 0.89 m
10.98 (*a*) steep S-3; (*b*) S-2; (*c*) S-1
10.106 No entry depth leads to critical flow
10.108 (*a*, *b*) Both curves reach $y \approx y_n \approx 0.5$ m at $x = 250$ m
10.110 (*a*) $y_{crest} \approx 0.782$ m; (*b*) $y(L) \approx 0.909$ m
10.112 M-1 curve, with $y = 2$ m at $L \approx 214$ m
10.114 Vexing! Flow chokes at $Q \approx 17$ m^3/s
10.116 $Q \approx 9.51$ m^3/s
10.120 $Y = 0.64$ m, $\alpha = 34°$
10.122 5500 gal/min
10.124 M-1 curve, $y = 10$ ft at $x = -3040$ ft
10.126 At $x = -100$ m, $y = 2.81$ m
10.128 At 300 m upstream, $y = 2.37$ m

Chapter 11

11.6 This is a diaphragm pump
11.8 (*a*) $H = 112$ ft and $\Delta p = 49$ lb/in^2; (*b*) $H = 112$ ft (of gasoline); $P = 15$ hp
11.10 (*a*) 1300 r/min; (*b*) 2080 lbf/in^2
11.12 (*a*) 11.3 m; (*b*) 1520 W
11.14 1870 W
11.16 (*a*) 1450 W; (*b*) 1030 r/min
11.18 $V_{vane} = (1/3)V_{jet}$ for max power
11.20 (*a*) 2 roots: $Q = 7.5$ and 38.3 ft^3/s; (*b*) 2 roots; $H =$ 180 ft and 35 ft
11.22 (*a*) BEP ≈ 92 percent at $Q \approx 0.22$ m^3/s
11.26 Correlation is "fair," not geometrically similar
11.28 BEP at about 6 ft^3/s; $N_s \approx 1430$, $Q_{max} \approx 12$ ft^3/s
11.30 (*a*) 1700 r/min; (*b*) 8.9 ft^3/s; (*c*) 330 ft
11.32 Correlation "fair," not geometrically similar
11.34 (*a*) 11.5 in; (*b*) 28 hp; (*c*) 100 ft; (*d*) 78 percent
11.36 $D = 9.8$ in, $n = 2100$ r/min
11.38 (*a*) 18.5 hp; (*b*) 7.64 in; (*c*) 415 gal/min; (*d*) 81 percent
11.40 (*a*) $D_s = D(gH^*)^{1/4}/Q^{*1/2}$
11.42 $NPSH_{proto} \approx 23$ ft
11.44 No cavitation, required depth is only 5 ft
11.46 $D_s \approx C/N_s$, $C = 7800 \pm 7$ percent
11.52 (*a*) 7.97 m^3/s; (*b*) 14.6 kW; (*c*) 28.3°
11.54 Centrifugal pumps, $D \approx 7.2$ ft
11.56 (*a*) $D = 5.67$ ft, $n = 255$ r/min, $P = 700$ hp; (*b*) $D = 1.76$ ft, $n = 1770$ r/min, $P = 740$ hp
11.58 Centrifugal pump, $\eta = 67$ percent, $D = 0.32$ ft
11.60 (*a*) 623; (*b*) 762 gal/min; (*c*) 1.77 ft
11.62 $D = 18.7$ ft, $\Delta p = 1160$ Pa
11.64 *No* speed is able to get to BEP
11.66 $Q \approx 1240$ ft^3/min
11.68 $Q_{new} \approx 15{,}300$ gal/min
11.70 (*a*) 212 ft; (*b*) 5.8 ft^3/s
11.72 (*a*) 10 gal/min; (*b*) 1.3 in
11.74 (*a*) 14.9; (*b*) 15.9; (*c*) 20.7 kgal/min
11.76 $D_{pipe} \approx 1.70$ ft
11.78 $D_{pipe} \approx 1.67$ ft, $P \approx 2000$ hp
11.80 $Q_{32} \approx 22{,}900$ gal/min; $Q_{28} \approx 8400$ gal/min, $H \approx 343$ ft for both
11.84 Two turbines: (*a*) $D \approx 9.6$ ft; (*b*) $D \approx 3.3$ ft
11.86 $N_{sp} \approx 70$, hence Francis turbines
11.88 $Q \approx 52$ ft^3/s, $D \approx 10.5$ ft
11.90 $P \approx 800$ kW
11.92 Pelton and Francis wheels both OK
11.94 (*a*) 71 percent; (*b*) $N_{sp} \approx 19$
11.96 (*a*) 1.68 ft; (*b*) 0.78 ft
11.100 (*a*) 190 kW; (*b*) 24 r/min; (*c*) 9.3 ft/s
11.102 $Q \approx 29$ gal/min



ketabline.com Ebook.ketabline.com

Index

A

Acceleration of a particle, 15, 90, 216
  centripetal, 90, 157
  convective, 216
  Coriolis, 157
  local, 216
Ackeret airfoil theory, 635–636
Acoustics, 573
Actuator disk theory, 752–753
Added mass, 539–540
Adiabatic flow, 578–579
  atmospheric lapse rate, 102, 105
  with friction, 604–606, 776–780
Adverse pressure gradient, 430, 445–448, 501
Aerodynamic forces and moments, 452–453
  NACA designs, 471, 528–530, 565
Air-cushion vehicle, 206
Airfoil description, 468, 529
Airfoil theory, 523–534
  finite-span, 530–534
  supersonic flow, 632–637
  thick-cambered, 528–530
  thin-plate, 524–528
Andrade's equation, 49
Anemometer
  cup, 387, 485
  hot-wire and film, 387, 389
Angle of attack
  definition, 468
  in inviscid flow, 499, 517
Angular momentum theorem, 130, 158–159, 230
Angular velocity of a fluid, 246–247
Annulus
  flow in, 362–364
  laminar friction factors, 364
Answers to selected problems, 806–812
Archimedes' laws of buoyancy, 44, 84
Area, body reference, 453
Area change in a duct, 583–587
Aspect ratio
  of a diffuser, 384
  of a wing, 472, 473, 530
Atmosphere
  isothermal, 68
  U. S. standard, 69, 773
Automobile drag forces, 461–463
Average velocity, 143, 26
  in pipe flow, 144, 341, 344, 346
Avogadro's number, 46
Axial-flow pumps, 730–734
Axisymmetric potential flow, 534–540

B

Backwater curve, 693–695
Barometer, 66–67
Basic equations (*see* Differential equations of flow)
Basic laws of fluid motion, 35, 129–131
Bend losses, 371



ketabline.com Ebook.ketabline.com

Bernoulli, Daniel, 10, 174
Bernoulli constant, 176, 248
Bernoulli obstruction meters, 397–404
Bernoulli's equation, 10, 174–177, 230, 248–249
  outside a boundary layer, 435
  compared to the energy equation, 176, 580
  for irrotational flow, 230, 249, 496
  for isentropic flow, 580–581
  limitations and assumptions, 176, 177
  in rotating coordinates, 717
  for unsteady flow, 175, 248, 249, 496
Betz number, 753
BG units, 8
Bingham-plastic fluid, 28
Blasius flat-plate solution, 437–439, 478
Blasius pipe friction formula, 345
Blowdown analysis, 598, 643
Blower, 711
Blunt-body flows, 429
Body forces, 61, 224
Bore in a channel, 702
Boundary conditions, 34, 234–236
  for a boundary layer, 436
  free surface or interface, 234–236, 497
  at an inlet or outlet, 234, 496
  for inviscid flow, 496, 497
  kinematic, 235
  no-slip, 24, 34, 234
Boundary-element method, 546–548
Boundary layer, 23, 45, 250, 431, 496, 578
  displacement thickness, 433, 438, 443
  equations of, 434–436
  on a flat plate, 153–155, 266
  momentum thickness, 431, 438
  with pressure gradient, 445–450
  with rough walls, 443–444
  separation, 435, 447, 447–449
  shape factor, 438, 443, 448
  thickness, 428, 442
  transition, 298, 432, 439
Bourdon tube gage, 99–100
Brinkman number, 268
Broad-crested weir, 689, 690
Buckingham pi theorem, 280, 286–288
Bulk modulus, 49, 102, 577
  of various liquids, 772
Bump, channel flow over, 675–676
Butterfly valve, 370
Buoyancy, 84–86
Buoyant force, 85

C

Cambered airfoil, 468, 471, 528–530
Capillary effect, 31, 299–300
Cauchy-Riemann equations, 249
Cavitation, 32–33, 552
  of a pump, 720, 721
  of a turbine, 765
Cavitation erosion, 33
Cavitation number, 32, 294, 297
Center of buoyancy, 85, 88
Center of mass, 80
Center of pressure, 75–76
  of an airfoil, 527, 636
Centrifugal pump, 161–162, 200, 714–718
  dimensionless coefficients, 724–726
  performance curves, 720–723, 758, 759
  similarity rules, 727–729
Centripetal acceleration, 90, 157
Centroid, 75
  of various cross-sections, 76
Channel flow (*see* Open channel flow)
Chézy coefficient, 665
Chézy formulas, 664–666
Choked flow, 586, 598, 740
  due to friction, 608–609
  due to heat transfer, 617
  in an open channel, 676
Chord line, 452, 468
Circular section
  open channel, 668–669
  pipe flow, 338–357
Circulation, 499
  at airfoil trailing edge, 524
  on a cylinder, 509, 511
Classification of flow, 36–37
Colebrook pipe-friction formula, 348
Complex-variable potential theory, 516–521



ketabline.com Ebook.ketabline.com

Composite channel flows, 687–688
Compressibility criterion, 35, 221, 571
Compressible flow, 220, 315, 571
  with area change, 583–587, 774–776
  with friction, 603–613, 780–784
  with heat transfer, 613–618, 784–788
  tables, 774–788
Compressor, 711, 740–741
Computational fluid dynamics, 3, 434, 465, 540–555, 735–736
  commercial codes, 552–553
Concentric cylinder flows, 261–263
Cone flow, supersonic, 638
Conformal mapping, 516, 562
Conical diffuser, 373, 386
Conjugate depths, 699
Conservation laws, 35, 130–131
  for angular momentum, 130, 158–159
  for energy, 131, 163–165, 231
  for linear momentum, 130, 146
  for mass, 130, 141–146
  for salt or species, 35, 315
Consistent units, 11–13
Contact angle, 30–31
Continuity, equation of, 218
  cylindrical polar form, 219–220, 793
  incompressible flow, 220
  spherical polar form, 265
  turbulent flow, 334
Continuum, 6–7
Contraction losses, 372, 374
Control section of a channel, 687, 693
Control surface, 136
Control volume, 36, 133
  arbitrary but fixed, 135–136
  deformable, 137–138, 140
  differential-sized, 218
  guidelines for selection, 183
  moving, 133, 137, 152
  one-dimensional, 134–135
Convective acceleration, 15–16
Converging-diverging nozzle, 600–603
Converging nozzle, 598–600
Conversion factors, 8–9, 791–792
Coriolis acceleration, 156, 157, 250
Corner flow, inviscid, 242, 518–519
Correlations, turbulent, 334
Corresponding states, law of, 24
Couette flow
  between cylinders, 261–263
  instability of, 262–263
  between plates, 25–26, 258–259
  nonnewtonian, 272
Couple, concentrated, 268
Creeping motion, 25, 298, 315, 317, 328, 483
  past a sphere, 47, 457, 483
Critical channel flow, 671–674
Critical depth, 664, 672
Critical Reynolds number, 329–330
Critical slope of a channel, 674
Critical sonic-point properties, 581, 605
Critical state, 6, 24
Crossflow turbine, 764
Crump weir, 705
Cup anemometer, 387, 485
Cup-mixing temperature, 268
Curl of a vector, 247
Current meter, 387, 389
Curved surface, force on, 79–82
Curvilinear coordinate system, 267
Cylinder
  array of, 515
  in inviscid flow, 245, 508–510
  rotating, 512
  in viscous flow, 261–263, 295–296, 298, 455
Cylindrical coordinates, 219
  equations of motion, 793–794

D

da Vinci, Leonardo, 44, 143
d'Alembert paradox, 45, 510
Darcy friction factor, 340, 342, 344, 604
Darcy's law of porous flow, 420
Darcy-Weisbach equation, 340, 664
Decimal prefixes, 13
Deformable control volume, 133, 137
Deformation of a fluid el
Del operator, 216, 219



ketabline.com Ebook.ketabline.com

Density
  definition of, 6, 17
  of various fluids, 771–772
Detached shock wave, 624
Diaphragm transducer, 101
Differential equations of flow, 36, 215, 682, 793
  angular momentum, 230
  continuity or mass, 217–221
  cylindrical coordinates, 793–794
  energy, 231–233
  incompressible, 220, 228, 236–237
  linear momentum, 62, 223–227
Diffuser flows, 313, 381–385, 447
  head loss, 373
  performance maps, 385, 386
  separation and stall, 383, 447–448
  stability map, 382
  subsonic versus supersonic, 584
Digital computer (*see* Computational fluid dynamics)
Dilatant fluid, 28
Dimensional analysis, 7, 12, 277
  of the basic equations, 292–294
  of the boundary conditions, 293–294
  of pipe flow, 307–309
  pitfalls of, 305–307
  of turbomachines, 724–726, 744
Dimensional homogeneity, 11–12, 280
  nonhomogeneity, 285–286
Dimensional matrix, 313
Dimensionless groups, list of, 297
Dimensions, 7–13, 278
  list of, 8–9, 287
Discharge coefficient, 12, 179, 181, 398
  flow nozzle, 401
  orifice plate, 399–400
  sluice gate, 677
  venturi, 401, 402
  weir, 690–692
Displacement thickness, 433
  for a flat plate, 433, 438, 443
Dissipation function, 233
  of a hydraulic jump, 680
Divergence of a vector, 220, 226
Dot product, 133
Doublet
  line, 270, 505–506
  point, 536
Downwash on a wing, 531, 532
Draft tube, 765
Drag, 452–467
  biological adaptation, 467–468
  induced, 472, 533
Drag coefficient, 195, 297, 453, 468, 632
  of airfoils, 457, 468, 471–473
  of a cylinder, 298, 455, 457
    rotating, 511–512
  on a flat plate, 438, 442–443
  at high Mach numbers, 465–466
  of road vehicles, 461–463
  of a sphere, 298, 456, 457
    spinning, 487, 488
  of surface ships, 464–465
  of three-dimensional bodies, 457, 460
  of two-dimensional bodies, 457–458
Drag reduction, 456, 462, 464
Drowned channel flow, 678, 701
Duct flow, 325, 603
  compressible, with friction, 603–613, 780
    with heat transfer, 613–618, 784
Dynamic similarity, 304–305

E

Eckert number, 297
Eddy viscosity, 406
Effective duct diameter, 360
Efficiency, 47, 715
  of an open channel, 669–671
  of a turbomachine, 715, 734
  volumetric, 716, 757
  of wind turbines, 753
Elbows, losses in, 368, 369
Elliptical wing, 533
Energy, 18, 131, 163
Energy equation, 163–165, 231–233
  steady flow, 167–168
Energy flux, 165, 231
Energy grade line, 177–178, 339 672



ketabline.com Ebook.ketabline.com

Engineering Equation Solver (EES), 41
Enthalpy, 19, 165, 574
Entrance length, 331
Entrance losses, 331, 371, 372
Entrance region, 330–331
Entropy, of an ideal gas, 574
Entropy change, 574
  across a normal shock, 591
  across a weak oblique shock, 627
Equations of motion (*see* Differential equations of flow)
Equilibrium of forces, 61–62
Equivalent length, minor losses, 367
Erosion of particles, 313, 698
Euler, Leonhard, 45, 174, 294
Euler number, 294, 297
Euler turbine equations, 161–162, 717
Eulerian description, 14, 216
Euler's equation, 227, 237, 247
Exit pipe loss, 371, 372
Expansion losses, 372–373
Explicit numerical model, 549
External flow, 333, 427, 451–467

F

Falling-body problem, 12
  dimensional analysis of, 282–285, 289
Fanno line, 648
Favorable pressure gradient, 430, 445–447, 495, 502
Film of fluid draining
  down an inclined plane, 268
  down a vertical cylinder, 272
  down a vertical plate, 271
Finite-difference method, 541–543
Finite-element method, 541
Finite-span wings, 472–473, 530–534
First law of thermodynamics, 131, 163
Fittings, losses in, 368
Flap, airfoil, 471, 472, 474
Flat-plate flow,153–155, 428, 431–433
  Blasius solution, 437–439, 478
  integral theory,
    laminar, 432
    turbulent, 441–444
  normal to the stream, 457–459, 519–521
  with rough walls, 443–444
Flettner rotorship, 511–512, 559
Floating element shear measurement, 480
Flooding of channels, 698
Flow between plates, 25–27, 258–260, 359–360
Flow coefficient of a meter, 398
Flow meters (*see* Fluid meters)
Flow net, 497
Flow nozzle, 399, 400–401
Flow straighteners, 479
Flow visualization, 40, 426, 470, 515, 554
Fluctuation, turbulent, 326, 333–334
Fluid, definition of, 4
Fluid meters, 385–404
  Coriolis type, 395, 396
  electromagnetic, 389
  flow nozzle, 399, 400–401
  head losses, 402
  hot-wire, hot-film, 387, 389
  laminar-flow element, 396–397
  laser-doppler, 387, 389–390
  obstruction type, 397–404
  orifice plate, 398–400
  pitot-static tube, 387, 388–389
  rotameter, 395
  Savonius rotor, 387, 486
  turbine type, 392–393
  ultrasonic, 394–395
  venturi meter, 399, 401–402
  volume flow type, 391
  vortex type, 393–394
Fluid properties, 769–773
Force coefficient, 278, 310
Forces
  hydrostatic, 74–84
  on a turning vane, 150–151
Fourier's law of conduction, 27, 231
Francis turbine, 742
Free-body concept, 77, 133
Free overfall, 687, 688
Free-streamline theory, 5
Free-surface flows, 4–5,



ketabline.com Ebook.ketabline.com

Free vortex, 253
Friction drag, 154, 453
Friction losses, 168
Friction factor, 42, 340, 342, 604
  compressible flow, 606
Friction factor—*Cont.*
  laminar pipe-flow, 342
  noncircular ducts, 364, 365
  rocky channels, 665
  turbulent pipe-flow, 345, 348
Friction velocity, 336
Frictionless flow, 227, 495, 613
Frontal area, 453, 462
Froude, William, 45, 294
Froude number, 294, 297, 465–466, 662, 679, 683
Froude scaling laws, 303–304
Fully developed flow, 258, 330–331
Fully rough flow
  in channels, 665
  on a flat plate, 443–444
  in pipes, 347, 348
Fundamentals of Engineering (FE) Exam, 43

G

Gage pressure, 63, 77, 148
Gages, pressure, 97–101
Gas constant, 19, 573
  of various gases, 772
Gas dynamics (*see* Compressible flow)
Geometric similarity, 301–303
  violation of, 302, 303, 307
Glide angle, 489
Gradient operator, 61, 216, 219
Gradual contraction loss, 374
Gradual expansion loss, 373
Gradually varied flow, 662, 682–687
  classification, 683–685
  effect of width changes, 704
Grashof number, 297
Gravity
  acceleration of, 9, 64
  variation with radius, 65
Gravity force on an element, 61, 224
Grid, numerical, 542, 549, 553, 564

H

Hagen, G. L. H., 329
Hagen-Poiseuille flow, 341
Half-body, plane, 256–258, 501–502
  axisymmetric, 537–538
Halocline, 120
Hazen-Williams formula, 47, 285
Head loss, 168, 340, 661
  of a hydraulic jump, 680
  minor, 367–375
  in pipe flow, 340
Heat addition, flow with, 613–618, 784–788
Heat conduction equation, 233
Heat flux through an element, 232
Heat transfer coefficient, 312
Hele-Shaw flow, 513–514
Herschel-type venturi, 401
High-lift devices, 474
History of fluid mechanics, 44–46, 280
Hodograph for an oblique shock, 623, 624
Homologous points, 302, 727
Honeycomb flow straightener, 408
Horseshoe vortex, 555
Hot-wire or hot-film anemometer, 387, 389
Hydraulic diameter, 358, 363, 661
Hydraulic efficiency, 716
Hydraulic grade line, 177–178, 339, 659
Hydraulic jump, 198–199, 664, 678–681, 702
  classification, 679
  sloping, 702
Hydraulic model, 307
Hydraulic radius, 13, 358, 661
Hydraulically smooth wall, 347
Hydrodynamic mass, 539–540
Hydrogen bubble technique, 34
Hydrometer, 118
Hydrostatic condition, 4, 59, 62, 63
  in gases, 67–69
  in liquids, 65–66



ketabline.com Ebook.ketabline.com

Hydrostatic forces
on curved surfaces, 79–83
in layered fluids, 82–84
laboratory apparatus, 127
on plane surfaces, 74–79
Hydrostatic pressure distribution, 63–65
Hypersonic flow, 572, 639

I

Icebergs, 89–90
Ideal gas (*see* Perfect-gas law)
Images, 521–522
Implicit numerical model, 550
Impulse turbines, 745–749
Incompressible flow, 17, 142–143, 220, 236, 572
Induced drag, 533
Inertial coordinate system, 156
Initial conditions, 234
Integral equations (*see* Control volume)
Intensity of turbulence, 334, 405
Interface, 29
Internal energy, 18, 574
Internal flow, 330
Inviscid flow, 36, 496
Irrotational flow, 230, 247–249, 496
frictionless, 247, 579–582
Isentropic flow, 579–582, 529
with area change, 583–587, 774
compared to Bernoulli's equation, 580–581
tables, 774–776
Isentropic process, 574
Isothermal duct flow, 610–611
Isovelocity contours, 660

J

Jet exit pressure condition, 149
Jet flow, laminar and turbulent, 326–327
Jet pump, 189, 712
Jet-turning vane, 150–151
Joukowski transformation, 562

K

Kaplan turbine, 742, 746, 749
Kármán momentum-integral relation, 154, 431
Kármán vortex street, 295–296
Kelvin oval, 513–514
Kinematic properties, 15
Kinematic similarity, 303–304, 498
Kinematic viscosity, 24
of various fluids, 24, 770–772
Kinetic energy, 18, 164
correction factor, 170–171
Kline-Fogleman airfoil, 473, 474
Kutta condition, 523–524
Kutta-Joukowski lift theorem, 510–511

L

Lagrangian description, 14
Laminar flow, 34, 326, 327, 551
in a concentric annulus, 346–364
between parallel plates, 25–27, 258–260, 359–360
in a pipe, 341–344
between rotating cylinders, 261–263
Laplace's equation, 239, 251, 496, 497, 516, 793
numerical simulation, 541–543
in polar coordinates, 498, 564, 793
Lapse rate, 68
Large-eddy simulation, 554
Laser-Doppler anemometer, 387, 389
Law-of-the-wall, 336
Lawn sprinkler analysis, 163
Layered fluids, 70, 82–84
Lift
definition of, 452, 468
in flow past a cylinder,



ketabline.com Ebook.ketabline.com

Lift coefficient
of airfoils, 470–474, 527, 529–530, 533
supersonic, 632–637
definition, 297, 468, 632
maximum, 473, 528
of a rotating cylinder, 511–512
of a rotating sphere, 488
Lift-drag polar plot, 472
Lifting line theory, 532
Lifting vane, 150–151, 469
Linear momentum, 130, 146–158, 223–227
Liquids versus gases, 4–6
Local acceleration, 216
Local mass-flow function, 586–587
Logarithmic velocity profile, 336, 344
Loss
minor, 367–375
in pumps, 723
Lubricating oil properties, 769, 770, 772
Lubrication theory, 271

M

Mach angle, 619
Mach cone, 619
Mach number, 35, 221, 295, 297, 306, 572, 579, 592
effect on body drag, 467
Mach waves, 594, 618–621, 628
analogy to water waves, 663, 673, 681
Magnus effect, 510
Manifold flow, 422–423
Manning, Robert, 13, 665
Manning roughness factor, 13, 285, 665
for various channels, 667
Manometer, 70–73, 97, 99
two-fluid differential, 72, 108
Mass, units of, 8
Mass flow, 133, 142, 586, 599, 611
in choked flow, 586
MATLAB contouring, 506
Mean free path of a gas, 7, 46
Meniscus, 74
Metacenter, 87
Metacentric height, 87, 88
Meter (*see* Fluid meters)
Minor losses in pipe flow, 367–375
Mixing-length theory, 406
Model-testing principles, 278, 301–307
pitfalls and discrepancies, 296–297
Mohr's circle, 4–5, 59
Molecular weight, 19, 573
of various gases, 772
Moment of inertia, 76, 88, 131
for various areas, 76
Momentum
angular, 130, 158, 230
linear, 130, 146–148, 223–227
Momentum flux, 147, 224
correction factor, 155–156
Momentum integral theory, 155, 431–433, 448
Momentum thickness, 431
for a flat plate, 438, 442
Thwaites' parameter, 448
Moody chart, 349, 443, 606, 665
Moody pump-size formula, 728
Moving shock wave, 595–596
Multiple-pipe systems, 375–381

N

NACA airfoils, 470–471, 528, 567
Nappe, 687, 689
Natural convection, 312, 315, 573
Navier-Stokes equations, 45, 228, 789
nonuniqueness of, 263
Net positive suction head, 721–722
Network, piping, 380–381
Neutral buoyancy, 86, 386
Newton, Sir Isaac, 23, 45, 577
Newtonian fluid, 23, 227–228
Newton's second law, 8, 130, 146
for a fluid element, 62, 216, 224
in noninertial coordinates, 156–158
No-slip condition, 24, 34, 234, 259, 262, 340
No-temperature-jump condition, 34,
Noncircular duct flow, 357–366



ketabline.com Ebook.ketabline.com

Nondimensionalization (*see* Dimensional analysis)
Noninertial coordinate system, 156–158
Nonnewtonian fluids, 28, 272
Nonwetting liquid, 30, 31
Normal channel depth, 662, 667
Normal shock wave, 590–595, 618
  tables, 776–780
Normal stresses, 225
Nozzle flow, 598–601
  analogy with a sluice gate, 664, 677
  choked, 586, 600
  converging-diverging, 600–603
  design conditions, 600–601
Nozzle flow—*Cont.*
  subsonic versus supersonic, 584
Numerical analysis, 3, 434, 540–555
  instability, 549
  of inviscid flow, 540–548
  of open-channel flow, 685–687
  of pumps, 735–736
  of viscous flow, 548–555

O

Oblique shock wave, 620, 621–628, 789–790
  reflection of, 651
One-dimensional approximation, 134–135, 138, 147, 165, 583, 660–661
One-seventh power-law, 439, 442, 479
Open channel flow, 236, 659
  analogy with gas dynamics, 663, 664, 673, 677, 681
  classification of, 662–664
  critical flow, 671–674
  gradually varied flow, 682–687
  most efficient section, 669–671
  over weirs, 687–693
Orifice plate, 398–400
Orthogonality conditions, 249, 497–498, 516
Outer layer, turbulent, 335–336
Overlap layer, 335–336, 441
Overrelaxation, 543

P

Parallel plates, 26, 258–259, 359–360
Pascal unit, 9, 11
Pascal's law, 71
Pathline, 37–38
Pelton wheel turbine, 745, 747
Perfect-gas law, 19, 35, 67, 573, 585
Permeability of porous media, 315, 420
Physical properties of fluids, 769–773
Pi theorem, 286–288
Piezometer, 103
Pipe flow, 328, 338–357
  bend loss, 371
  compressible, 604–613, 780–788
  flow rate determination, 352–355
  head loss or pressure drop, 307, 339, 351
  laminar, 341–344
  minor losses, 367–375
  in a network, 380–381
  noncircular, 357–366
  in parallel, 376–378
  with rough walls, 346–349
  in series, 375–376
  sizing problem, 355–357
  turbulent, 344–348
Pipe standard sizes, 357
Pipelines, 168, 610
Pitching moment, 452, 527
Pitot-static tube, 387, 388, 642
Planform area, 299, 453, 468
Pode's angle, 487
Poiseuille, J. L. M., 10, 341
Poiseuille flow, 260, 341–342
Poisson's ratio, 577
Polar coordinates, 220, 243, 498, 499
Polar drag plot, 472
Positive-displacement pump, 711–714, 757
Potential energy, 18, 164
Potential flow, 252–257, 497
  analog methods, 513–515
  axisymmetric, 534–540
  complex variable, 516–521
  numerical analysis, 540–548
Potential lines, 248, 498
Potential vortex, 253, 498



ketabline.com Ebook.ketabline.com

Power coefficient, 724, 753, 761
Power-law correlation, for pipe flow, 309, 345
  for velocity profile, 155, 439, 442, 479
  for viscosity, 27, 772
Power product method, 286
Power specific speed, 744
Prandtl, Ludwig, 2, 45, 434, 629
  flat-plate formulas, 479
  lifting line theory, 532
Prandtl-Meyer angle, 630, 788
Prandtl-Meyer expansion waves, 628–631, 788
Prandtl number, 297, 579
Prefixes for units, 13
Pressure, 17, 59–61
  absolute versus gage, 63
  at a point, 60
  stagnation, 312, 580
  vacuum, 63
  vapor, 31–32, 772, 773
Pressure coefficient, 297, 454, 526, 546
Pressure condition at a jet exit, 149
Pressure distribution, 62, 89
  hydrostatic, 63–65
  in irrotational flow, 249
  in a nozzle, 599, 601
  in rigid-body translation, 91–93
  in rotating rigid-body motion, 93–97
Pressure drop in pipes, 339, 345
Pressure drag, 453
Pressure force
  on a control volume, 147–148
  on a curved surface, 79–82
  on an element, 60–61
  on a plane surface, 74–79
Pressure gradient, 61, 96, 259, 341
  adverse and favorable, 430, 445–448, 501
Pressure head, 65, 102, 168
Pressure measurement, 97–101
Pressure recovery of a diffuser, 373, 382, 385, 386
Pressure transducers, 99–101
Primary dimensions, 8, 278
Principle of corresponding sates, 24–25
Principle of dimensional homogeneity, 10–11, 280
Problem-solving techniques, 44
Product of inertia, 76
Propeller turbine, 742, 746, 749
Properties of fluids, 769–773
Propulsion, rocket, 158
Prototype, 36, 278
Pseudoplastic fluid, 28
Pump-system matching, 735–740
Pump-turbine system, 203, 746
Pumps, 47, 711
  axial-flow, 729–733
  centrifugal, 161–162, 714–718
  dimensionless, 724
  effect of blade angle, 719
  effect of viscosity, 729, 730
  multistage, 740
  net positive-suction head, 721–722
  in parallel, 738–739
  performance curves, 204, 212, 714, 720–722, 733–735, 758, 759
  positive-displacement, 711–714
  in series, 739–740
  similarity rules, 727–728
  size effects, 728

R

Radius of curvature, 29, 235
Rankine half-body, plane, 256–258, 501–502
  axisymmetric, 537–538
Rankine oval, plane, 507–508
  axisymmetric, 563
Rankine-Hugoniot relations, 590
Rapidly varied channel flow, 662, 687
Rarefaction shock, 593, 624
Rayleigh line, 649
Reaction turbines, 742
Rectangular duct flow, 365, 366
Relative roughness, 349
Relative velocity, 137–138, 152
Reversible adiabatic flow (*see* Isentropic flow)
Reynolds, Osborne, 45, 294, 330
Reynolds number, 24, 278, 294, 297, 325, 427
  for an airfoil, 469
  local, 429
Reynolds pipe-flow experiment, 330
Reynolds time-averaging concept, 33



ketabline.com Ebook.ketabline.com

Reynolds transport theorem, 133–141
Rheology, 5, 28
Rheopectic fluid, 28
Rigid-body fluid motion, plane, 89–97
Rocket motion, 158
Rolling moment, 452
Rotameter, 395
Rotating cylinder, 512
  sphere, 488
Rotationality, generation of, 249–250
Rough-wall effects
  on channels, 665–667
  on cylinder drag, 298
  on a flat plate, 443–444
  on pipe flow, 346–348
  on pumps, 726
  sand-grain tests, 347
  on sphere drag, 321, 456
Roughness
  of commercial pipes, 349
  of open channels, 667

S

Salinity, 22
Sandgrain roughness, 347
Savonius rotor, 387, 486
Saybolt viscosity, 286
Scaling laws, 278–279, 304, 306
Scaling parameters, 282
Schedule-40 pipe sizes, 357
Seawater properties, 22, 772
Second law of thermodynamics, 131, 233, 606, 624, 679, 680
Secondary dimensions, 8–9
Secondary flow, 365–366
Separated flow, 429, 455, 456, 502
Separation bubble, 469
Separation point
  on an airfoil, 525
  on a cylinder, 455
  definition of, 447
  in a diffuser, 447
  in a laminar boundary layer, 449, 501–502
  on a sphere, 456
Shaft work, 164
Shape factor, 438, 443, 448
Sharp-crested weir, 689–690
Shear stresses, 4–5, 23, 225
  turbulent, 334
Shear work, 164
Shock-expansion theory, 632–637
Shock polar, 623, 624
Shock-tube wind tunnel, 598
Shock wave, 250, 591, 521
  detached, 624
  linearized, 626
  moving, 595–596
  normal, 590–595, 776–780
  oblique, 621–628, 789–790
  rarefaction, 593, 624
  strong versus weak, 624–626
Shut-off head of a pump. 719–720
SI units, 7–8
Silicon resonance transducer, 67, 101
Similarity, 279, 301
  dynamic, 304–305
  geometric, 301–303
  violations, 302, 303, 307
  kinematic, 303–304, 498
  for pumps, 727–728
Sink
  line, 253, 498, 563
  point, 536
Siphon, 208, 406
Skin friction coefficient, 432, 438, 441, 442, 449
Slip conditions in inviscid flow, 237
Sluice gate, 664, 677–678
  drowned, 678, 701
Smoke-flow visualization, 40, 470
Soap bubble, 29
Sonic boom, 620, 621
Sonic point, 581, 605
Source
  line, 253, 498, 517
  point, 536
Spar buoy, 119
Specific diameter, 760–761
Specific energy, 671–672
Specific gravity, 12, 18
Specific heat, 19–20, 573



ketabline.com Ebook.ketabline.com

Specific-heat ratio, 19, 295, 297, 572
of common gases, 21, 772
Specific speed, 730–731, 734, 735
Specific weight, 17
of common fluids, 65, 772
Speed of sound, 35, 221, 575–577
in the atmosphere, 773
of a perfect gas, 35, 577
of various materials, 577
of water, 577, 769
Sphere
inviscid flow, 265, 538–539
viscous flow, 298, 321, 456, 457, 483, 488
Spherical droplet, 29
Spherical polar coordinates, 265, 535–536
Stability of floating bodies, 86–89
Stability of a pump, 720, 763
Stability map of a diffuser, 382
Stagnation density, 580
Stagnation enthalpy, 167, 578, 614
Stagnation point, 38, 249, 252, 256, 519
plane flow near, 39–40, 265
Stagnation pressure, 312, 580
Stagnation properties, 578–580
Stagnation speed of sound, 579
Stagnation temperature, 579
Stall angle of attack, 528
Stall speed, 473
Stalled airfoil, 470
Standard atmosphere, 69, 773
Stanton number, 312
Starting vortex, 469
State, equation of, 16, 18, 67, 131, 234, 573
for gases, 18–20, 573–574
for liquids, 21–22
van der Waals, 642
Static-pressure measurement, 97
Steady-flow energy equation, 167–168, 578, 661
Stokes flow past a sphere, 47, 457, 483, 487
Stokes' stream function, 269, 535
Stopping vortex, 469
Strain rate, 23, 247
Stratified flow, 221, 250
Streakline, 37–38
Stream function, 238–244, 497
axisymmetric flow, 243–244, 535
compressible flow, 243
geometric interpretation, 240–241
irrotational flow, 239, 497
polar coordinates, 243
of Stokes, 269, 535
Streamline, 37–40, 240, 498
Streamline coordinates, 267
Streamlining of bodies, 456
Streamtube, 38, 143, 174
Stress gradients, 225
Stress tensor, 225, 227, 794
symmetry condition, 231
Strouhal number, 295, 296, 297
Subcritical channel flow, 663, 672
Subsonic flow, 572
Substantial derivative, 216
Suction specific speed, 731
Sudden expansion or contraction, 192–193, 371–372
Supercritical channel flow, 663, 672–673
Superposition of potential flows, 254–257, 500–501
Supersonic airfoil theory, 632–637
Supersonic flow, 149, 572, 618
Surface forces, 61, 225
Surface tension, 29–31, 235, 693
of air-water, 30, 773
of various interfaces, 29, 772
Sutherland-law viscosity formula, 27, 771
Swallow float, 86
System, 16, 130
System-matching of pumps, 735–740
Systems of units, 7

T

Tainter gate, 115
Takeoff analysis for aircraft, 475
Taylor number, 262
Taylor vortices, 263
Tee-junction losses, 368
Temperature
definition, 17
rise due to dissipation, 238
Terminal velocity, 309, 483



ketabline.com Ebook.ketabline.com

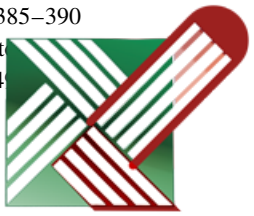
Thermal conductivity, 27, 231
Thermodynamic properties, 16, 131, 771–772
Thickness drag, supersonic, 635
Thin-airfoil theory, 524–527, 635
Thixotropic fluid, 28
Three-dimensional flow, 535–540, 637
  compressible, 637–640
Three-reservoir pipe junction, 376, 379
Throat in a duct, 585
Thwaites' integral method, 448–450
Time-averaging of turbulence, 333–334
Timeline, 37
Tornado flow model, 255, 501, 556
Torricelli's formula, 179
Total head, 168, 177
Trailing vortex, 469, 531–532
Transition to turbulence, 326–330
  in a boundary layer, 299, 432, 439
  on a flat plate, 405, 439
  in a jet exit stream, 327
  in pipe flow, 326, 328
  in sphere flow, 310, 405
Transitional roughness, 347
Transonic flow, 572
Transport properties, 16
Trapezoidal channel, 668, 670–671
Triangular duct flow, 365, 366
Tri-diagonal matrix, 550
Trip wire, 405
Troposphere, 68
Tube bundle, 412
Turbines, 742–749
  efficiency, 744, 748–749
  impulse, 745–749
  reaction, 742
  windmills, 750–754
Turbomachine classification, 711–714
Turbulent flow, 3, 34, 376
  on a flat plate, 441–444
  fluctuations 326, 333–334
  historical details, 328–330
  intensity, 405
  intermittency, 326
  numerical models, 552–553
  in a pipe, 328, 344–348
Turbulent puff, 328
Turbulent shear flow, 333–337
  logarithmic overlap layer, 335–337
  wall and outer layers, 335–336
Turbulent stresses, 334
Two-phase flow, 6, 219

U

Ultrasonic flowmeter, 394
Uncertainty of data, 42–43
Uncoupling of velocity and temperature, 236–237
Uniform channel flow, 662, 664–667
Uniform stream, 252–253, 498, 517, 536
Unit normal vector, 132, 136
U. S. Standard Atmosphere, 69, 773
Units, 7–10
Universal gas constant, 19, 573
Unsteady Bernoulli equation, 175, 248, 249, 496
Unsteady flow, 36, 40, 549
Upwind differencing, 552

V

V-notch weir, 692–693, 705
Vacuum pressure, 63
Valve flows, 12, 367–370
Van der Waals' equation, 642
Vane flow, 150–151
Vapor pressure, 31–32
  of various fluids, 772
  of water, 32, 773
Varied flow, 662, 682–687
Vector differentiation, 215–217
Velocity-defect law, 336
Velocity diagrams, 717, 732, 743
Velocity field, 14–15, 215
Velocity gradient, 23, 246
Velocity head, 168, 367
Velocity measurement, 385–390
Velocity of approach fact
Velocity potential, 248, 4



ketabline.com Ebook.ketabline.com

Velocity profile, 23, 34, 439, 449, 535
for the Blasius solution, 437, 439
Vena contracta, 391, 392, 397, 398, 678
VentureStar spacecraft, 639–640
Venturi flume, 704
Venturi meter, 180–181, 207, 399, 401–402
Virtual mass, 539–540
Viscometer, 50, 51, 203
Viscosity, 22–24
formula for liquids, 27
generalized chart, 25
Sutherland and power-law, 27, 772
of various fluids, 24, 769, 771–772
Viscous dissipation, 233
Viscous flow analysis, 258–263
Viscous force on an element, 226
Viscous stresses, 23, 225, 228
symmetry condition, 231
Viscous sublayer, 337–347
Viscous work, 164
Visualization of flow, 40
Volume expansion rate, 15
Volume flow, 132, 142
measurement of, 391–404
Von Kármán, Theodore, 45, 154, 406, 431, 567
Vortex, line, 253–254, 498, 503, 518
infinite row, 503–504
potential, 253, 498
starting and stopping, 469
trailing, 531–532
Vortex flowmeter, 393–394
Vortex shedding, 295–296
Vortex sheet, 504–505
for a thin airfoil, 524–527
Vorticity, 247

W

Wake flow, 190, 195, 250, 426, 429, 455
Wall roughness, 339–340
Wall shear stress, 341, 342, 438, 442
Waterline area, 88
Wave drag
of ships, 464–466
of supersonic bodies, 635
Wave motion, 494, 576, 663–664, 672
periodic, 696
Weber number, 294, 297, 693
Weirs, 47, 687–693
broad-crested, 689, 690
Crump type, 705
drowned, 196, 705
inviscid flow model, 560
sharp-crested, 689–690
Wetted area, 453, 465
Wetted perimeter, 358, 661
Wind turbines, 750–754
performance of, 753
typical designs, 751
world energy distribution, 754
Wing theory, two-dimensional, 523–534
finite span, 472, 530–534
Work, 164
due to viscous stresses, 232

X

X-33 spacecraft, 639–640

Y

Yawing moment, 452
Young's modulus, 577

Z

Zero-lift airfoil angle, 530
Zones of action and silence, 620, 672



ketabline.com Ebook.ketabline.com

StudyGuide for *Fluid Mechanics*

Preface

The following materials are provided as a study guide for the text *Fluid Mechanics* by Frank White. A brief summary of the key concepts and theory is presented for each chapter along with the final form of basic equations (without detailed derivations) used in the various analyses being presented. In most cases, a detailed explanation for the physical significance of each term in a fundamental governing equation is given (e.g., linear momentum, pg. III-8) to assist the student in identifying when a given term should be included in the analysis.

Example problems are provided for major sections. In each case, the starting general equation used in the solution is given followed by any necessary simplifications and the resulting complete solution. Where appropriate, the control volume and coordinate system used in the analysis are shown with the problem schematic. In many cases, an explanation is given with the final numerical answer to help the student understand the engineering significance of the answer (e.g., forces on curved surfaces, pg. II–18). In selected cases, computer based solutions to example problems are provided as an example to the student in the use of computer based problem solving techniques (e.g., parallel pipe sections, pg. VI-23).

For problems areas involving multiple steps in the solution, a summary of the steps used in a typical problem solution sequence is provided and enclosed in a boxed border (e.g., rigid body motion, pg. II-22). Areas where the author's experience has shown that mistakes in the analysis can easily occur are noted as **Key Points** (e.g., laminar flat plate boundary layer, pg. VII-5) throughout the material.

Finally, the author of this study guide appreciates the opportunity to contribute to the instructional materials provided with one of the leading texts in the area of fluid mechanics and to collaborate with an educator with whom he has long has the highest respect and had the privilege to further his education in fluid mechanics while a student at Georgia Tech.

Jerry R. Dunn, P.E.
Associate Professor,
Department of Mechanical Engineering
Texas Tech University



ketabline.com Ebook.ketabline.com

I. FLUID MECHANICS

I.1 Basic Concepts & Definitions:

Fluid Mechanics - Study of fluids at rest, in motion, and the effects of fluids on boundaries.

Note: This definition outlines the key topics in the study of fluids:

(1) fluid statics (fluids at rest), (2) momentum and energy analyses (fluids in motion), and (3) viscous effects and all sections considering pressure forces (effects of fluids on boundaries).

Fluid - A substance which **moves** and **deforms continuously** as a result of an **applied shear stress.**

The definition also clearly shows that viscous effects are not considered in the study of fluid statics.

Two important properties in the study of fluid mechanics are:

Pressure and Velocity

These are defined as follows:

Pressure - The **normal stress** on **any** plane through a fluid element **at rest.**

Key Point: The direction of pressure forces will **always** be perpendicular to the surface of interest.

Velocity - The rate of change of position at a point in a flow field. It is used not only to specify flow field characteristics but also to specify flow rate, momentum, and viscous effects for a fluid in motion.



ketabline.com Ebook.ketabline.com

I.4 Dimensions and Units

This text will use both the International System of Units (S.I.) and British Gravitational System (B.G.).

A key feature of both is that neither system uses g_c. Rather, in both systems the combination of units for mass * acceleration yields the unit of force, i.e. Newton's second law yields

S.I. 1 Newton (N) = 1 kg m/s^2 **B.G.** 1 lbf = 1 slug ft/s^2

This will be particularly useful in the following:

Concept	Expression	Units
momentum	$\dot{m}V$	kg/s * m/s = kg m/s^2 =N
		slug/s * ft/s = slug ft/s^2 = lbf
manometry	ρ g h	kg/m^3*m/s^2*m = (kg m/s^2)/ m^2 =N/m^2
		slug/ft^3*ft/s^2*ft = (slug ft/s^2)/ft^2 = lbf/ft^2
dynamic viscosity	μ	N s /m^2 = (kg m/s^2) s /m^2 = kg/m s
		lbf s /ft^2 = (slug ft/s^2) s /ft^2 = slug/ft s

Key Point: In the B.G. system of units, the mass unit is the slug and not the lbm. and 1 slug = 32.174 lbm. Therefore, be careful not to use conventional values for fluid density in English units without appropriate conversions, e.g., ρ_w = 62.4 lb/ft^3

For this case the manometer equation would be written as

$$\Delta P = \rho \frac{g}{g_c} h$$



ketabline.com Ebook.ketabline.com

Example:

Given: Pump power requirements are given by

$\dot{W}_p$ = fluid density*volume flow rate*g*pump head = ρ Q g h_p

For ρ = 1.928 slug/ft^3, Q = 500 gal/min, and h_p = 70 ft,

Determine: The power required in kW.

$\dot{W}_p$ = 1.928 slug/ft^3 * 500 gal/min*1 ft^3/s /448.8 gpm*32.2 ft/s^2 * 70 ft

$\dot{W}_p$ = 4841 ft$^-$lbf/s * 1.3558*10^{-3} kW/ft$^-$lbf/s = 6.564 kW

Note: We used the following: 1 lbf = 1 slug ft/s^2 to obtain the desired units

Recommendation: In working with problems with complex or mixed system units, at the start of the problem convert all parameters with units to the base units being used in the problem, e.g. for S.I. problems, convert all parameters to kg, m, & s; for BG problems, convert all parameters to slug, ft, & s. Then convert the final answer to the desired final units.

1.5 Properties of the velocity Field

Two important properties in the study of fluid mechanics are

Pressure and Velocity

The basic definition for velocity has been given previously, however, one of its most important uses in fluid mechanics is to specify both the volume and mass flow rate of a fluid.

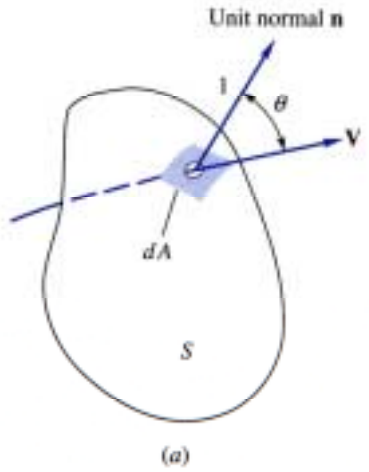


ketabline.com Ebook.ketabline.com

Volume flow rate:

$$\dot{Q} = \int_{cs} \bar{V} \cdot \bar{n}\, dA = \int_{cs} V_n\, dA$$

where V_n is the normal component of velocity at a point on the area across which fluid flows.



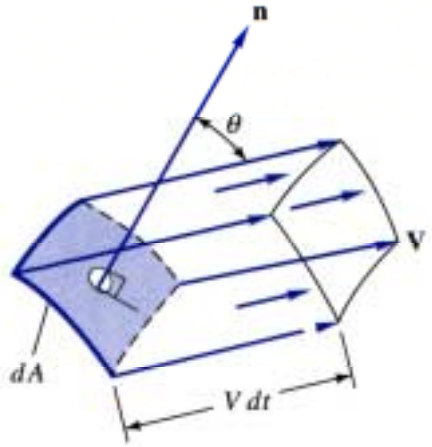
(a)

Key Point: Note that only the normal component of velocity contributes to flow rate across a boundary.

Mass flow rate:

$$\dot{m} = \int_{cs} \rho \bar{V} \cdot \bar{n}\, dA = \int_{cs} \rho V_n\, dA$$

NOTE: While not obvious in the basic equation, $\mathbf{V_n}$ must also be measured relative to any flow area boundary motion, i.e., if the flow boundary is moving, $\mathbf{V_n}$ is measured **relative to** the moving boundary.



(b)

This will be particularly important for problems involving moving control volumes in Ch. III.



ketabline.com Ebook.ketabline.com

1.6 Thermodynamic Properties

All of the usual thermodynamic properties are important in fluid mechanics

P - Pressure	(kPa, psi)
T- Temperature	(^{o}C, ^{o}F)
ρ ñ Density	(kg/m^3, slug/ft^3)

Alternatives for density

γ - specific weight = weight per unit volume (N/m^3, lbf/ft^3)

$\gamma = \rho\, g$ H_2O: $\gamma = 9790$ N/m^3 = 62.4 lbf/ft^3

Air: $\gamma = 11.8$ N/m^3 = 0.0752 lbf/ft^3

S.G. - specific gravity = ρ / ρ (ref)

where: ρ (ref) = ρ (water at 1 atm, 20˚C) for liquids = 998 kg/m^3

= ρ (air at 1 atm, 20˚C) for gases = 1.205 kg/m^3

Example: Determine the static pressure difference indicated by an 18 cm column of fluid (liquid) with a specific gravity of 0.85.

$\Delta P = \rho\, g\, h$ = S.G. $\gamma\, h$ = 0.85* 9790 N/m^3 0.18 m = 1498 N/m^2 = 1.5 kPa

I.7 Transport Properties

Certain transport properties are important as they relate to the diffusion of momentum due to shear stresses. Specifically:

$\mu \equiv$ coefficient of viscosity (dynamic viscosity) {M / L t }

$\nu \equiv$ kinematic viscosity (μ / ρ) { L^2 / t }



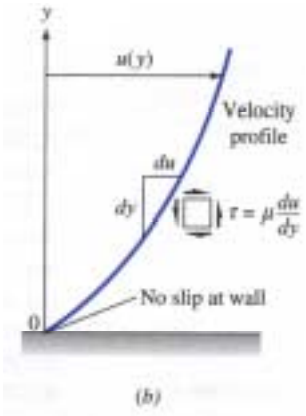
ketabline.com Ebook.ketabline.com

This gives rise to the definition of a Newtonian fluid.

Newtonian fluid: A fluid which has a **linear** relationship between shear stress and velocity gradient.

$$\tau = \mu \frac{dU}{dy}$$

The linearity coefficient in the equation is the coefficient of viscosity μ.



Flows constrained by solid surfaces can typically be divided into two regimes:

a. Flow near a bounding surface with
   1. significant velocity gradients
   2. significant shear stresses

   This flow region is referred to as a "**boundary layer**."

b. Flows far from bounding surface with
   1. negligible velocity gradients
   2. negligible shear stresses
   3. significant inertia effects

This flow region is referred to as "free stream" or "inviscid flow region."

An important parameter in identifying the characteristics of these flows is the

$$\text{Reynolds number} = \text{Re} = \frac{\rho V L}{\mu}$$

This physically represents the ratio of inertia forces in the flow to viscous forces. For most flows of engineering significance, both the characteristics of the flow and the important effects due to the flow, e.g., drag, pressure drop, aerodynamic loads, etc., are dependent on this parameter.



ketabline.com Ebook.ketabline.com

II. Fluid Statics

From a force analysis on a triangular fluid element at rest, the following three concepts are easily developed:
For a **continuous, hydrostatic, shear free** fluid:

1. Pressure is **constant** along a **horizontal plane**,
2. Pressure at a point is **independent of orientation**,
3. **Pressure change in any direction is proportional to the fluid density, local g, and vertical change in depth.**

These concepts are key to the solution of problems in fluid statics, e.g.

1. Two points at the same depth in a static fluid have the same pressure.
2. The orientation of a surface has no bearing on the pressure at a point in a static fluid.
3. Vertical depth is a key dimension in determining pressure change in a static fluid.

If we were to conduct a more general force analysis on a fluid in motion, we would then obtain the following:

$$\overline{\nabla}\,P = \rho\{\bar{g} - \bar{a}\} + \mu\nabla^2\overline{V}$$

Thus the pressure change in fluid in general depends on:

effects of fluid statics (ρ g), Ch. II

inertial effects (ρ a), Ch. III

viscous effects ($\mu\nabla^2 V$) Chs VI & VII

Note: For problems involving the effects of both (1) fluid statics and (2) inertial effects, it is the net $\vec{g} - \vec{a}$ acceleration vector that controls both the magnitude and direction of the pressure gradient.



ketabline.com Ebook.ketabline.com

This equation can be simplified for a fluid at rest (ie., no inertial or viscous effects) to yield

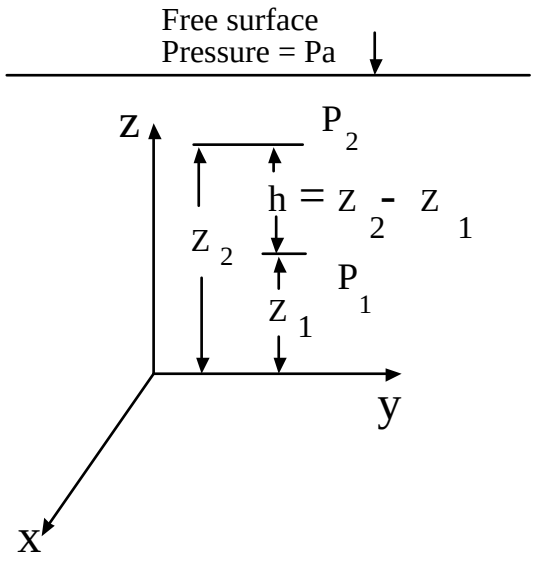
$$\overline{\nabla} p = \rho \, \overline{g}$$

$$\frac{\partial p}{\partial x} = 0 \; ; \quad \frac{\partial p}{\partial y} = 0 \; ; \quad \frac{\partial p}{\partial z} = \frac{dp}{dz} = -\rho g$$

$$P_2 - P_1 = -\int_1^2 \rho g \, dZ$$

For liquids and incompressible fluids, this integrates to

$$P_1 - P_2 = -\rho g \, (z_2 - z_1)$$



Note:

$z_2 - z_1$ is positive for z_2 above z_1.

but

$P_2 - P_1$ is negative for z_2 above z_1.

We can now define a new fluid parameter useful in static fluid analysis:

$$\gamma = \rho g \equiv \text{specific weight of the fluid}$$

With this, the previous equation becomes (for an incompressible, static fluid)

$$P_2 - P_1 = -\gamma \, (z_2 - z_1)$$

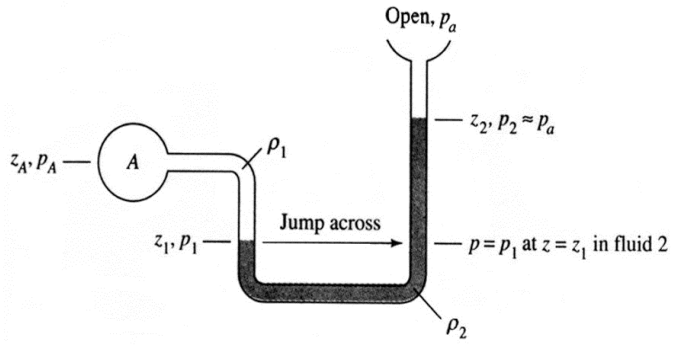
The most common application of this result is that of **manometry.**



ketabline.com Ebook.ketabline.com

Consider the U-tube, multi-fluid manometer shown on the right.

If we first label all intermediate points between A & a, we can write for the overall pressure change



$$P_A - P_a = (P_A - P_1) + (P_1 - P_2) + (P_2 - P_a)$$

This equation was obtained by adding and subtracting each intermediate pressure. The total pressure difference now is expressed in terms of a series of intermediate pressure differences. Substituting the previous result for static pressure difference, we obtain

$$P_A - P_B = -\rho g(Z_A - Z_1) - \rho g (Z_1 - Z_2) - \rho g (Z_2 - Z_B)$$

Again note: Z positive up and $Z_A > Z_1$, $Z_1 < Z_2$, $Z_2 < Z_a$.

In general, follow the following steps when analyzing manometry problems:

1. On manometer schematic, label points on each end of manometer and each intermediate point where there is a fluid-fluid interface: e.g., A – 1 – 2 - B
2. Express overall manometer pressure difference in terms of appropriate intermediate pressure differences.

   $$P_A - P_B = (P_A - P_1) + (P_1 - P_2) + (P_2 - P_B)$$

3. Express each intermediate pressure difference in terms of appropriate product of specific weight * elevation change (watch signs)

   $$P_A - P_B = -\rho g(z_A - z_1) - \rho g (z_1 - z_2) - \rho g (z_2 - z_B)$$

4. Substitute for known values and solve for remaining unknowns.

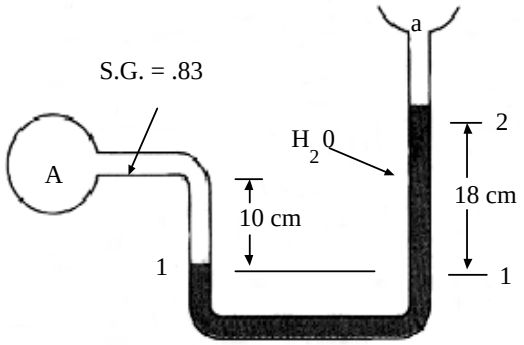
ketabline.com Ebook.ketabline.com

When developing a solution for manometer problems, take care to:

1. Include all pressure changes
2. Use correct Δz and γ with each fluid
3. Use correct signs with Δz. If pressure difference is expressed as $P_A - P_1$, the elevation change should be written as $z_A - z_1$
4. Watch units.

Manometer Example:

Given the indicated manometer, determine the gage pressure at A. Pa = 101.3 kPa. The fluid at A is Meriam red oil no. 3.



$\rho g_w = 9790\ N/m^3$

$\rho g_A = S.G.*\rho g_w = 0.83*9790\ N/m^3$

$\rho g_A = 8126\ N/m^3$

$\rho g_{air} = 11.8\ N/m^3$

With the indicated points labeled on the manometer, we can write

$$P_A - P_a = (P_A - P_1) + (P_1 - P_2) + (P_2 - P_a)$$

Substituting the manometer expression for a static fluid, we obtain

$$P_A - P_a = -\rho g_A(z_A - z_1) - \rho g_w(z_1 - z_2) - \rho g_a(z_2 - z_a)$$

Neglect the contribution due to the air column. Substituting values, we obtain

$$P_A - P_a = -8126\ N/m^3 * 0.10\ m - 9790\ N/m^3 * -0.18 = 949.6\ N/m^2$$

Note why: $(z_A - z_1) = 0.10$ m and $(z_1 - z_2) = -0.18$ m, & did not use P_a

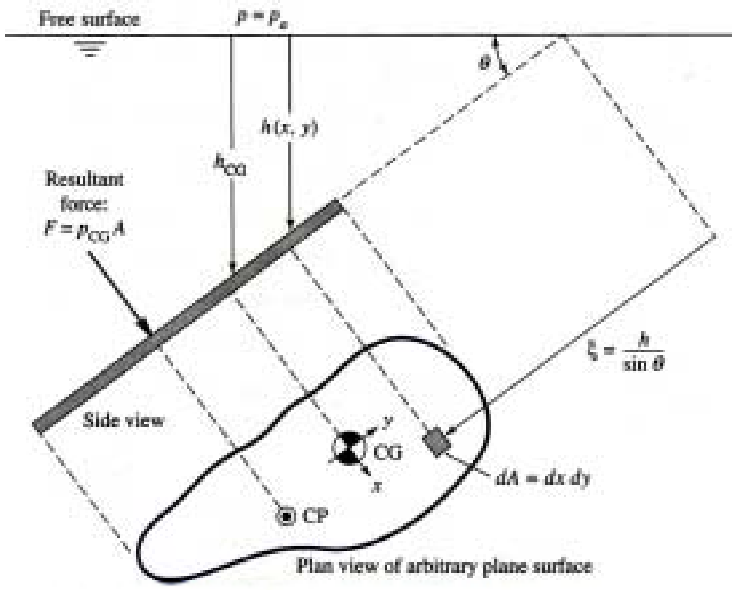
Review the text examples for manometry.



ketabline.com Ebook.ketabline.com

Hydrostatic Forces on Plane Surfaces

Consider a plane surface of arbitrary shape and orientation, submerged in a static fluid as shown:



If P represents the local pressure at any point on the surface and h the depth of fluid above any point on the surface, from basic physics we can easily show that

the net hydrostatic force on a plane surface is given by (see text for development):

$$F = \int_A PdA = P_{cg} A$$

The basic physics says that the hydrostatic force is a distributed load equal to the integral of the local pressure force over the area. This is equivalent to the following:

The hydrostatic force on one side of a plane surface submerged in a static fluid equals the product of the fluid pressure at the centroid of the surface times the surface area in contact with the fluid.

Also: Since pressure acts normal to a surface, the direction of the resultant force will always be **normal to the surface**.

Note: In most cases since it is the net hydrostatic force that is desired and the contribution of atmospheric pressure Pa will act on both sides of a surface, the result of atmospheric pressure P_a will cancel and the net force is obtained by

$$F = \rho g h_{cg} A$$

$$F = P_{cg} A$$



ketabline.com Ebook.ketabline.com

P_{cg} is now the **gage pressure** at the centroid of the area in contact with the fluid. Therefore, to obtain the net hydrostatic force F on a plane surface:

1. **Determine depth of centroid h_{cg} for the area in contact with the fluid**
2. **Determine the (gage) pressure at the centroid P_{cg}**
3. **Calculate $F = P_{cg}A$.**

The following page shows the centroid, and other geometric properties of several common areas.

It is noted that care must be taken when dealing with layered fluids. The required procedure is essentially that the force on the plane area in each layer of fluid must be determined individually for each layer using the steps listed above.

We must now determine the effective point of application of F. This is commonly called the "**center of pressure - cp**" of the hydrostatic force.

Define an x – y coordinate system whose origin is at the centroid, c.g, of the area.

The location of the resultant force is determined by integrating the moment of the distributed fluid load on the surface about each axis and equating this to the moment of the resultant force. Therefore, for the moment about the x axis:

$$F\, y_{cp} = \int_A y\, P\, dA$$

Applying a procedure similar to that used previously to determine the resultant force, and using the definition (see text for detailed development),

for I_{xx} defined as the ≡ moment of inertia, or 2nd moment of area we obtain

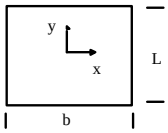
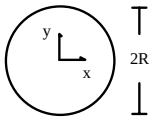
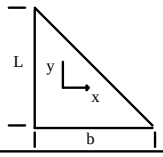
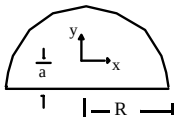
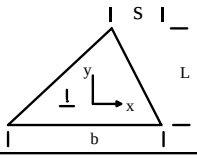
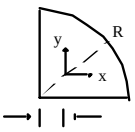
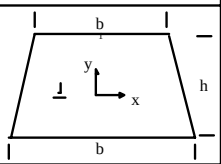
$$Y_{cp} = -\frac{\rho g \sin\theta\, I_{xx}}{P_{cg} A} \quad \leq \quad 0$$

Therefore, the resultant force will always act at a distance $\mathbf{y_{cp}}$ **below** the centroid of the surface (except for the special case of $\sin\theta = 0$).



ketabline.com Ebook.ketabline.com

PROPERTIES OF PLANE SECTIONS

Geometry	Centroid	Moment of Inertia I_{xx}	Product of Inertia I_{xy}	Area
	$b/2, L/2$	$\frac{bL^3}{12}$	0	$b \cdot L$
	0, 0	$\frac{\pi R^4}{4}$	0	πR^2
	$b/3, L/3$	$\frac{bL^3}{36}$	$-\frac{b^2L^2}{72}$	$\frac{b \cdot L}{2}$
	$0, a = \frac{4R}{3\pi}$	$R^4\left(\frac{\pi}{8} - \frac{8}{9\pi}\right)$	0	$\frac{\pi R^2}{2}$
	$a = \frac{L}{3}$	$\frac{bL^3}{36}$	$\frac{b(b-2s)L^2}{72}$	$\frac{1}{2} b \cdot L$
	$a = \frac{4R}{3\pi}$	$\left(\frac{\pi}{16} - \frac{4}{9\pi}\right) R^4$	$\left(\frac{1}{8} - \frac{4}{9\pi}\right) R^4$	$\frac{\pi R^2}{4}$
	$a = \frac{h(b+2b_1)}{3(b+b_1)}$	$\frac{h^3(b^2 + 4bb_1 + b_1^2)}{36(b+b_1)}$	0	$(b+b_1)\frac{h}{2}$

Fluid Specific Weight

	$1bf/ft^3$	N/m^3		$1bf/ft^3$	N/m^3
Air	.0752	11.8	Seawater	64.0	10,050
Oil	57.3	8,996	Glycerin	78.7	12,360
Water	62.4	9,790	Mercury	846.	133,100
Ethyl	49.2	7,733	Carbon	99.1	15,570

ketabline.com Ebook.ketabline.com

Proceeding in a similar manner for the x location, and defining I_{xy} = product of inertia, we obtain

$$X_{cp} = -\frac{\rho g \sin\theta \, I_{xy}}{P_{cg} A}$$

where X_{cp} can be either positive or negative since I_{xy} can be either positive or negative.

Note: For areas with a vertical plane of symmetry (e.g., squares, circles, isosceles triangles, etc.) through the centroid, i.e. the (y - axis), the center of pressure is located directly below the centroid along the plane of symmetry, i.e., **$X_{cp} = 0$**.

Key Points: The values X_{cp} and Y_{cp} are both measured with respect to the centroid of the area in contact with the fluid.

X_{cp} and Y_{cp} are both measured in the plane of the area; i.e., Y_{cp} is not necessarily a vertical dimension, unless $\theta = 90^{o}$.

Special Case: For most problems where (1) we have a single, homogeneous fluid (i.e., not applicable to layers of multiple fluids) and (2) the surface pressure is atmospheric, the fluid specific weight γ cancels in the equation for Y_{cp} and X_{cp} and we have the following simplified expressions:

$$F = \rho g h_{cg} A$$

$$Y_{cp} = -\frac{I_{xx} \sin\theta}{h_{cg} A} \qquad X_{cp} = -\frac{I_{xy} \sin\theta}{h_{cg} A}$$

However, for problems where we have either (1) multiple fluid layers, or (2) a container with surface pressurization > P_{atm} , these simplifications do not occur and t**he original, basic expressions** for F , Y_{cp} , and X_{cp} **must be used; i.e.,** take care to use the approximate expressions only for cases where they apply. The basic equations always work.



ketabline.com Ebook.ketabline.com

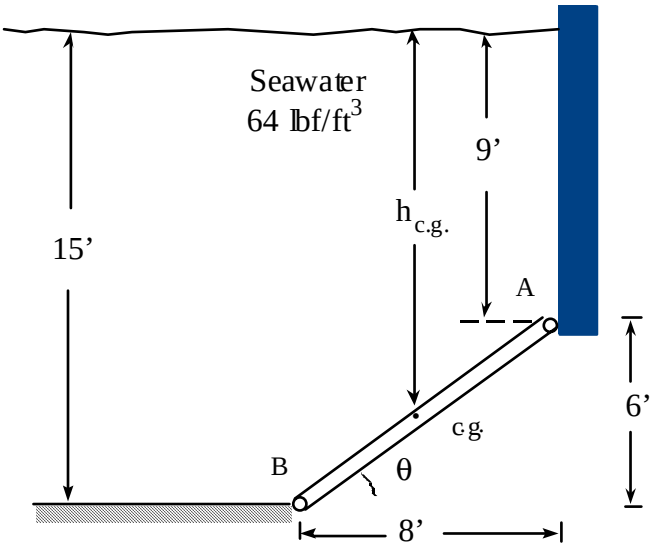
Summary:

1. The resultant force is determined from the product of the pressure at the centroid of the surface times the area in contact with the fluid
2. The centroid is used to determine the magnitude of the force. This is **not the location** of the resultant force
3. The location of the resultant force will be at the center of pressure which will be at a location $\mathbf{Y_{cp}}$ **below the centroid** and $\mathbf{X_{cp}}$ as specified previously
4. $\mathbf{X_{cp} = 0}$ for areas with a vertical plane of symmetry through the c.g.

Example 2.5

Given: Gate, 5 ft wide
Hinged at B
Holds seawater as shown

Find:
a. Net hydrostatic force on gate
b. Horizontal force at wall - A
c. Hinge reactions - B



a. By geometry: $\theta = \tan^{-1}(6/8) = 36.87^{o}$ Neglect P_{atm}

Since plate is rectangular, $h_{cg} = 9\text{ ft} + 3\text{ft} = 12\text{ ft}$ $A = 10 \times 5 = 50\text{ ft}^2$

$P_{cg} = \gamma h_{cg} = 64\text{ lbf/ft}^3 * 12\text{ ft} = 768\text{ lbf/ft}^2$

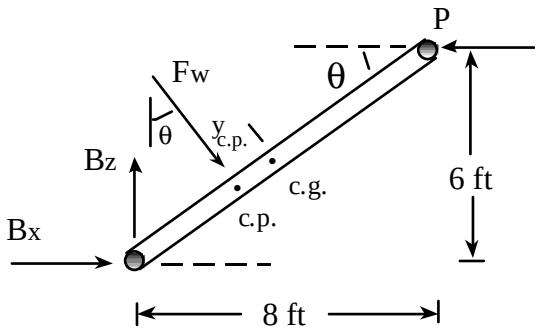
$\therefore$ $F_p = P_{cg} A = 768\text{ lbf/ft}^2 * 50\text{ ft}^2 = \underline{38{,}400\text{ lbf}}$

ketabline.com Ebook.ketabline.com

b. Horizontal Reaction at A

Must first find the location, c.p., for F_p

$$y_{cp} = -\rho g \sin\theta \frac{I_{xx}}{P_{cg} A} = -\frac{I_{xx} \sin\theta}{h_{cg} A}$$



For a rectangular wall:

$I_{xx} = bh^3/12$

$I_{xx} = 5 * 10^3/12 = 417\ ft^4$

Note: The relevant area is a rectangle, not a triangle.

Note: Do not overlook the hinged reactions at B.

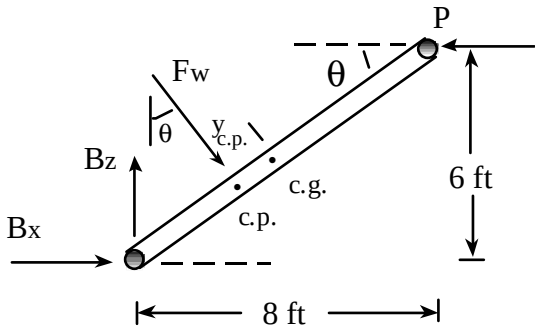
$$y_{cp} = -\frac{417 ft^4 0.6}{12 ft\, 50 ft^2} = -0.417 ft \quad y_{cp} = -\frac{417 ft^4 0.6}{12 ft\, 50 ft^2} = -0.417 ft$$ **below c.g.**

x_{cp} = 0 due to symmetry

$$\sum M_B = 0$$

$$(5 - 0.417) \cdot 38{,}400 - 6P = 0$$

P = 29,330 lbf ←





ketabline.com Ebook.ketabline.com

c. $\sum F_x = 0, \quad B_x + F\sin\theta - P = 0$

$B_x + 38{,}400*0.6 - 29{,}330 = 0$

$\underline{B_x = 6290 \text{ lbf}} \quad \rightarrow$

$$\sum F_z = 0, \quad B_z - F\cos\theta = 0$$

$B_z = 38{,}400 * 0.8 = \underline{30{,}720 \text{ lbf}} \quad \uparrow$

Note: Show the direction of all forces in final answers.

Summary: To find net hydrostatic force on a plane surface:

1. **Find area in contact with fluid.**
2. **Locate centroid of that area.**
3. **Find hydrostatic pressure P_{cg} at centroid, typically $= \gamma h_{cg}$ (generally neglect P_{atm}).**
4. **Find force $F = P_{cg} A$.**
5. **Location will not be at c.g., but at a distance y_{cp} below centroid. y_{cp} is in the plane of the area.**

Review all text examples for forces on plane surfaces.



ketabline.com Ebook.ketabline.com

Forces on Curved Surfaces

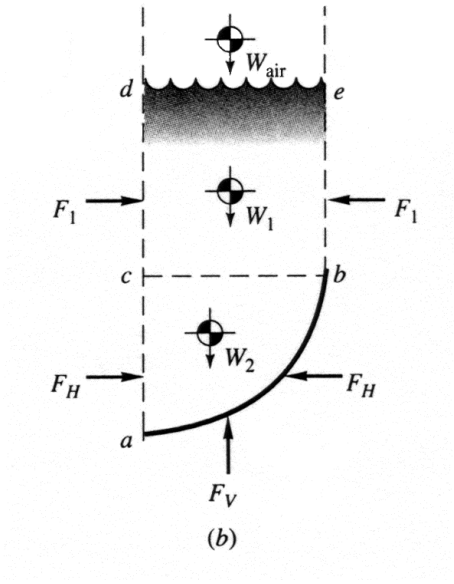
Since this class of surface is curved, the direction of the force is different at each location on the surface.

Therefore, we will evaluate separate x and y components of net hydrostatic force.

Consider curved surface, a-b. Force balances in x & y directions yields

$$F_h = F_H$$

$$F_V = W_{air} + W_1 + W_2$$

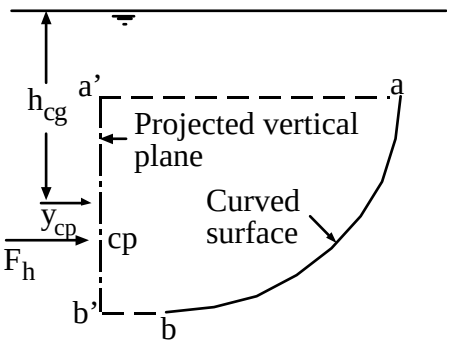


From this force balance, the basic rules for determining the horizontal and vertical component of forces on a curved surface in a static fluid can be summarized as follows:

Horizontal Component, F_h

The **horizontal** component of force on a curved surface equals the force on the plane area formed by the **projection of the curved surface** onto a **vertical plane** normal to the component.

The horizontal force will act through the c.p. (**not the centroid**) of the projected area.



ketabline.com Ebook.ketabline.com

Therefore, to determine the horizontal component of force on a curved surface in a hydrostatic fluid:

1. Project the curved surface into the appropriate vertical plane.
2. Perform all further calculations on the vertical plane.
3. Determine the location of the centroid - c.g. of the vertical plane.
4. Determine the depth of the centroid - h_{cg} of the vertical plane.
5. Determine the pressure - $P_{cg} = g\, h_{cg}$ at the centroid of the vertical plane.
6. Calculate $F_h = P_{cg} A$, where **A is the area of** the projection of the curved surface into the vertical plane, ie., **the area of the vertical plane**.
7. The location of F_h is through the center of pressure of the **vertical plane** , not the centroid.

Get the picture? All elements of the analysis are performed with the vertical plane. The original curved surface is important only as it is used to define the projected vertical plane.

Vertical Component - F_V

The **vertical** component of force on a curved surface equals the **weight** of the **effective** column of fluid **necessary to cause the pressure on the surface**.

The use of the words **effective column of fluid** is important in that there may not always actually be fluid directly above the surface. (See graphic that follows.)

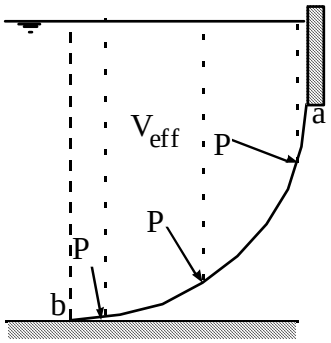
This effective column of fluid is specified by identifying the column of fluid that would be required to cause the pressure at each location on the surface.



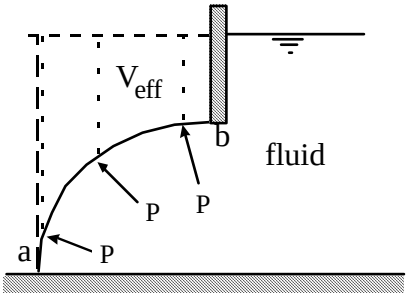
ketabline.com Ebook.ketabline.com

Thus to identify the effective volume - Veff:

1. Identify the curved surface in contact with the fluid.
2. Identify the pressure at each point on the curved surface.
3. Identify the height of fluid required to develop the pressure.
4. These collective heights combine to form V_{eff}.



Fluid above the surface



No fluid actually above surface

These two examples show two typical cases where this concept is used to determine V_{eff}.

The vertical force acts **vertically** through the centroid (center of mass) of the effective column of fluid. The vertical direction will be the direction of the vertical components of the pressure forces.

Therefore, to determine the vertical component of force on a curved surface in a hydrostatic fluid:

1. Identify the effective column of fluid necessary to cause the fluid pressure on the surface.
2. Determine the volume of the effective column of fluid.
3. Calculate the weight of the effective column of fluid - $F_V = \rho g V_{eff}$.
4. The location of F_V is through the centroid of V_{eff}.



ketabline.com Ebook.ketabline.com

Finding the Location of the Centroid

A second problem associated with the topic of curved surfaces is that of finding the location of the centroid of V_{eff}.

Recall:

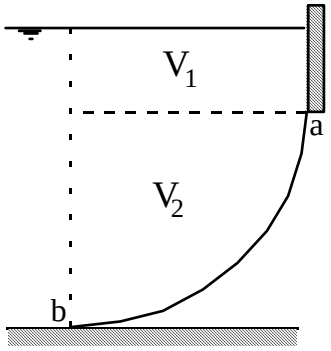
Centroid = the location where the first moment of a point area, volume, or mass equals the first moment of the distributed area, volume, or mass, e.g.

$$x_{cg}V_1 = \int_{V_1} x\,dV$$

This principle can also be used to determine the location of the centroid of complex geometries.

For example:

If $V_{eff} = V_1 + V_2$

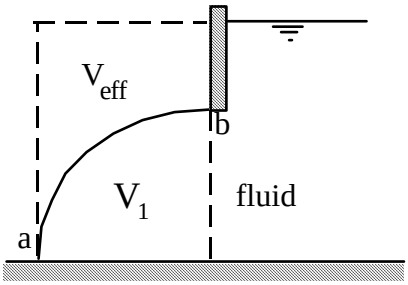


then

$x_{cg}V_{eff} = x_1V_1 + x_2V_2$

or

$V_T = V_1 + V_{eff}$



$x_TV_T = x_1V_1 + x_{cg}V_{eff}$

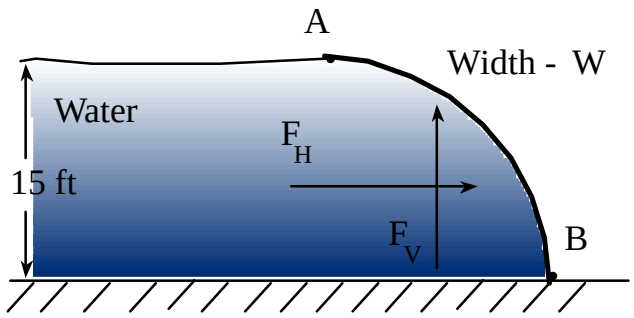
Note: In the figures shown above, each of the x values would be specified relative to a vertical axis through b since the cg of the quarter circle is most easily specified relative to this axis.



ketabline.com Ebook.ketabline.com

Example:

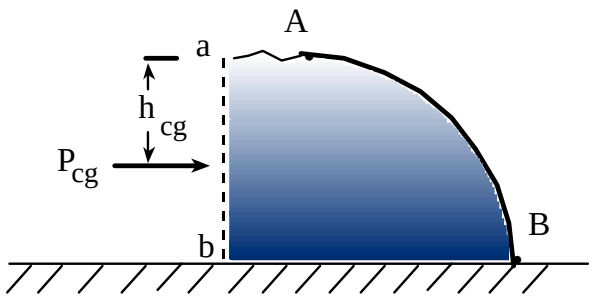
Gate AB holds back 15 ft of water. Neglecting the weight of the gate, determine the magnitude (per unit width) and location of the hydrostatic forces on the gate and the resisting moment about B.



a. Horizontal component $\gamma = \rho g = 62.4 \text{ lbf/ft}^3$

Rule: Project the curved surface into the vertical plane. Locate the centroid of the projected area. Find the pressure at the centroid of the vertical projection. $F = P_{cg} A_p$

Note: All calculations are done with the projected area. The curved surface is not used at all in the analysis.



The curved surface projects onto plane a - b and results in a **rectangle,** (not a quarter circle) 15 ft x W. For this rectangle:

$h_{cg} = 7.5$, $P_{cg} = \gamma h_{cg} = 62.4 \text{ lbf/ft}^3 * 7.5 \text{ ft} = 468 \text{ lbf/ft}^2$

$F_h = P_{cg} A = 468 \text{ lbf/ft}^2 * 15 \text{ ft} * W = \underline{7020 \, W \text{ lbf}}$ →

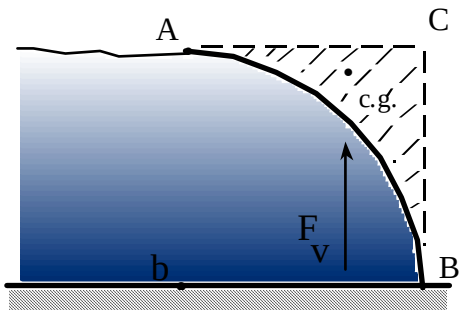
Location: $I_{xx} = bh^3/12 = W * 15^3/12 = 281.25 \, W \text{ ft}^4$

$$y_{cp} = -\frac{I_{xx} \sin\theta}{h_{cg} A} = -\frac{281.25 W \, ft^4 \sin 90^o}{7.5 \, ft \, 15 W \, ft^2} = -2.5 \, ft$$

The location is 2.5 ft below the c.g. or 10 ft below the surface, 5 ft above the bottom.

ketabline.com Ebook.ketabline.com

b. Vertical force:



Rule: F_v equals the weight of the effective column of fluid above the curved surface.

Q: What is the effective volume of fluid above the surface?

What volume of fluid would result in the actual pressure distribution on the curved surface?

Vol = A - B - C

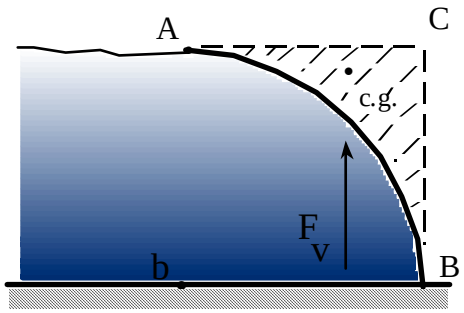
$V_{rec} = V_{qc} + V_{ABC}$, $V_{ABC} = V_{rec} - V_{qc}$

$V_{ABC} = V_{eff} = 15^2 W - \pi 15^2/4 * W = 48.29 W\ ft^3$

$F_v = \rho g V_{eff} = 62.4\ lbf/ft^3 * 48.29\ ft^3 = \underline{3013\ lbf}$ ↑

Note: F_v is directed upward even though the effective volume is above the surface.

c. What is the location?



Rule: F_v will act through the centroid of the "effective volume causing the force.

We need the centroid of volume A-B-C. How do we obtain this centroid?

Use the concept which is the basis of the centroid, the "first moment of an area."



ketabline.com Ebook.ketabline.com

Since: $A_{rec} = A_{qc} + A_{ABC}$ $M_{rec} = M_{qc} + M_{ABC}$ $M_{ABC} = M_{rec} - M_{qc}$

Note: We are taking moments about the left side of the figure, ie., point b. **WHY?**

(The c.g. of the quarter circle is known to be 4 R/ 3 π w.r.t. b.)

$$x_{cg} A = x_{rec} A_{rec} - x_{qc} A_{qc}$$

$$x_{cg} \{15^2 - \pi*15^2/4\} = 7.5*15^2 - \{4*15/3/\pi\}* \pi*15^2/4$$

x_{cg} = 11.65 ft { distance to rt. of b to centroid }

Q: Do we need a y location? Why?

d. Calculate the moment about B needed for equilibrium.

$\sum M_B = 0$ clockwise positive.

$$M_B + 5F_h + (15 - x_v)F_v = 0$$

$M_B + 5\times 7020W + (15 - 11.65)3013W = 0$ $M_B + 5\times 7020W + (15 - 11.65)3013W = 0$

$P_a \neq \rho g y \quad G \neq g$

$$M_B + 35{,}100W + 10{,}093.6W = 0$$

$$M_B = -45{,}194W \ ft - lbf$$ **Why negative?**

The hydrostatic forces will tend to roll the surface clockwise relative to B, thus a resisting moment that is counterclockwise is needed for static equilibrium.

Always review your answer (all aspects: magnitude, direction, units, etc.) to determine if it makes sense relative to physically what you understand about the problem. Begin to think like an engineer.



ketabline.com Ebook.ketabline.com

Buoyancy

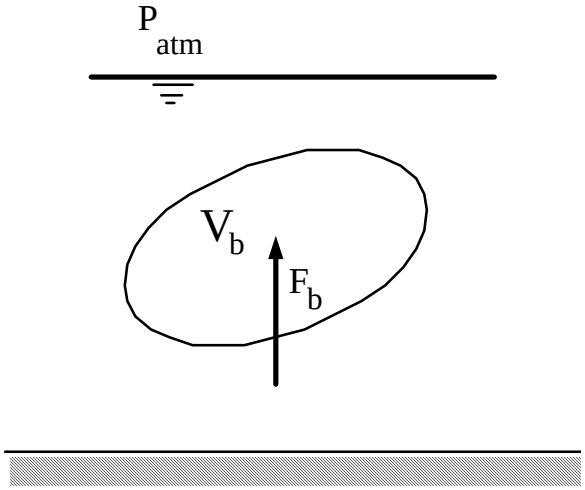
An important extension of the procedure for vertical forces on curved surfaces is that of the concept of buoyancy.

The basic principle was discovered by Archimedes.

It can be easily shown that (see text for detailed development) the buoyant force F_b is given by:

$$F_b = \rho g V_b$$

where V_b is the volume of the fluid displaced by the submerged body and ρg is the specific weight of the fluid displaced.



Thus, the **buoyant force** equals the **weight of the fluid displaced,** which is equal to the product of the specific weight times the volume of fluid displaced.

The location of the buoyant force is:

Through a vertical line of action, directed upward, which acts through the centroid of the volume of fluid displaced.

Review all text examples and material on buoyancy.

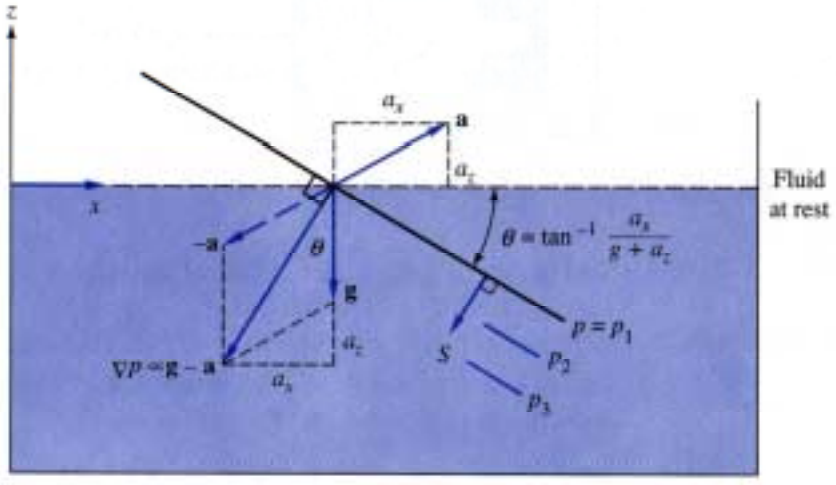


ketabline.com Ebook.ketabline.com

Pressure distribution in rigid body motion

All of the problems considered to this point were for static fluids. We will now consider an extension of our static fluid analysis to the case of rigid body motion, where the entire fluid mass moves and accelerates uniformly (as a rigid body).

The container of fluid shown below is accelerated uniformly up and to the right as shown.



From a previous analysis, the general equation governing fluid motion is

$$\overline{\nabla} P = \rho(\bar{g} - \bar{a}) + \mu \nabla^2 \overline{V}$$

For rigid body motion, there is no velocity gradient in the fluid, therefore

$$\mu \nabla^2 V = 0$$

The simplified equation can now be written as

$$\overline{\nabla} P = \rho(\bar{g} - \bar{a}) = \rho \overline{G}$$

where $\overline{G} = \bar{g} - \bar{a} \equiv$ the net acceleration vector acting on the fluid.

ketabline.com Ebook.ketabline.com

This result is similar to the equation for the variation of pressure in a hydrostatic fluid.

However, in the case of rigid body motion:

* $\overline{\nabla}P$ = f {fluid density & the **net** acceleration vector- $\overline{G} = \overline{g} - \overline{a}$ }

* $\overline{\nabla}P$ acts in the vector direction of $\overline{G} = \overline{g} - \overline{a}$

* Lines of constant pressure are perpendicular to $\overline{G}$. The new orientation of the free surface will also be perpendicular to $\overline{G}$.

The equations governing the analysis for this class of problems are most easily developed from an acceleration diagram.

Acceleration diagram:

For the indicated geometry:

$$\theta = \tan^{-1}\frac{a_x}{g + a_z} \qquad \theta = \tan^{-1}\frac{a_x}{g + a_z}$$

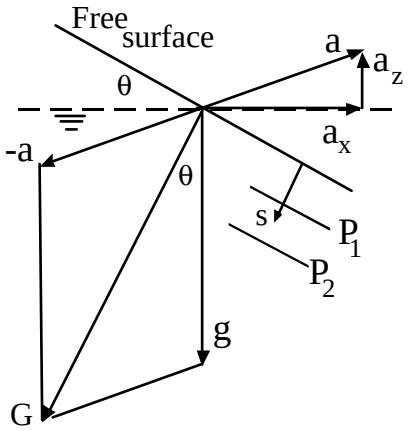
$$\frac{dP}{ds} = \rho G \qquad \text{where } G = \left\{a_x^2 + (g + a_z)^2\right\}^{1/2}$$

and $P_2 - P_1 = \rho G(s_2 - s_1)$

Note: $P_2 - P_1 \neq \rho g(z_2 - z_1)$

and

$s_2 - s_1$ is not a vertical dimension



Note: s is the depth to a given point **perpendicular** to the free surface or **its extension.** s is aligned with $\overline{G}$.



ketabline.com Ebook.ketabline.com

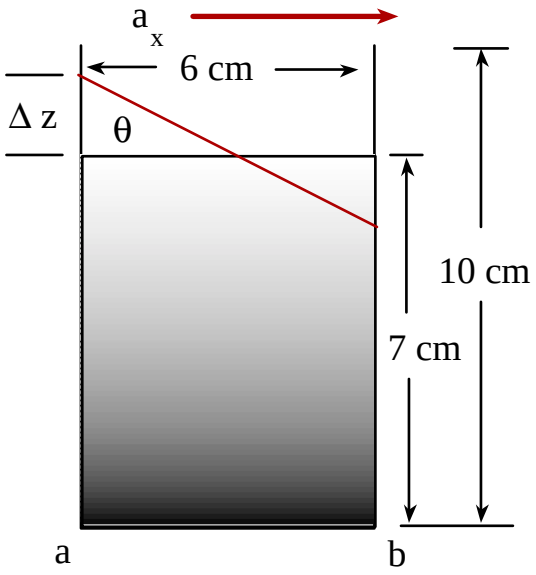
In analyzing typical problems with rigid body motion:

1. Draw the acceleration diagram taking care to correctly indicate –a, g, and θ, the inclination angle of the free surface.
2. Using the previously developed equations, solve for G and θ.
3. If required, use geometry to determine $s_2 - s_1$ (the perpendicular distance from the free surface to a given point) and then the pressure at that point relative to the surface using $P_2 - P_1 = \rho G (s_2 - s_1)$.

Key Point: Do not use ρg to calculate $P_2 - P_1$, use ρG.

Example 2.12

Given: A coffee mug, 6 cm x 6 cm square, 10 cm deep, contains 7 cm of coffee. Mug is accelerated to the right with $a_x = 7$ m/s^2 . Assuming rigid body motion. $\rho_c = 1010$ kg/m^3,



Determine: a. Will the coffee spill?

b. P_g at "a & b".

c. F_{net} on left wall.

a. First draw schematic showing original orientation and final orientation of the free surface.

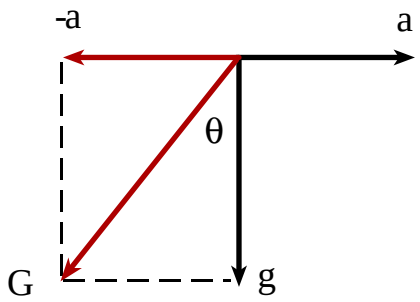
$\rho_c = 1010$ kg/m^3 $a_x = 7$m/s^2 $a_z = 0$ $g = 9.8907$ m/s^2

Have a new free surface angle θ where

$$\theta = \tan^{-1}\frac{a_x}{g + a_z}$$

$$\theta = \tan^{-1}\frac{7}{9.807} = 35.5°$$

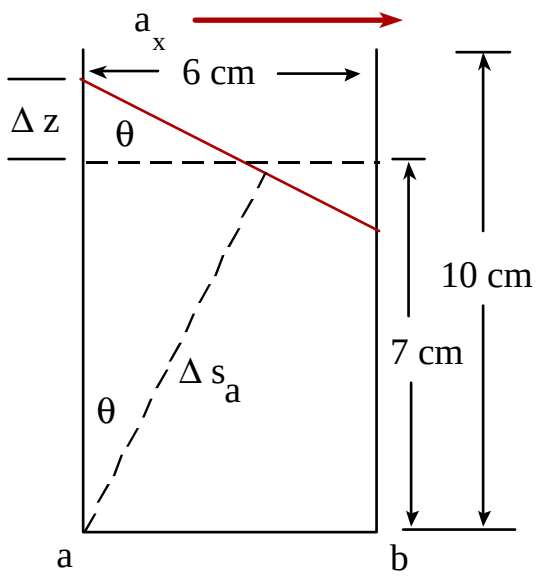
$\Delta z = 3 \tan 35.5 = 2.14$ cm



ketabline.com Ebook.ketabline.com

$h_{max} = 7 + 2.14 = 9.14 \text{ cm} < 10 \text{ cm}$ ∴ **Will not spill**.

b. Pressure at " a & b."



$P_a = \rho G \Delta s_a$

$G = \{a^2_x + g^2\}^{.5} = \{ 7^2 + 9.807^2\}^{.5}$

$G = 12.05 \text{ m/s}^2$

$\Delta s_a = \{7 + z\} \cos \theta$

$\Delta s_a = 9.14 \text{ cm} \cos 35.5 = 7.44 \text{ cm}$

$P_a = 1010 \text{ kg/m}^3 * 12.05 \text{m/s}^2 * 0.0744 \text{ m}$

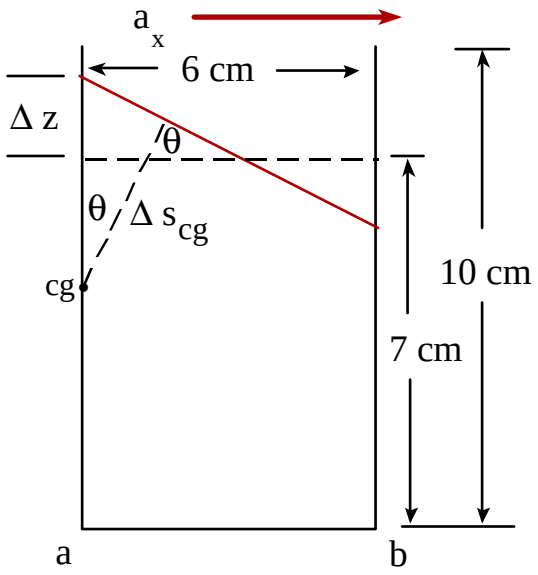
$P_a = 906 \text{ (kg m/s}^2\text{)/m}^2 =$ **906 Pa**

Note: $P_a \neq \rho g y \quad G \neq g$

Q: **How would you find the pressure at b**, P_b?

c. What is the force on the left wall?

We have a plane surface, what is the rule?



Find cg, P_{cg}, $F = P_{cg} \cdot A$

Vertical depth to cg is:

$z_{cg} = 9.14/2 = 4.57 \text{ cm}$

$\Delta s_{cg} = 4.57 \cos 35.5 = 3.72 \text{ cm}$

$P_{cg} = \rho G \Delta s_{cg}$

$P_{cg} = 1010 \text{ kg/m}^3 * 12.05 \text{ m/s}^2 * 0.0372 \text{ m}$

$P_{cg} = 452.7 \text{ N/m}^2$

$F = P_{cg} A = 452.7 \text{ N/m}^2 * 0.0914 * 0.06 \text{m}^2$

F = 2.48 N ←



ketabline.com Ebook.ketabline.com

What is the direction?

Horizontal, perpendicular to the wall;

i.e., **Pressure <u>always</u> acts normal to a surface.**

Q: How would you find the force on the right wall?



ketabline.com Ebook.ketabline.com

III. Control Volume Relations for Fluid Analysis

From consideration of hydrostatics, we now move to problems involving fluid flow with the addition of effects due to fluid motion, e.g. inertia and convective mass, momentum, and energy terms.

We will present the analysis based on a control volume (not differential element) formulation, e.g. similar to that used in thermodynamics for the first law.

Basic Conservation Laws:

Each of the following basic conservation laws is presented in its most fundamental, **fixed mass** form. We will subsequently develop an equivalent expression for each law that includes the effects of the flow of mass, momentum, and energy (as appropriate) across a control volume boundary. These transformed equations will be the basis for the control volume analyses developed in this chapter.

Conservation of Mass:

Defining m as the mass of a fixed mass system, the mass for a control volume V is given by

$$m_{sys} = \int_{sys} \rho dV$$

The basic equation for conservation of mass is then expressed as

$$\left(\frac{dm}{dt}\right)_{sys} = 0$$

The time rate of change of mass for the control volume is zero since at this point we are still working with a fixed mass system.

Linear Momentum:

Defining $\overline{P}_{sys}$ as the linear momentum of a fixed mass, the linear momentum of a fixed mass control volume is given by:



ketabline.com Ebook.ketabline.com

$$\overline{P}_{sys} = m\overline{V} = \int_{sys} \overline{V}\rho dV$$

where $\overline{V}$ is the local fluid velocity and dV is a differential volume element in the control volume.

The basic linear momentum equation is then written as

$$\sum \overline{F} = \left.\frac{d\overline{P}}{dt}\right)_{sys} = \left.\frac{d(m\overline{V})}{dt}\right)_{sys}$$

Moment of Momentum:

Defining $\overline{H}$ as the moment of momentum for a fixed mass, the moment of momentum for a fixed mass control volume is given by

$$\overline{H}_{sys} = \int_{sys} \overline{r} \times \overline{V}\rho dV$$

where $\overline{r}$ is the moment arm from an inertial coordinate system to the differential control volume of interest. The basic equation is then written as

$$\sum \overline{M}_{sys} = \sum \overline{r} \times \overline{F} = \left.\frac{d\overline{H}}{dt}\right)_{sys}$$

Energy:

Defining E_{sys} as the total energy of an element of fixed mass, the energy of a fixed mass control volume is given by

$$E_{sys} = \int_{sys} e\rho dV$$



ketabline.com Ebook.ketabline.com

where e is the total energy per unit mass (includes kinetic, potential, and internal energy) of the differential control volume element of interest.

The basic equation is then written as

$$\dot{Q} - \dot{W} = \frac{dE}{dt}\Big)_{sys} \qquad \text{(Note: written on a rate basis)}$$

It is again noted that each of the conservation relations as previously written applies only to fixed, constant mass systems.

However, since most fluid problems of importance are for open systems, we must transform each of these relations to an equivalent expression for a control volume which includes the effect of mass entering and/or leaving the system.

This is accomplished with the Reynolds transport theorem.

Reynolds Transport Theorem

We define a general, extensive property (an extensive property depends on the size or extent of the system) B_{sys} where

$$B_{sys} = \int_{sys} \beta \rho d\,V$$

B_{sys} could be total mass, total energy, total momentum, etc., of a system.

and B_{sys} per unit mass is defined as β or $\beta = \frac{dB}{dm}$

Thus, β is the intensive equivalent of B_{sys} .

Applying a general control volume formulation to the time rate of change of B_{sys} , we obtain the following (see text for detailed development):



ketabline.com Ebook.ketabline.com

$$\left.\frac{dB}{dt}\right)_{sys} = \frac{\partial}{\partial t}\int_{cv} \beta\,\rho\,dV + \int_{A_e} \beta_e\,\rho_e\,V_e\,dA_e - \int_{A_i} \beta_i\,\rho_i\,V_i\,dA_i$$

↓ ↓ ↓ ↓

System rate of change of B | **Rate of change of B in c.v.** | **Rate of B leaving c.v.** | **Rate of B entering c.v.**

↓ ↓

transient term | **convective terms**

where B is any conserved quantity, e.g. **mass, linear momentum, moment of momentum, or energy**.

We will now apply this theorem to each of the basic conservation equations to develop their equivalent open system, control volume forms.

Conservation of mass

For conservation of mass, we have that

$$B = m \qquad \text{and} \qquad \beta = 1$$

From the previous statement of conservation of mass and these definitions, Reynolds transport theorem becomes

$$\frac{\partial}{\partial t}\int_{cv} \rho\,dV + \int_{A_e} \rho_e\,V_e\,dA_e - \int_{A_i} \rho_i\,V_i\,dA_i = 0$$

or

$$\frac{\partial}{\partial t}\int_{cv} \rho\,dV + \int_{A_e} \rho_e\,V_e\,dA_e - \int_{A_i} \rho_i\,V_i\,dA_i = 0$$

↓ ↓ ↓

Rate of change of mass in c.v., | **Rate of mass leaving c.v.,** | **Rate of mass entering c.v.,**

↓ ↓ ↓

= 0 for steady-state | $\dot{m}_e$ | $\dot{m}_i$



ketabline.com Ebook.ketabline.com

This can be simplified to

$$\left.\frac{dm}{dt}\right)_{cv} + \sum \dot{m}_e - \sum \dot{m}_i = 0$$

Note that the exit and inlet velocities V_e and V_i are the local components of fluid velocities at the exit and inlet boundaries **relative to an observer standing on the boundary**. Therefore, if the boundary is moving, the velocity is measured relative to the boundary motion. The location and orientation of a coordinate system for the problem are not considered in determining these velocities.

Also, the result of $\overline{V}_e \cdot d\overline{A}_e$ and $\overline{V}_i \cdot d\overline{A}_i$ is the product of the normal velocity component times the flow area at the exit or inlet, e.g.

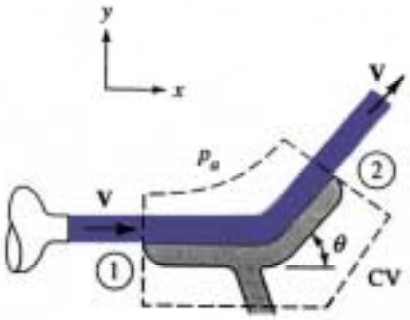
$$V_{e,n}\, dA_e \qquad \text{and} \qquad V_{i,n}\, dA_i$$

Special Case: For incompressible flow with a uniform velocity over the flow area, the previous integral expressions simplify to:

$$\dot{m} = \int_{cs} \rho V\, dA = \rho A V$$

Conservation of Mass Example

Water at a velocity of 7 m/s exits a stationary nozzle with D = 4 cm and is directed toward a turning vane with $\theta = 40^o$, Assume steady-state.



Determine:

a. Velocity and flow rate entering the c.v.
b. Velocity and flow rate leaving the c.v.

ketabline.com Ebook.ketabline.com

a. Find V_1 and $\dot{m}_1$

Recall that the mass flow velocity is the normal component of velocity measured **relative to the inlet or exit area**.

Thus, relative to the nozzle, V(nozzle) = 7 m/s and since there is no relative motion of point 1 relative to the nozzle, we also have **V_1 = 7 m/s ans.**

From the previous equation:

$$\dot{m} = \int_{cs} \rho V \, dA = \rho A V = 998 \text{ kg/m}^3 * 7 \text{ m/s} * \pi * 0.04^2/4$$

$\dot{m}_1$ = **8.78 kg/s ans.**

b. Find V_2 and $\dot{m}_2$

Determine the flow rate first.

Since the flow is steady state and no mass accumulates on the vane:

$\dot{m}_1 = \dot{m}_2$, $\dot{m}_2$ = **8.78 kg/s ans.**

Now: $\dot{m}_2 = 8.78 \text{ kg/s} = \rho A V)_2$

Since ρ and A are constant, **V_2 = 7 m/s ans.**

Key Point: For steady flow of a constant area, incompressible stream, the flow velocity and total mass flow are the same at the inlet and exit, even though the direction changes.

or alternatively:

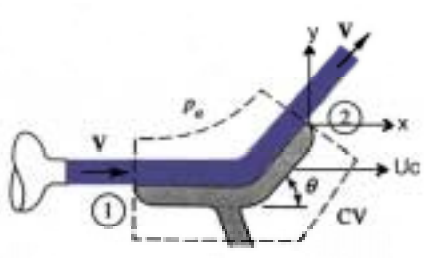
Rubber Hose Concept: For steady flow of an incompressible fluid, the flow stream can be considered as a rubber hose and if it enters a c.v. at a velocity of V, it exits at a velocity V, even if it is redirected.



ketabline.com Ebook.ketabline.com

Problem Extension:

Let the turning vane (and c.v.) now move to the right at a steady velocity of 2 m/s (other values remain the same); perform the same calculations.



Therefore:

Given: $U_c = 2$ m/s $V_J = 7$ m/s

For an observer standing at the c.v. inlet (point 1)

$V_1 = V_J - U_c = 7 - 2 = 5$ m/s

$\dot{m}_1 = \rho_1 V_1 A_1 = 998 \text{ kg/m}^3 * 5 \text{ m/s} * \pi * 0.04^2/4 = 6.271$ kg/s

Note: The inlet velocity used to specify the mass flow rate is again measured relative to the inlet boundary but now is given by $V_J - U_c$.

Exit:

$\dot{m}_1 = \dot{m}_2 = 6.271$ kg/s Again, since ρ and A are constant, $V_2 = 5$ m/s.

Again, the exit flow is most easily specified by conservation of mass concepts.

Note: The coordinate system could either have been placed on the moving cart or have been left off the cart with no change in the results.

Key Point: The location of the coordinate system does not affect the calculation of mass flow rate which is calculated relative to the flow boundary. It could have been placed at **Georgia Tech** with no change in the results.

Review material and work examples in the text on conservation of mass.



ketabline.com Ebook.ketabline.com

Linear Momentum

For linear momentum, we have that

$$\overline{B} = \overline{P} = m\overline{V} \quad \text{and} \quad \overline{\beta} = \overline{V}$$

From the previous statement of linear momentum and these definitions, Reynolds transport theorem becomes

$$\sum \overline{F} = \left.\frac{d\left(m\overline{V}\right)}{dt}\right)_{sys} = \frac{\partial}{\partial t}\int_{cv} \overline{V}\,\rho\, dV + \int_{A_e} \overline{V}\,\rho_e \overline{V}_e \cdot d\overline{A}_e - \int_{A_i} \overline{V}\,\rho_i \overline{V}_i \cdot d\overline{A}_i$$

or

$$\sum \overline{F} = \frac{\partial}{\partial t}\int_{cv} \overline{V}\,\rho\, dV + \int_{A_e} \overline{V}\, d\dot{m}_e - \int_{A_i} \overline{V}\, d\dot{m}_i$$

↓ ↓ ↓ ↓

= the $\sum$ of the external forces acting on the c.v.

= body + point + distributed, e.g. (pressure) forces

= the rate of change of momentum in the c.v.

= 0 for steady-state

= the rate of momentum leaving the c.v.

= the rate of momentum entering the c.v.

and where $\overline{V}$ is the vector momentum velocity relative to an inertial reference frame.

Key Point: Thus, the **momentum velocity has magnitude and direction** and is measured relative to the reference frame (coordinate system) being used for the problem. The **velocities in the mass flow terms** $\dot{m}_i$ and $\dot{m}_e$ **are scalars**, as noted previously, and are **measured relative to the inlet or exit boundary**.

Always clearly define a coordinate system and use it to specify the value of all inlet and exit momentum velocities when working linear momentum problems.



ketabline.com Ebook.ketabline.com

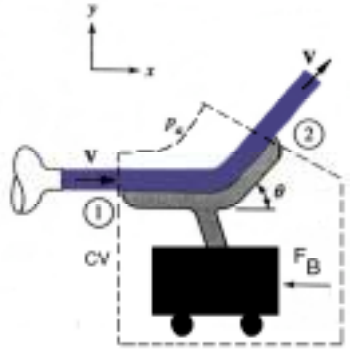
For the 'x' direction, the previous equation becomes

$$\sum \bar{F}_x = \frac{\partial}{\partial t}\int_{cv} \bar{V}_x \rho dV + \int_{A_e} \bar{V}_{x,e}\, d\dot{m}_e - \int_{A_i} \bar{V}_{x,i}\, d\dot{m}_i$$

Note that the above equation is also valid for control volumes moving at constant velocity with the coordinate system placed on the moving control volume. This is because an inertial coordinate system is a nonaccelerating coordinate system which is still valid for a c.s. moving at constant velocity.

Example:

A water jet 4 cm in diameter with a velocity of 7 m/s is directed to a stationary turning vane with $\theta = 40^o$. Determine the force F necessary to hold the vane stationary.



Governing equation:

$$\sum \bar{F}_x = \frac{\partial}{\partial t}\int_{cv} \bar{V}_x \rho dV + \int_{A_e} \bar{V}_{x,e}\, d\dot{m}_e - \int_{A_i} \bar{V}_{x,i}\, d\dot{m}_i$$

Since the flow is steady and the c.v. is stationary, the time rate of change of momentum within the c.v. is zero. Also with uniform velocity at each inlet and exit and a constant flow rate, the momentum equation becomes

$$-F_b = \dot{m}_e V_e - \dot{m}_i V_i$$

Note that the braking force, F_b, is written as negative since it is **assumed** to be in the negative x direction relative to positive x for the coordinate system.



ketabline.com Ebook.ketabline.com

From the previous example for conservation of mass, we can again write

$$\dot{m} = \int_{cs} \rho V \, dA = \rho A V = 998 \text{ kg/m}^3 * 7 \text{ m/s} * \pi * 0.04^2/4$$

$\dot{m}_1 =$ **8.78 kg/s** and $V_1 =$ **7 m/s**

and for the exit:

$\dot{m}_2 =$ **8.78 kg/s** and $V_2 =$ **7 m/s** inclined 40° above the horizontal.

Substituting in the momentum equation, we obtain

$$-F_b = 8.78 \text{ kg/s} * 7 \text{ m/s} * \cos 40^o - 8.78 \text{ kg/s} * 7 \text{ m/s}$$

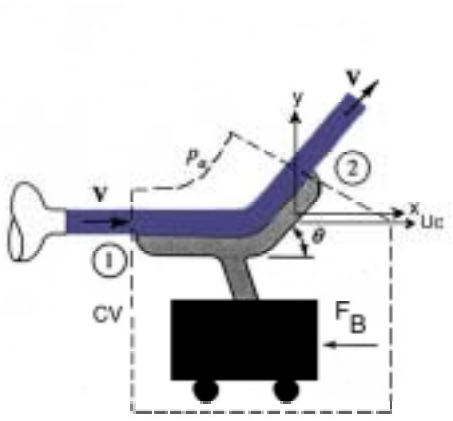
and $-F_b = -14.4 \text{ kg m/s}^2$ or $F_b =$ **14.4 N** ← **ans.**

Note: Since our final answer is positive, our original assumption of the applied force being to the left was correct. Had we assumed that the applied force was to the right, our answer would be negative, meaning that the direction of the applied force is opposite to what was assumed.

Modify Problem:

Now consider the same problem but with the cart moving to the right with a velocity $U_c = 2$ m/s. Again solve for the value of braking force F_b necessary to maintain a constant cart velocity of 2 m/s.

Note: The coordinate system for the problem has now been placed on the moving cart.



ketabline.com Ebook.ketabline.com

The transient term in the momentum equation is still zero. With the coordinate system on the cart, the momentum of the cart relative to the coordinate system is still zero. The fluid stream is still moving relative to the coordinate system, however, the flow is steady with constant velocity and the time rate of change of momentum of the fluid stream is therefore also zero. Thus

The momentum equation has the same form as for the previous problem (However the value of individual terms will be different.)

$$-F_b = \dot{m}_e V_e - \dot{m}_i V_i$$

$\dot{m}_1 = \rho_1 V_1 A_1 = 998 \text{ kg/m}^3 * 5 \text{ m/s} * \pi * 0.04^2/4 = 6.271 \text{ kg/s} = \dot{m}_2$

Now we must determine the momentum velocity at the inlet and exit. With the coordinate system on the moving control volume, the values of momentum velocity are

$V_1 = V_J - U_c = 7 - 2 = 5$ m/s and $V_2 = 5$ m/s inclined 40°

The momentum equation (x - direction) now becomes

$$-F_b = 6.271 \text{ kg/s} * 5 \text{ m/s} * \cos 40^o - 6.271 \text{ kg/s} * 5 \text{ m/s}$$

and $-F_b = -7.34 \text{ kg m/s}^2$ or $F_b =$ **7.34 N** ← **ans.**

Question: What would happen to the braking force F_b if the turning angle had been $> 90^o$, e.g., 130°? Can you explain based on your understanding of change in momentum for the fluid stream?

Review and work examples for linear momentum with fixed and non-accelerating (moving at constant velocity) control volumes.

Accelerating Control Volume

The previous formulation applies only to an inertial coordinate system, i.e., fixed or moving at constant velocity (non-accelerating).



ketabline.com Ebook.ketabline.com

We will now consider problems with accelerating control volumes. For these problems we will again place the coordinate system on the accelerating control volume, thus making it a non-inertial coordinate system.

For coordinate systems placed on an accelerating control volume, we must account for the acceleration of the c.s. by correcting the momentum equation for this acceleration. This is accomplished by including the term as shown below:

$$\sum \bar{F} - \int_{cv} \bar{a}_{cv}\, dm_{cv} = \frac{\partial}{\partial t}\int_{cv} \bar{V}\rho\, dV + \int_{A_e} \bar{V}\, d\dot{m}_e - \int_{A_i} \bar{V}\, d\dot{m}_i$$

$\bar{a}_{cv}\, dm_{cv}$ ↓

integral sum of
the local c.v. (c.s.)
acceleration * the c.v. mass

The added term accounts for the acceleration of the control volume and allows the problem to be worked with the coordinate system placed on the accelerating c.v.

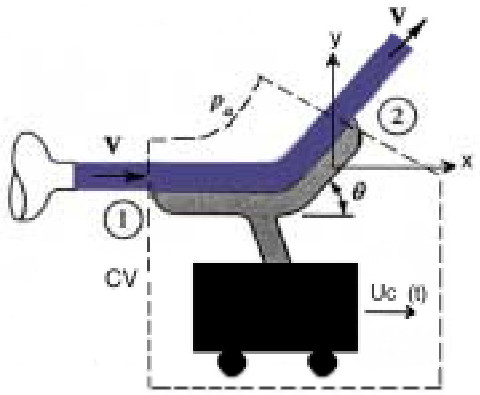
Note: Thus, all vector (momentum) velocities are then measured relative to an observer (coordinate system) on the accelerating control volume. For example, the velocity of a rocket as seen by an observer (c.s.) standing on the rocket is zero and the time rate of change of momentum is zero in this reference frame even if the rocket is accelerating.

Accelerating Control Volume Example

A turning vane with $\theta = 60^{o}$ accelerates from rest due to a jet of water ($V_J = 35$ m/s, $A_J = 0.003$ m^2). Assuming the mass of the cart m_c, is 75 kg and neglecting drag and friction effects, find:

a. Cart acceleration at t = 0.

b. U_c as a f(t)



ketabline.com Ebook.ketabline.com

Starting with the general equation shown above, we can make the following assumptions:

1. $\sum F_x = 0$, no friction or body forces.
2. The jet has uniform velocity and constant properties.
3. The entire cart accelerates uniformly over the entire control volume.
4. Neglect the relative momentum change of the jet stream that is within the control volume.

With these assumptions, the governing equation simplifies to

$$-a_c m_c = \dot{m}_e V_{x,e} - \dot{m}_i V_{x,i}$$

We thus have terms that account for the acceleration of the control volume, for the exit momentum, and for the inlet momentum (both of which change with time.)

Mass flow:

As with the previous example for a moving control volume, the mass flow terms are given by:

$$\dot{m}_i = \dot{m}_e = \dot{m} = \rho A_J (V_J - U_c)$$

Note that since the cart accelerates, U_c is not a constant but rather changes with time.

Momentum velocities:

$$U_{x,i} = V_J - U_c \qquad U_{x,e} = (V_J - U_c)\cos\theta$$

Substituting, we now obtain

$$-a_c m_c = \rho A_J (V_J - U_c)^2 \cos\theta - \rho A_J (V_J - U_c)$$

Solving for the cart acceleration, we obtain

$$a_c = \frac{\rho A_J (1 - \cos\theta)(V_J - U_c)^2}{m_c}$$



ketabline.com Ebook.ketabline.com

Substituting for the given values at t = 0, i.e., $U_c = 0$, we obtain

$$a_c\,(t = 0) = 24.45 \text{ m/s}^2 = 2.49 \text{ g's}$$

Note: The acceleration at any other time can be obtained once the cart velocity U_c at that time is known.

To determine the equation for cart velocity as a function of time, the equation for the acceleration must be written in terms of U_c (t) and integrated.

$$\frac{dU_c}{dt} = \frac{\rho A_J (1 - \cos\theta)(V_J - U_c)^2}{m_c}$$

Separating variables, we obtain

$$\int_0^{U_c(t)} \frac{dU_c}{(V_J - U_c)^2} = \int_0^t \frac{\rho A_J (1 - \cos\theta)}{m_c} dt$$

Completing the integration and rearranging the terms, we obtain a final expression of the form

$$\frac{U_c}{V_J} = \frac{V_J\, b\, t}{1 + V_J\, b\, t} \qquad \text{where} \qquad b = \frac{\rho A_J (1 - \cos\theta)}{m_c}$$

Substituting for known values, we obtain $V_J\, b = 0.699 \text{ s}^{-1}$

Thus the final equation for U_c is give by

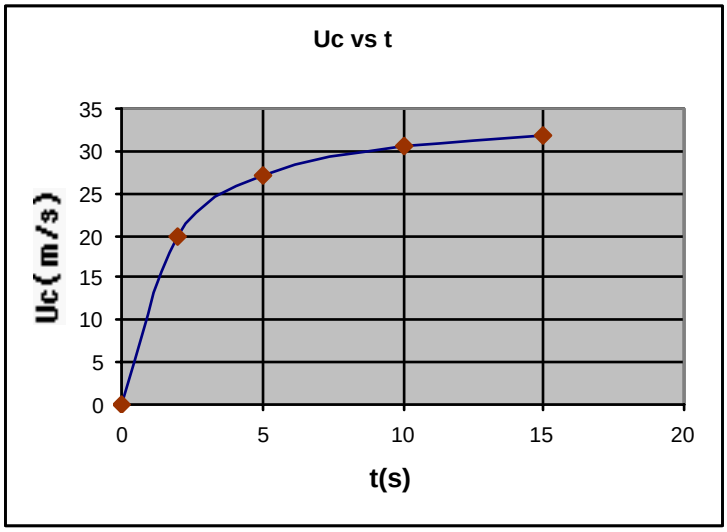
$$\frac{U_c}{V_J} = \frac{0.699\, t}{1 + 0.699\, t}$$



ketabline.com Ebook.ketabline.com

The final results are now given as shown below:

t (s)	U_c/V_J	U_c (m/s)	a_c (m/s^2)
0	0.0	0.0	24.45
2	0.583	20.0	4.49
5	0.757	27.2	1.22
10	0.875	30.6	0.39
15	0.912	31.9	0.192
∞	1.0	35	0.0



Note that the limiting case occurs when the cart velocity reaches the jet velocity. At this point, the jet can impart no more momentum to the cart, the acceleration is now zero, and the terminal velocity has been reached.

Review the text example on accelerating control volumes.

Moment of Momentum (angular momentum)

For moment of momentum we have that

$$\bar{B} = \bar{H} = \bar{r} \times (m\,\bar{V}) \quad and \quad \bar{\beta} = \bar{r} \times \bar{V}$$

From the previous equation for moment of momentum and these definitions, Reynolds transport theorem becomes



ketabline.com Ebook.ketabline.com

$$\sum \bar{M} = \frac{\partial}{\partial t}\int_{cv} \bar{r} \times \bar{V}\, \rho\, dV + \int_{A_e} \bar{r} \times \bar{V}\, d\dot{m}_e - \int_{A_i} \bar{r} \times \bar{V}\, d\dot{m}_i$$

= the $\sum$ of all external moments acting on the c.v.	= the rate of change of momentum in the c.v. = 0 for steady state	= the rate of moment of momentum leaving the c.v.	= the rate of moment of momentum entering the c.v.

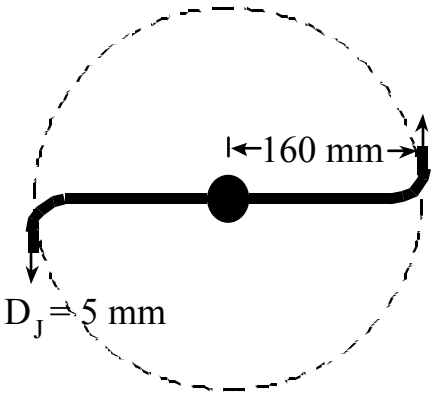
For the special case of steady-state, steady-flow and uniform properties at any exit or inlet, the equation becomes

$$\sum \bar{M} = \sum \dot{m}_e\, \bar{r} \times V_e - \sum \dot{m}_i\, \bar{r} \times V_i$$

For moment of momentum problems, we must be careful to correctly evaluate the moment of all applied forces and all inlet and exit momentum flows, with particular attention to the signs.

Moment of Momentum Example:

A small lawn sprinkler operates as indicated. The inlet flow rate is 9.98 kg/min with an inlet pressure of 30 kPa. The two exit jets direct flow at an angle of 40° above the horizontal.



For these conditions, determine the following:

a. Jet velocity relative to the nozzle.

b. Torque required to hold the arm stationary.

c. Friction torque if the arm is rotating at 35 rpm.

d. Maximum rotational speed if we neglect friction.



ketabline.com Ebook.ketabline.com

a. R = 160 mm, D_J = 5 mm, Therefore, for each of the two jets:

$$Q_J = 0.5 * 9.98 \text{ kg/min} / 998 \text{ kg/m}^3 = 0.005 \text{ m}^3/\text{min}$$

$$A_J = \pi \pi \ 0.0025^2 = 1.963 * 10^{-5} \text{ m}^2$$

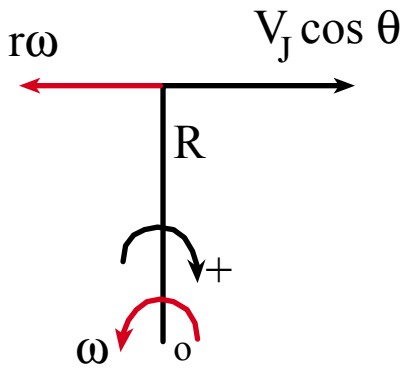
$$V_J = 0.005 \text{ m}^3/\text{min} / 1.963 * 10^{-5} \text{ m}^2 / 60 \text{ s/min}$$

V_J = 4.24 m/s relative to the nozzle exit **ans.**

b. Torque required to hold the arm stationary.

First develop the governing equations and analysis for the general case of the arm rotating.

With the coordinate system at the center of rotation of the arm, a general velocity diagram for the case when the arm is rotating is shown in the adjacent schematic.



Taking the moment about the center of rotation, the moment of the inlet flow is zero since the moment arm is zero for the inlet flow.

The basic equation then becomes

$$T_0 = 2\dot{m}_e R (V_J \cos\alpha - R\omega)$$

Note that the net momentum velocity is the difference between the tangential component of the jet exit velocity and the rotational speed of the arm. Also note that the direction of positive moments was taken as the same as for V_J and opposite to the direction of rotation.

For a stationary arm R ω = 0. We thus obtain for the stationary torque



ketabline.com Ebook.ketabline.com

$$T_o = 2\,\rho\,Q_J\,R\,V_J\cos\alpha$$

$$T_o = 2*998\frac{kg}{m^3}.005\frac{m^3}{\min}\frac{1\min}{60}m*4.24\frac{m}{s}\cos 4.160^o$$

$T_o = 0.0864$ N m clockwise. **ans.**

A resisting torque of 0.0864 N m must be applied in the clockwise direction to keep the arm from rotating in the counterclockwise direction.

c. At $\omega = 30$ rpm, calculate the friction torque T_f

$$\omega = 30\frac{rev}{\min}2\pi\frac{rad}{rev}\frac{1\min}{60} = \pi\frac{rad}{s}$$

$$T_o = 2*998\frac{kg}{m^3}0.005\frac{m^3}{\min}\frac{1\min}{60}0.16m\left[4.24\frac{m}{s}\cos 40^o - .16m*\pi\frac{rad}{s}\right]$$

ans.

Note; The resisting torque decreases as the speed increases.

d. Find the maximum rotational speed.

The maximum rotational speed occurs when the opposing torque is zero and all the moment of momentum goes to the angular rotation. For this case,

$$V_J\cos\theta - R\omega = 0$$

$$\omega = \frac{V_J\cos\theta}{R} = \frac{4.2\frac{rad}{s} = 193.8\,rpm\;4\,m/s\bullet\cos 40}{0.16\,m} = 20.3\frac{rad}{s} = 193.8\,rpm$$ **ans.**

Review material and examples on moment of momentum.



ketabline.com Ebook.ketabline.com

Energy Equation (Extended Bernoulli Equation)

For energy, we have that

$$B = E = \int_{cv} e\,\rho\,d\,V \qquad \text{and} \qquad \beta = e = u + \frac{1}{2}V^2 + g\,z$$

From the previous statement of conservation of energy and these definitions, Reynolds transport theorem becomes:

$$\dot{Q} - \dot{W} = \left.\frac{d\,E}{d\,t}\right)_{sys} = \frac{\partial}{\partial\,t}\int_{cv} e\,\rho\,dV + \int_{A_e} e_e\,\rho_e\,\bar{V}_e\cdot d\,A_e - \int_{A_i} e_i\,\rho_i\,\bar{V}_i\cdot d\,A_i$$

After extensive algebra and simplification (see text for detailed development), we obtain:

$$\frac{P_1 - P_2}{\rho\,g} = \frac{V_2^2 - V_1^2}{2\,g} + Z_2 - Z_1 + h_{f,1-2} - h_p$$

↓	↓	↓	↓	↓
Pressure drop from 1 – 2, in the flow direction	**Pressure drop due to acceleration of the fluid**	**Pressure drop due to elevation change**	**Pressure drop due to frictional head loss**	**Pressure drop due to mechanical work on fluid**

Note: this formulation must be written in the flow direction from 1 - 2 to be consistent with the sign of the mechanical work term and so that $h_{f,1\text{-}2}$ is always a positive term. Also note the following:

- The points 1 and 2 must be specific points along the flow path
- Each term has units of linear dimension, e.g., ft or meters, and $z_2 - z_1$ is positive for z_2 above z_1
- The term $h_{f,1\text{-}2}$ is always positive when written in the flow direction and for internal, pipe flow includes pipe or duct friction losses and fitting or piping component (valves, elbows, etc.) losses,



ketabline.com Ebook.ketabline.com

- The term h_p is positive for pumps and fans (i.e., pumps increase the pressure in the flow direction) and negative for turbines (turbines decrease the pressure in the flow direction)
- For pumps:

$$h_p = \frac{w_s}{g}$$ where w_S = the useful work per unit mass to the fluid

Therefore: $w_s = g\,h_p$ and $\dot{W}_f = \dot{m} w_s = \rho Q g\, h_p$

where $\dot{W}_f$ = the useful power delivered to the fluid

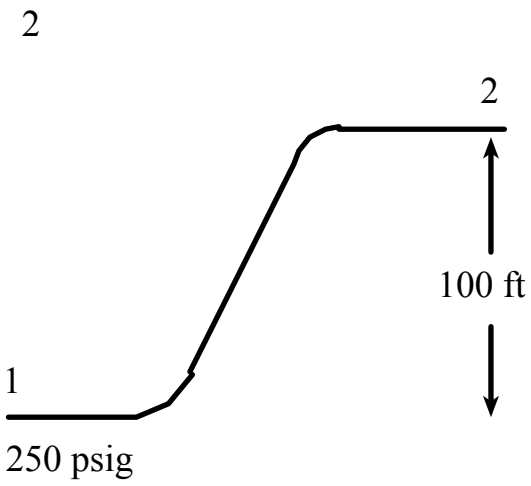
and $\dot{W}_p = \frac{\dot{W}_f}{\eta_p}$ where η_p is the pump efficiency

Example

Water flows at 30 ft/s through a 1000 ft length of 2 in diameter pipe. The inlet pressure is 250 psig and the exit is 100 ft higher than the inlet.

Assuming that the frictional loss is given by 18 $V^2/2g$,

Determine the exit pressure.



Given: $V_1 = V_2 = 30$ ft/s, $L = 1000$ ft, $Z_2 - Z_1 = 100$ ft, $P_1 = 250$ psig

Also, since there is no mechanical work in the process, the energy equation simplifies to

ketabline.com Ebook.ketabline.com

$$\frac{P_1 - P_2}{\rho g} = Z_2 - Z_1 \quad + \quad h_f$$

$$\frac{P_1 - P_2}{\rho g} = 100\ ft + 18\frac{30^2\ ft^2/s^2}{64.4\ ft/s^2} \quad = \quad 351.8\ ft$$

$$P_1 - P_2 = 62.4\ \text{lbf/ft}^3\ \ 351.8\ \text{ft} = 21{,}949\ \text{psf} = 152.4\ \text{psi}$$

$$P_2 = 250 - 152.4 = 97.6\ \text{psig} \quad \textbf{ans.}$$

Problem Extension

A pump driven by an electric motor is now added to the system. The motor delivers 10.5 hp. The flow rate and inlet pressure remain constant and the pump efficiency is 71.4 %, determine the new exit pressure.

$$Q = AV = \pi\pi\ (1/12)^2\ \text{ft}^2 * 30\ \text{ft/s} = 0.6545\ \text{ft}^3/\text{s}$$

$$W_f = \eta_p\ W_p = \rho\ Q\ g\ h_p$$

$$h_p = \frac{0.714 * 10.5 hp * 550 ft - lbf/s/hp}{62.4 lbm/ft^3 * 0.6545 ft^3/s} = 101 ft$$

The pump adds a head increase equal to 101 ft to the system and the exit pressure should increase.

Substituting in the energy equation, we obtain

$$\frac{P_1 - P_2}{\rho g} = 100\ ft + 18\frac{30^2\ ft^2/s^2}{64.4\ ft/s^2} \quad - 101\ ft = \quad 250.8\ ft$$

$$P_1 - P_2 = 62.4\ \text{lbf/ft}^3\ \ 250.8\ \text{ft} = 15{,}650\ \text{psf} = 108.7\ \text{psi}$$

$$P_2 = 250 - 108.7 = 141.3\ \text{psig} \quad \textbf{ans.}$$

Review examples for the use of the energy equation



ketabline.com Ebook.ketabline.com

Ch. IV Differential Relations for a Fluid Particle

This chapter presents the development and application of the basic differential equations of fluid motion. Simplifications in the general equations and common boundary conditions are presented that allow exact solutions to be obtained. Two of the most common simplifications are 1). steady flow and 2). incompressible flow.

The Acceleration Field of a Fluid

A general expression of the flow field velocity vector is given by:

$$\bar{V}(\bar{r},t) = \hat{i}\,u(x,y,z,t) + \hat{j}\,\mathrm{v}(x,y,z,t) + \hat{k}\,w(x,y,z,t)$$

One of two reference frames can be used to specify the flow field characteristics:

eulerian – the coordinates are fixed and we observe the flow field characteristics as it passes by the fixed coordinates.

lagrangian - the coordinates move through the flow field following individual particles in the flow.

Since the primary equation used in specifying the flow field velocity is based on Newton's second law, the acceleration vector is an important solution parameter. In cartesian coordinates, this is expressed as

$$\bar{a} = \frac{d\bar{V}}{dt} = \underbrace{\frac{\partial \bar{V}}{\partial t}}_{\text{local}} + \underbrace{\left(u\frac{\partial \bar{V}}{\partial x} + \mathrm{v}\frac{\partial \bar{V}}{\partial y} + w\frac{\partial \bar{V}}{\partial z} \right)}_{\text{convective}} = \frac{\partial \bar{V}}{\partial t} + (\bar{V}\cdot\bar{\nabla})\bar{V}$$

total

The acceleration vector is expressed in terms of three types of derivatives:

Total acceleration = total derivative of velocity vector

= local derivative + convective derivative of velocity vector



ketabline.com Ebook.ketabline.com

Likewise, the total derivative (also referred to as the substantial derivative) of other variables can be expressed in a similar form, e.g.,

$$\frac{dP}{dt} = \frac{\partial P}{\partial t} + \left(u\frac{\partial P}{\partial x} + v\frac{\partial P}{\partial y} + w\frac{\partial P}{\partial z} \right) = \frac{\partial P}{\partial t} + \left(\overline{V}\cdot\overline{\nabla}\right)P$$

Example 4.1

Given the eulerian velocity-vector field

$$\overline{V} = 3t\,\hat{i} + xz\,\hat{j} + t\,y^2\,\hat{k}$$

find the acceleration of the particle.

For the given velocity vector, the individual components are

$$u = 3t \qquad v = xz \qquad w = t\,y^2$$

Evaluating the individual components, we obtain

$$\frac{\partial \overline{V}}{\partial t} = 3\,\mathbf{i} + y^2\,\mathbf{k}$$

$$\frac{\partial \overline{V}}{\partial x} = z\,\mathbf{j} \qquad \frac{\partial \overline{V}}{\partial y} = 2ty\,\mathbf{k} \qquad \frac{\partial \overline{V}}{\partial z} = x\,\mathbf{j}$$

Substituting, we obtain

$$\frac{d\overline{V}}{dt} = (3\,\mathbf{i} + y^2\,\mathbf{k}) + (3t)(z\,\mathbf{j}) + (xz)(2ty\,\mathbf{k}) + (t\,y^2)(x\,\mathbf{j})$$

After collecting terms, we have

$$\frac{d\overline{V}}{dt} = 3\,\mathbf{i} + (3tz + txy^2)\,\mathbf{j} + (2xyzt + y^2)\,\mathbf{k} \quad \textbf{ans.}$$



ketabline.com Ebook.ketabline.com

The Differential Equation of Conservation of Mass

If we apply the basic concepts of conservation of mass to a differential control volume, we obtain a differential form for the continuity equation in cartesian coordinates

$$\frac{\partial \rho}{\partial t} + \frac{\partial}{\partial x}(\rho u) + \frac{\partial}{\partial y}(\rho \mathrm{v}) + \frac{\partial}{\partial z}(\rho w) = 0$$

and in cylindrical coordinates

$$\frac{\partial \rho}{\partial t} + \frac{1}{r}\frac{\partial}{\partial r}(r\,\rho \mathrm{v}_r) + \frac{1}{r}\frac{\partial}{\partial \theta}(\rho \mathrm{v}_\theta) + \frac{\partial}{\partial z}(\rho \mathrm{v}_z) = 0$$

Steady Compressible Flow

For steady flow, the term $\frac{\partial}{\partial t} = 0$ and all properties are function of position only.

The previous equations simplify to

Cartesian: $$\frac{\partial}{\partial x}(\rho u) + \frac{\partial}{\partial y}(\rho \mathrm{v}) + \frac{\partial}{\partial z}(\rho w) = 0$$

Cylindrical: $$\frac{1}{r}\frac{\partial}{\partial r}(r\,\rho \mathrm{v}_r) + \frac{1}{r}\frac{\partial}{\partial \theta}(\rho \mathrm{v}_\theta) + \frac{\partial}{\partial z}(\rho \mathrm{v}_z) = 0$$

Incompressible Flow

For incompressible flow, density changes are negligible, ρ = const., and $\frac{\partial \rho}{\partial t} = 0$

In the two coordinate systems, we have

Cartesian: $$\frac{\partial u}{\partial x} + \frac{\partial \mathrm{v}}{\partial y} + \frac{\partial w}{\partial z} = 0$$



ketabline.com Ebook.ketabline.com

Cylindrical: $$\frac{1}{r}\frac{\partial}{\partial r}(r\,v_r)+\frac{1}{r}\frac{\partial}{\partial \theta}(v_\theta)+\frac{\partial}{\partial z}(v_z)=0$$

Key Point:

It is noted that the assumption of incompressible flow is not restricted to fluids which cannot be compressed, e.g. liquids. Incompressible flow is valid for (1) when the fluid is essentially incompressible (liquids) and (2) for compressible fluids for which compressibility effects are not significant for the problem being considered.

The second case is assumed to be met when the Mach number is less than 0.3:

Ma = V/c < 0.3 Gas flows can be considered incompressible

The Differential Equation of Linear Momentum

If we apply Newton's Second Law of Motion to a differential control volume we obtain the three components of the differential equation of linear momentum. In cartesian coordinates, the equations are expressed in the form:

$$\rho g_x - \frac{\partial p}{\partial x} + \frac{\partial \tau_{xx}}{\partial x} + \frac{\partial \tau_{yx}}{\partial y} + \frac{\partial \tau_{zx}}{\partial z} = \rho\left(\frac{\partial u}{\partial t} + u\frac{\partial u}{\partial x} + v\frac{\partial u}{\partial y} + w\frac{\partial u}{\partial z}\right)$$

$$\rho g_y - \frac{\partial p}{\partial y} + \frac{\partial \tau_{xy}}{\partial x} + \frac{\partial \tau_{yy}}{\partial y} + \frac{\partial \tau_{zy}}{\partial z} = \rho\left(\frac{\partial v}{\partial t} + u\frac{\partial v}{\partial x} + v\frac{\partial v}{\partial y} + w\frac{\partial v}{\partial z}\right)$$

$$\rho g_z - \frac{\partial p}{\partial z} + \frac{\partial \tau_{xz}}{\partial x} + \frac{\partial \tau_{yz}}{\partial y} + \frac{\partial \tau_{zz}}{\partial z} = \rho\left(\frac{\partial w}{\partial t} + u\frac{\partial w}{\partial x} + v\frac{\partial w}{\partial y} + w\frac{\partial w}{\partial z}\right)$$

Inviscid Flow: Euler's Equation

If we assume the flow is frictionless, all of the shear stress terms drop out. The resulting equation is known as Euler's equation and in vector form is given by:

$$\rho\mathbf{g} - \nabla P = \rho\frac{d\mathbf{V}}{dt}$$



ketabline.com Ebook.ketabline.com

where $\frac{d\mathbf{V}}{dt}$ is the total or substantial derivative of the velocity discussed previously and ∇P is the usual vector gradient of pressure. This form of Euler's equation can be integrated along a streamline to obtain the frictionless Bernoulli's equation (Sec. 4.9).

The Differential Equation of Energy

The differential equation of energy is obtained by applying the first law of thermodynamics to a differential control volume. The most complex element of the development is the differential form of the control volume work due to both normal and tangential viscous forces. When this is done, the resulting equation has the form

$$\rho\frac{du}{dt} + P(\nabla\cdot\mathbf{V}) = \nabla\cdot(k\nabla T) + \Phi$$

where Φ is the viscous dissipation function. The term for the total derivative of internal energy includes both the transient and convective terms seen previously.

Two common assumptions used to simplify the general equation are:

1. $du \approx Cv\ dT$ and 2. $Cv, \mu, k, \rho \approx$ constants

With these assumptions, the energy equation reduces to

$$\rho C_v\frac{dT}{dt} = k\nabla^2 T + \Phi$$

It is noted that the flow-work term was eliminated as a result of the assumption of constant density, ρ, for which the continuity equation becomes $\nabla\cdot V = 0$,thus eliminating the term $P(\nabla\cdot V)$.

We now have the three basic differential equations necessary to obtain complete flow field solutions of fluid flow problems.



ketabline.com Ebook.ketabline.com

Boundary Conditions for the Basic Equations

In vector form, the three basic governing equations are written as

Continuity: $$\frac{\partial \rho}{\partial t} + \nabla \cdot (\rho \mathbf{V}) = 0$$

Momentum: $$\rho \frac{d\mathbf{V}}{dt} = \rho \mathbf{g} - \nabla P + \nabla \cdot \tau_{ij}$$

Energy: $$\rho \frac{du}{dt} + P(\nabla \cdot \mathbf{V}) = \nabla \cdot (k \nabla T) + \Phi$$

We have three equations and five unknowns: ρ, V, P, u, and T ; and thus need two additional equations. These would be the equations of state describing the variation of density and internal energy as functions of P and T, i.e.,

$$\rho = \rho(P,T) \text{ and } u = u(P,T)$$

Two common assumptions providing this information are either:

1. Ideal gas: $\rho = P/RT$ and $du = Cv\, dT$

2. Incompressible fluid: ρ = constant and $du = C\, dT$

Time and Spatial Boundary Conditions

Time Boundary Conditions: If the flow is unsteady, the variation of each of the variables (ρ, V, P, u, and T) must be specified initially, t = 0, as functions of spatial coordinates e.g. x,y,z.

Spatial Boundary Conditions: The most common spatial boundary conditions are those specified at a fluid – surface boundary. This typically takes the form of assuming equilibrium (e.g., no slip condition – no property jump) between the fluid and the surface at the boundary.



ketabline.com Ebook.ketabline.com

This takes the form:

$$V_{fluid} = V_{wall} \qquad T_{fluid} = T_{wall}$$

Note that for porous surfaces with mass injection, the wall velocity will be equal to the injection velocity at the surface.

A second common spatial boundary condition is to specify the values of V, P, and T at any flow inlet or exit.

Example 4.6

For steady incompressible laminar flow through a long tube, the velocity distribution is given by

$$v_z = U\left(1 - \frac{r^2}{R^2}\right) \qquad v_r = 0 \qquad v_\theta = 0$$

where U is the maximum or centerline velocity and R is the tube radius. If the wall temperature is constant at Tw and the temperature T = T(r) only, find T(r) for this flow.

For the given conditions, the energy equation reduces to

$$\rho C_v v_r \frac{dT}{dr} = \frac{k}{r}\frac{d}{dr}\left(r\frac{dT}{dr}\right) + \mu\left(\frac{dv_z}{dr}\right)^2$$

Substituting for v_z and realizing the $v_r = 0$, we obtain

$$\frac{k}{r}\frac{d}{dr}\left(r\frac{dT}{dr}\right) = -\mu\left(\frac{dv_z}{dr}\right)^2 = -\frac{4U^2\mu r^2}{R^4}$$

Multiply by r/k and integrate to obtain



ketabline.com Ebook.ketabline.com

$$\frac{dT}{dr} = -\frac{\mu U^2 r^3}{k R^4} + C_1$$

Integrate a second time to obtain

$$T = -\frac{\mu U^2 r^4}{4 k R^4} + C_1 \ln r + C_2$$

Since the term, ln r, approaches infinity as r approaches 0, $C_1 = 0$.

Applying the wall boundary condition, $T = T_W$ at $r = R$, we obtain for C_2

$$C_2 = T_w + \frac{\mu U^2}{4 k}$$

The final solution then becomes

$$T(r) = T_w + \frac{\mu U^2}{4 k}\left(1 - \frac{r^4}{R^4}\right)$$

The Stream Function

The necessity to obtain solutions for multiple variables in multiple governing equations presents an obvious mathematical challenge. However, the stream function, Ψ , allows the continuity equation to be eliminated and the momentum equation solved directly for the single variable, Ψ . The use of the stream function works for cases when the continuity equation can be reduced to only two terms.

For example, for 2-D, incompressible flow, continuity becomes

$$\frac{\partial u}{\partial x} + \frac{\partial v}{\partial y} = 0$$



ketabline.com Ebook.ketabline.com

Defining the velocity components to be

$$u = \frac{\partial \Psi}{\partial y} \quad and \quad v = -\frac{\partial \Psi}{\partial x}$$

which when substituted into the continuity equation yields

$$\frac{\partial}{\partial x}\left(\frac{\partial \Psi}{\partial y}\right) + \frac{\partial}{\partial y}\left(-\frac{\partial \Psi}{\partial x}\right) = 0$$

and continuity is automatically satisfied.

Geometric interpretation of Ψ

It is easily shown that lines of constant Ψ are flow streamlines. Since flow does not cross a streamline, for any two points in the flow we can write

$$Q_{1\to 2} = \int_1^2 (V \cdot n)\, dA = \int_1^2 d\Psi = \Psi_2 - \Psi_1$$

Thus the volume flow rate between two points in the flow is equal to the difference in the stream function between the two points.

Steady Plane Compressible Flow

In like manner, for steady, 2-D, compressible flow, the continuity equation is

$$\frac{\partial}{\partial x}(\rho u) + \frac{\partial}{\partial y}(\rho v) = 0$$

For this problem, the stream function can be defined such that

$$\rho u = \frac{\partial \Psi}{\partial y} \quad and \quad \rho v = -\frac{\partial \Psi}{\partial x}$$



ketabline.com Ebook.ketabline.com

As before, lines of constant stream function are streamlines for the flow, but the change in stream function is now related to the local mass flow rate by

$$\dot{m}_{1-2} = \int_1^2 \rho (V \cdot n)\, dA = \int_1^2 d\Psi = \Psi_2 - \Psi_1$$

Vorticity and Irrotationality

The concept of vorticity and irrotationality are very useful in analyzing many fluid problems. The analysis starts with the concept of angular velocity in a flow field.

Consider three points, A, B, & C, initially perpendicular at time t, that then move and deform to have the position and orientation at t + dt.

The lines AB and BC have both changed length and incurred angular rotation dα and dβ relative to their initial positions.

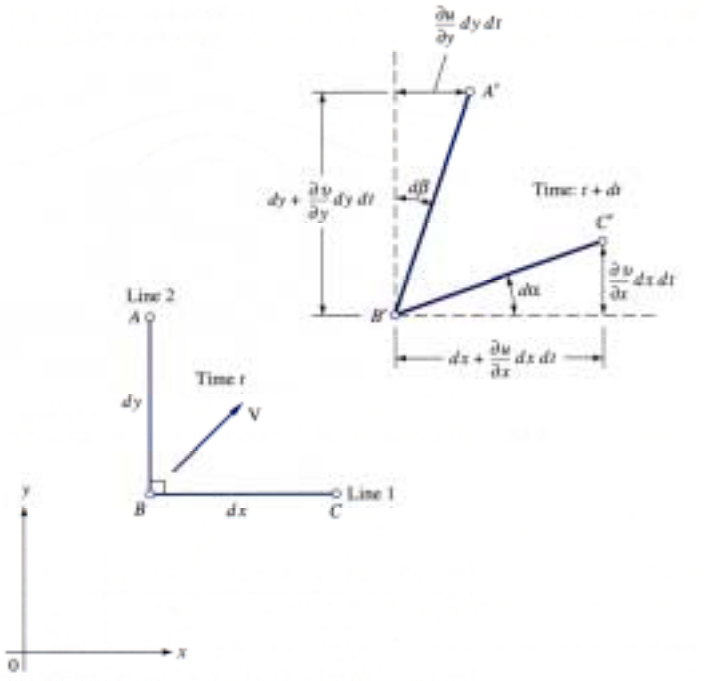


Fig. 4.10 Angular velocity and strain rate of two fluid lines deforming in the x-y plane

We define the angular velocity ω_z about the z axis as the average rate of counter-clockwise turning of the two lines expressed as

$$\omega_z = \frac{1}{2}\left(\frac{d\alpha}{dt} - \frac{d\beta}{dt}\right)$$



ketabline.com Ebook.ketabline.com

Applying the geometric properties of the deformation shown in Fig. 4.10 and taking the limit as $\Delta t \rightarrow 0$, we obtain

$$\omega_z = \frac{1}{2}\left(\frac{dv}{dx} - \frac{du}{dy}\right)$$

In like manner, the angular velocities about the remaining two axes are

$$\omega_x = \frac{1}{2}\left(\frac{dw}{dy} - \frac{dv}{dz}\right) \qquad \omega_y = \frac{1}{2}\left(\frac{du}{dz} - \frac{dw}{dx}\right)$$

From vector calculus, the angular velocity can be expressed as a vector with the form

$\boldsymbol{\omega} = \mathbf{i}\,\omega_x + \mathbf{j}\,\omega_y + \mathbf{k}\,\omega_z$ = 1/2 the curl of the velocity vector, e.g.

$$\omega = \frac{1}{2}(curl\,\mathbf{V}) = \frac{1}{2}\begin{vmatrix} i & j & k \\ \partial & \partial & \partial \\ \partial x & \partial y & \partial z \\ u & v & w \end{vmatrix}$$

The factor of 2 is eliminated by defining the vorticity, ξ, as follows:

$$\xi = 2\,\boldsymbol{\omega} = \text{curl}\,\mathbf{V}$$

Frictionless Irrotational Flows

When a flow is both frictionless and irrotational, the momentum equation reduces to Euler's equation given previously by

$$\rho\mathbf{g} - \nabla P = \rho\frac{d\mathbf{V}}{dt}$$



ketabline.com Ebook.ketabline.com

As shown in the text, this can be integrated along the path, ds, of a streamline through the flow to obtain

$$\int_1^2 \frac{\partial V}{\partial t}\, ds + \int_1^2 \frac{d\,P}{\rho} + \frac{1}{2}\left(V_2^2 - V_1^2\right) + g\left(z_2 - z_1\right) = 0$$

For steady, incompressible flow this reduces to

$$\frac{P}{\rho} + \frac{1}{2}V^2 + g\,z = \quad \text{constant along a streamline}$$



ketabline.com Ebook.ketabline.com

V. Modeling, Similarity, and Dimensional Analysis

To this point, we have concentrated on analytical methods of solution for fluids problems.

However, analytical methods are not always satisfactory due to:

(1) limitations due to simplifications required in the analysis,

(2) complexity and/or expense of a detailed analysis.

The most common alternative is to:

Use experimental test & verification procedures.

However, without planning and organization, experimental procedures can :

(a) be time consuming,
(b) lack direction,
(c) be expensive.

This is particularly true when the test program necessitates testing at one set of conditions, geometry, and fluid with the objective to represent a different but similar set of conditions, geometry, and fluid.

Dimensional analysis provides a procedure that will typically reduce both the time and expense of experimental work necessary to experimentally represent a desired set of conditions and geometry.

It also provides a means of "normalizing" the final results for a range of test conditions. A normalized (non-dimensional) set of results for one test condition can be used to predict the performance at different but fluid dynamically similar conditions (including even a different fluid).

The basic procedure for dimensional analysis can be summarized as follows:



ketabline.com Ebook.ketabline.com

1. Compile a list of relevant variables (dependent & independent) for the problem being considered,
2. Use an appropriate procedure to identify both the number and form of the resulting non-dimensional parameters.

This procedure is outlined as follows for the Buckingham Pi Theorem

Definitions:

n = the number of independent variables relevant to the problem

j' = the number of independent dimensions found in the n variables

j = the reduction possible in the number of variables necessary to be considered simultaneously

k = the number of independent pi terms that can be identified to describe the problem, $k = n - j$

Summary of Steps:

1. List and count the n variables involved in the problem.
2. List the dimensions of each variable using {MLTΘ} or {FLTΘ}. Count the number of basic dimensions (j') for the list of variables being considered.
3. Find j by initially assuming $j = j'$ and look for j repeating variables which do not form a pi product. If not successful, reduce j by 1 and repeat the process.
4. Select j scaling, repeating variables which do not form a pi product.
5. Form a pi term by adding one additional variable and form a power product. Algebraically find the values of the exponents which make the product dimensionless. Repeat the process with each of the remaining variables.
6. Write the combination of dimensionless pi terms in functional form:

$$\Pi_k = f(\Pi_1, \Pi_2, \ldots \Pi_i)$$

Consider the following example for viscous pipe flow. The relevant variables for this problem are summarized as follows:

ΔP = pressure drop ρ = density V = velocity D = diameter

μ = viscosity ε = roughness L = length

Seven pipe flow variables: $\{\Delta P \quad \rho, V, D, \mu, \varepsilon, L\}$

dependent independent



ketabline.com Ebook.ketabline.com

Use of the Buckingham Pi Theorem proceeds as follows:

1. Number of independent variables: $n = 7$

2. List the dimensions of each variable (use m L t Θ):

variables	ΔP	ρ	V	D	μ	ε	L
dimensions	$mL^{-1}t^{-2}$	mL^{-3}	Lt^{-1}	L	$mL^{-1}t^{-1}$	L	L

The number of basic dimensions is $j' = 3$.

3. Choose $j = 3$ with the repeating variables being ρ, V, and D. They do not form a dimensionless pi term. No combination of the 3 variables will eliminate the mass dimension in density or the time dimension in velocity.

4. This step described in the above step. The repeating variables again are ρ, V, and D and $j = 3$. Therefore, $k = n - j = 7 - 3 = 4$ independent Π terms.

5. Form the Π terms:

$$\Pi_1 = \rho^a V^b D^c \mu^{-1} = (mL^{-3})^a (Lt^{-1})^b L^c (mL^{-1}t^{-1})^{-1}$$

In order for the Π term to have no net dimensions, the sum of the exponents for each dimension must be zero. Therefore, we have:

mass: $a - 1 = 0$, $a = 1$
time: $-b + 1 = 0$, $b = 1$
length: $-3a + b + c + 1 = 0$, $c = 3 - 1 - 1 = 1$

We therefore have

$$\Pi_1 = \rho V D / \mu = Re = \text{Reynolds number}$$

Repeating the process by adding the roughness ε



ketabline.com Ebook.ketabline.com

$$\Pi_2 = \rho^a V^b D^c \varepsilon^1 = (mL^{-3})^a (Lt^{-1})^b L^c (L)^1$$

Solving:

mass: $a = 0$, $a = 0$
time: $-b = 0$, $b = 0$
Length: $-3a + b + c + 1 = 0$, $c = -1$

$\Pi_2 = \varepsilon / D$ Roughness ratio

Repeat the process by adding the length L.

$$\Pi_3 = \rho^a V^b D^c L^1 = (mL^{-3})^a (Lt^{-1})^b L^c (L)^1$$

Solving:

mass: $a = 0$, $a = 0$
time: $-b = 0$, $b = 0$
length: $-3a + b + c + 1 = 0$, $c = -1$

$\Pi_3 = L / D$ length-to-diameter ratio

These three are the independent Π terms.

Now obtain the dependent Π term by adding ΔP

$$\Pi_4 = \rho^a V^b D^c \Delta P^1 = (mL^{-3})^a (Lt^{-1})^b L^c (mL^{-1}t^{-2})^1$$

Solving:

mass: $a + 1 = 0$, $a = -1$
time: $-b - 2 = 0$, $b = -2$
length: $-3a + b + c - 1 = 0$, $c = 0$

$\Pi_4 = \Delta P / \rho V^2$ Pressure coefficient



ketabline.com Ebook.ketabline.com

Application of the Buckingham Pi Theorem to the previous list of variables yields the following non-dimensional combinations:

$$\frac{\Delta P}{\rho V^2} = f\left\{\frac{\rho VD}{\mu}, \frac{L}{D}, \frac{\varepsilon}{D}\right\}$$

or

$$C_p = f\left\{Re, \bar{L}, \bar{\varepsilon}\right\}$$

Thus, a non-dimensional pressure loss coefficient for viscous pipe flow would be expected to be a function of (1) the Reynolds number, (2) a non-dimensional pipe length, and (3) a non-dimensional pipe roughness. This will be shown to be exactly the case in Ch. VI, Viscous Internal Flow.

A list of typical dimensionless groups important in fluid mechanics is given in the accompanying table.

From these results, we would now use a planned experiment with data analysis techniques to get the exact form of the relationship among these non - dimensional parameters.

The next major step is concerned with the design and organization of the experimental test program

Two key elements in the test program are:

* design of the model
* specification of the test conditions, particularly when the test must be performed at conditions similar, but not the same as the conditions of interest.

Similarity and non-dimensional scaling

The basic requirement is in this process to achieve '**similarity**' between the 'experimental model and its test conditions' and the 'prototype and its test conditions' in the experiment.



ketabline.com Ebook.ketabline.com

Table 5.2 Dimensional Analysis and Similarity

Parameter	Definition	Qualitative ratio of effects	Importance
Reynolds number	$R_E = \frac{\rho UL}{\mu}$	$\frac{\text{Inertia}}{\text{Viscosity}}$	Always
Mach number	$MA = \frac{U}{A}$	$\frac{\text{Flow speed}}{\text{Sound speed}}$	Compressible flow
Froude number	$Fr = \frac{U^2}{gL}$	$\frac{\text{Inertia}}{\text{Gravity}}$	Free-surface flow
Weber number	$W_e = \frac{\rho U^2 L}{\gamma}$	$\frac{\text{Inertia}}{\text{Surface tension}}$	Free-surface flow
Cavitation number (Euler number)	$Ca = \frac{p - p_v}{\rho U^2}$	$\frac{\text{Pressure}}{\text{Inertia}}$	Cavitation
Prandtl number	$Pr = \frac{C_p \mu}{k}$	$\frac{\text{Dissipation}}{\text{Conduction}}$	Heat convection
Eckert number	$Ec = \frac{U^2}{c_p T_o}$	$\frac{\text{Kinetic energy}}{\text{Enthalpy}}$	Dissipation
Specific-heat ratio	$\gamma = \frac{c_p}{c_v}$	$\frac{\text{Enthalpy}}{\text{Internal energy}}$	Compressible flow
Strouhal number	$St = \frac{\omega L}{U}$	$\frac{\text{Oscillation}}{\text{Mean speed}}$	Oscillating flow
Roughness ratio	$\frac{\varepsilon}{L}$	$\frac{\text{Wall roughness}}{\text{Body length}}$	Turbulent,rough walls
Grashof number	$Gr = \frac{\beta \Delta T g L^3 \rho^2}{\mu^2}$	$\frac{\text{Buoyancy}}{\text{Viscosity}}$	Natural convection
Temperature ratio	$\frac{T_w}{T_o}$	$\frac{\text{Wall temperature}}{\text{Stream temperature}}$	Heat transfer
Pressure coefficient	$C_p = \frac{p - p_\infty}{1/2 \rho U^2}$	$\frac{\text{Static pressure}}{\text{Dynamic pressure}}$	Aerodynamics, hydrodynamics
Lift coefficient	$C_L = \frac{L}{1/2 \rho U^2 A}$	$\frac{\text{Lift force}}{\text{Dynamic force}}$	Aerodynamics hydrodynamics
Drag coefficient	$C_D = \frac{D}{1/2 \rho U^2 A}$	$\frac{\text{Lift force}}{\text{Dynamic force}}$	Aerodynamics, hydrodynamics



ketabline.com Ebook.ketabline.com

In this context, “similarity” is defined as

Similarity: **All relevant dimensionless parameters have the same values for the model & the prototype**.

Similarity generally includes three basic classifications in fluid mechanics:

(1) Geometric similarity
(2) Kinematic similarity
(3) Dynamic similarity

Geometric similarity

In fluid mechanics, geometric similarity is defined as follows:

Geometric Similarity **All linear dimensions of the model are related to the corresponding dimensions of the prototype by a constant scale factor** SF_G

Consider the following airfoil section (Fig. 5.4):

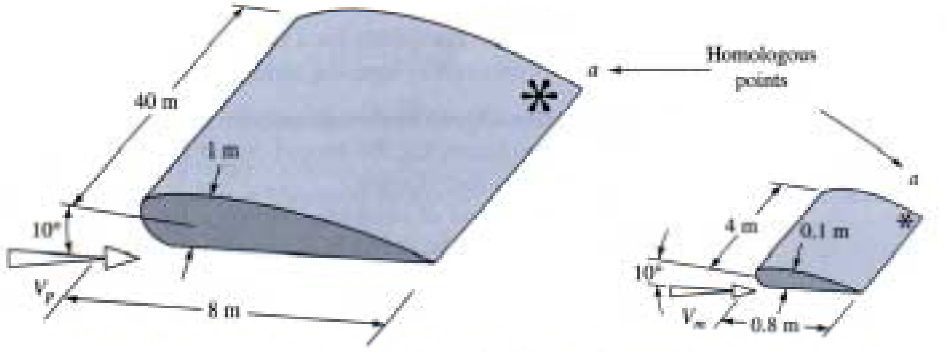


Fig. 5.4 Geometric Similarity in Model Testing

For this case, geometric similarity requires the following:

ketabline.com Ebook.ketabline.com

$$SF_G = \frac{r_m}{r_p} = \frac{L_m}{L_p} = \frac{W_m}{W_p} = \cdots$$

In addition, in geometric similarity,

All angles are preserved.

All flow directions are preserved.

Orientation with respect to the surroundings must be same for the model and the prototype, ie.,

Angle of attack)$_m$ = angle of attack)$_p$

Kinematic Similarity

In fluid mechanics, kinematic similarity is defined as follows:

Kinematic Similarity **The velocities at 'corresponding' points on the model & prototype are in the same direction and differ by a constant scale factor SF_k.**

Therefore, the flows must have similar streamline pattterns

Flow regimes must be the same.

These conditions are demonstrated for two flow conditions, as shown in the following kinematically similar flows (Fig. 5.6).

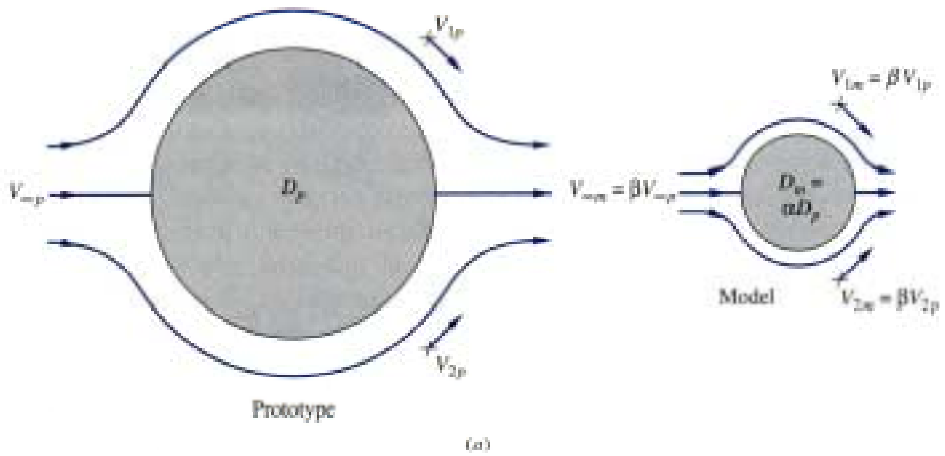


Fig. 5.6a Kinematically Similar Low Speed Flows

ketabline.com Ebook.ketabline.com

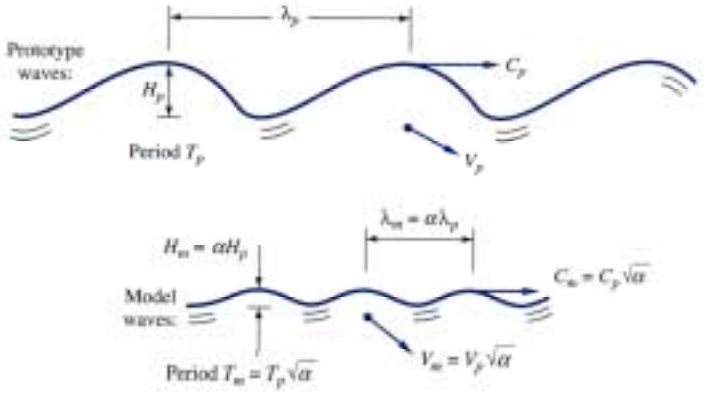


Fig. 5.6b Kinematically Similar Free Surface Flows

The conditions of kinematic similarity are generally met automatically when geometric and dynamic similarity conditions are satisfied.

Dynamic Similarity

In fluid mechanics, dynamic similarity is typically defined as follows:

Dynamic Similarity	**This is basically met if model and prototype forces differ by a constant scale factor at similar points.**

This is illustrated in the following figure for flow through a sluice gate (Fig. 5.7).

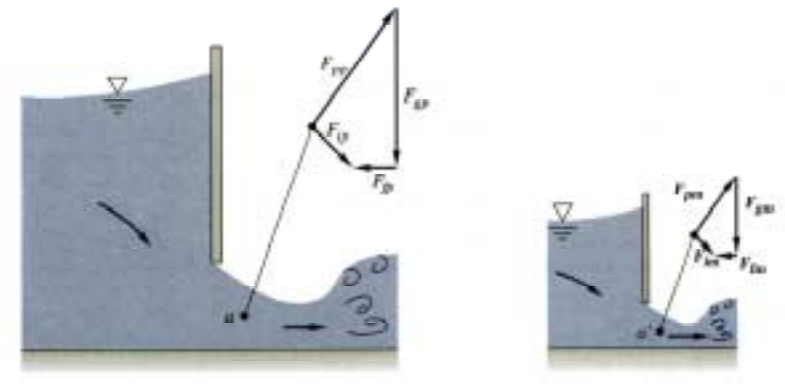


Fig. 5.7 Dynamic Similarity for Flow through a Sluice Gate



ketabline.com Ebook.ketabline.com

This is generally met for the following conditions:

1. Compressible flows: model & prototype Re, Ma, are equal

$$Re_m = Re_p, \quad Ma_m = Ma_p, \quad \gamma_m = \gamma_p$$

2. Incompressible flows

   a. No free surface

$$Re_m = Re_p$$

   b. Flow with a free surface

$$Re_m = Re_p \quad , \; Fr_m = Fr_p$$

Note: The parameters being considered, e.g., velocity, density, viscosity, diameter, length, etc., generally relate to the flow, geometry, and fluid characteristics of the problem and are considered to be independent variables for the subject problem.

The result of achieving similarity by the above means is that relevant non - dimensional dependent variables, e.g., C_D, C_p, C_f, or Nu, etc., are then equal for both the model and prototype.

This result would then indicate how the relevant dependent results, e.g. drag force, pressure forces, viscous forces, are to be scaled for the model to the prototype.

Equality of the relevant non-dimensional independent variables Re, Ma, x/L, etc., indicates how the various independent variables of importance should be scaled.



ketabline.com Ebook.ketabline.com

An example of this scaling is shown as follows:

Example: The drag on a sonar transducer prototype is to be predicted based on the following wind tunnel model data and prototype data requirements. Determine the model test velocity V_m necessary to achieve similarity and the expected prototype force F_p based on the model wind tunnel test results.

Given:	Prototype	Model
	sphere	sphere
D	1 ft	6 in
V	5 knots	unknown?
F	?	5.58 lb_f
ρ	1.98 $slugs/ft^3$	0.00238 $slugs/ft^3$
ν	$1.4 * 10^{-5}$ ft^2/s	$1.56 * 10^{-4}$ ft^2/s

From dimensional analysis:

$$C_D = f\{R_e\} \qquad \frac{F/D^2}{\rho V^2} = f\left\{\frac{VD}{\upsilon}\right\}$$

For the prototype, the actual operating velocity and Reynolds number are:

Prototype:

$$V_p = 5\frac{na \cdot mi}{hr}\,6080\frac{ft}{na \cdot mi}\,\frac{1hr}{3600s} = 8.44\frac{ft}{s} \quad V_p = 5\frac{na \cdot mi}{hr}\,6080\frac{ft}{na \cdot mi}\,\frac{1hr}{3600s} = 8.44\frac{ft}{s}$$



ketabline.com Ebook.ketabline.com

$$R_{e_p} = \left.\frac{VD}{\upsilon}\right)_p = \frac{8.44\,ft/s * 1ft}{1.4 * 10^{-5}\,ft^2/s} = 6.03 * 10^5$$

Equality of Reynolds number then yields the required model test velocity of

$$R_{e_m} = R_{e_p} = \left.\frac{VD}{\upsilon}\right)_m \Rightarrow V_m = 188\,ft/s$$

Based on actual test results for the model, i.e. measured F_m, equality of model and prototype drag coefficients yields

$$\therefore\ C_{D_p} = C_{D_m} \Rightarrow F_p = F_m \frac{\rho_p}{\rho_m} \frac{V_p^2}{V_m^2} \frac{D_p^2}{D_m^2} = 37.4\ lb_f$$

Note: All fluid dynamic flows and resulting flow characteristics are not Re dependent.

Example:

The drag coefficient for bluff bodies with a fixed point of separation; e.g., radar antennae, generally have a constant, fixed number for C_D which is not a function of Re.

$$C_D = const \neq f(R_e)$$



ketabline.com Ebook.ketabline.com

VI. VISCOUS INTERNAL FLOW

To date, we have considered only problems where the viscous effects were either:

a. known: i.e. - known F_D or h_f
b. negligible: i.e. - inviscid flow

This chapter presents methodologies for predicting viscous effects and viscous flow losses for internal flows in pipes, ducts, and conduits.

Typically, the first step in determining viscous effects is to determine the flow regime at the specified condition.

The two possibilities are:

a. **Laminar flow**
b. **Turbulent flow**

The student should read Section 6.1 in the text, which presents an excellent discussion of the characteristics of laminar and turbulent flow regions.

For steady flow at a known flow rate, these regions exhibit the following:

Laminar flow: A local velocity constant with time, but which varies spatially due to viscous shear and geometry.

Turbulent flow: A local velocity which has a constant mean value but also has a statistically random fluctuating component due to turbulence in the flow.

Typical plots of velocity time histories for laminar flow, turbulent flow, and the region of transition between the two are shown below.

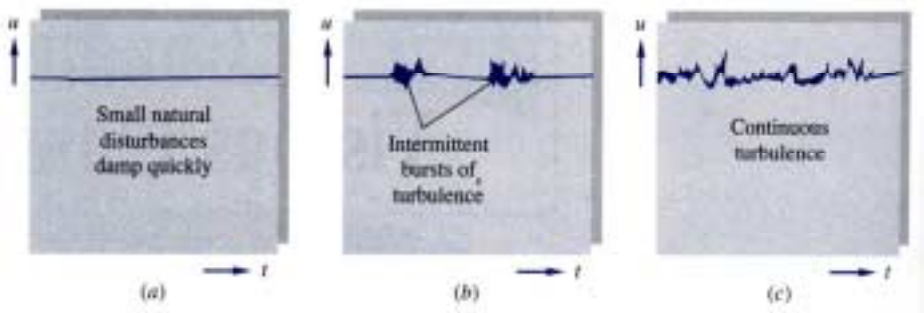


Fig. 6.1 (a) Laminar, (b)transition, and (c) turbulent flow velocity time histories.

ketabline.com Ebook.ketabline.com

Principal parameter used to specify the type of flow regime is the

$$\text{Reynolds number - Re} = \frac{\rho V D}{\mu} = \frac{V D}{\nu}$$

V - characteristic flow velocity
D - characteristic flow dimension
μ - dynamic viscosity
υ - kinematic viscosity = $\frac{\mu}{\rho}$

We can now define the

$Re_{cr} \equiv$ critical or transition Reynolds number

$Re_{cr} \equiv$ Reynolds number below which the flow is laminar, above which the flow is turbulent

While transition can occur over a range of Re, we will use the following for internal pipe or duct flow:

$$Re_{cr} \cong 2300 = \left.\frac{\rho VD}{\mu}\right)_{cr} = \left.\frac{VD}{\upsilon}\right)_{cr}$$

Internal Viscous Flow

A second classification concerns whether the flow has significant entrance region effects or is fully developed. The following figure indicates the characteristics of the entrance region for internal flows. Note that the slope of the streamwise pressure distribution is greater in the entrance region than in the fully developed region.

Typical criteria for the length of the entrance region are given as follows:

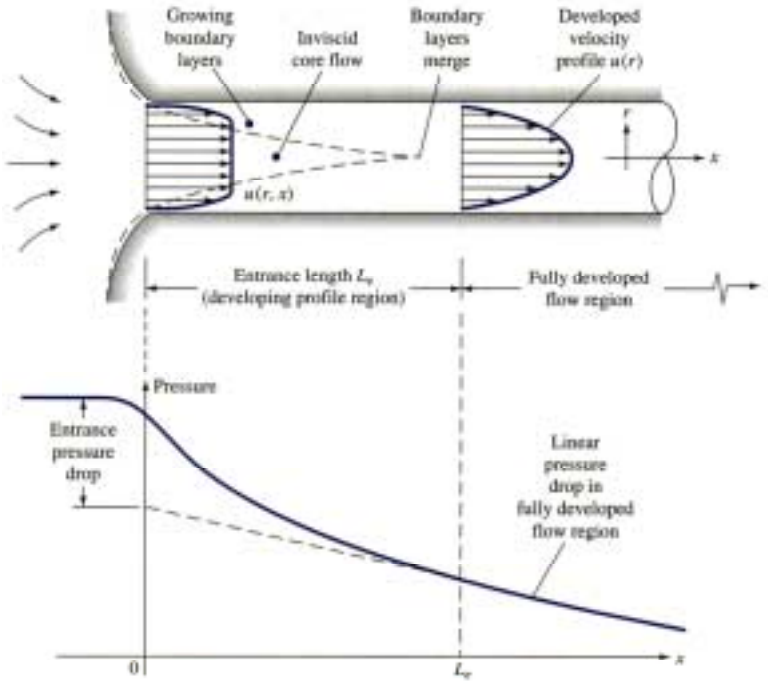
Laminar: $\frac{L_e}{D} \cong 0.06\,\text{Re}$



ketabline.com Ebook.ketabline.com

Turbulent $\frac{L_e}{D} \cong 4.4 Re^{1/6}$

where: L_e = length of the entrance region



Note: **Take care in neglecting entrance region effects**.

In the entrance region, frictional pressure drop/length > the pressure drop/length for the fully developed region. Therefore, if the effects of the entrance region are neglected, the overall predicted pressure drop will be low. This can be significant in a system with short tube lengths, e.g., some heat exchangers.

Fully Developed Pipe Flow

The analysis for **steady, incompressible, fully developed, laminar flow** in a circular horizontal pipe yields the following equations:

$$U(r) = -\frac{R^2}{4\mu}\frac{dP}{dx}\left\{1 - \frac{r^2}{R^2}\right\}$$



ketabline.com Ebook.ketabline.com

$$\frac{U}{U_{\max}} = \left\{1 - \frac{r^2}{R^2}\right\} \quad , \quad U_{\max} = 2V_{avg}$$

and

$$\mathbf{Q = A\,V_{avg} = \pi\,R^2\,V_{avg}}$$

Key Points: Thus for laminar, fully developed pipe flow (**not turbulent**):

a. The velocity profile is parabolic.
b. The maximum local velocity is at the centerline (r = 0).
c. The average velocity is one-half the centerline velocity.
d. The local velocity at any radius varies only with radius, not on the streamwise (x) location (due to the flow being fully developed).

Note: All subsequent equations will use the symbol V (no subscript) to represent the average flow velocity in the flow cross section.

Darcy Friction Factor:

We can now define the Darcy friction factor f as:

$$f \equiv \frac{\left(\frac{D}{L}\right)\Delta P_f}{\rho\frac{V^2}{2}}$$

where ΔP_f = the pressure drop due to friction only.

The general energy equation must still be used to determine total pressure drop.

Therefore, we obtain

$$\Delta P_f = \rho g h_f = f\frac{L}{D}\rho\frac{V^2}{2}$$

and the friction head loss h_f is given as

$$h_f = f\frac{L}{D}\frac{V^2}{2g}$$

Note: The definitions for f and h_f are **valid for either laminar or turbulent flow**. However, you must evaluate f for the correct flow regime, laminar or turbulent.



ketabline.com Ebook.ketabline.com

Key Point: It is common in industry to define and use a "fanning" friction factor f_f. The fanning friction factor differs from the Darcy friction factor by a factor of 4. Thus, care should be taken when using unfamiliar equations or data since use of f_f in equations developed for the Darcy friction factor will result in significant errors (a factor of 4). Your employer will not be happy if you order a 10 hp motor for a 2.5 hp application. The equation suitable for use with f_f I s

$$h_f = 4 f_f \frac{L}{D} \frac{V^2}{2g}$$

Laminar flow:

Application of the results for the laminar flow velocity profile to the definition of the Darcy friction factor yields the following expression:

$$f = \frac{64}{\mathrm{Re}} \qquad \text{laminar flow only (Re < 2300)}$$

Thus with the value of the Reynolds number, the friction factor for laminar flow is easily determined.

Turbulent flow:

A similar analysis is not readily available for turbulent flow. However, the Colebrook equation, shown below, provides an excellent representation for the variation of the Darcy friction factor in the turbulent flow regime. Note that the equation depends on both the pipe Reynolds number and the roughness ratio, is transcendental, and cannot be expressed explicitly for f .

$$f = -2\log\left[\frac{2.51}{\mathrm{Re}\, f^{1/2}} + \frac{\varepsilon / D}{3.7}\right] \qquad \text{turbulent flow only (Re > 2300)}$$



ketabline.com Ebook.ketabline.com

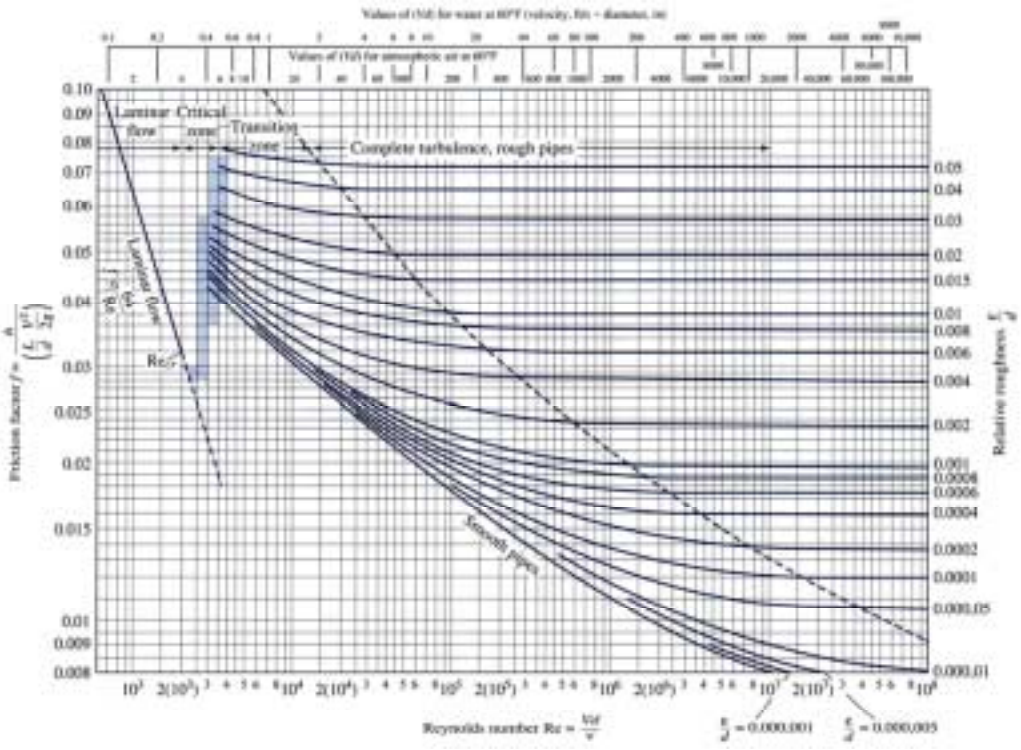
where ε = nominal roughness of pipe or duct being used. (Table 6.1, text)

(**Note**: Take care with units for ε; ε /D must be non-dimensional).

A good approximate equation for the turbulent region of the Moody chart is given by Haaland's equation:

$$f = \left\{-1.8\log\left[\frac{6.9}{\mathrm{Re}} + \left(\frac{\varepsilon/D}{3.7}\right)^{1.11}\right]\right\}^{-2}$$

Note again the roughness ratio ε/D must be non-dimensional in both equations. Graphically, the results for both laminar and turbulent flow pipe friction are represented by the Moody chart as shown below.



Typical roughness values are shown in the following table:

ketabline.com Ebook.ketabline.com

Table 6.1 Average roughness values of commercial pipe

Material	Condition	e, ft	e, mm	Uncertainty, %
Steel	Sheet metal, new	0.00016	0.05	± 60
	Stainless, new	0.000007	0.002	± 50
	Commercial, new	0.00015	0.046	± 30
	Riveted	0.01	3.0	± 70
	Rusted	0.007	2.0	± 50
Iron	Cast, new	0.00085	0.26	± 50
	Wrought, new	0.00015	0.046	± 20
	Galvanized, new	0.0005	0.15	± 40
	Asphalted cast	0.0004	0.12	± 50
Brass	Drawn, new	0.000007	0.002	± 50
Plastic	Drawn tubing	0.000005	0.0015	± 60
Glass	—	Smooth	Smooth	
Concrete	Smoothed	0.00013	0.04	± 60
	Rough	0.007	2.0	± 50
Rubber	Smoothed	0.000033	0.01	± 60
Wood	Stave	0.00016	0.5	± 40

Haaland's equation is valid for turbulent flow (Re > 2300) and is easily set up on a computer, spreadsheet, etc.

Key fluid system design considerations for laminar and turbulent flow

a. Most internal flow problems of engineering significance are turbulent, not laminar. Typically, a very low flow rate is required for internal pipe flow to be laminar. If you open your kitchen faucet and the outlet flow stream is larger than a kitchen match, the flow is probably turbulent. Thus, check your work carefully if your analysis indicates laminar flow.

b. The following can be easily shown:

Laminar flow: $$\Delta P_f \sim \{\mu, L, Q, D^{-4}\}$$

$$\dot{W}_f \sim \{\mu, L, Q^2, D^{-4}\}$$

Turbulent flow: $$\Delta P_f \sim \{\rho^{3/4}, \mu^{1/4}, L, Q^{1.75}, D^{-4.75}\}$$

$$\dot{W}_f \sim \{\rho^{3/4}, \mu^{1/4}, L, Q^{2.75}, D^{-4.75}\}$$

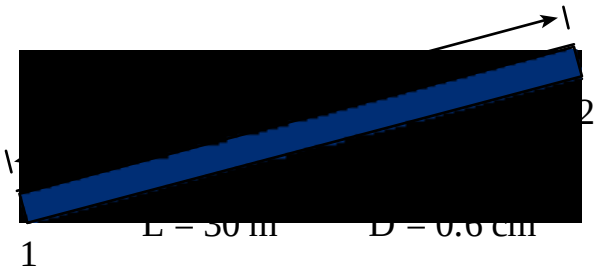
Thus both pressure drop and pump power are very dependent on flow rate and pipe/conduit diameter. Small changes in diameter and/or flow rate can significantly change circuit pressure drop and power requirements.



ketabline.com Ebook.ketabline.com

Example (Laminar flow):

Water, 20°C flows through a 0.6 cm tube, 30 m long, at a flow rate of 0.34 liters/min. If the pipe discharges to the atmosphere, determine the supply pressure if the tube is inclined 10° above the horizontal in the flow direction.



Water Properties:

ρ = 998 kg/m^3 ρg = 9790 N/m^3

ν = 1.005 E-6 m^2/s

Energy Equation

$$\frac{P_1 - P_2}{\rho g} = \frac{V_2^2 - V_1^2}{2g} + Z_2 - Z_1 + h_f - h_p$$

which for steady-flow in a constant diameter pipe with $P_2 = 0$ gage becomes,

$$\frac{P_1}{\rho g} = Z_2 - Z_1 + h_f = \text{L sin } 10^o + h_f$$

$$V = \frac{Q}{A} = \frac{0.34E^{-3}\, m^3/\min * 1\min/60\, s}{\pi (0.3/100)^2\, m^2} = 0.2\ m/s$$

$$\text{Re} = \frac{V D}{\upsilon} = \frac{0.2 * 0.006}{1.005\, E^{-6}} = 1197 \quad \rightarrow \quad \text{laminar flow}$$

$$f = \frac{64}{\text{Re}} = \frac{64}{1197} = 0.0535$$

$$h_f = f \frac{L}{D} \frac{V^2}{2g} = 0.0535 * \frac{30m}{0.006m} \frac{0.2^2}{2 * 9.807 m/s^2} = 0.545\, m$$

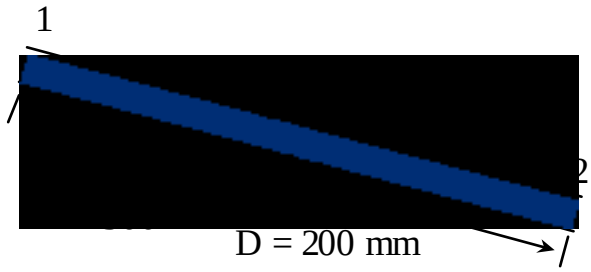
$$\frac{P_1}{\rho g} = 30 * \sin 10^o + 0.545 = \underset{\text{gravity head}}{5.21} + \underset{\text{friction head}}{0.545} = \underset{\text{total head loss}}{5.75m}$$

P_1 = 9790 N/m^3*5.75 m = 56.34 kN/m^3 (kPa) ~ 8.2 psig **ans.**

ketabline.com Ebook.ketabline.com

Example: (turbulent flow)

Oil, ρ = 900 kg/m^3, ν = 1 E-5 m^2/s, flows at 0.2 m^3/s through a 500 m length of 200 mm diameter, cast iron pipe. If the pipe slopes downward 10° in the flow direction, compute hf, total head loss, pressure drop, and power required to overcome these losses.



The energy equation can be written as follows where h_t = total head loss.

$$\frac{P_1 - P_2}{\rho g} = h_t = \frac{V_2^2 - V_1^2}{2g} + Z_2 - Z_1 + h_f - h_p$$

which reduces to

$$h_t = Z_2 - Z_1 + h_f$$

$$V = \frac{Q}{A} = \frac{0.2\, m^3/s}{\pi (.1)^2\, m^2} = 6.4\ m/s$$

Table 6.1, cast iron, ε = 0.26 mm

$$\text{Re} = \frac{VD}{\upsilon} = \frac{6.4 * .2}{1E^{-5}} = 128{,}000 \rightarrow \text{turbulent flow,} \qquad \frac{\varepsilon}{D} = \frac{0.26}{200} = 0.0013$$

Since flow is turbulent, use Haaland's equation to determine friction factor (check your work using the Moody chart).

$$f = \left\{-1.8 \log\left[\frac{6.9}{\text{Re}} + \left(\frac{\varepsilon/D}{3.7}\right)^{1.11}\right]\right\}^{-2}, \quad f = \left\{-1.8 \log\left[\frac{6.9}{128{,}000} + \left(\frac{0.0013}{3.7}\right)^{1.11}\right]\right\}^{-2}$$

$$f = 0.02257 \quad h_f = f \frac{L}{D} \frac{V^2}{2g} = 0.02257 * \frac{500m}{0.2m} \frac{6.4^2}{2 * 9.807 m/s^2} = 116.6\, m \quad \textbf{ans.}$$

$h_t = Z_2 - Z_1 + h_f = -500 \sin^0 + 116.6 = -86.8 + 116.6 = 29.8$ m ans.



ketabline.com Ebook.ketabline.com

Note that for this problem, there is a negative gravity head loss (i.e. a head increase) and a positive frictional head loss resulting in the net head loss of 29.8 m.

$$\Delta P = \rho g h_t = 900\,kg/m^3 * 9.807\,m/s^2 * 29.8\,m = 263\,kPa$$ **ans.**

$$\dot{W} = \rho Q g h_t = Q\Delta P = 0.2 m^3/s * 273{,}600\,N/m^2 = 54.7\,kw$$ **ans.**

Note that this is not necessarily the power required to drive a pump, as the pump efficiency will typically be less than 100%.

These problems are easily set up for solution in a spreadsheet as shown below. Make sure that the calculation for friction factor includes a test for laminar or turbulent flow with the result proceeding to the correct equation.

Always verify any computer solution with problems having a known solution.

FRICTIONAL HEAD LOSS CALCULATION

All Data are entered in S.I. Units e.g. (m, sec., kg), except as noted, ε

Ex. 6.7

	Input Data			Calculated Results		
L =	500	(m)		V =	6.37	(m/sec)
D =	0.2	(m)		Re =	127324	
ε =	0.26	(mm)		e/D =	0.0013	
ρ =	900	(kg/m^3)		f=	0.02258	
ν =	1.00E-05	(m^2/sec)		hf =	116.62	
Q =	0.2	(m^3/sec)		sum Ki =	0.00	
D1 =	0.08	(m)		hm =	0.00	(m)
D2 =	0.08	(m)				
d KE =	0.00	(m)		ht =	29.62	(m)
d Z =	-87	(m)				(m)
				P1-P2 =	261.43	(kPa)



ketabline.com Ebook.ketabline.com

Solution Summary:

To solve basic pipe flow frictional head loss problem, use the following procedure:

1. Use known flow rate to determine Reynolds number.
2. Identify whether flow is laminar or turbulent.
3. Use appropriate expression to determine friction factor (w Ɛ/D if necessary).
4. Use definition of hf to determine friction head loss.
5. Use general energy equation to determine total pressure drop.

Unknown Flow Rate and Diameter Problems

Problems involving unknown flow rate and diameter in general require iterative/ trial & error solutions due to the complex dependence of Re, friction factor, and head loss on velocity and pipe size.

Unknown Flow Rate:

For the special case of known friction loss hf a closed form solution can be obtained for the problem of unknown Q.

The solution proceeds as follows:

Given: Known values for D, L, h_f, ρ, and μ calculate V or Q.

Define solution parameter:

$$\varsigma = \frac{1}{2} f \mathrm{Re}_D^2 = \frac{g D^3 h_f}{L \upsilon^2}$$

Note that this solution does not contain velocity and the parameter ζ can be calculated from known values for D, L, h_f, ρ, and μ. The Reynolds number and subsequently the velocity can be determined from ζ and the following equations:

Turbulent: $$\mathrm{Re}_D = -(8\varsigma)^{1/2} \log\left\{\frac{\varepsilon/D}{3.7} + \frac{1.775}{\sqrt{\varsigma}}\right\}$$



ketabline.com Ebook.ketabline.com

Laminar: $\mathrm{Re}_D = \frac{\varsigma}{32}$

and laminar to turbulent transition can be assumed to occur approximately at ζ = 73,600 (check Re at end of calculation to confirm).

Note that this procedure is not valid (except perhaps for initial estimates) for problems involving significant minor losses where the head loss due only to pipe friction is not known.

For these problems a trial and error solution using a computer is best.

Example 6.9

Oil, with ρ = 950 kg/m^3 and ν = 2 E-5 m^2/s, flows through 100 m of a 30 cm diameter pipe. The pipe is known to have a head loss of 8 m and a roughness ratio ε/D = 0.0002. Determine the flow rate and oil velocity possible for these conditions.

Without any information to the contrary, we will neglect minor losses and KE head changes. With these assumptions, we can write:

$$\varsigma = \frac{g D^3 h_f}{L \upsilon^2} = \frac{9.807\,m/s^2 * 0.30^3\,m^3 * 8.0\,m}{100\,m * \left(2E{-}5\,m^2/s\right)^2} = 5.3E7 > \text{ 73,600; turbulent}$$

$$\mathrm{Re}_D = -(8*5.3E7)^{1/2} \log\left\{\frac{0.0002}{3.7} + \frac{1.775}{\sqrt{5.3E7}}\right\} = 72,600 \quad \text{checks, turbulent}$$

$$\mathrm{Re}_D = \frac{V D}{\upsilon}, \quad V = \frac{72{,}600 * 2E{-}5\,m^2/s}{0.3\,m} = 4.84\,\frac{m}{s} \quad \textbf{ans.}$$

$$Q = A\,V = \pi .15^2\ \mathrm{m}^2\, 4.84\ \mathrm{m/s} = 0.342\ \mathrm{m}^3/\mathrm{s} \quad \textbf{ans.}$$

This is the maximum flow rate and oil velocity that could be obtained through the given pipe and given conditions (hf = 8 m).



ketabline.com Ebook.ketabline.com

Note that this problem could have also been solved using a computer based trial and error procedure in which a value is assumed for the fluid flow rate until a flow rate is found which results in the specified head loss. Note also that with this procedure, the problem being solved can include the effects of minor losses, KE, and PE changes with no additional difficulty.

Unknown Pipe Diameter:

A similar difficulty arises for problems involving unknown pipe difficulty, except a closed form, analytical solution is not available. Again, a trial and error solution is appropriate for use to obtain the solution and the problem can again include losses due to KE, PE, and piping components with no additional difficulty.

Non-Circular Ducts:

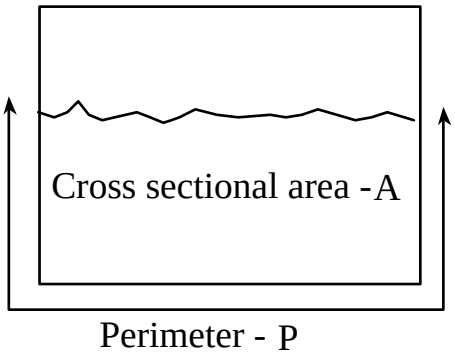
For flow in non-circular ducts or ducts for which the flow does not fill the entire cross-section, we can define the hydraulic diameter D_h as

$$D_h = \frac{4A}{P}$$

where

A = cross-sectional area of actual flow,

P = wetted perimeter, i.e. the perimeter on which viscous shear acts



With this definition, **<u>all previous equations</u>** for the Reynolds number Re friction factor f and head loss h_f are valid as previously defined and can be used on both circular and non-circular flow cross sections.

Minor Losses

In addition to frictional losses for a length L of pipe, we must also consider losses due to various fittings (valves, unions, elbows, tees, etc.). These losses are expressed as

$$h_m = K_i \frac{V^2}{2g}$$



ketabline.com Ebook.ketabline.com

where

h_m = the equivalent head loss across the fitting or flow component.

V = average flow velocity for the pipe size of the fitting

K_i = the minor loss coefficient for given flow component; valve, union, etc. See Sec. 6.7, Table 6.5, 6.6, Fig. 6.19, 6.20, 6.21, 6.22, etc.

Table 6.5 shows minor loss K values for several common types of valves, fully open, and for elbows and tees.

Table 6.5 Minor loss coefficient for common valves and piping components

	Nominal diameter, in								
	Screwed				Flanged				
	½	1	2	4	1	2	4	8	20
Valves (fully open):									
Globe	14	8.2	6.9	5.7	13	8.5	6.0	5.8	5.5
Gate	0.30	0.24	0.16	0.11	0.80	0.35	0.16	0.07	0.03
Swing check	5.1	2.9	2.1	2.0	2.0	2.0	2.0	2.0	2.0
Angle	9.0	4.7	2.0	1.0	4.5	2.4	2.0	2.0	2.0
Elbows:									
45° regular	0.39	0.32	0.30	0.29					
45° long radius					0.21	0.20	0.19	0.16	0.14
90° regular	2.0	1.5	0.95	0.64	0.50	0.39	0.30	0.26	0.21
90° long radius	1.0	0.72	0.41	0.23	0.40	0.30	0.19	0.15	0.10
180° regular	2.0	1.5	0.95	0.64	0.41	0.35	0.30	0.25	0.20
180° long radius					0.40	0.30	0.21	0.15	0.10
Tees:									
Line flow	0.90	0.90	0.90	0.90	0.24	0.19	0.14	0.10	0.07
Branch flow	2.4	1.8	1.4	1.1	1.0	0.80	0.64	0.58	0.41

Figure 6.18 shows minor loss K values for several types of common valves.

Note that the K valves shown here are for the indicated fractional opening. Also, fully open values may not be consistent with values indicated in Table 6.5 for fully open valves or for the valve of a particular manufacturer. In general, use specific manufacturer's data when available.



ketabline.com Ebook.ketabline.com

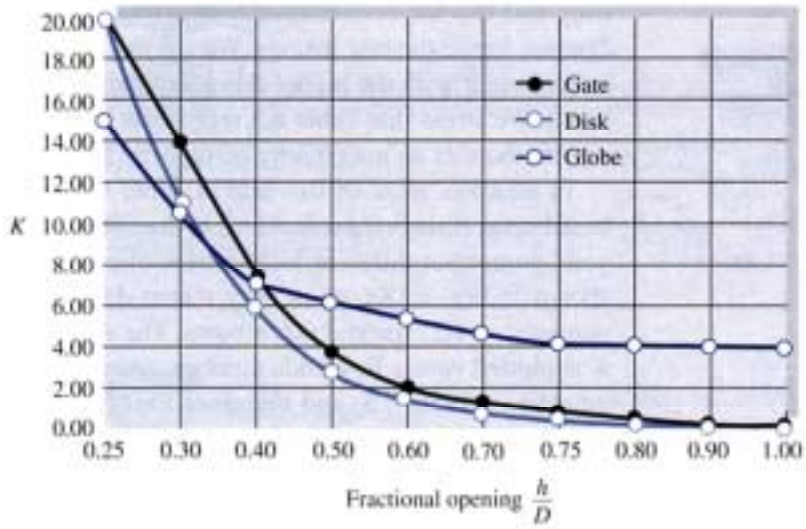


Fig. 6.18 Average loss coefficients for partially open valves

Note that exit losses are K ≅ 1 for all submerged exits, e.g., fluid discharged into a tank at a level below the fluid surface.

Also, for an open pipe discharge to the atmosphere, there is no loss coefficient when the energy equation is written only to the end of the pipe.

In general, do not take point 1 for an analysis to be in the plane of an inlet having an inlet loss. You do not know what fraction of the inlet loss to consider.

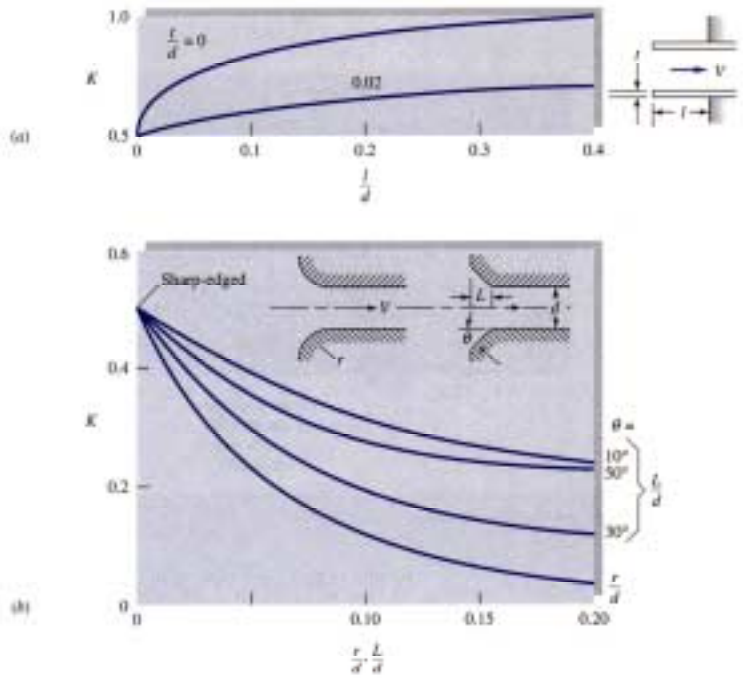


Fig. 6.21 Entrance and exit loss coefficients
(a) reentrant inlets; (b) rounded and beveled inlets



ketabline.com Ebook.ketabline.com

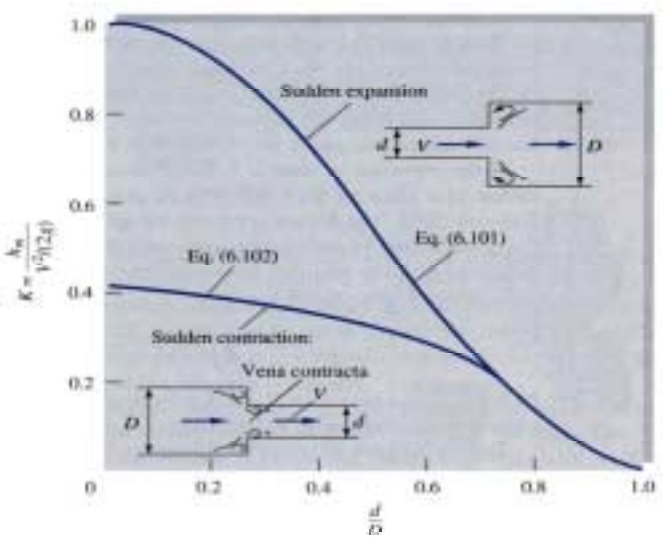


Fig. 6.22 Sudden contraction and expansion losses.

Note that the losses shown in Fig. 6.22 do not represent losses associated with pipe unions or reducers. These must be found in other sources in the literature.

Also note that the loss coefficient is always based on the velocity in the smaller diameter (d) of the pipe, irrespective of the direction of flow.

Assume that this is also true for reducers and similar area change fittings.

These and other sources of data now provide the ability to determine frictional losses for both the pipe and other piping/duct flow components.

The total frictional loss now becomes

$$h_f = f\frac{L}{D}\frac{V}{2g}^2 + \sum K_i \frac{V^2}{2g}$$

or

$$h_f = \left\{ f\frac{L}{D} + \sum K_i \right\} \frac{V}{2g}^2$$

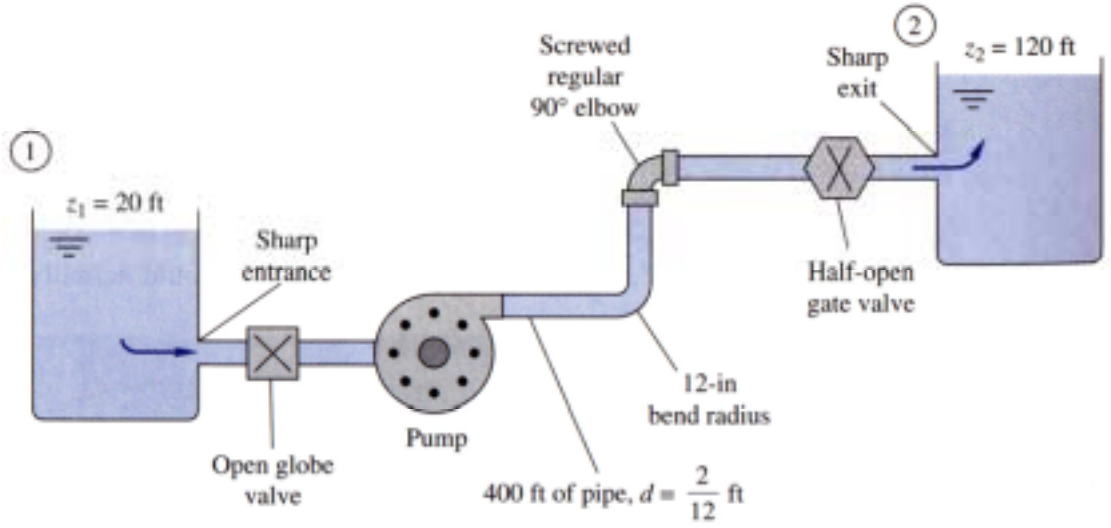
These equations would be appropriate for a single pipe size (with average velocity V). For multiple pipe/duct sizes, this term must be repeated for each pipe size.

Key Point: The energy equation must still be used to determine the total head loss and pressure drop from all possible contributions.



ketabline.com Ebook.ketabline.com

Example 6.16



Water, ρ = 1.94 slugs/ft^3 and ν = 1.1 E-5 ft^2/s, is pumped between two reservoirs at 0.2 ft^3/s through 400 ft of 2–in diameter pipe with ε/D = 0.001 having the indicated minor losses. Compute the pump horsepower (motor size) required.

Writing the energy equation between points 1 and 2 (the free surfaces of the two reservoirs), we obtain

$$\frac{P_1 - P_2}{\rho g} = \frac{V_2^2 - V_1^2}{2g} + Z_2 - Z_1 + h_f - h_p$$

For this problem, the pressure ($P_1 = P_2$) and velocity ($V_1 = V_2 = 0$) head terms are zero and the equation reduces to

$$h_p = Z_2 - Z_1 + h_f = Z_2 - Z_1 + \left\{ f\frac{L}{D} + \sum K_i \right\} \frac{V^2}{2g}$$

For a flow rate Q = 0.2 ft^3/s we obtain



ketabline.com Ebook.ketabline.com

$$V = \frac{Q}{A} = \frac{0.2\ ft^3/s}{\pi(1/12)^2\ ft^2} = 9.17\ ft/s$$

With ε/D = 0.001 and $\mathrm{Re} = \frac{VD}{\nu} = \frac{9.17\ ft/s(2/12)\ ft}{1.1E{-}5\ ft^2/s} = 139{,}000$

the flow is turbulent and Haaland's equation can be used to determine the friction factor:

$$f = \left\{-1.8\log\left[\frac{6.9}{139{,}000} + \left(\frac{.001}{3.7}\right)^{1.11}\right]\right\}^{-2} = 0.0214$$

the minor losses for the problem are summarized in the following table:

Note: The loss for a pipe bend is not the same as for an elbow fitting.

If there were no tank at the pipe discharge and point 2 were at the pipe exit, there would be no exit loss coefficient. However, there would be an exit K.E. term.

Loss element	Ki
Sharp entrance (Fig. 6.21)	0.5
Open globe valve (Table 6.5)	6.9
12 " bend, R/D = 12/6 = 2 (Fig. 6.19)	0.15
Threaded, 90Þ, reg. elbow, (Table 6.5)	0.95
Gate valve, 1/2 closed (Fig. 6.18)	2.7
Submerged exit (Fig. 6.20)	1
Ki =	12.2

Substituting in the energy equation we obtain

$$h_p = (120 - 20) + \left\{0.0214\frac{400}{2/12}\frac{9.17^2}{64.4}\right\} + \left\{12.2\frac{9.17^2}{64.4}\right\}$$

$$h_p = 100 + 67.1 + 15.9 = 183\,\mathrm{ft}$$



ketabline.com Ebook.ketabline.com

Note the distribution of the total loss between static, pipe friction, and minor losses.

The power required to be delivered to the fluid is give by

$$P_f = \rho Q g h_p = 1.94 \frac{slug}{ft^3} 32.2 \frac{ft}{s^2} 0.2 \frac{ft^3}{s} 183\ ft = 2286\ ft\ lbf$$

$$P_f = \frac{2286 ft lbf}{550 ft lbf/s/hp} = 4.2 hp$$

If the pump has an efficiency of 70 %, the power requirements would be specified by

$$\dot{W}_p = \frac{4.2 hp}{0.70} = 6 hp$$

Solution Summary:

To solve basic pipe flow pressure drop problem, use the following procedure:

1. Use known flow rate to determine Reynolds number.
2. Identify whether flow is laminar or turbulent.
3. Use appropriate expression to find friction factor (with ε/D if necessary).
4. Use definition of h_f to determine friction head loss.
5. Tabulate and sum minor loss coefficients for piping components.

6a. Use general energy equation to determine total pressure drop, or

6b. Determine pump head requirements as appropriate.

7. Determine pump power and motor size if required.



ketabline.com Ebook.ketabline.com

Multiple-Pipe Systems

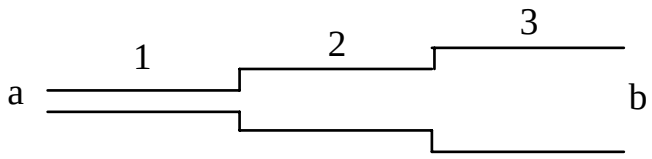
Basic concepts of pipe system analysis apply also to multiple pipe systems. However, the solution procedure is more involved and can be iterative.

Consider the following:

a. Multiple pipes in series
b. Multiple pipes in parallel

Series Pipe System:

The indicated pipe system has a steady flow rate Q through three pipes with diameters D_1, D_2, & D_3.



Two important rules apply to this problem.

1. The flow rate is the same through each pipe section. For incompressible flow, this is expressed as

$$Q_1 = Q_2 = Q_3 = Q \quad \text{or} \quad D_1^2 V_1 = D_2^2 V_2 = D_3^2 V_3$$

2. The total frictional head loss is the sum of the head losses through the various sections.

$$h_{f,a-b} = h_{f,1} + h_{f,2} + h_{f,3}$$

$$h_{f,a-b} = \left(f\frac{L}{D} + \sum K_i \right)_{D_1} \frac{V_1^2}{2g} + \left(f\frac{L}{D} + \sum K_i \right)_{D_2} \frac{V_2^2}{2g} + \left(f\frac{L}{D} + \sum K_i \right)_{D_3} \frac{V_3^2}{2g}$$

Note: Be careful how you evaluate the transitions from one section to the next. In general, loss coefficients for transition sections are based on the velocity of the smaller section.



ketabline.com Ebook.ketabline.com

Example: Given a pipe system as shown in the previous figure. The total pressure drop is $P_a - P_b = 150$ kPa and the elevation change is $Z_a - Z_b = -5$ m. Given the following data, determine the flow rate of water through the section.

Pipe	L (m)	D (cm)	e (mm)	e/D
1	100	8	0.24	0.003
2	150	6	0.12	0.02
3	80	4	0.2	0.005

The energy equation is written as where hf is given by the sum of the total frictional losses for three pipe sections.

$$\frac{P_a - P_b}{\rho g} = \frac{V_b^2 - V_a^2}{2g} + Z_b - Z_a + h_f - h_p$$

With no pump; hp is 0, $Z_b - Z_a$ = - 5 m and ht = 15.3 m for ΔP = 150 kPa

$$h_t = \frac{P_a - P_b}{\rho g} = \frac{150{,}000\ N/m^2}{9790\ N/m^2} = 15.3 m$$

Since the flow rate Q and thus velocity is the only remaining variable, the solution is easily obtained from a spreadsheet by assuming Q until ΔP = 150 kPa.

			1	2	3
Fluid		L(m)	100	150	80
ρ(kg/m^3) =	1000	D(m) =	0.08	0.06	0.04
ν(m^2/s) =	1.02E-06	ε(mm) =	0.24	0.12	0.20
inlet & exit		ε/D=	0.003	0.002	0.005
dZ (m) =	-5				
Da(m) =	0.08	V(m/s)=	0.56	1.00	2.25
Db(m) =	0.04	Re =	44082.8	58777.1	88165.6
Assume		f=	0.02872	0.02591	0.03139
Q (m^3/s)=	0.00283	hf =	0.58	3.30	16.18
Va(m/s)=	0.56	Ki	0	0	0
Vb(m/s)=	2.25	hm=	0	0	0
dKE(m) =	0.24				
hf (net) =	20.08	hf(calc) =	0.58	3.30	16.18
	Actual	Calculated			
Pa - Pb (kPa)	150	150.00	Q(m^3/hr) =	10.17	



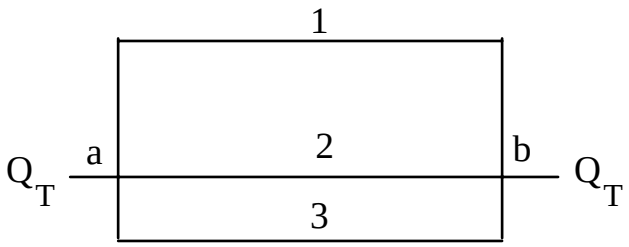
ketabline.com Ebook.ketabline.com

Thus it is seen that a flow rate of 10.17 m^3/hr produces the indicated head loss through each section and a net total ΔP = 150 kPa.

A solution can also be obtained by writing all terms explicitly in terms of a single velocity, however, the algebra is quite complex (unless the flow is laminar), and an iterative solution is still required. All equations used to obtained the solution are the same as those presented in previous sections.

Parallel Pipe Systems

A flow rate Q_T enters the indicated parallel pipe system. The total flow splits and flows through 3 pipe sections, each with different diameters and lengths.



Two basic rules apply to parallel pipe systems;

1. The total flow entering the parallel section is equal to the sum of the flow rates through the individual sections,
2. The total pressure drop across the parallel section is equal to the pressure drop across each individual parallel segment.

Note that if a common junction is used for the start and end of the parallel section, the velocity and elevation change is also the same for each section. Thus, the flow rate through each section must be such that the frictional loss is the same for each and the sum of the flow rates equals the total flow.

For the special case of no kinetic or potential energy change across the sections, we obtain:

$$h_t = (h_f + h_m)_1 = (h_f + h_m)_2 = (h_f + h_m)_3$$

and

$$Q_T = Q_1 + Q_2 + Q_3$$



ketabline.com Ebook.ketabline.com

Again, the equation used for both the pipe friction and minor losses is the same as previously presented. The flow and pipe dimensions used for the previous example are now applied to the parallel circuit shown above.

Example: A parallel pipe section consists of three parallel pipe segments with the lengths and diameters shown below. The total pressure drop is 150 kPa and the parallel section has an elevation drop of 5 m. Neglecting minor losses and kinetic energy changes, determine the flow rate of water through each pipe section.

The solution is iterative and is again presented in a spreadsheet. The net friction head loss of 20.3 m now occurs across each of the three parallel sections.

Fluid				1	2	3
ρ(kg/m^3) =	1000		L(m)	100	150	80
ν(m^2/s) =	1.02E-06		D(m) =	0.08	0.06	0.04
			ε(mm) =	0.24	0.12	0.20
inlet & exit			ε/D=	0.003	0.002	0.005
dZ (m) =	-5		Q(m^3/hr) =	62.54	25.95	11.41
Da(m) =	0.08		V(m/s)=	3.46	2.55	2.52
Db(m) =	0.04		Re =	271083.5	149977.8	98919.7
			f=	0.02666	0.02450	0.03129
Q (m^3/hr)=	99.91		hf =	20.30	20.30	20.30
Assume			Ki =	0	0	0
Q1 (m^3/s)=	62.54		hm=	0.00	0.00	0.00
Q2(m^3/s)=	25.95					
			hf,net(m) =	20.30	20.30	20.30
			hf + ΔZ=	15.30	15.30	15.30
Pa - Pb (kPa)	150.13					
ht(m) =	15.31		Q(m^3/hr) =	62.54	25.95	11.41

Total Flow, Qt(m^3/hr) =	99.91

The strong effect of diameter can be seen with the smallest diameter having the lowest flow rate, even though it also has the shortest length of pipe.



ketabline.com Ebook.ketabline.com

VII. Boundary Layer Flows

The previous chapter considered only viscous internal flows.

Viscous internal flows have the following major boundary layer characteristics:

* An entrance region where the boundary layer grows and dP/dx ≠ constant,
* A fully developed region where:
  - The boundary layer fills the entire flow area.
  - The velocity profiles, pressure gradient, and τ_w are constant; i.e., they are not equal to f(x),
  - The flow is either laminar or turbulent over the entire length of the flow , i.e., transition from laminar to turbulent is not considered.

However, viscous flow boundary layer characteristics for external flows are significantly different as shown below for flow over a flat plate:

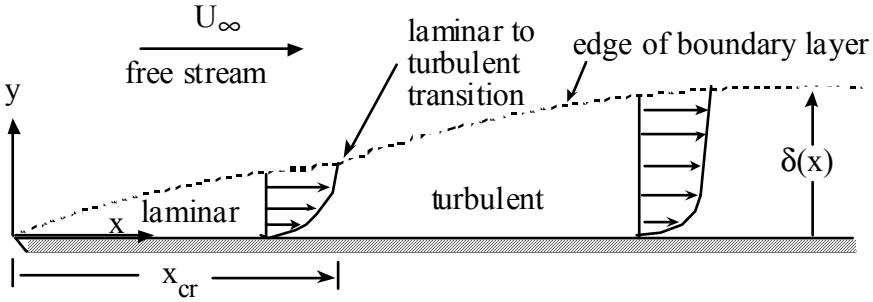


Fig. 7.1 Schematic of boundary layer flow over a flat plate

For these conditions, we note the following characteristics:

- The boundary layer thickness δ grows continuously from the start of the fluid-surface contact, e.g., the leading edge. It is a function of x, not a constant.
- Velocity profiles and shear stress τ are f(x,y).
- The flow will generally be laminar starting from x = 0.
- The flow will undergo laminar-to-turbulent transition if the streamwise dimension is greater than a distance x_{cr} corresponding to the location of the transition Reynolds number Re_{cr}.
- Outside of the boundary layer region, free stream conditions exist where velocity gradients and therefore viscous effects are typically negligible.



ketabline.com Ebook.ketabline.com

As it was for internal flows, the most important fluid flow parameter is the local Reynolds number defined as

$$\mathrm{Re}_x = \frac{\rho U_\infty x}{\mu} = \frac{U_\infty x}{\upsilon}$$

where

ρ = fluid density μ = fluid dynamic viscosity

ν = fluid kinematic viscosity U_∞ = characteristic flow velocity

x = characteristic flow dimension

It should be noted at this point that all external flow applications will not use a distance from the leading edge x and the characteristic flow dimension. For example, for flow over a cylinder, the diameter will be used as the characteristic dimension for the Reynolds number.

Transition from laminar to turbulent flow typically occurs at the local transition Reynolds number which for flat plate flows can be in the range of

$$500,000 \le \mathrm{Re}_{cr} \le 3,000,00$$

With x_{cr} = the value of x where transition from laminar to turbulent flow occurs, the typical value used for steady, incompressible flow over a flat plate is

$$\mathrm{Re}_{cr} = \frac{\rho U_\infty x_{cr}}{\mu} = 500,000$$

Thus for flat plate flows for which:

$x < x_{cr}$ the flow is laminar

$x \ge x_{cr}$ the flow is turbulent

The solution to boundary layer flows is obtained from the reduced "Navier – Stokes" equations, i.e., Navier-Stokes equations for which boundary layer assumptions and approximations have been applied.



ketabline.com Ebook.ketabline.com

Flat Plate Boundary Layer Theory

Laminar Flow Analysis

For steady, incompressible flow over a flat plate, the laminar boundary layer equations are:

Conservation of mass: $$\frac{\partial u}{\partial x}+\frac{\partial v}{\partial y}=0$$

'X' momentum: $$u\frac{\partial u}{\partial x}+v\frac{\partial u}{\partial y}=-\frac{1}{\rho}\frac{dp}{dx}+\frac{1}{\rho}\frac{\partial}{\partial y}\left(\mu\frac{\partial u}{\partial y}\right)$$

'Y' momentum: $$-\frac{\partial p}{\partial y}=0$$

The solution to these equations was obtained in 1908 by Blasius, a student of Prandtl's. He showed that the solution to the velocity profile, shown in the table below, could be obtained as a function of a single, non-dimensional variable η defined as

$$\eta = y\left(\frac{U_\infty}{\upsilon x}\right)^{1/2}$$

with the resulting ordinary differential equation:

$$f''' + \frac{1}{2} f f'' = 0$$

and $$f'(\eta)=\frac{u}{U_\infty}$$

$y[U/(\nu x)]^{1/2}$	u/U	$y[U/(\nu x)]^{1/2}$	u/U
0.0	0.0	2.8	0.81152
0.2	0.06641	3.0	0.84605
0.4	0.13277	3.2	0.87609
0.6	0.19894	3.4	0.90177
0.8	0.26471	3.6	0.92333
1.0	0.32979	3.8	0.94112
1.2	0.39378	4.0	0.95552
1.4	0.45627	4.2	0.96696
1.6	0.51676	4.4	0.97587
1.8	0.57477	4.6	0.98269
2.0	0.62977	4.8	0.98779
2.2	0.68132	5.0	0.99155
2.4	0.72899	∞	1.00000
2.6	0.77246		

Boundary conditions for the differential equation are expressed as follows:

at y = 0, v = 0 $\rightarrow$ f (0) = 0 ; y component of velocity is zero at y = 0

at y = 0 , u = 0 $\rightarrow f'(0)=0$; x component of velocity is zero at y = 0



ketabline.com Ebook.ketabline.com

The key result of this solution is written as follows:

$$\left.\frac{\partial^2 f}{\partial \eta^2}\right)_{y=0} = 0.332 = \frac{\tau_w}{\mu U_\infty \sqrt{U_\infty / \upsilon x}}$$

With this result and the definition of the boundary layer thickness, the following key results are obtained for the laminar flat plate boundary layer:

Local boundary layer thickness $\delta(x) = \frac{5x}{\sqrt{Re_x}}$

Local skin friction coefficient: (defined below) $C_{f_x} = \frac{0.664}{\sqrt{Re_x}}$

Total drag coefficient for length L (integration of τ_w dA over the length of the plate, per unit area, divided by 0.5 ρU_∞^2) $C_D = \frac{1.328}{\sqrt{Re_x}}$

where by definition $C_{f_x} = \frac{\tau_w(x)}{\frac{1}{2}\rho U_\infty^2}$ and $C_D = \frac{F_D / A}{\frac{1}{2}\rho U_\infty^2}$

With these results, we can determine local boundary layer thickness, local wall shear stress, and total drag force for laminar flow over a flat plate.

Example:

Air flows over a sharp edged flat plate with L = 1 m, a width of 3 m and U_∞ = 2 m/s . For one side of the plate, find: $\delta(L)$, $C_f(L)$, $\tau_w(L)$, C_D, and F_D.

Air: ρ = 1.23 kg/m^3 ν = 1.46 E-5 m^2/s

First check Re: $Re_L = \frac{U_\infty L}{\upsilon} = \frac{2m/s * 2.15m}{1.46E-5 m^2/s} = 294,520 < 500,000$

Key Point: Therefore, the flow is laminar over the entire length of the plate and calculations made for any x position from 0 - 1 m must be made using laminar flow equations.



ketabline.com Ebook.ketabline.com

Boundary layer thickness at x = L:

$$\delta(L) = \frac{5\,L}{\sqrt{\mathrm{Re}_L}} = \frac{5*2.15\,m}{\sqrt{294,520}} = 0.0198\,m = 1.98\,cm$$

Local skin friction coefficient at x = L:

$$C_f(L) = \frac{0.664}{\sqrt{\mathrm{Re}_L}} = \frac{0.664}{\sqrt{294,520}} = 0.00122$$

Surface shear stress at x = L:

$$\tau_w = 1/2\,\rho U_\infty^2\, C_f = 0.5*1.23\,kg/m^3 * 2^2\,m^2/s^2 * 0.00122$$

$$\tau_w = 0.0030\,N/m^2\,(Pa)$$

Drag coefficient over total plate, 0 – L:

$$C_D(L) = \frac{1.328}{\sqrt{\mathrm{Re}_L}} = \frac{1.328}{\sqrt{294,520}} = 0.00245$$

Drag force over plate, 0 – L:

$$F_D = 1/2\,\rho U_\infty^2\, C_D\, A = 0.5*1.23\,kg/m^3 * 2^2\,m^2/s^2 * 0.00245 * 2 * 2.15\,m^2$$

$$F_D = 0.0259\,N$$

Two key points regarding this analysis:

1. Each of these calculations can be made for any other location on the plate by simply using the appropriate x location for any $x \le L$.

2. Be careful not to confuse the calculation for C_f and C_D. C_f is a local calculation at a particular x location (including x = L) and can only be used to calculate local shear stress, not drag force. C_D is an integrated average over a specified length (including any $x \le L$) and can only be used to calculate the average shear stress and the integrated force over the length.



ketabline.com Ebook.ketabline.com

Turbulent Flow Equations

While the previous analysis provides an excellent representation of laminar, flat plate boundary layer flow, a similar analytical solution is not available for turbulent flow due to the complex nature of the turbulent flow structure. However, experimental results are available to provide equations for key flow field parameters.

A summary of the results for boundary layer thickness and local and average skin friction coefficient for a laminar flat plate and a comparison with experimental results for a smooth, turbulent flat plate are shown below.

Laminar	Turbulent	
$\delta(x) = \frac{5x}{\sqrt{Re_x}}$	$\delta(x) = \frac{0.37x}{Re_x^{.2}}$	
$C_{f_x} = \frac{0.664}{\sqrt{Re_x}}$	$C_{f_x} = \frac{0.0592}{Re_x^{.2}}$	
$C_D = \frac{1.328}{\sqrt{Re_L}}$	$C_D = \frac{0.074}{Re_L^{.2}}$	for turbulent flow over entire plate, 0 – L, i.e. assumes turbulent flow in the laminar region.

where

$$C_{f_x} = \frac{\tau_w}{\frac{1}{2}\rho U_\infty^2}$$

local drag coefficient based on local wall shear stress (laminar or turbulent flow region).

and

C_D = total drag coefficient based on the integrated force over the length 0 to L

$$C_D = \frac{F/A}{\frac{1}{2}\rho U_\infty^2} = \left(\frac{1}{2}\rho U_\infty^2 A\right)^{-1} \int_0^L \tau_w(x)\, w\, dx$$

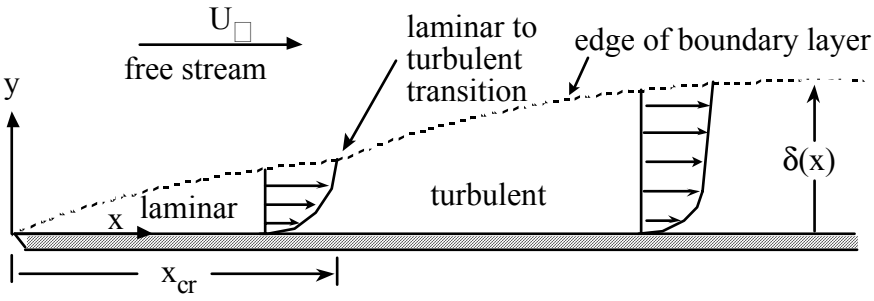
A careful study of these results will show that in general, boundary layer thickness grows faster for turbulent flow and wall shear and total friction drag are greater for turbulent flow than for laminar flow given the same Reynolds number.



ketabline.com Ebook.ketabline.com

It is noted that the expressions for turbulent flow are valid only for a flat plate with a smooth surface. Expressions including the effects of surface roughness are available in the text.

Combined Laminar and Turbulent Flow



Flat plate with both laminar and turbulent flow sections

For conditions (as shown above) where the length of the plate is sufficiently long that we have both laminar and turbulent sections:

* Local values for boundary layer thickness and wall shear stress for either the laminar or turbulent sections are obtained from the expressions for $\delta(x)$ and C_{f_x} for laminar or turbulent flow as appropriate for the given region.
* The result for average drag coefficient C_D and thus total frictional force over the laminar and turbulent portions of the plate is given by (assuming a transition Re of 500,000)

$$C_D = \frac{0.074}{\mathrm{Re}_L^{.2}} - \frac{1742}{\mathrm{Re}_L}$$

* Calculations assuming only turbulent flow can be made typically for two cases
  1. when some physical situation (a trip wire) has caused the flow to be leading from the leading edge or
  2. if the total length L of the plate is much greater than the length x_{cr} of the laminar section such that the total flow can be considered turbulent from x = 0 to L. Note that this will overpredict the friction drag force since turbulent drag is greater than laminar.

With these results, a detailed analysis can be obtained for laminar and/or turbulent flow over flat plates and surfaces that can be approximated as a flat plate.



ketabline.com Ebook.ketabline.com

Example:

Water flows over a sharp flat plate 2.55 m long, 1 m wide, with $U_\infty = 2$ m/s. Estimate the error in F_D if it is assumed that the entire plate is turbulent.

Water: $\rho = 1000\ kg/m^3$ $\nu = 1.02\ E\text{-}\ m^2/s$

Reynolds number: $$Re_L = \frac{U_\infty L}{\upsilon} = \frac{2\,m/s * 2.55\,m}{1.02E-6\,m^2/s} = 5E6 > 500,000$$

with $Re_{cr} = 500{,}000 \Rightarrow x_{cr} = 0.255m$ (or 10% laminar)

a. Assume that the entire plate is turbulent

$$C_D = \frac{0.074}{Re_L^{.2}} = \frac{0.074}{(5E6)^{.2}} = 0.00338$$

$$F_D = 0.5\rho U_\infty^2 C_D A = 0.5 * 1000\frac{kg}{m^3} * 2^2\frac{m^2}{s^2} * 0.00338 * 2.55m^2$$

$F_D = 17.26\,N$ **This should be high since we have assumed that the entire plate is turbulent and the first 10% is actually laminar.**

b. Consider the actual combined laminar and turbulent flow:

$$C_D = \frac{0.074}{Re_L^{.2}} - \frac{1742}{Re_L} = 0.00338 - \frac{1742}{5E6} = 0.00303$$

Note that the C_D has decreased when both the laminar and turbulent sections are considered.

$$F_D = 0.5\rho U_\infty^2 C_D A = 0.5 * 1000\frac{kg}{m^3} * 2^2\frac{m^2}{s^2} * 0.00303 * 2.55\,m^2$$



ketabline.com Ebook.ketabline.com

$$F_D = 15.46\,N \quad \{\text{Lower than the fully turbulent value}\}$$

$$Error = \frac{17.26 - 15.46}{15.46} * 100 = 11.6\%\ high$$

Question: Since $x_{cr} = 0.255$ m, what would your answers represent if you had calculated the Re, C_D, and F_D using $x = x_{cr} = 0.255$ m?

Answer: You would have the value of the transition Reynolds number and the drag coefficient and drag force over the laminar portion of the plate (assuming you used laminar equations). If you used turbulent equations, you would have red marks on your paper.



ketabline.com Ebook.ketabline.com

Von Karman Integral Momentum Analysis

While the previous results provide an excellent basis for the analysis of flat plate flows, complex geometries and boundary conditions make analytical solutions to most problems difficult.

An alternative procedure provides the basis for an approximate solution which in many cases can provide excellent results.

The key to practical results is to use a reasonable approximation to the boundary layer profile, u(x,y). This is used to obtain the following:

a. Boundary layer mass flow: $$\dot{m} = \int_0^{\delta} \rho u b \, dy$$

where b is the width of the area for which the flow rate is being obtained.

b. Wall shear stress: $$\tau_w = \mu \left(\frac{du}{dy} \right)_{y=0}$$

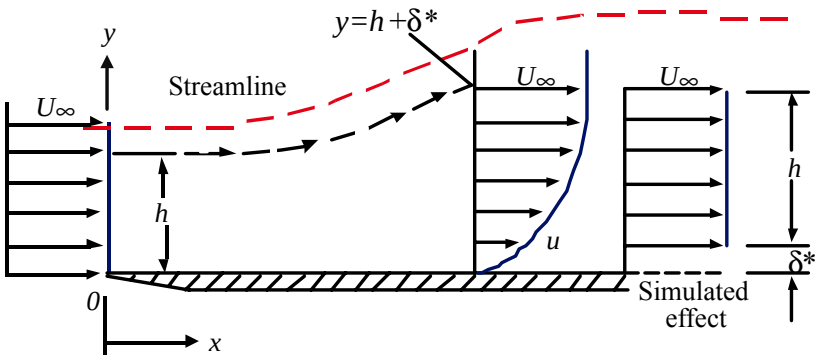
You will also need the streamwise pressure gradient $\frac{dP}{dx}$ for many problems.

The Von Karman integral momentum theory provides the basis for such an approximate analysis. The following summarizes this theory.

<u>Displacement thickness</u>:

Consider the problem indicated in the adjacent figure:

A uniform flow field with velocity U_∞ approaches a solid surface. As a result of viscous shear, a boundary layer velocity profile develops.



ketabline.com Ebook.ketabline.com

A viscous boundary layer is created when the flow comes in contact with the solid surface.

Key point: Compared to the uniform velocity profile approaching the solid surface, the effect of the viscous boundary layer is to displace streamlines of the flow outside the boundary layer away from the wall.

With this concept, we define δ^* = displacement thickness

δ^* = distance the solid surface would have to be displaced to maintain the same mass flow rate as for non-viscous flow.

From the development in the text, we obtain

$$\delta^* = \int_0^{\delta} \left(1 - \frac{u}{U_\infty}\right) dy$$

Therefore, with an expression for the local velocity profile we can obtain $\delta^* = f(\delta)$

Example:

Given: $\dfrac{u}{U_\infty} = 2\left(\dfrac{y}{\delta}\right) - \left(\dfrac{y}{\delta}\right)^2$ determine an expression for $\delta^* = f(\delta)$

Note that for this assumed form for the velocity profile:

1. At $y = 0$, $u = 0$ correct for no slip condition
2. At $y = \delta$, $u = U_\infty$ correct for edge of boundary layer
3. The form is quadratic

To simplify the mathematics,

let $\eta = y/\delta$, at $y = 0$, $\eta = 0$; at $y = \delta$, $\eta = 1$; $dy = \delta\, d\eta$

Therefore: $\dfrac{u}{U_\infty} = 2\eta - \eta^2$



ketabline.com Ebook.ketabline.com

Substituting: $$\delta^* = \int_0^1 \left(1 - 2\eta + \eta^2\right)\delta\, d\eta = \delta\left\{\eta - \frac{2\eta^2}{2} + \frac{\eta^3}{3}\right\}_0^1$$

which yields $$\delta^* = \frac{1}{3}\delta$$

Therefore, for flows for which the assumed quadratic equation approximates the velocity profile, streamlines outside of the boundary layer are displaced approximately according to the equation

$$\delta^* = \frac{1}{3}\delta$$

This closely approximates flow for a flat plate.

Key Point: When assuming a form for a velocity profile to use in the Von Karman analysis, make sure that the resulting equation satisfies both surface and free stream boundary conditions as well as has a form that approximates u(y).

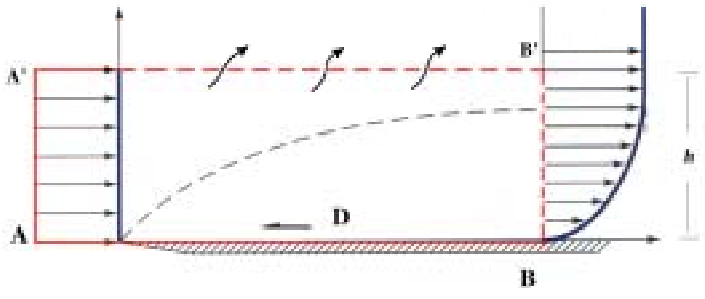
Momentum Thickness:

The second concept used in the Von Karman momentum analysis is that of

momentum thickness - θ

The concept is similar to that of displacement thickness in that θ is related to the loss of momentum due to viscous effects in the boundary layer.

Consider the viscous flow regions shown in the adjacent figure. Define a control volume as shown and integrate around the control volume to obtain the net change in momentum for the control volume.



ketabline.com Ebook.ketabline.com

If D = drag force on the plate due to viscous flow, we can write

$$-D = \sum (\text{momentum leaving c.v.}) - \sum (\text{momentum entering c.v.})$$

Completing an analysis shown in the text, we obtain

$$D = \rho U_\infty^2 \theta \qquad \theta = \int_0^\delta \frac{u}{U_\infty}\left(1 - \frac{u}{U_\infty}\right) dy$$

Using a drag coefficient defined as $C_D = \dfrac{D/A}{\frac{1}{2}\rho U_\infty^2}$

We can also show that $C_D = \dfrac{2\,\theta(L)}{L}$

where: θ(L) is the momentum thickness evaluated over the length L.

Thus, knowledge of the boundary layer velocity distribution u = f(y) allows the drag coefficient to be determined.

Momentum integral:

The final step in the Von Karman theory applies the previous control volume analysis to a differential length of surface. Performing an analysis similar to the previous analysis for drag D we obtain

$$\frac{\tau_w}{\rho} = \delta^* U_\infty \frac{dU_\infty}{dx} + \frac{d}{dx}\left(U_\infty^2 \theta\right)$$

This is the momentum integral for 2-D, incompressible flow and is valid for laminar or turbulent flow.



ketabline.com Ebook.ketabline.com

where $\delta^* U_\infty \frac{dU_\infty}{dx} = -\frac{\delta^*}{\rho}\frac{dP}{dx}$

Therefore, this analysis also accounts for the effect of freestream pressure gradient.

For a flat plate with non-accelerating flow, we can show that

$$P = const., \quad U_\infty = const., \quad \frac{dU_\infty}{dx} = 0$$

Therefore, for a flat plate, non-accelerating flow, the Von Karman momentum integral becomes

$$\frac{\tau_w}{\rho} = \frac{d}{dx}\left(U_\infty^2 \theta\right) = U_\infty^2 \frac{d\theta}{dx}$$

From the previous analysis and the assumed velocity distribution of

$$\frac{u}{U_\infty} = 2\left(\frac{y}{\delta}\right) - \left(\frac{y}{\delta}\right)^2 = 2\eta - \eta^2$$

The wall shear stress can be expressed as

$$\tau_w = \mu\left(\frac{du}{dy}\right)_w = 2U_\infty\left\{\frac{2}{\delta} - \frac{2y}{\delta^2}\right\}_{y=0} = \frac{2\mu U_\infty}{\delta} \qquad \text{(A)}$$

Also, with the assumed velocity profile, the momentum thickness θ can be evaluated as

$$\theta = \int_0^\delta \frac{u}{U_\infty}\left(1 - \frac{u}{U_\infty}\right) dy$$

or



ketabline.com Ebook.ketabline.com

$$\theta = \int_0^{\delta} (2\eta - \eta^2)(1 - 2\eta + \eta^2)\delta \, d\eta = \frac{2\delta}{15}$$

We can now write from the previous equation for τ_w

$$\tau_w = \rho U_\infty^2 \frac{d\theta}{dx} = \frac{2}{15}\rho U_\infty^2 \frac{d\delta}{dx}$$

Equating this result to Eqn. A we obtain

$$\tau_w = \frac{2}{15}\rho U_\infty^2 \frac{d\delta}{dx} = \frac{2\mu U_\infty}{\delta}$$

or

$$\delta \, d\delta = \frac{15\mu}{\rho U_\infty} dx \qquad \text{which after integration yields}$$

$$\delta = \left\{ \frac{30\mu x}{\rho U_\infty} \right\}^{1/2} \qquad \text{or} \qquad \delta = \frac{5.48}{\sqrt{\mathrm{Re}_x}}$$

Note that the this result is within 10% of the exact result from Blasius flat plate theory.

Since for a flat plate, we only need to consider friction drag (not pressure drag), we can write

$$C_{f_x} = \frac{\tau_w(x)}{\frac{1}{2}\rho U_\infty^2} = \frac{2\mu U_\infty}{\delta} \frac{1}{\frac{1}{2}\rho U_\infty^2}$$

Substitute for δ to obtain

$$C_{f_x} = \frac{2\mu U_\infty}{5.48} \frac{\sqrt{\mathrm{Re}}}{\frac{1}{2}\rho U_\infty^2} = \frac{0.73}{\sqrt{\mathrm{Re}_x}}$$



ketabline.com Ebook.ketabline.com

Exact theory has a numerical constant of 0.664 compared with 0.73 for the previous result.

It is seen that the von Karman integral theory provides the means to determine approximate expressions for

$$\delta,\ \tau_w, \text{ and } C_f$$

using only an assumed velocity profile.

Solution summary:

1. Assume an analytical expression for the velocity profile for the problem.
2. Use the assumed velocity profile to determine the solution for the displacement thickness for the problem.
3. Use the assumed velocity profile to determine the solution for the momentum thickness for the problem.
4. Use the previous results and the von Karman integral momentum equation to determine the solution for the drag/wall shear for the problem.

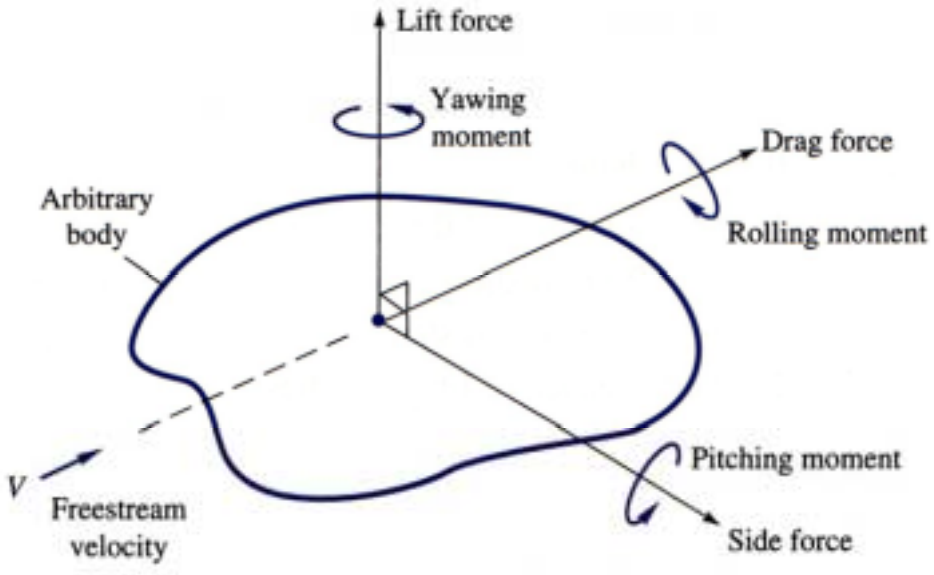


ketabline.com Ebook.ketabline.com

Bluff Body, Viscous Flow Characteristics
(Immersed Bodies)

In general, a body immersed in a flow will experience both externally applied forces and moments as a result of the flow about its external surfaces. The typical terminology and designation of these forces and moments are given in the diagram shown below.

The orientation of the axis for the drag force is typically along the principal body axis, although in certain applications, this axis is aligned with the principal axis of the free stream, approach velocity U.



Since in many cases the drag force is aligned with the principal axis of the body shape and not necessarily aligned with the approaching wind vector. Review all data carefully to determine which coordinate system is being used: body axis coordinate system or a wind axis coordinate system.

These externally applied forces and moments are generally a function of

a. Body geometry
b. Body orientation
c. Flow conditions



ketabline.com Ebook.ketabline.com

These forces and moments are also generally expressed in the form of a non-dimensional force/moment coefficient, e.g. the drag coefficient:

$$C_D = \frac{F_D/A}{\frac{1}{2}\rho U_\infty^2}$$

It is noted that it is common to see one of three reference areas used depending on the application:

1. Frontal (projected) area: Used for thick, stubby, non-aerodynamic shapes, e.g., buildings, cars, etc.

2. Planform (top view, projected) area: Used for flat, thin shapes, e.g., wings, hydrofoils, etc.

3. Wetted area: The total area in contact with the fluid. Used for surface ships, barges, etc.

The previous, flat plate boundary layer results considered only the contribution of viscous surface friction to drag forces on a body. However, a second major (and usually dominant) factor is **pressure or form drag**.

Pressure drag is drag due to the integrated surface pressure distribution over the body. Therefore, in general , the total drag coefficient of a body can be expressed as

$$C_D = C_{D,press} + C_{D,friction}$$

or

$$C_D = \frac{F_{D,total}/A}{\frac{1}{2}\rho U_\infty^2} = \frac{F_{D,press.}/A}{\frac{1}{2}\rho U_\infty^2} + \frac{F_{D,friction}/A}{\frac{1}{2}\rho U_\infty^2}$$

Which factor, pressure or friction drag, dominates depends largely on the aerodynamics (streamlining) of the shape and to a lesser extent on the flow conditions.

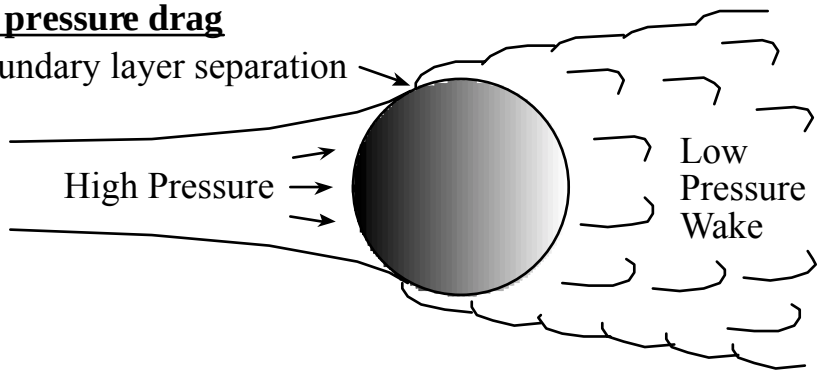


ketabline.com Ebook.ketabline.com

Typically the most important factor in the magnitude and significance of pressure or form drag is the boundary layer separation and resulting low pressure wake region associated with flow around non - aerodynamic shapes.

Consider the two shapes shown below:

large pressure drag



Low pressure drag no separated flow region



The flow around the streamlined airfoil remains attached, producing no boundary layer separation and comparatively small pressure drag. However, the flow around the less aerodynamic circular cylinder separates, resulting in an area of high surface pressure on the front side and low surface pressure on the back side and thus significant pressure drag.

This effect is shown very graphically in the following figures from the text.



ketabline.com Ebook.ketabline.com

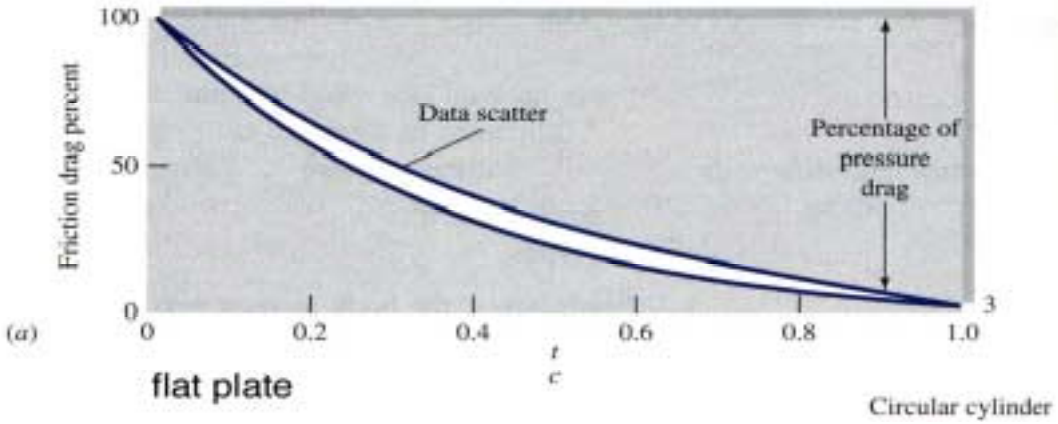


Fig. 7.12 Drag of a 2-D, streamlined cylinder

The previous figure shows the effect of streamlining and aerodynamics on the relative importance of friction and pressure drag. While for a thin flat plate (t/c = 0), all the drag is due to friction with no pressure drag, for a circular cylinder (t/c = 1), only 3% of the drag is due to friction with 97% due to pressure. Likewise for most bluff, non-aerodynamic bodies, pressure (also referred to as form drag) is the dominant contributor to the total drag.

However, the magnitude of the pressure (and therefore the total) drag can also be changed by reducing the size of the low pressure wake region. One way to do this is to change the flow conditions from laminar to turbulent. This is illustrated in the following figures from the text for a circular cylinder.

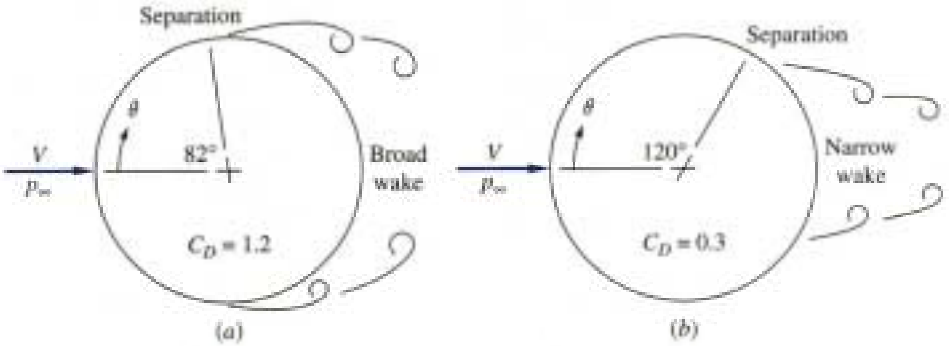


Fig. 7.13 Circular cylinder with (a) laminar separation and (b) turbulent separation

Note that for the cylinder on the left, the flow is laminar, boundary layer separation occurs at 82° and the C_D is 1.2, whereas for the cylinder on the right, the flow is turbulent and separation is delayed and occurs at 120°. The drag coefficient C_D is 0.3, a factor of 4 reduction due to a smaller wake region and reduced pressure drag.

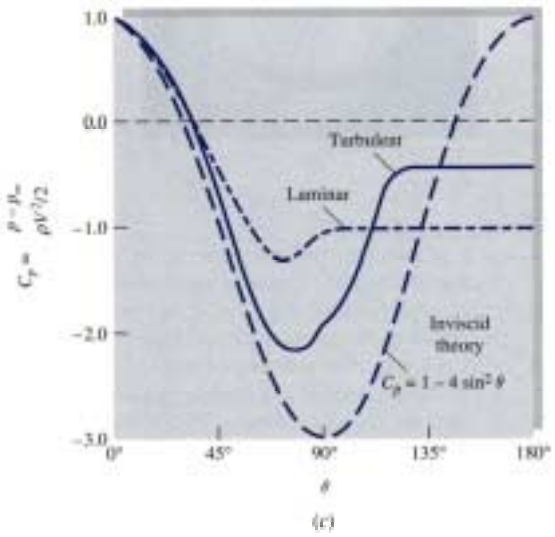


ketabline.com Ebook.ketabline.com

It should also be pointed out that the friction drag for the cylinder on the right is probably greater (turbulent flow conditions) than for the cylinder on the left (laminar flow conditions).

However, since pressure drag dominates, the net result is a significant reduction in the total drag.

The pressure distribution for laminar and turbulent flow over a cylinder is shown in Fig. 7.13c to the right. The front-to-rear pressure difference is greater for laminar flow, thus greater drag.



Finally, the effect of streamlining on total drag is shown very graphically with the sequence of modifications in Fig. 7.15.

Two observations can be made: (1) As body shape changes from a bluff body with fixed points of separation to a more aerodynamic shape, the effect of pressure drag and the drag coefficient will decrease.

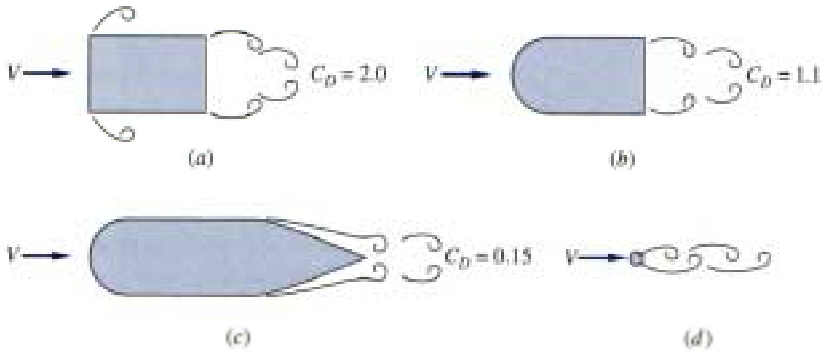


Fig. 7.15 The effect of streamlining on total drag

(2) The addition of surface area from (a) to (b) and (b) to (c) increases the friction drag, however, since pressure drag dominates, the net result is a reduction in the drag force and the C_D .

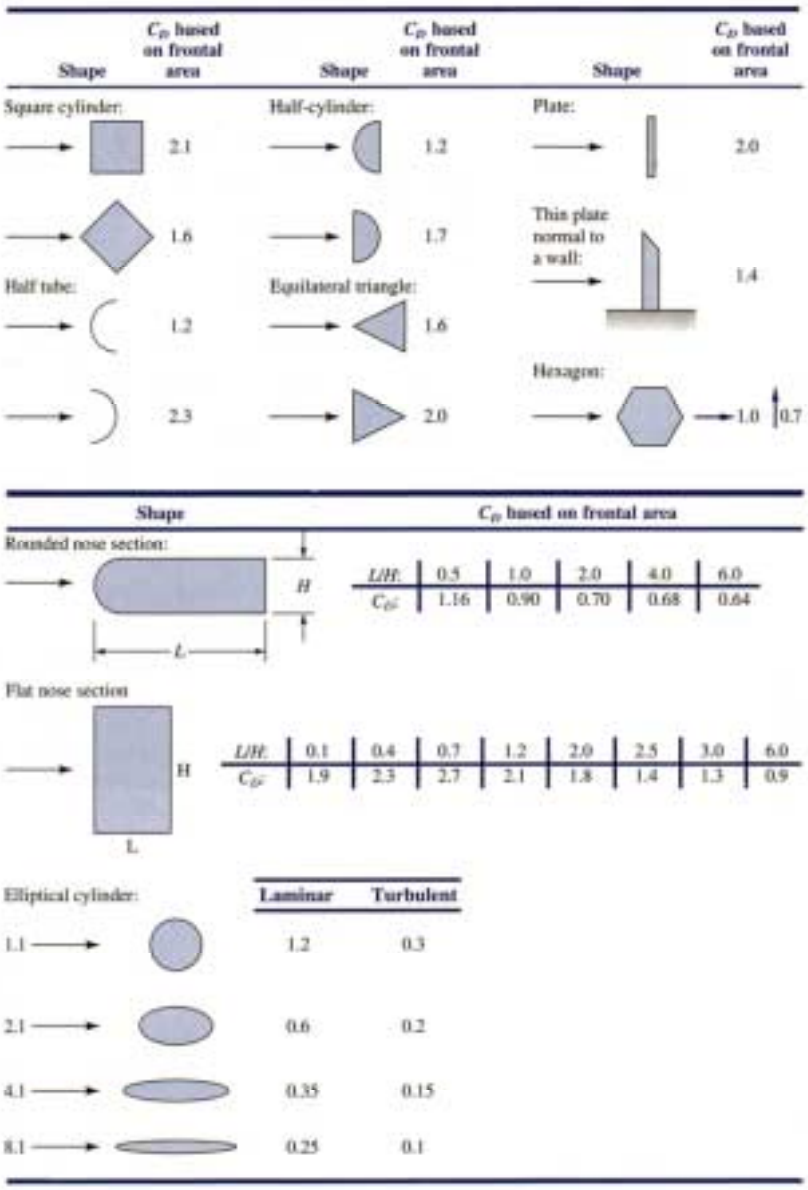


ketabline.com Ebook.ketabline.com

The final two figures show results for the drag coefficient for two and three dimensional shapes with various geometries.

Table 7.2 C_D for Two-Dimensional Bodies at Re $\geq 10^4$

First note that all values in Table 7.2 are for 2-D geometries, that is, the bodies are very long (compared to the cross-section dimensions) in the dimension perpendicular to the page.



Key Point: **Non – aerodynamic shapes with fixed points of separations (sharp corners) have a single value of C_D, irrespective of the value of the Reynolds number, e.g. square cylinder, half-tube, etc.**

Aerodynamic shapes generally have a reduction in C_D for a change from laminar to turbulent flow as a result of the shift in the point of boundary layer separation, e.g. elliptical cylinder.



ketabline.com Ebook.ketabline.com

Table 7.3 Drag of three-dimensional bodies at Re $\geq 10^4$

Body	C_D based on frontal area
Cube:	1.07
	0.81
Cup:	1.4
	0.4
Disk:	1.17
Parachute (Low porosity):	1.2

Body	C_D based on frontal area
Cone:	θ: 10° 20° 30° 40° 60° 75° 90°; C_D: 0.30 0.40 0.55 0.65 0.80 1.05 1.15
Short cylinder, laminar flow:	L/D: 1 2 3 5 10 20 40 ∞; C_D: 0.64 0.68 0.72 0.74 0.82 0.91 0.98 1.20
Porous parabolic dish [23]:	Porosity: 0 0.1 0.2 0.3 0.4 0.5; ← C_D: 1.42 1.33 1.20 1.05 0.95 0.82; → C_D: 0.95 0.92 0.90 0.86 0.83 0.80
Average person:	$C_DA = 9$ ft^2 ↑ $C_DA = 1.2$ ft^2
Pine and spruce trees [24]:	U, m/s: 10 20 30 40; C_D: 1.2 ± 0.2 1.0 ± 0.2 0.7 ± 0.2 0.5 ± 0.2

Body	Ratio	C_D based on frontal area
Rectangular plate:	b/h 1	1.18
	5	1.2
	10	1.3
	20	1.5
	∞	2.0

Body	Ratio	C_D based on frontal area
Flat-faced cylinder:	L/d 0.5	1.15
	1	0.90
	2	0.85
	4	0.87
	8	0.99

Ellipsoid:		Laminar	Turbulent
	L/d 0.75	0.5	0.2
	1	0.47	0.2
	2	0.27	0.13
	4	0.25	0.1
	8	0.2	0.08

The geometries in Table 7.3 are all 3-D and thus are finite perpendicular to the page. Similar to the results from the previous table, bluff body geometries with fixed points of separation have a single C_D, whereas aerodynamic shapes such as slender bodies of revolution have individual values of C_D for laminar and turbulent flow.

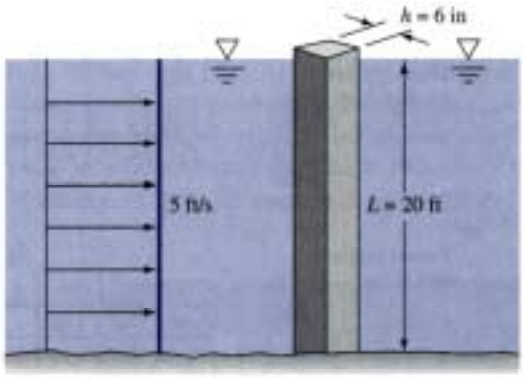


ketabline.com Ebook.ketabline.com

In summary, one must remember that broad generalizations such as saying that turbulent flow always increases drag, drag coefficients always depend on Reynolds number, or increasing surface area increases drag are not always valid. One must consider carefully all effects (viscous and pressure drag) due to changing flow conditions and geometry.

Example:

A square 6-in piling is acted on by a water flow of 5 ft/s that is 20 ft deep. Estimate the maximum bending stress exerted by the flow on the bottom of the piling.



Water: $\rho = 1.99$ slugs/ft^3

$\nu = 1.1\ E - 5$ ft^2/s

Assume that the piling can be treated as 2-D and thus end effects are negligible.

Thus for a width of 0.5 ft, we obtain:

$$\mathrm{Re} = \frac{5\ ft/s .5\ ft}{1.1E-5\ ft^2/s} = 2.3E5$$

In this range, Table 7.2 applies for 2-D bodies and we read $C_D = 2$ .1. The frontal area is A = 20*0.5 = 10 ft^2

$$F_D = 0.5\rho U_\infty^2 C_D A = 0.5 * 1.99 \frac{slug}{ft^3} * 5^2 \frac{ft^2}{s^2} * 2.1 * 10\ ft^2 = 522\ lbf$$

For uniform flow, the drag should be uniformly distributed over the total length with the net drag located at the mid-point of the piling.

Thus, relative to the bottom of the piling, the bending moment is given by

$$M_o = F * 0.5\ L = 522\ \text{lbf} * 10\ \text{ft} = 5220\ \text{ft-lbf}$$



ketabline.com Ebook.ketabline.com

From strength of materials, we can write

$$\sigma = \frac{M_o\, c}{I} = \frac{5220\ ft - lbf * 0.25\ ft}{\frac{1}{12} 0.5\ ft * 0.5^3\ ft^3} = 251{,}000\ psf = 1740\ psi$$

where c = distance to the neutral axis, I = moment of inertia = b h^3/12

Question: Since pressure acts on the piling and increases with increasing depth, why wasn't a pressure load considered?

Answer: Static pressure does act on the piling, but it acts uniformly around the piling at every depth and thus cancels. Dynamic pressure is considered in the drag coefficients of Tables 7.2 and 7.3 and does not have to be accounted for separately.



ketabline.com Ebook.ketabline.com

Ch. VIII Potential Flow and Computational Fluid Dynamics

Review of Velocity-Potential Concepts

This chapter presents examples of problems and their solution for which the assumption of potential flow is appropriate.

For low speed flows where viscous effects are neglected, the flow is irrotational and

$$\nabla \times \mathrm{V} = 0 \qquad \mathrm{V} = \nabla \phi \qquad \mathrm{u} = \frac{\partial \phi}{\partial \mathrm{x}} \qquad \mathrm{v} = \frac{\partial \phi}{\partial \mathrm{y}} \qquad \mathrm{w} = \frac{\partial \phi}{\partial \mathrm{z}}$$

The continuity equation , $\nabla \cdot \mathrm{V} = 0$, now reduces to

$$\nabla^2 \mathrm{V} = \frac{\partial^2 \phi}{\partial \mathrm{x}^2} + \frac{\partial^2 \phi}{\partial \mathrm{y}^2} + \frac{\partial^2 \phi}{\partial \mathrm{z}^2} = 0$$

The momentum equation reduces to Bernoulli's equation:

$$\frac{\partial \phi}{\partial t} + \frac{P}{\rho} + \frac{1}{2} V^2 + g z = \text{const}$$

Review of Stream Function Concepts

For plane incompressible flow in x-y coordinates a stream function exists such that

$$\mathrm{u} = \frac{\partial \Psi}{\partial \mathrm{y}} \quad \textit{and} \quad \mathrm{v} = -\frac{\partial \Psi}{\partial \mathrm{x}}$$

The condition of irrotationality reduces to Lapace's equation for Ψ and

$$\frac{\partial^2 \Psi}{\partial \mathrm{x}^2} + \frac{\partial^2 \Psi}{\partial \mathrm{y}^2} = 0$$



ketabline.com Ebook.ketabline.com

Elementary Plane-Flow Solutions

Three useful plane-flow solutions that are very useful in developing more complex solutions are:

Uniform stream, **i**U, in the x direction: $\Psi = \mathrm{U}\,\mathrm{y}$ $\phi = \mathrm{U}\,\mathrm{x}$

Line source or sink: $\Psi = \mathrm{m}\,\theta$ $\phi = m \ln \mathrm{r}$

Line vortex: $\Psi = -\mathrm{K} \ln \mathrm{r}$ $\phi = \mathrm{K}\,\theta$

In these expressions, the source strength, 'm' and vortex strength, ' K ', have the dimensions of velocity times length, or $[L^2/t]$.

If the uniform stream is written in plane polar coordinates, we have

Uniform stream, **i**U: $\Psi = \mathrm{U}\,\mathrm{r}\sin\theta$ $\phi = \mathrm{U}\,\mathrm{r}\cos\theta$

For a uniform stream moving at an angle, a , relative to the x-axis, we can write

$$u = \mathrm{U}\cos\alpha = \frac{\partial \Psi}{\partial \mathrm{y}} = \frac{\partial \phi}{\partial \mathrm{x}} \qquad \mathrm{v} = \mathrm{U}\sin\alpha = -\frac{\partial \Psi}{\partial \mathrm{x}} = \frac{\partial \phi}{\partial \mathrm{y}}$$

After integration, we obtain the following expressions for the stream function and velocity potential:

$$\Psi = U(y\cos\alpha - x\sin\alpha) \qquad \phi = U(x\cos\alpha + y\sin\alpha)$$

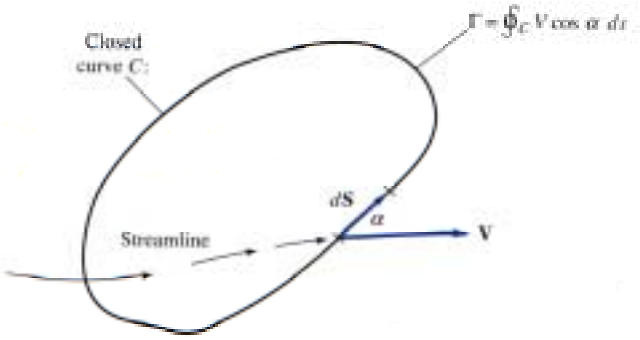
Circulation

The concept of fluid circulation is very useful in the analysis of certain potential flows, in particular those useful in aerodynamics analyses. Consider Figure 8.3 shown below:



ketabline.com Ebook.ketabline.com

We define the circulation, Γ , as the counterclockwise line integral of the arc length, ds times the velocity component tangent to the closed curve, C, e.g.



$$\Gamma = \oint_c V \cos\alpha \, d\,s = \int_c V \cdot ds$$

$$\Gamma = \int_c (u\,dx + \mathrm{v}\,\mathrm{dy} + \mathrm{w}\,\mathrm{dz})$$

For most flows, this line integral around a closed path, starting and stoping at the same point, yields $\Gamma = 0$. However,

for a vortex flow for which $\phi = K\,\theta$

the integral yields $\Gamma = 2\,\pi\,K$

An equivalent calculation can by made by defining a circular path of radius r around the vortex center to yield

$$\Gamma = \int_c \mathrm{v}_\theta \, d\,s = \int_0^{2\pi} \frac{K}{r} r \, d\,\phi = 2\,\pi\,K$$

Superposition of Potential Flows

Due to the mathematical character of the equations governing potential flows, the principle of superposition can be used to determine the solution of the flow which results from combining two individual potential flow solutions.

Several classic examples of this are presented as follows:



ketabline.com Ebook.ketabline.com

1. Source m at (-a,0) added to an equal sink at (+a, 0).

$$\psi = -m\tan^{-1}\frac{2ay}{x^2+y^2-a^2} \qquad \phi = \frac{1}{2}m\ln\frac{(x+a)^2+y^2}{(x-a)^2+y^2}$$

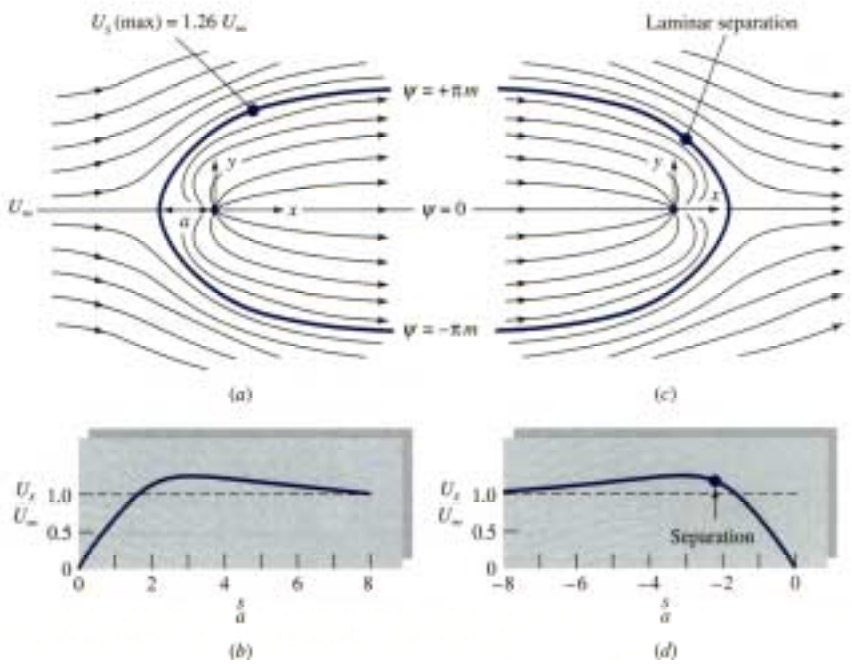
The streamlines and potential lines are two families of orthogonal circles (Fig. 4.13).

2. Sink m plus a vortex K, both at the origin.

$$\psi = m\theta - K\ln r \qquad \phi = m\ln r + K\theta$$

The streamlines are logarithmic spirals swirling into the origin (Fig. 4.14). They resemble a tornado or a bathtub vortex.

3. Uniform steam **i** U_∞ plus a source m at the origin (Fig. 4.15), the Ranking half body. If the origin contains a source, a plane half-body is formed with its nose to the left as shown below. If the origin contains a sink, m < 0, the half-body nose is to the right.. For both cases, the stagnation point is at a position $a = m / U_\infty$ away from the origin.



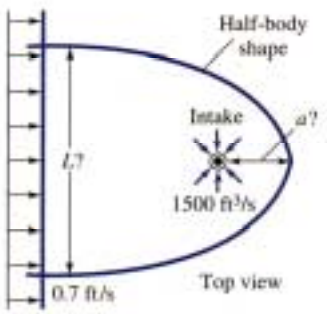
ketabline.com Ebook.ketabline.com

Example 8.1

An offshore power plant cooling water intake has a flow rate of 1500 ft^3/s in water 30 ft deep as in Fig. E8.1. If the tidal velocity approaching the intake is 0.7 ft/s, (a) how far downstream does the intake effect extend and (b) how much width of tidal flow in entrained into the intake?

The sink strength is related to the volume flow, Q and water depth by

$$m = \frac{Q}{2\pi b} = \frac{1500\ ft^3/s}{2\pi 30\ ft} = 7.96\ ft^2/s$$



E8.1

The lengths a and L are given by

$$a = \frac{m}{U_\infty} = \frac{7.96\ ft^2/s}{0.7\ ft/s} = 11.4\ ft$$

$$L = 2\pi a = 2\pi 11.4\ ft = 71\ ft$$

Flow Past a Vortex

Consider a uniform stream, U_∞ flowing in the x direction past a vortex of strength K with the center at the origin. By superposition the combined stream function is

$$\psi = \psi_{stream} + \psi_{vortex} = U_\infty r\sin\theta - K\ln r$$

The velocity components of this flow are given by

$$v_r = \frac{1}{r}\frac{\partial\psi}{\partial\theta} = U_\infty\cos\theta \qquad v_\theta = -\frac{\partial\psi}{\partial r} = -U_\infty\sin\theta + \frac{K}{r}$$

Setting v_r and $v_\theta = 0$, we find the stagnation point at $\theta = 90^\circ$, $r = a = K/U_\infty$ or (x,y) = (0,a).



ketabline.com Ebook.ketabline.com

An Infinite Row of Vortices

Consider an infinite row of vortices of equal strength K and equal spacing a. A single vortex, i , has a stream function given by

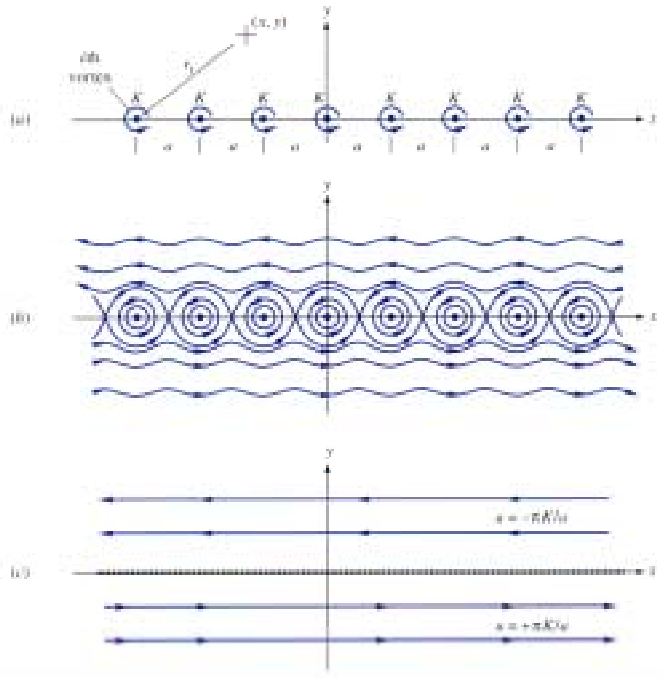


Fig. 8.7 Superposition of vortices

$$\psi_i = -K \sum_{i=1}^{\infty} \ln r_i$$

This infinite sum can also be expressed as

$$\psi = -\frac{1}{2} K \ln\left[\frac{1}{2}\left(\cosh\frac{2\pi y}{a} - \cosh\frac{2\pi x}{a}\right)\right]$$

The resulting left and right flow above and below the row of vortices is given by

$$u = \left.\frac{\partial \psi}{\partial y}\right|_{|y|>a} = \pm\frac{\pi K}{a}$$



ketabline.com Ebook.ketabline.com

Plane flow past Closed-Body Shapes

Various types of external flows over a closed-body can be constructed by superimposing a uniform stream with sources, sinks, and vortices.

Key Point: The body shape will be closed only if the net source of the outflow equals the net sink inflow.

Two examples of this are presented below.

The Rankine Oval

A Rankine Oval is a cylindrical shape which is long compared to its height. It is formed by a source-sink pair aligned parallel to a uniform stream.

The individual flows used to produce the final result and the combined flow field are shown in Fig. 8.9. The combined stream function is given by

$$\psi = U_\infty y - m\tan^{-1}\frac{2ay}{x^2+y^2-a^2}$$

or

$$\psi = U_\infty r\sin\theta + m(\theta_1 - \theta_2)$$

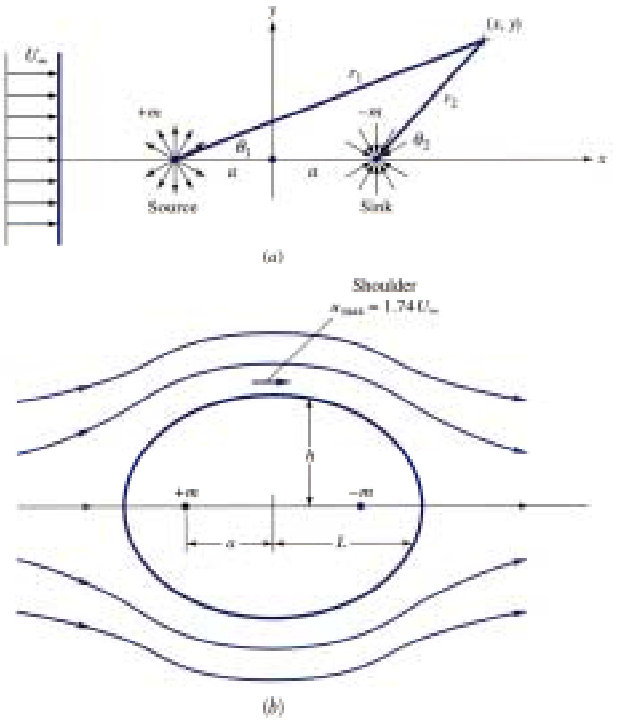


Fig. 8.9 The Rankine Oval

The oval shaped closed body is the streamline, $\psi = 0$. Stagnation points occur at the front and rear of the oval, $x = \pm L, y = 0$. Points of maximum velocity and minimum pressure occur at the shoulders, $x = 0, y = \pm h$. Key geometric and flow parameters of the Rankine Oval can be expressed as follows:



ketabline.com Ebook.ketabline.com

$$\frac{h}{a} = \cot\frac{h/a}{2m/(U_\infty a)} \qquad \frac{L}{a} = \left(1 + \frac{2m}{U_\infty a}\right)^{1/2}$$

$$\frac{u_{max}}{U_\infty} = 1 + \frac{2m/(U_\infty a)}{1 + h^2/a^2}$$

As the value of the parameter $m/(U_\infty a)$ is increased from zero, the oval shape increases in size and transforms from a flat plate to a circular cylinder at the limiting case of $m/(U_\infty a) = \infty$.

Specific values of these parameters are presented in Table 8.1 for four different values of the dimensionless vortex strength, $K/(U_\infty a)$.

Table 8.1 Rankine-Oval Parameters

$m/(U_\infty a)$	h/a	L/a	L/h	u_{max}/U_∞
0.0	0.0	1.0	∞	1.0
0.01	0.31	1.10	32.79	1.020
0.1	0.263	1.095	4.169	1.187
1.0	1.307	1.732	1.326	1.739
10.0	4.435	4.458	1.033	1.968
10.0	14.130	14.177	1.003	1.997
∞	∞	∞	1.000	2.000

Flow Past a Circular Cylinder with Circulation

It is seen from Table 8.1 that as source strength m becomes large, the Rankine Oval becomes a large circle, much greater in diameter than the source-sink spacing 2a. Viewed, from the scale of the cylinder, this is equivalent to a uniform stream plus a doublet. To add circulation, without changing the shape of the cylinder, we place a vortex at the doublet center. For these conditions the stream function is given by



ketabline.com Ebook.ketabline.com

$$\psi = U_\infty \sin\theta\left(r - \frac{a^2}{r}\right) - K \ln\frac{r}{a}$$

Typical resulting flows are shown in Fig. 8.10 for increasing values of non-dimensional vortex strength $K / U_\infty a$.

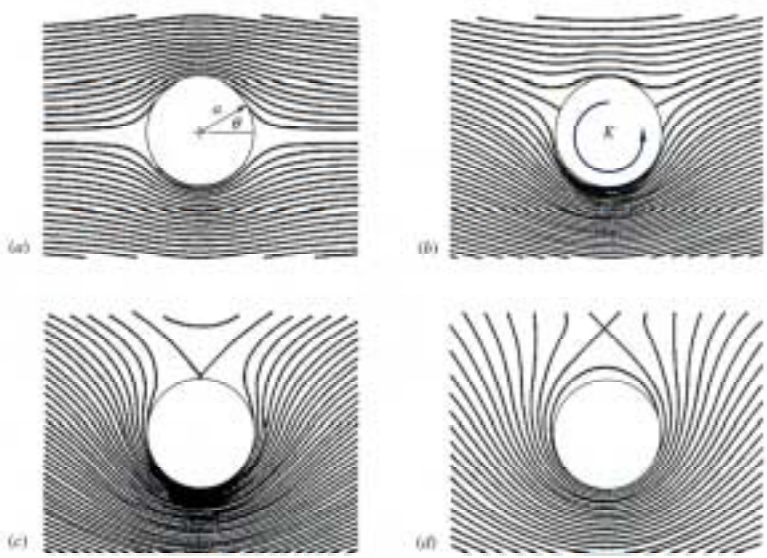


Fig. 8.10 Flow past a cylinder with circulation for values of $K / U_\infty a$ of (a) 0, (b) 1.0, (c) 2.0, and (d) 3.0

Again the streamline $\psi = 0$ is corresponds to the circle r = a. As the counter-clockwise circulation $\Gamma = 2\pi K$ increases, velocities below the cylinder increase and velocities above the cylinder decrease. In polar coordinates, the velocity components are given by

$$v_r = \frac{1}{r}\frac{\partial\psi}{\partial\theta} = U_\infty \cos\theta\left(1 - \frac{a^2}{r^2}\right)$$

$$v_\theta = -\frac{\partial\psi}{\partial r} = -U_\infty \sin\theta\left(1 + \frac{a^2}{r^2}\right) + \frac{K}{r}$$

For small K, two stagnation points appear on the surface at angles θ_s or for which



ketabline.com Ebook.ketabline.com

$$\sin\theta_s = \frac{K}{2U_\infty a}$$

Thus for K = 0, θ_s = 0 and 180°. For $K/U_\infty a = 1$, θ_s = 30 and 150° . Figure 8.10c is the limiting case for which with $K/U_\infty a = 2$, $\theta_s = 90°$ and the two stagnation points meet at the top of the cylinder.

The Kutta-Joukowski Lift Theorem

The development in the text shows that from inviscid flow theory,

> The lift per unit depth of any cylinder of any shape immersed in a uniform stream equals to $\rho U_\infty \Gamma$ where Γ is the total net circulation contained within the body shape. The direction of the lift is 90o from the stream direction, rotating opposite to the circulation.

This is the well known Kutta-Joukowski lift theorem.



ketabline.com Ebook.ketabline.com

IX. Compressible Flow

Compressible flow is the study of fluids flowing at speeds comparable to the local speed of sound. This occurs when fluid speeds are about 30% or more of the local acoustic velocity. Then, the fluid density no longer remains constant throughout the flow field. This typically does not occur with fluids but can easily occur in flowing gases.

Two important and distinctive effects that occur in compressible flows are (1) *choking* where the flow is limited by the sonic condition that occurs when the flow velocity becomes equal to the local acoustic velocity and (2) *shock waves* that introduce discontinuities in the fluid properties and are highly irreversible.

Since the density of the fluid is no longer constant in compressible flows, there are now four dependent variables to be determined throughout the flow field. These are pressure, temperature, density, and flow velocity. Two new variables, temperature and density, have been introduced and two additional equations are required for a complete solution. These are the *energy equation* and the fluid *equation of state*. These must be solved simultaneously with the *continuity* and *momentum* equations to determine all the flow field variables.

Equations of State and Ideal Gas Properties:

Two equations of state are used to analyze compressible flows: the *ideal gas* equation of state and the *isentropic flow* equation of state. The first of these describe gases at low pressure (relative to the gas critical pressure) and high temperature (relative to the gas critical temperature). The second applies to ideal gases experiencing isentropic (adiabatic and frictionless) flow.

The ideal gas equation of state is

$$\rho = \frac{P}{R\,T}$$

In this equation, R is the gas constant, and P and T are the absolute pressure and absolute temperature respectively. Air is the most commonly incurred compressible flow gas and its gas constant is R_{air} = 1717 $ft^2/(s^2\text{-}^oR)$ = 287 $m^2/(s^2\text{-}K)$.



ketabline.com Ebook.ketabline.com

Two additional useful ideal gas properties are the constant volume and constant pressure specific heats defined as

$$C_v = \frac{du}{dT} \quad and \quad C_p = \frac{dh}{dT}$$

where u is the specific internal energy and h is the specific enthalpy. These two properties are treated as constants when analyzing elemental compressible flows. Commonly used values of the specific heats of air are: c_v = 4293 ft^2/(s^2-^{o}R) = 718 m^2/(s^2-K) and c_p = 6010 ft^2/(s^2-^{o}R) = 1005 m^2/(s^2-K). Additional specific heat relationships are

$$R = C_p - C_v \quad and \quad k = \frac{C_p}{C_v}$$

The *specific heat ratio k* for air is 1.4.

When undergoing an isentropic process (constant entropy process), ideal gases obey the isentropic process equation of state:

$$\frac{P}{\rho^k} = \text{constant}$$

Combining this equation of state with the ideal gas equation of state and applying the result to two different locations in a compressible flow field yields

$$\frac{P_2}{P_1} = \left(\frac{T_2}{T_1}\right)^{k/(k-1)} = \left(\frac{\rho_2}{\rho_1}\right)^k$$

Note: The above equations may be applied to any ideal gas as it undergoes an isentropic process.

Acoustic Velocity and Mach Number

The *acoustic velocity* (speed of sound) is the speed at which an infinitesimally small pressure wave (sound wave) propagates through a fluid. In general, the acoustic velocity is given by



ketabline.com Ebook.ketabline.com

$$a^2 = \frac{\partial P}{\partial \rho}$$

The process experienced by the fluid as a sound wave passes through it is an isentropic process. The speed of sound in an ideal gas is then given by

$$a = \sqrt{k\,RT}$$

The *Mach number* is the ratio of the fluid velocity and speed of sound,

$$Ma = \frac{V}{a}$$

This number is the single most important parameter in understanding and analyzing compressible flows.

Mach Number Example:

An aircraft flies at a speed of 400 m/s. What is this aircraft's Mach number when flying at standard sea-level conditions (T = 289 K) and at standard 15,200 m (T = 217 K) atmosphere conditions?

At standard sea-level conditions, $a = \sqrt{k\,RT} = \sqrt{(1.4)(287)(289)} = 341\,m/s$ and at 15,200 m, $a = \sqrt{(1.4)(287)(217)} = 295\,m/s$. The aircraft Mach numbers are then

$$sea-level: \quad Ma = \frac{V}{a} = \frac{400}{341} = 1.17$$

$$15{,}200\ m: \quad Ma = \frac{V}{a} = \frac{400}{295} = 1.36$$

Note: Although the aircraft speed did not change, the Mach number did change because of the change in the local speed of sound.



ketabline.com Ebook.ketabline.com

Ideal Gas Steady Isentropic Flow

When the flow of an ideal gas is such that there is no heat transfer (i.e., adiabatic) or irreversible effects (e.g., friction, etc.), the flow is isentropic. The steady-flow energy equation applied between two points in the flow field becomes

$$h_1 + \frac{V_1^2}{2} = h_2 + \frac{V_2^2}{2} = h_o = \text{constant}$$

where h_0 is called the *stagnation enthalpy* that remains constant throughout the flow field. Observe that the stagnation enthalpy is the enthalpy at any point in an isentropic flow field where the fluid velocity is zero or very nearly so.

The enthalpy of an ideal gas is given by $h = C_p T$ over reasonable ranges of temperature. When this is substituted into the adiabatic, steady-flow energy equation, we see that $h_o = C_p T_o = \text{constant}$ and

$$\frac{T_o}{T} = 1 + \frac{k-1}{2} Ma^2$$

Thus, the stagnation temperature T_o remains constant throughout an isentropic or adiabatic flow field and the relationship of the local temperature to the field stagnation temperature only depends upon the local Mach number.

Incorporation of the acoustic velocity equation and the ideal gas equations of state into the energy equation yields the following useful results for steady isentropic flow of ideal gases.

$$\frac{T_o}{T} = 1 + \frac{k-1}{2} Ma^2$$

$$\frac{a_o}{a} = \left(\frac{T_o}{T}\right)^{1/2} = \left(1 + \frac{k-1}{2} Ma^2\right)^{1/2}$$

$$\frac{P_o}{P} = \left(\frac{T_o}{T}\right)^{k/(k-1)} = \left(1 + \frac{k-1}{2} Ma^2\right)^{k/(k-1)}$$

$$\frac{\rho_o}{\rho} = \left(\frac{T_o}{T}\right)^{1/(k-1)} = \left(1 + \frac{k-1}{2} Ma^2\right)^{1/(k-1)}$$



ketabline.com Ebook.ketabline.com

The values of the ideal gas properties when the Mach number is 1 (i.e., sonic flow) are known as the *critical or sonic properties* and are given by

$$\frac{T_o}{T^*} = 1 + \frac{k-1}{2}$$

$$\frac{a_o}{a^*} = \left(\frac{T_o}{T^*}\right)^{1/2} = \left(1 + \frac{k-1}{2}\right)^{1/2}$$

$$\frac{P_o}{P^*} = \left(\frac{T_o}{T^*}\right)^{k/(k-1)} = \left(1 + \frac{k-1}{2}\right)^{k/(k-1)}$$

$$\frac{\rho_o}{\rho^*} = \left(\frac{T_o}{T^*}\right)^{1/(k-1)} = \left(1 + \frac{k-1}{2}\right)^{1/(k-1)}$$

given by

Isentropic Flow Example:

Air flowing through an adiabatic, frictionless duct is supplied from a large supply tank in which P = 500 kPa and T = 400 K. What are the Mach number Ma. the temperature T, density _, and fluid V at a location in this duct where the pressure is 430 kPa?

The pressure and temperature in the supply tank are the stagnation pressure and temperature since the velocity in this tank is practically zero. Then, the Mach number at this location is

$$Ma = \sqrt{\frac{2}{k-1}\left[\left(\frac{P_o}{P}\right)^{(k-1)/k} - 1\right]}$$

$$Ma = \sqrt{\frac{2}{0.4}\left[\left(\frac{500}{430}\right)^{0.4/1.4} - 1\right]}$$

$$Ma = 0.469$$

and the temperature is given by



ketabline.com Ebook.ketabline.com

$$T = \frac{T_o}{1 + \frac{k-1}{2} Ma^2}$$

$$T = \frac{400}{1 + 0.2(0.469)^2}$$

$$T = 383\,K$$

The ideal gas equation of state is used to determine the density,

$$\rho = \frac{P}{R\,T} = \frac{430{,}000}{(287)(383)} = 3.91\,kg/m^3$$

Using the definition of the Mach number and the acoustic velocity,

$$V = Ma\sqrt{k\,RT} = 0.469\sqrt{(1.4)(287)(383)} = 184\,m/s$$

Solving Compressible Flow Problems

Compressible flow problems come in a variety of forms, but the majority of them can be solved by

1. Use the appropriate equations and reference states (i.e., stagnation and sonic states) to determine the Mach number at all the flow field locations involved in the problem.
2. Determine which conditions are the same throughout the flow field (e.g., the stagnation properties are the same throughout an isentropic flow field).
3. Apply the appropriate equations and constant conditions to determine the necessary remaining properties in the flow field.
4. Apply additional relations (i.e., equation of state, acoustic velocity, etc.) to complete the solution of the problem.

Most compressible flow equations are expressed in terms of the Mach number. You can solve these equations explicitly by rearranging the equation, by using tables, or by programming them with spreadsheet or EES software.



ketabline.com Ebook.ketabline.com

Isentropic Flow with Area Changes

All flows must satisfy the continuity and momentum relations as well as the energy and state equations. Application of the continuity and momentum equations to a differential flow (see textbook for derivation) yields:

$$\frac{dV}{V} = \frac{1}{Ma^2 - 1}\frac{dA}{A}$$

This result reveals that when $Ma < 1$ (subsonic flow) velocity changes are the opposite of area changes. That is, increases in the fluid velocity require that the area decrease in the direction of the flow. For supersonic flow ($Ma > 1$), the area must increase in the direction of the flow to cause an increase in the velocity. Changes in the fluid velocity dV can only be finite in sonic flows ($Ma = 1$) when $dA = 0$. The effect of the geometry upon velocity, Mach number, and pressure is illustrated in Figure 1 below.

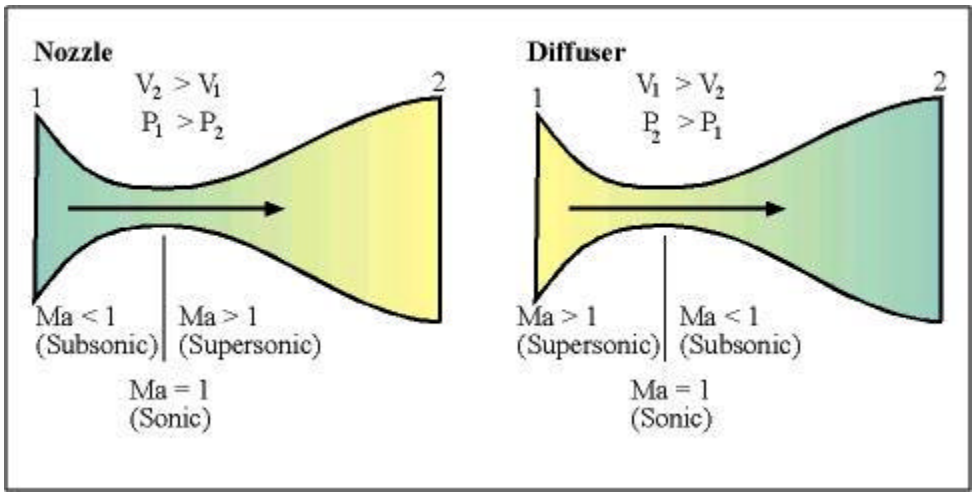


Figure 1

Combining the mass flow rate equation $\dot{m} = \rho A V = \text{constant}$ with the preceding isentropic flow equations yields

$$\frac{\rho^*}{\rho} = \left[\frac{2}{k+1}\left(1 + \frac{k-1}{2}Ma^2\right)\right]^{1/(k-1)}$$

ketabline.com Ebook.ketabline.com

$$\frac{V^*}{V} = \frac{1}{Ma}\left[\frac{2}{k+1}\left(1+\frac{k-1}{2}Ma^2\right)\right]^{1/2}$$

$$\frac{A}{A^*} = \frac{1}{Ma}\left[\frac{1+0.5(k-1)Ma^2}{0.5(k+1)}\right]^{(k+1)/[2(k-1)]}$$

where the sonic state (denoted with *) may or may not occur in the duct. If the sonic condition does occur in the duct, it will occur at the duct minimum or maximum area. If the sonic condition occurs, the flow is said to be choked since the mass flow rate $\dot{m} = \rho A V = \rho^* A^* V^*$ is the maximum mass flow rate the duct can accommodate without a modification of the duct geometry.

Review Example 9.4 of the textbook.

Normal Shock Waves

Under the appropriate conditions, very thin, highly irreversible discontinuities can occur in otherwise isentropic compressible flows. These discontinuities are known as *shock waves* which when they are perpendicular to the flow velocity vector are called *normal shock waves*. A normal shock wave in a one-dimensional flow channel is illustrated in Figure 2.

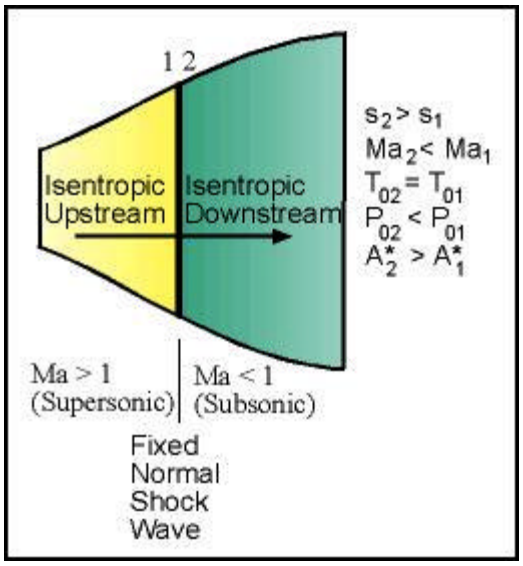


Figure 2

ketabline.com Ebook.ketabline.com

Application of the second law of thermodynamics to the thin, adiabatic normal shock wave reveals that normal shock waves can only cause a sharp rise in the gas pressure and must be supersonic upstream and subsonic downstream of the normal shock. *Rarefaction waves* that result in a decrease in pressure and increase in Mach number are impossible according to the second law.

Application of the conservation of mass, momentum, and energy equations along with the ideal gas equation of state to a thin, adiabatic control volume surrounding a normal shock wave yields the following results.

$$Ma_2^2 = \frac{(k-1)Ma_1^2 + 2}{2k\,Ma_1^2 - (k-1)}, \quad Ma_1 > 1$$

$$\frac{P_2}{P_1} = \frac{1 + k\,Ma_1^2}{1 + k\,Ma_2^2}$$

$$\frac{\rho_2}{\rho_1} = \frac{V_1}{V_2} = \frac{(k+1)\,Ma_1^2}{(k-1)\,Ma_1^2 + 2}$$

$$T_{o1} = T_{o2}$$

$$\frac{T_2}{T_1} = \left[2 + (k-1)Ma_1^2\right]\frac{2k\,Ma_1^2 - (k-1)}{(k+1)^2 Ma_1^2}$$

$$\frac{P_{o2}}{P_{o1}} = \frac{\rho_{o2}}{\rho_{o1}} = \left[\frac{(k+1)\,Ma_1^2}{2 + (k-1)\,Ma_1^2}\right]^{k/(k-1)}\left[\frac{k+1}{2k\,Ma_1^2 - (k-1)}\right]^{1/(k-1)}$$

$$\frac{A_2^*}{A_1^*} = \frac{Ma_2}{Ma_1}\left[\frac{2 + (k-1)\,Ma_1^2}{2 + (k-1)\,Ma_2^2}\right]^{(k+1)/[2(k-1)]}$$

When using these equations to relate conditions upstream and downstream of a normal shock wave, keep the following points in mind:

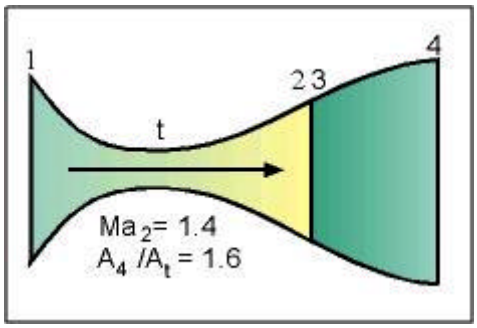


ketabline.com Ebook.ketabline.com

1. Upstream Mach numbers are always supersonic while downstream Mach numbers are subsonic.
2. Stagnation pressures and densities decrease as one moves downstream across a normal shock wave while the stagnation temperature remains constant.
3. Pressures increase greatly while temperature and density increase moderately across a shock wave in the downstream direction.
4. The effective throat area increases across a normal shock wave in the downstream direction.
5. Shock waves are very irreversible causing the specific entropy downstream of the shock wave to be greater than the specific entropy upstream of the shock wave.

Moving normal shock waves such as those caused by explosions, spacecraft reentering the atmosphere, and others can be analyzed as stationary normal shock waves by using a frame of reference that moves at the speed of the shock wave in the direction of the shock wave.

Converging-Diverging Nozzle Example: **Also see Example 9.6 of textbook**



Air is supplied to the converging-diverging nozzle shown here from a large tank where P = 2 Mpa and T = 400 K. A normal shock wave in the diverging section of this nozzle forms at a point $P_{o1} = P_{o2} = 2\,MPa$ where the upstream Mach number is 1.4. The ratio of the nozzle exit area to the throat area is 1.6. Determine (a) the Mach number downstream of the shock wave, (b) the Mach number at the nozzle exit, (c) the pressure at the nozzle exit, and (d) the temperature at the nozzle exit.

This flow is isentropic from the supply tank (1) to just upstream of the normal shock (2) and also from just downstream of the shock (3) to the exit (4). Stagnation temperatures do not change in isentropic flows or across shock waves, $T_{o1} = T_{o2} = T_{o3} = T_{o4} = 400\,K$. Stagnation pressures do not change in isentropic flows, $P_{o1} = P_{o2} = 2\,MPa$ and $P_{o3} = P_{o4}$, but stagnation pressures change across shocks, $P_{o2} > P_{o3}$.



ketabline.com Ebook.ketabline.com

Based upon the Mach number at 2 and the isentropic relations,

$$\frac{A_2}{A_t} = \frac{A_3}{A_t} = \frac{A_2}{A_t^*} = \frac{1}{Ma_2}\frac{\left(1+0.2\,Ma_2^2\right)^3}{1.728} = 1.115$$

The normal shock relations can be used to work across the shock itself. The answer to (a) is then:

$$Ma_3 = \left[\frac{(k-1)Ma_2^2+2}{2k\,Ma_2^2-(k-1)}\right]^{1/2} = \left[\frac{(0.4)(1.4)^2+2}{2(1.4)(1.4)^2-0.4}\right]^{1/2} = 0.740$$

Continuing to work across the shock,

$$P_{o4} = P_{o3} = P_{o2}\left[\frac{(k+1)Ma_2^2}{2+(k-1)Ma_2^2}\right]^{k/(k-1)}\left[\frac{k+1}{2k\,Ma_2^2-(k-1)}\right]^{1/(k-1)}$$

$$P_{o4} = P_{o3} = 2\left[\frac{(2.4)(0.74)^2}{2+(0.4)(0.74)^2}\right]^{3.5}\left[\frac{2.4}{2(1.4)(0.74)^2-0.4}\right]^{2.5} = 1.92\,MPa$$

$$\frac{A_3^*}{A_2^*} = \frac{Ma_3}{Ma_2}\left[\frac{2+(k-1)Ma_2^2}{2+(k-1)Ma_3^2}\right]^{(k+1)/[2(k-1)]} = 1.044$$

Now, we know A_4/A_t, and the flow is again isentropic between states 3 and 4. Writing an expression for the area ratio between the exit and the throat, we have

$$\frac{A_4}{A_t} = 1.6 = \frac{A_4}{A_4^*}\frac{A_4^*}{A_3^*}\frac{A_3^*}{A_2^*}\frac{A_2^*}{A_t} = \frac{A_4}{A_4^*}(1)(1.044)(1.115)$$

Solving for $\frac{A_4}{A_4^*}$ we obtain $\frac{A_4}{A_4^*} = 1.374$

Using a previously developed equation for choked, isentropic flow, we can write



ketabline.com Ebook.ketabline.com

$$\frac{A_4}{A_4^*} = 1.374 = \frac{1}{Ma}\left[\frac{1+0.5(k-1)Ma^2}{0.5(k+1)}\right]^{(k+1)/[2(k-1)]}$$

or

$$1.374 = \frac{1}{Ma_4}\frac{\left(1+0.2Ma_4^2\right)^3}{1.728}$$

The solution of this equation gives answer (b) $Ma_4 = 0.483$.

Now that the Mach number at 4 is known, we can proceed to apply the isentropic relations to obtain answers (c) and (d).

$$P_4 = \frac{P_{o4}}{\left[1+0.5(k-1)Ma_4^2\right]^{k/(k-1)}} = \frac{1.92\,MPa}{\left[1+0.2(0.483)^2\right]^{3.5}} = 1.637\,MPa$$

$$T_4 = \frac{T_{o4}}{1+0.5(k-1)Ma_4^2} = \frac{400\,K}{1+0.2(0.483)^2} = 382\,K$$

Note: Observe how the sonic area downstream from the shock is not the same as upstream of the shock. Also, observe the use of the area ratios to determine the Mach number at the nozzle exit.

The following steps can be used to solve most one-dimensional compressible flow problems.

1. Clearly identify the flow conditions:e.g., isentropic flow, constant stagnation temperature, constant stagnation pressure, etc.
2. Use the flow condition relationships, tables, or software to determine the Mach number at major locations in the flow field.
3. Once the Mach number is known at the principal flow locations, one can proceed to use the flow relations, tables, or software to determine other flow properties such as fluid velocity, pressure, and temperature. This may require the reduction of property ratios to the product of several ratios, as was done with the area ratio in the above example to obtain the answer.



ketabline.com Ebook.ketabline.com

Operation of Converging-Diverging Nozzles

A converging-diverging nozzle like that shown in Figure 3 can operate in several different modes depending upon the ratio of the discharge and supply pressure P_d/P_s. These modes of operation are illustrated on the pressure ratio – axial position diagram of Figure 3.

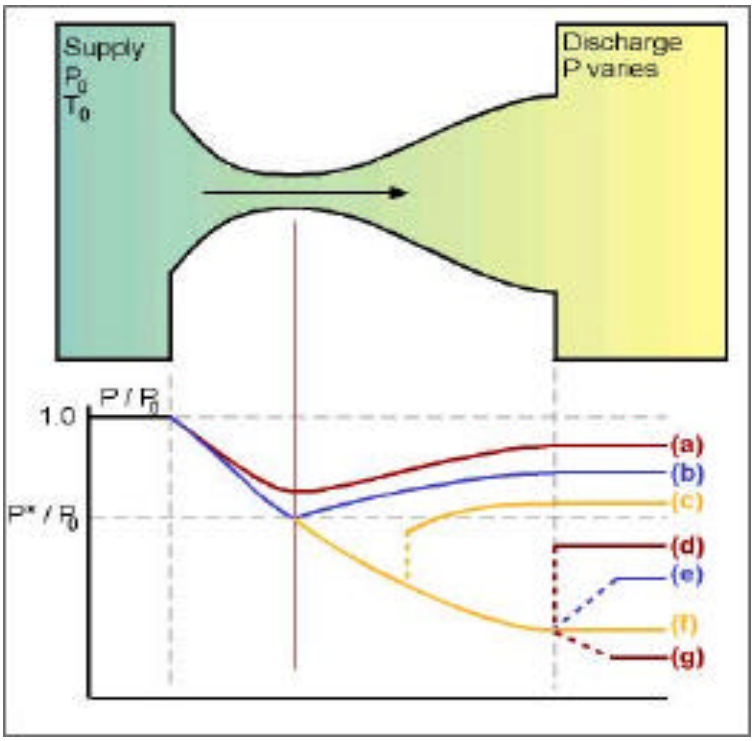
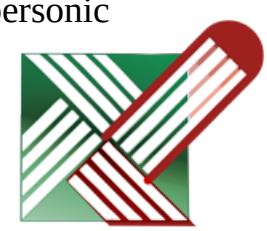


Figure 3

Mode (a) The flow is subsonic throughout the nozzle, supply, and discharge chambers. Without friction, this flow is also isentropic and the isentropic flow equations may be used throughout the nozzle.

Mode (b) The flow is still subsonic and isentropic throughout the nozzle and chambers. The Mach number at the nozzle throat is now unity. At the throat, the flow is sonic, the throat is choked, and the mass flow rate through the nozzle has reached its upper limit. Further reductions in the discharge tank pressure will not increase the mass flow rate any further.

Mode (c) A shock wave has now formed in the diverging section of the nozzle. The flow is subsonic before the throat, same as mode (b), the throat is choked, same as mode (b), and the flow is supersonic



ketabline.com Ebook.ketabline.com

and accelerating between the throat and just upstream of the shock. The flow is isentropic between the supply tank and just upstream of the shock. The flow downstream of the shock is subsonic and decelerating. The flow is also isentropic downstream of the shock to the discharge tank. The flow is not isentropic across the shock. Isentropic flow methods can be applied upstream and downstream of the shock while normal shock methods are used to relate conditions upstream to those downstream of the shock.

Mode (d) The normal shock is now located at the nozzle exit. Isentropic flow now exists throughout the nozzle. The flow at the nozzle exit is subsonic and adjusts to flow conditions in the discharge tank, not the nozzle. Isentropic flow methods can be applied throughout the nozzle.

Mode (e) A series of two-dimensional shocks are established in the discharge tank downstream of the nozzle. These shocks serve to decelerate the flow. The flow is isentropic throughout the nozzle, same as mode (d).

Mode (f) The pressure in the discharge tank equals the pressure predicted by the supersonic solution of the nozzle isentropic flow equations. The pressure ratio is known as the supersonic design pressure ratio. Flow is isentropic everywhere in the nozzle, same as mode (d) and (e), and in the discharge tank.

Mode (g) A series of two-dimensional shocks are established in the discharge tank downstream of the nozzle. These shocks serve to decelerate the flow. The flow is isentropic throughout the nozzle, same as modes (d), (e), and (f).

Review Example 9.9 of the textbook.



ketabline.com Ebook.ketabline.com

Adiabatic, Constant Duct Area Compressible Flow with Friction

When compressible fluids flow through insulated, constant-area ducts, they are subject to Moody-like pipe-friction which can be described by an average Darcy-Weisbach friction factor $\bar{f}$. Application of the conservation of mass, momentum, and energy principles as well as the ideal gas equation of state yields the following set of working equations.

$$\frac{\bar{f}\,L^*}{D} = \frac{1-Ma^2}{k\,Ma^2} + \frac{k+1}{2k}\ln\frac{(k+1)Ma^2}{2+(k-1)Ma^2}$$

$$\frac{P}{P^*} = \frac{1}{Ma}\left[\frac{(k+1)}{2+(k-1)Ma^2}\right]^{1/2}$$

$$\frac{\rho}{\rho^*} = \frac{V^*}{V} = \frac{1}{Ma}\left[\frac{2+(k-1)Ma^2}{k+1}\right]^{1/2}$$

$$\frac{T}{T^*} = \frac{a}{a^{*2}} = \frac{(k+1)}{2+(k-1)Ma^2}$$

$$\frac{P}{P_o^*} = \frac{\rho_o}{\rho_o^*} = \frac{1}{Ma}\left[\frac{2+(k-1)Ma^2}{k+1}\right]^{(k+1)/[2(k-1)]}$$

where the asterisk state is the sonic state at which the flow Mach number is one. This state is the same throughout the duct and may be used to relate conditions at one location in the duct to those at another location. The length of the duct enters these calculations by

$$\frac{\bar{f}\,\Delta L}{D} = \left(\frac{\bar{f}\,L^*}{D}\right)_1 - \left(\frac{\bar{f}\,L^*}{D}\right)_2$$

Thus, given the length ΔL of the duct and the Mach number at the duct entrance or exit, the Mach number at the other end (or location) of the duct can be determined.



ketabline.com Ebook.ketabline.com

Compressible Flow with Friction Example:

Air enters a 0.01-m-diameter duct ($\bar{f} = 0.05$) with *Ma* = 0.05. The pressure and temperature at the duct inlet are 1.5 MPa and 400 K. What are the (a) Mach number, (b) pressure, and (c) temperature in the duct 50 m from the entrance?

At the duct entrance, with $\bar{f} = 0.05$, D = 0.01 m, and Ma = 0.05, we obtain

$$\left(\frac{\bar{f}L^*}{D}\right)_1 = \left[\frac{1-Ma^2}{k\,Ma^2} + \frac{k+1}{2k}\ln\frac{(k+1)\,Ma^2}{2+(k-1)\,Ma^2}\right]$$

$$\left(\frac{\bar{f}L^*}{D}\right)_1 = \left[\frac{1-0.05^2}{1.4\,(0.05)^2} + \frac{2.4}{2.8}\ln\frac{(2.4)\,0.05^2}{2+(0.4)\,0.05^2}\right] = 280$$

Then, at the duct exit we obtain

$$\left(\frac{\bar{f}L^*}{D}\right)_2 = \left(\frac{\bar{f}L^*}{D}\right)_1 - \frac{\bar{f}\,\Delta L}{D} = 280 - \frac{(0.05)\,50}{0.01} = 30$$

We can not write for the duct exit that

$$\left(\frac{\bar{f}L^*}{D}\right)_2 = 30 = \left[\frac{1-Ma^2}{k\,Ma^2} + \frac{k+1}{2k}\ln\frac{(k+1)\,Ma^2}{2+(k-1)\,Ma^2}\right]_2$$

or

$$30 = \frac{1-Ma_2^2}{1.4\,Ma_2^2} + \frac{2.4}{2.8}\ln\frac{2.4\,Ma_2^2}{2+0.4\,Ma_2^2}$$

The solution of the second of these equations gives answer (a) $Ma_2 = 0.145$. Writing the following expression for pressure ratios yields for (b),

$$P_2 = P_1\,\frac{P_2}{P_2^*}\,\frac{P_2^*}{P_1^*}\,\frac{P_1^*}{P_1}$$



ketabline.com Ebook.ketabline.com

$$P_2 = (1.5)\frac{1}{Ma_2}\left[\frac{(k+1)}{2+(k-1)Ma_2^2}\right]^{1/2}(1)\frac{Ma_1}{1}\left[\frac{2+(k-1)Ma_1^2}{k+1}\right]^{1/2}$$

$$P_2 = (1.5)\frac{1}{0.145}\left[\frac{2.4}{2+(0.4)0.145^2}\right]^{1/2}(1)\frac{0.05}{1}\left[\frac{2+(0.4)0.05^2}{2.4}\right]^{1/2} = 0.516$$

Application of the temperature ratios yields answer (c),

$$T_2 = T_1\frac{T_1^*}{T_1}\frac{T_2^*}{T_1^*}\frac{T_2}{T_2^*} = 400\frac{2+(k-1)Ma_1^2}{2+(k-1)Ma_2^2} = 400\frac{2+(0.4)0.05^2}{2+(0.4)0.145^2} = 399$$

This example demonstrates what happens when the flow at the inlet to the duct is subsonic, the Mach number increases as the duct gets longer. When the inlet flow is supersonic, the Mach number decreases as the duct gets longer. A plot of the specific entropy of the fluid as a function of the duct Mach number (length) is presented in Figure 4 for both subsonic and supersonic flow.

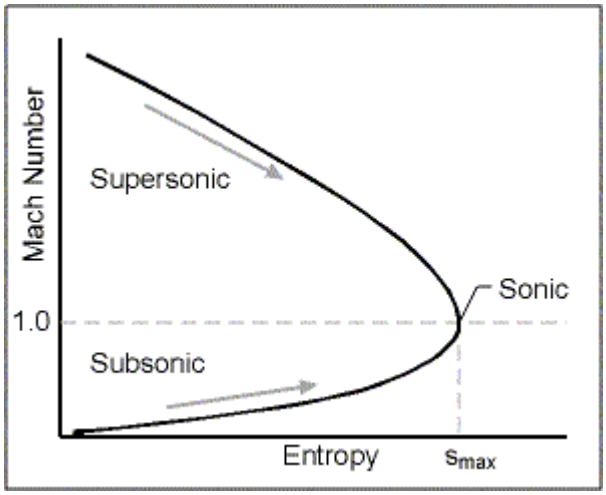


Figure 4

These results clearly illustrate that the Mach number in the duct approaches unity as the length of the duct is increased. Once the sonic condition exists at the duct exit, the flow becomes choked. This figure also demonstrates that the flow can never proceed from subsonic to supersonic (or supersonic to subsonic) flow, as this would result in a violation of the second law of thermodynamics.



ketabline.com Ebook.ketabline.com

Other compressible flows in constant area ducts such as isothermal flow with friction and frictionless flow with heat addition may be analyzed in a similar manner using the equations appropriate to each flow. Many of these flows also demonstrate choking behavior.

Oblique Shock Waves

Bodies moving through a compressible fluid at speeds exceeding the speed of sound create a shock system shaped like a cone. The half-angle of this *shock cone* is given by

$$\mu = \sin^{-1}\frac{1}{Ma}$$

This angle is known as the *Mach angle*. The interior of the shock cone is called the *zone of action*. Inside the zone of action, it is possible to hear any sounds produced by the moving body. Outside the Mach cone, in what is known as the *zone of silence*, sounds produced by the moving body cannot be heard.

An oblique shock wave at angle β with respect to the approaching compressible fluid whose Mach number is supersonic is shown in Figure 5. Observe that the streamlines (parallel to the velocity vector) have been turned by the deflection angle θ by passing through the oblique shock wave.

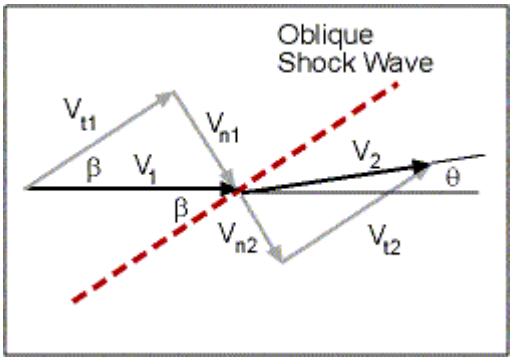


Figure 5

ketabline.com Ebook.ketabline.com

This flow is readily analyzed by considering the normal velocity components $V_{n1} = V_1 \sin\beta$ *and* $V_{n2} = V_2 \sin(\beta - \theta)$ and the tangential components V_{t1} *and* V_{t2}. Application of the momentum principle in the tangential direction (along which there are no pressure changes) verifies that

$$V_{t1} = V_{t2}$$

By defining the normal Mach numbers as

$$Ma_{n1} = \frac{V_{n1}}{a_1} = Ma_1 \sin\beta \quad and \quad Ma_{n2} = \frac{V_{n2}}{a_2} = Ma_2 \sin(\beta - \theta)$$

The simultaneous solution of the conservation of mass, momentum, and energy equations in the normal direction along with the ideal gas equation of state are the same as those of the normal shock wave with Ma_1 replaced with Ma_{n1} and Ma_2 replaced with Ma_{n2}. In this way, all the results developed in the normal shock wave section can be applied to two-dimensional oblique shock waves.

Oblique Shock Example:

A two-dimensional shock wave is created at the leading edge of an aircraft flying at *Ma* = 1.6 through air at 70 kPa, 300 K. If this oblique shock forms a 55° angle with respect to the approaching air, what is (a) the Mach number of the flow after the oblique shock (this is not the normal Mach number) and (b) the streamline deflection angle θ?

The velocity of the fluid upstream of the oblique shock wave is

$$V_1 = Ma_1 a_1 = Ma_1 \sqrt{k R T} = 1.6\sqrt{(1.4)(287)(300)} = 556\, m/s$$

whose components are

$$V_{n1} = V_1 \sin\beta = 556 \sin 55 = 455\, m/s$$

$$V_{t1} = V_{t2} = V_1 \cos\beta = 556 \cos 55 = 319\, m/s$$



ketabline.com Ebook.ketabline.com

The upstream normal Mach number is then

$$Ma_{n1} = Ma_1 \sin\beta = 1.6 \sin 54° = 1.311$$

and the downstream normal Mach number is

$$Ma_{n2} = \left[\frac{(k-1)Ma_{n1}^2 + 2}{2k\,Ma_{n1}^2 - (k-1)}\right]^{1/2} = \left[\frac{(0.4)(1.311)^2 + 2}{2(1.4)(1.311)^2 - 0.4}\right]^{1/2} = 0.780$$

and the downstream temperature is

$$T_2 = T_1\left[(k-1)Ma_{n1}^2 + 2\right]\frac{2\,k\,Ma_{n1}^2 - (k-1)}{(k+1)^2\,Ma_{n1}^2}$$

$$T_2 = 300\left[(0.4)1.311^2 + 2\right]\frac{2(1.4)1.311^2 - 0.4}{(2.4)^2 1.311^2} = 359\,K$$

Now, the downstream normal velocity is

$$V_{n2} = Ma_{n2}\,a_2 = Ma_{n2}\sqrt{k\,R\,T_2} = 0.780\sqrt{(1.4)(287)(359)} = 296\,m/s$$

and the downstream fluid velocity is

$$V_2 = \sqrt{V_{n2}^2 + V_{t2}^2} = \sqrt{296^2 + 319^2} = 435\,m/s$$

and the downstream Mach number is

$$Ma_2 = \frac{V_2}{a_2} = \frac{435}{\sqrt{(1.4)(287)(359)}} = 1.15$$

According to the geometry of Figure 5,



ketabline.com Ebook.ketabline.com

$$\theta = \beta - \tan^{-1}\frac{V_{n2}}{V_{t2}} = 55 - \tan^{-1}\frac{296}{319} = 12.1$$

Other downstream properties can be calculated in the same way as the downstream temperature by using the normal Mach numbers in the normal shock relations.

Prandl-Meyer Expansion Waves

The preceding section demonstrated that when the streamlines of a supersonic flow are turned into the direction of the flow an oblique compression shock wave is formed. Similarly, when the streamlines of a supersonic flow are turned away from the direction of flow as illustrated in Figure 6, an expansion wave system is established. Unlike shock waves (either normal or oblique) which form a strong discontinuity to change the flow conditions, expansion waves are a system of infinitesimally weak waves distributed in such a manner as required to make the required changes in the flow conditions.

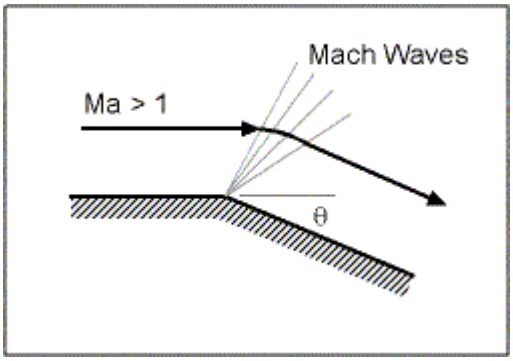


Figure 6

The Mach waves that accomplish the turning of supersonic flows form an angle with respect to the local flow velocity equal to the Mach angle $\mu = \sin^{-1}(1/Ma)$ and are isentropic. Application of the governing conservation equations and equation of state to an infinitesimal turning of the supersonic flow yields



ketabline.com Ebook.ketabline.com

$$-\theta(Ma) = \omega(Ma) = \left(\frac{k+1}{k-1}\right)^{1/2} \tan^{-1}\left[\frac{(k-1)(Ma^2-1)}{k+1}\right]^{1/2} - \tan^{-1}\left(Ma^2-1\right)^{1/2}$$

where $\omega(Ma)$ is the *Prandl-Meyer expansion function*. The overall change in the flow angle as a supersonic flow undergoes a Prandl-Meyer expansion is then

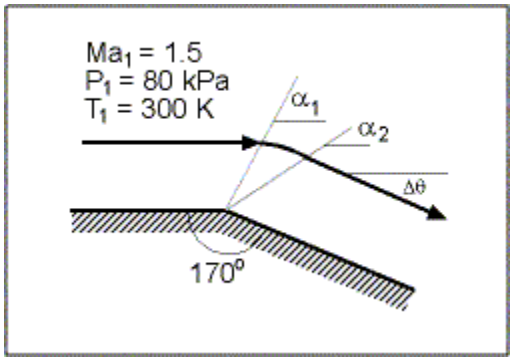
$$\Delta\theta = \omega(Ma_1) - \omega(Ma_2)$$

where 1 refers to the upstream condition and 2 refers to the downstream condition.

The flow through a Prandl-Meyer expansion fan is isentropic flow. The isentropic flow equations can then be used to relate the fluid properties upstream and downstream of the expansion fan.

Example:

Air at 80 kPa, 300 K with a Mach number of 1.5 turns the sharp corner of an airfoil as shown here. Determine the angles of the initial and final Mach waves, and the downstream pressure and temperature of this flow.



The initial angle between the flow velocity vector and the Prandtl-Meyer fan is the Mach angle.

$$\alpha_1 = \sin^{-1}\frac{1}{Ma_1} = \sin^{-1}\frac{1}{1.5} = 41.8^0$$



ketabline.com Ebook.ketabline.com

The upstream Prandtl-Meyer function is

$$\omega(Ma_1) = \left(\frac{k+1}{k-1}\right)^{1/2} \tan^{-1}\left[\frac{(k-1)\left(Ma_1^2-1\right)}{k+1}\right]^{1/2} - \tan^{-1}\left(Ma_1^2-1\right)^{1/2}$$

$$\omega(Ma_1) = \left(\frac{2.4}{0.4}\right)^{1/2} \tan^{-1}\left[\frac{(0.4)\left(1.5^2-1\right)}{2.4}\right]^{1/2} - \tan^{-1}\left(1.5^2-1\right)^{1/2}$$

$$\omega(Ma_1) = 11.90^0$$

The downstream Prandtl-Meyer function is then

$$\omega(Ma_2) = \omega(Ma_1) - \Delta\theta = 11.9^0 - 10^0 = 1.90^0$$

Solving the Prandtl-Meyer function gives the downstream Mach number $Ma_2 = 1.13$. The downstream Mach angle is then $\mu_2 = 62.2^0$. According to the geometry of the above figure,

$$\alpha_2 = \mu_2 - \Delta\theta = 62.2^0 - 10^0 = 52.2^0$$

Since T_0 and P_0 remain constant, the isentropic flow relations yield

$$T_2 = T_1 \frac{T_{01}}{T_1}\frac{T_2}{T_{02}} = T_1 \frac{1+\dfrac{k-1}{2}Ma_1^2}{1+\dfrac{k-1}{2}Ma_2^2} = 300\,\frac{1+0.2(1.5)^2}{1+0.2(1.13)} = 346\,K$$

$$P_2 = P_1 \frac{P_{01}}{P_1}\frac{P_2}{P_{02}} = P_1 \frac{\left[1+\dfrac{k-1}{2}Ma_1^2\right]^{k/(k-1)}}{\left[1+\dfrac{k-1}{2}Ma_2^2\right]^{3.5}} = 80\left[\frac{1+0.2(1.5)^2}{1+0.2(1.13)}\right]^{3.5} = 132\,MPa$$

Students are encouraged to examine the flow visualization photographs in Ch 9.



ketabline.com Ebook.ketabline.com

Ch. 10 Open-Channel Flow

Previous internal flow analyses have considered only closed conduits where the fluid typically fills the entire conduit and may be either a liquid or a gas.

This chapter considers only partially filled channels of liquid flow referred to as open-channel flow.

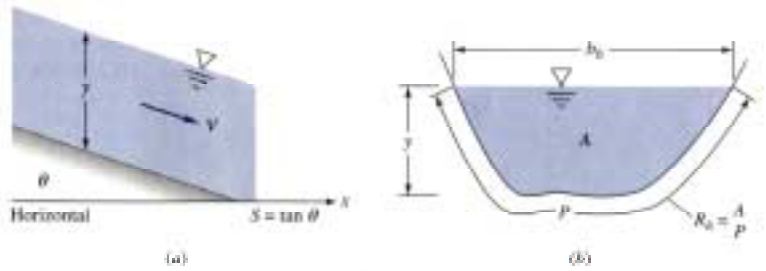
Open-Channel Flow: Flow of a liquid in a conduit with a free surface.

Open-channel flow analysis basically results in the balance of *gravity and friction forces*.

One Dimensional Approximation

While open-channel flow can, in general, be very complex (three dimensional and transient), one common approximation in basic analyses is the

One-D Approximation:
The flow at any local cross section can be treated as uniform and at most varies only in the principal flow direction.



This results in the following equations.

Conservation of Mass (for ρ = constant)

$$Q = V(x)\,A(x) = \text{constant}$$

Energy Equation

$$\frac{V_1^2}{2g} + Z_1 = \frac{V_2^2}{2g} + Z_2 + h_f$$

ketabline.com Ebook.ketabline.com

The equation in this form is written between two points (1 – 2) on the free surface of the flow. Note that along the free surface, the pressure is a constant, is equal to local atmospheric pressure, and does not contribute to the analysis with the energy equation.

The friction head loss h_f is analogous to the head loss term in duct flow, Ch. VI, and can be represented by

$$h_f = f\frac{x_2 - x_1}{D_h}\frac{V_{avg}^2}{2g}$$

where P = wetted perimeter

D_h = hydraulic diameter = $\frac{4A}{P}$

Note: One of the most commonly used formulas uses the hydraulic radius:

$$R_h = \frac{1}{4}D_h = \frac{A}{P}$$

Flow Classification by Depth Variation

The most common classification method is by rate of change of free-surface depth. The classes are summarized as

1. Uniform flow (constant depth and slope)
2. Varied flow
   a. Gradually varied (one-dimensional)
   b. Rapidly varied (multidimensional)

Flow Classification by Froude Number: Surface Wave Speed

A second classification method is by the dimensionless Froude number, which is a dimensionless surface wave speed. For a rectangular or very wide channel we have

$$Fr = \frac{V}{c_o} = \frac{V}{(gy)^{1/2}}$$ where y is the water depth

and c_o = the speed of a surface wave as the wave height approaches zero.

There are three flow regimes of incompressible flow. These have analogous flow regimes in compressible flow as shown below:



ketabline.com Ebook.ketabline.com

Incompressible Flow		Compressible Flow	
Fr < 1	subcritical flow	Ma < 1	subsonic flow
Fr = 1	critical flow	Ma = 1	sonic flow
Fr > 1	supercritical flow	Ma > 1	supersonic flow

Hydraulic Jump

Analogous to a normal shock in compressible flow, a hydraulic jump provides a mechanism by which an incompressible flow, once having accelerated to the supercritical regime, can return to subcritical flow. This is illustrated by the following figure.

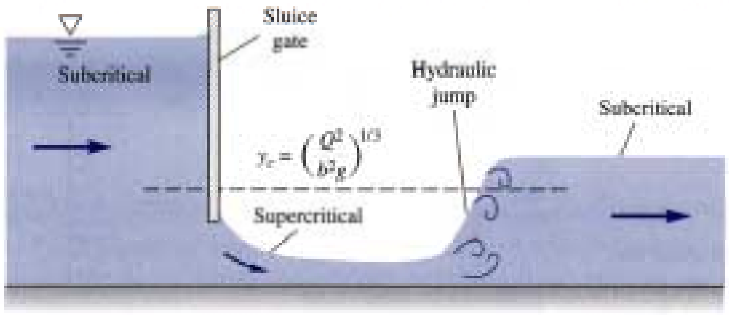


Fig. 10.5 Flow under a sluice gate accelerates from subcritical to critical to supercritical and then jumps back to subcritical flow.

The critical depth $y_c = \left(\frac{Q}{b^2 g}\right)^{1/3}$ is an important parameter in open-channel flow and is used to determine the local flow regime (Sec. 10.4).

Uniform Flow; the Chezy Formula

Uniform flow

1. Occurs in long straight runs of constant slope
2. The velocity is constant with $V = V_o$
3. Slope is constant with $S_o = \tan\theta$

ketabline.com Ebook.ketabline.com

From the energy equation with $V_1 = V_2 = V_o$, we have

$$h_f = Z_1 - Z_2 = S_o L$$

Since the flow is fully developed, we can write from Ch. VI

$$h_f = f\frac{L}{D_h}\frac{V_o^2}{2g} \qquad \text{and} \qquad V_o = \left(\frac{8g}{f}\right)^{1/2} R_h^{1/2} S_o^{1/2}$$

For fully developed, uniform flow, the quantity $\left(\frac{8g}{f}\right)^{1/2}$ is a constant and can be denoted by C. The equations for velocity and flow rate thus become

$$V_o = C R_h^{1/2} S_o^{1/2} \qquad \text{and} \qquad Q = C A R_h^{1/2} S_o^{1/2}$$

The quantity C is called the Chezy coefficient, and varies from 60 $ft^{1/2}/s$ for small rough channels to 160 $ft^{1/2}/s$ for large rough channels (30 to 90 $m^{1/2}/s$ in SI).

The Manning Roughness Correlation

The friction factor f in the Chezy equations can be obtained from the Moody chart of Ch. VI. However, since most flows can be considered fully rough, it is appropriate to use Eqn 6.64:

fully rough flow: $$f \approx \left(2.0 \log \frac{3.7 D_h}{\varepsilon}\right)^{-2}$$

However, most engineers use a simple correlation by Robert Manning:

S.I. Units $$V_o(m/s) \approx \frac{\alpha}{n}\left[R_h(m)\right]^{2/3} S_o^{1/2}$$

B.G. Units $$V_o(ft/s) \approx \frac{\alpha}{n}\left[R_h(ft)\right]^{2/3} S_o^{1/2}$$



ketabline.com Ebook.ketabline.com

where n is a roughness parameter given in Table 10.1 and is the same in both systems of units and α is a dimensional constant equal to 1.0 in S.I. units and 1.486 in B.G. units. The volume flow rate is then given by

Uniform flow $$Q = V_o A \approx \frac{\alpha}{n} A R_h^{2/3} S_o^{1/2}$$

Table 10.1 Experimental Values for Manning's n Factor

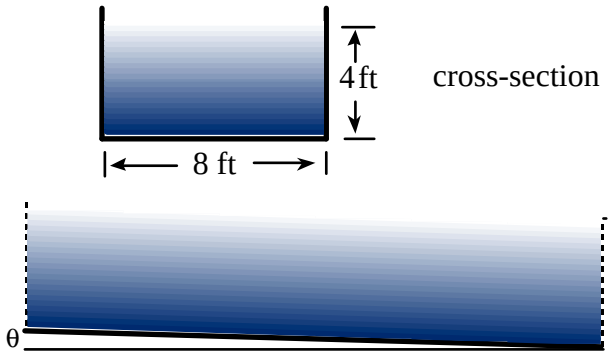
		Average roughness height ϵ	
	n	ft	mm
Artificial lined channels:			
Glass	0.010 ± 0.002	0.0011	0.3
Brass	0.011 ± 0.002	0.0019	0.6
Steel, smooth	0.012 ± 0.002	0.0032	1.0
Painted	0.014 ± 0.003	0.0080	2.4
Riveted	0.015 ± 0.002	0.012	3.7
Cast iron	0.013 ± 0.003	0.0051	1.6
Cement, finished	0.012 ± 0.002	0.0032	1.0
Unfinished	0.014 ± 0.002	0.0080	2.4
Planed wood	0.012 ± 0.002	0.0032	1.0
Clay tile	0.014 ± 0.003	0.0080	2.4
Brickwork	0.015 ± 0.002	0.012	3.7
Asphalt	0.016 ± 0.003	0.018	5.4
Corrugated metal	0.022 ± 0.005	0.12	37
Rubble masonry	0.025 ± 0.005	0.26	80
Excavated earth channels:			
Clean	0.022 ± 0.004	0.12	37
Gravelly	0.025 ± 0.005	0.26	80
Weedy	0.030 ± 0.005	0.8	240
Stony, cobbles	0.035 ± 0.010	1.5	500
Natural channels:			
Clean and straight	0.030 ± 0.005	0.8	240
Sluggish, deep pools	0.040 ± 0.010	3	900
Major rivers	0.035 ± 0.010	1.5	500
Floodplains:			
Pasture, farmland	0.035 ± 0.010	1.5	500
Light brush	0.05 ± 0.02	6	2000
Heavy brush	0.075 ± 0.025	15	5000
Trees	0.15 ± 0.05	?	?



ketabline.com Ebook.ketabline.com

Example 10.1

Given:
Rectangular channel,
finished concrete, slope = 0.5˚
water depth: y = 4 ft, width: b = 8 ft
Find:
Volume flow rate (ft^3/s)



For the given conditions: n = 0.012 $S_o = \tan 0.5^\circ = 0.0873$

$A = b\,y = (8\text{ ft})(4\text{ ft}) = 32\text{ ft}^2$ $P = b + 2y = 8 + 2(4) = 16\text{ ft}$

$$R_h = \frac{A}{P} = \frac{32\text{ ft}^2}{16\text{ ft}} = 2\text{ ft} \qquad D_h = 4R_h = 8\text{ ft}$$

Using Manning's formula in BG units, we obtain for the flow rate

$$Q \approx \frac{1.486}{0.012}(32\text{ ft}^2)(2\text{ ft})^{2/3}(0.00873)^{1.2} \approx 590\text{ ft}^3/\text{s}$$ **ans.**

Alternative Problem

The previous uniform problem can also be formulated where the volume flow rate Q is given and the fluid depth is unknown. For these conditions, the same basic equations are used and the area A and hydraulic radius R_h are expressed in terms of the unknown water depth y_n.

The solution is then obtained using iterative or systematic trial and error techniques that are available in several math analysis/ math solver packages such as EES (provided with the text) or Mathcad ®.



ketabline.com Ebook.ketabline.com

Uniform Flow in a Partly Full, Circular Pipe

Fig. 10.6 shows a partly full, circular pipe with uniform flow. Since frictional resistance increases with wetted perimeter, but volume flow rate increases with cross sectional flow area,

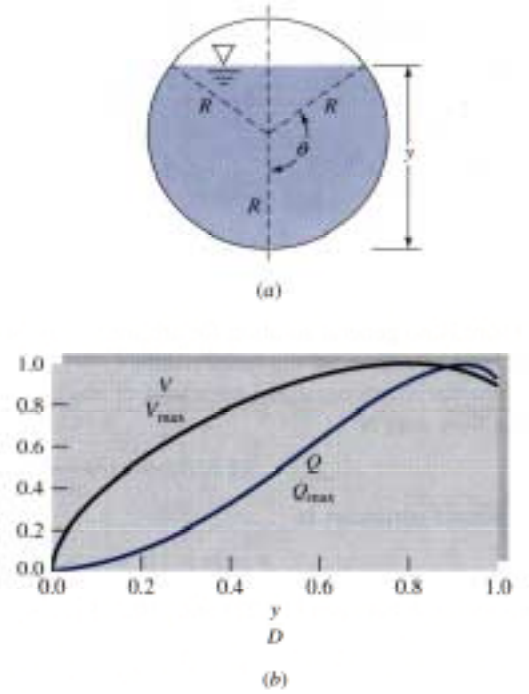


Fig. 10.6 Uniform Flow in a Partly Full, Circular Channel

the maximum velocity and flow rate occur before the pipe is completely full.

For this condition, the geometric properties of the flow are given by the equations below.

$$A = R^2\left(\theta - \frac{\sin 2\theta}{2}\right) \qquad P = 2R\theta \qquad R_h = \frac{R}{2}\left(1 - \frac{\sin 2\theta}{2\theta}\right)$$

The previous Manning formulas are used to predict V_o and Q for uniform flow when the above expressions are substituted for A, P, and R_h.

$$V_o \approx \frac{\alpha}{n}\left[\frac{R}{2}\left(1 - \frac{\sin 2\theta}{2\theta}\right)\right]^{2/3} S_o^{1/2} \qquad Q = V_o R^2\left(\theta - \frac{\sin 2\theta}{2}\right)$$

These equations have respective maxima for V_o and Q given by

ketabline.com Ebook.ketabline.com

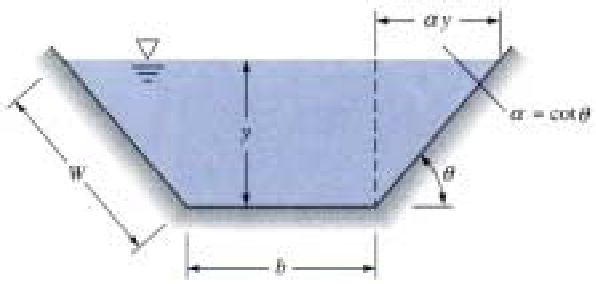
$$V_{max} = 0.718\frac{\alpha}{n} R^{2/3} S_o^{1/2} \quad \text{at} \quad \theta = 128.73^\circ \quad \text{and} \quad y = 0.813\,D$$

$$Q_{max} = 2.129\frac{\alpha}{n} R^{8/3} S_o^{1/2} \quad \text{at} \quad \theta = 151.21^\circ \quad \text{and} \quad y = 0.938\,D$$

Efficient Uniform Flow Channels

A common problem in channel flow is that of finding the most efficient low-resistance sections for given conditions.

This is typically obtained by maximizing R_h for a given area and flow rate. This is the same as minimizing the wetted perimeter.



Note: Minimizing the wetted perimeter for a given flow should minimize the frictional pressure drop per unit length for a given flow.

It is shown in the text that for constant value of area A and $\alpha = \cot\theta$, the minimum value of wetted perimeter is obtained for

$$A = y^2\left[2\left(1+\alpha^2\right)^{1/2} - \alpha\right] \qquad P = 4y\left(1+\alpha^2\right)^{1/2} - 2\alpha y \qquad R_h = \frac{1}{2}y$$

Note: For any trapezoid angle, the most efficient cross section occurs when the hydraulic radius is one-half the depth.

For the special case of a rectangle ($a = 0$, $q = 90^\circ$), the most efficient cross section occurs with

$$A = 2y^2 \qquad P = 4y \qquad R_h = \frac{1}{2}y \qquad b = 2y$$



ketabline.com Ebook.ketabline.com

Best Trapezoid Angle

The general equations listed previously are valid for any value of α. For a given, fixed value of area A and depth y the best trapezoid angle is given by

$$\alpha = \cot\theta = \frac{1}{3^{1/2}} \qquad or \qquad \theta = 60^{o}$$

Example 10.3

What are the best dimensions for a rectangular brick channel designed to carry 5 m^3/s of water in uniform flow with $S_o = 0.001$?

Taking n = 0.015 from Table 10.1, $A = 2y^2$, and $R_h = 1/2\ y$; Manning's formula is written as

$$Q \approx \frac{1.0}{n} A R_h^{2/3} S_o^{1/2} \quad or \quad 5 m^3/s = \frac{1.0}{0.015}(2y^2)\left(\frac{1}{2}y\right)^{2/3}(0.001)^{1/2}$$

This can be solved to obtain

$$y^{8/3} = 1.882\ m^{8/3} \qquad or \qquad y = 1.27 m$$

The corresponding area and width are

$$A = 2y^2 = 3.21 m^2 \qquad and \qquad b = \frac{A}{y} = 2.53 m$$

Note: The text compares these results with those for two other geometries having the same area.



ketabline.com Ebook.ketabline.com

Specific Energy: Critical Depth

One useful parameter in channel flow is the specific energy E, where y is the local water depth.

$$E = y + \frac{V^2}{2g}$$

Defining a flow per unit channel width as $q = Q/b$ we write

$$E = y + \frac{q^2}{2gy^2}$$

Fig. 10.8b is a plot of the water depth y vs. the specific energy E.

The water depth for which E is a minimum is referred to as the critical depth y_c.

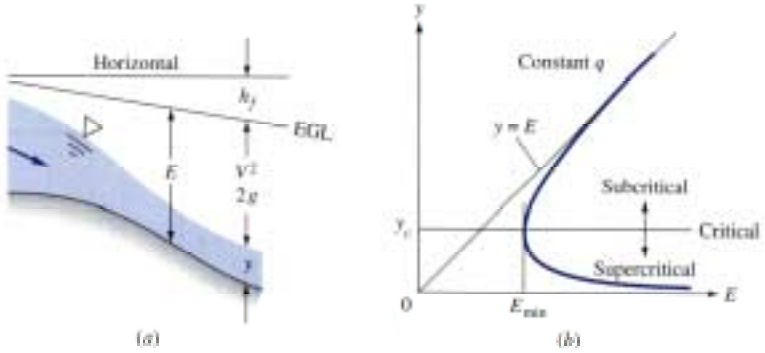


Fig. 10.8 Specific Energy Illustration

E_{min} occurs at

$$y = y_c = \left(\frac{q^2}{g}\right)^{1/3} = \left(\frac{Q^2}{b^2 g}\right)^{1/3}$$

The value of E_{min} is given by

$$E_{min} = \frac{3}{2} y_c$$

At this value of minimum energy and minimum depth we can write

$$V_c = (g y_c)^{1/2} = C_o \quad \text{and} \quad Fr = 1$$



ketabline.com Ebook.ketabline.com

Depending on the value of E_{min} and V, one of several flow conditions can exist.

For a given flow, if

$E < E_{min}$	No solution is possible
$E = E_{min}$	Flow is critical, $y = y_c$, $V = V_c$
$E > E_{min}$, $V < V_c$	Flow is subcritical, $y > y_c$,disturbances can propagate upstream as well as downstream
$E > E_{min}$, $V > V_c$	Flow is supercritical, $y < y_c$, disturbances can only propagate downstream within a wave angle given by $\mu = \sin^{-1}\frac{C_o}{V} = \sin^{-1}\frac{(gy)^{1/2}}{V}$

Nonrectangular Channels

For flows where the local channel width varies with depth y, critical values can be expressed as

$$A_c = \left(\frac{b_o Q^2}{g}\right)^{1/3} \quad \text{and} \quad V_c = \frac{Q}{A_c} = \left(\frac{g A_c}{b_o}\right)^{1/2}$$

where b_o = channel width at the free surface.

These equations must be solved iteratively to determine the critical area A_c and critical velocity V_c.

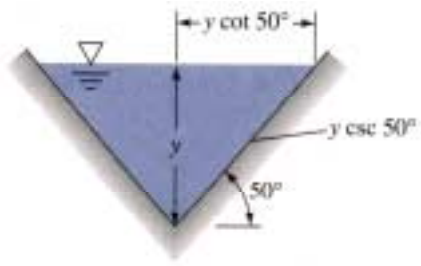
For critical channel flow that is also moving with constant depth (y_c), the slope corresponds to a critical slope S_c given by



ketabline.com Ebook.ketabline.com

$$S_c = \frac{n^2 g A_c}{\alpha^2 b_o R_{h,c}}$$ and α = 1. for S I units and 2.208 for B. G. units

Example 10.5



Given: a 50˚, triangular channel has a flow rate of Q = 16 m^3/s.

Compute: (a) y_c, (b) V_c,

(c) S_c for n = 0.018

a. For the given geometry, we have

P = 2 (y csc 50˚) A = 2[y (1/2 y cot 50˚)]

R_h = A/P = y/2 cos 50˚ b_o = 2 (y cot 50˚)

For critical flow, we can write

$$g A_c^3 = b_o Q^2 \quad or \quad g\left(y_c^2 \cot 50°\right) = \left(2 y_c \cot 50°\right) Q^2$$

y_c = 2.37 m **ans.**

b. With y_c, we compute

P_c = 6.18 m A_c = 4.70 m^2 $b_{o,c}$ = 3.97 m

The critical velocity is now $$V_c = \frac{Q}{A} = \frac{16\, m^3/s}{4.70\, m} = 3.41\, m/s$$ **ans.**

c. With n = 0.018, we compute the critical slope as

$$S_c = \frac{g\, n^2 P}{\alpha^2 b_o R_h^{1/3}} = \frac{9.81(0.018)^2 (6.18)}{1.0^2 (3.97)(0.76)^{1/3}} = 0.0542$$



ketabline.com Ebook.ketabline.com

Frictionless Flow over a Bump

Frictionless flow over a bump provides a second interesting analogy, that of compressible gas flow in a nozzle.

The flow can either increase or decrease in depth depending on whether the initial flow is subcritical or supercritical.

The height of the bump can also change the results of the downstream flow.

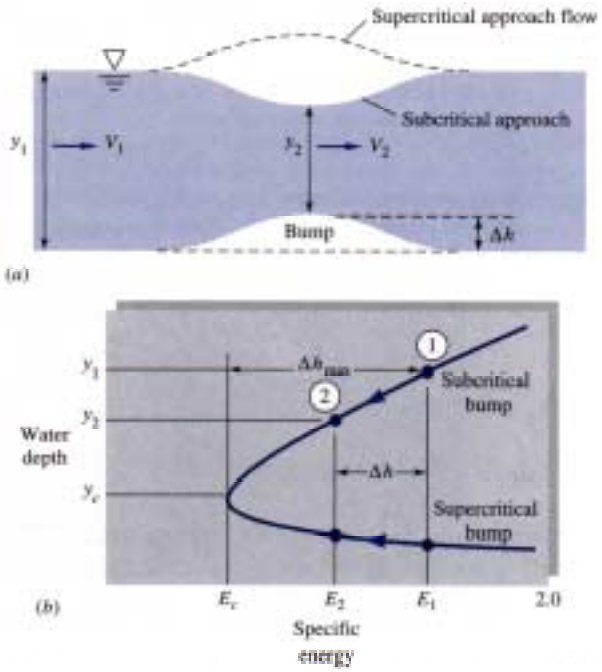


Fig. 10.9 Frictionless, 2-D flow over a bump

Writing the continuity and energy equations for two dimensional, frictionless flow between sections 1 and 2 in Fig. 10.10, we have

$$V_1 y_1 = V_2 y_2 \quad and \quad \frac{V_1^2}{2g} + y_1 = \frac{V_2^2}{2g} + y_2 + \Delta h$$

Eliminating V_2, we obtain

$$y_2^3 - E_2 y_2^2 + \frac{V_1^2 y_1^2}{2g} = 0 \quad where \quad E_2 = \frac{V_1^2}{2g} + y_1 - \Delta h$$

The problem has the following solutions depending on the initial flow condition and the height of the jump:



ketabline.com Ebook.ketabline.com

Key Points:

1. The specific energy E_2 is exactly Δh less than the approach energy E_1.
2. Point 2 will lie on the same leg of the curve as point 1.
3. For Fr < 1, subcritical approach — The water level will decrease at the bump. Flow at point 2 will be subcritical.
4. For Fr > 1, supercritical approach — The water level will increase at the bump. Flow at point 2 will be supercritical.
5. For bump height equal to $\Delta h_{max} = E_1 - E_c$ — Flow at the crest will be exactly critical (Fr =1).
6. For $\Delta h > \Delta h_{max}$ — No physically correct, frictionless solutions are possible. Instead, the channel will choke and typically result in a hydraulic jump.

Flow under a Sluice Gate

A sluice gate is a bottom opening in a wall as shown below in Fig. 10.10a. For free discharge through the gap, the flow smoothly accelerates to critical flow near the gap and the supercritical flow downstream.

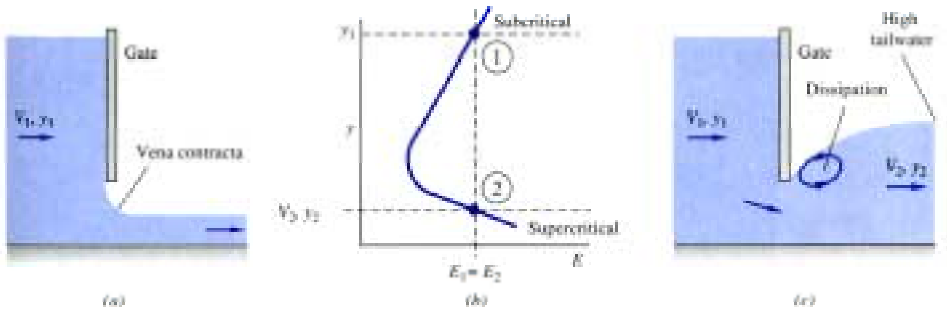


Fig. 10.10 Flow under a sluice gate

This is analogous to the compressible flow through a converging-diverging nozzle. For a free discharge, we can neglect friction. Since this flow has no bump ($\Delta h = 0$) and $E_1 = E_2$, we can write



ketabline.com Ebook.ketabline.com

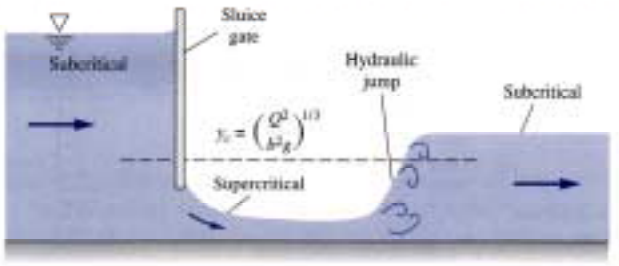
$$y_2^3 - \left(\frac{V_1^2}{2g} + y_1\right) y_2^2 + \frac{V_1^2 y_1^2}{2g} = 0$$

This equation has the following possible solutions.

Subcritical upstream flow and low to moderate tailwater (downstream water level)	One positive, real solution. Supercritical flow at y_2 with the same specific energy $E_2 = E_1$. Flow rate varies as y_2/y_1. Maximum flow is obtained for $y_2/y_1 = 2/3$.
Subcritical upstream flow and high tailwater	The sluice gate is drowned or partially drowned (analogous to a choked condition in compressible flow). Energy dissipation will occur downstream in the form of a hydraulic jump and the flow downstream will be subcritical.

The Hydraulic Jump

The hydraulic jump is an irreversible, frictional dissipation of energy which provides a mechanism for super-critical flow to transition (jump) to subcritical flow analogous to a normal shock in compressible flow.



The development of the theory is equivalent to that for a strong fixed wave (Sec 10.1) and is summarized for a hydraulic jump in the following section.



ketabline.com Ebook.ketabline.com

Theory for a Hydraulic Jump

If we apply the continuity and momentum equations between points 1 and 2 across a hydraulic jump, we obtain

$$\frac{2\,y_2}{y_1} = -1 + \left(1 + 8\,Fr_1^2\right)^{1/2}$$ which can be solved for y_2.

We obtain V_2 from continuity: $$V_2 = \frac{V_1\,y_1}{y_2}$$

The dissipation head loss is obtained from the energy equation as

$$h_f = E_1 - E_2 = \left(\frac{V_1^2}{2\,g} + y_1\right) - \left(\frac{V_2^2}{2\,g} + y_2\right)$$

or

$$h_f = \frac{\left(y_2 - y_1\right)^3}{4\,y_1\,y_2}$$

Key points:

1. Since the dissipation loss must be positive, y_2 must be > y_1.
2. The initial Froude number Fr_1 must be > 1 (supercritical flow).
3. The downstream flow must be subcritical and $V_2 < V_1$.

Example 10.7

Water flows in a wide channel at q = 10 m^3/(s m) and y_1 = 1.25 m. If the flow undergoes a hydraulic jump, compute: (a) y_2, (b) V_2, (c) Fr_2, (d) h_f, (e) the percentage dissipation, (f) power dissipated/unit width, and (g) temperature rise.



ketabline.com Ebook.ketabline.com

a. The upstream velocity is $$V_1 = \frac{q}{y_1} = \frac{10\,m^3/(s\cdot m)}{1.25\,m} = 8.0\,m/s$$

The upstream Froude number is $$Fr_1 = \frac{V_1}{(g\,y_1)^{1/2}} = \frac{8.0}{[9.81(1.25)]^{1/2}} = 2.285$$

This is a weak jump and y_2 is given by

$$\frac{2\,y_2}{y_1} = -1 + \left(1 + 8\,(2.285)^2\right)^{1/2} = 5.54$$

and

$$y_2 = 1/2\; y_1(5.54) = 3.46\,m$$

b. The downstream velocity is $$V_2 = \frac{V_1\,y_1}{y_2} = \frac{8.0(1.25)}{3.46} = 2.89\,m/s$$

c. The downstream Froude number is

$$Fr_2 = \frac{V_2}{(g\,y_2)^{1/2}} = \frac{2.89}{[9.81(3.46)]^{1/2}} = 0.496$$

and Fr_2 is subcritical as expected.

d. The dissipation loss is given by

$$h_f = \frac{(y_2 - y_1)^3}{4\,y_1\,y_2} = \frac{(3.46 - 1.25)^3}{4(3.46)(1.25)} = 0.625\,m$$

e. The percentage dissipation is the ratio of h_f/E_1.

$$E_1 = \frac{V_1^2}{2g} + y_1 = 1.25 + \frac{8.0^2}{2\,(9.81)} = 4.51m$$



ketabline.com Ebook.ketabline.com

The percentage loss is thus given by

$$\% \, Loss = \frac{h_f}{E_1} 100 = \frac{0.625}{4.51} 100 = 14\%$$

f. The power dissipated per unit width is

$$\text{Power} = \rho \, Q \, g \, h_f = 9800 \text{ M/m}^3 * 10 \text{ m}^3/(\text{s m}) * 0.625 \text{ m} = 61.3 \text{ kw/m}$$

g. Using C_p = 4200 J/kg K, the temperature rise is given by

$$Power \; dissipated = \dot{m} C_p \Delta T$$

or

$$61{,}300 \text{ W/m} = 10{,}000 \text{ kg/s m} * 4200 \text{ J/kg K} * \Delta T$$

$$\Delta T = 0.0015^{\circ}\text{K}$$

negligible temperature rise



ketabline.com Ebook.ketabline.com

XI. Turbomachinery

This chapter considers the theory and performance characteristics of the mechanical devices associated with the fluid circulation.

General Classification:

Turbomachine - A device which adds or extracts energy from a fluid.

Adds energy:	Pump
Extracts energy:	Turbine

In this context, a pump is a generic classification that includes any device that adds energy to a fluid, e.g. fans, blowers, compressors.

We can classify pumps by operating concept:

1. Positive displacement
2. Dynamic (momentum change)

General Performance Characteristics

Positive Displacement Pumps

1. Delivers pulsating or periodic flow (cavity opens, fluid enters, cavity closes, decreasing volume forces fluid out exit opening.
2. Not sensitive to wide viscosity changes.
3. Delivers a moderate flow rate.
4. Produces a high pressure rise.
5. Small range of flow rate operation (fixed pump speed).

Dynamic Pumps

1. Typically higher flow rates than PD's.
2. Comparatively steady discharge.
3. Moderate to low pressure rise.
4. Large range of flow rate operation.
5. Very sensitive to fluid viscosity.



ketabline.com Ebook.ketabline.com

Typical Performance Curves (at fixed impeller speed)

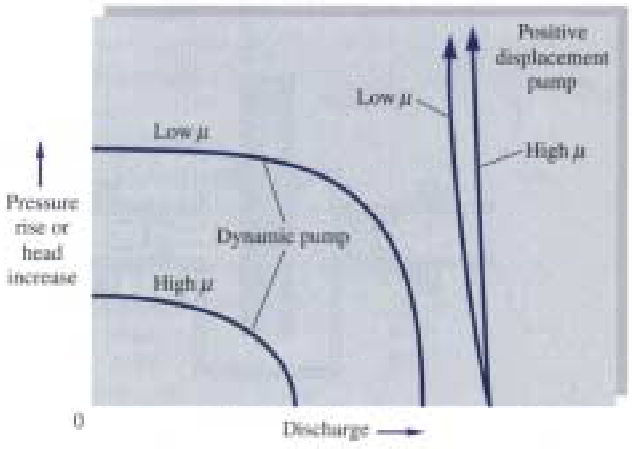


Fig. 11.2 Performance curves for dynamic and positive displacement pumps

Centrifugal Pumps

Most common turbomachine used in industry. Includes the general categories of (a) liquid pumps, (b) fans, (c) blowers, etc.

They are momentum change devices and thus fall within the dynamic classification.

Typical schematic shown as

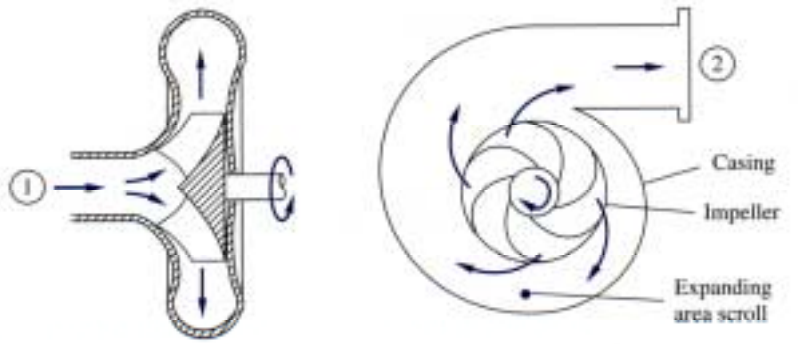


Fig. 11.3 Cutaway schematic of a typical centrifugal pump

ketabline.com Ebook.ketabline.com

Writing the energy equation across the device and solving for $h_p - h_f$,we have

$$H = h_p - h_f = \frac{P_2 - P_1}{\rho g} + \frac{V_2^2 - V_1^2}{2g} + Z_2 - Z_1$$

where H is the net useful head delivered to the fluid, the head that results in pressure, velocity, and static elevation change.

Since for most pumps (not all), $V_1 = V_2$ and ΔZ is small, we can write

$$H \cong \frac{\Delta P}{\rho g}$$

Since friction losses have already been subtracted, this is the ideal head delivered to the fluid. Note that velocity head has been neglected and can be significant at large flow rates where pressure head is small.

The ideal power to the fluid is given by

$$P_w = \rho\, Q\, g\, H$$

The pump efficiency is given by

$$\eta = \frac{P_w}{BHP} = \frac{\rho Q g H}{BHP} = \frac{\rho Q g H}{\omega T}$$

where BHP = shaft power necessary to drive the pump

ω = angular speed of shaft

T = torque delivered to pump shaft

Note that from the efficiency equation, pump efficiency is zero at zero flow rate Q and at zero pump head,H.



ketabline.com Ebook.ketabline.com

Basic Pump Theory

Development of basic pump theory begins with application of the integral conservation equation for moment-of-momentum previously presented in Ch. III.

Applying this equation to a centrifugal pump with one inlet, one exit, and uniform properties at each inlet and exit, we obtain

$$\bar{T} = \dot{m}_e \, \bar{r} \times \bar{V}_e - \dot{m}_i \, \bar{r} \times \bar{V}_i$$

where $\bar{T}$ is the shaft torque needed to drive the pump

$\bar{V}_i$, $\bar{V}_e$ are the absolute velocities at the inlet and exit of the pump

This is used to determine the change of angular momentum across the device.

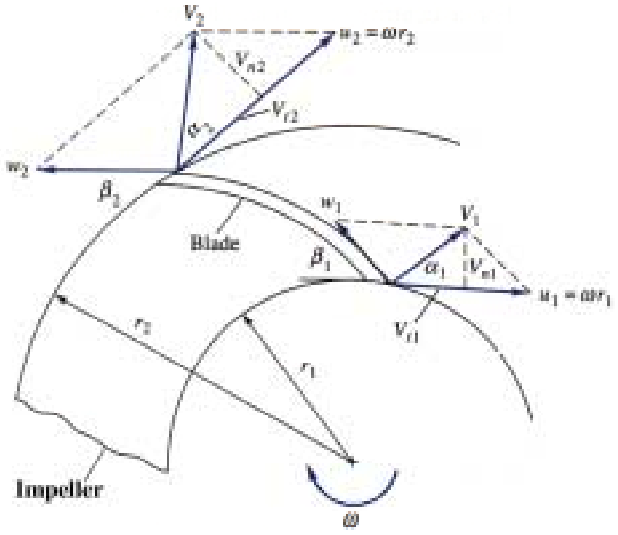


Fig. 11.4 Inlet and exit velocity diagrams for an idealized impeller

Since the velocity diagram is key to the analysis of the device, we will discuss the elements in detail.



ketabline.com Ebook.ketabline.com

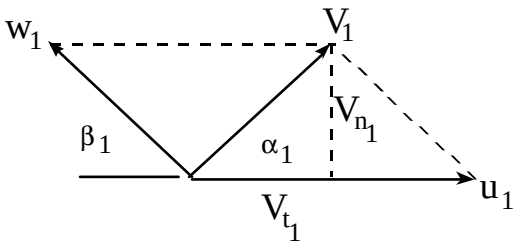
1. At the inner radius r_1 have two velocity components:

a. the circumferential velocity due to the impeller rotation

$u_1 = r_1 \omega$ blade tip speed at inner radius

b. relative flow velocity tangent to the blade

w_1 tangent to the blade angle β_1



These combine to yield the absolute inlet velocity V_1 at angle α_1

The absolute velocity can be resolved into two absolute velocity components:

1. Normal (radial) component:

$V_{n_1} = V_1 \sin\alpha_1 = w_1 \sin\beta_1$

Note that for ideal pump design,

$V_{n_1} = V_1$ *and* $\alpha_1 = 90^o$

2. Absolute tangential velocity:

$V_{t_1} = V_1 \cos\alpha_1 = u_1 - w_1 \cos\beta_1$ again, ideally $V_{t_1} = 0$

It is also important to note that V_{n_1} is use to determine the inlet flow rate, i.e.,

$$Q = A_1 V_{n_1} = 2\pi r_1 b_1 V_{n_1}$$

where b_1 is the inlet blade width



ketabline.com Ebook.ketabline.com

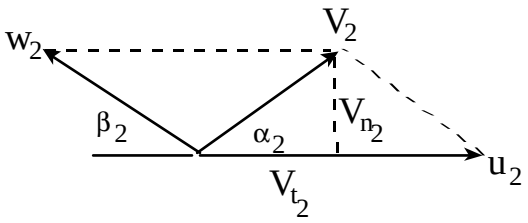
Likewise for the outer radius r_2 we have the following:

a. the circumferential velocity due to the impeller rotation

$u_2 = r_2 \omega$ blade tip speed at outer radius

b. relative flow velocity tangent to the blade

w_2 tangent to the blade angle β_2



These again combine to yield the absolute outlet velocity V_2 at angle α_2

The exit absolute velocity can also be resolved into two absolute velocity components:

1. Normal (radial) component:

$$V_{n_2} = V_2 \sin\alpha_2 = w_2 \sin\beta_2 = \frac{Q}{2\pi r_2 b_2}$$

Note that Q is the same as for the inlet flow rate

2. Absolute tangential velocity:

$$V_{t_2} = V_2 \cos\alpha_2 = u_2 - w_2 \cos\beta_2$$

$$V_{t_2} = u_2 - \frac{V_{n_2}}{\tan\beta_2} = u_2 - \frac{Q}{2\pi r_2 b_2 \tan\beta_2}$$

where $Q = A_1 V_{n_1} = 2\pi r_1 b_1 V_{n_1} = A_2 V_{n_2} = 2\pi r_2 b_2 V_{n_2}$

Again, each of the above expressions follows easily from the velocity diagram, and the student should draw and use the diagram with each pump theory problem.



ketabline.com Ebook.ketabline.com

We can now apply moment - of – momentum equation.

$$\overline{T} = \rho Q\left\{r_2 * V_{t_2} - r_1 * V_{t_1}\right\}$$ (again V_{t1} is zero for the ideal design)

For a sign convention, we have assumed that V_{t1} and V_{t2} are positive in the direction of impeller rotation.

The " ideal" power supplied to the fluid is given by

$$P_w = \omega\overline{T} = \rho Q\left\{\omega r_2\ V_{t_2} - \omega r_1\ V_{t_1}\right\}$$

or

$$P_w = \omega\overline{T} = \rho Q\left\{u_2\ V_{t_2} - u_1\ V_{t_1}\right\} = \rho Q g H$$

Since these are ideal values, the shaft power required to drive a non-ideal pump is given by

$$BHP = \frac{P_w}{\eta_p}$$

The head delivered to the fluid is

$$H = \frac{\rho Q\left\{u_2\ V_{t_2} - u_1\ V_{t_1}\right\}}{\rho Q g} = \frac{\left\{u_2\ V_{t_2} - u_1\ V_{t_1}\right\}}{g}$$

For the special case of purely radial inlet flow

$$H^* = \frac{u_2\ V_{t_2}}{g}$$



ketabline.com Ebook.ketabline.com

From the exit velocity diagram, substituting for V_{t2} we can show that

$$H = \frac{u_2^2}{g} - \frac{\omega Q}{2\pi b_2 g \tan\beta_2}$$ has the form $C_1 - C_2 Q$

where: $C_1 = \frac{u_2^2}{g}$ shutoff head, the head produced at zero flow, Q = 0

Example:

A centrifugal water pump operates at the following conditions:

speed = 1440 rpm, r_1 = 4 in, r_2 = 7 in, $\beta_1 = 30^o$, $\beta_2 = 20^o$, $b_1 = b_2$ = 1.75 in

Assuming the inlet flow enters normal to the impeller (zero absolute tangential velocity):

find: (a) Q, (b) T, (c) W_p, (d) h_p, (e) ΔP

$$\omega = 1440 \frac{\text{rev}}{\text{min}} \frac{2\pi}{60} = 150.8 \frac{\text{rad}}{\text{s}}$$

Calculate blade tip velocities:

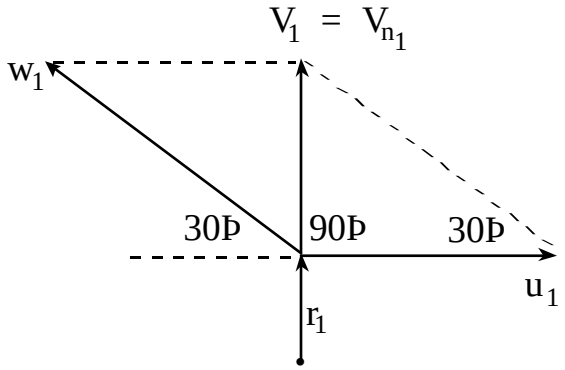
$$u_1 = r_1 \omega = \frac{4}{12} \text{ft} \, 150.8 \frac{\text{rad}}{\text{s}} = 50.3 \frac{\text{ft}}{\text{s}} \qquad u_2 = r_2 \omega = \frac{7}{12} \text{ft} \, 150.8 \frac{\text{rad}}{\text{s}} = 88 \frac{\text{ft}}{\text{s}}$$

Since design is ideal, at inlet

$\alpha_1 = 90^o$, $V_{t1} = 0$

$V_{n1} = U_1 \tan 30^0 = 50.3 \tan 30^o = 29.04$ ft/s

$$Q = 2\pi r_1 b_1 V_{n_1}$$



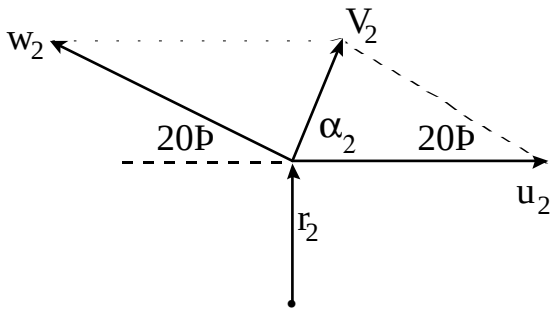
ketabline.com Ebook.ketabline.com

$$Q = 2\pi\frac{4}{12}\,\text{ft}\,1.75\,\text{ft}\,29.04\frac{\text{ft}}{\text{s}} = 8.87\frac{\text{ft}^3}{\text{s}}$$

$$Q = 8.87\frac{\text{ft}^3}{\text{s}}\,60\frac{s}{\text{min}}\,7.48\frac{\text{gal}}{\text{ft}^3} = 3981\frac{\text{gal}}{\text{min}}$$

Repeat for the outlet:

$$V_{n_2} = \frac{Q}{2\pi r_2 b_2} = \frac{8.87\frac{\text{ft}^3}{\text{s}}}{2\pi\frac{7}{12}\,\text{ft}\,\frac{1.75}{12}\,\text{ft}}$$



$$V_{n_2} = 16.6\frac{\text{ft}}{\text{s}}$$

$$w_2 = \frac{V_{n_2}}{\sin 20^o} = \frac{16.6\,\text{ft/s}}{\sin 20^o} = 48.54\frac{\text{ft}}{\text{s}}$$

$$V_{t_2} = u_2 - w_2\cos\beta_2 = 88 \quad - 48.54\cos 20^o = 42.4\frac{\text{ft}}{\text{s}}$$

We are now able to determine the pump performance parameters. Since for the centrifugal pump, the moment arm r_1 at the inlet is zero, the momentum equation becomes

Ideal moment of momentum delivered to the fluid:

$$T = \rho Q\{r_2 * V_{t_2}\} = 1.938\frac{\text{slug}}{\text{ft}^3}\,8.87\frac{\text{ft}^3}{\text{s}}\,\frac{7}{12}\,\text{ft}\,42.4\frac{\text{ft}}{\text{s}} = 425.1\,\text{ft}-\text{lbf}$$

Ideal power delivered to the fluid:

$$P = \omega T = 150.8\frac{\text{rad}}{\text{s}}\,425.1\,\text{ft}-\text{lbf} = 64{,}103\frac{\text{ft}-\text{lbf}}{\text{s}} = 116.5\,\text{hp}$$



ketabline.com Ebook.ketabline.com

Head produced by the pump (ideal):

$$H = \frac{P}{\rho g Q} = \frac{64{,}103\,\text{ft} - \text{lbf/s}}{62.4\,\frac{\text{lbf}}{\text{ft}^3}\,8.87\,\frac{\text{ft}^3}{\text{s}}} = 115.9\,\text{ft}$$

Pressure increase produced by the pump:

$$\Delta P = \rho g H = 62.4\,\frac{\text{ft}^3}{\text{s}}\,115.9\,\text{ft} = 7226\,\text{psf} = 50.2\,\text{psi}$$

Pump Performance Curves and Similarity Laws

Pump performance results are typically obtained from an experimental test of the given pump and are presented graphically for each performance parameter.

- Basic independent variable - Q {usually gpm or cfm }
- Dependent variables typically

  H – head pressure rise, in some cases ΔP

  BHP – input power requirements (motor size)

  η – pump efficiency
- These typically presented at fixed pump speed and impeller diameter

Typical performance curves appear as



ketabline.com Ebook.ketabline.com

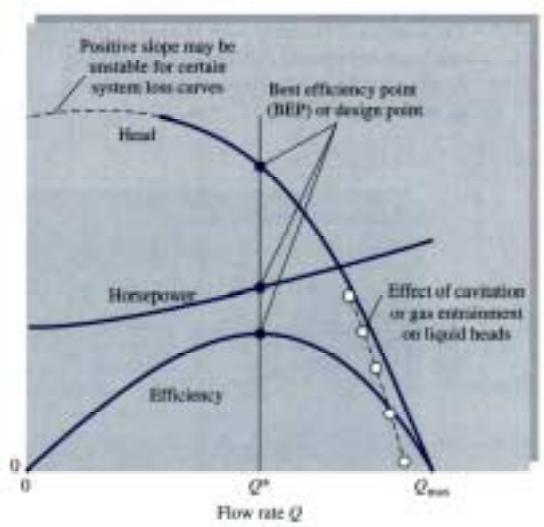


Fig. 11.6 Typical Centrifugal Pump Performance Curves at Fixed Pump Speed and diameter

These curves are observed to have the following characteristics:

1. h_p is approximately constant at low flow rate.
2. $h_p = 0$ at Q_{max}.
3. BHP is not equal to 0 at Q = 0.
4. BHP increases monotonically with the increase in Q.
5. $\eta_p = 0$ at Q = 0 and at Q_{max}.
6. Maximum pump efficiency occurs at approximately $Q^* = 0.6\ Q_{max}$. This is the best efficiency point BEP. At any other operating point, efficiency is less, pump head can be higher or lower, and BHP can be higher or lower.
7. At the BEP, $Q = Q^*$, $h_p = h_p^*$, $BHP = BHP^*$.

Measured Performance Data

Actual pump performance data will typically be presented graphically as shown in Fig. 11.7. Each graph will usually have curves representing the pump head vs flow rate for two or more impeller diameters for a given class/model of pumps having a similar design. The graphs will also show curves of constant efficiency and constant pump power (BHP) for the impeller diameters shown. All curves will be for a fixed pump impeller speed.



ketabline.com Ebook.ketabline.com

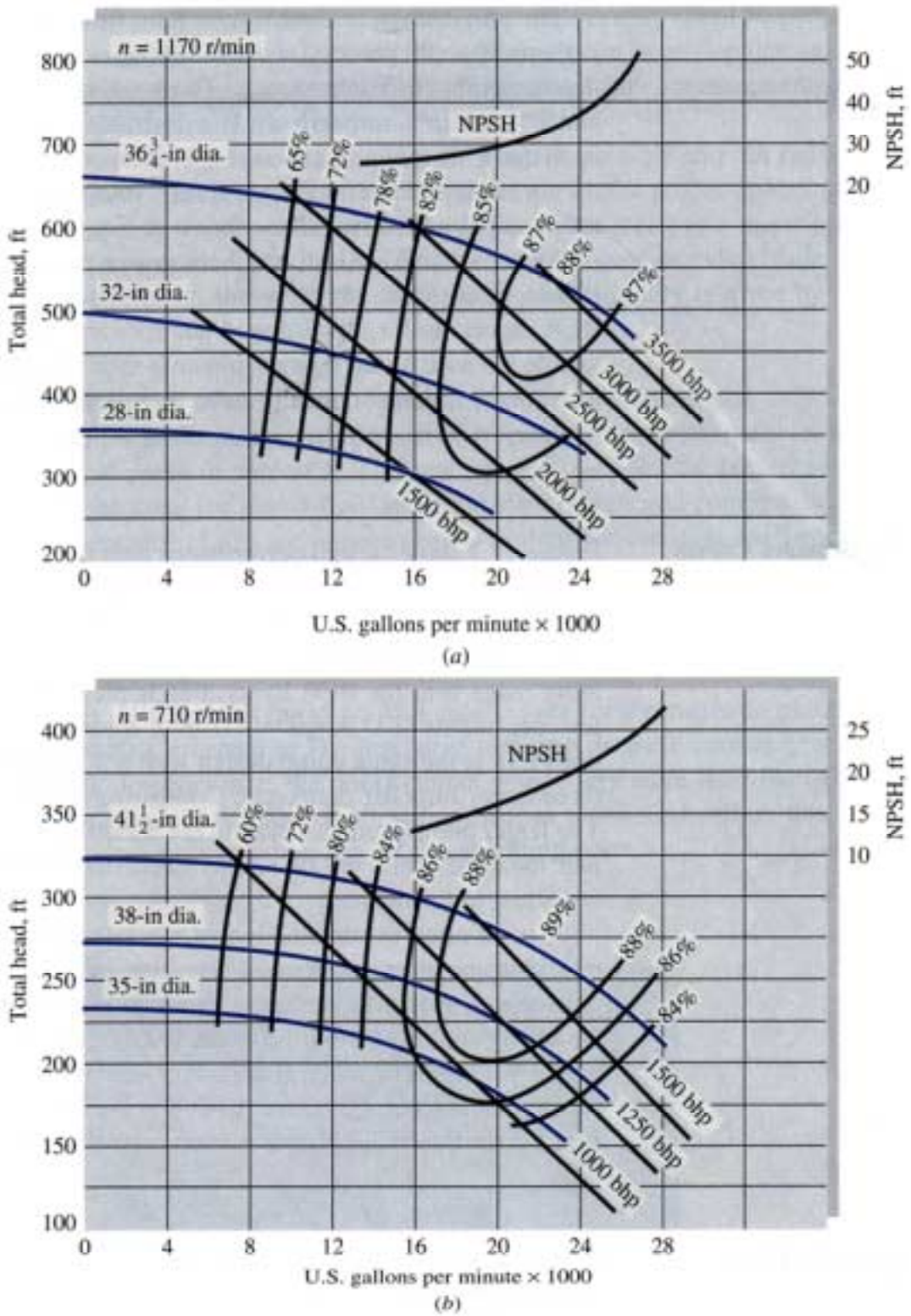


Fig. 11.7 Measured performance curves for two models of a centrifugal water pump

ketabline.com Ebook.ketabline.com

How to Read Pump Performance Curves

Care must be taken to correctly read the performance data from pump curves. This should be done as follows:

(1) For a given flow rate Q

(2) Read vertically to a point on the pump head curve h for the impeller diameter D of interest.

(3) All remaining parameters (efficiency & BHP) are read at this point; i.e., graphically interpolate between adjacent curves for BHP to obtain the pump power at this point.

Note that the resulting values are valid only for the conditions of these curves:

(1) pump model and design, (2) pump speed – N, (3) impeller size – D, (4) fluid (typically water)

Thus for the pump shown in Fig. 11.7a with an impeller diameter D = 32 in, we obtain the following performance at Q = 20,000 gpm:

$$Q = 20{,}000 \text{ gpm}, \; D = 32 \text{ in}, \; N = 1170 \text{ rpm}$$

$$H \cong 385 \text{ ft}, \; BHP \cong 2300 \text{ bhp}, \; \eta_p \cong 86.3 \%$$

Note that points that are not on an h vs. Q curve are not valid operating points. Thus for Fig. 11.7b, the conditions

$$Q = 22{,}000 \text{ gpm}, \; BHP = 1500 \text{ bhp}, \; hp = 250 \text{ ft}$$

do not correspond to a valid operating point because they do not fall on one of the given impeller diameter curves. However, for the same figure, the point

$$Q = 20{,}000 \text{ gpm}, \; BHP = 1250 \text{ bhp}$$

is a valid point because it coincidentally also falls on the D = 38 in impeller curve at hp = 227 ft.



ketabline.com Ebook.ketabline.com

Net Positive Suction Head - NPH

One additional parameter is typically shown on pump performance curves:

NPSH = head required at the pump inlet to keep the fluid from cavitating.

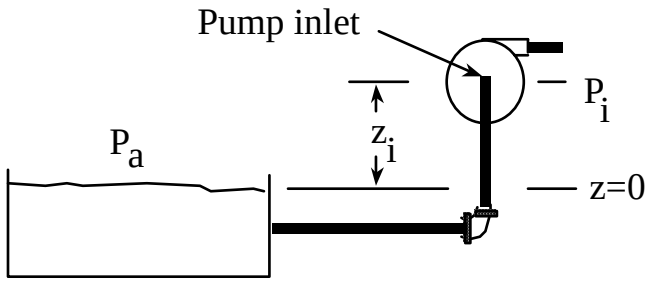
NPSH is defined as follows:

$$NPSH = \frac{P_i}{\rho g} + \frac{V_i^2}{2g} - \frac{P_v}{\rho g}$$

where P_i = pump inlet pressure

P_v = vapor pressure of fluid

Considering the adjacent figure, write the energy equation between the fluid surface and the pump inlet to obtain the following:

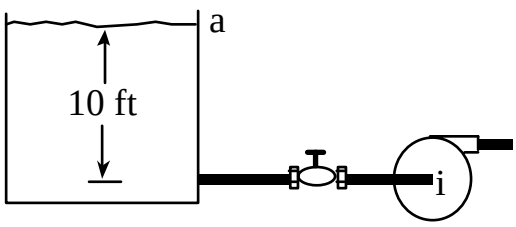


$$NPSH = \frac{P_i}{\rho g} + \frac{V_i^2}{2g} - \frac{P_v}{\rho g} = \frac{P_a}{\rho g} - Z_i - h_{f,a-i} - \frac{P_v}{\rho g}$$

For a pump installation with this configuration to operate as intended, the right-hand-side of the above equation must be > the NPSH value for the operating flow rate for the pump.

Example:

A water supply tank and pump are connected as shown. P_a = 13.6 psia and the water is at 20 °C with P_v = 0.34 psia. The system has a friction loss of 4.34 ft. Will the NPSH of the pump of Fig. 11.7a at 20,000 gpm work?





ketabline.com Ebook.ketabline.com

Applying the previous equation we obtain

$$NPSH = \frac{P_a}{\rho g} - Z_i - h_{f,a-i} - \frac{P_v}{\rho g}$$

$$NPSH = \frac{(13.6 - 0.34)\,lbf/in^2 * 144\,in^2/ft^2}{62.4\,lbf/ft^3} - (-10\,ft) - 4.34\,ft$$

$NPSH = 36.26\,ft$ The pump will work because the system NPSH as shown in Fig. 11.7a is 30 ft which provides a 6.3 ft safety margin. Conversely, the pump could be located as close as 3.7 ft below the water surface and meet NPSH requirements.

Pump Similarity Laws

Application of the dimensional analysis procedures of Ch. V will yield the following three dimensionless performance parameters:

Dimensionless flow coefficient: $C_Q = \frac{Q}{\omega D^3}$

Dimensionless head coefficient: $C_H = \frac{g H}{\omega^2 D^2}$

Dimensionless power coefficient: $C_P = \frac{BHP}{\rho \omega^3 D^5}$

where ω is the pump speed in radians/time and other symbols are standard design and operating parameters with units that make the coefficients dimensionless.

How are these used?

These terms can be used to estimate design and performance changes between two pumps of similar design.



ketabline.com Ebook.ketabline.com

Stated in another way:

If pumps 1 and 2 are from the same geometric design family and are operating at similar operating conditions, the flow rates, pump head, and pump power for the two pumps will be related according to the following expressions:

$$\frac{Q_2}{Q_1} = \frac{N_2}{N_1}\left(\frac{D_2}{D_1}\right)^3$$

Use to predict the new flow rate for a design change in pump speed N and impeller diameter D.

$$\frac{H_2}{H_1} = \left(\frac{N_2}{N_1}\right)^2\left(\frac{D_2}{D_1}\right)^2$$

Used to predict the new pump head H for a design change in pump speed, N and impeller diameter D.

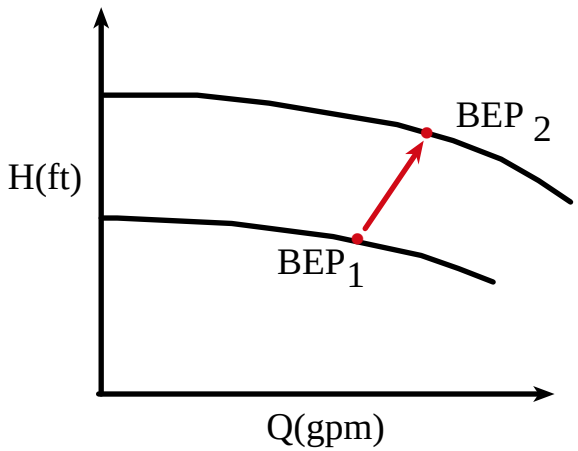
$$\frac{BHP_2}{BHP_1} = \left(\frac{\rho_2}{\rho_1}\right)\left(\frac{N_2}{N_1}\right)^3\left(\frac{D_2}{D_1}\right)^5$$

Used to predict the new pump power BHP for a design change in fluid, ρ, pump speed N and impeller diameter D.

Example

It is desired to modify the operating conditions for the 38 in diameter impeller pump of Fig. 11.7b to a new pump speed of 900 rpm and a larger impeller diameter of 40 in.

Determine the new pump head and power for the new pump speed at the BEP.





ketabline.com Ebook.ketabline.com

For the D = 38 in impeller of Fig. 11.7b operating at 710 rpm, we read the best efficiency point (BEP) values as

$$Q^* = 20{,}000 \text{ gpm}, \quad H^* = 225 \text{ ft}, \quad BHP^* = 1250 \text{ hp}$$

Applying the similarity laws for $N_2 = 900$ rpm and $D_2 = D_1 = 38$ in, we obtain

$$\frac{Q_2}{Q_1} = \frac{N_2}{N_1}\left(\frac{D_2}{D_1}\right)^3 = \frac{900}{710}\left(\frac{40}{38}\right)^3 = 1.478$$

$$Q_2 = 20{,}000*1.478 = 29{,}570 \text{ gpm} \qquad \textbf{ans.}$$

$$\frac{H_2}{H_1} = \left(\frac{N_2}{N_1}\right)^2\left(\frac{D_2}{D_1}\right)^2 = \left(\frac{900}{710}\right)^2\left(\frac{40}{38}\right)^2 = 1.78$$

$$H_2 = 225*1.78 = 400.5 \text{ ft} \qquad \textbf{ans.}$$

$$\frac{BHP_2}{BHP_1} = \left(\frac{\rho_2}{\rho_1}\right)\left(\frac{N_2}{N_1}\right)^3\left(\frac{D_2}{D_1}\right)^5 = (1)\left(\frac{900}{710}\right)^3\left(\frac{40}{38}\right)^5 = 2.632$$

$$BHP2 = 3290 \text{ hp} \qquad \textbf{ans.}$$

Thus, even small changes in the speed and size of a pump can result in significant changes in flow rate, head, and power.

It is noted that every point on the original 38 in diameter performance curve exhibits a similar translation to a new operating condition.

The similarity laws are obviously useful to predict changes in the performance characteristics of an existing pump or to estimate the performance of a modified pump design prior to the construction of a prototype.



ketabline.com Ebook.ketabline.com

Matching a Pump to System Characteristics

The typical design/sizing requirement for a pump is to select a pump which has a pump head which matches the required system head at the design/operating flow rate for the piping system.

Key Point

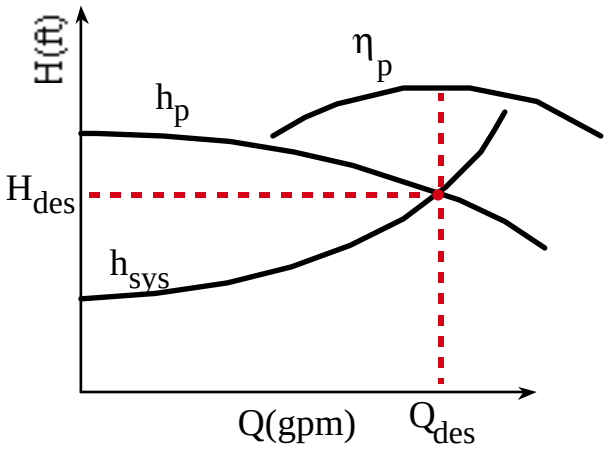
$h_p = h_{sys}$ at Q_{des}.

It is noted that pump selection should occur such that the operating point of the selected pump should occur on the pump curve near or at the BEP.

From the energy equation in Ch. VI, the system head is typically expressed as

$$h_{sys} = \frac{P_2 - P_1}{\rho g} + \frac{V_2^2 - V_1^2}{2g} + Z_2 - Z_1 + \left\{ f\frac{L}{D} + \sum K_i \right\} \frac{V^2}{2g}$$

Thus the selection of a pump for a piping system design should result in a pump for which the pump head h_p at the design flow rate Q_{des} is equal (or very close) to the head requirements h_{sys} of the piping system at the same flow rate, and this should occur at or near the point of maximum efficiency for the chosen pump.



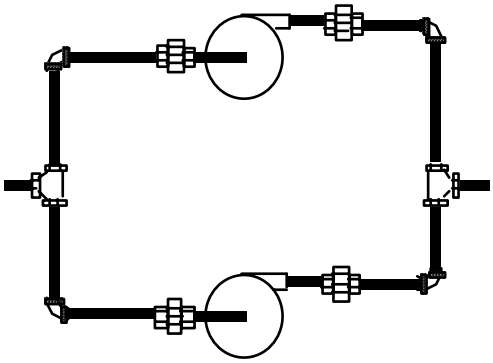
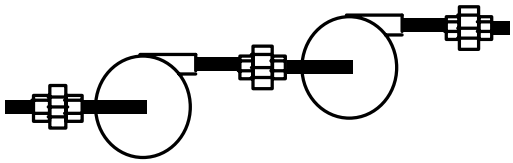
Other operating and performance requirements (such as NPSH) are obviously also a part of the selection criteria for a pump.

ketabline.com Ebook.ketabline.com

Pumping Systems: Parallel and Series Configurations

For some piping system designs, it may be desirable to consider a multiple pump system to meet the design requirements. Two typical options include parallel and series configurations of pumps. Specific performance criteria must be met when considering these options.

Given a piping system which has a known design flow rate and head requirements, Q_{des}, h_{des}. The following pump selection criteria apply.

Pumps in Parallel: Assuming that the pumps are identical, each pump must provide the following: $Q(pump) = 0.5\ Q_{des}$ $h(pump) = h_{des}$	
Pumps in Series: Assuming that the pumps are identical, each pump must provide the following: $Q\ (pump) = Q_{des}$ $h(pump) = 0.5\ h_{des}$	

For example, if the design point for a given piping system were Q_{des} = 600 gpm, and h_{sys} = 270 ft, the following pump selection criteria would apply:

1. Single pump system — Q(pump) = 600 gpm, h_p = 270 ft
2. Parallel pump system — Q(pump) = 300 gpm, h_p = 270 ft for each of the two pumps
3. Series pump system — Q(pump) = 600 gpm, h_p = 135 ft for each of the two pumps

